

UC San Diego

UC San Diego Electronic Theses and Dissertations

Title

Development of Atroposelective Nucleophilic Substitutions Towards Pharmaceutically Relevant N-Heterocyclic Scaffolds

Permalink

<https://escholarship.org/uc/item/6xg5f4qc>

Author

Cardenas, Mariel Manaloto

Publication Date

2024

Peer reviewed|Thesis/dissertation

UNIVERSITY OF CALIFORNIA SAN DIEGO

SAN DIEGO STATE UNIVERSITY

**Development of Atroposelective Nucleophilic Substitutions Towards Pharmaceutically
Relevant *N*-Heterocyclic Scaffolds**

A dissertation submitted in partial satisfaction of the requirements
for the degree Doctor of Philosophy

in

Chemistry

by

Mariel Manaloto Cardenas

Committee in charge:

University of California San Diego

Professor Stacey Brydges
Professor Åsa Gustafsson
Professor Emmanuel Theodorakis

San Diego State University

Professor Jeffrey Gustafson, Chair
Professor Byron Purse

2024

Copyright

Mariel Manaloto Cardenas, 2024

All rights reserved.

The dissertation of Mariel Manaloto Cardenas is approved, and it is acceptable in quality and form for publication on microfilm and electronically.

Chair

University of California San Diego

San Diego State University

2024

DEDICATION

I dedicate my dissertation to God,
to my parents Maria and Mike Cardenas,
to my little sisters Melisa and Melarie Cardenas,
to my relatives,
and to all my friends for
their love and support.

TABLE OF CONTENTS

DISSERTATION APPROVAL PAGE	iii
DEDICATION	iv
TABLE OF CONTENTS.....	v
LIST OF FIGURES	viii
LIST OF EQUATIONS	x
LIST OF TABLES.....	xiii
LIST OF ABBREVIATIONS	xv
ACKNOWLEDGEMENTS.....	xviii
VITA.....	xxiii
PUBLICATIONS.....	xxiv
ORAL PRESENTATIONS.....	xxv
POSTER PRESENTATIONS.....	xxvi
LEADERSHIP AND AFFILIATIONS	xxviii
HONORS AND AWARDS	xxviii
ABSTRACT OF THE DISSERTATION	xxix
Chapter 1 INTRODUCTION.....	1
Copyright	1
1.1 Atropisomerism in Drug Discovery	1
1.2 Atropisomerism and its Role in Chemotherapeutics	5
1.3 Addressing Unmet Needs for Developing Atroposelective Synthetic Methodologies to Obtain Pharmaceutically Relevant Compounds.....	9
Acknowledgments.....	10
Chapter 2 APPLICATIONS OF ATROPOSELECTIVE NUCLEOPHILIC AROMATIC SUBSTITUTION TOWARDS PHARMACEUTICALLY RELEVANT <i>N</i> -HETEROCYCLES	11
Section 1. Synthesizing Class-3 Atropisomeric PPYs.....	11

Copyright	11
2.1 Background: Atroposelective S _N Ar towards PPYs	11
2.2 Addressing the Shortcomings for Current Atroposelective S _N Ar Synthetic Methods to Access PPYs	14
2.3 Reaction Development: Optimizing Atroposelective S _N Ar for 3-aryl PPYs	17
2.4 Atroposelective S _N Ar of Thiophenol towards 3-aryl PPYs.....	23
2.5 Enantiodivergent Syntheses Towards Selective Kinase Inhibitor PPYs.....	29
2.6 Conclusion and Future Directions for this Work	34
Acknowledgements	36
2.7 Experimental Section.....	37
Section 2. Accessing Class-3 Atropisomeric 3-aryl-2-thioquinolines.....	216
Copyright	216
2.9 Background: Atroposelective S _N Ar towards 3-arylquinolines.....	216
2.10 Reaction Optimization for Atroposelective S _N Ar towards 3-arylquinolines.....	220
2.11 Atroposelective S _N Ar of 3-arylquinolines via DKR.....	226
2.12 Dynamic and Classical Kinetic Resolution Hybrid Mechanism	229
2.12 Atroposelective S _N Ar of 3-arylquinolines via Classical KR	233
2.13 Post-functionalization of Atropisomeric 3-arylquinolines	235
2.14 Proposed Transition State Model of the S _N Ar of 3-arylquinolines	238
2.15 Conclusion.....	247
Acknowledgements	247
2.15 Experimental Section.....	248
Chapter 3 ACCESSING ATROPISOMERIC CHEMICAL PROBES FOR NEW DISEASE TARGETS.....	516
Copyright	516
3.1 Background – Chemical Probes Role in Medicinal Chemistry.....	516

3.2	Diazirine Atropoprobes – Activated by UV Light	519
3.3	Current Results and Future Directions	521
3.3	Experimental Section.....	523
	Acknowledgements	556
Chapter 4 FUTURE DIRECTIONS FOR NEW ATROPOSELECTIVE NUCLEOPHILIC SUBSTITUTIONS.....		557
	Copyright	557
4.1	Background Information	557
4.2	Preliminary Results: Minisci Chemistry	560
	Acknowledgements	561
	REFERENCES	562

LIST OF FIGURES

Figure 1. Example of dynamic chirality. Thalidomide as a drug exists only as a racemic mixture due to tautomerization in the bloodstream.....	1
Figure 2. a. Comparison of “Single-Point” Chirality to Atropisomerism. b. Example of biaryl atropisomerism. c. Examples of non-biaryl atropisomerism.	2
Figure 3. Classification of atropisomerism. A pharmaceutically relevant atropisomer represents each class based on stereochemical stability. Figure shown was adapted from LaPlante’s seminal research. ^{1,7,20}	3
Figure 4. Examples of atropisomerism in drug discovery. ^{2,4,21,22,24–28} Examples shown range from FDA-approved drugs, chemical probes, and/or pharmaceutically relevant compounds. Red arrow represents the axis of chirality. In green indicates <i>N</i> -heterocycles. ²⁹	4
Figure 5. Sample dataset from leveraging atropisomerism towards kinase inhibiting PPYs. ^{7,33} ...	6
Figure 6. Summary of medicinal chemistry effort towards synthesizing a potent and selective RET kinase inhibiting PPY through leveraging atropisomerism (i.e., precluding non-relevant yet accessible low energy binding conformations). IC ₅₀ s presented in the table are reported in nanomolar (nM).	7
Figure 7. Proposed kinetic resolution pathway towards enantioenriched PPY sulfides. ^{18,62–68}	15
Figure 8. Evaluation of enantioenriched PPYs across Src and Brk kinases. ^{55,56} IC ₅₀ s were determined using Promega’s ATP Glo Kinase Inhibition Assay in duplicate. Please see Section 2.1.25 for more details.	33
Figure 9. Barrier to Racemization of 21 at 140 °C, Ph ₂ O (1st order Racemization)	98
Figure 10. Barrier to Racemization of 22 at 140 C, Ph ₂ O (1st order Racemization).....	99
Figure 11. Barrier to Racemization of 60 at 125 °C, Ph ₂ O (1st order Racemization)	100
Figure 12. Barrier to Racemization of 61 at 125 °C, Ph ₂ O (1st order Racemization)	101
Figure 13. Barrier to Racemization of 64 at 127 °C, Ph ₂ O (1st order Racemization)	102
Figure 14. Barrier to Racemization of 57 at 140 °C, Ph ₂ O (1st order Racemization)	103
Figure 15. Barrier to Racemization of 58 at 140 °C, Ph ₂ O (1st order Racemization)	104
Figure 16. ADP-Glo™ Kinase Assay (Image Reference: https://www.promega.com/products/cell-signaling/kinase-assays-and-kinase-biology/adp-glo-kinase-assay/?catNum=V6930).....	105
Figure 17. Dose-response curve for enantioenriched 57 in [a] Brk and [Src] kinase.....	106
Figure 18. Dose-response curve for enantioenriched 59 in [a] Brk and [Src] kinase.....	107
Figure 19. Dose-response curve for enantioenriched 59 in [a] Brk and [Src] kinase.....	108
Figure 20. Examples of Biaryl Heterocyclic Atropisomers in Drug Discovery. Each compound is drawn where they lie in stereochemical stability determined by the barrier to racemization, ΔG_{rac} . ^{23,28,30,87}	217
Figure 21. Examples of Pharmaceutically Relevant Biarylquinoline Atropisomers	218

Figure 22. a. Atroposelective S _N Ar of 3-aryl-2-fluoroquinolines. b. Example of a classical DKR and a classical KR substrate; C-2 fluoroquinoline substrates with barrier to racemization.	219
Figure 23. Early hypotheses and proposed model of transition state towards atroposelective S _N Ar of C-3 arylquinolines. Shown is the urea-based quinine catalyst engaging in H-bonding with the quinoline to allow direct substitution from fluoro to S-aryl.	221
Figure 24. ¹⁹ F NMR Singleton Experiments to Study Catalyst-Starting Material Complex.....	240
Figure 25. ¹⁹ H- ¹⁵ N HSQC Singleton Experiments to Study Catalyst-Starting Material Complex	241
Figure 26. ¹⁹ H- ¹⁵ N HSQC Singleton Experiments to Study Catalyst-Starting Material Complex	242
Figure 27. Unfavored interactions between starting material 3-arylquinoline 72 interaction with catalyst 77 obtained from minimization of MOE. The proposed model is represented in a 2-D and 3-D structure.	245
Figure 28. Favored interactions between starting material 3-arylquinoline 72 interaction with catalyst 77 obtained from minimization of MOE. The proposed model is represented in a 2-D and 3-D structure.	246
Figure 29. Barrier to Racemization of 72 at 80 °C, PhMe.....	335
Figure 30. Barrier to Racemization of 96 at 80 °C, PhMe.....	336
Figure 31. Barrier to Racemization of 98 at 55 °C, PhMe.....	337
Figure 32. Barrier to Racemization of 97 at 100 °C, PhMe.....	338
Figure 33. Barrier to Racemization of 103 at 100 °C, PhMe.....	339
Figure 34. Barrier to Racemization of 105 at 118 °C, PhMe.....	340
Figure 35. Barrier to Racemization of 108 at 81 °C , PhMe.....	341
Figure 36. Barrier to Racemization of 112 at 81 °C, PhMe.....	342
Figure 37. Barrier to Racemization of 73 at 130 °C, Ph ₂ O.....	343
Figure 38. Crystal structures of compound 107 produced from the asymmetric syntheses. The thermal ellipsoids are drawn at the 50% probability level.....	391
Figure 39. Crystal structures of compound 86 produced from the asymmetric syntheses. The thermal ellipsoids are drawn at the 50% probability level.....	391
Figure 40. Crystal structures of compound 72 showing one of the enantiomers found in the racemic crystals. The thermal ellipsoids are drawn at the 50% probability level.	392
Figure 41. Crystal structures of compound 85 showing one of the enantiomers found in the racemic crystals. The thermal ellipsoids are drawn at the 50% probability level.	392
Figure 42. Chemical Probes via Fragment-Based Ligand and Targeted Discovery ^{108,119}	519
Figure 43. Scope of Chemical Probes.....	549

LIST OF EQUATIONS

Equation 1. Proposal of alternative synthetic route to access pharmaceutically relevant PPYs... 11	11
Equation 2. Atroposelective nucleophilic aromatic substitution of biaryl pyrimidines. ⁶⁰	13
Equation 3. An overview of atroposelective S _N Ar methodology. Compound 15 was found to be the optimal catalyst for both yield and enantioselectivity. ⁹	14
Equation 4. a. Transformation of enantioenriched starting materials, and b. transformation of enantioenriched products towards C-4 aminated kinase inhibitors. Reported ^[a] isolated yields and ^[b] enantioselectivity via e.r. are for one trial. c. Modification of the C-2 position using modern Pd-coupling reaction conditions. See Section 2.1.17 for more details.	30
Equation 5. Atroposelective S _N Ar towards PPY-based Kinase Inhibitors	34
Equation 6. Atroposelective S _N Ar towards PPY-based kinase inhibitors via Dynamic Kinetic Resolution (DRK)	34
Equation 7. From every trial, conversion is calculated using the methods of Fiaud. ⁷²	38
Equation 8. Calculating s-factor from conversion and enantioenriched percentage. ⁷²	38
Equation 9. Synthesis of PPY Core	41
Equation 10. Synthesis of 3-aryl PPY Intermediate	46
Equation 11. Scheme for the Chlorination of PPY towards PPY Starting Materials for Atroposelective S _N Ar	55
Equation 12. General Scheme for C-2 Bromination of PPY	62
Equation 13. General Scheme for Stille Coupling.....	63
Equation 14. Ketone to DAST Synthesis towards Difluoromethyl Analogue.....	64
Equation 15. EAS towards Nitro-group at C-2 position of PPY	65
Equation 16. General Scheme for Atroposelective S _N Ar of 3-aryl PPYs.....	66
Equation 17. General Scheme for Amination of PPYs to Final Kinase Inhibitors.....	79
Equation 18. General Scheme for Oxidation of Sulfide PPY to Sulfone	84
Equation 19. General Scheme for Boc-protection to Further Elaborate Kinase Inhibitor PPY ...	88
Equation 20. C-2 Methylation of PPYs (1).....	90
Equation 21. Arylation of PPYs.....	92
Equation 22. Methylation of PPYs (2).....	94
Equation 23. First-order kinetics for racemization of atropisomers with respect to time.....	96
Equation 24. Rate constant for the degradation of enantiomeric ratio.	97
Equation 25. Calculating barrier to racemization (otherwise known as the barrier to rotation of atropisomeric compounds), ΔG_{rac}	97
Equation 26. Half-life to racemization for atropisomeric compounds.	97

Equation 27. Optimized reaction conditions of the dynamic kinetic resolution of atropisomeric 3-arylquinolines.....	225
Equation 28. Optimized reaction conditions of atroposelective S _N Ar towards 3-arylquinolines via classical kinetic resolution. Enantioenriched sulfide and recovered starting materials were isolated.	233
Equation 29. Post-translational modifications with enantioenriched products. Refer to Sections 2.2.14 to 2.2.17 for more details regarding the above syntheses.	236
Equation 30. (Prep 1.) Synthesis of Cinchona Alkaloid-Based Quinine Catalysts via Isocyanates and Isothiocyanates.....	251
Equation 31. (Prep 2.) Synthesis of Catalyst 78	258
Equation 32. General Reaction for Catalyst Evaluation	258
Equation 33. General Reaction for the Solvent Evaluation	260
Equation 34. General Reaction for the Concentration and Temperature Evaluation	262
Equation 35. General Reaction for the Base Evaluation.....	263
Equation 36. General Reaction for the Catalyst Load Evaluation.....	264
Equation 37. General Reaction for the Catalyst Load Evaluation.....	265
Equation 38. General Reaction for the Catalyst Load Evaluation.....	267
Equation 39. General Reaction for the Catalyst Load Evaluation.....	268
Equation 40. Buchwald Coupling to yield 3-aryl quinoline intermediates.....	270
Equation 41. Suzuki Coupling to yield 3-aryl quinoline intermediates.....	271
Equation 42. General Fluorination Method Towards Substrate 70. Adapted from Hartwig and coworkers' selective C-H fluorination. ^[14]	286
Equation 43. Atroposelective S _N Ar optimization can be found in ' Section 2.2.7 Reaction Development. '	301
Equation 44. Oxidation to yield enantioenriched 3-aryl-2-(phenylsulfonyl)quinolines 124	324
Equation 45. Amination of 3-arylquinolines. Procedure was followed according to the procedure reported in Cardenas and coworkers. ^[17]	330
Equation 46. S _N Ar procedure towards 3-arylquinolin-2-ols (5) was adapted from work by Patel and coworkers. ^[18]	331
Equation 47. Synthesis of Intermediate 123	333
Equation 48. General Syntheses for Atropoprobes. a. Synthesis of the control chemical probes. b. Synthesis of chemical probes.....	521
Equation 49. Method A. Buchwald-Hartwig Cross-Coupling	531
Equation 50. Method B. Suzuki-Miyaura Cross-Coupling	531

Equation 51. The modified Hartwig fluorination procedure is followed in accordance conditions reported in Cardenas, M. M. ; Saputra, M. A.; Gordon, D. A.; Sanchez, A. N.; Yamamoto, N.; Gustafson, J. L. <i>Chem. Commun.</i> , 2021 , 57, 10087–10090.	535
Equation 52. The nucleophilic aromatic substitution of thiophenol into a 3-aryl-2-fluoroquinoline was reported by Section “ 2.2.6.11 General S _N Ar Strategy to yield enantioenriched 3-aryl-2-(phenylthio)quinolines (2).” A modification was used where 10.0 equiv of potassium phosphate is used and the reaction is heated at 95 °C.....	541
Equation 53. The nucleophilic aromatic substitution of thiophenol into a 3-aryl-2-fluoroquinoline was reported by Cardenas, M. M. ; Saputra, M. A.; Gordon, D. A.; Sanchez, A. N.; Yamamoto, N.; Gustafson, J. L. <i>Chem. Commun.</i> , 2021 , 57, 10087–10090. A modification was used where 10.0 equiv of potassium phosphate is used and the reaction is heated at 95 °C.	543
Equation 54. Amide coupling was conducted in accordance with the report from Conway, L. P.; Jadhav, A.M.; Homan, R. A.; Li, W.; Rubiano, J.S.; Hawkins, R.; Lawrence, R.M.; Parker, C.G. <i>Chem. Sci.</i> , 2021, 12, 7839–7847 (<i>i.e.</i> , General Procedure 2 of ‘Synthesis of Diazirine Containing Tags’).	549
Equation 55. S _N Ar of atroposelective pharmaceutically relevant scaffolds. a. Synthesis of Enantioenriched Scaffold derived from Sotorasib. b. Synthesis of scaffold derived from MRTX1719.....	558
Equation 56. General synthetic scheme of atroposelective S _N Ar of Quinazolinones.....	559
Equation 57. General synthetic scheme of atroposelective Minisci on 3-arylquinolines	560

LIST OF TABLES

Table 1. S _N Ar Reaction Optimization Summary Towards 3-aryl PPY sulfides.....	18
Table 2. Solvent Evaluation and Permittivity Constants for the Reaction Optimization of Atroposelective S _N Ar.....	20
Table 3. Scope of Enantioenriched PPY Sulfides obtained from Atroposelective S _N Ar	26
Table 4. Catalyst Index	39
Table 5. Complete Reaction Optimization for S _N Ar of PPYs	40
Table 6. Time-dependent Enantiodegradation of 21.....	98
Table 7. Time-dependent Enantiodegradation of 22.....	99
Table 8. Time-dependent Enantiodegradation of 60.....	100
Table 9. Time-dependent Enantiodegradation of 61.....	101
Table 10. Time-dependent Enantiodegradation of 64.....	102
Table 11. Time-dependent Enantiodegradation of 57.....	103
Table 12. Time-dependent Enantiodegradation of 58.....	104
Table 13. S _N Ar Reaction Optimization Summary Towards 3-arylquinolines.....	223
Table 14. 3-arylquinoline Analogues Obtained via Dynamic Kinetic Resolution (Classical DKR)	227
Table 15. 3-arylquinoline Analogues Obtained via Hybrid Dynamic Kinetic Resolution and Kinetic Resolution (DKR/KR Hybrid)	230
Table 16. 3-arylquinoline Analogues Obtained via Kinetic Resolution (Classical KR)	235
Table 17. Full Catalyst Evaluation towards Atroposelective S _N Ar of 3-arylquinoline	259
Table 18. Solvent Evaluation.....	261
Table 19. Concentration and Temperature Evaluation	262
Table 20. Base Evaluation	263
Table 21. Catalyst Load Evaluation.....	264
Table 22. Time-dependent Enantiodegradation of 72	335
Table 23. Time-dependent Enantiodegradation of 96	336
Table 24. Time-dependent Enantiodegradation of 98	337
Table 25. Time-dependent Enantiodegradation of 97	338
Table 26. Time-dependent Enantiodegradation of 103	339
Table 27. Time-dependent Enantiodegradation of 105	340
Table 28. Time-dependent Enantiodegradation of 108	341
Table 29. Time-dependent Enantiodegradation of 112	342

Table 30. Time-dependent Enantiodegradation of 73	343
Table 31. Crystallographic data of compounds 107 and 86	389
Table 32. Crystallographic data of compounds 72 and 85	390
Table 33. 3-aryl Pyrrolopyrimidine-based diazirines	522
Table 34. 3-aryl Quinoline-based diazirines	522

LIST OF ABBREVIATIONS

S _N Ar	Nucleophilic aromatic substitution
VNS	Vicarious nucleophilic substitution
rxn	Reaction
DKR	Dynamic kinetic resolution
KR	Kinetic resolution
SM	Starting material
PR	Product
e.r. <i>or</i> er	Enantiomeric ratio
e.e. <i>or</i> ee	Enantiomeric excess (%)
equiv.	Equivalence
conv.	Conversion
<i>s</i> or <i>k</i> _{rel}	<i>s</i> -factor, selectivity factor
Conc.	Concentration
Temp.	Temperature
r.t. <i>or</i> rt	Room temperature, ambient temperature
°C	Celsius
aq.	Aqueous
org.	Organic
mol%	Molar percent
nM	Nanomolar
FCC	Flash column chromatography
TLC	Thin-layer chromatography

CD	Circular dichroism
NMR	Nuclear magnetic resonance
PPY	Pyrrolopyrimidine
(<i>R</i> _a)-	Asymmetric, enantioenriched to the (<i>R</i>)-atropisomer
(<i>S</i> _a)-	Asymmetric, enantioenriched to the (<i>S</i>)-atropisomer
N/A	Not applicable
<i>n.d.</i>	Not determined, no data for this entry
IPA	Isopropyl alcohol, isopropanol
EtOH	Ethyl alcohol, ethanol
MeOH	Methanol
PhMe	Toluene
MTBE	Methyl tert-butyl ether
CH ₂ Cl ₂	Dichloromethane, DCM
MeCN	Acetonitrile, ACN
CCl ₄	Carbon tetrachloride
EtOAc	Ethyl acetate
Hex	<i>n</i> -Hexanes
<i>i</i> Pr ₂ O	Diisopropyl ether
<i>m</i> -Xyl	<i>m</i> -Xylenes
K ₂ HPO ₄	Potassium phosphate, dibasic
DMF	(<i>N,N</i>)-Dimethylformamide
K ₂ CO ₃	Potassium carbonate
Cs ₂ CO ₃	Cesium carbonate

Na ₂ CO ₃	Sodium carbonate
KHCO ₃	Potassium bicarbonate
K ₃ PO ₄	Potassium phosphate, tribasic
NaOH	Sodium hydroxide
KOH	Potassium hydroxide
NEt ₃	Triethylamine
N.B.	No base was used in the reaction.
HSPh	Thiophenol
TFA	Trifluoroacetic acid
TFFA	Trifluoroacetic anhydride

ACKNOWLEDGEMENTS

From the challenges and struggles I faced throughout my academic journey, I have been very loved and supported in it all. I am blessed to be in this humbling position to receive this prestigious titleship of Joint Doctor of Philosophy, Organic Chemistry. I would like to thank my family, friends, mentors, colleagues, and collaborators throughout this huge milestone in my life. First and foremost, as a devout Christian I give thanks and glory to God. Achieving this highest academic honor is just the means to further praise Him. I give gratitude and all my love to my family for their support. For my mom (Maria) and dad (Mike): thank you for believing, encouraging, and loving me throughout everything. You've both sacrificed so much of yourselves to get me further in my life. I am who I am today because of you both. To my two little sisters Melisa and Melarie: thank you for keeping me grounded. I am excited to watch you both carry out your own Ph.D. journeys and advance your individual careers. To my relatives and extended family: I am grateful for your love and prayers throughout my Ph.D.

I've also been blessed to have inspiring and selfless mentors that openly shared their wisdom and teachings. Thank you to my high school teacher Dr. Erika Senegar-Mitchell who encouraged my love of pursuing science and becoming my source of inspiration that women have a place in STEAM research. Thank you to Dr. Kirk Webley and the rest of the dedicated counselors at San Diego Miramar College for being my support system during my community college years. At the University of California at San Diego, I thank Professor Bob Ternansky for your teachings and inspiring me to pursue Organic Chemistry as a career. I sincerely thank Professor Eduardo Caro for your mentorship when I was an undergraduate researcher in Professor Emmanuel Theodorakis's research group. You were the one who taught me the joy of research in an academic setting and gave me a firm foundation for lab skills. Finally, thank you Professor Emmanuel

Theodorakis. I pursued graduate studies in Organic Chemistry with confidence because of your determination in me. Your guidance, support, and care throughout my career even after graduating from UCSD has shaped who I am today.

My journey in the Gustafson lab began even before I formally started in the group, in Chem 695. I am grateful for Dr. Andrew Dinh, Dr. Sean Toenjes and Ryan Noorbehesht – we forged a squad ever since that class into what eventually became a golden era of the Gustafson lab. To Dinhe and Toenny specifically: thank you both so much for being 2/3 of the Three Musketeers. You both are two of my greatest friends, and a huge part of my graduate school journey. I was fortunate to be mentored by senior Ph.D. students at the time: Dr. Sean Maddox and Professor Chris Nalbandian. Thank you both for letting me begin chemistry before I started in the lab! I thank you both for deepening my understanding of skills and techniques in organic chemistry research. All of you “OG” Gustafson group graduate students gave me so much, and now I reflect on all those memories that I can treasure in Polaroids and past Instagram posts.

I thank our postdoctoral students Dr. Della Saputra and Dr. Sagar Vaidya. You have both much insight from all your experiences, talents, and contributions that led towards the development of many projects under my dissertation. To the graduate students I was fortunate to overlap with: Ashley Nguyen, Zach Brown, Mariam Basilaia, Bahar and Beeta Heydari, Ryan Zanolini – I’m excited to watch the future research of the Gustafson group shape in this new era. I leave you with my wisdom: graduate school can be challenging but remain vigilant and focus purely on your science. When it gets hard, never forget to take moments of respite and go with confidence in your research. To the army of many Gustafson group current and alumni undergraduates: each one of you has shaped a huge part of this group, and some of you had massive impacts in the projects I’ve done. I’m very excited to watch you transcend your own individual careers in science post-SDSU.

Thank you to Professor Jeff Gustafson, who I've always been told "just call me Jeff, Dr. Gustafson is my wife." Jeff, thank you so much for everything you've done for me. Every day I think "I'm very thankful I had you as my graduate advisor and mentor." You know that my time as a graduate student was not always easy for me. Almost every season carried a new burden or challenge that tested my ability to make it through to the end. Every time I was down, I got back up much stronger, confident, and more passionate about my future in a scientific career because of you. From the humble beginnings where we both simultaneously deepened our understanding of DKRs/KRs, to coaching me about data integrity and responsible science; overseeing my gaps to fill, getting me through all those hard times, feeding my Harry Potter addiction, and appreciating that classic rock and 80's rock anthems are superior to any genre. My Ph.D. journey reflects your investment and efforts in me as a scientist. My research serves as a standard for your current program behind atroposelective syntheses and is a platform for future grants and new students under your visage. I wish you and your future group all the best, Jeff. (At the time of this writing, you're moving your group to the East Coast. Wishing you the best, and I'm looking forward to the new scientific pursuits from Gustafson Lab v2.0!)

Outside of the Gustafson group, I want to thank other mentors who were integral in my graduate studies. First, I dedicate this dissertation to the late Professor Douglas (Doug) Grotjahn. Doug was integral to my career as the late JDP coordinator at SDSU, and my committee member from 2017-2023. I also thank Doug for allowing me access to his group's glovebox; thanks to Dr. Greg Elliott in support of HRMS. Professor Christal Sohl, you remain a huge role model in my life and were a huge support system in my time at SDSU. I'm grateful for the opportunity to also mentor your MINDSET mentees. Lastly, thank you to my life coach and professional career

mentor Dr. Angie Angeles. Auntie Gigi – I’m truly blessed that you consistently provide constructive critiques and teachings such that I will have a fruitful professional life.

I’m grateful to have been supported by several fellowships and scholarships throughout my career – including CalVet, the SDSU University Graduate Fellowship, and NIGMS grant R35GM124637 (Gustafson). Specifically, thank you to everyone in the ARCS Foundation – Mrs. Robin Luby for your gift of financial support for the years I was your ARCS Scholar. I hope that you’re doing well and that I will continue to make you excited to watch research in America take form. Thank you to Rachel Collins for leading SDSU San Diego Chapter. Finally, thank you to Dr. Cathie Atkins for being my supporter throughout the years for this scholarship.

Chapter 1 contains material in part as a reformatted reprint of the following book chapter, with permission from the Wiley VCH: Saputra, M. A.; Cardenas, M. M.; Gustafson, J. L. “Asymmetric Synthesis of Nonbiaryl Atropisomers.” in *Axially Chiral Compounds: Asymmetric Synthesis and Applications.*; Tan, B.; Wiley-VCH., ISBN: 978-3-527-34712-4. The dissertation author reviewed the literature and was a co-author of this material. In addition, Chapter 1 also contains material that is in part a reformatted reprint of the following review, with permission from ARKAT USA, Inc.: Cardenas, M. M.; Nguyen, A. N.; Brown, Z. E.; Heydari, B. S.; Heydari, B. S.; Vaidya, S. D.; Gustafson, J. L. “Atropisomerism as Inspiration for New Chemistry.” *Arkivoc*, **2021**, *i*, 20-47. The dissertation author reviewed the literature and lead author of this material. Support of these works by the National Institute of General Medical Sciences are acknowledged (R35GM124637).

The contents in Chapter 2, Section 1 are in part a reformatted reprint of the following manuscript, with permission from the American Chemical Society: Cardenas, M. M.; Toenjes, S. T.; Nalbandian, C. J.; Gustafson, J. L. “Enantioselective Synthesis of Pyrrolopyrimidine Scaffolds

through Cation-Directed Nucleophilic Aromatic Substitution.” *Org. Lett.* **2018**, *20*, 2037-2041.

The dissertation author is the primary researcher for the data presented, and lead author of this material. Support of this work by the National Institute of General Medical Science (R35GM124637) is acknowledged.

The contents in Chapter 2, Section 2 are in part a reformatted reprint of the following manuscript, with permission from the Royal Society of Chemistry: Cardenas, M. M.; Saputra, M. A.; Gordon, D. A.; Sanchez, A. N.; Yamamoto, N.; Gustafson, J. L. “Catalytic Atroposelective Dynamic Kinetic Resolutions and Kinetic Resolutions towards 3-arylquinolines via S_NAr .” *Chem. Commun.*, **2021**, *57*, 10087–10090. The dissertation author is the primary researcher for the data presented, and lead author of this material. Support of this work by the National Institute of General Medical Science (R35GM124637) is acknowledged.

The contents in Chapter 3 were work performed primarily by Cardenas, M. M. The dissertation author was the primary researcher for the data presented. Support of this work by the National Institute of General Medical Science (R35GM124637) is acknowledged.

Chapter 4 is a compilation of material that may be utilized in future publications. This work was primarily led by Cardenas, M. M. and Gustafson, J. L. The dissertation author was the primary researcher for the data presented. Support of this work by the National Science Foundation (CHE-1664565) and the National Institute of General Medical Science (R35GM124637) are acknowledged.

VITA

- 2011 Analytical Chemistry Lab Assistant and Intern, ADME Department, Ferring
Pharmaceuticals Research Institute, San Diego, CA.
- 2013 Associate of Arts in Mathematical Studies, San Diego Miramar College
- 2013 Associate of Science in Pre-engineering (Chemistry), San Diego Miramar College
- 2014 Bachelor of Science in Chemistry (Chemistry), University of California at San Diego
- 2014 Chemistry Teaching Assistant, Department of Chemistry and Biochemistry at San
Diego State University
- 2021 Senior Scientist, Chemical Process R&D, Mirati Therapeutics, San Diego, CA.
- 2024 Doctor of Philosophy Chemistry (Chemistry), Joint Doctoral Program between
University of California at San Diego and San Diego State University
- 2022-present: Medicinal Chemistry Research Scientist, Vertex Pharmaceuticals, San Diego,
CA.

PUBLICATIONS

Cardenas, M. M.; Toenjes, S. T.; Nalbandian, C. J.; Gustafson, J. L. “Enantioselective Synthesis of Pyrrolopyrimidine Scaffolds through Cation-Directed Nucleophilic Aromatic Substitution.” *Org. Lett.* **2018**, *20*, 2037-2041. [PMID: 29561161]

Cardenas, M. M.; Nguyen, A. D.; Brown, Z. E.; Heydari, B. S.; Heydari, B. S.; Vaidya, S. D.; Gustafson, J. L. “Atropisomerism as Inspiration for New Chemistry.” *Arkivoc*, **2021**, *i*, 20-47. [<https://doi.org/10.24820/ark.5550190.p011.382>]

Saputra, M. A.*; **Cardenas, M. M.**;* Gustafson, J. L. “Asymmetric Synthesis of Nonbiaryl Atropisomers.” in *Axially Chiral Compounds: Asymmetric Synthesis and Applications.*; Tan, B.; Wiley-VCH., ISBN: 978-3-527-34712-4. [*authors contributed equally to this work]

Cardenas, M. M.; Saputra, M. A.; Gordon, D. A.; Sanchez, A. N.; Yamamoto, N.; Gustafson, J. L. “Catalytic Atroposelective Dynamic Kinetic Resolutions and Kinetic Resolutions towards 3-arylquinolines via S_NAr .” *Chem. Commun.*, **2021**, *57*, 10087–10090.

ORAL PRESENTATIONS

Cardenas, M. M. "Development of Atroposelective Syntheses Towards Pharmaceutically Relevant N-Heterocyclic Scaffolds." Presented at Research Seminar (Hiring Initiative) Mirati Therapeutics, La Jolla, CA, February 3, 2021.

Cardenas, M. M. "Development of Atroposelective Syntheses to Access Pharmaceutically Relevant Scaffolds." Presented at gRED Research Seminar (Postdoctoral Fellow Candidate) for Genetech (a Member of the Roche Group), Google Meet, January 19, 2021.

Cardenas, M. M. "Enantioselective Synthesis of Pharmaceutically Relevant Scaffolds through Cation-Directed Nucleophilic Aromatic Substitution." Presented at the Department of Chemistry & Biochemistry, Guest Seminar Speaker Graduate Student Sessions. San Diego State University, San Diego, CA, March 2017-March 2021.

Cardenas, M. M. "Syntheses of Pharmaceutically Relevant N-Heterocyclic Atropisomers via Nucleophilic Substitutions." Presented at the SDSU MINDSET Seminars in partnership with the ACS Miramar Chemistry Affiliate at San Diego Miramar College, San Diego CA, November 14, 2019.

Cardenas, M. M. "Developing Atroposelective Syntheses to Access Pharmaceutically Relevant Compounds." Presented at the Annual Student Research Symposium at San Diego State University, San Diego CA, March 1, 2019.

Cardenas, M. M. "What to Look Forward to After Transferring to a Research University." Presented at the SDSU Undergraduate Research Information Session from the ACS Miramar Chemistry Affiliate at San Diego Miramar College, San Diego CA, February 23, 2018.

Cardenas, M. M.; Nalbandian, C. J.; Mattocks, J. A.; Gustafson, J. L. "Cation-Directed Catalysis Towards the Atroposelective Nucleophilic Kinetic Resolution of Promiscuous

Pyrrolopyrimidine Kinase Inhibitors.” Presented at the Annual Student Research Symposium at San Diego State University, San Diego CA, March 3, 2017.

POSTER PRESENTATIONS

Cardenas, M. M.; Saputra, M. A.; Sanchez, A. N.; Robinson, C. J.; Valle, E.; Gustafson, J. L. “Accessing pharmaceutically relevant 3-arylated N-heterocycles via atroposelective synthetic methodologies.” Presented at the ACS National Meeting & Exposition, Fall 2019 at San Diego Convention Center, San Diego CA, Sci-Mix: August 26, 2019, Divisional: Aug 29, 2019.

Cardenas, M. M.; Saputra, M. A.; Sanchez, A. N.; Robinson, C. J.; Valle, E.; Gustafson, J. L. “Development of Atroposelective Syntheses of Pharmaceutically Relevant N-Heterocycles.” Presented at the 46th NOS at Indiana University, Bloomington IN, Jun 26, 2019.

Cardenas, M. M.; Saputra, M. A.; Sanchez, A. N.; Robinson, C. J.; Valle, E.; Gustafson, J. L. “Developing atroposelective syntheses to access diverse pharmaceutically relevant scaffolds.” Presented at the ACS National Meeting & Exposition, Spring 2019 at Orange County Convention Center, Orlando FA, Sci-Mix: April 1, 2019, Divisional: April 3, 2019.

Cardenas, M. M.; Toenjes, S. T.; Nalbandian, C. J.; Duong, T. M.; Gustafson, J. L.* “The Enantioselective Synthesis of Pyrrolopyrimidine Scaffolds Through Cation-directed Nucleophilic Aromatic Substitution.” Presented at the IRACDA UC San Diego/SDSU at San Diego State University, San Diego, CA, April 11, 2018.

Cardenas, M. M.; Toenjes, S. T.; Nalbandian, C. J.; Duong, T. M.; Gustafson, J. L. “The Enantioselective Synthesis of Pyrrolopyrimidine Scaffolds Through Cation-directed Nucleophilic Aromatic Substitution.” Presented at the ACS National Meeting & Exposition, Spring 2018 at New Orleans Convention Center, New Orleans LA, March 19, 2018.

Cardenas, M. M.; Toenjes, S. T.; Nalbandian, C. J.; Duong, T. M.; Gustafson, J. L. “The Enantioselective Synthesis of Pyrrolopyrimidine Scaffolds Through Cation-directed Nucleophilic Aromatic Substitution.” Presented at the Annual Student Research Symposium at San Diego State University, San Diego CA, March 3, 2018.

Cardenas, M. M.; Nalbandian, C. J.; Toenjes, S. T.; Gustafson, J. L. “The Enantioselective Synthesis of Pyrrolopyrimidine Scaffolds through Cation-Directed Nucleophilic Aromatic Substitution.” 45th NOS at UC Davis, Davis CA, June 25, 2017

Cardenas, M. M.*; Dinh, A. N.*; Gustafson, J. L. “Atropisomeric Synthesis of Selective Kinase Inhibitors: A Scalable Solution to a Problem in Drug Discovery” Presented at the 29th CSU Annual Biotechnology Symposium at Santa Clara Marriott, Santa Clara, CA, January 4, 2017.

[*authors contributed equally to this work]

FIELD OF STUDY

Major Field: Organic Chemistry, Medicinal Chemistry

Studies in Development of Atroposelective Syntheses to Access Pharmaceutically Relevant Scaffolds

Graduate Advisor: Professor Jeffrey L. Gustafson

LEADERSHIP AND AFFILIATIONS

- i. 2022 National Organic Symposium Committee Member and Local Community Organizer (Hosted by the ACS Division of Organic Chemistry) (2019-present).
- ii. Stanford PRISM Student (cohort for October 2020).
- iii. Maximizing INclusion and Diversity in Science, Engineering, and Technology (MINDSET) Mentor (2018-2021).
- iv. ARCS Advancing Science in America Scholar, San Diego Chapter (2017-2021).
- v. Chemistry Graduate Student Association (CGSA), Public Relations at San Diego State University (2018-2020).
- vi. ACS Division of Organic Chemistry Member (2013-present).
- vii. Phi Theta Kappa Honors Member at San Diego Miramar College (2011-2012).

HONORS AND AWARDS

- i. University Graduate Fellowship Awardee, San Diego State University (2019-2020).
- ii. Library Award Winner of the 2018 SDSU Student Research Symposium (2018).
- iii. ARCS Advancing Science in America Scholar, San Diego Chapter (2017-2021).
- iv. NIH Funded Student (eRA ID: 15522888, grant R35GM124637) (2017-2021).
- v. Cal Vet Student, Cal Veteran Services (2010-2020).
- vi. Neel Endowed Scholarship, San Diego State University (2017).
- vii. Harry E. Hamber Memorial Scholarship, San Diego State University (2016).

ABSTRACT OF THE DISSERTATION

Development of Atroposelective Nucleophilic Substitutions Towards Access Pharmaceutically Relevant Scaffolds

by

Mariel Manaloto Cardenas

Doctor of Philosophy in Chemistry

University of California San Diego, 2024
San Diego State University, 2024

Professor Jeffrey L. Gustafson, Chair

Atropisomerism (or axial chirality) arises from restricted bond rotation most typically in a Csp^2-Csp^2 σ bonds, wherein the neighboring substitutions across the atropisomeric bond contribute energy differences through steric strain. Also referred to as axial chirality, stable atropisomerism (i.e., creating significant steric strain across the bond to give rise to two isolable enantiomers) can

be very challenging to achieve.¹ However, in stabilizing the atropisomeric axis this leads to two unique compounds that have been shown to possess profound activities in many areas of research. Within the last decade, the Gustafson group at San Diego State University²⁻⁴ has since focused on leveraging atropisomerism^{5,6} on its importance to drug discovery with emphasis of exploring *N*-heterocyclic pharmaceutically relevant scaffolds. Along with challenges to achieving stable atropisomerism within a compound, it is very often equally difficult to then furnish enantiopure atropisomers. Traditional resolution methods such as chiral separation can be inconducive in time and resources and sometimes impractical for scaffold exploration.

To address this bottleneck, the Gustafson group began a marital chemistry program in developing new chemical reactions that expedite access to these atropisomeric compounds (Chapter 1^{7,8}). Currently, we have several atroposelective synthetic strategies via nucleophilic aromatic substitutions ($S_{\text{N}}\text{Ar}$, Chapter 2^{9,10}) which have successfully furnished atropisomeric 3-arylpyrrolopyrimidines and 3-arylquinolines. Post-functionalization from the atroposelective $S_{\text{N}}\text{Ar}$ methods have also potentially are useful to synthesize chemical probes (Chapter 3). Furthermore, nucleophilic substitutions outside of $S_{\text{N}}\text{Ar}$ have also been widely used for the synthesis of pharmaceutically relevant compounds (Chapter 4, vicarious nucleophilic substitution (VNS) and atroposelective alkylation by acid-catalyzed directed ‘nucleophilic radicals’ (Minisci chemistry)). We believe our research will impact the current need for atroposelective nucleophilic substitution strategies towards pharmaceutically relevant scaffolds in the field of asymmetric catalysis. Lastly, we shared that these chemistries furnished enantioenriched pharmaceutically relevant scaffolds in desired yields that would be useful to ongoing medicinal chemistry efforts.

Chapter 1 INTRODUCTION

Copyright

Chapter 1 is in part a reformatted reprint with permission from a book chapter titled “Asymmetric Synthesis of Nonbiaryl Atropisomers.” in *Axially Chiral Compounds: Asymmetric Synthesis and Applications.*; Tan, B.; Wiley-VCH., ISBN: 978-3-527-34712-4. Copyright 2021 Wiley VCH. Chapter 1 also contains material that is in part a reformatted reprint of the following review, with permission from *Arkivoc*, **2021**, *i*, 20-47. Copyright 2021 ARKAT USA, Inc.

1.1 Atropisomerism in Drug Discovery

One of the long-standing problems that continues to elude medicinal chemistry arises from complications related to dynamic (otherwise referred to as “unstable”) chirality. Molecules which exhibit dynamic chirality are usually isolated as enantiopure compounds but are susceptible to racemization in various mechanisms (e.g., pH sensitivity, heat intolerance, short half-life, etc.). An example of this phenomenon is in the tragic case of thalidomide, which was once a drug intended to treat morning sickness in pregnant women during the early 1960s (Figure 1).^{11,12}

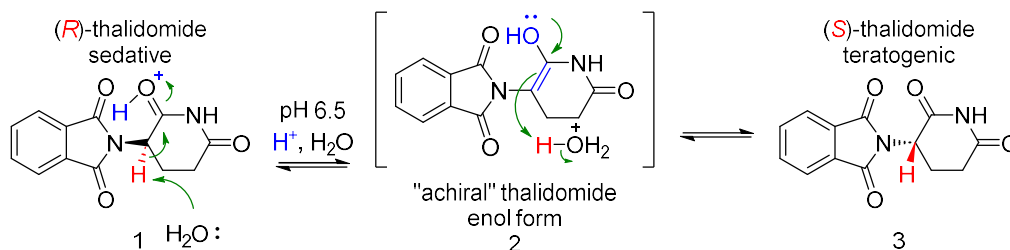


Figure 1. Example of dynamic chirality. Thalidomide as a drug exists only as a racemic mixture due to tautomerization in the bloodstream.

While one enantiomer of thalidomide had an acceptable toxicological profile, the other enantiomer bound promiscuously to an enzyme that was important in embryonic development

resulting in fatal birth defects. There were efforts to deliver the enantiopure drug after preparation and purification, but it was later found that ease of tautomerization under biological conditions led back to the racemic mixture. While thalidomide and other examples of unstable “single point” chiral drugs (Figure 2.a.) show promiscuous biological activities, there are other types of chirality in drugs which are becoming increasingly prevalent in the current pipeline.

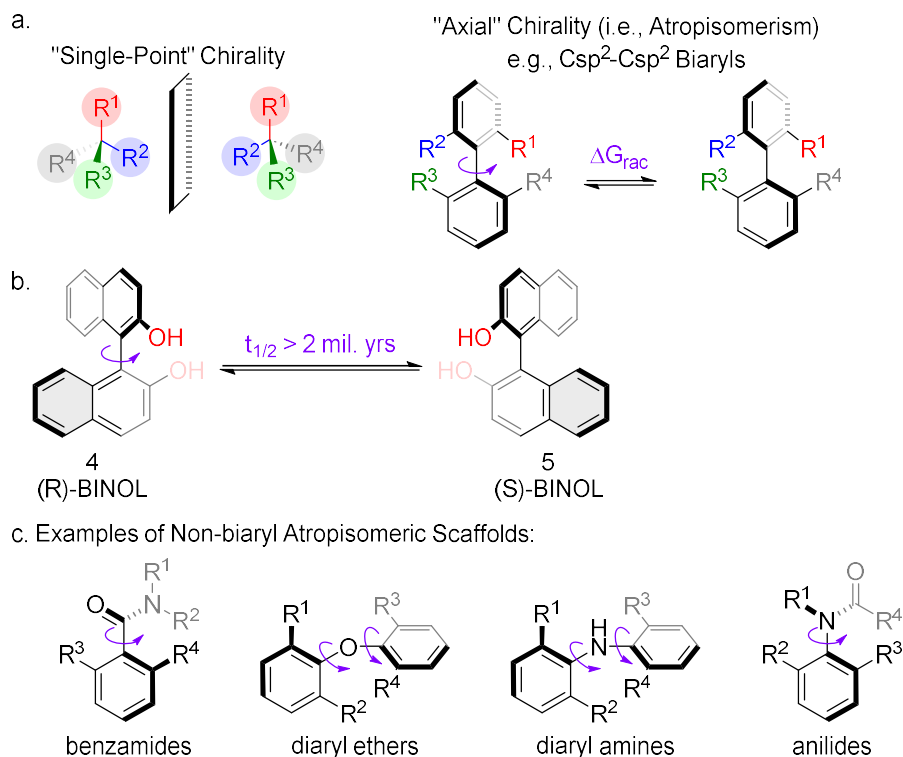


Figure 2. a. Comparison of “Single-Point” Chirality to Atropisomerism. b. Example of biaryl atropisomerism. c. Examples of non-biaryl atropisomerism.

Atropisomerism^{5-7,13-15} is a form of spatial chirality that results from a molecule’s restricted rotation, also referred to as “axial chirality.” Atropisomerism differs from point and other instances of chirality due to spontaneous racemization that can occur via bond rotation, particularly observed in a σ -bond between two Csp^2-Csp^2 atoms (Figure 2.a). Racemization is typically determined by the magnitude of steric hindrance that is adjacent to the atropisomeric bond. Size, shape, and/or electronics of the substituents about the chiral axis contribute to the stability of the

atropisomer, allowing the compound to exist as either stable isolable enantiomers or a rapidly interconverting mixture. A classic example is (*R*) and (*S*)-BINOL^{16–19} (a privileged scaffold in asymmetric catalysis) which possesses a half-life of racemization (i.e., $t_{1/2}$ (rt)) of ~2 million years (Figure 2.b. compounds 4 and 5). Additionally, there are other types of atropisomerism that are non-biaryl scaffolds. These compounds also pervade drug discovery, including scaffolds such as *N*-heterocyclic biaryls, diaryl ethers, diaryl amines, benzamides and anilides (Figure 2.c).

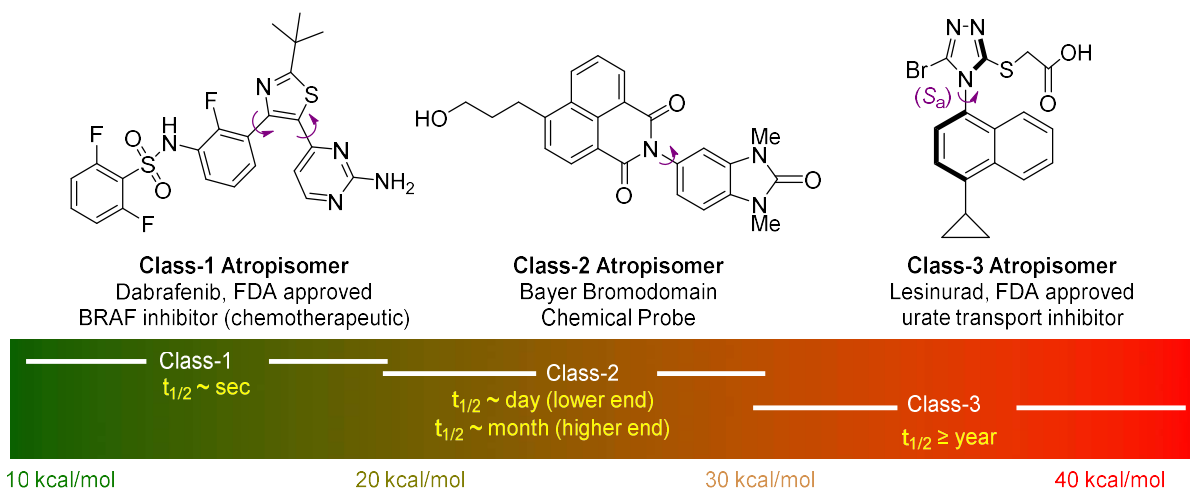


Figure 3. Classification of atropisomerism. A pharmaceutically relevant atropisomer represents each class based on stereochemical stability. Figure shown was adapted from LaPlante's seminal research.^{1,7,20}

In 2011, Professor LaPlante and coworkers^{1,20} studied the effects of atropisomerism on a variety of different compounds (including those FDA-approved and potential drug candidates). LaPlante evaluated their stereochemical stabilities, and developed a system which has become the modern standard to classify atropisomerism (Figure 3). Like BINOL, atropisomers with similar magnitudes of stereochemical stability are referred to as Class-3 atropisomers. Compounds of this classification possess barriers to rotation (i.e., ΔG_{rac} , energy to lead to racemization) above 30 kcal/mol, and thus leads to a $t_{1/2}$ to racemization at room temperature on the “year or greater” time scale. An example of Class-3 atropisomeric FDA-approved drug is the urate transport inhibitor

(+)-Lesinurad,²¹ which does not racemize nor enantiodegrade when heated in DMSO to 120 °C for 24 hours. MRTX1719²² from Mirati Therapeutics (a PMRT5 agonist) and FDA-approved Sotorasib²³ from Amgen (a mutant KRAS inhibitor) were two recent examples of Class-3 atropisomers.

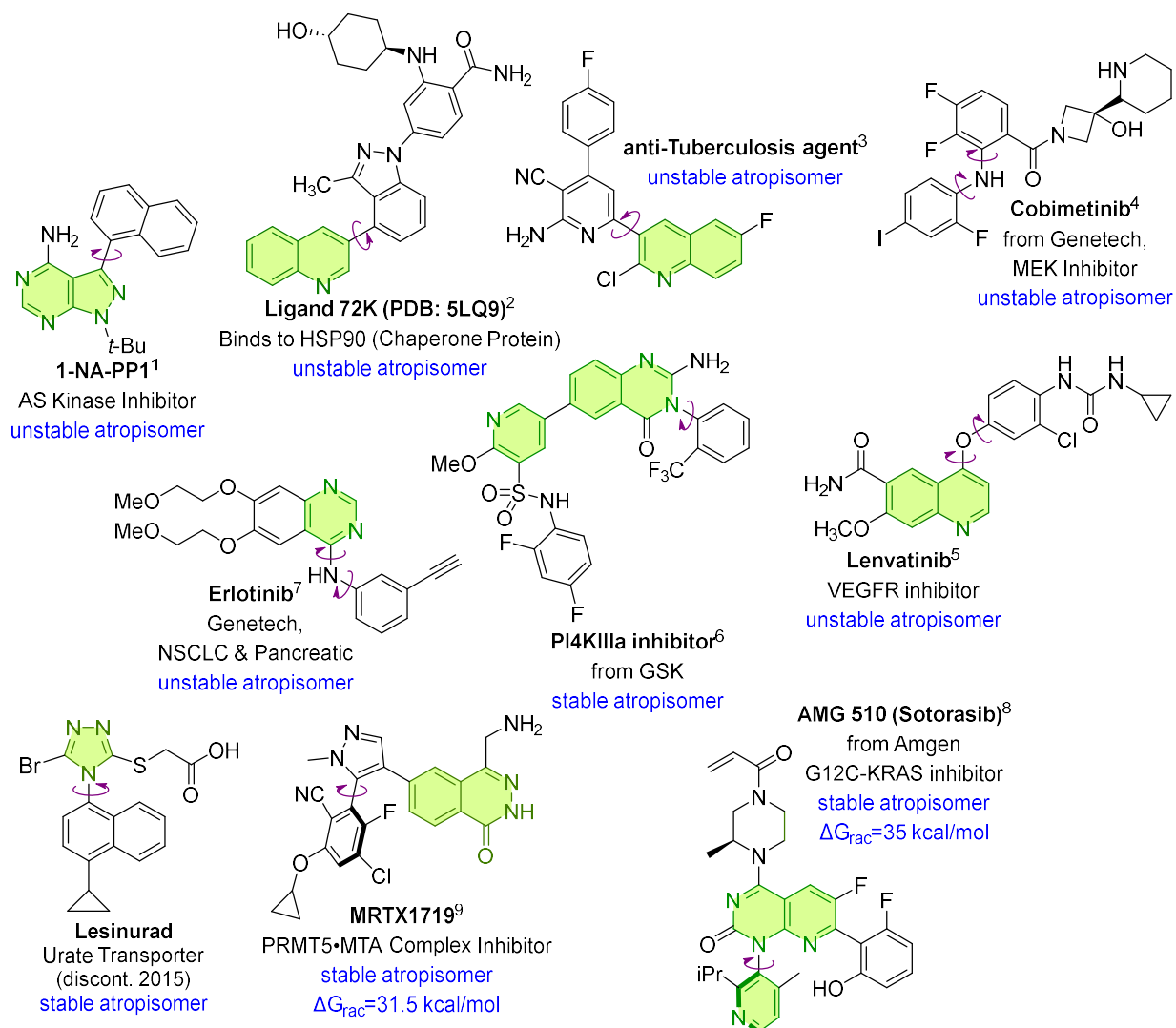


Figure 4. Examples of atropisomerism in drug discovery.^{2,4,21,22,24–28} Examples shown range from FDA-approved drugs, chemical probes, and/or pharmaceutically relevant compounds. Red arrow represents the axis of chirality. In green indicates *N*-heterocycles.²⁹

Conversely, Class-1 atropisomerism refers to compounds where the enantiomers cannot be isolated from rapid racemization at room temperature due to a significantly lower ΔG_{rac} Class-1

atropisomers can access all conformations in 360° rotation. Class-1 atropisomers are also referenced as “unstable” atropisomers. Some examples are the FDA-approved drugs Cobimetinib (Genentech’s MEK inhibitor) and Lenvatinib (a VEGFR inhibitor),³⁰ where the substituents across the atropisomeric axis each biaryl system are smaller in atomic radii (e.g., proton, fluorine). The final category Class-2 atropisomers possess stereochemical stabilities wherein the atropisomers can be isolated in enantiopure form. However, Class-2 atropisomers can readily become enantiodegraded because racemization occurs within “hours, days, to months” timescale at room temperature. There are some examples of pharmaceuticals and chemical probes which span the gamut of the Class-2 atropisomeric scale. Many of these compounds reside closer to the lower end and resemble more of Class-1 atropisomerism (i.e., $t_{1/2}$ (r.t.) within 6 hours).

1.2 Atropisomerism and its Role in Chemotherapeutics

An in-depth study (along with following work) from our group found that roughly 30% of FDA-approved pharmaceuticals since 2011^{2,31} possessed at least one atropisomeric axis. Amongst this 30%, our studies unveiled 85% were FDA-approved kinase inhibitors (i.e., chemotherapeutics).^{2,4} The number of FDA-approved atropisomeric drugs is quite striking, however modern medicinal chemistry typically has cautioned against creating stable atropisomers whenever possible, and often shows a preference for Class-1 rapidly interconverting atropisomers (i.e., achiral molecules). There are many reasons that attributed to this ‘industry standard,’ but can be generally summarized into three main points. The first roadblock is accessing Class-3 atropisomerism (i.e., synthesizing compounds with $\Delta G_{\text{rac}} > 30 \text{ kcal/mol}$ ³²), especially if there are also limitations to key functionalities that are integral for the lead compound. If the first problem is resolved and Class-3 atropisomerism is indeed possible, this yields two distinct compounds as

many occasions have a pair of atropisomers show differing biological activities. The final problem (and persists as the most important to highlight) is access to each atropisomer is limited to what can be isolated in chiral SFC or other analogous purification methods.

While atropisomerism can sometimes pose many challenges in medicinal chemistry, many companies have (especially within this last decade) delivered FDA-approved “blockbuster” Class-3 atropisomeric drugs. These pharmaceuticals are great examples where improved potency and selectivity is defined as a function for introducing high stereochemical stabilities when compared to their respective non-atropisomeric variants. Class-3 atropisomers typically possess divergent activities, with one atropisomer possessing most of the desired activity and the non-relevant atropisomer often contributing little to the desired activity. It has also been shown that the non-relevant atropisomeric confirmation of the ligand may also lend itself to promiscuous off-targeted activities. Much like in the case of thalidomide, this phenomenon often results in undesirable side effects from patients undergoing these types of chemotherapies.

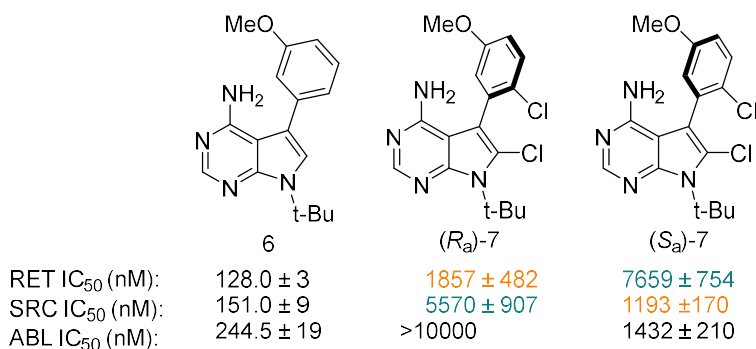


Figure 5. Sample dataset from leveraging atropisomerism towards kinase inhibiting PPYs.^{7,33}

The Gustafson group focuses on finding new types of kinase inhibiting scaffolds, since we found that this class of drugs encompasses the largest scope of Class-1 to Class-2 atropisomeric FDA-approved pharmaceuticals. The Gustafson group’s earliest work predates my tenure (est. 2014) and serves as the foundation of many projects that I pursued during my thesis. This initial

work examined the effect of pre-organization of the atropisomeric axis of known Class-1 promiscuous kinase inhibiting scaffold, a pyrrolopyrimidine (i.e., PPY) against a panel of mutated kinases (i.e., exhibiting cancer derived phenotype(s)) (Figure 5).³³ The Gustafson group selected this series of inhibiting scaffold, as it is an analogue of the venerable chemical probe from Dr. Kevan Shokat and coworkers' NA-PP1 (Figure 4).²⁶ These compounds are quite modular and can be easily diversified since there were three unique vectors to explore. Lastly there is a rich literature that follows the PPY scaffolds³⁴ and related analogues regarding the synthesis of these compounds, which makes exploration of this scaffold very forthcoming.

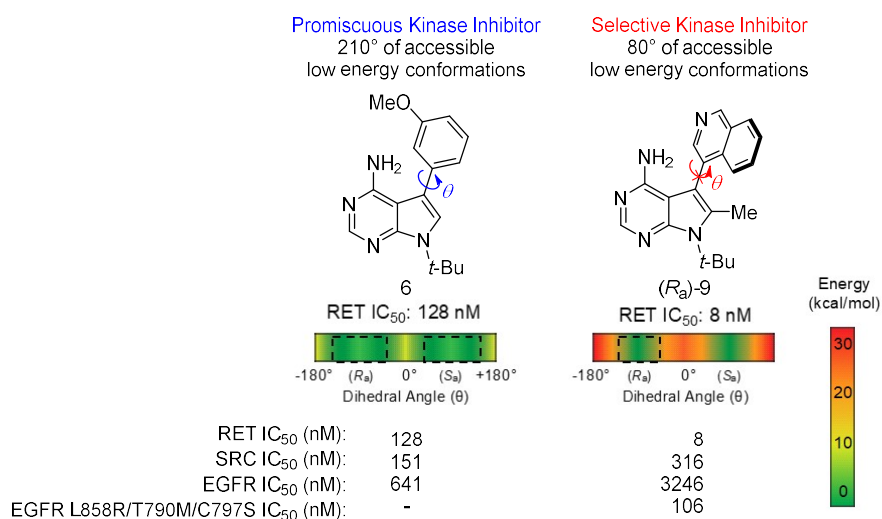


Figure 6. Summary of medicinal chemistry effort towards synthesizing a potent and selective RET kinase inhibiting PPY through leveraging atropisomerism (i.e., precluding non-relevant yet accessible low energy binding conformations). IC₅₀s presented in the table are reported in nanomolar (nM).

Each analogue consisted of two isolable Class-3 atropisomers, which were then isolated via preparatory chiral HPLC. The Gustafson group was quite excited, as these results of this exploration implicated that selectivity for the PPY scaffold could be highly improved through synthesizing the atropisomeric conformation biasing its target (Figure 5, compounds (R_a)-7 and (S_a)-7). While exciting, the contributors of this project did find that many of these compounds led

to an average <10-fold loss in potency compared to the respective Class-1 atropisomeric analogues. By introducing large, halogen substituents the data obtained suggested these types of functionalities were not generally tolerated for kinases. At the time of this first study, our group found that installing chloride or bromide across the atropisomeric axes of PPYs were the only known methods to achieving high stereochemical stability.

To further understand the role of atropisomerism and how it can lead to enhanced selectivities, the Gustafson group focused on RET kinase as a potential target. Finding an effective compound both potent and selective³⁵⁻³⁷ for RET kinase has remained a long-standing challenge within drug discovery. It was an interesting target, as aberrant RET kinase is attributed to many aggressive cancers such as breast, thyroid, and non-small cell lung cancers.³⁸⁻⁴² To begin, our research team had studied many PDB crystallographic models of various kinases^{30,33,34,42-57} and learned that specific residues within said targets could be expressly targeted wherein one atropisomeric confirmation would appropriately bind. In addition, we theorized that specific tuning of the dihedral angle of the atropisomeric axis by introducing key functionalities to the PPY would recapitulate or improve selectivity towards our desired kinase, and potentially would increase the potency. Indeed, our hypotheses were confirmed after iterative structural activity relationships (i.e., SAR) towards potent and functionally selective atropisomeric PPY (*R_a*)-9 that inhibits RET kinase (est. 2020, Figure 6). Importantly, this “second-generation” Class-3 atropisomeric PPY³⁷ (Figure 6) had exquisite potency compared to the “first-generation” set of Class-3 PPYs 7 and 8 (Figure 5). Interestingly as well, (*R_a*)-9 also possessed secondary activities to only mutant EGFR kinases. Currently, the Gustafson group is investigating the effect of these emerging activities for oncogenic RET and EGFR kinases and other mutagenic kinase targets.^{37,58}

1.3 Addressing Unmet Needs for Developing Atroposelective Synthetic Methodologies to Obtain Pharmaceutically Relevant Compounds

Before the discovery of RET kinase inhibitor (R_a)-9, our lab had a dire need for more efficient access to atropisomerically pure (i.e., enantiopure) samples of these PPY kinase inhibiting scaffolds. We found that the inaccessibility to the direct atropisomer of our interest was not just an exclusive problem observed in industry. The Gustafson group began a dedicated program for exploring and developing novel atroposelective chemistries towards pharmaceutically relevant atropisomeric scaffolds. Outside of our research group, there are other contributions to this emerging field of asymmetric syntheses – a growing literature for the enantioselective syntheses biaryl and non-biaryl Class-3 atropisomeric compounds. It should be noted that I and colleagues have since reviewed the primary literature and have dedicated a chapter in “Asymmetric Synthesis of Nonbiaryl Atropisomers.” in *Axially Chiral Compounds: Asymmetric Synthesis and Applications.*; Tan, B.; Wiley-VCH., ISBN: 978-3-527-34712-4. Copyright 2021 Wiley VCH. This mentioned, there are many other reviews that go into analysis of various atroposelective synthetic strategies and their applications towards specific scaffolds.

When I started in the Gustafson group, I began with the development of an enantioselective reaction to access a library of atropisomeric PPYs. Medicinal chemistry efforts were being delayed because of a heavy reliance on chiral HPLC separation which was both timely and unsustainable for the ongoing projects. In the next chapter, I will discuss how we developed an atroposelective synthesis of diverse PPYs (and related *N*-heterocyclic biaryl scaffolds) by nucleophilic aromatic substitution (i.e., abbreviated as S_NAr).

Acknowledgments

Chapter 1, in full, is a reprint of the material as it appears in “Asymmetric Synthesis of Nonbiaryl Atropisomers.” in *Axially Chiral Compounds: Asymmetric Synthesis and Applications.*; Tan, B.; Wiley-VCH., ISBN: 978-3-527-34712-4. Copyright 2021 Wiley VCH. Saputra, Mirza A.; Cardenas; Mariel M., Gustafson, Jeffrey L.; **2021**.⁵⁹ The dissertation author was the primary investigator and co-author of this paper.

Chapter 1 also contains material that is in part a reformatted reprint of the following review, with permission from *Arkivoc*, **2021**, *i*, 20-47. Copyright 2021 ARKAT USA, Inc. Cardenas, Mariel M.; Nguyen, Mariel M. Cardenas, Ashley D.; Brown, Zachary E.; Heydari, Beeta S.; Heydari, Bahar S.; Vaidya, Sagar D.; Gustafson, Jeffrey L.⁷ The dissertation author was the primary investigator and author of this paper.

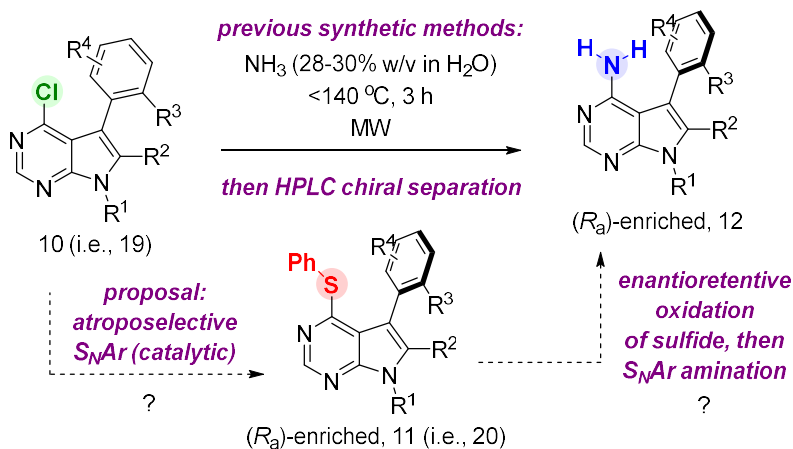
Chapter 2 APPLICATIONS OF ATROPOSELECTIVE NUCLEOPHILIC AROMATIC SUBSTITUTION TOWARDS PHARMACEUTICALLY RELEVANT *N*-HETEROCYCLES

Section 1. Synthesizing Class-3 Atropisomeric PPYs

Copyright

Chapter 2, Section 1 is reformatted in part with permissions from *Organic Letters*, **2018**, 20, 2037–2041. Copyright 2018 American Chemical Society. Chapter 2, Section 1 also contains material that is in part a reformatted reprint of the following review, with permission from *Arkivoc*, **2021**, *i*, 20-47. Copyright 2021 ARKAT USA, Inc.

2.1 Background: Atroposelective S_NAr towards PPYs



Equation 1. Proposal of alternative synthetic route to access pharmaceutically relevant PPYs.

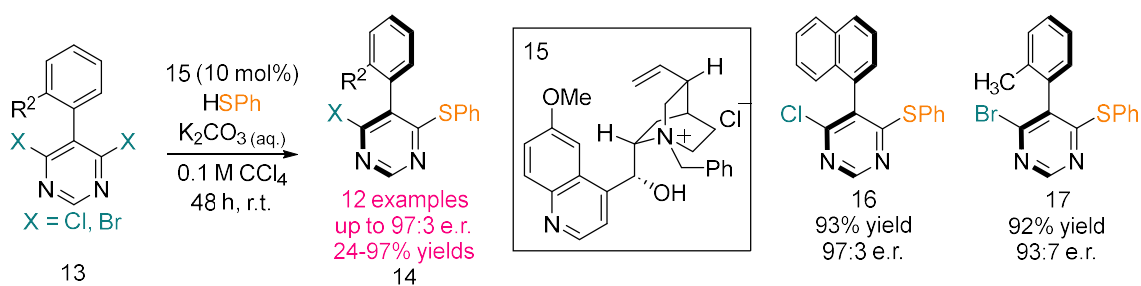
The last step before accessing the racemic mixture of atropisomeric kinase inhibiting PPYs requires amination via nucleophilic substitution of the preceding chloro-group at the C4 position of the pyrimidine (Equation 1). This step requires ammonia addition at elevated temperatures in non-atroposelective conditions. After this reaction, the (R)_a- and (S)_a-compounds are then

separated and isolated via chiral HPLC. This synthetic approach was trivial during the earliest exploration of these PPYs, however research efforts in the RET kinase inhibitor project became more focused and demanded a lot of compounds for cell studies. In addition, many of these early PPYs were not near the desired potency or selectivity profile to target RET kinase.

There were two major problems that we encountered once we had evaluated the process for this new medicinal chemistry campaign. These problems were becoming increasingly more frustrating to deal with as it often led to some delays in timelines and exhaustive, labor-intensive resyntheses. One of the major bottlenecks was related to the overall reaction scales since the final yields were limited to how much we could comfortably purify via HPLC chiral separation. At the time, our group did not have a proper budget to afford a preparatory chiral column to accommodate higher volumes of separated materials. The second problem was that (at the time of this project) the separation of both atropisomers was still necessary. My colleagues primarily working on that medicinal chemistry effort were unsure which atropisomer was contributing to the desired activity, specifically towards our target RET kinase. Our team needed to deconvolute the observed biological activity of the active atropisomer to the non-relevant atropisomer. The excessive need for more experiments and assays required even higher amounts of compounds that were already quite challenging to access in a timely fashion. It is important to note, we eventually confirmed in X-ray crystallographic structural elucidation which atropisomer was the most active conformation towards RET kinase when we accumulated enough material of the most promising lead compound.

For these reasons, I and my colleagues believed it would be very desirable to optimize and improve our existing S_NAr strategy described above to be able to obtain a large quantity of desired atropisomer for further studies. I suspected that redesigning the S_NAr reaction to undergo some atroposelective process would allow us to sterically control which atropisomer product we would

obtain, without the direct reliance on preparatory chiral HPLC separation. I wanted to know if we could somehow bias the S_NAr reaction to favor one atropisomeric product, and if this was possible then we may also be able to obtain the opposite atropisomer by biasing the reaction for the other. The first thing that immediately came to mind was the inclusion of a chiral catalyst, which allows us to facilitate faster reactions but can also influence the stereochemical outcome of the product. Many studies supported that a catalyst would likely engage at the interface of reaction, and directly transpose its stereochemistry to the final atropisomeric enriched product in sufficient yields. The other atropisomer could then be obtained from the enantiomer of the chiral catalyst (Equation 1).

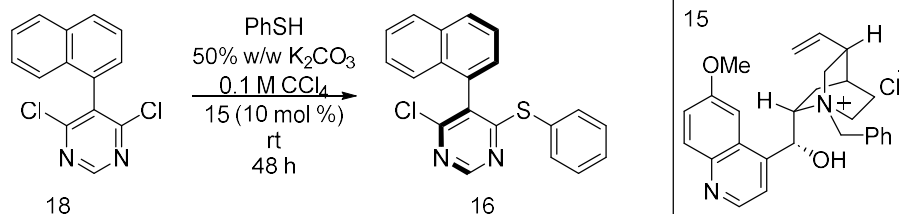


Equation 2. Atroposelective nucleophilic aromatic substitution of biaryl pyrimidines.⁶⁰

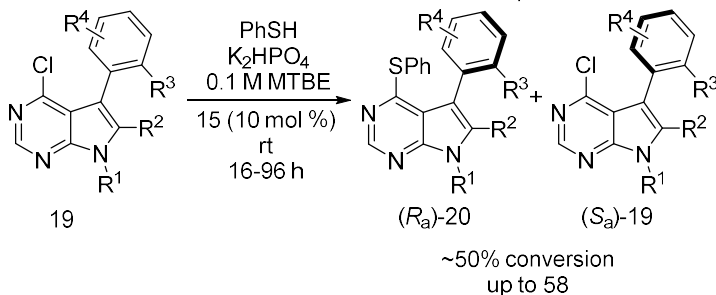
I and my colleagues had also been inspired by work from Dr. Martin Smith's group at the University of Oxford. Dr. Smith and coworkers' (est. 2015) had disclosed an atroposelective desymmetrization of biaryl pyrimidines (i.e., a similar scaffold to PPYs) via chiral cation directed S_NAr of thiophenol (Equation 2).⁶¹ This work represented the first example of atroposelective S_NAr and furnished atropisomeric pyrimidines such as 16 and 17 in excellent yields and enantioselectivities. While this work served as a great foundation, there were several factors that we needed to address and improve upon to make a plausible strategy amenable for our PPYs.

2.2 Addressing the Shortcomings for Current Atroposelective S_NAr Synthetic Methods to Access PPYs

a. Smith's Cation-directed Desymmetrization of pyrimidines



b. Cation-directed Kinetic Resolution to access atropisomeric PPYs



Equation 3. An overview of atroposelective S_NAr methodology. Compound 15 was found to be the optimal catalyst for both yield and enantioselectivity.⁹

2.1.1 Enantioselective Reaction Pathways: Desymmetrization vs. Kinetic Resolution

Smith and coworkers performed a desymmetrization of biaryl pyrimidines, which was indeed a very useful synthetic approach to access these types of atropisomeric scaffolds. The Smith group found higher yields of enantioenriched biaryl pyrimidines across several of their substrates. In desymmetrization, the starting material is prochiral which leads the chiral catalyst to possess no bias of reacting with one atropisomeric conformation over the other. However, our PPYs are asymmetric and therefore will not proceed S_NAr using this unique reaction pathway.

Our chloro-PPY starting materials exhibited high stereochemical stability, as a racemic mixture of both (*R*)_a- and (*S*)_a- Class-3 atropisomers. Instead, the reaction pathway biases one of the two atropisomers via the chiral catalyst complexation which lowers its transition state relative to the other atropisomer (Figure 7). Compared to the mechanism of a desymmetrization, S_NAr of

our chloro-PPY starting materials underwent what is referred to as a kinetic resolution (i.e., KR).⁶² In this case, I and my colleagues working on this project hypothesized that our catalyst 15 would likely bias one atropisomer over the other. The most favorable catalyst-substrate complex would then facilitate directed substitution of the nucleophilic thiophenol to yield desired atropisomeric sulfide PPY. At the end of the reaction, the unreacted atropisomer would remain with high enantiopurity. Both product and recovered starting material would be easier to isolate since we would be able to use very standard, and achiral purification techniques.

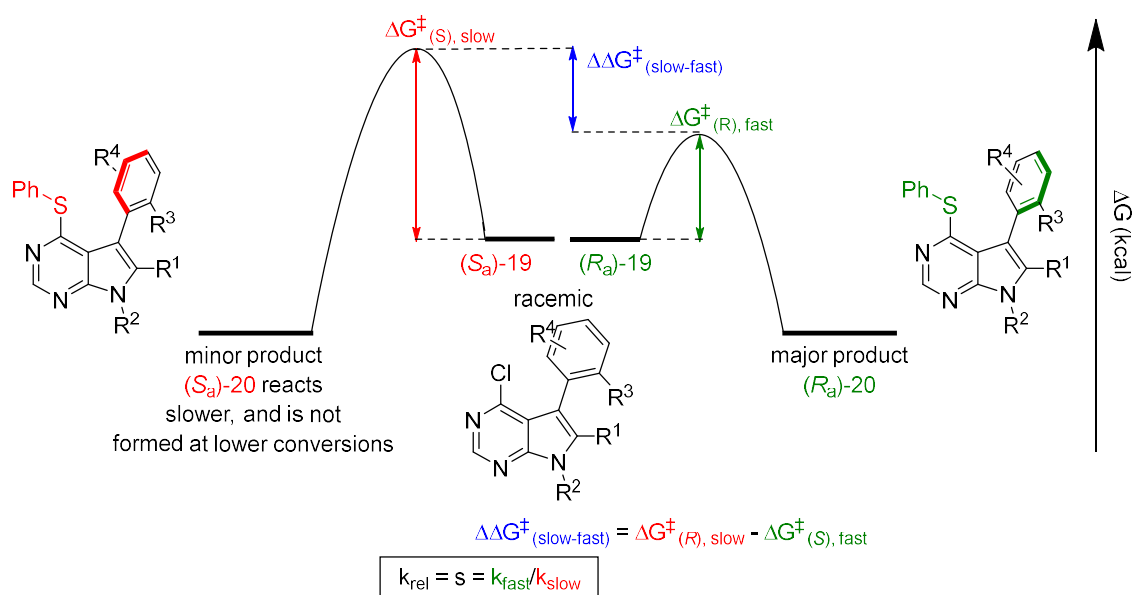


Figure 7. Proposed kinetic resolution pathway towards enantioenriched PPY sulfides.^{18,62–68}

The optimization for this atroposelective S_NAr presented many complex challenges. As a kinetic resolution there is a limitation of 50% of desired conversion^{63,65} since the purpose of the catalyst is to favor the reaction of one the atropisomers from the racemic mixture. Over conversion to achieve yields that compare to Smith and coworkers' desymmetrization work would negatively impact the enantiopurity of the final product. As the biased atropisomer is theoretically completely depleted at 50% (i.e., has been fully converted into the product), the unreacted starting material

would start getting consumed. This ultimately causes degradation of enantiopurity of the desired product. To ensure that we were representing the data consistently across various PPYs, I monitored our S_NAr using the selectivity factor (i.e., often referred to as *s*-factor, or k_{rel}) – a calculated value based on the relative rates of the reaction from both atropisomers the chiral catalyst-directed thiophenol substitution. Atroposelectivity of the reaction is directly proportional to the *s*-factor, it is desirable to see larger magnitude for this measurement of enantioselectivity.

2.1.2 Broader Exploration of the PPY Scaffolds

We designed an S_NAr approach to incorporate broader diversity and explore a wider chemical space around the PPY scaffold. I and my colleagues were primarily focused on common perturbations that would appeal to a general medicinal chemistry campaign. Being able to take resulting atropisomeric products and convert them in a post-functionalization approach applying more chemistry without observable racemization (i.e., possessing stable Class-3 atropisomerism) would also allow for larger enumeration of SAR⁴³ of these PPYs. I wanted a diverse panel of substrates, where the PPY substitutions went beyond simple aryl-based substitution permutations. Examples of this were adding potentially reactive functional groups during synthesis, making PPYs which range in different atropisomeric stereochemical stabilities. Importantly, we wanted to then test these products against the current SAR to increase potency or selectivity.

Lastly, the product sulfides are considered widely in drug discovery as an ‘esoteric’ group (apart from very few yet specific examples in different areas of pharmaceutical research, refer to Lesinuard from Figure 4 in Section 1.1). The sulfide group itself is often leveraged as a precursor intermediate towards the final active compounds. This is particularly observed with these thiopyrimidine products which can be easily oxidizable in biological conditions. This is evidenced

by Smith and colleagues, as they successfully twice oxidized their corresponding sulfide products under *m*CPBA (a common oxidizing agent)^{60,61} towards sulfones at room temperature. Especially in the PPY, we found that the C-4 amine functionality is one of the main drivers for potency and selectivity while the sulfide products were largely inactive in kinase assays. For this reason, we wanted to demonstrate the synthetic utility of these sulfides obtained from the S_NAr approach as key building blocks for facile access to desired aminated, atropisomeric PPYs.

2.3 Reaction Development: Optimizing Atroposelective S_NAr for 3-aryl PPYs

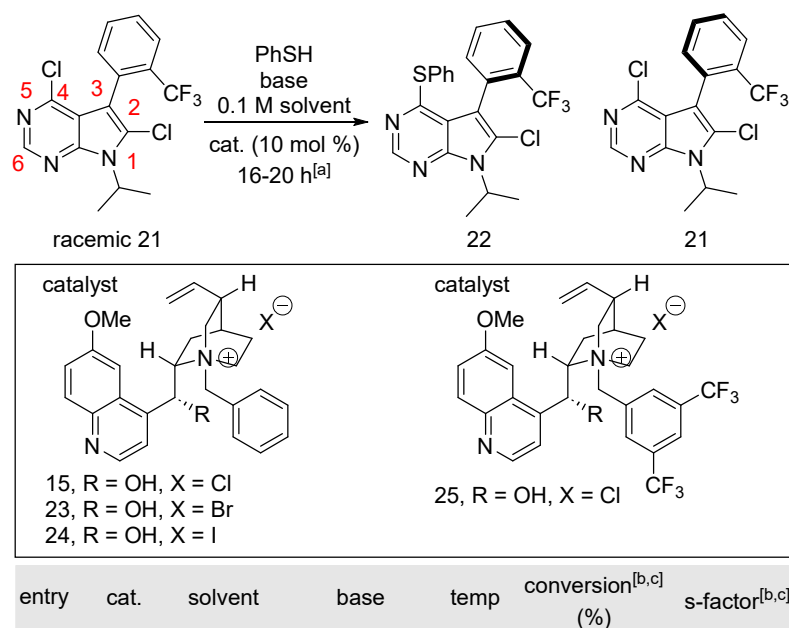
2.1.3 Substrate Development PPY

We began these studies first by optimizing the catalyst and reaction conditions for this atroposelective S_NAr of 3-arylated PPYs. I and my colleagues desired this S_NAr via kinetic resolution strategy to outcompete the previous workflow of the racemic synthesis followed by chiral HPLC separation towards atropisomeric PPYs. Also, we wanted consistent and comparable tests during the reaction development phase. Based on these two reasons, I restricted the total reaction time of this atroposelective S_NAr and kept it constant of around 24 hours and kept the reaction scale to 25 mg of starting material. Lastly, each S_NAr experiment was performed as a total of at least 3 trials (see Section 2.1.9 for more information regarding the overall procedure).

PPY 21 possesses a trifluoromethyl group adjacent to the axis of chirality and was chosen as the starting material to optimize our atroposelective S_NAr strategic approach (Table 1). The trifluoromethyl group is ubiquitous in many pharmaceutically relevant ligands and is often used by medicinal chemists during lead optimization of a scaffold. Also at the time of this S_NAr development, the Gustafson group was interested in testing trifluoromethyl-containing PPY^{69,70}

analogues based on the predicted property space. We thought introduction of these functional groups would lead to improved potency of these potential kinase inhibiting scaffolds.

Table 1. S_NAr Reaction Optimization Summary Towards 3-aryl PPY sulfides



^[a]Reactions were performed on a 0.0267 mmol scale of 21 with 7.5 equiv thiophenol and 12 equiv base. ^[b]Conversions and *s*-factors were determined using HPLC. ^[c]Results are reported as an average of at least 3 trials. See the Supporting information (SI) for more details.

Most importantly, we also thought the trifluoromethyl substituent would provide sufficient bulkiness about the atropisomeric axis to prevent potential racemization over the course of S_NAr

reaction. After making the starting material core PPY 21, we measured the barrier to racemization and we were delighted to find that this compound possessed $\Delta G_{\text{rac}} = 33.5$ kcal/mol. In addition, I also measured the barrier to racemization of the resulting sulfide product from this PPY which was $\Delta G_{\text{rac}} = 32.8$ kcal/mol. Both compounds correspond to a $t_{(1/2)}$ of racemization at 37 °C (i.e., biologically significant temperatures) of over 1000 years.

2.1.4 Solvent Screening and Evaluating Reaction Concentration

Using starting material PPY 21, we performed a control atroposelective $S_{\text{N}}\text{Ar}$ experiment using Smith's optimal conditions: a biphasic $S_{\text{N}}\text{Ar}$ reaction where the solvent system is a 1:1 CCl_4 in a solution of aqueous potassium carbonate, which is catalyzed by a readily available quinine based quaternary ammonium salt (i.e., a privileged scaffold⁷¹ in enantioselective catalysis which is also commercially available, *N*-benzylquininium chloride).⁶¹ After the 24-hour reaction time limitation, the overall conversion was lower than the KR's 50% conversion limit. I also recovered a decent amount of unreacted, starting material after this reaction. However, this control test did yield promising enantioselectivity with an *s*-factor of 5 (Table 2, entry 1). Doing a comparison reaction, we removed the aqueous component (using solid inorganic base, which is insoluble in CCl_4) (Table 2, entry 2). Results had little effect on the reaction conversion, however I did notice around a 2-fold increase in the *s*-factor which was very promising. I and my colleagues decided to forgo a biphasic reaction in favor of reducing reaction complexity, and allowing for quicker reaction development since there were no stark differences found from the homogeneous mixture.

We next screened various solvents that are commonly used to perform $S_{\text{N}}\text{Ar}$ (i.e., please refer to Section 2.1.9, Table 5), and as we expected was an important factor for both conversion and enantioselectivity (Table 1, entries 2-5). We wanted to find more similar but more cost

effective, eco-friendly solvents compared to CCl₄ which Smith and coworkers found to be an optimal solvent for atroposelective S_NAr. After testing different reactions in different solvents, I noticed a trend where nonpolar, aprotic solvents like CCl₄ performed better as these S_NAr reactions led to sulfide products with higher atroposelectivity.

Table 2. Solvent Evaluation and Permittivity Constants for the Reaction Optimization of Atroposelective S_NAr

Solvent	Permittivity, ϵ ^[a]	Conversion (%) ^[b]	<i>s</i> -factor ^[c]
CCl ₄	2.24	25.8	9.48
CDCl ₃	4.81	30.7	1.64
CH ₃ C ₆ H ₅	2.38	20.7	11.2
CH ₂ Cl ₂	8.93	41.3	2.25
THF	7.58	67.5	1.53
MTBE	2.6 ^[d]	50.7	27.9

^[a] Dielectric constants reported in this table were obtained and adapted from https://depts.washington.edu/eo optic/linkfiles/dielectric_chart%5B1%5D.pdf ^[b] Conversions and ^[c] *s*-factors are calculated using methods from Kagan and coworkers.⁷² Methods can be found in Section 2.1.8. ^[d] Dielectric constants reported in this table were obtained and adapted from https://monumentchemical.com/uploads/files/TDS/MTBE_TDS.pdf?v=1635378633113

To understand this correlation, I compared these solvents based on their permittivity or the measurement of how each solvent can sustain charged substrates in solution. Examining the data, these nonpolar solvents possessed similar dielectric constants (i.e., ϵ) to that of CCl₄. These nonpolar solvents like CCl₄ which possess $\epsilon < 3$ likely are unable to promote a stabilization of charges generated over the course of the reaction. Because of this reason, the cationic charge from the quaternary ammonium salt-based catalyst becomes less insulated by these types of solvents. From this, I inferred that the cationic catalyst may be encouraged to form a tighter salt bridge with the anionic thiophenol and lead to stronger H-bonding interactions with PPY 21 over the course of the S_NAr reaction. While atroposelectivity was improved, I found that the yields for these

reactions tend to be slower since the substrate, base, and sometimes catalyst were not very soluble in these solvents.

We also examined solvents with larger dielectric constants of $\epsilon > 3$ and found that these S_NAr reactions led to overall better yields (based on the limit of 50% conversion). This was anticipated: generally, nucleophilic substitutions perform better in polar, aprotic solvents as the nucleophile (which in this case is deprotonated thiophenol) is more exposed and the overall reaction is more soluble. However, these experiments observed overall poor enantioselectivity for these S_NAr reactions. For example, the *s*-factor was completely degraded in chloroform (i.e., $\epsilon = 4.81$, slightly improved in toluene (i.e., $\epsilon = 2.38$, and significantly improved at a faster rate in MTBE (i.e., $\epsilon = 2.6$). From these studies, MTBE possessed the physical properties that facilitated the most optimal atroposelective S_NAr based on the *s*-factor, and the reaction components were by far more soluble to make the reaction more homogenized for overall better yields. I and the team could have continued to focus on a screen of ether-based solvents that would possess similar characteristics to MTBE. However, we thought that MTBE was quite accessible and cost advantageous while still being quite optimal to performing these S_NAr reactions.

2.1.5. Catalyst and Base Evaluation (i.e., Charged Species in the Atroposelective S_NAr)

With MTBE as the most optimal solvent, we next screened catalysts that were similar in properties to that of *N*-benzylquininium chloride (i.e., catalyst 15). I examined catalysts with various counter anions, catalysts that diversify the electronics of the benzyl substitution off the quaternary ammonium, and catalysts that change the chiral hydroxyl-group into other moieties (Table 1, entries 5-8). In many of these changes, the *s*-factors for these reactions were significantly lowered suggesting that these three factors impart crucial atroposelectivity. Many of these

reactions also found poor conversions. As we were urgently pushing this project forward in favor of impacting the medicinal chemistry efforts of atroposelective PPY syntheses, I and the team decided that this catalyst screen would suffice. We were content to affect enantioselectivity of this reaction with the general substrate with *s*-factor > 20. From this catalyst screening, we decided that *N*-benzylquininium chloride was the most tolerated for this atroposelective S_NAr. For the completed catalyst screen, please refer to Section 2.1.9, Table 4.

After this short catalyst evaluation, we examined a set of various bases (Table 1, entries 5 and 9-12). Weaker bases (i.e., higher pK_b) generally performed better, with dibasic potassium phosphate as the most desirable near 50% conversion with an *s*-factor of over 27. Conversely, the S_NAr conversion was slightly improved with stronger bases, but also led to a 10-fold drop in *s*-factor. Please refer to Section 2.1.9, Table 5 for more information about the base optimization of this S_NAr reaction.

2.1.6. Temperature and Reaction Concentration

Second to last, I studied the temperature profile of this reaction and was unsurprised to find that enantioselectivity was completely degraded at elevated temperatures (Table 13-15). S_NAr is much faster under the higher reaction temperatures as there is no bias for either enantiomer of the starting material PPY 21 to yield the corresponding sulfide atropisomeric PPY 21. Essentially, the chiral catalyst for KR becomes inconsequential. I and my colleagues were a bit surprised however to find that the colder S_NAr reactions did lose selectivity. From this observation, we think the atroposelective S_NAr reaction is perhaps too sluggish for this desired KR to occur via the catalyst interaction with the starting material. As such, a background reaction might be happening over the course of the S_NAr, which will scramble the enantiopurity of the final product PPY. This is

evidenced when we ran a test reaction at a starting temperature of -78 °C, which was then gradually warmed to ambient reaction conditions over 24 hours. The result of this experiment led to a modest 40% conversion to product PPY 22, yet poor enantioselectivity of an *s*-factor of 2.30.

Lastly, we explored the potential effect of reaction concentration for this atroposelective S_NAr. Generally, nucleophilic substitution reactions are dependent on reaction concentration; wherein the success of this kinetic resolution is greatly affected ability of the chiral catalyst to engage with the starting material PPY. We thought it would be important to see what effect concentration would have on the overall enantioselectivity. I was a bit surprised to see the conversions seemingly fluctuate between 0.01 and 0.05 M MTBE runs (which I equate as within error averaging between several trials per experiment). More interestingly, I found that the most ideal condition for S_NAr was in the middle of range of concentrations. From these conclusions, we decided to stick with the original dilution of 0.1 M anhydrous MTBE.

After a few months of developing this atroposelective S_NAr, we were eager to see if this would be a viable method for our group's medicinal chemistry efforts about PPY-based kinase inhibiting scaffolds. We next designed and tested a varied substrate scope which served to perform library syntheses using our antiquated atroposelective S_NAr synthetic strategy.

2.4 Atroposelective S_NAr of Thiophenol towards 3-aryl PPYs

From readily available 4-chloro-7H-pyrrolo[2,3-d]pyrimidine, we prepared our C-4 chlorinated, racemic PPY substrates through this below general synthesis (i.e., numbering of atoms in the PPY is shown in Table 1, compound 19):

- 1) Iodination of the C-3 position via electrophilic aromatic substitution (i.e., EAS)

- 2) *N*-alkylation of the pyrrole (i.e., changing the substitution off the N-1 nitrogen; adding R² functionality that mimic the ribose of the native kinase ligand ATP).
- 3) A selective Ar-Ar coupling where the iodinated C-3 position is via Suzuki-Miyaura conditions establishes the atropisomeric bond, which is stabilized lastly via
- 4) Functionalization of the C-2 position (e.g., halogenation via Lewis-base catalyzed EAS, Stille couplings, etc.).⁷³ Please refer to Sections 2.1.10 to 2.1.16 for more details of the syntheses towards the PPY substrates involved in the atroposelective S_NAr library.

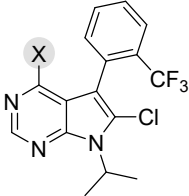
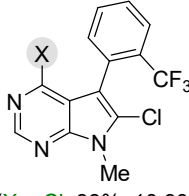
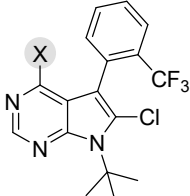
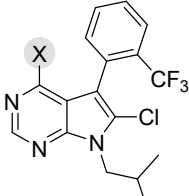
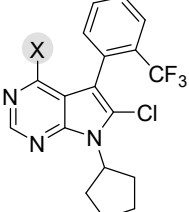
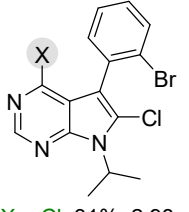
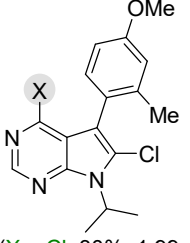
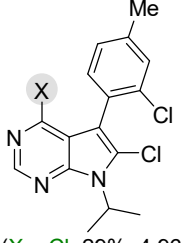
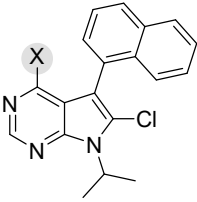
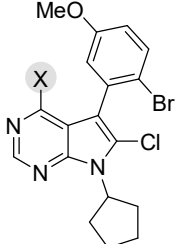
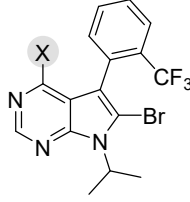
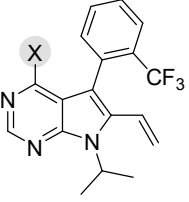
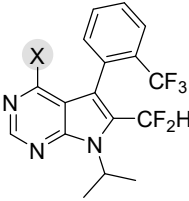
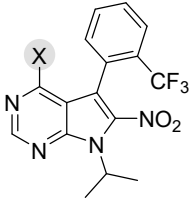
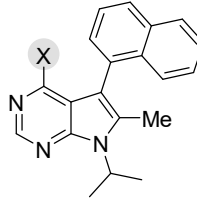
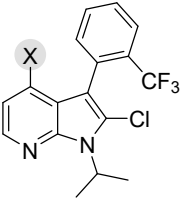
As mentioned in Section 2.3, the first round of chloro-PPY substrates were primarily focused on trifluoromethyl substitution off the 3-aryl (i.e., adjacent to atropisomeric axis). We synthesized a set of analogues that switched the pyrrole's *N*-1 aliphatic groups, as these were features that were desirable to test in potential kinase inhibiting compounds. There were no observable differences in the enantioselectivity between analogues, wherein the optimal S_NAr conditions led to excellent *s*-factors ranging from ~15-40. These results were extremely exciting and very promising, since the success for atroposelective S_NAr towards the desired sulfide products was unaffected from these changes made to the PPY scaffold.

During the time of this project, our group was focused on the C-3 aryl-group of the atropisomeric PPY scaffold as a key driver of the ongoing medicinal chemistry campaign. Straying away from the trifluoromethyl group, we synthesized many analogues that changed the size and electronics off the R³-group about the 3-aryl (i.e., adjacent to the axis of chirality, Equation 2). From relevant work of similar PP scaffolds and from our previous studies, it is shown that this

moiety acts as an anchor to engage the ‘gatekeeper’ (i.e., a unique residue embedded in the hydrophobic region) of the kinase.⁵³ By tuning the substitution off the 3-aryl (i.e., the R³-group), our team hypothesized this would likely result in the most marked improvement of kinase inhibitor selectivity for this scaffold. We were particularly eager to apply the atroposelective S_NAr to synthesize these types of PPY analogues. Another consideration was that changing the substitution off this 3-aryl position (i.e., adjacent to the atropisomeric axis of the PPY) would drastically affect the stereochemical stability for these compounds. To confirm this we took barrier to racemization measurements for some of the starting material PPYs, and found that all of them existed as Class-3 atropisomers which means that these compounds would still be KR viable substrates for atroposelective S_NAr. More details for the synthetic exploration can be found in Section 2.1.24 for Racemization Kinetics of some of the PPY scaffolds.

After examining S_NAr across this panel of substrates, we found that compared to the reaction of PPY 21 there was about a 2 to 5-fold loss of enantioselectivity at the optimal KR conversion. For example, changing the trifluoromethyl to a naphthyl group in PPY 37 yielded a modest *s*-factor about 13 at the 50% KR conversion limit. This PPY represented an atropisomerically stable analogue of the chemical probe NA-PP1 (i.e., binds strongly to kinases, closely resembles ATP). Across many of these substrates, we found decent enantioselectivities with *s*-factors >10. Despite the lowered selectivity of the S_NAr to access these PPYs, I and my colleagues found that limiting the conversion from the 50% threshold to around 40-45% allowed us to achieve workable enantiopurity for both the isolated sulfide products and recovered starting material PPYs.

Table 3. Scope of Enantioenriched PPY Sulfides obtained from Atroposelective S_NAr

 21 (X = Cl, 41% ^[d] , 7:94 e.r. ^[b]) 22 (X = SPh, 42% ^[d] , 8:92 e.r. ^[b]) conversion ^[c,d] = 51% s ^[c,d] = 28 [S _{1g} scale] = 15]	 23 (X = Cl, 38%, 10:90 e.r.) 24 (X = SPh, 46%, 87:17 e.r.) conversion = 46% s = 15	 25 (X = Cl, 30%, 18:82 e.r.) 26 (X = SPh, 43%, 6:94 e.r.) conversion = 49% s = 29	 27 (X = Cl, 46%, 5:95 e.r.) 28 (X = SPh, 48%, 83:17 e.r.) conversion = 54% s = 37
 29 (X = Cl, 43%, 6:94 e.r.) 30 (X = SPh, 34%, 9:91 e.r.) conversion = 52% s = 40	 31 (X = Cl, 31%, 2:98 e.r.) 32 (X = SPh, 48%, 13:87 e.r.) conversion = 54% s = 36	 33 (X = Cl, 30%, 1:99 e.r.) 34 (X = SPh, 48%, 27:73 e.r.) conversion = 65% s = 6.0	 35 (X = Cl, 29%, 4:96 e.r.) 36 (X = SPh, 50%, 17:83 e.r.) conversion = 63% s = 14
 37 (X = Cl, 40%, 8:92 e.r.) 38 (X = SPh, 46%, 24:76 e.r.) conversion = 51.2% s = 13 [S _{1g} scale] = 15.0]	 39 (X = Cl, 34%, 94:6 e.r.) 40 (X = SPh, 47%, 88:11 e.r.) conversion = 54% s = 17	 41 (X = Cl, 41%, 11:90 e.r.) 42 (X = SPh, 42%, 7:93 e.r.) conversion = 47% s = 16 [S _{3g} scale] = 58]	 43 (X = Cl, 23%, 22:80 e.r.) 44 (X = SPh, 24%, 72:28 e.r.) conversion = 40% s = 9.0
 45 (X = Cl, 30%) 47 (X = NH ₂ , 0.3:99.7 e.r. ^[e]) 46 (X = SPh, 68%, 17:83 e.r.) conversion = 70% s ^[e] = 12 (from 47)	 48 (X = Cl, 44%, 36:64 e.r.) 49 (X = SPh, 41%, 72:28 e.r.) conversion = 41% s = 2.0	 50 (X = Cl, n.d.) 51 (X = SPh, n.d.) conversion = >5% s = n.d.	 52 (X = Cl, n.d.) 53 (X = SPh, n.d.) conversion = >5% s = n.d.

^[a]Reactions were performed on a 25 mg scale of 1. ^[b]Reported isolated yield and e.r. are determined for one trial of the S_NAr of each substrate and its product. ^[c]Conversion and s-factors were determined using HPLC. ^[d]Results are reported as an average of at least 3 trials. ^[e]e.r. and s-factor were determined from the aminated substrate. *n.d.* means value was not determined. Please refer to Section 2.1.17 for more details.

We next synthesized a few PPYs that varied the C-2 position (i.e., the R²-group from the pyrrole that is adjacent to the atropisomeric axis) and evaluated each correspondent S_NAr reaction. Firstly, this position of the PPY required substitution to achieve Class-3 atropisomeric stability. In addition, our group found that we could exploit this C-2 substitution to gain further selectivity by engaging non-conserved residues. Lastly, this substitution can greatly regulate electrophilicity of the pyrimidine ring that forms crucial hydrogen bonding interactions with the hinge region of the kinase. Upon experimentation, we found that these substitutions had led to the most drastic changes in enantioselectivity. For one, this S_NAr chemistry was amenable to substitutions such as a C-2 bromide (i.e., *s*-factor = 16) or alkenyl group, to even a difluoromethyl group (an important functional group within the pantheon of drug discovery, much like the trifluoromethyl group). I observed S_NAr reactions with *s*-factors in modest conversions comparable to PPY 21. At scaling the reaction from the ‘mg to gram’-scale, I and my colleagues found that the S_NAr performed better, yielding an *s*-factor of almost 60 for the synthesis of C-2 bromo-PPY 41. This example represented the first time our lab was able to access a large quantity of atropoisomerically enriched, Class-3 stereochemically stable PPY.

Straying away from this, I and my colleagues tested PPY substrates with stronger electron withdrawing groups (e.g., C-2 nitro-group, PPY 48) which found small *s*-factors (i.e., within >20-fold loss in enantioselectivities). This was a noteworthy departure from the enantioselectivities we previously observed, and we considered that introducing these substitutions made the pyrimidine ring more electrophilic, thus making these PPY substrates more reactive towards S_NAr. I and my colleagues thought that perhaps a significant background reaction was able to outcompete the chiral catalyst’s influence to undergo the desired KR. To test this theory, I had set up the exact reaction using PPY 48 in the absence of any catalyst and found racemic sulfide product PPY 49

was being formed. This result suggested that the S_NAr reaction would need to be reoptimized to suit highly reactive PPYs, and lead to desirable yields and observed enantioselectivities.

While it may be that atroposelectivity of our S_NAr approach would be negatively influenced by a competing background reaction from such reactive substrates, this was not the only source of interest for substrates within this class. In some instances, we recovered the starting material PPYs after the atroposelective S_NAr reactions in unexpectedly poor enantiopurity. More specifically, this conundrum was spurred after we recovered the starting material PPY 48 at 36:64 e.r.; an isolated enantiopurity that would be useful for the ongoing medicinal chemistry campaign. From canonical KR, this recovered starting material should (based on theory, and as mentioned earlier) be isolated in a higher enantiopurity around (or at) the 50% conversion limit. This striking and perplexing result of 28 ee% for PPY 48, at the time of this reporting, did not have a complete hypothesis to understand what potentially might be happening. Our working theory was that these PPY substrates that contained these reactive substrates were somehow unstable (despite how all S_NAr reactions led to clean purifications of product sulfide PPY and recovered starting material chloride PPY during FCC normal phase separation). This observation was reencountered within the context of a completely different project (i.e., the atroposelective syntheses of 3-aryl quinolines, Section 2.12). From more in-depth interrogation and furthered exploration in that future project, we were able to propose a more comprehensive and plausible theory. I and my colleagues working on these atroposelective methodologies had later learned that kinetic resolution was more multilayered than what the current field of enantioselective catalysis perceives.

Regardless, I and my colleagues moved forward with these results and synthesized PPYs fashioned with electron donating substituents (e.g., alkyl groups like the C-2 methyl PPY 50). Running in parallel, our medicinal chemistry efforts found that putting more electron donating

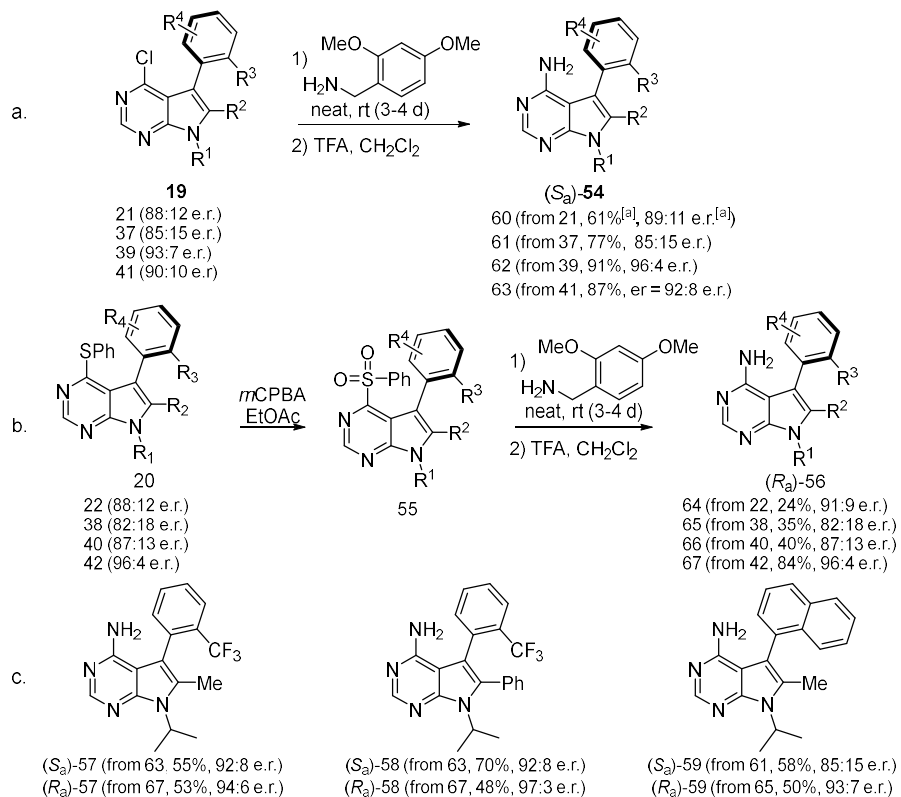
groups would impart more potency towards kinases of interest. After evaluating our S_NAr approach in the context of these PPYs, we were dismayed as we found minimal to no conversions to sulfide product PPYs. Unlike in the previous set of molecules, we attributed these PPYs as weakly reactive substrates for successful atroposelective S_NAr . Running a test reaction, I took PPY 50 (which possesses the C-3 naphthyl group and a C-2 methyl) and found no conversion even after a week of allowing the reaction to stir at room temperature.

Lastly, I tested one of the most common *N*-heterocyclic analogues to the PPY scaffold, an azaindole scaffold compound 52. This switched the reactive pyrimidine to a pyridine, which should reduce the electrophilicity. The result of this test was within our expectation, and I found no conversion to product using these S_NAr conditions upon this substrate.

2.5 Enantiodivergent Syntheses Towards Selective Kinase Inhibitor PPYs

The typical amination conditions required microwave conditions: a pressure sealed reaction of the PPY in ammonium hydroxide, at 140 °C with stirring (Equation 1). It would be remiss to perform this procedure on our newly acquired enantioenriched PPYs, since these extremely hot amination conditions would indubitably cause racemization. After isolating the recovered starting material and respective sulfide products, I found that these could be transformed into the final kinase inhibiting aminopyrimidines (i.e., $-NH_2$ at C-4 position) with no observed racemization via a different 2 (or 3-step in the case of the sulfide) amination process (Equation 4). Before I began developing an alternative amination method, I required a more substantial amount of both the sulfide product and recovered chloride starting material PPYs. Because I was able to perform an S_NAr reaction towards enantioenriched PPY sulfide 22 on ‘gram-scale’ (with large improvement in enantioselectivity based on the resulting *s*-factor), I synthesized PPYs 37, 39, and

41 in larger yields successfully. I was happy to find these results comparable to the small-scale syntheses of these compounds, but also to see that in some cases enantioselectivity of the final product was greatly improved.



Equation 4. a. Transformation of enantioenriched starting materials, and b. transformation of enantioenriched products towards C-4 aminated kinase inhibitors. Reported ^[a]isolated yields and ^[b]enantioselectivity via e.r. are for one trial. c. Modification of the C-2 position using modern Pd-coupling reaction conditions. See Section 2.1.17 for more details.

Taking inspirations from “PMB-protection followed by deprotection” of amines, I found that quantitative aminated intermediate to the atropisomerically enriched, chloride PPY occurred via S_NAr in neat 2,4-dimethoxybenzylamine within 24-48 hours at room temperature (Equation 4.a.). Upon reaction completion and then a subsequent purification, I treated the isolated 2,4-dimethoxybenzyl substituted aniline intermediate with TFA to expose the -NH₂ amine over the course of an hour. These steps resulted in aminated PPYs without observable enantiodegradation

for any of the cases evaluated. Moreover learnings from Smith and coworker's desymmetrization work, we then oxidized a handful of sulfide products to sulfone based PPYs using *m*CPBA⁶¹ in ethyl acetate at room temperature (Equation 4.b.). Making the sulfide into a sulfone made for a better leaving group, which then immediately transformed to the aminated PPYs also with no observable degradation in enantiopurity. This synthetic sequence represents how the sulfide PPY from the atroposelective S_NAr and its counterpart recovered starting material chloride PPY can lead to aminated products in an enantiodivergent manner. In principle, I and my colleagues were successful in separating the (*R*)_a- and (*S*)_a- atropisomers of the kinase inhibiting PPY.

It is also worth noting that we found increased enantioenrichment (i.e., improved e.r.) after the amination, which we believe is because these compounds were likely isolated after an *in-situ* trituration. Trituration is using a solvent with low solubility for the substrate to either dissolve or crash out the enantiomer in excess. This leaves the other enantiomer as the precipitate or in the solution, respectively. As the last step requires deprotection of the PMB-like group, the aminated PPY was isolated as a TFA salt which was then trituated during workup of the final reaction. For example, we performed the above-described synthetic sequence to yield PPY 66 from PPY 40 and found the enantiopurity of this material was slightly improved. This PPY 66 was vital to make into the aminated PPY since this substrate was already previously characterized from the original 2014 PPY work via small molecule crystallography from enantiopure material. Using this information, we assigned the stereoinduction traced back to atroposelective S_NAr of thiophenol. From the investigation, the final sulfide product obtained from the kinetic resolution was the (*R*)_a- atropisomer.

Atroposelective S_NAr towards analogues that changed the C-2 substitutions were limited, since enantioselectivity often was within *s*-factor < 10. To address this shortcoming, alternative

methods were used to install these electrons donating C-2 substitutions through using these final products obtained from this atroposelective S_NAr reaction. In doing these chemistries, I and my colleagues hoped to avoid racemization. We examined PPYs 65 and 67 which possess either chloride or bromide at the C-2 position, respectively. Using these as launching points, we fully protected the C-4 amine using Boc anhydride to avoid further synthetic complications. The Boc-protected 67 was readily functionalized to C-2 methylated 57 using chemistry developed from Schoenebeck⁷⁴ and C-2 arylated 58 using conditions from Buchwald⁷⁵ each in good yields. Once we confirmed we had these desired PPY products, we removed the Boc-group using acid and found that over these two steps there was no observed racemization. Separately, we took the naphthyl based aminated PPY 61 easily transformed the chloride at this C-2 chloride to a methylated analogue (PPY 59) using Organ's PEPPSI-*i*Pent catalyst⁷⁶ with no observed degradation in e.r.

Upon removal of the Boc-group, as in the previous case we found that the enantiomeric purity could be further improved from trituration using a mixture of hexanes in IPA. In this work, we measured that the many of these aminated PPYs possessed lower barriers to racemization compared to the chloride or sulfone (i.e., $\Delta G_{rac} = 28$ kcal/mol). For this reason, we decided that PPYs that such as 57 and 59 which correspond to $t_{(1/2)}$ of racemization of over a year at room temperature (2-3 months at 37 °C), stabilities that would be appropriate for chemical probes and to subject to test in kinase inhibition assays.

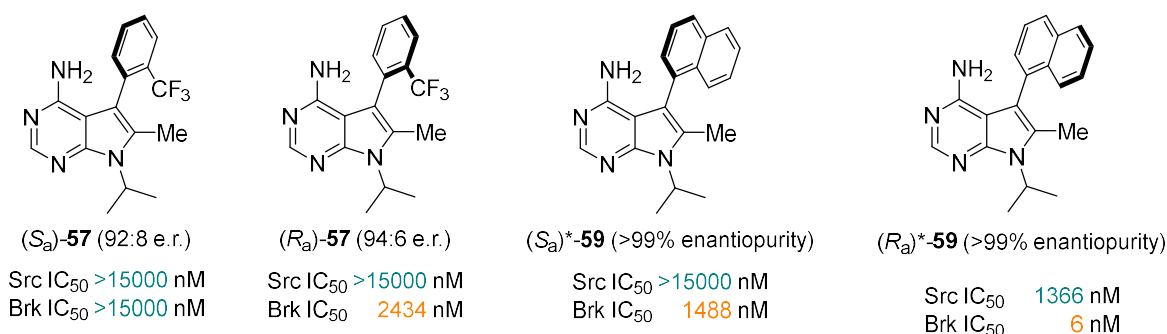
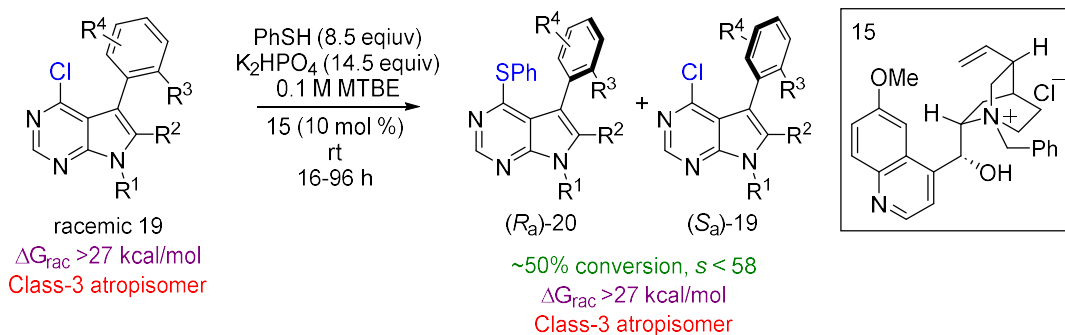


Figure 8. Evaluation of enantioenriched PPYs across Src and Brk kinases.^{55,56} IC₅₀s were determined using Promega's ATP Glo Kinase Inhibition Assay in duplicate. Please see Section 2.1.25 for more details.

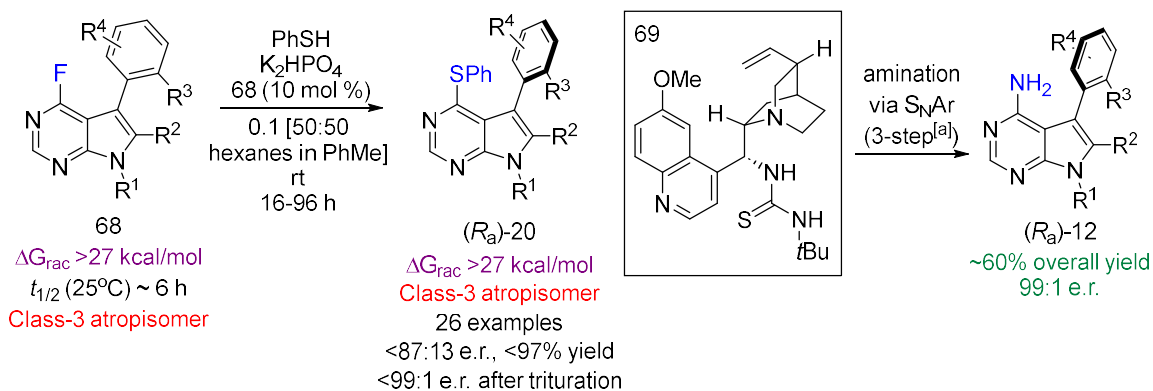
We examined PPYs 63 (and its atropisomer 67), both atropisomers of 57 (enantioenriched), and both atropisomers of 59 (enantiopure, after trituration) for inhibitory activity across kinases Src (which in the previous study had a preference to bind the (*S*)_a-atropisomer of the PPY scaffold) and Breast Tumor kinase (Brk).^{56,77} From these experiments, we found that the C-2 brominated (*S*_a)-63 or (*R*_a)-67 were inactive as neither atropisomer for this PPY inhibited these kinases. However, the (*R*)-atropisomer of C-2 methylated 57 led to a IC₅₀ of 25 μM towards Brk kinase. Based on these results, we evaluated the C-2 methylated 59, with the putative (*R*)_a-atropisomer inhibiting Src with an IC₅₀ of 13 μM and Brk with an IC₅₀ of 0.005 μM. This exciting >250-fold preference for Brk over Src was very promising, and (*R*)-atropisomer of 59 became an intriguing lead towards a selective Brk inhibitor. Eventually, this work served to springboard the medicinal chemistry exploration towards our best PPY inhibitor of RET kinase.

2.6 Conclusion and Future Directions for this Work



Equation 5. Atroposelective $\text{S}_{\text{N}}\text{Ar}$ towards PPY-based Kinase Inhibitors

I and my colleagues disclosed an atroposelective selective $\text{S}_{\text{N}}\text{Ar}$ approach to the kinetic resolution of an important class of kinase inhibitors. This chemistry proved quite robust and became a standard for accessing large quantities of enantioenriched PPY analogues. In addition, these compounds were amenable to post asymmetric induction modification. Excitingly, this work accelerated the medicinal chemistry campaigns, highlighted by the discovery of sub-digit nM potent and selective inhibitor of Breast Tumor Kinase (Brk).



Equation 6. Atroposelective $\text{S}_{\text{N}}\text{Ar}$ towards PPY-based kinase inhibitors via Dynamic Kinetic Resolution (DRK)

It should be mentioned that since this atroposelective synthetic strategy towards atropisomeric PPYs was published, other group members quickly followed up on this work and

modified this strategy to make it more accessible. While a viable strategy to access both atropisomers of the PPY scaffold on gram-scale, we found that the 50% conversion limitation was not going to be a sustainable, long-term solution. Also at this point, we wanted to focus our efforts on synthesizing the more active (*R*)_a-atropisomer of our PPY analogues and effectively ‘throwing away half of the material’ seemed egregious. To address this, we reoptimized my S_NAr strategy to undergo dynamic kinetic resolution (i.e., DKR).^{78–86} DKR is a subtype of the kinetic resolution – an enantioselective reaction in which the asymmetrical starting material (i.e., yielding two distinct enantiomers) is stereochemically unstable due to various factors such as epimerization, planarization, etc. Due to this instability, the highly reactive enantiomer depletes over the course of the reaction which then facilitates equilibration of the starting material via Le Châtelier's principle. As a result, this cycle drives the reaction further achieving higher conversions while retaining high enantioselectivity.

In the case of these PPYs, we found replacing the leaving group C-4 chloride with a smaller C-4 fluoride group would possess a rate of racemization that is faster than the rate of S_NAr. After reoptimizing the atroposelective S_NAr conditions and subjecting a set of PPYs (some new and some from the original substrate scope), enantioselectivities were very comparable. Additionally, trituration of the recovered products after following my general amination procedure led to 99:1 e.r.s in <70% yield, proving DKR as more efficient to access this class of kinase inhibitors. As of this thesis report, this work is still ongoing.

Acknowledgements

Chapter 2, Section 1 in full, is a reprint of the material as it appears in *Organic Letters*, **2018**, *20*, 2037–2041. Cardenas, Mariel M.; Toenjes, Sean. T.; Nalbandian, Chris J.; Gustafson, Jeffrey L.⁹ The dissertation author was the primary investigator and first author of this paper.

Chapter 2 also contains material that is in part a reformatted reprint of the following review, with permission from *Arkivoc*, **2021**, *i*, 20-47. Copyright 2021 ARKAT USA, Inc. Cardenas, Mariel M.; Nguyen, Mariel M. Cardenas, Ashley D.; Brown, Zachary E.; Heydari, Beeta S.; Heydari, Bahar S.; Vaidya, Sagar D.; Gustafson, Jeffrey L.⁷ The dissertation author was the primary investigator and author of this paper.

2.7 Experimental Section

This section is a reformatting of the Supporting Information from the original manuscript. Compound numbering is bolded to represent the preparation of that substrate. In other cases, the numbering format is not bolded.

^1H and ^{13}C NMR spectra were recorded on Varian VNMRs 400 MHz, Varian Inova 500 MHz and Varian VNMRs 600 MHz at room temperature. All chemical shifts were reported in parts per million (δ) and were internally referenced to residual protio solvents unless otherwise noted. All spectral data were reported as follows: δ = chemical shift (J = multiplicity [singlet (*s*), doublet (*d*), triplet (*t*), quartet (*q*), quintet (*p*), and multiplet (*m*)], coupling constants [Hz], integration). ^{13}C spectra were recorded with complete ^1H and ^{19}F decoupling. ^{19}F spectra were recorded with internal fluorine standards (trifluoroacetic acid or trifluorotoluene). Conventional mass spectra were obtained using Advion expression^s CMS APCI/ASAP.

For cross-coupling reactions, 1,4-dioxane and deionized H_2O were sparged with N_2 for 30 minutes. For the chlorination of substrates, purchased (*N*)-chlorosuccinimide was recrystallized before use. Chemicals were purchased from Sigma Aldrich, TCI, Frontier Scientific, Acros Organics, Strem, Oakwood, Cambridge Isotope Laboratories, or Fischer and were used as received without further purification. All flash column chromatography (FCC) was performed using Grade 60 Silica gel (230-400 mesh) purchased from Fisher Scientific. TLC preparatory plates were performed from Grade 60 Silica gel with fluorescent indicator F₂₅₄ and purchased from Fischer.

Enantiomeric ratios (*er* or e.r.) were determined by HPLC analysis employing chiral stationary phase column specified for each individual experiment. All data acquired was recorded on HP Agilent 1100 HPLC using Chiral Technologies Inc. Daicel Group Chiralpak IA, IB, and IC Normal Phase chiral columns.

2.1.7 Helpful Tips and Tricks

1. We found that K_2HPO_4 is universally the most effective base for the cation-directed S_NAr of anionic thiophenol based on highest determined selectivity factor (s). However, K_2CO_3 and $KHCO_3$ also provided comparable conversions and selectivity.
2. Our developed reaction ratio is 1.0:1.7 thiophenol to K_2HPO_4 as more non-nucleophilic base is necessary to acquire comparable ~50% conversions.
3. Our optimized reaction conditions are 8.5 equiv of thiophenol and 14.5 equiv of K_2HPO_4 . However, each PPY analogue yielded varying conversions at these reaction conditions.
4. In general, we found that more electron deficient PPY substrates required ≥ 3.0 equiv of thiophenol, and more electron rich PPY substrates required ≤ 3.0 equiv of thiophenol.

2.1.8 Formula to Determine All Conversions and s -factors of Each Substrate:

Equation 7. From every trial, conversion is calculated using the methods of Fiaud.⁷²

$$\text{conversion}(\%) = \left(\frac{ee_{SM}}{ee_{SM} + ee_{PR}} \right) 100$$

where ee_{SM} is the ee of the starting material

and ee_{PR} is the ee of the product

The reported conversion for this dissertation represents every substrate as an average of >3 trials.

For each trial, s is calculated from ee_{SM} and the calculated conversion (not percentage) *for that given trial* using the following equation.

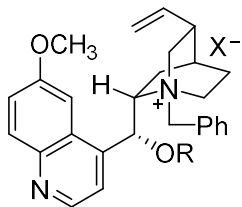
Equation 8. Calculating s -factor from conversion and enantioenriched percentage.⁷²

$$s = k_{rel} = \frac{\ln[(1 - conv)(1 - ee_{SM})]}{\ln[(1 - conv)(1 + ee_{SM})]}$$

The reported s for this dissertation represents every substrate as an average of >3 trials.

2.1.9 Reaction Development and Optimization

Table 4. Catalyst Index



A1 R = H, X = Cl (conv^[a] = 55.9%, s^[b] = 23.7)

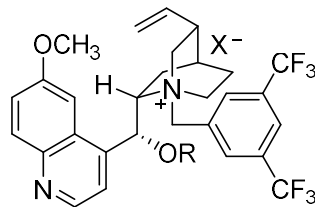
A2 R = H, X = Br (conv = 38.0%, s = 12.0)

A3 R = H, X = I (conv = 34.0%, s = 6.00)

A4 R = H, X = F (conv >5.0%, s NTD)

A5 R = Ac, X = Br (conv >5.0%, s NTD)

A6 R = CH₃, X = F (conv >5.0%, s NTD)

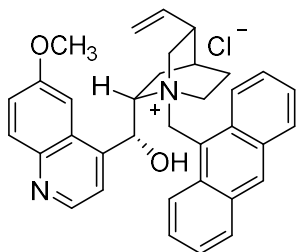


B1 R = H, X = Cl (conv = 28.0%, s = 3.00)

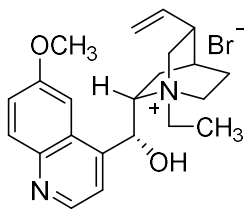
B2 R = H, X = Br (conv = 26.0%, s = 2.00)

B3 R = H, X = F (conv = 8.54%, s = 1.88)

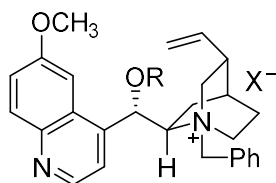
B4 R = Ac, X = Br (conv = 8.71%, s = 1.08)



C1 (conv >5.0%, s NTD)



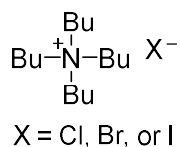
C2 (conv = 28.2%, s = 2.52)



D1 R = H, X = Cl (conv = 40.0%, s = 1.00)

D2 R = Ac, X = Br (conv = 27.9%, s = 1.45)

achiral catalyst
for standards:



With 0.0267 mmol (10 mg, 1.0 equiv) **74**, 0.0027 mmol of catalyst, and 0.1 M solvent, 0.167 mmol HSPH and 0.878 mmol base were added to the reaction and stirred overnight. See **Table 1. Reaction Optimization for S_NAr of PPYs** for more details on the rest of the reaction development.

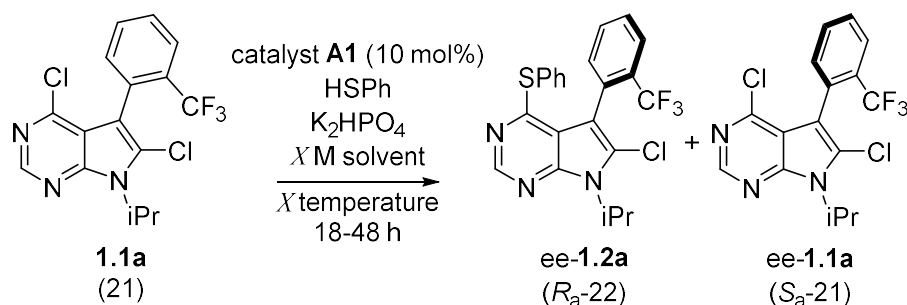
Catalyst Legend (Referenced to Section 1 of this Dissertation):

A1 = Compound 15

A2 = Compound 23

A3 = Compound 24

B1 = Compound 25

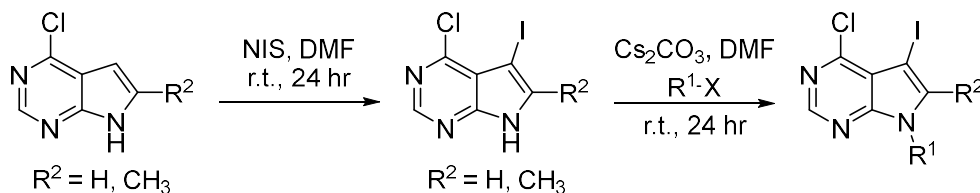
Table 5. Complete Reaction Optimization for S_NAr of PPYs

Entry	Solvent	Base	Temp. (°C)	Conc.(M)	conv(%)	<i>s</i> ^[h,i]
1 ^[a,g]	CCl ₄	K ₂ CO ₃	r.t.	0.1	22.2	5.64
2 ^[a]	CCl ₄	K ₂ CO ₃	r.t.	0.1	25.8	9.48
3 ^[b]	CDCl ₃	K ₂ CO ₃	r.t.	0.1	30.7	1.64
4 ^[c]	CH ₃ C ₆ H ₅	K ₂ CO ₃	r.t.	0.1	20.7	11.2
5 ^[a]	CH ₂ Cl ₂	K ₂ CO ₃	r.t.	0.1	41.3	2.25
6 ^[d]	THF	K ₂ CO ₃	r.t.	0.1	67.5	1.53
7	MTBE	Cs ₂ CO ₃	r.t.	0.1	14.5	2.93
8	MTBE	K ₃ PO ₄	r.t.	0.1	7.77	1.51
9	MTBE	NaHCO ₃	r.t.	0.1	21.8	2.23
10 ^[e]	MTBE	KHCO ₃	r.t.	0.1	48.2	16.3
11^[f]	MTBE	K₂HPO₄	r.t.	0.1	50.7	27.9
12 ^[f,h]	MTBE	K ₂ HPO ₄	95	0.1	81.7	1.02
13 ^[f]	MTBE	K ₂ HPO ₄	60	0.1	62.8	1.09
14 ^[f]	MTBE	K ₂ HPO ₄	4	0.1	16.4	5.99
15 ^[f]	MTBE	K ₂ HPO ₄	-78 to r.t.	0.1	40.4	2.30
16 ^[f]	MTBE	K ₂ HPO ₄	r.t.	0.01	43.6	1.35
17 ^[f]	MTBE	K ₂ HPO ₄	r.t.	0.05	25.1	8.16
18 ^[f]	MTBE	K ₂ HPO ₄	r.t.	0.13	66.5	2.50

^[a]0.0267 mmol (10 mg, 1.0 equiv) **74**, 0.0027 mmol of catalyst (10 mol%), and 0.1 M solvent, 0.167 mmol HSPH and 0.878 mmol base were added to the reaction and stirred overnight. ^[a]0.401 mmol HSPH and 0.878 mmol base were added instead of previous conditions. ^[b]0.251 mmol HSPH and 0.351 mmol base were added instead of previous conditions. ^[c]0.401 mmol HSPH and 0.561 mmol were added instead of previous conditions. ^[d]0.0335 mmol HSPH and 0.0468 mmol base were added instead of previous conditions. ^[e]0.234 mmol HSPH and 1.54 mmol base were added instead of previous conditions. ^[f]0.488 mmol HSPH and 0.802 mmol base were added instead of previous conditions. ^[g]K₂CO₃(aq.) was added as 50% w/w aqueous solution. ^[h]Pressure vial was used. Results are reported as an average of at least 3 trials. ^[h,i]Conversions and *s*-factors are determined using HPLC. Percent conversion is calculated by Equation 7. *s*-factors are calculated from the isolated starting materials via Equation 8.

2.1.10 General Procedure for PPY Substrates Prior to Suzuki Coupling

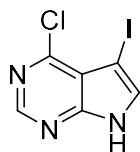
Equation 9. Synthesis of PPY Core



Step 1. To PPY (1.0 equiv) in a 25-mL Erlenmeyer was (*N*)-iodosuccinimide (i.e., NIS, 1.1 equiv) added and dissolved in 2.6 M DMF. The reaction was stirred at *r.t.* for 30 min to overnight. The resulting mixture was added to a 125-mL Erlenmeyer flask with distilled room temperature water. The desired precipitate was obtained after vacuum filtration.

Step 2. To PPY (1.0 equiv) in a 250-mL round-bottom flask was added Cs_2CO_3 (1.5 equiv) and 0.36 M DMF. The mixture was stirred at *r.t.* for 5 minutes, and alkyl halide $\text{R}^2\text{-X}$ (1.1 equiv) was added. The reaction was left to stir overnight. The resulting mixture was added to 125-mL Erlenmeyer flask with distilled room temperature water. The desired precipitate was filtered by vacuum filtration to yield product (yield varies amongst different alkyl halides) as a yellowish sienna colored solid. If the solid did precipitate out, the mixture was taken in 50-mL EtOAc and extracted, dried with Na_2SO_4 and concentrated in *vacuo* to yield product. Column chromatography was used to purify these PPYs via 15:1 Hexanes:EtOAc or 100% dichloromethane.

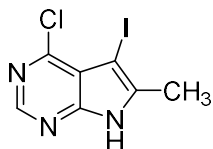
4-chloro-5-iodo-7*H*-pyrrolo[2,3-*d*]pyrimidine



Following the general procedure: to 4-chloro-7*H*-pyrrolo[2,3-*d*]pyrimidine (1.00 g, 6.5 mmol, 1.0 equiv) was NIS (1.61 g, 7.15 mmol, 1.1 equiv) added and stirred for 30 minutes in DMF. The product was recrystallized from DMF by the addition of water to yield pure 4-chloro-3-iodo-7*H*-pyrrolo[2,3-*d*]pyrimidine as a yellow solid. Quantitative

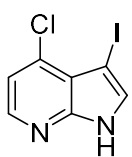
yield. Spectral data for this compound is attained in agreeance in U.S. patent: Goldstein, D. M.; Al Brameld, K. *Preparation of substituted pyrazolopyrimidinamines as tyrosine kinase inhibitors*, **2015**, Application Number: US 2013-13859569.

4-chloro-5-iodo-6-methyl-7H-pyrrolo[2,3-d]pyrimidine



Following the general procedure: to 4-chloro-6-methyl-7H-pyrrolo[2,3-d]pyrimidine (1.70 g, 10.2 mmol, 1.0 equiv) was NIS (2.52 g, 11.2 mmol, 1.1 equiv) added and stirred overnight in 5 mL DMF. The crude product was diluted with water and extracted with EtOAc. The collected organic layers were rinsed with brine, dried with Na₂SO₄, concentrated in *vacuo*. Trituration with hexanes afforded **4-chloro-3-iodo-2-methyl-7H-pyrrolo[2,3-d]pyrimidine** moved on without any methods of purification. Spectral data for this compound is attained in agreeance with Singer, M.; Jäschke, A. *J. Am. Chem. Soc.* **2010**, *132* (24), 8372.

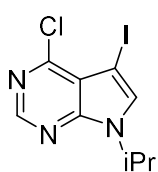
4-chloro-3-iodo-1H-pyrrolo[2,3-b]pyridine



Following the general procedure: to 4-chloro-1H-pyrrolo[2,3-b]pyridine (1.00 g, 6.5 mmol, 1.0 equiv) was NIS (1.61 g, 7.15 mmol, 1.1 equiv) added and stirred for 30 minutes in DMF. The product was recrystallized from DMF by the addition of water to yield crude **4-chloro-3-iodo-1H-pyrrolo[2,3-b]pyridine** as a brown solid. Quantitative yield. Spectral data for this compound is attained in agreeance in U.S. patent: Bahceci, S.; Chan, B.; Diva, S.; Chen, J.; Forsyth, T. P.; Franzini, M.; Jammalamadaka, V.; Jeong, J. W.; Jones, L. R.; Kelley, R. M.; Kim, M. H.; Leahy, J. W.; Mac, M. B.; Noguchi, R. T.; Rao, P.; Ridgway, B. H.; Xu, W.; Wang, Y. *Preparation of pyrrolo[2,3-b]pyridine, 1H-pyrazolo[3,4-d]pyrimidine, and 3H-*

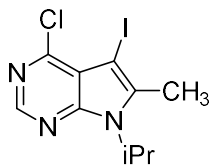
imidazo[4,5-b]pyridine derivatives as cyclin-dependent kinase (CDK) modulators, **2010**. PCT Int. Appl., 2010003133.

4-chloro-5-iodo-7-isopropyl-7H-pyrrolo[2,3-d]pyrimidine



Following the general procedure: to 4-chloro-5-iodo-7H-pyrrolo[2,3-d]pyrimidine (5.59 g, 20.03 mmol, 1.0 equiv) was Cs₂CO₃ (9.79 g, 30.05 mmol, 1.5 equiv) added and dissolved into 55.9 mL DMF. After 3 minutes, 2-iodopropane (2.20 mL, 22.04 mmol, 1.1 equiv) was added. The reaction was left to stir overnight. The product was recrystallized from DMF by the addition of water to yield pure **4-chloro-5-iodo-7-isopropyl-7H-pyrrolo[2,3-d]pyrimidine** as a yellow solid. 100% isolated yield. Spectral data for this compound is attained in agreeance in U.S. patent: Buffa, L.; Menichincheri, M.; Motto, I.; Quartieri, F. *Preparation of 6-amino-7-bicyclo-7-deazapurine derivatives as protein kinase inhibitors*, **2016**. Application No. WO 2016075224.

4-chloro-5-iodo-7-isopropyl-6-methyl-7H-pyrrolo[2,3-d]pyrimidine



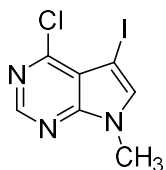
Following the general procedure: to crude 4-chloro-5-iodo-2-methyl-7H-pyrrolo[2,3-d]pyrimidine (6.9 g, 23.5 mmol, 1.0 equiv) was Cs₂CO₃ (10.50 g, 32.3 mmol, 1.5 equiv) added and dissolved into 38 mL DMF. After 3 minutes, 2-iodopropane (1.5 mL, 15.0 mmol, 1.1 equiv) was added. The reaction was left to stir overnight. The crude product was diluted with water and then extracted with EtOAc x5 times. The collected EtOAc layers were rinsed with brine, dried with Na₂SO₄. After filtering, the combined organic layers were concentrated in *vacuo*. Trituration with hexanes afforded **4-chloro-5-iodo-7-isopropyl-6-methyl-7H-pyrrolo[2,3-d]pyrimidine** without the need for any methods of purification.

¹H NMR (400 MHz, CDCl₃) δ (ppm) = 8.54 (s, 1H), 4.99 – 4.90 (m, 1H), 2.58 (s, 3H), 1.65 (d, 6H).

¹³C NMR (101 MHz, CDCl₃) δ (ppm) = 151.5, 150.7, 149.6, 148.9, 140.7, 117.1, 49.2, 21.4, 15.2.

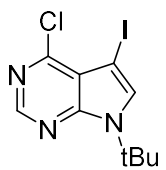
MS (APCI) = 336.0 [M+H]⁺ for C₁₀H₁₂ClIN₃; experimental 336.0 m/z.

4-chloro-5-iodo-7-methyl-7H-pyrrolo[2,3-d]pyrimidine



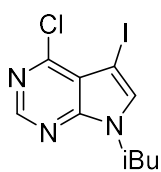
Following the general procedure: to 4-chloro-5-iodo-7H-pyrrolo[2,3-d]pyrimidine (5.59 g, 20.03 mmol, 1.0 equiv) was Cs₂CO₃ (9.79 g, 30.05 mmol, 1.5 equiv) added and dissolved into 55.9 mL DMF. After 3 minutes, iodomethane (2.20 mL, 22.04 mmol, 1.1 equiv) was added. The reaction was left to stir overnight. The product was recrystallized from DMF by the addition of water to yield pure **4-chloro-5-iodo-7-methyl-7H-pyrrolo[2,3-d]pyrimidine** as a yellow solid. Quantitative yield. Spectral data for this compound is attained in agreeance with Maddox, S. M.; Nalbandian, C. J.; Smith, D. E.; Gustafson, J. L. *Org. Lett.* **2015**, *17* (4), 1042.

7-(tert-butyl)-4-chloro-5-iodo-7H-pyrrolo[2,3-d]pyrimidine



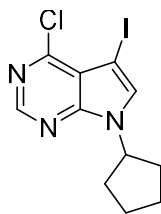
The synthesis and spectra data of **7-(tert-butyl)-4-chloro-5-iodo-7H-pyrrolo[2,3-d]pyrimidine** was prepared and obtained in agreeance with Smith, D. E.; Marquez, I.; Lokensgard, M. E.; Rheingold, A. L.; Hecht, D. a.; Gustafson, J. L. *Angew. Chem., Int. Ed.* **2015**, *54* (40), 11754. **2015**. Quantitative yield.

4-chloro-5-iodo-7-isobutyl-7H-pyrrolo[2,3-d]pyrimidine



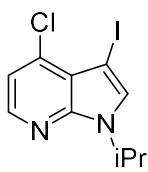
Following the general procedure: to 4-chloro-5-iodo-7H-pyrrolo[2,3-d]pyrimidine (7.3 g, 26.17 mmol, 1.0 equiv) was Cs₂CO₃ (12.8 g, 39.3 mmol, 1.5 equiv) added and dissolved into 87 mL DMF. After 3 minutes, 1-iodo-2-methylpropane (7.85 mL, 78.51 mmol, 3.0 equiv) was added. The reaction was left to stir overnight. The product was ran through a silica plug and flushed with dichloromethane to yield pure **4-chloro-5-iodo-7-isobutyl-7H-pyrrolo[2,3-d]pyrimidine** as a yellowish-orange solid. 100% isolated yield. Spectral data for this compound is attained in agreeance with Angiolini, M.; Buffa, L.; Menichincheri, M.; Motto, I.; Polucci, P.; Traquandi, G.; Zuccotto, F. Preparation of pyrrolo[2,3-d]pyrimidine derivatives as kinase inhibitors, **2014**. PCT Int. Appl., 2014184069.

4-chloro-7-cyclopentyl-5-iodo-7H-pyrrolo[2,3-d]pyrimidine



The synthesis and spectra data of **4-chloro-7-cyclopentyl-5-iodo-7H-pyrrolo[2,3-d]pyrimidine** was prepared and obtained in agreeance with Smith, D. E.; Marquez, I.; Lokensgard, M. E.; Rheingold, A. L.; Hecht, D. a.; Gustafson, J. L. *Angew. Chem., Int. Ed.* **2015**, 54 (40), 11754. Quantitative yield.

4-chloro-3-iodo-1-isopropyl-1H-pyrrolo[2,3-b]pyridine



Following the general procedure: to 4-chloro-3-iodo-1H-pyrrolo[2,3-b]pyridine (1.0 g, 3.59 mmol, 1.0 equiv) was Cs₂CO₃ (1.75 g, 5.39 mmol, 1.5 equiv) added and dissolved into 11 mL DMF. After 3 minutes, 2-iodopropane (395 μL, 3.95 mmol, 1.1 equiv) was added. The reaction stirred overnight. Purification through column chromatography afforded pure **4-chloro-3-iodo-1-isopropyl-1H-pyrrolo[2,3-b]pyridine** as a yellow-orange solid. 21% isolated yield.

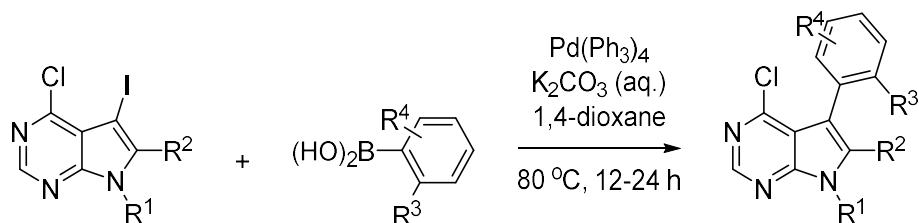
$^1\text{H NMR}$ (500 MHz, CDCl_3) δ (ppm) = 8.15 (d, J = 5.1 Hz, 1H), 7.45 (s, 1H), 7.02 (d, J = 5.1 Hz, 1H), 5.16 (hept, J = 6.6 Hz, 1H), 1.47 (d, J = 6.8 Hz, 6H).

$^{13}\text{C NMR}$ (101 MHz, CDCl_3) δ (ppm) = 147.0, 143.1, 136.5, 130.8, 117.7, 117.4, 117.4, 46.4, 22.8.

MS (APCI) = 321.0 $[\text{M}+\text{H}]^+$ for $\text{C}_{10}\text{H}_{11}\text{ClIN}_3$; experimental 321.0 m/z.

2.1.11 General Procedure for the Suzuki Coupling of PPY Substrates

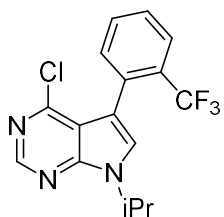
Equation 10. Synthesis of 3-aryl PPY Intermediate



To PPY (1.0 equiv) in a 100-mL round-bottom flask was added (*o*)- R^3 - R^4 -phenylboronic acid (1.1 eq), $\text{Pd}(\text{Ph}_3)_4$ (0.05 equiv), and K_2CO_3 (2.5 equiv). The mixture was thoroughly purged with vacuum then argon. To this mixture was added degassed 1,4-dioxane (100 mg/mL) and distilled, deionized water (300 mg/mL). The reaction was refluxed 12-48 hours at $80\text{ }^\circ\text{C}$. To the resulting mixture was added 5% w/w lithium chloride (aq.) and partitioned in EtOAc. The organic layer was collected, and the aqueous was extracted twice with EtOAc. The organic layers were combined, dried with Na_2SO_4 and concentrated in *vacuo* to yield crude products. Purification through FCC (99:1 \rightarrow 9:1) Hexanes/EtOAc afforded the desired product (\sim 40-95% comparable yields). In some of our reported NMR spectra, we observed 5-10% of protio-dehalogenated side products and $>90\%$ of the product of the Suzuki coupling. Products that contained these minor

impurities were taken onto the last steps of the syntheses to yield the (\pm)-**1** analogues for our substrate scope and were rigorously purified at that stage.

4-chloro-7-isopropyl-5-(2-(trifluoromethyl)phenyl)-7H-pyrrolo[2,3-d]pyrimidine



Following the general procedure: to 4-chloro-5-iodo-7-isopropyl-7H-pyrrolo[2,3-d]pyrimidine (4.61 g, 14.35 mmol, 1.0 equiv), was added 2-trifluoromethylphenylboronic acid (3.00 g, 15.78 mmol, 1.1 equiv), Pd(Ph₃)₄ (828 mg, 0.717 mmol, 0.05 equiv), and K₂CO₃ (4.96 g, 35.88 mmol, 2.5 equiv).

The mixture was thoroughly purged with vacuum then argon. To this mixture were added degassed 1,4-dioxane (46.1 mL) and water (15.4 mL). The reaction was refluxed 48 hours at 80 °C. Workup and purification were followed according to the general procedure to afford **4-chloro-7-isopropyl-5-(2-(trifluoromethyl)phenyl)-7H-pyrrolo[2,3-d]pyrimidine** as a yellowish-orange semi-solid. 70% isolated yield.

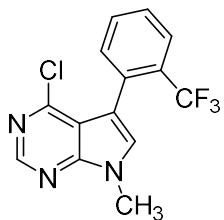
¹H NMR (400 MHz, CDCl₃) δ (ppm) = 8.65 (s, 1H), 7.78 (d, J = 7.8 Hz, 1H), 7.58 (t, J = 7.0 Hz, 1H), 7.52 (t, J = 7.3 Hz, 1H), 7.46 (d, J = 7.5 Hz, 1H), 7.32 (s, 1H), 5.21 (hept, J = 6.7 Hz, 1H), 1.57 (d, J = 6.8 Hz, 6H).

¹³C NMR (126 MHz, CDCl₃) δ (ppm) = 151.6, 150.1, 150.0, 134.0, 131.7 (q, J = 1.8 Hz), 130.5, 130.1 (q, J = 29 Hz), 127.7, 125.4 (q, J = 5.3 Hz), 125.3 (q, J = 2.1 Hz), 122.8, 116.0, 111.7, 46.6, 22.2.

¹⁹F NMR (470 MHz, CDCl₃) δ (ppm) = -58.29.

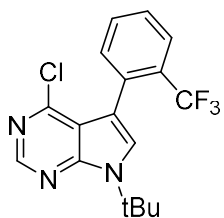
MS (APCI) = 340.1 [M+H]⁺ for C₁₆H₁₄ClF₃N₃; experimental 340.3 m/z.

4-chloro-7-methyl-5-(2-(trifluoromethyl)phenyl)-7H-pyrrolo[2,3-d]pyrimidine



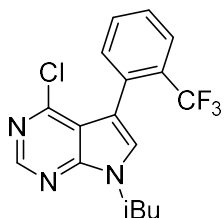
The synthesis and spectral data for compound **4-chloro-7-methyl-5-(2-(trifluoromethyl)phenyl)-7H-pyrrolo[2,3-d]pyrimidine** is attained in agreeance with Maddox, S. M.; Nalbandian, C. J.; Smith, D. E.; Gustafson, J. *L. Org. Lett.* **2015**, *17* (4), 1042. 29% isolated yield.

7-(tert-butyl)-4-chloro-5-(2-(trifluoromethyl)phenyl)-7H-pyrrolo[2,3-d]pyrimidine



The synthesis and spectral data for compound **7-(tert-butyl)-4-chloro-5-(2-(trifluoromethyl)phenyl)-7H-pyrrolo[2,3-d]pyrimidine** is attained in agreeance with Maddox, S. M.; Nalbandian, C. J.; Smith, D. E.; Gustafson, J. *L. Org. Lett.* **2015**, *17* (4), 1042. 63% isolated yield.

4-chloro-7-isobutyl-5-(2-(trifluoromethyl)phenyl)-7H-pyrrolo[2,3-d]pyrimidine



Following the general procedure: to 4-chloro-5-iodo-7-isobutyl-7H-pyrrolo[2,3-d]pyrimidine (1.3023 g, 3.88 mmol, 1.0 equiv), was added 2-trifluoromethylphenylboronic acid (885 mg, 4.66 mmol, 1.2 equiv), Pd(Ph₃)₄ (224.2 mg, 4.66 mmol, 0.12 equiv), and K₂CO₃ (1.34 g, 9.7 mmol, 2.5 equiv).

The mixture was thoroughly purged with vacuum then argon. To this mixture were added degassed 1,4-dioxane (12.5 mL) and water (4.16 mL). The reaction was refluxed for 2 days at 80 °C. Workup and purification were followed according to the general procedure to afford **4-chloro-7-isobutyl-5-(2-(trifluoromethyl)phenyl)-7H-pyrrolo[2,3-d]pyrimidine** as a yellowish-white solid. 36% isolated yield.

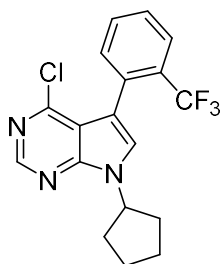
¹H NMR (400 MHz, CDCl₃) δ (ppm) = 8.61 (s, 1H), 7.72 (d, *J* = 8.3 Hz, 1H), 7.55 – 7.44 (m, 2H), 7.42 (d, *J* = 7.5 Hz, 1H), 7.19 (s, 1H), 4.10 (ddd, *J* = 91.1, 13.2, 7.4 Hz, 2H), 2.22 (dh, *J* = 13.6, 6.8 Hz, 1H), 0.90 (d, *J* = 6.7 Hz, 6H).

¹³C NMR (101 MHz, CDCl₃) δ (ppm) = 152.0, 151.0, 150.7, 134.3, 131.7 (q, *J* = 1.4 Hz), 130.8, 130.2 (q, *J* = 29.3 Hz), 129.2 (q, *J* = 2.4 Hz), 128.1, 125.7 (q, *J* = 5.3 Hz), 122.7 (q, *J* = 274.5 Hz), 116.0, 111.7, 52.5, 29.5, 19.9.

¹⁹F NMR (376 MHz, CDCl₃) δ (ppm) = -58.27.

MS (APCI) = 354.1 [M+H]⁺ for C₁₇H₁₆ClF₃N₃; experimental 354.4 m/z.

4-chloro-7-cyclopentyl-5-(2-(trifluoromethyl)phenyl)-7H-pyrrolo[2,3-d]pyrimidine



Following the general procedure: to 4-chloro-7-cyclopentyl-5-iodo-7H-pyrrolo[2,3-d]pyrimidine (500 mg, 1.44 mmol, 1.0 equiv), was added 2-trifluoromethylphenylboronic acid (355 mg, 1.82 mmol, 1.3 equiv), Pd(Ph₃)₄ (161.7 mg, 0.14 mmol, 0.1 equiv), and K₂CO₃ (457 mg, 3.312 mmol, 2.3 equiv).

The mixture was thoroughly purged with vacuum then argon. To this mixture were added degassed 1,4-dioxane (7.2 mL) and water (1.8 mL). The reaction was refluxed overnight at 80 °C. Workup and purification were followed according to the general procedure to afford **4-chloro-7-cyclopentyl-5-(2-(trifluoromethyl)phenyl)-7H-pyrrolo[2,3-d]pyrimidine** as a white solid. 45% isolated yield.

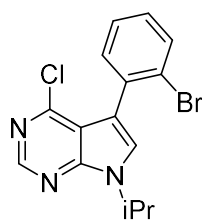
¹H NMR (400 MHz, CDCl₃) δ (ppm) = 8.65 (s, 1H), 7.77 (d, *J* = 7.8 Hz, 1H), 7.61 – 7.49 (m, 2H), 7.47 – 7.43 (m, 1H), 7.29 (s, 1H), 5.31 (dt, *J* = 13.8, 7.3 Hz, 1H), 2.36 – 2.23 (m, 2H), 1.97 – 1.85 (m, 4H), 1.84 – 1.77 (m, 2H).

^{13}C NMR (101 MHz, CDCl_3) δ (ppm) = 151.8, 150.7, 150.3, 134.2, 131.8 (q, $J = 2.1$ Hz), 130.7 (q, $J = 1.1$ Hz), 130.4, 130.1, 127.9, 126.1 (q, $J = 2.17$ Hz), 125.7 (q, $J = 5.2$ Hz), 124.0 (q, $J = 273.9$ Hz), 111.9, 55.8, 33.0, 24.1.

^{19}F NMR (376 MHz, CDCl_3) δ (ppm) = -58.25.

MS (APCI) = 366.1 $[\text{M}+\text{H}]^+$ for $\text{C}_{18}\text{H}_{16}\text{ClF}_3\text{N}_3$; experimental 366.0 m/z.

5-(2-bromophenyl)-4-chloro-7-isopropyl-7H-pyrrolo[2,3-d]pyrimidine



Following the general procedure: to 4-chloro-5-iodo-7-isopropyl-7H-pyrrolo[2,3-d]pyrimidine (363.88 mg, 1.13 mmol, 1.0 equiv), was added 2-bromophenylboronic acid (250 mg, 1.245 mmol, 1.1 equiv), $\text{Pd}(\text{Ph}_3)_4$ (65 mg, 0.057 mmol, 0.05 equiv), and K_2CO_3 (390.44 mg, 2.825 mmol, 2.5 equiv). The

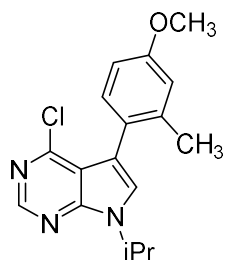
mixture was thoroughly purged with vacuum then argon. To this mixture were added degassed 1,4-dioxane (3.66 mL) and water (1.64 mL). The reaction was refluxed overnight at 80 °C. Workup and purification were followed according to the general procedure to afford **5-(2-bromophenyl)-4-chloro-7-isopropyl-7H-pyrrolo[2,3-d]pyrimidine** as a white solid. 80% isolated yield.

^1H NMR (400 MHz, CDCl_3) δ (ppm) = 8.57 (s, 1H), 7.60 (dd, $J = 8.0, 0.9$ Hz, 1H), 7.35 – 7.23 (m, 3H), 7.21 – 7.14 (m, 1H), 5.12 (hept, $J = 6.8$ Hz, 1H), 1.50 (d, $J = 6.8$ Hz, 6H).

^{13}C NMR (126 MHz, CDCl_3) δ (ppm) = 152.1, 150.4, 150.3, 134.2, 133.0, 132.5, 129.3, 126.8, 125.8, 125.1, 115.8, 115.0, 46.8, 22.7.

MS (APCI) = 350.0 $[\text{M}+\text{H}]^+$ for $\text{C}_{15}\text{H}_{14}\text{BrClN}_3$; experimental 350.3 m/z.

4-chloro-7-isopropyl-5-(4-methoxy-2-methylphenyl)-7H-pyrrolo[2,3-d]pyrimidine



Following the general procedure: to 4-chloro-5-iodo-7-isopropyl-7H-pyrrolo[2,3-d]pyrimidine (500 mg, 1.56 mmol, 1.0 equiv), was added 2-methyl-4-methoxyphenylboronic acid (335 mg, 2.02 mmol, 1.3 equiv), Pd(Ph₃)₄ (180.18 mg, 0.156 mmol, 0.1 equiv), and K₂CO₃ (495 mg, 3.58 mmol,

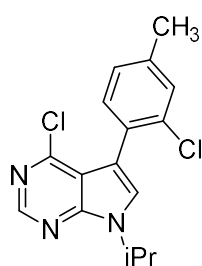
2.3 equiv). The mixture was thoroughly purged with vacuum then argon. To this mixture were added degassed 1,4-dioxane (10 mL) and water (2.5 mL). The reaction was refluxed overnight at 80 °C. Workup and purification were followed according to the general procedure to afford **4-chloro-7-isopropyl-5-(4-methoxy-2-methylphenyl)-7H-pyrrolo[2,3-d]pyrimidine** as a white solid. 62% isolated yield.

¹H NMR (500 MHz, CDCl₃) δ (ppm) = 8.55 (s, 1H), 7.17 (s, 1H), 7.11 (d, *J* = 8.3 Hz, 1H), 6.77 (s, 1H), 6.70 (d, *J* = 8.3 Hz, 1H), 5.12 (hept, *J* = 6.6 Hz, 1H), 3.75 (s, 3H), 2.10 (s, 3H), 1.50 (d, *J* = 6.9 Hz, 6H).

¹³C NMR (101 MHz, CDCl₃) δ (ppm) = 159.3, 152.1, 150.4, 150.2, 139.5, 132.4, 131.5, 125.0, 124.2, 116.2, 115.2, 110.4, 55.2, 46.6, 22.7, 20.8.

MS (APCI) = 316.1 [M+H]⁺ for C₁₇H₁₉ClN₃O; experimental 316.1 m/z.

4-chloro-5-(2-chloro-4-methylphenyl)-7-isopropyl-7H-pyrrolo[2,3-d]pyrimidine



Following the general procedure: to 4-chloro-5-iodo-7-isopropyl-7H-pyrrolo[2,3-d]pyrimidine, (500 mg, 1.56 mmol, 1.0 equiv) was added 2-chloro-4-methylboronic acid (291 mg, 1.71 mmol, 1.1 equiv), Pd(Ph₃)₄ (90 mg, 0.078 mmol, 0.05 equiv), and K₂CO₃ (328 mg, 2.34 mmol, 1.5 equiv). The mixture was

thoroughly purged with vacuum then argon. To this mixture were added degassed 1,4-dioxane (5.00 mL) and water (1.67 mL). The reaction was refluxed overnight at 80 °C. Workup and purification were followed according to the general procedure to afford **4-chloro-5-(2-chloro-4-**

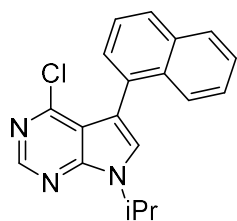
methylphenyl)-7-isopropyl-7H-pyrrolo[2,3-d]pyrimidine as a yellowish-orange semi-solid. 85% isolated yield.

$^1\text{H NMR}$ (400 MHz, CDCl_3) δ (ppm) = 8.57 (s, 1H), 7.23 (s, 2H), 7.21 (s, 1H), 7.03 (d, $J = 7.6$ Hz, 1H), 5.12 (p, $J = 6.8$ Hz, 1H), 2.31 (s, 3H), 1.50 (d, $J = 6.8$ Hz, 6H).

$^{13}\text{C NMR}$ (101 MHz, CDCl_3) δ (ppm) = 152.0, 150.4, 150.2, 139.3, 134.7, 132.7, 129.7, 129.0, 127.0, 125.2, 115.9, 113.0, 46.8, 22.6, 20.9.

MS (APCI) = 320.1 $[\text{M}+\text{H}]^+$ for $\text{C}_{16}\text{H}_{16}\text{Cl}_2\text{N}_3$; experimental 320.3 m/z.

4-chloro-7-isopropyl-5-(naphthalen-1-yl)-7H-pyrrolo[2,3-d]pyrimidine



Following the general procedure: to 4-chloro-5-iodo-7-isopropyl-7H-pyrrolo[2,3-d]pyrimidine, (1.0 g, 3.11 mmol, 1.0 equiv) was added 1-naphthylboronic acid (535 mg, 3.11 mmol, 1.0 equiv), $\text{Pd}(\text{Ph}_3)_4$ (113 mg, 0.078 mmol, 0.05 equiv), and K_2CO_3 (1.3 g, 0.098 mmol, 0.3 equiv). The

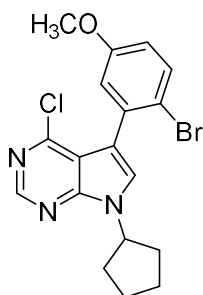
mixture was thoroughly purged with vacuum then argon. To this mixture were added degassed 1,4-dioxane (5.00 mL) and water (1.67 mL). The reaction was refluxed overnight at 80 °C. Workup and purification were followed according to the general procedure to afford **4-chloro-7-isopropyl-5-(naphthalen-1-yl)-7H-pyrrolo[2,3-d]pyrimidine** as a yellowish-orange semi-solid. 55% isolated yield.

$^1\text{H NMR}$ (500 MHz, CDCl_3) δ (ppm) = 8.69 (s, 1H), 7.92 (d, $J = 8.1$ Hz, 2H), 7.68 (d, $J = 8.6$ Hz, 1H), 7.56 – 7.47 (m, 3H), 7.43 – 7.39 (m, 2H), 5.26 (hept, $J = 6.8$ Hz, 1H), 1.62 (t, $J = 6.9$ Hz, 6H).

$^{13}\text{C NMR}$ (126 MHz, CDCl_3) δ (ppm) = 152.2, 150.4, 150.3, 133.5, 133.3, 130.7, 128.9, 128.2, 128.0, 126.0, 126.0, 125.7, 125.2, 124.9, 116.6, 114.1, 46.7, 22.6.

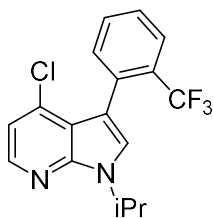
MS (APCI) = 322.1 [M+H]⁺ for C₁₉H₁₇ClN₃; experimental 322.3 m/z.

5-(2-bromo-5-methoxyphenyl)-4-chloro-7-cyclopentyl-7H-pyrrolo[2,3-d]pyrimidine



The synthesis and spectra data of **5-(2-bromo-5-methoxyphenyl)-4-chloro-7-cyclopentyl-7H-pyrrolo[2,3-d]pyrimidine** was prepared and obtained in agreeance with Smith, D. E.; Marquez, I.; Lokensgard, M. E.; Rheingold, A. L.; Hecht, D. a.; Gustafson, J. L. *Angew. Chem. Int. Ed.* **2015**, *54* (40), 11754.

4-chloro-1-isopropyl-3-(2-(trifluoromethyl)phenyl)-1H-pyrrolo[2,3-b]pyridine



Following the general procedure: to 4-chloro-3-iodo-1-isopropyl-1H-pyrrolo[2,3-b]pyridine, (330.4 mg, 1.03 mmol, 1.0 equiv) was added 2-chloro-4-methylboronic acid (235 mg, 1.24 mmol, 1.2 equiv), Pd(Ph₃)₄ (60 mg, 0.052 mmol, 0.05 equiv), and K₂CO₃ (356 mg, 2.58 mmol, 2.5 equiv). The mixture was thoroughly purged with vacuum then argon. To this mixture were added degassed 1,4-dioxane (3 mL) and water (1.5 mL). The reaction was refluxed at 80 °C for 48 hours. Workup and purification were followed according to the general procedure to afford **4-chloro-1-isopropyl-3-(2-(trifluoromethyl)phenyl)-1H-pyrrolo[2,3-b]pyridine** as an orange semi-solid. 88% isolated yield.

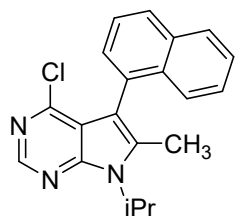
¹H NMR (400 MHz, CDCl₃) δ (ppm) = 8.23 (d, *J* = 5.1 Hz, 1H), 7.76 (d, *J* = 7.8 Hz, 1H), 7.54 – 7.48 (m, 2H), 7.48 – 7.41 (m, 1H), 7.34 (s, 1H), 7.03 (d, *J* = 5.1 Hz, 1H), 5.34 – 5.25 (m, 1H), 1.56 (d, *J* = 6.8 Hz, 6H).

^{13}C NMR (101 MHz, CDCl_3) δ (ppm) = 147.5, 143.0, 136.1, 134.6, 133.6 (q, J = 1.9 Hz), 130.7, 130.5, 127.5, 125.6 (q, J = 5.4 Hz), 124.7 (q, J = 2.2 Hz), 122.9 (q, J = 274.4 Hz), 118.1, 117.0, 98.2, 46.0, 22.8, 22.7.

^{19}F NMR (376 MHz, CDCl_3) δ (ppm) = -58.28.

MS (APCI) = 339.1 $[\text{M}+\text{H}]^+$ for $\text{C}_{17}\text{H}_{15}\text{ClF}_3\text{N}_2$; experimental 339.3 m/z.

4-chloro-7-isopropyl-6-methyl-5-(naphthalen-1-yl)-7H-pyrrolo[2,3-d]pyrimidine (**1.1o**)



Following the general procedure: to 4-chloro-5-iodo-7-isopropyl-6-methyl-7H-pyrrolo[2,3-d]pyrimidine (175 mg, 0.566 mmol, 1.0 equiv) was added 2-naphthylboronic acid (116.86 mg, 0.68 mmol, 1.2 equiv), $\text{Pd}(\text{Ph}_3)_4$ (64.76 mg, 0.056 mmol, 0.1 equiv), and K_3PO_4 (276.9 mg, 1.302 mmol, 2.3 equiv). The

mixture was thoroughly purged with vacuum then argon. To this mixture were added degassed 1,4-dioxane (2.3 mL) and water (0.75 mL). The reaction was refluxed overnight at 80 °C. Workup and purification were followed according to the general procedure to afford **1.1o** as a white solid.

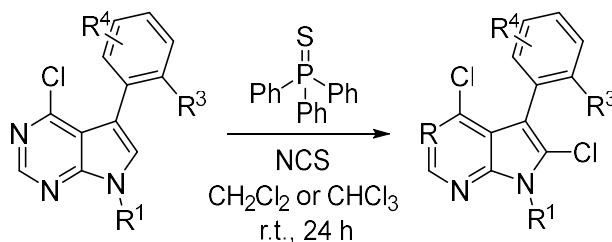
^1H NMR (400 MHz, CDCl_3) δ (ppm) = 8.60 (s, 1H), 7.92 (d, J = 8.2 Hz, 2H), 7.57 – 7.36 (m, 5H), 5.01 (dq, J = 13.9, 6.8 Hz, 1H), 2.26 (s, 3H), 1.79 (t, J = 6.6 Hz, 6H).

^{13}C NMR (101 MHz, CDCl_3) δ (ppm) = 151.3, 150.5, 149.1, 137.3, 134.1, 133.6, 131.0, 129.8, 128.4, 128.3, 126.3, 126.1, 125.9, 125.2, 117.1, 110.9, 48.2, 21.6, 21.6, 12.1.

MS (APCI) = 336.1 $[\text{M}+\text{H}]^+$ for $\text{C}_{20}\text{H}_{19}\text{ClN}_3$; experimental 336.1 m/z.

2.1.12 General Chlorination Procedure to Generate Racemic PPYs ($R^1 = H$)

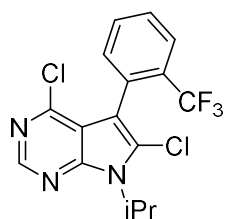
Equation 11. Scheme for the Chlorination of PPY towards PPY Starting Materials for Atroposelective S_NAr



Chlorination method is adapted from Maddox, S. M.; Nalbandian, C. J.; Smith, D. E.; Gustafson, J. L. *Org. Lett.* **2015**, *17* (4), 1042.⁷³

To PPY (1.0 equiv) in a 20-gram vial was added 10% mol triphenylphosphine sulfide catalyst (TPPS) and (*N*)-chlorosuccinimide (i.e., NCS, 1.1 equiv) in 0.1 M CH_2Cl_2 or $CHCl_3$. The resulting mixture was stirred for 24 hours at room temperature. The resulting mixture was concentrated in *vacuo* and purified in FCC (99:1 \rightarrow 9:1) Hexanes/EtOAc. Isolated yields were between 60-90%.

4,6-dichloro-7-isopropyl-5-(2-(trifluoromethyl)phenyl)-7H-pyrrolo[2,3-d]pyrimidine (**21**)



Following the general procedure: to 4-chloro-7-isopropyl-5-(2-(trifluoromethyl)phenyl)-7H-pyrrolo[2,3-d]pyrimidine (1.47 g, 4.32 mmol, 1.0 equiv), was added TPPS (254 mg, 0.864 mmol, 0.2 equiv) and dissolved in 21.6 mL CH_2Cl_2 . After 3 minutes, NCS (750 mg, 5.62 mmol, 1.3 equiv) was added and the reaction was stirred for 5 hours at room temperature. Workup and purification were followed according to the general procedure to afford **21** as a white solid. 97% isolated yield.

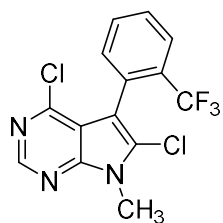
¹H NMR (400 MHz, CDCl₃) δ (ppm) = 8.62 (s, 1H), 7.80 (d, *J* = 7.5 Hz, 1H), 7.59 (dq, *J* = 14.9, 7.3 Hz, 2H), 7.38 (d, *J* = 7.3 Hz, 1H), 5.19 (hept, *J* = 6.7 Hz, 1H), 1.74 (d, *J* = 5.6 Hz, 6H).

¹³C NMR (101 MHz, CDCl₃) δ (ppm) = 160.1, 150.6, 147.6, 135.3, 134.0, 131.6 (q, *J* = 1.2 Hz), 129.2, 129.0, 128.5, 126.3 (q, *J* = 5.18 Hz), 125.3 (q, *J* = 274.5 Hz), 115.6, 109.5, 48.5, 21.3, 21.3.

¹⁹F NMR (376 MHz, CDCl₃) δ (ppm) = -61.82.

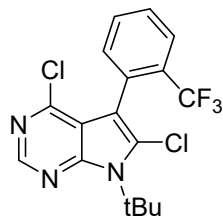
MS (APCI) = 374.0 [M+H]⁺ for C₁₆H₁₃Cl₂F₃N₃; experimental 374.1 m/z.

4,6-dichloro-7-methyl-5-(2-(trifluoromethyl)phenyl)-7H-pyrrolo[2,3-d]pyrimidine (**23**)



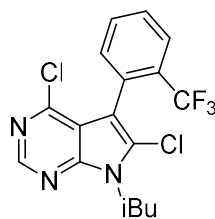
The synthesis and spectral data for compound **23** is attained in agreeance with Maddox, S. M.; Nalbandian, C. J.; Smith, D. E.; Gustafson, J. L. *Org. Lett.* **2015**, *17* (4), 1042. 29% isolated yield.⁷³

-(tert-butyl)-4,6-dichloro-5-(2-(trifluoromethyl)phenyl)-7H-pyrrolo[2,3-d]pyrimidine (**25**)



The synthesis and spectral data for compound **25** is attained in agreeance with Maddox, S. M.; Nalbandian, C. J.; Smith, D. E.; Gustafson, J. L. *Org. Lett.* **2015**, *17* (4), 1042. 76% isolated yield.⁷³

4,6-dichloro-7-isobutyl-5-(2-(trifluoromethyl)phenyl)-7H-pyrrolo[2,3-d]pyrimidine (**27**)



Following the general procedure: to 4-chloro-7-isobutyl-5-(2-(trifluoromethyl)phenyl)-7H-pyrrolo[2,3-d]pyrimidine (488 mg, 1.38 mmol, 1.0 equiv), was added TPPS (41 mg, 0.138 mmol, 0.1 equiv) and dissolved in 11.38 mL CH₂Cl₂. After 3 minutes, NCS (203 mg, 1.52 mmol, 1.1 equiv) was

added and the reaction was stirred overnight at room temperature. Workup and purification were followed according to the general procedure to afford **27** as a white solid. 89% isolated yield.

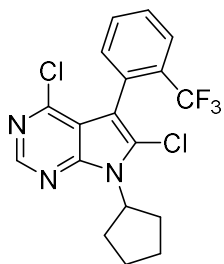
¹H NMR (400 MHz, CDCl₃) δ (ppm) = 8.51 (s, 1H), 7.63 (d, *J* = 7.3 Hz, 1H), 7.38 (dd, *J* = 28.7, 7.1 Hz, 3H), 4.02 (d, *J* = 92.8 Hz, 2H), 2.26 – 2.02 (m, 1H), 0.81 (d, *J* = 6.3 Hz, 6H).

¹³C NMR (101 MHz, CDCl₃) δ (ppm) = 151.0, 150.8, 150.2, 133.6, 131.6 (q, *J* = 1.0 Hz), 131.0 (q, *J* = 29.6 Hz), 130.0 (q, *J* = 2.1 Hz), 129.0, 128.5, 126.2 (q, *J* = 5.0 Hz), 122.5 (q, *J* = 274.0 Hz), 116.1, 109.0, 50.4, 29.0, 19.9, 19.8.

¹⁹F NMR (376 MHz, CDCl₃) δ (ppm) = -61.50.

MS (APCI) = 388.1 [M+H]⁺ for C₁₇H₁₅Cl₂F₃N₃; experimental 387.5 m/z.

4,6-dichloro-7-cyclopentyl-5-(2-(trifluoromethyl)phenyl)-7H-pyrrolo[2,3-d]pyrimidine (**29**)



Following the general procedure: to 4-chloro-7-cyclopentyl-5-(2-(trifluoromethyl)phenyl)-7H-pyrrolo[2,3-d]pyrimidine (245 mg, 0.671 mmol, 1.0 equiv), was added TPPS (19.7 mg, 0.067 mmol, 0.1 equiv) and dissolved in 5 mL CH₂Cl₂. After 3 minutes, NCS (116.4 mg, 0.872 mmol, 1.3 equiv) was

added and the reaction was stirred overnight at room temperature. Workup and purification were followed according to the general procedure to afford **29** as a white solid. 79% isolated yield.

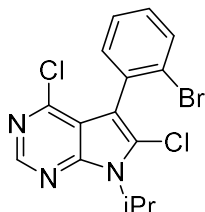
¹H NMR (400 MHz, CDCl₃) δ (ppm) = 8.61 (s, 1H), 7.79 (d, *J* = 7.7 Hz, 1H), 7.64 – 7.53 (m, 2H), 7.38 (d, *J* = 8.0 Hz, 1H), 5.30 – 5.21 (m, 1H), 2.44 (ddd, *J* = 20.0, 15.5, 8.0 Hz, 2H), 2.19 – 2.02 (m, 4H), 1.80 – 1.68 (m, 2H).

¹³C NMR (101 MHz, CDCl₃) δ (ppm) = 150.9, 150.1, 149.9, 133.6, 131.5, 130.9 (q, *J* = 30.2 Hz), 130.2 (q, *J* = 2.1 Hz), 128.9, 128.2, 126.1 (q, *J* = 6.0 Hz), 122.5 (q, *J* = 274.7 Hz), 116.5, 109.4, 56.8, 30.7, 25.1.

^{19}F NMR (376 MHz, CDCl_3) δ (ppm) = -61.59.

MS (APCI) = 400.1 $[\text{M}+\text{H}]^+$ for $\text{C}_{18}\text{H}_{15}\text{Cl}_2\text{F}_3\text{N}_3$; experimental 400.1 m/z.

5-(2-bromophenyl)-4,6-dichloro-7-isopropyl-7H-pyrrolo[2,3-d]pyrimidine (31)



Following the general procedure: to 5-(2-bromophenyl)-4-chloro-7-isopropyl-7H-pyrrolo[2,3-d]pyrimidine (319 mg, 0.909 mmol, 1.0 equiv), was added TPPS (27 mg, 0.0909 mmol, 0.1 equiv) and dissolved in 9.09 mL CHCl_3 . After 3

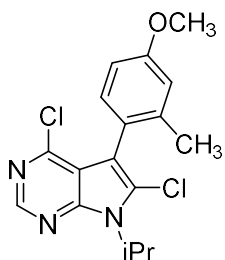
minutes, NCS (158 mg, 1.18 mmol, 1.3 equiv) was added and the reaction was stirred overnight at room temperature. Workup and purification were followed according to the general procedure to afford **31** as a white solid. 87% isolated yield.

^1H NMR (500 MHz, CDCl_3) δ (ppm) = 8.63 (s, 1H), 7.74 – 7.68 (m, 1H), 7.42 – 7.35 (m, 2H), 7.34 – 7.28 (m, 1H), 5.21 (dq, $J = 13.9, 6.9$ Hz, 1H), 1.76 (dd, $J = 6.9, 4.2$ Hz, 6H).

^{13}C NMR (126 MHz, CDCl_3) δ (ppm) = 150.8, 150.0, 149.8, 133.0, 132.5, 132.4, 130.0, 127.4, 127.0, 126.2, 115.7, 112.0, 49.0, 21.1, 21.1.

MS (APCI) = 384.0 $[\text{M}+\text{H}]^+$ for $\text{C}_{15}\text{H}_{13}\text{BrCl}_2\text{N}_3$; experimental 386.0 m/z.

4,6-dichloro-7-isopropyl-5-(4-methoxy-2-methylphenyl)-7H-pyrrolo[2,3-d]pyrimidine (33)



Following the general procedure: to 4-chloro-7-isopropyl-5-(4-methoxy-2-methylphenyl)-7H-pyrrolo[2,3-d]pyrimidine (300 mg, 0.950 mmol, 1.0 equiv), was added TPPS (27.3 mg, 0.095 mmol, 0.1 equiv) and dissolved in 9.5 mL CH_2Cl_2 . After 3 minutes, NCS (127 mg, 0.950 mmol, 1.0 equiv) was added and

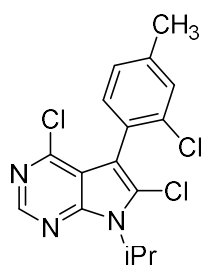
the reaction was stirred overnight at room temperature. Workup and purification were followed according to the general procedure to afford **33** as a white solid. 57% isolated yield.

¹H NMR (400 MHz, CDCl₃) δ (ppm) = 8.61 (s, 1H), 7.14 (d, *J* = 8.4 Hz, 1H), 6.86 (d, *J* = 2.7 Hz, 1H), 6.81 (dd, *J* = 8.4, 2.7 Hz, 1H), 5.20 (hept, *J* = 7.0 Hz, 1H), 3.85 (s, 3H), 2.10 (s, 3H), 1.74 (dd, *J* = 7.0, 3.1 Hz, 6H).

¹³C NMR (126 MHz, CDCl₃) δ (ppm) = 159.9, 151.0, 150.1, 150.0, 140.0, 132.7, 127.0, 122.9, 116.1, 115.4, 112.0, 111.0, 55.3, 49.0, 21.3, 20.6.

MS (APCI) = 350.1 [M+H]⁺ for C₁₇H₁₈Cl₂N₃O; experimental 350.2 m/z.

4,6-dichloro-5-(2-chloro-4-methylphenyl)-7-isopropyl-7H-pyrrolo[2,3-d]pyrimidine (**35**)



Following the general procedure: to 4-chloro-5-(2-chloro-4-methylphenyl)-7-isopropyl-7H-pyrrolo[2,3-d]pyrimidine (425 mg, 1.327 mmol, 1.0 equiv), was added TPPS (39 mg, 0.1327 mmol, 0.1 equiv) and dissolved in 13.27 mL CHCl₃.

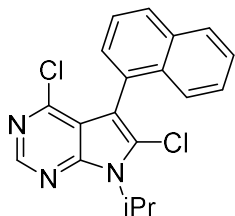
After 3 minutes, NCS (177 mg, 1.327 mmol, 1.0 equiv) was added and the reaction was stirred overnight at room temperature. Workup and purification were followed according to the general procedure to afford **35** as a white solid. 79% isolated yield.

¹H NMR (500 MHz, CDCl₃) δ (ppm) = 8.64 (s, 1H), 7.36 (s, 1H), 7.28 (s, 1H), 7.18 (d, *J* = 7.8 Hz, 1H), 5.22 (hept, *J* = 6.9 Hz, 1H), 2.44 (s, 3H), 1.83 – 1.75 (m, 6H).

¹³C NMR (126 MHz, CDCl₃) δ (ppm) = 150.9, 150.1, 150.0, 140.4, 135.5, 132.9, 130.0, 127.4, 127.3, 127.2, 116.0, 110.2, 49.2, 21.3, 21.3, 21.3.

MS (APCI) = 354.0 [M+H]⁺ for C₁₆H₁₅Cl₃N₃; experimental 354.1 m/z.

4,6-dichloro-7-isopropyl-5-(naphthalen-1-yl)-7H-pyrrolo[2,3-d]pyrimidine (37)



Following the general procedure: to 4-chloro-7-isopropyl-5-(naphthalen-1-yl)-7H-pyrrolo[2,3-d]pyrimidine (425 mg, 1.327 mmol, 1.0 equiv), was added

TPPS (39 mg, 0.1327 mmol, 0.1 equiv) and dissolved in 13.27 mL CHCl₃.

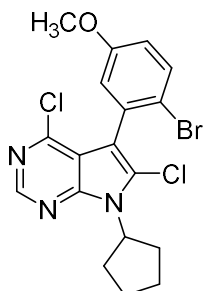
After 3 minutes, NCS (177 mg, 1.327 mmol, 1.0 equiv) was added and the reaction was stirred overnight at room temperature. Workup and purification were followed according to the general procedure to afford **37** as a whitish solid. 84% isolated yield.

¹H NMR (400 MHz, CDCl₃) δ (ppm) = 8.67 (s, 1H), 8.01 – 7.90 (m, 2H), 7.62 – 7.55 (m, 1H), 7.55 – 7.46 (m, 3H), 7.46 – 7.39 (m, 1H), 5.27 (hept, *J* = 7.1 Hz, 1H), 1.92 – 1.71 (m, 6H).

¹³C NMR (101 MHz, CDCl₃) δ (ppm) = 151.2, 150.2, 133.6, 133.3, 129.9, 129.0, 128.8, 128.5, 127.8, 127.3, 126.5, 126.0, 125.8, 125.2, 116.7, 110.8, 49.2, 21.3, 21.3.

MS (APCI) = 356.1 [M+H]⁺ for C₁₉H₁₆Cl₂N₃; experimental 335.9 m/z.

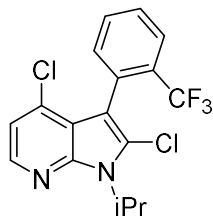
5-(2-bromo-5-methoxyphenyl)-4,6-dichloro-7-cyclopentyl-7H-pyrrolo[2,3-d]pyrimidine (39)



The synthesis and spectra data of **39** was prepared and obtained in agreeance with Smith, D. E.; Marquez, I.; Lokensgard, M. E.; Rheingold, A. L.; Hecht, D.;

Gustafson, J. L. *Angew. Chem. Int. Ed.* **2015**, *54* (40), 11754.³³ Yield is in agreeance with report, 81% isolated yield.⁷³.

2,4-dichloro-1-isopropyl-3-(2-(trifluoromethyl)phenyl)-1H-pyrrolo[2,3-b]pyridine (**52**)



Following the general procedure: to 4-chloro-1-isopropyl-3-(2-(trifluoromethyl)phenyl)-1H-pyrrolo[2,3-b]pyridine (425 mg, 1.327 mmol, 1.0 equiv), was added TPPS (39 mg, 0.1327 mmol, 0.1 equiv) and dissolved in 13.27 mL CHCl₃. After 3 minutes, NCS (177 mg, 1.327 mmol, 1.0 equiv) was added and the reaction was stirred overnight at room temperature. Workup and purification were followed according to the general procedure to afford **52** as a white solid. 56% isolated yield.

¹H NMR (400 MHz, CDCl₃) δ (ppm) = 8.17 (d, *J* = 5.2 Hz, 1H), 7.79 (d, *J* = 8.8 Hz, 1H), 7.64 – 7.51 (m, 2H), 7.41 (d, *J* = 7.1 Hz, 1H), 7.02 (d, *J* = 5.2 Hz, 1H), 5.32 (hept, *J* = 7.0 Hz, 1H), 1.74 (d, *J* = 7.0 Hz, 6H).

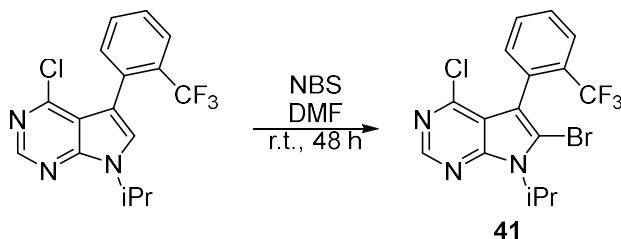
¹³C NMR (101 MHz, CDCl₃) δ (ppm) = 146.5, 142.5, 135.3, 134.0, 131.8, 131.5 (q, *J* = 2.0 Hz), 131.3 (q, *J* = 1.0 Hz), 128.5, 126.8, 126.0 (q, *J* = 5.3 Hz), 125.4 (q, *J* = 274.3 Hz), 118.4, 117.5, 109.0, 48.3, 21.3, 21.2.

¹⁹F NMR (376 MHz, CDCl₃) δ (ppm) = -60.90.

MS (APCI) = 373.1 [M+H]⁺ for C₁₇H₁₄Cl₂F₃N₃; experimental 372.0 m/z.

2.1.13 Bromination Procedure of 4-chloro-7-isopropyl-5-(2-(trifluoromethyl)phenyl)-7H-pyrrolo[2,3-d]pyrimidine Towards 41

Equation 12. General Scheme for C-2 Bromination of PPY



To -chloro-7-isopropyl-5-(2-(trifluoromethyl)phenyl)-7H-pyrrolo[2,3-d]pyrimidine (534 mg, 1.57 mmol, 1.0 eq) was added (*N*)-bromosuccinimide (i.e., NBS, 336 mg, 1.886 mmol, 1.2 eq) in 0.314 mL DMF. The resulting mixture was stirred for 48 hours at room temperature. The resulting mixture was concentrated in *vacuo* and purified in FCC (40:1 → 4:1) Hexanes/EtOAc) to yield **6-bromo-4-chloro-7-isopropyl-5-(2-(trifluoromethyl)phenyl)-7H-pyrrolo[2,3-d]pyrimidine (41)** as a light yellow solid. 98% isolated yield.

¹H NMR (500 MHz, CDCl₃) δ (ppm) = 8.60 (s, 1H), 7.80 (d, *J* = 7.7 Hz, 1H), 7.60 (dt, *J* = 22.2, 7.6 Hz, 2H), 7.37 (d, *J* = 7.4 Hz, 1H), 5.15 (m, *J* = 9.7, 5.1 Hz, 1H), 1.76 (d, *J* = 6.9 Hz, 6H).

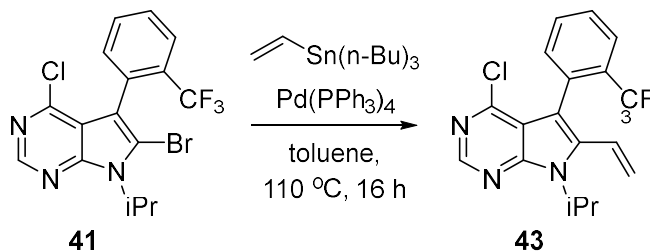
¹³C NMR (126 MHz, CDCl₃) δ (ppm) = 150.9, 150.5, 150.0, 133.5, 131.5 (q, *J* = 2.0 Hz), 131.3, 131.0 (q, *J* = 30.0 Hz), 129.1, 128.8, 126.1 (q, *J* = 5.2 Hz), 124.8 (q, *J* = 274.2 Hz), 117.3, 112.7, 50.7, 21.1, 21.0.

¹⁹F NMR (376 MHz, CDCl₃) δ (ppm) = -60.62.

MS (APCI) = 418.0 [M+H]⁺ for C₁₆H₁₃BrClF₃N₃; experimental 420.0 m/z.

2.1.14 Stille Coupling Procedure of 41 to yield 43

Equation 13. General Scheme for Stille Coupling



To (\pm)-**41** (2.0 g, 4.80 mmol, 1.0 equiv) was added vinyl- $\text{Sn}(\text{nBu}_3)$ (1.0 mL, 3.42 mmol, 0.713 equiv) in 68 mL PhMe. The resulting mixture was stirred for 10 minutes with bubbling argon through, and then $\text{Pd}(\text{PPh}_3)_4$ (554.5 mg, 0.48 mmol, 0.1 equiv) was added. The reaction was left overnight to stir (\sim 16 hrs) at 110°C . The mixture was filtered through a Celite plug. The filtrate was rinsed with brine and then extracted 3x with EtOAc. The combined organic layers were dried over Na_2SO_4 and then concentrated in vacuo. The crude product was purified in FCC (100:0 \rightarrow 95:5) Hexanes/EtOAc to afford **4-chloro-7-isopropyl-5-(2-(trifluoromethyl)phenyl)-6-vinyl-7H-pyrrolo[2,3-d]pyrimidine (43)** as a white solid. 57% isolated yield.

$^1\text{H NMR}$ (400 MHz, CDCl_3) δ (ppm) = 8.58 (s, 1H), 7.77 (d, $J = 8.6$ Hz, 1H), 7.62 – 7.49 (m, 2H), 7.40 (d, $J = 7.4$ Hz, 1H), 6.63 (dd, $J = 17.7, 11.8$ Hz, 1H), 5.37 (dd, $J = 11.8, 1.1$ Hz, 1H), 5.17 (dd, $J = 17.7, 1.1$ Hz, 1H), 5.06 (hept, $J = 6.9$ Hz, 1H), 1.72 (dd, $J = 7.0, 2.4$ Hz, 6H).

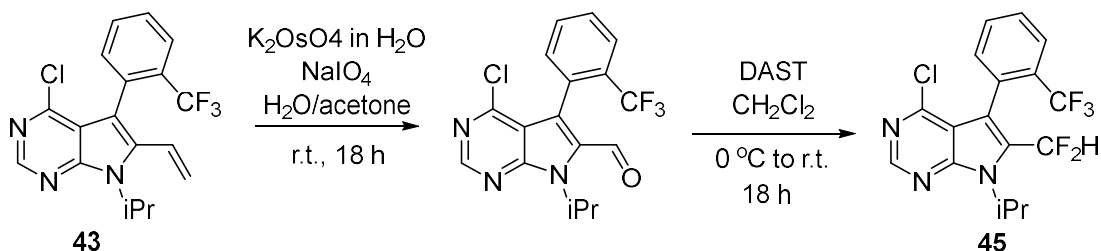
$^{13}\text{C NMR}$ (126 MHz, CDCl_3) δ (ppm) = 151.6, 150.8, 149.9, 136.6, 133.9, 132.7 (q, $J = 2.1$ Hz), 131.3, 130.9 (q, $J = 29.4$ Hz), 128.2, 126.1 (q, $J = 5.1$ Hz), 124.9, 123.0 (q, $J = 274.3$ Hz), 122.8, 116.9, 110.0, 48.2, 21.6, 21.5.

$^{19}\text{F NMR}$ (470 MHz, CDCl_3) δ (ppm) = -60.58.

MS (APCI) = 366.1 $[\text{M}+\text{H}]^+$ for $\text{C}_{18}\text{H}_{16}\text{ClF}_3\text{N}_3$; experimental 365.6 m/z.

2.1.15 Procedure for the -CF₂H addition Towards 46

Equation 14. Ketone to DAST Synthesis towards Difluoromethyl Analogue



Step 1. To **1.11** (495 mg, 1.35 mmol, 1.0 equiv) was added K₂OsO₄ (49.7 mg, 0.135 mmol, 0.1 equiv) and NaIO₄ (1.01 g, 4.73 mmol, 3.5 equiv) in 1:1 mixture of deionized, distilled water:acetone (13.5 mL total solvent mixture). The reaction was stirred at room temperature, overnight. The solids were filtered off in Celite plug, and the resulting filtrate was concentrated in *vacuo*. The crude product was dissolved in dichloromethane, and then rinsed with thiosulfate. The resulting organic layer was rinsed with brine, and then dried with Na₂SO₄. The combined organic layers were concentrated in *vacuo*. The crude product was purified in FCC (100:0 → 80:20) Hexanes/EtOAc to afford **4-chloro-7-isopropyl-5-(2-(trifluoromethyl)phenyl)-7H-pyrrolo[2,3-d]pyrimidine-6-carbaldehyde** as a white solid. 40% isolated yield. This PPY intermediate was immediately taken on to Step 2 without any further characterization.

MS (APCI) = 368.1 [M+H]⁺ for C₁₇H₁₄ClF₃N₄O; experimental 365.6 m/z.

Step 2. To crude 4-chloro-7-isopropyl-5-(2-(trifluoromethyl)phenyl)-7H-pyrrolo[2,3-d]pyrimidine-6-carbaldehyde (203 mg, 0.557 mmol, 1.0 equiv) was added DAST (120 μL, 0.908 mmol, 1.6 equiv) in 4.25 mL CH₂Cl₂. The reaction was stirred at 0°C, and then warmed to room temperature overnight. The resulting mixture was quenched with saturated NaHCO₃ and extracted with dichloromethane. The organic layer was rinsed with brine, and the combined organic layers were dried over Na₂SO₄. The dried organic layer was concentrated in *vacuo*. The crude product was purified in 97:3 to 80:20 Hexanes:EtOAc to afford **45** as a white solid. 54% isolated yield.

¹H NMR (400 MHz, CDCl₃) δ (ppm) = 8.71 (s, 1H), 7.85 – 7.79 (m, 1H), 7.66 – 7.58 (m, 2H), 7.41 (d, *J* = 6.2 Hz, 1H), 6.39 (t, 1H), 5.04 (p, *J* = 6.9 Hz, 1H), 1.83 (s, 6H).

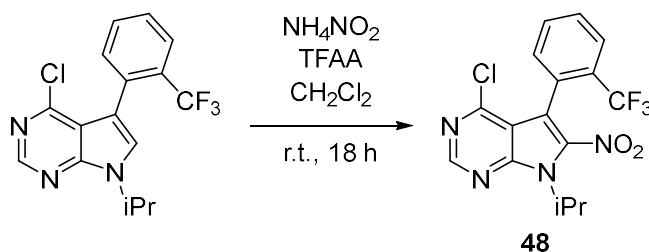
¹³C NMR (126 MHz, CDCl₃) δ (ppm) = 154.1, 151.8, 151.4, 133.8, 131.6 (q, *J* = 29.2 Hz), 131.2, 129.8, 129.6, 129.4, 126.3 (q, *J* = 5.43 Hz), 122.6 (q, *J* = 274.2 Hz), 116.4, 114.4 (t, *J* = 9.5 Hz), 109.8 (t, *J* = 236.6 Hz), 51.4, 51.4, 21.2.

¹⁹F NMR (376 MHz, CDCl₃) δ (ppm) = -60.00, -110.07, -111.04, -113.34, -114.17.

MS (APCI) = 390.1 [M+H]⁺ for C₁₇H₁₄ClF₅N₃; experimental 389.5 m/z.

2.1.16 Nitration Procedure Towards 48

Equation 15. EAS towards Nitro-group at C-2 position of PPY



To 4-chloro-7-isopropyl-5-(2-(trifluoromethyl)phenyl)-7H-pyrrolo[2,3-d]pyrimidine (1.20 g, 3.53 mmol, 1.0 equiv) was added NH₄NO₂ (1.27 mg, 15.89 mmol, 4.5 equiv), 9.0 mL TFAA, and 35 mL dry CH₂Cl₂. The reaction was stirred at room temperature overnight. After about 20 hrs, the resulting mixture was neutralized with saturated sodium bicarbonate, and the crude product was extracted into an organic layer with dichloromethane. The resulting organic layer was rinsed with brine; the combined organic layers were dried over Na₂SO₄ and then concentrated in *vacuo*. The crude product was purified with FCC (100:0 → 70:30) Hexanes/EtOAc to afford **48** as a white solid. 70% isolated yield.

¹H NMR (500 MHz, CDCl₃) δ (ppm) = 8.85 (s, 1H), 7.83 (dd, *J* = 7.8, 1.5 Hz, 1H), 7.71 – 7.60 (m, 2H), 7.46 (ddd, *J* = 7.3, 1.6, 0.8 Hz, 1H), 5.34 (p, *J* = 6.9 Hz, 1H), 1.84 (t, *J* = 7.1 Hz, 6H).

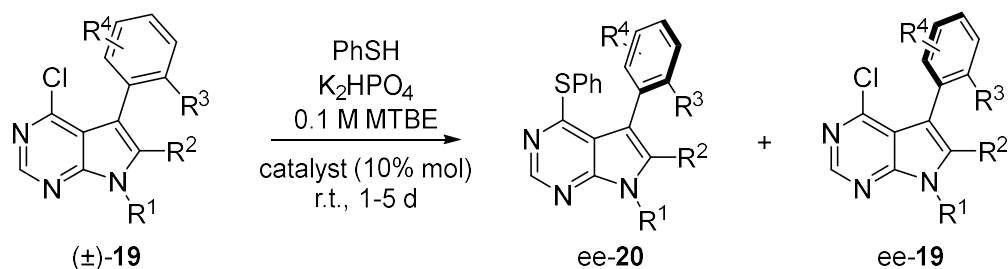
^{13}C NMR (126 MHz, CDCl_3) δ (ppm) = 156.3, 153.7, 149.1, 140.1, 132.3, 131.6, 129.6 (q, J = 30.3), 129.3, 128.4 (q, J = 2.1), 126.3 (q, J = 5.2), 123.7 (q, J = 273.3), 114.8, 112.8, 51.7, 21.1.

^{19}F NMR (376 MHz, CDCl_3) δ (ppm) = -61.88.

MS (APCI) = 385.1 $[\text{M}+\text{H}]^+$ for $\text{C}_{16}\text{H}_{13}\text{ClF}_3\text{N}_4\text{O}_2$; experimental 384.5 m/z.

2.1.17 General Procedure for the Cation-Directed $\text{S}_{\text{N}}\text{Ar}$ of (\pm)-PPYs

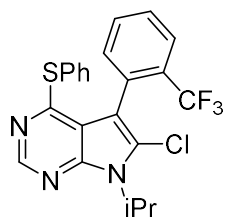
Equation 16. General Scheme for Atroposelective $\text{S}_{\text{N}}\text{Ar}$ of 3-aryl PPYs



To the reaction vessel containing the (\pm)-**19**, 10% mol catalyst and the base was added. MTBE was then added to the reaction. The reaction was stirred until all the non-dissolved solids were suspended and then followed with the addition of thiophenol (PhSH). The reaction was sealed and then stirred vigorously (up to 1500 rpm) at room temperature. The reaction was left to stir for ~1-5 days. (Note: Reaction time is substrate dependent). The reaction was filtered through a Celite plug to remove excess base, and the reaction filtrate was diluted in dichloromethane. 1 M NaOH was added to the reaction to remove excess thiophenol. The organic layer was isolated and re-extracted again with additional 1 M NaOH. The organic layer was extracted with brine rinse and dried over sodium sulfate. The reaction was concentrated in *vacuo* at 25 °C to afford the crude mixture of enantioenriched **20** and **19**. Purification was performed via FCC (99:1 \rightarrow 9:1) Hexanes/EtOAc or TLC preparatory plate (9:1) Hexanes/EtOAc. HPLC spectra used for

determination of ee% for each substrate are included in this Experimental Section of this dissertation.

6-chloro-7-isopropyl-4-(phenylthio)-5-(2-(trifluoromethyl)phenyl)-7H-pyrrolo[2,3-d]pyrimidine (22)



Following the general procedure: to **21** (25 mg, 0.0668 mmol, 1.0 equiv), was added 10% mol catalyst **15** (3.01 mg, 0.00686 mmol, 0.1 equiv) and K_2HPO_4 (169.0 mg, 0.970 mmol, 14.5 equiv). The mixture was suspended in 668 μ L MTBE. After 3 minutes of stirring, PhSH (58 μ L, 0.568 mmol, 8.5 equiv) was added and the reaction at room temperature for 20 h. Workup and purification was followed according to the general procedure to afford **22** and **21** as white solids. Isolated Yield (**22**): 42.3%, Isolated Yield (**19**): 40.6%. (Conversion = 51.2%, $s = 28.3$).

Scale-up Procedure of 22: To **21** (1.0 g, 2.67 mmol, 1.0 equiv), was added 10% mol catalyst **15** (120.6 mg, 0.267 mmol, 0.1 equiv) and K_2HPO_4 (6.75 g, 38.8 mmol, 14.5 equiv). The mixture was suspended in 26.7 mL MTBE. After 3 minutes of stirring, PhSH (2.32 mL, 22.7 mmol, 8.5 equiv) was added and the reaction at room temperature for 96 h. Workup and purification was followed according to the general procedure to afford **22** and **21** as white solids. Isolated Yield (**22**): 38.6%, Isolated Yield (**21**): 38.2%. (Conversion = 46.8%, $s = 14.4$).

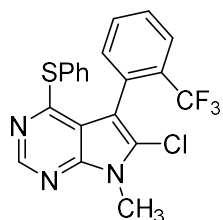
1H NMR (400 MHz, $CDCl_3$) δ (ppm) = 8.52 (s, 1H), 7.83 (d, $J = 7.7$ Hz, 1H), 7.69 – 7.57 (m, 2H), 7.48 (d, $J = 7.7$ Hz, 1H), 7.46 – 7.39 (m, 2H), 7.39 – 7.32 (m, 3H), 5.19 (hept, $J = 6.7$ Hz, 1H), 1.73 (dd, $J = 7.0, 1.8$ Hz, 6H).

^{13}C NMR (126 MHz, CDCl_3) δ (ppm) = 160.0, 150.4, 147.4, 135.2, 133.8, 131.5, 131.4, 131.2, 131.1 (q, J = 2.3 Hz), 129.1, 129.1, 128.9, 128.3, 126.2 (q, J = 5.3 Hz), 125.5, 123.8 (q, J = 274.2 Hz), 115.5, 109.5, 48.4, 21.2, 21.1.

^{19}F NMR (376 MHz, CDCl_3) δ (ppm) = -61.56.

MS (APCI) = 448.1 $[\text{M}+\text{H}]^+$ for $\text{C}_{22}\text{H}_{13}\text{ClF}_3\text{N}_3\text{S}$; experimental 448.1 m/z.

6-chloro-7-methyl-4-(phenylthio)-5-(2-(trifluoromethyl)phenyl)-7H-pyrrolo[2,3-d]pyrimidine (24)



Following the general procedure: to **23** (25 mg, 0.0723 mmol, 1.0 equiv), was added 10% mol catalyst **15** (3.26 mg, 0.00723 mmol, 0.1 equiv) and K_2HPO_4 (182.0 mg, 0.105 mmol, 14.5 equiv). The mixture was suspended in 722 μL

MTBE. After 3 minutes of stirring, PhSH (63 μL , 0.0614 mmol, 8.5 equiv) was added and the reaction at room temperature for 43 h. Workup and purification was followed according to the general procedure to afford **24** and **23** as white solids. Isolated Yield (**24**): 45.6%, Isolated Yield (**23**): 38.1%. (Conversion = 46.2%, s = 14.9).

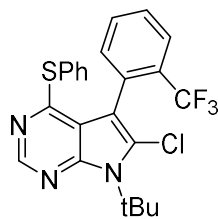
^1H NMR (500 MHz, CDCl_3) δ (ppm) = 8.56 (s, 1H), 7.85 (d, J = 7.7 Hz, 1H), 7.64 (dt, J = 27.6, 7.5 Hz, 2H), 7.49 – 7.42 (m, 3H), 7.39 – 7.34 (m, 3H), 3.88 (s, 3H).

^{13}C NMR (126 MHz, CDCl_3) δ (ppm) = 160.3, 151.2, 147.9, 135.4, 134.0, 131.6, 131.3, 130.9, 129.3, 129.2, 129.1, 128.4, 127.2, 127.1, 126.3, 125.0, 115.4, 109.1, 29.1.

^{19}F NMR (470 MHz, CDCl_3) δ (ppm) = -60.71.

MS (APCI) = 420.1 $[\text{M}+\text{H}]^+$ for $\text{C}_{20}\text{H}_{14}\text{ClF}_3\text{N}_3\text{S}$; experimental 420.4 m/z.

7-(tert-butyl)-6-chloro-4-(phenylthio)-5-(2-(trifluoromethyl)phenyl)-7H-pyrrolo[2,3-d]pyrimidine (26)



Following the general procedure: to **25** (25 mg, 0.0644 mmol, 1.0 equiv), was added 10% mol catalyst **15** (2.91 mg, 0.00644 mmol, 0.1 equiv) and K_2HPO_4 (163.0 g, 0.0935 mmol, 14.5 equiv). The mixture was suspended in 644 mL MTBE. After 3 minutes of stirring, PhSH (56 μ L, 0.0548 mmol, 8.5 equiv) was added and the reaction at room temperature for 40 h. Workup and purification was followed according to the general procedure to afford **26** and **25** as white solids. Isolated Yield (**26**): 42.8%, Isolated Yield (**25**): 30.0%. (Conversion = 48.8%, $s = 29.9$).

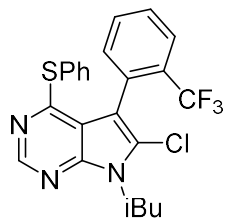
1H NMR (500 MHz, $CDCl_3$) δ (ppm) = 8.51 (s, 1H), 7.83 (d, $J = 7.6$ Hz, 1H), 7.62 (dt, $J = 29.3$, 7.6 Hz, 2H), 7.45 (d, $J = 7.5$ Hz, 1H), 7.41 (dd, $J = 7.0$, 2.7 Hz, 2H), 7.36 (dd, $J = 5.2$, 1.8 Hz, 3H), 2.01 (s, 9H).

^{13}C NMR (126 MHz, $CDCl_3$) δ (ppm) = 159.8, 149.6, 149.3, 135.4, 133.9, 131.7, 131.7, 131.6, 131.6, 131.6, 131.3, 129.3, 129.0, 128.6, 126.7, 126.4, 125.1, 115.7, 111.8, 63.2, 31.4.

^{19}F NMR (376 MHz, $CDCl_3$) δ (ppm) = -61.89.

MS (APCI) = 462.1 $[M+H]^+$ for $C_{23}H_{20}ClF_3N_3S$; experimental 461.2 m/z.

6-chloro-7-isobutyl-4-(phenylthio)-5-(2-(trifluoromethyl)phenyl)-7H-pyrrolo[2,3-d]pyrimidine (27)



Following the general procedure: to **27** (25 mg, 0.0644 mmol, 1.0 equiv), was added 10% mol catalyst **15** (2.91 g, 0.00644 mmol, 0.1 equiv) and K_2HPO_4 (163.0 g, 0.0935 mmol, 14.5 equiv). The mixture was suspended in 644 mL

MTBE. After 3 minutes of stirring, PhSH (56 μ L, 0.0548 mmol, 8.5 equiv) was added and the reaction at room temperature for 26 h. Workup and purification was followed according to the general procedure to afford **28** and **27** as white solids. Isolated Yield (**28**): 47.5%, Isolated Yield (**27**): 45.6%. (Conversion = 53.7%, $s = 36.9$).

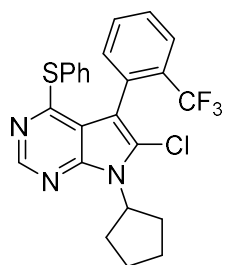
$^1\text{H NMR}$ (500 MHz, CDCl_3) δ (ppm) = 8.55 (s, 1H), 7.84 (d, $J = 7.7$ Hz, 1H), 7.64 (dt, $J = 28.3$, 7.4 Hz, 2H), 7.48 (d, $J = 7.4$ Hz, 1H), 7.44 (dd, $J = 6.9$, 2.7 Hz, 2H), 7.37 (dd, $J = 5.1$, 1.8 Hz, 3H), 4.17 (ddd, $J = 68.2$, 13.9, 7.7 Hz, 2H), 2.38 (dh, $J = 14.0$, 6.7 Hz, 1H), 0.95 (d, $J = 7.7$ Hz, 6H).

$^{13}\text{C NMR}$ (126 MHz, CDCl_3) δ (ppm) = 160.2, 151.0, 147.8, 135.3, 133.9, 131.7, 131.5, 131.4, 131.3, 131.0, 130.9 (q, $J = 1.9$ Hz), 129.2, 129.1, 129.0, 128.3, 126.2 (q, $J = 5.3$ Hz), 124.9 (q, $J = 274.2$ Hz), 115.1, 109.0, 50.0, 28.9, 19.8, 19.8.

$^{19}\text{F NMR}$ (470 MHz, CDCl_3) δ (ppm) = -60.61.

MS (APCI) = 462.1 $[\text{M}+\text{H}]^+$ for $\text{C}_{23}\text{H}_{20}\text{ClF}_3\text{N}_3\text{S}$; experimental 461.5 m/z.

6-chloro-7-cyclopentyl-4-(phenylthio)-5-(2-(trifluoromethyl)phenyl)-7H-pyrrolo[2,3-d]pyrimidine (**30**)



Following the general procedure: to **29** (25 mg, 0.0625 mmol, 1.0 equiv), was added 10% mol catalyst **15** (2.82 mg, 0.00625 mmol, 0.1 equiv) and K_2HPO_4 (332.2 mg, 0.906 mmol, 14.5 equiv). The mixture was suspended in 625 μ L MTBE. After 3 minutes of stirring, PhSH (54 μ L, 0.531 mmol, 8.5 equiv) was

added and the reaction at room temperature for 46 h. Workup and purification was followed according to the general procedure to afford **30** and **29** as white solids. Isolated Yield (**30**): 34.0%, Isolated Yield (**29**): 43.0%. (Conversion = 52.0%, $s = 39.8$).

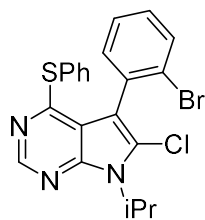
¹H NMR (400 MHz, CDCl₃) δ (ppm) = 8.53 (s, 1H), 7.84 (d, *J* = 7.2 Hz, 1H), 7.69 – 7.57 (m, 2H), 7.48 (d, *J* = 6.7 Hz, 1H), 7.44 – 7.40 (m, 2H), 7.36 (dd, *J* = 5.1, 1.8 Hz, 3H), 5.27 (m, *J* = 8.7 Hz, 1H), 2.51 – 2.36 (m, 2H), 2.18 – 2.02 (m, 4H), 1.80 – 1.69 (m, 2H).

¹³C NMR (126 MHz, CDCl₃) δ (ppm) = 160.0, 150.4, 147.6, 135.2, 133.9, 131.5, 131.4, 131.2 (q, *J* = 1.9 Hz), 131.1, 131.1, 129.1, 129.1, 128.9, 128.4, 126.2 (q, *J* = 5.1 Hz), 125.8, 123.8 (q, *J* = 274.1 Hz), 115.5, 109.6, 56.3, 30.6, 30.6, 25.0, 25.0.

¹⁹F NMR (470 MHz, CDCl₃) δ (ppm) = -61.66.

MS (APCI) = 474.1 [M+H]⁺ for C₂₄H₂₀ClF₃N₃S; experimental 473.5 m/z.

5-(2-bromophenyl)-6-chloro-7-isopropyl-4-(phenylthio)-7H-pyrrolo[2,3-d]pyrimidine (**32**)



Following the general procedure: to **31** (25 mg, 0.0649 mmol, 1.0 equiv), was added 10% mol catalyst **15** (2.93 mg, 0.00649 mmol, 0.1 equiv) and K₂HPO₄ (164 mg, 0.942 mmol, 0.1 equiv). The mixture was suspended in 649 μL MTBE.

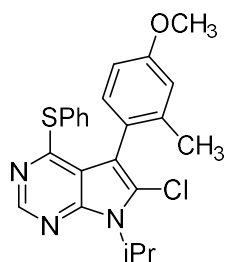
After 3 minutes of stirring, PhSH (56 μL, 0.552 mmol, 14.5 equiv) was added and the reaction at room temperature for 16 h. Workup and purification was followed according to the general procedure to afford **32** and **31** as white solids. Isolated Yield (**32**): 48.3%, Isolated Yield (**31**) 30.8%. (Conversion = 54.2%, *s* = 36.4).

¹H NMR (500 MHz, CDCl₃) δ (ppm) = 8.55 (s, 1H), 7.73 (d, *J* = 8.7 Hz, 1H), 7.50 – 7.41 (m, 4H), 7.38 (qd, *J* = 3.9, 1.9 Hz, 3H), 7.34 (ddd, *J* = 8.0, 6.8, 2.4 Hz, 1H), 5.20 (p, *J* = 7.0 Hz, 1H), 1.74 (dd, *J* = 7.0, 2.1 Hz, 6H).

¹³C NMR (126 MHz, CDCl₃) δ (ppm) = 160.1, 158.8, 150.4, 147.6, 135.3, 133.4, 133.3, 132.5, 130.1, 129.1, 129.1, 128.4, 127.1, 126.6, 126.6, 125.1, 114.7, 112.1, 48.4, 21.2, 21.2.

MS (APCI) = 458.0 [M+H]⁺ for C₂₁H₁₈BrClN₃S; experimental 459.4 m/z.

6-chloro-7-isopropyl-5-(4-methoxy-2-methylphenyl)-4-(phenylthio)-7H-pyrrolo[2,3-d]pyrimidine (34)



Following the general procedure: to **33** (25 mg, 3.22 mmol, 1.0 equiv), was added 10% mol catalyst **15** (3.22 mg, 0.00714 mmol, 0.1 equiv) and K_2HPO_4 (180.3 mg, 0.607 mmol, 14.5 equiv). The mixture was suspended in 714 μL MTBE. After 3 minutes of stirring, PhSH (62 μL , 0.607 mmol, 8.5 equiv) was

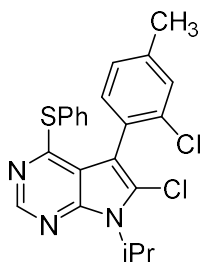
added and the reaction at room temperature for 16 h. Workup and purification was followed according to the general procedure to afford **34** and **33** as white solids. Isolated Yield (**34**): 48.0%, Isolated Yield (**33**): 30.0%. (Conversion = 65.4%, $s = 6.06$).

1H NMR (400 MHz, $CDCl_3$) δ (ppm) = 8.51 (s, 1H), 7.46 (dd, $J = 6.6, 3.1$ Hz, 2H), 7.41 – 7.35 (m, 3H), 7.23 (d, $J = 8.3$ Hz, 1H), 6.89 (d, $J = 2.8$ Hz, 1H), 6.85 (dd, $J = 8.3, 2.7$ Hz, 1H), 5.20 (dq, $J = 14.0, 6.9$ Hz, 1H), 3.87 (s, 3H), 2.18 (s, 3H), 1.73 (dd, $J = 7.0, 2.0$ Hz, 6H).

^{13}C NMR (126 MHz, $CDCl_3$) δ (ppm) = 160.2, 159.9, 150.2, 147.5, 140.2, 135.3, 135.3, 132.8, 129.1, 129.1, 128.4, 124.5, 123.7, 115.3, 115.0, 111.9, 110.9, 110.8, 55.2, 48.3, 21.2, 20.6.

MS (APCI) = 424.1 $[M+H]^+$ for $C_{23}H_{23}ClN_3OS$; experimental 423.5 m/z.

6-chloro-5-(2-chloro-4-methylphenyl)-7-isopropyl-4-(phenylthio)-7H-pyrrolo[2,3-d]pyrimidine (36)



Following the general procedure: to **35** (25 mg, 0.0705 mmol, 1.0 equiv), was added 10% mol catalyst **15** (3.18 mg, 0.00705 mmol, 0.1 equiv) and K_2HPO_4 (178.0 mg, 1.02 mmol, 14.5 equiv). The mixture was suspended in 705 μL MTBE. After 3 minutes of stirring, PhSH (61 μL , 0.599 mmol, 8.5 equiv) was

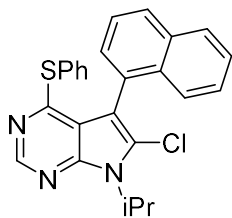
added and the reaction at room temperature for 16 h. Workup and purification was followed according to the general procedure to afford **36** and **35** as white solids. Isolated Yield (**36**): 49.5%, Isolated Yield (**35**) 29.4%. (Conversion = 63.2%, *s* = 13.9).

¹H NMR (500 MHz, CDCl₃) δ (ppm) = 8.53 (s, 1H), 7.48 (dd, *J* = 6.6, 3.0 Hz, 2H), 7.38 (d, *J* = 2.5 Hz, 4H), 7.34 (d, *J* = 7.8 Hz, 1H), 7.19 (d, *J* = 8.7 Hz, 1H), 5.20 (h, *J* = 6.9 Hz, 1H), 2.43 (s, 3H), 1.74 (dd, *J* = 7.0, 3.7 Hz, 6H).

¹³C NMR (101 MHz, CDCl₃) δ (ppm) = 160.1, 150.3, 147.6, 140.3, 135.6, 135.3, 135.3, 133.0, 129.9, 129.1, 129.1, 128.4, 128.1, 127.3, 127.3, 125.2, 114.9, 110.1, 48.4, 21.2.

MS (APCI) = 428.1 [M+H]⁺ for C₂₂H₂₀Cl₂N₃S; experimental 428.1 m/z.

6-chloro-7-isopropyl-5-(naphthalen-1-yl)-4-(phenylthio)-7H-pyrrolo[2,3-d]pyrimidine (**38**)



Following the general procedure: to **37** (25 mg, 0.0702 mmol, 1.0 equiv), was added 10% mol catalyst **15** (3.16 mg, 0.00702 mmol, 0.1 equiv) and K₂HPO₄ (177.2 g, 1.02 mmol, 14.5 equiv). The mixture was suspended in 702 μL MTBE. After 3 minutes of stirring, PhSH (61 μL, 0.596 mmol, 8.5 equiv) was

added and the reaction at room temperature for 18 h. Workup and purification was followed according to the general procedure to afford **38** and **37** as white solids. Isolated Yield (**38**): 45.6%, Isolated Yield (**37**): 39.7%. (Conversion = 51.2%, *s* = 12.7).

Scale-up Procedure of 38: to **37** (1.25 mg, 3.51 mmol, 1.0 equiv), was added 10% mol catalyst **15** (158.25 mg, 0.351 mmol, 0.1 equiv) and K₂HPO₄ (8.86 g, 50.9 mmol, 14.5 equiv). The mixture was suspended in 35 mL MTBE. After 3 minutes of stirring, PhSH (3.04 mL, 29.8 mmol, 8.5 equiv) was added and the reaction at room temperature for 96 h. Workup and purification was

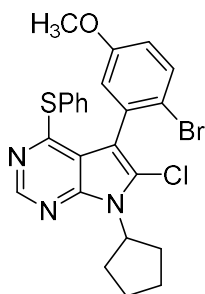
followed according to the general procedure. Isolated Yield (**38**): 47.8%, Isolated Yield (**37**): 40.8%. (Conversion = 50.9%, *s* = 15.0).

¹H NMR (500 MHz, CDCl₃) δ (ppm) = 8.57 (s, 1H), 7.97 (dd, *J* = 18.4, 7.8 Hz, 2H), 7.66 – 7.56 (m, 3H), 7.56 – 7.44 (m, 2H), 7.31 (d, *J* = 2.4 Hz, 5H), 5.27 (hept, *J* = 6.8, 6.4 Hz, 1H), 1.79 (dd, *J* = 6.9, 5.0 Hz, 6H).

¹³C NMR (126 MHz, CDCl₃) δ (ppm) = 160.5, 150.4, 147.9, 135.4, 133.7, 133.5, 130.1, 129.7, 129.2, 129.1, 129.1, 128.5, 128.4, 127.2, 126.5, 126.2, 126.1, 125.6, 125.3, 115.6, 111.0, 48.6, 21.4, 21.4.

MS (APCI) = 430.1 [M+H]⁺ for C₂₅H₂₁ClN₃S; experimental 429.5 m/z.

5-(2-bromo-5-methoxyphenyl)-6-chloro-7-cyclopentyl-4-(phenylthio)-7H-pyrrolo[2,3-d]pyrimidine (**40**)



Following the general procedure: to **39** (100 mg, 0.227 mmol, 1.0 equiv), was added 10% mol catalyst **15** (10.2 mg, 0.0227 mmol, 0.1 equiv) and K₂HPO₄ (572 mg, 3.29 mmol, 14.5 equiv). The mixture was suspended in 2.27 mL MTBE. After 3 minutes of stirring, PhSH (197 μL, 1.93 mmol, 8.5 equiv) was added and the reaction at room temperature for 30 h. Workup and purification was followed

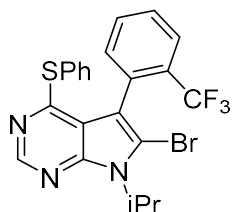
according to the general procedure to afford **40** and **39** as white solids. Isolated Yield (**40**) 46.7%, Isolated Yield (**39**): 33.6%. (Conversion = 54.1%, *s* = 17.1).

¹H NMR (400 MHz, CDCl₃) δ (ppm) = 8.55 (s, 1H), 7.60 (d, *J* = 8.8 Hz, 1H), 7.49 (pd, *J* = 4.3, 1.3 Hz, 2H), 7.41 – 7.35 (m, 3H), 7.00 (d, *J* = 3.1 Hz, 1H), 6.90 (dd, *J* = 8.8, 3.1 Hz, 1H), 5.28 (p, *J* = 8.8 Hz, 1H), 3.85 (s, 3H), 2.53 – 2.39 (m, 2H), 2.10 (ddd, *J* = 12.9, 10.7, 6.4 Hz, 4H), 1.74 (dt, *J* = 13.4, 6.8 Hz, 2H).

^{13}C NMR (101 MHz, CDCl_3) δ (ppm) = 160.1, 158.6, 150.5, 147.8, 135.4, 134.2, 133.2, 129.3, 129.3, 129.2, 128.5, 127.6, 125.7, 118.7, 117.1, 116.3, 114.7, 112.3, 56.4, 55.7, 30.8, 30.7, 25.1.

MS (APCI) = 514.0 $[\text{M}+\text{H}]^+$ for $\text{C}_{24}\text{H}_{22}\text{BrClN}_3\text{S}$; experimental 515.3 m/z.

6-bromo-7-isopropyl-4-(phenylthio)-5-(2-(trifluoromethyl)phenyl)-7H-pyrrolo[2,3-d]pyrimidine (42)



Following the general procedure: to **41** (50 mg, 0.119 mmol, 1.0 equiv), was added 10% mol catalyst **15** (5.39 mg, 0.0119 mmol, 0.1 equiv) and K_2HPO_4 (301.6 mg, 1.73 mmol, 14.5 equiv). The mixture was suspended in 1.19 mL

MTBE. After 3 minutes of stirring, PhSH (104 μL , 1.02 mmol, 8.5 equiv) was added and the reaction at room temperature for 40 h. Workup and purification was followed according to the general procedure to afford **42** and **41** as white solids. Isolated Yield (**42**): 42.0%, Isolated Yield (**41**): 41.0%. (Conversion = 47.1%, $s = 15.5$).

Scale-up Procedure of 42: to **41** (3.0 g, 7.17 mmol, 1.0 equiv), was added 10% mol catalyst **15** (323.2 mg, 0.717 mmol, 0.1 equiv) and K_2HPO_4 (18.1 g, 104.0 mmol, 14.5 equiv). The mixture was suspended in 72 mL MTBE. After 3 minutes of stirring, PhSH (6.2 mL, 60.9 mmol, 8.5 equiv) was added and the reaction at room temperature for 50 h. Workup and purification was followed according to the general procedure to afford **42** and **41** as a white solid. Isolated Yield (**42**): 41.6%, Isolated Yield (**41**) 44.0%. (Conversion = 46.7%, $s = 58.0$).

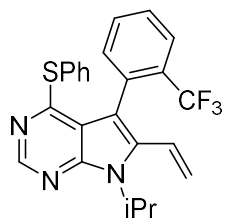
^1H NMR (400 MHz, CDCl_3) δ (ppm) = 8.53 (s, 1H), 7.84 (d, $J = 8.1$ Hz, 1H), 7.72 – 7.56 (m, 2H), 7.52 – 7.39 (m, 3H), 7.39 – 7.31 (m, 3H), 5.15 (ddd, $J = 26.6, 13.4, 6.5$ Hz, 1H), 1.76 (dd, $J = 7.0, 2.2$ Hz, 6H).

^{13}C NMR (126 MHz, CDCl_3) δ (ppm) = 160.0, 150.5, 150.3, 148.4, 135.2, 133.8, 132.2, 131.4, 131.4, 131.1, 130.9, 129.1, 128.9, 128.5, 126.2 (q, $J = 5.24$), 124.9, 123.8 (q, $J = 273.49$), 116.3, 112.9, 50.1, 48.4, 21.1.

^{19}F NMR (376 MHz, CDCl_3) δ (ppm) = -60.39.

MS (APCI) = 492.0 $[\text{M}+\text{H}]^+$ for $\text{C}_{22}\text{H}_{18}\text{BrF}_3\text{N}_3$; experimental 493.3 m/z.

7-isopropyl-4-(phenylthio)-5-(2-(trifluoromethyl)phenyl)-6-vinyl-7H-pyrrolo[2,3-d]pyrimidine (44)



Following the general procedure: to **43** (50 mg, 0.137 mmol, 1.0 equiv), was added 10% mol catalyst **15** (6.16 mg, 0.00137 mmol, 0.1 equiv) and K_2HPO_4 (345 mg, 1.98 mmol, 14.5 equiv). The mixture was suspended in 6.16 mL MTBE. After 3 minutes of stirring, PhSH (118.5 μL , 1.16 mmol, 8.5 equiv) was added and the reaction at room temperature for 48 h. Workup and purification was followed according to the general procedure to afford **44** and **43** as white solids. Isolated Yield (**44**): 24.3%, Isolated Yield (**43**): 22.9%. (Conversion = 39.5%, $s = 8.74$).

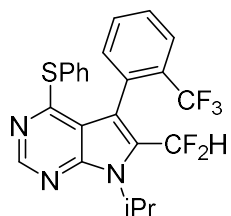
^1H NMR (400 MHz, CDCl_3) δ (ppm) = 8.51 (s, 1H), 7.80 (d, $J = 7.8$ Hz, 1H), 7.65 – 7.60 (m, 1H), 7.54 (dd, $J = 20.4, 7.5$ Hz, 2H), 7.45 – 7.39 (m, 2H), 7.35 (dt, $J = 3.7, 2.2$ Hz, 3H), 6.65 (dd, $J = 17.7, 11.8$ Hz, 1H), 5.30 (dd, $J = 11.8, 1.1$ Hz, 1H), 5.13 (dd, $J = 17.7, 1.2$ Hz, 1H), 5.10 – 5.00 (m, 1H), 1.71 (dd, $J = 7.0, 3.5$ Hz, 6H).

^{13}C NMR (101 MHz, CDCl_3) δ (ppm) = 150.1, 148.7, 135.7, 134.7, 131.8, 131.6, 131.3, 130.4, 129.8, 129.6, 129.5, 128.9, 127.2, 126.8 (q, $J = 7.45$ Hz), 125.6, 123.0 (q, $J = 273.5$ Hz), 122.5, 116.5, 111.1, 48.3, 30.2, 22.1, 22.1.

^{19}F NMR (376 MHz, CDCl_3) δ (ppm) = -60.45.

MS (APCI) = 440.1 [M+H]⁺ for C₂₄H₂₁F₃N₃S; experimental 439.5 m/z.

6-(difluoromethyl)-7-isopropyl-4-(phenylthio)-5-(2-(trifluoromethyl)phenyl)-7H-pyrrolo[2,3-d]pyrimidine (46)



Following the general procedure: to **45** (25 mg, 0.0641 mmol, 1.0 equiv), was added 10% mol catalyst **15** (2.89 mg, 0.00641 mmol, 0.1 equiv) and K₂HPO₄ (76.2 mg, 0.438 mmol, 6.83 equiv). The mixture was suspended in 641 mL MTBE. After 3 minutes of stirring, PhSH (56 μL, 0.257 mmol, 4.0 equiv) was added and the reaction at room temperature for 20 h. Workup and purification was followed according to the general procedure to afford **46** and **45** as white solids. Isolated Yield (**46**): 68.3%, Isolated Yield (**45**): 29.9%. *Note*: ee-SM **46** was aminated to yield (*S*_a)-**47** for *s*-factor determination via HPLC analysis. (Conversion = 69.8%, Determined *s* = 11.5).

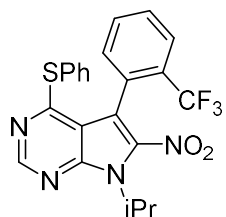
¹H NMR (400 MHz, CDCl₃) δ (ppm) = 8.61 (s, 1H), 7.85 (d, *J* = 7.4 Hz, 1H), 7.65 (p, *J* = 7.6, 7.0 Hz, 2H), 7.51 (d, *J* = 6.8 Hz, 1H), 7.46 – 7.35 (m, 5H), 6.39 (t, *J* = 52.1 Hz, 2H), 5.03 (dq, *J* = 13.7, 6.8 Hz, 1H), 1.82 (t, *J* = 6.7 Hz, 6H).

¹³C NMR (101 MHz, CDCl₃) δ (ppm) = 163.3, 151.6, 149.0, 135.4, 134.0, 131.5, 131.3, 131.0, 130.0, 129.5, 129.3, 129.2, 127.8, 127.6, 126.2 (q, *J* = 5.1 Hz), 125.0, 122.3 (q, *J* = 275.1 Hz), 115.1, 114.6 (t, *J* = 7.7 Hz), 109.9 (t, *J* = 233.5 Hz), 50.8, 21.2, 21.1.

¹⁹F NMR (376 MHz, CDCl₃) δ (ppm) = -59.77, -109.23, -110.20, -112.67, -113.50.

MS (APCI) = 464.1 [M+H]⁺ for C₂₃H₂₈F₅N₃S; experimental 463.5 m/z.

7-isopropyl-6-nitro-4-(phenylthio)-5-(2-(trifluoromethyl)phenyl)-7H-pyrrolo[2,3-d]pyrimidine (49)



Following the general procedure: to **48** (25 mg, 0.0650 mmol, 1.0 equiv), was added 10% mol catalyst **15** (5.86 mg, 0.130 mmol, 0.2 equiv) and K_2HPO_4 (9.65 mg, 0.056 mmol, 0.85 equiv). The mixture was suspended in 578 mL MTBE. The reaction was cooled to 4 °C and stirred for 3 minutes. PhSH (72 μ L, 0.0325 mmol, 0.5 equiv) from a 50 mg/mL stock solution in MTBE was then added to the reaction. The reaction was left to stir at 4 °C for 20 h. Workup and purification was followed according to the general procedure to afford **49** and **48** as white solids. Isolated Yield (**49**): 40.5%, Isolated Yield (**48**): 44.4%. (Conversion = 40.8%, $s = 2.02$).

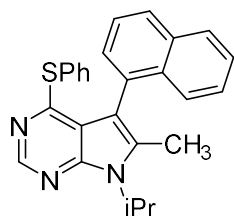
1H NMR (500 MHz, $CDCl_3$) δ (ppm) = 8.64 (s, 1H), 7.84 (d, $J = 7.7$ Hz, 1H), 7.67 (dt, $J = 33.9$, 7.4 Hz, 2H), 7.54 (d, $J = 7.4$ Hz, 1H), 7.44 – 7.37 (m, 5H), 5.38 (hept, $J = 6.3$ Hz, 1H), 1.82 – 1.78 (m, 6H).

^{13}C NMR (126 MHz, $CDCl_3$) δ (ppm) = 167.1, 154.0, 147.5, 138.9, 135.6, 135.4, 132.5, 131.9, 130.0, 129.8, 129.7, 129.5, 129.4, 129.3, 127.2, 126.6 (q, $J = 5.4$ Hz), 125.0 (q, $J = 274.6$ Hz), 114.2, 113.7, 51.1, 21.3, 21.3.

^{19}F NMR (376 MHz, $CDCl_3$) δ (ppm) = -61.87.

MS (APCI) = 459.1 $[M+H]^+$ for $C_{22}H_{18}F_3N_4O_2S$; experimental 458.5 m/z.

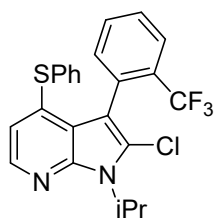
7-isopropyl-6-methyl-5-(naphthalen-1-yl)-4-(phenylthio)-7H-pyrrolo[2,3-d]pyrimidine (51)



Following the general procedure: to **50** (45 mg, 0.149 mmol, 1.0 equiv), was added 10% mol catalyst **15** (6.04 mg, 0.0149 mmol, 0.1 equiv) and K_2HPO_4 (1.13 mg, 6.48 mmol, 43.5 equiv). The mixture was suspended in 1.34 mL

MTBE. After 3 minutes of stirring, PhSH (387 μ L, 3.8 mmol, 25.5 equiv) was added and the reaction at room temperature for 48 h. Workup and purification was followed according to the general procedure. Conversion is >5%, and thus isolated yields of **51** and **50** and *s*-factor were not determined.

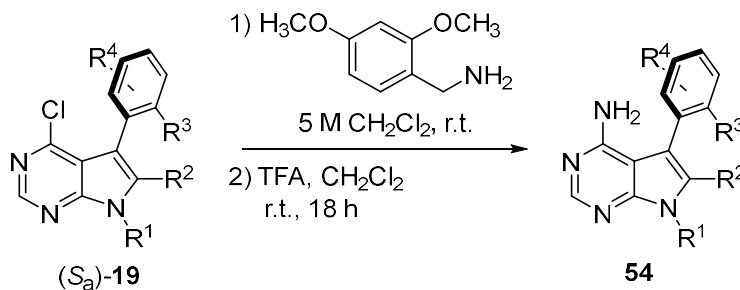
2-chloro-1-isopropyl-4-(phenylthio)-3-(2-(trifluoromethyl)phenyl)-1H-pyrrolo[2,3-b]pyridine (**53**)



Following the general procedure: to **52** (25 mg, 0.0670 mmol, 1.0 equiv), was added 10% mol catalyst **15** (3.02 mg, 0.00670 mmol, 0.1 equiv) and K_2HPO_4 (169 mg, 0.972 mmol, 14.5 equiv). The mixture was suspended in 670 μ L MTBE. After 3 minutes of stirring, PhSH (58 μ L, 0.569 mmol, 8.5 equiv) was added and the reaction at room temperature for 96 h. Workup and purification was followed according to the general procedure. Conversion is >5%, and thus the isolated yields of **53** and **52** and *s*-factor were not determined.

2.1.18 General Procedure for the Amination of (*S_a*)-**19** to **54**

Equation 17. General Scheme for Amination of PPYs to Final Kinase Inhibitors

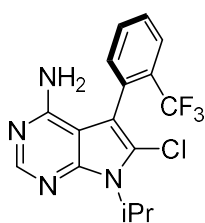


Step 1. To 1.0 equiv of (*S_a*)-**19** was added 20.0 equiv of 2,4-dimethoxybenzylamine and ~0.4 M CH_2Cl_2 . The reaction was stirred at room temperature for 2-4 days. The reaction was quenched with saturated aqueous citric acid and diluted with CH_2Cl_2 . The organic layer was extracted out

and then partitioned with brine. The organic layers were recombined, dried with Na₂SO₄, and then concentrated in *vacuo*. The crude product was purified in FCC (90:10 → 6:4) Hexanes/EtOAc to afford the intermediate PPY. The intermediate PPY was taken onto Step 2 without characterization.

Step 2. To 1.0 equiv of intermediate PPY was added 0.15 M TFA and 0.45 M CH₂Cl₂, and the reaction was stirred at room temperature. After about 5 hours to overnight, the resulting mixture was cooled down to 0 °C and diluted with CH₂Cl₂. The reaction was slowly quenched with saturated aqueous NaHCO₃, and the mixture was slowly warmed up to room temperature. The organic layer was rinsed with brine, and the combined organic layers were dried over Na₂SO₄. The dried organic layer was concentrated in *vacuo*. The crude product was purified in FCC (8:2 → 2:8) Hexanes/EtOAc to afford **54** with the (**S_a**) configuration as a white solid. Isolated yields varied between 60-90%.

S-atropisomer of 6-chloro-7-isopropyl-5-(2-(trifluoromethyl)phenyl)-7H-pyrrolo[2,3-d]pyrimidin-4-amine (60)



Following the general procedure: To ee-**21** (386.2 mg, 1.03 mmol, 1.0 equiv) was added 2,4-dimethoxybenzylamine (3.05 mL, 20.6 mmol, 20.0 equiv) and 0.53 M (1.96 mL) CH₂Cl₂, and the reaction was left to stir for 96 h at room temperature. Workup and purification were followed according to Step 1. To this intermediate PPY (373.1 mg, 0.74 mmol, 1.0 equiv) was added 4.9 mL TFA and 1.64 mL CH₂Cl₂. The reaction was left to stir at room temperature for 16 h. Workup and purification was followed according to Step 2 to afford **60** as a white solid. 61% overall yield.

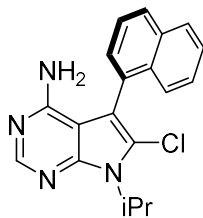
¹H NMR (500 MHz, CDCl₃) δ (ppm) = 8.26 (s, 1H), 7.86 – 7.80 (m, 1H), 7.62 (dt, *J* = 30.6, 7.5 Hz, 2H), 7.45 (d, *J* = 7.5 Hz, 1H), 5.15 (hept, *J* = 6.9 Hz, 1H), 4.68 (s, 2H), 1.69 (d, *J* = 7.0 Hz, 6H).

¹³C NMR (101 MHz, CDCl₃) δ (ppm) = 155.1, 149.9, 148.6, 133.6, 132.2 (q, *J* = 1.25 Hz), 131.4, 131.1, 129.4, 126.8 (q, *J* = 5.3 Hz), 125.0 (q, *J* = 273.5 Hz), 122.3, 108.7, 102.9, 48.3, 21.4, 21.3.

¹⁹F NMR (376 MHz, CDCl₃) δ (ppm) = -60.72.

MS (APCI) = 355.1 [M+H]⁺ for C₁₆H₁₅ClF₃N₄; experimental 354.6 m/z.

S-atropisomer of 6-chloro-7-isopropyl-5-(naphthalen-1-yl)-7H-pyrrolo[2,3-d]pyrimidin-4-amine (61)



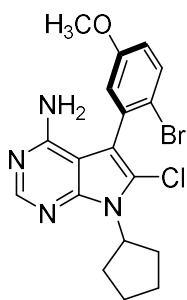
Following the general procedure: To ee-**37** (510.8 mg, 1.43 mmol, 1.0 equiv) was added 2,4-dimethoxybenzylamine (4.23 mL, 28.6 mmol, 20.0 equiv) and 0.72 M (2.0 mL) CH₂Cl₂, and the reaction was left to stir for 60 h at room temperature. Workup and purification were followed according to Step 1. To this intermediate PPY (613.2 mg, 1.26 mmol, 1.0 equiv) was added 8.0 mL TFA and 3.0 mL CH₂Cl₂. The reaction was left to stir at room temperature for 16 h. Workup and purification was followed according to Step 2 to afford **61** as a white solid. 77% overall yield.

¹H NMR (400 MHz, CDCl₃) δ (ppm) = 8.29 (s, 1H), 7.96 (t, *J* = 7.6 Hz, 2H), 7.66 (d, *J* = 8.4 Hz, 1H), 7.62 – 7.51 (m, 3H), 7.48 (ddd, *J* = 8.2, 6.8, 1.4 Hz, 1H), 5.23 (hept, *J* = 6.8 Hz, 1H), 4.96 (s, 2H), 1.77 (dd, *J* = 7.0, 3.9 Hz, 6H).

¹³C NMR (101 MHz, CDCl₃) δ (ppm) = 155.0, 149.6, 148.9, 134.0, 132.4, 129.5, 129.4, 129.3, 128.7, 127.1, 126.6, 125.8, 125.6, 122.2, 110.3, 102.8, 48.4, 21.5, 21.4.

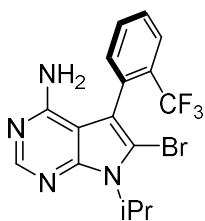
MS (APCI) = 337.1 [M+H]⁺ for C₁₉H₁₈ClN₄; experimental 336.7 m/z.

S-atropisomer of 5-(2-bromo-5-methoxyphenyl)-6-chloro-7-cyclopentyl-7H-pyrrolo[2,3-d]pyrimidin-4-amine (62)



Following the general procedure: To ee-**39** (64.6 mg, 0.146 mmol, 1.0 equiv) was added 2,4-dimethoxybenzylamine (433 μ L, 2.93 mmol, 20.0 equiv) and 0.25 M (260 μ L) CH_2Cl_2 , and the reaction was left to stir for 96 h at room temperature. Workup and purification were followed according to Step 1. To this intermediate PPY (75.5 mg, 0.138 mmol, 1.0 equiv) was added 922 μ L TFA and 307 μ L dichloromethane. The reaction was left to stir at room temperature for 16 h. Workup and purification was followed according to Step 2 to afford **62** as a white solid. 91% overall yield. Spectral data agrees with Smith, D. E.; Marquez, I.; Lokensgard, M. E.; Rheingold, A. L.; Hecht, D. a.; Gustafson, J. L. *Angew. Chem., Int. Ed.* **2015**, 54 (40), 11754. **2015**.³³

S-atropisomer of 6-bromo-7-isopropyl-5-(2-(trifluoromethyl)phenyl)-7H-pyrrolo[2,3-d]pyrimidin-4-amine (63)



Following the general procedure: To **41** (1.32 g, 3.14 mmol, 1.0 equiv) was added 2,4-dimethoxybenzylamine (9.30 mL, 62.7 mmol, 20.0 equiv) and 0.31 M (9.30 mL) CH_2Cl_2 , and the reaction was left to stir for 112 h at room temperature. Workup and purification was followed according to Step 1. To this intermediate PPY (2.5 g, 4.6 mmol, 1.0 equiv) was added 30.7 mL TFA and 10.2 mL CH_2Cl_2 . The reaction was left to stir at room temperature for 16 h. Workup and purification was followed according to Step 2 to afford **63** as a white solid. 87% overall yield.

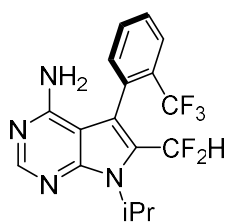
$^1\text{H NMR}$ (400 MHz, CDCl_3) δ (ppm) = 8.24 (s, 1H), 7.85 (d, $J = 7.0$ Hz, 1H), 7.70 – 7.58 (m, 2H), 7.44 (d, $J = 7.4$ Hz, 1H), 5.17 – 5.04 (m, 1H), 4.87 (s, 2H), 1.73 (d, $J = 7.0$ Hz, 6H).

^{13}C NMR (101 MHz, CDCl_3) δ (ppm) = 154.9, 149.7, 149.6, 133.6, 132.2 (q, J = 1.2 Hz), 132.1 (q, J = 2.0 Hz), 131.2 (q, J = 29.7 Hz), 129.4, 126.8 (q, J = 5.2 Hz), 125.0 (q, J = 273.7 Hz), 112.1, 111.2, 103.9, 50.0, 21.4, 21.3.

^{19}F NMR (376 MHz, CDCl_3) δ (ppm) = -60.50.

MS (APCI) = 399.0 $[\text{M}+\text{H}]^+$ for $\text{C}_{16}\text{H}_{15}\text{BrF}_3\text{N}_4$; experimental 400.7 m/z.

S-atropisomer of 6-(difluoromethyl)-7-isopropyl-5-(2-(trifluoromethyl)phenyl)-7H-pyrrolo[2,3-d]pyrimidin-4-amine (47)



Following the general procedure: To ee-**45** (5.26 mg, 0.0135 mmol, 1.0 equiv) was added 2,4-dimethoxybenzylamine (41 μL , 0.27 mmol, 20.0 equiv) and 0.2 M (65 μL) CH_2Cl_2 , and the reaction was left to stir for 48 h at room temperature. Workup and purification were followed according to Step 1. To

this intermediate PPY (2.03 mg, 0.00401 mmol, 1.0 equiv) was added 26.7 μL TFA and 9.0 μL dichloromethane. The reaction was left to stir at room temperature for 16 h. Workup and purification was followed according to Step 2 to afford **47** as a white solid. 28% isolated yield.

^1H NMR (500 MHz, CDCl_3) δ (ppm) = 8.23 (s, 1H), 7.85 (d, J = 9.2 Hz, 1H), 7.70 – 7.63 (m, 2H), 7.45 – 7.40 (m, 1H), 6.24 (t, J = 51.9 Hz, 1H), 4.94 (hept, J = 6.9 Hz, 1H), 3.72 (s, 2H), 1.73 (d, J = 6.9 Hz, 6H).

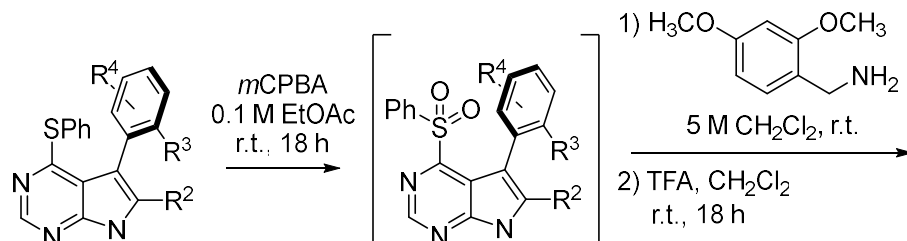
^{13}C NMR (126 MHz, CDCl_3) δ (ppm) = 156.6, 155.7, 149.8, 148.5 (q, J = 6.7 Hz), 133.4, 132.4, 130.1, 129.5, 127.0 (q, J = 6.4 Hz), 124.5 (q, J = 273.5 Hz), 111.6, 109.7 (t, J = 240.0 Hz), 102.6, 56.0, 32.1, 29.9, 22.8, 21.5, 21.4.

^{19}F NMR (470 MHz, CDCl_3) δ (ppm) = -60.03, -109.86, -110.0, -110.52, -110.63, -112.57, -112.68, -113.23, -113.34.

MS (APCI) = 371.1 $[\text{M}+\text{H}]^+$ for $\text{C}_{17}\text{H}_{16}\text{F}_5\text{N}_4$; experimental 370.6 m/z.

2.1.19 General Procedure for the Amination of 1.2 to (R_a)-1.3

Equation 18. General Scheme for Oxidation of Sulfide PPY to Sulfone

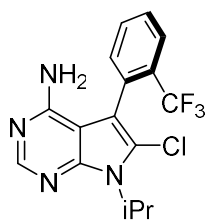


Step 1. To 1.0 equiv of (R_a)-20 was added 4.5 equiv of (*m*)-chloroperoxybenzoic acid (*m*CPBA) and 0.1 M EtOAc. The reaction was stirred at room temperature for 1-3 days. The reaction was quenched with saturated aqueous sodium bicarbonate and diluted with EtOAc. The organic layer was extracted out, and then quenched with additional wash of aqueous sodium bicarbonate. The organic layers were recollected and subsequently rinsed with brine. The organic layers were recombined, and then dried with Na₂SO₄. The combined organic layers were concentrated in *vacuo*. The crude product was purified in FCC (99:1 → 9:1) Hexanes/EtOAc to afford the intermediate PPY (sulfone). This sulfone was then taken onto Step 2 without characterization.

Step 2. To 1.0 equiv of the sulfone was added 20.0 equiv of 2,4-dimethoxybenzylamine and ~0.4 M CH₂Cl₂. The reaction was stirred at room temperature for 2-4 days. The reaction was quenched with saturated aqueous citric acid and diluted with CH₂Cl₂. The organic layer was extracted out and then partitioned with brine. The organic layers were recombined, dried with Na₂SO₄, and then concentrated in *vacuo*. The crude product was purified in FCC (90:10 → 6:4) Hexanes/EtOAc to afford the intermediate PPY. The intermediate PPY was taken onto Step 2 without characterization.

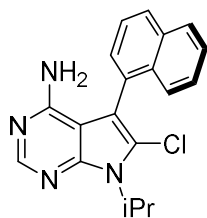
Step 3. To 1.0 equiv of intermediate PPY was added 0.15 M TFA and 0.45 M CH₂Cl₂, and the reaction was stirred at room temperature. After about 5 hours to overnight, the resulting mixture was cooled down to 0 °C and diluted with CH₂Cl₂. The reaction was slowly quenched with saturated aqueous NaHCO₃, and the mixture slowly warmed up to room temperature. The organic layer was rinsed with brine, and the combined organic layers were dried over Na₂SO₄. The dried organic layer was concentrated in *vacuo*. The crude product was purified in FCC (8:2 → 2:8) Hexanes/EtOAc to afford **56** with the (*R*_a)-configuration as a white solid. Isolated yields varied between 60-90%.

***R*-atropisomer of 6-chloro-7-isopropyl-5-(2-(trifluoromethyl)phenyl)-7H-pyrrolo[2,3-d]pyrimidin-4-amine (64)**



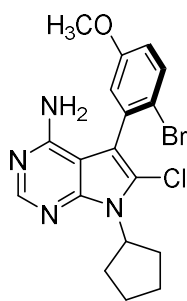
Following the general procedure: To ee-**22** (458.2 mg, 1.023 mmol, 1.0 equiv) was added *m*CPBA (794 mg, 4.603 mmol, 4.5 equiv) and 10 mL EtOAc. The reaction was stirred at room temperature for 50 h. Workup and purification was followed according to Step 1. To this sulfone (282 mg, 0.588 mmol, 1.0 equiv) was added 2,4-dimethoxybenzylamine (1.74 mL, 11.8 mmol, 20.0 equiv) and 0.6 M (1.0 mL) CH₂Cl₂, and the reaction was left to stir for 48 h at room temperature. Workup and purification were followed according to Step 2. To this intermediate PPY (236 mg, 0.467 mmol, 1.0 equiv) was added 3.11 mL TFA and 1.04 mL CH₂Cl₂. The reaction was left to stir at room temperature for 16 h. Workup and purification was followed according to Step 3 to afford **64** as a white solid. 28% overall yield. All spectral data was obtained in agreement with **60**.

***R*-atropisomer of 6-chloro-7-isopropyl-5-(naphthalen-1-yl)-7H-pyrrolo[2,3-d]pyrimidin-4-amine (65)**



Following the general procedure: To **38** (598 mg, 1.39 mmol, 1.0 equiv) was added *m*CPBA (1.08 g, 6.26 mmol, 4.5 equiv) and 11.4 mL EtOAc. The reaction was stirred at room temperature for 90 h. Workup and purification was followed according to Step 1. To this sulfone (377.2 mg, 0.820 mmol, 1.0 equiv) was added 2,4-dimethoxybenzylamine (2.43 mL, 16.4 mmol, 20.0 equiv) and 0.6 M (1.5 mL) CH₂Cl₂, and the reaction was left to stir for 98 h at room temperature. Workup and purification were followed according to Step 2. To this intermediate PPY (269.2 mg, 0.553 mmol, 1.0 equiv) was added 3.5 mL TFA and 1.23 mL CH₂Cl₂. The reaction was left to stir at room temperature for 16 h. Workup and purification was followed according to Step 3 to afford **65** as a white solid. 24% overall yield. All spectral data was obtained in agreement with **61**.

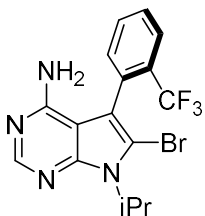
***R*-atropisomer of 5-(2-bromo-5-methoxyphenyl)-6-chloro-7-cyclopentyl-7H-pyrrolo[2,3-d]pyrimidin-4-amine (66)**



Following the general procedure: To **40** (87.2 mg, 0.178 mmol, 1.0 equiv) was added *m*CPBA (138 mg, 0.802 mmol, 4.5 equiv) and 1.78 mL EtOAc. The reaction was stirred at room temperature for 20 h. Workup and purification was followed according to Step 1. To this sulfone (94.5 mg, 0.181 mmol, 1.0 equiv) was added 2,4-dimethoxybenzylamine (573 μL, 3.63 mmol, 20.0 equiv) and 0.7 M (260 μL) CH₂Cl₂, and the reaction was left to stir for 96 h at room temperature. Workup and purification were followed according to Step 2. To this intermediate PPY (39.7 mg, 0.071 mmol, 1.0 equiv) was added 475 μL TFA and 158 μL CH₂Cl₂. The reaction was left to stir at room

temperature for 16 h. Workup and purification was followed according to Step 3 to afford **66** as a white solid. 40% overall yield. Spectral data was obtained in agreement with Smith, D. E.; Marquez, I.; Lokensgard, M. E.; Rheingold, A. L.; Hecht, D. a.; Gustafson, J. L. *Angew. Chem., Int. Ed.* **2015**, *54* (40), 11754.

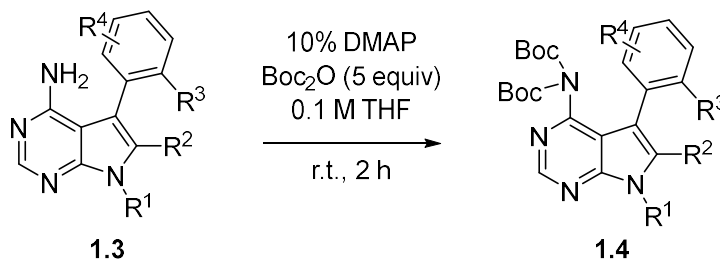
R-atropisomer of 6-bromo-7-isopropyl-5-(2-(trifluoromethyl)phenyl)-7H-pyrrolo[2,3-d]pyrimidin-4-amine (67)



Following the general procedure: To **42** (1.47 g, 2.98 mmol, 1.0 equiv) was added *m*CPBA (2.32 g, 13.4 mmol, 4.5 equiv) and 16.6 mL EtOAc. The reaction was stirred at room temperature for 40 h. Workup and purification were followed according to Step 1. To intermediate PPY (3.3 g, 6.29 mmol, 1.0 equiv) was added 2,4-dimethoxybenzylamine (18.6 mL, 125.9 mmol, 20.0 equiv) and 1.26 M (5.0 mL) CH₂Cl₂, and the reaction was left to stir for 98 h at room temperature. Workup and purification were followed according to Step 2. To this intermediate PPY (1.56 g, 2.84 mmol, 1.0 eq) was added 19 mL TFA and 6.3 mL CH₂Cl₂. The reaction was left to stir at room temperature for 16 h. Workup and purification was followed according to Step 3 to afford **67** as a white solid. 24% overall yield. All spectral data was obtained in agreement with the **64**.

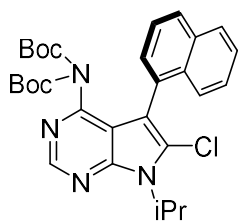
2.1.20 General Procedure for the Boc-protection of Both (*R*_a)- and (*S*_a)-1.3

Equation 19. General Scheme for Boc-protection to Further Elaborate Kinase Inhibitor PPY



To 1.0 equiv of **1.3** in ~0.1 M THF was added 5.0 eq di-*tert*-butyl dicarbonate (Boc_2O) and 10% mol 4-(dimethyl)aminopyridine (DMAP). The reaction was stirred at room temperature for 2-4 hours. The reaction was quenched with distilled water and extracted with EtOAc. The organic layers were recollected, and then rinsed with brine. The resulting organic layers were recombined, and then dried with Na_2SO_4 . The subsequent organic layers were concentrated in *vacuo*, and the product was immediately taken onto further functionalization.

(*S*)-atropisomer of *tert*-butyl (*tert*-butoxycarbonyl)(6-chloro-7-isopropyl-5-(naphthalen-1-yl)-7H-pyrrolo[2,3-*d*]pyrimidin-4-yl)carbamate



Following the general procedure: to **61** (280 mg, 0.83 mmol, 1.0 equiv) in 1.0 mL THF was added Boc_2O (904 mg, 4.15 mmol, 5.0 equiv) and DMAP (10 mg, 0.08 mmol, 0.13 equiv). The reaction was stirred at room temperature for 3 h. Workup and purification were followed accordingly to afford product as

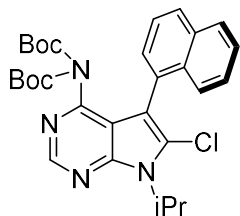
a white solid. 62% overall yield.

$^1\text{H NMR}$ (400 MHz, CDCl_3) δ (ppm) = 8.85 (s, 1H), 7.92 (dd, $J = 6.1, 3.4$ Hz, 1H), 7.89 (d, $J = 7.7$ Hz, 1H), 7.59 (d, $J = 7.7$ Hz, 1H), 7.53 – 7.48 (m, 2H), 7.48 – 7.37 (m, 2H), 5.27 (hept, $J = 6.7$ Hz, 1H), 1.80 (dd, $J = 7.0, 4.2$ Hz, 6H), 1.42 (s, 9H), 0.80 (s, 9H).

^{13}C NMR (101 MHz, CDCl_3) δ (ppm) = 152.3, 150.6, 150.2, 134.0, 132.3, 129.1, 128.8, 128.7, 128.4, 128.1, 126.4, 126.4, 126.0, 125.4, 115.5, 109.9, 48.9, 28.1, 27.3, 21.3, 21.3.

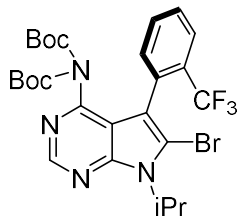
MS (APCI) = 537.2 $[\text{M}+\text{H}]^+$ for $\text{C}_{29}\text{H}_{34}\text{ClN}_4\text{O}_4$; experimental 536.4 m/z.

(R)-atropisomer of tert-butyl (tert-butoxycarbonyl)(6-chloro-7-isopropyl-5-(naphthalen-1-yl)-7H-pyrrolo[2,3-d]pyrimidin-4-yl)carbamate



Following the general procedure: to **65** (120 mg, 0.224 mmol, 1.0 equiv) in 1.0 mL THF was added Boc_2O (244 mg, 1.12 mmol, 5.0 equiv) and DMAP (4 mg, 0.03 mmol, 0.13 equiv). The reaction was stirred at room temperature for 3 h. Workup and purification were followed accordingly to afford product as a white solid. 70% overall yield. All spectral data was obtained in agreement with the (S_a)-configuration.

(S)-atropisomer of 6-bromo-7-isopropyl-5-(2-(trifluoromethyl)phenyl)-7H-pyrrolo[2,3-d]pyrimidin-4-amine



Following the general procedure: to **63** (~200 mg, 0.5 mmol, 1.0 equiv) in 2.0 mL THF was added Boc_2O (450 mg, 2.0 mmol, 4.0 equiv) and DMAP (11.0 mg, 0.05 mmol, 0.1 equiv). The reaction was stirred at room temperature for 3 h. Workup and purification were followed accordingly to afford product as a white-beige solid. 83% overall yield.

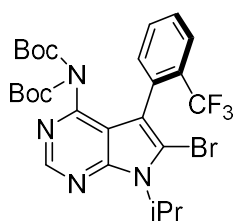
^1H NMR (400 MHz, CDCl_3) δ (ppm) = 8.81 (s, 1H), 7.77 (dt, $J = 7.6, 3.7$ Hz, 1H), 7.59 – 7.53 (m, 2H), 7.38 (dd, $J = 5.4, 3.6$ Hz, 1H), 5.16 (dt, $J = 13.7, 6.4$ Hz, 1H), 1.76 (d, $J = 7.0$ Hz, 6H), 1.32 (s, 18H).

^{13}C NMR (101 MHz, CDCl_3) δ (ppm) = 152.8, 150.6, 149.8, 133.4, 131.7 (q, $J = 2.0$ Hz), 131.3, 131.0 (q, $J = 29.9$ Hz), 128.7, 126.6 (q, $J = 4.83$ Hz), 125.2 (q, $J = 274.8$ Hz), 117.9, 116.5, 112.1, 83.5, 50.6, 28.0, 21.2, 21.2.

^{19}F NMR (470 MHz, CDCl_3) δ (ppm) = -60.07.

MS (APCI) = 600.4 $[\text{M}+\text{H}]^+$ for $\text{C}_{26}\text{H}_{31}\text{BrF}_3\text{N}_4\text{O}_4$; experimental 600.0 m/z.

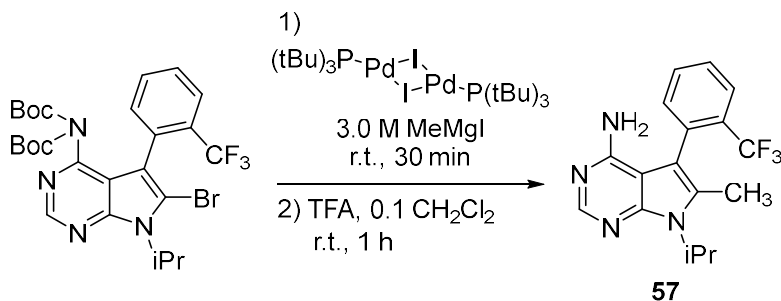
(*R*)-atropisomer of 6-bromo-7-isopropyl-5-(2-(trifluoromethyl)phenyl)-7H-pyrrolo[2,3-d]pyrimidin-4-amine



Following the general procedure: to **67** (108 mg, 0.27 mmol, 1.0 equiv) in 2.7 mL THF was added Boc_2O (589 mg, 1.35 mmol, 5.0 equiv) and DMAP (4.3 mg, 0.035 mmol, 0.13 equiv). The reaction was stirred at room temperature for 3 h. Workup and purification were followed accordingly to afford product as a white solid. 83% overall yield. All spectral data was obtained in agreement with the (*S_a*)-configuration.

2.1.21 Methylation of Both (*R_a*)- and (*S_a*)-4k via Schoenebeck Conditions

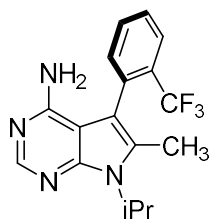
Equation 20. C-2 Methylation of PPYs (1)



To either enantiomer of 6-bromo-7-isopropyl-5-(2-(trifluoromethyl)phenyl)-7H-pyrrolo[2,3-d]pyrimidin-4-amine (1.0 equiv) in 0.2 M dry toluene was 2.5 mol% Pd(I) dimer catalyst added, followed by the slow addition of 3 M MeMgI (150 mL, 1.5 equiv) at room

temperature. After 30 minutes of stirring, the reaction was then quenched with 0.1 M TFA and then stirred for an additional 1.5 h. The resulting reaction mixture was then concentrated in *vacuo*, and then purified with FCC (10:1 → 1:1) Hexanes/EtOAc to afford both atropisomers of **57** as pure white solids.

***S*-atropisomer of 7-isopropyl-6-methyl-5-(2-(trifluoromethyl)phenyl)-7H-pyrrolo[2,3-d]pyrimidin-4-amine (*S_a*-57)**



Following the general procedure: to (*S_a*)-atropisomer of 6-bromo-7-isopropyl-5-(2-(trifluoromethyl)phenyl)-7H-pyrrolo[2,3-d]pyrimidin-4-amine (60 mg, 0.1 mmol, 1.0 equiv) in 0.5 mL (0.2 M) dry toluene was 2.5 mol% Pd(I) dimer catalyst (2.0 mg, 0.0025 mmol) added, followed by the slow addition of 3 M MeMgI (150 mL, 1.5 equiv) at room temperature. Workup and purification were followed accordingly to afford (*S_a*)-**1.3q** as a white solid. 55% overall yield.

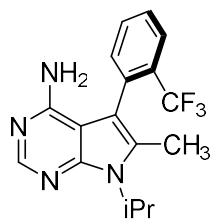
¹H NMR (400 MHz, CDCl₃) δ (ppm) = 8.20 (s, 1H), 7.82 (d, *J* = 7.8 Hz, 1H), 7.60 (dt, *J* = 26.5, 7.3 Hz, 2H), 7.42 (d, *J* = 7.4 Hz, 1H), 5.03 (s, 2H), 4.93 – 4.84 (m, 1H), 2.15 (s, 3H), 1.68 (dd, *J* = 7.0, 2.4 Hz, 6H).

¹³C NMR (126 MHz, CDCl₃) δ (ppm) = 154.7, 149.5, 147.7, 134.0, 133.5, 132.7, 132.3 (q, *J* = 1.0 Hz), 131.7 (q, *J* = 2.2 Hz), 129.1, 126.9 (q, *J* = 5.2 Hz), 123.0 (q, *J* = 274.2 Hz), 109.3, 103.1, 47.9, 22.0, 21.9, 12.1.

¹⁹F NMR (376 MHz, CDCl₃) δ (ppm) = -61.99.

MS (APCI) = 335.2 [M+H]⁺ for C₁₇H₁₈F₃N₄; experimental 334.7 m/z.

R-atropisomer of 7-isopropyl-6-methyl-5-(2-(trifluoromethyl)phenyl)-7H-pyrrolo[2,3-d]pyrimidin-4-amine [(R_a)-1.3q]

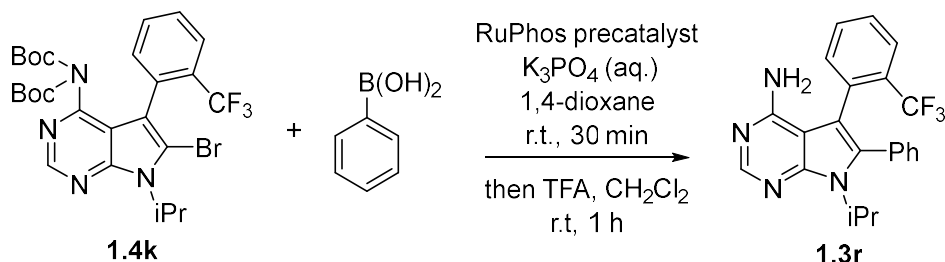


overall yield.

The synthesis and spectra data of (*R_a*)-**57** was prepared from the (*R_a*)-atropisomer of 6-bromo-7-isopropyl-5-(2-(trifluoromethyl)phenyl)-7H-pyrrolo[2,3-d]pyrimidin-4-amine and obtained in agreeance with (*S_a*)-**57**. 53%

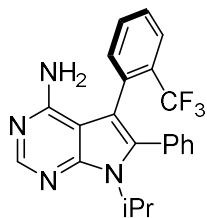
2.1.22 Arylation of Both (*R_a*)- and (*S_a*)-4k via Buchwald conditions

Equation 21. Arylation of PPYs



To either atropisomer of 6-bromo-7-isopropyl-5-(2-(trifluoromethyl)phenyl)-7H-pyrrolo[2,3-d]pyrimidin-4-amine (1.0 equiv) was added phenylboronic acid (2.0 equiv), 0.3 mol% RuPhos precatalyst, and K₃PO₄ (3.0 equiv). The mixture was thoroughly purged with vacuum then argon. To this mixture was added degassed 1.6 M 1,4-dioxane and 3.3 M distilled, deionized water. After addition of the solvents, the biphasic reaction was left to stir at 30 minutes at room temperature. The resulting reaction was then diluted in water and partitioned with CH₂Cl₂. The resulting organic layer was extracted out, dried with Na₂SO₄ and then concentrated *in vacuo*. Purification through TLC preparatory plate (9:1) Hexanes/EtOAc afforded both atropisomers of **58** as white solids.

***S*-atropisomer of 7-isopropyl-6-phenyl-5-(2-(trifluoromethyl)phenyl)-7H-pyrrolo[2,3-d]pyrimidin-4-amine (*S_a*-58)**



Following the general procedure: to (*S_a*)-atropisomer of 6-bromo-7-isopropyl-5-(2-(trifluoromethyl)phenyl)-7H-pyrrolo[2,3-d]pyrimidin-4-amine (60 mg, 0.1 mmol, 1.0 equiv) was added phenylboronic acid (24 mg, 0.2 mmol, 2.0 equiv), 0.3 mol% RuPhos precatalyst (2.5 mg, 0.3 mmol), and K₃PO₄ (50 mg, 0.4 mmol, 3.0 equiv). The mixture was thoroughly purged with vacuum then argon. To this mixture was added degassed 0.6 mL (1.6 M) dioxane and 0.3 mL (3.3 M) water. Workup and purification were followed accordingly to afford (*S_a*)-58 as a white solid. 70% overall yield.

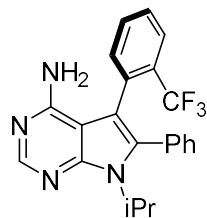
¹H NMR (400 MHz, CDCl₃) δ (ppm) = 8.21 (s, 1H), 7.72 (d, *J* = 8.5 Hz, 1H), 7.60 – 7.49 (m, 2H), 7.41 (d, *J* = 7.0 Hz, 1H), 7.38 – 7.31 (m, 3H), 7.21 (dd, *J* = 7.5, 1.9 Hz, 2H), 4.78 (s, 2H), 4.50 (hept, *J* = 6.9 Hz, 1H), 1.68 (dd, *J* = 28.5, 6.9 Hz, 6H).

¹³C NMR (101 MHz, CDCl₃) δ (ppm) = 162.9, 162.5, 152.0, 147.1, 140.3, 138.7, 134.0, 132.2, 130.6, 130.4, 129.6 (q, *J* = 5.3 Hz), 129.5, 129.1, 128.7, 127.0, 124.9 (q, *J* = 275.5 Hz), 117.4, 112.0, 102.2, 50.3, 21.8, 21.7.

¹⁹F NMR (376 MHz, CDCl₃) δ (ppm) = -60.25.

MS (APCI) = 397.2 [M+H]⁺ for C₂₂H₂₀F₃N₄; experimental 397.1 m/z.

***R*-atropisomer of 7-isopropyl-6-phenyl-5-(2-(trifluoromethyl)phenyl)-7H-pyrrolo[2,3-d]pyrimidin-4-amine (*R_a*-58)**

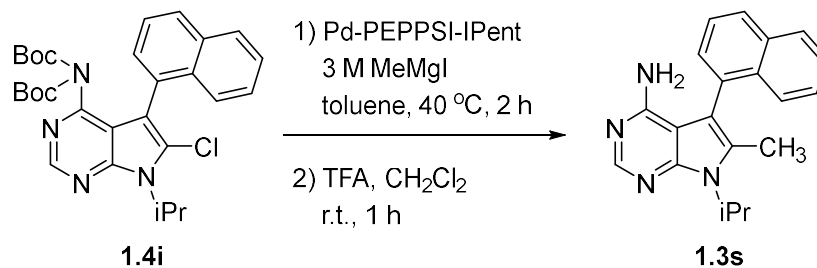


overall yield.

The synthesis and spectra data of (*R_a*)-58 was prepared from the (*R_a*)-atropisomer of 6-bromo-7-isopropyl-5-(2-(trifluoromethyl)phenyl)-7H-pyrrolo[2,3-d]pyrimidin-4-amine and obtained in agreeance with (*S_a*)-58. 48%

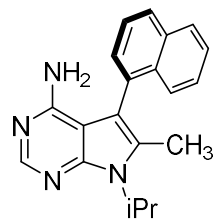
2.1.23 Methylation of Both (*R*_a)- and (*S*_a)-4i via Organ conditions

Equation 22. Methylation of PPYs (2)



To a reaction vial equipped with a stirbar was added either atropisomer of tert-butyl (tert-butoxycarbonyl)(6-chloro-7-isopropyl-5-(naphthalen-1-yl)-7H-pyrrolo[2,3-d]pyrimidin-4-yl)carbamate (1.0 equiv) and 5 mol% Pd-PEPPSI-IPent catalyst. The reaction apparatus was then purged of O₂ to argon, and degassed toluene was subsequently added. After two minutes of stirring at r.t., 3.4 equiv of 3 M MeMgI was added dropwise. The reaction was heated to 40 °C and stirred at this temperature for 1 h. An additional 3.4 equiv of 3 M MeMgI was added, and the reaction was stirred for an additional 30 min. The resulting reaction mixture was first cooled to r.t., and then subsequently quenched with 0.45 M TFA. The reaction was stirred at this temperature for an additional hour. The resulting reaction mixture was then concentrated in *vacuo*, and then pulled through a silica plug to remove excess TFA. Purification through TLC preparatory plate (4:1) Hexanes/EtOAc afforded both atropisomers of **1.3s** as white solids.

***S*-atropisomer of 7-isopropyl-6-methyl-5-(naphthalen-1-yl)-7H-pyrrolo[2,3-d]pyrimidin-4-amine (*S*_a-59)**



To a reaction vial equipped with a stirbar was added (*S*_a)-atropisomer of tert-butyl (tert-butoxycarbonyl)(6-chloro-7-isopropyl-5-(naphthalen-1-yl)-7H-pyrrolo[2,3-d]pyrimidin-4-yl)carbamate (60 mg, 0.11 mmol, 1.0 equiv) and 5 mol% Pd-PEPPSI-IPent catalyst (4.4 mg, 0.005 mmol). The reaction apparatus

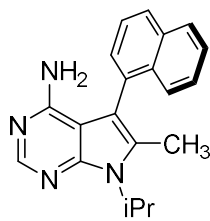
was then purged of O₂ to argon, and degassed toluene was subsequently added. After two minutes of stirring at r.t., 3.4 equiv of 3 M MeMgI was added dropwise. The reaction was heated to 40 °C and stirred at this temperature for 1 h. An additional 125 μL 3 M MeMgI (0.374 mmol, 3.4 equiv) was added, and the reaction was stirred for an additional 30 min. Workup and purification were followed accordingly to afford **(S_a)-59** as a white solid. 58% overall yield.

¹H NMR (400 MHz, CDCl₃) δ (ppm) = 8.13 (s, 1H), 7.98 (t, *J* = 7.8 Hz, 3H), 7.60 – 7.56 (m, 2H), 7.53 – 7.46 (m, 3H), 7.44 (dd, *J* = 7.0, 1.2 Hz, 1H), 4.96 – 4.90 (m, 1H), 2.26 (s, 3H), 1.77 (t, *J* = 7.0 Hz, 6H).

¹³C NMR (126 MHz, CDCl₃) δ (ppm) = 155.9, 150.4, 150.0, 134.2, 133.5, 132.5, 131.9, 129.5, 128.8, 128.6, 127.0, 126.6, 126.6, 125.8, 110.3, 103.5, 47.6, 30.1, 22.1, 12.2.

MS (APCI) = 317.2 or C₂₀H₂₁N₄; experimental 317.3 m/z.

***R*-atropiosomer of 7-isopropyl-6-methyl-5-(naphthalen-1-yl)-7H-pyrrolo[2,3-d]pyrimidin-4-amine (*R_a*-59)**



The synthesis and spectra data of **(R_a)-59** was prepared from *(R_a)-atropiosomer* of tert-butyl (tert-butoxycarbonyl)(6-chloro-7-isopropyl-5-(naphthalen-1-yl)-7H-pyrrolo[2,3-d]pyrimidin-4-yl)carbamate and obtained in agreeance with **(S_a)-1.3s**. 50% overall yield.

2.1.24 Racemization Kinetics

Enantiomerically enriched atropisomeric analogues post-S_NAr were tested for barrier to rotation (ΔG_{rac}) measurements using the similar procedures from Smith, D. E.; Marquez, I.; Lokensgard, M. E.; Rheingold, A. L.; Hecht, D. a.; Gustafson, J. L. *Angew. Chem., Int. Ed.* **2015**, *54* (40), 11754.³³

General Procedure:⁹

Enantiomerically enriched atropisomeric analogue of interest (<50 mg) was dissolved in ~1.5 mL of high boiling solvents i.e., toluene (PhMe), diphenylether (Ph₂O). This solution was then heated at a constant temperature for 2.5 h. A total of about 5 time points were recorded. At each time point, a 100-200 μL aliquot was isolated and quenched in an HPLC vial with room temperature 100% hexanes. Each sample was then injected into the chiral HPLC system. Each ΔG_{rac} measurement is determined from an average of two experiments.

Barrier to Racemization (ΔG_{rac}) and Half-Life to Racemization ($t_{1/2}$) of Atropisomers:

The ee% vs. time (sec, s) was plotted to determine the rate constant k_{obs} (i.e. the slope of the pseudo first-order kinetics) at this constant temperature using the following equation:

$$k_{\text{obs}} = \frac{\ln\left(\frac{1}{ee\%}\right)}{t}$$

Equation 23. First-order kinetics for racemization of atropisomers with respect to time.

From this, the racemization rate constant k_{rac} was determined using the following equation:

$$k_{rac} = \frac{k_{obs}}{2}$$

Equation 24. Rate constant for the degradation of enantiomeric ratio.

The average k_{rac} was determined by taking the average of the k_{rac} of each trial. From this, substitution into the Eyring equation was performed to determine the barrier to rotation, in which ΔG is the barrier to rotation measurement, R is the gas constant, T is the constant temperature, k_b is the Boltzmann distribution constant, and h is Planck's constant.:

$$\Delta G_{rac} = RT \ln \left(\frac{Tk_b}{k_{rac}h} \right)$$

Equation 25. Calculating barrier to racemization (otherwise known as the barrier to rotation of atropisomeric compounds), ΔG_{rac} .

To determine $t_{1/2}$ at 37 °C (physiological temperatures), the calculated ΔG_{rac} is then factored into this below equation in which $t_{1/2}$ is the half-life to racemization in seconds. This unit can be converted into hours (h), days (d), or years (y):

$$t_{1/2} = \frac{\left(\frac{k_b T e^{-\frac{\Delta G_{rac}}{RT}}}{\ln 2} \right)}{\ln 2}$$

Equation 26. Half-life to racemization for atropisomeric compounds.

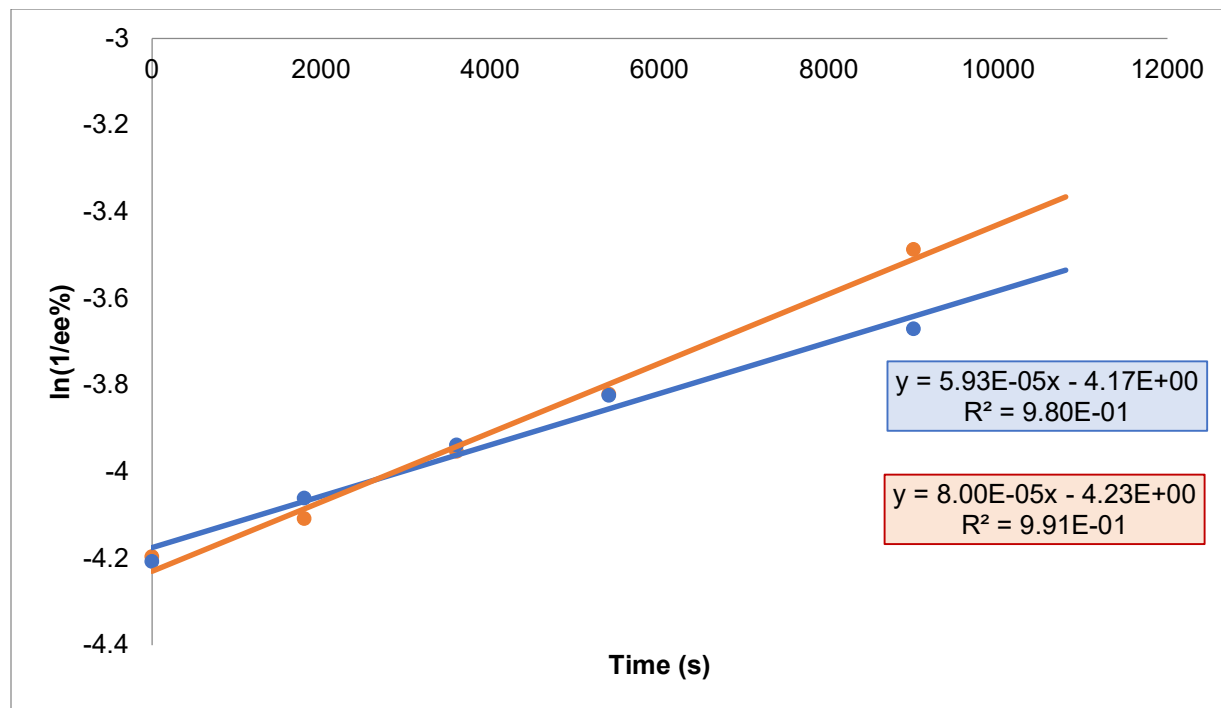
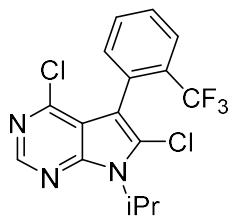


Figure 9. Barrier to Racemization of 21 at 140 °C, Ph₂O (1st order Racemization)

Table 6. Time-dependent Enantiodegradation of 21

Time (s)	Trial Run 1 (ee%)	Trial 1 [ln(1/ee%)]	Trial Run 2 (ee%)	Trial 2 [ln(1/ee%)]
0	67.154	-4.20698849	66.428	-4.196118654
1800	58.012	-4.06064989	60.822	-4.107951566
3600	51.334	-3.93835330	52.070	-3.952588967
5400	45.778	-3.82380363	45.652	-3.821047418
9000	39.258	-3.67015525	32.678	-3.486702069

Average k_{obs} = 6.97×10^{-5} , Average k_{rac} = 3.48×10^{-5}

Calculated Average ΔG = 33 kcal mol⁻¹ (i.e., 32.9 kcal mol⁻¹)

Calculated $t_{1/2}$ (37 °C) = 505.2 yr (or 184,386 d)

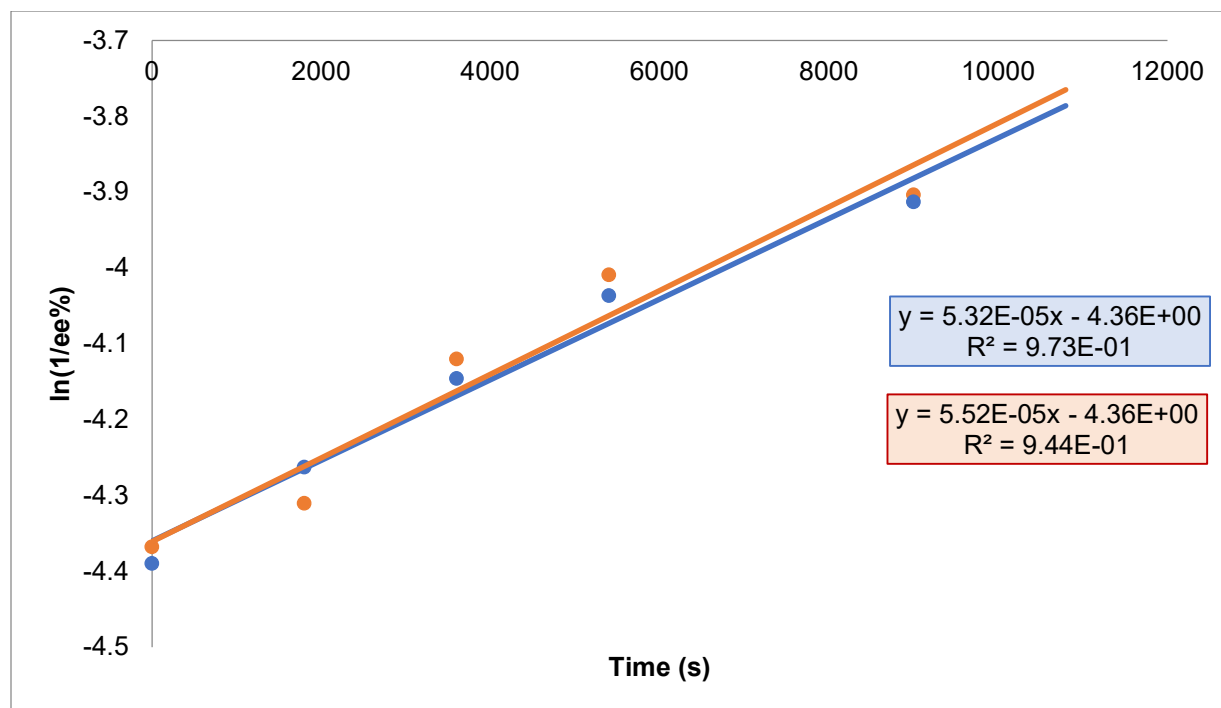
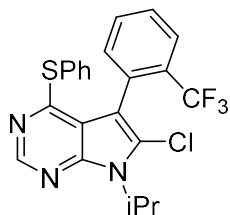


Figure 10. Barrier to Racemization of 22 at 140 C, Ph₂O (1st order Racemization)

Table 7. Time-dependent Enantiodegradation of 22

Time (s)	Trial Run 1 (ee%)	Trial 1 [ln(1/ee%)]	Trial Run 2 (ee%)	Trial 2 [ln(1/ee%)]
0	80.620	-4.38974676	78.888	-4.368029125
1800	71.008	-4.26279255	74.460	-4.310262068
3600	63.174	-4.14589282	61.568	-4.120142255
5400	56.638	-4.03668014	55.090	-4.008968211
9000	50.050	-3.91302251	49.568	-3.903345464

Average k_{obs} = 5.42×10^{-5} , Average k_{rac} = 2.71×10^{-5}

Calculated Average ΔG = 33 kcal mol⁻¹ (i.e., 33.1 kcal mol⁻¹)

Calculated $t_{1/2}$ (37 °C) = 706.6 yr (or 259,914 d)

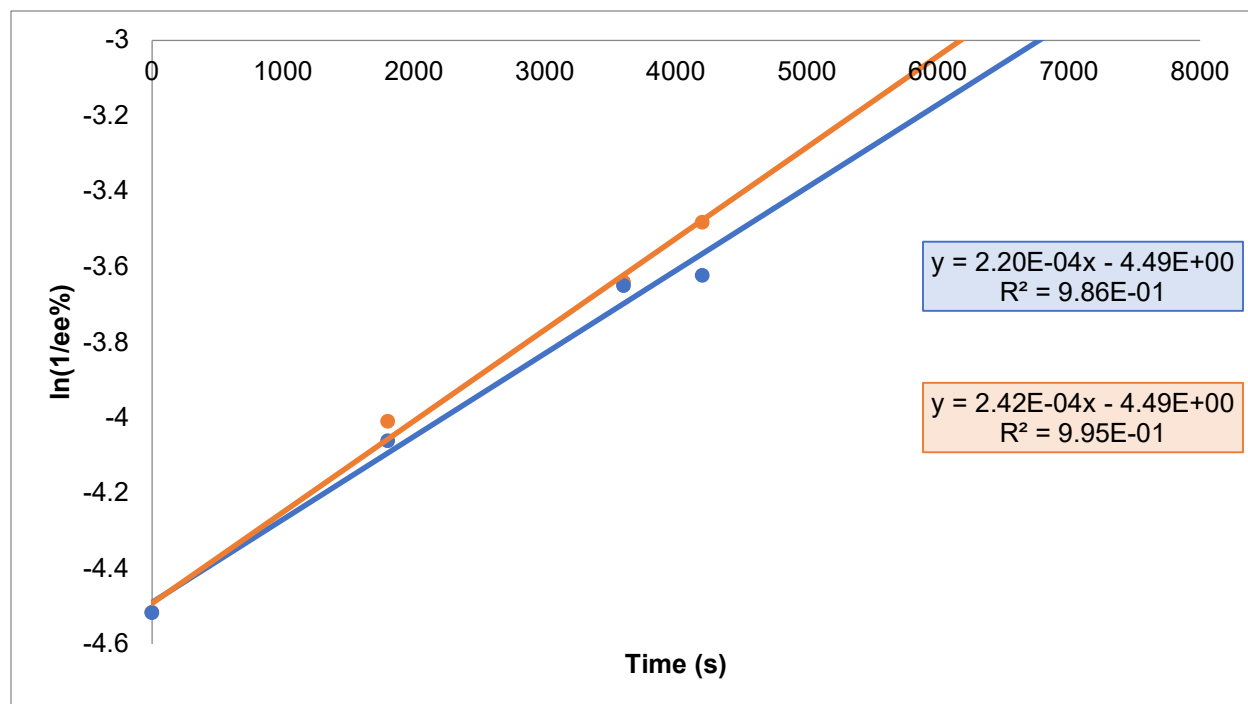
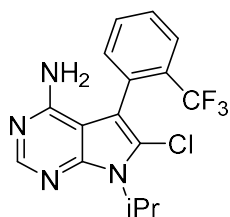


Figure 11. Barrier to Racemization of 60 at 125 °C, Ph₂O (1st order Racemization)

Table 8. Time-dependent Enantiodegradation of 60

Time (s)	Trial Run 1 (ee%)	Trial 1 [ln(1/ee%)]	Trial Run 2 (ee%)	Trial 2 [ln(1/ee%)]
0	91.476	-4.51607664	91.528	-4.516645
1800	57.998	-4.06040853	55.074	-4.008678
3600	38.442	-3.64915061	38.098	-3.640162
4200	37.430	-3.62247252	32.514	-3.481671
7500	34.534	N/A*	35.876	N/A*

Average $k_{\text{obs}} = 2.31 \times 10^{-5}$, Average $k_{\text{rac}} = 1.15 \times 10^{-5}$

Calculated Average $\Delta G = 31 \text{ kcal mol}^{-1}$ (i.e., 30.7 kcal mol⁻¹)

Calculated $t_{1/2}$ (37 °C) = 14.9 yr (or 5,441 d)

*At steady-state kinetics, no observable ee% change is observed

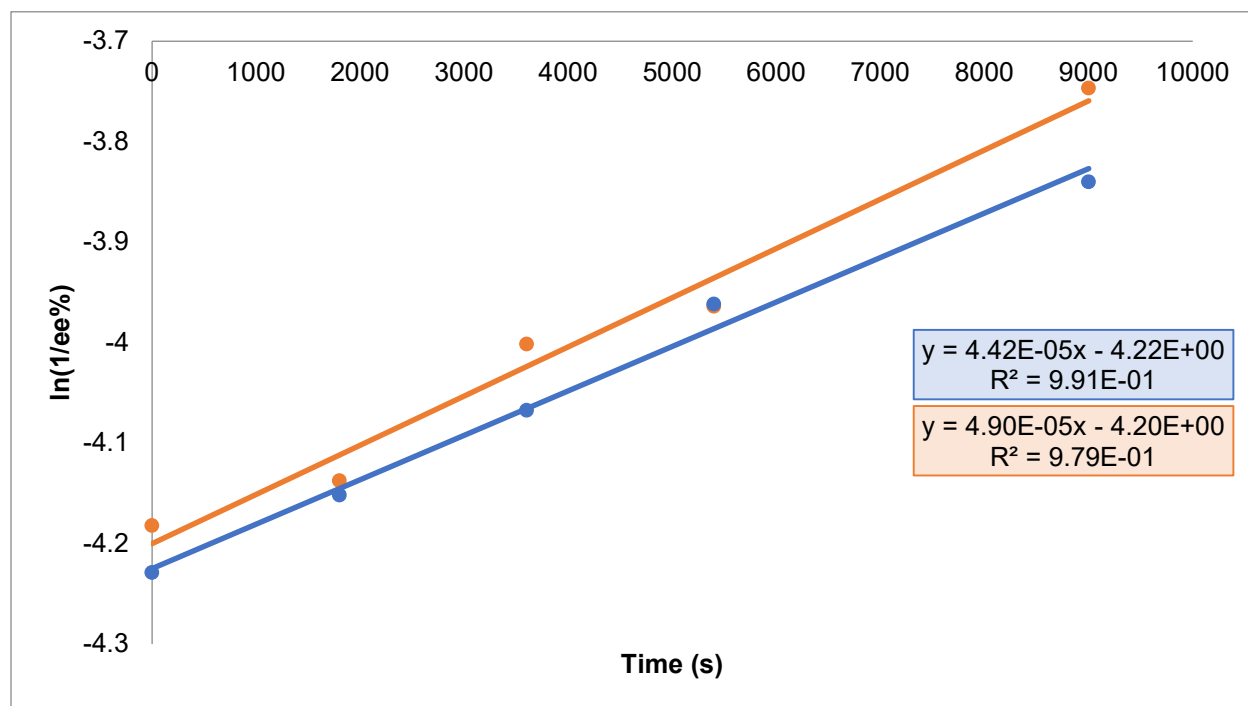
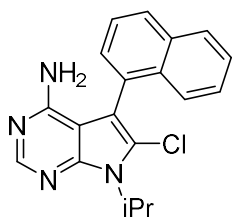


Figure 12. Barrier to Racemization of 61 at 125 °C, Ph₂O (1st order Racemization)

Table 9. Time-dependent Enantiodegradation of 61

Time (s)	Trial Run 1 (ee%)	Trial 1 [ln(1/ee%)]	Trial Run 2 (ee%)	Trial 2 [ln(1/ee%)]
0	68.612	-4.22846745	65.498	-4.182020
1800	63.524	-4.15141779	62.626	-4.137181
3600	58.388	-4.06711039	54.656	-4.001059
5400	52.532	-3.96142251	52.652	-3.963704
9000	46.512	-3.83971034	42.366	-3.746346

Average $k_{\text{obs}} = 4.66 \times 10^{-5}$, Average $k_{\text{rac}} = 2.23 \times 10^{-5}$
 Calculated Average $\Delta G = 28$ kcal/mol (i.e., 27.9 kcal/mol)
 Calculated $t_{1/2}$ (37 °C) = 0.148 yr (or 54 d)

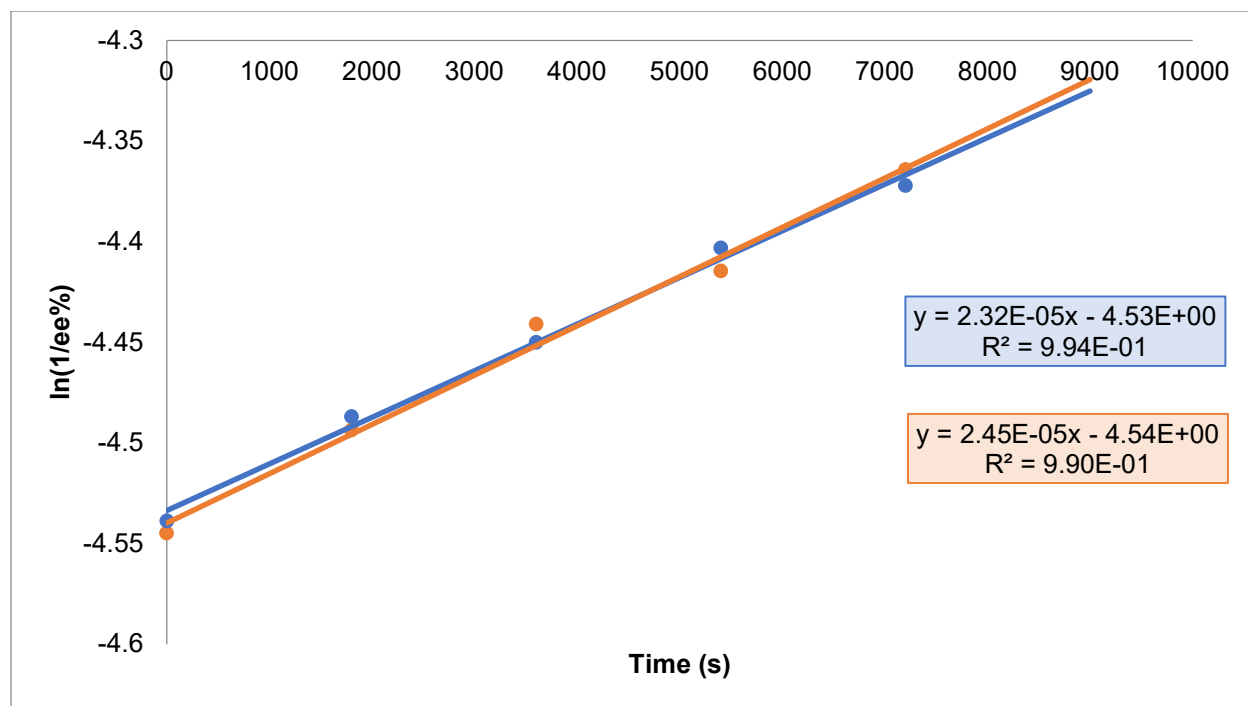
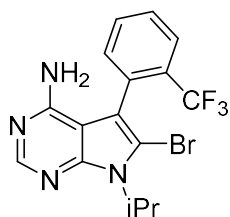


Figure 13. Barrier to Racemization of 64 at 127 °C, Ph₂O (1st order Racemization)

Table 10. Time-dependent Enantiodegradation of 64

Time (s)	Trial Run 1 (ee%)	Trial 1 [ln(1/ee%)]	Trial Run 2 (ee%)	Trial 2 [ln(1/ee%)]
0	93.576	-4.53877394	94.146	-4.544846769
1800	88.852	-4.48697206	89.440	-4.493568009
3600	85.626	-4.44998898	84.858	-4.440979271
5400	81.708	-4.40315192	82.638	-4.414469623
7200	79.210	-4.37210255	78.582	-4.364142666

Average k_{obs} = 2.39×10^{-5} , Average k_{rac} = 1.19×10^{-5}
Calculated Average ΔG = 33 kcal/mol (i.e., 32.7 kcal/mol)
Calculated $t_{1/2}$ (37 °C) = 360.5 yr (or 131,580 d)

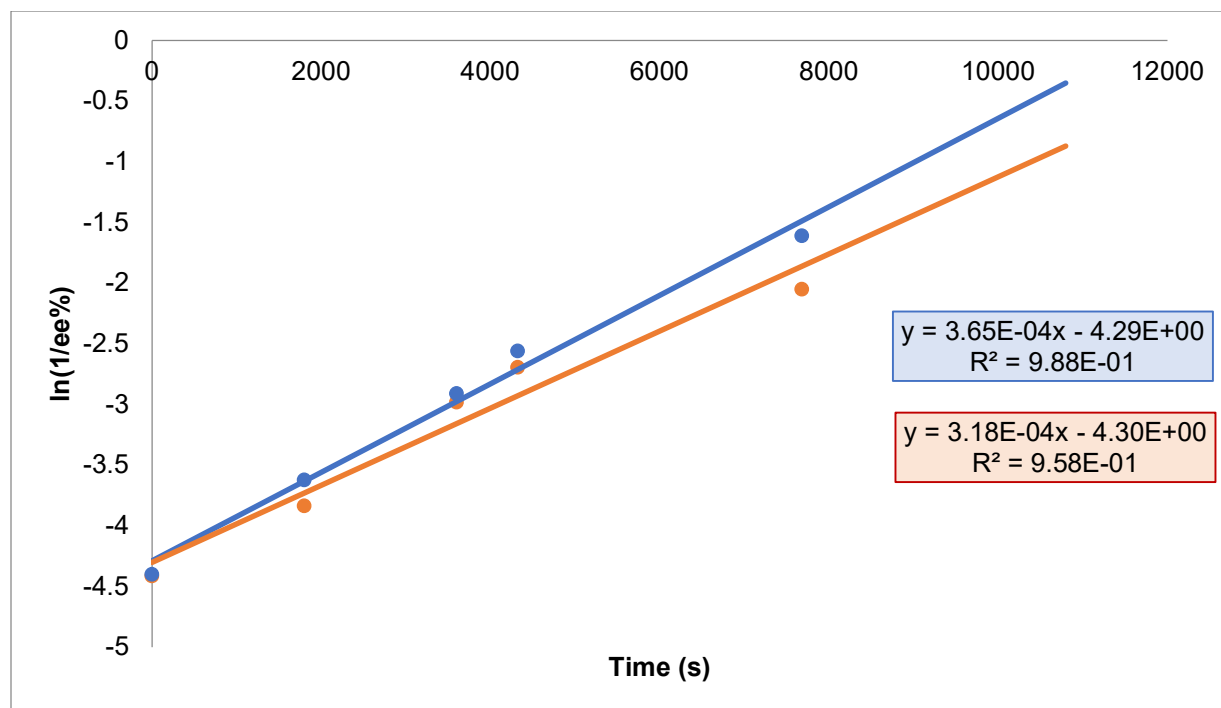
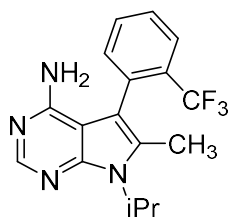


Figure 14. Barrier to Racemization of 57 at 140 °C, Ph₂O (1st order Racemization)

Table 11. Time-dependent Enantiodegradation of 57

Time (s)	Trial Run 1 (ee%)	Trial 1 [ln(1/ee%)]	Trial Run 2 (ee%)	Trial 2 [ln(1/ee%)]
0	81.386	-4.399203268	82.686	-4.415050301
1800	37.456	-3.623166911	46.366	-3.836566432
3600	18.360	-2.910174385	19.722	-2.981734764
4320	12.928	-2.559395502	14.800	-2.694627181
7680	5.000	-1.609437912	7.772	-2.050527532

Average k_{obs} = 3.41×10^{-4} , Average k_{rac} = 1.71×10^{-4}
Calculated Average ΔG = 32 kcal/mol (i.e., 31.6 kcal/mol)
Calculated $t_{1/2}$ (37 °C) = 60.9 yr (or 22,217 d)

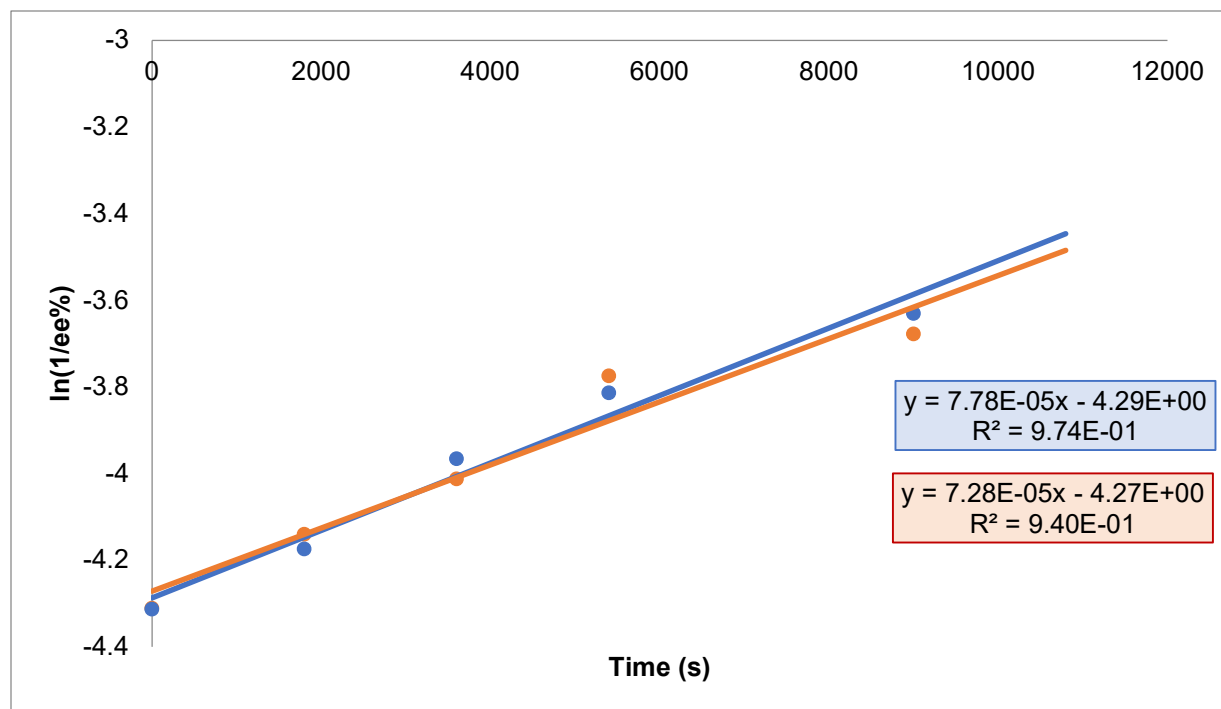
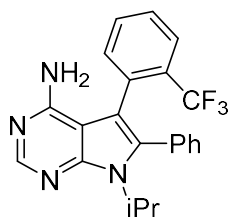


Figure 15. Barrier to Racemization of 58 at 140 °C, Ph₂O (1st order Racemization)

Table 12. Time-dependent Enantiodegradation of 58

Time (s)	Trial Run 1 (ee%)	Trial 1 [ln(1/ee%)]	Trial Run 2 (ee%)	Trial 2 [ln(1/ee%)]
0	74.588	-4.31197964	74.534	-4.311255397
1800	64.920	-4.17315574	62.780	-4.139636551
3600	52.724	-3.96507076	55.252	-4.011904539
5400	45.275	-3.81275500	43.536	-3.773588182
9000	37.710	-3.62992531	39.536	-3.677211649

Average $k_{\text{obs}} = 7.53 \times 10^{-5}$, Average $k_{\text{rac}} = 3.77 \times 10^{-5}$
Calculated Average $\Delta G = 33$ kcal/mol (i.e., 32.9 kcal/mol)
Calculated $t_{1/2}$ (37 °C) = 455.4 yr (or 166,221 d)

2.1.25 Dose-Response Data of Kinase Inhibitors

Human recombinant, full-length SRC and BRK kinase expressed in Sf9 insect cells were purchased from SignalChem. SRC substrate (KVEKIGEGTYGVVYK-amide) was purchased from Biomatik. BRK substrate Poly (Glu:Tyr, 4:1) was purchased from Sigma Aldrich. ATP, reaction buffers, ADP-Glo and Kinase Detection reagents were purchased in an assay ready kit from Promega (Promega Corporation, Madison WI 53711 USA) and used as received. Brief procedure: Incubations were performed in 40 mM Tris buffer (pH 7.4, 1% DMSO) supplemented with 50 μ M DTT, 25 mM MgCl₂, and 2mM MnCl₂ in a white flat-bottom 96-well plate. Kinase (1.2 μ g/mL), substrate (200 μ g/mL), ATP (50 μ M) and inhibitor were combined in a total reaction volume of 25 μ L and incubated for 60min at room temperature. ADP-Glo reagent was then added and incubated for 40min. Kinase Detection reagent was then added and after 45min the luminescence was recorded on a Tecan Infinite M200 luminometer. The light generated is proportional to the amount ADP present and, consequently, to the kinase activity. All incubations were done in duplicates.

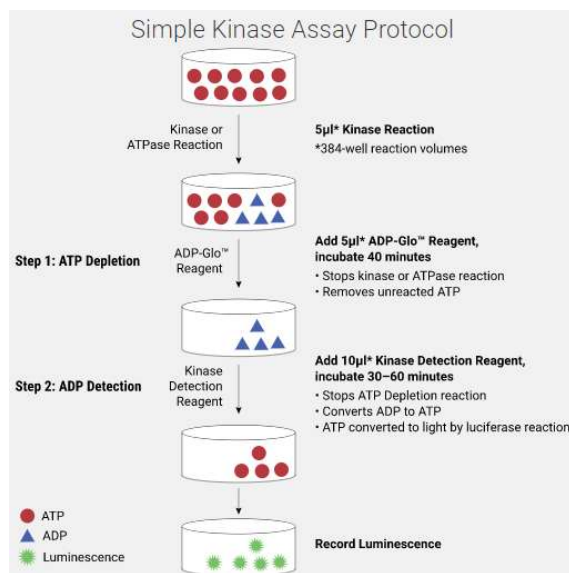


Figure 16. ADP-Glo™ Kinase Assay (Image Reference: <https://www.promega.com/products/cell-signaling/kinase-assays-and-kinase-biology/adp-glo-kinase-assay/?catNum=V6930>)

Cell-free kinase incubation with corresponding inhibitors. The activity readout of inhibitors was referenced to a negative control (without inhibitor). Error bars mean \pm standard deviation of duplicate samples. Sigmoidal dose-response curves were generated by GraphPad software using non-linear fitting of experimental data points.

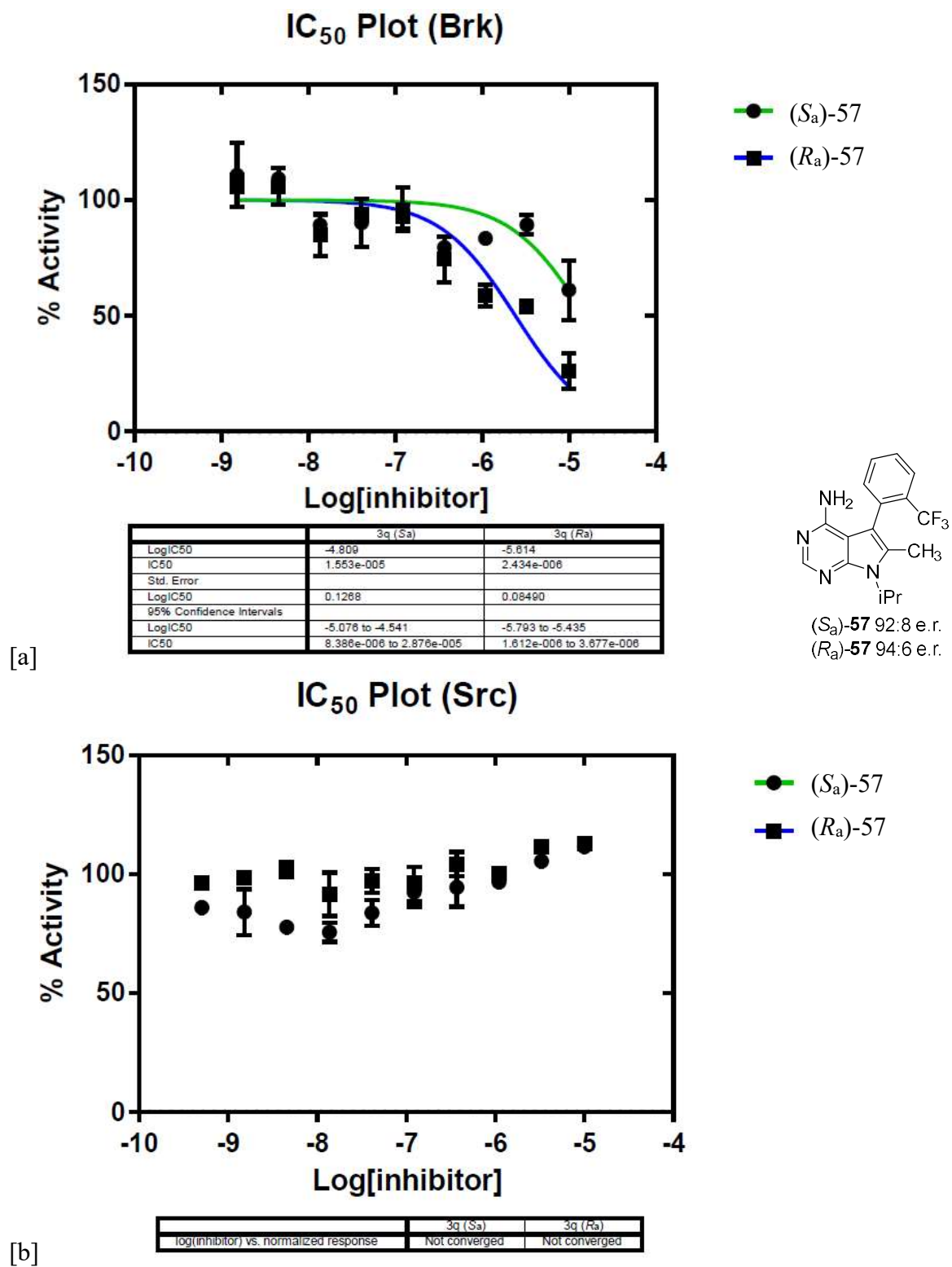


Figure 17. Dose-response curve for enantioenriched 57 in [a] Brk and [Src] kinase.

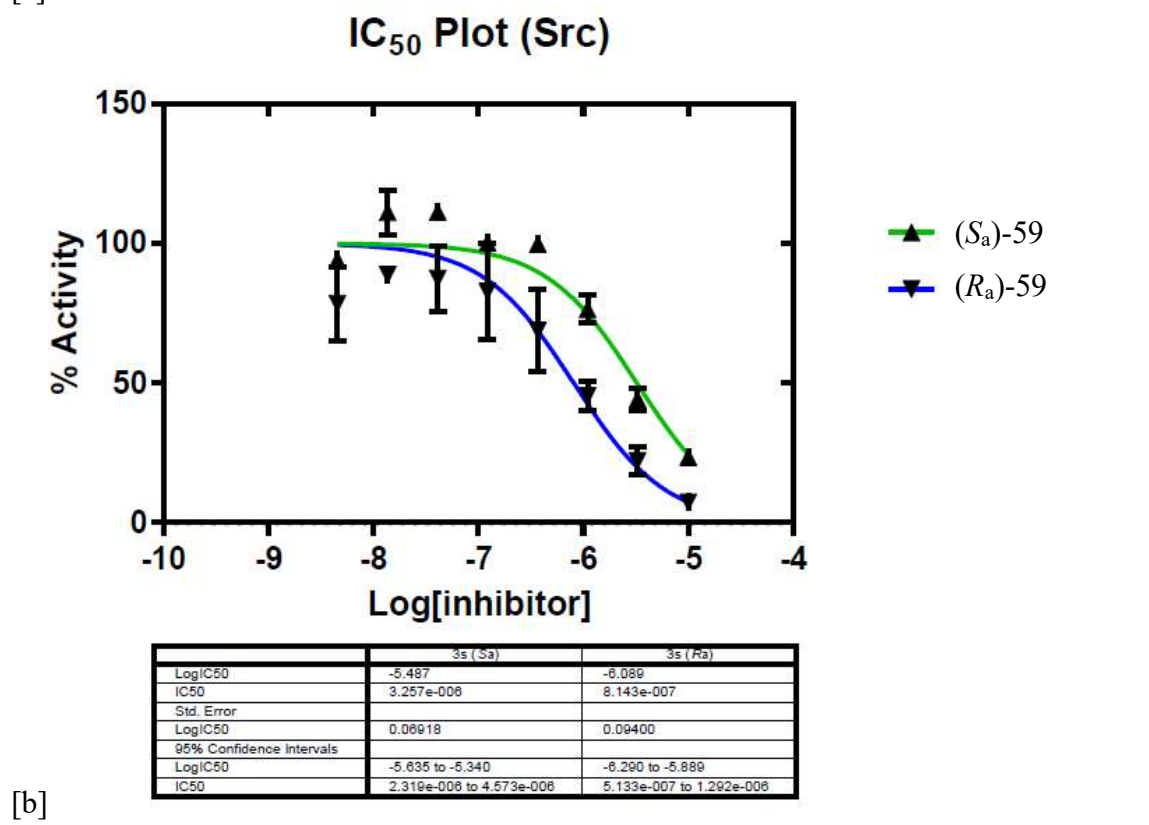
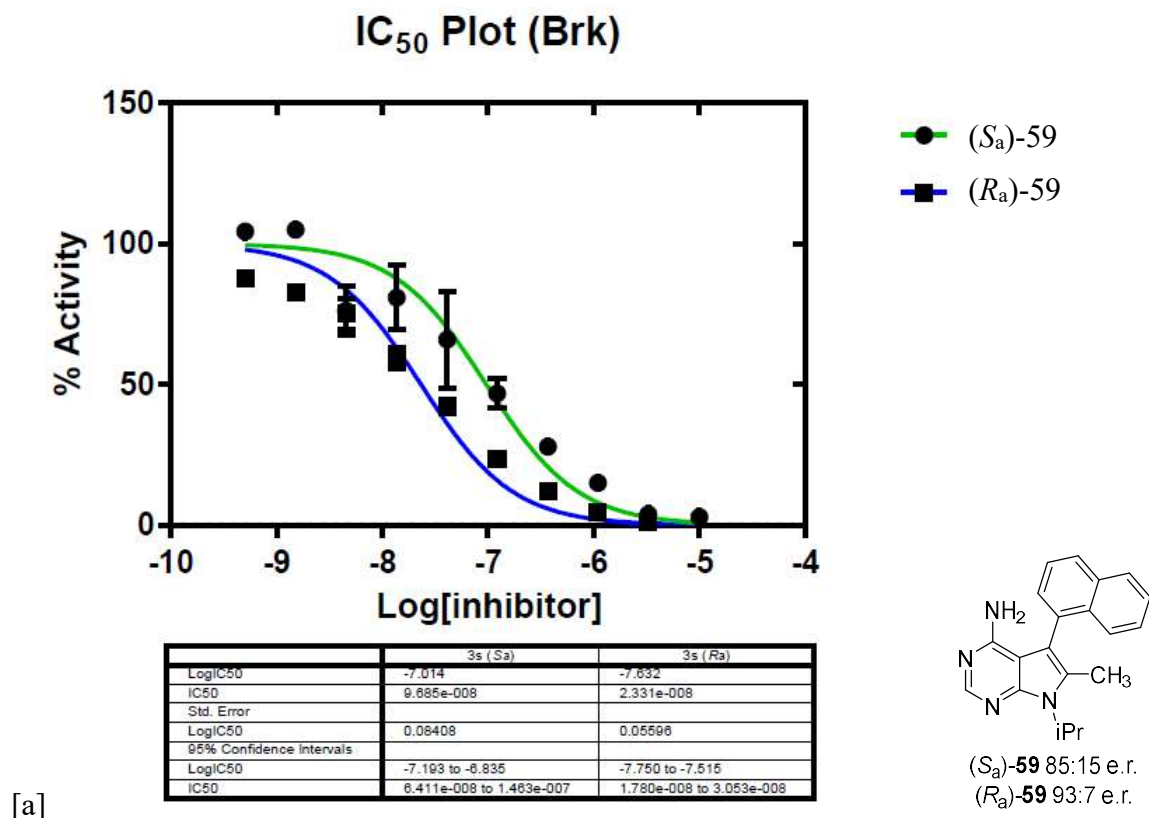


Figure 18. Dose-response curve for enantioenriched 59 in [a] Brk and [Src] kinase.

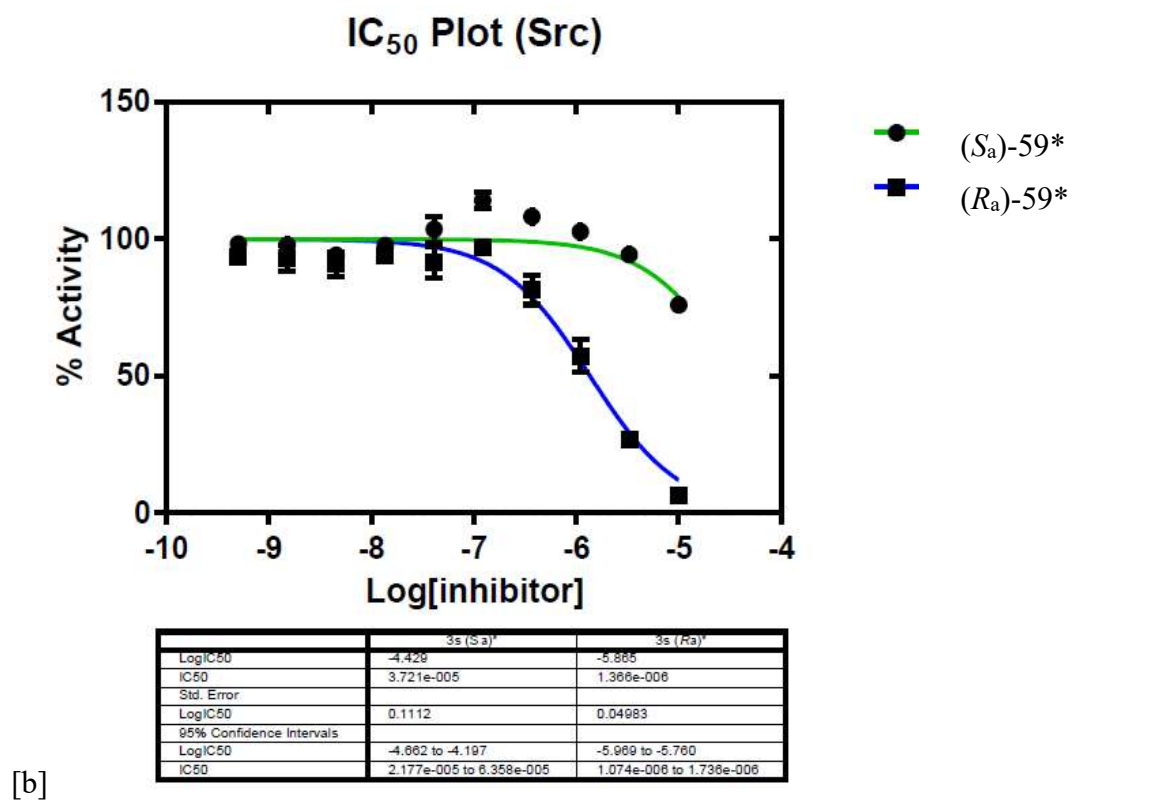
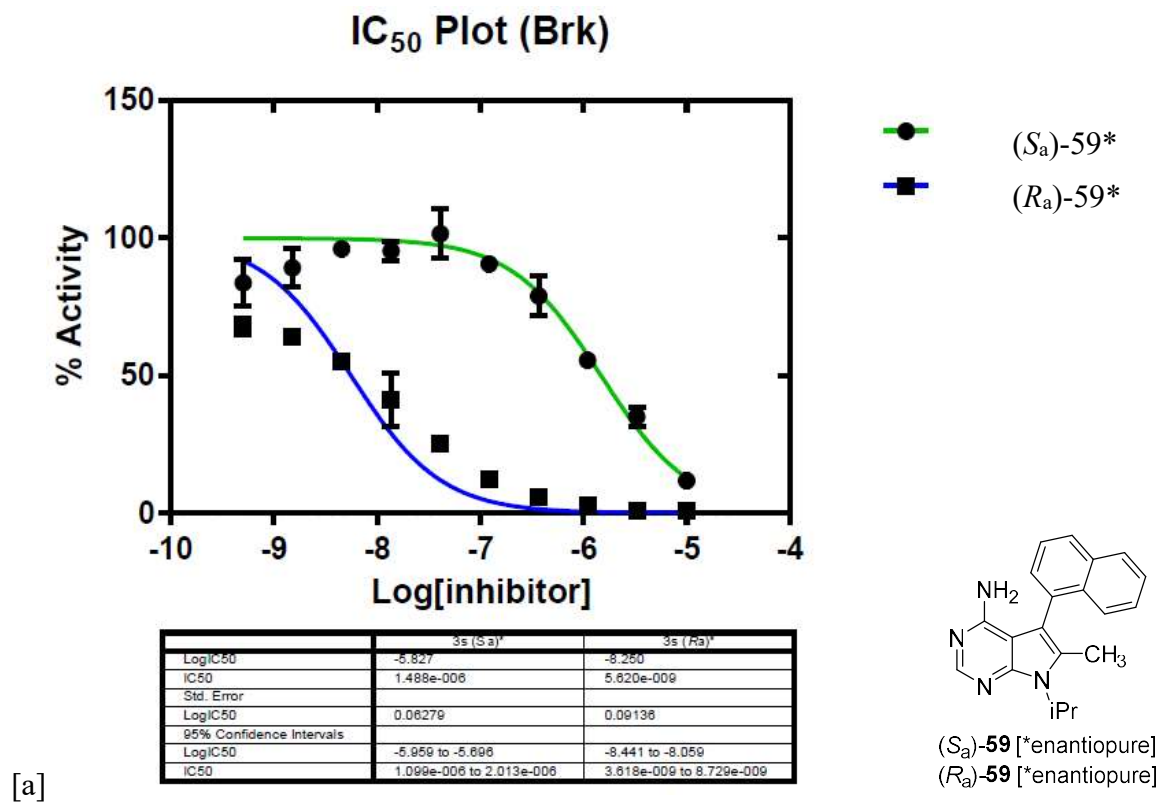
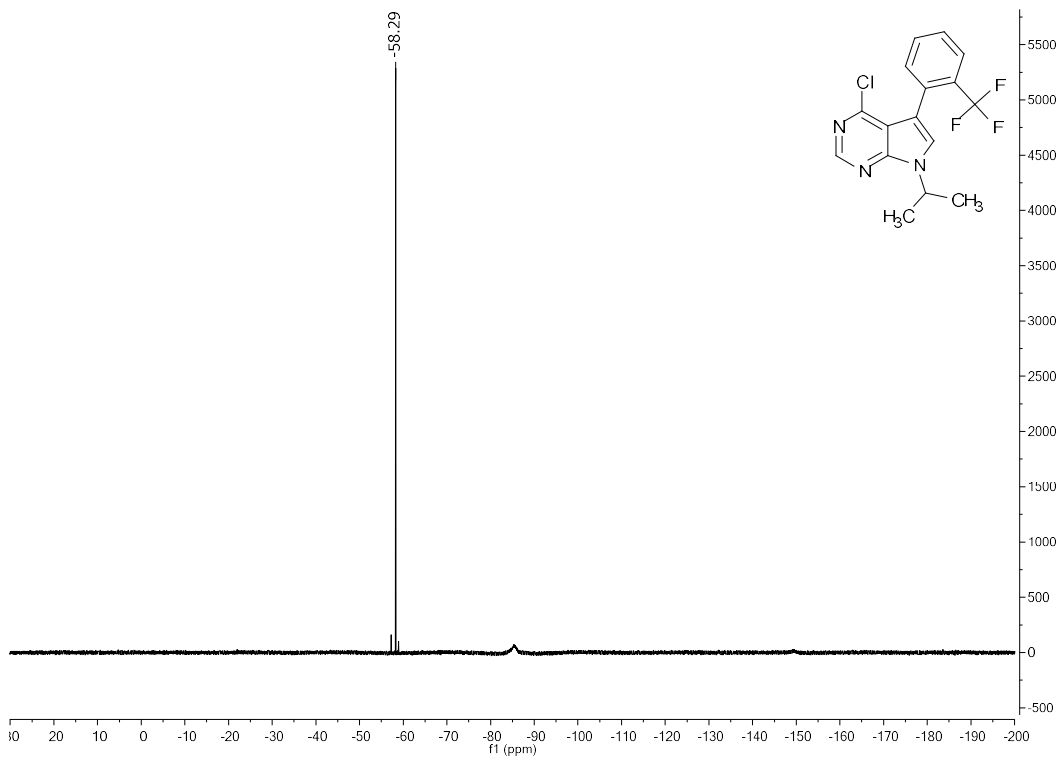
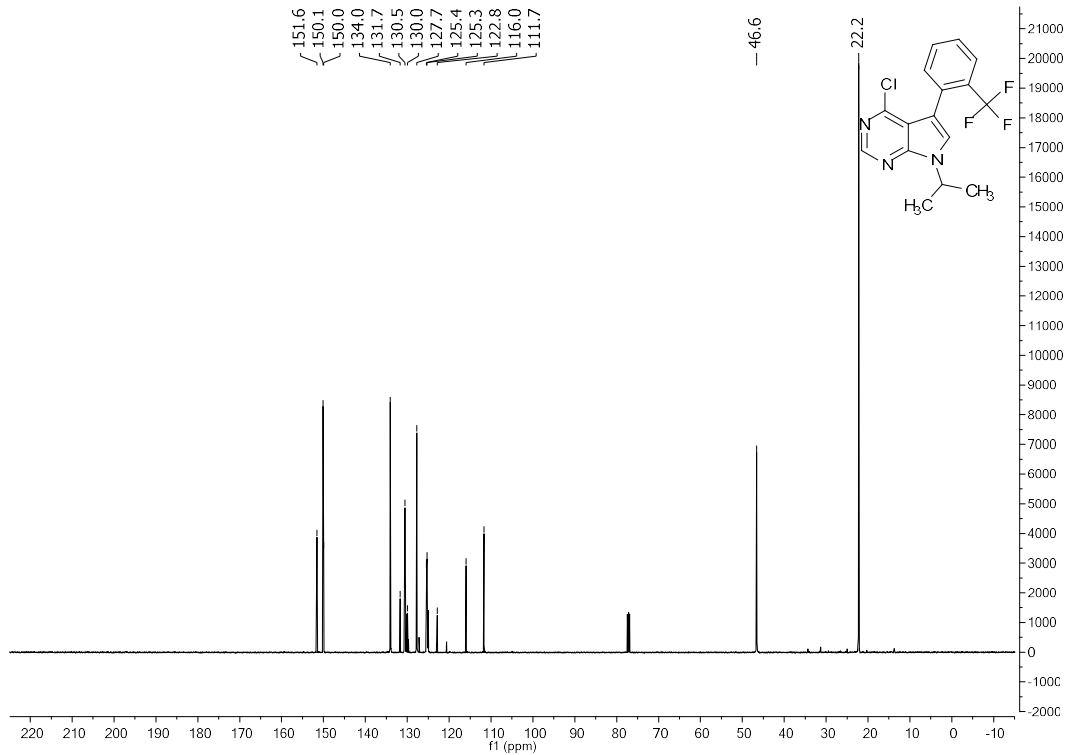


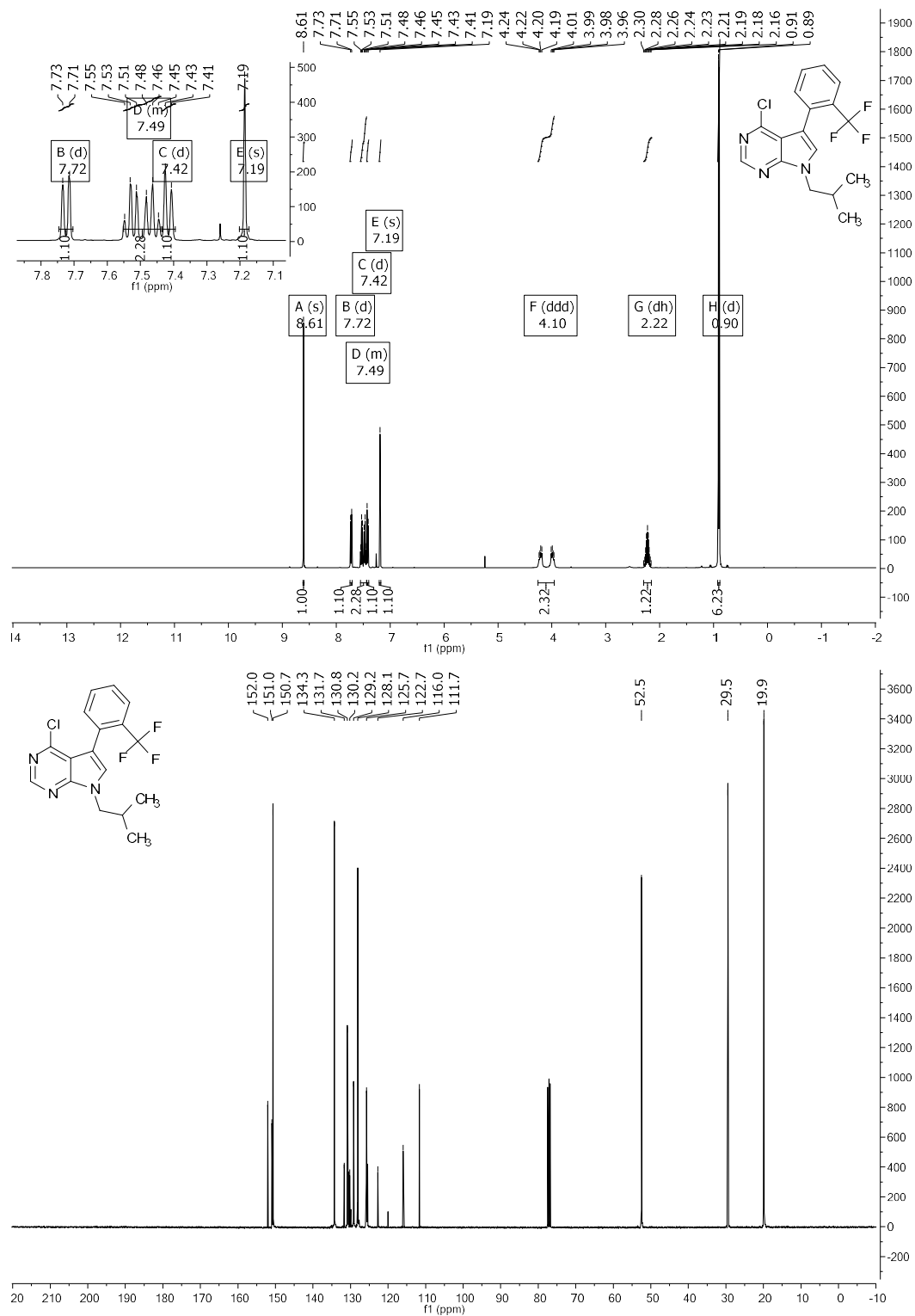
Figure 19. Dose-response curve for enantioenriched 59 in [a] Brk and [Src] kinase.

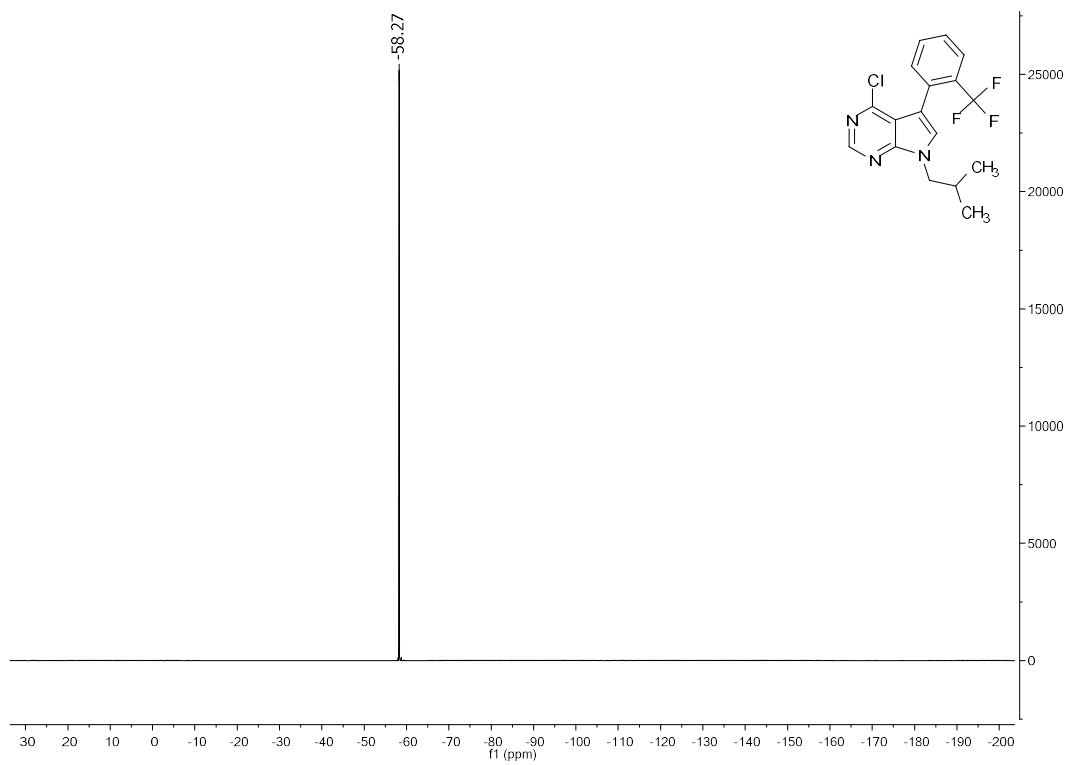
2.1.26 NMR Spectra

^1H , ^{13}C , and ^{19}F Spectral Data of 4-chloro-7-isopropyl-5-(2-(trifluoromethyl)phenyl)-7*H*-pyrrolo[2,3-d]pyrimidine

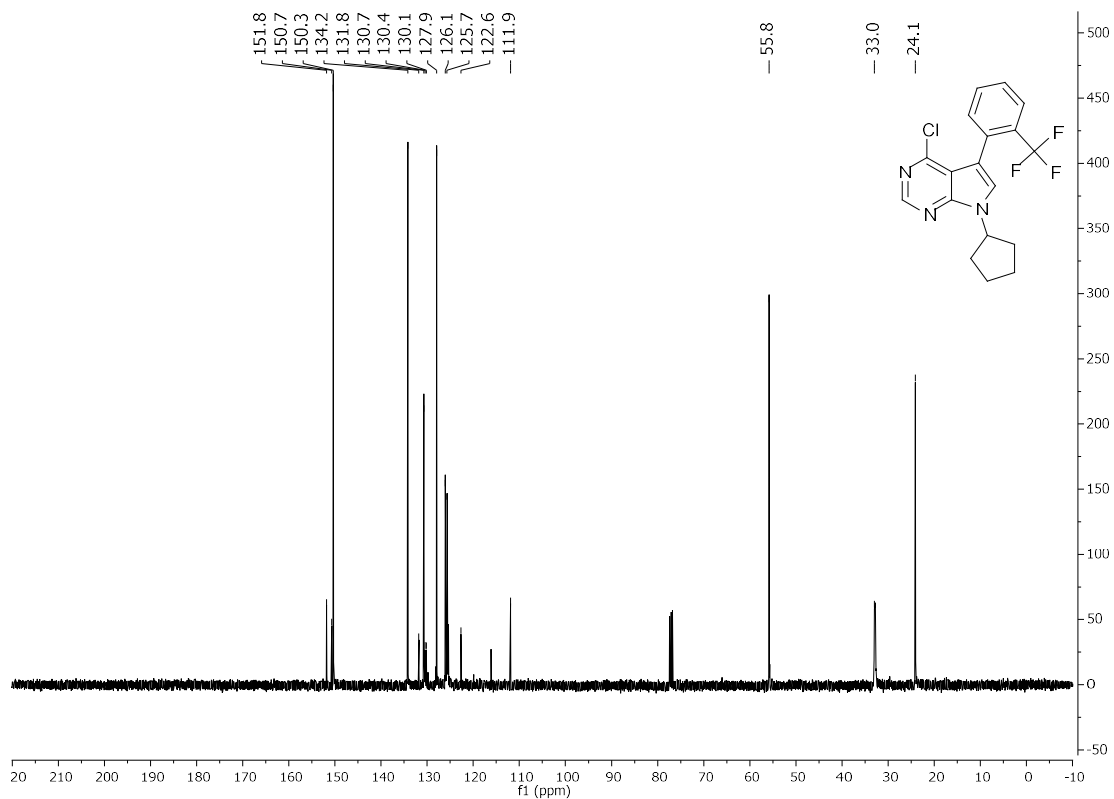
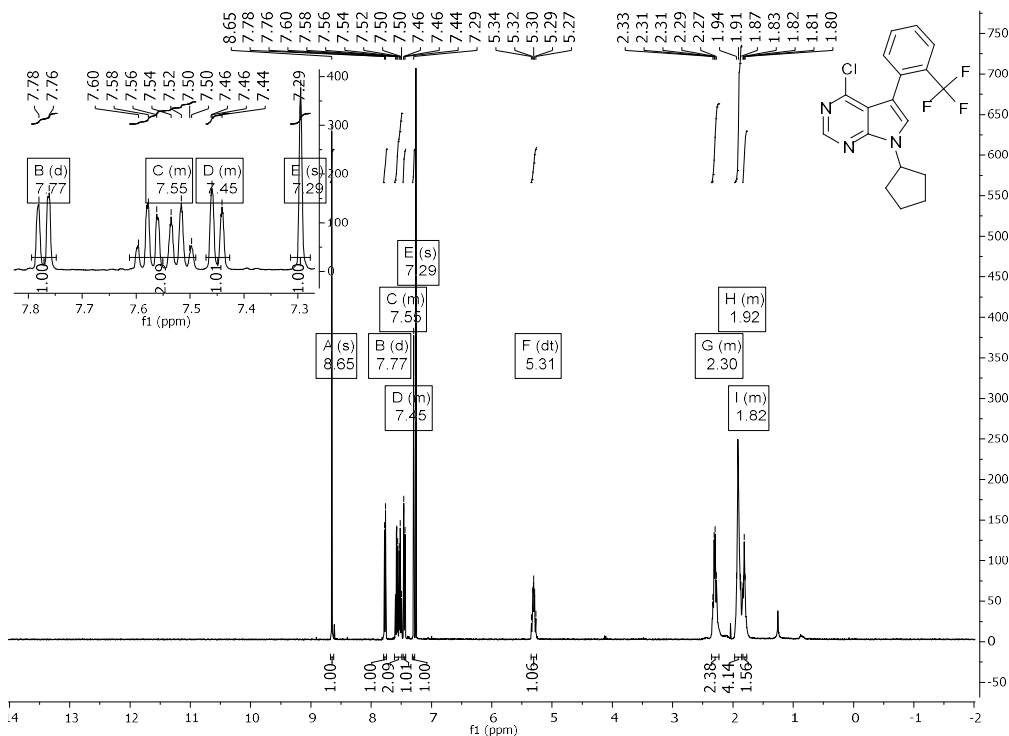


^1H , ^{13}C , and ^{19}F Spectral Data of 4-chloro-7-isobutyl-5-(2-(trifluoromethyl)phenyl)-7H-pyrrolo[2,3-d]pyrimidine



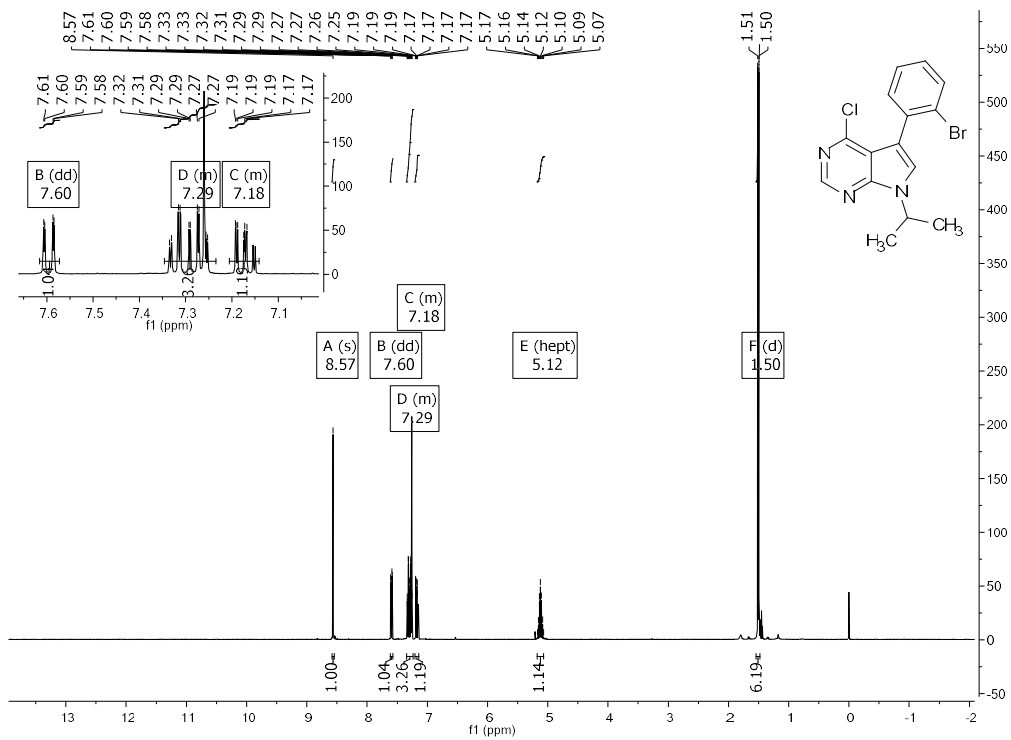


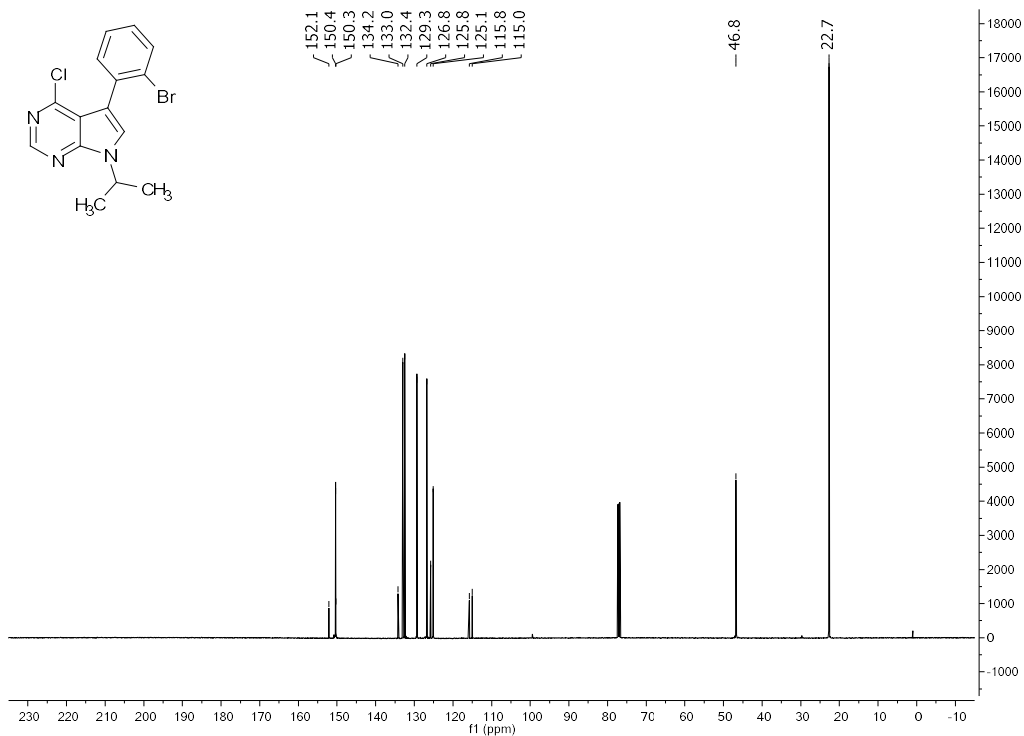
^1H , ^{13}C , and ^{19}F Spectral Data of 4-chloro-7-cyclopentyl-5-(2-(trifluoromethyl)phenyl)-*7H*-pyrrolo[2,3-*d*]pyrimidine



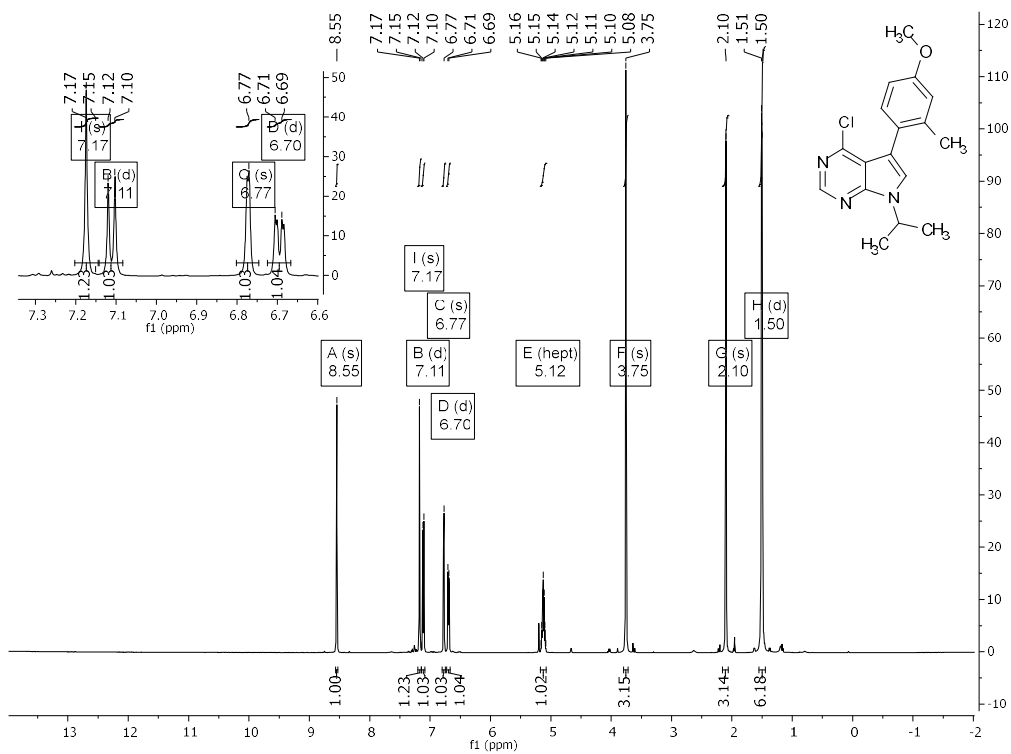


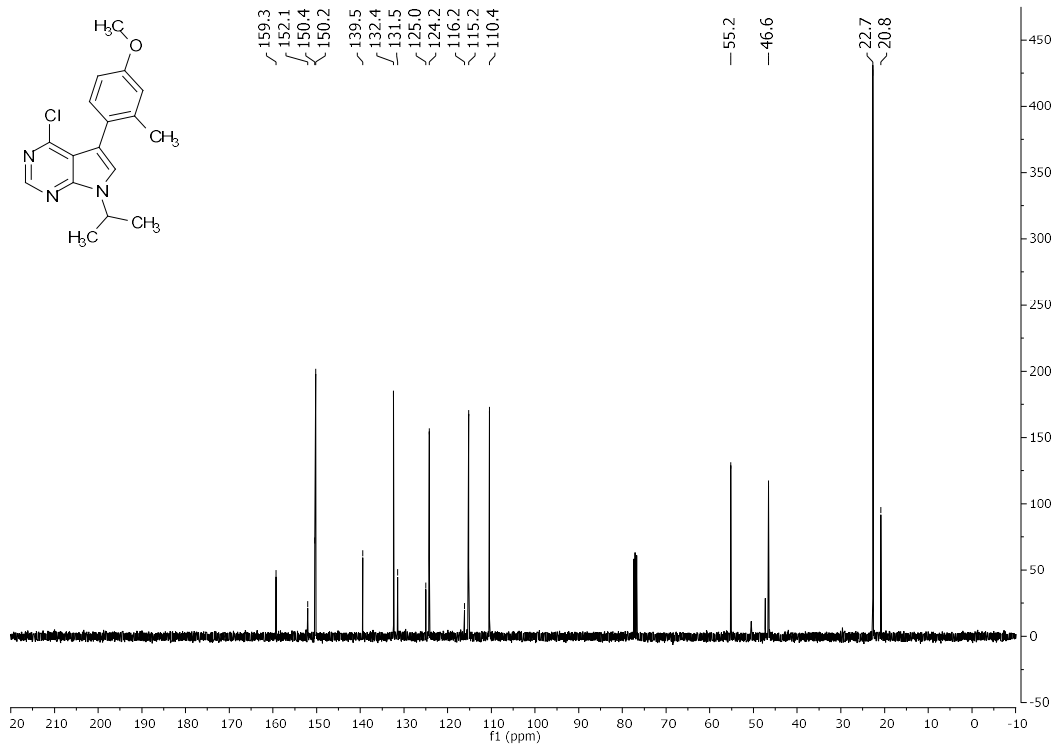
¹H and ¹³C Spectral Data of 5-(2-bromophenyl)-4-chloro-7-isopropyl-7H-pyrrolo[2,3-d]pyrimidine



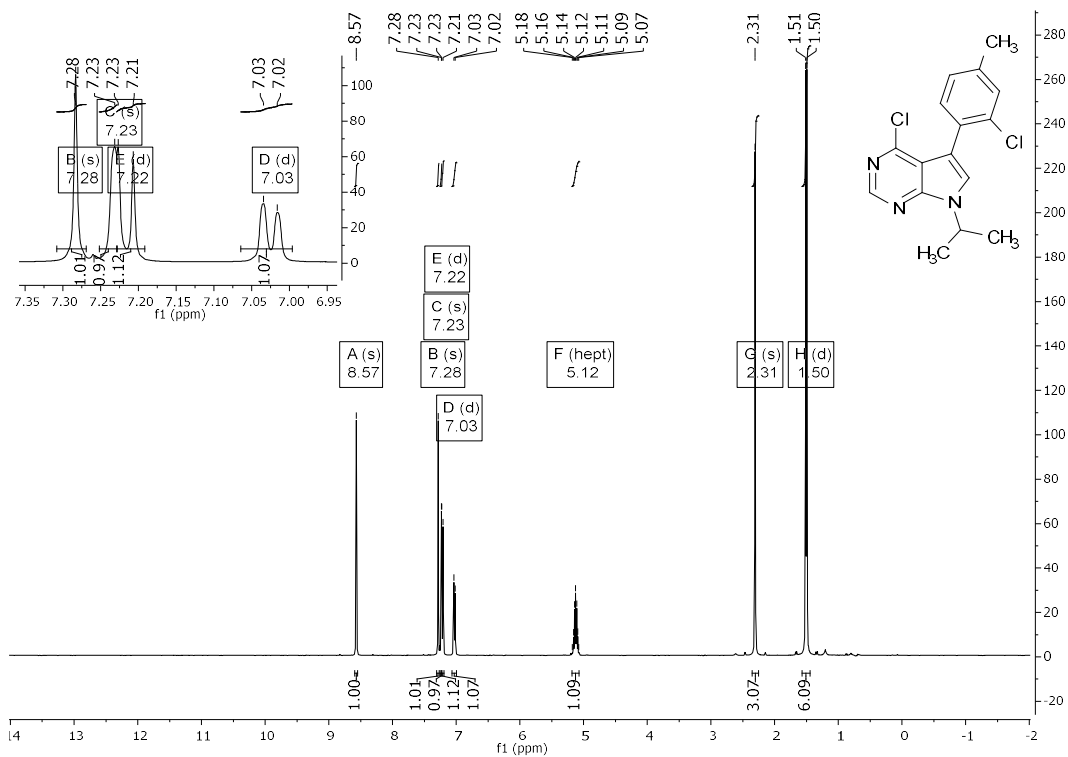


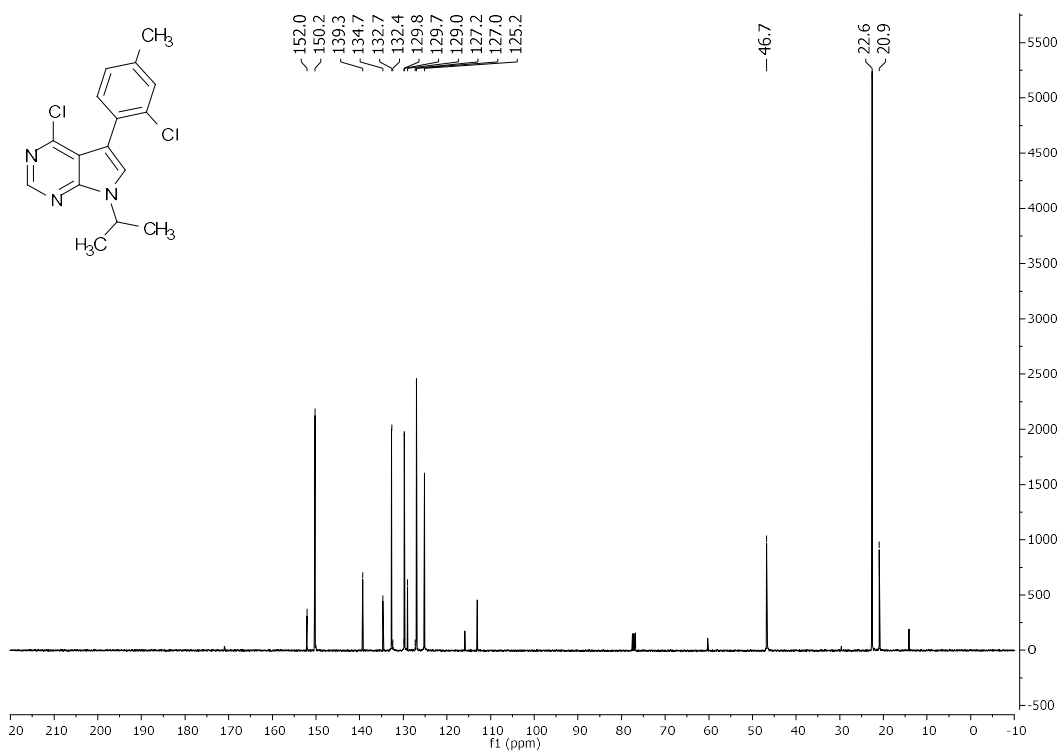
¹H and ¹³C Spectral Data of 4-chloro-7-isopropyl-5-(4-methoxy-2-methylphenyl)-7H-pyrrolo[2,3-d]pyrimidine



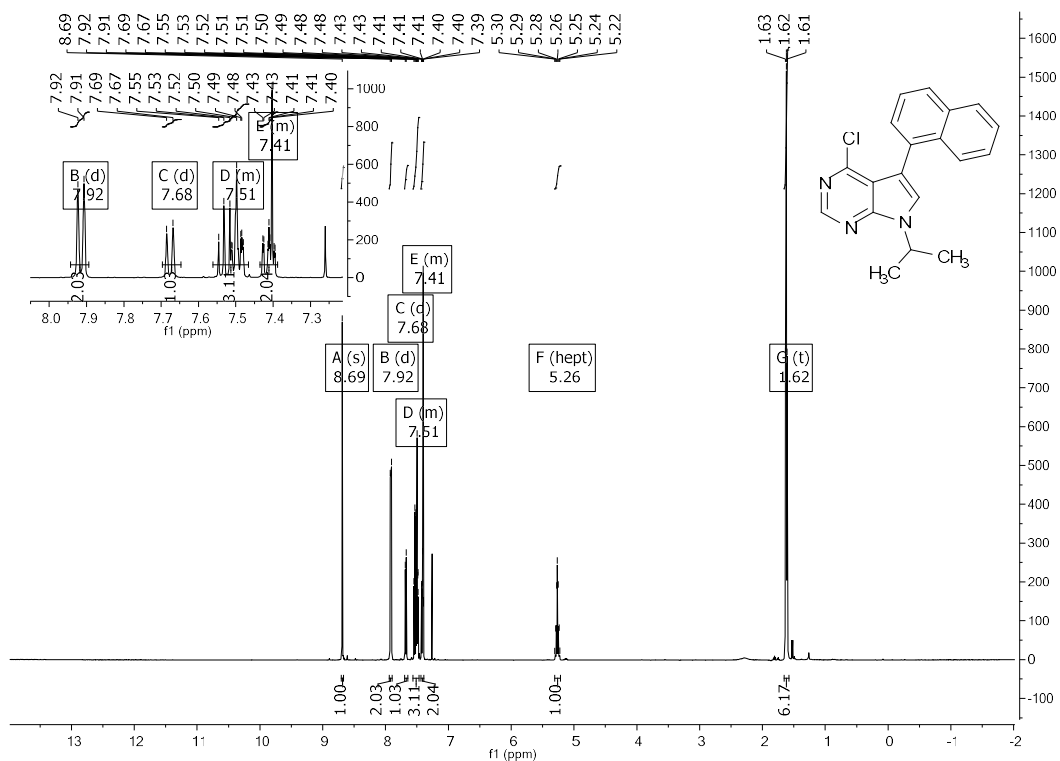


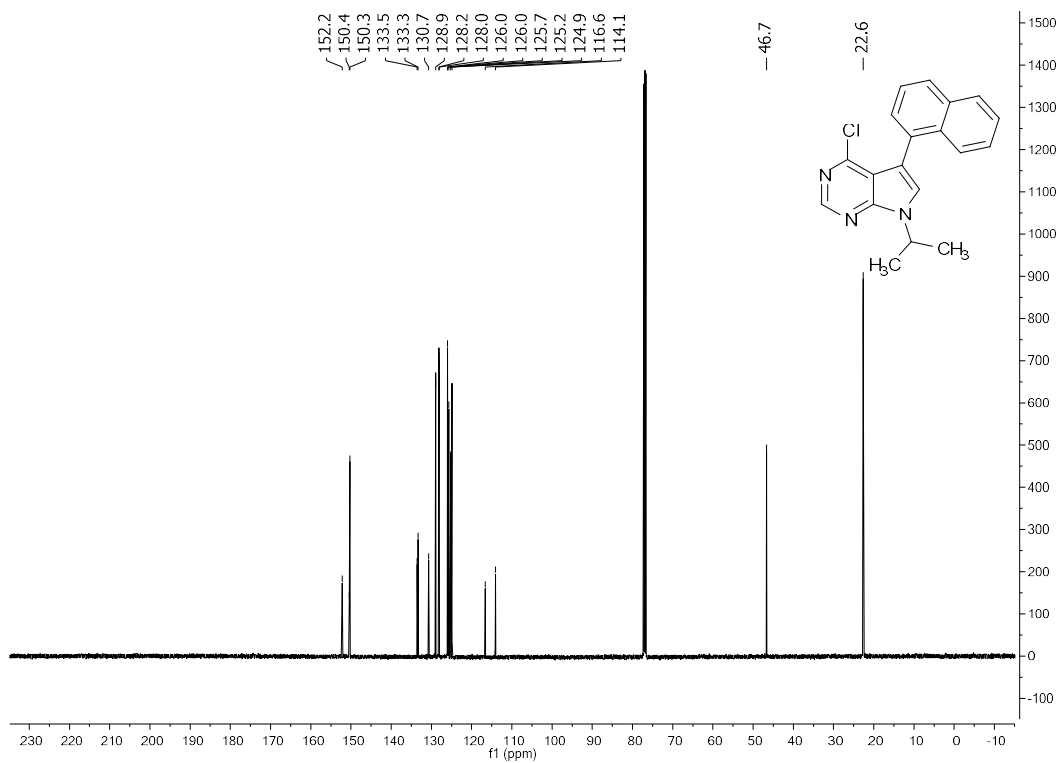
^1H and ^{13}C Spectral Data of 4-chloro-5-(2-chloro-4-methylphenyl)-7-isopropyl-7H-pyrrolo[2,3-d]pyrimidine



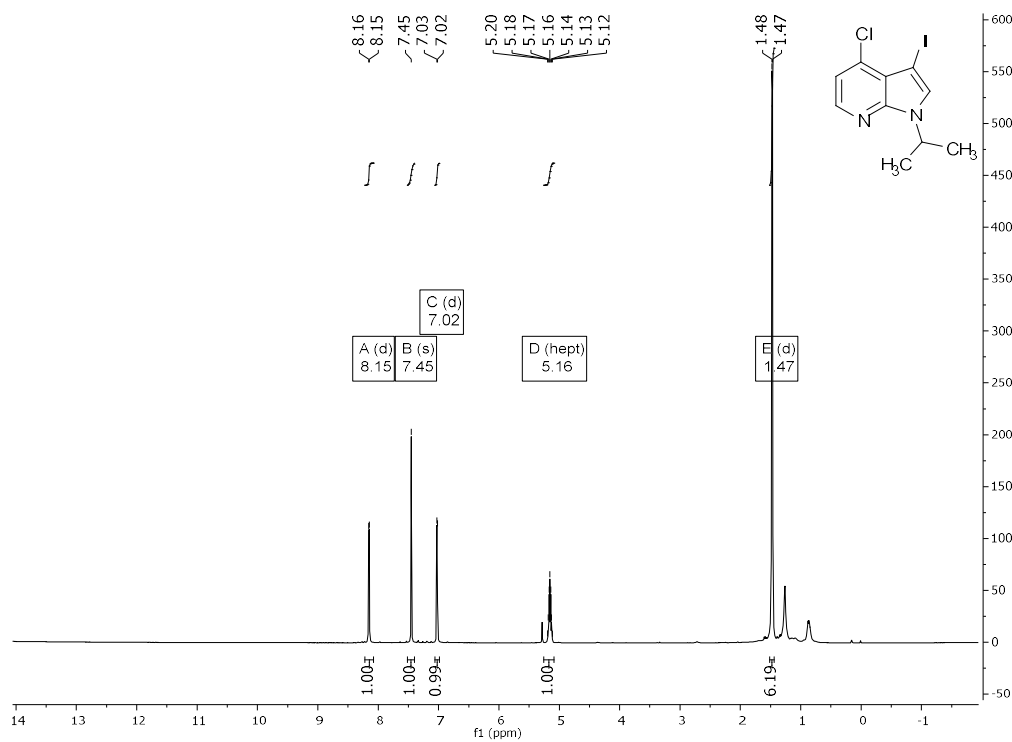


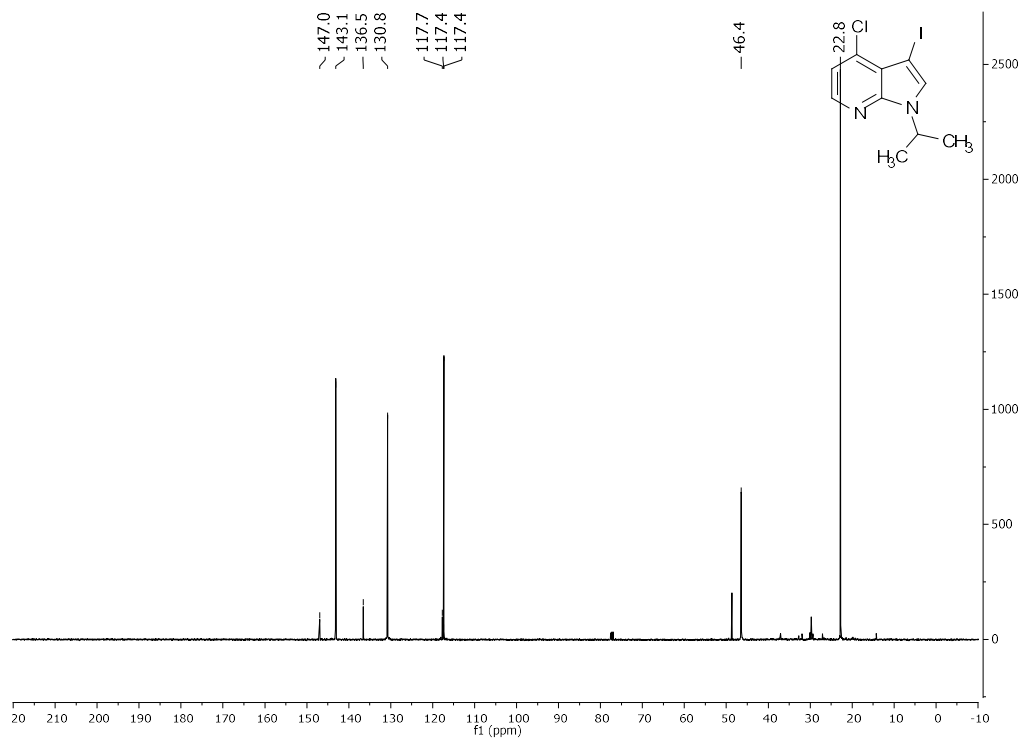
^1H and ^{13}C Spectral Data of 4-chloro-7-isopropyl-5-(naphthalen-1-yl)-7H-pyrrolo[2,3-d]pyrimidine



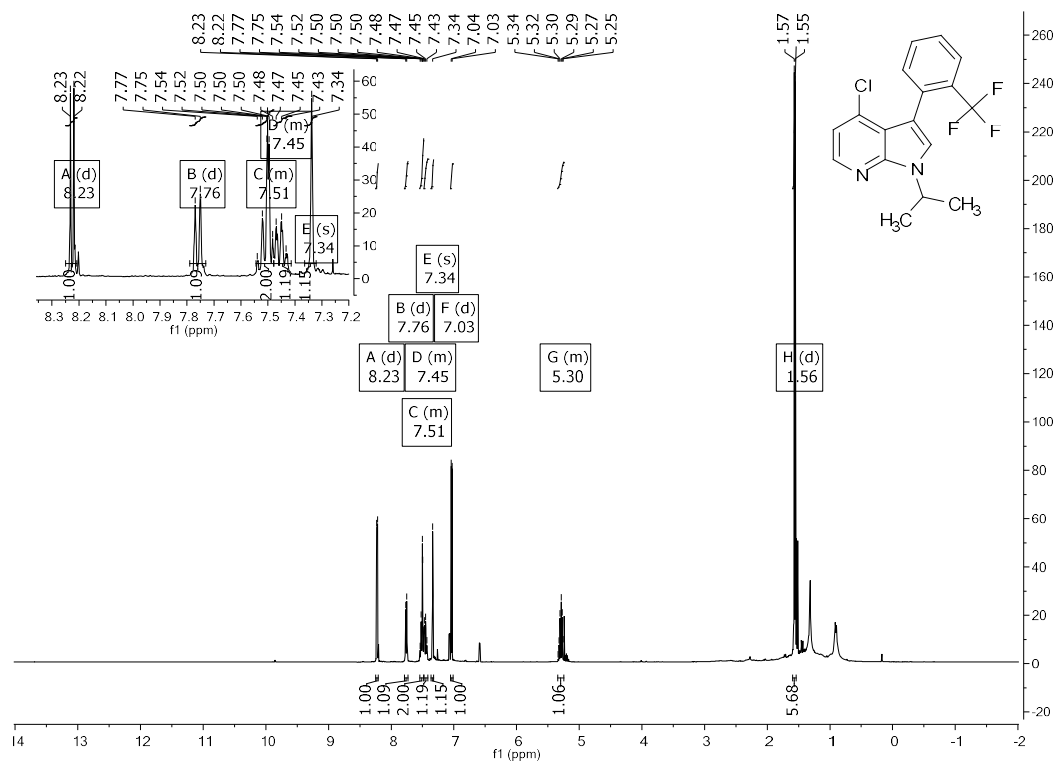


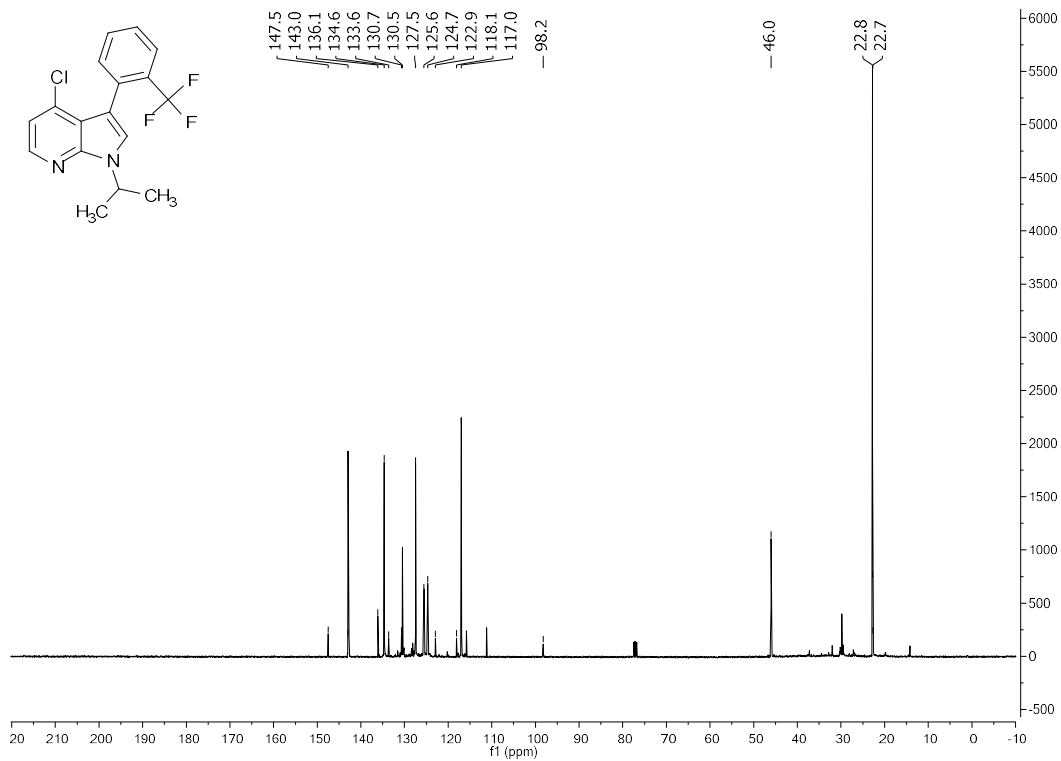
$^1\text{H} / ^{13}\text{C}$ Spectral data of 4-chloro-3-iodo-1-isopropyl-1*H*-pyrrolo[2,3-*b*]pyridine



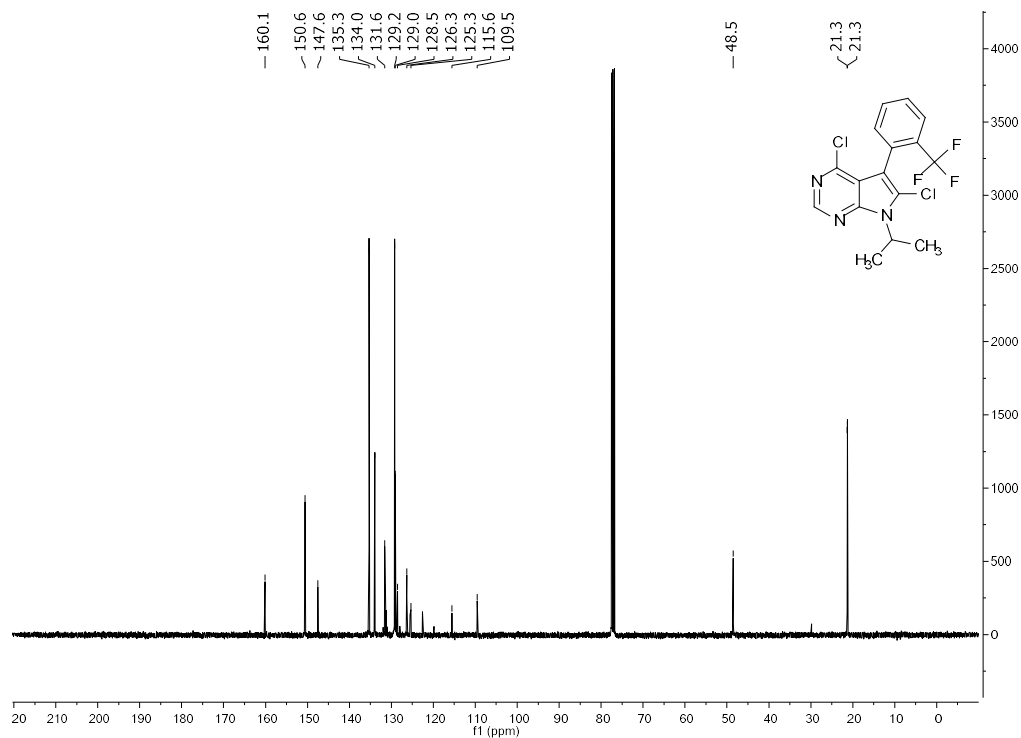
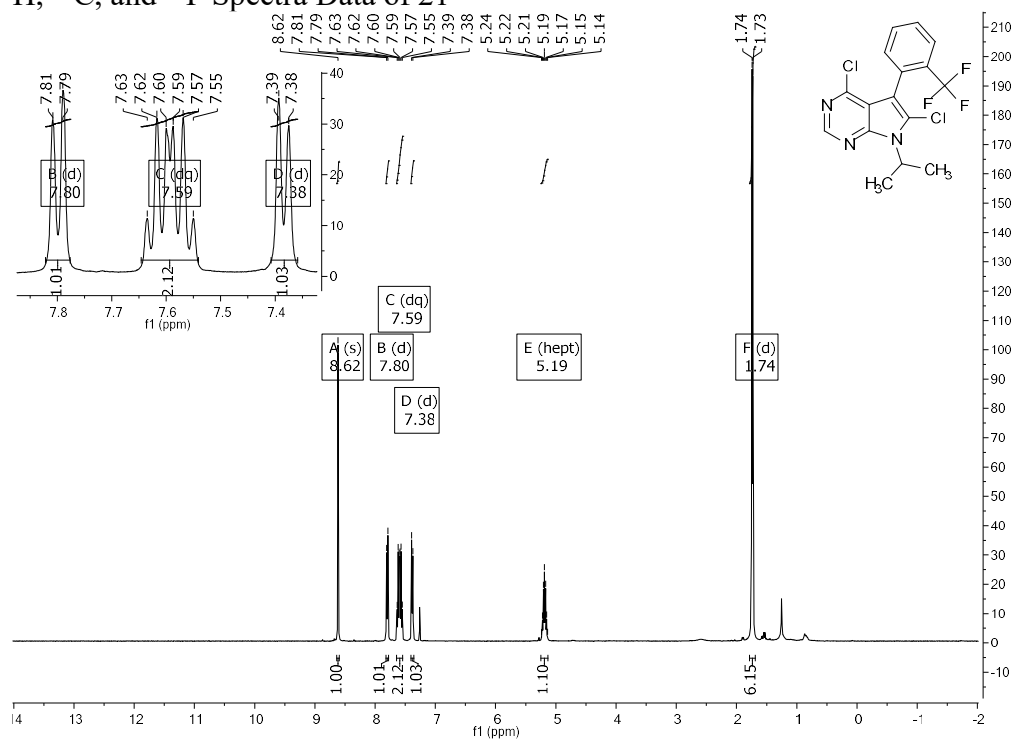


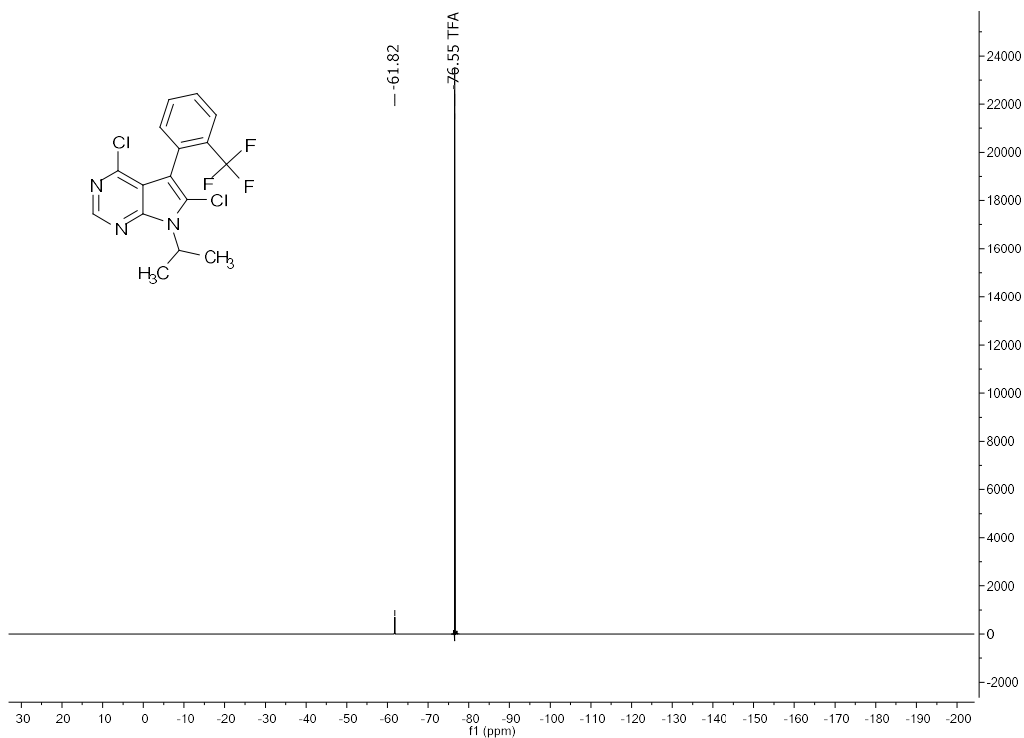
^1H , ^{13}C , and ^{19}F Spectral data of 4-chloro-1-isopropyl-3-(2-(trifluoromethyl)phenyl)-1H-pyrrolo[2,3-b]pyridine



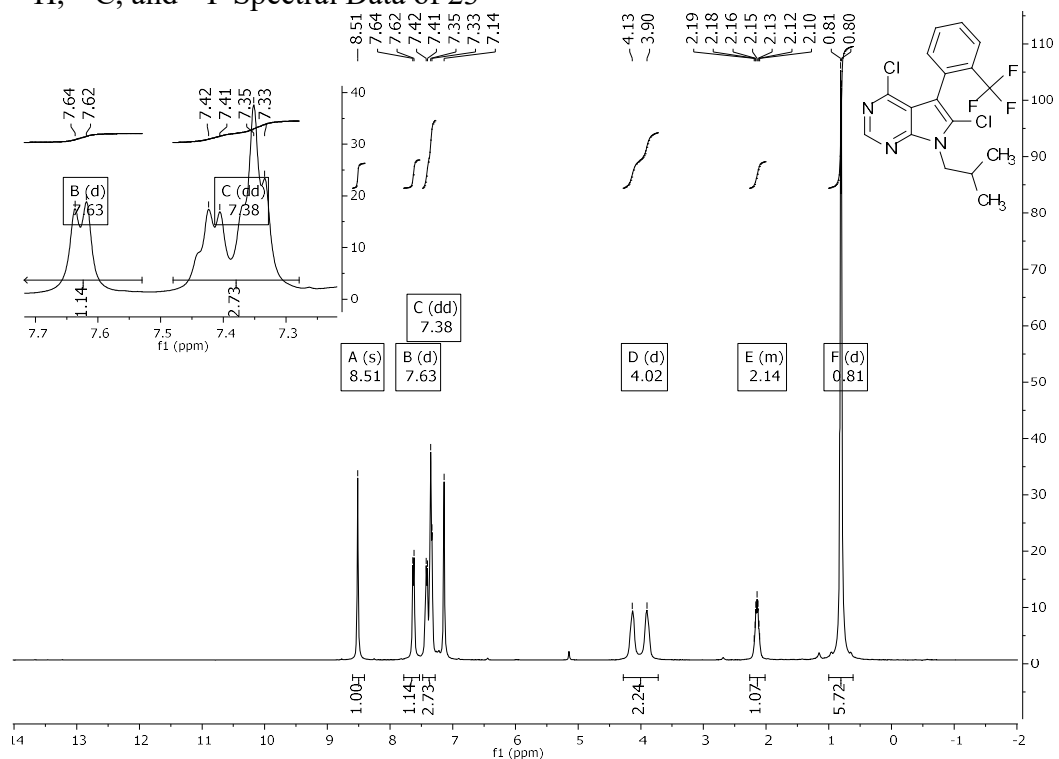


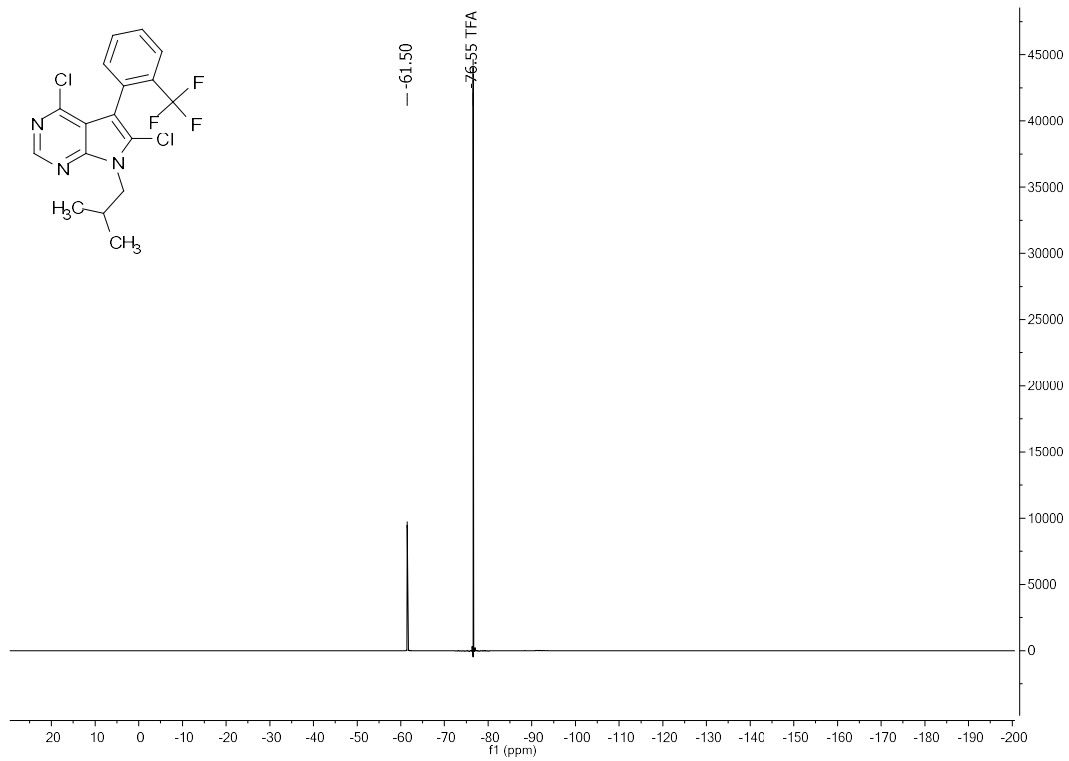
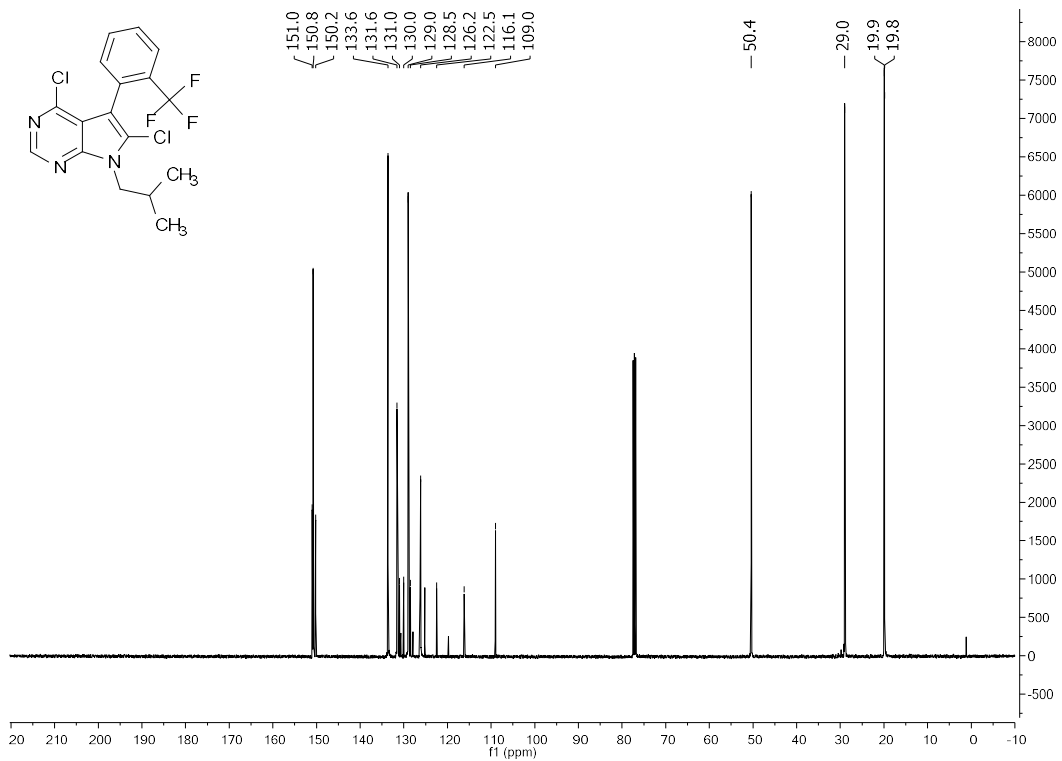
^1H , ^{13}C , and ^{19}F Spectra Data of 21



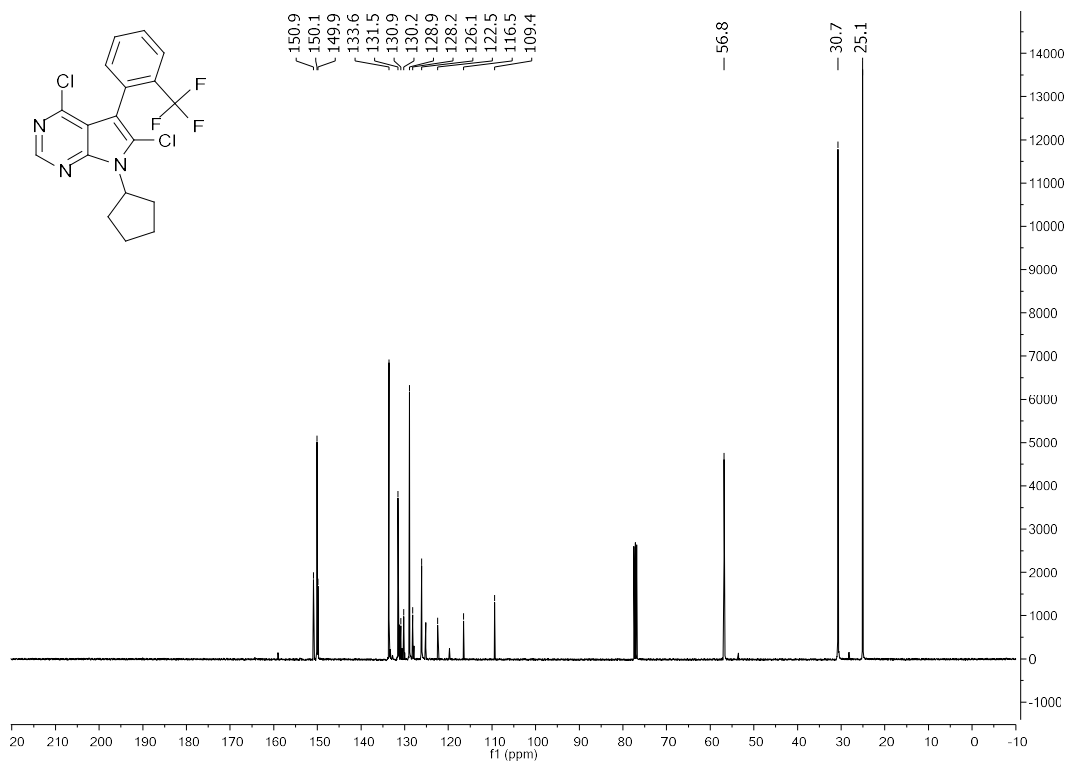
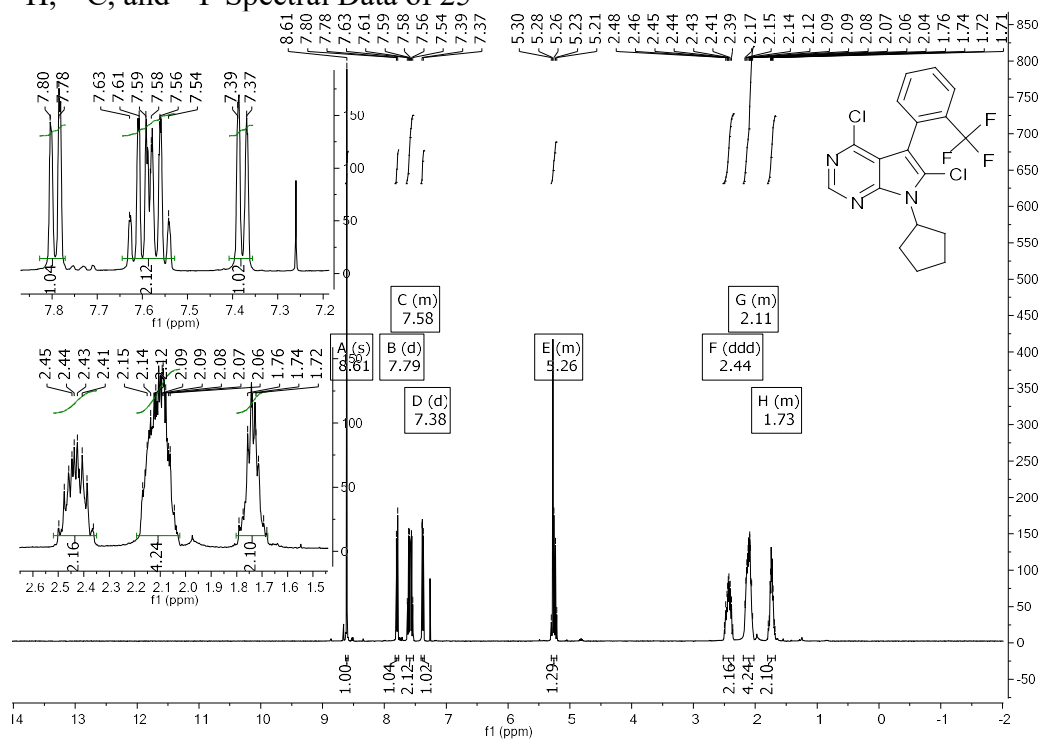


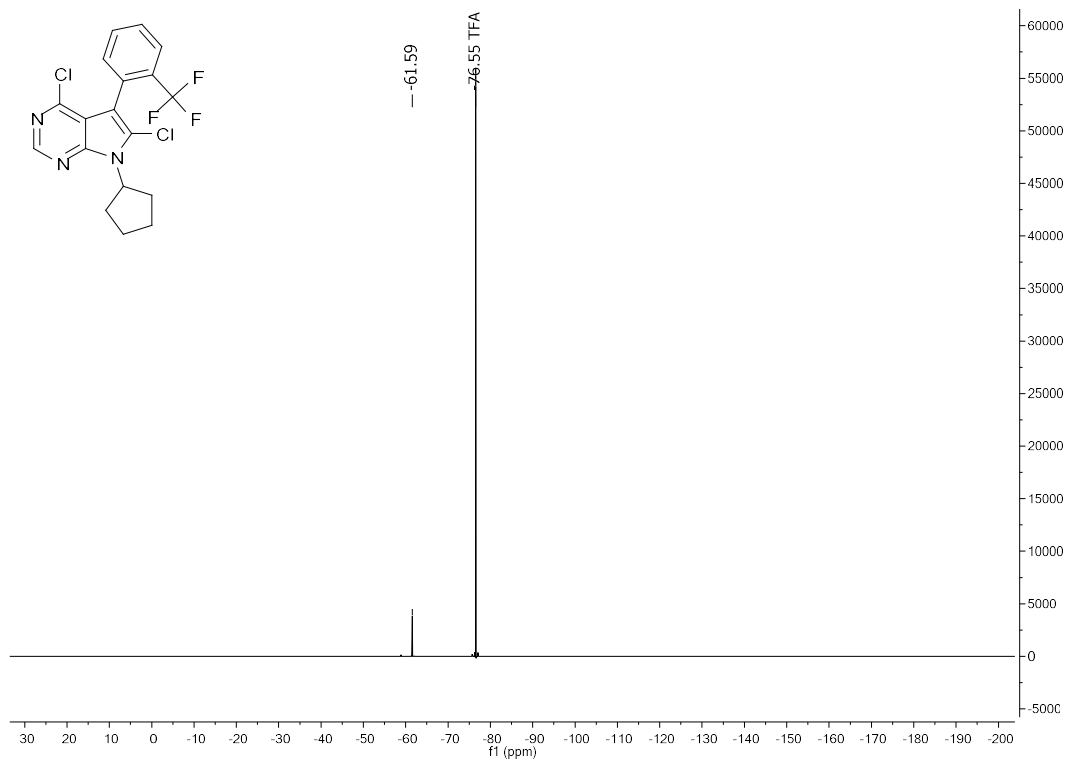
¹H, ¹³C, and ¹⁹F Spectral Data of 23



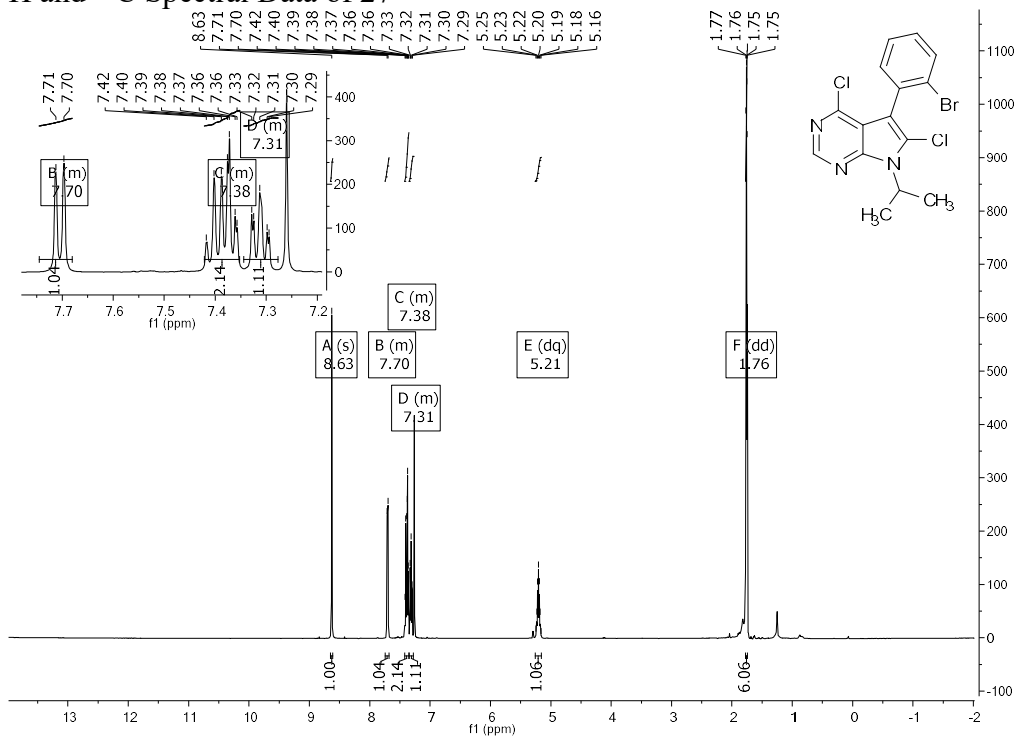


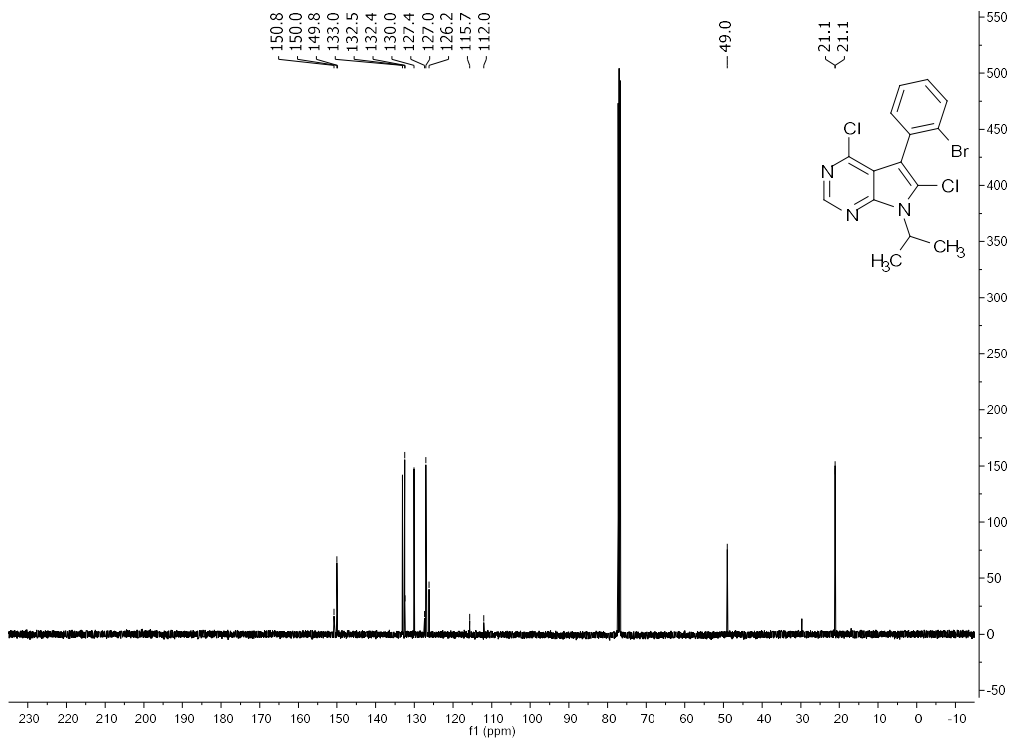
¹H, ¹³C, and ¹⁹F Spectral Data of 25



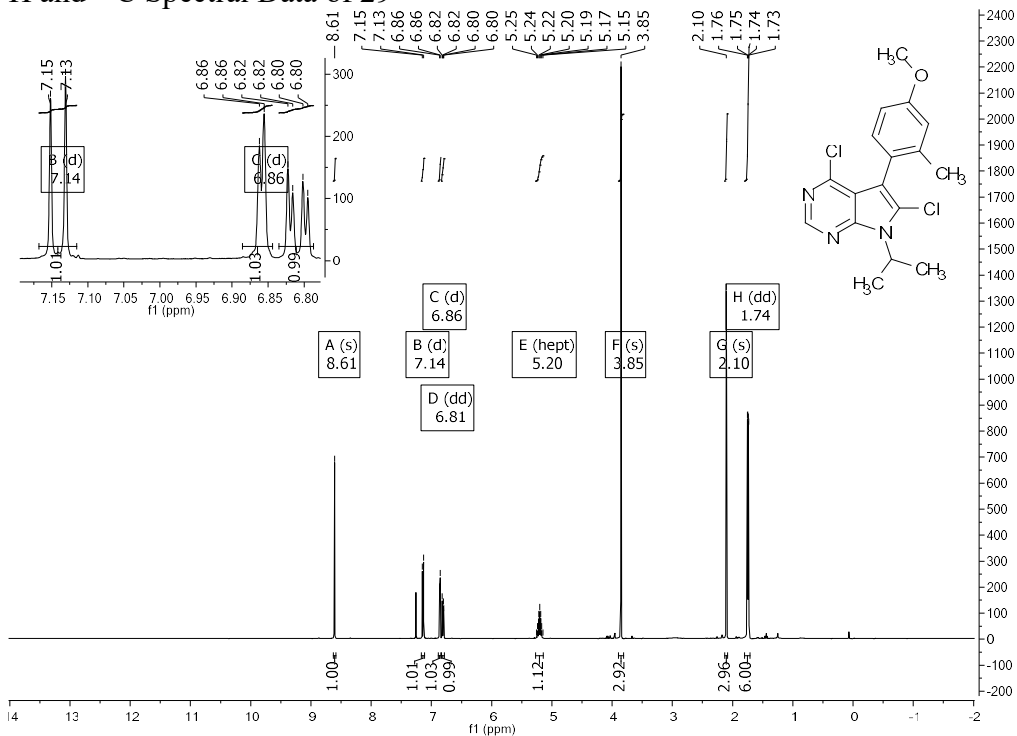


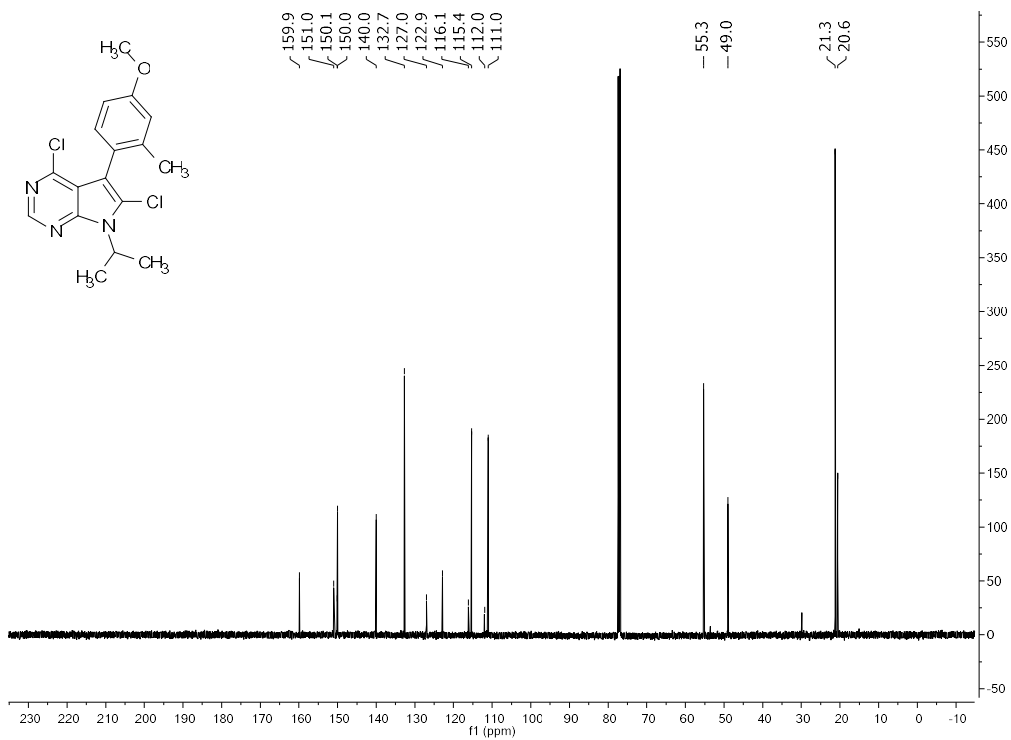
¹H and ¹³C Spectral Data of 27



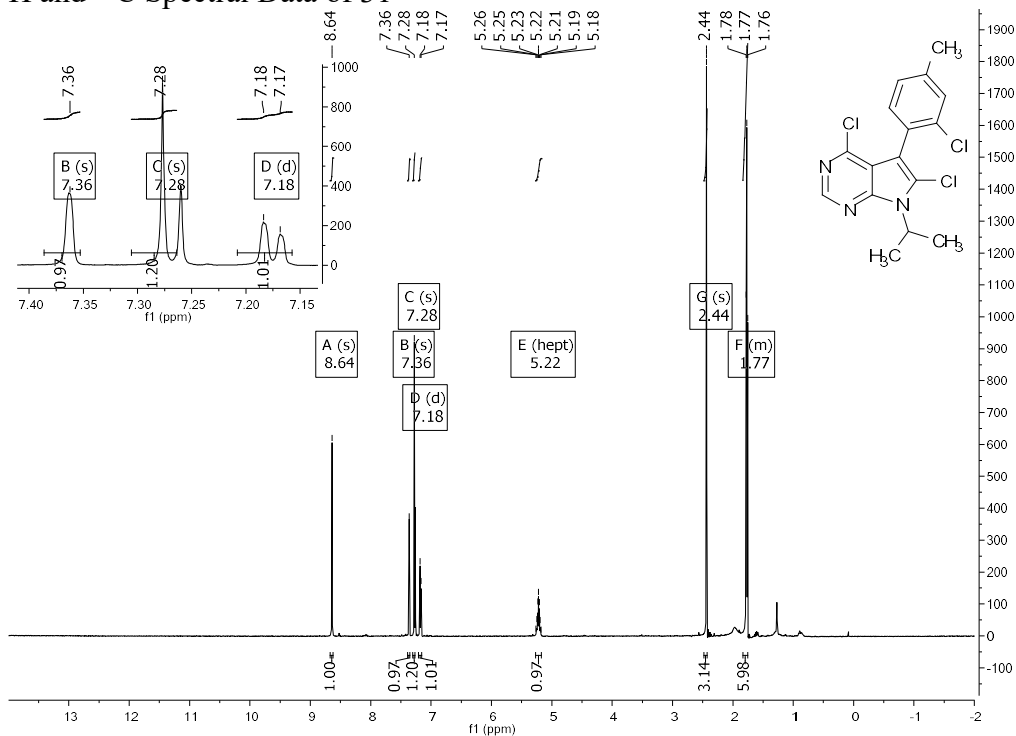


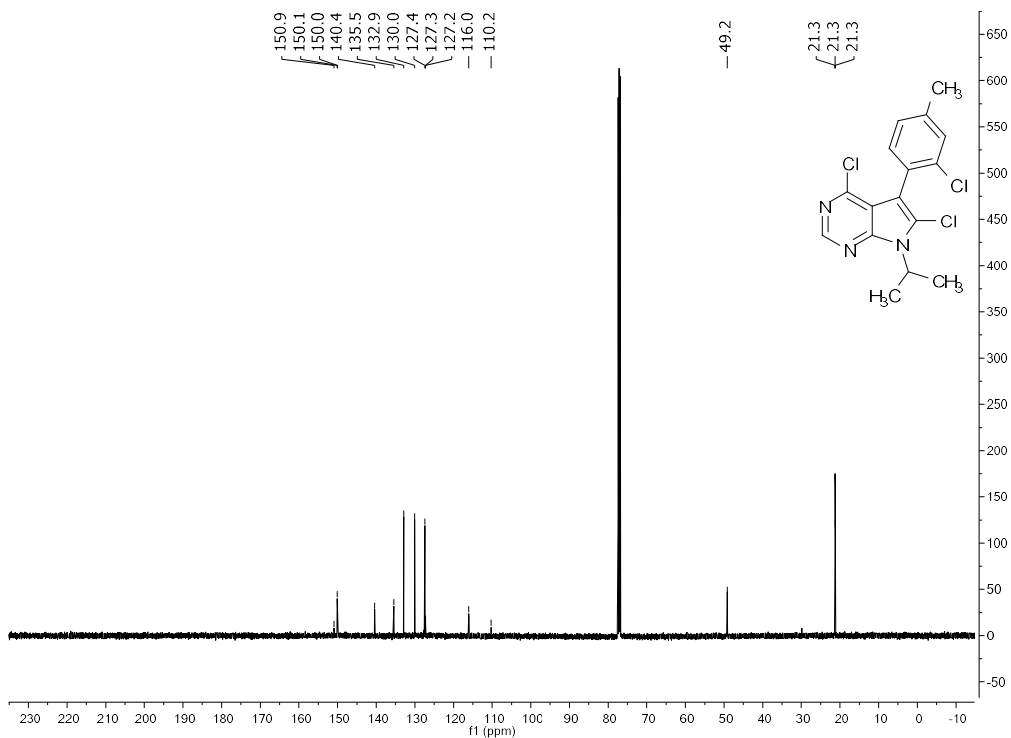
¹H and ¹³C Spectral Data of 29



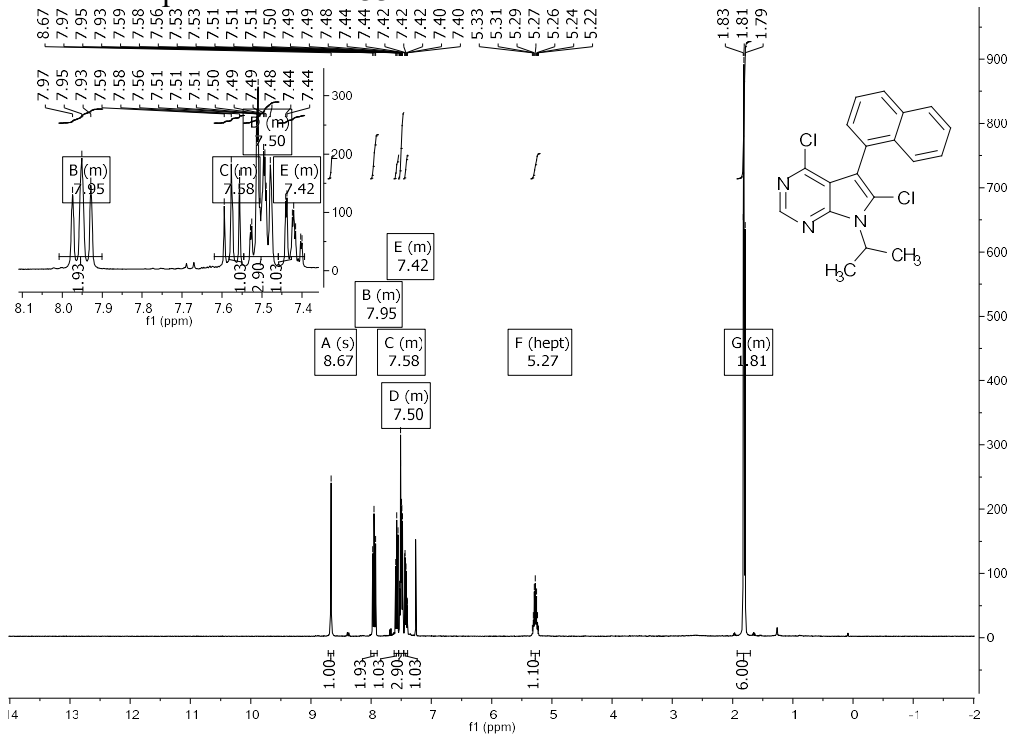


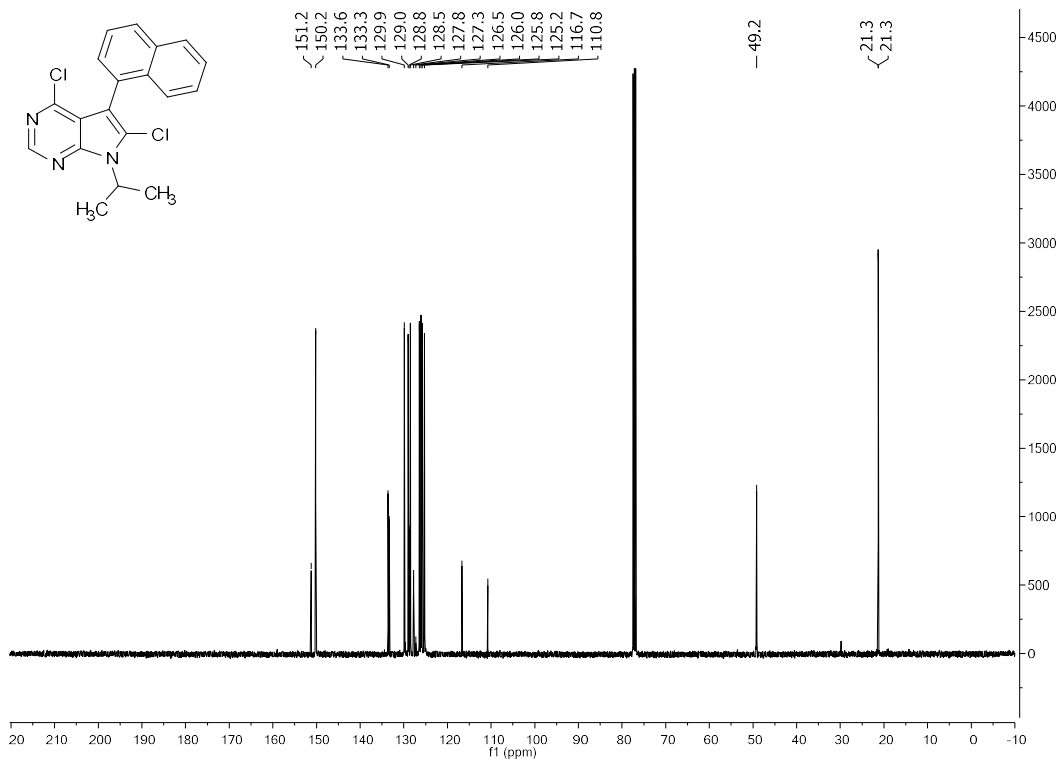
¹H and ¹³C Spectral Data of 31



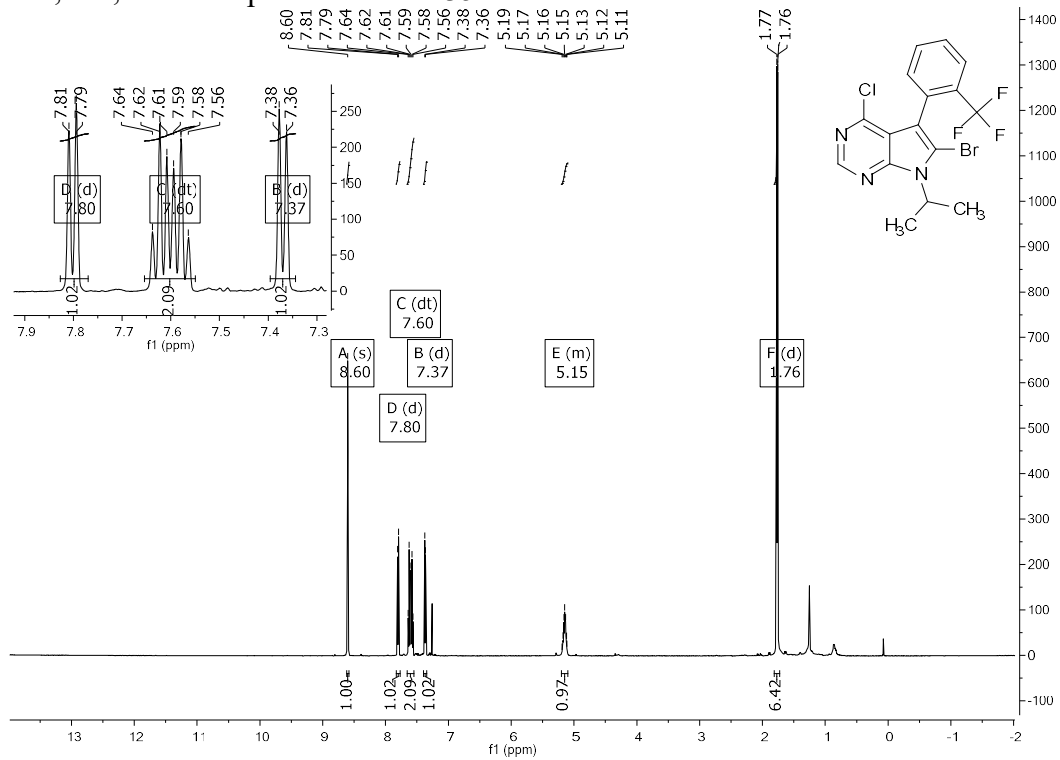


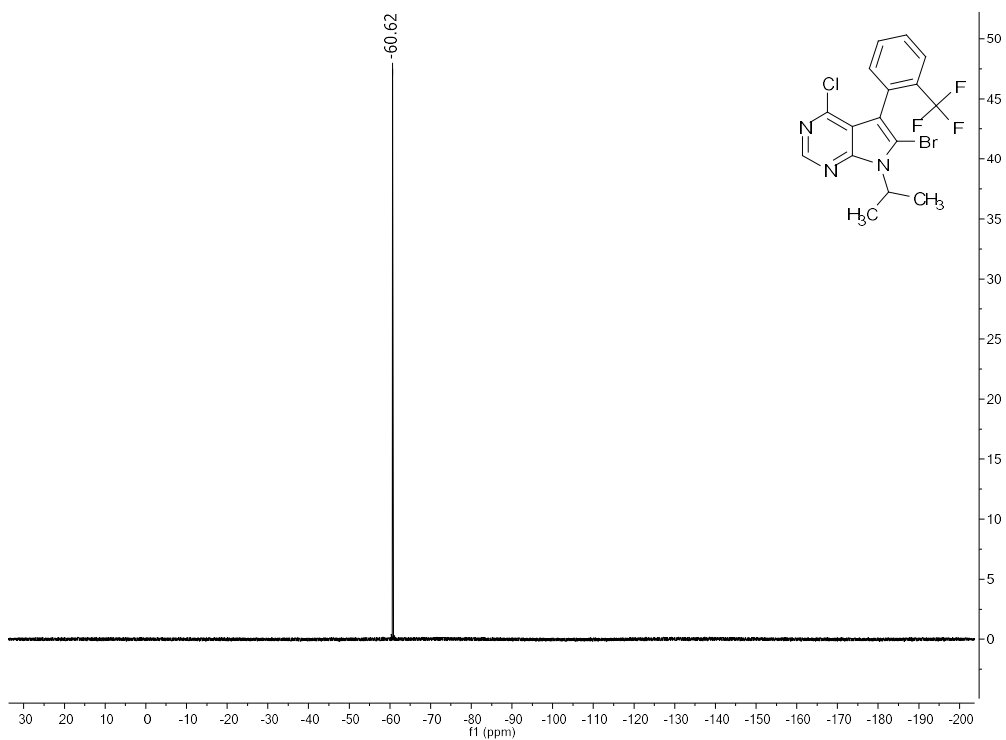
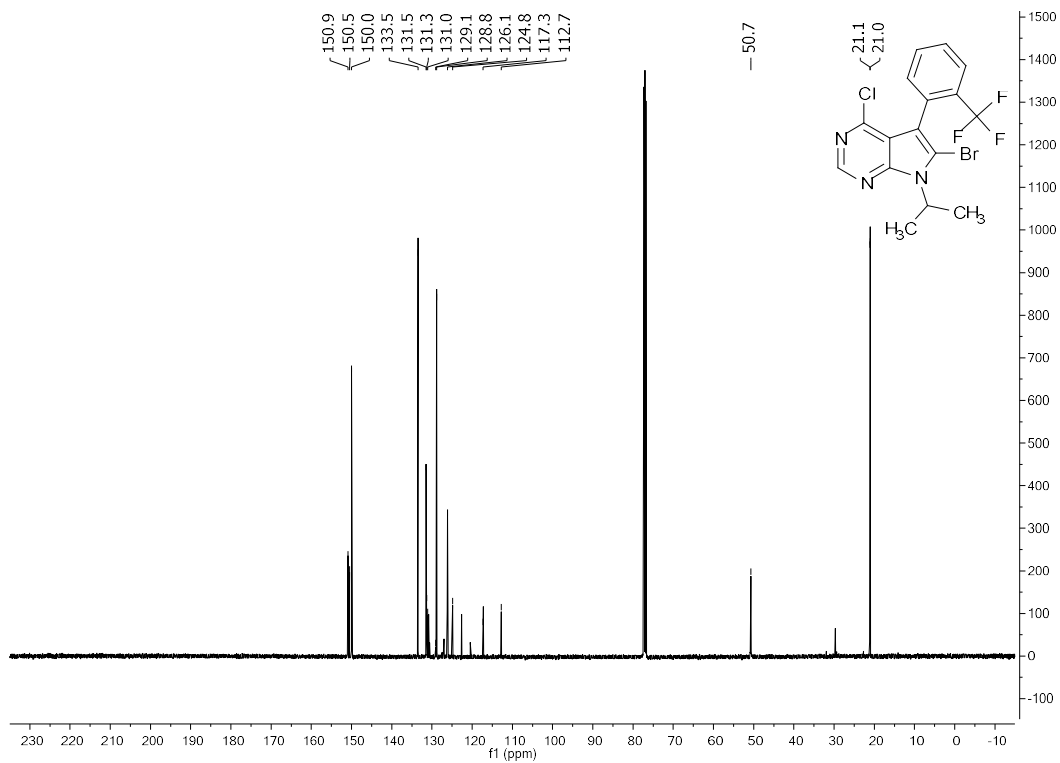
¹H and ¹³C Spectral Data of 33



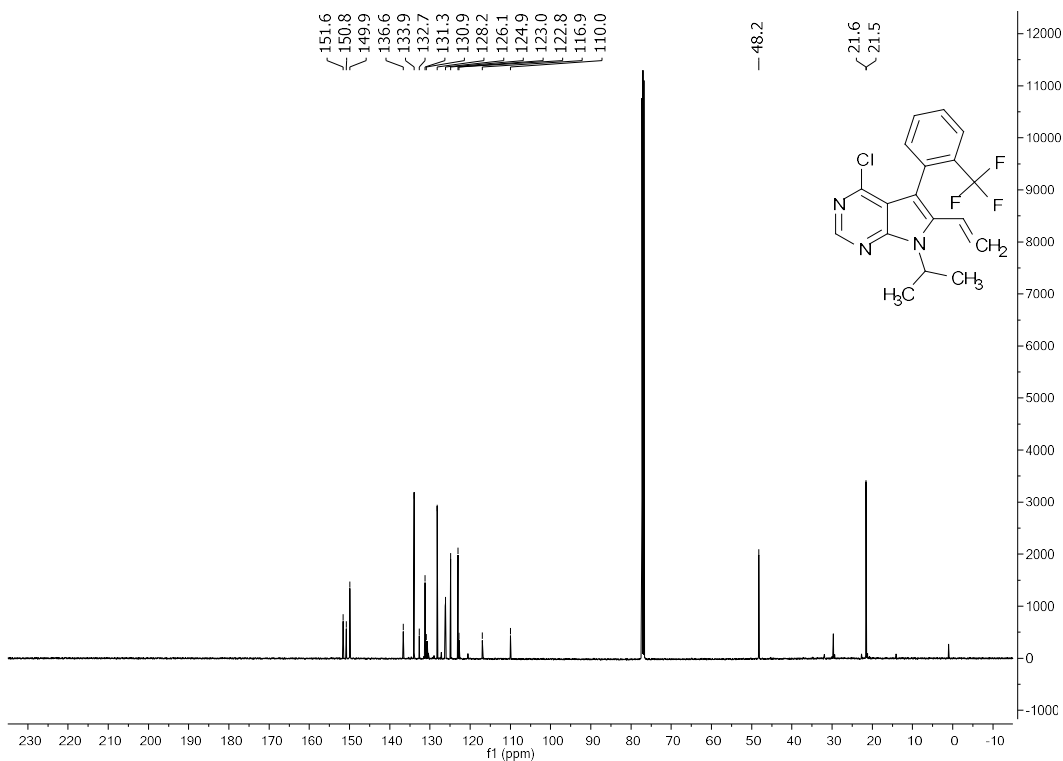
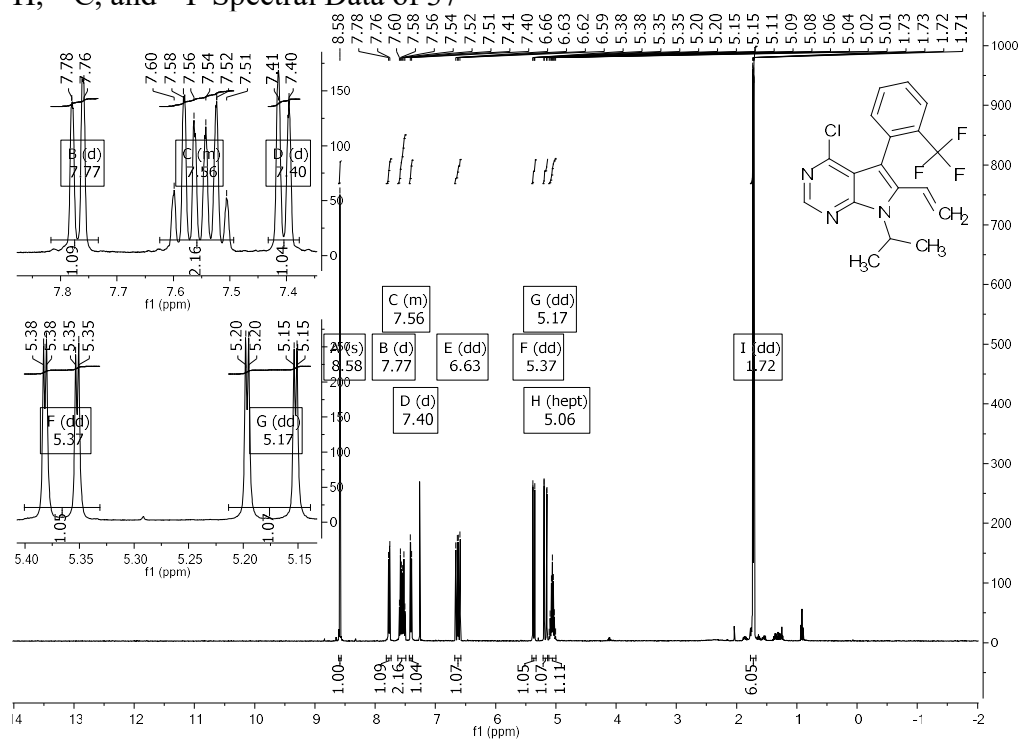


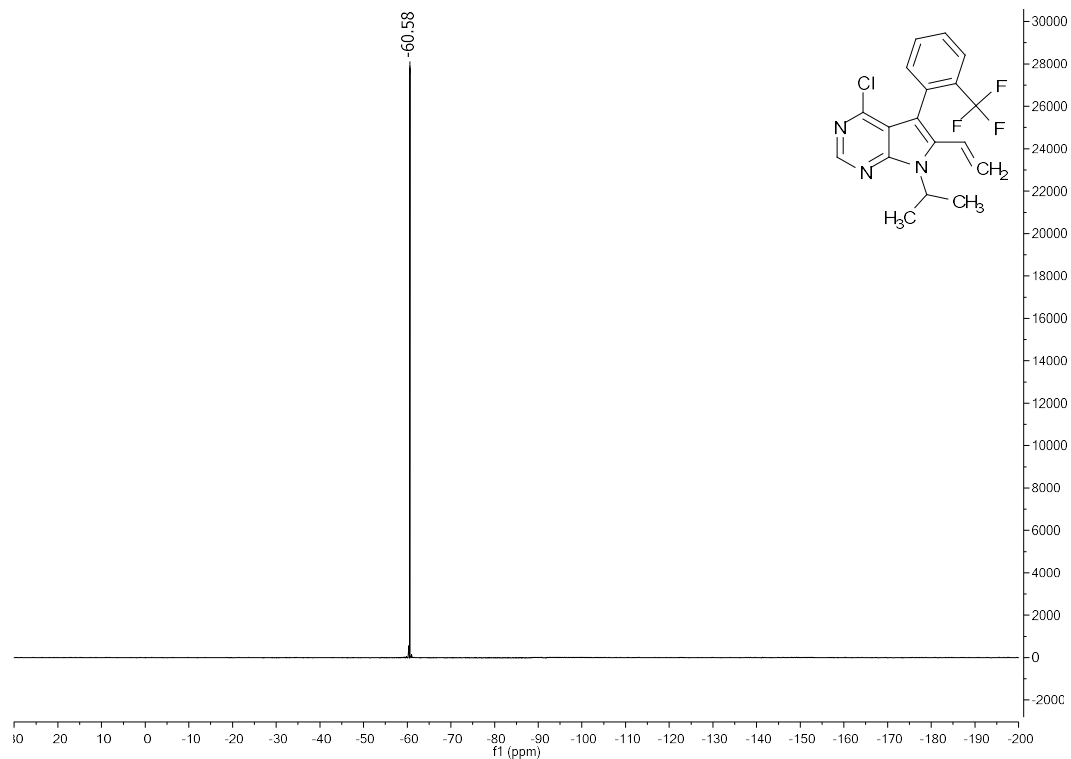
¹H, ¹³C, and ¹⁹F Spectral Data of 35



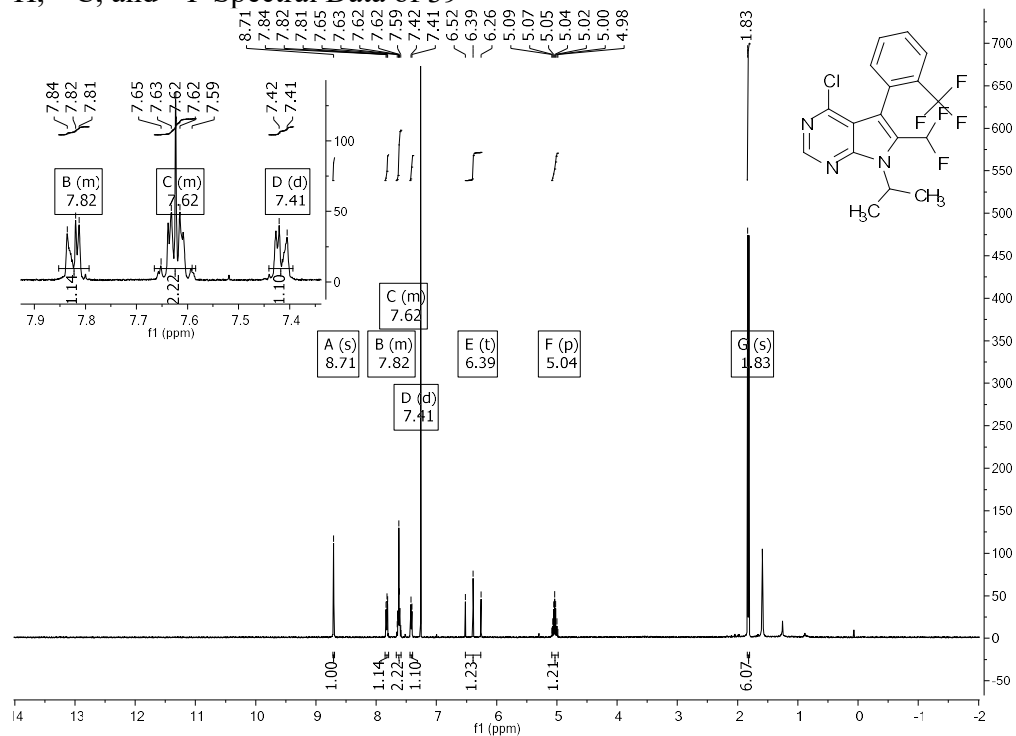


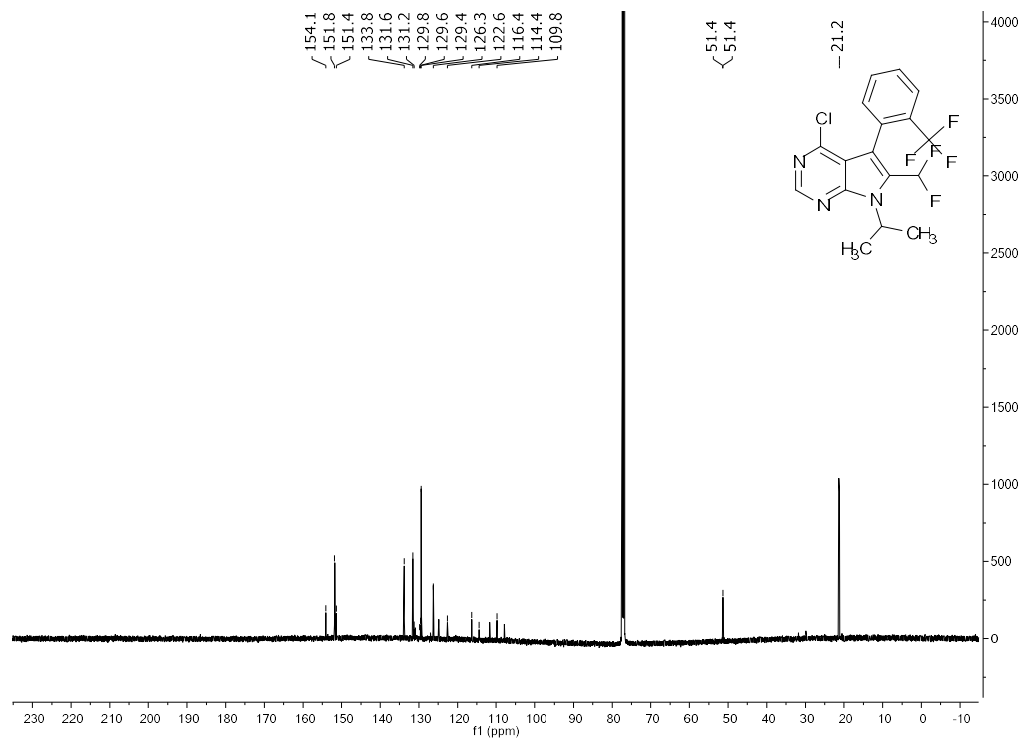
^1H , ^{13}C , and ^{19}F Spectral Data of 37



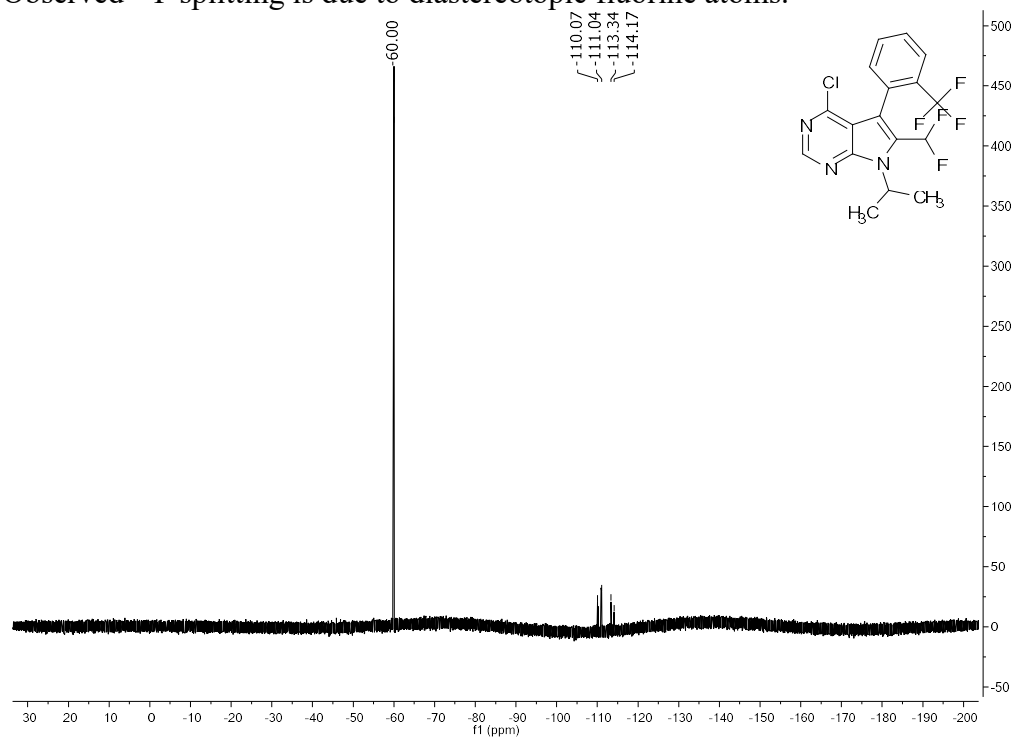


^1H , ^{13}C , and ^{19}F Spectral Data of 39

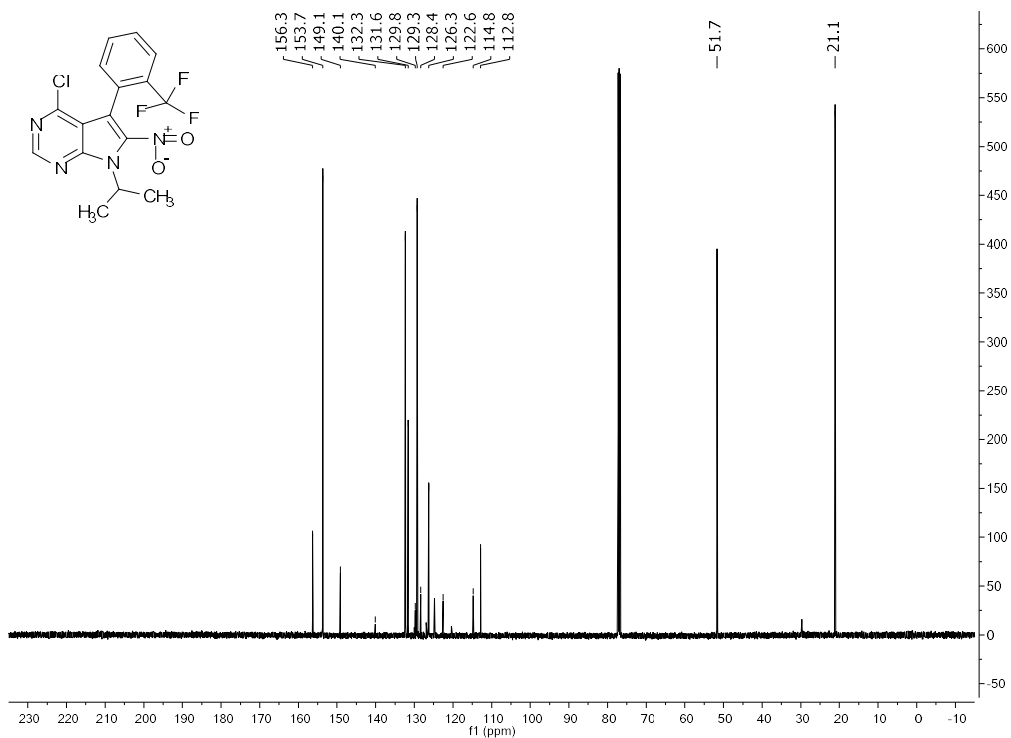
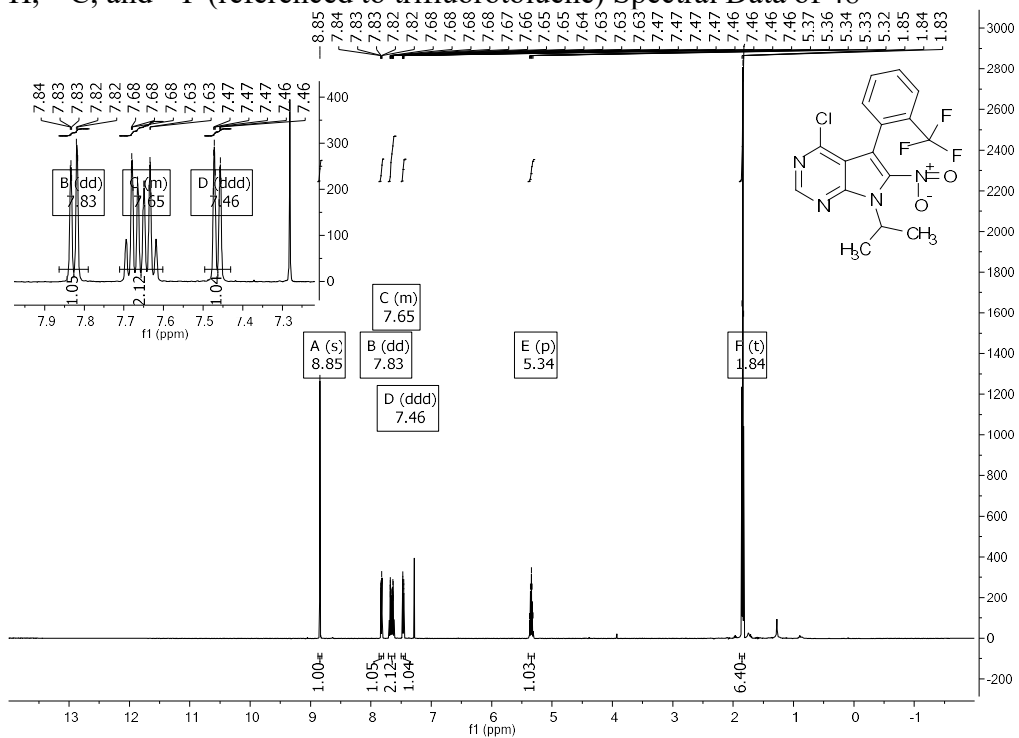


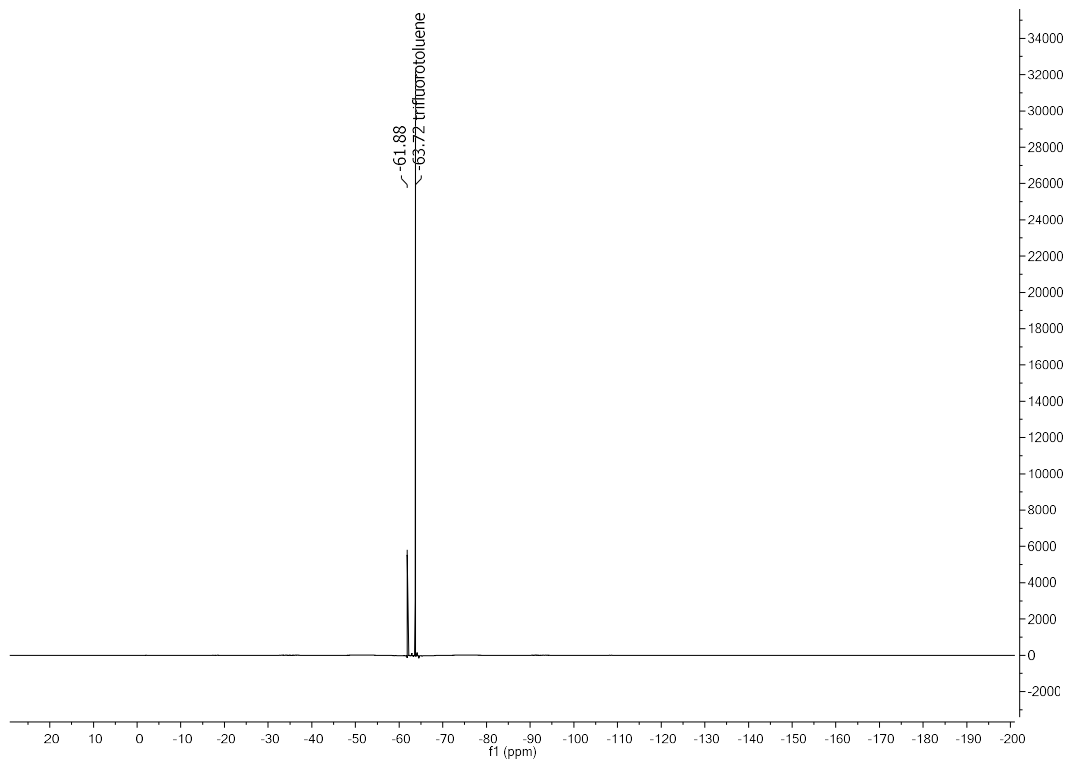


Observed ^{19}F splitting is due to diastereotopic fluorine atoms.

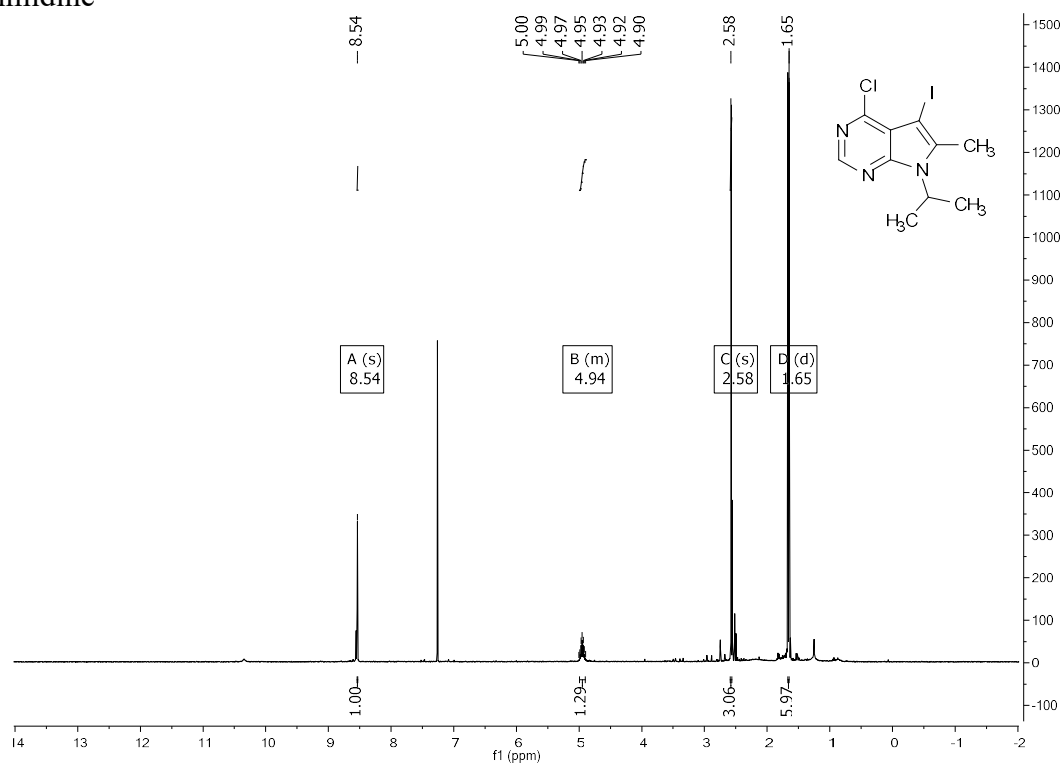


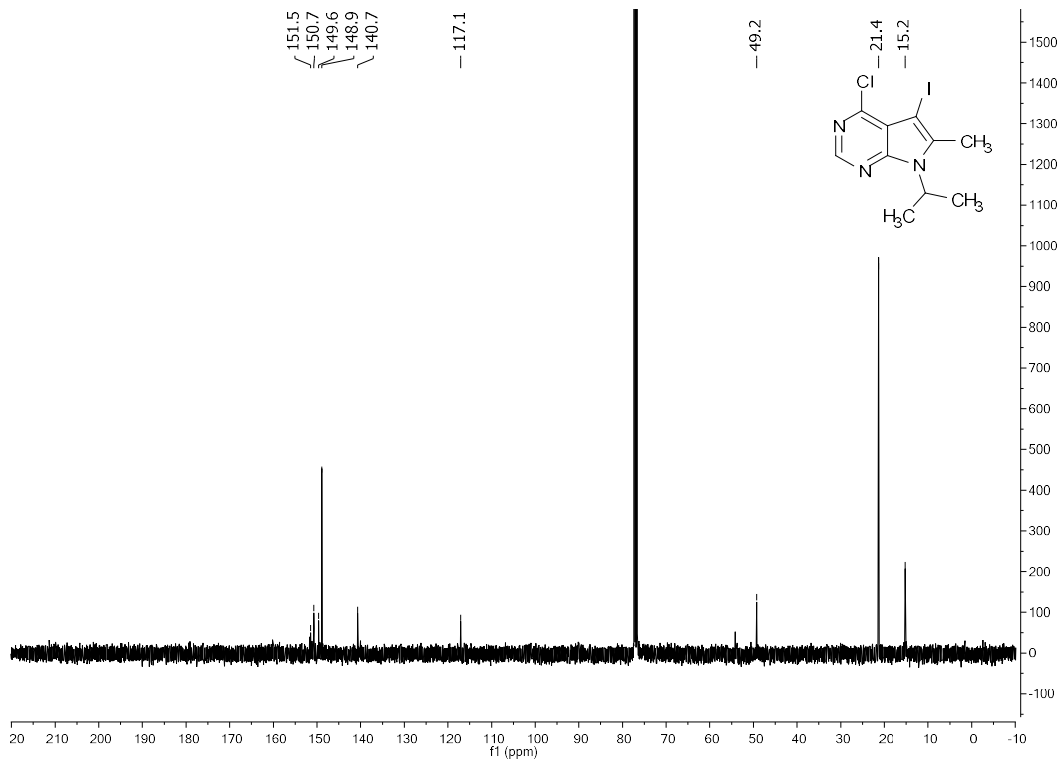
^1H , ^{13}C , and ^{19}F (referenced to trifluorotoluene) Spectral Data of 48



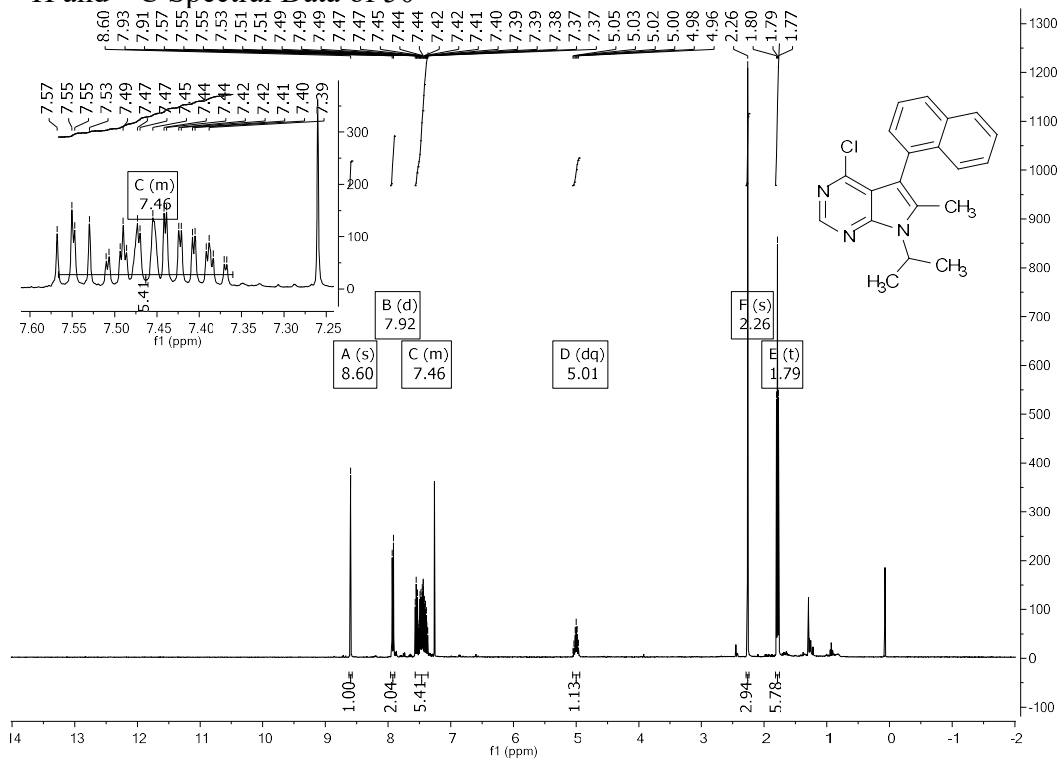


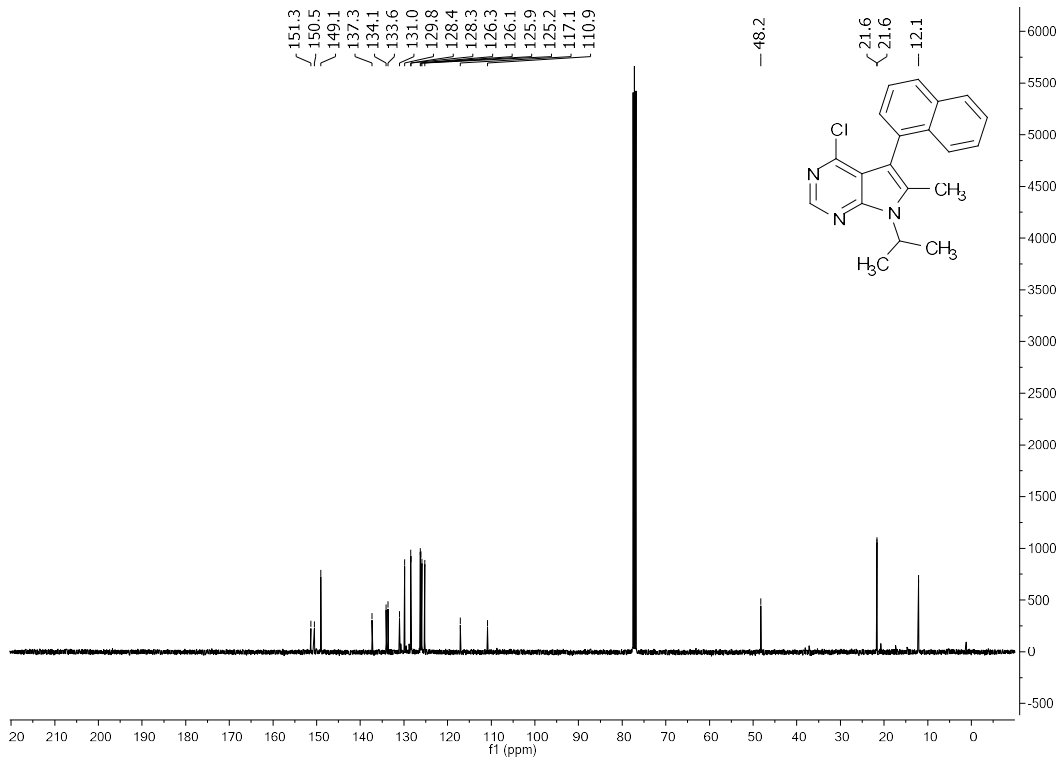
¹H and ¹³C Spectral Data of 4-chloro-5-iodo-7-isopropyl-6-methyl-7H-pyrrolo[2,3-d]pyrimidine



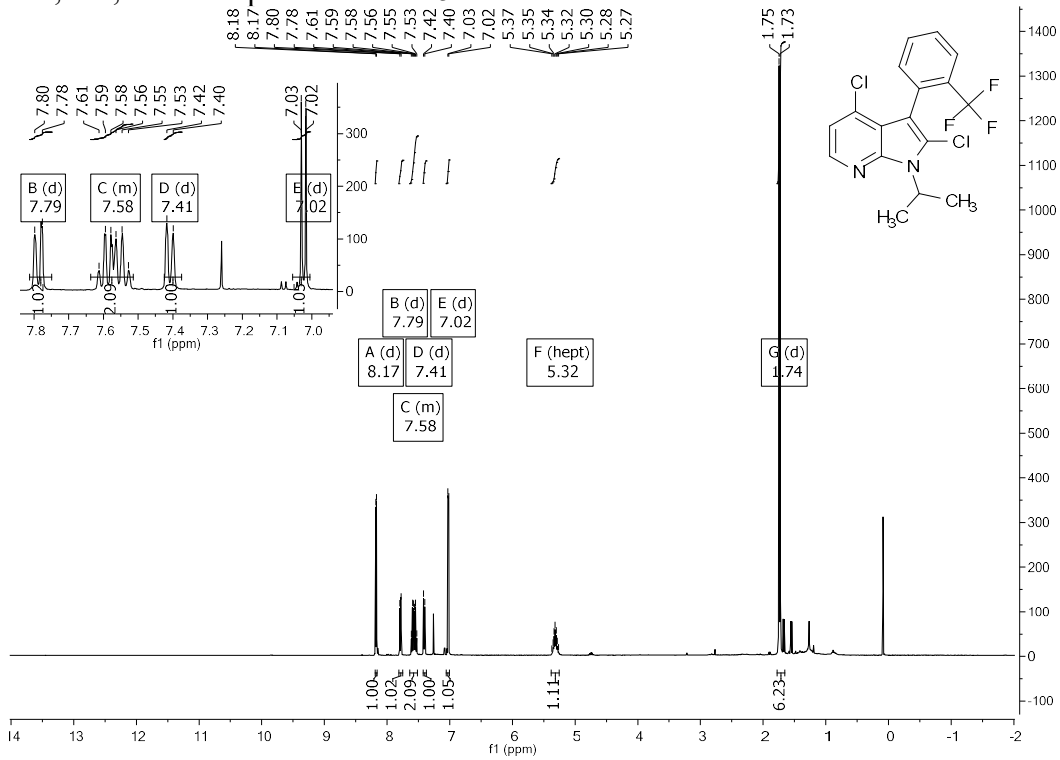


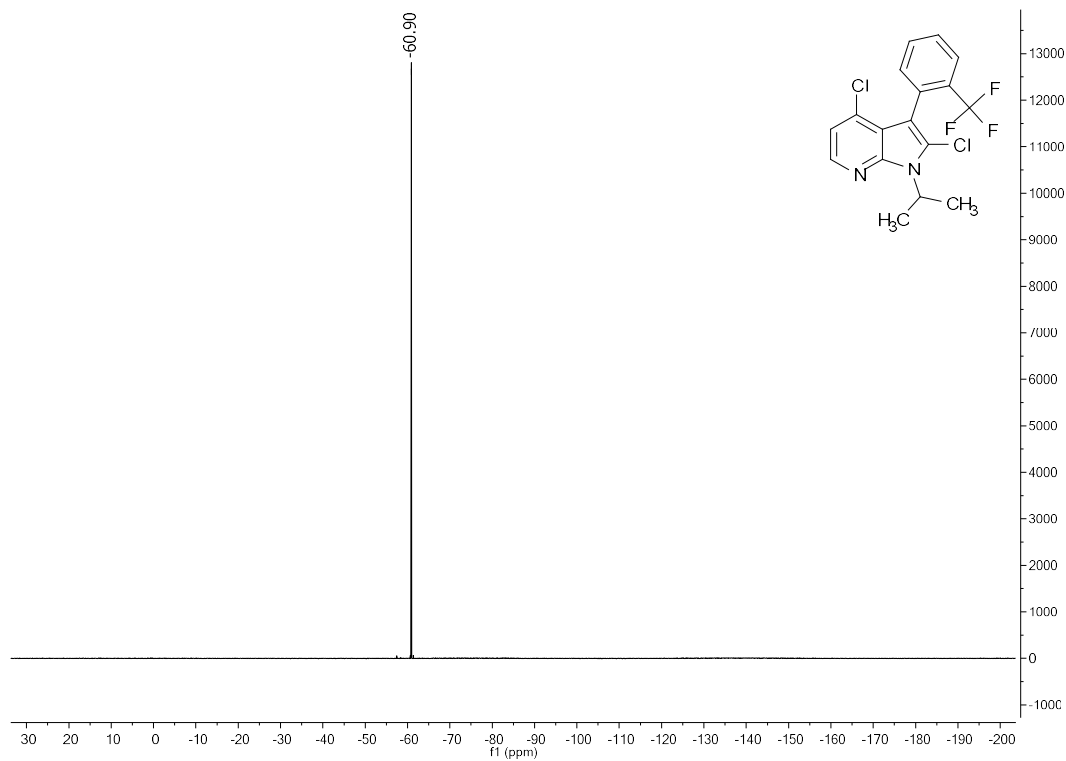
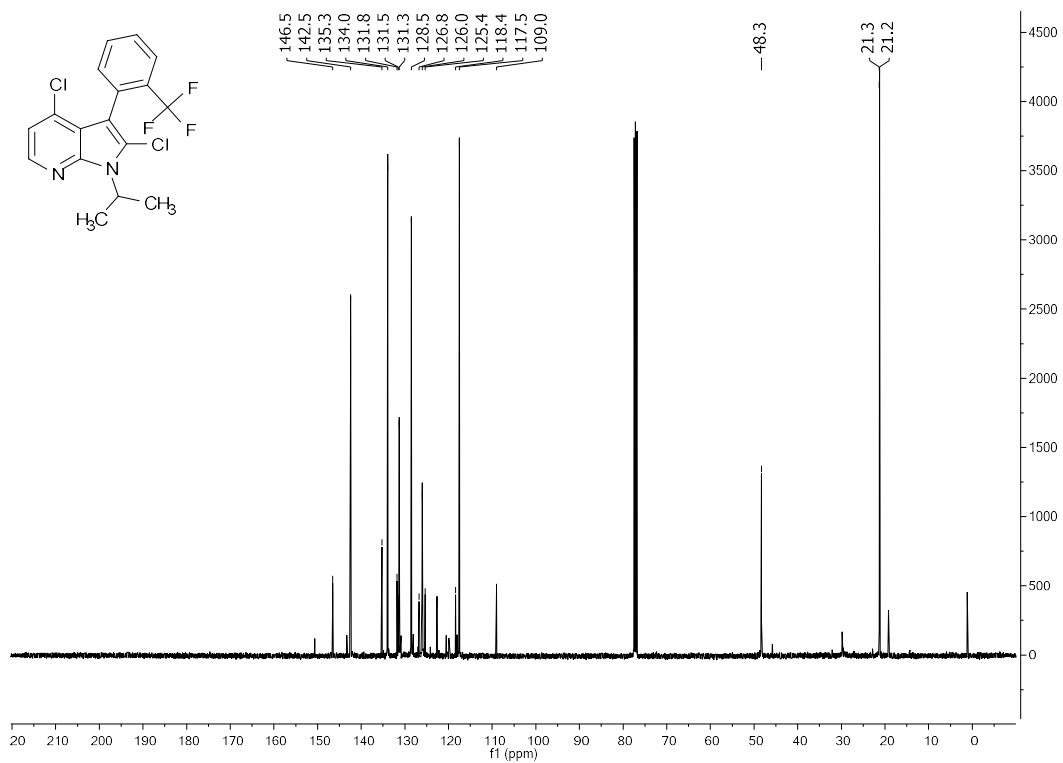
¹H and ¹³C Spectral Data of 50



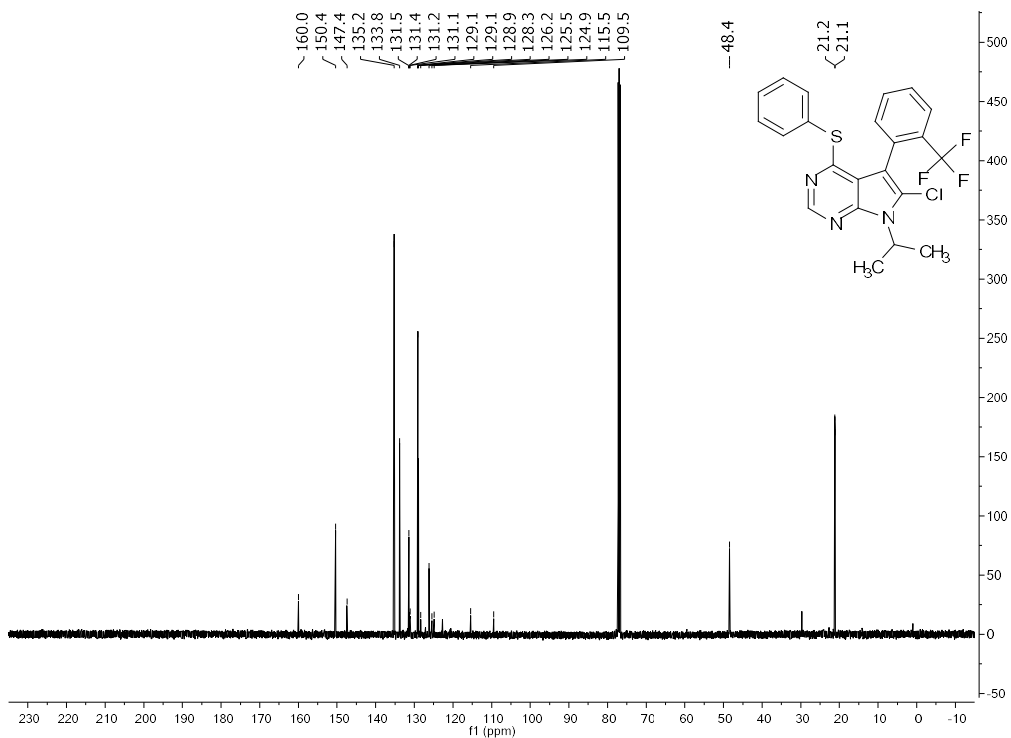
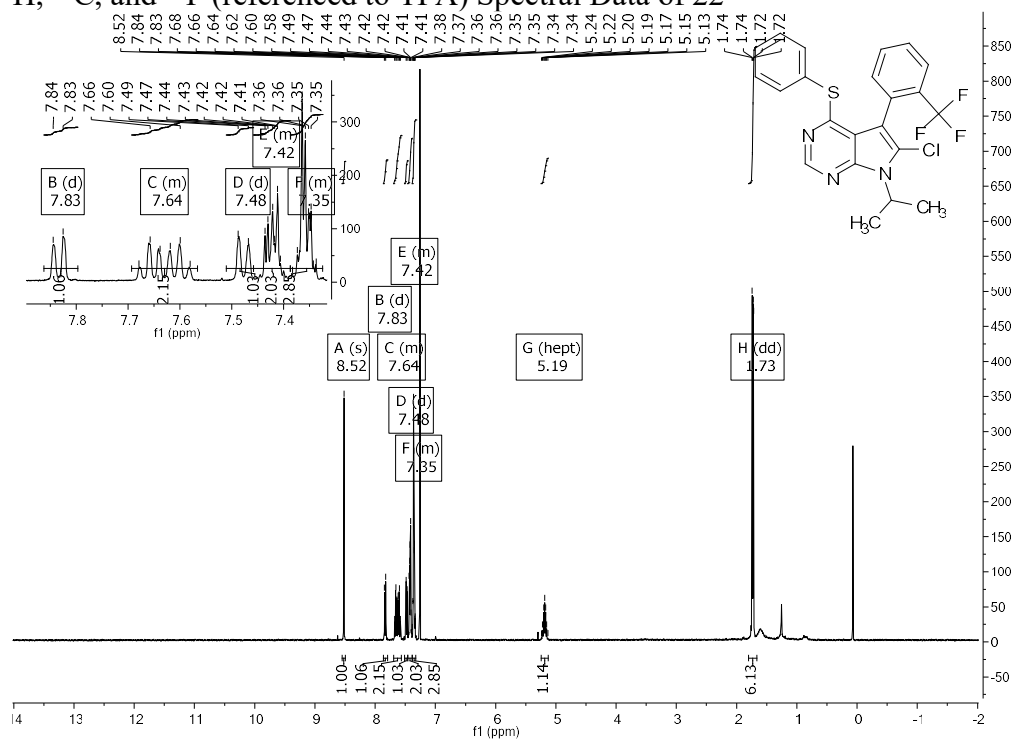


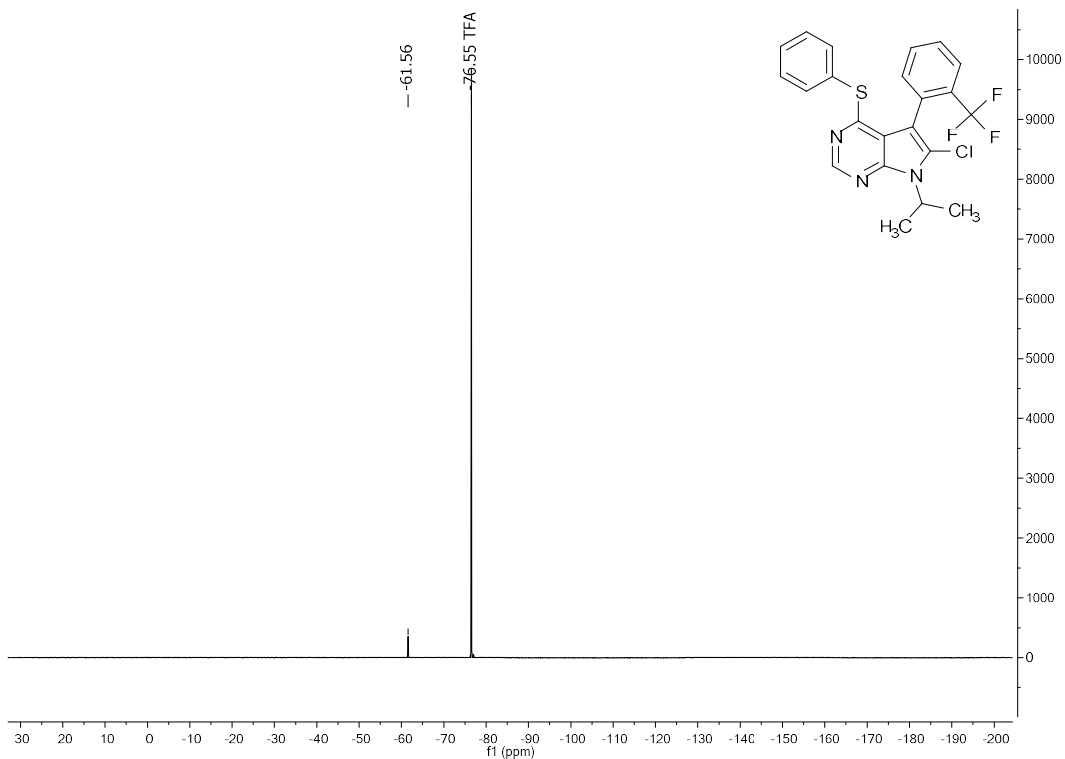
¹H, ¹³C, and ¹⁹F Spectral data of 52



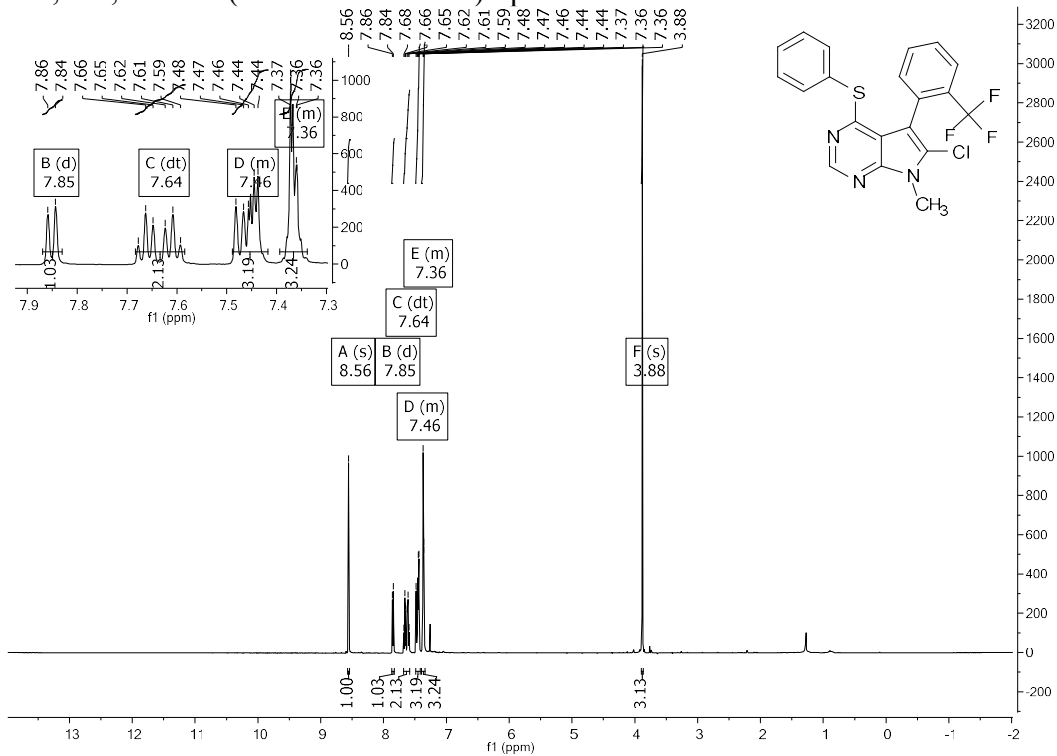


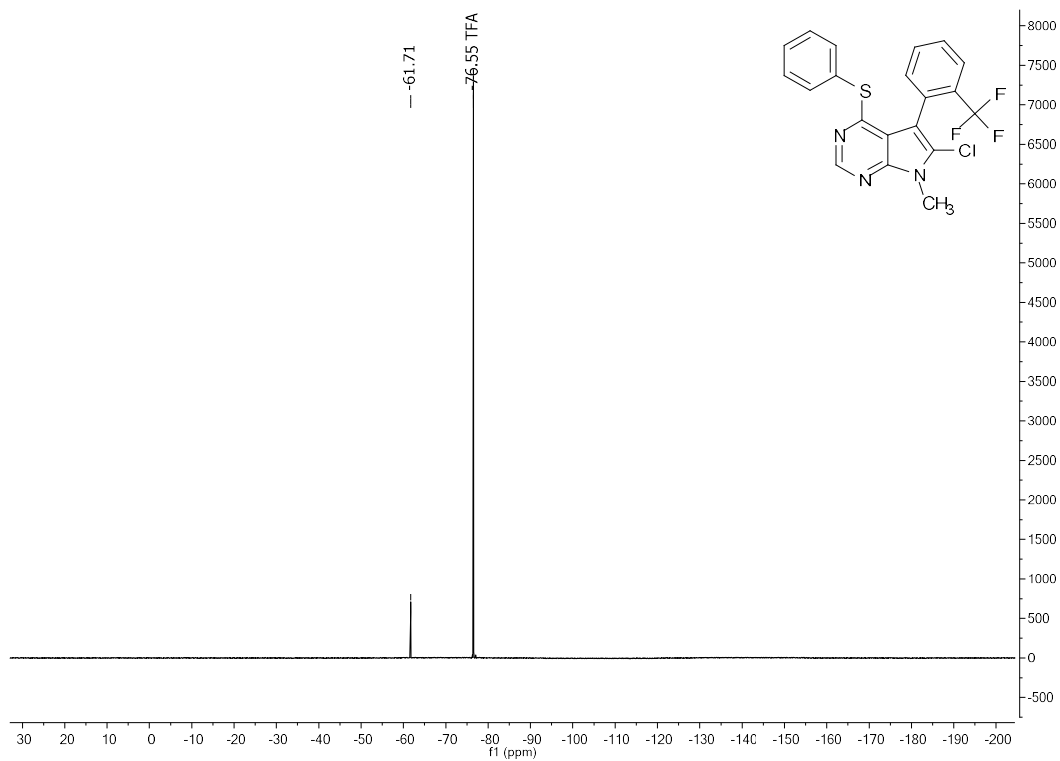
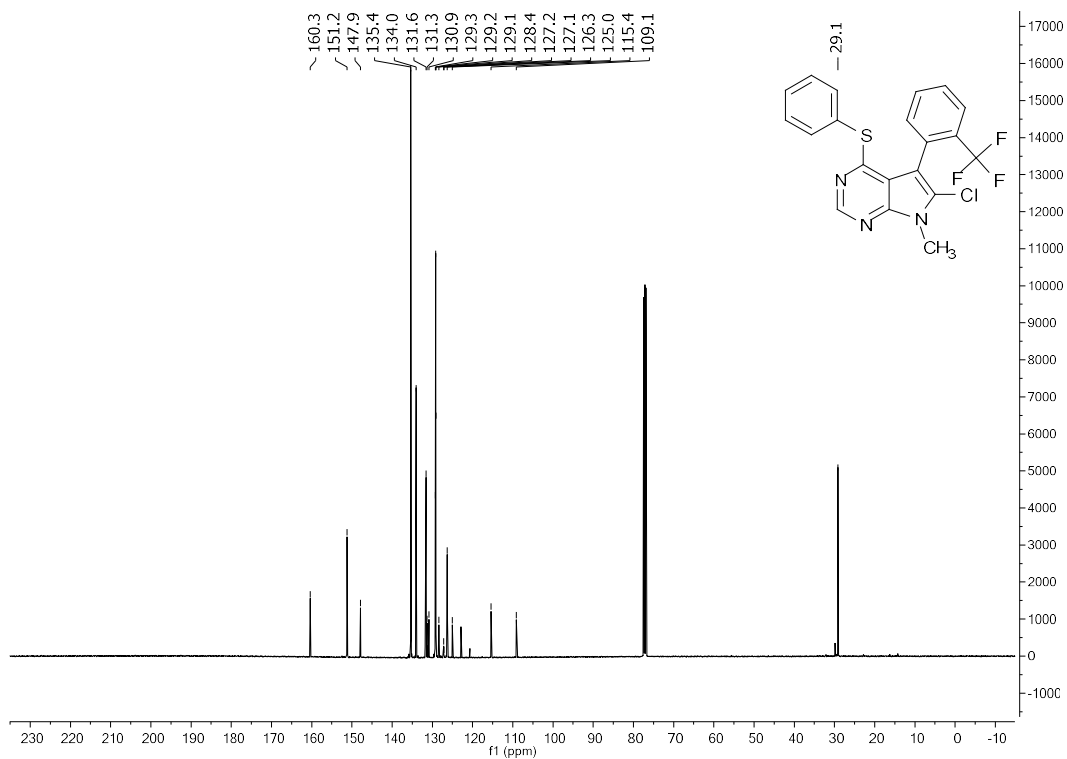
^1H , ^{13}C , and ^{19}F (referenced to TFA) Spectral Data of 22



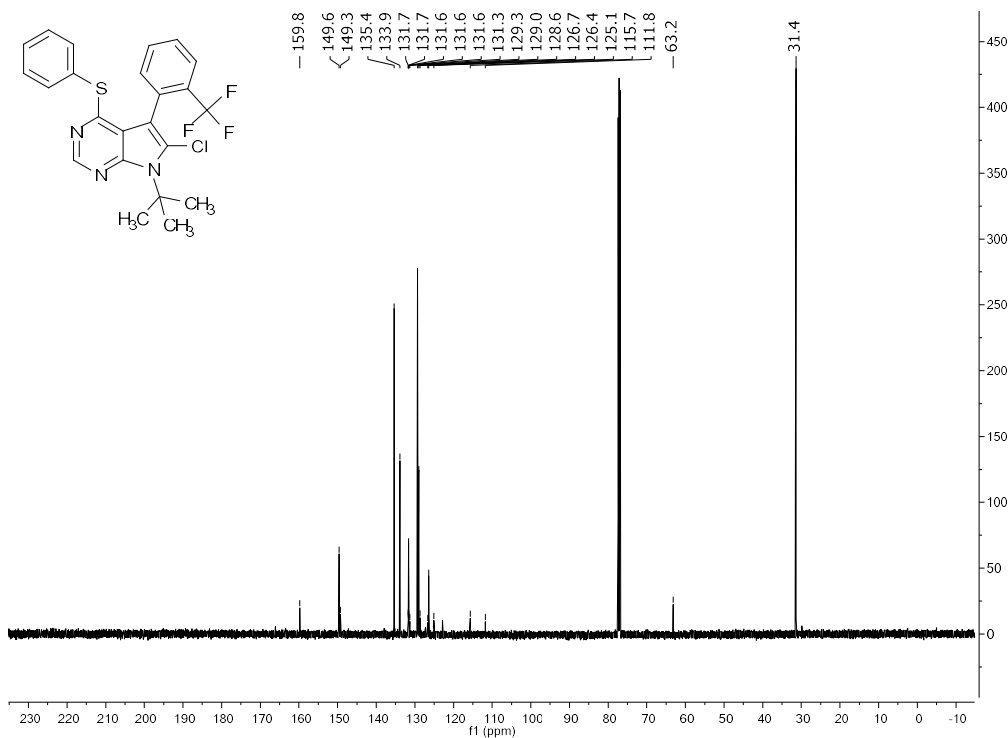
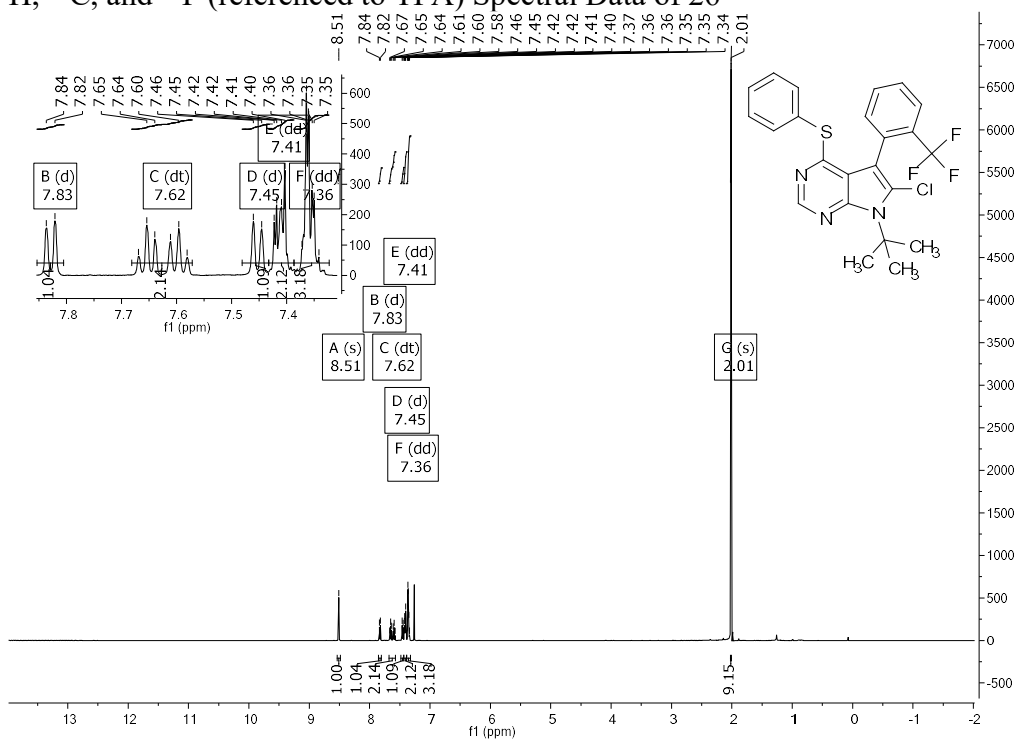


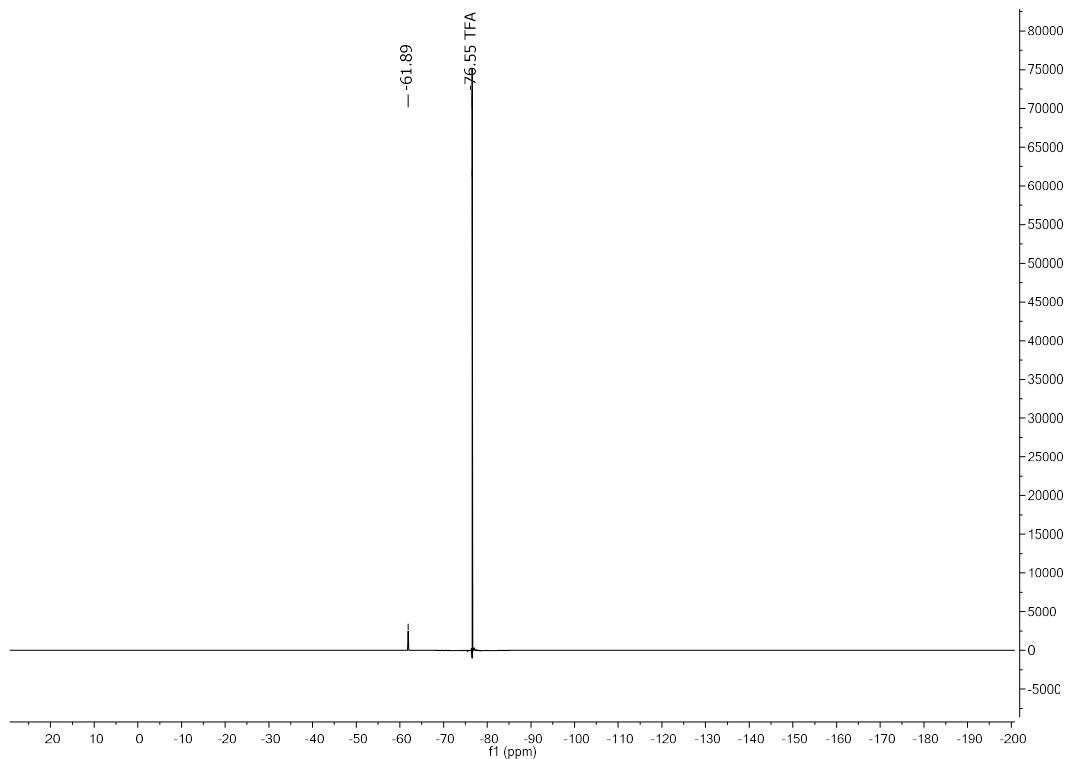
¹H, ¹³C, and ¹⁹F (referenced to TFA) Spectral Data of 24



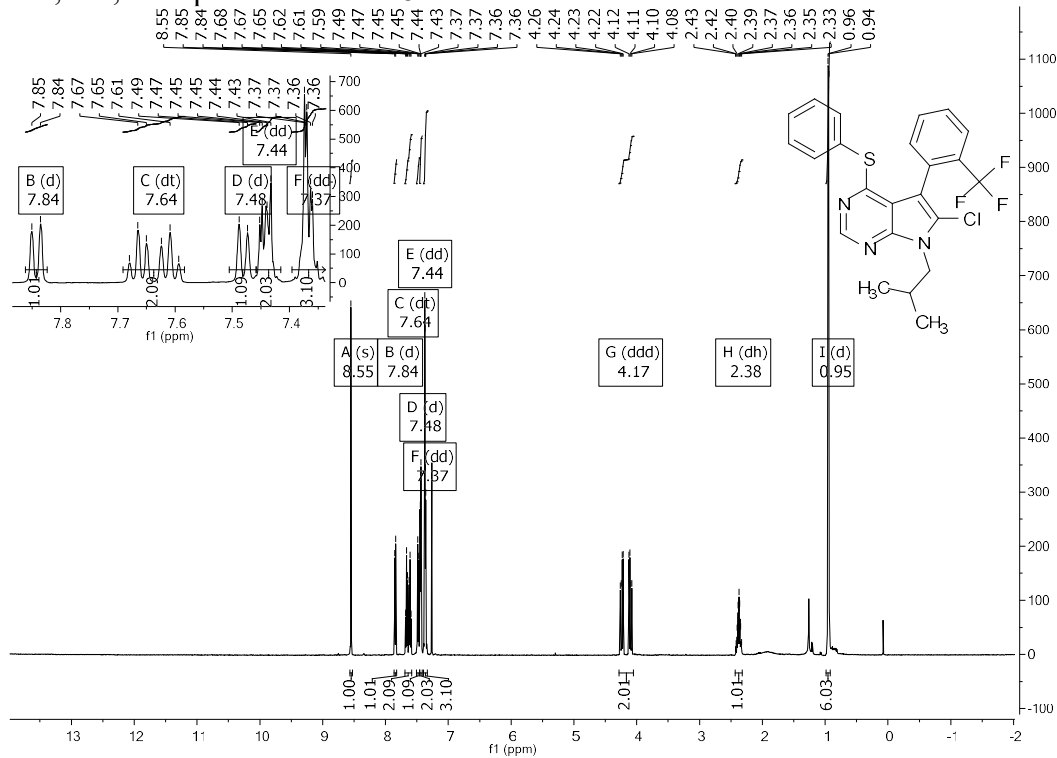


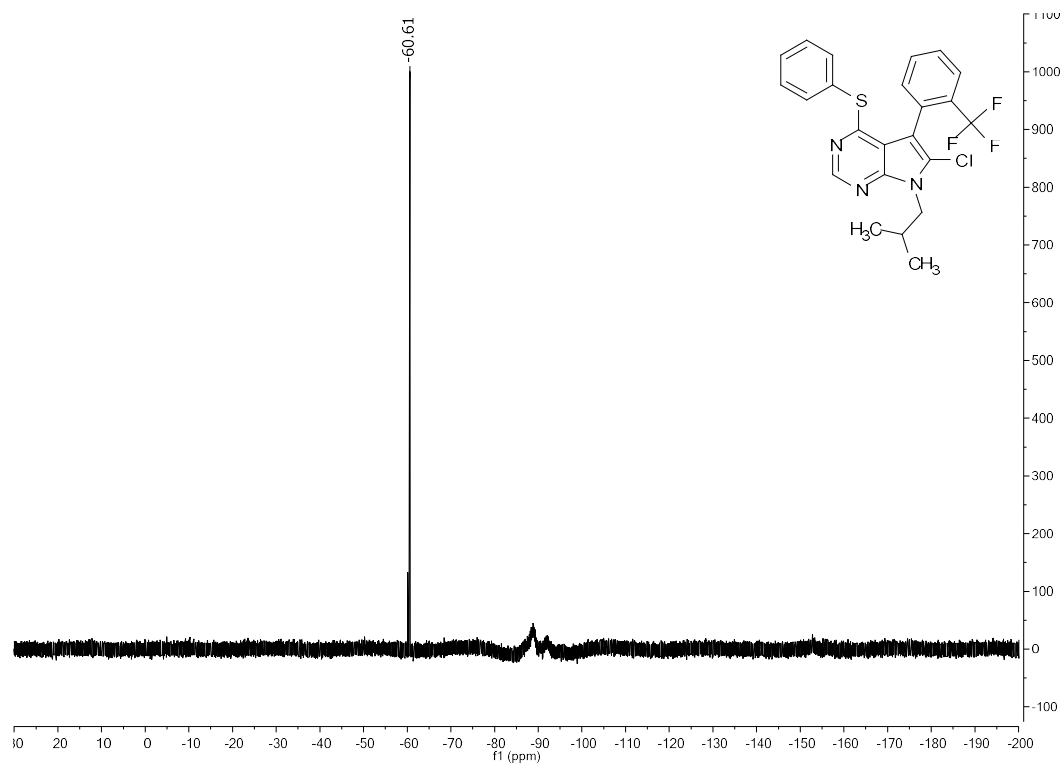
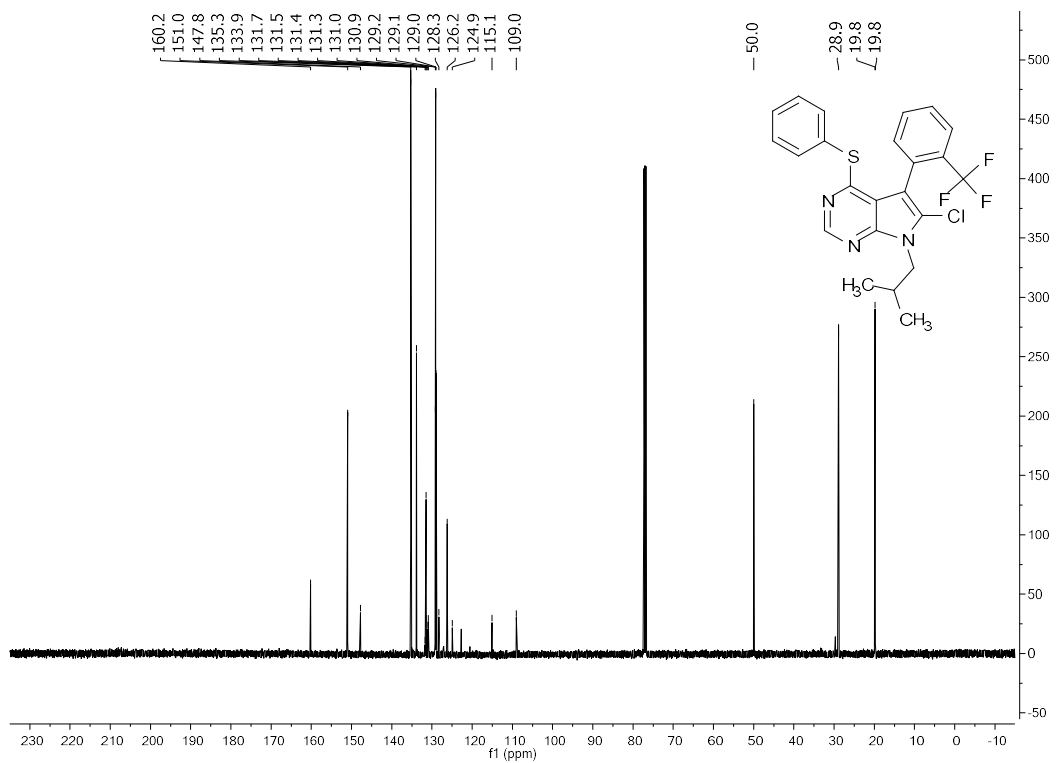
^1H , ^{13}C , and ^{19}F (referenced to TFA) Spectral Data of 26



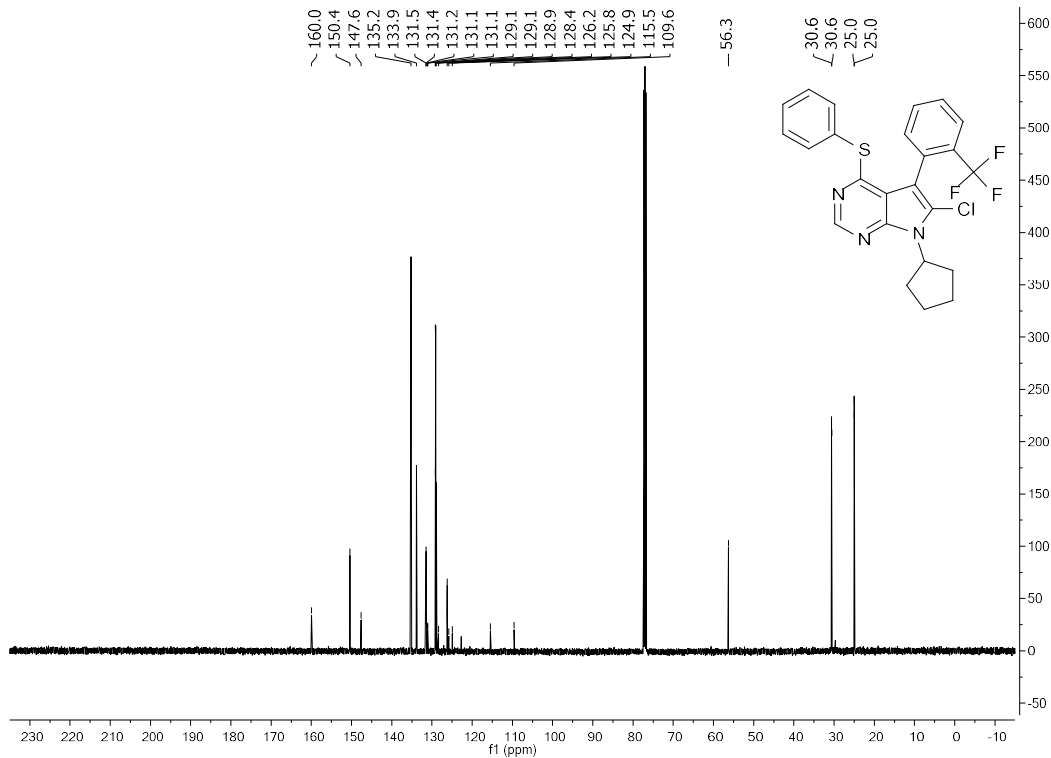
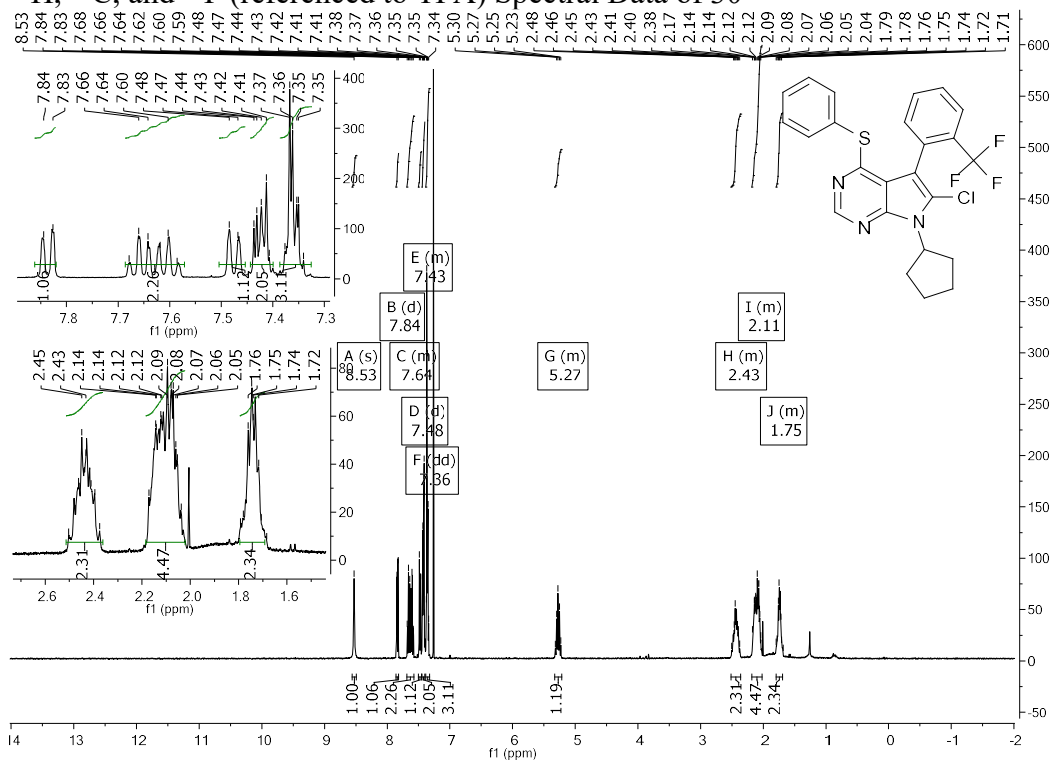


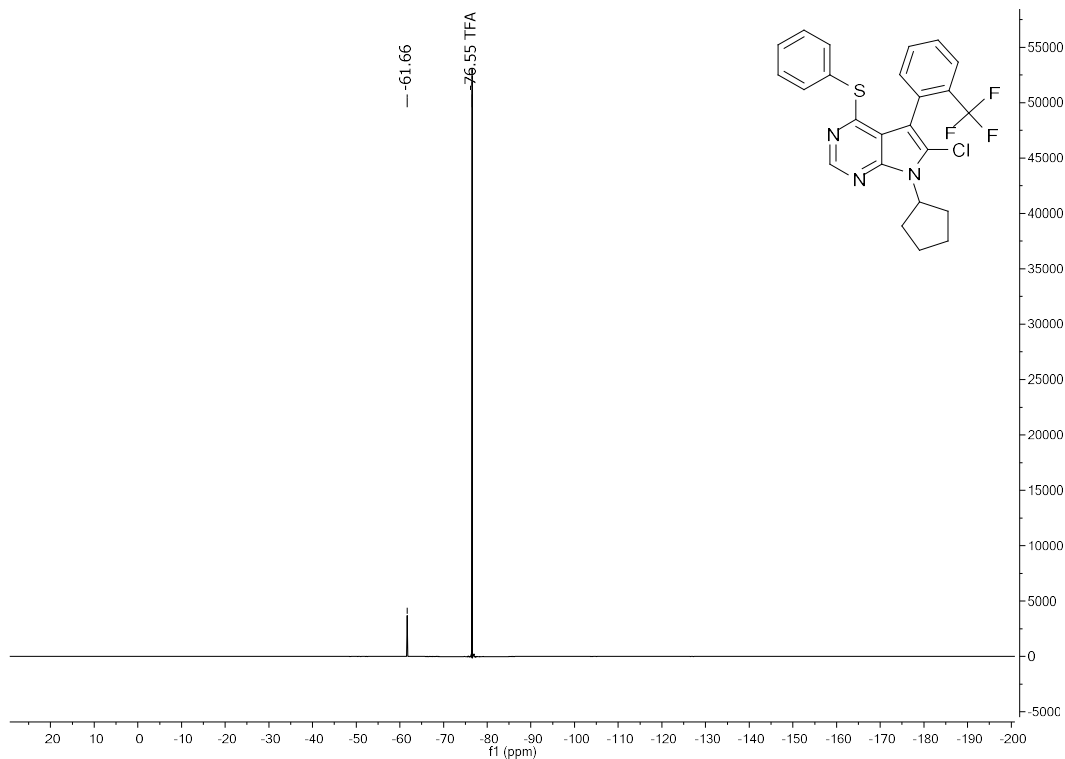
^1H , ^{13}C , ^{19}F Spectral data of 28



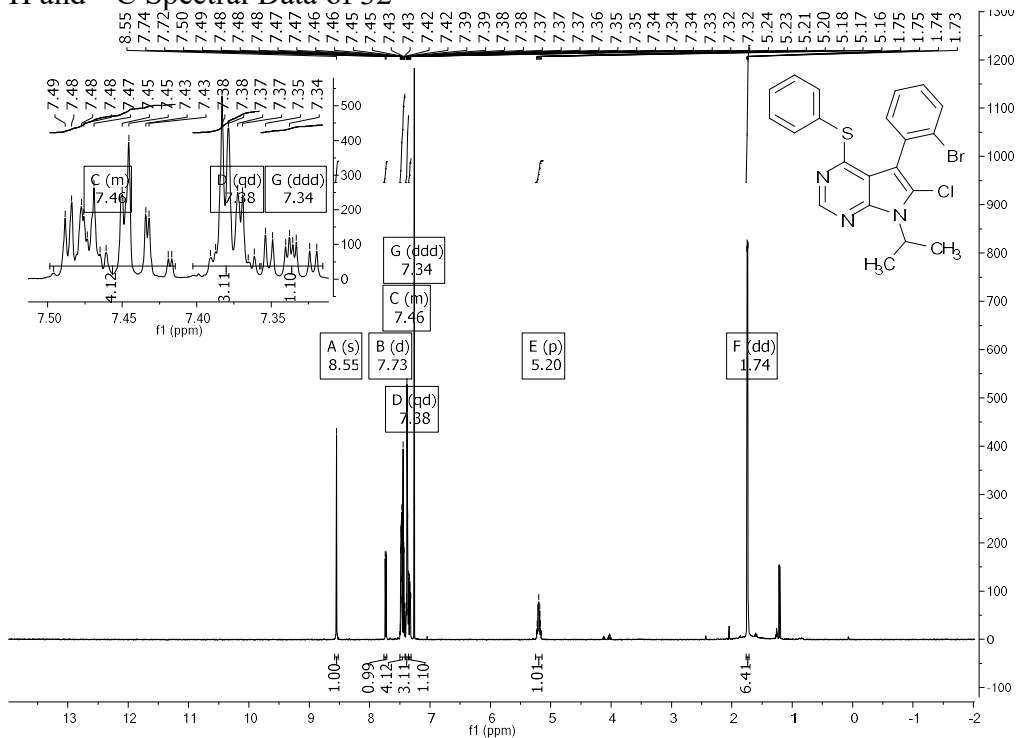


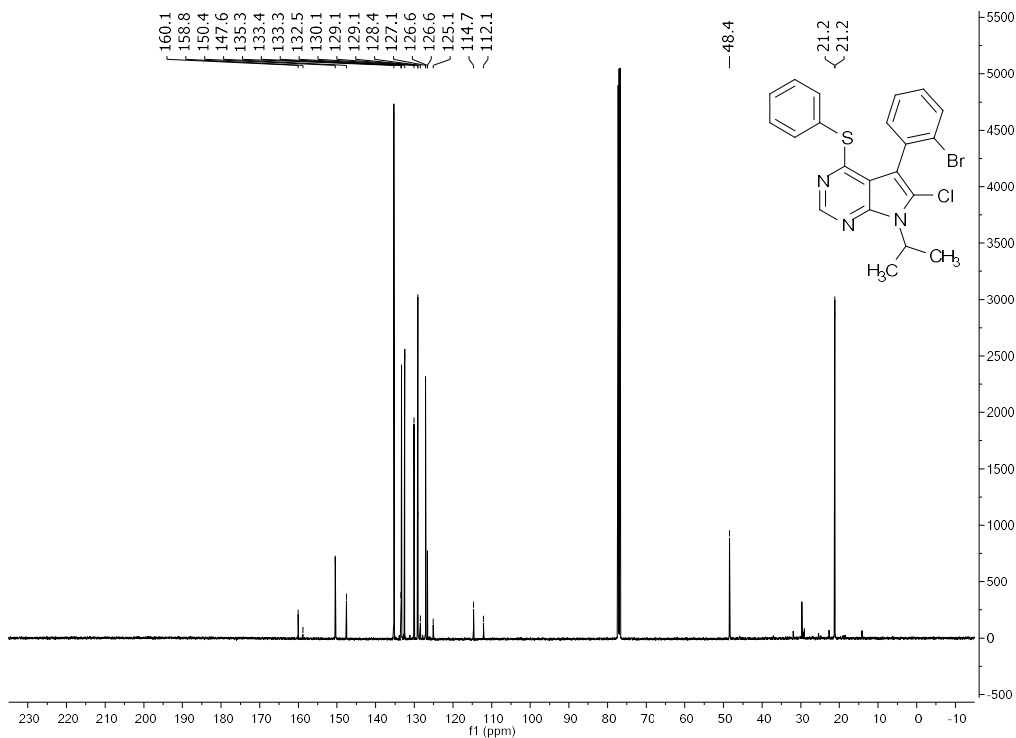
¹H, ¹³C, and ¹⁹F (referenced to TFA) Spectral Data of 30



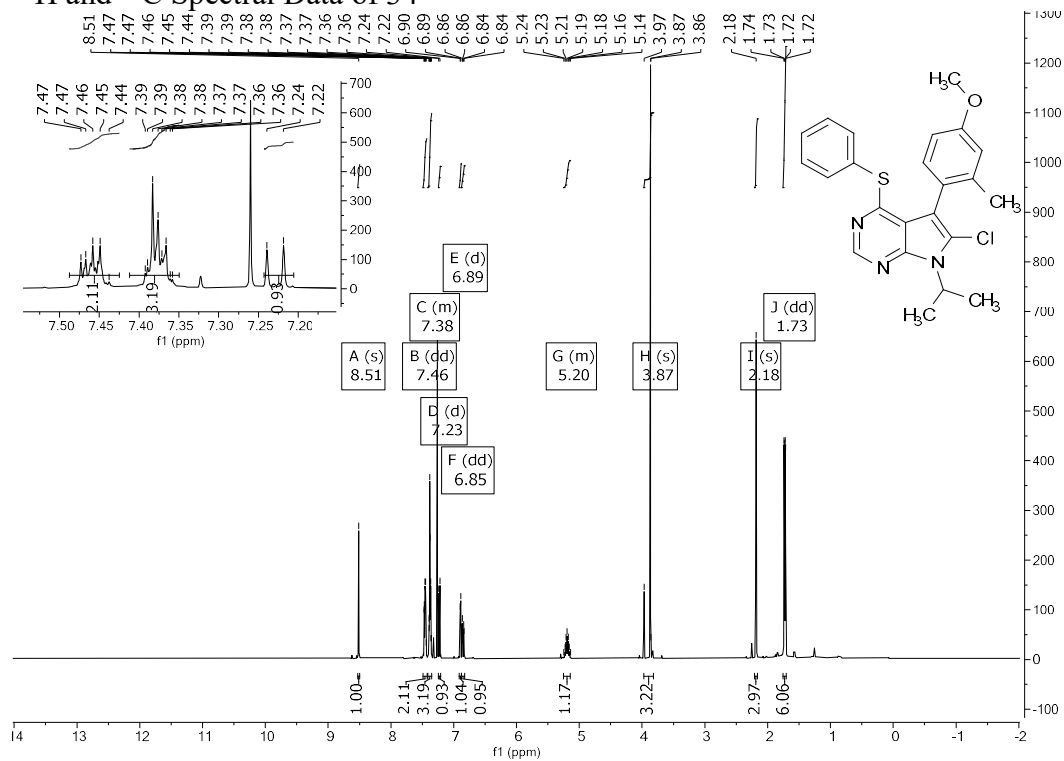


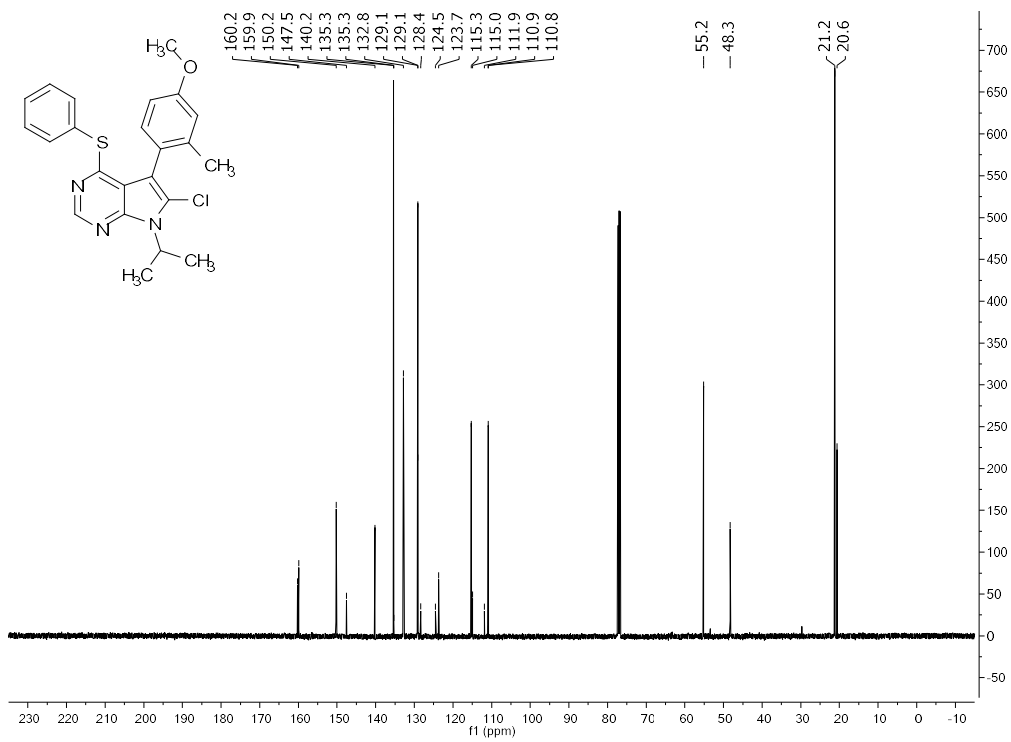
¹H and ¹³C Spectral Data of 32



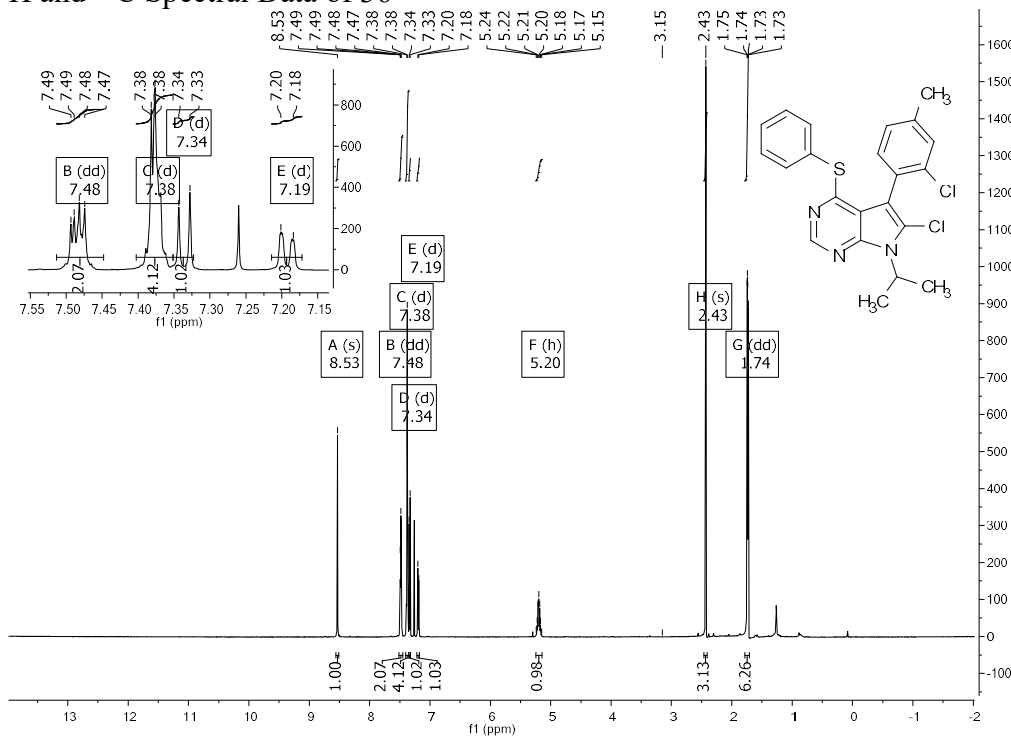


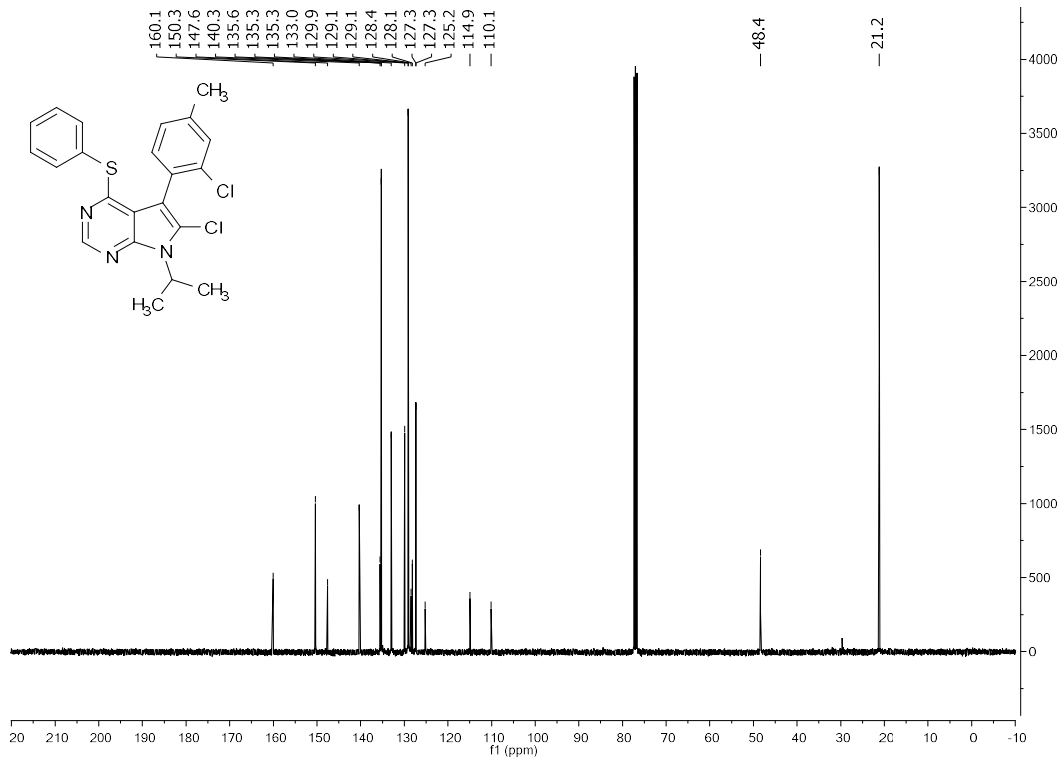
¹H and ¹³C Spectral Data of 34



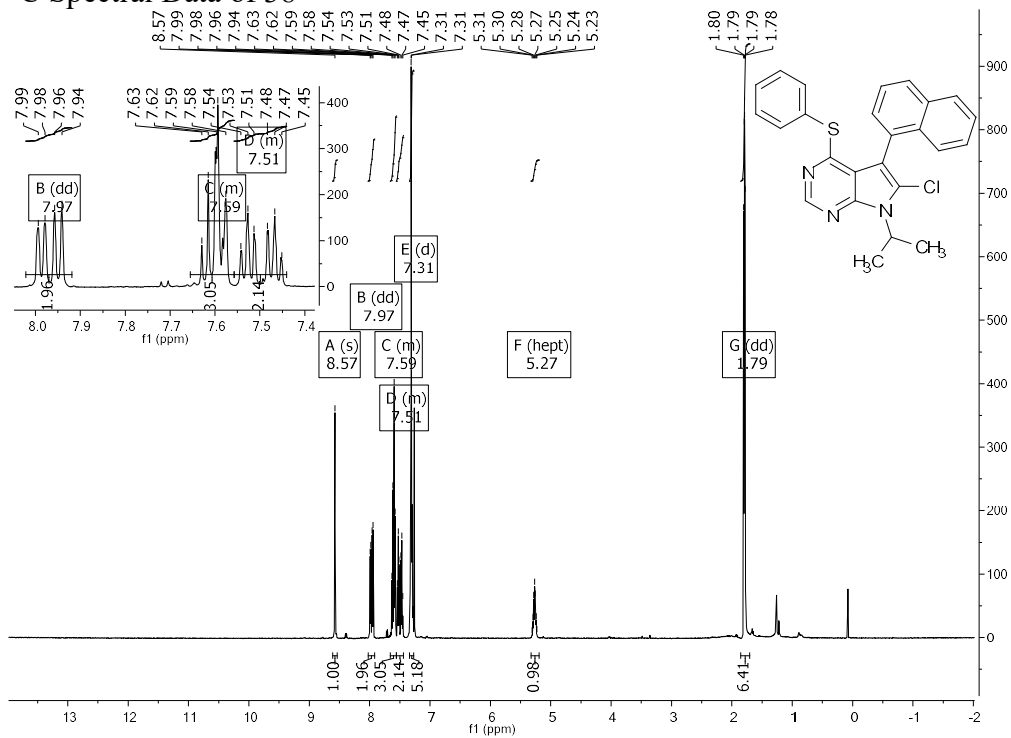


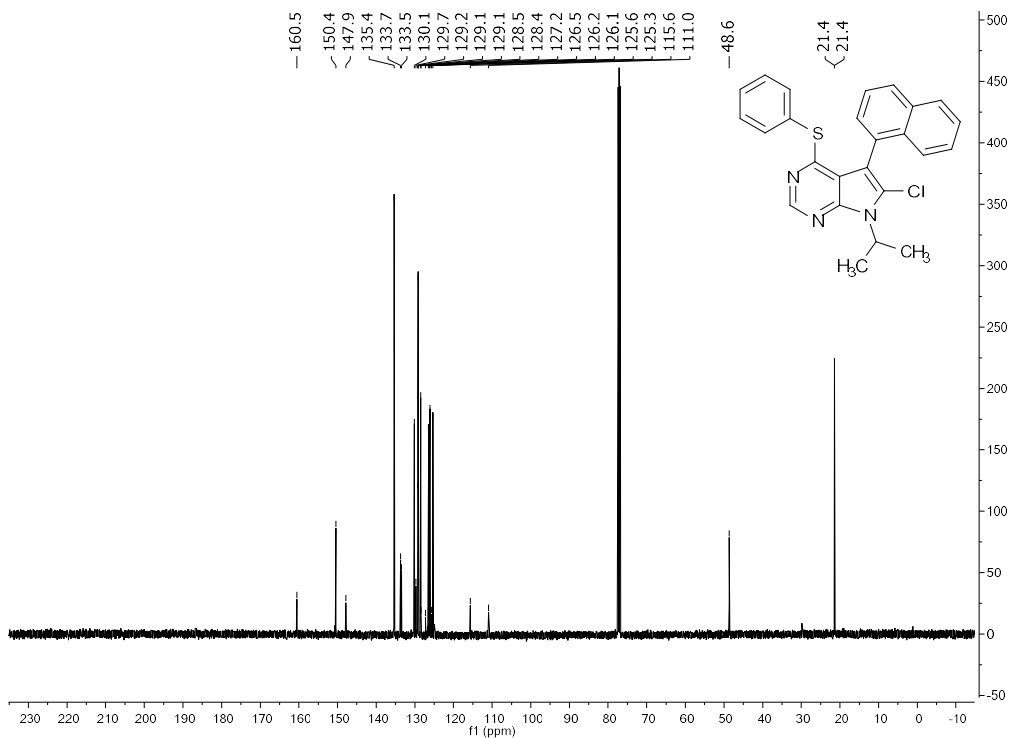
¹H and ¹³C Spectral Data of 36



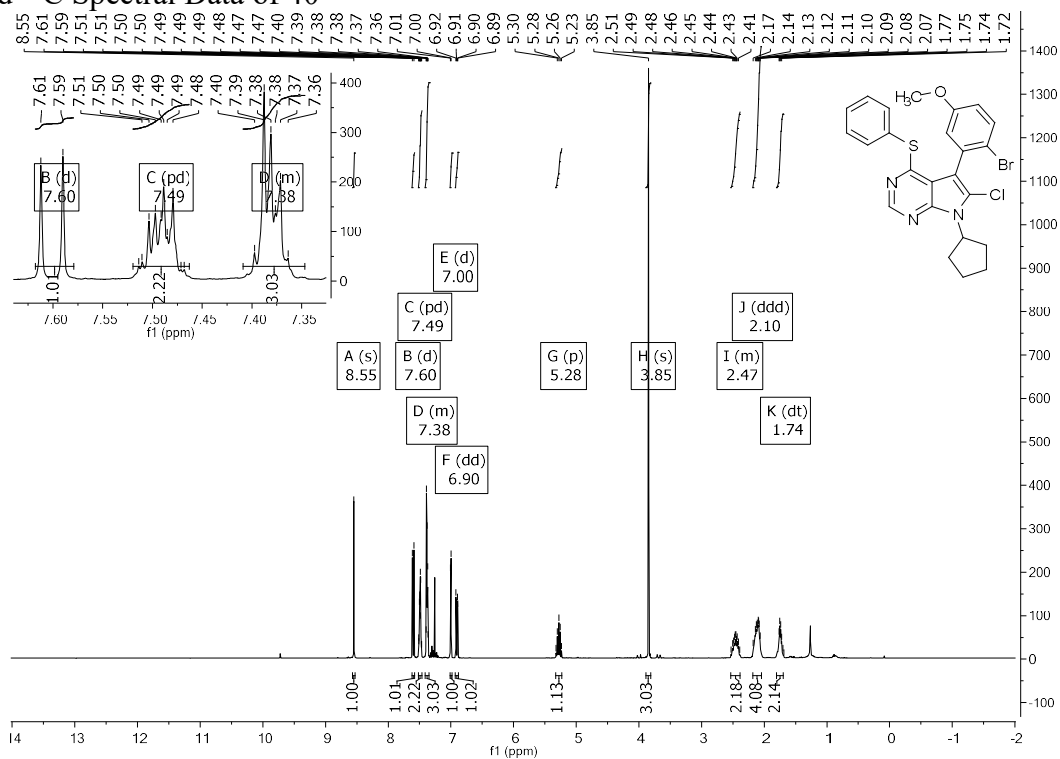


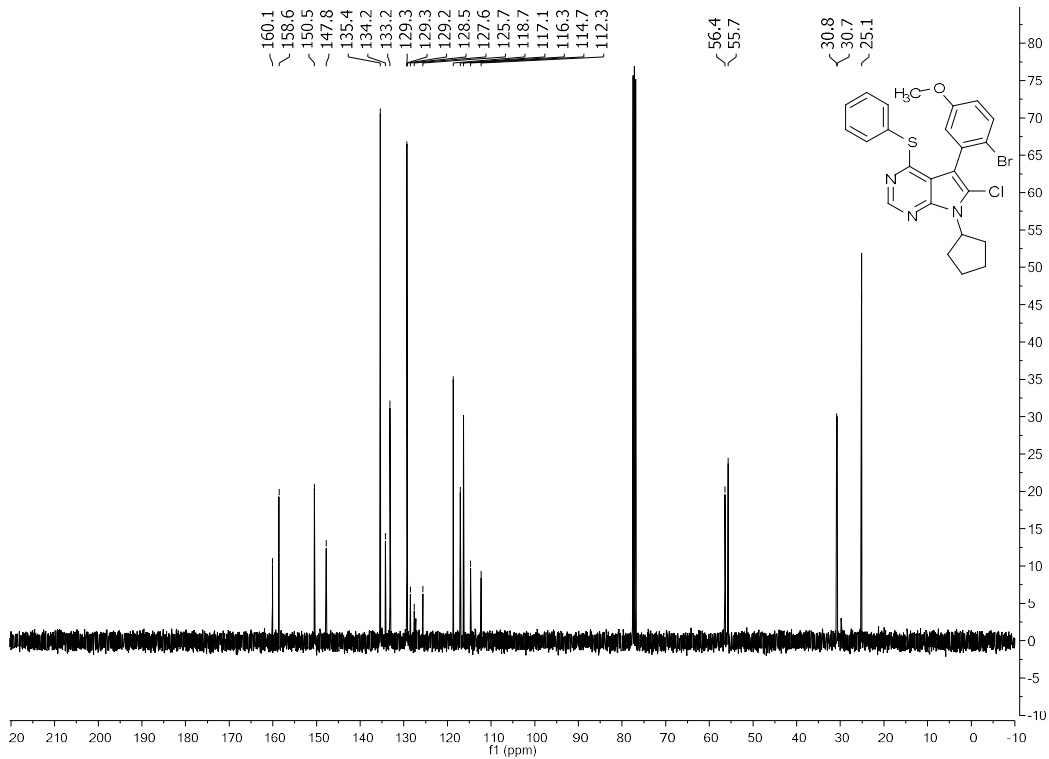
¹H and ¹³C Spectral Data of 38



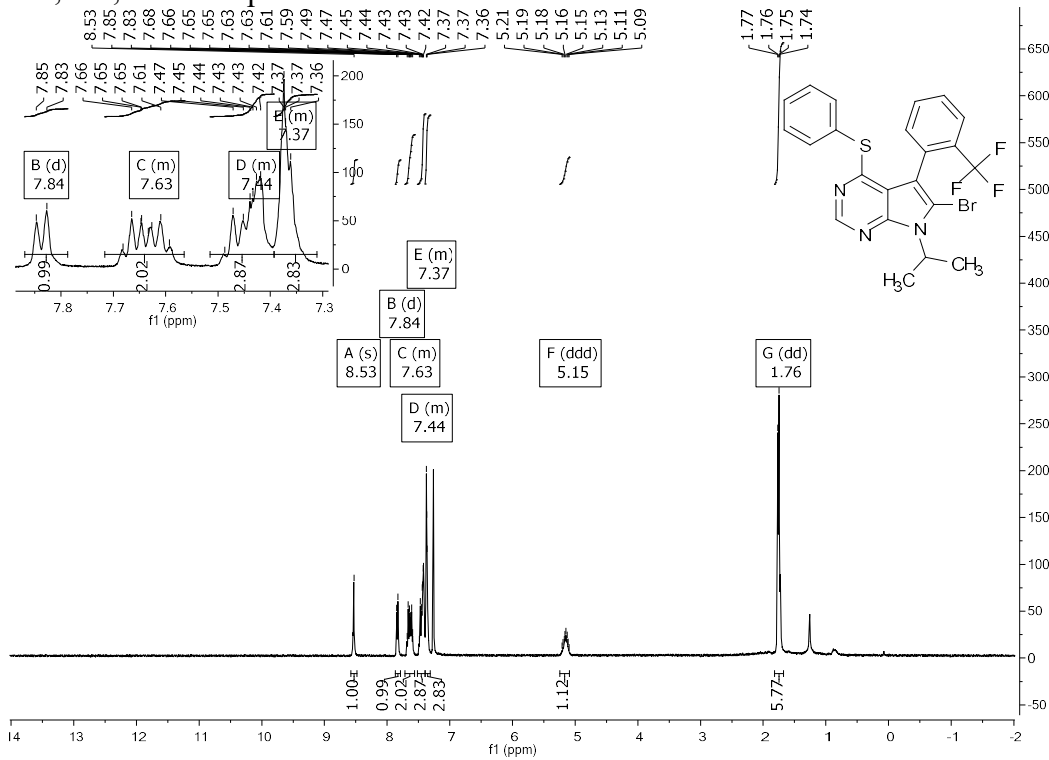


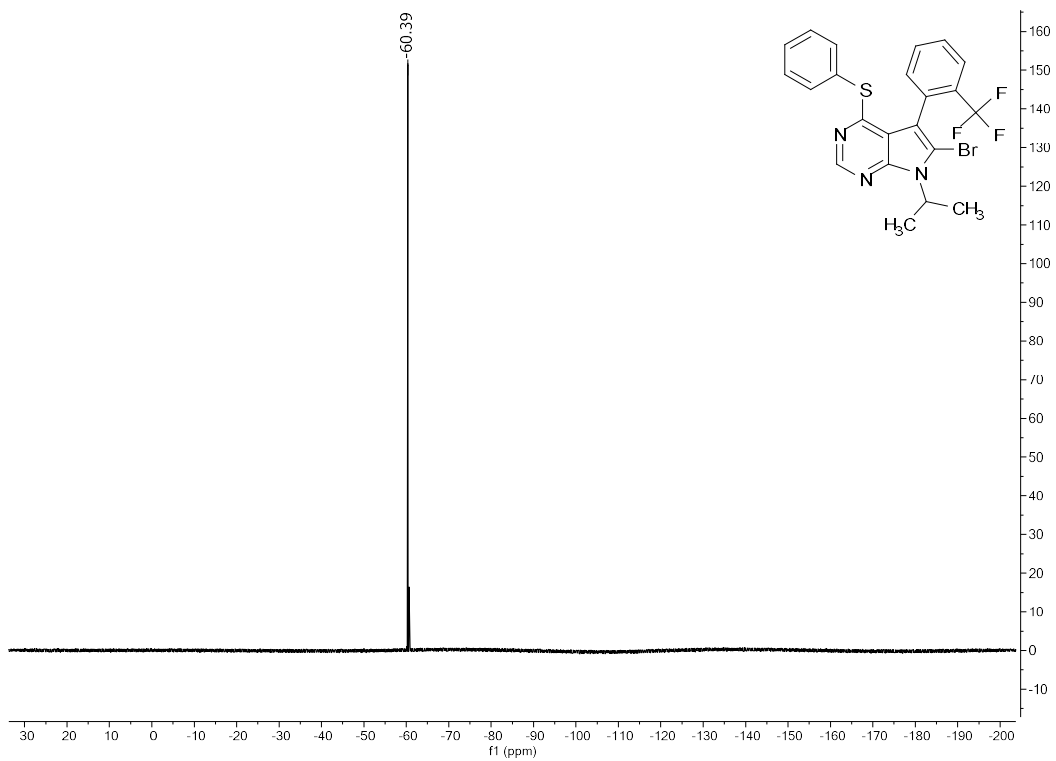
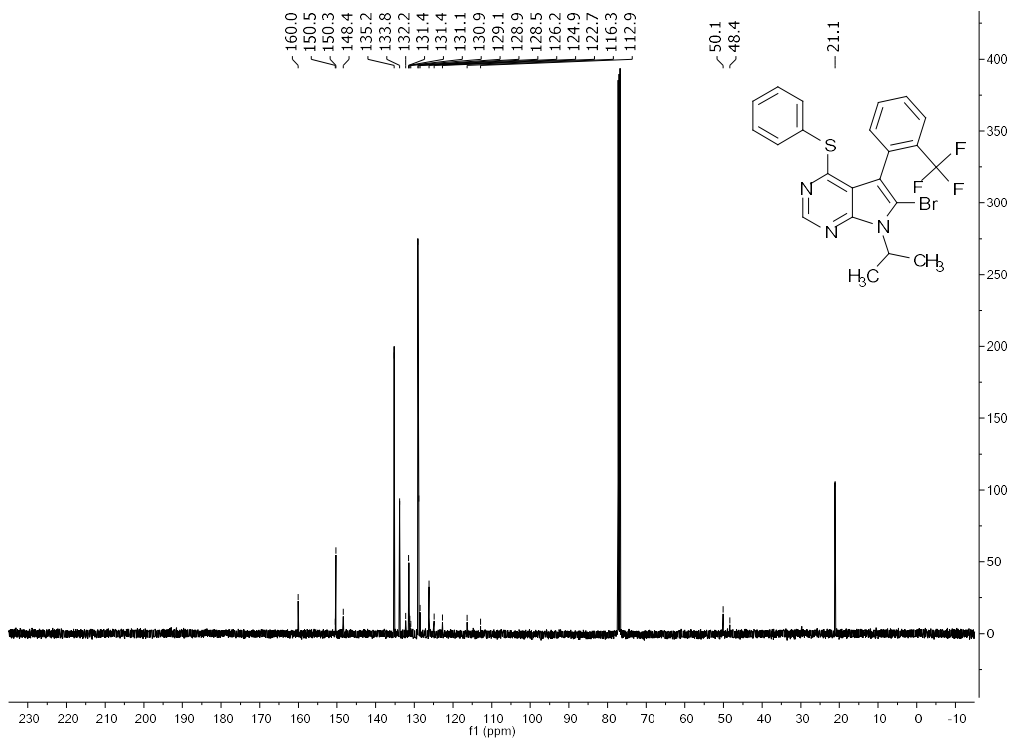
¹H and ¹³C Spectral Data of 40



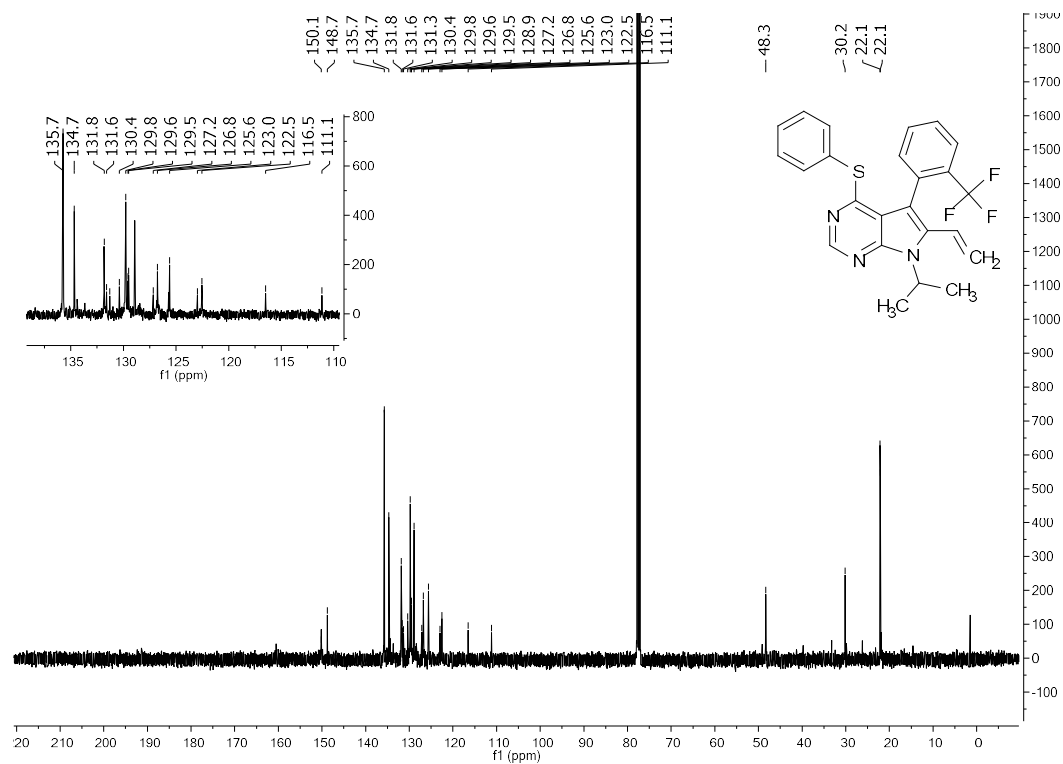
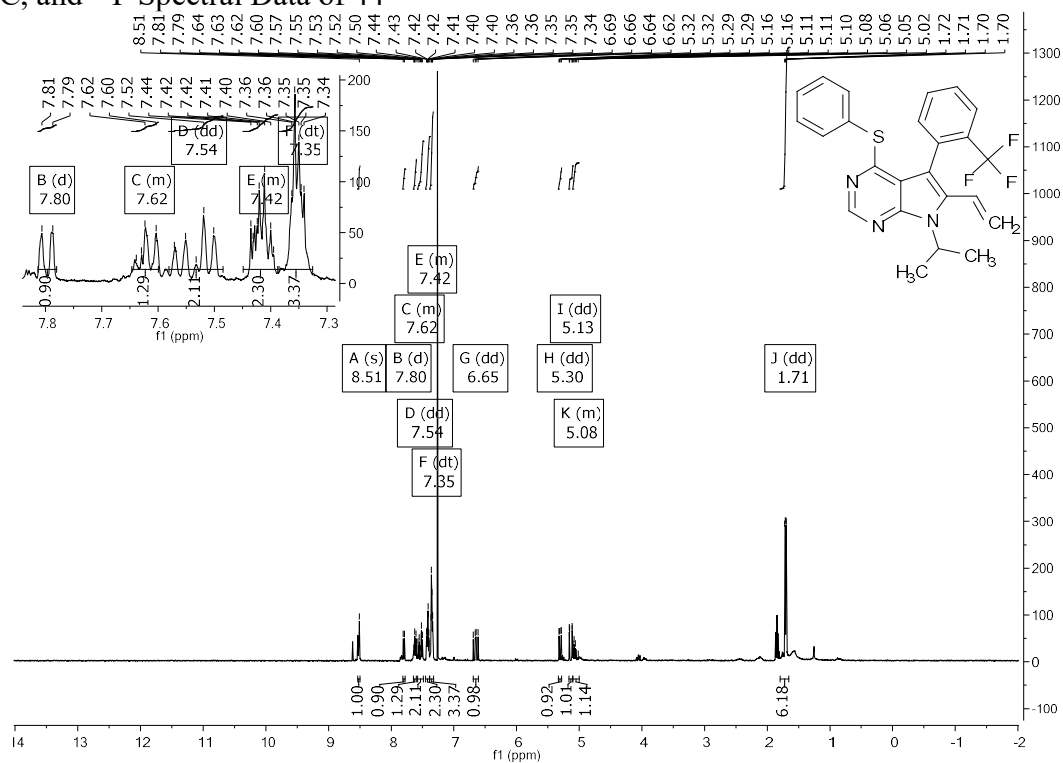


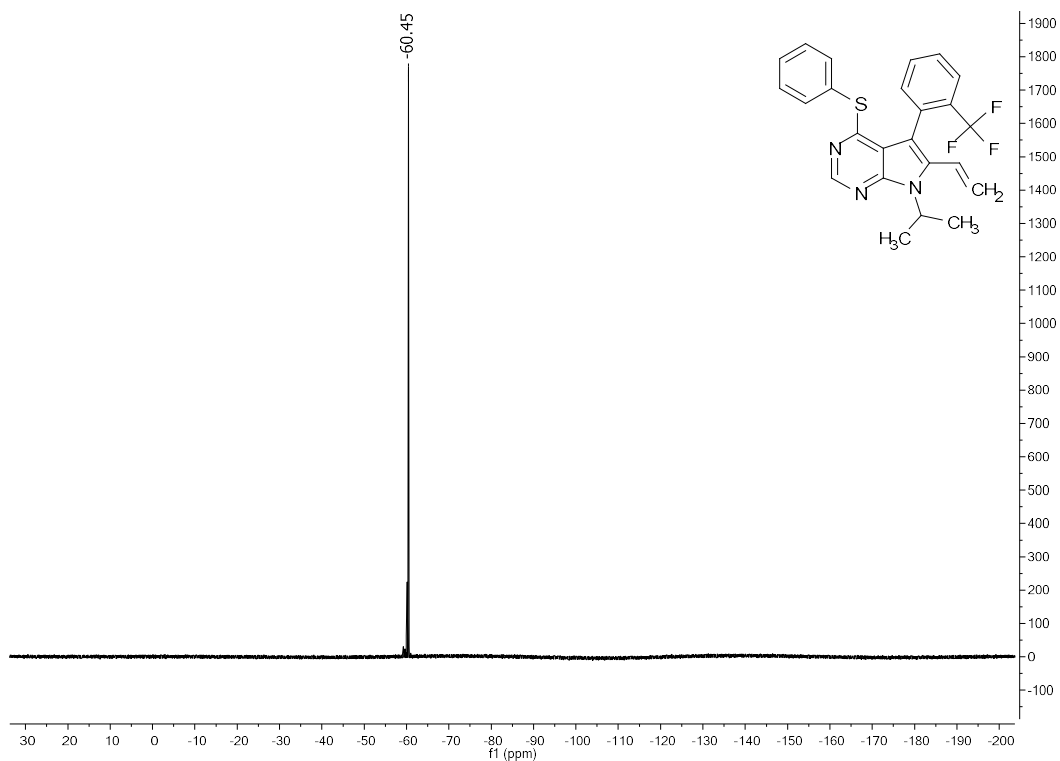
¹H, ¹³C, and ¹⁹F Spectral Data of 42



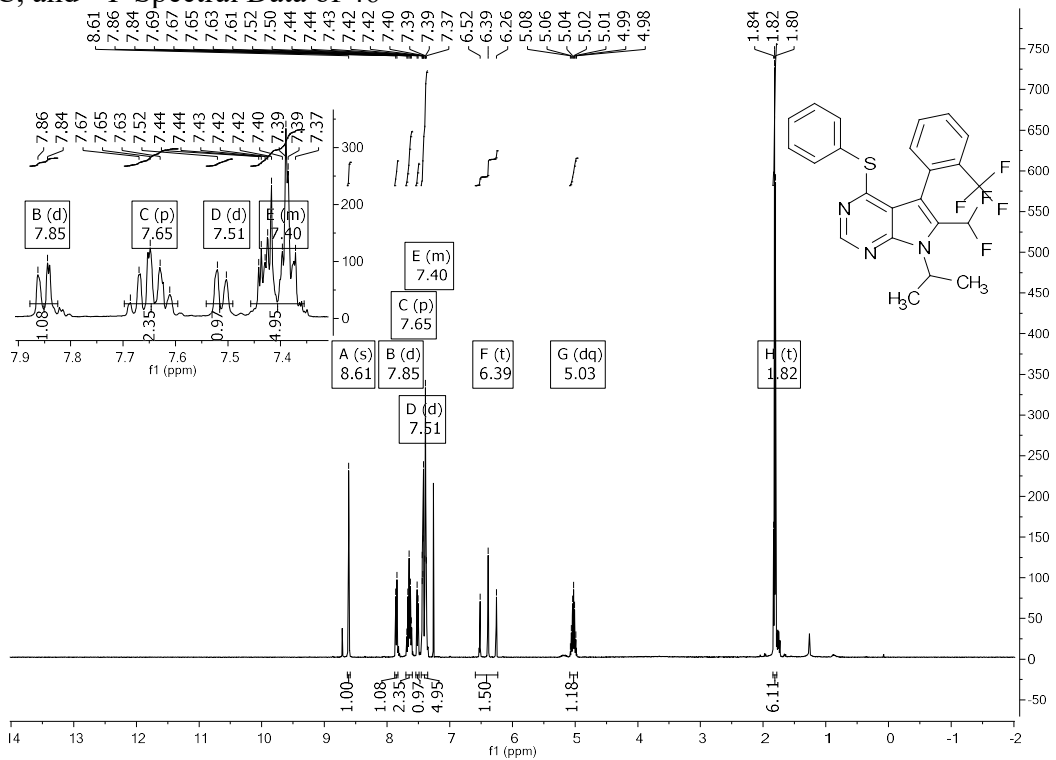


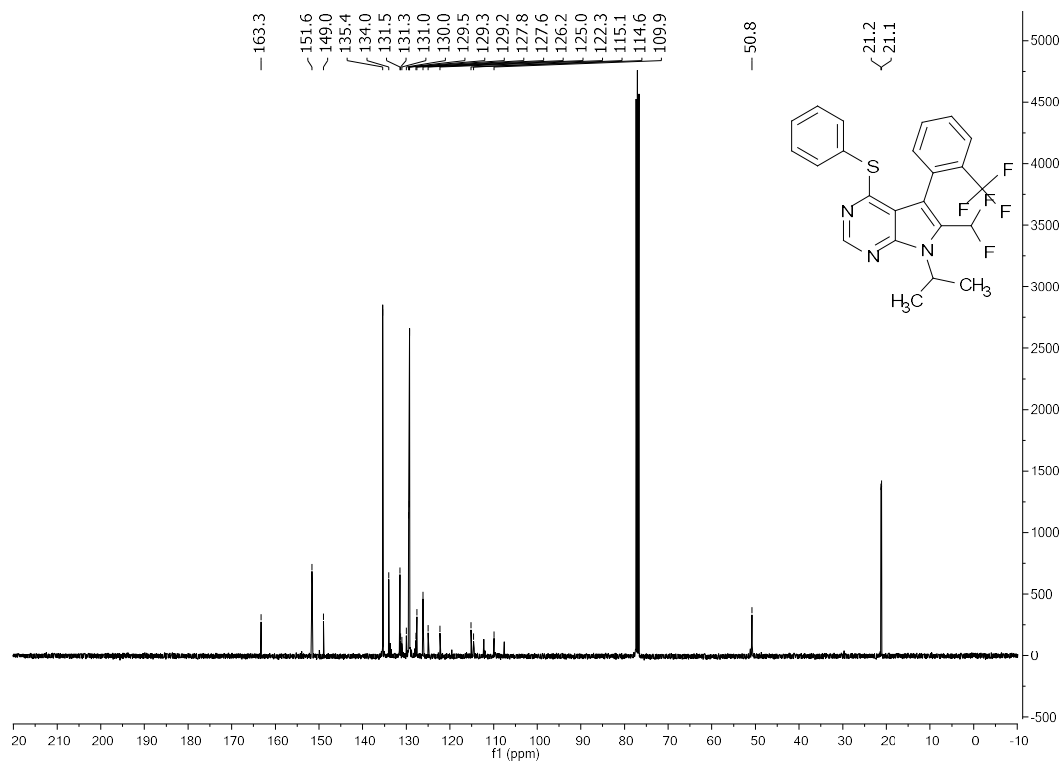
¹H, ¹³C, and ¹⁹F Spectral Data of 44



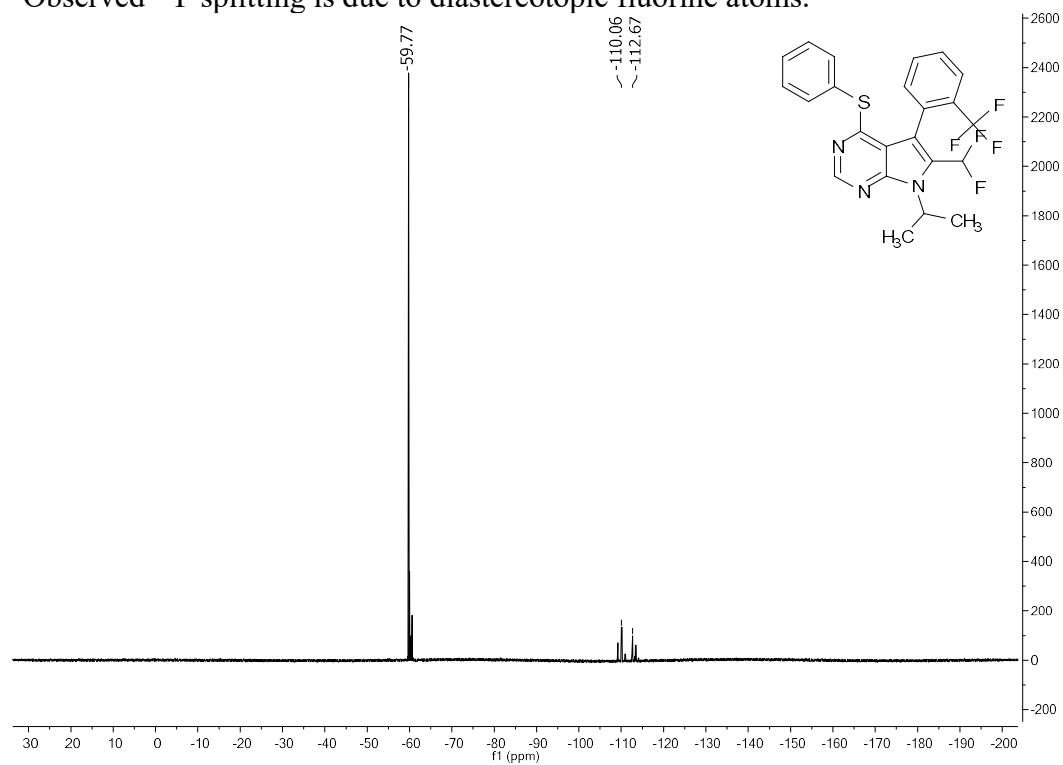


¹H, ¹³C, and ¹⁹F Spectral Data of 46

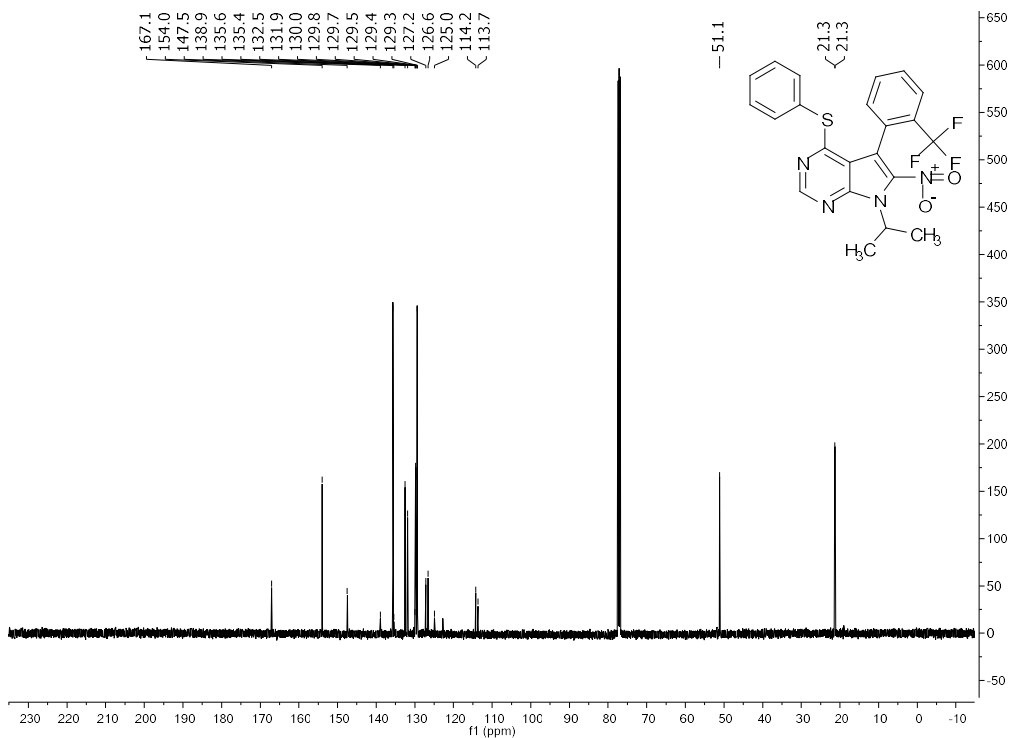
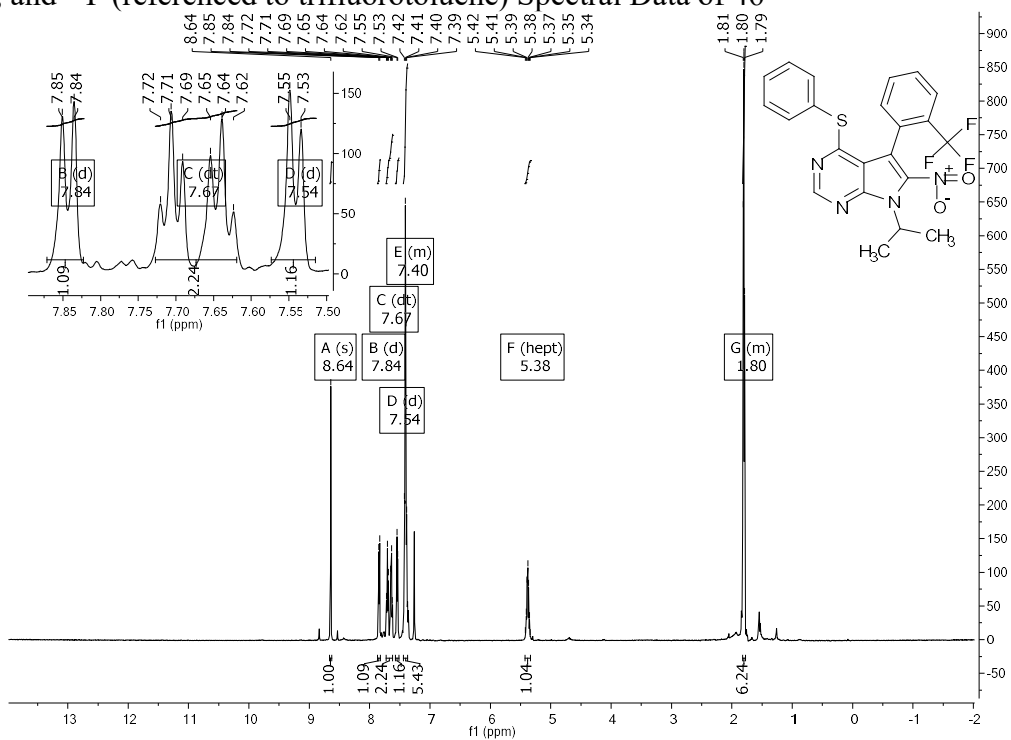


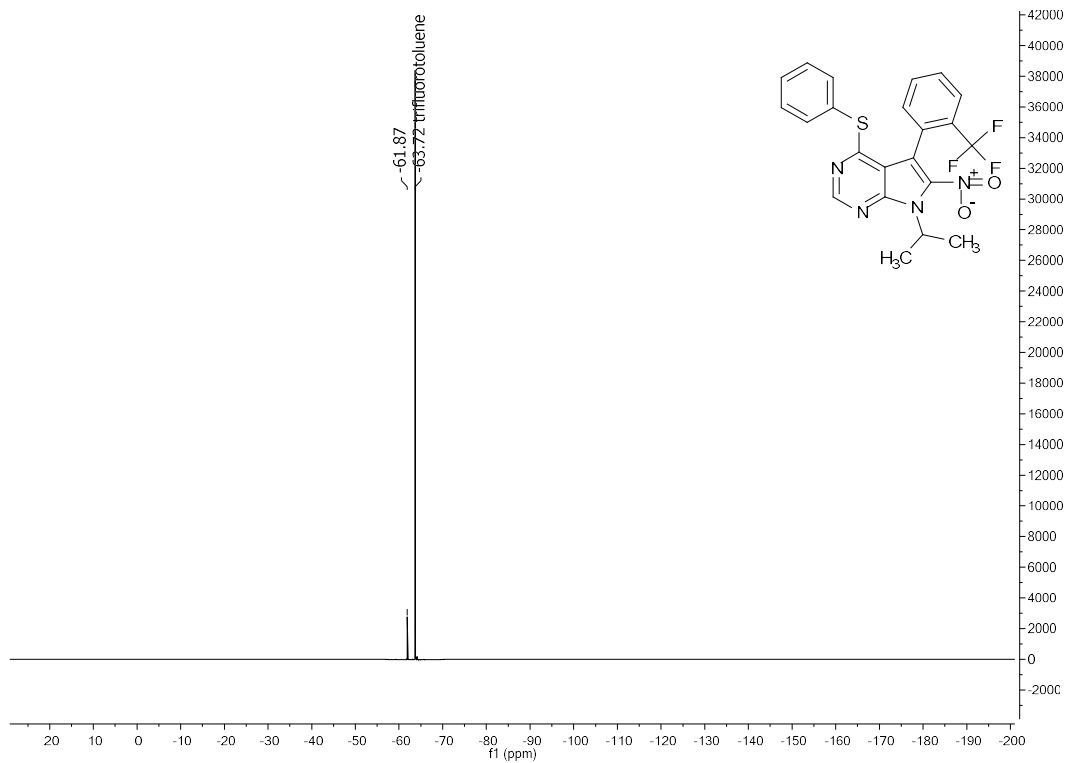


Observed ^{19}F splitting is due to diastereotopic fluorine atoms.

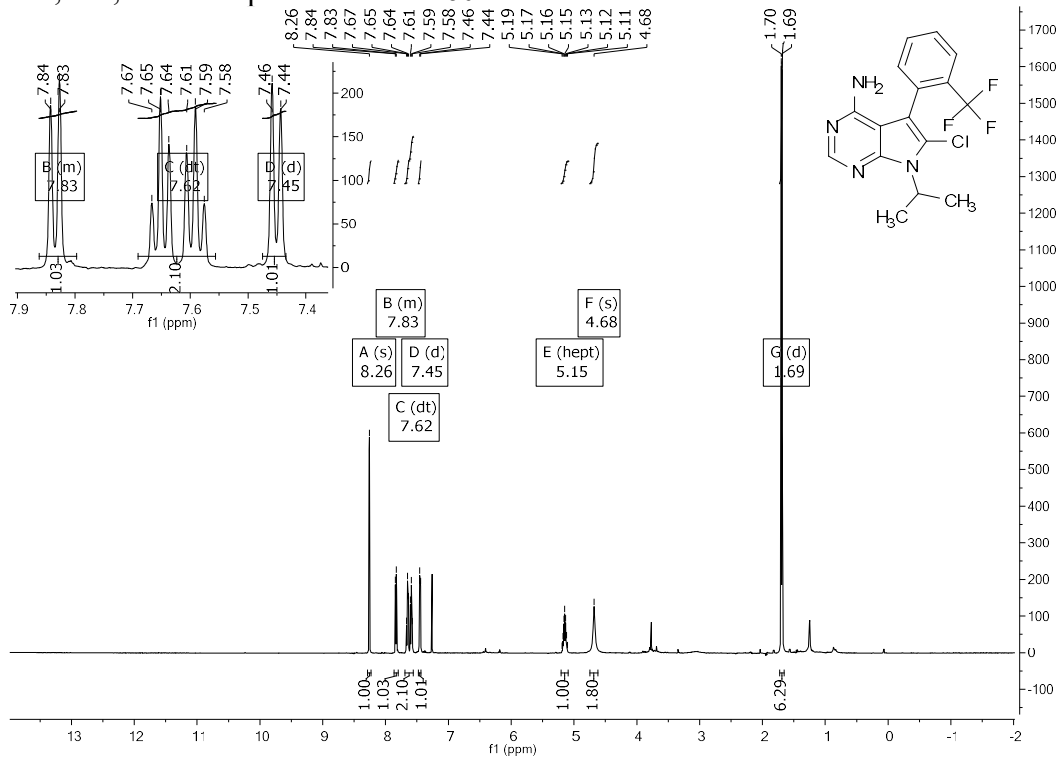


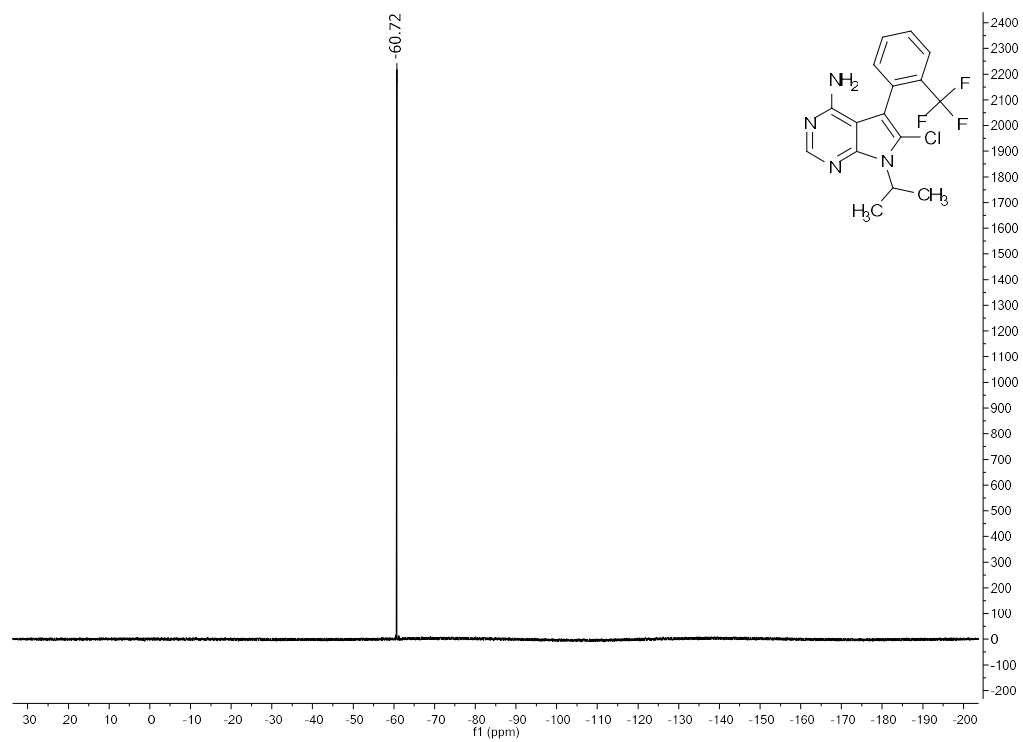
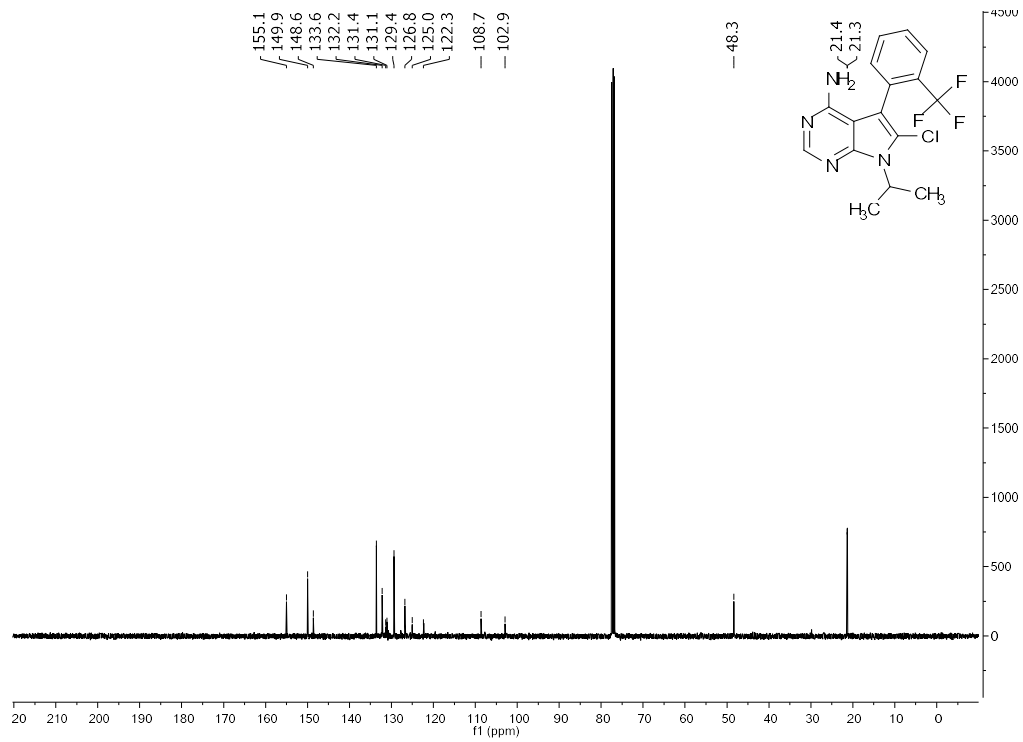
^1H , ^{13}C , and ^{19}F (referenced to trifluorotoluene) Spectral Data of 46



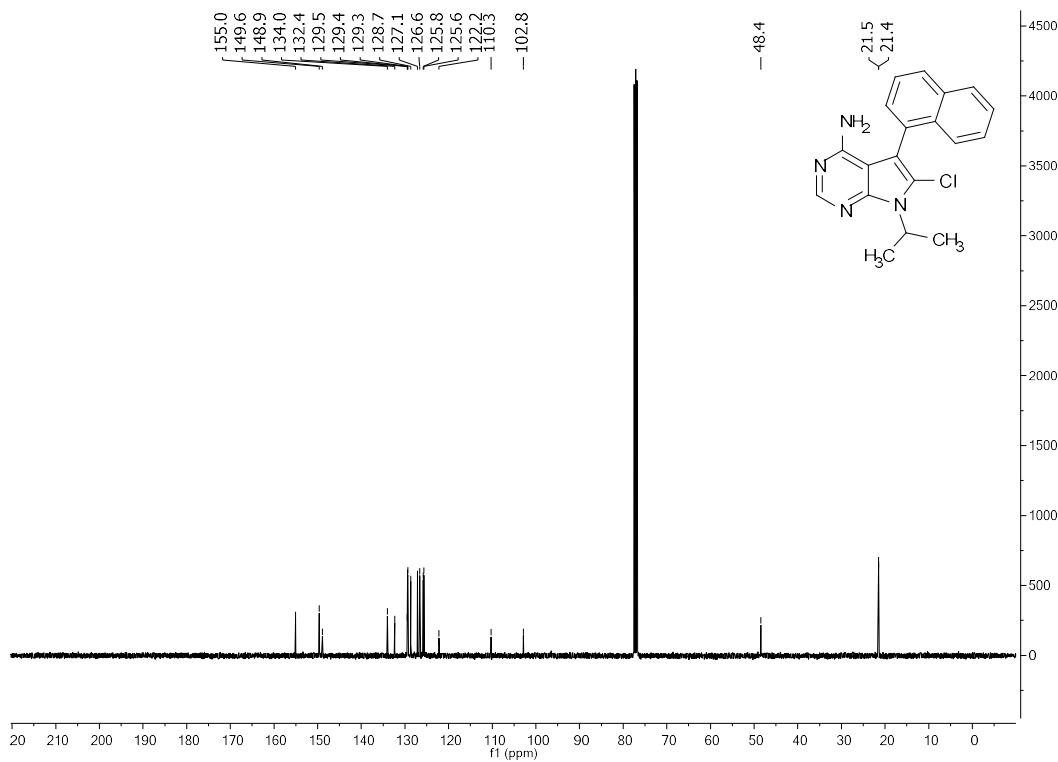
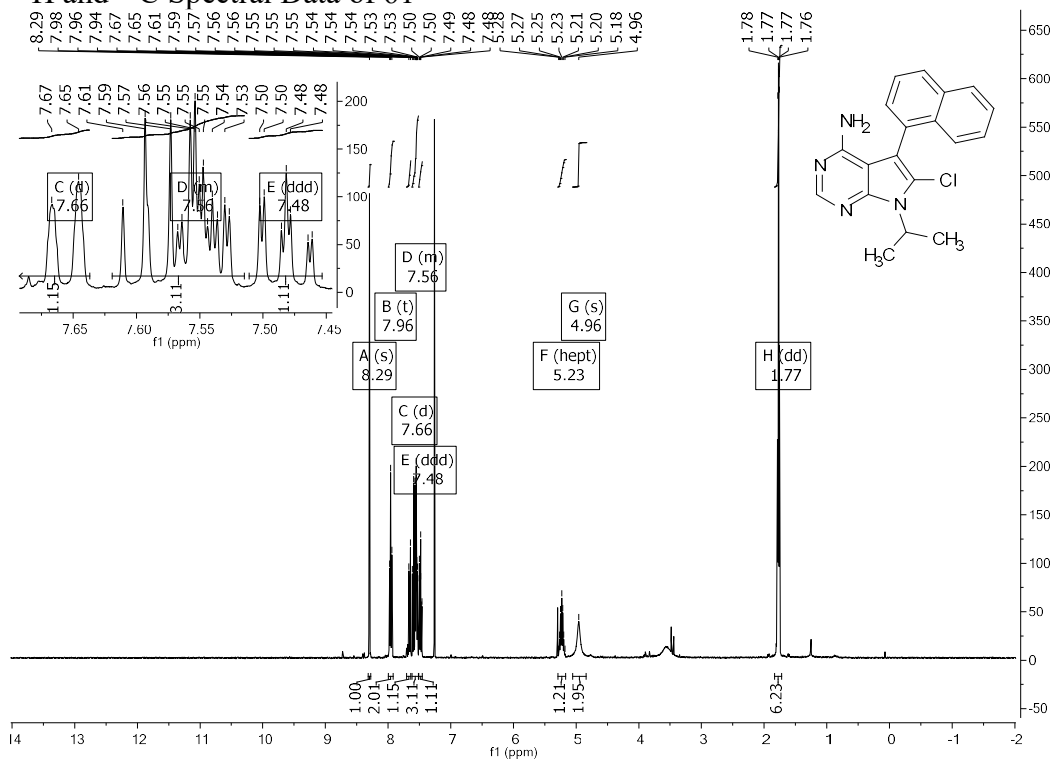


¹H, ¹³C, and ¹⁹F Spectral Data of 60

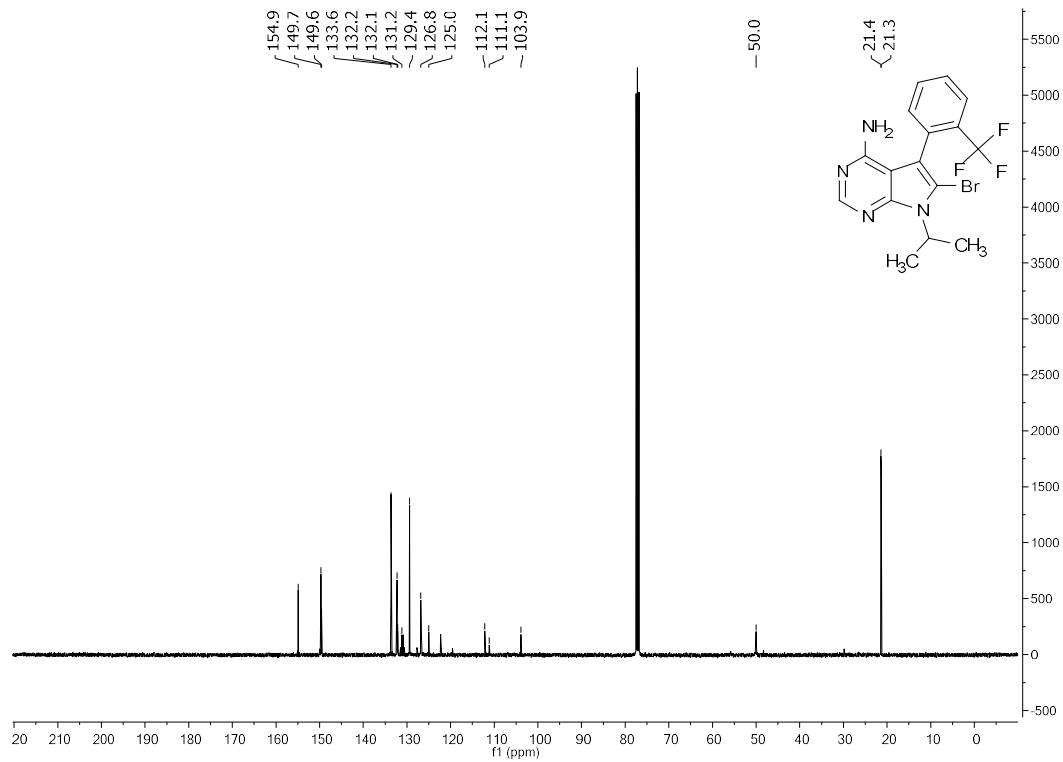
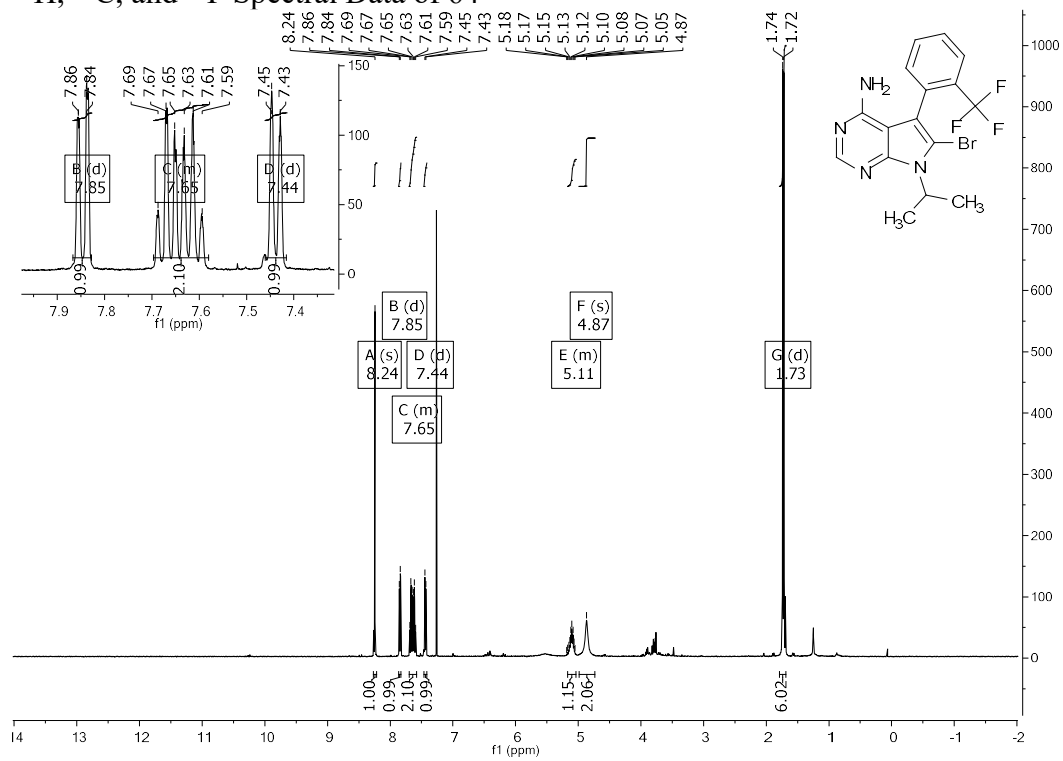


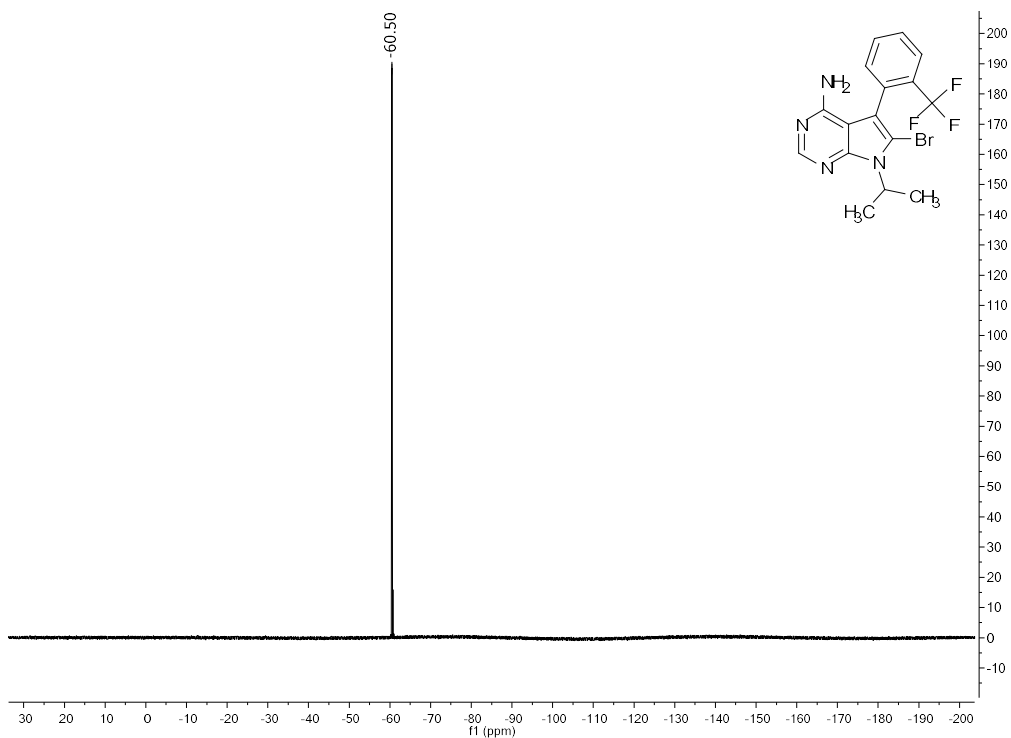


¹H and ¹³C Spectral Data of 61

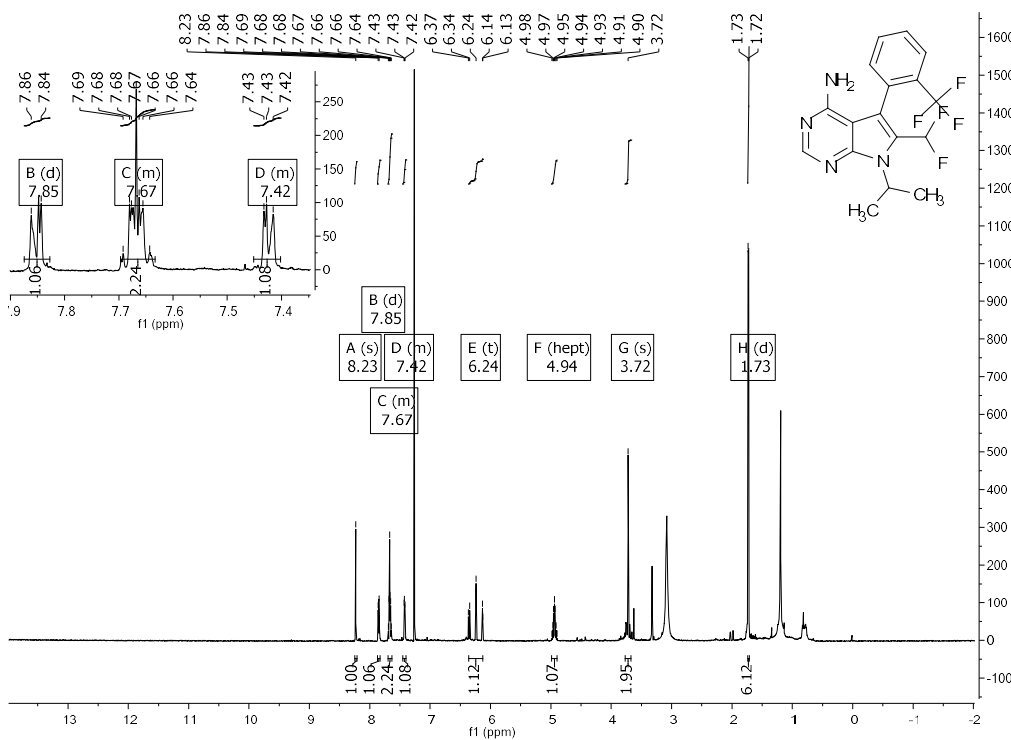


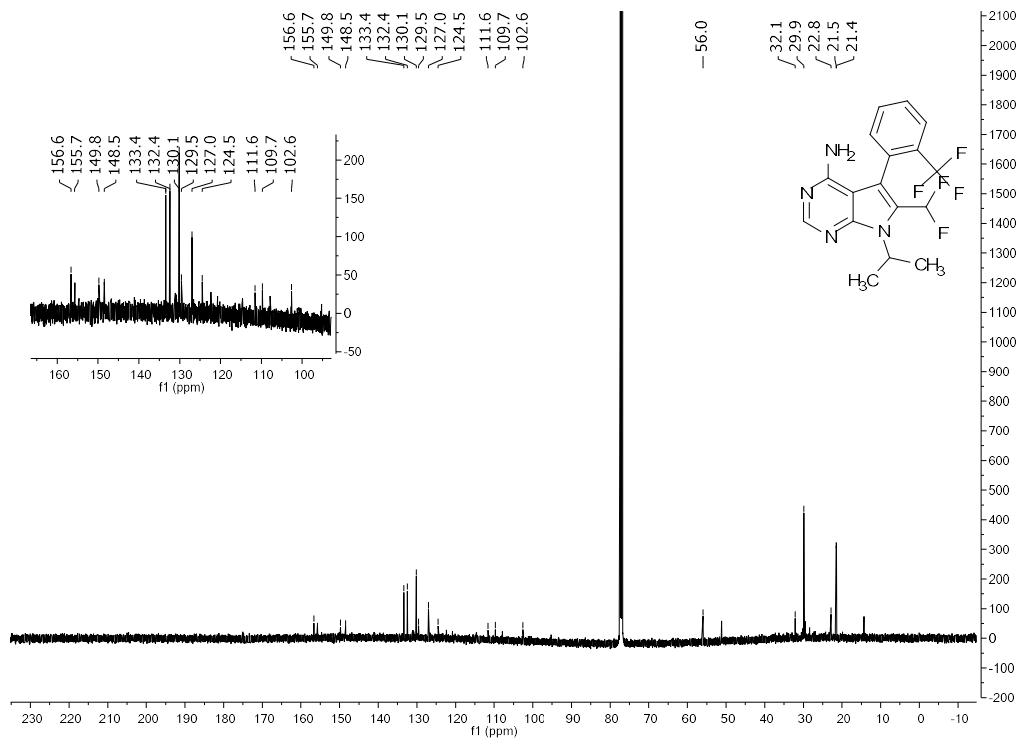
¹H, ¹³C, and ¹⁹F Spectral Data of 64



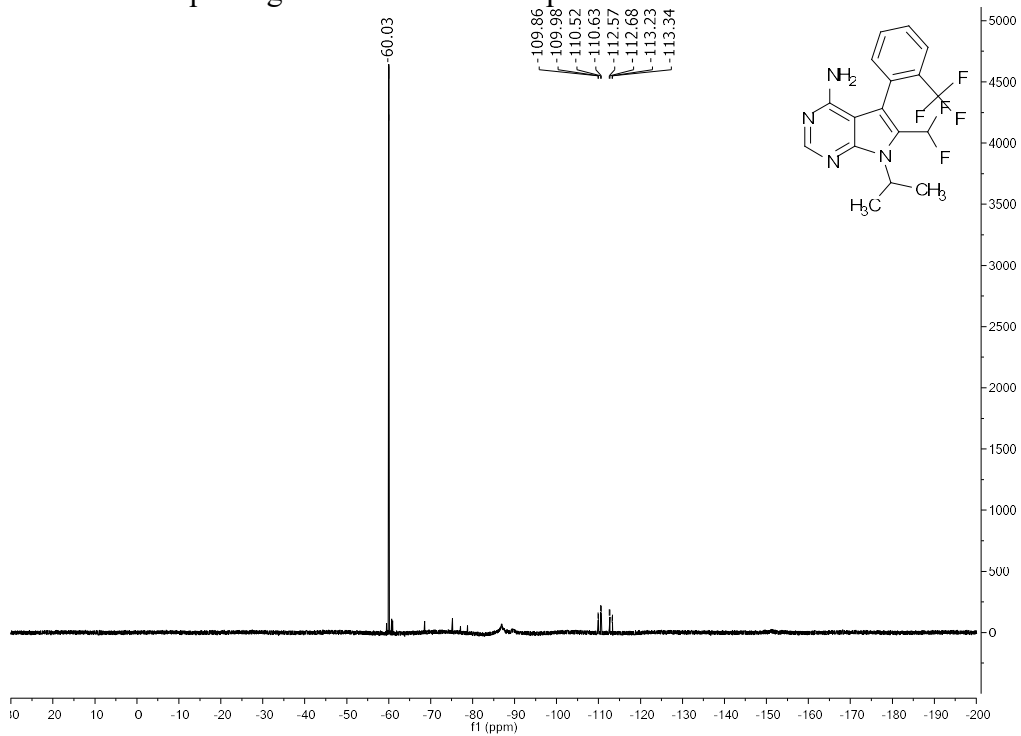


¹H, ¹³C, and ¹⁹F Spectral Data of 47
 ee-SM 45 was aminated to yield (*S_a*)-47 for *s*-factor determination via HPLC analysis.

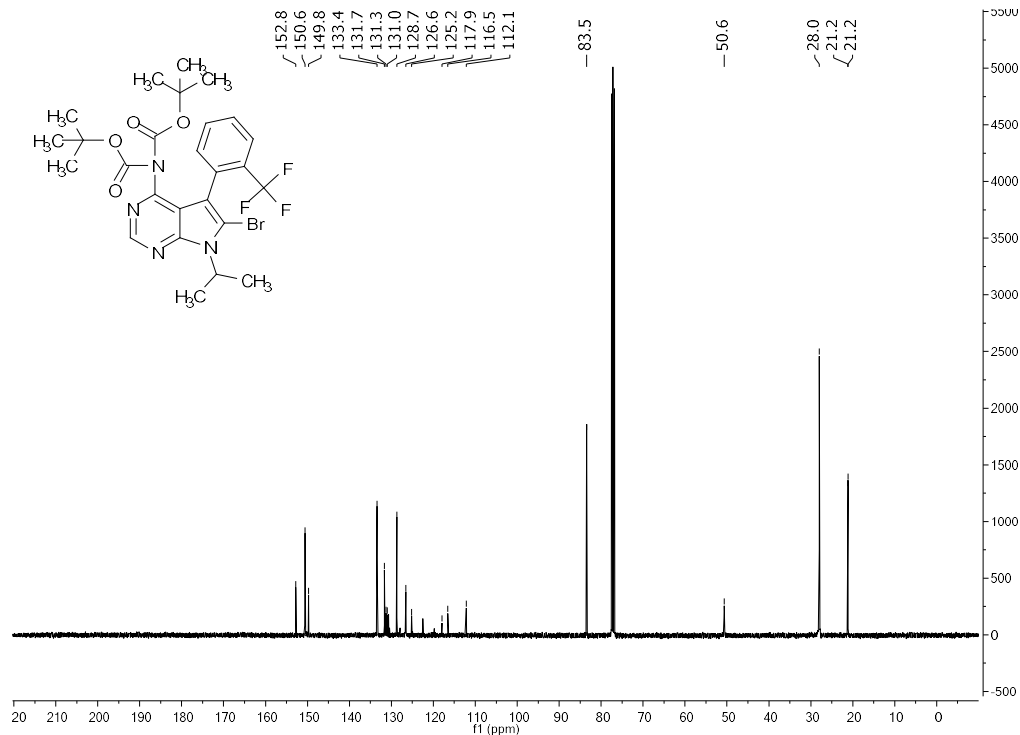
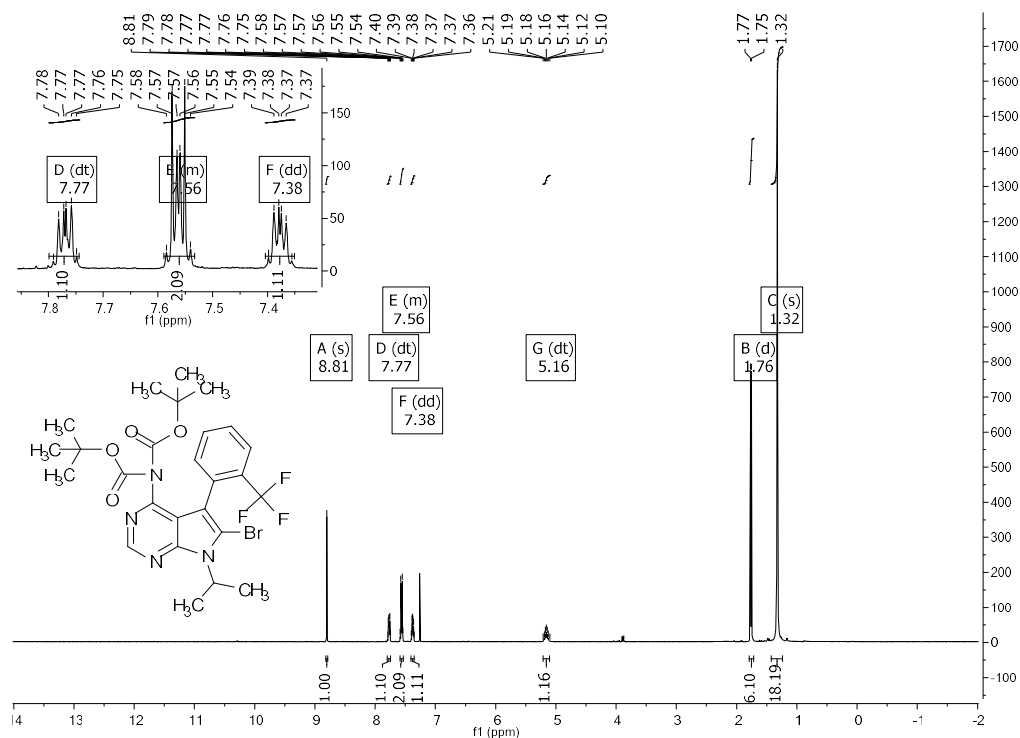


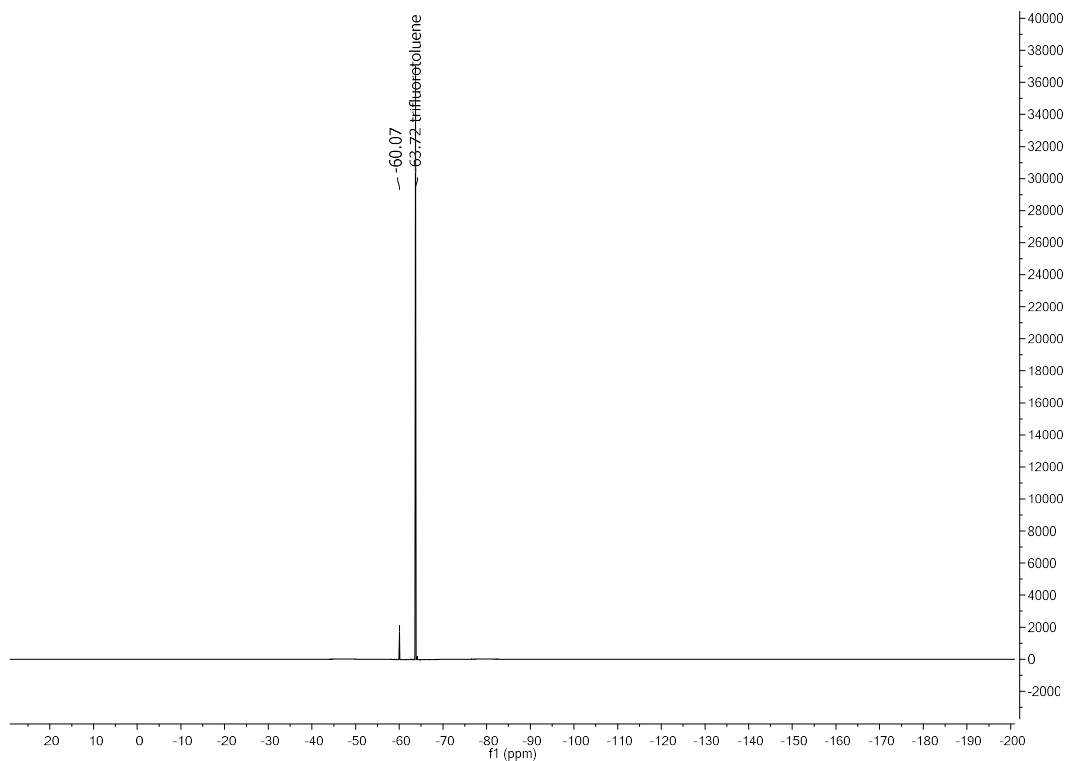


Observed ^{19}F splitting is due to diastereotopic fluorine atoms.

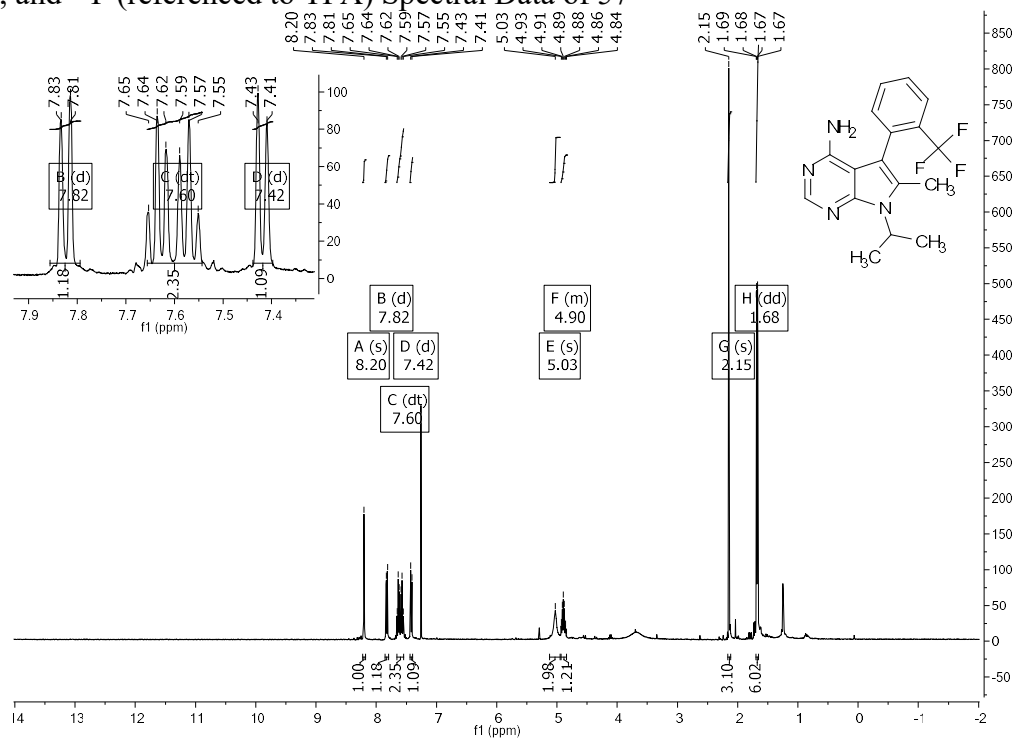


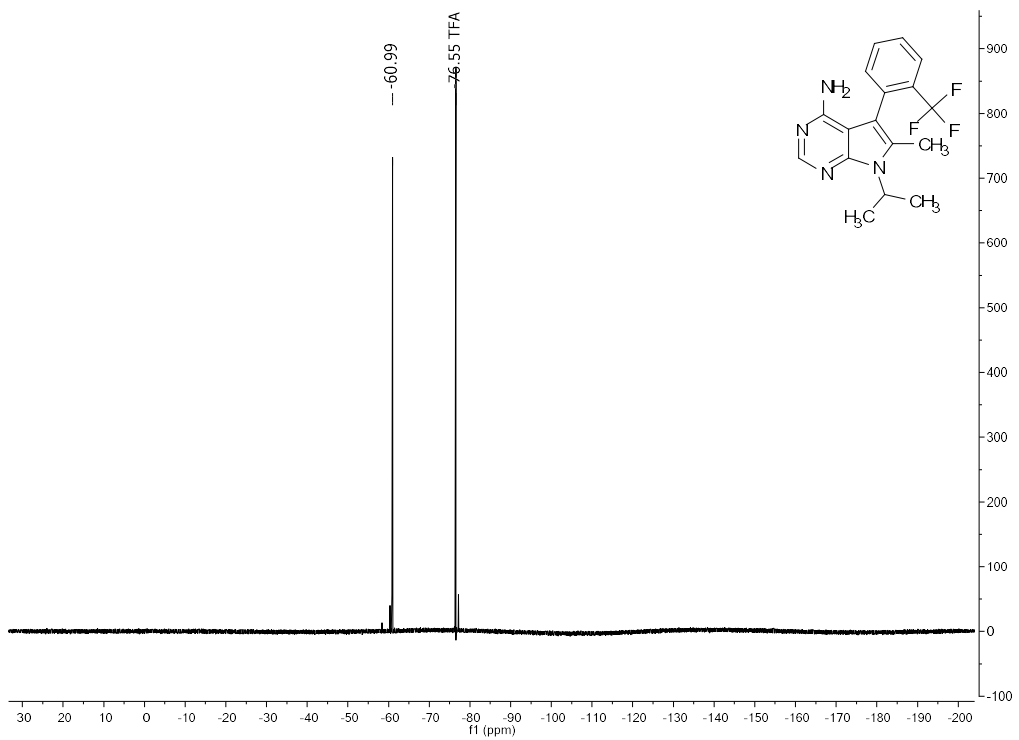
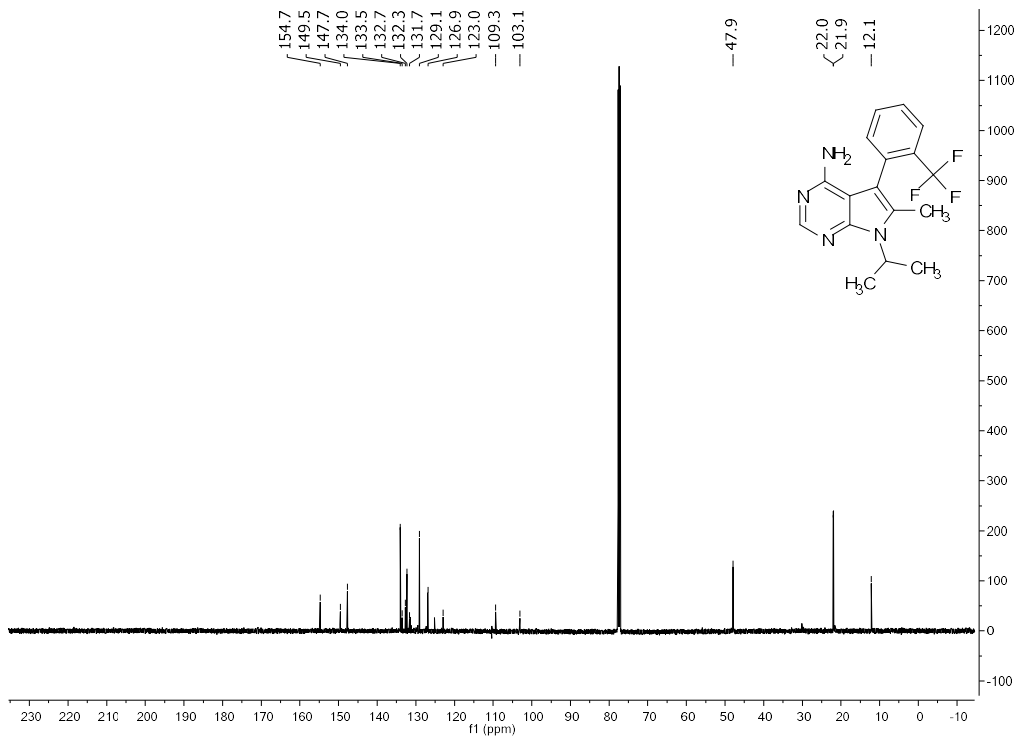
^1H , ^{13}C , and ^{19}F (referenced to trifluorotoluene) Spectral Data of 6-bromo-7-isopropyl-5-(2-(trifluoromethyl)phenyl)-7H-pyrrolo[2,3-d]pyrimidin-4-amine



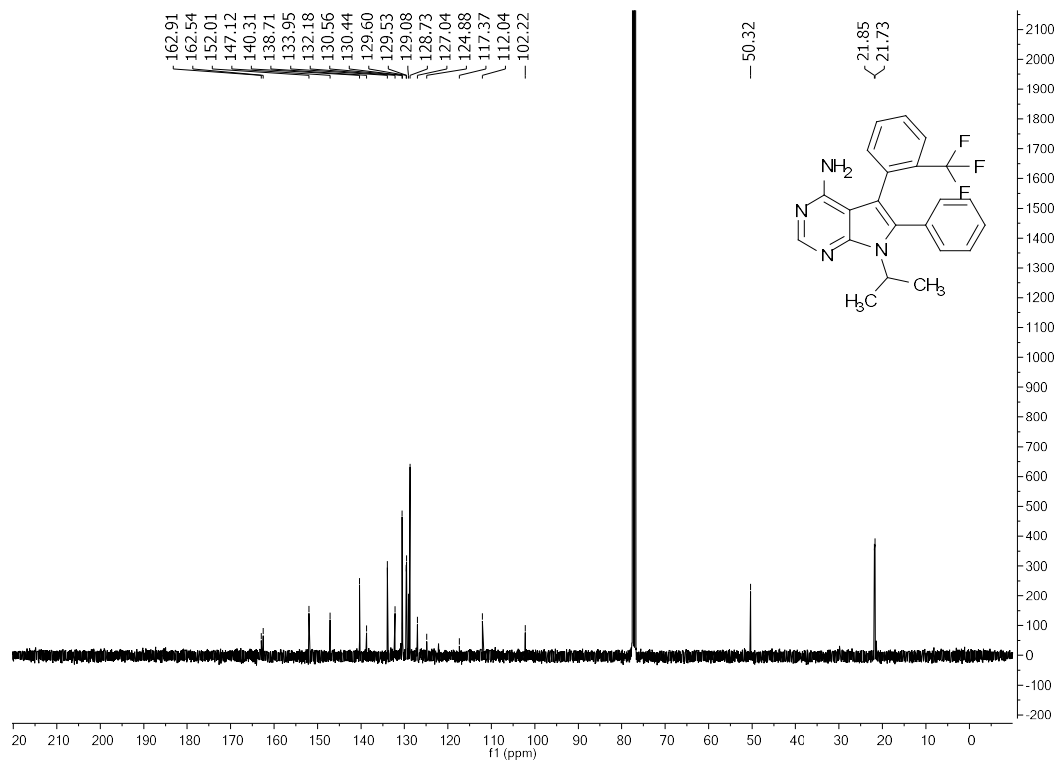
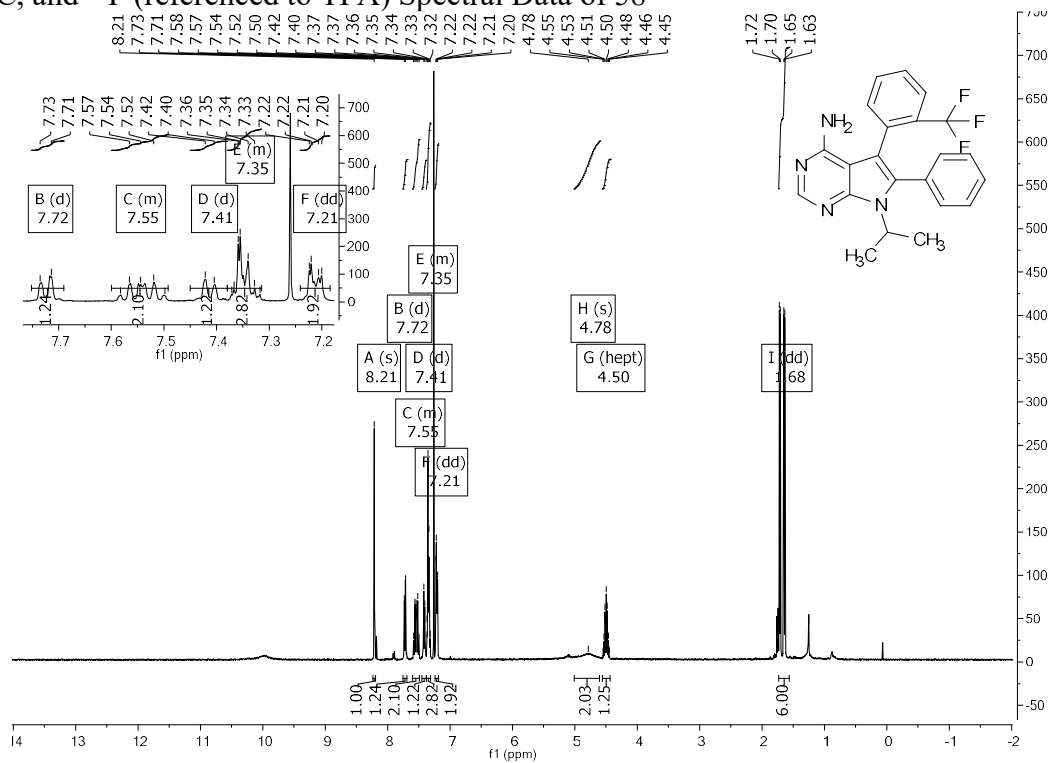


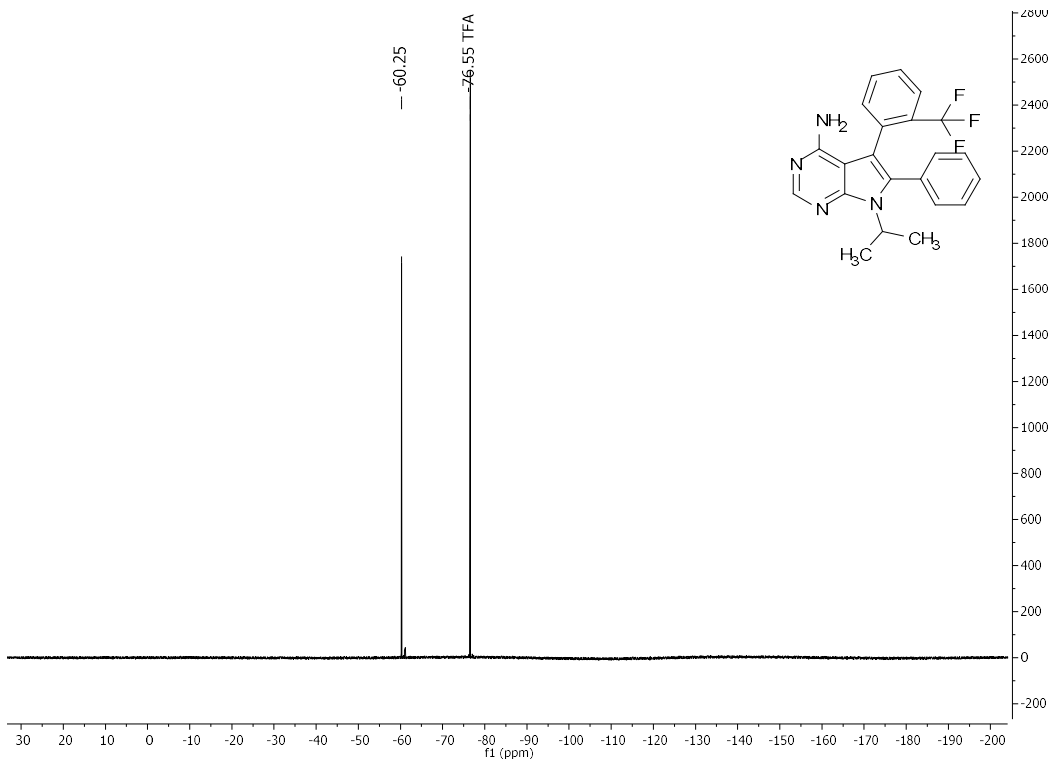
^1H , ^{13}C , and ^{19}F (referenced to TFA) Spectral Data of 57



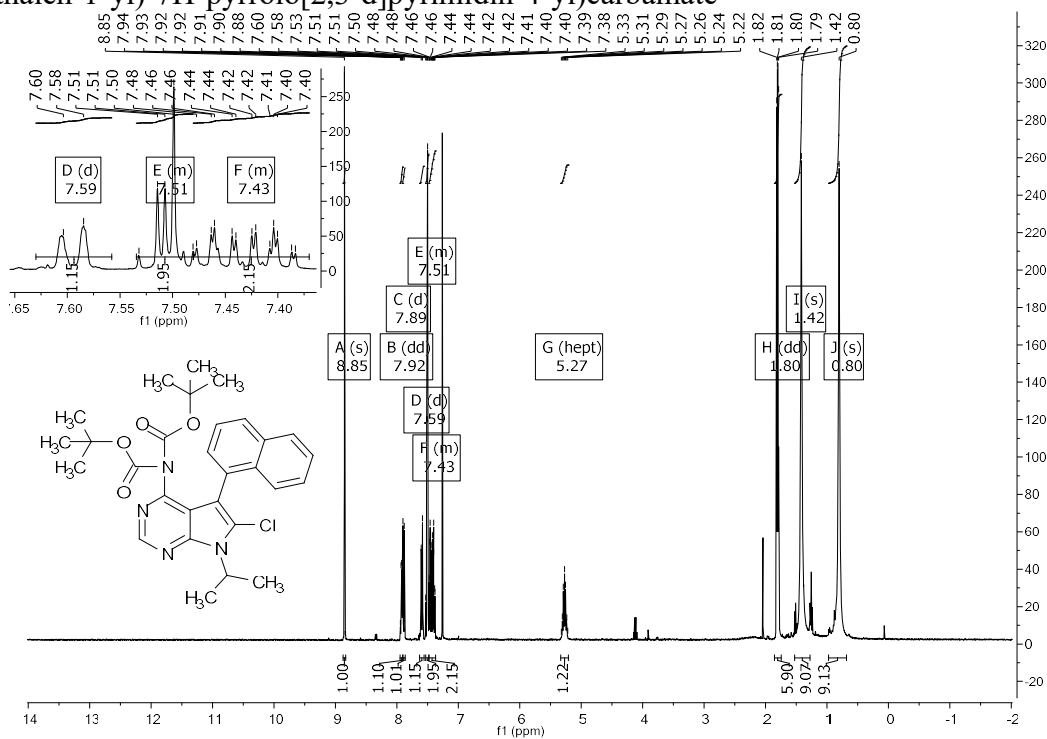


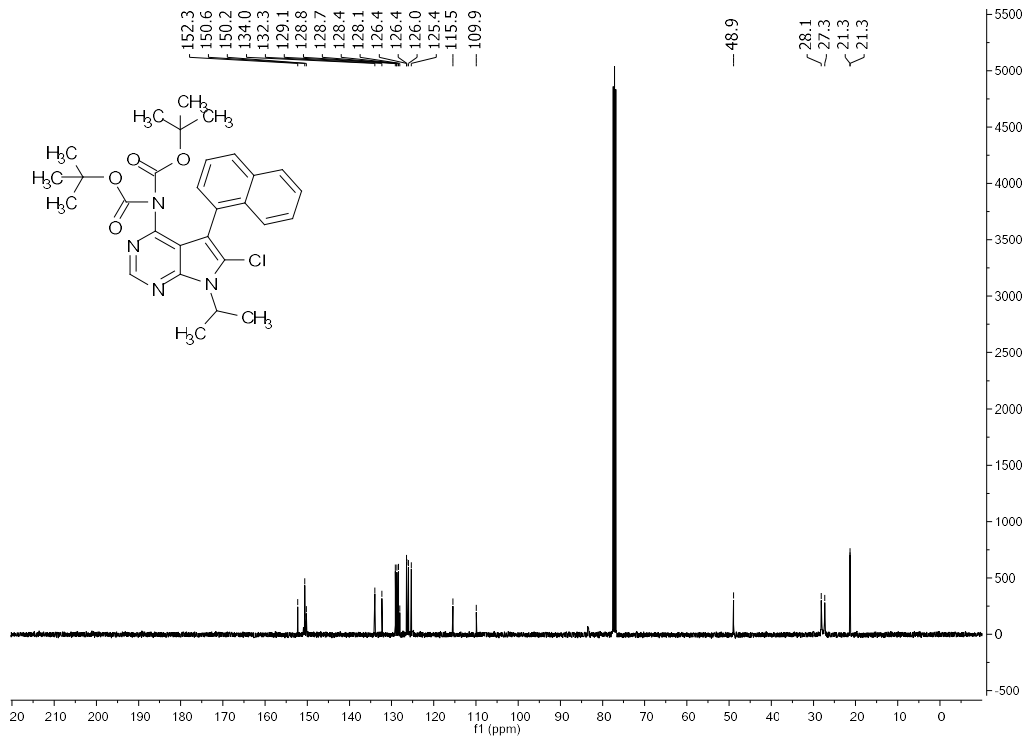
^1H , ^{13}C , and ^{19}F (referenced to TFA) Spectral Data of 58



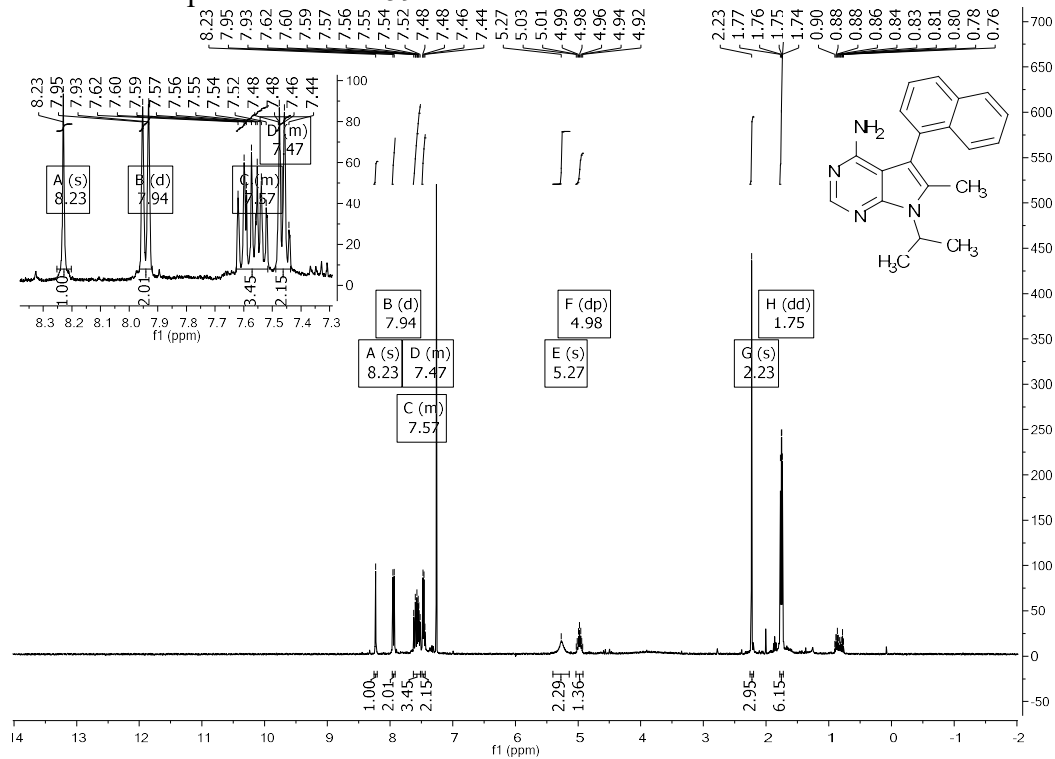


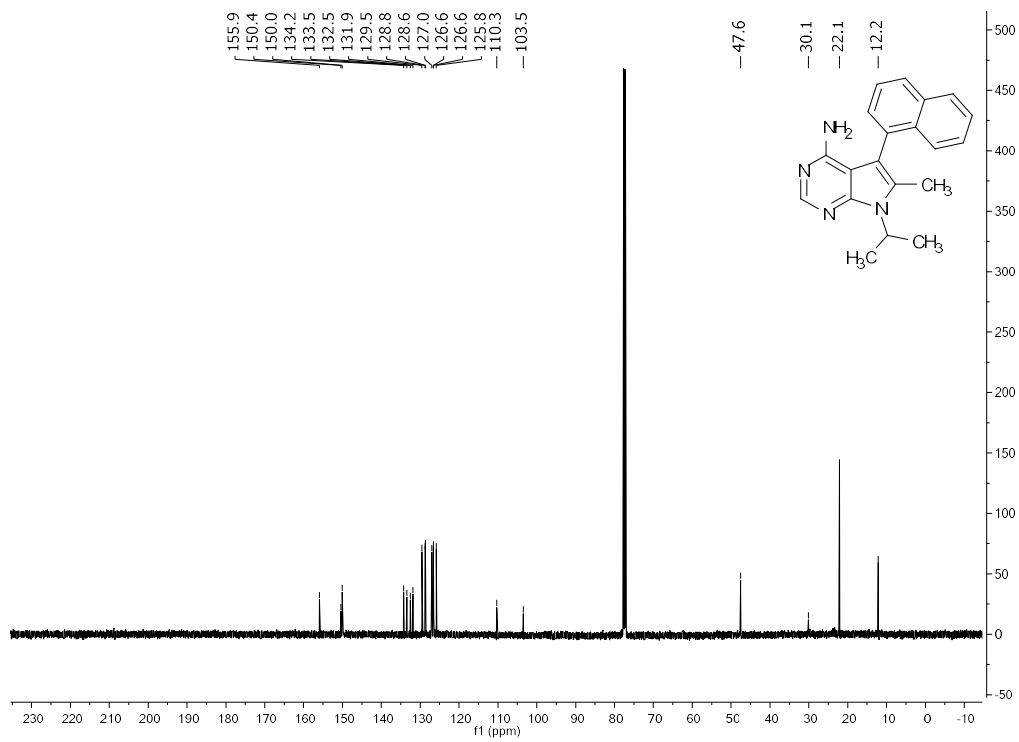
^1H , ^{13}C , and ^{19}F Spectral Data of tert-butyl (tert-butoxycarbonyl)(6-chloro-7-isopropyl-5-(naphthalen-1-yl)-7H-pyrrolo[2,3-d]pyrimidin-4-yl)carbamate



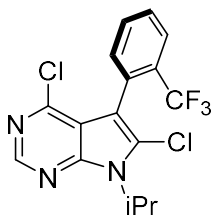


¹H and ¹³C Spectral Data of 59





2.1.27 Chiral HPLC Traces

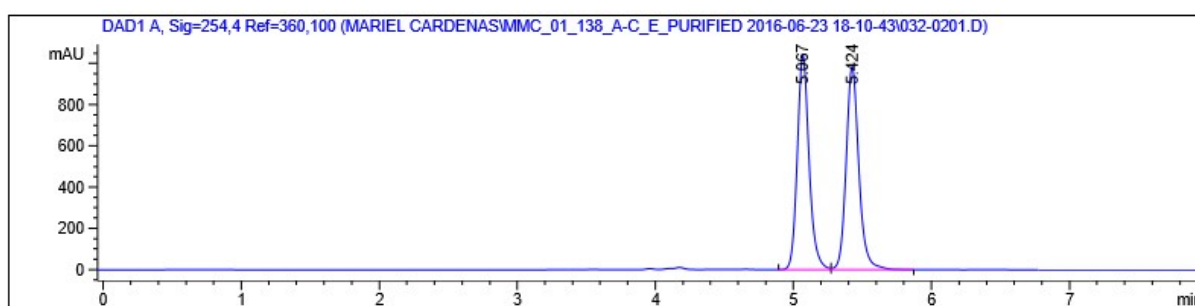


major enantiomer,
(*S_a*)-21

21 was measured with HPLC analysis using Chiralpak IA Hexanes/IPA (98:2), flow rate = 1.0 mL/min, tR = 5.1 min (minor) and tR = 5.4 min (major).

→ Determined 6.5:93.5 e.r., 87 ee%

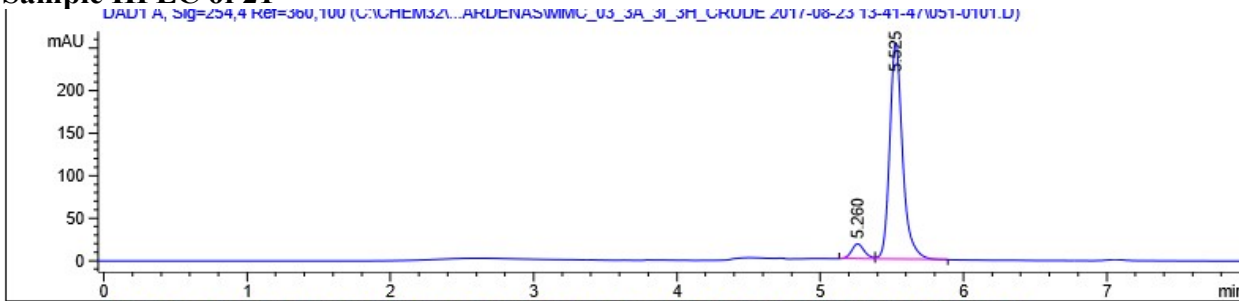
Racemic Standard of 21



Signal 1: DAD1 A, Sig=254,4 Ref=360,100

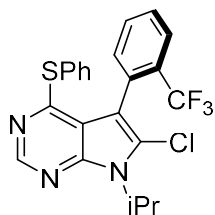
Peak #	RetTime [min]	Type	Width [min]	Area [mAU*s]	Height [mAU]	Area %
1	5.067	BV	0.0914	6203.22168	1042.72803	49.5136
2	5.424	VB	0.0966	6325.10791	988.85168	50.4864
Totals :				1.25283e4	2031.57971	

Sample HPLC of 21



Signal 1: DAD1 A, Sig=254,4 Ref=360,100

Peak #	RetTime [min]	Type	Width [min]	Area [mAU*s]	Height [mAU]	Area %
1	5.260	BV	0.0953	111.02058	17.66045	6.5183
2	5.525	VB	0.0948	1592.20068	255.17557	93.4817
Totals :				1703.22127	272.83602	

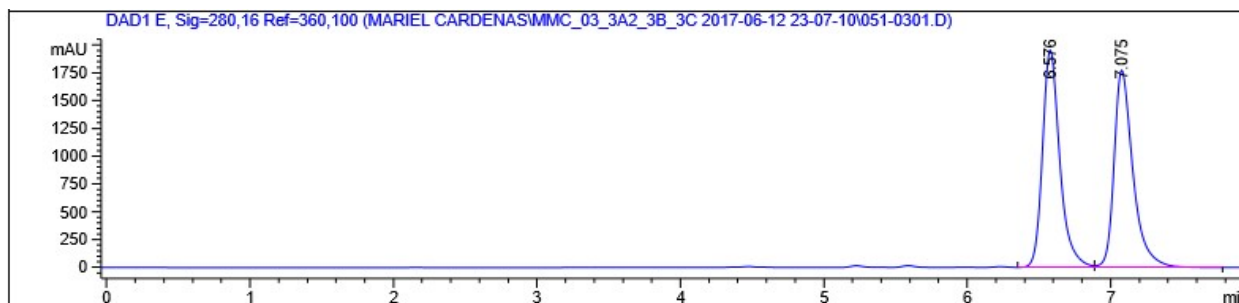


major enantiomer,
(*R_a*)-22

22 was measured with HPLC analysis using Chiralpak IA Hexanes/IPA (98:2), flow rate = 1.0 mL/min, *t*_R = 6.6 min (minor) and *t*_R = 7.1 min (major).

→ Determined 7.9:92.1 e.r., 84.2 ee%

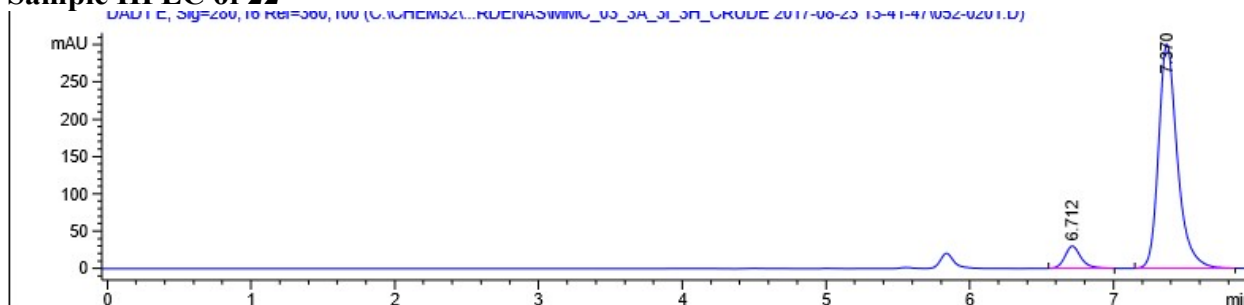
Racemic Standard of 22



Signal 5: DAD1 E, Sig=280,16 Ref=360,100

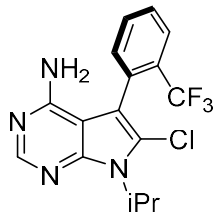
Peak #	RetTime [min]	Type	Width [min]	Area [mAU*s]	Height [mAU]	Area %
1	6.576	VV	0.1282	1.64532e4	1955.50183	50.2751
2	7.075	VB	0.1390	1.62731e4	1774.10095	49.7249
Totals :				3.27262e4	3729.60278	

Sample HPLC of 22



Signal 5: DAD1 E, Sig=280,16 Ref=360,100

Peak #	RetTime [min]	Type	Width [min]	Area [mAU*s]	Height [mAU]	Area %
1	6.712	BB	0.1195	235.29710	30.00303	7.9080
2	7.370	BB	0.1382	2740.13989	301.02481	92.0920
Totals :				2975.43700	331.02784	



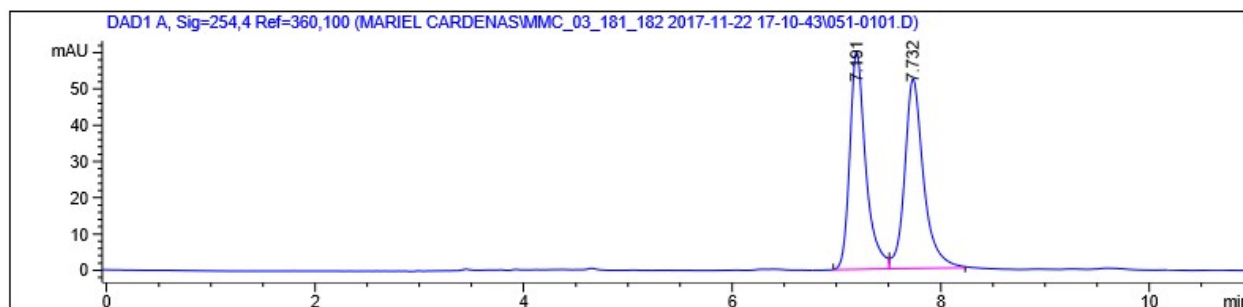
major enantiomer,

60

60 was measured with HPLC analysis using Chiralpak IA Hexanes/EtOH (80:20), flow rate = 1.0 mL/min, tR = 7.2 min (major) and tR = 7.7 min (minor).

→ Determined 88.9:11.1 e.r., 77.8 ee%

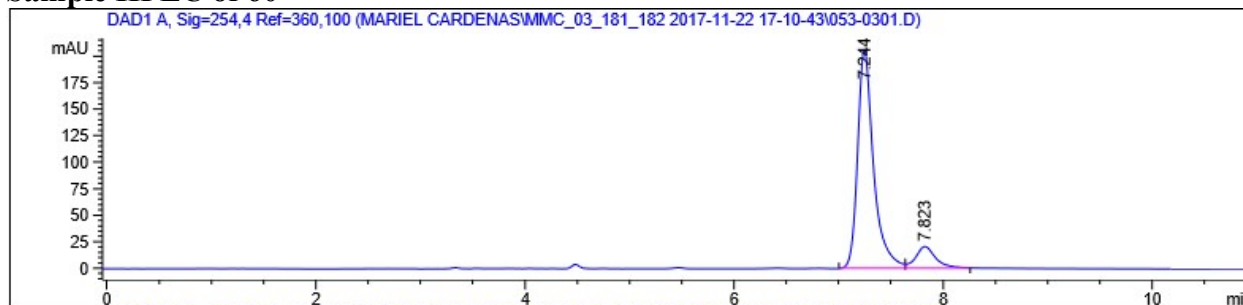
Racemic Standard of 60



Signal 1: DAD1 A, Sig=254,4 Ref=360,100

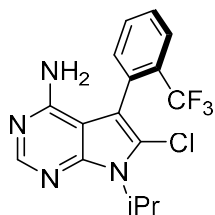
Peak #	RetTime [min]	Type	Width [min]	Area [mAU*s]	Height [mAU]	Area %
1	7.191	BV	0.1589	642.98181	60.04250	49.2519
2	7.732	VB	0.1875	662.51392	52.41048	50.7481
Totals :				1305.49573	112.45297	

Sample HPLC of 60



Signal 1: DAD1 A, Sig=254,4 Ref=360,100

Peak #	RetTime [min]	Type	Width [min]	Area [mAU*s]	Height [mAU]	Area %
1	7.244	BV	0.1573	2183.22290	206.62021	88.8514
2	7.823	VB	0.1978	273.93884	20.51527	11.1486
Totals :				2457.16174	227.13548	



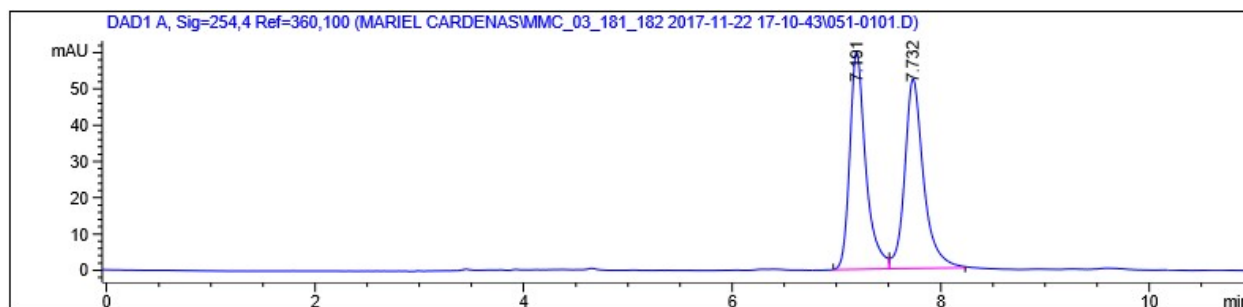
major enantiomer,

64

64 was measured with HPLC analysis using Chiralpak IA Hexanes/EtOH (80:20), flow rate = 1.0 mL/min, tR = 7.2 min (minor) and tR = 7.7 min (major).

→ Determined 8.4:91.6 e.r., 83.2 ee%

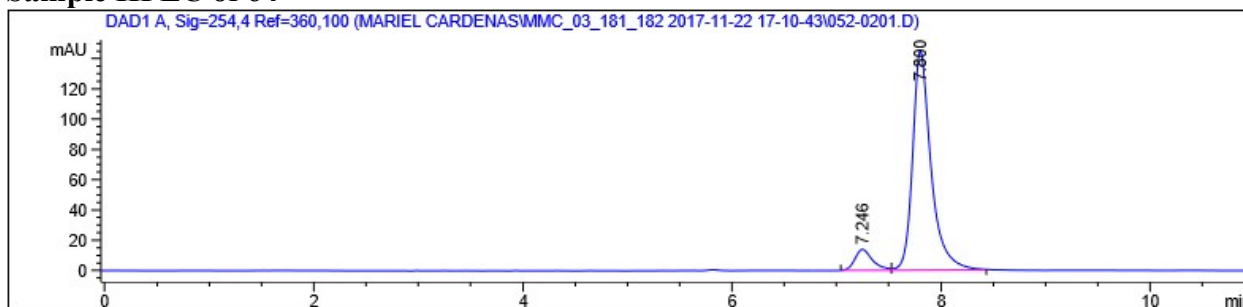
Racemic Standard of 64



Signal 1: DAD1 A, Sig=254,4 Ref=360,100

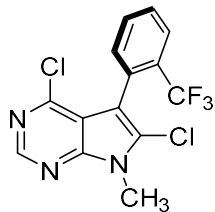
Peak #	RetTime [min]	Type	Width [min]	Area [mAU*s]	Height [mAU]	Area %
1	7.191	BV	0.1589	642.98181	60.04250	49.2519
2	7.732	VB	0.1875	662.51392	52.41048	50.7481
Totals :				1305.49573	112.45297	

Sample HPLC of 64



Signal 1: DAD1 A, Sig=254,4 Ref=360,100

Peak #	RetTime [min]	Type	Width [min]	Area [mAU*s]	Height [mAU]	Area %
1	7.246	BV	0.1778	163.63228	13.85399	8.4263
2	7.800	VB	0.1812	1778.29932	144.87025	91.5737
Totals :				1941.93159	158.72425	

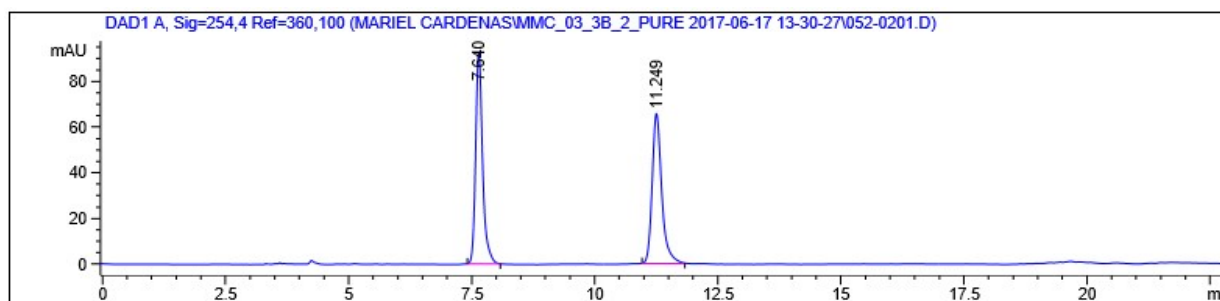


major enantiomer,
(*S_a*)-23

23 was measured with HPLC analysis using Chiralpak IA Hexanes/IPA (98:2), flow rate = 1.0 mL/min, t_R = 7.6 min (minor) and t_R = 11.2 min (major).

→ Determined 10.4:89.6 e.r., 79.2 ee%

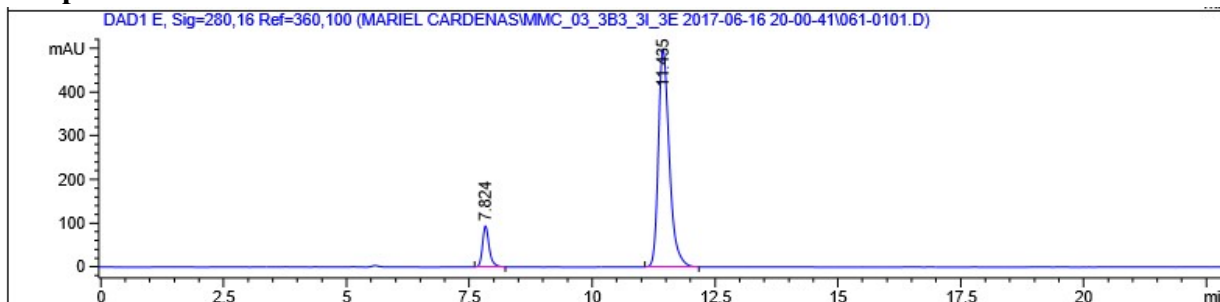
Racemic Standard of 23



Signal 1: DAD1 A, Sig=254,4 Ref=360,100

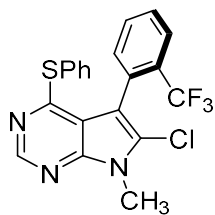
Peak #	RetTime [min]	Type	Width [min]	Area [mAU*s]	Height [mAU]	Area %
1	7.640	BB	0.1491	917.96295	93.07886	50.6082
2	11.249	BB	0.2051	895.89917	65.71040	49.3918
Totals :				1813.86212	158.78925	

Sample HPLC of 23



Signal 5: DAD1 E, Sig=280,16 Ref=360,100

Peak #	RetTime [min]	Type	Width [min]	Area [mAU*s]	Height [mAU]	Area %
1	7.824	BB	0.1453	895.23553	93.82450	10.3794
2	11.435	BB	0.2393	7729.90381	497.43048	89.6206
Totals :				8625.13934	591.25498	

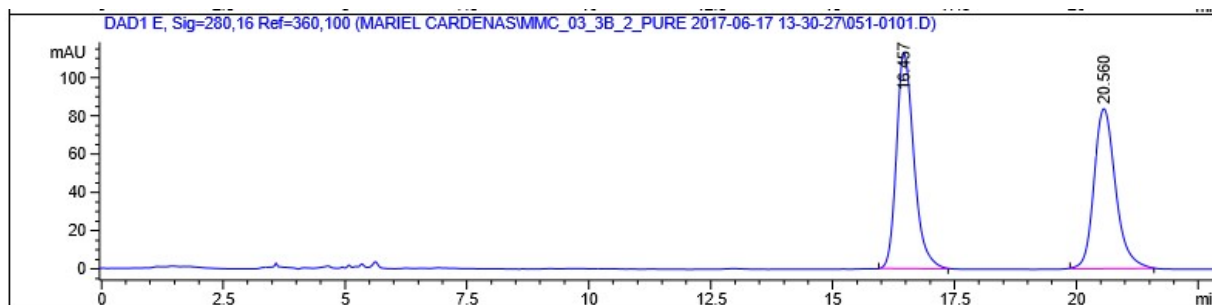


major enantiomer,
(*R*_a)-24

24 was measured with HPLC analysis using Chiralpak IA Hexanes/IPA (98:2), flow rate = 1.0 mL/min, t_R = 16.5 min (major) and t_R = 20.6 min (minor).

→ Determined 87.4:12.6 e.r., 74.8 ee%

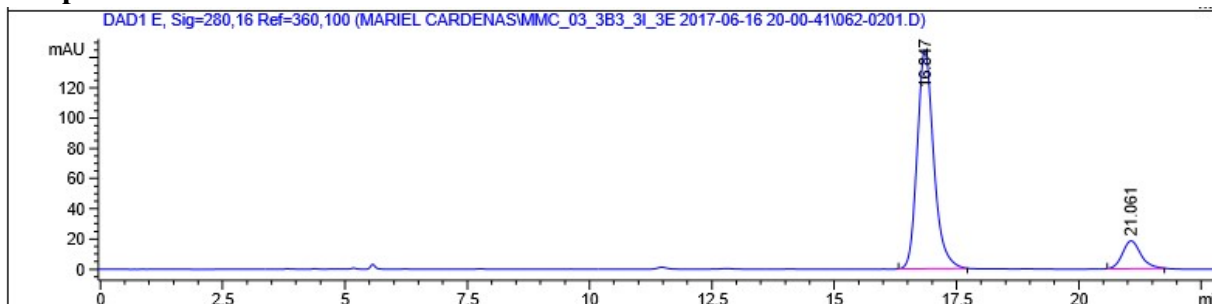
Racemic Standard of 24



Signal 5: DAD1 E, Sig=280,16 Ref=360,100

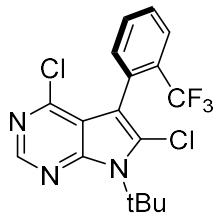
Peak #	RetTime [min]	Type	Width [min]	Area [mAU*s]	Height [mAU]	Area %
1	16.457	BB	0.3861	2825.44019	112.83447	52.1721
2	20.560	BB	0.4751	2590.17310	83.68762	47.8279
Totals :				5415.61328	196.52209	

Sample HPLC of 24



Signal 5: DAD1 E, Sig=280,16 Ref=360,100

Peak #	RetTime [min]	Type	Width [min]	Area [mAU*s]	Height [mAU]	Area %
1	16.847	BB	0.3542	3406.83887	144.94890	87.3735
2	21.061	BB	0.4038	492.32932	18.54117	12.6265
Totals :				3899.16818	163.49007	

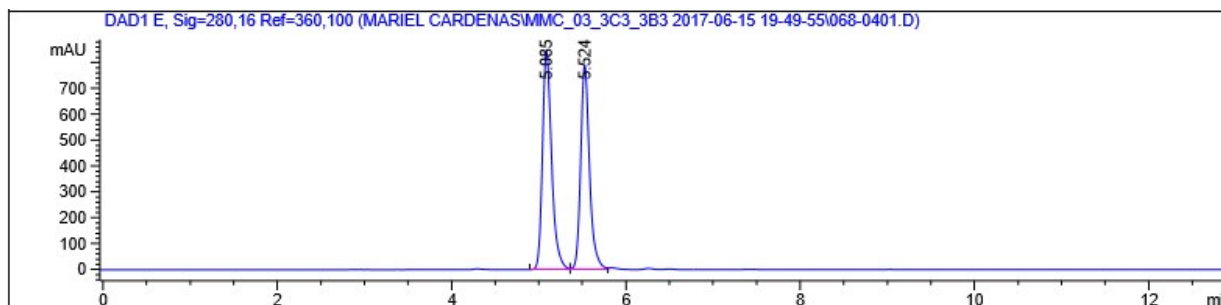


major enantiomer,
(*S*_a)-25

25 was measured with HPLC analysis using Chiralpak IA Hexanes/IPA (98:2), flow rate = 1.0 mL/min, t_R = 5.1 min (minor) and t_R = 5.5 min (major).

→ Determined 18.1:81.9 e.r., 63.8 ee%

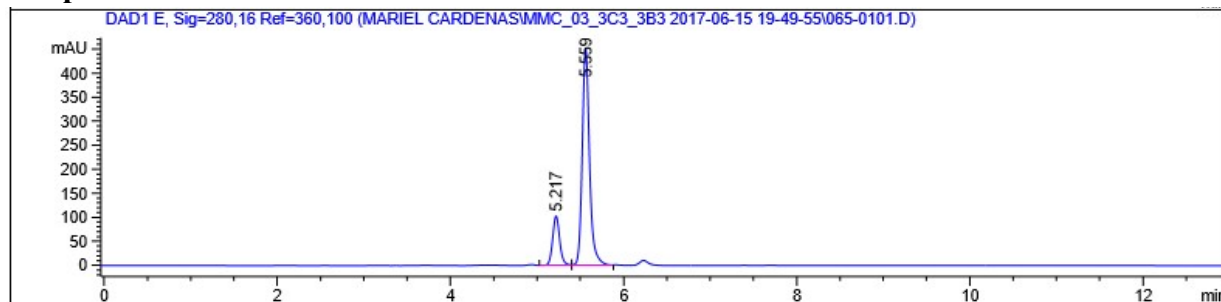
Racemic Standard of 25



Signal 5: DAD1 E, Sig=280,16 Ref=360,100

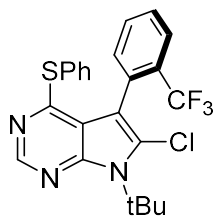
Peak #	RetTime [min]	Type	Width [min]	Area [mAU*s]	Height [mAU]	Area %
1	5.085	BV	0.1112	6189.62842	848.01636	52.3991
2	5.524	VV	0.1068	5622.83691	792.26917	47.6009
Totals :				1.18125e4	1640.28552	

Sample HPLC of 25



Signal 5: DAD1 E, Sig=280,16 Ref=360,100

Peak #	RetTime [min]	Type	Width [min]	Area [mAU*s]	Height [mAU]	Area %
1	5.217	VV	0.0866	587.82611	102.93880	18.1392
2	5.559	VB	0.0885	2652.81299	451.58722	81.8608
Totals :				3240.63910	554.52602	

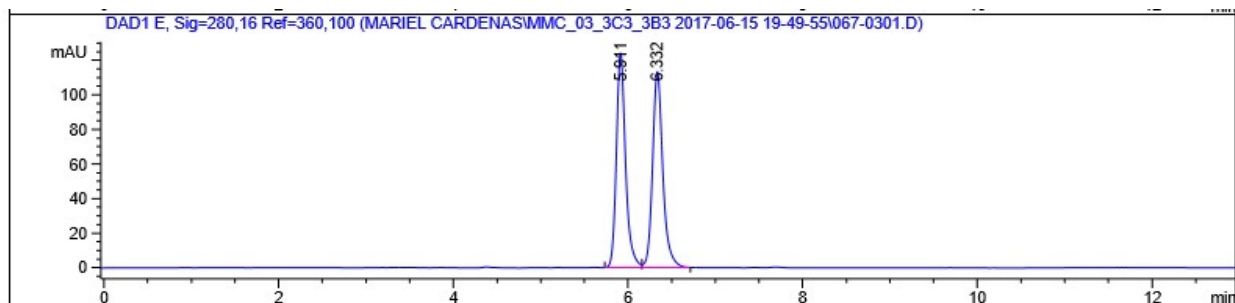


major enantiomer,
(*R*_a)-26

26 was measured with HPLC analysis using Chiralpak IA Hexanes/IPA (98:2), flow rate = 1.0 mL/min, t_R = 5.9 (minor) and t_R = 6.3 min (major).

→ Determined 6.3:93.7 e.r., 87.4 ee%

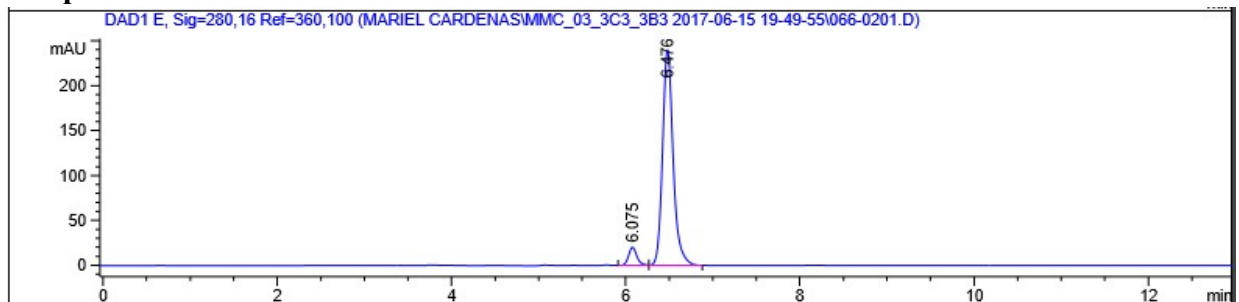
Racemic Standard of 26



Signal 5: DAD1 E, Sig=280,16 Ref=360,100

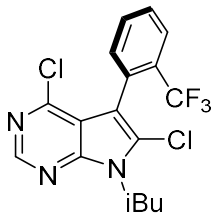
Peak #	RetTime [min]	Type	Width [min]	Area [mAU*s]	Height [mAU]	Area %
1	5.911	BV	0.1111	907.68311	124.42542	49.4178
2	6.332	VB	0.1235	929.07104	113.48219	50.5822
Totals :				1836.75415	237.90761	

Sample HPLC of 26



Signal 5: DAD1 E, Sig=280,16 Ref=360,100

Peak #	RetTime [min]	Type	Width [min]	Area [mAU*s]	Height [mAU]	Area %
1	6.075	VV	0.1029	137.30356	20.30781	6.3192
2	6.476	VB	0.1288	2035.48792	240.39420	93.6808
Totals :				2172.79147	260.70200	

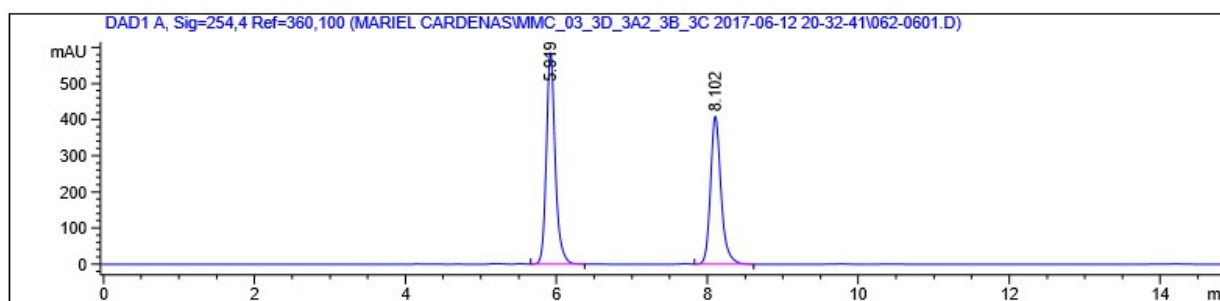


major enantiomer,
(*S*_a)-27

27 was measured with HPLC analysis using Chiralpak IA Hexanes/IPA (98:2), flow rate = 1.0 mL/min, t_R = 5.9 (minor) and t_R = 8.1 min (major).

→ Determined 4.9:95.1 e.r., 90.2 ee%

Racemic Standard of 27

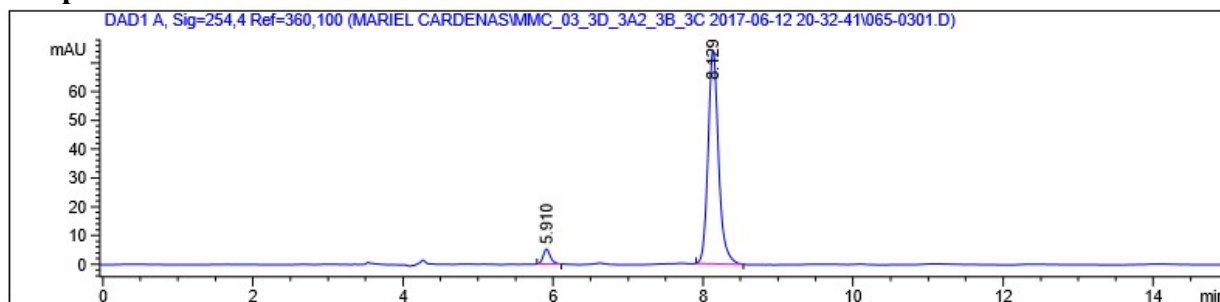


Signal 1: DAD1 A, Sig=254,4 Ref=360,100

Peak #	RetTime [min]	Type	Width [min]	Area [mAU*s]	Height [mAU]	Area %
1	5.919	VB	0.1230	4774.09570	586.03693	54.6016
2	8.102	VB	0.1450	3969.40869	409.91248	45.3984

Totals : 8743.50439 995.94940

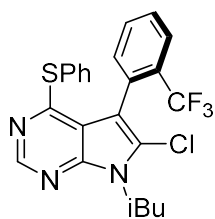
Sample HPLC of 27



Signal 1: DAD1 A, Sig=254,4 Ref=360,100

Peak #	RetTime [min]	Type	Width [min]	Area [mAU*s]	Height [mAU]	Area %
1	5.910	BB	0.1051	36.91776	5.30790	4.8638
2	8.129	BB	0.1472	722.10583	74.44534	95.1362

Totals : 759.02359 79.75324

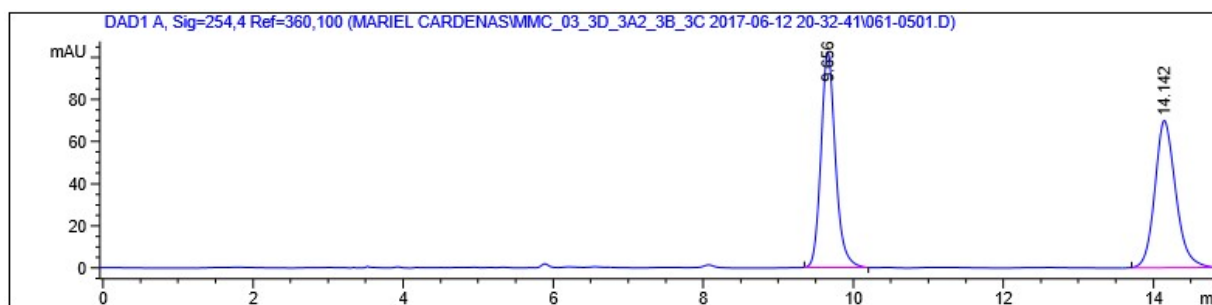


major enantiomer,
(*R*_a)-28

28 was measured with HPLC analysis using Chiralpak IA Hexanes/IPA (98:2), flow rate = 1.0 mL/min, t_R = 9.7 (major) and t_R = 14.1 min (minor).

→ Determined 82.6:17.4 e.r., 65.2 ee%

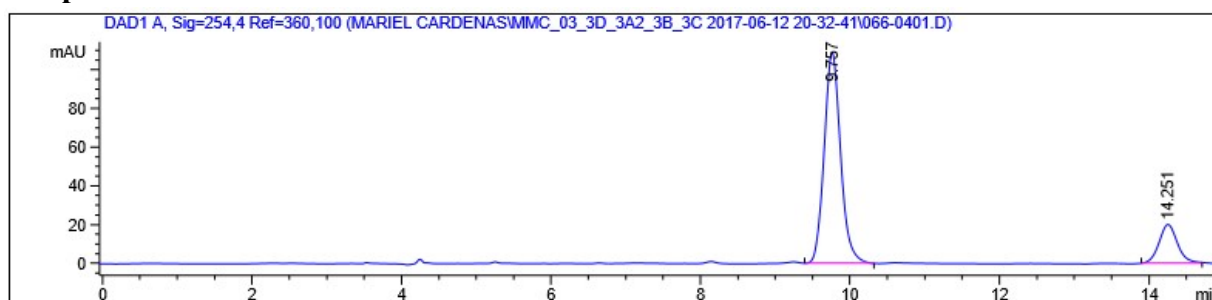
Racemic Standard of 28



Signal 1: DAD1 A, Sig=254,4 Ref=360,100

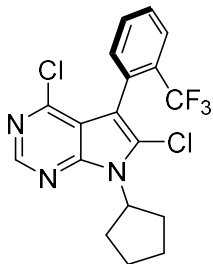
Peak #	RetTime [min]	Type	Width [min]	Area [mAU*s]	Height [mAU]	Area %
1	9.656	BB	0.2047	1376.22229	102.49348	50.2947
2	14.142	BB	0.2964	1360.09290	70.08131	49.7053
Totals :				2736.31519	172.57479	

Sample HPLC of 28



Signal 1: DAD1 A, Sig=254,4 Ref=360,100

Peak #	RetTime [min]	Type	Width [min]	Area [mAU*s]	Height [mAU]	Area %
1	9.757	VB	0.2320	1660.45508	108.81732	82.6328
2	14.251	BB	0.2623	348.98288	20.12815	17.3672
Totals :				2009.43796	128.94547	

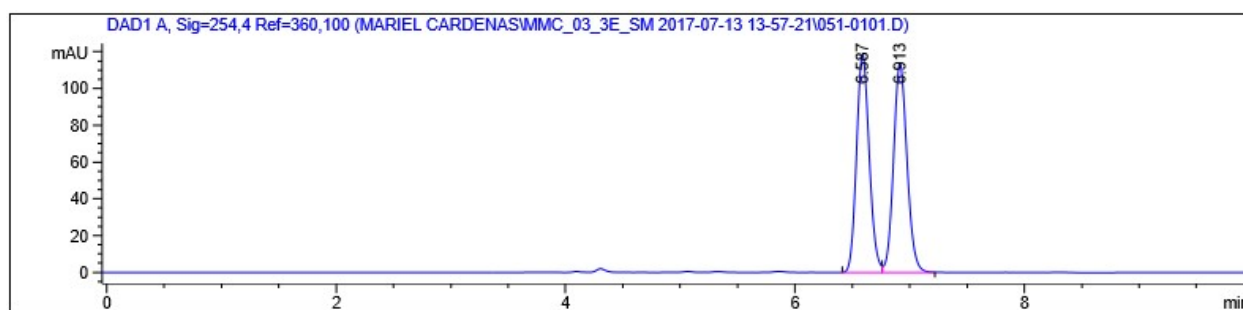


major enantiomer,
(*S_a*)-29

29 was measured with HPLC analysis using Chiralpak IC Hexanes/IPA (98:2), flow rate = 1.0 mL/min, *t_R* = 6.6 (major) and *t_R* = 6.9 min (minor).

→ Determined 6.0:94.0 e.r., 88 ee%

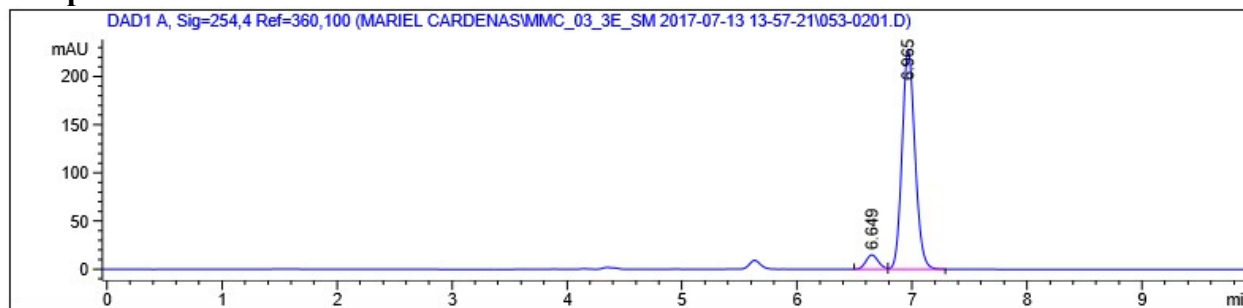
Racemic Standard of 29



Signal 1: DAD1 A, Sig=254,4 Ref=360,100

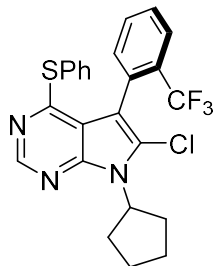
Peak #	RetTime [min]	Type	Width [min]	Area [mAU*s]	Height [mAU]	Area %
1	6.587	BV	0.1198	914.09552	118.81230	49.5156
2	6.913	VB	0.1256	931.98181	113.75684	50.4844
Totals :				1846.07733	232.56915	

Sample HPLC of 29



Signal 1: DAD1 A, Sig=254,4 Ref=360,100

Peak #	RetTime [min]	Type	Width [min]	Area [mAU*s]	Height [mAU]	Area %
1	6.649	BV	0.1162	112.76811	14.92136	5.9631
2	6.965	VB	0.1213	1778.33374	227.19728	94.0369
Totals :				1891.10185	242.11864	

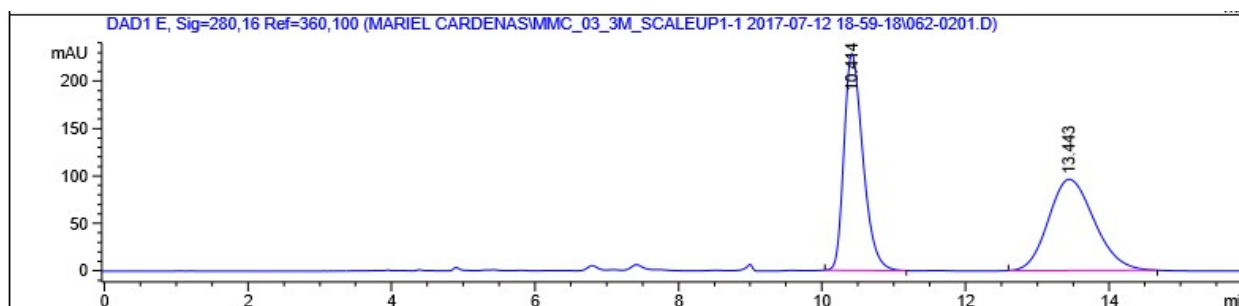


major enantiomer,
(*R*_a)-30

30 was measured with HPLC analysis using Chiralpak IA Hexanes/IPA (98:2), flow rate = 1.0 mL/min, t_R = 10.4 (minor) and t_R = 13.6 min (major).

→ Determined 9.2:90:8 e.r., 81.6 ee%

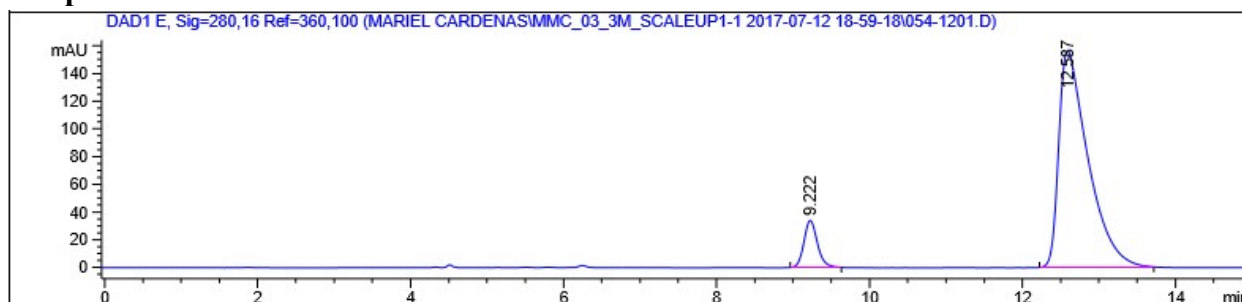
Racemic Standard of 30



Signal 5: DAD1 E, Sig=280,16 Ref=360,100

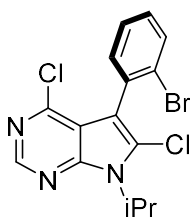
Peak #	RetTime [min]	Type	Width [min]	Area [mAU*s]	Height [mAU]	Area %
1	10.414	BB	0.2834	4217.74707	228.48947	49.4399
2	13.443	BB	0.6923	4313.30859	96.35287	50.5601
Totals :				8531.05566	324.84235	

Sample HPLC of 30



Signal 5: DAD1 E, Sig=280,16 Ref=360,100

Peak #	RetTime [min]	Type	Width [min]	Area [mAU*s]	Height [mAU]	Area %
1	9.222	BB	0.1886	422.72644	34.10819	9.2344
2	12.587	BB	0.3901	4154.99707	156.30141	90.7656
Totals :				4577.72351	190.40960	

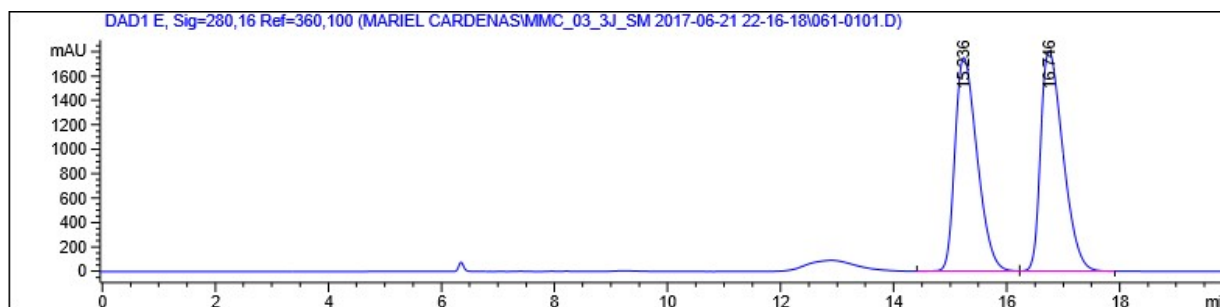


major enantiomer,
(*S_a*)-31

31 was measured with HPLC analysis using Chiralpak IC Hexanes/EtOH (99.5:0.5), flow rate = 0.7 mL/min, t_R = 15.2 (minor) and t_R = 16.7 min (major).

→ Determined 1.7:98:3 e.r., 96.6 ee%

Racemic Standard of 31

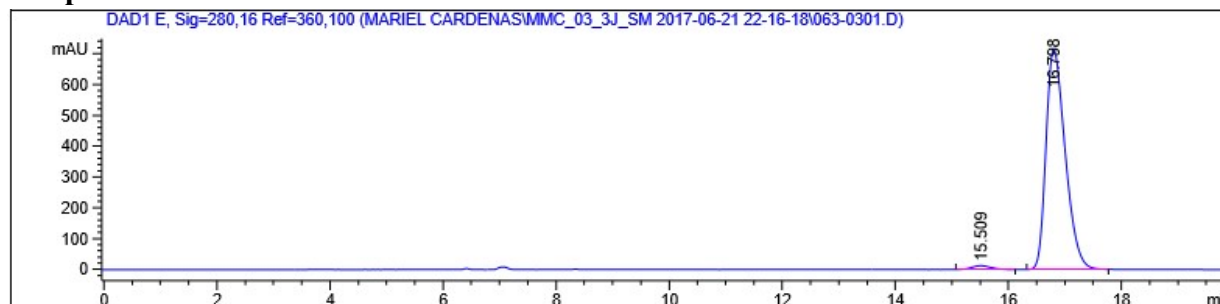


Signal 5: DAD1 E, Sig=280,16 Ref=360,100

Peak #	RetTime [min]	Type	Width [min]	Area [mAU*s]	Height [mAU]	Area %
1	15.236	VV	0.4233	4.79134e4	1750.52527	49.0603
2	16.746	VB	0.4258	4.97488e4	1803.58862	50.9397

Totals : 9.76622e4 3554.11389

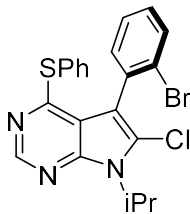
Sample HPLC of 31



Signal 5: DAD1 E, Sig=280,16 Ref=360,100

Peak #	RetTime [min]	Type	Width [min]	Area [mAU*s]	Height [mAU]	Area %
1	15.509	BB	0.3628	300.52310	12.66845	1.7494
2	16.798	BB	0.3640	1.68785e4	713.51758	98.2506

Totals : 1.71790e4 726.18603

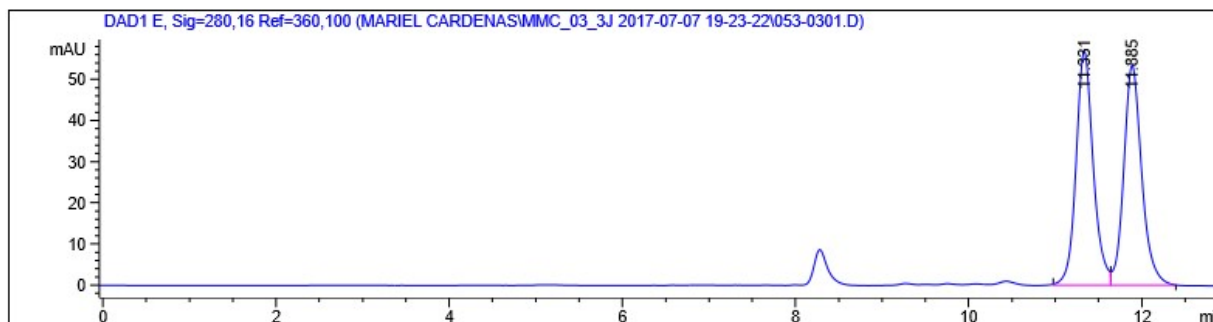


major enantiomer,
(*R_a*)-32

32 was measured with HPLC analysis using Chiralpak IA Hexanes/EtOH (98:2), flow rate = 0.5 mL/min, t_R = 11.3 (minor) and t_R = 11.9 min (major).

→ Determined 12.6:87.4 e.r., 74.8 ee%

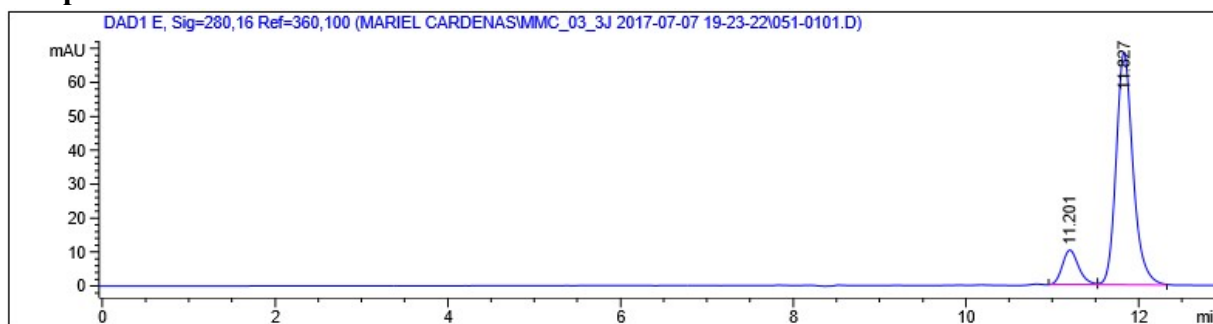
Racemic Standard of 32



Signal 5: DAD1 E, Sig=280,16 Ref=360,100

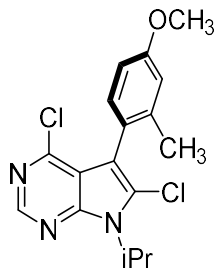
Peak #	RetTime [min]	Type	Width [min]	Area [mAU*s]	Height [mAU]	Area %
1	11.331	BV	0.2076	788.54047	56.91887	50.4579
2	11.885	VB	0.2188	774.22992	53.50144	49.5421
Totals :				1562.77039	110.42031	

Sample HPLC of 32



Signal 5: DAD1 E, Sig=280,16 Ref=360,100

Peak #	RetTime [min]	Type	Width [min]	Area [mAU*s]	Height [mAU]	Area %
1	11.201	BV	0.2021	134.90135	10.21548	12.6157
2	11.827	VB	0.2072	934.41309	68.48373	87.3843
Totals :				1069.31444	78.69922	

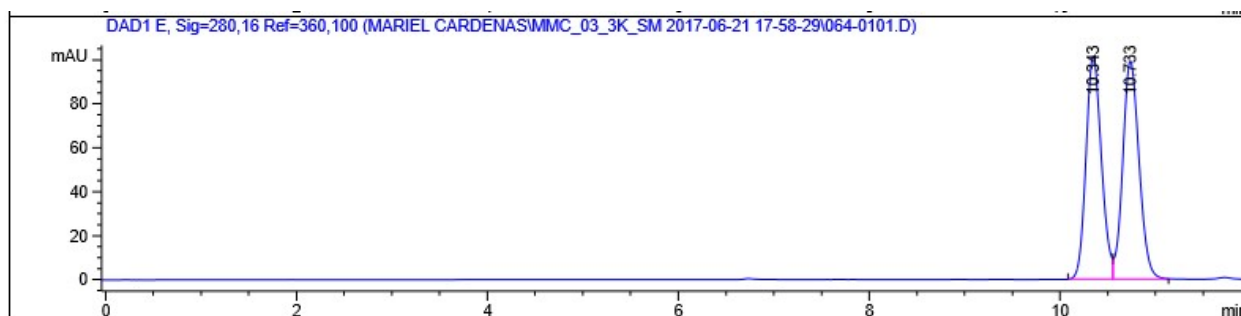


major enantiomer,
(*S_a*)-33

33 was measured with HPLC analysis using Chiralpak IC Hexanes/EtOH (99.5:0.5), flow rate = 0.7 mL/min, t_R = 10.3 (minor) and t_R = 10.7 min (major).

→ Determined 1.0:99.0 e.r., 98 ee%

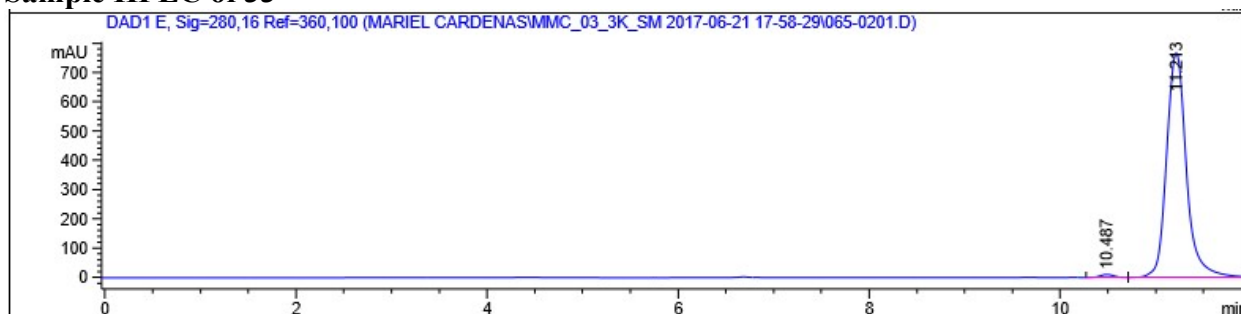
Racemic Standard of 33



Signal 5: DAD1 E, Sig=280,16 Ref=360,100

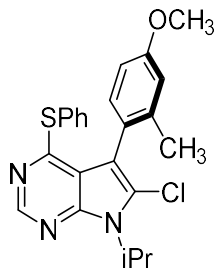
Peak #	RetTime [min]	Type	Width [min]	Area [mAU*s]	Height [mAU]	Area %
1	10.343	BV	0.1731	1138.88867	101.37023	49.1583
2	10.733	VB	0.1845	1177.88867	99.20670	50.8417
Totals :				2316.77734	200.57693	

Sample HPLC of 33



Signal 5: DAD1 E, Sig=280,16 Ref=360,100

Peak #	RetTime [min]	Type	Width [min]	Area [mAU*s]	Height [mAU]	Area %
1	10.487	VV	0.1641	114.87145	10.79732	1.0226
2	11.213	VBA	0.2249	1.11183e4	767.77875	98.9774
Totals :				1.12332e4	778.57606	

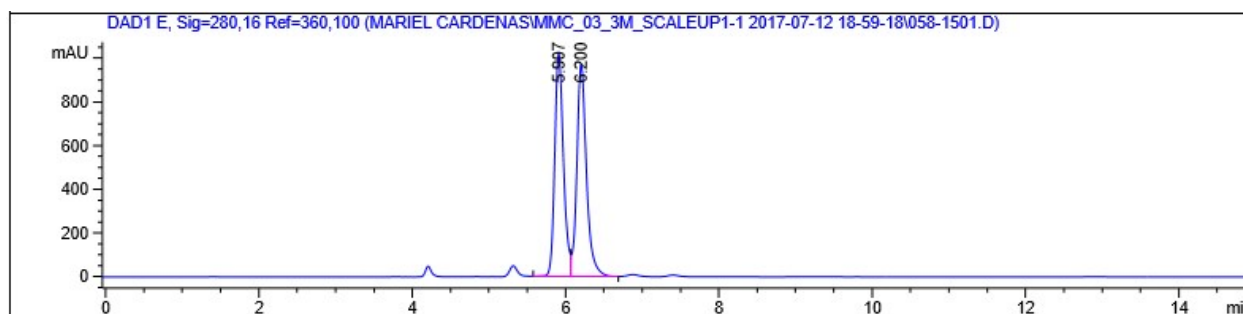


major enantiomer,
(*R*_a)-34

34 was measured with HPLC analysis using Chiralpak IC Hexanes/EtOH (99.5:0.5), flow rate = 0.7 mL/min, t_R = 10.3 (minor) and t_R = 10.7 min (major).

→ Determined 27.3:72.7 e.r., 45.4 ee%

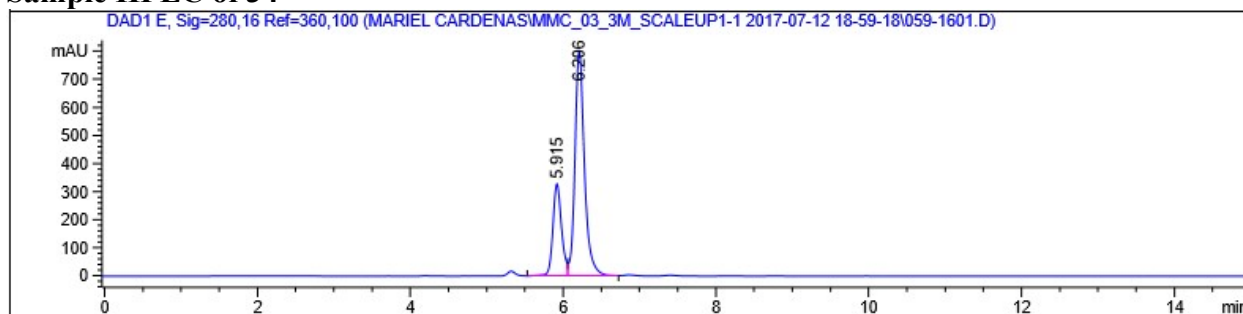
Racemic Standard of 34



Signal 5: DAD1 E, Sig=280,16 Ref=360,100

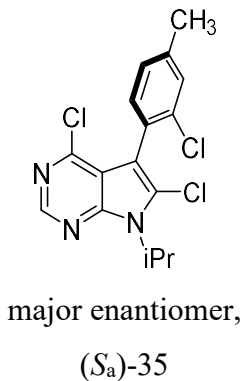
Peak #	RetTime [min]	Type	Width [min]	Area [mAU*s]	Height [mAU]	Area %
1	5.907	VV	0.1210	8166.60889	1024.95251	48.9583
2	6.200	VV	0.1299	8514.12598	974.86908	51.0417
Totals :				1.66807e4	1999.82159	

Sample HPLC of 34



Signal 5: DAD1 E, Sig=280,16 Ref=360,100

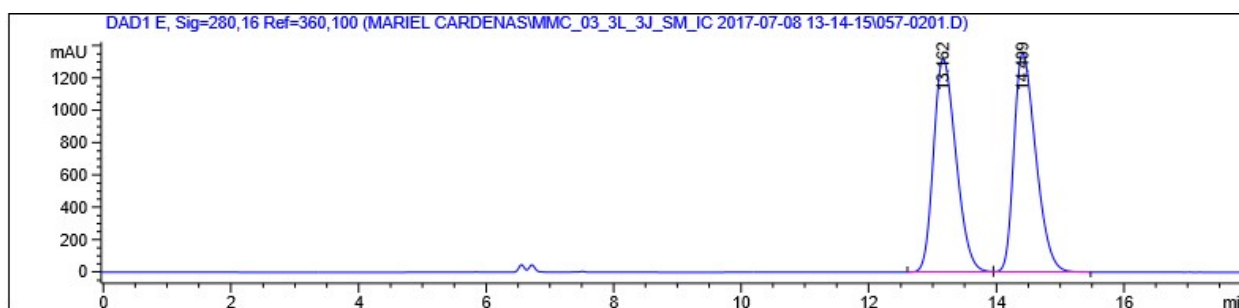
Peak #	RetTime [min]	Type	Width [min]	Area [mAU*s]	Height [mAU]	Area %
1	5.915	VV	0.1212	2623.96655	328.30048	27.3487
2	6.206	VV	0.1295	6970.52930	801.21320	72.6513
Totals :				9594.49585	1129.51367	



35 was measured with HPLC analysis using Chiralpak IC Hexanes/EtOH (99.5:0.5), flow rate = 1.0 mL/min, tR = 13.2 (minor) and tR = 14.4 min (major).

→ Determined 4.4:95.6 e.r., 91.2 ee%

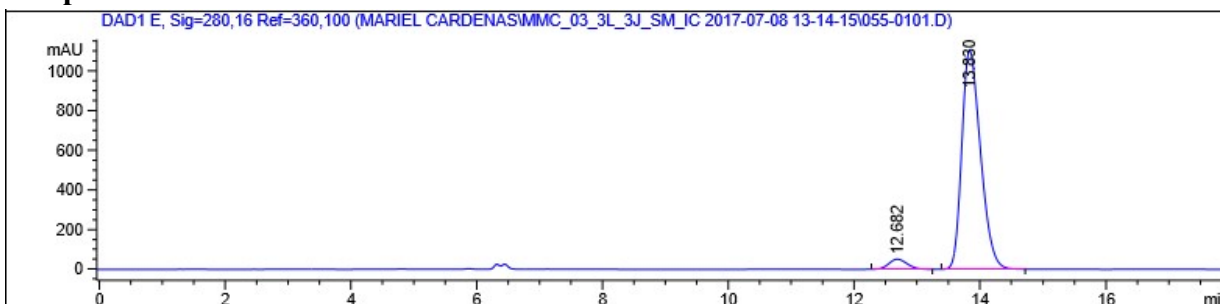
Racemic Standard of 35



Signal 5: DAD1 E, Sig=280,16 Ref=360,100

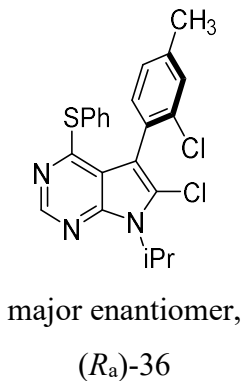
Peak #	RetTime [min]	Type	Width [min]	Area [mAU*s]	Height [mAU]	Area %
1	13.162	BV	0.3825	3.23789e4	1318.70020	49.9950
2	14.409	VB	0.3686	3.23854e4	1355.97021	50.0050
Totals :				6.47643e4	2674.67041	

Sample HPLC of 35



Signal 5: DAD1 E, Sig=280,16 Ref=360,100

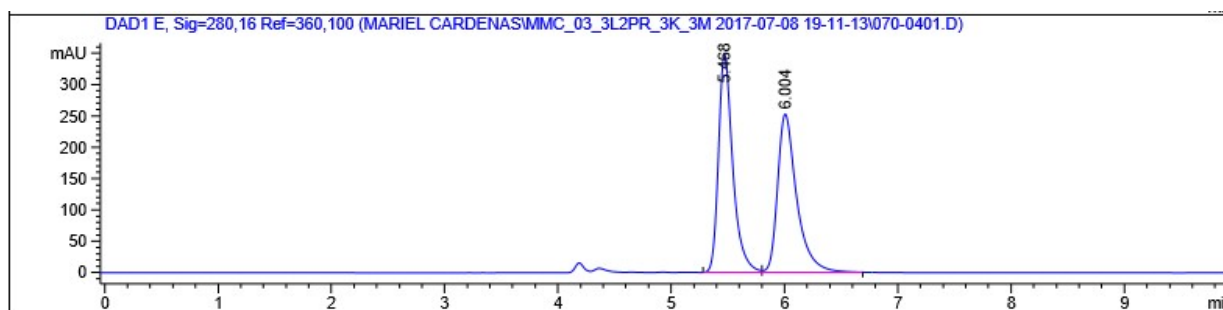
Peak #	RetTime [min]	Type	Width [min]	Area [mAU*s]	Height [mAU]	Area %
1	12.682	BB	0.3193	1051.63245	51.26130	4.3987
2	13.830	BB	0.3196	2.28563e4	1103.76050	95.6013
Totals :				2.39079e4	1155.02179	



36 was measured with HPLC analysis using Chiralpak IA Hexanes/IPA (98.2), flow rate = 0.7 mL/min, *t*_R = 5.5 (minor) and *t*_R = 6.0 min (major).

→ Determined 16.9:83.1 e.r., 66.2 ee%

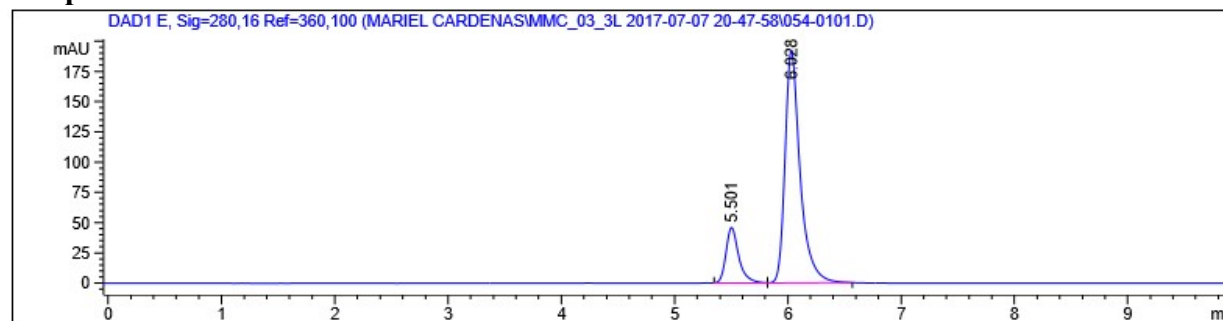
Racemic Standard of 36



Signal 5: DAD1 E, Sig=280,16 Ref=360,100

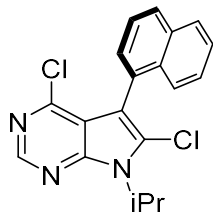
Peak #	RetTime [min]	Type	Width [min]	Area [mAU*s]	Height [mAU]	Area %
1	5.468	BV	0.1326	3069.30859	348.90720	50.7428
2	6.004	VB	0.1755	2979.44995	252.87904	49.2572
Totals :				6048.75854	601.78624	

Sample HPLC of 36



Signal 5: DAD1 E, Sig=280,16 Ref=360,100

Peak #	RetTime [min]	Type	Width [min]	Area [mAU*s]	Height [mAU]	Area %
1	5.501	BV	0.1182	363.07425	45.94283	16.8945
2	6.028	VB	0.1405	1785.99182	192.06075	83.1055
Totals :				2149.06607	238.00357	

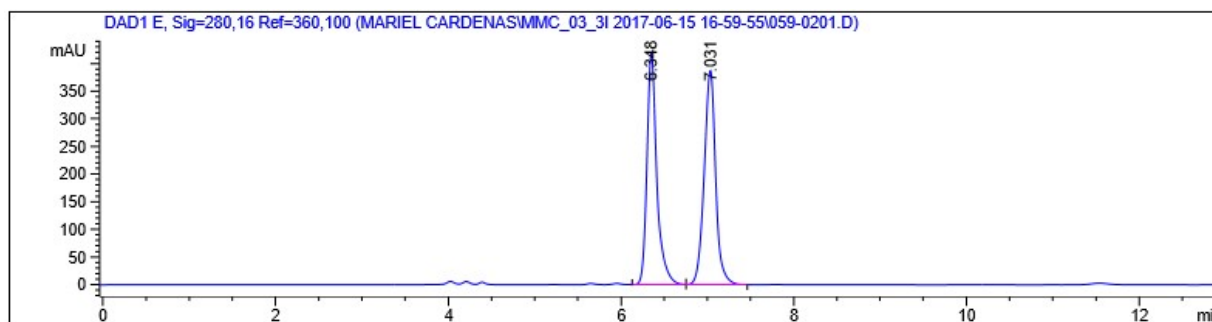


major enantiomer,
(*S*_a)-37

37 was measured with HPLC analysis using Chiralpak IA Hexanes/IPA (98:2), flow rate = 1.0 mL/min, t_R = 6.3 (minor) and t_R = 7.0 min (major).

→ Determined 8.0:92.0 e.r., 84 ee%

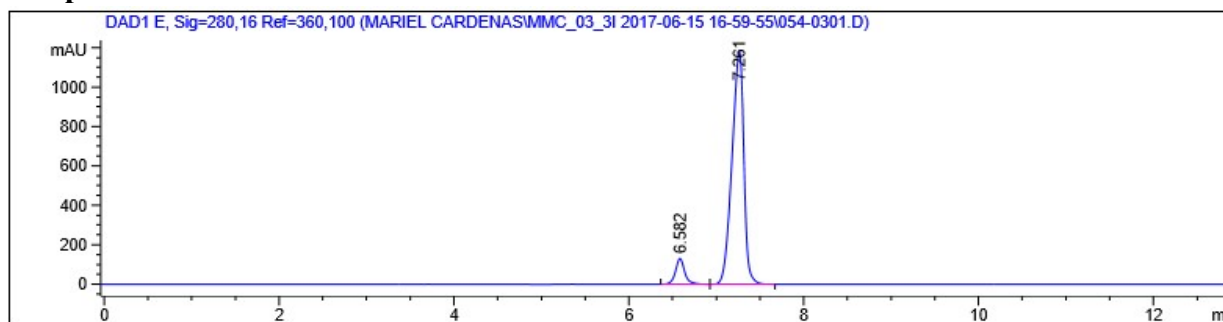
Racemic Standard of 37



Signal 5: DAD1 E, Sig=280,16 Ref=360,100

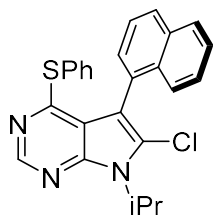
Peak #	RetTime [min]	Type	Width [min]	Area [mAU*s]	Height [mAU]	Area %
1	6.348	VV	0.1189	3350.29126	420.54169	48.3500
2	7.031	VB	0.1416	3578.95850	387.96466	51.6500
Totals :				6929.24976	808.50635	

Sample HPLC of 37



Signal 5: DAD1 E, Sig=280,16 Ref=360,100

Peak #	RetTime [min]	Type	Width [min]	Area [mAU*s]	Height [mAU]	Area %
1	6.582	BV	0.1105	973.80792	131.28720	8.0321
2	7.261	VB	0.1462	1.11502e4	1180.51123	91.9679
Totals :				1.21240e4	1311.79843	

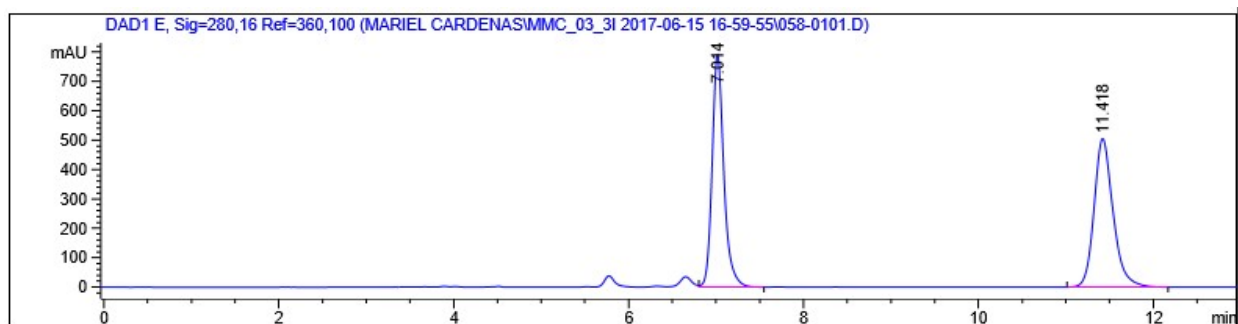


major enantiomer,
(*R*_a)-38

38 was measured with HPLC analysis using Chiralpak IA Hexanes/IPA (98:2), flow rate = 1.0 mL/min, t_R = 6.3 (minor) and t_R = 7.0 min (major).

→ Determined 23.5:76.5 e.r., 53 ee%

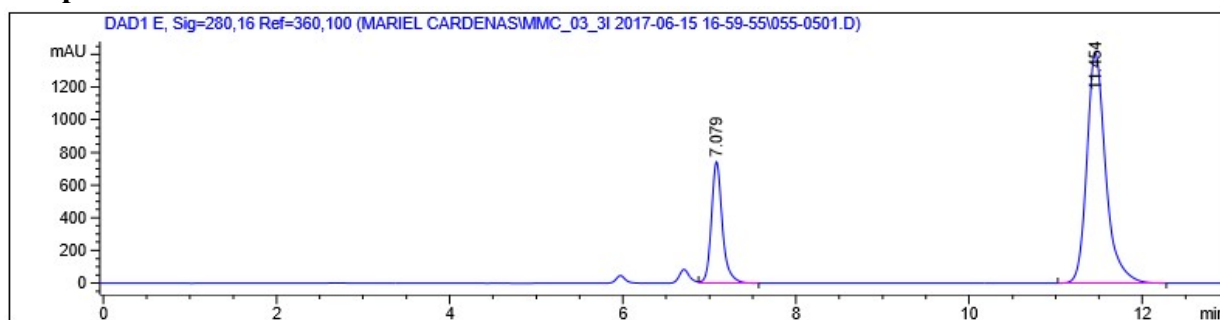
Racemic Standard of 38



Signal 5: DAD1 E, Sig=280,16 Ref=360,100

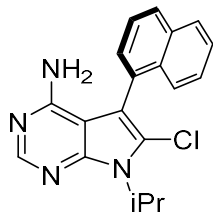
Peak #	RetTime [min]	Type	Width [min]	Area [mAU*s]	Height [mAU]	Area %
1	7.014	VB	0.1407	7392.16162	793.31683	49.1212
2	11.418	BB	0.2245	7656.66406	506.04010	50.8788
Totals :				1.50488e4	1299.35693	

Sample HPLC of 38



Signal 5: DAD1 E, Sig=280,16 Ref=360,100

Peak #	RetTime [min]	Type	Width [min]	Area [mAU*s]	Height [mAU]	Area %
1	7.079	VB	0.1330	6571.87256	744.08899	23.4674
2	11.454	BB	0.2292	2.14324e4	1410.85071	76.5326
Totals :				2.80043e4	2154.93970	

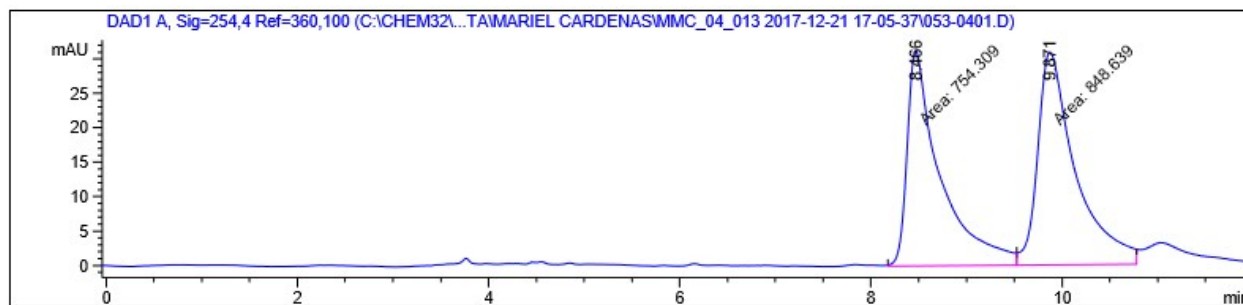


major enantiomer,
(*S*_a)-62

62 was measured with HPLC analysis using Chiralpak IA Hexanes/IPA (90:10), flow rate = 1.0 mL/min, t_R = 8.5 (major) and t_R = 9.9 min (minor).

→ Determined 86.3:13.7 e.r., 72.6 ee%

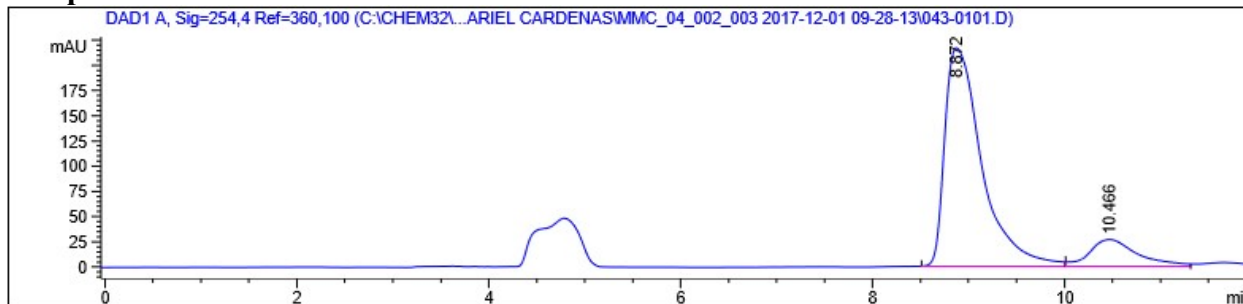
Racemic Standard of 62



Signal 1: DAD1 A, Sig=254,4 Ref=360,100

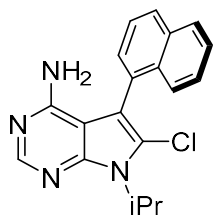
Peak #	RetTime [min]	Type	Width [min]	Area [mAU*s]	Height [mAU]	Area %
1	8.466	MF	0.4022	754.30908	31.26097	47.0576
2	9.871	FM	0.4578	848.63879	30.89629	52.9424
Totals :				1602.94788	62.15726	

Sample HPLC of 62



Signal 1: DAD1 A, Sig=254,4 Ref=360,100

Peak #	RetTime [min]	Type	Width [min]	Area [mAU*s]	Height [mAU]	Area %
1	8.872	BB	0.4135	5821.42725	216.67093	86.2790
2	10.466	BB	0.5180	925.78375	26.60163	13.7210
Totals :				6747.21100	243.27256	

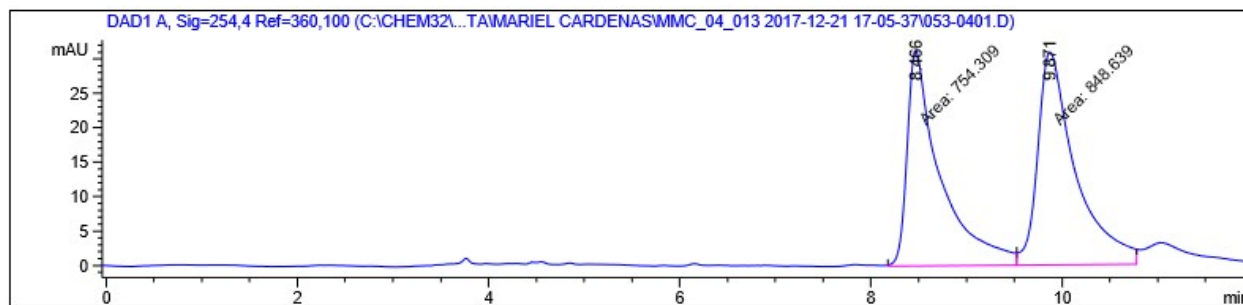


major enantiomer,
(*R*_a)-65

65 was measured with HPLC analysis using Chiralpak IA Hexanes/IPA (90:10), flow rate = 1.0 mL/min, t_R = 8.5 (major) and t_R = 9.9 min (minor).

→ Determined 15.5:84.5 e.r., 69 ee%

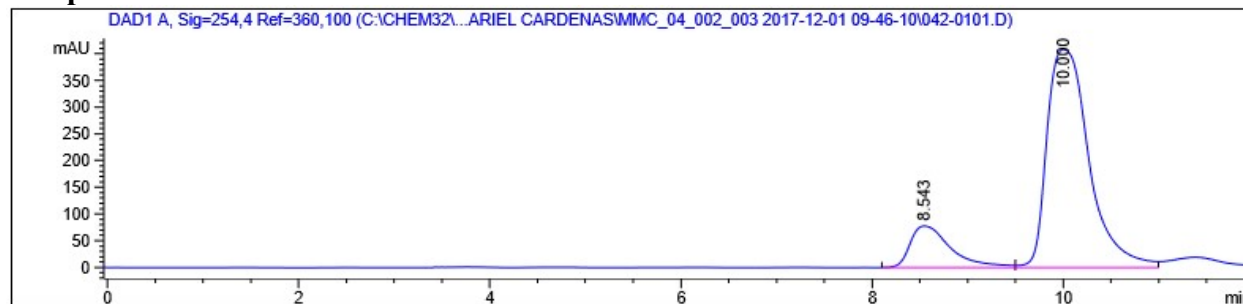
Racemic Standard of 65



Signal 1: DAD1 A, Sig=254,4 Ref=360,100

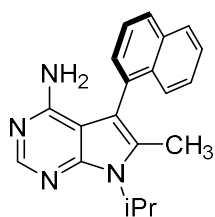
Peak #	RetTime [min]	Type	Width [min]	Area [mAU*s]	Height [mAU]	Area %
1	8.466	MF	0.4022	754.30908	31.26097	47.0576
2	9.871	FM	0.4578	848.63879	30.89629	52.9424
Totals :				1602.94788	62.15726	

Sample HPLC of 65



Signal 1: DAD1 A, Sig=254,4 Ref=360,100

Peak #	RetTime [min]	Type	Width [min]	Area [mAU*s]	Height [mAU]	Area %
1	8.543	BB	0.4463	2295.52637	77.77354	15.5277
2	10.000	BV	0.4828	1.24879e4	408.36307	84.4723
Totals :				1.47834e4	486.13660	

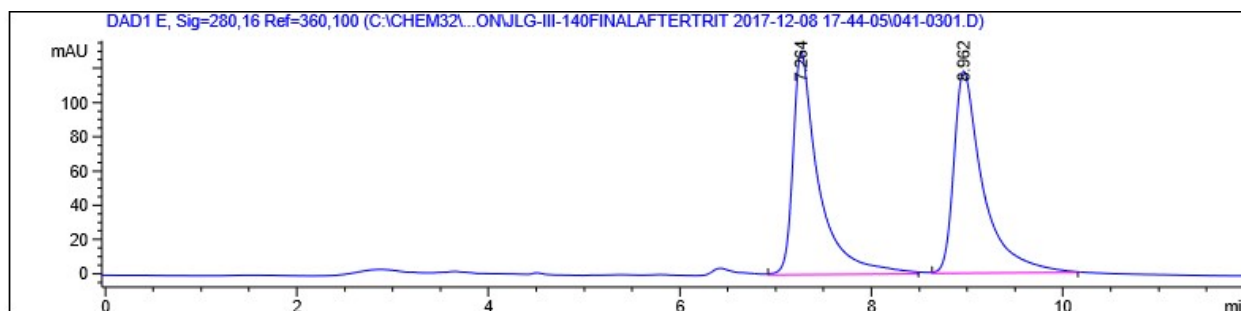


major enantiomer,
(*S_a*)-59

59 was measured with HPLC analysis using Chiralpak IA Hexanes/IPA (80:20), flow rate = 1.0 mL/min, t_R = 7.3 (minor) and t_R = 9.0 min (major).

→ Determined 15.6:84.4 e.r., 68.8 ee%

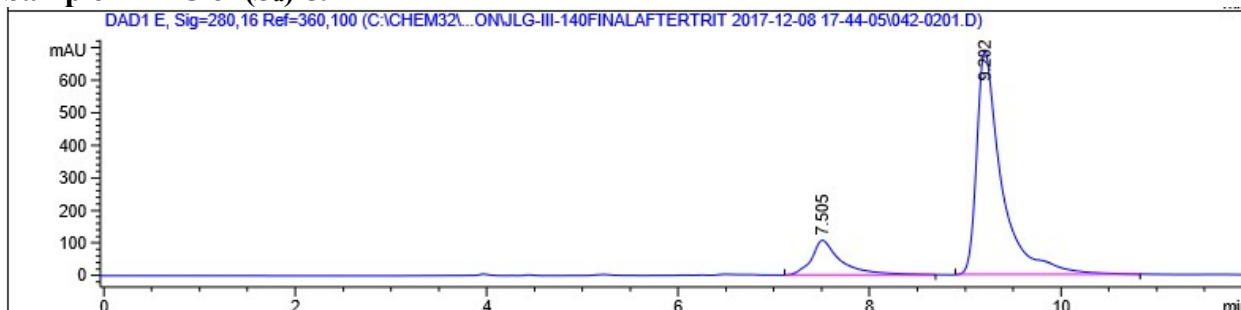
Racemic Standard of 59



Signal 5: DAD1 E, Sig=280,16 Ref=360,100

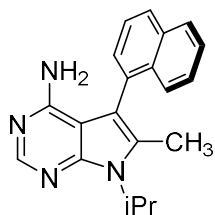
Peak #	RetTime [min]	Type	Width [min]	Area [mAU*s]	Height [mAU]	Area %
1	7.264	BB	0.2647	2441.09473	130.23062	49.3104
2	8.962	BB	0.3038	2509.36963	118.16527	50.6896
Totals :				4950.46436	248.39589	

Sample HPLC of (*S_a*)-59



Signal 5: DAD1 E, Sig=280,16 Ref=360,100

Peak #	RetTime [min]	Type	Width [min]	Area [mAU*s]	Height [mAU]	Area %
1	7.505	BB	0.2978	2301.27783	106.61762	15.5680
2	9.202	BB	0.2600	1.24808e4	686.94769	84.4320
Totals :				1.47821e4	793.56532	

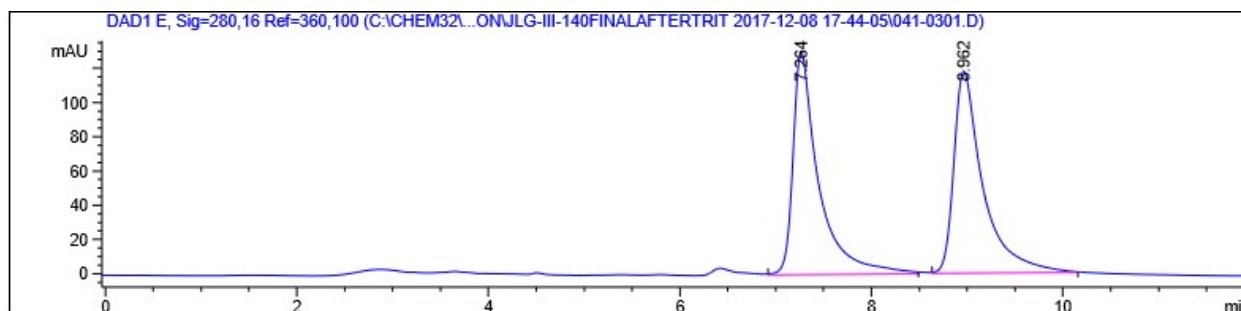


major enantiomer,
(*R_a*)-59

(*R_a*)-59 was measured with HPLC analysis using Chiralpak IA Hexanes/IPA (80:20), flow rate = 1.0 mL/min, *t*_R = 7.3 (minor) and *t*_R = 9.0 min (major).

→ Determined 93.0:7.0 e.r., 86.0 ee%

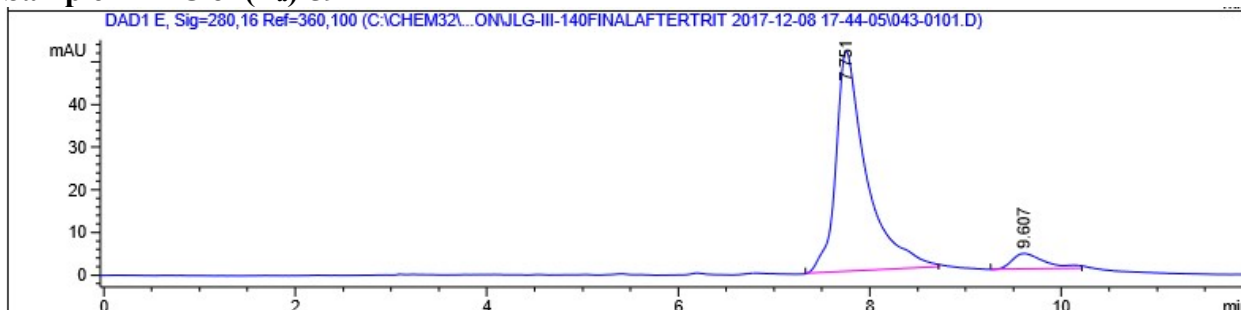
Racemic Standard of 59



Signal 5: DAD1 E, Sig=280,16 Ref=360,100

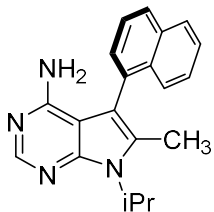
Peak #	RetTime [min]	Type	Width [min]	Area [mAU*s]	Height [mAU]	Area %
1	7.264	BB	0.2647	2441.09473	130.23062	49.3104
2	8.962	BB	0.3038	2509.36963	118.16527	50.6896
Totals :				4950.46436	248.39589	

Sample HPLC of (*R_a*)-59



Signal 5: DAD1 E, Sig=280,16 Ref=360,100

Peak #	RetTime [min]	Type	Width [min]	Area [mAU*s]	Height [mAU]	Area %
1	7.751	BB	0.3142	1152.31311	51.66392	92.9890
2	9.607	BB	0.3541	86.87988	3.61854	7.0110
Totals :				1239.19299	55.28245	



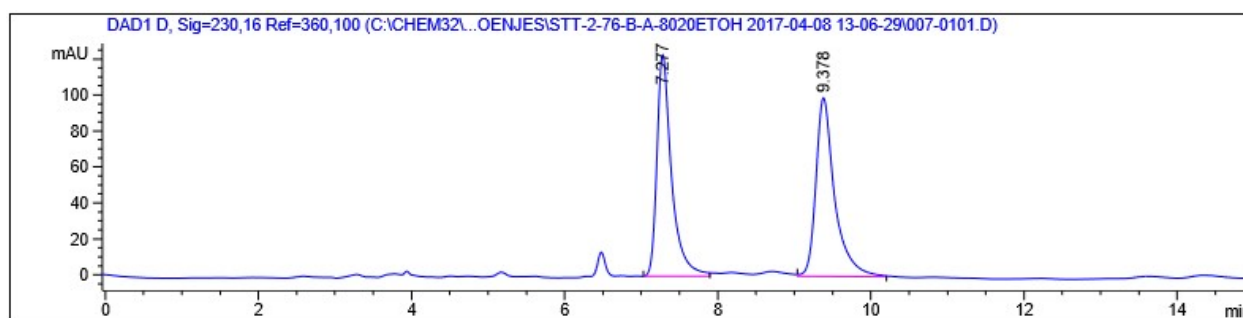
(*S_a*)*59 [*enantiopure]

Chiral Trace of (*S_a*)*59 after further purification on a semi-preparative Chiralpak IA column (Hexanes/EtOH (80:20), flow rate = 3.0 mL/min).

(*S_a*)*59 was measured with HPLC analysis using Chiralpak IA Hexanes/EtOH (80:20), flow rate = 1.0 mL/min, t_R = 7.3 (minor) and t_R = 9.4 min (major).

→ Determined 100 ee%

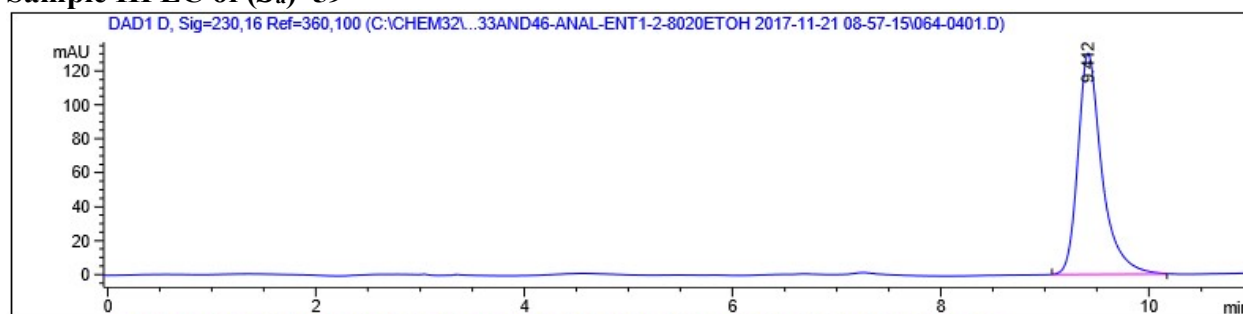
Racemic Standard of 59



Signal 4: DAD1 D, Sig=230,16 Ref=360,100

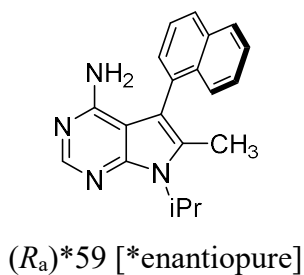
Peak #	RetTime [min]	Type	Width [min]	Area [mAU*s]	Height [mAU]	Area %
1	7.277	BB	0.1949	1636.35400	123.27943	48.9874
2	9.378	VB	0.2517	1704.00061	99.53017	51.0126
Totals :				3340.35461	222.80960	

Sample HPLC of (*S_a*)*59



Signal 4: DAD1 D, Sig=230,16 Ref=360,100

Peak #	RetTime [min]	Type	Width [min]	Area [mAU*s]	Height [mAU]	Area %
1	9.412	BB	0.2392	2093.19067	130.46901	100.0000
Totals :				2093.19067	130.46901	

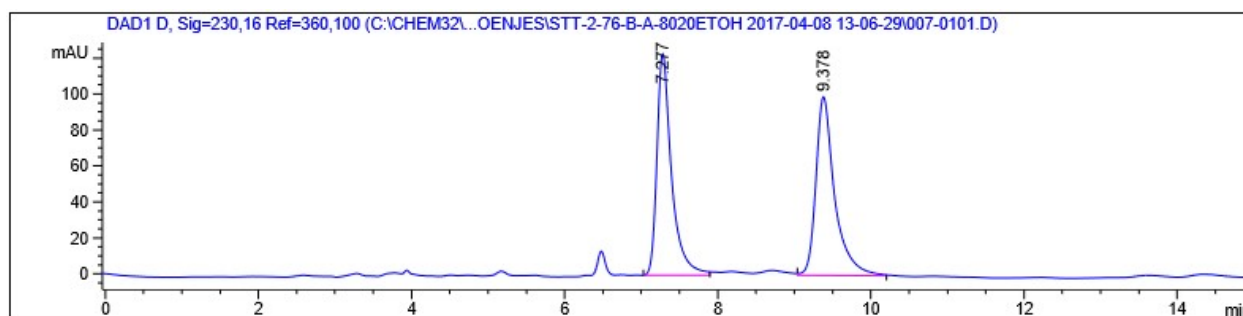


Chiral Trace of (*R_a*)*59 after further purification on a semi-preparative Chiralpak IA column (Hexanes/EtOH (80:20), flow rate = 3.0 mL/min).

(*R_a*)*59 was measured with HPLC analysis using Chiralpak IA Hexanes/EtOH (80:20), flow rate = 1.0 mL/min, t_R = 7.3 (minor) and t_R = 9.4 min (major).

→ Determined 100 ee%

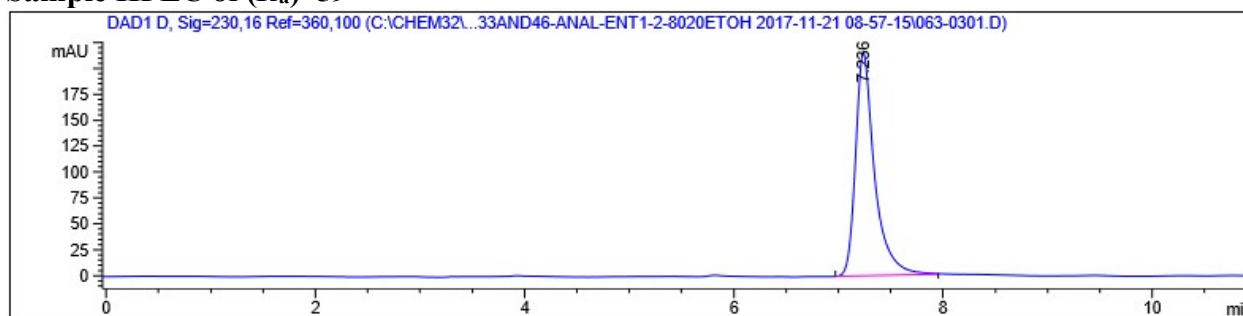
Racemic Standard of 59



Signal 4: DAD1 D, Sig=230,16 Ref=360,100

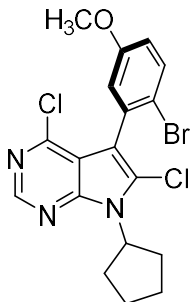
Peak #	RetTime [min]	Type	Width [min]	Area [mAU*s]	Height [mAU]	Area %
1	7.277	BB	0.1949	1636.35400	123.27943	48.9874
2	9.378	VB	0.2517	1704.00061	99.53017	51.0126
Totals :				3340.35461	222.80960	

Sample HPLC of (*R_a*)*59



Signal 4: DAD1 D, Sig=230,16 Ref=360,100

Peak #	RetTime [min]	Type	Width [min]	Area [mAU*s]	Height [mAU]	Area %
1	7.236	BB	0.1882	2737.07080	215.42680	100.0000
Totals :				2737.07080	215.42680	

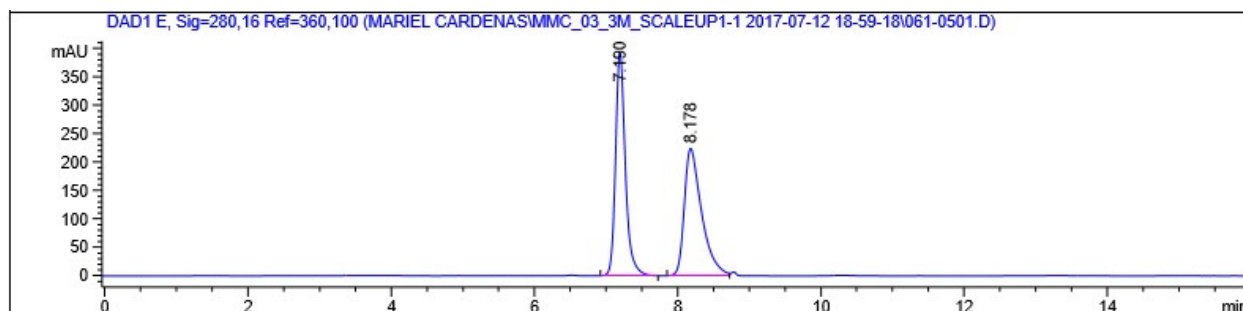


major enantiomer,
(*S_a*)-39

39 was measured with HPLC analysis using Chiralpak IA Hexanes/EtOH (98.2), flow rate = 1.0 mL/min, tR = 7.2 (minor) and tR = 8.2 min (major).

→ Determined 93.9:6.1 e.r., 87.8 ee%

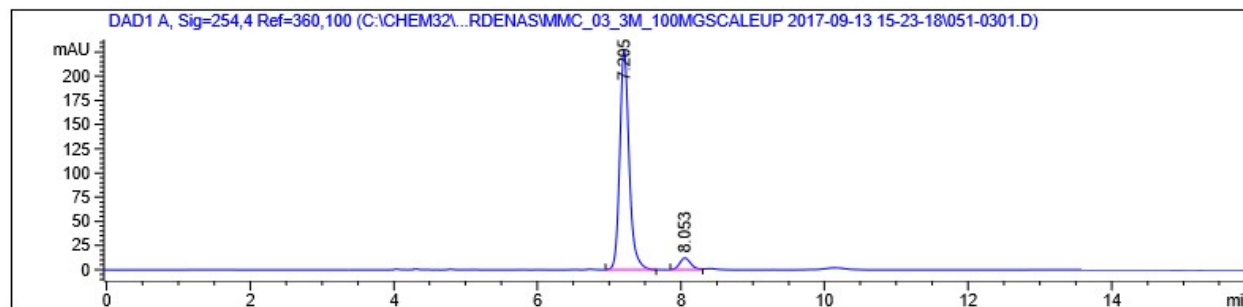
Racemic Standard of 39



Signal 5: DAD1 E, Sig=280,16 Ref=360,100

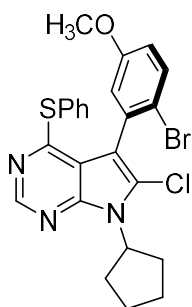
Peak #	RetTime [min]	Type	Width [min]	Area [mAU*s]	Height [mAU]	Area %
1	7.190	BB	0.1432	3750.91138	393.46307	49.7688
2	8.178	BV	0.2489	3785.76367	224.29826	50.2312
Totals :				7536.67505	617.76134	

Sample HPLC of (*R_a*)-39



Signal 1: DAD1 A, Sig=254,4 Ref=360,100

Peak #	RetTime [min]	Type	Width [min]	Area [mAU*s]	Height [mAU]	Area %
1	7.205	BB	0.1381	2063.89233	226.85533	93.8502
2	8.053	BV	0.1669	135.24295	12.24392	6.1498
Totals :				2199.13528	239.09925	

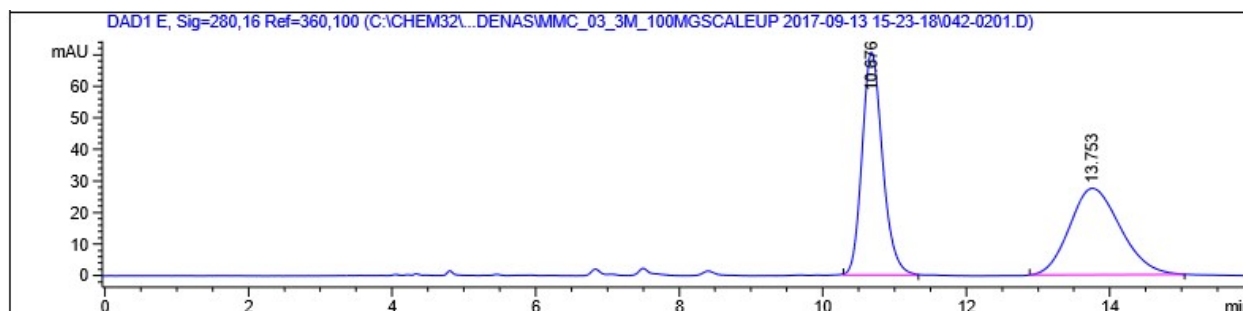


major enantiomer,
(*R_a*)-40

40 was measured with HPLC analysis using Chiralpak IA Hexanes/EtOH (98.2), flow rate = 1.0 mL/min, t_R = 10.7 min (major) and t_R = 13.8 min (major).

→ Determined 88.4:11.6 e.r., 76.8 ee%

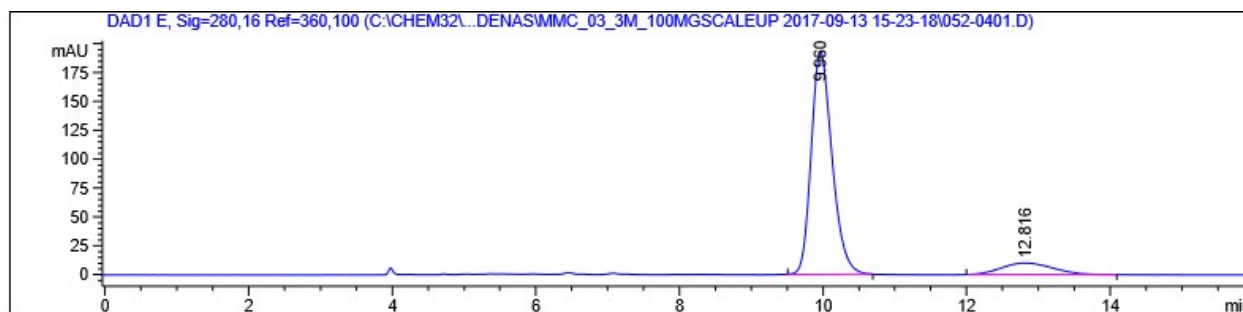
Racemic Standard of 40



Signal 5: DAD1 E, Sig=280,16 Ref=360,100

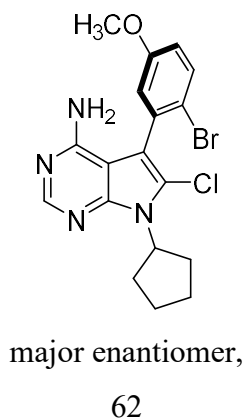
Peak #	RetTime [min]	Type	Width [min]	Area [mAU*s]	Height [mAU]	Area %
1	10.676	BB	0.3057	1401.69092	70.57632	50.6645
2	13.753	BB	0.7506	1364.92456	27.52290	49.3355
Totals :				2766.61548	98.09922	

Sample HPLC of (*R_a*)-40



Signal 5: DAD1 E, Sig=280,16 Ref=360,100

Peak #	RetTime [min]	Type	Width [min]	Area [mAU*s]	Height [mAU]	Area %
1	9.960	BB	0.3119	3903.35742	193.06070	88.4188
2	12.816	BB	0.7176	511.26465	10.11664	11.5812
Totals :				4414.62207	203.17734	

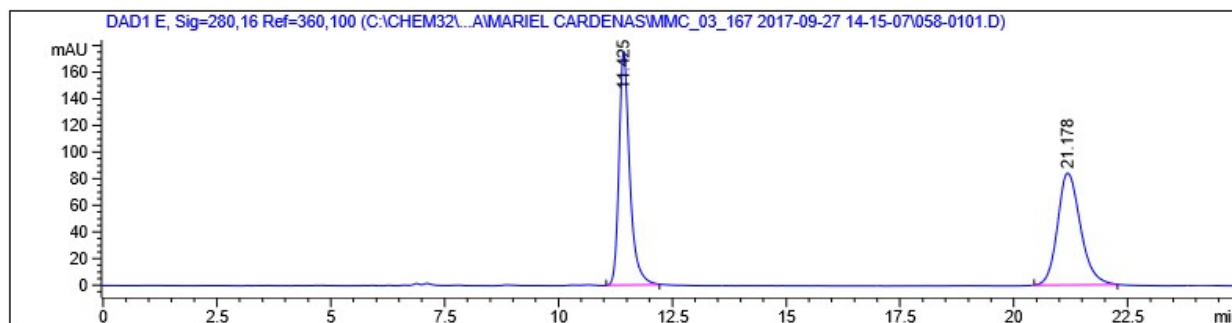


For the assignment of stereochemistry, please see crystal structure of 62 in Smith, D. E.; Marquez, I.; Lokensgard, M. E.; Rheingold, A. L.; Hecht, D.; Gustafson, J. L. *Angew. Chem. Int. Ed.* **2015**, *54* (40), 11754.

66 was measured with HPLC analysis using Chiralpak IA Hexanes/EtOH (98.2), flow rate = 1.0 mL/min, tR = 7.2 (minor) and tR = 8.2 min (major).

→ Determined 96.7:3.3 e.r., 93.4 ee%

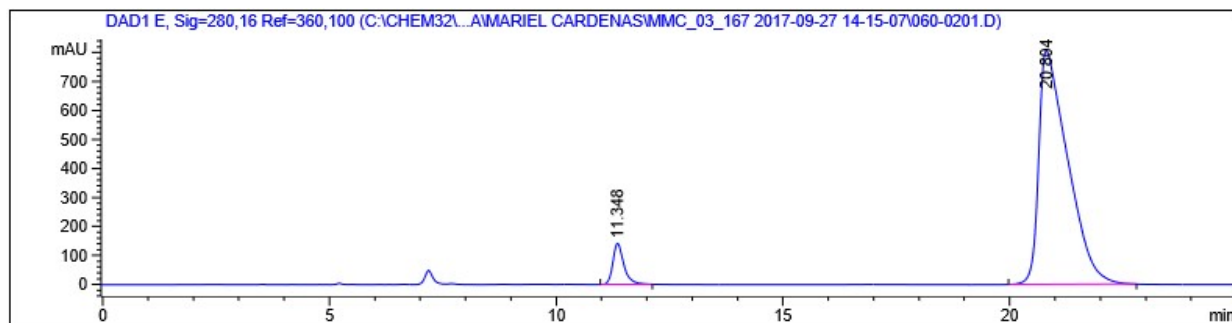
Racemic Standard of 62



Signal 5: DAD1 E, Sig=280,16 Ref=360,100 (C:\CHEM32\...AWMARIEL CARDENAS\MMC_03_167 2017-09-27 14-15-07\058-0101.D)

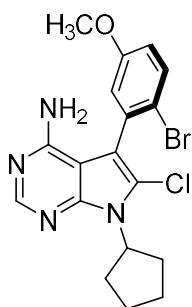
Peak #	RetTime [min]	Type	Width [min]	Area [mAU*s]	Height [mAU]	Area %
1	11.425	BB	0.2434	2878.31030	175.42651	49.1411
2	21.178	BB	0.5424	2978.92505	84.27662	50.8589
Totals :				5857.23535	259.70313	

Sample HPLC of 62



Signal 5: DAD1 E, Sig=280,16 Ref=360,100 (C:\CHEM32\...AWMARIEL CARDENAS\MMC_03_167 2017-09-27 14-15-07\060-0201.D)

Peak #	RetTime [min]	Type	Width [min]	Area [mAU*s]	Height [mAU]	Area %
1	11.348	BB	0.2524	2406.21387	141.51419	6.2917
2	20.804	BB	0.6312	3.58378e4	805.34216	93.7083
Totals :				3.82440e4	946.85635	



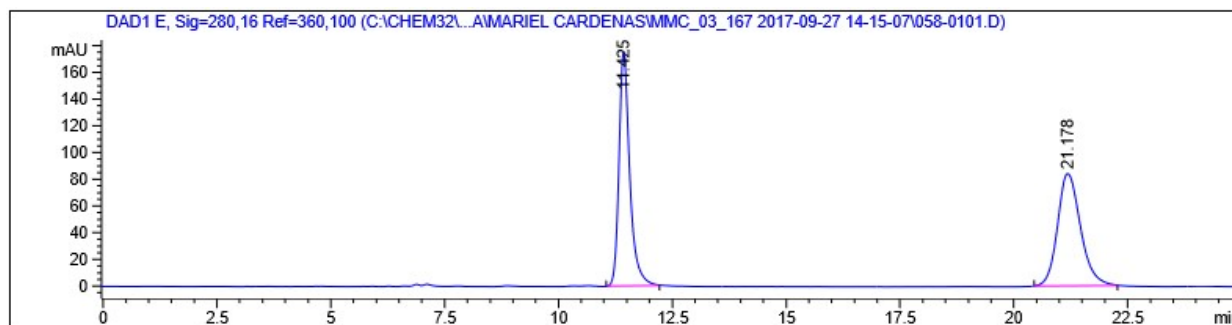
major enantiomer,
66

For the assignment of stereochemistry, please see crystal structure of 66 in Smith, D. E.; Marquez, I.; Lokensgard, M. E.; Rheingold, A. L.; Hecht, D.; Gustafson, J. L. *Angew. Chem. Int. Ed.* **2015**, 54 (40), 11754.

66 was measured with HPLC analysis using Chiralpak IA Hexanes/EtOH (98.2), flow rate = 1.0 mL/min, tR = 7.2 (minor) and tR = 8.2 min (major).

→ Determined 96.7:3.3 e.r., 93.4 ee%

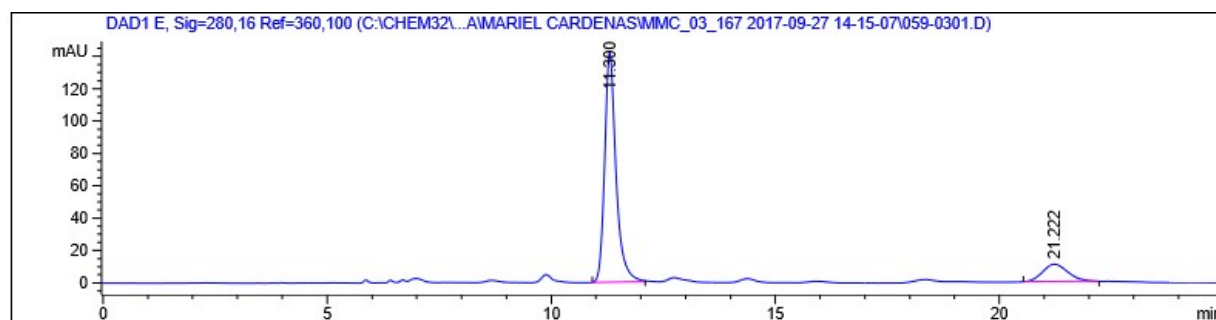
Racemic Standard of 66



Signal 5: DAD1 E, Sig=280,16 Ref=360,100

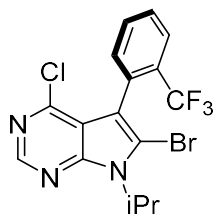
Peak #	RetTime [min]	Type	Width [min]	Area [mAU*s]	Height [mAU]	Area %
1	11.425	BB	0.2434	2878.31030	175.42651	49.1411
2	21.178	BB	0.5424	2978.92505	84.27662	50.8589
Totals :				5857.23535	259.70313	

Sample HPLC of 66



Signal 5: DAD1 E, Sig=280,16 Ref=360,100

Peak #	RetTime [min]	Type	Width [min]	Area [mAU*s]	Height [mAU]	Area %
1	11.300	BB	0.2610	2493.12842	141.85727	85.3154
2	21.222	BB	0.6117	429.12198	10.79597	14.6846
Totals :				2922.25040	152.65324	

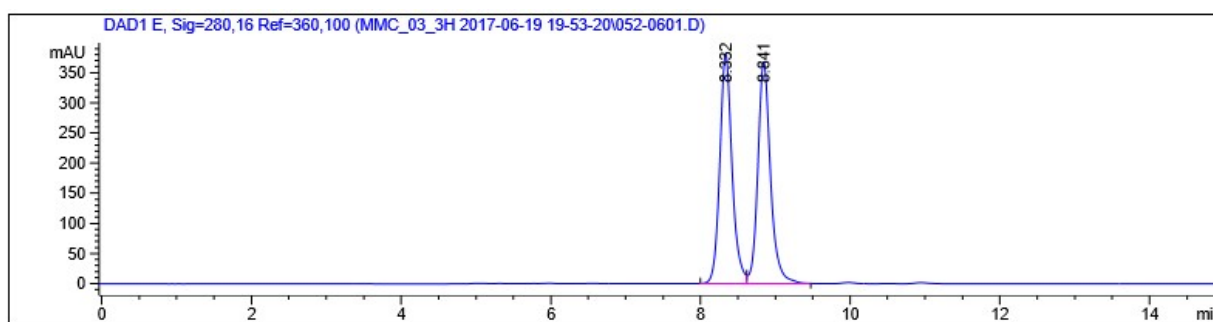


major enantiomer,
(*S_a*)-41

41 was measured with HPLC analysis using Chiralpak IA Hexanes/IPA (98.5:1.5), flow rate = 0.7 mL/min, tR = 8.3 (minor) and tR = 8.8 min (major).

→ Determined 11.0:89.0, 78 ee%

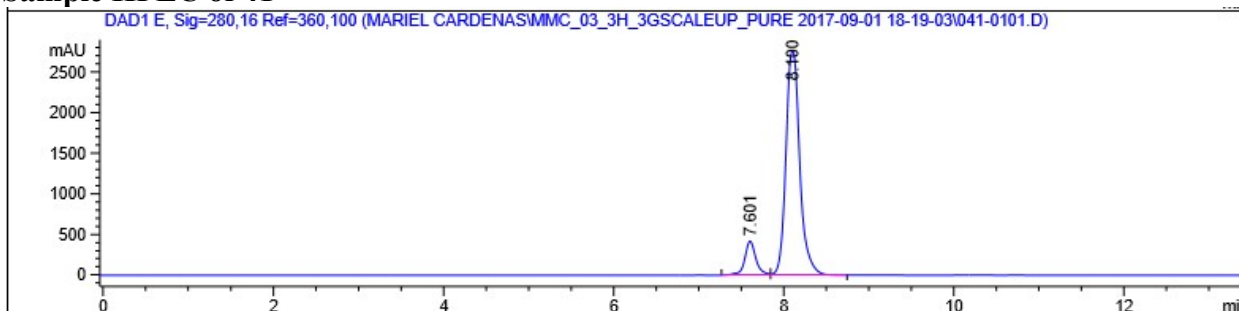
Racemic Standard of 41



Signal 5: DAD1 E, Sig=280,16 Ref=360,100

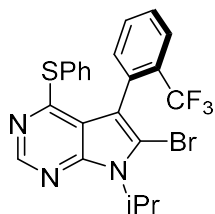
Peak #	RetTime [min]	Type	Width [min]	Area [mAU*s]	Height [mAU]	Area %
1	8.332	BV	0.1731	4342.45801	380.76401	50.0818
2	8.841	VB	0.1772	4328.27783	368.05478	49.9182
Totals :				8670.73584	748.81879	

Sample HPLC of 41



Signal 5: DAD1 E, Sig=280,16 Ref=360,100

Peak #	RetTime [min]	Type	Width [min]	Area [mAU*s]	Height [mAU]	Area %
1	7.601	BV	0.1371	3851.95630	419.44180	10.9779
2	8.100	VB	0.1740	3.12364e4	2761.27148	89.0221
Totals :				3.50884e4	3180.71329	

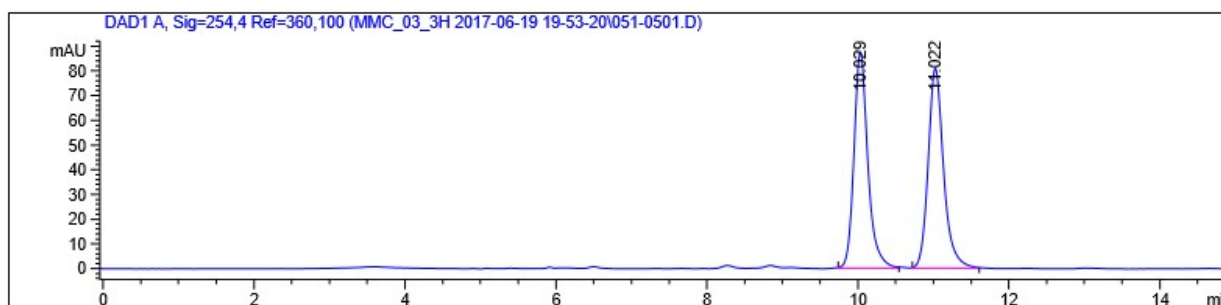


major enantiomer,
(*S_a*)-42

42 was measured with HPLC analysis using Chiralpak IA Hexanes/IPA (98.5:1.5), flow rate = 0.7 mL/min, tR = 10.0 (minor) and tR = 11.0 min (major).

→ Determined 7.2:92.8, 85.6 ee%

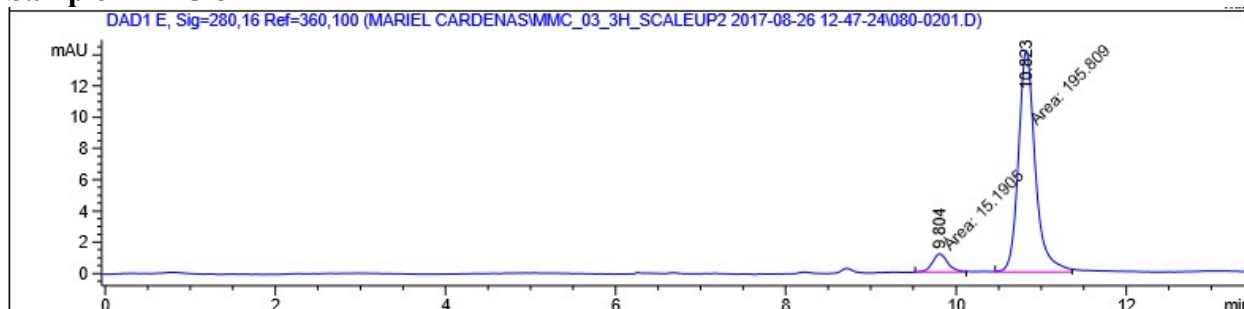
Racemic Standard of 42



Signal 1: DAD1 A, Sig=254,4 Ref=360,100

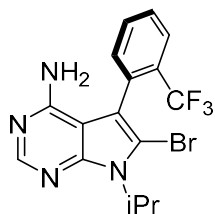
Peak #	RetTime [min]	Type	Width [min]	Area [mAU*s]	Height [mAU]	Area %
1	10.029	BB	0.1938	1125.01282	87.59054	49.3876
2	11.022	BB	0.2140	1152.91248	81.03737	50.6124
Totals :				2277.92529	168.62791	

Sample HPLC of 42



Signal 5: DAD1 E, Sig=280,16 Ref=360,100

Peak #	RetTime [min]	Type	Width [min]	Area [mAU*s]	Height [mAU]	Area %
1	9.804	MF	0.2161	15.19055	1.17180	7.1993
2	10.823	FM	0.2300	195.80908	14.18752	92.8007
Totals :				210.99963	15.35932	



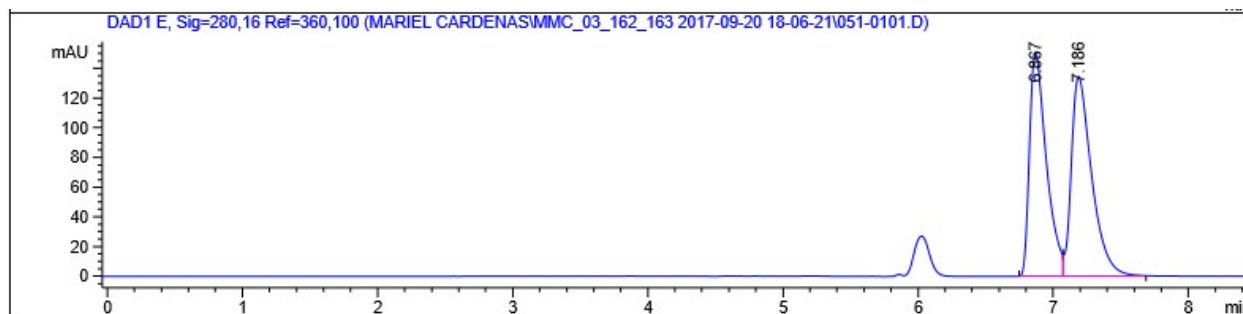
major enantiomer,

63

63 was measured with HPLC analysis using Chiralpak IC Hexanes/IPA (98.5:1.5), flow rate = 0.7 mL/min, tR = 6.9 (major) and tR = 7.2 min (minor).

→ Determined 92.9:7.1, 85.8 ee%

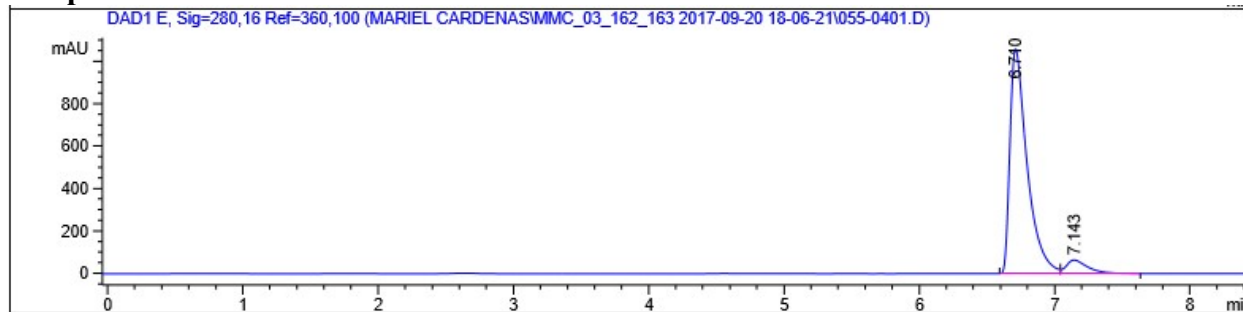
Racemic Standard of 63



Signal 5: DAD1 E, Sig=280,16 Ref=360,100

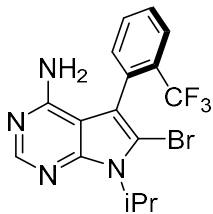
Peak #	RetTime [min]	Type	Width [min]	Area [mAU*s]	Height [mAU]	Area %
1	6.867	BV	0.1313	1306.16406	150.40356	48.1356
2	7.186	VB	0.1581	1407.34741	134.48869	51.8644
Totals :				2713.51147	284.89226	

Sample HPLC of 63



Signal 5: DAD1 E, Sig=280,16 Ref=360,100

Peak #	RetTime [min]	Type	Width [min]	Area [mAU*s]	Height [mAU]	Area %
1	6.710	BV	0.1310	9362.99023	1060.30054	92.8969
2	7.143	VB	0.1639	715.91504	64.30420	7.1031
Totals :				1.00789e4	1124.60474	



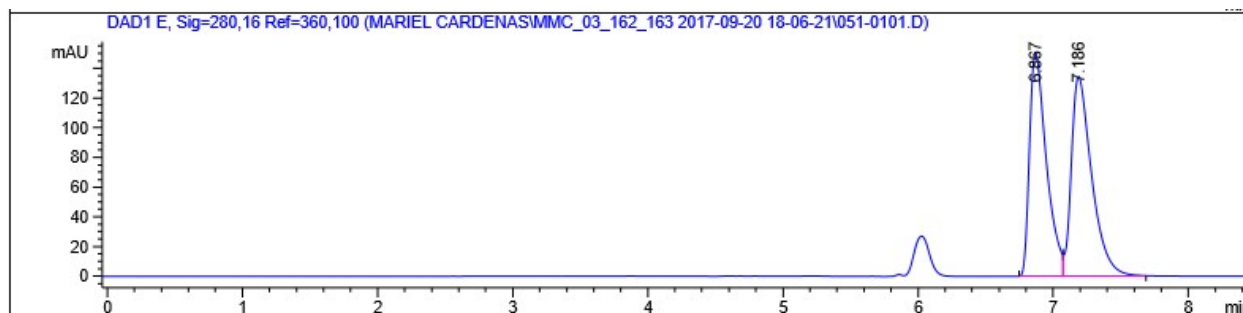
major enantiomer,

67

67 was measured with HPLC analysis using Chiralpak IC Hexanes/IPA (98.5:1.5), flow rate = 0.7 mL/min, tR = 6.9 (major) and tR = 7.2 min (minor).

→ Determined 2.1:97.9, 95.8 ee%

Racemic Standard of 67

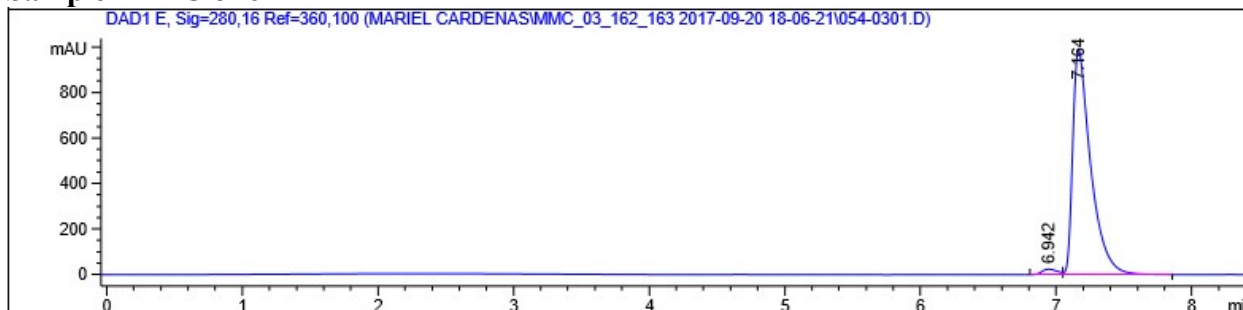


Signal 5: DAD1 E, Sig=280,16 Ref=360,100

Peak #	RetTime [min]	Type	Width [min]	Area [mAU*s]	Height [mAU]	Area %
1	6.867	BV	0.1313	1306.16406	150.40356	48.1356
2	7.186	VB	0.1581	1407.34741	134.48869	51.8644

Totals : 2713.51147 284.89226

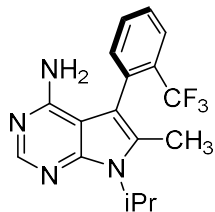
Sample HPLC of 67



Signal 5: DAD1 E, Sig=280,16 Ref=360,100

Peak #	RetTime [min]	Type	Width [min]	Area [mAU*s]	Height [mAU]	Area %
1	6.942	BV	0.1211	192.26782	24.63406	2.0634
2	7.164	VB	0.1357	9125.91699	988.87976	97.9366

Totals : 9318.18481 1013.51382

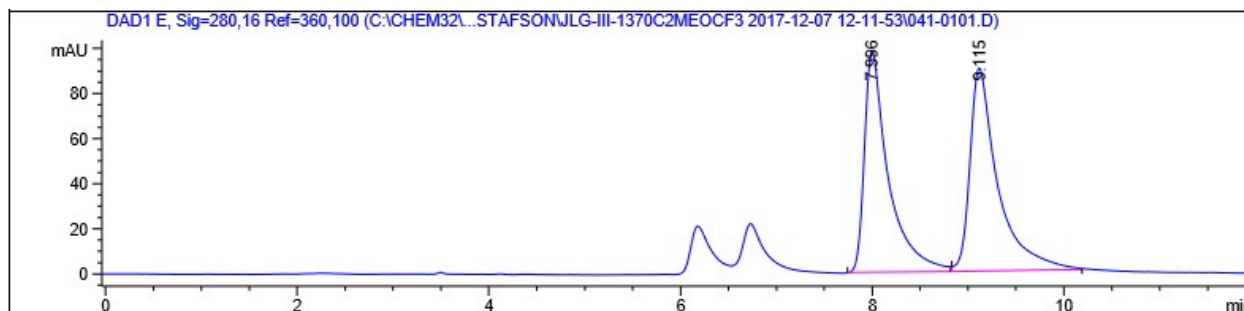


major enantiomer,
(*S_a*)-57

(*S_a*)-57 was measured with HPLC analysis using Chiralpak IA Hexanes/EtOH (80:20), flow rate = 1.0 mL/min, t_R = 8.0 min (minor) and t_R = 9.1 min (major).

→ Determined 8.8:91.2, 82.4 ee%

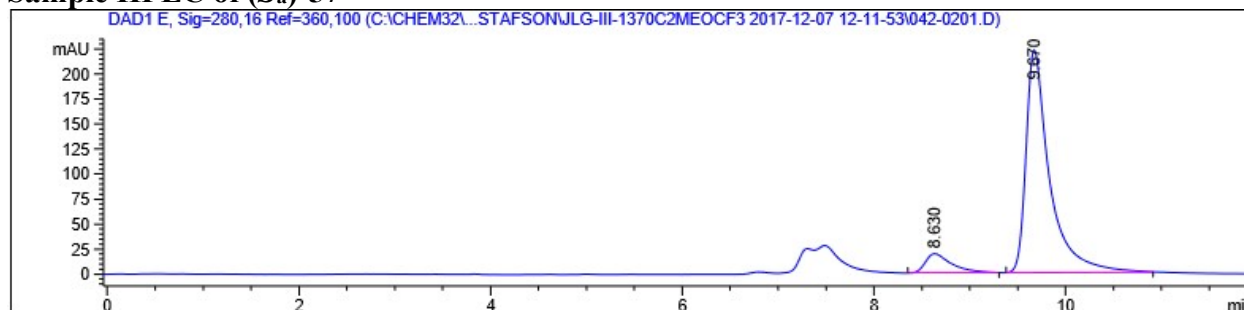
Racemic Standard of 57



Signal 5: DAD1 E, Sig=280,16 Ref=360,100

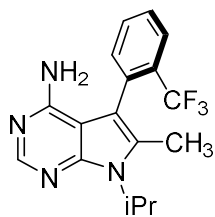
Peak #	RetTime [min]	Type	Width [min]	Area [mAU*s]	Height [mAU]	Area %
1	7.996	BB	0.2490	1708.43250	98.18758	48.2984
2	9.115	BB	0.2889	1828.81494	90.06945	51.7016
Totals :				3537.24744	188.25703	

Sample HPLC of (*S_a*)-57



Signal 5: DAD1 E, Sig=280,16 Ref=360,100

Peak #	RetTime [min]	Type	Width [min]	Area [mAU*s]	Height [mAU]	Area %
1	8.630	BB	0.2790	367.92255	19.25073	8.7977
2	9.670	BB	0.2478	3814.12256	222.68596	91.2023
Totals :				4182.04510	241.93669	

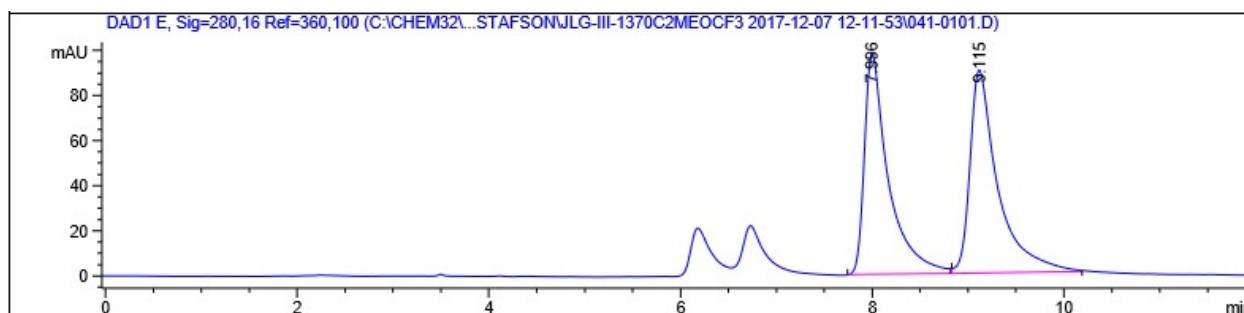


major enantiomer,
(*R_a*)-57

(*R_a*)-57 was measured with HPLC analysis using Chiralpak IA Hexanes/EtOH (80:20), flow rate = 1.0 mL/min, t_R = 8.0 min (minor) and t_R = 9.1 min (major).

→ Determined 95.7:4.3, 91.4 ee%

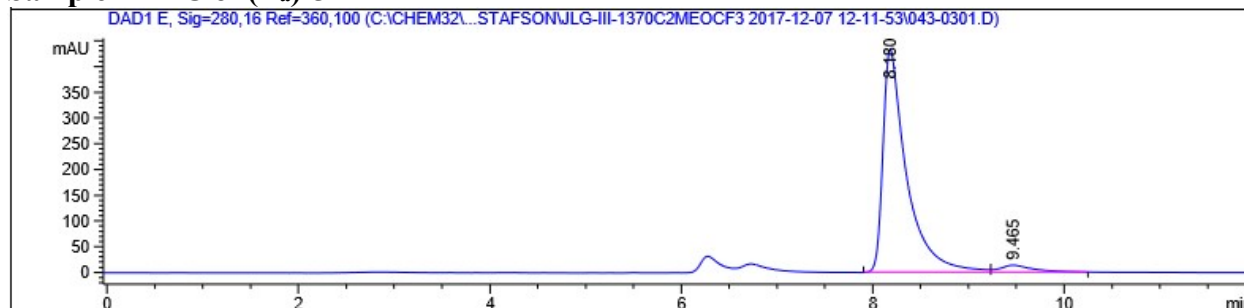
Racemic Standard of 57



Signal 5: DAD1 E, Sig=280,16 Ref=360,100

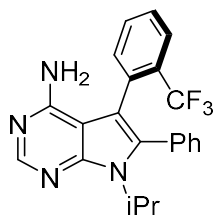
Peak #	RetTime [min]	Type	Width [min]	Area [mAU*s]	Height [mAU]	Area %
1	7.996	BB	0.2490	1708.43250	98.18758	48.2984
2	9.115	BB	0.2889	1828.81494	90.06945	51.7016
Totals :				3537.24744	188.25703	

Sample HPLC of (*R_a*)-57



Signal 5: DAD1 E, Sig=280,16 Ref=360,100

Peak #	RetTime [min]	Type	Width [min]	Area [mAU*s]	Height [mAU]	Area %
1	8.180	BB	0.2468	7457.65625	433.37958	95.7186
2	9.465	BB	0.3430	333.57629	13.65464	4.2814
Totals :				7791.23254	447.03422	

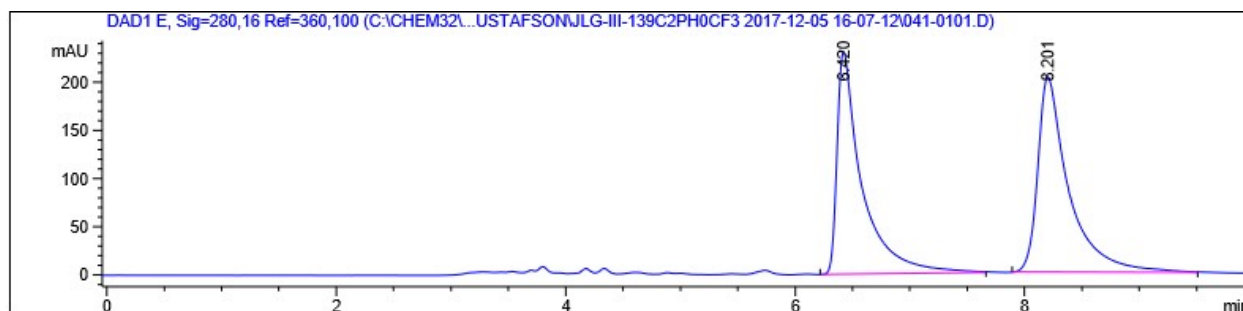


major enantiomer,
(*R*_a)-58

(*S*_a)-58 was measured with HPLC analysis using Chiralpak IA Hexanes/IPA (90:10), flow rate = 1.0 mL/min, t_R = 6.4 min (minor) and t_R = 8.2 min (major).

→ Determined 97.2:2.8, 82.6 ee%

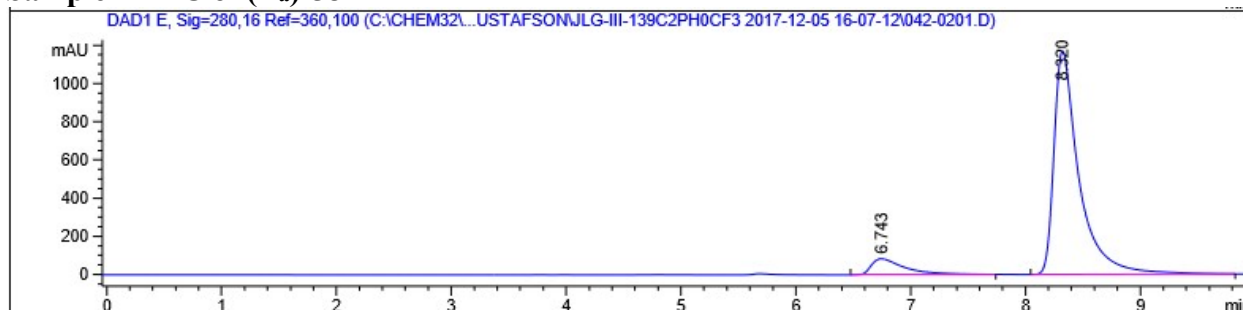
Racemic Standard of 58



Signal 5: DAD1 E, Sig=280,16 Ref=360,100

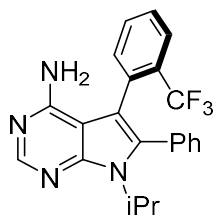
Peak #	RetTime [min]	Type	Width [min]	Area [mAU*s]	Height [mAU]	Area %
1	6.420	VB	0.2100	3480.53809	230.78078	47.7418
2	8.201	BB	0.2656	3809.79590	202.43517	52.2582
Totals :				7290.33398	433.21594	

Sample HPLC of (*R*_a)-58



Signal 5: DAD1 E, Sig=280,16 Ref=360,100

Peak #	RetTime [min]	Type	Width [min]	Area [mAU*s]	Height [mAU]	Area %
1	6.743	BB	0.2977	1700.92932	83.46830	8.7206
2	8.320	BB	0.2236	1.78039e4	1169.79285	91.2794
Totals :				1.95048e4	1253.26115	

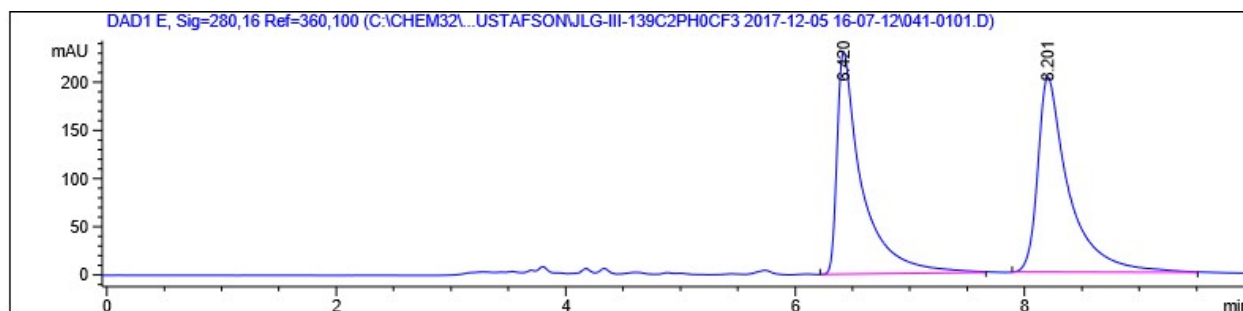


major enantiomer,
(*S*_a)-58

(*S*_a)-58 was measured with HPLC analysis using Chiralpak IA Hexanes/IPA (90:10), flow rate = 1.0 mL/min, t_R = 6.4 min (minor) and t_R = 8.2 min (major).

→ Determined 97.2:2.8, 94.4 ee%

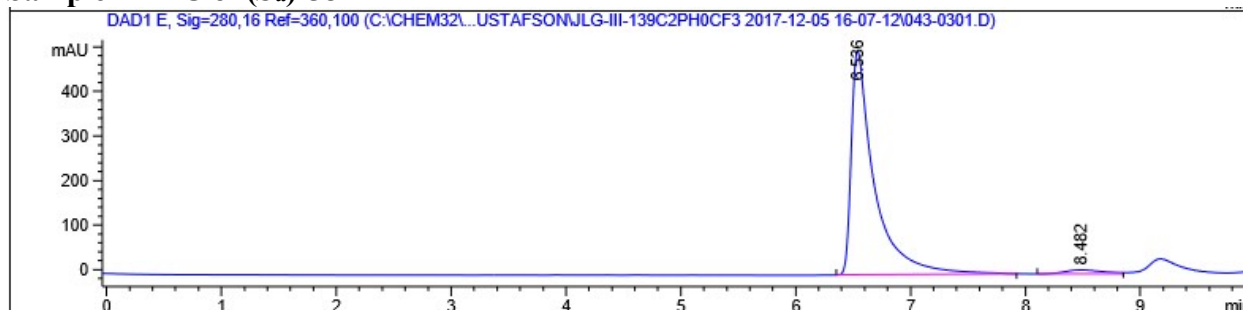
Racemic Standard of 58



Signal 5: DAD1 E, Sig=280,16 Ref=360,100

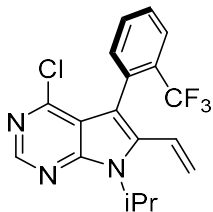
Peak #	RetTime [min]	Type	Width [min]	Area [mAU*s]	Height [mAU]	Area %
1	6.420	VB	0.2100	3480.53809	230.78078	47.7418
2	8.201	BB	0.2656	3809.79590	202.43517	52.2582
Totals :				7290.33398	433.21594	

Sample HPLC of (*S*_a)-58



Signal 5: DAD1 E, Sig=280,16 Ref=360,100

Peak #	RetTime [min]	Type	Width [min]	Area [mAU*s]	Height [mAU]	Area %
1	6.536	BB	0.1979	7058.39111	502.58072	97.1657
2	8.482	BV	0.3530	205.89063	8.86271	2.8343
Totals :				7264.28174	511.44343	

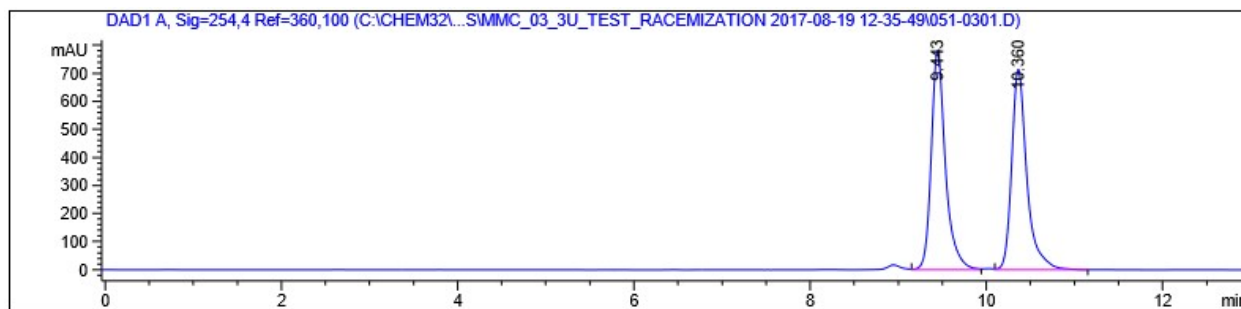


major enantiomer,
(*S*_a)-43

43 was measured with HPLC analysis using Chiralpak IA Hexanes/IPA (95:5), flow rate = 1.0 mL/min, t_R = 9.4 (minor) and t_R = 10.4 min (major).

→ Determined 22.1:77.9, 55.8 ee%

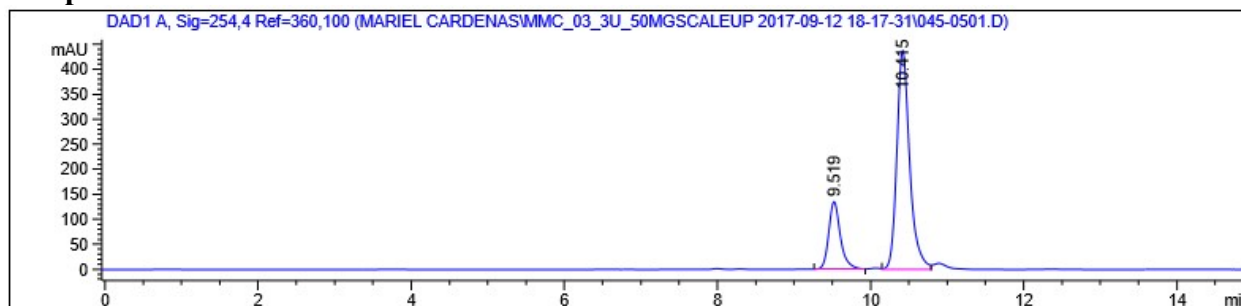
Racemic Standard of 43



Signal 1: DAD1 A, Sig=254,4 Ref=360,100

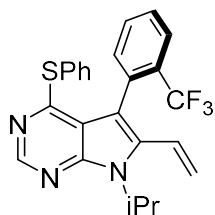
Peak #	RetTime [min]	Type	Width [min]	Area [mAU*s]	Height [mAU]	Area %
1	9.443	VV	0.1670	8764.99805	780.77112	50.5594
2	10.360	VB	0.1779	8571.03809	714.81744	49.4406
Totals :				1.73360e4	1495.58856	

Sample HPLC of 43



Signal 1: DAD1 A, Sig=254,4 Ref=360,100

Peak #	RetTime [min]	Type	Width [min]	Area [mAU*s]	Height [mAU]	Area %
1	9.519	BV	0.1607	1446.35999	135.28400	22.0877
2	10.415	VV	0.1760	5101.91016	437.77911	77.9123
Totals :				6548.27014	573.06311	

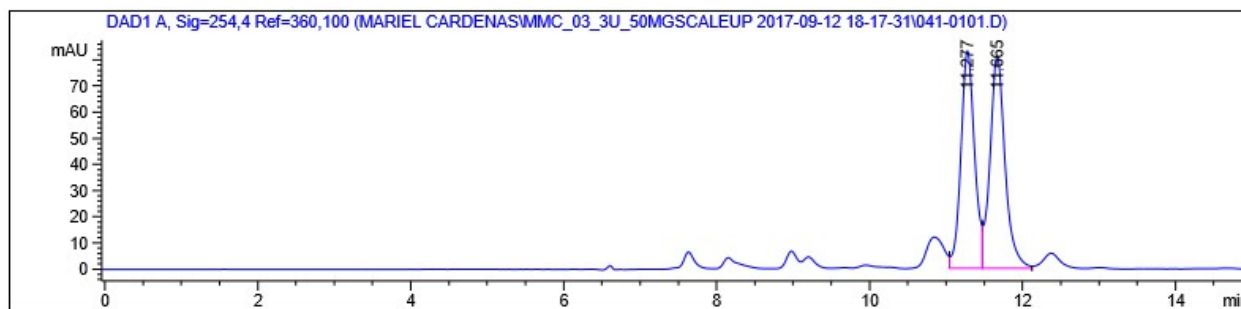


major enantiomer,
(*R*_a)-44

44 was measured with HPLC analysis using Chiralpak IA Hexanes/IPA (99:1), flow rate = 0.7 mL/min, t_R = 11.4 (major) and t_R = 12.7 min (minor).

→ Determined 16.8:83.2, 66.4 ee%

Racemic Standard of 44



Signal 1: DAD1 A, Sig=254,4 Ref=360,100

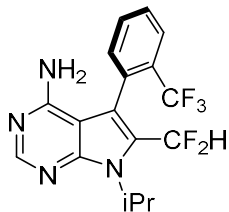
Peak #	RetTime [min]	Type	Width [min]	Area [mAU*s]	Height [mAU]	Area %
1	11.277	VV	0.1893	1034.62756	83.05152	48.2331
2	11.665	VV	0.2055	1110.43127	81.24649	51.7669
Totals :				2145.05884	164.29801	

Sample HPLC of 44



Signal 1: DAD1 A, Sig=254,4 Ref=360,100

Peak #	RetTime [min]	Type	Width [min]	Area [mAU*s]	Height [mAU]	Area %
1	11.242	VV	0.1801	157.71895	13.32198	16.8049
2	11.627	VV	0.1986	780.80933	58.92472	83.1951
Totals :				938.52827	72.24670	



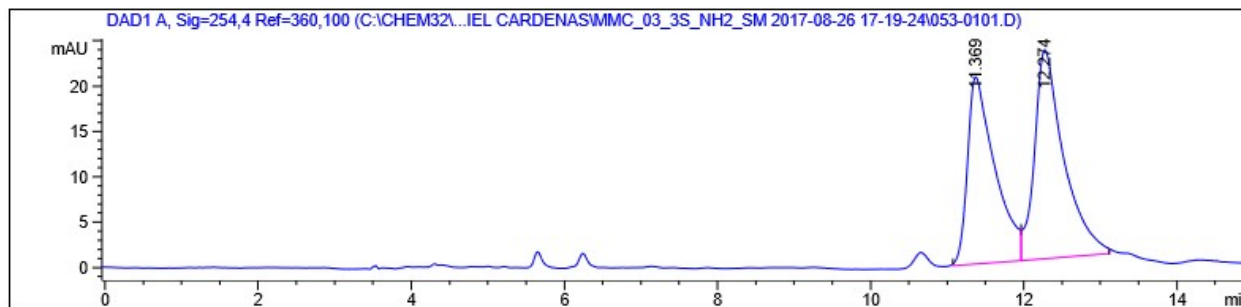
major enantiomer,
(*S*_a)-47

Note: 45 was aminated to yield (*S*_a)-47 for *s*-factor determination via HPLC analysis. 45 was not observable on HPLC.

(*S*_a)-47 was measured with HPLC analysis using Chiralpak IA Hexanes/IPA (95:5), flow rate = 1.0 mL/min, *t*_R = 11.4 (minor) and *t*_R = 12.3 min (major).

→ Determined 0.3:99.7, 99.4 ee%

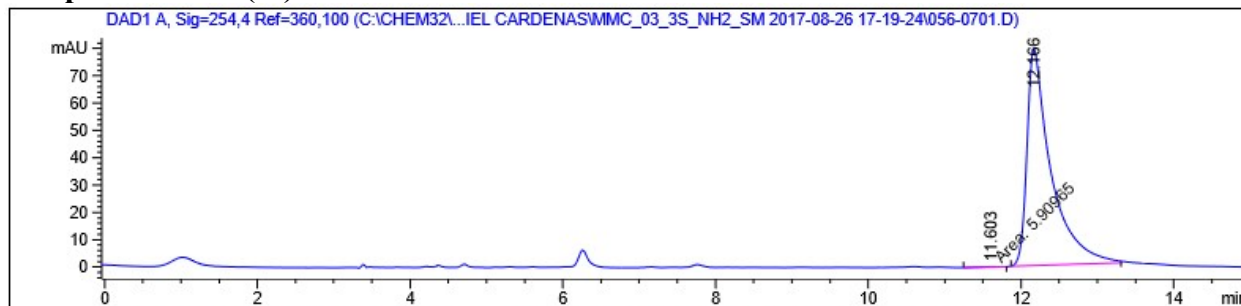
Racemic Standard of 47



Signal 1: DAD1 A, Sig=254,4 Ref=360,100

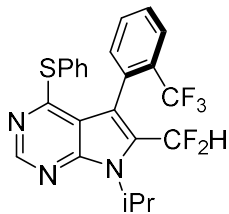
Peak #	RetTime [min]	Type	Width [min]	Area [mAU*s]	Height [mAU]	Area %
1	11.369	BV	0.3393	511.62524	20.63073	45.4438
2	12.274	VB	0.3773	614.21722	23.01890	54.5562
Totals :				1125.84247	43.64963	

Sample HPLC of (*S*_a)-47



Signal 1: DAD1 A, Sig=254,4 Ref=360,100

Peak #	RetTime [min]	Type	Width [min]	Area [mAU*s]	Height [mAU]	Area %
1	11.603	MM	0.4029	5.90965	2.44466e-1	0.3391
2	12.166	BB	0.3056	1736.79553	79.27777	99.6609
Totals :				1742.70518	79.52224	

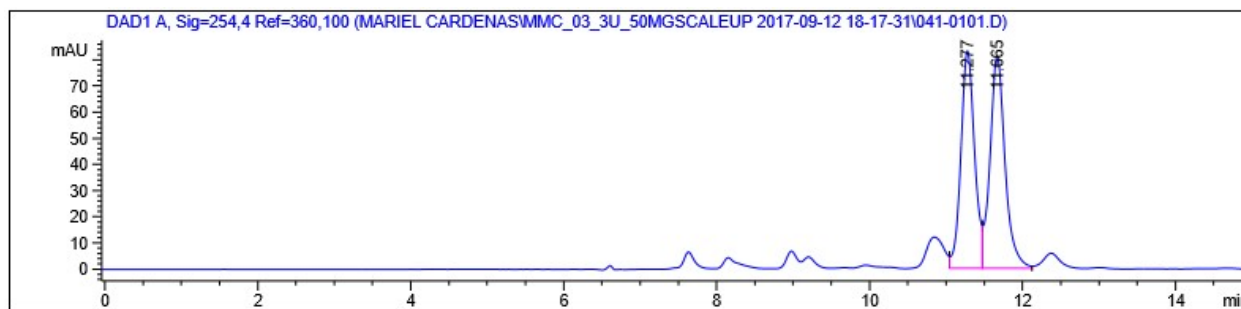


major enantiomer,
(*S_a*)-46

46 was measured with HPLC analysis using Chiralpak IA Hexanes/IPA (99:1), flow rate = 0.7 mL/min, t_R = 11.3 (minor) and t_R = 11.7 min (major).

→ Determined 16.8:83.2, 66.4 ee%

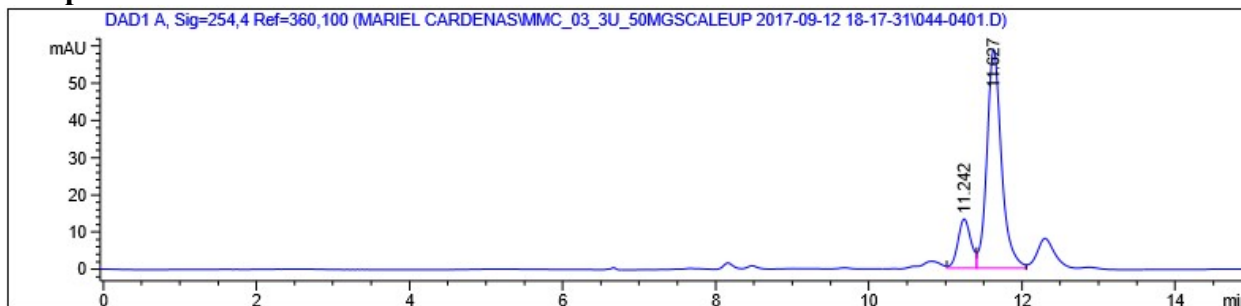
Racemic Standard of 46



Signal 1: DAD1 A, Sig=254,4 Ref=360,100

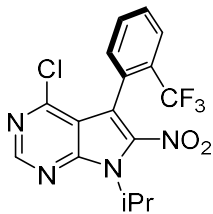
Peak #	RetTime [min]	Type	Width [min]	Area [mAU*s]	Height [mAU]	Area %
1	11.277	VV	0.1893	1034.62756	83.05152	48.2331
2	11.665	VV	0.2055	1110.43127	81.24649	51.7669
Totals :				2145.05884	164.29801	

Sample HPLC of 46



Signal 1: DAD1 A, Sig=254,4 Ref=360,100

Peak #	RetTime [min]	Type	Width [min]	Area [mAU*s]	Height [mAU]	Area %
1	11.242	VV	0.1801	157.71895	13.32198	16.8049
2	11.627	VV	0.1986	780.80933	58.92472	83.1951
Totals :				938.52827	72.24670	

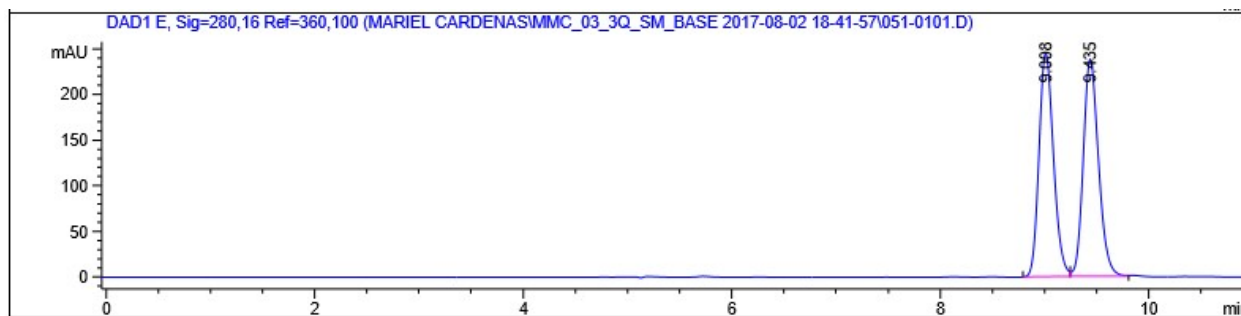


major enantiomer,
(*S_a*)-48

48 was measured with HPLC analysis using Chiralpak IC Hexanes/IPA (99:01), flow rate = 0.7 mL/min, t_R = 9.0 (minor) and t_R = 9.4 min (major).

→ Determined 36.0:64.0, 28 ee%

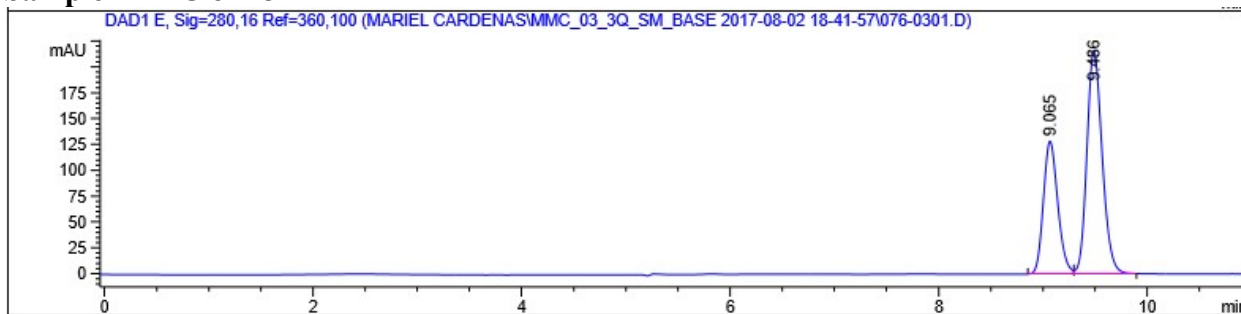
Racemic Standard of 48



Signal 5: DAD1 E, Sig=280,16 Ref=360,100

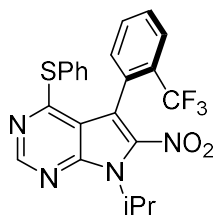
Peak #	RetTime [min]	Type	Width [min]	Area [mAU*s]	Height [mAU]	Area %
1	9.008	BV	0.1487	2370.74512	245.32623	49.4216
2	9.435	VB	0.1568	2426.23535	238.26570	50.5784
Totals :				4796.98047	483.59193	

Sample HPLC of 48



Signal 5: DAD1 E, Sig=280,16 Ref=360,100

Peak #	RetTime [min]	Type	Width [min]	Area [mAU*s]	Height [mAU]	Area %
1	9.065	BV	0.1481	1235.78638	128.61526	35.9702
2	9.486	VB	0.1570	2199.79492	215.68462	64.0298
Totals :				3435.58130	344.29988	

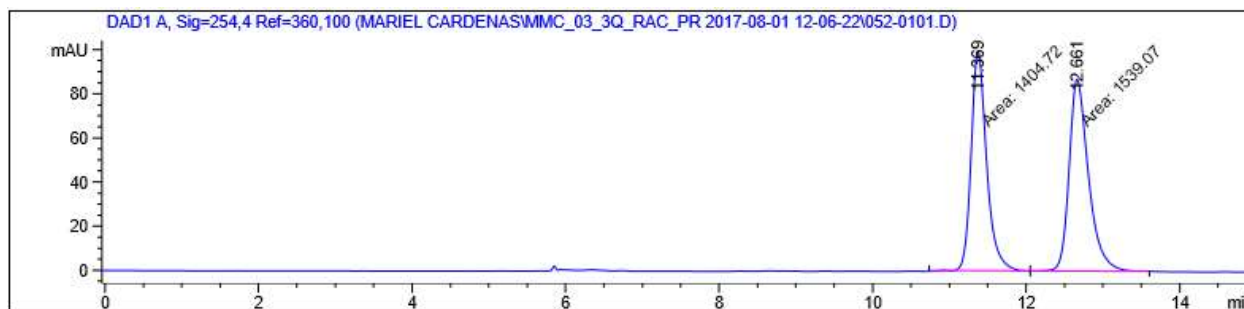


major enantiomer,
(*R_a*)-49

49 was measured with HPLC analysis using Chiralpak IA Hexanes/IPA (99:1), flow rate = 0.7 mL/min, t_R = 11.4 (major) and t_R = 12.7 min (minor).

→ Determined 71.5:28.5, 43 ee%

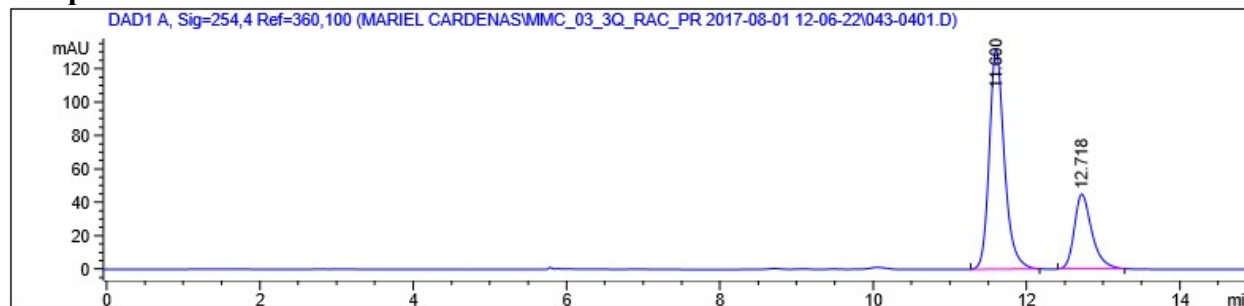
Racemic Standard of 49



Signal 1: DAD1 A, Sig=254,4 Ref=360,100

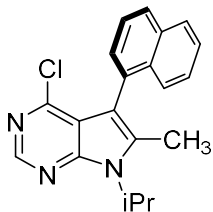
Peak #	RetTime [min]	Type	Width [min]	Area [mAU*s]	Height [mAU]	Area %
1	11.369	MF	0.2352	1404.72375	99.52377	47.7181
2	12.661	FM	0.2948	1539.07007	87.00592	52.2819
Totals :				2943.79382	186.52969	

Sample HPLC of 49



Signal 1: DAD1 A, Sig=254,4 Ref=360,100

Peak #	RetTime [min]	Type	Width [min]	Area [mAU*s]	Height [mAU]	Area %
1	11.600	BB	0.2081	1807.10181	131.72208	71.4523
2	12.718	BB	0.2416	721.99976	44.90083	28.5477
Totals :				2529.10156	176.62291	

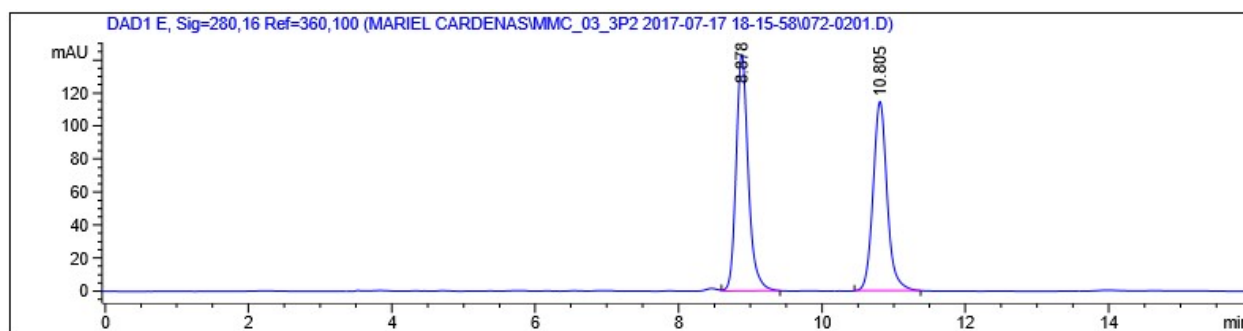


s-factor NTD for 59

59 was measured with HPLC analysis using Chiralpak IA Hexanes/IPA (98:2), flow rate = 1.0 mL/min, tR = 8.9 (minor) and tR = 10.8 min (major).

→ Determined 44.3:55.7, 11.4 ee%

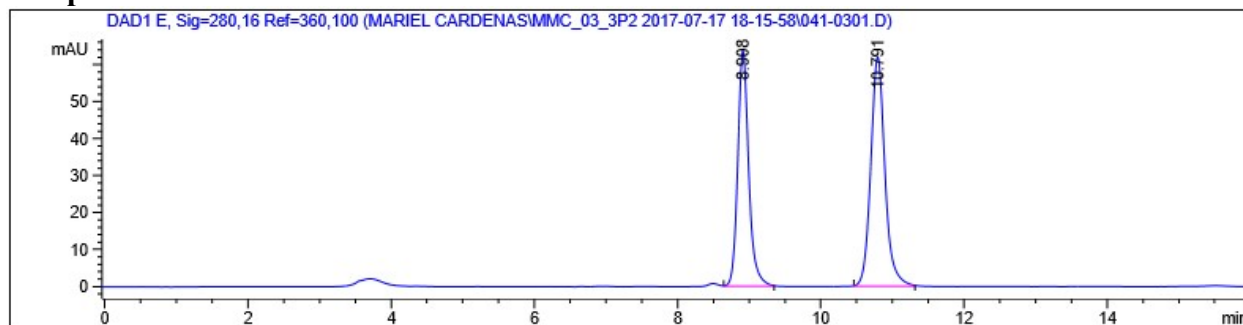
Racemic Standard of 59



Signal 5: DAD1 E, Sig=280,16 Ref=360,100

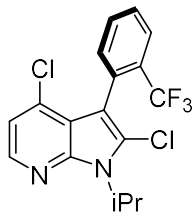
Peak #	RetTime [min]	Type	Width [min]	Area [mAU*s]	Height [mAU]	Area %
1	8.878	VB	0.1797	1693.81445	143.46536	51.8973
2	10.805	BB	0.2096	1569.96826	114.77440	48.1027
Totals :				3263.78271	258.23976	

Sample HPLC of 59



Signal 5: DAD1 E, Sig=280,16 Ref=360,100

Peak #	RetTime [min]	Type	Width [min]	Area [mAU*s]	Height [mAU]	Area %
1	8.908	VB	0.1625	679.93652	63.72921	44.3165
2	10.791	BB	0.2087	854.33691	62.01492	55.6835
Totals :				1534.27344	125.74413	

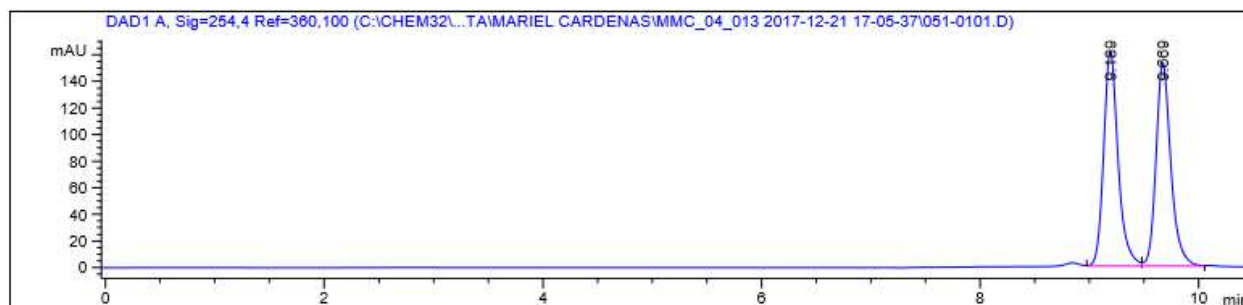


s-factor NTD for 59

59 was measured with HPLC analysis using Chiralpak IA Hexanes/EtOH (98.2), flow rate = 1.0 mL/min, tR = 7.2 (minor) and tR = 8.2 min (major).

→ Determined 46.9:53.1, 6.2 ee%

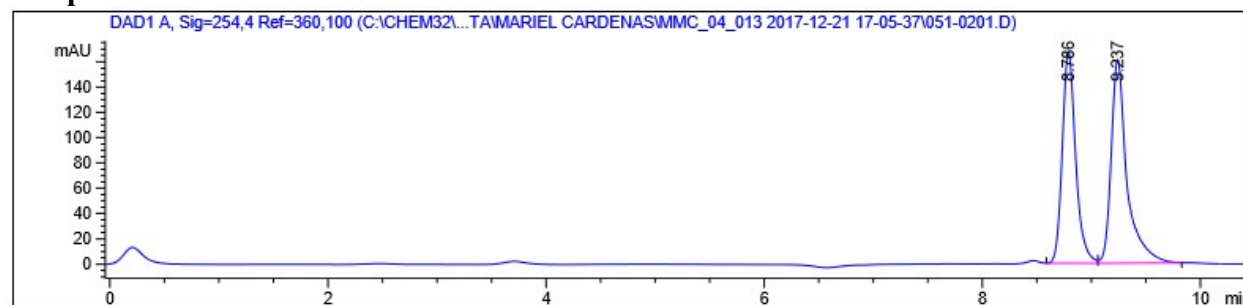
Racemic Standard of 59



Signal 1: DAD1 A, Sig=254,4 Ref=360,100

Peak #	RetTime [min]	Type	Width [min]	Area [mAU*s]	Height [mAU]	Area %
1	9.189	VV	0.1393	1493.79102	162.39738	50.7802
2	9.669	VB	0.1443	1447.89124	153.08092	49.2198
Totals :				2941.68225	315.47830	

Sample HPLC of 59



Signal 1: DAD1 A, Sig=254,4 Ref=360,100

Peak #	RetTime [min]	Type	Width [min]	Area [mAU*s]	Height [mAU]	Area %
1	8.786	VV	0.1298	1433.06519	167.50496	46.9132
2	9.237	VB	0.1492	1621.64819	161.36833	53.0868
Totals :				3054.71338	328.87329	

Copyright

Chapter 2, Section 2 is reformatted in part with permissions from *Chemical Communications*, **2021**, 57, 10087–10090. Copyright 2021 Royal Chemical Society.

2.9 Background: Atroposelective S_NAr towards 3-arylquinolines

With the learnings and successes of atroposelective S_NAr to obtain PPY-based kinase inhibiting scaffolds, we were interested in expanding this chemistry in other pharmaceutically relevant scaffolds. In addition, we were able to reoptimize the atroposelective S_NAr strategy to incorporate DKR which allowed us to synthesize less reactive substrates compared to PPYs as well. One of the key standouts from the PPY exploration was azaindole compound 52 (Table 3), which had not led to any desired S_NAr product using these original conditions. One important consideration was that this pyridine core was not as electrophilic as the pyrimidine. Because of this, it would be pertinent to reoptimize the atroposelective S_NAr through testing many diverse, reactive catalysts as well as other conditions.

A similar known bioisostere of azaindole is quinoline, an *N*-heterocycle which consists of a 6-membered benzene ring fused with pyridine. Quinolines are considered an important building block in the field of medicinal chemistry and are widely found in many pharmaceutically relevant scaffolds. As such, it was much easier to design new compounds and increase our substrate scope based on availability of starting materials. Also, quinoline possesses significant electrophilic character to perform reactions such as nucleophilic substitutions. Inspired by the azaindole, biaryl quinoline-based scaffolds became the focus for this new exploration. Based on the general

reactivity of these heterocycles, we examined a variety of 3-arylquinolines in which the pyridine-type *N*-1 nitrogen is meta to the C-3 arylated position. Within this scaffold, the C-2 position of the quinoline core (i.e., the carbon adjacent to the atropisomeric axis) would therefore be the most electrophilic position and most reactive position to facilitate an atroposelective S_NAr .

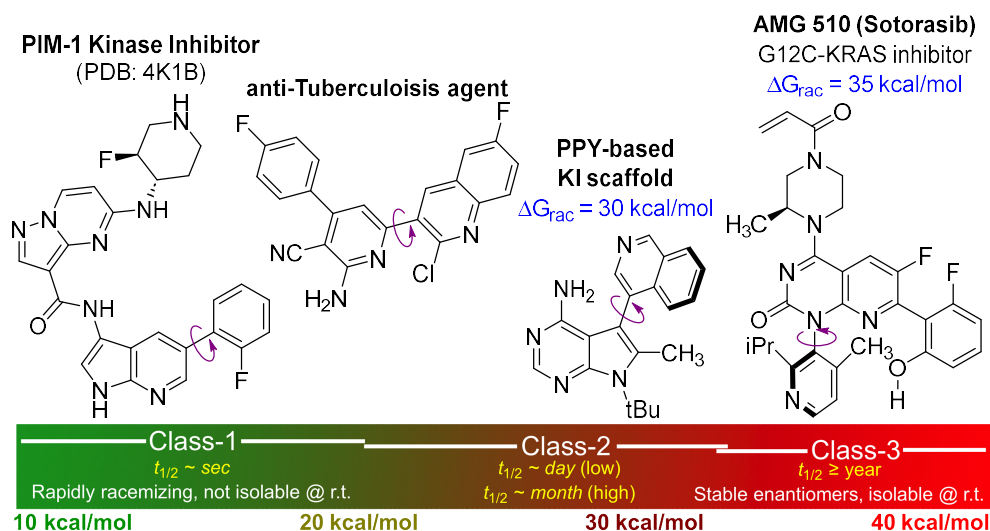


Figure 20. Examples of Biaryl Heterocyclic Atropisomers in Drug Discovery. Each compound is drawn where they lie in stereochemical stability determined by the barrier to racemization, ΔG_{rac} .^{23,28,30,87}

A cursory search of the literature found that 3-arylquinolines are among some of the most represented classes of quinolines in drug discovery. Some examples of known diverse bioactive atropisomeric pyridines and quinolines include an inhibitor of BACE1⁸⁸ (with prevalence to treating Alzheimer's disease), quinolines associated with targeting HIV-1,⁸⁹⁻⁹² molecules exhibiting antibacterial properties and a new ligand that binds to HSP90 (a chaperone protein that participates in protein degradation) (Figure 4). As suspected, an overwhelming majority existed as Class-1 atropisomers according to LaPlante's scale (Figures 3 and 4). However, there are some inspiring examples of Class-3 atropisomeric quinolines (Figures 16 and 17). An example is Ripretinib,⁹³ a 'first-in-class' switch-controlled kinase inhibitor of both KIT and PDGFR α kinases

which are implicated in gastrointestinal stromal tumor (from Deciphera Pharmaceuticals, LLC). Our best PPY-based kinase inhibiting scaffold of RET kinase also features an atropisomeric quinoline of the 3-aryl position finding Class-3 atropisomerism.

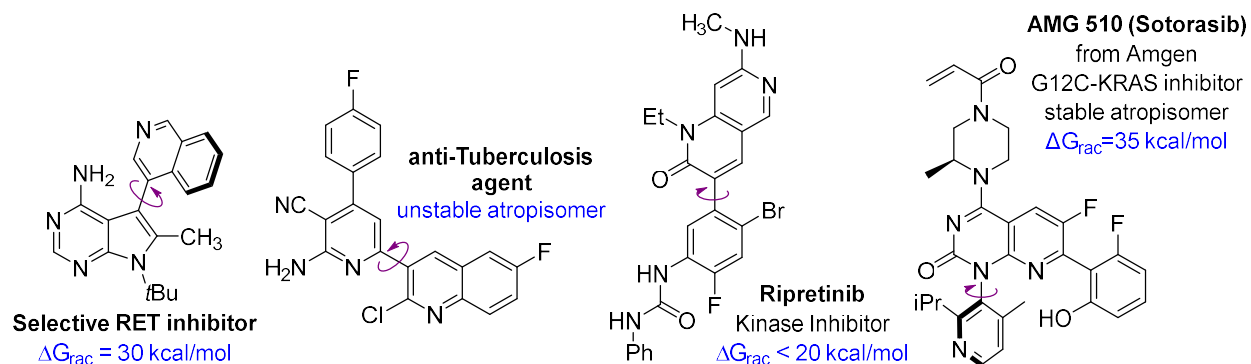


Figure 21. Examples of Pharmaceutically Relevant Biarylquinoline Atropisomers

At the time of this work, there were no amenable atroposelective routes towards 3-arylquinolines outside of S_NAr . Many of these examples in the literature utilized the pyridine or quinoline or motif as a directing group for C-H functionalization. In a different strategy, Zhou and coworkers⁹⁴ disclosed a kinetic resolution via transfer hydrogenation of racemic atropisomeric quinolines that allowed for access to enantioenriched 5- or 8- substituted quinolines. Finally, Cheng and coworkers⁹⁵ have also recently disclosed an atroposelective Friedländer quinoline heteroannulation towards 4-aryl quinolines.

Additionally, the 3-arylquinoline scaffold presented a similar challenge since many of the starting materials may exhibit Class-3 atropisomerism. Much like PPYs, any stereoinduction would occur via a kinetic resolution (KR) process as the barrier to racemization would be much higher (i.e., a 6-6 biaryl axis of chirality typically has higher stereochemically stability than a 6-5 biaryl axis). However, if the starting material can racemize faster than the reaction occurs and the resulting product is stereochemically stable, then a dynamic kinetic resolution (DKR) would be

possible. This would be a more desirable approach to perform enantioselective reactions. DKR would allow for near quantitative yields of highly enantioenriched products much like in the optimization on the PPY-scaffold. Thiophenol was our nucleophile for this strategy due to repeated success for using respective enantiomerically enriched sulfide products as activated intermediates to the sulfone. From here, any second S_NAr with any nucleophile was expected to yield no observable racemization.

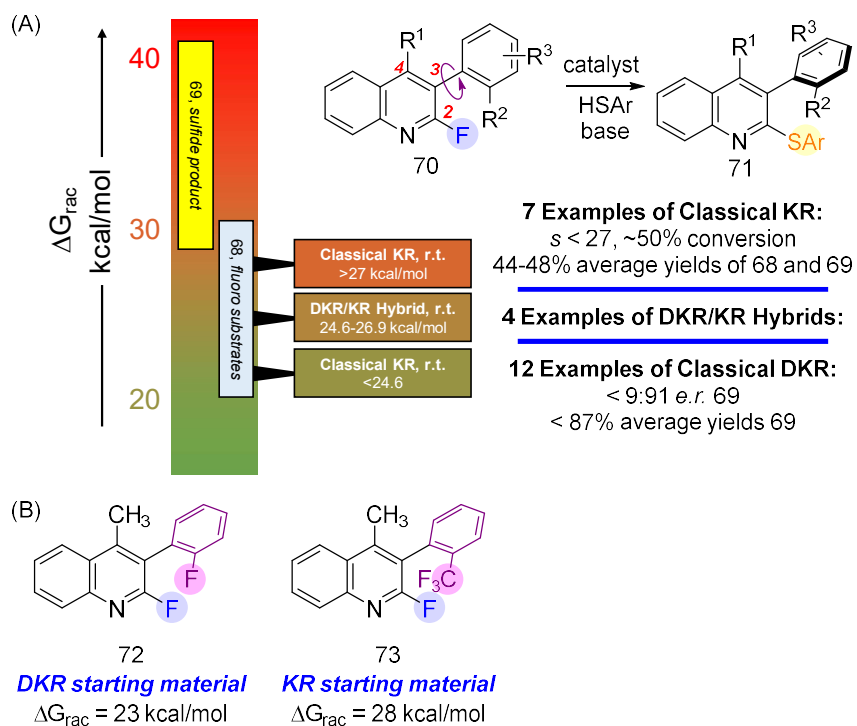


Figure 22. a. Atroposelective S_NAr of 3-aryl-2-fluoroquinolines. b. Example of a classical DKR and a classical KR substrate; C-2 fluoroquinoline substrates with barrier to racemization.

In the previously discussed examples of atroposelective S_NAr , the C4-chloride was replaced with an S-aryl group on the PPY scaffold (Chapter 2, Section 2.6). As chlorine and sulfur are similar in atomic radii, there is little difference in stereochemical stability from the starting material and product. We confirmed this after measuring barriers to racemization of both the S-aryl PPY and recovered starting material chloride PPY and found that they possessed similarly

around 30 kcal/mol stereochemical stability. In contrast, we learned that if the leaving group is a fluoride then the difference in steric bulk imparted to the axis between it and sulfur can be approximated to result to an increase in barrier to rotation of 5 kcal/mol. This would put the atroposelective S_NAr reaction at a range to allow for DKR. For example, if the starting material is a Class-1 atropisomer that has a $\Delta G_{\text{rac}} = 24$ kcal/mol, the resulting product will be a Class-3 atropisomer with a $\Delta G_{\text{rac}} = 29$ kcal/mol.

To test this hypothesis, we synthesized quinoline 72 (Figure 22, part b.) – a simple biaryl quinoline system containing the smallest group across on the 3-aryl axis aside from hydrogen (i.e., fluoride).^{5,96,97} The stereochemical stability of this compound was atropisomerically unstable at room temperature (i.e., Class-1 atropisomerism). This was later confirmed when we attempted to perform barrier to racemization studies and were largely unsuccessful. From here, quinoline 72 had proved to be amenable to S_NAr with thiophenol to give product 74, which possessed low Class-3 atropisomerism after determining the barrier to racemization to be $\Delta G_{\text{rac}} = 28$ kcal/mol. This stereochemical instability and ability to racemize to the functionally reactive atropisomer was an exciting start for S_NAr reaction optimization in a DKR approach (more details are in Section 2.12).

2.10 Reaction Optimization for Atroposelective S_NAr towards 3-arylquinolines

2.2.1 Catalyst Evaluation

For a control experiment, I attempted to synthesize compound 74 using the quaternary ammonium (i.e., derived from quinine) organocatalyst⁹⁸ 15 that was originally used in our kinetic resolution of the PPY scaffold⁹ (Table 1, entry 1). Unlike in the recent atroposelective strategy we used to obtain enantioenriched PPYs (Equation 5), this previously optimal catalyst 15 led performed poorly with low enantioselectivity in the S_NAr, as the product sulfide possessed an

55:45 e.r. (Table 6, entry 1). Also, the reaction had comprised of mostly unreacted starting material; this outcome being very comparable to the results of the azaindole scaffold.

At such low conversion, we redeveloped our catalytic strategy to activate the *N*-heterocycle of the 3-arylquinoline more optimally for this successful S_NAr . We initially thought that incorporating an H-bond donor into the quaternary ammonium catalyst might allow for increased S_NAr reactivity. However, there are other mechanisms to which stronger intramolecular H-bonding interactions may be formed with this class of privileged catalysts through specifically engaging the *N*-1 and the C2-F of the starting material. Higher conversions would be possible. We also proposed that through the mechanism model in Figure 23, we can direct the nucleophilic thiophenol to the explicit site where the S_NAr reaction takes place during the catalyst-substrate transition state. A search into the literature had supported these early hypotheses, as many cases solved poor reactivity for nucleophilic substitutions by increasing substrate-catalyst interactions through hydrogen bonding.

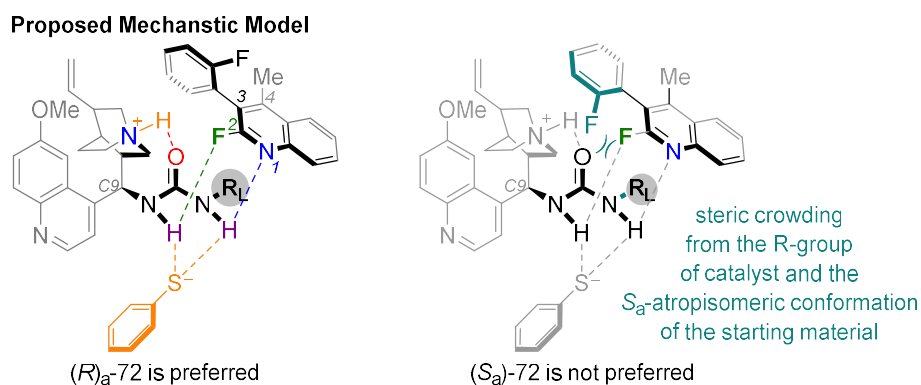


Figure 23. Early hypotheses and proposed model of transition state towards atroposelective S_NAr of C-3 arylquinolines. Shown is the urea-based quinine catalyst engaging in H-bonding with the quinoline to allow direct substitution from fluoro to *S*-aryl.

Work led by other research groups found that a urea was the best H-bond donor group for these catalysts. We first explored a traditional library of various quinines catalysts since these are generally very activated for enantioselective S_NAr . I and my colleagues had synthesized many

analogues of these C-9 epi-quinine derived urea catalysts, and evaluated all of these in the atroposelective S_NAr towards 3-arylquinoline 72. Many of the catalysts we applied in reaction optimization had been directly curated from previous literature, such as catalysts used by Professor Ken Houk's^{99,100} group from the University of California, at Los Angeles. The Houk group examined what features of the urea-based Cinchona^{98,100,101} alkaloid organocatalysts led to diverse yet consistently high catalytic activity across different reactions. To support their findings, Houk and coworkers had performed their Gaussian calculations to propose a transition state for how quinine-based organocatalysts exist in the lowest energy conformation. Their work was an integral reference for designing many different catalyst analogues. The preparation of all catalysts of this project can be found in Section 2.2.6.

Taking in the inspiration from Houk and others, quaternary ammonium salt urea-based catalyst 75 had indeed led to greater atroposelectivity as it effected the S_NAr in 18:82 e.r. 23% yield of sulfide product (Table 7, entry 2) but only slightly improved 23% isolated yield. The non-substituted quinuclidine (i.e., the “free amine variant”) catalyst 76 was by far more effective, with similar enantioselectivity to the quaternary ammonium salt yet greatly improved yield (Table 7, entry 3) likely due to solubility and homogeneity in the reaction. The most optimal catalyst was when we relaxed the steric effects from the urea, where we changed the group from an *N*-tertbutyl to an *N*-isopropyl R-group (i.e., catalyst 77). This had increased the yield to 75% at 10:90 e.r. (i.e., enantioselectivity at 80 ee%). Other substitutions such as R-group ethyl led to similar reactivity. Aromatic R-groups (such as 76) or cycloalkyl-based R-groups (such as 77) gave lower e.r.s and lower yields (Table 1, entries 5-6). In addition to understanding sterics for these catalysts, I and my colleagues also wanted to understand the importance of urea in the context of the H-bond donor. We synthesized then tested a thiourea variant and amide variant (that provides only one

hydrogen-bond donor site) of the catalyst. In each respective catalyst, enantioselectivity was markedly worse (i.e., e.r. of 35:65, please refer to Section 2.2.7, Table 17) which suggested that the urea moiety must be optimally tuned for the stereoinduction.

Table 13. S_NAr Reaction Optimization Summary Towards 3-arylquinolines

racemic-72 $\xrightarrow[\text{X M solvent, Temp., 60 h}]{\text{catalyst (X mol%), HSPh base}}$ 73

15

75

76: R = *t*Bu
77: R = *i*Pr
78: R = Ph
79: R = *cyc*-Pe

Entry ^[a]	Cat.	Solvent	Temp. (°C)	Conc. (M)	Base	Cat. Load (mol%)	72 e.r. ^[b]	72 %yield ^[c]
1	15	PhMe	r.t.	0.1	K ₂ HPO ₄	10	55:45	<5%
2	75	PhMe	r.t.	0.1	K ₂ HPO ₄	10	18:82	23
3	76	PhMe	r.t.	0.1	K ₂ HPO ₄	10	14:85	43
4	77	PhMe	r.t.	0.1	K ₂ HPO ₄	10	10:90	75
5	78	PhMe	r.t.	0.1	K ₂ HPO ₄	10	23:77	50
6	79	PhMe	r.t.	0.1	K ₂ HPO ₄	10	11:89	58
7	77	PhMe	r.t.	0.1	KHCO ₃	10	12:88	<5
8	77	PhMe	r.t.	0.1	KOH	10	10:90	15
9	77	PhMe	r.t.	0.1	-	10	15:85	29
10	77	mXy	r.t.	0.1	K ₂ HPO ₄	10	10:90	79
11	77	Hex/mXy	r.t.	0.1	K ₂ HPO ₄	10	10:90	82
12	77	Hex/mXy	r.t.	0.1	K ₂ HPO ₄	5	9:91	49
13	77	Hex/PhMe	r.t.	0.1	K ₂ HPO ₄	20	10:90	91

^[a]Reactions were performed on a 0.10 mmol scale of 74 with 10.0 equiv of thiophenol and 20.0 equiv of base. ^[b]e.r.s are determined from chiral stationary phase HPLC; reported as average of at least two trials. ^[c]Yields are reported as an average of at least two trials. Hex is an acronym for *n*-hexanes. mXy is an acronym for *m*-xylene. See Section 2.2.7 for further details on this reaction optimization.

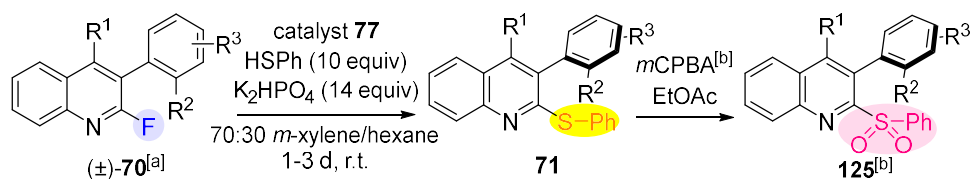
Other privileged urea-containing catalyst scaffolds, particularly a biphenyl urea-based catalyst derived (which can be synthesized from enantiopure BINAM) inspired by pivotal works from Professor Maruoka's¹⁰² group and Professor Gouverneur's group were screened and tested.^{103–105} Likened to the quinine-based catalysts, these biphenyl urea catalysts can facilitate an H-bonding interaction with pyridinyl type scaffolds and then lead to S_NAr using the adjacent fluoride as a secondary handle. When we evaluated these urea catalysts towards the desired 3-arylquinoline sulfide 72, we observed mostly racemic products at very low yield. From these results, we selected catalyst 77 as our most optimal to use for the atroposelective S_NAr of many 3-arylquinoline compounds. As mentioned before, the complete summary of all these catalyst results can be found in Section 2.2.7, Table 17.

2.2.2 Summary of the Reaction Optimization

With the optimal reaction catalyst, we next examined reaction temperature, concentration, and base (Table 6, entries 7-14) for the best enantioselectivity and yield from this DKR of 3-arylquinolines. The enantioselectivities across these S_NAr reactions had remained largely unchanged, however the yields were marginally impacted in some of these cases. To help explain these findings, we tested the absence of the external base to see if the atroposelective S_NAr would still occur. In essence, we wanted to understand if the catalyst was the main driver for the observed trend of higher conversions in the reaction optimization. Inherently, the catalyst itself can also act as the non-nucleophilic base since the quinuclidine amine would be basic enough to deprotonate thiophenol. From this experiment, comparable e.r. albeit in 29% yield (Table 1, entry 9) was observed – an outcome that was very departed from the atroposelective S_NAr strategy utilized in the PPY series. Even though it was possible to perform this reaction without base, the inclusion of external non-nucleophilic base K₂HPO₄ was critical for improved and consistent conversions

(something that would be important for evaluation of other types of 3-arylquinoline substrates). In support of these findings, we performed a catalyst loading screen for this S_NAr and found no fold improved atroposelectivity. Notably, reaction conversion was indeed increased in a linear trend, where 20 mol% catalyst loading resulting in the highest isolated yield.

The optimized atroposelective S_NAr towards these 3-arylquinolines was also very solvent dependent. In a similar fashion to the PPYs, non-polar, aprotic solvents which possessed a dielectric constant $\epsilon \sim 2.5$ were the most optimal (the complete solvent screen is found in Section 2.2.7, Table 18). Our studies found improved yields with xylenes over toluene (entry 10); specifically, mixtures of xylene/hexanes (entries 11-13) led to the best result of this reaction optimization. Specifically, we found a mixture of 30% *n*-hexane and 70% *m*-xylene was determined to yield the most optimal combination of yield and enantioselectivity (91% yield of **74** with 80 ee%) in DKR, though a mixture of *n*-hexane and toluene also yielded comparable results.



Equation 27. Optimized reaction conditions of the dynamic kinetic resolution of atropisomeric 3-arylquinolines.

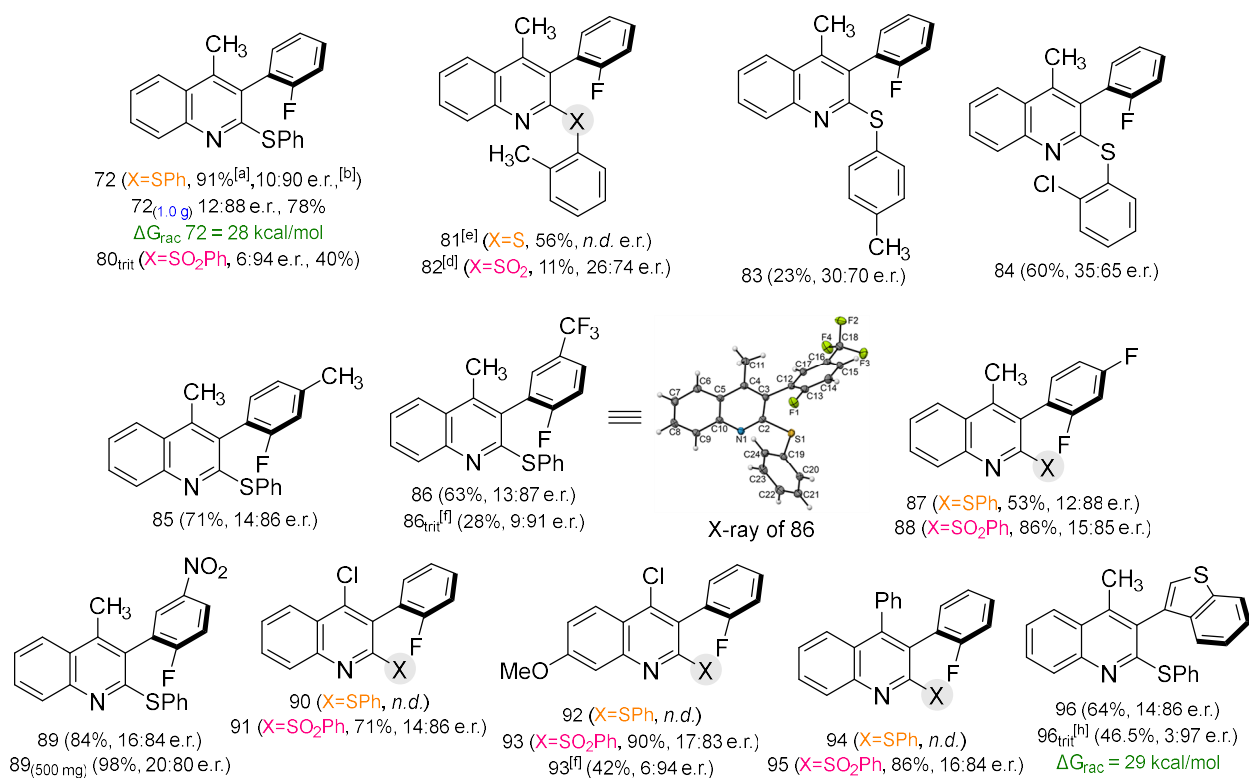
In summary, our most optimal reaction conditions used 20 mol% catalyst C4 and K₂HPO₄ in 0.1 M solution of 70% *m*-xylene and 30% *n*-hexanes. Adding a significant excess of both thiophenol and inorganic base increased the atroposelective S_NAr conversion but did not impact the enantioselectivity of the reaction.

2.11 Atroposelective S_NAr of 3-arylquinolines via DKR

We next evaluated the scope of this DKR (Equation 27 and Table 7). It is worth noting that in some cases, oxidation of the product sulfide 72 to sulfones 80 using *m*CPBA was needed to separate products from starting material and assess enantioselectivities. These sulfide product 3-arylquinolines (when compared to the PPY scaffold) were very nonpolar, and as a result had poor resolution on analytical chiral HPLC. Also, another departure from the initial PPY exploration – we examined the effects of S_NAr using different thiophenols. From another project in our group, more electronic rich thiophenol derivatives had resulted in optimal enantioselective vicarious nucleophilic substitution (i.e., VNS, a more reactive S_NAr where the leaving group is a proton).

The nucleophilicity of these different thiophenols might greatly improve our nucleophilic aromatic substitution for this scaffold and facilitate higher atroposelectivity at the transition state of the catalyst-substrate interaction. We were not agnostic to our source for establishing the S-aryl bond, as it would only serve as an intermediate towards any future enantioselective post-functionalization. From these experiments, S_NAr using chloro-substituted thiophenols (81) had resulted in sulfide products with larger decreased enantioselectivity and relatively similar yields to that of 72. These thiophenols would be less nucleophilic, and therefore resulted in poor enantioselectivity at 35:65 e.r. at 60% yield. Notably, the experiments using *ortho*-cresol (as in 81) and *para*-cresol (as in 83) thiophenol derivatives as our nucleophile also decreased enantioselectivity and yield. From these results, added steric bulk at this site of S_NAr reaction resulted in low conversion and no improved enantioselectivity. We concluded that the unsubstituted thiophenol was the most optimal for the nucleophile.

Table 14. 3-arylquinoline Analogues Obtained via Dynamic Kinetic Resolution (Classical DKR)



S_NAr reactions were performed with 1.0 equiv racemic 3-arylquinoline 70, 20 mol% catalyst 77, 10.0 equiv HSPH, 20.0 equiv K₂HPO₄, and 70:30 *m*-xylene/*n*-hexanes (0.1 M) at room temperature for up to 80 h (~3 days). ^[a]Reported overall yields and ^[b]enantiomeric ratio (e.r.) are an average of at least 2 trials. ^[c]Barrier to rotations are an average of at least 2 trials. ^[d]Oxidation to sulfone 80 used 1.0 equiv sulfide 72, 2.1 equiv mCPBA in 0.1 M EtOAc at room temperature for 18 h. ^[e]E.r. was *n.d.* = not determined for this substrate. ^[f]Trituration from 100% *n*-hexanes or 80:20 *n*-Hexanes/DCE, yields are overall from starting material 70. ^[g]Stereochemical outcome of our S_NAr elucidated by X-ray crystal structure. For more details please refer to Section 2.2.13.

Using the optimized atroposelective S_NAr conditions, we examined several 3-aryl 2-fluoroquinolines (Table 7) with mildly electron-donating groups on the 3-aryl ring (e.g., the *para*-methyl group in 85), or electron-withdrawing groups (e.g., examples 86-89, and 96). These S_NAr reactions resulted in products of moderate enantioselectivities, comparable to 72. For example, sulfide product 85 was isolated in 71% yield at 14:86 e.r., while sulfide 86 was isolated at 13:87 e.r. in 63% yield. This data suggests that the efficiency for this atroposelective S_NAr was not

largely impacted by the other 3-aryl substitution (i.e., groups that are not adjacent to the axis of chirality). Highly enantioenriched, solid crystals were obtained through trituration – as previously mentioned in Section 1, a method of rinsing enantioenriched crystals to increase the purity of the sample; in this case, producing a solution or solid crystals of high enantiopurity. Through trituration of the resulting sulfide product 86, we were enabled to X-ray crystallographic methods which elucidated absolute stereochemical assignment. We surmised that the major atropisomer for the enantioselective S_NAr strategy was in the (R_a)-configuration, which strengthened our hypotheses for mechanism of this reaction (see Section 2.14).

We also synthesized enantioenriched sulfide product containing a benzothiophene adjacent to the chiral axis (i.e., an example of a Class-1 ‘6-5’ atropisomeric biaryl). From the PPY work, we knew that the ‘6-6’ biaryl system typically results in higher stereochemical stability than ‘6-5’ biaryl atropisomers.¹⁰⁶ Indeed DKR was observed, yielding compound 96 in 14:86 e.r. and 64% yield while existing as a stereochemically Class-3 atropisomer ($\Delta G_{rac} = 29$ kcal/mol). With such modest enantioselectivity for this reaction, trituration of in *n*-hexane improved the enantiopurity of the sulfide to 3:97 e.r. in 52% overall yield. With success from trituration, we were able to take S_NAr products and increase enantiopurity in a robust process.

Moving away from R^1 -methyl, we changed the R^1 -group on the quinoline scaffold to a more electron withdrawing group (example quinolines 90-94). Changing the electronics of the quinoline by induction of such functional groups impacted the enantioselectivities and yields for the S_NAr . From the data, these changes also yielded comparable enantioselectivities to 72. Some examples were switching the C-4 methyl to a C-4 chloro-group such in substrates 90 (sulfone 91 was obtained in 79% yield, 12:88 e.r.) and 92 (sulfone 93 was obtained in 90% yield, 17:83 e.r.), or phenyl as in 94 (sulfone 95 was obtained in 86% yield, 16:84 e.r.).

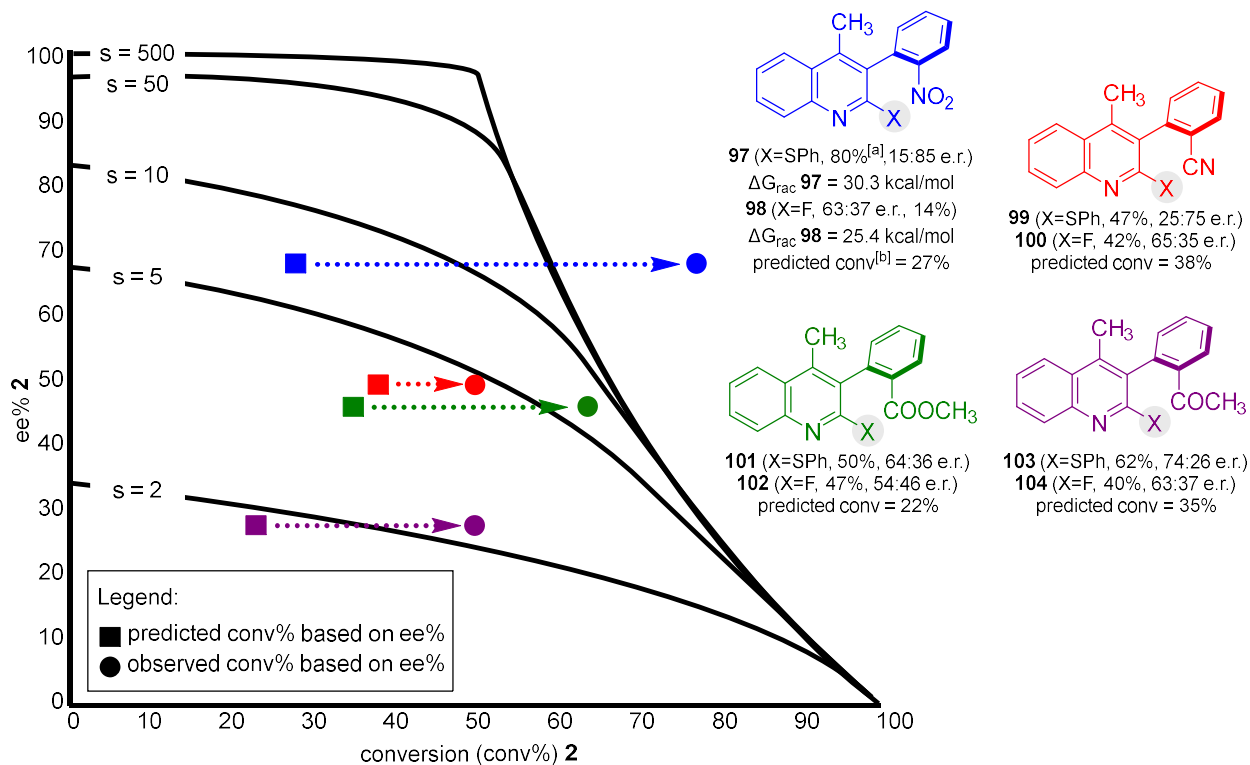
Many of these sulfide products were oxidized to the respective sulfone (illustrated in Equation 27), due to poor available analytical methods at the time of our measurements. There were no observed losses in enantioselectivity when telescoped to the sulfone. Also, these 3-arylquinoline sulfides were typically amorphous solids (in some cases, were oils); while many of the sulfone products were now crystalline solids. Enantiopurity of the products were increased through simple trituration of the sulfones via our defined protocols. This was a helpful strategy for the pursuit of these 3-arylquinoline based substrates which after the atroposelective S_NAr led to modest (sometimes less than 80 ee%) enantioselectivities. An example was that trituration allowed us to improve enantiopurity of 72 to 6:94 e.r. in 40% telescoped yield from its starting fluoroquinoline 74. Another example is that sulfone 93 was isolated in 6:94 e.r. in 42% yield telescoped from S_NAr . As a countermeasure, recovered the starting materials after the reaction which were racemic after examining analytical chiral HPLC traces. This offered further evidence that these reactions are largely proceeding via DKR (see Section 2.2.19 for more details).

2.12 Dynamic and Classical Kinetic Resolution Hybrid Mechanism

Broadening our substrate scope for other analogues of 3-arylquinolines would be more desirable in Future Med. Chem. Straying away from *ortho*-fluorinated analogues of our 3-arylquinolines, we next examined substrates with increased the size of the substituent adjacent to the atropisomeric axis (i.e., increasing the atomic radii off the R²-group). We performed atroposelective S_NAr on a *ortho*-nitro substrate 97, *ortho*-cyano substrate 99, and *ortho*-carbonylated substrates 101 and 107. Across this suite of compounds, there appeared to be a huge loss in enantioselectivity for the S_NAr reactions towards the resulting sulfide products. These

observations were reminiscent of substrate 48 from the original PPY atroposelective S_NAr work (please refer to Section 2.4, Table 3) – where a loss of enantioselectivity was also observed with the C-2 nitro-group. I wanted to investigate if there might be more to the kinetic resolution towards atropisomers, since these substrates were just slightly larger than the *ortho*-fluoro groups used in the DKR. I and my colleagues hypothesized that there was likely some competing background reaction – where we proposed that the product PPY 49 was unstable causing racemization or enantiodegradation) occurs when using these types of functionalities that result poor observed enantioselectivities in the final products.

Table 15. 3-arylquinoline Analogues Obtained via Hybrid Dynamic Kinetic Resolution and Kinetic Resolution (DKR/KR Hybrid)



S_NAr reactions were performed under the same conditions as reported in Equation 27. ^[a]Reported e.r.s above are of one trial for simplicity. Reported yields are obtained from isolated and purified products and starting material, as an average of at least three trials. ^[b]To determine the theoretical conversion, the Fiaud equation (Section 2.1.8) was used (Section 2.1.8). Please refer to Section 2.2.13 for more details about the syntheses towards these compounds in this table.

To understand this, our strategy was to study the enantioselective S_NAr towards these types of products in the context of classical kinetic resolution (KR). It was entirely possible when this result was found that these substrates were possibly at higher stereochemical stability. For classical kinetic resolution, the reaction conversions for these experiments were limited to nearly 50% conversion in order to study the enantiopurity of both the sulfide and recovered starting materials. I designed these experiments to keep all the S_NAr reaction times consistent across all substrates within this set, which would greatly impact overall reaction conversions. This would prevent huge invariabilities between all the S_NAr reactions and provide more direct comparisons. This method was like our previous KR approach for atroposelective S_NAr towards the PPY scaffold. On one hand, we were able to control the reaction yields towards *ortho*-cyano 100 and the *ortho*-carbonyl substrates 102 and 104. However, the atroposelective S_NAr of this *ortho*-nitro 98 happened much faster than the total reaction time we allotted. Because of this discrepancy, we thought that the product sulfide would not be as optimally enantioenriched caused by this superseding of the 50% conversion limit in classical KR. Nonetheless I examined the resulting analytical chiral HPLC traces of all these substrates and was shocked to find that the resulting enantioselectivities (despite containing most of them to the optimal KR conversion) remained largely unchanged. I was even more surprised that the recovered starting materials resulted in enantioselectivities of about 30 ee%. However, most intriguing of all were the results from the reference compound, this *ortho*-nitro-group series. I had captured the final sulfide product 98 in 15:85 e.r. in 80% yield, but also recovered the enantioenriched starting material 97 in 63:37 e.r. at 14% yield.

All these results did not align with the classical methods, and these observations obtained were not indicative of a classical kinetic resolution reaction pathway. With the yield of 98 superseding the 50% limit yet possessing moderately higher enantioselectivities compared to the

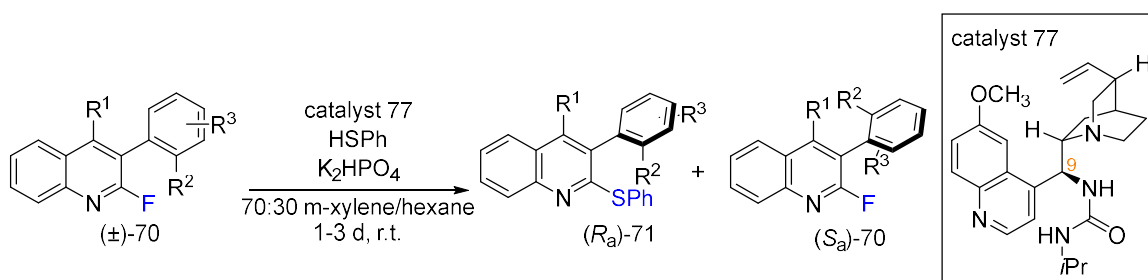
starting material, this especially does not align with the methods of dynamic kinetic resolution either. To better understand what was happening, we measured the barrier of racemization for each of these entities. We examined the post-S_NAr enantioenriched mixtures of several isolated, recovered starting materials and resulting sulfide quinolines 98 and 97. The recovered, enantioenriched nitro-group 97 starting material had possessed a ΔG_{rac} of ~ 25 kcal/mol (Table 8), corresponding to racemization on the hour to day timescale at room temperature. Its product sulfide 98 was found to exist as a Class-3 atropisomer of $\Delta G_{\text{rac}} \sim 30$ kcal/mol. Comparing these results to the other substrates, the *ortho*-cyano 100 and *ortho*-carbonyl 102 and 104 substrates possessed similar barriers to racemization. For example, I calculated the ΔG_{rac} for the *ortho*-ketone 3-arylquinoline sulfide product 104 to be around 29 kcal/mol – which puts its preceding starting material within the stereochemical range of the *ortho*-nitro 3-arylquinoline 97). All these results show that these starting materials possess ΔG_{rac} between 24.5 to 26 kcal/mol, which correlates with how long these reactions typically take.

To understand this correlation better, we revisited the classical Fiaud and Kagan equations⁷² (please refer to Section 2.1.8, Equations 7 and 8) in order to determine the predicted conversions based on the observed enantiomeric excess (ee) of starting material and product. In the context of a canonical kinetic resolution, both overall yield towards product and reaction conversion should associate very closely (i.e., enantioselectivity is a direct function of the conversion). From these equations, calculated *s*-factors from the enantioselectivities were a function of the observed from the recovered, isolated starting material 98 and corresponding sulfide product 97. The projected, predicted S_NAr reaction should be around 27% conversion. However, the observed isolated yield of 80% significantly outperforms this calculated conversion. Using this same analysis, I calculated the expected conversions based on the observed

enantioselectivities for products and substrates 99-104 as well. While these substrates yielded attenuated enantioselectivities, we observed similar perturbations in isolated yield from the expected conversions for a purely kinetic resolution process. This is perhaps represented most clearly when plotted onto a graphic representation of product e.r. degradation depending on the various *s*-factors for this transformation.

One likely conclusion is that because the starting materials may be racemizing in accordance with the reaction time, a “nebulous” type of reaction occurs. These observations lead to the idea that these S_NAr reactions display both hallmarks of DKR and KR. As these reactions progress, there is a significant background of DKR that can alter the enantiopurity of the innate KR-character in the S_NAr reaction. This type of reaction mechanism can be coupled with the fact that these substrates contain electron-withdrawing groups that are also likely competing with our catalyst-driven atroposelective S_NAr reaction. A future study that I would leave the Gustafson group to understand would be to examine alternative S_NAr substrates with electron-donating groups that fall within this dynamic range of stereochemical stability.

2.12 Atroposelective S_NAr of 3-arylquinolines via Classical KR

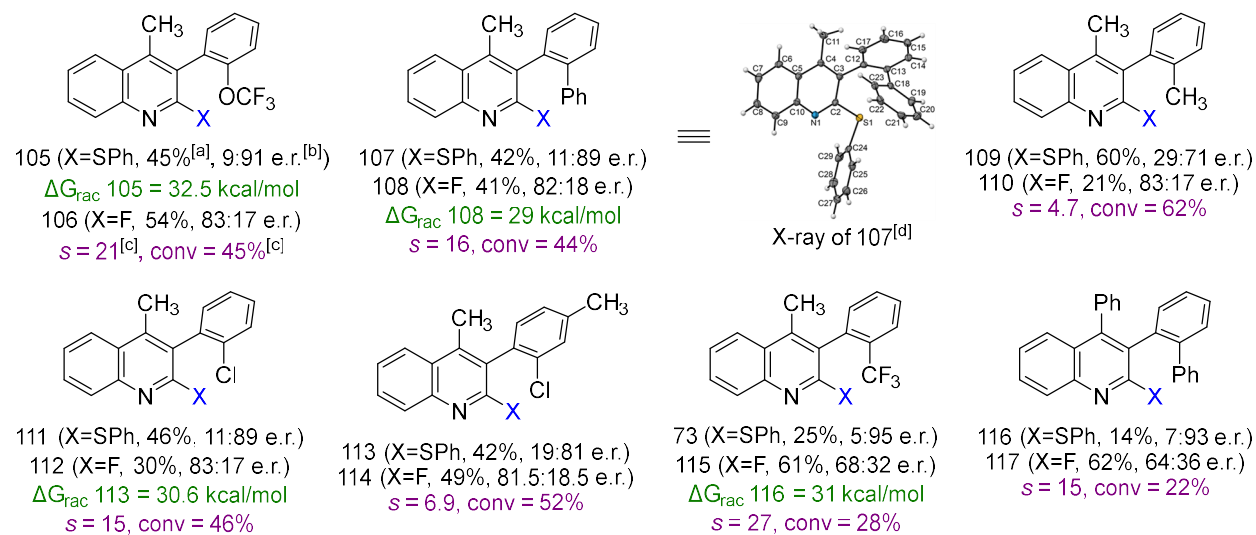


Equation 28. Optimized reaction conditions of atroposelective S_NAr towards 3-arylquinolines via classical kinetic resolution. Enantioenriched sulfide and recovered starting materials were isolated.

Finally, I and my colleagues evaluated stereochemically stable substrates with diverse, larger *ortho*-substitutions (i.e., $\Delta G_{\text{rac}} > 26.9$ kcal/mol). Unsurprisingly, I observed classical kinetic resolutions under our optimal $S_{\text{N}}\text{Ar}$ conditions. Stereochemical stabilities calculated from these starting materials ensured that there was no background racemization over the course of the reaction. An example of this is substrate 106 (with an *ortho*-trifluoromethoxy group, a higher Class-2 atropisomer), yielded sulfide 105 with a $\Delta G_{\text{rac}} = 33$ kcal/mol in 45% yield in 9:91 e.r.; recovered 106 being isolated in 87:17 e.r in 54% yield. The $S_{\text{N}}\text{Ar}$ reaction of this substrate calculated to an *s*-factor of 21 (and importantly a 45% conversion that aligns with the product yield). Another example is substrate 108 with an *ortho*-phenyl possesses a surprisingly (likely due to steric clashing resulting in an orientational planarity) high ΔG_{rac} of 29 kcal/mol and led to a KR with a *s*-factor of 16 in 44% conversion under our optimal conditions. *Ortho*-methyl (a sp^3 -group that is typically very large as a substituent) substrate 110 led to an $S_{\text{N}}\text{Ar}$ reaction of *s*-factor of 4.7 and 62% conversion.

Substrate 112, with *ortho*-chloride, yielded a *s*-factor of 15, however the incorporation of a *para*-methyl on the 3-aryl in substrate 114 led to a drop in *s*-factor to 6.9. One likely reason is that the $S_{\text{N}}\text{Ar}$ reaction is sensitive to a fine balance of steric and electronic factors (which matches with previous findings of the other two substrate scopes). Substrate 116, which possesses an *ortho*-trifluoromethyl group, yielded a *s*-factor of 27 at 28% conversion under our optimal conditions, allowing for the isolation of compound 73 in 5:95 e.r. albeit in only 25% yield. Finally, substrate 117 resulted in a *s*-factor of 15. Overall, the observed level of selectivities across these substrates suggests that enantioselective $S_{\text{N}}\text{Ar}$ can yield synthetically useful yields and enantioselectivities of diverse 3-arylquinolines regardless of the size of steric hinderance imparted by the neighboring functional groups.

Table 16. 3-arylquinoline Analogues Obtained via Kinetic Resolution (Classical KR)



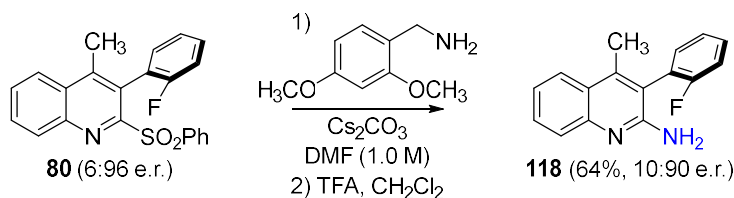
Substrate scope: Kinetic resolution. Reactions were performed on 50 mg substrate. ^[a]Isolated yields are reported as an average of at least two trials. ^[b]Exemplary e.r.s of starting material and product are included above for one trial. ^[c]Conversions and *s*-factors are reported as an average of at least 2 trials and were determined from chiral stationary phase HPLC using the Fiaud and Kagan equations 7 and 8 (Section 2.1.8). ^[d]X-ray crystallography still confirms that the sulfide product was obtained as the (*R*_a)-atropisomer.

2.13 Post-functionalization of Atropisomeric 3-arylquinolines

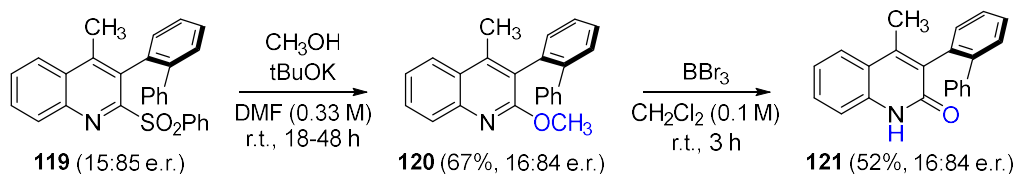
From the sulfides, oxidation to the corresponding sulfones using *m*CPBA with minimal to no observable racemization was trivial. Sulfones have been shown to be good leaving groups for S_NAr, thus we first evaluated whether we could leverage this activity to incorporate functionalities that are commonly seen in pharmaceutically relevant quinolines. Taking advantage of this sulfone as a useful synthetic handle, we performed subsequent S_NAr with other nucleophiles. Firstly we subjected enantioenriched sulfone 80 (4:96 e.r.) to our previously reported, two-step amination procedure (Equation 29, part a), isolating enantioenriched 2-aminoquinoline 118, with minimal racemization, in 10:90 e.r. and 64% overall yield.

We next sought to determine if we could access enantioenriched 3-aryl-2-hydroxyquinolones (can also be referred to as naphthyridones), which are among the most common moieties in pharmaceutically relevant scaffolds. These types of groups are often exploited in drug discovery for their likeness to amides due to a similar pKa of the N-H, but are more rigid as the H-donor is locked in a stable aromatic ring. We were inspired by recent work from Patel and Wei,¹⁰⁷ where they show S_NAr towards a variety 4-quinolinyll ethers can be accessed from 4-(phenylsulfonyl)quinoline. We leveraged a similar two-step strategy, wherein the sulfone is first subjected to S_NAr using methanol and tert-butoxide at room temperature then followed by a demethylation using BBr₃ to give the desired 2-quinolones (Equation 29, part b).

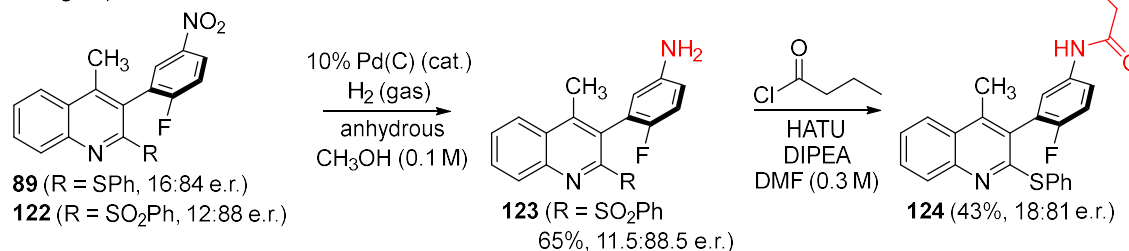
a. S_NAr towards 2-amino-3-arylquinoline



b. S_NAr towards 3-arylquinolin-2-ols



c. Aryl Nitro-group Reduction



Equation 29. Post-translational modifications with enantioenriched products. Refer to Sections 2.2.14 to 2.2.17 for more details regarding the above syntheses.

One consideration before I attempted this reaction was to be mindful that the methoxy-substituted quinolines (or 2-quinolones as well) are much smaller in size compared to the 2-sulfide or the 2-amino substitutions. Because of this, we expected a net loss in the overall stereochemical stability which would then find these products racemized within minutes. Sulfone 80 was used as a control test, and we found complete enantio-degradation of its final 2-quinolone¹⁰⁷ since the enantiopurity was very close to 0 ee%. Stereochemically stable substrates from the scope within the classical kinetic resolution were the most optimal to use for this type of post-functionalization strategy. Choosing sulfide 107, we oxidized this to its corresponding sulfone 119 which possesses very high Class-3 stereochemical stability and is amenable to this transformation sequence. I synthesized its *ortho*-methoxy product 120 and then shortly after obtained 2-quinolone 121 with very good yields throughout this synthesis, and no observed racemization.

Lastly, we reduced the *para*-nitro group of either the sulfide 89 or its oxidized corresponding sulfone 122 using standard Pd(C)/H₂ conditions. Sulfone 122 was not reduced under these conditions. These reductions also led to no huge losses in racemization, in overall ~65% yields. Standard peptide coupling conditions of acyl chloride or carboxylic acid, HATU, and excess DIPEA were then pursued immediately to yield amide 124 in minimal observed racemization. In general, the amide coupling reaction is extremely ubiquitous across medicinal chemistry and is arguably the important transformation in drug discovery. Amide groups provide an H-bond donor that is often exploited in medicine to target specific key residues for potency and selectivity, but also link various functionalities that can make these scaffolds more pharmaceutically relevant. We synthesized this butyryl-group¹⁰⁸ as a control to use for a chemical probe collaboration with Professor Chris Parker's group at TSRI San Diego (Chapter 3). Much the same, 2-amino groups that were obtained from the S_NAr of the sulfones were also susceptible for

amide formation using these methods. This final synthetic sequence demonstrates the extensive utility of sulfide products for other common functionalities in drug discovery, with minimal racemization and good yields.

2.14 Proposed Transition State Model of the S_NAr of 3-arylquinolines

This S_NAr project was being concluded yet unfortunately in February 2020 there was a global shutdown due to the extreme devastations caused by the COVID-19 pandemic. I had been finishing final experiments which required resyntheses and trituration of enantioenriched materials starting from the atroposelective S_NAr. This was important since a lot of this material was used frequently for optimizing our post-functionalization chemistries (Section 2.13). With this minimal access and time to our research lab as well as limited resources, we were unable to pursue more experiments and discussion in our final publication of this work. Many of these experiments included mechanistic studies that I and my colleagues investigated into understanding our catalytic atroposelective S_NAr. Many of these studies in this section were towards understanding how the catalyst **77** was found to be the most optimal. We proposed many experiments to provide insight on how our optimal catalyst outcompeted the entire suite of other catalysts tested from the beginning of this entire project.

2.2.3 Preliminary Results from NMR Experiments to Study Catalyst-Substrate Complex

Based on our data from the catalyst screening, potential H-bonding interactions between our optimal urea-containing catalyst and the 2-fluorinated quinoline **72** would likely be the key driver of enantioselectivity in S_NAr. We previously hypothesized that the transition-state

mechanistic model on findings from the primary literature would lead to a potentially stronger H-bonding network and bring the thiophenol closer to the site of activated S_NAr in a stereospecific manner (see Section 2.2.1 for an explanation of many catalysts). This engagement then would result in enantioenriched sulfide product, favoring the reactive atropisomer that participated in the H-bonding network through a potentially unique N-H and H-F bonding interaction. To determine more empirically if the urea -NH chiral catalyst can engage in an H-bonding network with our quinoline substrate through this -N and -F bidentate interaction, we ran several preliminary ¹⁹F NMR¹⁰⁹⁻¹¹¹ and ¹H-¹⁵N HSQC experiments each examining the quinoline starting material in the presence or absence of the urea catalyst.

We felt that NMR experiments would be the most visually accessible since a chemical shift (in ppm) in these nuclei NMR experiments suggested a change due to catalyst engagement with the starting material. These studies would require further in-depth analysis through follow-up NMR runs. Given more time, we would have liked to run variable time-dependent NMR experiments to study the emerging NMR shifts after addition of the catalyst. Also, each of these NMR experiments were taken with only one trial, so these experiments should be repeated to solidify any interesting findings. Following this point, these NMR experiments were performed in deuterated toluene (i.e., not a feasible timeline to access “30:70 deuterated *n*-hexane in deuterated *m*-xylenes”) which while comparable in the optimization of the reaction conditions was not the optimal solvent system we pursued in the totality of the of the atroposelective S_NAr strategy of these fluorinated quinolines. Finally, it was difficult to access proper NMR processing software given the short time, so we were only able to provide scans of the spectra due to limited resources. For all these reasons, these mechanistic NMR experiments are not included in the final delivery of this manuscript. These experiments are exclusively in this dissertation to springboard and inspire

future exploration for the Gustafson research group in other projects that may include these catalysts.

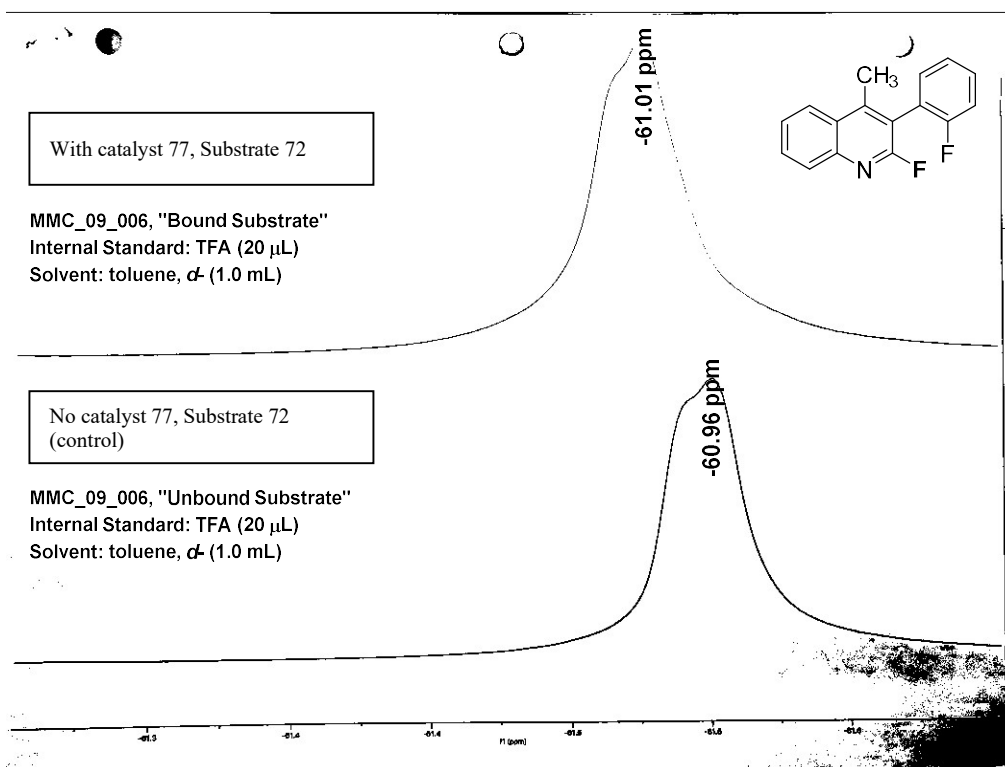


Figure 24. ^{19}F NMR Singleton Experiments to Study Catalyst-Starting Material Complex

We conducted these rudimentary ^{19}F NMR experiments^{111,112} since at the time these were the most straightforward and accessible given our then resources. TFA was selected to be the internal standard for these studies since its chemical shift does not overlap with our 2-fluoroquinoline substrate. However, if we were to include TFA into the NMR tube ‘as is,’ it would likely react with the catalyst which could alter the ^{19}F NMR substrate-catalyst interaction. In addition, TFA is quite volatile at room temperatures so the concentration and consistency across the experiment would be too variable. To circumvent this, we prepared a 20 μL TFA sealed glass ampoule that could then be equipped to the sample (i.e., slowly, and carefully lowering the

ampoule inside the NMR tube). After taking the ^{19}F NMR (standard experiment, 4 scans), we assigned the quinoline's C-2 fluorine to engage in $\text{S}_{\text{N}}\text{Ar}$ (Figure 24, highlighted in green) possessed a shift of -60.96 ppm. To this NMR tube was then added catalyst 77 in the matching stoichiometry to what we typically run our $\text{S}_{\text{N}}\text{Ar}$ at (i.e., catalyst loading of 20 mol%). After retaking ^{19}F NMR after 16 hours, I observed a 0.05 ppm ^{19}F NMR shift more downfield. Looking at this data, we have not observed a drastic change in this ^{19}F NMR. In addition, this value is within the error of the probe during the recording of these experiments. These experiments were a bit inconclusive, so future experiments that were described will only help to better solidify our new learnings. It is likely that choosing another starting material that is faster and more reactive would see these shifts more obviously. Unfortunately, no pursuits cannot be recorded at this time.

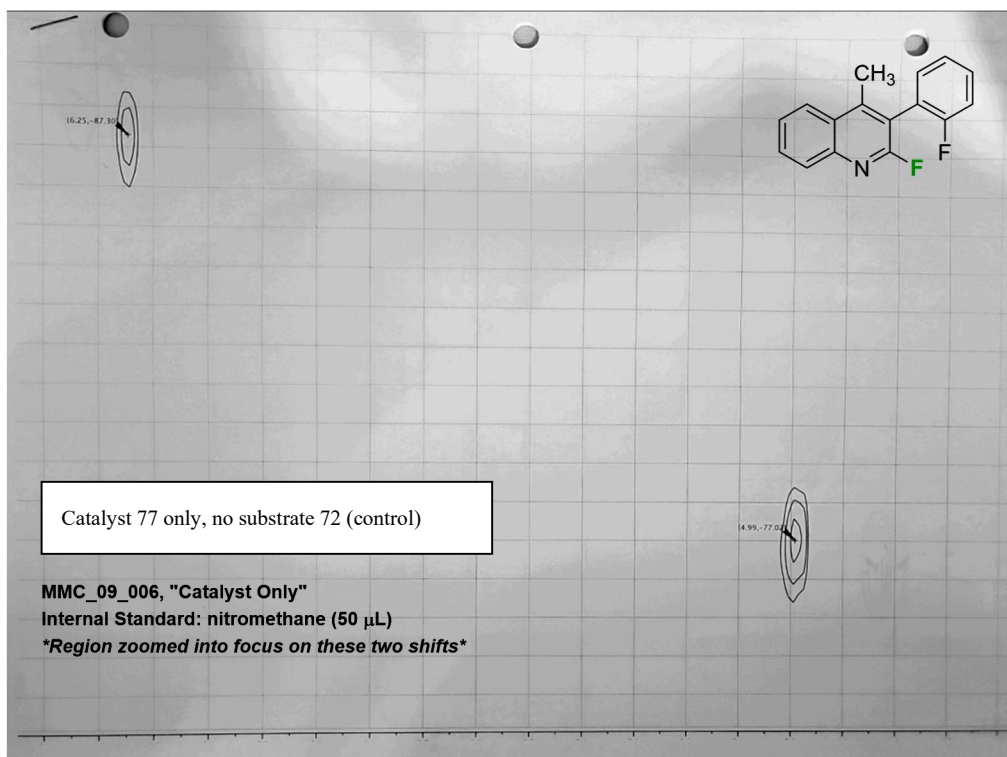


Figure 25. ^{19}H - ^{15}N HSQC Singleton Experiments to Study Catalyst-Starting Material Complex

Single nuclei ^{15}N NMR experiments for the starting material as the to probe a potential for a H-bonding interaction through the fluoride could theoretically be possible using this approach. However, these experiments were not convincing as standalone; further NMR studies would have offered a fresher perspective in understanding this catalyst-substrate complex. We performed preliminary ^1H - ^{15}N HSQC to examine the urea from the catalyst when in the presence and or absence of starting material 72. In theory, if these two -NH from the urea were engaging in what we believe is H-bonding (i.e., effects of the electric field from the substrate engaging with the catalyst) we might see shifts in the 2-D spectra. To carry out this experiment, 16.2 mg of the catalyst to deuterated toluene was performed to dissolution. More loading of the catalyst was necessary since ^{15}N is the rarest isotope and would require more sample and longer scans. Then, internal standard nitromethane was prepared in a glass ampoule and equipped in the sample NMR tube (i.e., for similar reasons to the case of ^{19}F NMR experiments).

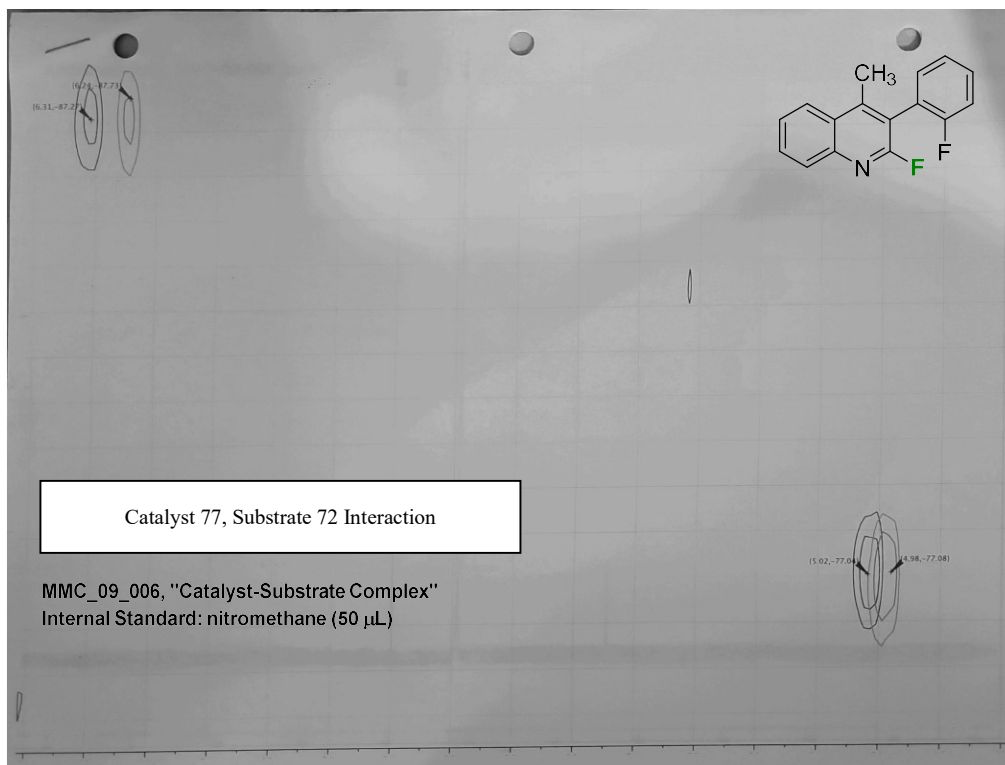


Figure 26. ^1H - ^{15}N HSQC Singleton Experiments to Study Catalyst-Starting Material Complex

After recording the 2-D NMR at this stage, I added substrate 74 to this NMR sample ensuring dissolution, and then performed this analysis again. After studying the ^1H - ^{15}N HSQC, once again I found the spectral data had minor NMR shifts. One of the signals at around [^1H δ 6.25 ppm, ^{15}N δ -87.30 ppm] had shifted more downfield [^1H δ 0.07 ppm, ^1H δ 0.46 ppm]. The other signal (corresponding to the other urea -NH) appeared around [^1H δ 4.98 ppm, ^{15}N δ -77.08 ppm], but showed a much more subtle differential of [^1H δ 0.04 ppm, ^{15}N δ 0.04 ppm] more downfield after the addition of the substrate. This subtle difference in the HSQC also pairs with the measurement of the minimal ^{19}F NMR shift. To strengthen these findings more experiments that were earlier proposed would need to be performed before using this observation as a solid basis of understanding the catalyst-substrate complex.

There has been many new NMR experiments that continue to be developed, redeveloped, and implemented into many areas of research. One may also envision some of these new experiments being useful to study our catalyst-substrate interaction. For example, the most recent prevalence of fluorination throughout medicinal chemistry has warranted new methods for ^{19}F NMR based 2-D experiments. ^{19}F is quite an attractive NMR-active nuclide as it is 100% natural abundance with high detection efficiency (i.e., less time to run experiments), and typically has fidelity due to low spectral overlap. For example, 2-D NMR experiments such as ^{19}F NOESY or ^1H - ^{19}F HOESY are quite popular for structural elucidation of pharmaceuticals containing fluorine. Both (i.e., Overhauser Effect) are highly sensitive NMR experiments for studying “through-space” effects (i.e., long distances), it might be possible to observe changes if detection for the catalyst H and substrate C2-F is observed.

Other potential experiments could be 2-D NMR experiments such as ^{13}C - ^{19}F HSQC/HMBC (i.e., “through-bond,” 1-2 bond distance detection limit) – becoming increasingly

popular studies which may aid in seeing any differences made to the C2-site where S_NAr takes place (i.e., where the catalyst engages with C2-fluoride can affect the C-F bond). In all cases, everything that was previously discussed can aid in our understanding of our S_NAr using empirical data. Especially when paired with powerful computational tools like Gaussian, all the empirical findings from the NMR experiments would be quite helpful to solidify our understanding of the catalyst-substrate complex.

2.2.4 Molecular Docking Tools to Visualize Atropisomeric Preference

Gaussian or newer computation tools today would likely be more quantitative and precise, and in addition S_NAr reactions study transition states (which require higher-order, longer computation experiments). In addition, higher-order computation tools are necessary to properly align “through-space” and provide a 3-D model of how the catalyst and substrate orient themselves in respect to each other present in the experiment. For example, computational software considers calculations from geometry or electronics. From our X-ray crystallography, we learned that our major product was the (R_a)-atropisomer and then minor enantiomer in the mixture was the (S_a)-atropisomer. Gaussian calculations using our (R_a)-atropisomer in the presence of the catalyst were attempted, but unfortunately were not able to get solutions due to a low processing power from the CPU. Unfortunately, because of all these situations I and my colleagues decided to deprioritize our efforts in working on any of these mechanistic studies altogether.

We turned our attention to using other approaches to examine our transition state in 3-D. At the time of finalizing this project, my other colleagues from our research group were using other molecular docking software in their other studies. At the time of my reporting, MOE (i.e., Molecular Operating Environment) was used heavily by the members of the Gustafson group to model their atropisomeric products in 3-D space. For example, this molecular docking software is

very helpful and is used by many research institutions and industries to visualize these structures in space. Our group was primarily using MOE for SBDD towards a more suitable PPY-analogue for the RET-inhibiting kinase project.

Proposed Model Transition State (Unfavored)

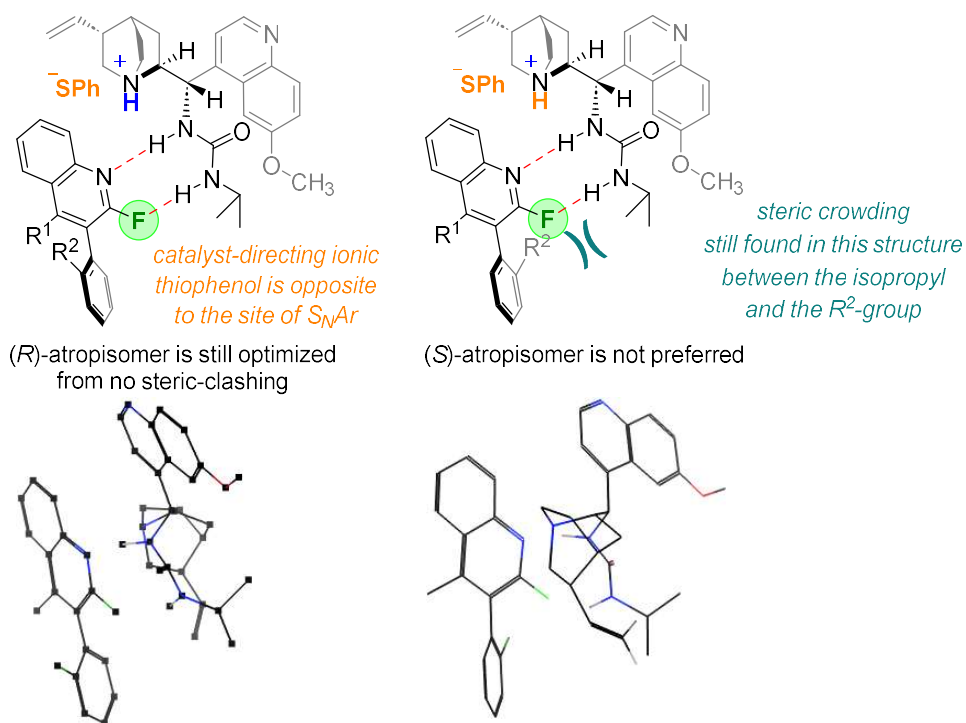


Figure 27. Unfavored interactions between starting material 3-arylquinoline 72 interaction with catalyst 77 obtained from minimization of MOE. The proposed model is represented in a 2-D and 3-D structure.

I was inspired by a postdoctoral student in our group at this time in the project, Dr. Sagar Vaidya, who suggested using MOE to model the catalyst and substrate transition-state “in-space,” then allow MOE to run minimization energy calculations. In doing this, the MOE prediction should reflect how each catalyst-substrate complex is with some degree of confidence. Running these calculations could also provide an estimation for the preference of our S_NAr reaction to proceed via the (R_a)-atropisomer over the (S_a)-atropisomer. To see higher degrees of confidence in this

MOE approach, one would have to run multiple minimization experiments for all the compounds used in our three different substrate scopes. Due to limited resources and time, this would not be feasible. I then focused our efforts on prediction using starting material 72.

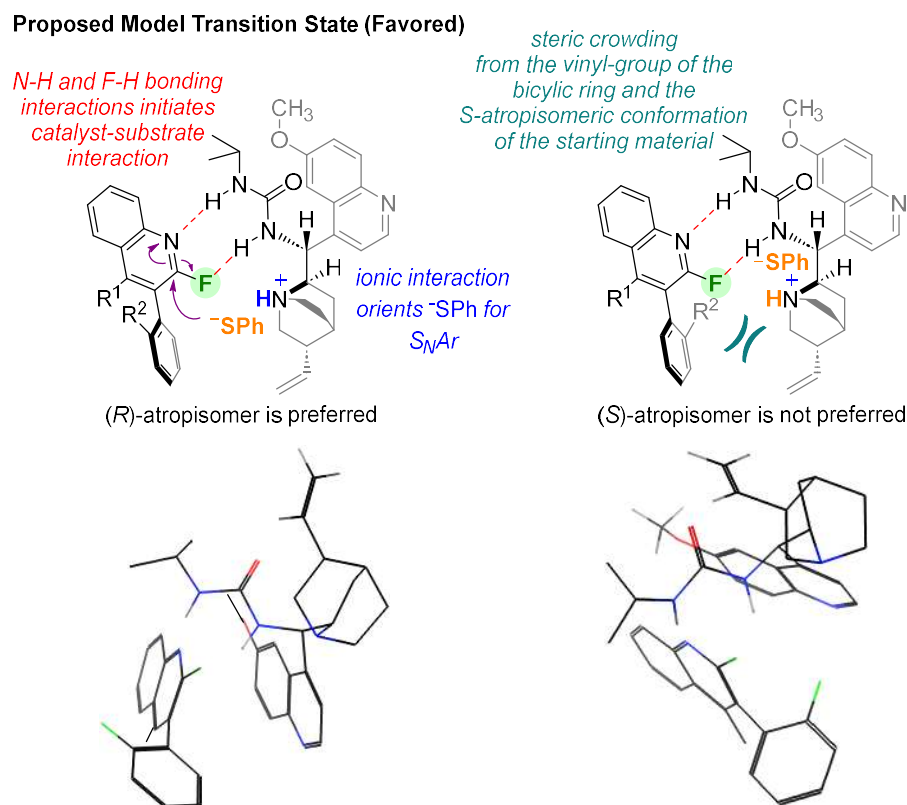


Figure 28. Favored interactions between starting material 3-arylquinoline 72 interaction with catalyst 77 obtained from minimization of MOE. The proposed model is represented in a 2-D and 3-D structure.

From the start of our project, we have always presumed that the catalyst-substrate interaction is where the -NHR group (e.g., isopropyl) of the *epi*-quinine urea catalyst is orientated to “push the C3-aryl out of plane” giving us the (R_a)-atropisomer due to steric-clashing (see Section 2.2.1, Figure 23). Several calculations supported two-working models where one is likely more viable. A more favored catalyst-substrate prediction was found to be the opposite orientation. In this model, MOE minimization found that the quinuclidine of the catalyst biases the (R_a)-atropisomer over the (S_a)-atropisomer due to steric crowding. This also better optimizes the H-

bonding network, and this MOE 3-D prediction finds that the catalytic-directed thiophenol is closer in this orientation to facilitate the atropisomeric S_NAr. I also think this can potentially explain our relatively flat enantioselectivity trends from our earliest catalyst screens. Especially when looking at other more branched R-groups, enantioselectivity was very conserved across different R-group changes (e.g., even for larger R-groups like isobutyl and adamantyl). Future experiments to test this hypothesis would be to explore catalysts that monitor that quinuclidine (e.g., changing the vinyl-substitution, changing the core quinuclidine into other groups, etc.).

2.15 Conclusion

Overall, this work provides access to enantioenriched 3-aryl quinolines in synthetically useful yields and enantiopurities, with the sulfide products transformable to pharmaceutically relevant pharmacophores with little racemization in most cases. As these and related heterocyclic motifs are ‘pharmaceutically privileged’, this work can have numerous applications towards biologically active atropisomeric heterocycles.

Acknowledgements

Chapter 2, Section 2 in full, is a reprint of the material as it appears in *Chemical Communications*, **2021**, 57, 10087–10090. Cardenas, Mariel M; Saputra, Mirza A.; Gordon, Deane A; Sanchez, Andreas N.; Yamamoto, Nobuyuki; Gustafson, Jeffrey L.¹⁰ The dissertation author was the primary investigator and author of this paper.

2.15 Experimental Section

This section is a reformatting of the Supporting Information from the original manuscript. Compound numbering is bolded to represent the preparation of that substrate. In other cases, the numbering format is not bolded.

^1H , ^{13}C , and ^{19}F NMR spectra are recorded from Varian VNMRS 400 MHz, Varian Inova 500 MHz and Bruker VNMRS 400 MHz at room temperature. All chemical shifts are reported in parts per million (δ) and were internally referenced to residual protio solvents (otherwise noted). All spectral data were reported as follows: chemical shift (multiplicity [singlet (s), doublet (d), triplet (t), quartet (q), quintet (p), and multiplet (m)], coupling constants [Hz], integration). ^{13}C NMR spectra were recorded with complete ^1H and ^{19}F decoupling. Some fluorine spectra are recorded with internal fluorine standards (i.e. trifluoroacetic acid, trifluorotoluene). Conventional mass spectra are obtained using Advion expressions CMS APCI/ASAP and HRMS were taken on Agilent 6530 Accurate Mass QTOF ESI. Enantiomeric ratios (*er* or e.r.) are determined from analytical HPLC on chiral stationary phase. Comparison with the appropriate racemic mixtures of each substrate allowed us to confirm the HPLC spectra. In some cases, we have trace amounts of solvents such as CH_2Cl_2 , CHCl_3 , and/or toluene.

All ‘Racemization Kinetics’ studies (also referred to as ‘Barrier to Rotation’) were conducted via a time-dependent study of e.r. degradation at an indicated temperature. All data is acquired from an HP Agilent 1100 HPLC using Chiral Technologies Inc. Daicel Group Chiralpak IA, IB, and IC Normal Phase chiral columns (otherwise noted).

For all cross-coupling reactions (i.e. Suzuki-Miyaura coupling, Buchwald coupling, etc.) to obtain 3-aryl quinoline intermediates: 1,4-dioxane and deionized, distilled H_2O are rigorously degassed under nitrogen flushing 30 minutes prior to use. See Section 2.15 for more details. For

Hartwig's fluorination to obtain the 2-fluorinated quinolines: all reactions are conducted under inert, anhydrous conditions using a nitrogen-filled glovebox. Anhydrous and degassed acetonitrile (MeCN) is stored over molecular sieves in the nitrogen-filled glovebox. All reactions were conducted in a 21 mL dram vial fitted with a Teflon-lined screw cap, along with parafilm coating of the reaction apparatus. After the addition of the reagents and solvent (the reaction was sealed appropriately), the reactions could be taken out of the glovebox to stir outside in ambient conditions (please refer to Section 2.2.12 for more details). For the S_NAr of 2-fluoro-3-aryl quinoline substrates **70**, our chiral Cinchona alkaloid catalysts were synthesized from readily purchased chemicals. See section "2.2.6. Synthesis of Catalysts" for more details. Solvents were dried over molecular sieves prior to addition into the reaction (please refer to Sections 2.15, 2.2.13 for more details on the syntheses of these compounds).

All other chemicals were purchased from Sigma Aldrich, TCI, Frontier Scientific, Acros Organics, Strem, Oakwood, Cambridge Isotope Laboratories, or Fisher Scientific and were used as received without further purification. All flash column chromatography (FCC) is performed using Grade 60 Silica gel (230-400 mesh) from Fisher Scientific. All preparatory plates are performed using Grade 60 Silica gel with fluorescent indicator F254 thin-layer chromatography (TLC) plates. In many cases, these materials were the source of grease seen in reported 1H -NMR spectra δ (ppm) = ~ 1.2 (s), ~ 0.5 (s).

2.2.5 Helpful Tips and Tricks

1. We found that K_2HPO_4 is universally the most effective base for the S_NAr of anionic HSPh based on highest determined product e.r. in DKR, or highest *s* in KR. However, Na_2CO_3 and $KHCO_3$ also provide comparable isolated yields and enantioselectivities.

2. We found that a 0.1 M solvent mixture of 70% *m*-xylene and 30% hexane is universally the most effective for the S_NAr of anionic HSPh by the determined product e.r. in DKR, or highest *s* in KR. Additionally this solvent also provided the most consistent yields. However, 70:30 CCl₄/hexanes or 70:30 PhMe/hexanes also provide comparable isolated yields and enantioselectivities.
3. Our developed reaction ratio is 1:2 HSPh to K₂HPO₄, as we found that significantly more non-nucleophilic base is necessary to acquire comparable yields. Our optimized reaction conditions are 10.0 equiv of thiophenol and 20.0 equiv of K₂HPO₄.

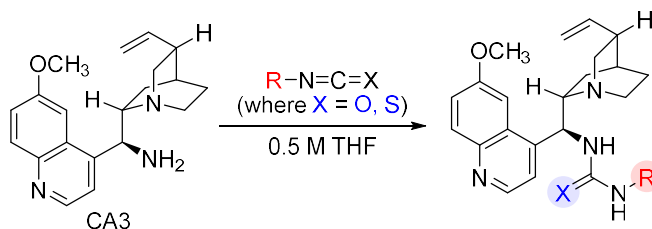
2.2.6 Synthesis of Catalysts

Quinine (CA1) is purchased from vendors supported by Fisher Scientific (i.e. Alfa Aesar, Acros Organics, 99%) and used as is. Catalyst 75 was synthesized from CA1 according to the general procedure outlined from Armstrong and coworkers.^[1] This catalyst was most optimal in our earlier report of an atroposelective S_NAr of thiophenol towards 3-aryl PPYs.^[2] Note that this catalyst is also purchasable and can be used as is (i.e. Sigma Aldrich).

epi-Aminoquinine (CA3) was synthesized from CA1 according to a general protocol reported by Cassani and coworkers.^[3] Catalysts 76 and 75 were synthesized and purified according to general protocols reported from Dinh and coworkers.^[4] Catalyst CA6 was synthesized and purified according to the general procedure reported from Bassas and coworkers.^[5] Catalyst CA25 was synthesized and purified according to the general procedure reported from Bella and coworkers.^[6] Catalyst CA26 was synthesized and purified according to the general procedure reported from Oh and coworkers.^[7]

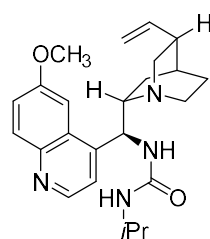
All spectral data of the described catalysts above agree with their reports. Please see ‘section 2.2.6. Reaction Development: Catalyst Index’ for the completed list as well as the optimization of these catalysts towards the atroposelective S_NAr of thiophenol towards sulfide product 74.

epi-Aminoquinine (CA3) was placed in a 21 mL dram vial equipped with a stir bar, and then dissolved into 0.5 to 0.8 M anhydrous THF. The isocyanate was then added, and the reaction is left to stir at r.t. overnight. The resulting reaction was then concentrated *in vacuo* and purified via FCC eluting with $CH_2Cl_2/MeOH$ (100:0 to 80:20). Catalysts were obtained in 60-80% average isolated yields. *Note*: We report catalysts that we included in the manuscript with corresponding characterization (along selected additional examples) that were synthesized using this described method. Other catalysts were obtained through other synthetic methods.



Equation 30. (Prep 1.) Synthesis of Cinchona Alkaloid-Based Quinine Catalysts via Isocyanates and Isothiocyanates

1-isopropyl-3-((S)-(6-methoxyquinolin-4-yl)((1S,2S,4S,5R)-5-vinylquinuclidin-2-



yl)methyl)urea, 77

To CA3 (1.40 g, 3.09 mmol, 1.0 equiv) was added 4.0 mL of anhydrous THF and isopropyl isocyanate (478 μ L, 4.87 mmol, 1.5 equiv). The reaction (with workup and purification) was followed according to the general procedure

described above to yield **77** as a light beige solid (1.5 g, 85%). This catalyst was the most optimal. See section “2.2.7. Reaction Development” for more details.

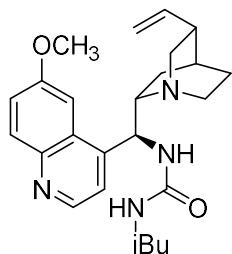
¹H NMR (400 MHz, CDCl₃) δ (ppm) = 8.72 (d, *J* = 4.6 Hz, 1H), 8.00 (d, *J* = 9.2 Hz, 1H), 7.72 (d, *J* = 2.7 Hz, 1H), 7.37 (dd, *J* = 9.3, 3.4 Hz, 2H), 5.97 (s, 1H), 5.68 (ddd, *J* = 17.4, 10.0, 7.3 Hz, 1H), 5.27 (s, 1H), 4.99 (d, *J* = 5.8 Hz, 1H), 4.96 (d, *J* = 1.1 Hz, 1H), 4.64 (d, *J* = 7.7 Hz, 1H), 3.97 (s, 3H), 3.75 (dq, *J* = 13.0, 6.5 Hz, 1H), 3.23 (dd, *J* = 13.8, 10.2 Hz, 3H), 2.79 – 2.69 (m, 2H), 2.36 – 2.28 (m, 1H), 1.73 – 1.58 (m, 3H), 1.50 – 1.40 (m, 1H), 1.03 (dd, *J* = 10.9, 6.5 Hz, 6H).

¹³C NMR (101 MHz, CDCl₃) δ (ppm) = 158.01, 157.49, 147.70, 144.91, 140.49, 131.83, 121.86, 115.27, 101.97, 55.86, 55.64, 42.35, 41.06, 39.09, 27.35, 25.90, 23.51, 23.41.

MS (APCI) = 409.5 calculated [M]⁺ for C₂₄H₃₂N₄O₂; experimental 409.0.

HRMS (ESI) = 409.2604 calculated [M]⁺ found 409.2616 for C₂₄H₃₂N₄O₂.

1-isobutyl-3-((S)-(6-methoxyquinolin-4-yl)((1S,2S,4S,5R)-5-vinylquinuclidin-2-yl)methyl)urea, CA10,

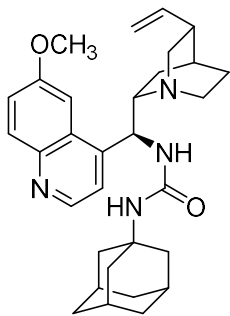


To CA3 (65 mg, 0.201 mmol, 1.0 equiv) was added 2.0 mL of anhydrous THF and *sec*-butyl isocyanate (35 μL, 0.301 mmol, 1.5 equiv). The reaction (with workup and purification) was followed according to the general procedure described above to yield CA10 as a yellow amorphous solid (69.5 mg, 82%).

¹H NMR (400 MHz, CDCl₃) δ (ppm) = 8.73 (d, *J* = 4.6 Hz, 1H), 8.02 (dd, *J* = 9.2, 0.8 Hz, 1H), 7.74 (d, *J* = 2.7 Hz, 1H), 7.42 – 7.35 (m, 2H), 6.22 (d, *J* = 16.0 Hz, 1H), 5.70 (ddd, *J* = 17.3, 10.1, 7.1 Hz, 1H), 5.36 (s, 1H), 5.06 (d, *J* = 5.7 Hz, 1H), 5.02 (d, *J* = 1.2 Hz, 1H), 4.67 (dd, *J* = 7.9, 3.9 Hz, 1H), 3.98 (d, *J* = 2.0 Hz, 3H), 3.63 – 3.55 (m, 1H), 3.35 (dd, *J* = 13.8, 10.2 Hz, 3H), 3.03 (s, 2H), 2.92 – 2.82 (m, 2H), 2.47 – 2.40 (m, 1H), 1.79 (s, 3H), 1.57 – 1.50 (m, 1H), 1.35 (dtd, *J* = 11.2, 6.8, 4.2 Hz, 2H), 1.02 (dd, *J* = 17.6, 6.6 Hz, 4H), 0.80 (dt, *J* = 12.4, 7.4 Hz, 3H).

MS (APCI) = 423.6 calculated [M]⁺ for C₂₅H₃₄N₄O₂; experimental 423.7.

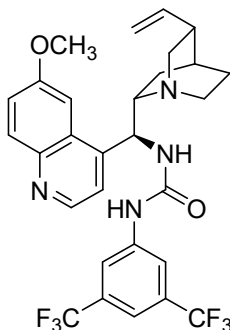
1-((3R,5R,7R)-adamantan-1-yl)-3-((S)-(6-methoxyquinolin-4-yl)((1S,2S,4S,5R)-5-vinylquinuclidin-2-yl)methyl)urea, CA11



To CA3 (50 mg, 0.155 mmol, 1.0 equiv) was added 1.6 mL of anhydrous THF and adamantyl isocyanate (33 mg, 0.186 mmol, 1.2 equiv). The reaction (with workup and purification) was followed according to the general procedure described above to yield CA11 as a yellow solid (66 mg, 85%).

The spectral data obtained for this catalyst are in agreement with Greenaway and coworkers' report.^[8]

1-(3,5-bis(trifluoromethyl)phenyl)-3-((S)-(6-methoxyquinolin-4-yl)((1S,2S,4S,5R)-5-vinylquinuclidin-2-yl)methyl)urea, CA13

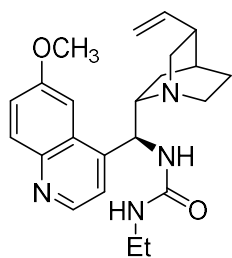


To CA3 (27 mg, 0.083 mmol, 1.0 equiv) was added 0.8 mL of anhydrous DCM and 1-isocyanato-3,5-bis(trifluoromethyl)benzene (21 mg, 0.083 mmol, 1.0 equiv). The reaction was then stirred at room temperature overnight. The reaction (with workup and purification) was followed according to the general procedure described above to yield CA13 as a light beige foam (18 mg, 37%).

The spectral data obtained for this catalyst agrees with Greenaway and coworkers' report.^[8]

1-ethyl-3-((S)-(6-methoxyquinolin-4-yl)((1S,2S,4S,5R)-5-vinylquinuclidin-2-yl)methyl)urea,

CA16



To CA3 (511 mg, 1.58 mmol, 1.0 equiv) was added 3.2 mL of anhydrous THF and ethyl isocyanate (188 μ L, 2.37 mmol, 1.5 equiv). The reaction (with workup and purification) was followed according to the general procedure to afford, CA16 as a light beige foam (367.7 mg, 59%).

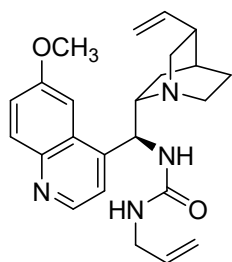
$^1\text{H NMR}$ (400 MHz, CDCl_3) δ (ppm) = 8.70 (d, J = 4.6 Hz, 1H), 7.99 (d, J = 9.2 Hz, 1H), 7.73 (d, J = 2.7 Hz, 1H), 7.37 – 7.34 (m, 2H), 5.95 (s, 1H), 5.73 – 5.65 (m, 1H), 5.27 (s, 1H), 4.98 – 4.96 (m, 1H), 4.93 (s, 1H), 4.78 (t, J = 5.4 Hz, 1H), 4.47 (s, 1H), 3.96 (s, 3H), 3.26 (s, 1H), 3.20 – 3.14 (m, 1H), 3.08 (dd, J = 7.2, 5.6 Hz, 2H), 2.73 – 2.62 (m, 2H), 2.56 (s, 2H), 2.31 – 2.25 (m, 1H), 1.65 (t, J = 3.1 Hz, 1H), 1.61 (dd, J = 6.3, 3.0 Hz, 1H), 1.44 – 1.37 (m, 1H), 0.99 (t, J = 7.2 Hz, 3H), 0.92 (dd, J = 13.9, 6.6 Hz, 1H).

$^{13}\text{C NMR}$ (101 MHz, CDCl_3) δ (ppm) = 158.22, 157.96, 147.62, 144.85, 140.94, 131.73, 128.50, 121.84, 114.95, 102.08, 55.82, 41.03, 39.31, 35.32, 27.66, 27.39, 26.14, 15.47.

MS (APCI) = 395.5 calculated $[\text{M}]^+$ for $\text{C}_{23}\text{H}_{30}\text{N}_4\text{O}_2$; experimental 394.1.

1-allyl-3-((S)-(6-methoxyquinolin-4-yl)((1S,2S,4S,5R)-5-vinylquinuclidin-2-yl)methyl)urea,

CA18



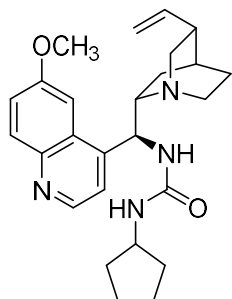
To CA3 (1.2 g, 3.726 mmol, 1.0 equiv) was added 5.0 mL of anhydrous THF and allyl isocyanate (0.5 mL, 5.59 mmol, 1.5 equiv). The reaction (with workup and purification) was followed according to the general procedure to afford CA18 as a light beige foam (554.2 mg, 37%).

¹H NMR (400 MHz, CDCl₃) δ (ppm) = 8.70 (d, *J* = 4.6 Hz, 1H), 7.99 (d, *J* = 9.2 Hz, 1H), 7.71 (d, *J* = 2.7 Hz, 1H), 7.37 – 7.34 (m, 2H), 6.16 (s, 1H), 5.77 – 5.63 (m, 2H), 5.28 (s, 1H), 5.12 (s, 1H), 5.07 – 4.93 (m, 4H), 3.95 (s, 3H), 3.66 (t, *J* = 5.6 Hz, 2H), 3.25 (s, 1H), 3.14 (dd, *J* = 13.7, 10.2 Hz, 2H), 2.95 (s, 1H), 2.71 – 2.61 (m, 2H), 2.28 (d, *J* = 4.0 Hz, 1H), 1.68 – 1.65 (m, 1H), 1.61 (dd, *J* = 6.2, 3.1 Hz, 1H), 1.47 – 1.39 (m, 1H), 0.93 (dd, *J* = 13.4, 6.6 Hz, 1H).

¹³C NMR (101 MHz, CDCl₃) δ (ppm) = 158.15, 157.97, 147.64, 144.87, 140.78, 135.37, 131.77, 128.44, 121.86, 115.55, 115.05, 102.02, 55.83, 55.70, 42.99, 41.03, 39.21, 27.54, 27.35, 26.09.

MS (APCI) = 407.5 calculated [M]⁺ for C₂₄H₃₀N₄O₂; experimental 407.1.

1-cyclopentyl-3-((S)-(6-methoxyquinolin-4-yl)((1S,2S,4S,5R)-5-vinylquinuclidin-2-yl)methyl)urea, 79



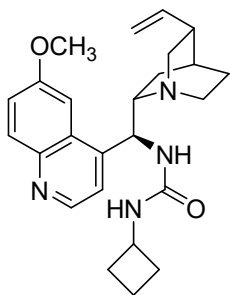
To CA3 (530 mg, 1.64 mmol, 1.0 equiv) was added 3.3 mL of anhydrous THF and cyclopentyl isocyanate (0.277 mL, 2.46 mmol, 1.5 equiv). The reaction (with workup and purification) was followed according to the general procedure to afford **77** as a light beige foam (306 mg, 43%).

¹H NMR (400 MHz, CDCl₃) δ (ppm) = 8.71 (d, *J* = 4.5 Hz, 1H), 8.00 (d, *J* = 9.2 Hz, 1H), 7.72 (d, *J* = 2.7 Hz, 1H), 7.44 – 7.31 (m, 2H), 5.91 (s, 1H), 5.72 – 5.63 (m, 1H), 5.22 (s, 1H), 4.96 (dd, *J* = 3.0, 1.1 Hz, 1H), 4.94 – 4.86 (m, 1H), 4.74 (d, *J* = 7.2 Hz, 1H), 3.96 (s, 3H), 3.88 (h, *J* = 6.5 Hz, 1H), 3.25 (dd, *J* = 13.7, 7.0 Hz, 1H), 3.17 (dd, *J* = 13.8, 10.2 Hz, 1H), 3.14 – 3.05 (m, 1H), 2.77 – 2.60 (m, 3H), 2.27 (q, *J* = 7.5, 6.7 Hz, 1H), 1.90 – 1.77 (m, 2H), 1.61 (dddd, *J* = 21.9, 12.5, 6.4, 3.4 Hz, 3H), 1.49 (dt, *J* = 8.6, 4.3 Hz, 3H), 1.40 (dd, *J* = 12.7, 11.0 Hz, 1H), 1.22 (dp, *J* = 12.0, 5.9 Hz, 2H), 0.92 (dd, *J* = 13.9, 6.5 Hz, 1H).

^{13}C NMR (101 MHz, CDCl_3) δ (ppm) = 157.97, 147.66, 144.89, 140.98, 131.79, 128.47, 121.81, 114.92, 102.02, 55.82, 52.19, 41.02, 39.36, 33.69, 33.53, 27.69, 27.41, 26.13, 23.67.

MS (APCI) = 435.6 calculated $[\text{M}]^+$ for $\text{C}_{26}\text{H}_{34}\text{N}_4\text{O}_2$; experimental 435.1.

1-cyclobutyl-3-((S)-(6-methoxyquinolin-4-yl)((1S,2S,4S,5R)-5-vinylquinuclidin-2-yl)methyl), CA21



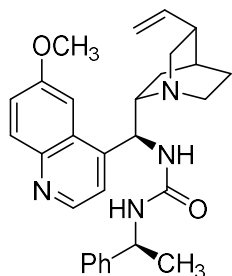
To CA3 (222 mg, 0.684 mmol, 1.0 equiv) was added 2.5 mL of anhydrous THF and cyclobutyl isocyanate (0.1 mL, 1.0 mmol, 1.5 equiv). The reaction (with workup and purification) was followed according to the general procedure to afford CA21 as a light beige foam (130 mg, 45%).

^1H NMR (400 MHz, CDCl_3) δ (ppm) = 8.71 (d, J = 4.6 Hz, 1H), 7.99 (d, J = 9.2 Hz, 1H), 7.70 (d, J = 2.7 Hz, 1H), 7.47 – 7.28 (m, 2H), 6.19 (d, J = 4.7 Hz, 1H), 5.68 (ddd, J = 17.4, 10.1, 7.2 Hz, 1H), 5.30 (s, 1H), 5.21 (d, J = 7.6 Hz, 1H), 5.01 (d, J = 5.4 Hz, 1H), 4.97 (d, J = 1.1 Hz, 1H), 4.07 (q, J = 7.9 Hz, 1H), 3.96 (s, 3H), 3.42 – 3.24 (m, 2H), 3.19 (dd, J = 13.7, 10.2 Hz, 2H), 2.84 – 2.64 (m, 2H), 2.38 – 2.29 (m, 1H), 2.28 – 2.09 (m, 2H), 1.81 – 1.53 (m, 6H), 1.52 – 1.43 (m, 1H), 1.01 – 0.88 (m, 1H).

^{13}C NMR (101 MHz, CDCl_3) δ (ppm) = 158.06, 157.14, 147.69, 144.89, 140.10, 131.81, 128.37, 121.91, 115.51, 102.00, 55.88, 55.45, 45.78, 41.10, 38.84, 31.68, 31.50, 27.28, 27.07, 25.78, 15.96.

MS (APCI) = 421.6 calculated $[\text{M}]^+$ for $\text{C}_{25}\text{H}_{32}\text{N}_4\text{O}_2$; experimental 420.9.

1-((S)-(6-methoxyquinolin-4-yl)((1S,2S,4S,5R)-5-vinylquinuclidin-2-yl)methyl)-3-((S)-1-phenylethyl)urea, CA24

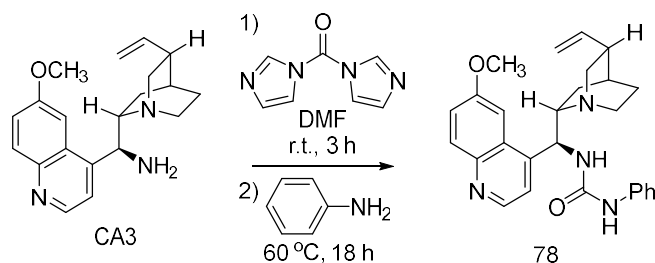


To CA3 (385 mg, 1.19 mmol, 1.0 equiv) was added 2.38 mL of anhydrous THF and (*R*)-(+)- α -methylbenzyl isocyanate (0.25 mL, 1.78 mmol, 1.5 equiv). The reaction (with workup and purification) was followed according to the general procedure to afford CA24 as a light beige solid (193 mg, 35%).

^1H NMR (400 MHz, CDCl_3) δ (ppm) = 8.67 (d, J = 4.4 Hz, 1H), 8.00 (d, J = 9.2 Hz, 1H), 7.69 (s, 1H), 7.37 (dd, J = 9.2, 2.6 Hz, 1H), 7.34 – 7.27 (m, 4H), 7.24 (s, 1H), 7.20 – 7.15 (m, 1H), 6.82 (s, 1H), 5.92 (s, 1H), 5.70 (dd, J = 19.6, 6.9 Hz, 1H), 5.54 (s, 1H), 5.12 (s, 1H), 5.08 (d, J = 4.9 Hz, 1H), 4.77 (p, J = 7.1 Hz, 1H), 4.29 (s, 2H), 3.96 (s, 3H), 3.84 (s, 1H), 3.56 – 3.48 (m, 1H), 3.40 – 3.31 (m, 1H), 3.13 (s, 1H), 2.82 – 2.72 (m, 1H), 2.51 – 2.45 (m, 1H), 1.82 (d, J = 11.1 Hz, 2H), 1.76 (d, J = 14.8 Hz, 1H), 1.64 (d, J = 15.4 Hz, 1H), 1.34 (d, J = 6.9 Hz, 3H), 1.06 (d, J = 13.9 Hz, 1H).

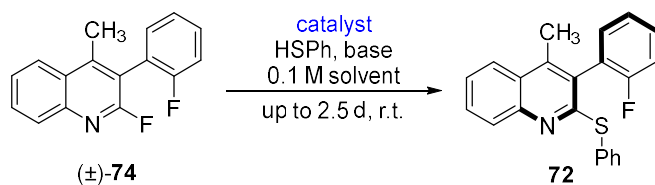
^{13}C NMR (101 MHz, CDCl_3) δ (ppm) = 158.45, 157.00, 147.73, 145.06, 144.89, 137.94, 131.88, 128.59, 126.95, 125.97, 122.24, 116.97, 101.79, 59.62, 56.11, 54.49, 50.60, 41.21, 37.52, 27.03, 25.45, 24.98, 23.53.

MS (APCI) = 471.6 calculated $[\text{M}]^+$ for $\text{C}_{29}\text{H}_{34}\text{N}_4\text{O}_2$; experimental 470.9.



Equation 31. (Prep 2.) Synthesis of Catalyst 78

To a solution of CA3 (170 mg, 0.527 mmol, 1.0 equiv) in 2.6 mL DMF was added carbonyldiimidazole (103 mg, 0.632 mmol, 1.2 equiv) at room temperature. The reaction was stirred for 3 hours, and then heated to 60 °C. To this reaction was added aniline (96 μ L, 1.05 mmol, 2.0 equiv), and the reaction was refluxed overnight. The resulting reaction was concentrated *in vacuo*, followed by purification via FCC eluting with CH₂Cl₂/MeOH (100:0 to 80:20) to afford *l*-((*S*)-(6-methoxyquinolin-4-yl)((1*S*,2*S*,4*S*,5*R*)-5-vinylquinuclidin-2-yl)methyl)-3-phenylurea, C12 (in manuscript, C5) as a yellow amorphous solid (168 mg, 72% yield). All spectral data of this catalyst is in agreeance with Jiang and coworkers' report.^[9]



Equation 32. General Reaction for Catalyst Evaluation

In each reaction, **74** (0.0979 mmol, 1.0 equiv) and catalyst (0.00979 mmol, 10 mol%) was used unless stated otherwise. Each reaction (after the addition of the reagents listed below) was left to stir at room temperature for up to 2.5 days. See “**Section 2.2.13**” for more details about the reaction, workup, and purification.

2.2.7 Reaction Development of Atroposelective S_NAr Towards 3-arylquinolines

In this section we report the full reaction optimization for the atroposelective S_NAr. The final transformation is detailed in Section 2.2.13.

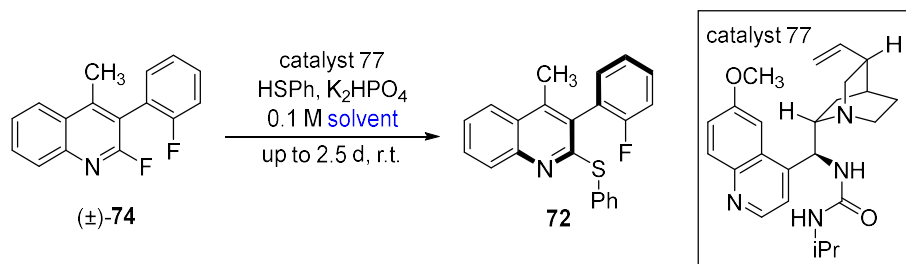
Table 17. Full Catalyst Evaluation towards Atroposelective S_NAr of 3-arylquinoline

CA1 ^[a] 64:36 e.r., 28 ee%, 20%	CA2 (15) ^[a] 55:45 e.r., 10 ee%, >5%	CA3 ^[a] 32:68 e.r., 36 ee%, 21%	CA4 (76) ^[a] 13:87 e.r., 74 ee%, 43%	CA5 (75) ^[a] 18:82 e.r., 64 ee%, 23% 39:61 e.r. ^[c] 22 ee%, <8.5% 36:64 e.r. ^[f] 28 ee%, <7.4%	CA6 ^[a] 51:49 e.r., 1 ee%, 21%
CA7 ^[a] 50:50 e.r., 0 ee%, <5%	CA8 ^[a] 37:63 e.r., 26 ee%, 30%	CA9 (77) ^[a] 9:91 e.r., 82 ee%, 67% 10:90 e.r. ^[c] 80 ee%, 91%	CA10 ^[a] 12:88 e.r., 76 ee%, 51%	CA11 ^[a] 13:87 e.r., 76 ee%, 54%	CA12 (78) ^[a] 23:77 e.r., 54 ee%, 31%
CA13 ^[a] 20:80 e.r., 60 ee%, 24%	CA14 ^[a] 44:56 e.r., 12 ee%, 20%	CA15 ^[a] 47:53 e.r., 6 ee%, <5%	CA16 ^[a] 11:89 e.r., 78 ee%, 69%	CA17 ^[a] 17:83 e.r., 65 ee%, 72%	CA18 ^[a] 12:88 e.r., 76 ee%, 58%
CA19 ^[a] (79) 11:89 e.r., 78 ee%, 77%	CA20 ^[a] 19:81 e.r., 62 ee%, 65%	CA21 ^[a] 17:83 e.r., 66 ee%, 74%	CA22 ^[a] 49:51 e.r., 2 ee%, 23%	CA23 ^[a] 16:84 e.r., 68 ee%, 80%	CA24 ^[a] 14:86 e.r., 68 ee%, 64%
CA25 ^[a] 17:83 e.r., 66 ee%, <20%	CA26 ^[a] 83:17 e.r., 66 ee%, 19.7%	CA27 ^[a] 43:57 e.r., 14% ee%, 43%	(R)-CA28 ^[a] 25:75 e.r., 50 ee%, 43% (S)-CA28 ^[a] 40:60 e.r., 20 ee%, 24%		

[a] K₂HPO₄ (1.4 mmol, 14.5 equiv), 979 μL PhMe, and HSPh (0.979 mmol, 10.0 equiv) used. [b] K₂HPO₄ (1.97 mmol, 8.0 equiv), 489.5 μL *n*-hexane, 489.5 μL PhMe, and HSPh (0.196 mmol, 5.0 equiv) used. [c] Catalyst (0.0197 mmol, 20 mol%) was used for this reaction. K₂HPO₄ (0.3136 mmol, 8.0 equiv), 489.5 μL *n*-hexane, 489.5 μL PhMe, and HSPh (0.196 mmol, 5.0 equiv) used. [d] Catalyst (0.0197 mmol, 20 mol%) was used for this reaction. K₂HPO₄ (0.3136 mmol, 8.0 equiv), 294 μL *n*-hexane, 685 μL *m*-Xylene, and HSPh (0.196 mmol, 5.0 equiv) used. [e] K₂HPO₄ (1.4 mmol, 14.5 equiv), 979 μL MTBE, and HSPh (0.979 mmol, 10.0 equiv) used. [f] K₂HPO₄ (1.4 mmol, 14.5 equiv), 979 μL *i*Pr₂O, and HSPh (0.392 mmol, 10.0 equiv) used.

For determination of the optimal reaction catalyst, entries CA1-CA28 (in Table 17) were evaluated and compared for highest enantiomeric ratio (e.r.) and highest determined enantioenriched percentage (ee%). Reported ee% and e.r. are determined using HPLC analysis. Reported yields are represented as an average of at least $n = 2$ trials (optimally, ~70%). For catalyst 77, yields are reported for comparison of two conditions.

From this catalyst evaluation, we found that catalyst 77 was the most optimal and thus was used for further reaction development.



Equation 33. General Reaction for the Solvent Evaluation

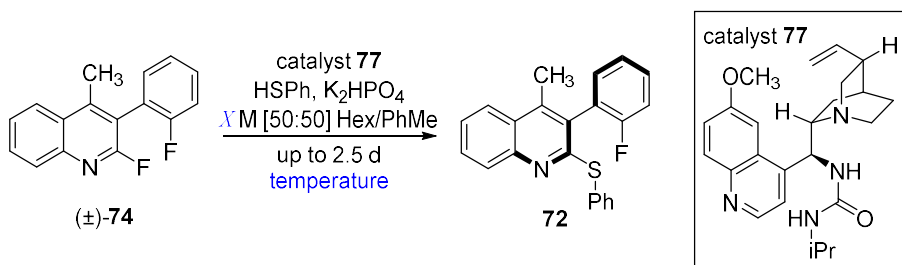
From selecting optimal catalyst, we next screened several different solvents and co-solvent mixtures (Equation 33). In each reaction (Table 18), substrate 74 (0.0392 mmol, 1.0 equiv) and catalyst 77 (0.00392 mmol, 10 mol%) is used. K₂HPO₄ (0.588 mmol, 14.5 equiv), 392 μ L solvent, HSPh (0.392 mmol, 10 equiv) is added to each reaction. The resulting reaction was left to stir at the ambient temperature for each trial of each entry up to 2.5 days. See “Section 2.2.13. General S_NAr Strategy to yield enantioenriched 3-aryl-2-thioquinolines (2)” for more details about the reaction, workup, and purification.

Based on our results, we concluded that entry 31 is found to be the most optimal and was thus used for this reaction development.

Table 18. Solvent Evaluation

Entry	Solvent	72 e.r. ^[h]	72 ee (%) ^[h]	72 Yield (%) ^[h]
1	PhMe	14:86	72	43
2		13:87	74	37
3	CH ₂ Cl ₂	23:77	54	24
4	MTBE	21:79	58	22
5	CCl ₄	49:51	2	73
6	THF	26:74	48	36
7	EtOAc	43:57	14	15
8	<i>i</i> Pr ₂ O	16:84	68	41
9 ^[b]	<i>n</i>-Hexanes in PhMe	12:88	76	54
10 ^[d]		10:90	80	61
11 ^[c]		10:90	80	78
12^[f]		10:90	80	74
13 ^[a,g]		10:90	80	40
14 ^[d]	<i>n</i> -Hexanes in CCl ₄	11:89	78	67
15 ^[c]		12:88	76	76
16 ^[f]		13:87	74	77
17	PhCF ₃	26:74	48	36
18 ^[a]	<i>n</i> -Hexanes in PhCF ₃	16:84	68	57
19 ^[c]		14:86	72	58
20 ^[a]	Pentane in PhMe	11:89	78	26
21 ^[d]		12:88	76	22
22 ^[c]		10:90	80	28
23 ^[f]		8:92	84	20
24 ^[d]		11:89	78	66
25 ^[c]	Pentane in CCl ₄	11:89	78	42
26 ^[f]		11:89	78	89
27 ^[d]		10:90	80	41
28 ^[c]	<i>m</i> -Xylenes in PhMe	10:90	80	37
29 ^[f]		10:90	80	67
30	<i>m</i> -Xylenes	9.5:90.5	80	79
31 ^[d]	<i>n</i>-Hexanes in <i>m</i>-Xylenes	9.5/90.5	80	41
32 ^[c]		10:90	80	37
33^[f]		9:91	82	82

^[a] 392 μ L of a 50:50 ratio of 2 solvents is used; 196 μ L solvent A and 196 μ L solvent B. ^[b] 392 μ L of a 25:75 ratio of 2 solvents is used; 98 μ L solvent A and 294 μ L solvent B is used. ^[c] 392 μ L of a 75:25 ratio of 2 solvents is used; 294 μ L solvent A and 98 μ L solvent B is used. ^[d] 392 μ L of a 10:90 ratio of 2 solvents is used; 39 μ L solvent A and 353 μ L solvent B is used. ^[e] 392 μ L of a 20:80 ratio of 2 solvents is used; 78 μ L solvent A and 314 μ L solvent B is used. ^[f] 392 μ L of a 30:70 ratio of 2 solvents is used; 118 μ L solvent A and 274 μ L solvent B is used. ^[g] Molecular sieves were included in the reaction, anhydrous solvent was used. ^[h] For determination of the optimal solvent (or bisolvent ratio), entries 1-31 were evaluated and compared for highest enantiomeric ratio (e.r.) and highest determined enantioenriched percentage (ee%). Reported ee% and e.r. are determined using HPLC analysis and reported as an average of at least $n = 3$ trials. Reported yields are represented as an average of at least $n = 3$ trials (optimally, ~70%). Please refer to below general procedure.



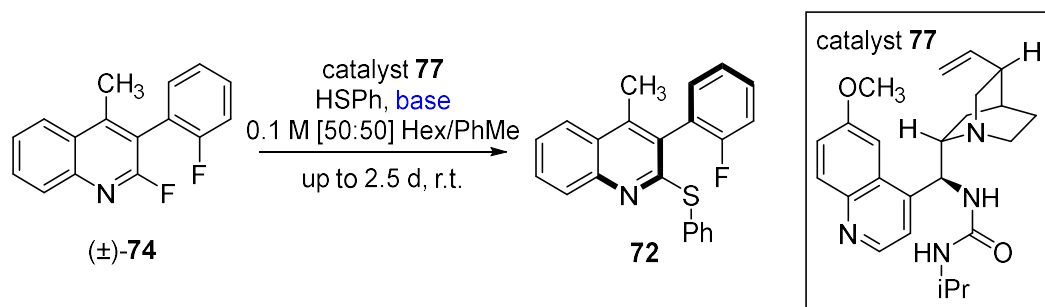
Equation 34. General Reaction for the Concentration and Temperature Evaluation

We examined the effects of concentration and temperature on the S_NAr , using substrate **74** and catalyst **77**. The reaction was performed in a 50:50 ratio of *n*-hexanes and PhMe (i.e. Hex/PhMe), unless stated otherwise (Table 19). The resulting reaction was left to stir at the indicated temperature for each entry up to 2.5 days. From this evaluation, Entry 1 is selected as the most optimal and was thus used for further reaction development.

Table 19. Concentration and Temperature Evaluation

Entry	Temp. (°C)	Conc. (M)	72 e.r. ^[f]	72 ee (%) ^[f]	72 Yield (%) ^[f]
1 ^[a]	r.t.	0.10	10:90	80	65
2 ^[b]	r.t.	0.10	10:90	80	30
3 ^[c]	r.t.	0.05	8:92	84	17
4 ^[d]	r.t.	0.20	12:88	76	82
5 ^[d]	r.t.	0.15	11:89	78	75
6 ^[a]	30	0.10	10:90	80	67
7 ^[a]	35	0.10	11:89	78	71
8 ^[a]	40	0.10	13:87	74	82
9 ^[a]	4	0.10	10:90	80	33

^[a] K_2HPO_4 (0.31 mmol, 8.0 equiv), 392 μ L Hex/PhMe, and HSPH (0.20 mmol, 5.0 equiv) used. ^[b] K_2HPO_4 (0.16 mmol, 4.0 equiv), 392 μ L Hex/PhMe, HSPH (0.10 mmol, 2.5 equiv) used. ^[c] K_2HPO_4 (0.31 mmol, 8.0 equiv), 784 μ L Hex/PhMe, and HSPH (0.10 mmol, 5.0 equiv) used. ^[d] K_2HPO_4 (0.31 mmol, 8.0 equiv), 196 μ L Hex/PhMe, and HSPH (0.2 mmol, 5.0 equiv) used. ^[e] K_2HPO_4 (0.31 mmol, 8.0 equiv), 261 μ L Hex/PhMe, and HSPH (0.2 mmol, 5.0 equiv) used. ^[f] For determination of the optimized reaction temperature and reaction concentration, entries 1-9 were evaluated and compared for highest enantiomeric ratio (e.r.) and highest determined enantioenriched percentage (ee%). Reported ee% and e.r. are determined using HPLC analysis and reported as an average of at least $n = 2$ trials. Reported yields are represented as an average of at least $n = 2$ trials (optimally, ~70%).



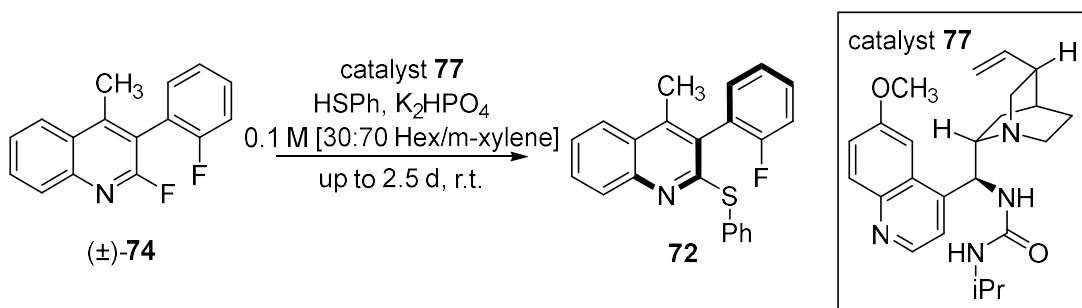
Equation 35. General Reaction for the Base Evaluation

Table 20. Base Evaluation

Entry	Base	72 e.r. ^[d]	72 ee% ^[d]	72 Yield (%) ^[d]
1 ^[a]	K ₂ HPO ₄	10:90	80	65
2 ^[b]	K ₂ HPO ₄	25:75	50	76
3 ^[a]	K ₃ PO ₄	44:56	12	<1.0
4 ^[a]	K ₂ CO ₃	11:89	78	9.7
5 ^[a]	Cs ₂ CO ₃	11:89	78	13
6 ^[a]	Na ₂ CO ₃	11:89	78	44
7 ^[a]	KHCO ₃	12:88	76	40
8 ^[a]	NaHCO ₃	14:86	72	37
9 ^[a]	NaOH	9:91	82	2.6
10 ^[b]	NaOH	24:77	53	47
11 ^[b]	KOH	26:74	58	49
12 ^[b]	LiOH	26:74	48	29
13 ^[b]	CsOH	<i>n.d.</i> ^[c]	<i>n.d.</i> ^[c]	<i>n.d.</i> ^[c]
14 ^[a]	NEt ₃	28:72	44	39
15 ^[a]	“No base”	15:85	70	29

^[a]72 (0.0392 mmol, 1.0 equiv) and catalyst 77 (0.00392 mmol, 10 mol%) was used. Base (0.3136 mmol, 8.0 equiv) was then added to the reaction. 194 μ L *n*-hexane and 194 μ L PhMe were used as the reaction solvent. HSPh (0.196 mmol, 5.0 equiv) was then added. ^[b]72 (0.09765 mmol, 1.0 equiv) and catalyst 77 (0.01953 mmol, 20 mol%) was used. Base (1.953 mmol, 20.0 equiv) was then added to the reaction. 488.5 μ L *n*-hexane and 488.5 μ L PhMe were used as the reaction solvent. HSPh (0.9765 mmol, 10.0 equiv) was then added. ^[c]There was no observed reaction (i.e., recovered starting material). ^[d] For determination of the optimized reaction temperature and reaction concentration, entries 1-15 were evaluated and compared for highest enantiomeric ratio (e.r.) and highest determined enantioenriched percentage (ee%). Reported ee% and e.r. are determined using HPLC analysis and reported as an average of at least *n* = 2 trials. Reported yields are represented as an average of at least *n* = 2 trials (optimally, ~70%).

The resulting reaction was left to stir at room temperature for each entry up to 2.5 days. See “Section 2.2.12. General S_NAr Strategy to yield enantioenriched 3-aryl-2-thioquinolines (2)” for more details about the reaction, workup, and purification. From this base evaluation, Entry 1 is selected most optimal.^[10,11]



Equation 36. General Reaction for the Catalyst Load Evaluation

Table 21. Catalyst Load Evaluation

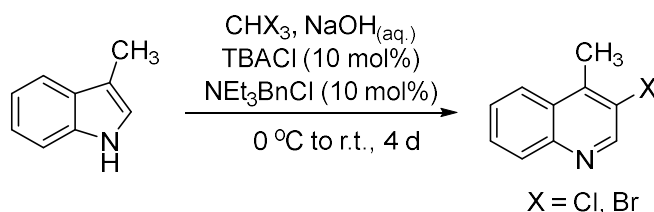
Entry	Catalyst Load (mol %)	72 e.r. ^[f]	72 ee% ^[f]	72 Yield (%) ^[f]
1 ^[a]	1	9:91	82	15
2 ^[b]	2	9:91	82	33
3 ^[c]	5	9:91	82	49
4 ^[d]	10	10:90	80	82
5 ^[e]	20	10:90	80	91

^[a]Catalyst 77 (0.000979 mmol, 0.01 equiv) was used. ^[b]Catalyst 77 (0.00196 mmol, 0.02 equiv) was used. ^[c]Catalyst 77 (0.0045 mmol, 0.05 equiv) was used. ^[d]Catalyst 77 (0.00979 mmol, 0.1 equiv) was used. ^[e]Catalyst 77 (0.0196 mmol, 0.2 equiv) was used. ^[f]For determination of the optimized reaction temperature and reaction concentration, entries 1-15 were evaluated and compared for highest enantiomeric ratio (e.r.) and highest determined enantioenriched percentage (ee%). Reported ee% and e.r. are determined using HPLC analysis and reported as an average of at least $n = 2$ trials. Reported yields are represented as an average of at least $n = 2$ trials (optimally, ~70%).

Results are reported as one of 2-3 trials for each entry. In each reaction, substrate **72** (0.0979 mmol, 1.0 equiv) and catalyst **77** was used (see below for each amount). K₂HPO₄ (1.4 mmol, 20.0 equiv) was then added to the reaction. 294 μ L *n*-hexane and 685 μ L *m*-xylene was

used as the reaction solvent. HSPh (0.979 mmol, 10.0 equiv) was then added. The resulting reaction was left to stir at room temperature for each entry up to 2.5 days. From this catalyst loading evaluation, Entry 5 is found to be the most optimal. With these conditions at hand, we pursued S_NAr on 3-arylquinoline **70**.

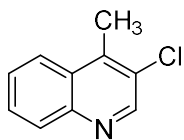
2.2.8 Synthesis of 3-halogenated quinoline intermediates



Equation 37. General Reaction for the Catalyst Load Evaluation

General Procedure: A 100-mL round bottom flask was equipped with a magnetic stir bar and charged with 3-methylindole (1.0 equiv), tetrabutylammonium chloride (0.1 equiv), benzyltriethylammonium chloride (0.1 equiv), and chloroform or bromoform (0.76 M). The mixture was cooled to $0\text{ }^\circ\text{C}$, and chilled solution of $NaOH$ (5.5 equiv) in H_2O (1.67 M) was then added in one portion. The reaction was let to stir vigorously at room temperature for four days and quenched with saturated citric acid. The aqueous layer was extracted with dichloromethane and the combined organic layers were washed with brine and dried over $NaSO_4$. After filtration and solvent evaporation, the crude was purified by flash column chromatography using *n*-hexanes:EtOAc = 0 \rightarrow 5% to afford the title compound.

3-chloro-4-methylquinoline



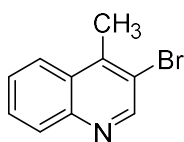
The reaction, workup and purification were followed according to the general procedure. The reaction of 3-methylindole (5.0 g, 38.12 mmol), TBACl (1.04 g, 3.812 mmol) and NEt_3BnCl (868.3 mg, 3.812 mmol) dissolved into 50.16 mL CHCl_3 , and 22.83 mL of 9 M NaOH afforded *3-chloro-4-methylquinoline*^[12] as a yellowish solid (4.37 g, 65%).

$^1\text{H NMR}$ (400 MHz, CDCl_3) δ (ppm) = 8.80 (s, 1H), 8.11 (dd, $J = 8.4, 1.6$ Hz, 1H), 8.01 (dt, $J = 8.5, 0.7$ Hz, 1H), 7.71 (ddd, $J = 8.3, 6.9, 1.4$ Hz, 1H), 7.62 (ddd, $J = 8.3, 6.9, 1.4$ Hz, 1H), 2.77 (s, 3H).

$^{13}\text{C NMR}$ (101 MHz, CDCl_3) δ (ppm) = 149.09, 145.36, 141.71, 129.53, 129.40, 128.50, 128.48, 127.62, 123.82, 15.14.

MS (APCI) = 178.0 calculated $[\text{M}+\text{H}]^+$ for $\text{C}_{10}\text{H}_9\text{ClN}$; experimental 177.5.

3-bromo-4-methylquinoline



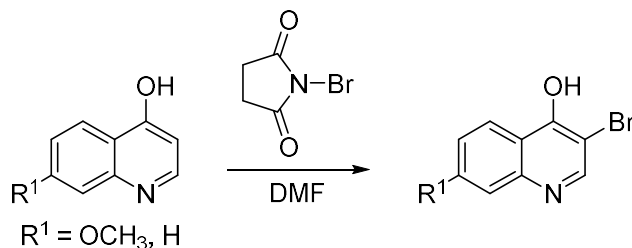
The reaction, workup and purification were followed according to the general procedure. The reaction of 3-methylindole (2.0 g, 15.25 mmol), TBACl (424 mg, 1.525 mmol) and NEt_3BnCl (347 mg, 1.525 mmol) dissolved into 20 mL CHBr_3 , and 9.1 mL of 9 M NaOH afforded *3-bromo-4-methylquinoline* as a yellowish solid (1.48 g, 44%).

$^1\text{H NMR}$ (400 MHz, CDCl_3) δ (ppm) = 8.90 (s, 1H), 8.09 (dt, $J = 8.4, 0.9$ Hz, 1H), 8.05 – 8.03 (dt, $J = 8.5, 0.8$ Hz, 1H), 7.72 (ddd, $J = 8.3, 6.9, 1.3$ Hz, 1H), 7.60 (ddd, $J = 8.3, 6.9, 1.2$ Hz, 1H), 2.80 (s, 3H).

$^{13}\text{C NMR}$ (101 MHz, CDCl_3) δ (ppm) = 151.71, 146.31, 143.13, 130.01, 129.27, 128.94, 127.40, 123.93, 119.99, 18.20.

MS (APCI) = 222.0 calculated $[\text{M}+\text{H}]^+$ for $\text{C}_{10}\text{H}_9\text{BrN}$; experimental 221.6.

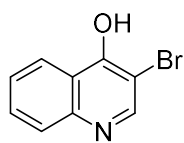
2.2.9 Bromination to yield 3-bromo-4-quinolol



Equation 38. General Reaction for the Catalyst Load Evaluation

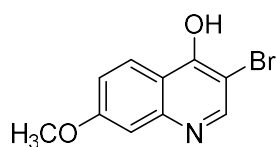
General Procedure: To 4-quinolol starting materials (1.0 equiv) was added *N*-bromosuccinimide (NBS, 1.0 equiv) in 0.7 to 1 M DMF. The reaction was then stirred at room temperature (unless otherwise stated) for up to 18 h. To this reaction was added ice water, and the product was recrystallized. Vacuum filtration afforded products in quantitative yields (>90%).

3-bromoquinolin-4-ol



The reaction, workup and purification were followed according to the general procedure. The reaction of 4-hydroxyquinoline (10.0 g, 70.0 mmol, 1.0 equiv), NBS (11.41 g, 70.0 mmol, 1.0 equiv) and 100 mL DMF afforded 3-bromoquinolin-4-ol as yellowish solid (quantitative). The spectral data for this compound were in agreement with Boudet and coworkers.^[13]

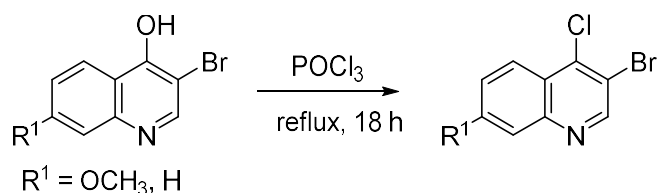
3-bromo-7-methoxyquinolin-4-ol



The reaction (at 55 °C), workup and purification were followed according to the general procedure. The reaction of 4-hydroxy-7-methoxyquinoline (1.00 g, 5.71 mmol), NBS (1.22 g, 6.85 mmol, 1.2 equiv) and 5.7 mL DMF

afforded *3-bromo-7-methoxyquinolin-4-ol* as a pale white solid (quantitative). The product was then taken to the next step (i.e., chlorination with POCl₃) without any characterization.

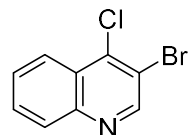
2.2.10 Chlorination to yield 3-bromo-4-chloroquinoline



Equation 39. General Reaction for the Catalyst Load Evaluation

General Procedure: To 3-bromoquinolin-4-ol (1.0 equiv) was added 0.7 to 1 M POCl₃, and then subjected to reflux from 2 to 18 h. The resulting reaction mixture was quenched very slowly with ice water, and then partitioned with CH₂Cl₂. The organic layer was extracted out and then subsequently rinsed with saturated aqueous NaCl. The organic layer was dried over anhydrous Na₂SO₄ and then concentrated *in vacuo* to afford the final 4-chloroquinoline intermediates for cross couplings.

3-bromo-4-chloroquinoline



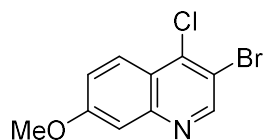
The reaction, workup and purification were followed according to the general procedure. The reaction of 3-bromoquinolin-4-ol (5.0 g, 22.3 mmol, 1.0 equiv) and 30 mL POCl₃ at room temperature afforded *3-bromo-4-chloroquinoline* as a sienna-colored solid (4.25 g, 79%).

¹H NMR (400 MHz, CDCl₃) δ (ppm) = 8.94 (s, 1H), 8.24 (ddd, $J = 8.5, 1.4, 0.7$ Hz, 1H), 8.11 (ddd, $J = 8.5, 1.3, 0.6$ Hz, 1H), 7.78 (ddd, $J = 8.4, 6.9, 1.4$ Hz, 1H), 7.67 (ddd, $J = 8.3, 6.9, 1.2$ Hz, 1H).

^{13}C NMR (101 MHz, CDCl_3) δ (ppm) = 151.56, 146.97, 141.64, 130.38, 129.78, 128.60, 127.38, 124.41, 117.97.

MS (APCI) = 243.9 calculated $[\text{M}+\text{H}]^+$ for $\text{C}_9\text{H}_6\text{BrClN}$; experimental 244.1.

3-bromo-4-chloro-7-methoxyquinoline



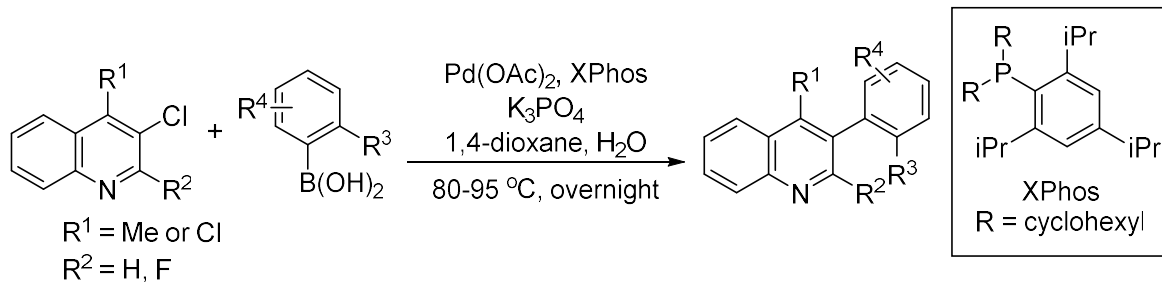
The reaction, workup and purification were followed according to the general procedure. The reaction of (1.14 g, 4.49 mmol) was dissolved in 9.0 mL of 1,4-dioxane, and POCl_3 (4.2 mL, 44.87 mmol) was then added in one portion. The reaction was stirred at 90 °C for 3 hours. The workup and purification were followed according to the general procedure. *3-bromo-4-chloro-7-methoxyquinoline* was obtained as a dark red solid product (1.12 g, 92%).

^1H -NMR (400 MHz, CD_3OD) δ (ppm) = 8.82 (s, 1H), 8.12 (d, $J = 9.0$ Hz, 1H), 7.38 – 7.31 (m, 2H), 3.97 (s, 3H).

^{13}C NMR (101 MHz, CD_3OD) δ (ppm) = 163.22, 152.94, 149.98, 142.75, 126.68, 123.52, 122.93, 116.13, 108.19, 56.37.

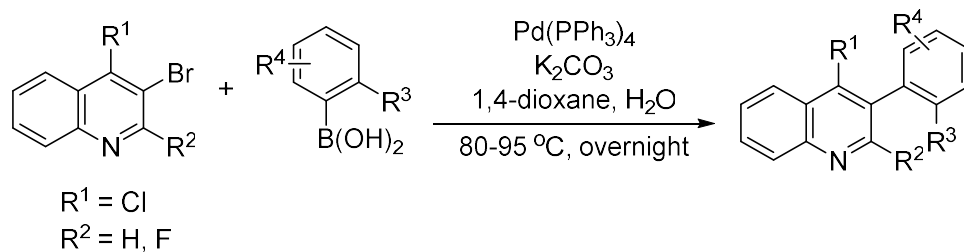
MS (APCI) = 272.5 calculated $[\text{M}]^+$ for $\text{C}_{10}\text{H}_7\text{BrClNO}$; experimental 272.4

2.2.11 Synthesis of 3-aryl quinoline intermediates



Equation 40. Buchwald Coupling to yield 3-aryl quinoline intermediates

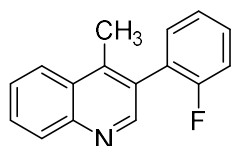
General Procedure – Buchwald Coupling: To 3-chloro-4-R¹-2-R²-quinoline (1.0 equiv) in a 100-mL round bottom flask equipped with magnetic stir bar, 2-R¹-(3, 4 or 5)-R²-phenylboronic acid (1.1 equiv), Pd(OAc)₂ (0.1 equiv), XPhos (0.2 equiv), and K₃PO₄ (2.0 equiv) were added. The mixture was thoroughly purged and refilled with argon. This mixture was then dissolved in degassed (bubbled with argon for 20 minutes) 1,4-dioxanes (0.25 M) and degassed H₂O (3:1 ratio of 1,4-dioxane/H₂O), and the reaction was let to stir under reflux at 90 °C for 12-24 hours. The reaction was quenched with deionized H₂O and partitioned with EtOAc. The aqueous layer was further extracted with EtOAc, and the combined organic layers were washed with brine and dried over NaSO₄. After filtration and solvent evaporation, the crude was purified by flash column chromatography using *n*-Hexanes:EtOAc = 0 → 5% or 10% to afford the desired coupling products in 33-97% yields. *Note: some of the reactions were performed in a 20-mL scintillation vial, which was quickly purged with argon after adding all reagents and solvent. The vial was then capped tightly and placed on a reaction block instead of an oil bath.*



Equation 41. Suzuki Coupling to yield 3-aryl quinoline intermediates

General Procedure 2 – Buchwald Coupling: To 3-bromo-4- R^1 -2- R^2 -quinoline (1.0 equiv) in a 100-mL round bottom flask equipped with magnetic stir bar, 2- R^1 -(3, 4 or 5)- R^2 -phenylboronic acid (1.1 equiv), $\text{Pd}(\text{PPh}_3)_4$ (0.05 equiv), and K_2CO_3 (2.5 equiv) were added. The mixture was thoroughly purged and refilled with argon. This mixture was then dissolved in degassed (bubbled with argon for 20 minutes) 1,4-dioxanes (0.3 M) and degassed H_2O (3:1 ratio of 1,4-dioxane/ H_2O), and the reaction was let to stir under reflux at 90 °C for 12-24 hours. The reaction was quenched with deionized H_2O and partitioned with EtOAc. The aqueous layer was further extracted with EtOAc, and the combined organic layers were washed with brine and dried over NaSO_4 . After filtration and solvent evaporation, the crude was purified by flash column chromatography using n -Hexanes:EtOAc = 0 \rightarrow 5% or 10% to afford the desired coupling products in 42-63% yields. *Note: some of the reactions were performed in a 20-mL scintillation vial, which was quickly purged with argon after adding all reagents and solvent. The vial was then capped tightly and placed on a reaction block instead of an oil bath.*

3-(2-fluorophenyl)-4-methylquinoline



The reaction, workup and purification were followed according to the General Procedure 1. The reaction with 3-chloro-4-methylquinoline (777 mg, 4.37

mmol), 2-fluorophenylboronic acid (796 mg, 5.69 mmol), Pd(OAc)₂ (98 mg, 0.44 mmol), XPhos (417 mg, 0.89 mmol), K₃PO₄ (1.86 g, 8.75 mmol) in 17.5 mL of degassed 1,4-dioxane and 5.8 mL of degassed deionized H₂O afforded the product as an orange oil (825 mg, 3.48 mmol, 80%).

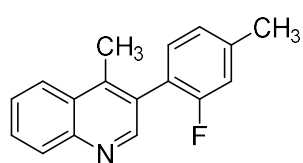
¹H NMR (400 MHz, CDCl₃) δ (ppm) = 8.77 (s, 1H), 8.17 (d, *J* = 8.4 Hz, 1H), 8.13 – 8.09 (m, 1H), 7.75 (ddd, *J* = 8.3, 6.8, 1.3 Hz, 1H), 7.63 (ddd, *J* = 8.3, 6.9, 1.2 Hz, 1H), 7.48 -7.42 (m, 1H), 7.35 (td, *J* = 7.4, 2.0 Hz, 1H), 7.29 (td, *J* = 7.4, 1.1 Hz, 1H), 7.22 (ddd, *J* = 9.5, 8.2, 1.1 Hz, 1H), 2.60 (d, *J* = 1.7 Hz, 3H).

¹³C NMR (101 MHz, CDCl₃) δ (ppm) = 160.01 (d, *J* = 247.0 Hz), 151.06, 146.97, 142.76, 131.88 (d, *J* = 3.2 Hz), 130.05 (d, *J* = 8.0 Hz), 129.78, 129.33, 128.41, 127.75, 126.87, 125.91 (d, *J* = 16.3 Hz), 124.34 (d, *J* = 3.8 Hz), 124.23, 115.85 (d, *J* = 22.2 Hz), 15.77 (d, *J* = 2.5 Hz).

¹⁹F NMR (376 MHz, CDCl₃) δ (ppm) = -40.16.

MS (APCI) = 238.1 calculated [M+H]⁺ for C₁₆H₁₃FN; experimental 237.5.

3-(2-fluoro-4-methylphenyl)-4-methylquinoline



The reaction, workup and purification were followed according to the General Procedure 1. The reaction with 3-chloro-4-methylquinoline (495 mg, 2.79 mmol), 2-fluoro-4-methoxyphenyl boronic acid (558 mg, 3.62 mmol), Pd(OAc)₂ (62 mg, 0.28 mmol), XPhos (266 mg, 0.56 mmol), K₃PO₄ (1.20 g, 5.57 mmol) in 11.1 mL of degassed 1,4-dioxane and 3.7 mL of degassed deionized H₂O afforded the product as a yellow solid (540 mg, 2.15 mmol, 77%).

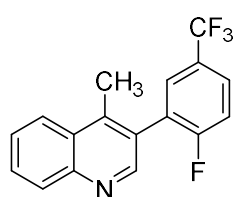
¹H NMR (400 MHz, CDCl₃) δ (ppm) = 8.75 (s, 1H), 8.16 – 8.08 (m, 2H), 7.74 (ddd, *J* = 8.3, 6.9, 1.4 Hz, 1H), 7.61 (ddd, *J* = 8.3, 6.8, 1.3 Hz, 1H), 7.23 (t, *J* = 7.7 Hz, 1H), 7.10 (ddd, *J* = 7.7, 1.6, 0.8 Hz, 1H), 7.04 (dt, *J* = 10.8, 1.1 Hz, 1H), 2.59 (d, *J* = 1.7 Hz, 3H), 2.45 (s, 3H).

¹³C NMR (101 MHz, CDCl₃) δ (ppm) = 159.88 (d, *J* = 246.5 Hz), 151.57, 147.25, 142.35, 140.64 (d, *J* = 7.8 Hz), 131.54 (d, *J* = 3.8 Hz), 130.02, 129.08, 128.49, 127.81, 126.71, 125.07 (d, *J* = 3.2 Hz), 124.22, 122.95 (d, *J* = 16.6 Hz), 116.35 (d, *J* = 22.0 Hz), 21.22 (d, *J* = 1.7 Hz), 15.74 (d, *J* = 2.5 Hz).

¹⁹F NMR (376 MHz, CDCl₃) δ (ppm) = -115.73.

MS (APCI) = 252.1 calculated [M+H]⁺ for C₁₇H₁₃FN; experimental 251.8.

3-(2-fluoro-5-(trifluoromethyl)phenyl)-4-methylquinoline



The reaction, workup and purification were followed according to the General

Procedure 1. The reaction with 3-chloro-4-methylquinoline (700 mg, 3.94

mmol), 2-fluoro-5-(trifluoromethyl)phenylboronic acid (1.07 g, 5.12 mmol),

Pd(OAc)₂ (88 mg, 0.39 mmol), XPhos (376 mg, 0.79 mmol), K₃PO₄ (1.70 g, 7.88 mmol) in 15.8 mL of degassed 1,4-dioxane and 5.3 mL of degassed deionized H₂O afforded the product as an orange oil (719 mg, 2.36 mmol, 60%).

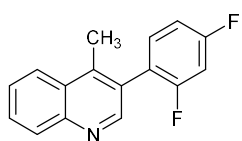
¹H NMR (400 MHz, CDCl₃) δ (ppm) = 8.74 (s, 1H), 8.16 (dd, *J* = 8.4, 0.7 Hz, 1H), 8.12 (ddd, *J* = 8.4, 1.4, 0.6 Hz, 1H), 7.78 (td, *J* = 7.6, 1.4 Hz, 1H), 7.75 – 7.71 (m, 1H), 7.68 – 7.62 (m, 2H), 7.35 (t, *J* = 8.7 Hz, 1H), 2.59 (d, *J* = 1.7 Hz, 3H).

¹³C NMR (101 MHz, CDCl₃) δ (ppm) = 161.82 (d, *J* = 253.5 Hz), 150.66, 147.54, 142.74, 130.09, 129.66, 129.36 (p, *J* = 3.7 Hz), 127.56, 127.47 (d, *J* = 3.6 Hz), 127.38 (d, *J* = 3.6 Hz), 127.09, 126.90 (d, *J* = 3.0 Hz), 124.97, 124.21, 122.26, 116.61 (d, *J* = 23.8 Hz), 15.79 (d, *J* = 2.4 Hz).

¹⁹F NMR (376 MHz, CDCl₃) δ (ppm) = -61.89 (d, *J* = 1.7 Hz), -108.38 (m).

MS (APCI) = 306.1 calculated [M+H]⁺ for C₁₇H₁₂F₄N; experimental 305.9.

3-(2,4-difluorophenyl)-4-methylquinoline



The reaction, workup and purification were followed according to the General Procedure 1. The reaction with 3-chloro-4-methylquinoline (600 mg, 3.38 mmol), 2,4-difluorophenylboronic acid (693 mg, 4.39 mmol), Pd(OAc)₂ (76

mg, 0.34 mmol), XPhos (322 mg, 0.68 mmol), K₃PO₄ (1.43 g, 6.76 mmol) in 13.5 mL of degassed 1,4-dioxane and 4.5 mL of degassed deionized H₂O afforded the product as a pale yellow solid (592 mg, 2.32 mmol, 69%).

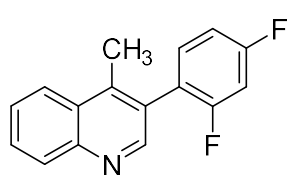
¹H NMR (500 MHz, CDCl₃) δ (ppm) = 8.72 (s, 1H), 8.14 (dd, *J* = 8.5, 1.2 Hz, 1H), 8.10 (dd, *J* = 8.4, 1.3 Hz, 1H), 7.75 (ddd, *J* = 8.3, 6.8, 1.4 Hz, 1H), 7.63 (ddd, *J* = 8.3, 6.8, 1.3 Hz, 1H), 7.32 (td, *J* = 8.4, 6.4 Hz, 1H), 7.04 (tdd, *J* = 8.3, 2.6, 1.0 Hz, 1H), 6.98 (ddd, *J* = 9.5, 8.8, 2.5 Hz, 1H), 2.57 (d, *J* = 1.7 Hz, 3H).

¹³C NMR (126 MHz, CDCl₃) δ (ppm) = 162.91 (dd, *J* = 249.4, 11.0 Hz), 160.11 (dd, *J* = 249.8, 12.3 Hz), 151.20, 147.37, 142.52, 132.56 (dd, *J* = 9.5, 4.7 Hz), 130.03, 129.30, 127.66, 127.48, 126.86, 124.17, 122.14 (dd, *J* = 16.8, 4.0 Hz), 111.64 (dd, *J* = 21.4, 3.7 Hz), 104.25 (td, *J* = 25.7, 2.3 Hz), 15.66 (t, *J* = 5.0 Hz).

¹⁹F NMR (470 MHz, CDCl₃) δ (ppm) = -108.33 (q, *J* = 9.0 Hz), -108.57 (p, *J* = 8.0 Hz).

MS (APCI) = 256.1 calculated [M+H]⁺ for C₁₆H₁₂F₂N; experimental 256.1.

3-(2-fluoro-5-nitrophenyl)-4-methylquinoline



The reaction, workup and purification were followed according to the General Procedure 1. The reaction with 3-chloro-4-methylquinoline (600 mg, 3.38 mmol), 2-fluoro-5-nitrophenylboronic acid (812 mg, 4.39 mmol), Pd(OAc)₂ (76 mg, 0.34 mmol), XPhos (322 mg, 0.68 mmol), K₃PO₄ (1.40 g, 6.76 mmol) in 13.5 mL of degassed 1,4-dioxane and 4.5 mL of degassed deionized H₂O afforded the product as an orange oil (476 mg, 1.69 mmol, 50%).

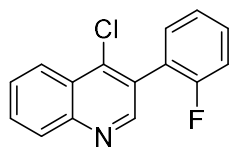
¹H NMR (500 MHz, CDCl₃) δ (ppm) = 8.74 (s, 1H), 8.37 (ddd, *J* = 9.0, 4.3, 2.8 Hz, 1H), 8.32 (dd, *J* = 6.2, 2.8 Hz, 1H), 8.17 (ddd, *J* = 8.4, 1.4, 0.6 Hz, 1H), 8.12 (ddd, *J* = 8.4, 1.4, 0.7 Hz, 1H), 7.79 (ddd, *J* = 8.3, 6.9, 1.4 Hz, 1H), 7.66 (ddd, *J* = 8.3, 6.9, 1.3 Hz, 1H), 7.39 (t, *J* = 8.6 Hz, 1H), 2.60 (s, 3H).

¹³C NMR (126 MHz, CDCl₃) δ (ppm) = 166.22 (d, *J* = 258.2 Hz), 153.00, 150.40, 147.01, 145.54, 132.87, 132.60, 130.50 (d, *J* = 5.0 Hz), 130.34 (d, *J* = 19.1 Hz), 129.96, 128.72, 128.50 (d, *J* = 9.9 Hz), 126.89, 119.67 (d, *J* = 25.1 Hz), 18.55, (d, *J* = 2.6 Hz).

¹⁹F NMR (470 MHz, CDCl₃) δ (ppm) = -102.27.

MS (APCI) = 283.1 calculated [M+H]⁺ for C₁₆H₁₂FN₂O₂; experimental 283.2.

4-chloro-3-(2-fluorophenyl)quinoline



The reaction, workup and purification were followed according to the General Procedure 2. The reaction with 3-bromo-4-chloroquinoline (1.0 g, 4.12 mmol), 2-fluorophenyl boronic acid (635 mg, 4.54 mmol), Pd(PPh₃)₄ (238 mg, 0.21 mmol), K₂CO₃ (1.42 g, 10.31 mmol) in 13.7 mL of degassed 1,4-dioxane and 4.6 mL of degassed deionized H₂O afforded the product as a light yellow oil (668 mg, 2.59 mmol, 63%).

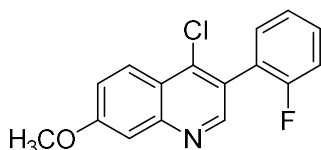
¹H NMR (400 MHz, CDCl₃) δ (ppm) = 8.82 (s, 1H), 8.36 (ddd, *J* = 8.4, 1.5, 0.7 Hz, 1H), 8.19 (dd, *J* = 8.4, 0.7 Hz, 1H), 7.85 – 7.78 (m, 1H), 7.71 (ddd, *J* = 8.2, 7.0, 1.2 Hz, 1H), 7.53 – 7.40 (m, 2H), 7.31 (td, *J* = 7.5, 1.1 Hz, 1H), 7.25 (ddd, *J* = 9.5, 8.5, 0.9 Hz, 1H).

¹³C NMR (101 MHz, CDCl₃) δ (ppm) = 159.93 (d, *J* = 248.7 Hz), 151.08, 148.07, 141.64, 131.77 (d, *J* = 2.8 Hz), 130.74 (d, *J* = 8.1 Hz), 130.49, 129.60, 128.06, 127.97, 126.27, 124.65, 124.24 (d, *J* = 3.8 Hz), 123.90 (d, *J* = 15.7 Hz), 116.02 (d, *J* = 21.7 Hz).

¹⁹F NMR (376 MHz, CDCl₃) δ (ppm) = -113.91.

MS (APCI) = 258.0 calculated [M+H]⁺ for C₁₅H₁₀ClFN; experimental 257.4.

4-chloro-3-(2-fluorophenyl)-7-methoxyquinoline



The reaction, workup and purification were followed according to the General Procedure 2. The reaction with 3-bromo-4-chloro-7-methoxyquinoline (1.12 g, 4.11 mmol), 2-fluorophenylboronic acid

(633 mg, 4.52 mmol), Pd(PPh₃)₄ (237 mg, 0.21 mmol), K₂CO₃ (1.42 g, 10.28 mmol) in 16.4 mL of degassed 1,4-dioxane and 5.5 mL of degassed deionized H₂O afforded the product as a white solid (513 mg, 1.78 mmol, 43%).

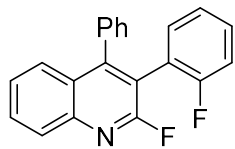
¹H-NMR (400 MHz, CDCl₃) δ (ppm) = 8.73 (s, 1H), 8.22 (d, *J* = 9.2 Hz, 1H), 7.49 – 7.44 (m, 2H), 7.42 (td, *J* = 7.4, 1.9 Hz, 1H), 7.33 (dd, *J* = 9.2, 2.5 Hz, 1H), 7.29 (td, *J* = 7.5, 1.2 Hz, 1H), 7.23 (ddd, *J* = 9.5, 8.2, 1.1 Hz, 1H), 3.99 (s, 3H).

¹³C NMR (101 MHz, CDCl₃) δ (ppm) = 161.45, 160.05 (d, *J* = 248.4 Hz), 151.51 (d, *J* = 1.5 Hz), 150.19, 141.29, 131.93 (d, *J* = 2.9 Hz), 130.49 (d, *J* = 8.1 Hz), 125.93, 125.85, 124.15 (d, *J* = 3.8 Hz), 124.13 (d, *J* = 15.8 Hz), 121.35, 121.03, 115.94 (d, *J* = 21.9 Hz), 107.61, 55.69.

¹⁹F NMR (376 MHz, CDCl₃) δ (ppm) = -112.25

HRMS (ESI) = 288.0586 calculated [M+H]⁺ for C₁₆H₁₂ClFNO; experimental 288.0578.

DKR Substrate, 1j



The reaction, workup and purification were followed according to the General

Procedure 1. The reaction with 4-chloro-2-fluoro-3-(2-fluorophenyl)quinoline, (\pm)-**1f** (435 mg, 1.37 mmol), phenylboronic acid (220

mg, 1.8 mmol), Pd(OAc)₂ (31.4 mg, 0.14 mmol), XPhos (130.6 mg, 0.274 mmol), K₃PO₄ (715 mg, 4.11 mmol, 3.0 equiv) in 5.5 mL of degassed 1,4-dioxane and 1.8 mL of degassed deionized H₂O afforded **2-fluoro-3-(2-fluorophenyl)-4-phenylquinoline, 1g** as a whitish solid (234.5 mg, 0.74 mmol, 54%).

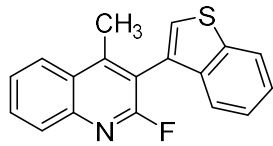
¹H NMR (500 MHz, CDCl₃) δ (ppm) = 8.06 (d, J = 8.4 Hz, 1H), 7.78 – 7.72 (m, 1H), 7.62 (d, J = 6.8 Hz, 1H), 7.48 – 7.44 (m, 1H), 7.37 – 7.27 (m, 3H), 7.26 – 7.21 (m, 2H), 7.15 (d, J = 7.8 Hz, 1H), 7.05 – 6.96 (m, 3H).

¹³C NMR (126 MHz, CDCl₃) δ (ppm) = 160.50 (d, J = 193.1 Hz), 158.56 (d, J = 188.4 Hz), 153.71 (d, J = 5.7 Hz), 145.68 (d, J = 17.2 Hz), 135.46 (d, J = 3.8 Hz), 132.39, 130.73, 130.26, 129.75 (d, J = 39.1 Hz), 128.48, 128.33, 127.91, 127.12 – 126.77 (m), 126.38, 123.79, 121.24 (d, J = 16.2 Hz), 117.25 (d, J = 36.7 Hz), 115.43 (d, J = 21.5 Hz).

¹⁹F NMR (470 MHz, CDCl₃) δ (ppm) = -62.58 (d, J = 7.5 Hz), -112.85 – -113.00 (m).

MS (APCI) = 258.0 calculated [M+H]⁺ for C₂₁H₁₃F₂N; experimental 257.4.

DKR Substrate, 1k



The reaction, workup and purification were followed according to the

General Procedure 1. The reaction with 3-chloro-2-fluoro-4-methylquinoline (430 mg, 2.20 mmol), benzo[b]thien-3-ylboronic acid

(470 mg, 2.64 mmol), Pd(OAc)₂ (49 mg, 0.22 mmol), XPhos (210 mg, 0.44 mmol), K₃PO₄ (933 g,

4.40 mmol) in 8.8 mL of degassed 1,4-dioxane and 2.9 mL of degassed deionized H₂O afforded **3-(benzo[b]thiophen-3-yl)-2-fluoro-4-methylquinoline**, (\pm)-**1h** as a pink solid (400 mg, 1.36 mmol, 62%).

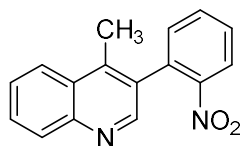
¹H-NMR (400 MHz, CDCl₃) δ (ppm) = 8.09 – 8.01 (m, 2H), 7.96 (dt, J = 8.0, 1.1 Hz, 1H), 7.78 (ddd, J = 8.4, 6.9, 1.4 Hz, 1H), 7.62 (ddd, J = 8.4, 6.9, 1.3 Hz, 1H), 7.47 (s, 1H), 7.41 (ddd, J = 8.1, 5.3, 3.0 Hz, 1H), 7.38 – 7.34 (m, 2H), 2.55 (s, 3H).

¹³C NMR (101 MHz, CDCl₃) δ (ppm) = 160.33, 157.93, 149.89 (d, J = 5.9 Hz), 144.94 (d, J = 17.3 Hz), 139.78, 138.59, 130.40, 128.65, 127.10 (d, J = 1.8 Hz), 126.72, 126.21 (d, J = 2.4 Hz), 124.60 (d, J = 13.4 Hz), 124.39, 122.82, 122.48, 117.03 (d, J = 36.3 Hz), 109.96 (d, J = 41.7 Hz), 16.29 (d, J = 3.7 Hz).

¹⁹F NMR (376 MHz, CDCl₃) δ (ppm) = -60.26.

MS (APCI) = 294.1 calculated [M+H]⁺ for C₁₈H₁₃FNS; experimental 294.2.

4-methyl-3-(2-nitrophenyl)quinoline



The reaction, workup and purification were followed according to the General Procedure 1. The reaction with 3-chloro-4-methylquinoline (500 mg, 2.82 mmol), 2-nitrophenylboronic acid (611 mg, 3.66 mmol), Pd(OAc)₂ (63 mg,

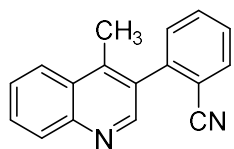
0.28 mmol), XPhos (268 mg, 0.56 mmol), K₃PO₄ (1.20 g, 5.63 mmol) in 11.3 mL of degassed 1,4-dioxane and 3.7 mL of degassed deionized H₂O afforded the product as a yellow crystal after washing with n-hexanes (302 mg, 1.14 mmol, 40%).

¹H NMR (400 MHz, CDCl₃) δ (ppm) = 8.67 (s, 1H), 8.17 – 8.12 (m, 2H), 8.06 (ddd, J = 8.5, 1.4, 0.6 Hz, 1H), 7.78 – 7.70 (m, 2H), 7.66 – 7.60 (m, 2H), 7.41 (dd, J = 7.6, 1.5 Hz, 1H), 2.47 (s, 3H).

^{13}C NMR (101 MHz, CDCl_3) δ (ppm) = 149.57, 149.24, 147.32, 141.35, 133.53, 133.03, 132.78, 130.57, 130.10, 129.40, 129.20, 127.48, 126.99, 124.62, 124.08, 15.65.

MS (APCI) = 265.1 calculated $[\text{M}+\text{H}]^+$ for $\text{C}_{16}\text{H}_{13}\text{N}_2\text{O}_2$; experimental 265.0.

3-(2-cyanophenyl)-4-methylquinoline



The reaction, workup and purification were followed according to the General

Procedure 1. The reaction with 3-chloro-4-methylquinoline (300 mg, 1.69

mmol), 2-cyanophenylboronic acid (323 mg, 2.20 mmol), $\text{Pd}(\text{OAc})_2$ (38 mg,

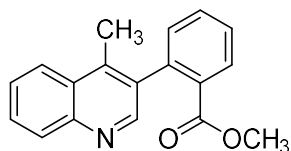
0.17 mmol), XPhos (161 mg, 0.34 mmol), K_3PO_4 (717 mg, 3.38 mmol) in 6.8 mL of degassed 1,4-dioxane and 2.3 mL of degassed deionized H_2O afforded the product as a yellow solid (134 mg, 0.55 mmol, 33%).

^1H NMR (400 MHz, CDCl_3) δ (ppm) = 8.74 (s, 1H), 8.16 (dd, J = 8.4, 1.3 Hz, 1H), 8.11 (dd, J = 8.4, 1.5 Hz, 1H), 7.83 (dd, J = 7.8, 1.4 Hz, 1H), 7.77 (td, J = 7.8, 1.5 Hz, 1H), 7.73 (td, J = 7.9, 1.6 Hz, 1H), 7.65 (ddd, J = 8.3, 6.8, 1.3 Hz, 1H), 7.56 (td, J = 7.7, 1.2 Hz, 1H), 7.47 (dd, J = 7.7, 1.2 Hz, 1H), 2.60 (s, 3H).

^{13}C NMR (101 MHz, CDCl_3) δ (ppm) = 150.17, 147.54, 142.41, 142.20, 133.03, 132.82, 131.11, 130.86, 130.06, 129.69, 128.38, 127.52, 127.13, 124.34, 117.68, 113.74, 15.74.

MS (APCI) = 245.1 calculated $[\text{M}+\text{H}]^+$ for $\text{C}_{17}\text{H}_{13}\text{N}_2$; experimental 244.7.

2-(4-methylquinolin-3-yl)benzoate



The reaction, workup and purification were followed according to the

General Procedure 1. The reaction with 3-chloro-4-methylquinoline (600

mg, 3.38 mmol, 1.0 equiv) were added (2-

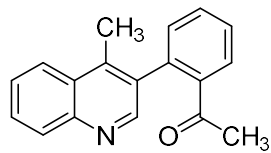
(methoxycarbonyl)phenyl)boronic acid (790 mg, 4.39 mmol, 1.3 equiv), Pd(OAc)₂ (76 mg, 0.34 mmol, 0.1 equiv), XPhos (322 mg, 0.68 mmol, 0.2 equiv), and K₃PO₄ (1.43 g, 6.76 mmol, 2.0 equiv) in 13.5 mL of degassed 1,4-dioxane and 4.5 mL of degassed deionized H₂O afforded product as a yellow solid (472 mg, 1.69 mmol, 50%).

¹H-NMR (400 MHz, CDCl₃) δ (ppm) = 8.65 (s, 1H), 8.14 (d, *J* = 8.4 Hz, 1H), 8.10 (dt, *J* = 7.8, 0.7 Hz, 1H), 8.07 (dt, *J* = 8.5, 0.8 Hz, 1H), 7.72 (ddd, *J* = 8.3, 6.9, 1.3 Hz, 1H), 7.65 – 7.58 (m, 2H), 7.53 (td, *J* = 7.6, 1.3 Hz, 1H), 7.30 (dt, *J* = 7.6, 0.7 Hz, 1H), 3.59 (s, 3H), 2.46 (s, 3H).

¹³C NMR (101 MHz, CDCl₃) δ (ppm) = 167.21, 150.46, 146.90, 140.49, 139.69, 134.20, 131.94, 131.73, 130.62, 130.52, 129.98, 128.78, 128.03, 127.66, 126.59, 124.09, 52.04, 15.56.

MS (APCI) = 278.1 calculated [M+H]⁺ for C₁₈H₁₆NO₂; experimental 277.7.

1-(2-(4-methylquinolin-3-yl)phenyl)ethanone



The reaction, workup and purification were followed according to the General Procedure 1. The reaction with 3-chloro-4-methylquinoline (736 mg, 4.14 mmol), (2-acetylphenyl)boronic acid (883 mg, 5.39 mmol),

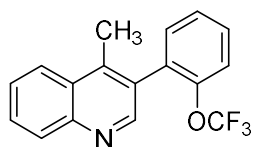
Pd(OAc)₂ (93 mg, 0.41 mmol), XPhos (395 mg, 0.83 mmol), K₃PO₄ (1.76 g, 8.29 mmol) in 16.6 mL of degassed 1,4-dioxane and 5.5 mL of degassed deionized H₂O afforded the product in as a bright orange oil (533 mg, 2.04 mmol, 49%).

¹H-NMR (400 MHz, CDCl₃) δ (ppm) = 8.67 (s, 1H), 8.14 (dd, *J* = 8.4, 0.8 Hz, 1H), 8.06 (ddd, *J* = 8.4, 1.5, 0.6 Hz, 1H), 7.81 (ddd, *J* = 7.7, 1.5, 0.5 Hz, 1H), 7.73 (ddd, *J* = 8.4, 6.9, 1.4 Hz, 1H), 7.64 – 7.57 (m, 2H), 7.53 (td, *J* = 7.6, 1.4 Hz, 1H), 7.30 (ddd, *J* = 7.5, 1.5, 0.5 Hz, 1H), 2.47 (s, 3H), 2.18 (s, 3H).

^{13}C NMR (100 MHz, CDCl_3) δ (ppm) = 201.29, 150.55, 147.15, 141.07, 139.89, 137.47, 133.84, 131.73, 131.38, 130.10, 129.09, 128.76, 128.20, 127.69, 126.88, 124.14, 29.67, 15.67.

MS (APCI) = 262.1 calculated $[\text{M}+\text{H}]^+$ for $\text{C}_{18}\text{H}_{16}\text{NO}$; experimental 262.2.

4-methyl-3-(2-(trifluoromethoxy)phenyl)quinoline



The reaction, workup and purification were followed according to the General Procedure 1. The reaction with 3-chloro-4-methylquinoline (700 mg, 3.94 mmol), 2-(trifluoromethoxy)phenylboronic acid (1.06 g, 5.12 mmol), $\text{Pd}(\text{OAc})_2$ (88 mg, 0.39 mmol), XPhos (376 mg, 0.79 mmol), K_3PO_4 (1.70 g, 7.88 mmol) in 15.8 mL of degassed 1,4-dioxane and 5.3 mL of degassed deionized H_2O afforded the product as an orange oil (1.04 g, 3.42 mmol, 87%).

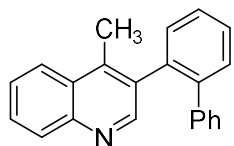
^1H NMR (400 MHz, CDCl_3) δ (ppm) = 8.72 (s, 1H), 8.16 (ddd, $J = 8.4, 1.3, 0.6$ Hz, 1H), 8.10 (ddd, $J = 8.4, 1.4, 0.6$ Hz, 1H), 7.75 (ddd, $J = 8.3, 6.9, 1.4$ Hz, 1H), 7.63 (ddd, $J = 8.3, 6.9, 1.3$ Hz, 1H), 7.53 – 7.47 (m, 1H), 7.46 – 7.40 (m, 2H), 7.39 – 7.34 (m, 1H), 2.52 (s, 3H).

^{13}C NMR (101 MHz, CDCl_3) δ (ppm) = 151.13, 147.26, 147.01 (d, $J = 1.7$ Hz), 142.13, 132.29, 131.94, 130.05, 129.65, 129.32, 129.23, 127.64, 126.87 (d, $J = 18.0$ Hz), 124.20, 121.07 (q, $J = 1.5$ Hz), 120.27 (d, $J = 258.2$ Hz), 15.60.

^{19}F NMR (376 MHz, CDCl_3) δ (ppm) = -56.34.

MS (APCI) = 304.1 calculated $[\text{M}+\text{H}]^+$ for $\text{C}_{17}\text{H}_{13}\text{F}_3\text{NO}$; experimental 303.9.

3-([1,1'-biphenyl]-2-yl)-4-methylquinoline



The reaction, workup and purification were followed according to the General Procedure 2. The reaction with 3-bromo-4-methylquinoline (450 mg, 2.03

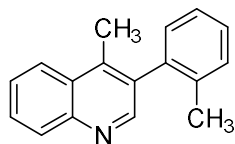
mmol), 2-biphenylboronic acid (441 mg, 2.23 mmol), Pd(PPh₃)₄ (117 mg, 0.10 mmol), K₂CO₃ (700 mg, 5.07 mmol) in 6.8 mL of degassed 1,4-dioxane and 2.3 mL of degassed deionized H₂O afforded product as orange oil (576 mg, 1.95 mmol, 96%).

¹H NMR (400 MHz, CDCl₃) δ (ppm) = 8.67 (s, 1H), 8.07 (dd, *J* = 8.4, 0.7 Hz, 1H), 7.92 (ddd, *J* = 8.4, 1.4, 0.6 Hz, 1H), 7.68 (ddd, *J* = 8.3, 6.8, 1.4 Hz, 1H), 7.56 – 7.51 (m, 3H), 7.51 – 7.45 (m, 1H), 7.36 (dt, *J* = 7.3, 1.1 Hz, 1H), 7.14 – 7.06 (m, 5H), 2.31 (s, 3H).

¹³C NMR (101 MHz, CDCl₃) δ (ppm) = 152.07, 146.62, 142.13, 141.18, 140.74, 136.77, 134.01, 131.33, 130.28, 129.85, 129.38, 128.73, 128.32, 128.01, 127.67, 127.33, 126.74, 126.49, 124.04, 15.61.

MS (APCI) = 296.1 calculated [M+H]⁺ for C₂₂H₁₈N; experimental 295.4.

4-methyl-3-(*o*-tolyl)quinoline



The reaction, workup and purification were followed according to the General Procedure 1. The reaction with 3-chloro-4-methylquinoline (600 mg, 3.38 mmol), *o*-tolylboronic acid (597 mg, 4.39 mmol), Pd(OAc)₂ (76 mg, 0.34

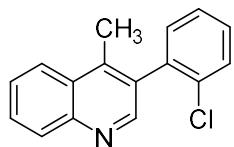
mmol), XPhos (322 mg, 0.68 mmol), K₃PO₄ (1.43 g, 6.76 mmol) in 13.5 mL of degassed 1,4-dioxane and 4.5 mL of degassed deionized H₂O afforded the product as a dark orange oil (716 mg, 3.07 mmol, 91%).

¹H NMR (400 MHz, CDCl₃) δ (ppm) = 8.71 (s, 1H), 8.19 (dt, *J* = 8.5, 0.8 Hz, 1H), 8.09 (dt, *J* = 8.5, 0.8 Hz, 1H), 7.75 (ddd, *J* = 8.4, 6.9, 1.4 Hz, 1H), 7.63 (ddd, *J* = 8.3, 6.8, 1.3 Hz, 1H), 7.38 – 7.33 (m, 2H), 7.33 – 7.28 (m, 1H), 7.18 (d, *J* = 7.2 Hz, 1H), 2.48 (s, 3H), 2.10 (s, 3H).

¹³C NMR (101 MHz, CDCl₃) δ (ppm) = 150.99, 146.65, 141.69, 137.88, 136.54, 134.12, 130.12, 129.98, 129.70, 129.00, 128.07, 127.89, 126.76, 125.85, 124.10, 20.01, 15.36.

MS (APCI) = 234.1 calculated $[M+H]^+$ for $C_{17}H_{16}N$; experimental 233.8.

3-(2-chlorophenyl)-4-methylquinoline



The reaction, workup and purification were followed according to the General

Procedure 1. The reaction with 3-chloro-4-methylquinoline (1.00 g, 5.63 mmol), 2-chlorophenylboronic acid (1.16 g, 7.32 mmol), $Pd(OAc)_2$ (126 mg,

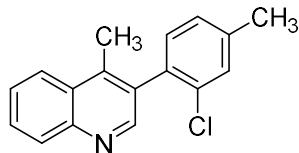
0.56 mmol), XPhos (537 mg, 1.13 mmol), K_3PO_4 (2.40 g, 11.26 mmol) in 22.5 mL of degassed 1,4-dioxane and 7.6 mL of degassed deionized H_2O afforded the product as an orange oil (651 mg, 2.57 mmol, 46%).

1H NMR (400 MHz, $CDCl_3$) δ (ppm) = 8.70 (s, 1H), 8.16 (ddd, $J = 8.4, 1.4, 0.6$ Hz, 1H), 8.10 (ddd, $J = 8.4, 1.4, 0.6$ Hz, 1H), 7.75 (ddd, $J = 8.4, 6.9, 1.4$ Hz, 1H), 7.62 (ddd, $J = 8.3, 6.8, 1.4$ Hz, 1H), 7.57 – 7.53 (m, 1H), 7.42 – 7.37 (m, 2H), 7.34 – 7.30 (m, 1H), 2.52 (s, 3H).

^{13}C NMR (101 MHz, $CDCl_3$) δ (ppm) = 151.01, 147.28, 142.02, 137.31, 134.18, 132.02, 131.66, 130.05, 129.67, 129.42, 129.17, 127.70, 126.84, 126.74, 124.21, 15.55.

MS (APCI) = 254.1 calculated $[M+H]^+$ for $C_{16}H_{13}ClN$; experimental 254.1.

3-(2-chloro-4-methylphenyl)-4-methylquinoline



The reaction, workup and purification were followed according to the

General Procedure 1. The reaction with 3-chloro-4-methylquinoline (800 mg, 4.60 mmol), 2-chloro-4-methylphenylboronic acid (860 mg, 5.06

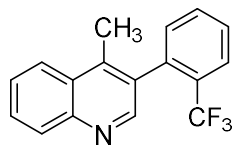
mmol), $Pd(OAc)_2$ (103 mg, 0.460 mmol), XPhos (438 mg, 0.920 mmol), K_3PO_4 (2.0 g, 11.5 mmol, 2.5 equiv) in 18 mL of degassed 1,4-dioxane and 6.0 mL of degassed deionized H_2O afforded the product as an orange oil (475.3 mg, 2.57 mmol, 46%).

¹H NMR (400 MHz, CDCl₃) δ (ppm) = 8.69 (s, 1H), 8.15 (d, *J* = 8.4 Hz, 1H), 8.10 (dd, *J* = 8.4, 1.3 Hz, 1H), 7.74 (ddd, *J* = 8.4, 6.9, 1.4 Hz, 1H), 7.62 (ddd, *J* = 8.3, 6.9, 1.3 Hz, 1H), 7.38 – 7.36 (m, 1H), 7.19 (d, *J* = 1.0 Hz, 2H), 2.52 (s, 3H), 2.43 (s, 3H).

¹³C NMR (101 MHz, CDCl₃) δ (ppm) = 151.35, 147.27, 142.37, 139.88, 134.35, 133.96, 132.19, 131.52, 130.26, 130.10, 129.26, 127.91, 127.83, 126.86, 124.36, 21.14, 15.72.

MS (APCI) = 267.8 calculated [M+H]⁺ for C₁₇H₁₄ClN; experimental 267.5.

4-methyl-3-(2-(trifluoromethyl)phenyl)quinoline



The reaction, workup and purification were followed according to the General

Procedure 1. The reaction with 3-chloro-4-methylquinoline (651 mg, 3.657 mmol), 2-(trifluoromethyl)phenylboronic acid (1.04 g, 5.486 mmol, 1.5

equiv), Pd(OAc)₂ (83 mg, 0.37 mmol), XPhos (353 mg, 0.74 mmol), K₃PO₄ (1.94 g, 9.143 mmol) in 14.6 mL of degassed 1,4-dioxane and 5.0 mL of degassed deionized H₂O afforded the product as a dark orange oil (681 mg, 2.37 mmol, 86%).

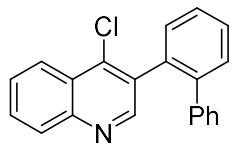
¹H NMR (400 MHz, CDCl₃) δ (ppm) = 8.69 (s, 1H), 8.17 (d, *J* = 8.4 Hz, 1H), 8.07 (d, *J* = 8.4 Hz, 1H), 7.83 (d, *J* = 7.9 Hz, 1H), 7.77 – 7.72 (m, 1H), 7.65 – 7.59 (m, 2H), 7.56 (t, *J* = 7.7 Hz, 1H), 7.30 (d, *J* = 7.5 Hz, 1H), 2.41 (s, 3H).

¹³C NMR (101 MHz, CDCl₃) δ (ppm) = 150.61 (q, *J* = 30.0 Hz), 147.34, 142.10, 137.53, 130.19 (q, *J* = 7.8 Hz), 129.76, 129.59, 129.47, 128.62, 128.15, 127.69, 127.20, 126.78 (d, *J* = 30 Hz), 126.16, 124.35, 124.18, 16.01 (d, *J* = 36.4 Hz).

¹⁹F NMR (376 MHz, CDCl₃) δ (ppm) = -59.37.

MS (APCI) = 287.3 calculated [M+H]⁺ for C₁₇H₁₂F₃N; experimental 287.3.

3-([1,1'-biphenyl]-2-yl)-4-chloroquinoline



The reaction, workup and purification were followed according to the General

Procedure 2. The reaction with 3-bromo-4-chloroquinoline (1.0 g, 4.12 mmol),

2-biphenylboronic acid (898 mg, 4.54 mmol), Pd(PPh₃)₄ (238 mg, 0.21 mmol),

K₂CO₃ (1.42 g, 10.31 mmol) in 13.7 mL of degassed 1,4-dioxane and 4.6 mL of degassed deionized

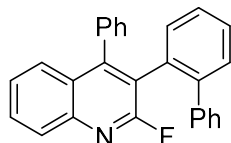
H₂O afforded the product as a light yellow oil (548 mg, 1.74 mmol, 42%).

¹H-NMR (400 MHz, CDCl₃) δ (ppm) = 8.53 (s, 1H), 8.25 (dd, *J* = 8.4, 1.4 Hz, 1H), 8.07 (dt, *J* = 8.6, 0.8 Hz, 1H), 7.74 (ddd, *J* = 8.4, 6.9, 1.4 Hz, 1H), 7.64 (ddd, *J* = 8.3, 6.9, 1.2 Hz, 1H), 7.57 – 7.54 (m, 2H), 7.53 – 7.44 (m, 2H), 7.17 – 7.12 (m, 5H).

¹³C NMR (101 MHz, CDCl₃) δ (ppm) = 152.04, 147.47, 141.99, 140.60, 140.38, 134.62, 133.42, 131.28, 130.37, 129.91, 129.60, 129.23 (2 x CH), 128.90, 128.09 (2 x CH), 127.72, 127.24, 127.01, 126.12, 124.43.

MS (APCI) = 316.1 calculated [M+H]⁺ for C₂₁H₁₅ClN; experimental 315.7.

KR Substrate, 117



The reaction, workup and purification were followed according to the General

Procedure 1. The reaction with 3-([1,1'-biphenyl]-2-yl)-4-chloro-2-

fluoroquinoline (333 mg, 1.00 mmol), phenylboronic acid (158 mg, 1.30

mmol), Pd(OAc)₂ (22 mg, 0.10 mmol), XPhos (95 mg, 0.20 mmol), K₃PO₄ (530 mg, 2.50 mmol)

in 4.0 mL of degassed 1,4-dioxane and 1.3 mL of degassed deionized H₂O afforded the product **3-**

([1,1'-biphenyl]-2-yl)-2-fluoro-4-phenylquinoline, (±)-117 as an orange solid (102 mg, 0.27

mmol, 27%).

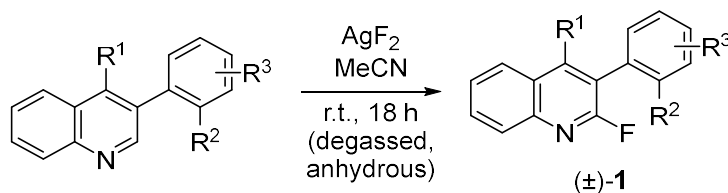
¹H-NMR (400 MHz, CDCl₃) δ (ppm) = 8.00 (dd, *J* = 8.4, 1.2 Hz, 1H), 7.69 (ddd, *J* = 8.4, 6.8, 1.5 Hz, 1H), 7.45 (dd, *J* = 8.5, 1.5 Hz, 1H), 7.39 – 7.31 (m, 4H), 7.28 – 7.23 (m, 2H), 7.21 – 7.15 (m, 2H), 7.12 (dddd, *J* = 6.8, 5.4, 4.2, 1.7 Hz, 3H), 6.95 (dt, *J* = 7.3, 1.8 Hz, 1H), 6.91 – 6.86 (m, 2H), 6.41 (dt, *J* = 7.6, 1.7 Hz, 1H).

¹³C NMR (101 MHz, CDCl₃) δ (ppm) = 160.37, 157.98, 152.07 (d, *J* = 5.8 Hz), 145.23 (d, *J* = 17.3 Hz), 141.16 (d, *J* = 145.4 Hz), 134.85 (d, *J* = 3.8 Hz), 131.93, 131.24 (d, *J* = 3.2 Hz), 130.08, 129.98 (d, *J* = 15.2 Hz), 129.96, 129.07, 128.45, 128.12, 128.03 (d, *J* = 1.6 Hz), 127.80, 127.72, 127.57 (d, *J* = 4.5 Hz), 126.70 (d, *J* = 13.1 Hz), 126.65, 126.57 (d, *J* = 1.9 Hz), 125.96 (d, *J* = 2.3 Hz), 122.56 (d, *J* = 36.0 Hz).

¹⁹F NMR (376 MHz, CDCl₃) δ (ppm) = -59.06.

MS (APCI) = 376.2 calculated [M+H]⁺ for C₂₇H₁₉FN; experimental 376.2.

2.2.12 Hartwig Fluorination to yield 2-fluoro-3-arylquinoline (1)

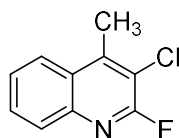


Equation 42. General Fluorination Method Towards Substrate 70. Adapted from Hartwig and coworkers' selective C-H fluorination.^[14]

To 3-aryl-2-R¹-quinoline (1.0 equiv) was dissolved in 0.5 - 0.1 M anhydrous MeCN in the glovebox. Once dissolved, silver (II) fluoride (3.5 equiv) was then added to the reaction and the vial was sealed with a Teflon-lined cap. Each fluorination reaction was brought out of the glovebox to stir at room temperature overnight (unless otherwise stated). The resulting reaction was gravity filtered, and the solid was thoroughly rinsed with EtOAc. The resulting filtrate was poured into a

separatory funnel containing saturated aqueous NaHCO₃, and then partitioned with EtOAc. The resulting organic layer was extracted and rinsed with more saturated aqueous NaHCO₃. The resulting organic layer was washed with saturated aqueous NaCl, then dried over Na₂SO₄. After filtration and solvent evaporation, the crude was purified by FCC using *n*-hexanes:EtOAc = 0 → 5% or 10% to afford (±)-**1** in ~20-90% yields.

3-chloro-2-fluoro-4-methylquinoline



To 3-chloro-4-methylquinoline (850 mg, 4.776 mmol) was added silver (II) fluoride (2.4 g, 16.71 mmol) in 10 mL anhydrous MeCN. The reaction (with workup and purification) was followed according to the general procedure to afford **3-chloro-2-fluoro-4-methylquinoline** as a whitish solid (203 mg, 1.03 mmol, 22%).

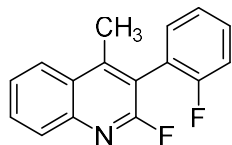
¹H NMR (500 MHz, CDCl₃) δ (ppm) = 7.97 – 7.93 (m, 1H), 7.91 (d, *J* = 8.0 Hz, 1H), 7.71 (ddd, *J* = 8.3, 7.0, 1.2 Hz, 1H), 7.60 – 7.55 (m, 1H), 2.79 (s, 3H).

¹³C NMR (101 MHz, CDCl₃) δ (ppm) = 156.03 (d, *J* = 239.5 Hz), 147.22 (d, *J* = 3.5 Hz), 143.13 (d, *J* = 16.2 Hz), 130.43 (d, *J* = 1.0 Hz), 128.82 (d), 127.55 (d, *J* = 2.0 Hz), 126.86 (d, *J* = 2.6 Hz), 124.14 (d), 116.17 (d, *J* = 37.8 Hz), 15.78 (d, *J* = 3.7 Hz).

¹⁹F NMR (470 MHz, CDCl₃) δ (ppm) = -68.24.

MS (APCI) = 196.6 calculated [M]⁺ for C₁₀H₇ClFN; experimental 195.9.

DKR Substrate, 74



To 3-(2-fluorophenyl)-4-methylquinoline (2.6 g, 11.0 mmol) was added silver (II) fluoride (5.6 g, 38.9 mmol) in 22.0 mL anhydrous MeCN. The reaction (with workup and purification) was followed according to the general

procedure to afford **2-fluoro-3-(2-fluorophenyl)-4-methylquinoline**, (\pm)-**74** as a pale beige solid (1.6 g, 6.6 mmol, 60%).

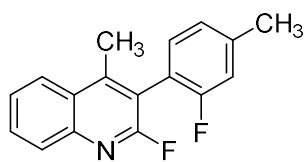
$^1\text{H NMR}$ (400 MHz, CDCl_3) δ (ppm) = 8.06 (d, $J = 8.3$ Hz, 1H), 8.01 (d, $J = 8.4$ Hz, 1H), 7.76 (t, $J = 7.6$ Hz, 1H), 7.60 (t, $J = 7.6$ Hz, 1H), 7.51 – 7.43 (m, 1H), 7.36 – 7.31 (m, 1H), 7.29 (d, $J = 7.3$ Hz, 1H), 7.25 – 7.20 (m, 1H), 2.57 (s, 3H).

$^{13}\text{C NMR}$ (101 MHz, CDCl_3) δ (ppm) = 161.48, 159.93, 159.02, 157.54, 149.44 (d, $J = 5.4$ Hz), 144.96 (d, $J = 17.2$ Hz), 132.26 (dd, $J = 2.8, 0.9$ Hz), 130.74 (d, $J = 8.1$ Hz), 130.63 (d, $J = 0.9$ Hz), 128.71 (d, $J = 1.6$ Hz), 127.13 (d, $J = 1.9$ Hz), 126.38 (d, $J = 2.4$ Hz), 124.59 (d, $J = 0.9$ Hz), 124.33 (d, $J = 3.7$ Hz), 116.06 (d, $J = 21.9$ Hz), 16.33 (dd, $J = 3.8, 1.4$ Hz).

$^{19}\text{F NMR}$ (376 MHz, CDCl_3) δ (ppm) = -61.50, -112.34.

MS (APCI) = 255.3 calculated $[\text{M}]^+$ for $\text{C}_{16}\text{H}_{11}\text{F}_2\text{N}$; experimental 255.8.

DKR Substrate, **1d**



To 3-(2-fluoro-4-methylphenyl)-4-methylquinoline (530 mg, 1.97 mmol) was added silver (II) fluoride (1.01 g, 6.89 mmol) in 4.0 mL anhydrous MeCN in the glovebox. The reaction (with workup and purification) was followed according to the general procedure to afford **2-fluoro-3-(2-fluoro-4-methylphenyl)-4-methylquinoline**, (\pm)-**1d** as a whitish solid (246 mg, 0.913 mmol, 43%).

$^1\text{H NMR}$ (500 MHz, CDCl_3) δ (ppm) = 8.03 (d, $J = 8.3$ Hz, 1H), 7.99 – 7.96 (m, 1H), 7.75 – 7.71 (m, 1H), 7.59 – 7.55 (m, 1H), 7.19 (t, $J = 7.7$ Hz, 1H), 7.10 – 7.06 (m, 1H), 7.04 (d, $J = 10.4$ Hz, 1H), 2.56 (d, $J = 0.9$ Hz, 3H), 2.43 (s, 3H).

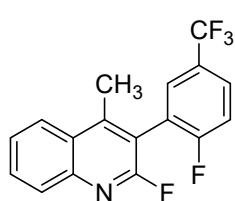
$^{13}\text{C NMR}$ (126 MHz, CDCl_3) δ (ppm) = 160.44 (d, $J = 149.1$ Hz), 158.50 (d, $J = 142.6$ Hz), 149.24 (d, $J = 5.8$ Hz), 144.98 (d, $J = 17.5$ Hz), 141.39 (d, $J = 7.9$ Hz), 131.80 (d, $J = 1.6$ Hz), 130.39,

128.71 (d, $J = 1.4$ Hz), 127.15 (d, $J = 1.7$ Hz), 126.22 (d, $J = 2.6$ Hz), 125.05, 124.52, 118.06 (dd, $J = 16.6, 3.2$ Hz), 117.49 (d, $J = 36.0$ Hz), 116.50 (dd, $J = 21.6, 4.1$ Hz), 21.38 (d, $J = 4.2$ Hz), 16.22.

^{19}F NMR (470 MHz, CDCl_3) δ (ppm) = -67.73 (d, $J = 4.7$ Hz), -115.09 (dt, $J = 11.6, 6.7$ Hz).

MS (APCI) = 269.3 calculated $[\text{M}]^+$ for $\text{C}_{17}\text{H}_{13}\text{F}_2\text{N}$; experimental 269.8.

DKR Substrate, **1e**



To 3-(2-fluoro-5-(trifluoromethyl)phenyl)-4-methylquinoline (700 mg, 2.40 mmol) was added silver (II) fluoride (1.23 g, 8.42 mmol) in 4.8 mL anhydrous MeCN in the glovebox. The reaction (with workup and purification) was followed according to the general procedure to afford **2-fluoro-3-(2-fluoro-5-(trifluoromethyl)phenyl)-4-methylquinoline**, (\pm)-**1e** as a golden amorphous solid (309 mg, 0.963 mmol, 40%)

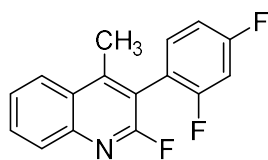
^1H NMR (500 MHz, CDCl_3) δ (ppm) = 8.06 (d, $J = 8.4$ Hz, 1H), 8.00 (d, $J = 8.4$ Hz, 1H), 7.81 – 7.76 (m, 1H), 7.76 – 7.72 (m, 1H), 7.64 (dd, $J = 6.6, 2.1$ Hz, 1H), 7.60 (d, $J = 7.4$ Hz, 1H), 7.35 (t, $J = 8.7$ Hz, 1H), 2.57 (s, 3H).

^{13}C NMR (101 MHz, CDCl_3) δ (ppm) = 162.06 (dd, $J = 253.6, 1.2$ Hz), 158.22 (d, $J = 240.3$ Hz), 149.56 (d, $J = 5.4$ Hz), 145.28 (d, $J = 17.5$ Hz), 130.99, 129.83 (p, $J = 4.2$ Hz), 128.84 (d, $J = 1.6$ Hz), 128.34 – 127.93 (m), 127.32 (d, $J = 3.7$ Hz), 126.94 (d, $J = 1.9$ Hz), 126.60 (d, $J = 2.4$ Hz), 124.58 (d, $J = 0.8$ Hz), 123.69 (q, $J = 271.6$ Hz), 122.39 (d, $J = 3.3$ Hz), 122.29 (dd, $J = 3.3, 15.9$ Hz), 16.44.

^{19}F NMR (376 MHz, CDCl_3) δ (ppm) = -60.73, -61.62, -106.43.

MS (APCI) = 323.3 calculated $[\text{M}]^+$ for $\text{C}_{17}\text{H}_{11}\text{F}_4\text{NO}$; experimental 323.9.

DKR Substrate, 1f



To 3-(2,4-difluorophenyl)-4-methylquinoline (588 mg, 2.30 mmol) was added silver (II) fluoride (1.18 g, 8.06 mmol) in 4.6 mL anhydrous MeCN in the glovebox. The reaction (with workup and purification) was followed according to the general procedure to afford **3-(2,4-difluorophenyl)-2-fluoro-4-methylquinoline**, (\pm)-**1f** as a pale-yellow solid (465 mg, 1.7 mmol, 74%).

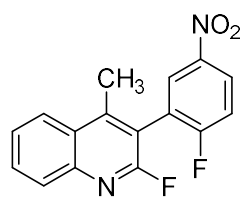
^1H NMR (500 MHz, CDCl_3) δ (ppm) = 8.06 – 8.03 (m, 1H), 7.98 (d, J = 8.4 Hz, 1H), 7.76 (t, J = 7.6 Hz, 1H), 7.60 (t, J = 7.7 Hz, 1H), 7.30 (q, J = 7.6, 7.2 Hz, 1H), 7.03 (ddd, J = 8.6, 6.6, 2.4 Hz, 1H), 6.99 (td, J = 9.2, 2.5 Hz, 1H), 2.56 (s, 3H).

^{13}C NMR (126 MHz, CDCl_3) δ (ppm) = 163.39 (dd, J = 250.9, 11.9 Hz), 161.43 (d, J = 12.4 Hz), 159.50 (d, J = 28.9 Hz), 157.70, 149.48 (d, J = 5.9 Hz), 145.15 (d, J = 17.6 Hz), 133.05 (t, J = 7.0 Hz), 130.71 (d, J = 1.0 Hz), 128.82 (d, J = 1.6 Hz), 127.08 (d, J = 1.9 Hz), 126.44 (dd, J = 2.4, 0.5 Hz), 124.57 (d, J = 1.0 Hz), 116.50 (d, J = 36.2 Hz), 111.79 (d, J = 25.3 Hz), 104.55 (t, J = 25.7 Hz), 16.27 (d, J = 3.5 Hz).

^{19}F NMR (470 MHz, CDCl_3) δ (ppm) = -61.61 (t, J = 4.0 Hz), -76.59, -107.65 (dt, J = 14.9, 8.1 Hz).

MS (APCI) = 273.3 calculated $[\text{M}]^+$ for $\text{C}_{16}\text{H}_{10}\text{F}_3\text{N}$; experimental 273.8.

DKR Substrate, 1g



To 3-(2-fluoro-5-nitrophenyl)-4-methylquinoline (460 mg, 1.63 mmol) was added silver (II) fluoride (831.8 mg, 5.70 mmol) in 3.3 mL anhydrous MeCN in the glovebox. The reaction (with workup and purification) was followed

according to the general procedure to afford **2-fluoro-3-(2-fluoro-5-nitrophenyl)-4-methylquinoline**, (\pm)-**1g** as yellow solid (206 mg, 0.684 mmol, 42%)

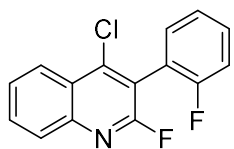
$^1\text{H NMR}$ (400 MHz, CDCl_3) δ (ppm) = 8.38 (ddd, $J = 9.1, 4.3, 2.9$ Hz, 1H), 8.29 (dd, $J = 6.0, 2.8$ Hz, 1H), 8.08 – 8.05 (m, 1H), 7.99 (d, $J = 8.3$ Hz, 1H), 7.82 – 7.77 (m, 1H), 7.66 – 7.60 (m, 1H), 7.42 – 7.37 (m, 1H), 2.59 (d, $J = 0.9$ Hz, 3H).

$^{13}\text{C NMR}$ (101 MHz, CDCl_3) δ (ppm) = 163.77 (d, $J = 258.9$ Hz), 157.91 (d, $J = 240.2$ Hz), 149.70 (d, $J = 5.2$ Hz), 145.37 (d, $J = 17.5$ Hz), 144.34, 128.88 (d, $J = 1.7$ Hz), 128.36 (d, $J = 4.8$ Hz), 127.15 (d, $J = 10.1$ Hz), 126.83 (d, $J = 1.9$ Hz), 126.78 (d, $J = 2.5$ Hz), 126.52 (d, $J = 10.1$ Hz), 124.62, 122.92 (dd, $J = 19.1, 3.3$ Hz), 117.18 (d, $J = 24.8$ Hz), 114.95 (d, $J = 36.3$ Hz), 16.41 (dd, $J = 3.9, 1.4$ Hz).

$^{19}\text{F NMR}$ (376 MHz, CDCl_3) δ (ppm) = -61.69 (d, $J = 5.6$ Hz), -100.89 (p, $J = 5.7$ Hz).

MS (APCI) = 300.3 calculated $[\text{M}]^+$ for $\text{C}_{16}\text{H}_{10}\text{F}_2\text{N}_2\text{O}_2$; experimental 300.8.

DKR Substrate, **1h**



To 4-chloro-3-(2-fluorophenyl)quinoline (562 mg, 2.18 mmol) was added silver (II) fluoride (636.12 mg, 7.63 mmol) and dissolved in anhydrous 4.4 mL MeCN in the glovebox. The reaction (with workup and purification) was

followed according to the general procedure to afford **4-chloro-2-fluoro-3-(2-fluorophenyl)quinoline**, (\pm)-**1h** as a pale yellowish solid (346 mg, 1.25 mmol, 43%).

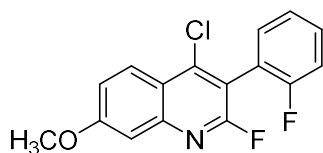
$^1\text{H NMR}$ (400 MHz, CDCl_3) δ (ppm) = 8.27 – 8.20 (m, 1H), 7.99 (d, $J = 8.3$ Hz, 1H), 7.78 (ddd, $J = 8.4, 7.0, 1.3$ Hz, 1H), 7.64 – 7.59 (m, 1H), 7.47 (dddd, $J = 8.3, 7.2, 5.3, 1.8$ Hz, 1H), 7.41 (td, $J = 7.4, 1.7$ Hz, 1H), 7.28 (td, $J = 7.6, 1.1$ Hz, 1H), 7.26 – 7.20 (m, 1H).

^{13}C NMR (101 MHz, CDCl_3) δ (ppm) = 160.31 (d, J = 191.3 Hz), 157.87 (d, J = 184.0 Hz), 145.65 (d, J = 7.5 Hz), 145.10 (d, J = 18.3 Hz), 131.99 (d, J = 2.5 Hz), 131.65 (d, J = 1.1 Hz), 131.29 (d, J = 8.2 Hz), 128.42 (d, J = 1.7 Hz), 127.34 (d, J = 2.6 Hz), 125.42 (d, J = 2.5 Hz), 124.91 (d, J = 1.3 Hz), 124.23 (d, J = 3.7 Hz), 119.51 (dd, J = 16.0, 3.5 Hz), 117.61 (d, J = 39.8 Hz), 115.99 (d, J = 21.5 Hz).

^{19}F NMR (376 MHz, CDCl_3) δ (ppm) = -60.57 (d, J = 6.7 Hz), -112.66 – -112.74 (m).

MS (APCI) = 275.7 calculated $[\text{M}]^+$ for $\text{C}_{15}\text{H}_8\text{ClF}_2\text{N}$; experimental 276.1

DKR Substrate, **1i**



To 3-(2-fluorophenyl)-7-methoxy-4-methylquinoline (500 mg, 1.738 mmol) was added silver (II) fluoride (887.4 mg, 6.08 mmol, 3.5 equiv) and dissolved in anhydrous 17.0 mL MeCN in the glovebox. The

reaction (with workup and purification) was followed according to the general procedure to afford **4-chloro-3-(2-fluorophenyl)-7-methoxyquinoline**, (\pm)-**1i** as a white solid (249 mg, 0.815 mmol, 47%).

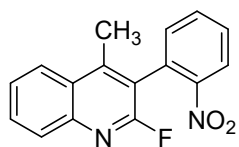
^1H NMR (400 MHz, CDCl_3) δ (ppm) = 8.15 (d, J = 9.2 Hz, 1H), 7.51 – 7.45 (m, 1H), 7.42 – 7.38 (m, 1H), 7.33 – 7.29 (m, 2H), 7.28 – 7.26 (m, 1H), 7.24 (d, J = 9.3 Hz, 1H), 3.97 (d, J = 0.8 Hz, 3H).

^{13}C NMR (101 MHz, CDCl_3) δ (ppm) = 162.62, 160.80 (d, J = 136.7 Hz), 158.36 (d, J = 128.9 Hz), 147.38 (d, J = 19.1 Hz), 145.44 (d, J = 7.8 Hz), 131.71 (d, J = 109.1 Hz), 126.22 (d, J = 5.3 Hz), 124.22, 120.45 (d, J = 2.8 Hz), 120.10 (d, J = 7.8 Hz), 116.04 (d, J = 21.5 Hz), 114.79 (d, J = 39.2 Hz), 107.14 (d, J = 8.5 Hz), 55.91 (d, J = 10.2 Hz).

^{19}F NMR (376 MHz, CDCl_3) δ (ppm) = -61.07 (d, J = 6.8 Hz), -112.76 – -112.85 (m).

MS (APCI) = 305.7 calculated $[M+H]^+$ for $C_{16}H_{10}ClF_2NO$; experimental 306.1.

DKR/KR Hybrid Substrate, 98



To 4-methyl-3-(2-nitrophenyl)quinoline (390 mg, 1.477 mmol) was added silver (II) fluoride (754 mg, 5.169 mmol) and dissolved in anhydrous 14.7 mL MeCN in the glovebox. The reaction (with workup and purification) was

followed according to the general procedure to afford **2-fluoro-4-methyl-3-(2-nitrophenyl)quinoline**, (\pm)-**98** as a pale yellowish solid (202 mg, 0.716 mmol, 49%).

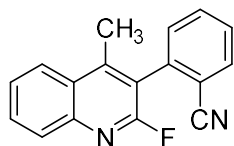
1H NMR (400 MHz, $CDCl_3$) δ (ppm) = 8.24 (d, J = 8.2 Hz, 1H), 8.03 – 7.96 (m, 2H), 7.76 (t, J = 7.2 Hz, 2H), 7.65 (t, J = 7.8 Hz, 1H), 7.59 (t, J = 7.6 Hz, 1H), 7.39 (d, J = 7.5 Hz, 1H), 2.47 (s, 3H).

^{13}C NMR (101 MHz, $CDCl_3$) δ (ppm) = 157.78 (d, J = 238.8 Hz), 148.78, 147.32 (d, J = 5.5 Hz), 144.96 (d, J = 17.5 Hz), 133.66, 132.96, 130.65, 129.91, 129.21 (d, J = 3.2 Hz), 128.84 (d, J = 1.6 Hz), 127.03 (d, J = 1.7 Hz), 126.49 (d, J = 2.4 Hz), 125.21, 124.43, 120.19 (d, J = 36.7 Hz), 16.29 (d, J = 3.8 Hz).

^{19}F NMR (376 MHz, $CDCl_3$) δ (ppm) = -62.59.

MS (APCI) = 283.3 calculated $[M]^+$ for $C_{16}H_{11}FN_2O$; experimental 282.8.

DKR/KR Hybrid Substrate, 100



To 2-(4-methylquinolin-3-yl)benzonitrile (76 mg, 0.310 mmol) was added silver (II) fluoride (159.0 mg, 1.09 mmol) in 1.0 mL anhydrous MeCN in the glovebox. The reaction (with workup and purification) was followed

according to the general procedure to afford **2-(2-fluoro-4-methylquinolin-3-yl)benzonitrile**, (\pm)-**100** as a pale yellowish oil (52 mg, 0.198 mmol, 64%).

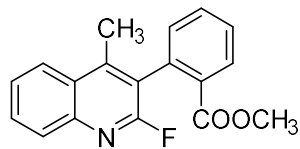
$^1\text{H NMR}$ (400 MHz, CDCl_3) δ (ppm) = 7.99 – 7.93 (m, 3H), 7.72 (ddd, J = 8.4, 6.9, 1.6 Hz, 2H), 7.61 – 7.50 (m, 2H), 6.94 (d, J = 1.0 Hz, 1H), 2.73 (d, J = 1.0 Hz, 3H).

$^{13}\text{C NMR}$ (101 MHz, CDCl_3) δ (ppm) = 149.36 (d, J = 2.1 Hz), 145.86, 140.39, 136.33, 129.80, 128.76 (d, J = 2.8 Hz), 128.18, 128.12, 127.06 (d, J = 2.1 Hz), 123.54 – 123.39 (m), 121.72 (d, J = 1.8 Hz), 121.44, 118.70, 118.56, 110.98 (d, J = 10.6 Hz), 14.66 (q, J = 3.9 Hz), 9.57 (d, J = 4.2 Hz).

$^{19}\text{F NMR}$ (470 MHz, CDCl_3) δ (ppm) = -65.81.

MS (APCI) = 262.3 calculated $[\text{M}]^+$ for $\text{C}_{17}\text{H}_{11}\text{FN}_2$; experimental 262.8.

DKR/KR Hybrid Substrate, 102



To methyl 2-(4-methylquinolin-3-yl)benzoate (644 mg, 2.32 mmol) was added silver (II) fluoride (1.11 g, 7.63 mmol) and dissolved in 4.4 mL anhydrous MeCN in the glovebox. The reaction (with workup and purification) was followed according to the general procedure to afford **methyl 2-(2-fluoro-4-methylquinolin-3-yl)benzoate**, (\pm)-**102** as a whitish solid (337 mg, 49% yield).

$^1\text{H NMR}$ (500 MHz, CDCl_3) δ (ppm) = 8.18 (dd, J = 7.9, 1.1 Hz, 1H), 8.01 (d, J = 8.4 Hz, 1H), 7.99 – 7.97 (m, 1H), 7.72 (ddd, J = 8.3, 7.0, 1.3 Hz, 1H), 7.65 (td, J = 7.5, 1.4 Hz, 1H), 7.56 (dtd, J = 9.1, 8.0, 1.3 Hz, 2H), 7.29 (dd, J = 7.8, 1.1 Hz, 1H), 3.66 (s, 3H), 2.45 (s, 3H).

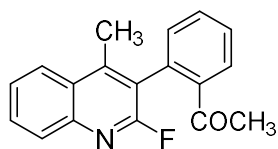
$^{13}\text{C NMR}$ (101 MHz, CDCl_3) δ (ppm) = 166.48, 158.30 (d, J = 239.1 Hz), 146.34 (d, J = 6.0 Hz), 144.44 (d, J = 17.3 Hz), 135.08 (d, J = 2.8 Hz), 132.38, 131.69, 130.91, 130.02, 129.83, 128.55,

128.48 (d, $J = 1.8$ Hz), 125.93 (d, $J = 2.5$ Hz), 124.30, 123.50 (d, $J = 36.7$ Hz), 52.04, 15.98 (d, $J = 3.9$ Hz).

^{19}F NMR (376 MHz, CDCl_3) δ (ppm) = -62.51.

MS (APCI) Calculated: 295.3 calculated $[\text{M}]^+$ for $\text{C}_{18}\text{H}_{14}\text{FNO}_2$; experimental 294.9.

DKR/KR Hybrid Substrate, 104



To 1-(2-(4-methylquinolin-3-yl)phenyl)ethanone (440 mg, 1.68 mmol) was added silver (II) fluoride (860 mg, 5.89 mmol) and dissolved in 3.4 mL anhydrous MeCN in the glovebox. The reaction (with workup and purification) was followed according to the general procedure to afford **1-(2-(2-fluoro-4-methylquinolin-3-yl)phenyl)ethenone**, (\pm)-**104** as a whitish solid (55 mg, 12% yield).

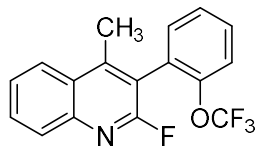
^1H NMR (500 MHz, CDCl_3) δ (ppm) = 8.02 – 7.99 (m, 1H), 7.99 – 7.95 (m, 1H), 7.91 (dd, $J = 7.7, 1.0$ Hz, 1H), 7.72 (ddd, $J = 8.3, 7.1, 1.2$ Hz, 1H), 7.62 (td, $J = 7.5, 1.4$ Hz, 1H), 7.56 (tt, $J = 7.6, 1.5$ Hz, 2H), 7.31 – 7.27 (m, 0H), 2.44 (s, 3H), 2.44 (s, 3H).

^{13}C NMR (126 MHz, CDCl_3) δ (ppm) = 202.5, 161.7, 159.8, 149.5 (d, $J = 6.4$ Hz), 147.3 (d, $J = 18.2$ Hz), 141.2, 135.7 (d, $J = 3.0$ Hz), 134.7 (d, $J = 3.8$ Hz), 134.5, 132.6, 132.0, 131.3 (d, $J = 1.4$ Hz), 129.8 (d, $J = 1.5$ Hz), 128.7, 126.9, 126.1 (d, $J = 38.8$ Hz), 31.3, 18.7.

^{19}F NMR (376 MHz, CDCl_3) δ (ppm) = -83.83.

MS (APCI) Calculated: 279.3 calculated $[\text{M}]^+$ for $\text{C}_{18}\text{H}_{14}\text{FNO}$; experimental 279.1.

KR Substrate, 106



To 4-methyl-3-(2-(trifluoromethoxy)phenyl)quinoline (1.0 g, 3.30 mmol) was added silver (II) fluoride (1.69 g, 11.55 mmol) in 6.6 mL anhydrous

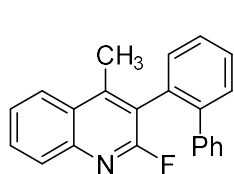
MeCN in the glovebox. The reaction (with workup and purification) was followed according to the general procedure to afford *4-methyl-3-(2-(trifluoromethoxy)phenyl)quinoline*, (\pm)-**106** as a yellow oil (628 mg, 1.94 mmol, 59%).

^1H NMR (500 MHz, CDCl_3) δ (ppm) = 8.04 (d, J = 8.3 Hz, 1H), 8.00 (d, J = 8.4 Hz, 1H), 7.78 – 7.73 (m, 1H), 7.59 (t, J = 7.7 Hz, 1H), 7.53 – 7.49 (m, 1H), 7.42 (t, J = 7.4 Hz, 2H), 7.35 (dd, J = 7.6, 1.7 Hz, 1H), 2.51 (s, 3H).

^{13}C NMR (126 MHz, CDCl_3) δ (ppm) = 158.54 (d, J = 240.5 Hz), 149.02 (d, J = 5.7 Hz), 147.36 (d, J = 1.9 Hz), 145.12 (d, J = 17.6 Hz), 132.39, 130.57, 130.33, 128.78 (d, J = 1.5 Hz), 127.21 (d, J = 3.2 Hz), 127.04, 126.97 (d, J = 1.8 Hz), 126.32 (d, J = 2.3 Hz), 124.55, 121.14, 120.44 (q, J = 258.7 Hz), 118.36 (d, J = 36.3 Hz), 16.11 (q, J = 3.3 Hz).

^{19}F NMR (376 MHz, CDCl_3) δ (ppm) = -56.47, -61.43.

MS (APCI) = 321.3 calculated $[\text{M}]^+$ for $\text{C}_{17}\text{H}_{11}\text{F}_4\text{NO}$; experimental 321.9.



KR Substrate, 108

To 3-([1,1'-biphenyl]-2-yl)-4-methylquinoline (576 mg, 1.96 mmol) was added silver (II) fluoride (1.0 g, 6.85 mmol) in 3.9 mL anhydrous MeCN in the glovebox. The reaction (with workup and purification) was followed according to the general procedure to afford *3-([1,1'-biphenyl]-2-yl)-2-fluoro-4-methylquinoline*, (\pm)-**108** as a yellow solid (205 mg, 0.651 mmol, 33.5%).

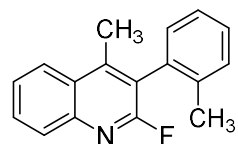
^1H NMR (500 MHz, CDCl_3) δ (ppm) = 7.91 (d, J = 8.4 Hz, 1H), 7.87 (d, J = 8.0 Hz, 1H), 7.70 – 7.65 (m, 1H), 7.55 – 7.46 (m, 4H), 7.32 (d, J = 7.7 Hz, 1H), 7.14 (ddd, J = 10.4, 4.5, 2.2 Hz, 5H), 2.32 (s, 3H).

¹³C NMR (126 MHz, CDCl₃) δ (ppm) = 159.88, 157.98, 147.97 (d, *J* = 6.1 Hz), 144.70 (d, *J* = 17.5 Hz), 141.78 (d, *J* = 231.2 Hz), 132.12 (d, *J* = 3.0 Hz), 131.02, 130.31, 129.99, 128.87, 128.80, 128.62 (d, *J* = 1.6 Hz), 128.14 (d, *J* = 0.6 Hz), 127.48, 127.09, 126.93 (d, *J* = 1.8 Hz), 126.00 (d, *J* = 2.2 Hz), 124.38, 123.30 (d, *J* = 36.2 Hz), 16.14 (dd, *J* = 4.1, 2.2 Hz).

¹⁹F NMR (376 MHz, CDCl₃) δ (ppm) = -86.27.

MS (APCI) = 313.4 calculated [M]⁺ for C₂₂H₁₆FN; experimental 313.9.

KR Substrate, 110



To 4-methyl-3-(*o*-tolyl)quinoline (654 mg, 2.80 mmol) was added silver (II) fluoride (1.43 g, 9.82 mmol) in 5.6 mL anhydrous MeCN in the glovebox. The reaction (with workup and purification) was followed according to the general procedure to afford **2-fluoro-4-methyl-3-(*o*-tolyl)quinoline**, (±)-**110** as a pale-yellow amorphous solid (336 mg, 1.33 mmol, 48%).

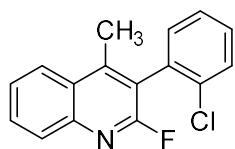
¹H NMR (500 MHz, CDCl₃) δ (ppm) = 8.04 (d, *J* = 8.4 Hz, 1H), 8.00 (d, *J* = 8.4 Hz, 1H), 7.77 – 7.72 (m, 1H), 7.62 – 7.57 (m, 1H), 7.36 (dd, *J* = 6.2, 1.3 Hz, 2H), 7.30 (td, *J* = 6.7, 6.0, 2.8 Hz, 1H), 7.16 (d, *J* = 7.6 Hz, 1H), 2.46 (s, 3H), 2.10 (s, 3H).

¹³C NMR (126 MHz, CDCl₃) δ (ppm) = 158.91 (d, *J* = 240.0 Hz), 148.19 (d, *J* = 6.5 Hz), 144.88 (d, *J* = 17.2 Hz), 137.00, 133.27 (d, *J* = 2.9 Hz), 130.30, 130.15, 130.09, 128.71, 128.63, 127.23 (d, *J* = 1.7 Hz), 126.16 (d, *J* = 2.4 Hz), 126.06, 124.43, 122.99 (d, *J* = 36.8 Hz), 19.83 (d, *J* = 0.7 Hz), 15.88 (dt, *J* = 6.0, 2.6 Hz).

¹⁹F NMR (376 MHz, CDCl₃) δ (ppm) = -86.29.

MS (APCI) = 251.3 calculated [M]⁺ for C₁₇H₁₄FN; experimental 251.9.

KR Substrate, 112



To 3-(2-chlorophenyl)-4-methylquinoline (466 mg, 1.8395 mmol) was added silver (II) fluoride (938 mg, 6.428 mmol) and dissolved in 3.7 mL anhydrous MeCN in the glovebox. The reaction (with workup and purification) was

followed according to the general procedure to afford **3-(2-chlorophenyl)-2-fluoro-4-methylquinoline**, (\pm)-**112** as a pale yellowish oil (321 mg, 1.12 mmol, 65%).

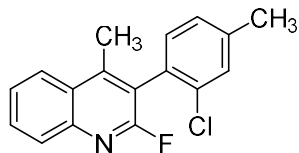
^1H NMR (400 MHz, CDCl_3) δ (ppm) = 8.05 (d, J = 8.4 Hz, 1H), 8.00 (d, J = 7.7 Hz, 1H), 7.75 (ddd, J = 8.4, 6.9, 1.5 Hz, 1H), 7.58 (d, J = 6.9 Hz, 1H), 7.56 – 7.54 (m, 1H), 7.43 – 7.37 (m, 2H), 7.32 – 7.28 (m, 1H), 2.49 (s, 3H).

^{13}C NMR (126 MHz, CDCl_3 , X-C coupling where X = F, Cl) δ (ppm) = 159.69 – 157.70 (m), 148.95 (d, J = 5.7 Hz), 147.45, 145.05 (d, J = 17.2 Hz), 142.13, 140.38, 136.10, 134.92, 134.69, 134.13, 132.10, 131.37 (d, J = 11.0 Hz), 130.75, 130.49 – 130.22 (m), 129.98 (d, J = 9.1 Hz), 129.27 – 128.55 (m), 128.37 – 127.83 (m), 127.15 (d, J = 18.1 Hz), 126.25 (d, J = 12.9 Hz), 125.09 (d, J = 140.2 Hz), 124.19, 15.56 (d, J = 2.9 Hz).

^{19}F NMR (470 MHz, CDCl_3) δ (ppm) = -62.15.

MS (APCI) = 271.2 calculated $[\text{M}]^+$ for $\text{C}_{16}\text{H}_{11}\text{ClFN}$; experimental 271.8.

KR Substrate, 114



To 3-(2-chloro-4-methylphenyl)-4-methylquinoline (475 mg, 1.78 mmol) was added silver (II) fluoride (906 mg, 6.21 mmol) and dissolved in 17.7 mL anhydrous MeCN in the glovebox. The reaction (with workup and purification) was followed according to the general procedure to afford **3-(2-chloro-4-**

methylphenyl)-2-fluoro-4-methylquinoline, (\pm)-**114** as a pale yellowish oil (321 mg, 1.18 mmol, 65%).

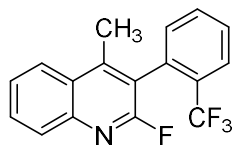
$^1\text{H NMR}$ (400 MHz, CDCl_3) δ (ppm) = 8.04 (d, $J = 8.4$ Hz, 1H), 7.99 (d, $J = 8.4$ Hz, 1H), 7.75 (t, $J = 8.4$ Hz, 1H), 7.59 (t, $J = 8.4$ Hz, 1H), 7.38 (s, 1H), 7.19 (d, $J = 4.3$ Hz, 2H), 2.50 (s, 3H), 2.43 (s, 3H).

$^{13}\text{C NMR}$ (101 MHz, CDCl_3) δ (ppm) = 158.75 (d, $J = 240.2$ Hz), 148.97 (d, $J = 5.7$ Hz), 145.11 (d, $J = 17.3$ Hz), 140.42, 134.18, 131.45, 130.41, 130.34 (d, $J = 1.8$ Hz), 129.75 (d, $J = 3.2$ Hz), 128.80, 127.91, 127.11 (d, $J = 1.8$ Hz), 126.22 (d, $J = 2.2$ Hz), 124.56, 121.07 (d, $J = 36.4$ Hz), 21.20, 16.01.

$^{19}\text{F NMR}$ (376 MHz, CDCl_3) δ (ppm) = -62.24.

MS (APCI) = 285.7 calculated $[\text{M}]^+$ for $\text{C}_{17}\text{H}_{13}\text{ClFN}$; experimental 285.8.

KR Substrate, 73



To 4-methyl-3-(2-(trifluoromethyl)phenyl)quinoline (595 mg, 2.07 mmol) was added silver (II) fluoride (1.06 g, 7.25 mmol) and dissolved in 4.1 mL anhydrous MeCN in the glovebox. The reaction (with workup and

purification) was followed according to the general procedure to afford *2-fluoro-4-methyl-3-(2-(trifluoromethyl)phenyl)quinoline*, (\pm)-**115** as a pale yellowish oil (561 mg, 1.84 mmol, 89%).

$^1\text{H NMR}$ (500 MHz, CDCl_3) δ (ppm) = 8.02 (d, $J = 6.8$ Hz, 1H), 8.00 (d, $J = 8.4$ Hz, 1H), 7.83 (d, $J = 8.1$ Hz, 1H), 7.78 – 7.73 (m, 1H), 7.67 – 7.64 (m, 1H), 7.61 – 7.57 (m, 2H), 7.31 (d, $J = 7.2$ Hz, 1H), 2.41 (d, $J = 2.1$ Hz, 3H).

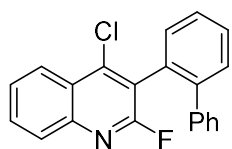
$^{13}\text{C NMR}$ (126 MHz, CDCl_3) δ (ppm) = 158.50 (d, $J = 239.8$ Hz), 148.86 (d, $J = 5.7$ Hz), 145.19 (d, $J = 17.2$ Hz), 132.70, 132.18, 131.85, 130.59, 129.79 (q, $J = 29.8$ Hz), 128.87 (d, $J = 11.0$ Hz),

126.84, 126.52 (q, $J = 5.2$ Hz), 126.38 (d, $J = 2.3$ Hz), 124.51, 122.75 (q, $J = 274.1$ Hz), 120.77 (d, $J = 37.2$ Hz).

^{19}F NMR (376 MHz, CDCl_3) δ (ppm) = -60.64, -61.02.

MS (APCI) = 305.3 calculated $[\text{M}]^+$ for $\text{C}_{17}\text{H}_{11}\text{F}_4\text{N}$; experimental 305.9.

3-([1,1'-biphenyl]-2-yl)-4-chloro-2-fluoroquinoline (starting material for DKR substrate 117)



To 4-chloro-3-(2-(trifluoromethyl)phenyl)quinoline (595 mg, 2.07 mmol) was added silver (II) fluoride (1.06 g, 7.25 mmol, 3.5 equiv) and dissolved in 4.1 mL anhydrous MeCN in the glovebox. The reaction (with workup and

purification) was followed according to the general procedure to afford **3-([1,1'-biphenyl]-2-yl)-4-chloro-2-fluoroquinoline** as a pale yellowish oil (602 mg, 1.803 mmol, 87%).

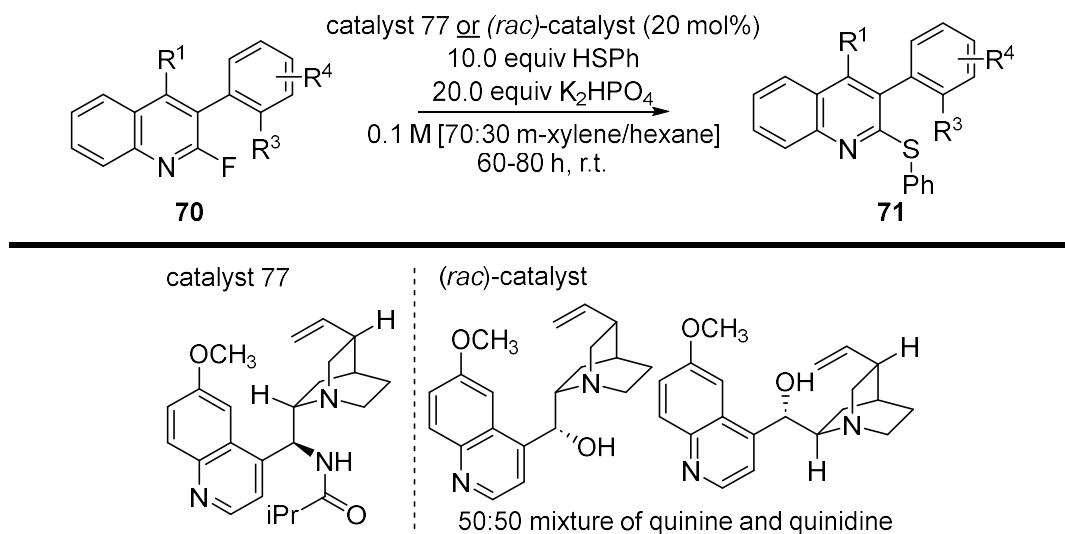
^1H NMR (400 MHz, CDCl_3) δ (ppm) = 8.18 (d, $J = 8.5$ Hz, 1H), 7.93 (d, $J = 7.0$ Hz, 1H), 7.74 (ddd, $J = 8.4, 6.9, 1.5$ Hz, 1H), 7.61 – 7.49 (m, 4H), 7.40 (dd, $J = 7.5, 1.4$ Hz, 1H), 7.25 – 7.20 (m, 2H), 7.20 – 7.13 (m, 3H).

^{13}C NMR (101 MHz, CDCl_3) δ (ppm) = 158.23 (d, $J = 241.2$ Hz), 144.88 (d, $J = 1.8$ Hz), 141.60 (d, $J = 217.9$ Hz), 130.47 (d, $J = 3.9$ Hz), 128.40 (d, $J = 1.8$ Hz), 127.15 (d, $J = 2.5$ Hz), 125.30 (d, $J = 2.5$ Hz), 124.80 (d, $J = 1.8$ Hz), 123.54 (d, $J = 39.6$ Hz), 115.15 (d, $J = 21.5$ Hz).

^{19}F NMR (376 MHz, CDCl_3) δ (ppm) = -58.60.

MS (APCI) = 333.8 calculated $[\text{M}+\text{H}]^+$ for $\text{C}_{21}\text{H}_{13}\text{ClFN}$; experimental 334.1.

2.2.13 General S_NAr Strategy to yield enantioenriched 3-aryl-2-(phenylthio)quinolines (2)



Equation 43. Atroposelective S_NAr optimization can be found in ‘**Section 2.2.7 Reaction Development.**’

To fluoroquinoline **70** (1.0 equiv) in a 1.6-dram vial equipped with a stir bar was added K₂HPO₄ (20.0 equiv) and 20 mol% catalyst 77. The reaction was then taken into 0.1 M solvent mixture of anhydrous 70% *m*-xylene and 30% *n*-hexanes (anhydrous, HPLC grade) and stirred until all the non-dissolved solids were suspended. Thiophenol (10.0 equiv) was then added to the reaction. The S_NAr reaction was stirred vigorously (up to 1500 rpm) at room temperature for up to 60-80 h (*generally, the reactions stirred for 60 h, but other substrates required more time to reach optimal conversions and yields*).

The resulting reaction was then diluted with CH₂Cl₂ and subsequently quenched with deionized H₂O. The organic layer was isolated through liquid extraction, and subsequently partitioned with 1.0 N NaOH (aq.). The resulting organic layer was extracted, washed with saturated aqueous NaCl, re-extracted, and dried over Na₂SO₄. After filtration, the filtrate was isolated *in vacuo* at 25 °C. The crude was then purified by FCC using *n*-hexanes:EtOAc = 0% →

5-10% to afford the pure enantioenriched (R_a)-71 (and recovered enantioenriched (S_a)-70 for KR) in optimal yields.

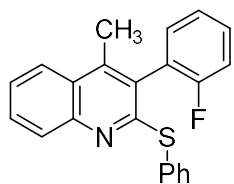
In some cases, the determined R_s of both 2 and 1 were very similar, resulting in mixtures that were either difficult to purify or had led to co-elution. For these cases, the resulting mixture was first isolated *in vacuo* at 25 °C. The purified mixture was then oxidized to sulfone 3. This afforded a larger difference in polarity and allowed us to purify our products. For more details regarding our oxidation method, see “Section 2.2.14 Post-translational Modifications of 2 (and enantioenriched-1).”

For racemic HPLC standards: We either 1) switched catalyst 77 to (*rac*)-catalyst, or 2) heated our enantioenriched compounds to racemization. For our racemization via heating methods, see “Section 2.2.18 Racemization Kinetics” for more details regarding procedure.

Analytical chiral HPLC was used for determination of e.r., ee%, conversions, and *s*-factors of enantioenriched 2. To improve e.r. (or achieve enantiopurity) post-DKR, enantioenriched products were either:

- (1) triturated using 100% HPLC grade *n*-hexanes, or
- (2) partially dissolving the product in small amounts of reagent-pure DCE and then recrystallization with slow addition of HPLC grade *n*-hexane. The resulting liquor and precipitate were isolated and separated.

DKR Product, 74



Following the general procedure: **72** (50 mg, 0.2033 mmol, 1.0 equiv), catalyst **77** (16.6 mg, 0.04065 mmol, 0.2 equiv) and K_2HPO_4 (707 mg, 4.065 mmol, 20.0 equiv) were added into a vial and dissolved in 1.42 mL *m*-xylene and 609

μ L *n*-hexanes. Thiophenol (228 μ L, 2.236 mmol, 11.0 equiv) was then added to the reaction. The workup and purification following the general procedure afforded **3-(2-fluorophenyl)-4-methyl-2-(phenylthio)quinoline, 74** as a white solid (64 mg, 0.185 mmol, 91%, 10:90 e.r.).

For racemic standards: 20 mol% (*rac*)-catalyst (13.2 mg, 0.04065 mmol) was used. The reaction was stirred at room temperature for 4 days.

Scale-up Procedure of **74**: Following the general procedure, **72** (1.0 g, 3.906 mmol, 1.0 equiv), catalyst **77** (318 mg, 0.781 mmol, 0.2 equiv) and K_2HPO_4 (13.6 g, 78.12 mmol, 20.0 equiv) were added into a 250 mL round-bottom flask that was equipped with a stir bar. A mixture of 28 mL *m*-xylene and 12 mL *n*-hexanes was then added. Thiophenol (10 mL, 9.8 mmol, 10.0 equiv) was added to the reaction, and the reaction was left to stir for 3 days at room temperature. The workup and purification following the general procedure afforded the final product **74** as a white solid (1.05 g, 3.04 mmol, 78%, 13:87 e.r.).

1H NMR (500 MHz, $CDCl_3$) δ (ppm) = δ 7.99 (d, J = 8.4 Hz, 1H), 7.85 (d, J = 8.4 Hz, 1H), 7.67 – 7.61 (m, 3H), 7.55 – 7.48 (m, 2H), 7.46 – 7.40 (m, 4H), 7.35 (td, J = 7.5, 1.1 Hz, 1H), 7.29 (t, J = 8.8 Hz, 1H), 2.46 (s, 3H).

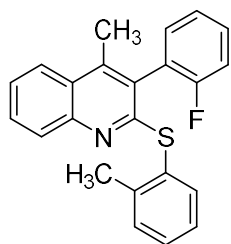
^{13}C NMR (126 MHz, $CDCl_3$) δ (ppm) = 160.12 (d, J = 246.7 Hz), 158.94, 147.41, 142.61, 134.86, 132.41, 131.30, 130.65 (d, J = 8.0 Hz), 129.33, 129.22, 128.74, 128.29, 127.17, 126.24, 125.66, 124.67 (d, J = 17.0 Hz), 124.43, 124.40, 124.15, 115.99 (d, J = 21.8 Hz), 15.78 (d, J = 3.1 Hz).

^{19}F NMR (376 MHz, $CDCl_3$) δ (ppm) = -112.02 (q, J = 7.4 Hz).

MS (APCI) = 345.4 calculated $[M]^+$ for $C_{22}H_{16}FNS$; experimental 344.9.

HRMS (ESI) = 346.1066 calculated $[M+H]^+$ found 346.1075.

DKR Product, **81**



Following the general procedure: **72** (50 mg, 0.2033 mmol, 1.0 equiv), catalyst **77** (16.6 mg, 0.04065 mmol, 0.2 equiv) and K_2HPO_4 (707 mg, 4.065 mmol, 20.0 equiv) were used. 1.42 mL *m*-xylene and 609 μ L hexane were added. 2-tolylthiol (208.3 μ L, 2.033 mmol, 10.0 equiv) was added to the reaction. The

reaction vial was capped, and then left to stir up to 3 days at room temperature. More 2-tolylthiol (104 μ L, 1.02 mmol, 5.0 equiv) and K_2HPO_4 (354 mg, 2.033 mmol, 10.0 equiv) was added at this temperature, and the resulting reaction stirred for an additional 18 hours. The workup and purification following the general procedure afforded **3-(2-fluorophenyl)-4-methyl-2-(o-tolylthio)quinoline**, **81** as a white solid (37 mg, 0.103 mmol, 56%). Sulfide **81** was taken onto oxidation to sulfone **82** without determination of e.r. See Section K for more details.

For racemic standards: 20 mol% (*rac*)-catalyst (13.2 mg, 0.04065 mmol) was used. The reaction was stirred at room temperature for 2.5 days. The racemic standard was isolated and then subsequently oxidized to the sulfone *rac*-**82**.

1H NMR (500 MHz, $CDCl_3$) δ (ppm) = 7.97 (d, J = 8.3 Hz, 1H), 7.59 (d, J = 7.2 Hz, 1H), 7.49 (d, J = 7.0 Hz, 2H), 7.37 – 7.31 (m, 2H), 7.29 (d, J = 8.8 Hz, 2H), 7.21 (d, J = 8.4 Hz, 1H), 7.19 – 7.14 (m, 3H), 2.42 (s, 3H), 2.29 (s, 3H).

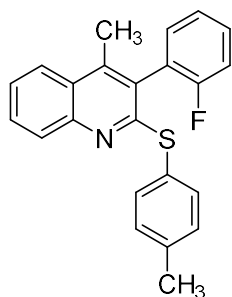
^{13}C NMR (126 MHz, $CDCl_3$) δ (ppm) = 158.90 (s), 142.98 (s), 137.56 (s), 136.18 (s), 135.57 (s), 132.33 (d, J = 3.5 Hz), 130.75 (s), 130.70 (s), 130.50 (s), 130.45 (s), 129.72 (s), 129.70 (s), 129.30

– 129.27 (m), 128.83 (s), 127.57 (s), 127.47 (s), 126.78 (d, $J = 11.5$ Hz), 126.44 (s), 126.22 (s), 125.93 (d, $J = 1.0$ Hz), 124.55 (d, $J = 3.6$ Hz), 124.25 (s).

^{19}F NMR (470 MHz, CDCl_3) δ (ppm) = -113.08.

MS (APCI) = 360.3 calculated $[\text{M}]^+$ for $\text{C}_{23}\text{H}_{18}\text{FNS}$; experimental 359.5.

DKR Product, 83



Following the general procedure: **74** (50 mg, 0.2033 mmol, 1.0 equiv), catalyst **77** (16.6 mg, 0.04065 mmol, 0.2 equiv) and K_2HPO_4 (707 mg, 4.065 mmol, 20.0 equiv) were used. 1.42 mL *m*-xylene and 609 μL *n*-hexanes was added. 2-tolylthiol (208.3 μL , 2.033 mmol, 10.0 equiv) was added to the reaction. The reaction vial was capped, and then left to stir up to 3 days at room temperature.

More 2-tolylthiol (104 μL , 1.02 mmol, 5.0 equiv) and K_2HPO_4 (354 mg, 2.033 mmol, 10.0 equiv) was added at this temperature, and the resulting reaction stirred for an additional 18 hours. The workup and purification followed according to the general procedure afforded **3-(2-fluorophenyl)-4-methyl-2-(*p*-tolylthio)quinoline, 83** as a pale yellow solid (17 mg, 0.047 mmol, 23%, 30:70 e.r.).

For racemic standards: 20 mol% (*rac*)-catalyst (13.2 mg, 0.04065 mmol) was used. The reaction was stirred at room temperature for 2.5 days. The racemic standard was isolated and then subsequently oxidized to the sulfone *rac*-83.

^1H NMR (400 MHz, CDCl_3) δ (ppm) = 7.95 (d, $J = 8.3$ Hz, 1H), 7.77 (d, $J = 8.4$ Hz, 1H), 7.59 (ddt, $J = 8.4, 6.8, 1.5$ Hz, 1H), 7.50 – 7.45 (m, 2H), 7.43 (dd, $J = 8.4, 1.4$ Hz, 2H), 7.37 – 7.34 (m, 1H), 7.31 (d, $J = 7.2$ Hz, 1H), 7.24 (d, $J = 8.9$ Hz, 1H), 7.22 – 7.18 (m, 2H), 2.44 – 2.37 (m, 6H).

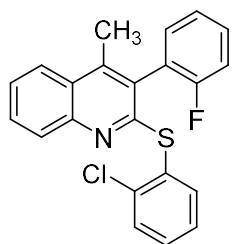
^{13}C NMR (101 MHz, CDCl_3) δ (ppm) = 161.48, 159.45, 159.02, 147.55, 142.50, 138.43, 135.06, 132.51, 130.69 (d, $J = 7.8$ Hz), 129.65, 129.34, 128.81, 127.65, 127.15, 126.29, 125.60, 124.91, 124.74, 124.46, 124.19, 116.10 (d, $J = 21.9$ Hz), 21.47 (d, $J = 3.2$ Hz), 15.81 (d, $J = 3.5$ Hz).

^{19}F NMR (376 MHz, CDCl_3) δ (ppm) = -127.21 (dt, $J = 8.9, 5.8$ Hz).

MS (APCI) = 360.3 calculated $[\text{M}]^+$ for $\text{C}_{23}\text{H}_{18}\text{FN}$ S; experimental 359.5.

HRMS (ESI) = 359.4624 calculated $[\text{M}+\text{H}]^+$ found 360.1223.

DKR Product, 84



Following the general procedure: **74** (25 mg, 0.2033 mmol, 1.0 equiv), catalyst **77** (16.6 mg, 0.04065 mmol, 0.2 equiv) and K_2HPO_4 (707 mg, 4.065 mmol, 20.0 equiv) were used. A mixture of 1.42 mL *m*-xylene and 609 μL *n*-hexanes was added. 2-chlorothiophenol (240 μL , 2.033 mmol, 10.0 equiv) was then

added to the reaction. The reaction vial was capped, and then left to stir up to 3.5 days at room temperature. The workup and purification following the general procedure afforded **2-((2-chlorophenyl)thio)-3-(2-fluorophenyl)-4-methylquinoline**, **84** as a white solid (46 mg, 0.122 mmol, 60%, 35:65 e.r.).

For racemic standards: 20 mol% (*rac*)-catalyst (13.2 mg, 0.04065 mmol) was used. The reaction was stirred at room temperature for 2.5 days.

^1H NMR (400 MHz, CDCl_3) δ (ppm) = 7.97 (d, $J = 6.9$ Hz, 1H), 7.73 (d, $J = 8.6$ Hz, 1H), 7.59 (t, $J = 7.5$ Hz, 2H), 7.48 (t, $J = 6.6$ Hz, 3H), 7.41 (d, $J = 7.4$ Hz, 1H), 7.34 – 7.29 (m, 2H), 7.28 – 7.22 (m, 3H), 2.43 (s, 3H).

^{13}C NMR (126 MHz, CDCl_3) δ (ppm) = 161.28, 159.32, 157.92, 147.38, 143.21, 139.16, 137.21, 132.40 (d, $J = 2.9$ Hz), 131.47, 130.97, 130.84 (d, $J = 8.1$ Hz), 130.07, 130.03 (d, $J = 2.4$ Hz),

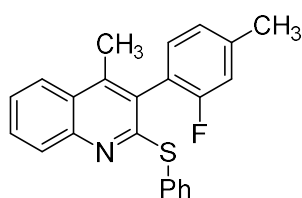
129.55, 129.27, 128.29, 127.41 (d, $J = 7.6$ Hz), 127.07, 126.40, 125.95, 124.72, 124.57 (d, $J = 3.8$ Hz), 124.27, 116.16 (d, $J = 21.9$ Hz), 29.85.

^{19}F NMR (470 MHz, CDCl_3) δ (ppm) = -113.08.

MS (APCI) = 379.9 calculated $[\text{M}]^+$ for $\text{C}_{22}\text{H}_{15}\text{ClFNS}$; experimental 379.8.

HRMS (ESI) = 379.8774 calculated $[\text{M}+\text{H}]^+$ found 380.0635.

DKR Product, **85**



Following the general procedure: **1d** (50 mg, 0.1851 mmol, 1.0 equiv), catalyst **77** (15.1 mg, 0.0370 mmol, 0.2 equiv) and K_2HPO_4 (644 mg, 3.70 mmol, 20.0 equiv) were used. 1.3 mL *m*-xylene and 550 μL *n*-

hexanes were added. Thiophenol (189 μL , 1.851 mmol, 10.0 equiv) was added to the reaction. The reaction vial was capped, and then left to stir up to 4.5 days at room temperature. The workup and purification followed according to the general procedure afforded **3-(2-fluoro-4-methylphenyl)-4-methyl-2-(phenylthio)quinoline, 85** as a white solid (47.5 mg, 0.131 mmol, 71%, 14:86 e.r.).

For racemic standards: 20 mol% (*rac*)-catalyst (12.0 mg, 0.0370 mmol) was used. The reaction was stirred at room temperature for 2.5 days.

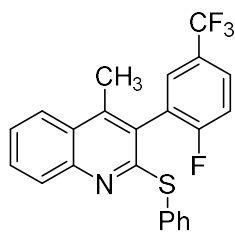
^1H NMR (400 MHz, CDCl_3) δ (ppm) = 7.96 (dd, $J = 8.1, 1.1$ Hz, 1H), 7.76 (dd, $J = 8.2, 1.0$ Hz, 1H), 7.61 – 7.58 (m, 1H), 7.57 – 7.54 (m, 2H), 7.46 (ddd, $J = 8.3, 6.9, 1.3$ Hz, 1H), 7.38 (dd, $J = 5.1, 1.9$ Hz, 3H), 7.23 (d, $J = 7.7$ Hz, 1H), 7.13 (d, $J = 7.1$ Hz, 1H), 7.06 (d, $J = 10.3$ Hz, 1H), 2.48 (d, $J = 0.7$ Hz, 3H), 2.42 (d, $J = 0.6$ Hz, 3H).

^{13}C NMR (101 MHz, CDCl_3) δ (ppm) = 161.23, 159.30, 158.78, 147.41, 142.73, 141.41 (d, $J = 7.8$ Hz), 134.97, 132.03, 131.39, 129.26, 128.76, 128.32, 127.26, 126.35, 125.62, 125.24, 124.19, 121.54 (d, $J = 17.3$ Hz), 116.74, 116.52, 21.53, 15.84.

^{19}F NMR (376 MHz, CDCl_3) δ (ppm) = -122.13 – -122.36 (m).

MS (APCI) = 360.1 calculated $[\text{M}]^+$ for $\text{C}_{23}\text{H}_{18}\text{FNS}$; experimental 359.4.

DKR Product, **86**



Following the general procedure: **1e** (50 mg, 0.155 mmol, 1.0 equiv), catalyst

77 (12.5 mg, 0.03095 mmol, 0.2 equiv) and K_2HPO_4 (538.5 mg, 3.095 mmol,

20.0 equiv) was used. 1.09 mL *m*-xylene and 460 μL hexane was added.

Thiophenol (158 μL , 1.55 mmol, 10.0 equiv) was added to the reaction. The

reaction vial was capped, and then left to stir up to 4.5 days at room temperature. The workup and purification followed according to the general procedure afforded **3-(2-fluoro-5-(trifluoromethyl)phenyl)-4-methyl-2-(phenylthio)quinoline, 86** as a pale yellowish oil (40.6 mg, 0.0980 mmol, 63%, 13:87 e.r.). Trituration was followed according to the general procedure to improve e.r. of **86** (11.2 mg, 0.025 mmol, 9:91 e.r., 28%, recovered solid).

For racemic standards: 20 mol% (*rac*)-catalyst (10.0 mg, 0.03095 mmol) was used. The reaction was stirred at room temperature for 2.5 days.

^1H NMR (400 MHz, CDCl_3) δ (ppm) = 7.97 (dt, J = 8.4, 1.3 Hz, 1H), 7.82 (dt, J = 8.5, 1.3 Hz, 1H), 7.77 – 7.74 (m, 1H), 7.66 – 7.62 (m, 1H), 7.48 (d, J = 1.4 Hz, 1H), 7.37 – 7.34 (m, 1H), 7.32 (d, J = 17.2 Hz, 15H), 2.42 (d, J = 1.5 Hz, 1H).

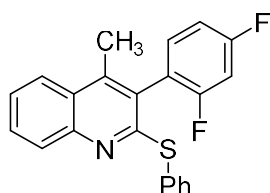
^{13}C NMR (101 MHz, CDCl_3) δ (ppm) = 164.69 (d, J = 10.6 Hz), 162.21 (d, J = 10.6 Hz), 161.61 (d, J = 12.6 Hz), 159.19, 159.06, 147.52, 143.10, 134.81, 133.29 (d, J = 4.5 Hz), 133.20 (d, J = 4.5 Hz), 131.22, 129.58, 129.34, 128.85, 128.42, 126.39, 126.27, 125.86, 124.20, 120.79 (dd, J = 17.4, 4.0 Hz), 111.87 (dd, J = 21.3, 3.7 Hz), 104.58 (t, J = 25.6 Hz), 15.86.

^{19}F NMR (376 MHz, CDCl_3) δ (ppm) = -23.55 (q, J = 8.5 Hz), -23.85 (dt, J = 16.7, 8.4 Hz).

MS (APCI) = 414.1 calculated $[M]^+$ for $C_{23}H_{15}F_4NS$; experimental 413.9.

HRMS (ESI) = 414.0940 calculated $[M+H]^+$ found 414.0953.

DKR Product, 87



Following the general procedure: **1f** (50 mg, 0.183 mmol, 1.0 equiv), 20 mol% catalyst **77** (14.9 mg, 0.0366 mmol) and K_2HPO_4 (637 mg, 3.66 mmol, 20.0 equiv) were used. 1.28 mL *m*-xylene and 549 μ L *n*-hexanes

were added. Thiophenol (187 μ L, 1.83 mmol, 10.0 equiv) was added to the reaction. The reaction vial was capped, and then left to stir up to 4.5 days at room temperature. The workup and purification followed according to the general procedure afforded **3-(2,4-difluorophenyl)-4-methyl-2-(phenylthio)quinoline, 87** as a pale yellowish oil (35 mg, 0.096 mmol, 53%, 12:88 e.r.).

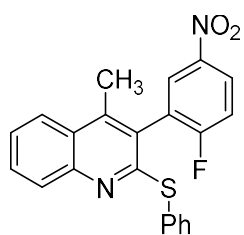
For racemic standards: 20 mol% (*rac*)-catalyst (11.9 mg, 0.0366 mmol) was used. The reaction was stirred at room temperature for 2.5 days.

1H NMR (400 MHz, $CDCl_3$) δ (ppm) = 7.96 (dd, J = 8.7, 1.3 Hz, 1H), 7.77 (dd, J = 8.8, 1.6 Hz, 1H), 7.61 (ddd, J = 8.3, 6.9, 1.4 Hz, 1H), 7.54 – 7.46 (m, 3H), 7.39 – 7.35 (m, 3H), 7.34 – 7.29 (m, 1H), 7.05 (tdd, J = 8.2, 2.5, 1.0 Hz, 1H), 6.98 (td, J = 9.1, 2.5 Hz, 1H), 2.41 (s, 3H).

^{13}C NMR (101 MHz, $CDCl_3$) δ (ppm) = 164.70 (d, J = 10.6 Hz), 162.22 (d, J = 10.6 Hz), 161.62 (d, J = 12.4 Hz), 159.20, 159.07, 147.53, 143.11, 134.98, 134.81, 133.25 (dd, J = 9.5, 4.6 Hz), 131.23, 129.47 (d, J = 23.3 Hz), 128.86, 128.43, 126.39, 126.27, 125.86, 124.22, 120.80 (dd, J = 17.5, 4.1 Hz), 111.87 (dd, J = 21.2, 3.5 Hz), 104.58 (t, J = 25.6 Hz), 15.86.

^{19}F NMR (376 MHz, $CDCl_3$) δ (ppm) = -108.36 (q, J = 8.5 Hz), -108.60 – -108.71 (m).

HRMS (ESI) = 364.0972 calculated $[M+H]^+$ for $C_{22}H_{16}F_2NS$ found 364.0980.



Following the general procedure: **1g** (50 mg, 0.166 mmol, 1.0 equiv), CA9 (in manuscript, **C4**) (13.6 mg, 0.0332 mmol, 0.2 equiv) and K₂HPO₄ (577.7 mg, 3.32 mmol, 20.0 equiv) were used. 1.16 mL *m*-xylene and 498 μL *n*-hexanes were added. Thiophenol (169 μL, 1.66 mmol, 10.0 equiv) was added

to the reaction. The reaction vial was capped, and then left to stir up to 4.5 days at room temperature. The workup and purification followed according to the general procedure afforded **3-(2-fluoro-5-nitrophenyl)-4-methyl-2-(phenylthio)quinoline, 2g** as a pale yellowish oil (55 mg, 0.140 mmol, 84%, 16:84 e.r.).

For racemic standards: 20 mol% (*rac*)-catalyst (10.8 mg, 0.0332 mmol) was used. The reaction was stirred at room temperature for 2.5 days.

Scale-up Procedure of **2g**: Following the general procedure, **1g** (500 mg, 1.66 mmol, 1.0 equiv), CA9 (in manuscript, **C4**) (135.7 mg, 0.332 mmol, 0.2 equiv) and K₂HPO₄ (5.78 g, 33.2 mmol, 20.0 equiv) were added into a 20 mL dram vial that was equipped with a stir bar. 11.6 mL *m*-xylene and 5.0 mL *n*-hexanes were added. Thiophenol (1.7 mL, 16.6 mmol, 10.0 equiv) was added to the reaction, and the reaction was left to stir for 3 days at room temperature. The workup and purification followed according to the general procedure afforded **2g** as a pale yellowish, amorphous solid (635 mg, 98%, 20:80 e.r.).

¹H NMR (400 MHz, CDCl₃) δ (ppm) = 8.36 (ddt, J = 3.5, 2.6, 1.8 Hz, 1H), 8.25 (s, 1H), 7.98 (dt, J = 8.3, 1.3 Hz, 1H), 7.85 – 7.81 (m, 1H), 7.68 – 7.63 (m, 1H), 7.55 – 7.50 (m, 1H), 7.47 – 7.44 (m, 1H), 7.34 (t, J = 1.8 Hz, 1H), 2.42 (d, J = 1.5 Hz, 1H).

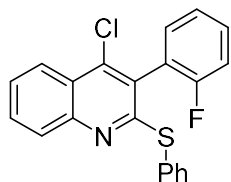
^{13}C NMR (101 MHz, CDCl_3) δ (ppm) = 165.14, 162.57, 157.89, 147.70, 144.45, 143.41, 134.47, 130.90, 130.13, 129.48, 128.97, 128.68 (d, $J = 5.0$ Hz), 128.57, 126.51, 126.48, 126.38, 126.31, 126.09, 125.24, 124.23, 117.12 (d, $J = 24.8$ Hz), 16.07.

^{19}F NMR (376 MHz, CDCl_3) δ (ppm) = -100.80 (q, $J = 5.7$ Hz).

MS (APCI) Calculated: 391.1 calculated $[\text{M}]^+$ for $\text{C}_{16}\text{H}_{10}\text{F}_2\text{N}_2\text{O}_2$; experimental 389.9.

HRMS (ESI) = 391.0917 calculated $[\text{M}+\text{H}]^+$ found 391.0924.

DKR Product, 90



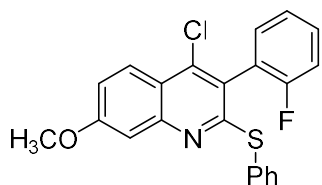
Following the general procedure: **1h** (50 mg, 0.181 mmol, 1.0 equiv), catalyst **77** (14.8 mg, 0.0363 mmol, 0.2 equiv) and K_2HPO_4 (631.6 mg, 3.63 mmol, 20.0 equiv) were used. 1.27 mL *m*-xylene and 543 μL *n*-hexanes were added.

Thiophenol (185 μL , 1.81 mmol, 10.0 equiv) was added to the reaction. The reaction vial was capped, and then left to stir up to 4.5 days at room temperature. The workup and purification were followed according to the general procedure and afforded crude **4-chloro-3-(2-fluorophenyl)-2-(phenylthio)quinoline**, **90**. Crude sample of **90** was then immediately taken oxidized to sulfone **91** without any clean isolation of **91**. See Section K for more details.

For racemic standards: 20 mol% (*rac*)-catalyst (11.8 mg, 0.0363 mmol) was used. The reaction was stirred at room temperature for 2.5 days. The resulting sulfide racemic **2h** was also taken to the oxidized sulfone **3h**.

MS (APCI) Calculated: 365.9 calculated $[\text{M}]^+$ for $\text{C}_{21}\text{H}_{13}\text{ClFNS}$; experimental 365.9.

DKR Product, 92

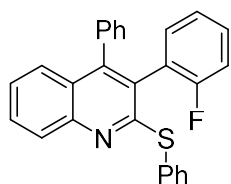


Following the general procedure: **1i** (50 mg, 0.163 mmol, 1.0 equiv), 20 mol% catalyst **77** (13.3 mg, 0.0327 mmol) and K₂HPO₄ (569 mg, 3.27 mmol, 20.0 equiv) were used. 1.14 mL *m*-xylene and 490 μ L *n*-

hexanes were added. Thiophenol (167 μ L, 1.64 mmol, 10.0 equiv) was added to the reaction. The reaction vial was capped, and then left to stir up to 4.5 days at room temperature. The workup and purification were followed according to the general procedure and afforded crude **4-chloro-3-(2-fluorophenyl)-7-methoxy-2-(phenylthio)quinoline, 92**. The crude sample of **92** was then immediately taken oxidized to sulfone **93** without any clean isolation of **2i**. See Section 2.2.14 for more details.

For racemic standards: Enantioenriched **92** was heated to racemization. See Section 2.2.18 for more details. **MS (APCI) Calculated:** 395.9 calculated [M]⁺ for C₂₂H₁₅ClFNOS; experimental 396.5.

DKR Product, 94



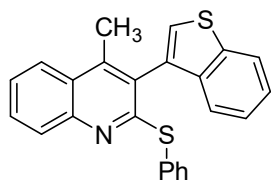
Following the general procedure: **1j** (50 mg, 0.158 mmol, 1.0 equiv), catalyst **77** (13.0 mg, 0.0315 mmol, 0.2 equiv) and K₂HPO₄ (548.6 mg, 3.15 mmol, 20.0 equiv) were used. 1.11 mL *m*-xylene and 471 μ L *n*-hexanes were added.

Thiophenol (161 μ L, 1.58 mmol, 10.0 equiv) was added to the reaction. The reaction vial was capped, and then left to stir up to 4.5 days at room temperature. The workup and purification were followed according to the general procedure and afforded crude **3-(2-fluorophenyl)-4-phenyl-2-(phenylthio)quinoline, 94**. Crude sample of **94** was then immediately taken oxidized to sulfone **95** without any clean isolation of **94**. See Section 2.2.14 for more details. For racemic standards:

Enantioenriched **94** was heated to racemization. See Section 2.2.18 for more details. **MS (APCI)**

Calculated: 407.5 calculated $[M]^+$ for $C_{27}H_{18}FNS$; experimental 407.6.

DKR Product, **96**



Following the general procedure: **1k** (50 mg, 0.166 mmol, 1.0 equiv), catalyst **77** (13.6 mg, 0.0332 mmol, 0.2 equiv) and K_2HPO_4 (577.7 mg, 3.32 mmol, 20.0 equiv) were used. 1.16 mL *m*-xylene and 498 μ L *n*-hexanes

were added. Thiophenol (169 μ L, 1.66 mmol, 10.0 equiv) was added to the reaction. The reaction vial was capped, and then left to stir up to 4.5 days at room temperature. The workup and purification followed according to the general procedure afforded **3-(benzo[b]thiophen-3-yl)-4-methyl-2-(phenylthio)quinoline, 96** as a pale yellowish oil (42 mg, 0.11 mmol, 64%, 14:86 er).

96 was then triturated using 100% HPLC grade *n*-hexanes. The resulting solid and filtrate were isolated; the resulting solid was reportedly more enantioenriched (30 mg, 52%, 3:97 e.r.). Overall yield beginning from **1k** is 46.5%.

For racemic standards: Enantioenriched **96** was heated to racemization. See Section 2.2.18 for more details.

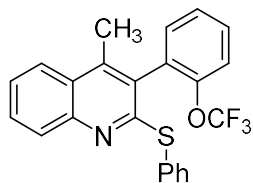
1H NMR (400 MHz, $CDCl_3$) δ (ppm) = 7.99 – 7.95 (m, 2H), 7.78 (d, J = 8.5 Hz, 1H), 7.62 (ddd, J = 8.3, 6.8, 1.4 Hz, 1H), 7.52 – 7.48 (m, 4H), 7.42 (dt, J = 8.0, 4.0 Hz, 1H), 7.36 – 7.32 (m, 5H), 2.38 (s, 3H).

^{13}C NMR (101 MHz, $CDCl_3$) δ (ppm) = 147.53, 140.14, 138.78, 135.00, 132.54, 129.47, 129.36, 128.75, 128.34, 127.20, 125.74, 124.86, 124.69, 124.21, 123.01, 122.80, 113.91, 15.99.

MS (APCI) = 383.5 calculated $[M]^+$ for $C_{24}H_{17}NS_2$; experimental 382.9.

HRMS (ESI) = 384.0887 calculated $[M+H]^+$ found 384.0895.

KR Product, 105



Following the general procedure: **106** (50 mg, 0.187 mmol, 1.0 equiv), catalyst **77** (15.3 mg, 0.0374 mmol, 0.2 equiv) and K_2HPO_4 (551 mg, 3.74 mmol, 20.0 equiv) were used. 1.31 mL *m*-xylene and 561 μ L *n*-hexanes were

added. Thiophenol (190.7 μ L, 1.87 mmol, 10.0 equiv) was added to the reaction. The reaction vial was capped, and then left to stir up to 2.5 days at room temperature. The workup and purification followed according to the general procedure afforded *4-methyl-2-(phenylthio)-3-(2-(trifluoromethoxy)phenyl)quinoline*, **105** as a pale yellowish oil (34 mg, 0.0839 mmol, 45%, 9:91 e.r.) and recovered **1p** as a beige foam (32 mg, 0.101 mmol, 54%, 83:17 e.r.). Conv = 45%, *s* = 21. For racemic standards: 20 mol% (*rac*)-catalyst (12 mg, 0.0374 mmol) was used. The reaction was stirred at room temperature for 4 days.

1H NMR (400 MHz, $CDCl_3$) δ (ppm) = 7.98 (dd, *J* = 8.3, 1.6 Hz, 1H), 7.79 (d, *J* = 8.2 Hz, 1H), 7.62 (ddd, *J* = 8.4, 6.9, 1.4 Hz, 1H), 7.56 (tq, *J* = 4.9, 2.3 Hz, 3H), 7.51 – 7.42 (m, 4H), 7.41 (d, *J* = 3.7 Hz, 1H), 7.39 (d, *J* = 1.8 Hz, 2H), 2.40 (s, 3H).

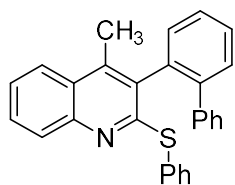
^{13}C NMR (101 MHz, $CDCl_3$) δ (ppm) = 158.96, 147.50 (q, *J* = 1.5 Hz), 147.45, 142.43, 134.93, 132.84, 131.39, 130.35, 130.13, 129.42, 129.31, 128.82, 128.38, 128.09, 126.97, 126.23, 124.23, 121.87 (q, *J* = 274.3), 120.67 (q, *J* = 1.7 Hz), 15.84.

^{19}F NMR (470 MHz, $CDCl_3$) δ (ppm) = -57.66.

MS (APCI) Calculated: 411.4 calculated $[M]^+$ for $C_{23}H_{16}F_3NOS$; experimental 411.4.

HRMS (ESI) = 411.0905 calculated $[M+H]^+$ found 412.1002 (2.5 ppm).

KR Product, 108



Following the general procedure: **107** (25 mg, 0.0798 mmol, 1.0 equiv), catalyst **77** (6.52 mg, 0.016 mmol, 0.2 equiv) and K_2HPO_4 (278 mg, 1.596 mmol, 20.0 equiv) were used. 559 μL *m*-xylene and 239 μL *n*-hexanes were

added. Thiophenol (81 μL , 0.798 mmol, 10.0 equiv) was added to the reaction. The reaction vial was capped, and then left to stir up to 2.5 days at room temperature. The workup and purification followed according to the general procedure afforded **3-([1,1'-biphenyl]-2-yl)-4-methyl-2-(phenylthio)quinoline, 108** as a pale yellowish oil (13.5 mg, 0.0335 mmol, 42%, 11:89 e.r.) and recovered **108** (10 mg, 0.0327 mmol, 41%, 82:18 e.r.). Conv = 44%, $s = 16$.

For racemic standards: 20 mol% (*rac*)-catalyst (5.2 mg, 0.016 mmol) was used. The reaction was stirred at room temperature for 3 days.

Scale-up Procedure of **108**: **107** (265 mg, 0.839 mmol, 1.0 equiv), 20% mol catalyst **77** (68.4 mg, 0.1677 mmol) and K_2HPO_4 (2.92 g, 16.772 mmol, 20.0 equiv) were added into a 20 mL dram vial equipped with a stir bar. 5.82 mL *m*-xylene and 2.5 mL *n*-hexanes were then added. Thiophenol (855.5 μL , 8.386 mmol, 10.0 equiv) was added to the reaction, and the reaction was left to stir for 3 days at room temperature. The workup and purification followed according to the general procedure afforded ee-**108** as a pale yellowish oil (58 mg, 0.033 mmol, 17%, 15:85 e.r.) and ee-**107** (168 mg, 0.531 mmol, 63%, 93:7 e.r.). Conv = 55%, $s = 15$.

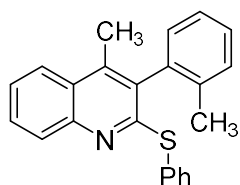
1H NMR (400 MHz, $CDCl_3$) δ (ppm) = 7.79 (d, $J = 8.4$ Hz, 1H), 7.67 (d, $J = 8.4$ Hz, 1H), 7.57 (d, $J = 2.5$ Hz, 3H), 7.51 (s, 3H), 7.39 (s, 2H), 7.38 (s, 3H), 7.35 – 7.32 (m, 2H), 7.14 (d, $J = 5.5$ Hz, 3H), 2.21 (s, 3H).

^{13}C NMR (101 MHz, CDCl_3) δ (ppm) = 159.52, 147.09, 144.95, 142.77, 142.49, 141.34, 141.08, 135.29, 135.08, 134.91, 132.58, 131.68, 131.60, 130.60, 130.36, 129.47, 128.95, 128.78, 128.31, 128.18, 127.95, 127.62, 127.52, 127.04, 126.18, 125.34, 124.10, 15.94.

MS (APCI) Calculated: 403.5 calculated $[\text{M}]^+$ for $\text{C}_{28}\text{H}_{21}\text{NS}$; experimental 403.5.

HRMS (ESI) = 403.1395 calculated $[\text{M}+\text{H}]^+$ found 404.1490

KR Product, **109**



Following the general procedure: **110** (25 mg, 0.0995 mmol, 1.0 equiv), catalyst **77** (8.0 mg, 0.0199 mmol, 0.2 equiv) and K_2HPO_4 (346 mg, 1.99 mmol, 20.0 equiv) were used. 299 μL *m*-xylene and 299 μL *n*-hexanes were

added. Thiophenol (101.5 μL , 0.995 mmol, 10.0 equiv) was added to the reaction. The reaction vial was capped, and then left to stir up to 4.5 days at room temperature. The workup and purification followed according to the general procedure afforded **4-methyl-2-(phenylthio)-3-(o-tolyl)quinoline, 109** as a pale yellowish oil (20 mg, 0.0597 mmol, 60%, 29:71 e.r.) and recovered **110** (4.5 mg, 0.0179 mmol, 21%, 83:17 e.r.). Conv = 62%, $s = 4.7$.

For racemic standards: 20 mol% (*rac*)-catalyst (6.4 mg, 0.0199 mmol) was used. The reaction was stirred at room temperature for about 3 days.

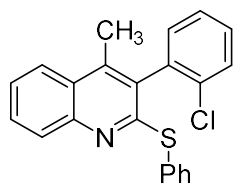
^1H NMR (400 MHz, CDCl_3) δ (ppm) = 7.96 (d, $J = 8.3$ Hz, 1H), 7.76 (d, $J = 8.3$ Hz, 1H), 7.61 – 7.56 (m, 3H), 7.47 (t, $J = 6.9$ Hz, 1H), 7.41 – 7.35 (m, 6H), 7.22 (d, $J = 7.4$ Hz, 1H), 2.34 (s, 3H), 2.15 (s, 3H).

^{13}C NMR (101 MHz, CDCl_3) δ (ppm) = 159.25, 146.88, 141.80, 137.28, 136.52, 135.12, 132.74, 131.23, 130.43, 128.85, 128.49, 126.55, 126.43, 125.73, 124.19, 124.12, 19.88, 19.81, 15.60, 15.53.

MS (APCI) Calculated: 341.5 calculated $[M]^+$ for $C_{23}H_{19}NS$; experimental 341.4.

HRMS (ESI) = 341.1238 calculated $[M+H]^+$ found 342.1331

KR Product, **111**



Following the general procedure: **112** (50 mg, 0.1845 mmol, 1.0 equiv), catalyst **77** (15.1 mg, 0.03689 mmol, 0.2 equiv) and K_2HPO_4 (641.9 mg, 3.69 mmol, 20.0 equiv) were used. 1.3 mL *m*-xylene and 553.5 μ L *n*-hexanes were

added. Thiophenol (188 μ L, 1.845 mmol, 10.0 equiv) was added to the reaction. The reaction vial was capped, and then left to stir up to 4.5 days at room temperature. The workup and purification followed according to the general procedure afforded **3-(2-chlorophenyl)-4-methyl-2-(phenylthio)quinoline**, **111** as a pale yellowish oil (31 mg, 0.0849 mmol, 46%, 11:89 e.r.) and recovered **112** (15 mg, 0.05535 mmol, 30%, 83:17 e.r.). Conv = 46%, *s* = 15.

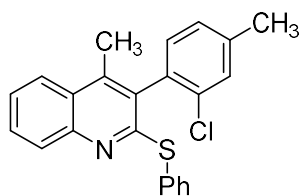
For racemic standards: 20 mol% (*rac*)-catalyst (12 mg, 0.03689 mmol) was used. The reaction was stirred at room temperature for about 3 days.

1H NMR (400 MHz, $CDCl_3$) δ (ppm) = 7.97 (d, *J* = 8.3 Hz, 1H), 7.79 (d, *J* = 8.6 Hz, 1H), 7.77 – 7.51 (m, 5H), 7.51 – 7.42 (m, 3H), 7.42 – 7.29 (m, 5H), 2.38 (s, 3H).

^{13}C NMR (101 MHz, $CDCl_3$) δ (ppm) = 158.75, 147.38, 142.37, 136.13, 134.94, 134.75, 132.14, 131.35, 130.89, 130.06, 129.42, 129.24, 128.83, 128.40, 127.25, 126.37, 125.76, 124.24, 124.22, 29.85, 15.61.

MS (APCI) Calculated: 361.9 calculated $[M]^+$ for $C_{22}H_{16}ClNS$; experimental 361.9.

KR Product, 113



Following the general procedure: **114** (50 mg, 0.1754 mmol, 1.0 equiv), catalyst **77** (14.3 mg, 0.03507 mmol, 0.2 equiv) and K_2HPO_4 (610 mg, 3.51 mmol, 20.0 equiv) were used. 1.23 mL *m*-xylene and 525 μ L *n*-

hexanes were added. Thiophenol (179 μ L, 1.75 mmol, 10.0 equiv) was added to the reaction. The reaction vial was capped, and then left to stir up to 4.5 days at room temperature. The reaction vial was capped, and then left to stir up to 4.5 days at room temperature. The workup and purification followed according to the general procedure afforded **3-(2-chloro-4-methylphenyl)-4-methyl-2-(phenylthio)quinoline**, **114** as a pale yellowish oil (27 mg, 0.07367 mmol, 42%, 19:81 e.r.) and recovered **113** (24.5 mg, 0.0859 mmol, 49%, 81.5:18.5 e.r.). Conv = 52%, $s = 6.9$.

For racemic standards: 20 mol% (*rac*)-catalyst (11.4 mg, 0.03507 mmol) was used. The reaction was stirred at room temperature for about 3 days.

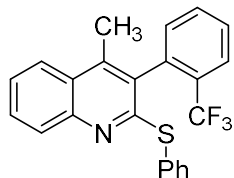
1H NMR (400 MHz, $CDCl_3$) δ (ppm) = 7.95 (ddd, $J = 8.4, 1.4, 0.6$ Hz, 1H), 7.75 (ddd, $J = 8.4, 1.4, 0.6$ Hz, 1H), 7.59 (ddd, $J = 8.3, 6.9, 1.5$ Hz, 1H), 7.56 – 7.53 (m, 2H), 7.46 (ddd, $J = 8.2, 6.8, 1.4$ Hz, 1H), 7.39 – 7.36 (m, 3H), 7.22 (d, $J = 7.6$ Hz, 1H), 7.12 (ddd, $J = 7.7, 1.7, 0.7$ Hz, 1H), 7.06 (dd, $J = 10.3, 0.8$ Hz, 1H), 2.47 (s, 3H), 2.42 (s, 3H).

^{13}C NMR (101 MHz, $CDCl_3$) δ (ppm) = 161.24, 159.32, 158.79, 147.43, 142.74, 141.46, 141.38, 134.98, 132.01, 131.41, 129.29, 128.82, 128.33, 127.27, 126.36, 125.64, 125.28, 124.20, 121.64, 121.47, 116.75, 116.53, 21.52, 15.84.

MS (APCI) Calculated: 375.9 calculated $[M]^+$ for $C_{23}H_{18}ClNS$; experimental 374.7

HRMS (ESI) = 376.0927 calculated $[M+H]^+$ found 376.0936 (2.5 ppm).

KR Product, 73



Following the general procedure: **115** (50 mg, 0.163 mmol, 1.0 equiv), catalyst **77** (16.1 mg, 0.0326 mmol, 0.2 equiv) and K_2HPO_4 (567 mg, 3.26 mmol, 20.0 equiv) were used. 1.14 mL *m*-xylene and 489 μ L *n*-hexanes were added.

Thiophenol (166.3 μ L, 1.63 mmol, 10.0 equiv) was added to the reaction. The reaction vial was capped, and then left to stir up to 2.5 days at room temperature. The workup and purification followed according to the general procedure afforded **4-methyl-2-(phenylthio)-3-(2-(trifluoromethyl)phenyl)quinoline, 73** as a pale yellowish oil (16 mg, 0.0408 mmol, 25%, 5:95 e.r.) and recovered **115** (30 mg, 0.099 mmol, 61%, 68:32 e.r.). Conv = 28%, $s = 27$.

For racemic standards: 20 mol% (*rac*)-catalyst (10.5 mg, 0.0326 mmol) was used. The reaction was stirred at room temperature for about 3 days.

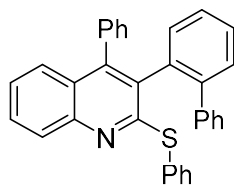
1H NMR (500 MHz, $CDCl_3$) δ (ppm) = 7.95 (dd, $J = 8.4, 1.7$ Hz, 1H), 7.89 (d, $J = 7.9$ Hz, 1H), 7.78 (d, $J = 8.6$ Hz, 1H), 7.70 (t, $J = 7.5$ Hz, 1H), 7.64 – 7.59 (m, 2H), 7.55 – 7.52 (m, 2H), 7.50 – 7.46 (m, 1H), 7.39 (d, $J = 4.5$ Hz, 2H), 7.37 (d, $J = 1.6$ Hz, 2H), 2.33 (s, 3H).

^{13}C NMR (126 MHz, $CDCl_3$) δ (ppm) = 153.17 (d, $J = 1462.9$ Hz), 142.43 – 135.73 (m), 134.92, 132.66 (d, $J = 3.8$ Hz), 132.24, 131.46, 130.53, 129.97 (q, $J = 30.3$ Hz), 129.37 (d, $J = 23.8$ Hz), 128.89 (d, $J = 9.5$ Hz), 128.41, 127.24 (q), 126.87 (q, $J = 5.0$ Hz), 126.21, 125.80, 124.20, 16.39.

^{19}F NMR (470 MHz, $CDCl_3$) δ (ppm) = -60.78.

MS (APCI) Calculated: 395.4 calculated $[M]^+$ for $C_{23}H_{16}F_3NS$; experimental 395.1.

KR Product, 117



Following the general procedure: **116** (50 mg, 0.1538 mmol, 1.0 equiv), catalyst **77** (12.6 mg, 0.03076 mmol, 0.2 equiv) and K_2HPO_4 (522.3 mg, 3.002 mmol, 20.0 equiv) were used. 1.05 mL *m*-xylene and 450 μ L *n*-hexanes were

added. Thiophenol (153.1 μ L, 1.501 mmol, 10.0 equiv) was added to the reaction. The reaction vial was capped, and then left to stir up to 2.5 days at room temperature. The workup and purification followed according to the general procedure afforded **3-([1,1'-biphenyl]-2-yl)-4-phenyl-2-(phenylthio)quinoline, 117** as a pale yellowish oil (16 mg, 0.0215 mmol, 14%, 7:93 e.r.) and enantioenriched **116** (16 mg, 0.408 mmol, 62%, 64:36 e.r.). Conv = 15%, $s = 22$.

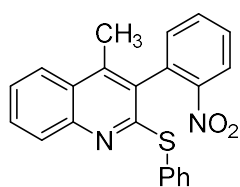
$^1\text{H NMR}$ (400 MHz, CDCl_3) δ (ppm) = 7.77 (d, $J = 8.5$ Hz, 1H), 7.66 (dd, $J = 6.3, 1.9$ Hz, 2H), 7.54 – 7.43 (m, 5H), 7.41 – 7.36 (m, 3H), 7.30 – 7.27 (m, 2H), 7.22 – 7.17 (m, 2H), 7.14 – 7.06 (m, 5H), 7.02 (t, $J = 1.8$ Hz, 1H), 7.00 (t, $J = 2.0$ Hz, 1H), 6.85 (d, $J = 7.6$ Hz, 1H), 6.21 (d, $J = 7.6$ Hz, 1H).

$^{13}\text{C NMR}$ (101 MHz, CDCl_3) δ (ppm) = 160.34, 147.57, 146.24, 141.72, 140.73, 135.62, 135.24, 135.11, 134.36, 132.90, 131.68, 131.43, 130.66, 130.52, 130.04, 129.42, 128.87, 128.62, 127.77, 127.52, 127.31, 126.86, 125.84, 125.46, 29.85.

MS (APCI) Calculated: 465.6 calculated $[\text{M}]^+$ for $\text{C}_{33}\text{H}_{23}\text{NS}$; experimental 465.4.

HRMS (ESI) = 465.6140 calculated $[\text{M}+\text{H}]^+$ found 466.1631 (2.5 ppm).

DKR/KR Hybrid Product, **97**



Following the general procedure: **98** (50 mg, 0.177 mmol, 1.0 equiv), (15.6 mg, 0.0354 mmol) and K_2HPO_4 (616 mg, 3.54 mmol, 20.0 equiv) were used. 1.24 mL *m*-xylene and 531 μ L *n*-hexanes were added. Thiophenol (180.6 μ L,

1.77 mmol, 10.0 equiv) was added to the reaction. The reaction vial was capped, and then left to stir up to 2 days at room temperature. The workup and purification followed according to the general procedure afforded **4-methyl-3-(2-nitrophenyl)-2-(phenylthio)quinoline, 97** as a bright

yellow solid (53 mg, 0.1416 mmol, 80%, 15:85 e.r.) and recovered **98** (7 mg, 0.02478 mmol, 14%, 63:37 e.r.). Conv_p = 27%.

For racemic standards: 20 mol% (*rac*)-catalyst (11.5 mg, 0.0354 mmol) was used. The reaction was stirred at room temperature for 2.5 days.

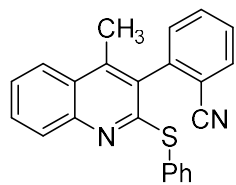
¹H NMR (400 MHz, CDCl₃) δ (ppm) = 8.18 (d, *J* = 8.2 Hz, 1H), 7.88 (d, *J* = 8.3 Hz, 1H), 7.75 (d, *J* = 8.6 Hz, 1H), 7.71 – 7.66 (m, 1H), 7.60 (dt, *J* = 8.2, 1.4 Hz, 1H), 7.56 – 7.52 (m, 1H), 7.41 – 7.38 (m, 2H), 7.32 – 7.25 (m, 5H), 2.29 (d, *J* = 1.2 Hz, 3H).

¹³C NMR (101 MHz, CDCl₃) δ (ppm) = 157.47, 148.84, 147.19, 141.57, 134.57, 133.41, 132.63, 131.06, 130.25, 128.94, 126.37, 125.19, 125.14, 124.16, 29.85, 16.11.

MS (APCI) = 372.4 calculated [M]⁺ for C₂₂H₁₆N₂O₂S; experimental 371.8.

HRMS (ESI) = 373.1011 calculated [M+H]⁺ found 373.1018 (2.0 ppm).

DKR/KR Hybrid Product, **99**



Following the general procedure: **100** (50 mg, 0.1906 mmol, 1.0 equiv), catalyst **77** (15.6 mg, 0.0381 mmol, 0.2 equiv) and K₂HPO₄ (663 mg, 3.81 mmol, 20.0 equiv) were used. 1.32 mL *m*-xylene and 573 μL *n*-hexanes were

added. Thiophenol (195 μL, 1.91 mmol, 10.0 equiv) was added to the reaction. The reaction vial was capped, and then left to stir up to 2.5 days at room temperature. The workup and purification followed according to the general procedure afforded **2-(4-methyl-2-(phenylthio)quinolin-3-yl)benzonitrile, 99** as a light beige solid (29 mg, 0.0896 mmol, 47%, 25:75 e.r.) and recovered **100** (21 mg, 0.0801 mmol, 42%, 65:35 e.r.). Conv_p = 38%.

For racemic standards: 20 mol% (*rac*)-catalyst (12.3 mg, 0.0381 mmol) was used. The reaction was stirred at room temperature for 2.5 days.

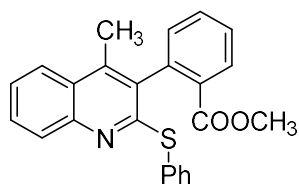
¹H NMR (400 MHz, CDCl₃) δ (ppm) = 7.97 (d, *J* = 9.9 Hz, 1H), 7.83 (d, *J* = 7.9 Hz, 1H), 7.79 – 7.72 (m, 2H), 7.63 (d, *J* = 6.8 Hz, 1H), 7.60 – 7.56 (m, 1H), 7.53 – 7.47 (m, 4H), 7.38 – 7.35 (m, 3H), 2.41 (s, 3H).

¹³C NMR (101 MHz, CDCl₃) δ 157.99, 147.73, 142.56, 141.38, 134.85, 133.34, 133.01, 131.81, 131.04, 129.87, 129.45, 128.95, 128.52, 126.23, 126.08, 124.33, 117.55, 114.46, 15.89.

MS (APCI) = 352.5 calculated [M]⁺ for C₂₃H₁₆N₂S; experimental 352.6.

HRMS (ESI) = 352.4550 calculated [M+H]⁺ found 353.1110

DKR/KR Hybrid Product, 101



Following the general procedure: **102** (25 mg, 0.0847 mmol, 1.0 equiv), catalyst **77** (7 mg, 0.0169 mmol, 0.2 equiv) and K₂HPO₄ (295 mg, 1.69 mmol, 20.0 equiv) were used. 593 μL *m*-xylene and 254 μL *n*-hexanes

were added. Thiophenol (86 μL, 0.847 mmol, 10.0 equiv) was added to the reaction. The reaction vial was capped, and then left to stir up to 2.5 days at room temperature. The workup and purification followed according to the general procedure afforded **methyl 2-(4-methyl-2-(phenylthio)quinolin-3-yl)benzoate**, **101** as a white foamy solid (16.3 mg, 0.0424 mmol, 50%, 64:36 e.r.) and recovered **102** (12 mg, 0.0398 mmol, 47%, 54:46 e.r.). Conv_p = 22%.

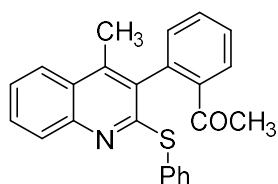
For racemic standards: 20 mol% (*rac*)-catalyst (5.5 mg, 0.0354 mmol) was used. The reaction was stirred at room temperature for 2.5 days.

¹H NMR (400 MHz, CDCl₃) δ (ppm) = 8.17 (dd, *J* = 8.0, 1.6 Hz, 1H), 7.95 (dd, *J* = 8.3, 1.9 Hz, 1H), 7.78 (dd, *J* = 8.4, 1.8 Hz, 1H), 7.66 (td, *J* = 7.5, 1.4 Hz, 1H), 7.57 (tdd, *J* = 7.7, 4.2, 1.4 Hz, 2H), 7.52 – 7.44 (m, 3H), 7.33 (dd, *J* = 5.1, 2.0 Hz, 3H), 7.29 (dd, *J* = 7.6, 1.5 Hz, 1H), 3.64 (s, 3H), 2.33 (s, 3H).

^{13}C NMR (126 MHz, CDCl_3) δ (ppm) = 161.25, 159.29, 158.95, 147.60, 143.14, 142.47, 136.28, 132.39, 130.63, 130.53, 130.38, 129.36, 129.27, 129.17, 127.22, 126.32, 126.14, 125.56, 125.03, 124.90, 124.50, 124.19, 116.03, 20.96, 15.81.

MS (APCI) = 385.5 calculated $[\text{M}]^+$ for $\text{C}_{24}\text{H}_{19}\text{NO}_2\text{S}$; experimental 384.9.

DKR/KR Hybrid Product, 103



Following the general procedure: **104** (50 mg, 0.179 mmol, 1.0 equiv), catalyst **77** (14.6 mg, 0.0358 mmol, 0.2 equiv) and K_2HPO_4 (622.9 mg, 3.58 mmol, 20.0 equiv) were used. 1.25 mL *m*-xylene and 537 μL *n*-

hexanes were added. Thiophenol (183 μL , 1.79 mmol, 10.0 equiv) was added to the reaction. The reaction vial was capped, and then left to stir up to 2.5 days at room temperature. The workup and purification followed according to the general procedure afforded **1-(2-(4-methyl-2-(phenylthio)quinolin-3-yl)phenyl)ethan-1-one**, **103** as a light yellow solid (41 mg, 0.111 mmol, 62%, 74:26 e.r.) and recovered **104** (20 mg, 0.0716 mmol, 40%, 63:37 e.r.). $\text{Conv}_p = 35\%$.

For racemic standards: 20 mol% (*rac*)-catalyst (12 mg, 0.0358 mmol) was used. The reaction was stirred at room temperature for 4 days.

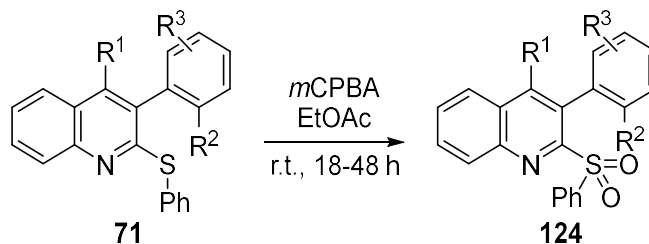
^1H NMR (400 MHz, CDCl_3) δ 7.96 – 7.92 (m, 1H), 7.89 (dd, $J = 7.6, 1.3$ Hz, 1H), 7.77 – 7.72 (m, 1H), 7.63 (td, $J = 7.4, 1.6$ Hz, 1H), 7.58 (ddt, $J = 8.4, 6.9, 1.6$ Hz, 2H), 7.53 – 7.43 (m, 3H), 7.36 (qd, $J = 3.8, 1.6$ Hz, 3H), 7.30 (dd, $J = 7.2, 1.5$ Hz, 1H), 2.36 (s, 3H), 2.33 (s, 3H).

^{13}C NMR (101 MHz, CDCl_3) δ (ppm) = 200.62, 158.01, 147.23, 141.43, 139.66, 136.23, 134.76, 132.68, 132.21, 131.96, 131.34, 129.32, 129.14, 128.83, 128.80, 128.37, 126.45, 125.72, 124.14, 29.15.

MS (APCI) = 369.5 calculated $[\text{M}]^+$ for $\text{C}_{24}\text{H}_{19}\text{NOS}$; experimental 369.5.

HRMS (ESI) = 369.4820 calculated $[\text{M}+\text{H}]^+$ found 370.1283.

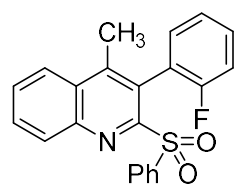
2.2.14 Post Functionalization of Enantioenriched **71** towards Sulfones



Equation 44. Oxidation to yield enantioenriched 3-aryl-2-(phenylsulfonyl)quinolines **124**

To **71** (1.0 equiv) was added (*m*)-chloroperoxybenzoic acid (i.e., *m*CPBA, ~2.0 equiv) and 0.1 M EtOAc. The reaction was stirred at room temperature up to 2 days. The resulting reaction was then quenched with saturated aqueous sodium bicarbonate and diluted with EtOAc. The organic layer was extracted out, and subsequently rinsed with brine. The organic layers were recombined, and then dried over Na₂SO₄. The combined organic layers were concentrated *in vacuo*. The resulting crude residue was then purified by FCC using *n*-hexanes:EtOAc = 0% → 30% to afford the purified **124** (and in some cases, recovered enantioenriched **70**) in 60-80% yields. Yields and e.r.s are reported as an average of at least 2 trials; the amount shown is reported of 1 trial for simplicity.

Sulfone Product, **80**



Following the general procedure: **72** (1.05 g, 3.04 mmol, 78%, 13:87 e.r., 1.0 equiv), *m*CPBA (1.2 g, 6.38 mmol, 2.1 equiv) and 30.4 mL EtOAc were used.

The workup and purification following the general procedure afforded **3-(2-fluorophenyl)-4-methyl-2-(phenylsulfonyl)quinoline**, **80** as a white solid (942 mg, 2.5 mmol, 82%, 15:85 e.r.). **80** was then triturated using 80:20 HPLC grade *n*-hexanes/DCE. The resulting

solid and filtrate were isolated; the resulting solid was more enantioenriched (594 mg, 1.57 mmol, 63%, 6:94 e.r.). The overall yield beginning from **74**(1.0 g) is 40%.

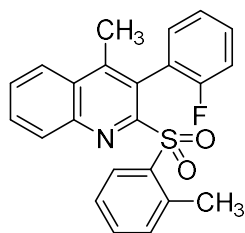
¹H NMR (500 MHz, CDCl₃) δ 8.13 (d, *J* = 8.2 Hz, 1H), 8.07 (d, *J* = 8.1 Hz, 1H), 7.80 – 7.77 (m, 1H), 7.74 – 7.70 (m, 3H), 7.56 (t, *J* = 7.5 Hz, 1H), 7.45 (dd, *J* = 9.8, 5.6 Hz, 1H), 7.41 (t, *J* = 7.9 Hz, 2H), 7.29 (td, *J* = 7.4, 1.8 Hz, 1H), 7.24 (dd, *J* = 7.5, 0.9 Hz, 1H), 7.04 (t, *J* = 8.8 Hz, 1H), 2.42 (s, 3H).

¹³C NMR (126 MHz, CDCl₃) δ (ppm) = 160.22 (d, *J* = 246.5 Hz), 156.04, 147.82, 145.42, 139.33, 133.25, 133.03, 131.20, 130.85 (d, *J* = 8.0 Hz), 130.62, 129.34, 129.00, 128.65, 128.56, 125.53, 124.33, 123.90 (d, *J* = 3.5 Hz), 122.66 (d, *J* = 16.9 Hz), 115.33 (d, *J* = 21.8 Hz), 15.87.

¹⁹F NMR (376 MHz, CDCl₃) δ (ppm) = -110.93.

MS (APCI) Calculated: 377.4 calculated [M]⁺ for C₂₂H₁₆FNO₂S; experimental 377.3.

Sulfone Product, **82**



Following the general procedure: **81** (37 mg, 0.1027 mmol, 1.0 equiv), *m*CPBA (35.4 mg, 0.2054 mmol, 2.0 equiv) and 1.02 mL EtOAc were used.

The workup and purification following the general procedure afforded **3-(2-fluorophenyl)-4-methyl-2-(o-tolylsulfonyl)quinoline**, **82** as a white solid

(6.04 mg, 0.0308 mmol, 15%, 26:74 e.r.). The overall yield beginning from **81** is 11%.

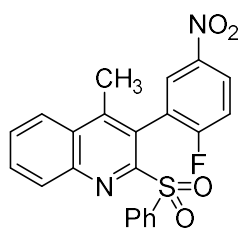
¹H NMR (400 MHz, CDCl₃) δ (ppm) = 7.99 – 7.95 (m, 1H), 7.74 – 7.69 (m, 1H), 7.58 (ddd, *J* = 8.3, 6.9, 1.4 Hz, 1H), 7.54 – 7.49 (m, 2H), 7.47 (ddd, *J* = 8.2, 6.9, 1.4 Hz, 1H), 7.39 (td, *J* = 7.4, 2.0 Hz, 1H), 7.36 – 7.31 (m, 3H), 7.27 (d, *J* = 7.1 Hz, 1H), 7.21 (td, *J* = 7.0, 6.4, 2.7 Hz, 1H), 2.43 (s, 3H), 2.32 (s, 3H).

^{13}C NMR (126 MHz, CDCl_3) δ (ppm) = 160.27 (d, J = 246.8 Hz), 158.95, 145.37 (d, J = 560.6 Hz), 142.47, 136.28, 132.40 (d, J = 2.2 Hz), 130.66 (d, J = 8.5 Hz), 130.53, 130.39 (d, J = 3.0 Hz), 129.36, 129.27, 129.17 (d, J = 1.8 Hz), 127.22, 126.32 (d, J = 1.4 Hz), 126.14, 125.56, 124.96 (d, J = 17.2 Hz), 124.50 (t, J = 4.4 Hz), 124.19, 116.20 (d, J = 3.2 Hz), 116.04 (d, J = 2.5 Hz), 20.95 (d, J = 2.3 Hz), 15.82 (q, J = 3.1, 2.4 Hz).

^{19}F NMR (376 MHz, CDCl_3) δ (ppm) = -112.07 – -112.16 (m).

MS (APCI) Calculated: 391.5 calculated $[\text{M}]^+$ for $\text{C}_{23}\text{H}_{18}\text{FNO}_2\text{S}$; experimental 391.6

Sulfone Product, 122



Following the general procedure: **89** (635 mg, 1.62 mmol, 98%, 20:80 e.r., 1.0 equiv), *m*CPBA (505 mg, 2.93 mmol, 2.1 equiv) and 16.2 mL EtOAc were used. The workup and purification followed according to the general procedure afforded **3-(2-fluoro-5-nitrophenyl)-4-methyl-2-(phenylsulfonyl)quinoline, 122** as a white solid. **122** was then triturated using 80:20 HPLC grade *n*-hexanes/DCE. The resulting solid and filtrate were isolated; the resulting solid was more enantioenriched (225 mg, 0.534 mmol, 33%, 12:88 e.r.). The overall yield beginning from **1g**(500 mg) is 32%.

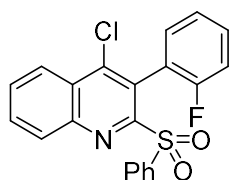
^1H NMR (400 MHz, CDCl_3) δ (ppm) = 8.39 (ddd, J = 9.1, 4.4, 2.8 Hz, 1H), 8.12 – 8.08 (m, 3H), 7.99 (d, J = 7.8 Hz, 1H), 7.82 (d, J = 7.2 Hz, 2H), 7.76 – 7.72 (m, 1H), 7.63 – 7.58 (m, 1H), 7.48 (t, J = 7.7 Hz, 2H), 7.42 (t, J = 7.9 Hz, 1H), 7.37 – 7.32 (m, 1H), 2.46 (s, 3H).

^{13}C NMR (101 MHz, CDCl_3) δ (ppm) = 165.32, 162.75, 155.74, 147.80, 145.68, 143.98, 138.91, 134.83, 133.97, 133.82, 131.21, 130.39, 129.99, 129.84, 129.20, 128.82, 128.69, 128.47, 126.75 (d, J = 10.2 Hz), 124.40, 116.57 (d, J = 25.1 Hz), 16.12.

^{19}F NMR (376 MHz, CDCl_3) δ (ppm) = -99.14 (dd, J = 10.2, 3.4 Hz).

MS (APCI) Calculated: 422.4 calculated $[\text{M}]^+$ for $\text{C}_{22}\text{H}_{15}\text{FN}_2\text{O}_4\text{S}$; experimental 422.2

Sulfone Product, 91



Following the general procedure: Crude mixture of **90** (70.6 mg, 0.181 mmol, 1.0 equiv), *m*CPBA (66 mg, 0.380 mmol, 2.1 equiv) and 2.0 mL EtOAc were used. The workup and purification following the general procedure afforded

4-chloro-3-(2-fluorophenyl)-2-(phenylsulfonyl)quinoline, 91 as a white solid (65 mg, 0.162 mmol, 79%, 12:88 e.r.). The overall yield from **1h** is 79%.

^1H NMR (400 MHz, CDCl_3) δ (ppm) = 8.37 (d, J = 8.4 Hz, 1H), 8.23 (d, J = 8.4 Hz, 1H), 8.15 (s, 1H), 8.06 (d, J = 7.8 Hz, 1H), 7.95 – 7.84 (m, 2H), 7.80 (d, J = 7.4 Hz, 1H), 7.65 (d, J = 7.5 Hz, 2H), 7.57 – 7.45 (m, 5H), 7.42 – 7.37 (m, 1H), 7.36 – 7.32 (m, 1H), 7.14 (t, J = 8.9 Hz, 1H).

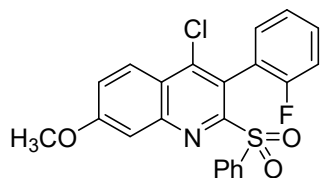
^{13}C NMR (101 MHz, CDCl_3 , X-C coupling where X = F, Cl) δ (ppm) = 170.78, 160.17 (d, J = 247.6 Hz), 156.51, 138.80, 134.44 (d, J = 84.8 Hz), 133.65, 132.77 (d, J = 2.5 Hz), 131.86, 131.44 (d, J = 8.1 Hz), 131.02 (d, J = 21.5 Hz), 130.57, 130.19 (d, J = 41.3 Hz), 129.21, 128.75, 128.45, 127.24, 125.73, 124.93, 123.93 (d, J = 3.5 Hz), 121.22 (d, J = 17.0 Hz), 115.45 (d, J = 21.5 Hz).

^{19}F NMR (376 MHz, CDCl_3) δ (ppm) = -111.84 (ddd, J = 9.5, 7.2, 5.1 Hz).

MS (APCI) Calculated: 397.9 calculated $[\text{M}]^+$ for $\text{C}_{21}\text{H}_{13}\text{ClFNO}_2\text{S}$; experimental 398.0

HRMS (ESI) = 397.8484 calculated $[\text{M}+\text{H}]^+$ found 398.0427.

Sulfone Product, 93



Following the general procedure: **92** (64.5 mg, 0.163 mmol, 1.0 equiv), *m*CPBA (51 mg, 0.295 mmol, 2.0 equiv) and 1.6 mL EtOAc were used.

The workup and purification following the general procedure afforded

4-chloro-3-(2-fluorophenyl)-7-methoxy-2-(phenylsulfonyl)quinoline, 93 as a white solid (63 mg, 0.147 mmol, 90%, 17:83 e.r.). The resulting solid and filtrate were isolated; the resulting solid was more enantioenriched (30 mg, 0.0685 mmol, 42%, 6:94 e.r.). Overall yield from **92** is 42%.

¹H NMR (400 MHz, CDCl₃) δ (ppm) = 8.19 (d, *J* = 9.2 Hz, 1H), 7.66 (d, *J* = 8.0 Hz, 2H), 7.56 (d, *J* = 7.3 Hz, 1H), 7.52 (d, *J* = 1.8 Hz, 1H), 7.48 – 7.28 (m, 5H), 7.23 (d, *J* = 9.2 Hz, 1H), 7.01 (t, *J* = 8.9 Hz, 1H), 3.99 (s, 3H).

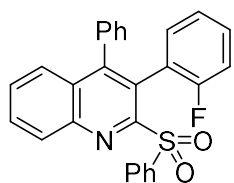
¹³C NMR (101 MHz, CDCl₃) δ (ppm) = 162.62, 161.50, 160.12, 159.00, 157.72, 147.47, 147.28, 145.47, 145.41, 132.60, 131.94, 131.50, 130.87, 126.32, 126.11, 124.58, 123.89, 120.46, 119.79, 115.00, 114.61, 77.16, 55.96.

¹⁹F NMR (376 MHz, CDCl₃) δ (ppm) = -111.82 (dt, *J* = 9.3, 5.9 Hz).

MS (APCI) Calculated: 427.9 calculated [M]⁺ for C₂₂H₁₅ClFNO₃S; experimental 428.1.

HRMS (ESI) = 427.8744 calculated [M+H]⁺ found 428.0497.

Sulfone Product, **95**



Following the general procedure: **94** (37 mg, 0.1027 mmol, 1.0 equiv), *m*CPBA (35 mg, 0.2054 mmol, 2.0 equiv) and 1.02 mL EtOAc were used. The workup and purification following the general procedure afforded **3-(2-**

fluorophenyl)-4-phenyl-2-(phenylsulfonyl)quinoline, 95 as a white solid (27 mg, 0.0652 mmol, 40%, 12:88 e.r.). The overall yield from **94** is 40%.

¹H NMR (400 MHz, CDCl₃) δ (ppm) = 8.19 (t, *J* = 8.7 Hz, 1H), 8.10 (t, *J* = 1.9 Hz, 1H), 8.00 (dt, *J* = 7.8, 1.4 Hz, 1H), 7.87 – 7.66 (m, 3H), 7.60 – 7.52 (m, 3H), 7.42 (t, *J* = 7.9 Hz, 3H), 7.30 – 7.12 (m, 5H), 7.00 (d, *J* = 7.3 Hz, 1H), 6.75 (t, *J* = 8.3 Hz, 1H).

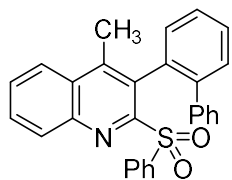
^{13}C NMR (101 MHz, CDCl_3) δ (ppm) = 170.81, 160.04 (d, J = 245.8 Hz), 154.42 (d, J = 359.2 Hz), 146.01, 139.31, 135.32, 134.41 (d, J = 84.8 Hz), 133.42 (d, J = 2.8 Hz), 133.36, 131.03 (d, J = 25.4 Hz), 130.53 (d, J = 5.7 Hz), 130.44 – 130.29 (m), 129.99 (d, J = 1.4 Hz), 129.55, 129.41, 129.16, 129.07 (d, J = 1.8 Hz), 128.63, 128.59, 128.45, 128.16 (d, J = 5.3 Hz), 127.82, 126.87, 125.34, 123.09 (d, J = 3.2 Hz), 122.49 (d, J = 16.6 Hz), 114.76 (d, J = 21.9 Hz).

^{19}F NMR (376 MHz, CDCl_3) δ (ppm) = -109.32 (dtd, J = 9.5, 6.1, 2.0 Hz).

MS (APCI) Calculated: 439.5 calculated $[\text{M}]^+$ for $\text{C}_{27}\text{H}_{18}\text{FNO}_2\text{S}$; experimental 440.1.

HRMS (ESI) = 439.5044 calculated $[\text{M}+\text{H}]^+$ found 440.1157.

Sulfone Product, 119



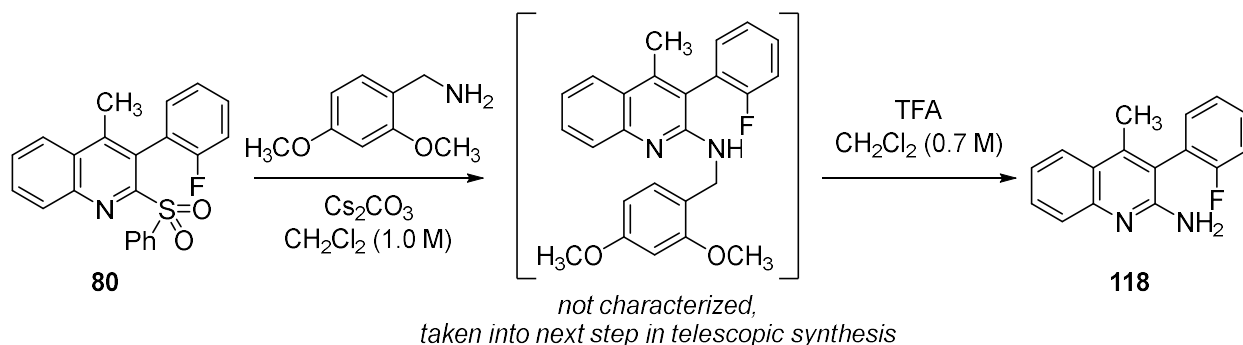
Following the general procedure: **107** was split into three trials (37 mg, 0.1027 mmol, 1.0 equiv), and then *m*CPBA (35.4 mg, 0.2054 mmol, 2.0 equiv) and 1.02 mL EtOAc were used for each trial. The workup and purification following the general procedure afforded **3-((1,1'-biphenyl)-2-yl)-4-methyl-2-(phenylsulfonyl)quinoline, 119** as a white solid. Samples were then combined towards the end to perform future post-translational modifications (20.4 mg, 55%, 15:85 e.r.).

^1H NMR (400 MHz, CDCl_3) δ (ppm) = 8.10 (t, J = 1.9 Hz, 2H), 8.02 – 7.99 (m, 2H), 7.93 (d, J = 1.5 Hz, 2H), 7.84 (d, J = 7.2 Hz, 1H), 7.66 (ddd, J = 8.3, 6.8, 1.4 Hz, 1H), 7.61 – 7.58 (m, 3H), 7.54 – 7.49 (m, 3H), 7.42 (d, J = 7.9 Hz, 3H), 7.09 (d, J = 7.1 Hz, 2H), 2.15 (s, 3H).

^{13}C NMR (126 MHz, CDCl_3) δ (ppm) = 170.66, 167.07, 146.56, 143.71 (d, J = 323.3 Hz), 140.01, 135.11 (d, J = 54.8 Hz), 134.58, 134.02, 133.34, 131.58, 131.12, 130.94, 130.42, 130.37, 130.25, 129.99, 129.73, 129.52, 129.41, 129.06 (d, J = 12.4 Hz), 128.57, 128.47, 127.90, 127.51, 127.12, 126.91 (d, J = 20.5 Hz), 124.26, 16.06.

MS (APCI) Calculated: 435.5 calculated $[\text{M}]^+$ for $\text{C}_{28}\text{H}_{21}\text{NO}_2\text{S}$; experimental 434.8.

2.2.15 Amination to yield enantioenriched 2-amino-3-arylquinoline 118



Equation 45. Amination of 3-arylquinolines. Procedure was followed according to the procedure reported in Cardenas and coworkers.^[17]

Step 1. To **80** (594 mg, 1.57 mmol, 63%, 6:94 e.r., 1.0 equiv) was added 2,4-dimethoxybenzylamine (20 mL, 31.7 mmol, 20.0 equiv), Cs_2CO_3 (2.3 g, 7.0 mmol, 20.0 equiv) and 16 mL CH_2Cl_2 . The resulting reaction was stirred at room temperature for up to 3.5 days. The resulting reaction was then diluted with more CH_2Cl_2 , and then partitioned with distilled, deionized water. The organic layer was extracted out, and subsequently rinsed with brine. The resulting organic layers were recombined, dried over Na_2SO_4 , recollected after filtration, and concentrated *in vacuo*. The crude product of this step was then purified by FCC using *n*-hexanes:EtOAc = 5% \rightarrow 80% to afford *N*-(2,4-dimethoxybenzyl)-3-(2-fluorophenyl)-4-methylquinolin-2-amine as a pure white solid.

Step 2. To the vial containing this substrate was charged 3.0 mL CH_2Cl_2 . TFA was then dropwise added to the reaction (0.15 mL, 1.87 mmol, 1.2 equiv). The reaction stirred up to 36 h and was purified by 1) FCC using *n*-hexanes:EtOAc = 5% \rightarrow 80% (in some cases, the solvent system was switched to CH_2Cl_2 : CH_3OH = 0% \rightarrow 13%, or 2) preparatory plate (60:40 *n*-hexanes:EtOAc) to afford 3-(2-fluorophenyl)-4-methylquinolin-2-amine, **4a** as a white solid (346.1 mg, 1.0 mmol, 64%, 10:90 e.r.).

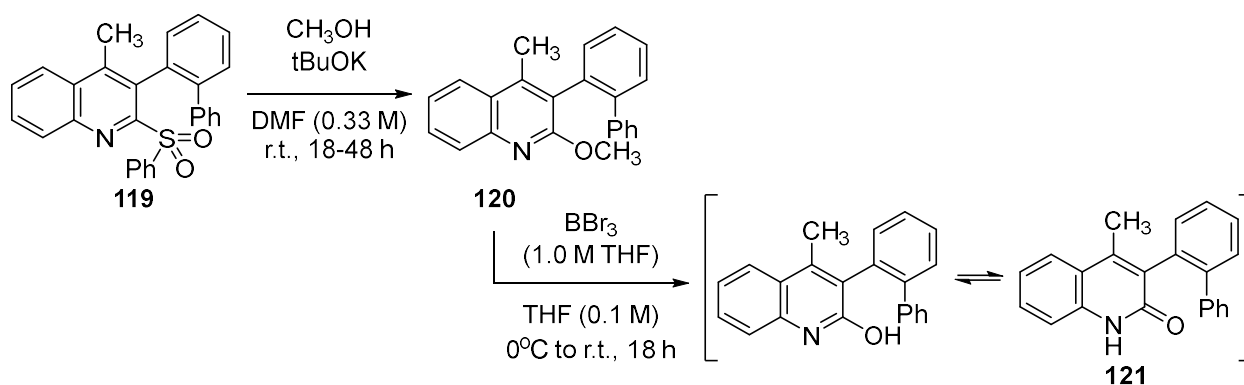
$^1\text{H NMR}$ (400 MHz, CDCl_3) δ (ppm) = 11.37 (s, 1H), 7.76 (d, J = 8.2 Hz, 1H), 7.48 (t, J = 7.7 Hz, 1H), 7.44 – 7.37 (m, 1H), 7.36 – 7.18 (m, 6H), 2.36 (s, 3H).

$^{13}\text{C NMR}$ (101 MHz, CDCl_3) δ (ppm) = 165.02, 164.76, 163.39, 162.35, 152.83, 146.85, 145.26, 137.71, 132.55, 130.66, 129.05, 126.40, 125.22, 123.65, 120.75, 17.03.

$^{19}\text{F NMR}$ (376 MHz, CDCl_3) δ (ppm) = -113.63.

MS (APCI) Calculated: 252.3 calculated $[\text{M}]^+$ for $\text{C}_{16}\text{H}_{13}\text{FN}_2$; experimental 252.1

2.2.16 Enantioenriched 3-([1,1'-biphenyl]-2-yl)-2-methoxy-4-methylquinoline 121



Equation 46. $\text{S}_{\text{N}}\text{Ar}$ procedure towards 3-arylquinolin-2-ols (**5**) was adapted from work by Patel and coworkers.^[18]

Step 1. To **119** (50 mg, 0.115 mmol, 1.0 equiv) was added MeOH (15 μL , 0.138 mmol, 1.2 equiv), and 350 μL DMF (0.33 M). The reaction was cooled to 0 °C, and $t\text{BuOK}$ (10 mg, 0.115 mmol, 1.2 equiv) was slowly added. The resulting reaction was warmed slowly to room temperature over the course of 2 days. The resulting reaction was then diluted with EtOAc and partitioned with saturated ammonium chloride. The organic layer was extracted out, and subsequently rinsed with brine. The resulting organic layers were recombined, dried over Na_2SO_4 , recollected after filtration, and concentrated *in vacuo*. The crude product of this step was then purified by FCC using n -hexanes: EtOAc = 5% \rightarrow 80% to afford enantioenriched 3-([1,1'-

biphenyl]-2-yl)-2-methoxy-4-methylquinoline 120 as a white solid (30 mg, 0.0921 mmol, 80%, 16:84 e.r.).

¹H NMR (500 MHz, CDCl₃) δ (ppm) = 7.87 (d, J = 8.1 Hz, 1H), 7.81 (dd, J = 8.3, 1.5 Hz, 1H), 7.61 – 7.57 (m, 1H), 7.51 – 7.50 (m, 1H), 7.49 (d, J = 1.0 Hz, 1H), 7.45 (ddd, J = 7.3, 5.3, 3.6 Hz, 1H), 7.37 (ddd, J = 8.3, 7.0, 1.3 Hz, 1H), 7.26 (dt, J = 7.3, 1.2 Hz, 1H), 7.15 – 7.10 (m, 5H), 3.91 (s, 3H), 2.26 (s, 3H).

¹³C NMR (126 MHz, CDCl₃) δ (ppm) = 160.25, 145.48, 143.90, 142.57, 141.55, 134.85, 131.10, 130.03, 129.04, 128.68, 128.13, 127.88, 127.51, 127.28, 126.82, 125.54, 125.27, 124.24, 123.96, 53.71, 29.84, 15.92.

MS (APCI) Calculated: 325.4 calculated [M]⁺ for C₂₃H₁₉NO; experimental 325.1

Step 2. Substrate **120** was added to a 20 mL dram vial equipped with a stir bar and then dissolved in 1.0 mL of anhydrous THF (0.1 M). The reaction was then cooled to 0 °C, and then BBr₃ (69 μL, 0.111 mmol, 1.2 equiv, solution of 1.64 M THF) was added dropwise. After addition of the BBr₃, the reaction was slowly heated to room temperature, and left to stir overnight. The resulting reaction was cooled back to 0 °C, quenched slowly with diH₂O, and slowly warmed to room temperature. The reaction was then diluted with EtOAc and then poured to a separatory funnel. The resulting organic layer was obtained, rinsed with brine, and then recollected. The resulting organic layer was dried with Na₂SO₄, collected, and concentrated *in vacuo*. The crude residue containing desired product was purified in FCC using *n*-hexanes:EtOAc = 10% → 80% to afford enantioenriched **3-([1,1'-biphenyl]-2-yl)-4-methylquinolin-2(1H)-one 5q** as a white solid (15 mg, 0.048 mmol, 52%, 16:84 e.r.).

To prepare NMR samples, 10% MeOH was added to achieve solubility.

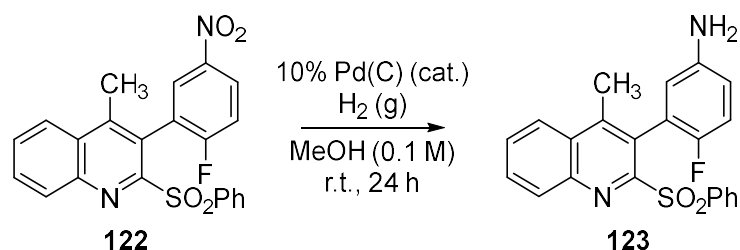
¹H NMR (400 MHz, CDCl₃) δ (ppm) = 7.81 (t, J = 8.2 Hz, 2H), 7.58 (dd, J = 8.3, 7.0 Hz, 1H), 7.50 – 7.43 (m, 3H), 7.38 – 7.33 (m, 1H), 7.26 – 7.23 (m, 1H), 7.14 – 7.09 (m, 5H), 2.25 (s, 3H).

¹³C NMR (101 MHz, CDCl₃) δ (ppm) = 160.28, 145.70, 143.69, 142.57, 141.58, 134.94, 131.12, 130.03, 128.97, 128.69, 128.11, 127.87, 127.63, 127.27, 126.81, 125.52, 125.31, 124.24, 123.88, 53.54, 29.85, 15.90, 15.87.

MS (APCI) Calculated: 311.4 calculated [M]⁺ for C₂₂H₁₇NO; experimental 312.4

HRMS (ESI) = 311.3840 calculated [M+H]⁺ found 312.1387.

2.2.17 Reduction of Nitro-groups to Yield 3-Anilines



Equation 47. Synthesis of Intermediate 123

Under degassed conditions, a 2 dram vial equipped with a stir bar was added 5-nitrophenyl sulfone **122** (225 mg, 0.53 mmol, 1.0 equiv). 10% Pd(C) (56 mg, 0.4664 mmol, 0.88 equiv) was then added in one portion. To the reaction, a H₂ balloon was equipped and slowly purged into the reaction vessel. Under this atmosphere, slow addition of 5.30 mL anhydrous, degassed MeOH (MeOH was dried over activated molecular sieves). The resulting reaction equipped with the H₂ balloon was then stirred at room temperature for at least 1 day. The resulting reaction was diluted with MeOH and filtered through Celite plug. The crude organic was concentrated *in vacuo* and purified by FCC using *n*-hexanes:EtOAc = 15% → 80% to afford **4-fluoro-3-(4-methyl-2-**

(phenylsulfonyl)quinolin-3-yl)aniline, **123** as a white solid (209 mg, 0.3445 mmol, 65%, 11.5:88.5 e.r.).

¹H NMR (400 MHz, CDCl₃) δ (ppm) = 8.10 (t, *J* = 1.9 Hz, 3H), 8.02 – 7.99 (m, 3H), 7.62 – 7.56 (m, 5H), 7.44 (d, *J* = 7.8 Hz, 3H), 2.80 (s, 3H).

¹³C NMR (101 MHz, CDCl₃) δ (ppm) = 169.93, 155.03, 145.22, 139.14, 138.10, 134.66, 133.74, 133.03, 131.04, 130.41, 130.22, 129.80, 129.30, 128.99, 128.89, 128.86, 128.55, 128.40, 128.37, 128.26, 124.21, 29.68.

¹⁹F NMR (376 MHz, CDCl₃) δ (ppm) = -122.54, -127.92 (impurity from slight over reduction).

MS (APCI) Calculated: 392.4 calculated [M]⁺ for C₂₂H₁₇FN₂O₂S; experimental 393.5

2.2.18 Racemization Kinetics

Enantiomerically enriched (or enantiopure) compound (<50 mg) was dissolved in ~1.5 mL of high boiling solvents (i.e., PhMe, diphenyl ether or Ph₂O). This solution was then heated at a constant temperature for indicated times. At each time point, a 100-200 μL aliquot was isolated in an HPLC vial and quenched with room temperature HPLC grade *n*-hexanes. Each sample was then injected into the chiral HPLC system.

The determination of the barrier to racemization (ΔG_{rac}) is followed according to the procedure outlined in work by Cardenas and coworkers.^[2] Please refer to Section 2.1.24 for more details. Each ΔG_{rac} per substrate is obtained from averaging two trials.

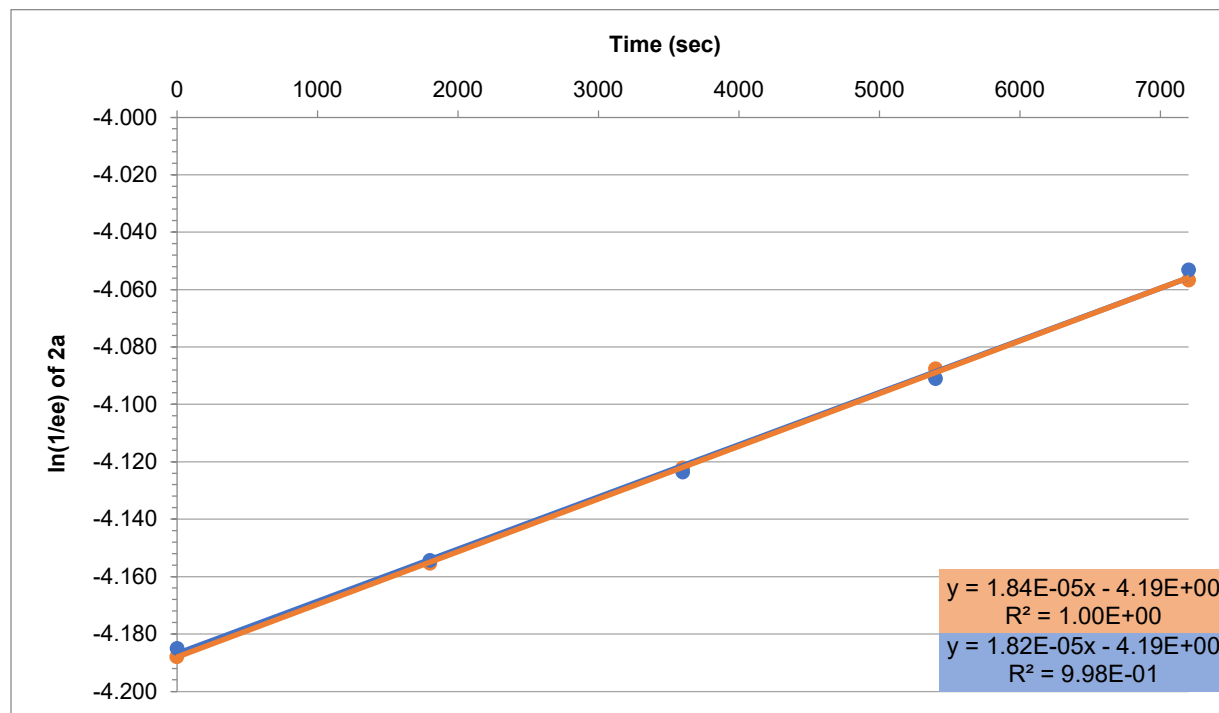
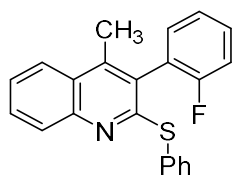


Figure 29. Barrier to Racemization of **72** at 80 °C, PhMe

Table 22. Time-dependent Enantiodegradation of **72**

Time (s)	Trial Run 1 (ee%)	Trial 1 [ln(1/ee%)]	Trial Run 2 (ee%)	Trial 2 [ln(1/ee%)]
0	71.106	-4.26417172	71.832	-4.274330
1800	62.512	-4.13535854	61.874	-4.125100
3600	54.812	-4.00390915	51.532	-3.942203
5400	47.402	-3.85866442	44.444	-3.794230
7200	35.834	-3.57889716	40.440	-3.699819

Average $k_{\text{obs}} = 8.69 \times 10^{-5}$, Average $k_{\text{rac}} = 4.34 \times 10^{-5}$

Calculated, Average $\Delta G_{\text{rac}} = 27.87 \text{ kcal mol}^{-1}$ (116.61 kJ mol^{-1})

Calculated $t_{1/2}$ (37 °C) = 0.141 y (or 52 d)

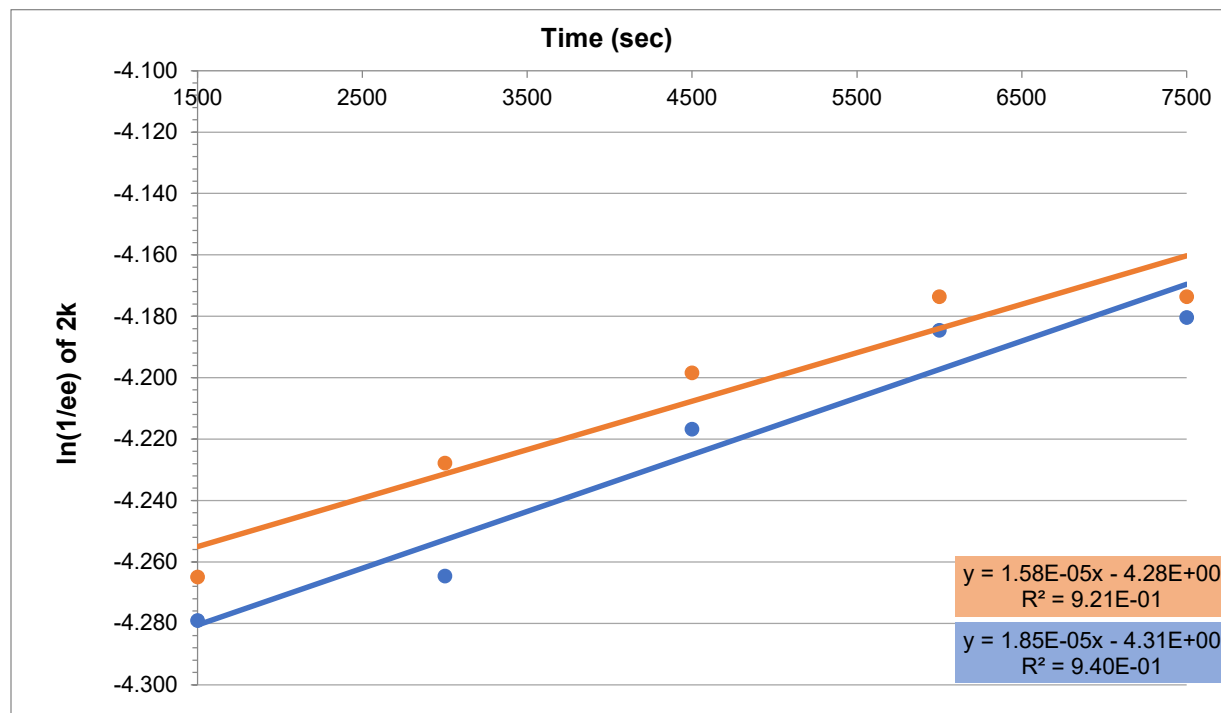
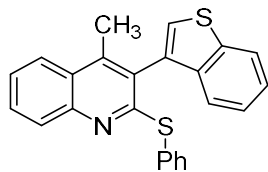


Figure 30. Barrier to Racemization of **96** at 80 °C, PhMe

Table 23. Time-dependent Enantiodegradation of **96**

Time (s)	Trial Run 1 (ee%)	Trial 1 [ln(1/ee%)]	Trial Run 2 (ee%)	Trial 2 [ln(1/ee%)]
1500	72.170	-4.2790244	71.968	-4.264847
3000	71.132	-4.2645373	71.154	-4.22768
4500	67.806	-4.2166507	68.558	-4.198314
6000	65.656	-4.1844351	66.574	-4.173495
7500	65.385	-4.1802929	64.942	-4.173495

Average $k_{\text{obs}} = 1.71 \times 10^{-5}$, Average $k_{\text{rac}} = 8.57 \times 10^{-6}$

Calculated, Average $\Delta G_{\text{rac}} = 29.01 \text{ kcal mol}^{-1}$ (121.37 kJ mol^{-1})

Calculated $t_{1/2}$ (37 °C) = 0.897 y (or 327 d)

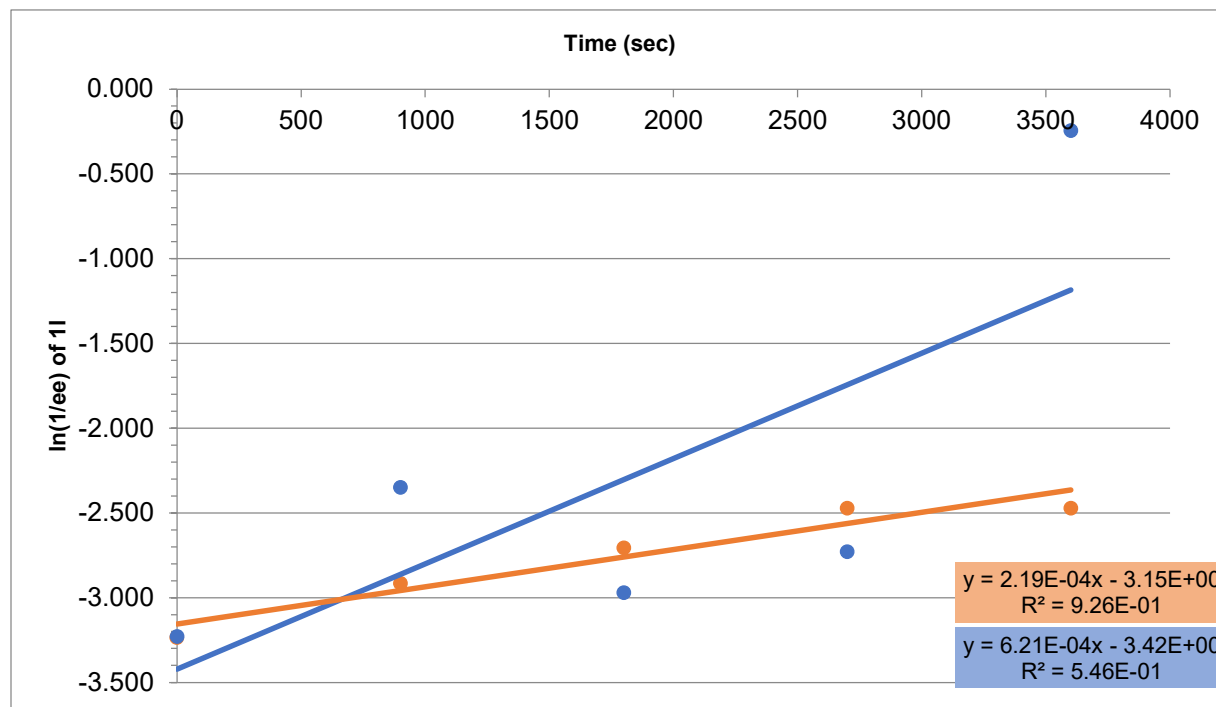
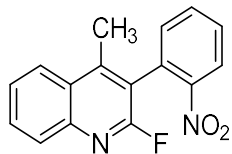


Figure 31. Barrier to Racemization of **98** at 55 °C, PhMe

Table 24. Time-dependent Enantiodegradation of **98**

Time (s)	Trial Run 1 (ee%)	Trial 1 [ln(1/ee%)]	Trial Run 2 (ee%)	Trial 2 [ln(1/ee%)]
0	25.198	-3.22676463	25.440	-3.236323
900	19.456	-2.34774964	21.732	-2.914088
1800	15.282	-2.96815551	18.432	-2.705246
2700	10.462	-2.72667567	14.958	-2.470470
3600	1.274	-0.24216866	11.828	-2.470470

Average $k_{\text{obs}} = 4.20 \times 10^{-4}$, Average $k_{\text{rac}} = 2.10 \times 10^{-4}$

Calculated, Average $\Delta G_{\text{rac}} = 24.81 \text{ kcal mol}^{-1}$ (103.81 kJ mol^{-1})

Calculated $t_{1/2}$ (37 °C) = 8.8 h

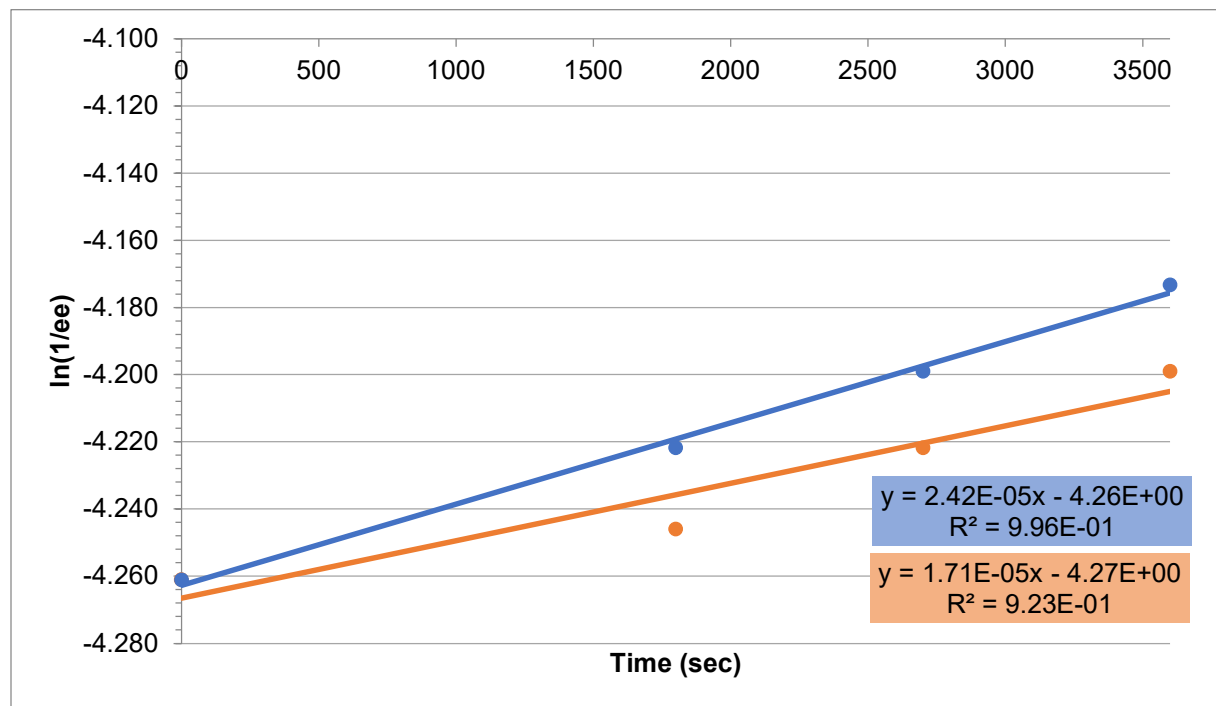
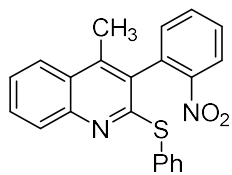


Figure 32. Barrier to Racemization of **97** at 100 °C, PhMe

Table 25. Time-dependent Enantiodegradation of **97**

Time (s)	Trial Run 1 (ee%)	Trial 1 [ln(1/ee%)]	Trial Run 2 (ee%)	Trial 2 [ln(1/ee%)]
0	70.884	-4.26104474	70.884	-4.261045
1800	68.150	-4.22171116	69.818	-4.245892
2700	66.612	-4.19888474	68.150	-4.221711
3600	64.920	-4.17315574	66.612	-4.198885

Average $k_{\text{obs}} = 2.06 \times 10^{-5}$, Average $k_{\text{rac}} = 1.03 \times 10^{-5}$

Calculated, Average $\Delta G_{\text{rac}} = 30.6 \text{ kcal mol}^{-1}$ (127.84 kJ mol^{-1})

Calculated $t_{1/2}$ (37 °C) = 11 y

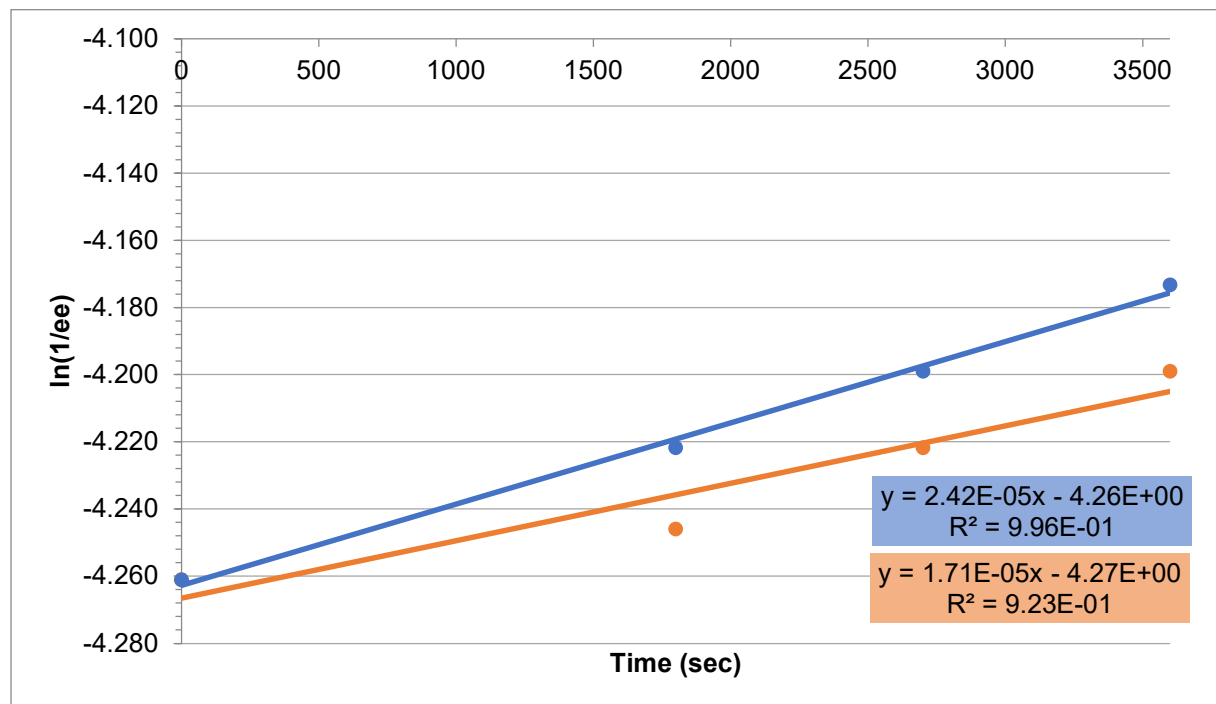
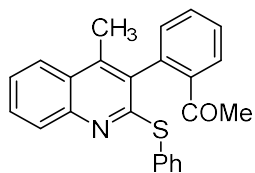


Figure 33. Barrier to Racemization of **103** at 100 °C, PhMe

Table 26. Time-dependent Enantiodegradation of **103**

Time (s)	Trial Run 1 (ee%)	Trial 1 [ln(1/ee%)]	Trial Run 2 (ee%)	Trial 2 [ln(1/ee%)]
0	25.197	-3.22674081	25.439	-3.236299
1800	19.463	-2.96849468	21.733	-3.078823
3600	15.282	-2.72670184	14.957	-2.705193
5400	12.047	-2.48853340	11.827	-2.470402

Average $k_{\text{obs}} = 1.42 \times 10^{-4}$, Average $k_{\text{rac}} = 7.12 \times 10^{-5}$

Calculated, Average $\Delta G_{\text{rac}} = 29.12 \text{ kcal mol}^{-1}$ (121.84 kJ mol⁻¹)

Calculated $t_{1/2}$ (37 °C) = 1.08 y (or 393 d)

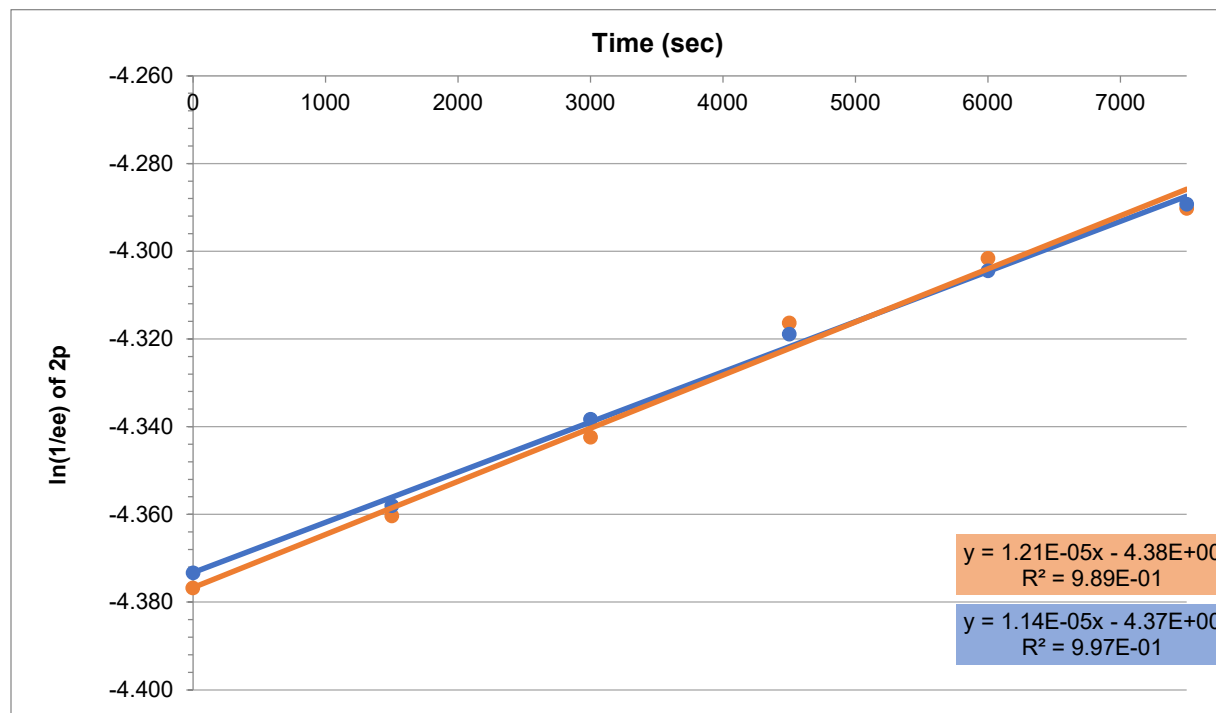
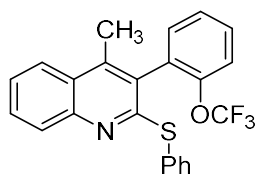


Figure 34. Barrier to Racemization of **105** at 118 °C, PhMe

Table 27. Time-dependent Enantiodegradation of **105**

Time (s)	Trial Run 1 (ee%)	Trial 1 [ln(1/ee%)]	Trial Run 2 (ee%)	Trial 2 [ln(1/ee%)]
0	79.304	-4.3732886	79.584	-4.376813
1500	78.098	-4.3579644	78.280	-4.360292
3000	76.574	-4.3382576	76.888	-4.34235
4500	75.102	-4.3188472	74.910	-4.316287
6000	74.022	-4.3043623	73.812	-4.301521
7500	72.910	-4.2892258	72.976	-4.290131

Average $k_{\text{obs}} = 1.18 \times 10^{-5}$, Average $k_{\text{rac}} = 5.89 \times 10^{-6}$

Calculated, Average $\Delta G_{\text{rac}} = 32.50 \text{ kcal mol}^{-1}$ (135.99 kJ mol^{-1})

Calculated $t_{1/2}$ (37 °C) = 258.83 y (or 94,472 d)

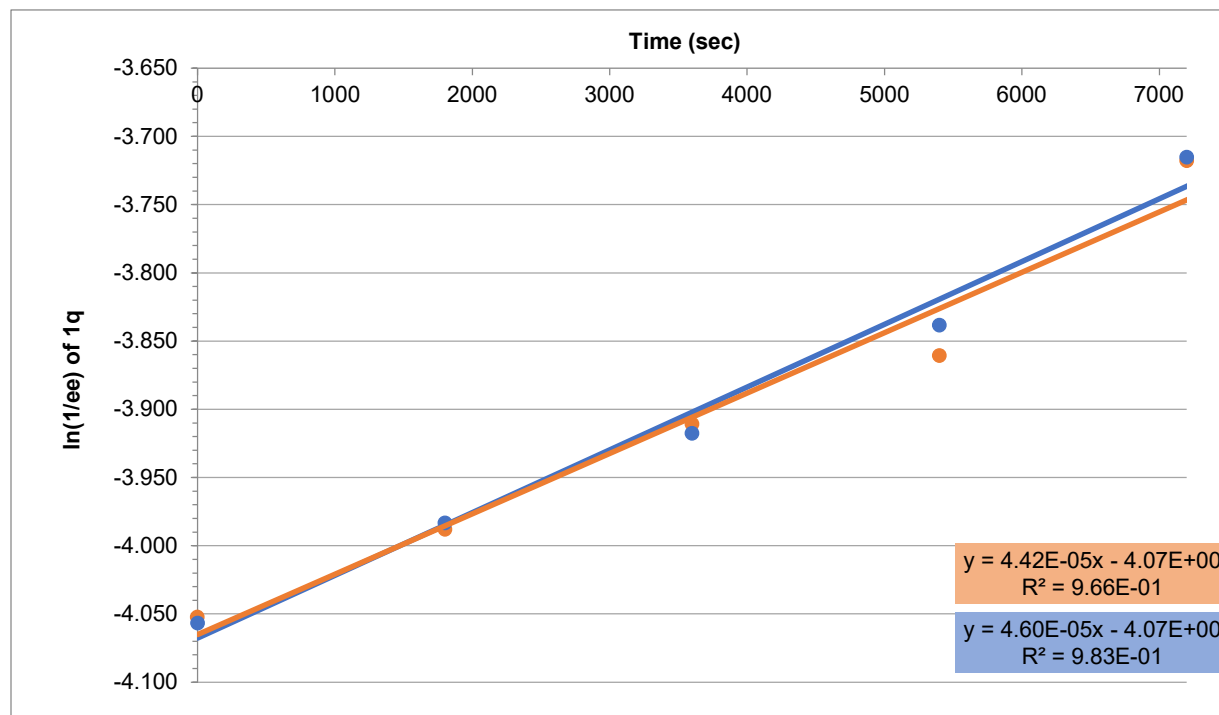
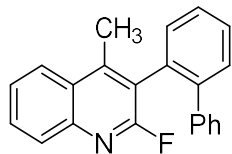


Figure 35. Barrier to Racemization of **108** at 81 °C , PhMe

Table 28. Time-dependent Enantiodegradation of **108**

Time (s)	Trial Run 1 (ee%)	Trial 1 [ln(1/ee%)]	Trial Run 2 (ee%)	Trial 2 [ln(1/ee%)]
0	57.768	-4.0564350	57.526	-4.052237
1800	53.676	-3.9829660	53.928	-3.987650
3600	50.266	-3.9173289	49.932	-3.910662
5400	46.440	-3.8381612	47.486	-3.860435
7200	41.060	-3.7150344	41.166	-3.717613

Average $k_{obs} = 4.51 \times 10^{-5}$, Average $k_{rac} = 2.26 \times 10^{-5}$

Calculated, Average $\Delta G_{rac} = 28.41 \text{ kcal mol}^{-1}$ (118.87 kJ mol⁻¹)

Calculated $t_{1/2}$ (37 °C) = 0.341 y (or 124 d)

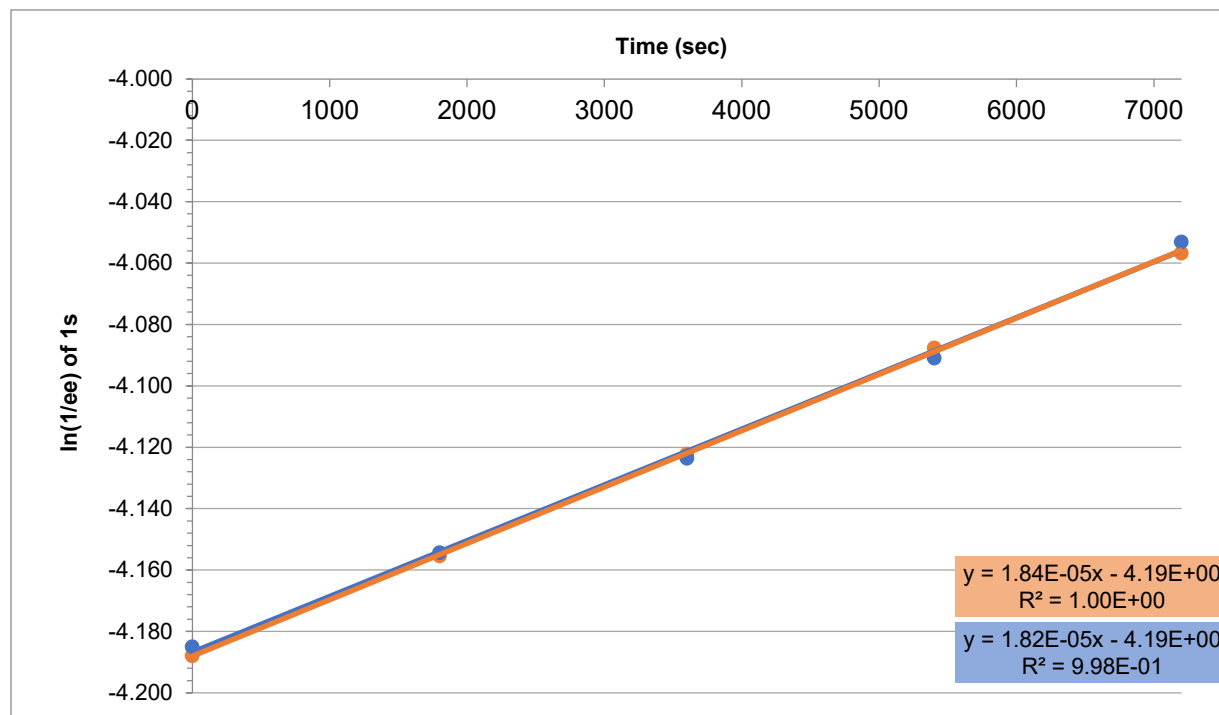
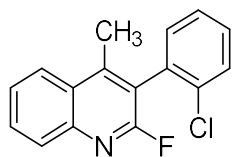


Figure 36. Barrier to Racemization of **112** at 81 °C, PhMe

Table 29. Time-dependent Enantiodegradation of **112**

Time (s)	Trial Run 1 (ee%)	Trial 1 [ln(1/ee%)]	Trial Run 2 (ee%)	Trial 2 [ln(1/ee%)]
0	65.688	-4.1849163	65.890	-4.187987
1800	63.703	-4.1542317	63.772	-4.155314
3600	61.776	-4.1235149	61.688	-4.122089
5400	59.794	-4.0909053	59.590	-4.087488
7200	57.569	-4.0529842	57.780	-4.056643

Average $k_{obs} = 1.83 \times 10^{-5}$, Average $k_{rac} = 9.03 \times 10^{-6}$

Calculated, Average $\Delta G_{rac} = 30.64 \text{ kcal mol}^{-1}$ (128.20 kJ mol^{-1})

Calculated $t_{1/2}$ (37 °C) = 12.75 y (or 4,558 d)

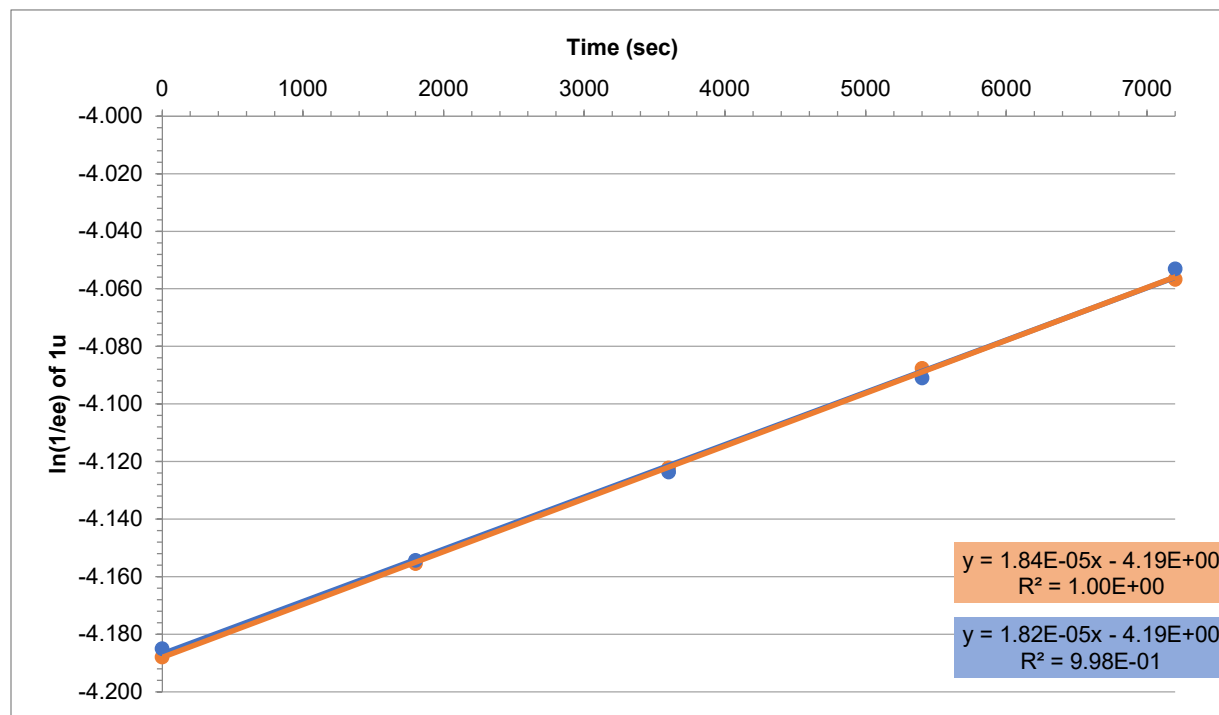
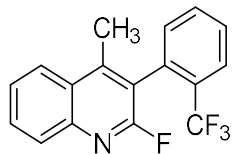


Figure 37. Barrier to Racemization of **73** at 130 °C, Ph₂O

Table 30. Time-dependent Enantiodegradation of **73**

Time (s)	Trial Run 1 (ee%)	Trial 1 [ln(1/ee%)]	Trial Run 2 (ee%)	Trial 2 [ln(1/ee%)]
0	84.430	-4.43592279	85.380	-4.447112
1800	81.724	-4.40334772	82.234	-4.409569
3600	77.670	-4.35246908	77.324	-4.348004
5400	73.858	-4.30214433	74.390	-4.309322
7200	70.864	-4.26076255	70.816	-4.260085

Average $k_{obs} = 2.57 \times 10^{-5}$, Average $k_{rac} = 1.29 \times 10^{-5}$

Calculated Average $\Delta G_{rac} = 32.90$ kcal mol⁻¹ (137.65 kJ mol⁻¹)

Calculated $t_{1/2}$ (37 °C) = 491.2 y (or 179,282 d)

2.2.19 Chiral HPLC Traces of Enantioenriched Products and Starting Materials

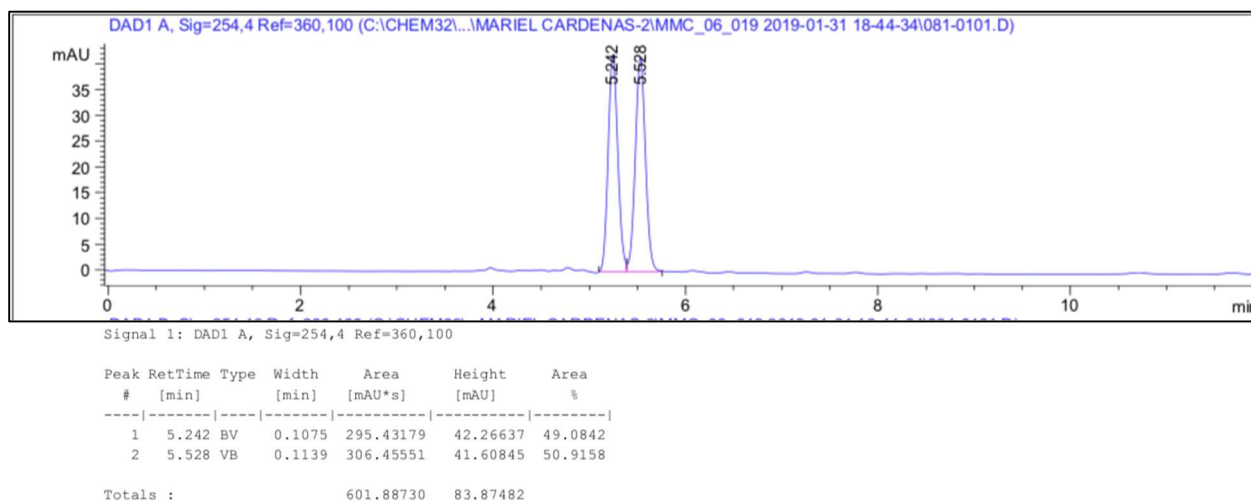
major enantiomer,
(*R*_a)-**72**

Enantioselectivity of **72** was measured using a Daicel Corp. Chiralpak IC Column (4.6 mm ϕ \times 250 mL, Particle Size 5 μ M, Part No. 83325). *Method*: Hexanes:IPA (98:2), flow rate = 0.7 mL/min, *t*_R = 5.1 min (minor) and *t*_R = 5.4 min (major).

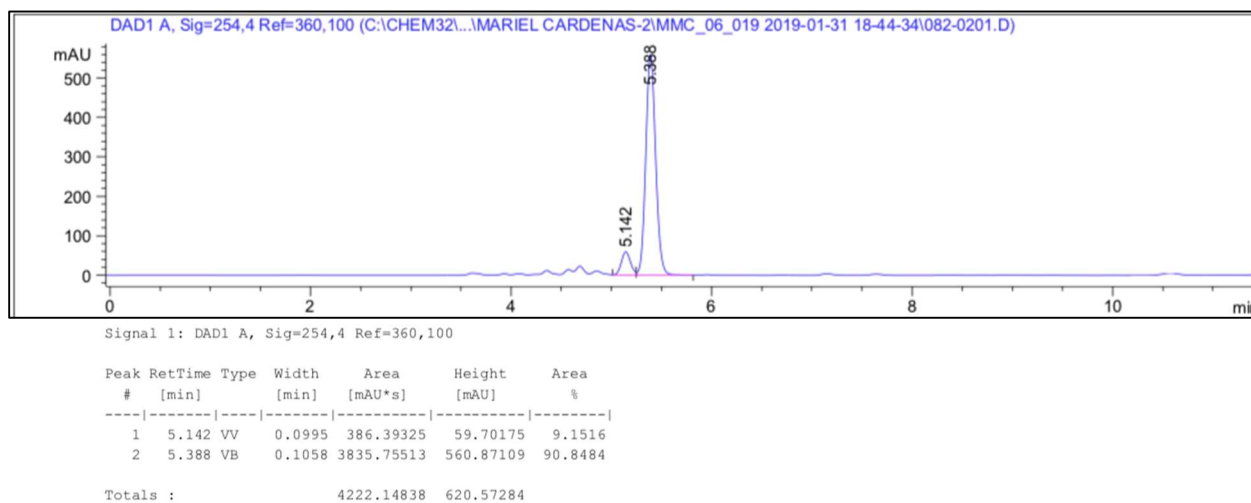
→ Determined, averaged of 9 trials: 9:91 e.r., 82 ee%

Sample Trace: 9:91 e.r., 82 ee%

Racemic Standard of **72**



Sample HPLC of **72**



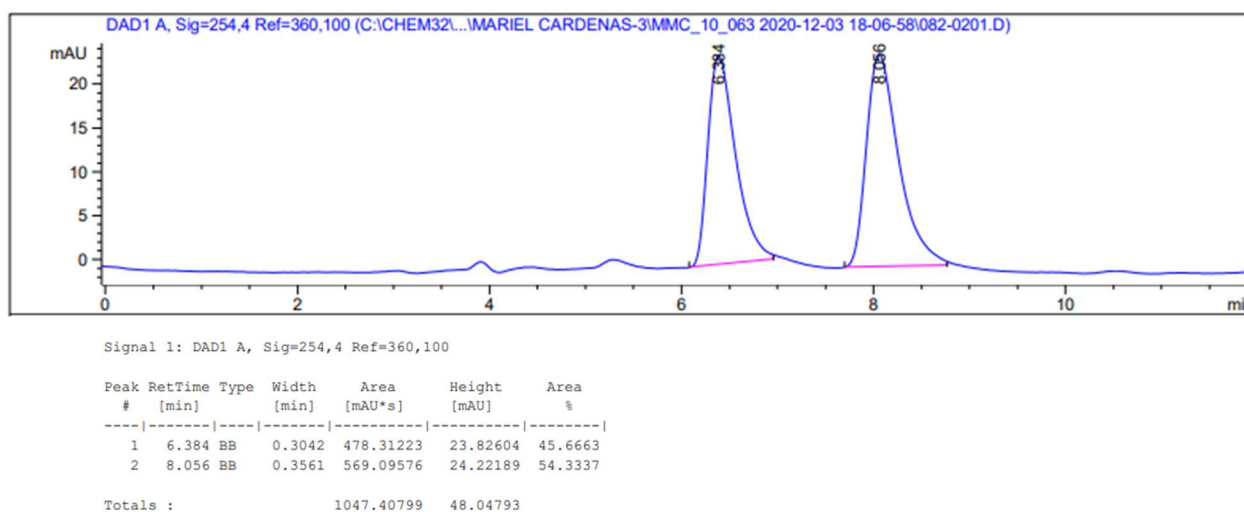
major enantiomer,
(*R*_a)-**80**

Enantioselectivity of **80** was measured with chiral HPLC analysis using a Daicel Corp. Chiralpak IA Column (4.6 mm ϕ \times 250 mL, Particle Size 5 μ M, Part No. 80325). *Method*: Hexanes:IPA (70:30), flow rate = 1.0 mL/min, *t*_R = 6.3 min (minor) and *t*_R = 8.1 min (major).

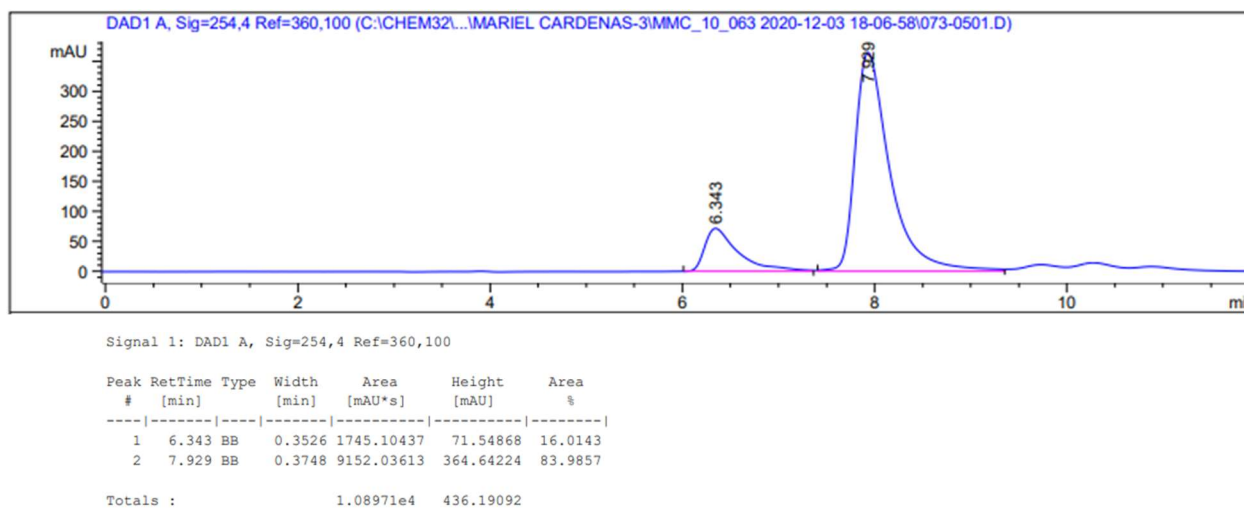
→ Determined, averaged of 5 trials: 16:84 e.r., 68 ee%

Sample Trace: 16:84 e.r., 68 ee%

Racemic Standard of **80**



Sample HPLC of **80**

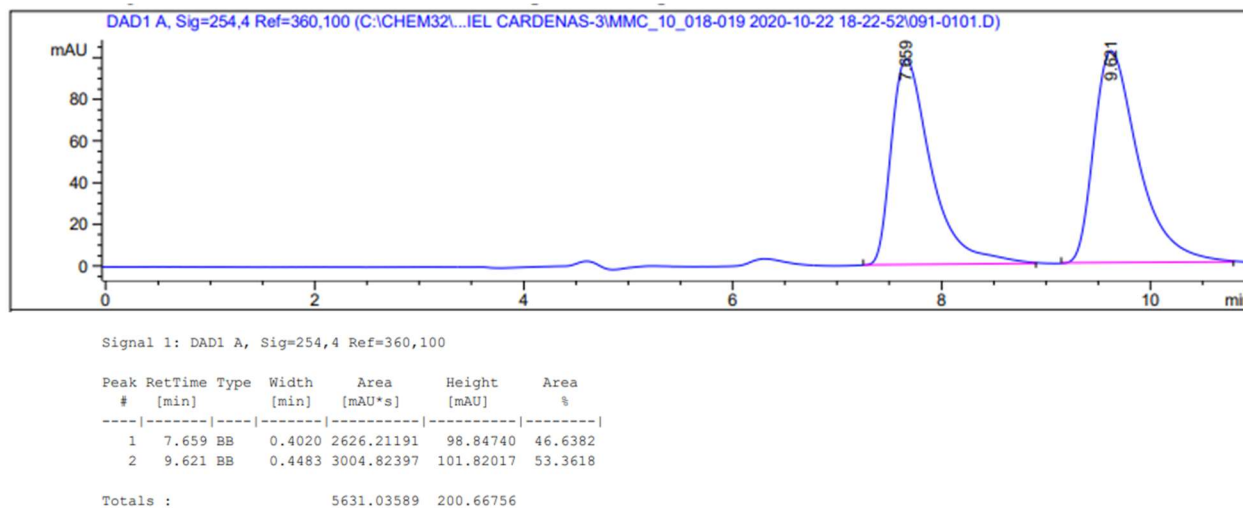


major enantiomer,
(*R*_a)-**80**

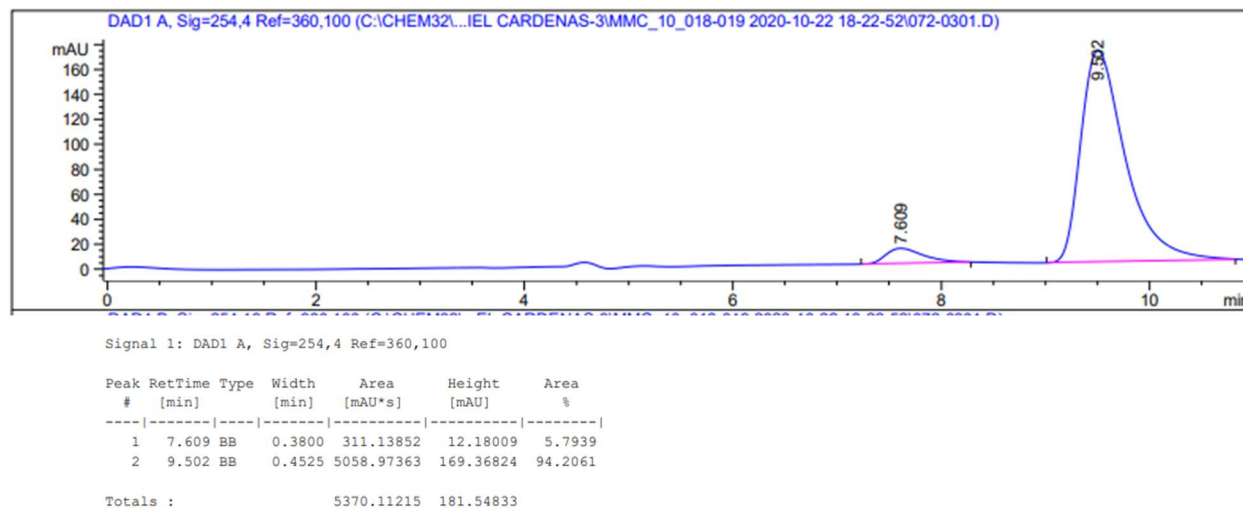
Enantioselectivity of **80** was measured with chiral HPLC analysis using a Daicel Corp. Chiralpak IA Column (4.6 mm ϕ \times 250 mL, Particle Size 5 μ M, Part No. 80325). *Method*: Hexanes:IPA (70:30), flow rate = 1.0 mL/min, *t*_R = 7.6 min (minor) and *t*_R = 9.6 min (major). Retention times were altered with polarity of the dissolved materials. Recrystallization was done using 80:20 HPLC grade *n*-Hexanes/DCE. The solid and filtrate were separated, and the solid is found to be higher e.r.

→ Determined from **80** (1.0 g): 6:94 e.r., 88 ee%

Racemic Standard of **80**



Recrystallization HPLC of **80**



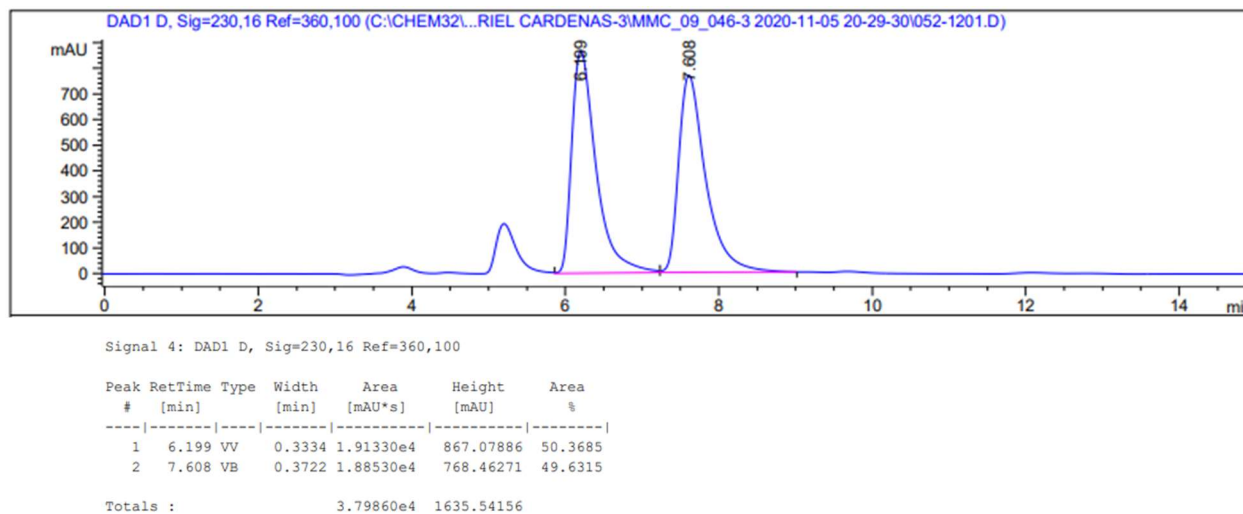
major enantiomer,
(*R*_a)-**118**

Enantioselectivity of **118** was measured with chiral HPLC analysis using a Daicel Corp. Chiralpak IA Column (4.6 mm ϕ \times 250 mL, Particle Size 5 μ M, Part No. 80325). *Method*: Hexanes:IPA (70:30), flow rate = 1.0 mL/min, *t*_R = 6.2 min (minor) and *t*_R = 7.6 min (major). Impurity that appears around 5.5 min is dichloromethane (necessary to dissolve compound).

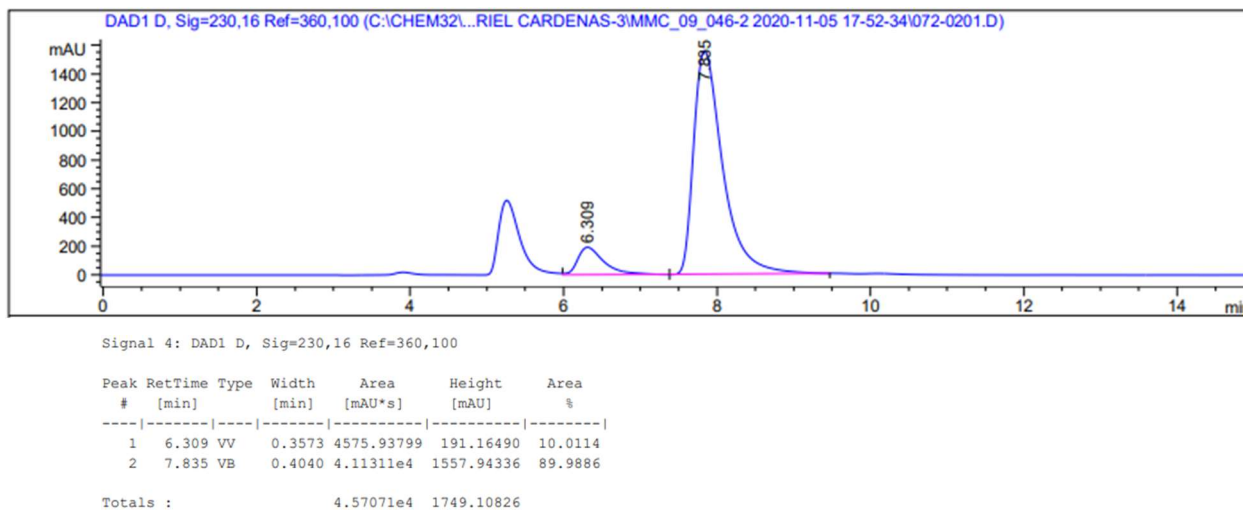
→ Determined, averaged of 3 trials: 10:90 e.r., 80 ee%

Sample Trace: 10:90 e.r., 80 ee%

Racemic Standard of **118**



Sample HPLC of **118**



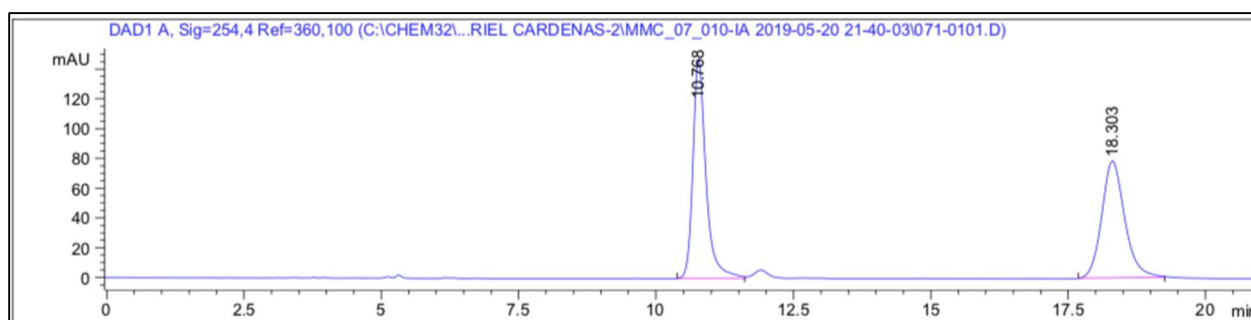
major enantiomer,
(*R*_a)-**82**

Enantioselectivity of **82** was measured with chiral HPLC analysis using a Daicel Corp. Chiralpak IA Column (4.6 mm ϕ \times 250 mL, Particle Size 5 μ M, Part No. 80325). *Method*: Hexanes:IPA (90:10), flow rate = 1.0 mL/min, *t*_R = 10.7 min (minor) and *t*_R = 18.3 min (major).

→ Determined, averaged of 3 trials: 26:74 e.r., 48 ee%

Sample Trace: 9:91 e.r., 82 ee%

Racemic Standard of **82**

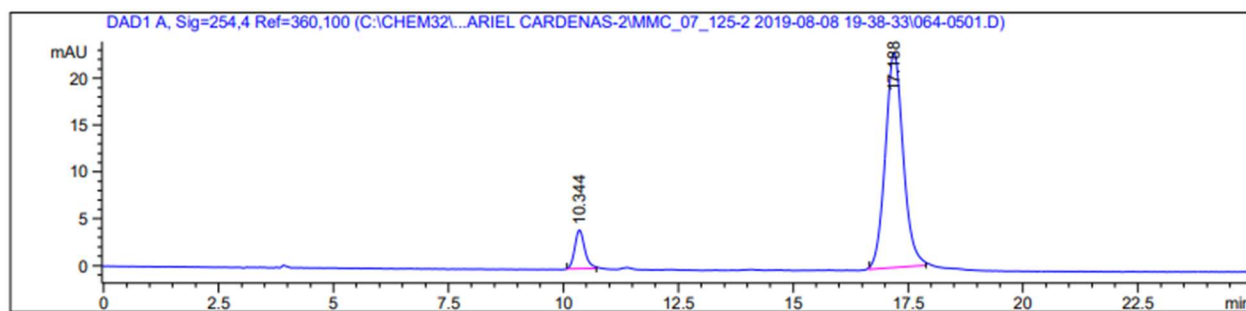


Signal 1: DAD1 A, Sig=254,4 Ref=360,100

Peak #	RetTime [min]	Type	Width [min]	Area [mAU*s]	Height [mAU]	Area %
1	10.768	BB	0.2488	2437.14453	147.46245	51.5322
2	18.303	BB	0.4442	2292.22241	78.61761	48.4678

Totals : 4729.36694 226.08006

Sample HPLC of **82**



Signal 1: DAD1 A, Sig=254,4 Ref=360,100

Peak #	RetTime [min]	Type	Width [min]	Area [mAU*s]	Height [mAU]	Area %
1	10.344	BB	0.2247	62.64346	4.13610	9.1477
2	17.188	BB	0.4100	622.15765	22.96848	90.8523

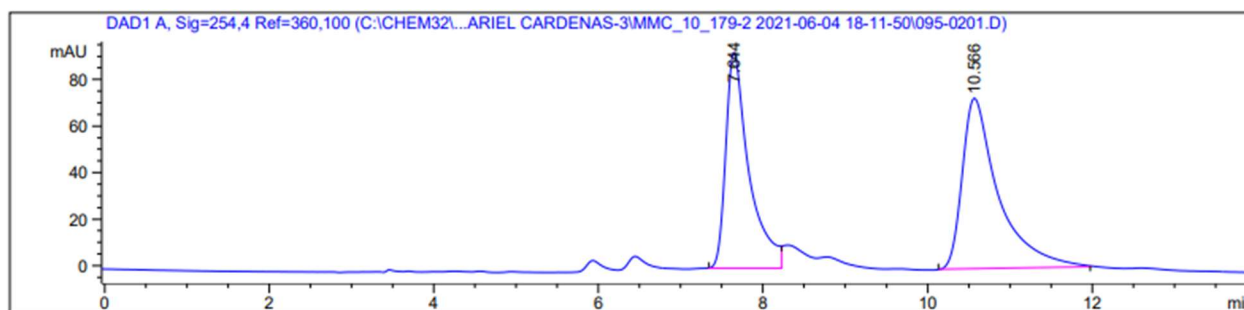
Totals : 684.80111 27.10457

Enantioselectivity of **83** was measured with chiral HPLC analysis using a Daicel Corp. Chiralpak IA Column (4.6 mm ϕ \times 250 mL, Particle Size 5 μ M, Part No. 83325). *Method*: Hexanes:IPA (99.5:0.5), flow rate = 0.7 mL/min, t_R = 7.6 min (minor) and t_R = 10.6 min (major).

major enantiomer,
(*R*_a)-**83**

→ Determined, averaged of 2 trials: 30:70 e.r., 40 ee%
Sample Trace: 31:69 e.r., 38 ee%

Racemic Standard of **83**

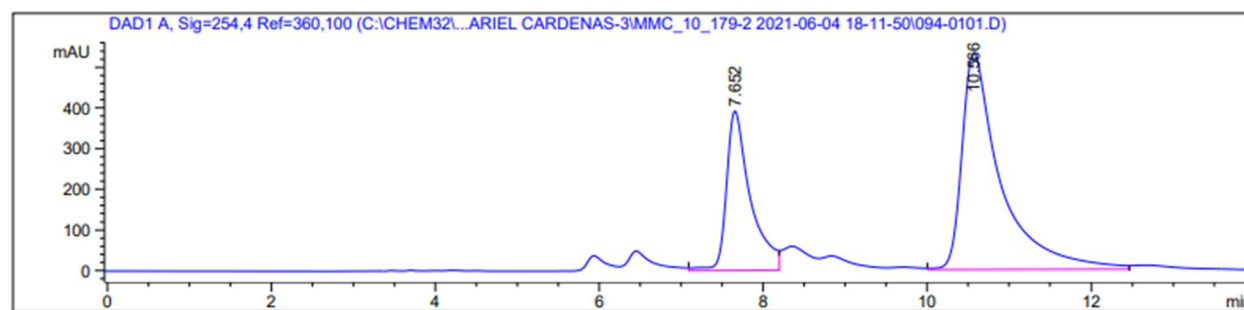


Signal 1: DAD1 A, Sig=254,4 Ref=360,100

Peak #	RetTime [min]	Type	Width [min]	Area [mAU*s]	Height [mAU]	Area %
1	7.644	BB	0.2834	1825.26208	92.81421	44.7838
2	10.566	BB	0.4398	2250.45410	73.37851	55.2162

Totals : 4075.71619 166.19272

Sample HPLC of **83**



Signal 1: DAD1 A, Sig=254,4 Ref=360,100

Peak #	RetTime [min]	Type	Width [min]	Area [mAU*s]	Height [mAU]	Area %
1	7.652	VV	0.2919	7992.03271	391.88425	31.3012
2	10.566	VB	0.4661	1.75407e4	532.80676	68.6988

Totals : 2.55327e4 924.69101

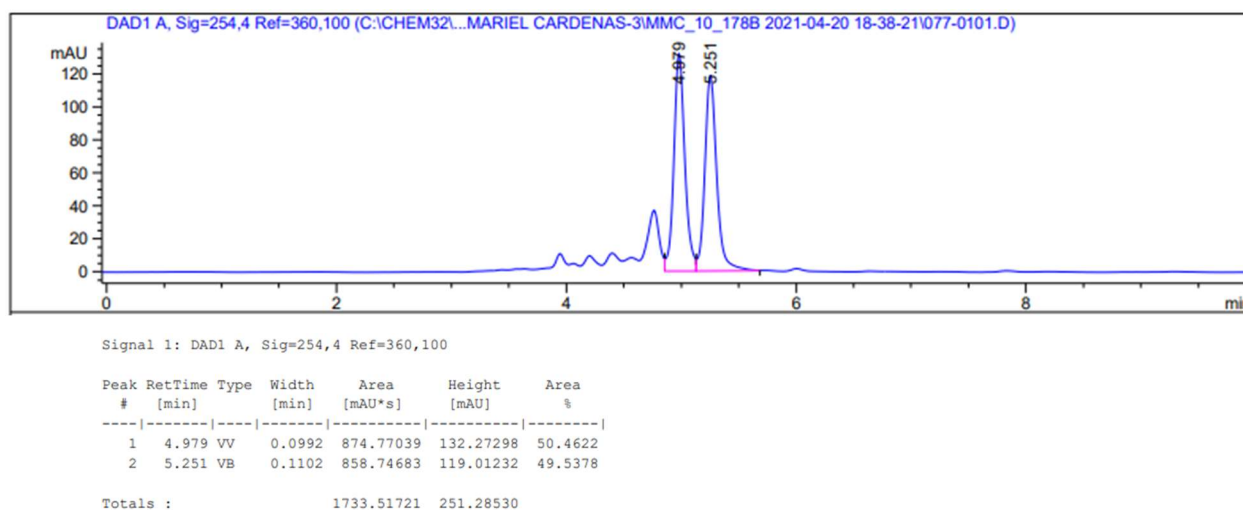
major enantiomer,
(*R*_a)-**84**

Enantioselectivity of **84** was measured with chiral HPLC analysis using a Daicel Corp. Chiralpak IC Column (4.6 mm ϕ \times 250 mL, Particle Size 5 μ M, Part No. 83325). *Method*: Hexanes:IPA (98:2), flow rate = 1.0 mL/min, *t*_R = 5.0 min (minor) and *t*_R = 5.3 min (major).

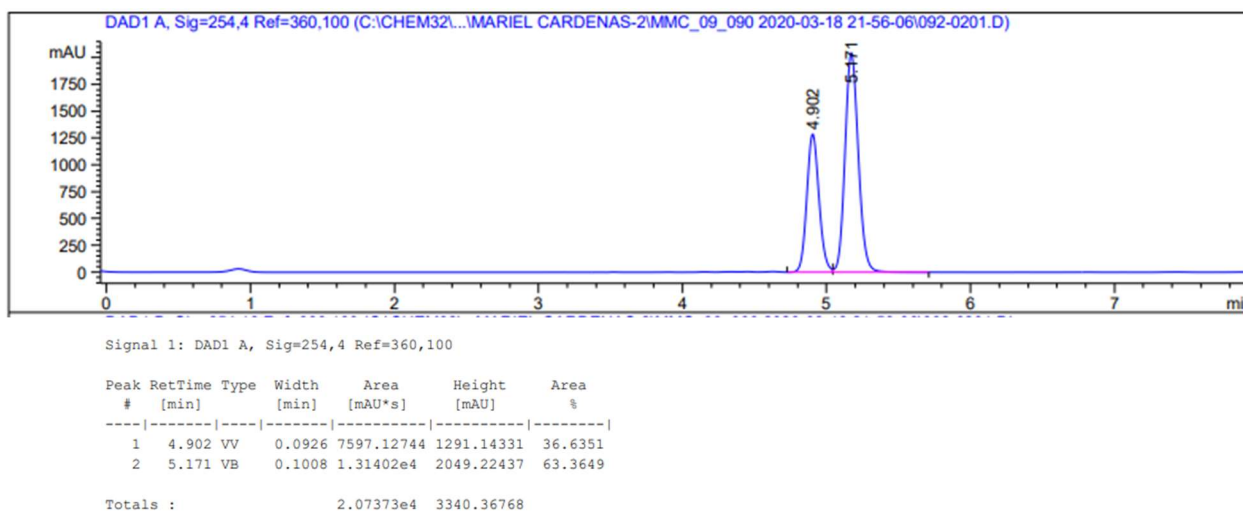
→ Determined, averaged of 4 trials: 35:65 e.r., 30 ee%

Sample Trace: 37:63 e.r., 26 ee%

Racemic Standard of **84**



Sample HPLC of **84**



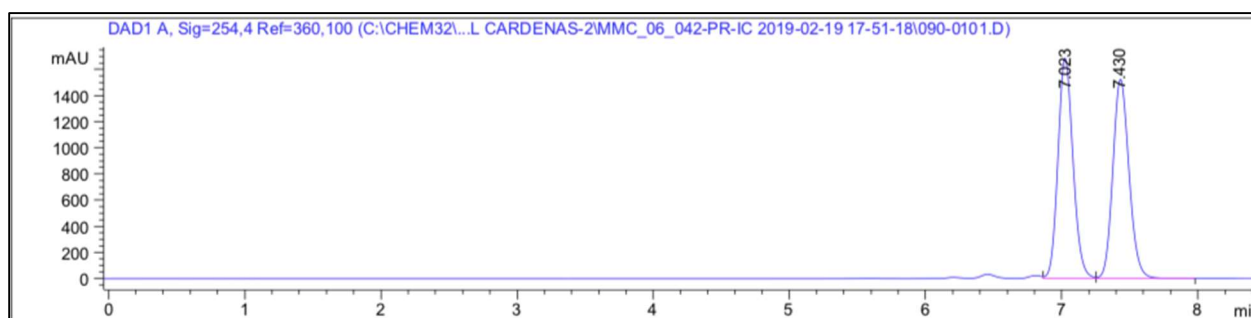
major enantiomer,
(*R*_a)-**85**

Enantioselectivity of **85** as measured with chiral HPLC analysis using a Daicel Corp. Chiralpak IC Column (4.6 mm ϕ \times 250 mL, Particle Size 5 μ M, Part No. 83325). *Method*: Hexanes:IPA (98:2), flow rate = 0.7 mL/min, *t*_R = 7.0 min (minor) and *t*_R = 7.4 min (major).

→ Determined, averaged of 4 trials: 14:86 e.r., 72 ee%

Sample Trace: 14:86 e.r., 72 ee%

Racemic Standard of **85**

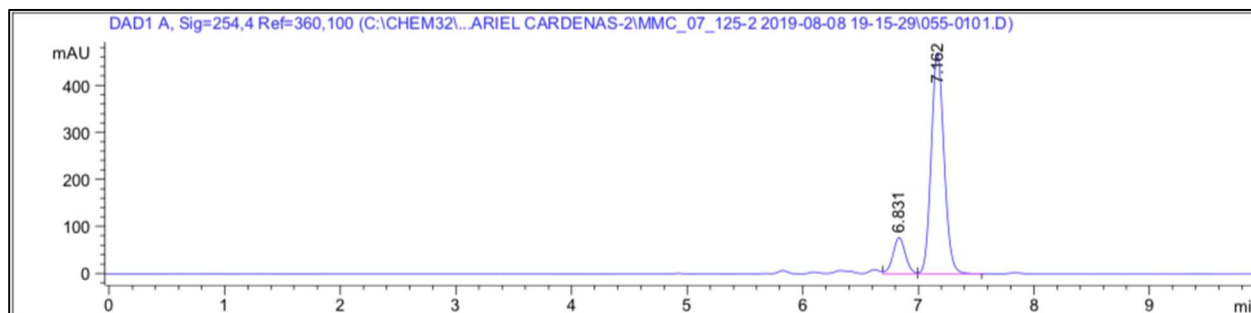


Signal 1: DAD1 A, Sig=254,4 Ref=360,100

Peak #	RetTime [min]	Type	Width [min]	Area [mAU*s]	Height [mAU]	Area %
1	7.023	VV	0.1196	1.29600e4	1687.56140	50.5657
2	7.430	VV	0.1288	1.26700e4	1526.49841	49.4343

Totals : 2.56300e4 3214.05981

Sample HPLC of **85**



Signal 1: DAD1 A, Sig=254,4 Ref=360,100

Peak #	RetTime [min]	Type	Width [min]	Area [mAU*s]	Height [mAU]	Area %
1	6.831	VV	0.1157	583.86658	77.64782	13.8582
2	7.162	VB	0.1201	3629.27271	470.17639	86.1418

Totals : 4213.13928 547.82421

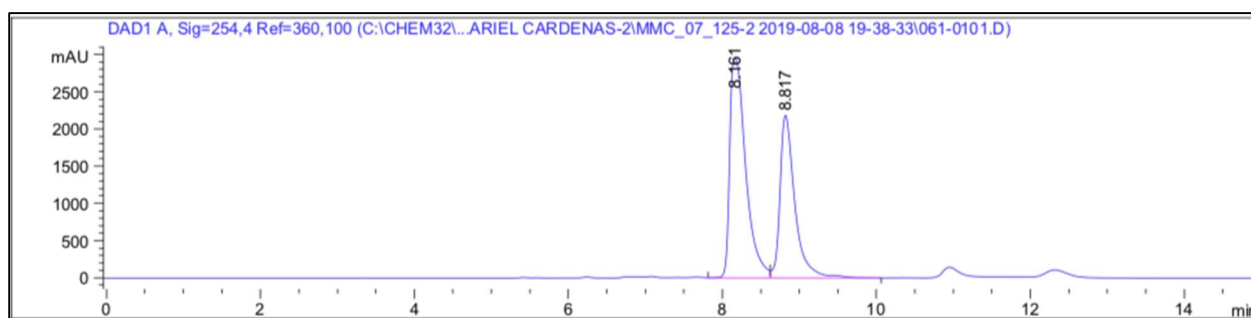
major enantiomer,
(*R*_a)-**86**

Enantioselectivity of **86** was measured with chiral HPLC analysis using a Daicel Corp. Chiralpak IA Column (4.6 mm ϕ \times 250 mL, Particle Size 5 μ M, Part No. 80325). *Method*: Hexanes:IPA (99.5:0.5), flow rate = 0.7 mL/min, *t*_R = 8.2 min (major) and *t*_R = 8.8 min (minor).

→ Determined, averaged of 6 trials: 13:87 e.r., 74 ee%

Sample Trace: 87:13 e.r., 74 ee%

Racemic Standard of **86**

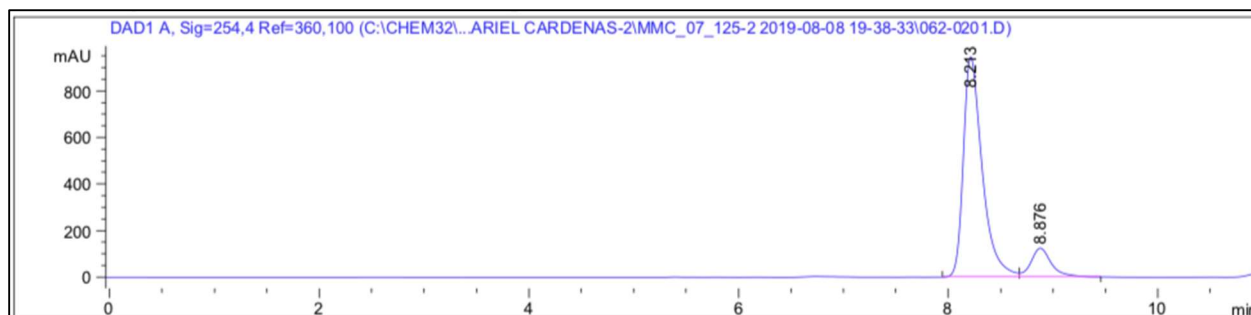


Signal 1: DAD1 A, Sig=254,4 Ref=360,100

Peak #	RetTime [min]	Type	Width [min]	Area [mAU*s]	Height [mAU]	Area %
1	8.161	VV	0.2199	4.25977e4	2959.98877	59.2020
2	8.817	VB	0.2007	2.93554e4	2185.83984	40.7980

Totals : 7.19532e4 5145.82861

Sample HPLC of **86**



Signal 1: DAD1 A, Sig=254,4 Ref=360,100

Peak #	RetTime [min]	Type	Width [min]	Area [mAU*s]	Height [mAU]	Area %
1	8.213	BV	0.1878	1.18203e4	946.12091	87.3910
2	8.876	VB	0.2061	1705.45642	124.28365	12.6090

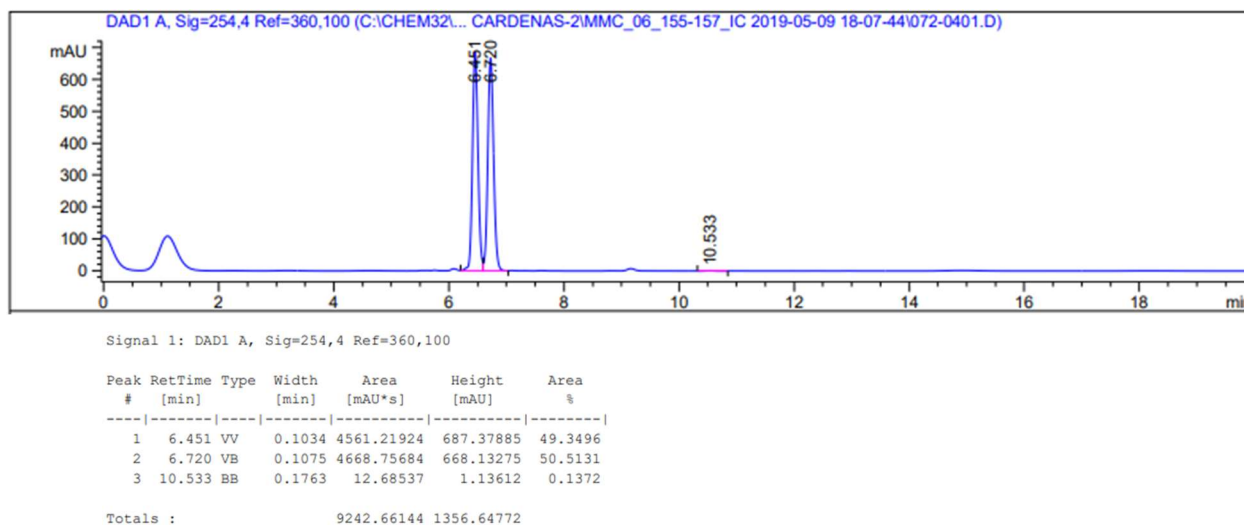
Totals : 1.35257e4 1070.40456

major enantiomer,
(*R*_a)-**87**

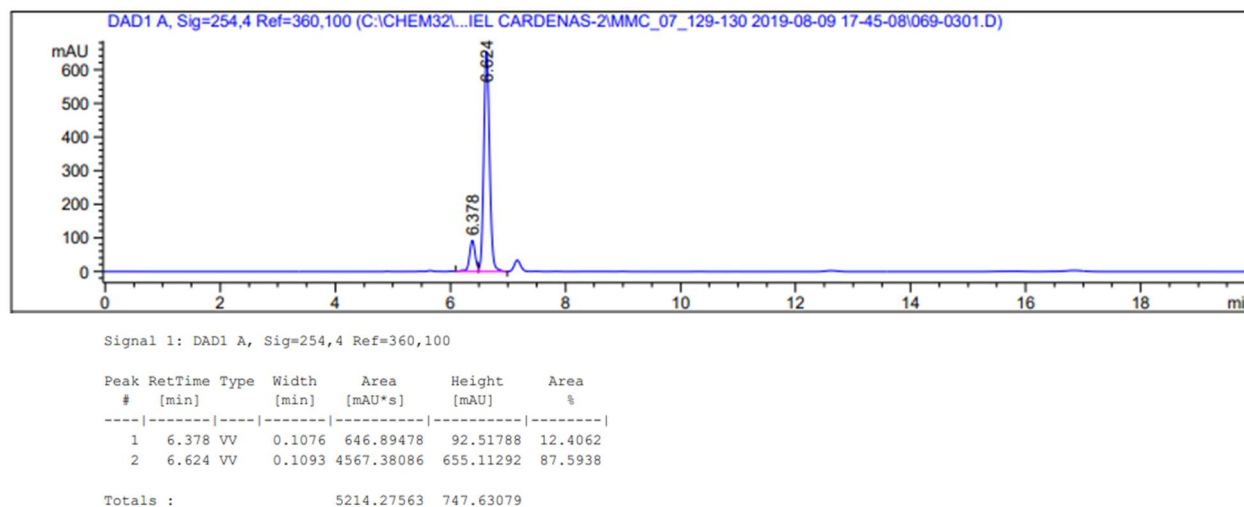
Enantioselectivity of **87** was measured with using a Daicel Corp. Chiralpak IC Column (4.6 mm ϕ \times 250 mL, Particle Size 5 μ M, Part No. 83325). *Method*: Hexanes:IPA (98:2), flow rate = 0.7 mL/min, *t*_R = 6.5 min (minor) and *t*_R = 6.7 min (major).

→ Determined, averaged of 3 trials: 12:88 e.r., 76 ee%
Sample Trace: 12:88 e.r., 76 ee%

Racemic Standard of **87**



Sample HPLC of **87**



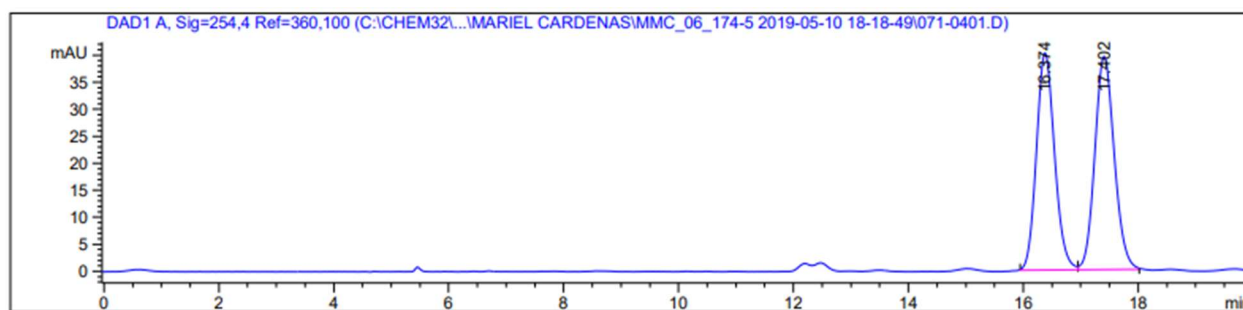
major enantiomer,
(*R*_a)-**89**

Enantioselectivity of **89** was measured with chiral HPLC analysis using a Daicel Corp. Chiralpak IC Column (4.6 mm ϕ \times 250 mL, Particle Size 5 μ M, Part No. 83325). *Method*: Hexanes:IPA (98:2), flow rate = 0.7 mL/min, *t*R = 16.4 min (major) and *t*R = 17.4 min (minor).

→ Determined, averaged of 3 trials: 16:84 e.r., 68 ee%

Sample Trace: 18:82 e.r., 64 ee%

Racemic Standard of **89**

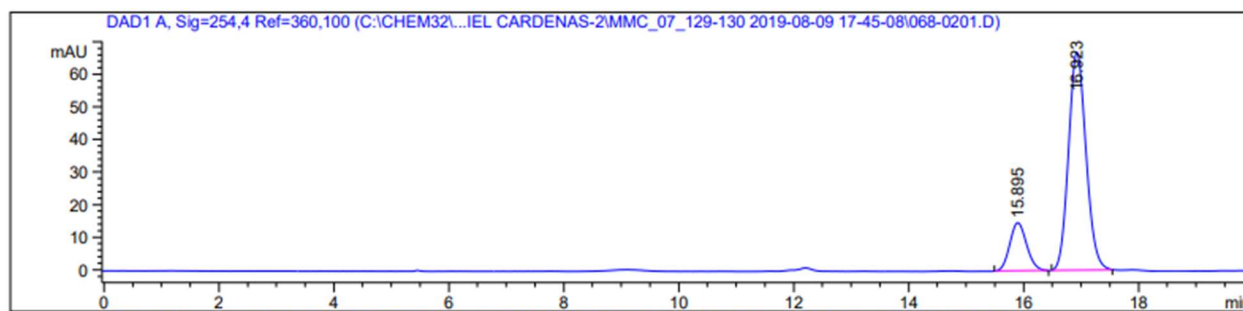


Signal 1: DAD1 A, Sig=254,4 Ref=360,100

Peak #	RetTime [min]	Type	Width [min]	Area [mAU*s]	Height [mAU]	Area %
1	16.374	BB	0.3427	885.19928	40.22905	48.7786
2	17.402	BB	0.3666	929.52887	39.49314	51.2214

Totals : 1814.72815 79.72219

Sample HPLC of **89**



Signal 1: DAD1 A, Sig=254,4 Ref=360,100

Peak #	RetTime [min]	Type	Width [min]	Area [mAU*s]	Height [mAU]	Area %
1	15.895	BB	0.3198	304.54974	14.81926	17.6505
2	16.923	BB	0.3273	1420.89368	67.02037	82.3495

Totals : 1725.44342 81.83963

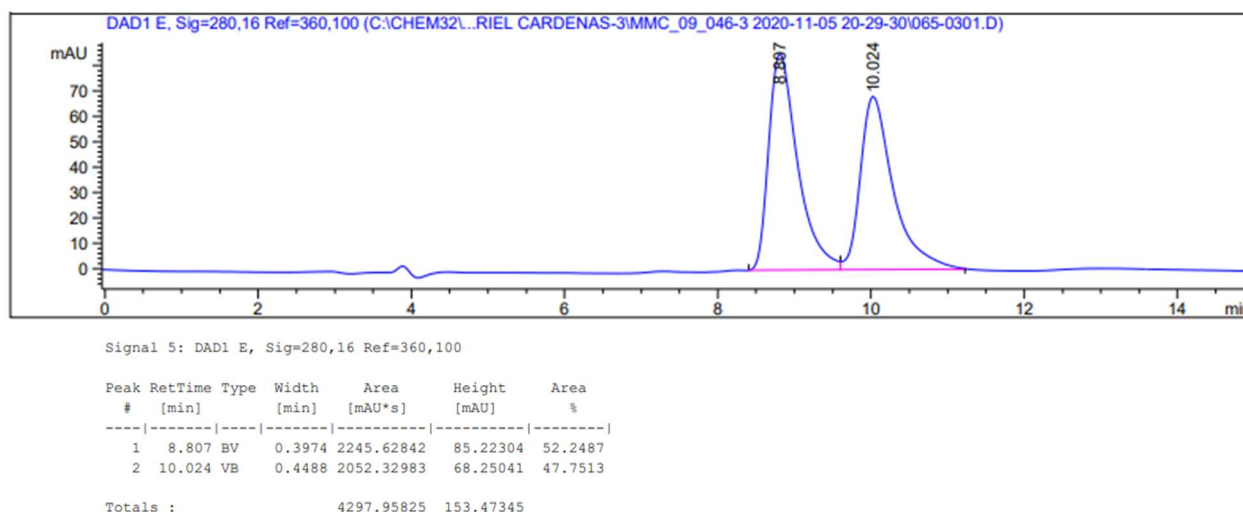
major enantiomer,
(*R*_a)-**122**

Enantioselectivity of **122** was measured with chiral HPLC analysis using a Daicel Corp. Chiralpak IA Column (4.6 mm ϕ \times 250 mL, Particle Size 5 μ M, Part No. 80325). *Method*: Hexanes:IPA (70:30), flow rate = 1.0 mL/min, *t*_R = 8.8 min (major) and *t*_R = 10.0 min (minor).

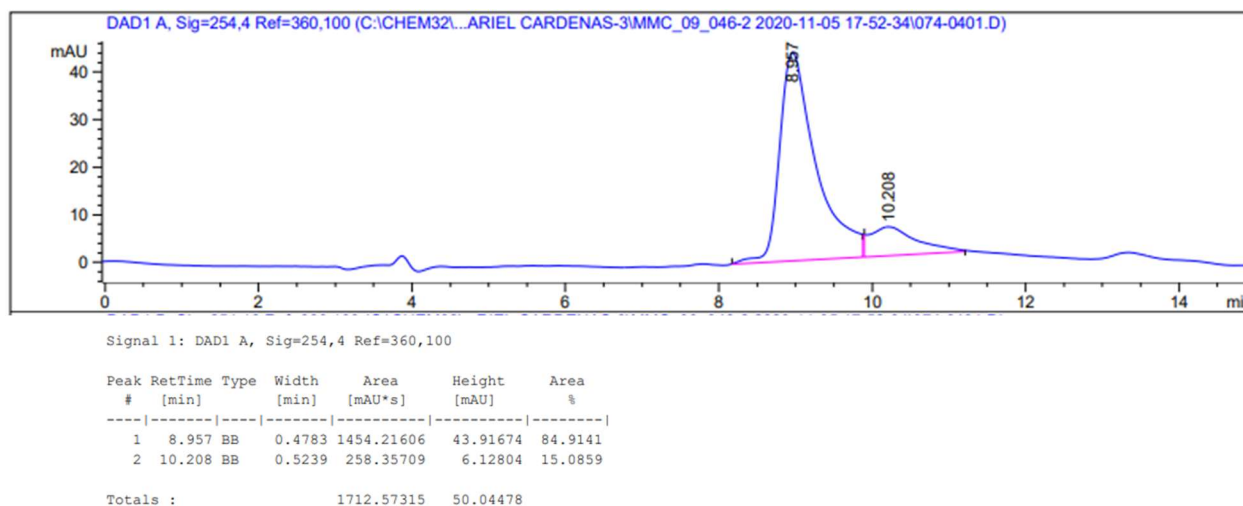
Recrystallization was done using 80:20 HPLC grade *n*-Hexanes/DCE. The solid and filtrate were separated, and the solid is found to be higher e.r.

→ Determined from **122** (500 mg): 15:85 e.r., 70 ee%

Racemic Standard of **122**



Sample → Trituration HPLC of **122**

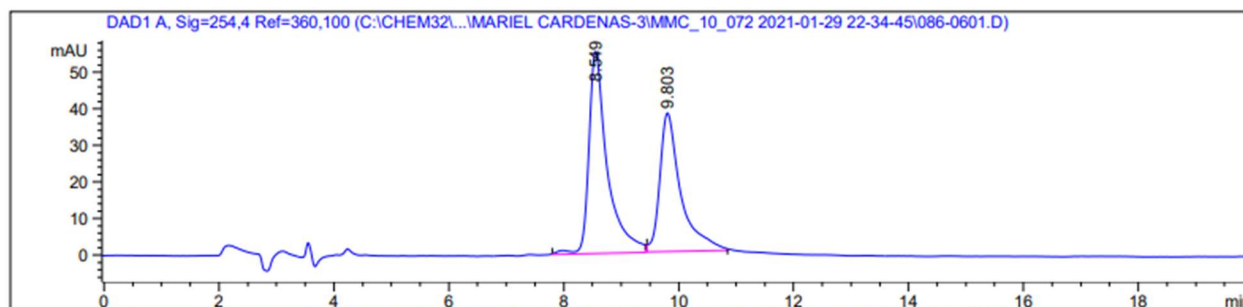


major enantiomer,
(*R*_a)-**123**

Enantioselectivity of **123** was measured with chiral HPLC analysis using a Daicel Corp. Chiralpak IA Column (4.6 mm ϕ \times 250 mL, Particle Size 5 μ M, Part No. 80325). *Method*: Hexanes:IPA (70:30), flow rate = 1.0 mL/min, *t*_R = 8.55 min (major) and *t*_R = 9.8 min (minor).

→ Determined from **123** (500 mg): 88.5:11.5 e.r., 77 ee%

Racemic Standard of **123**

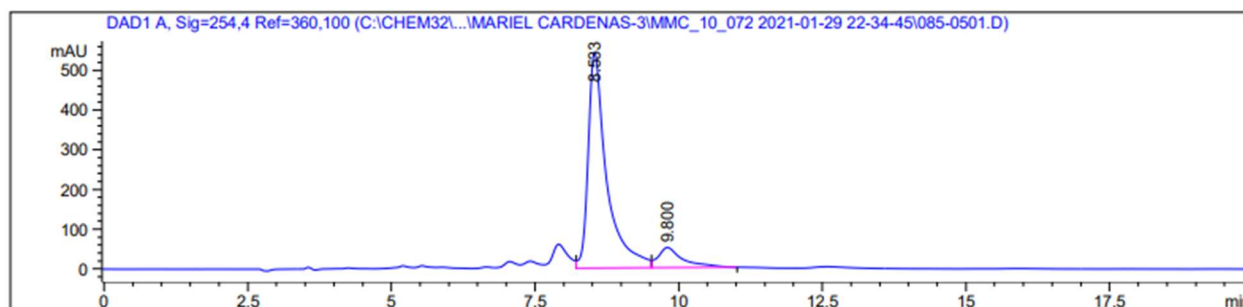


Signal 1: DAD1 A, Sig=254,4 Ref=360,100

Peak #	RetTime [min]	Type	Width [min]	Area [mAU*s]	Height [mAU]	Area %
1	8.549	BB	0.3202	1232.14343	55.25118	56.0780
2	9.803	BB	0.3648	965.05194	37.93866	43.9220

Totals : 2197.19537 93.18984

Sample HPLC of **123**



Signal 1: DAD1 A, Sig=254,4 Ref=360,100

Peak #	RetTime [min]	Type	Width [min]	Area [mAU*s]	Height [mAU]	Area %
1	8.533	VV	0.3226	1.22814e4	545.58502	88.4579
2	9.800	VB	0.4311	1602.48962	51.76992	11.5421

Totals : 1.38838e4 597.35494

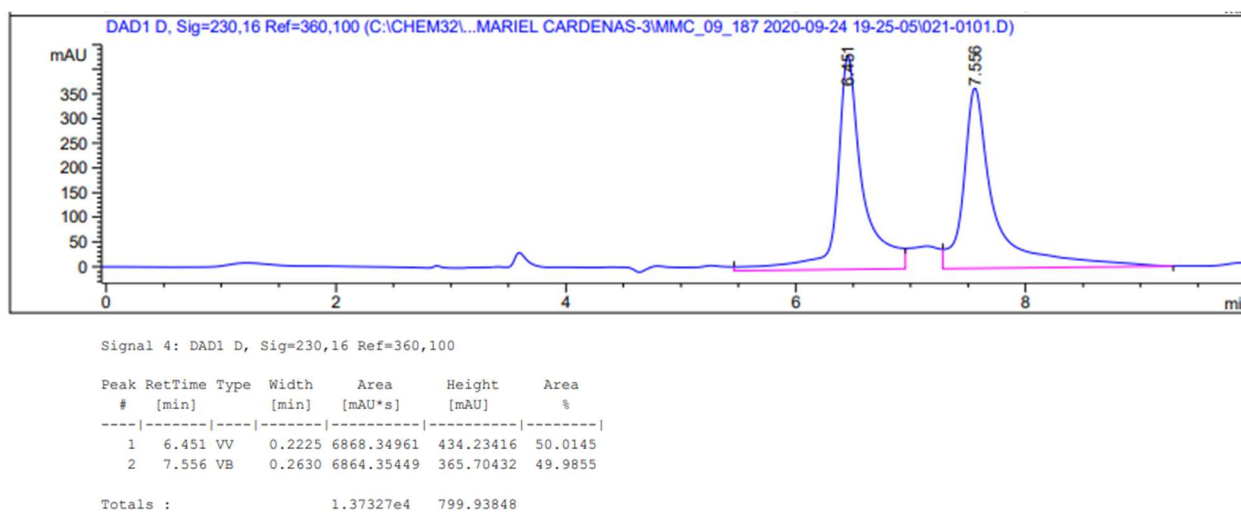
major enantiomer,
(*R*_a)-**91**

Enantioselectivity of **91** was measured with chiral HPLC analysis using a Daicel Corp. Chiralpak IA Column (4.6 mm ϕ \times 250 mL, Particle Size 5 μ M, Part No. 80325). Method: Hexanes:IPA (75:25), flow rate = 1.0 mL/min, *t*_R = 6.5 min (major) and *t*_R = 7.6 min (minor).

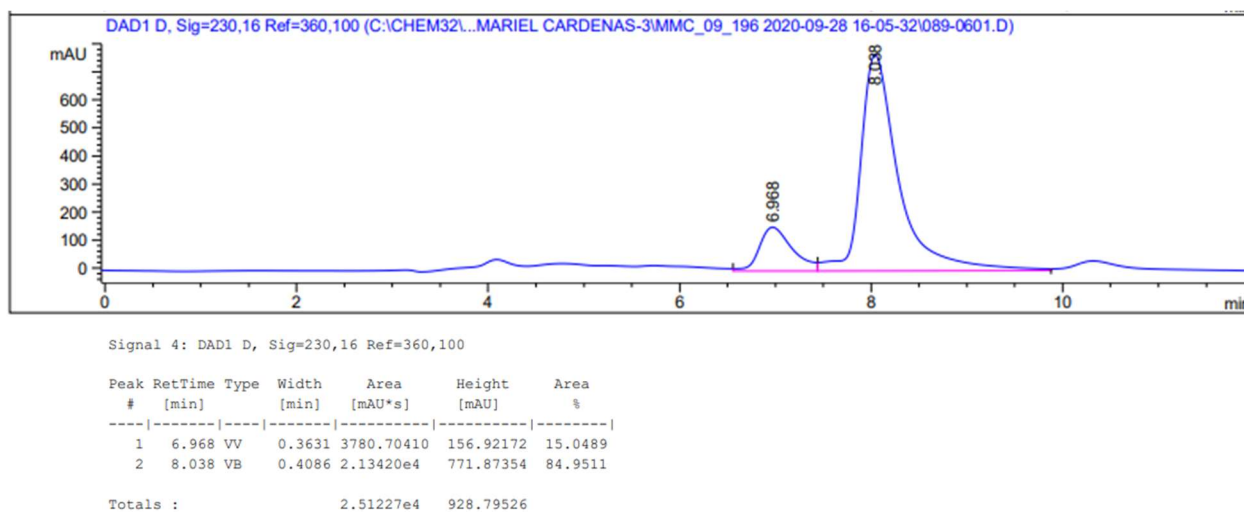
→ Determined, averaged of 3 trials: 12:88 e.r., 76 ee%

Sample Trace: 15:85 e.r., 70 ee%

Racemic Standard of **91**



Sample HPLC of **91**



major enantiomer,
(*R*_a)-**93**

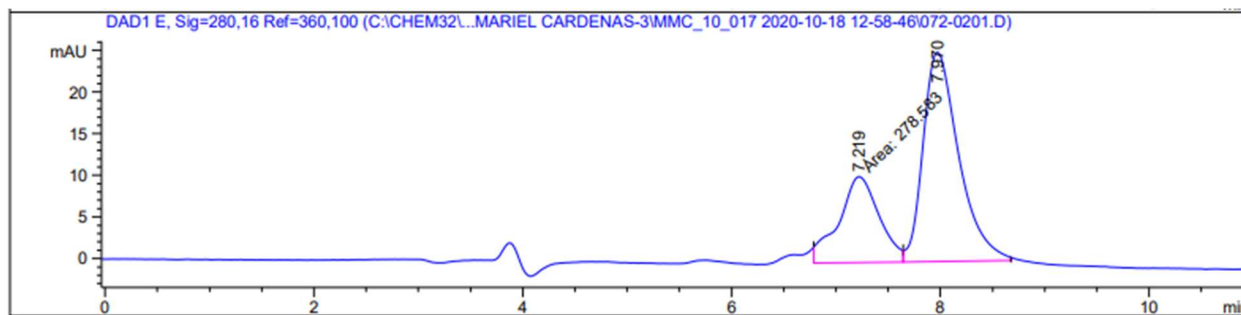
Enantioselectivity of **93** was measured with chiral HPLC analysis using a Daicel Corp. Chiralpak IA Column (4.6 mm ϕ \times 250 mL, Particle Size 5 μ M, Part No. 80325). Method: Hexanes:IPA (70:30), flow rate = 1.0 mL/min, *t*_R = 7.2 min (minor) and *t*_R = 8.0 min (major).

→ Determined, averaged of 2 trials: 13:87 e.r., 74 ee%

Sample Trace: 13:87 e.r., 74 ee%

HPLC Standard of **93**

Racemized enantioenriched material using heat, and observed enantiomer growing in.

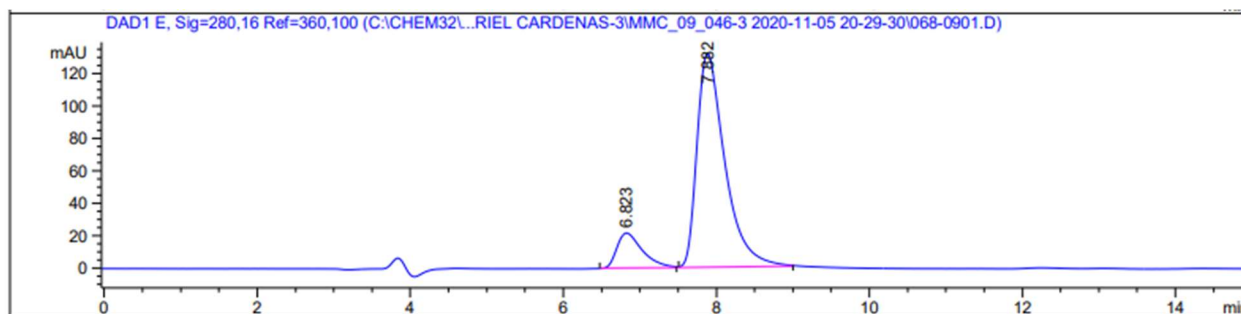


Signal 5: DAD1 E, Sig=280,16 Ref=360,100

Peak #	RetTime [min]	Type	Width [min]	Area [mAU*s]	Height [mAU]	Area %
1	7.219	FM	0.4491	278.58328	10.33797	31.7321
2	7.970	VB	0.3661	599.33844	25.14007	68.2679

Totals : 877.92172 35.47804

Sample HPLC of **93**



Signal 5: DAD1 E, Sig=280,16 Ref=360,100

Peak #	RetTime [min]	Type	Width [min]	Area [mAU*s]	Height [mAU]	Area %
1	6.823	BB	0.3490	503.51254	21.67638	13.1036
2	7.882	BB	0.3815	3339.05322	131.82666	86.8964

Totals : 3842.56577 153.50304

major enantiomer,
(*R_a*)-**93**

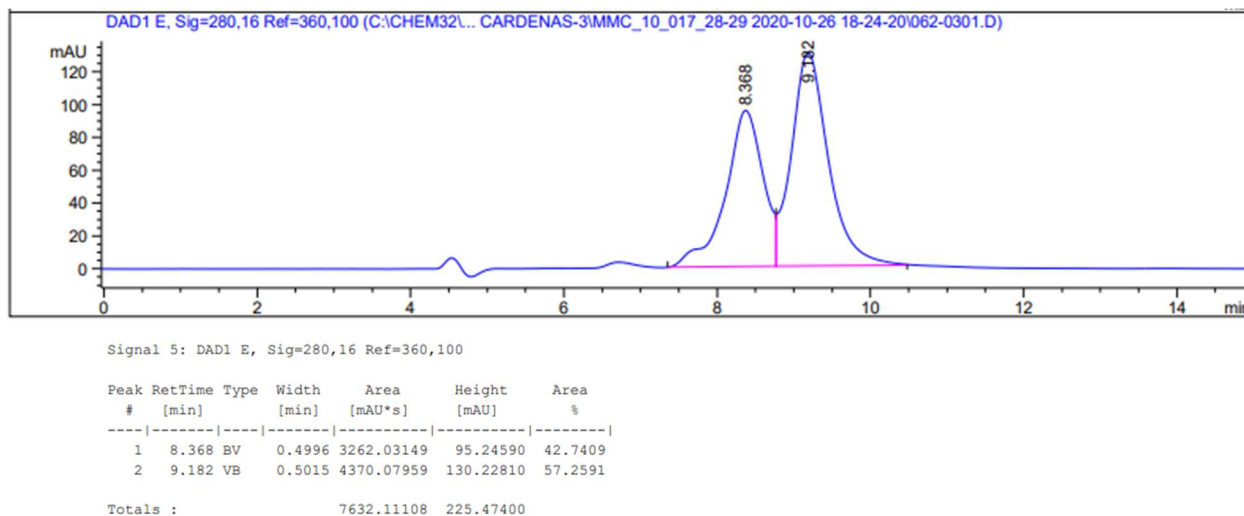
Enantioselectivity of **93** was measured with chiral HPLC analysis using a Daicel Corp. Chiralpak IA Column (4.6 mm ϕ \times 250 mL, Particle Size 5 μ M, Part No. 80325). *Method*: Hexanes:IPA (75:25), flow rate = 1.0 mL/min, *t*_R = 8.4 min (minor) and *t*_R = 9.2 min (minor).

→ Determined, averaged of 2 trials: 6:94 e.r., 88 ee%

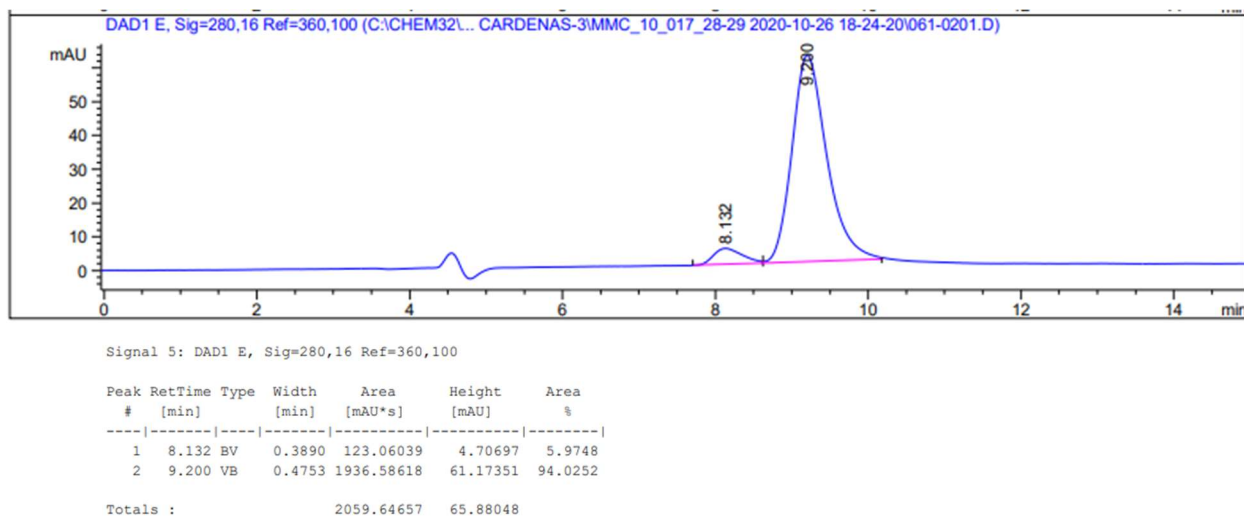
Sample Trace: 6:94 e.r., 88 ee%

HPLC Standard of **93**

Racemized enantioenriched material using heat, and observed enantiomer growing in.



Trituration HPLC of **93**



major enantiomer,
(*R*_a)-**95**

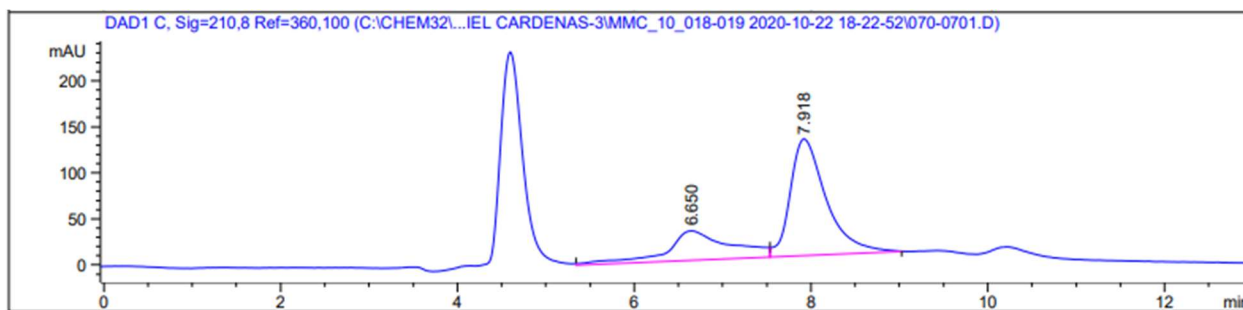
Enantioselectivity of **95** was measured with chiral HPLC analysis using a Daicel Corp. Chiralpak IA Column (4.6 mm ϕ \times 250 mL, Particle Size 5 μ M, Part No. 80325). *Method*: Hexanes:IPA (75:25), flow rate = 1.0 mL/min, *t*_R = 6.7 min (major) and *t*_R = 7.9 min (minor). Impurity that appears around 5.0 min is dichloromethane (necessary to dissolve compound).

→ Determined, averaged of 2 trials: 12:88 e.r., 76 ee%

Sample Trace: 12:88 e.r., 76 ee%

HPLC Standard of **95**

Racemized enantioenriched material using heat, and observed enantiomer growing in.

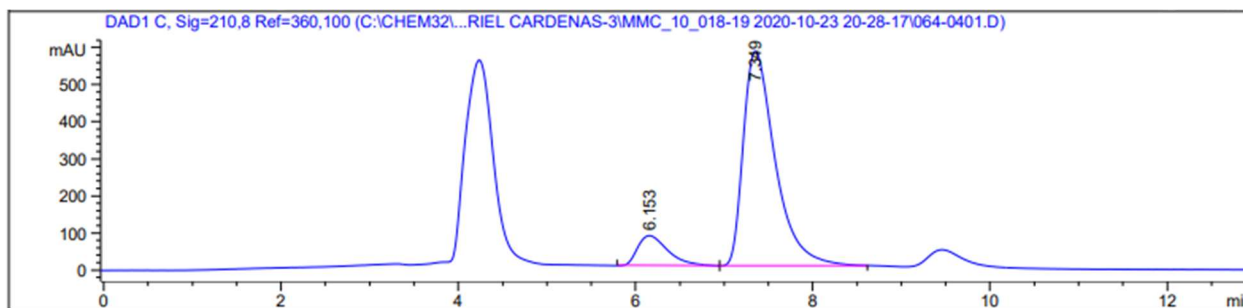


Signal 3: DAD1 C, Sig=210,8 Ref=360,100

Peak #	RetTime [min]	Type	Width [min]	Area [mAU*s]	Height [mAU]	Area %
1	6.650	BV	0.6203	1629.57349	32.20629	31.0442
2	7.918	VB	0.4206	3619.62427	126.98035	68.9558

Totals : 5249.19775 159.18663

Sample HPLC of **95**



Signal 3: DAD1 C, Sig=210,8 Ref=360,100

Peak #	RetTime [min]	Type	Width [min]	Area [mAU*s]	Height [mAU]	Area %
1	6.153	BV	0.3555	1926.83716	80.99856	11.7327
2	7.349	VB	0.3822	1.44960e4	578.79230	88.2673

Totals : 1.64228e4 659.79086

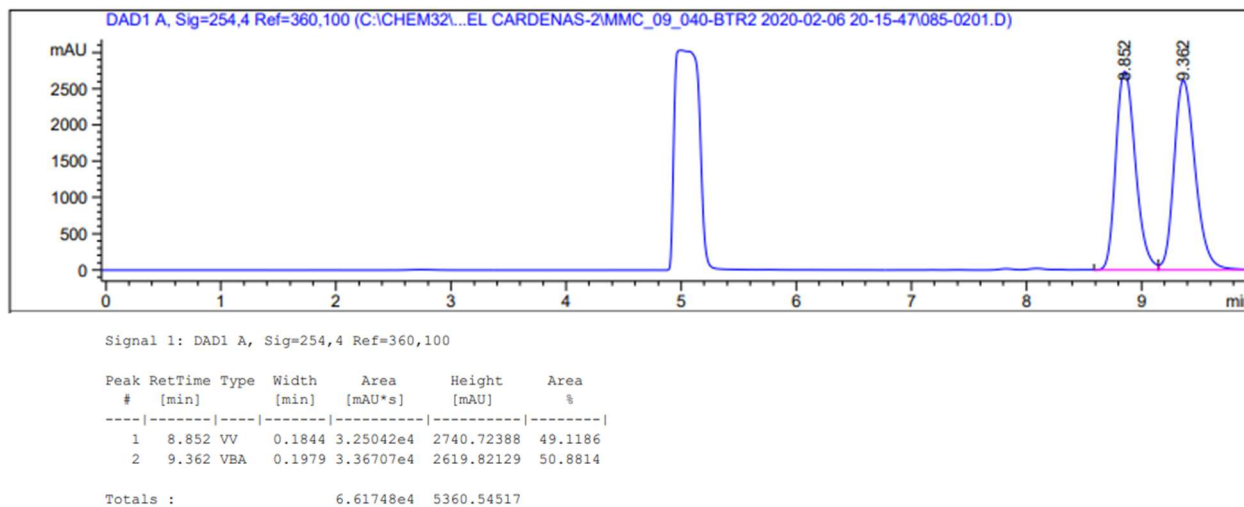
major enantiomer,
(*R*_a)-**96**

Enantioselectivity of **96** was measured with chiral HPLC analysis using a Daicel Corp. Chiralpak IC Column (4.6 mm ϕ \times 250 mL, Particle Size 5 μ M, Part No. 83325). *Method*: Hexanes:IPA (99:1), flow rate = 0.7 mL/min, *t*R = 16.4 min (major) and *t*R = 17.4 min (minor). Impurity that appears around 5.0 min is toluene (necessary to dissolve compound).

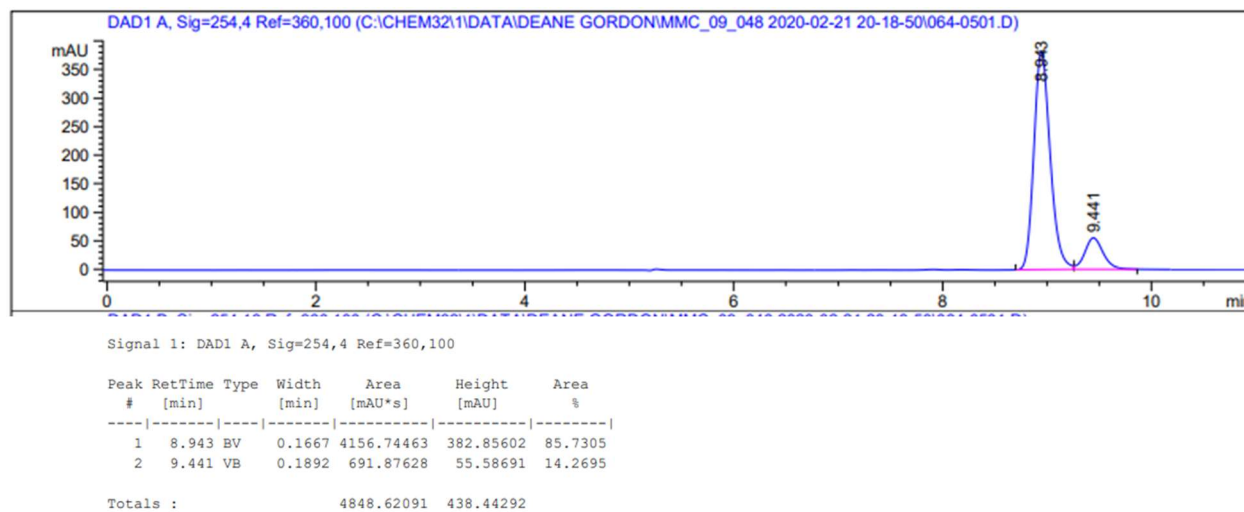
→ Determined, averaged of 6 trials: 14:86 e.r., 72 ee%

Sample Trace: 86:14 e.r., 72 ee%

Racemic Standard of **96**



Sample HPLC of **96**

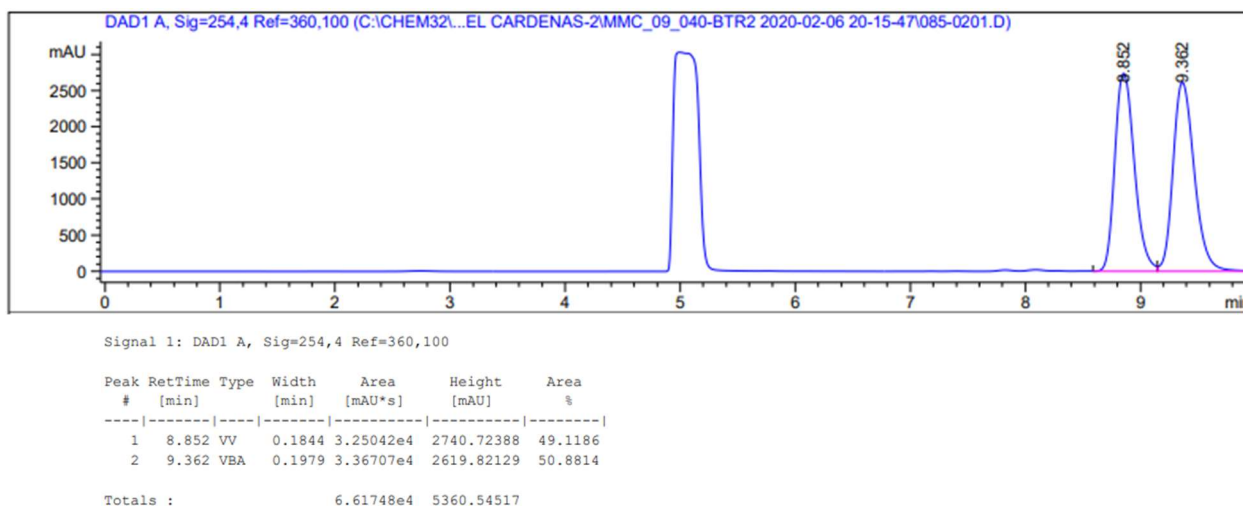


major enantiomer,
(*R*_a)-**96**

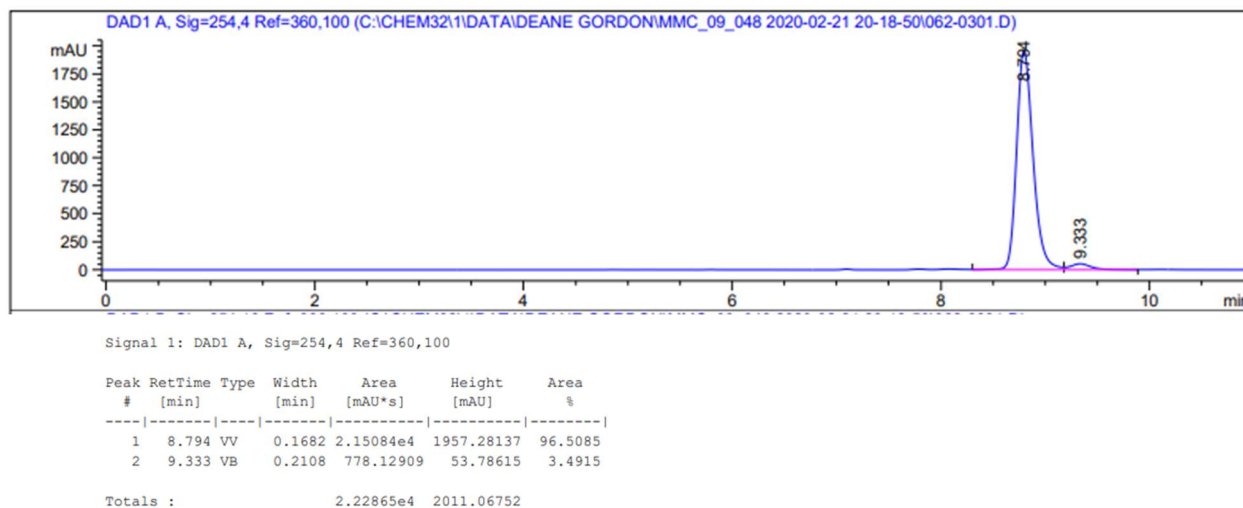
Enantioselectivity of **96** was measured with chiral HPLC analysis using a Daicel Corp. Chiralpak IC Column (4.6 mm ϕ \times 250 mL, Particle Size 5 μ M, Part No. 83325). *Method*: Hexanes:IPA (99:1), flow rate = 0.5 mL/min, *t*R = 16.4 min (major) and *t*R = 17.4 min (minor). Impurity that appears around 5.0 min is dichloromethane (necessary to dissolve compound). Recrystallization was done using 80:20 HPLC grade *n*-Hexanes/DCE. The solid and filtrate were separated, and the solid is found to be higher e.r.

→ Determined 3:97 e.r., 94 ee%

Racemic Standard of **96**



Trituration HPLC of **96**



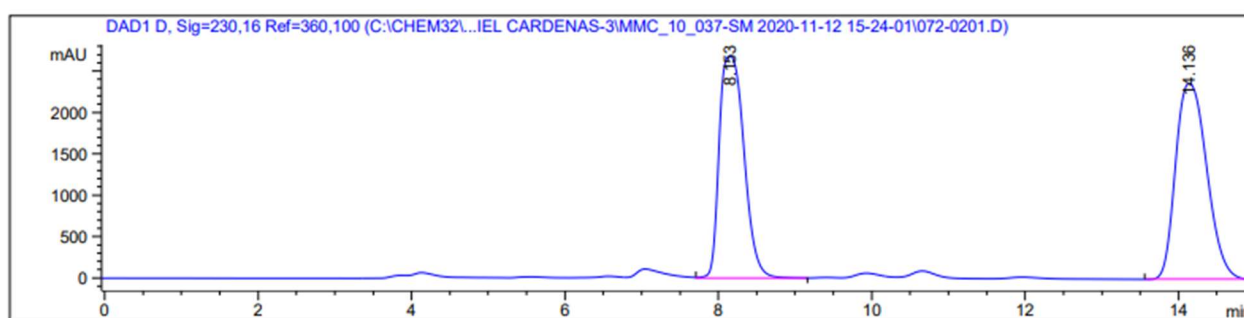
major enantiomer,
(S_a)-**98**

Enantioselectivity of **98** was measured with chiral HPLC analysis using a Daicel Corp. Chiralpak IC Column (4.6 mm ϕ \times 250 mL, Particle Size 5 μ M, Part No. 83325). *Method*: Hexanes:IPA (70:30), flow rate = 1.0 mL/min, *t*R = 8.2 min (major) and *t*R = 14.1 min (minor).

→ Determined, averaged of 5 trials: 63:37 e.r., 26 ee%

Sample Trace: 55:45 e.r., 10 ee%

Racemic Standard of **98**

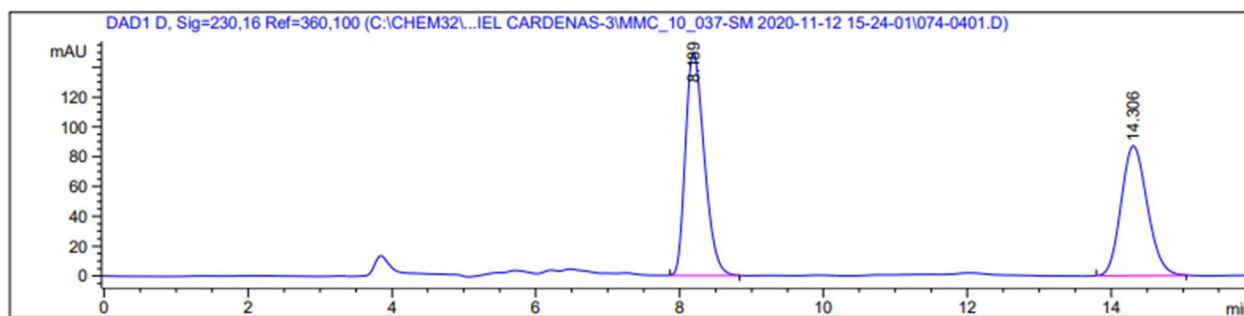


Signal 4: DAD1 D, Sig=230,16 Ref=360,100

Peak #	RetTime [min]	Type	Width [min]	Area [mAU*s]	Height [mAU]	Area %
1	8.153	VB	0.3600	6.04026e4	2689.37500	47.4296
2	14.136	VBA	0.4512	6.69494e4	2372.55176	52.5704

Totals : 1.27352e5 5061.92676

Sample HPLC of **98**



Signal 4: DAD1 D, Sig=230,16 Ref=360,100

Peak #	RetTime [min]	Type	Width [min]	Area [mAU*s]	Height [mAU]	Area %
1	8.189	BB	0.2822	2720.96216	149.58224	55.1007
2	14.306	BB	0.3970	2217.19775	87.09694	44.8993

Totals : 4938.15991 236.67918

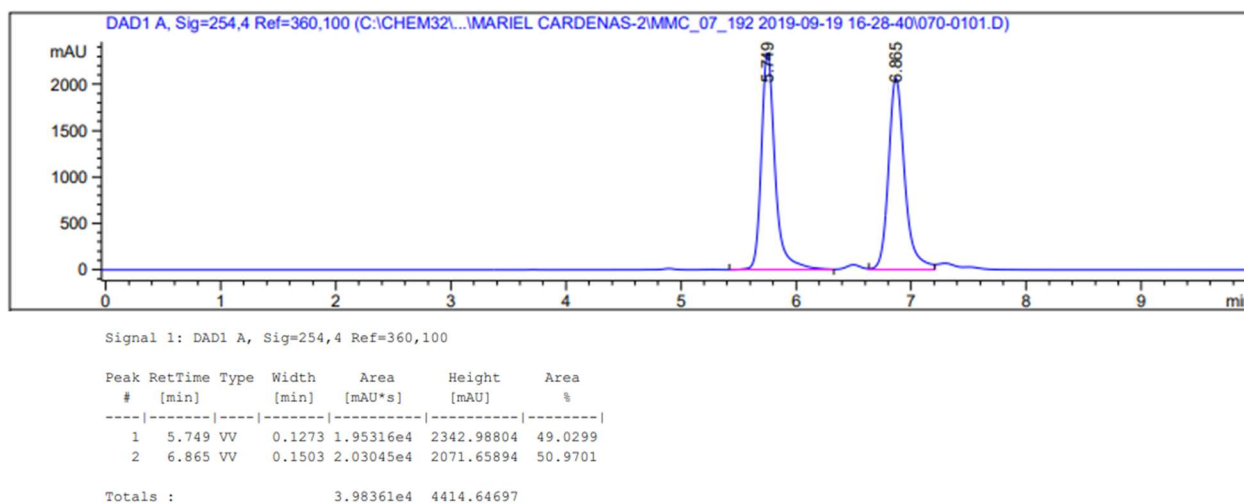
major enantiomer,
(*R*_a)-**97**

Enantioselectivity of **97** was measured with chiral HPLC analysis using a Daicel Corp. Chiralpak IC Column (4.6 mm ϕ \times 250 mL, Particle Size 5 μ M, Part No. 83325). *Method*: Hexanes:IPA (75:25), flow rate = 1.0 mL/min, *t*_R = 5.6 min (major) and *t*_R = 6.7 min (minor).

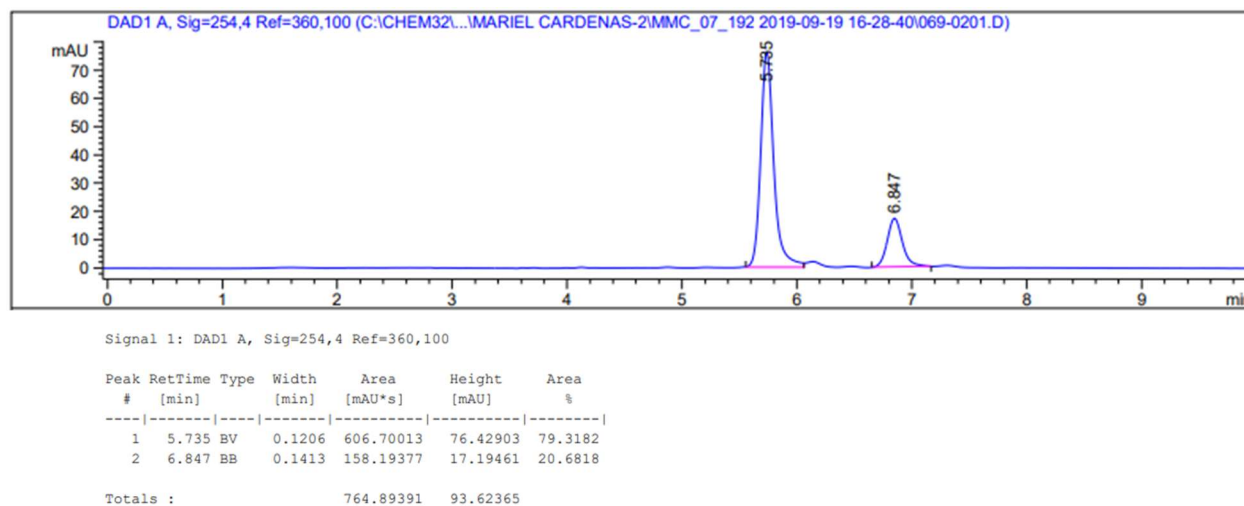
→ Determined, averaged of 5 trials: 15:85 e.r., 70 ee%

Sample Trace: 79:21 e.r., 58 ee%

Racemic Standard of **97**



Sample HPLC of **97**



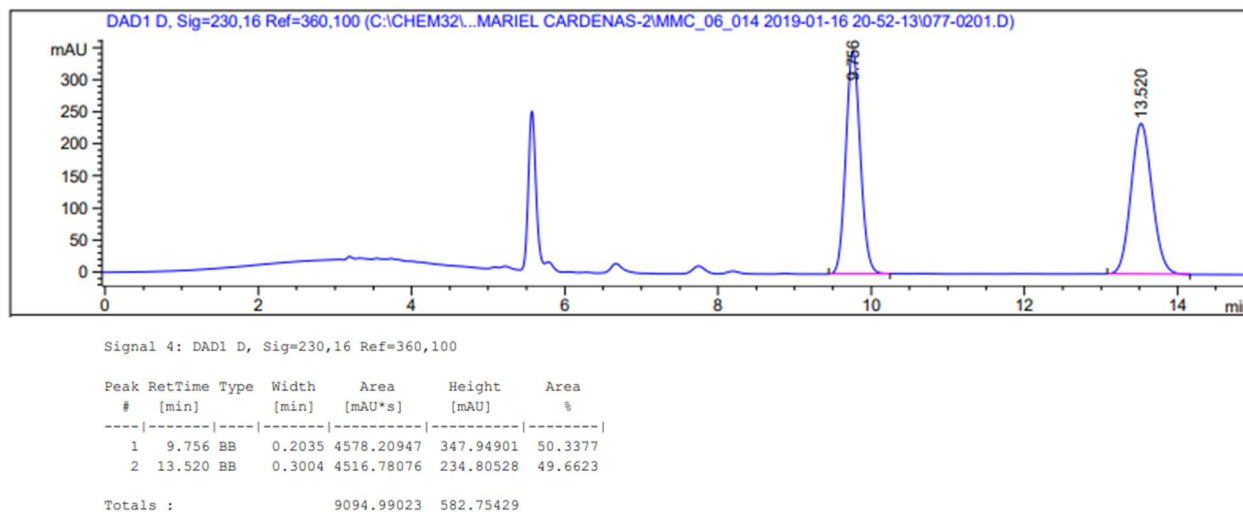
major enantiomer,
(S_a)-**100**

Enantioselectivity of **100** was measured with chiral HPLC analysis using a Daicel Corp. Chiralpak IC Column (4.6 mm ϕ \times 250 mL, Particle Size 5 μ M, Part No. 83325). *Method*: Hexanes:IPA (70:30), flow rate = 1.0 mL/min, *t*_R = 9.8 min (major) and *t*_R = 13.5 min (minor). Trace amount of CH₂Cl₂ (used to dissolve the compound is around 5.8 min).

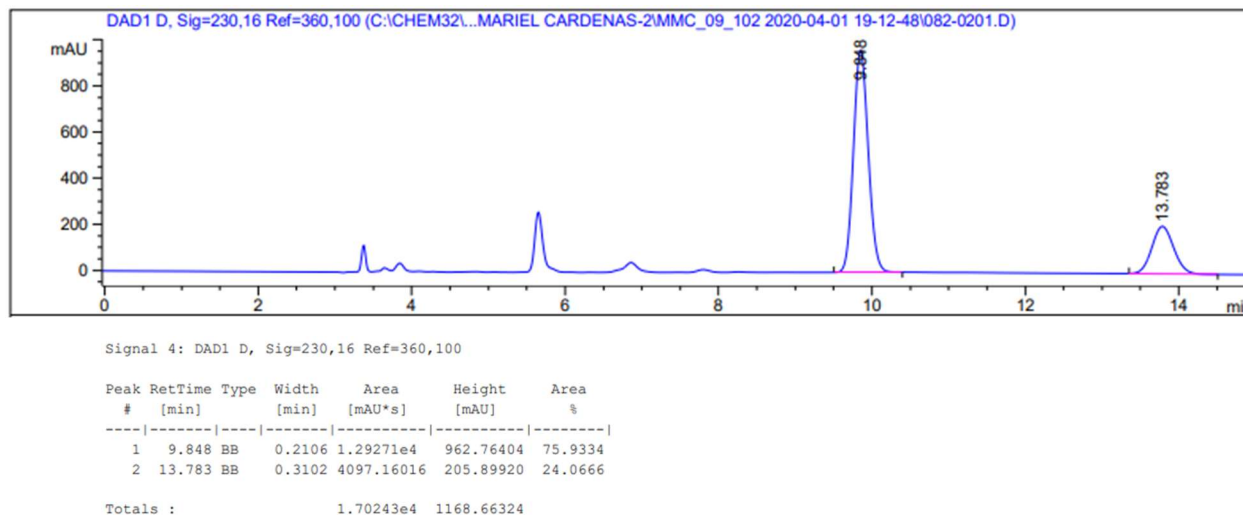
→ Determined, average of 4 trials: 65:35 e.r., 30 ee%

Sample Trace: 76:24 e.r., 52 ee%

Racemic Standard of **100**



Sample HPLC of **100**



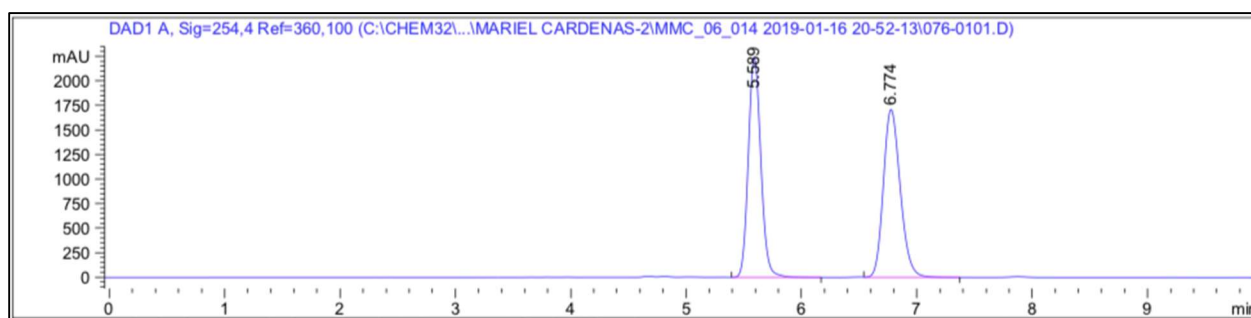
major enantiomer,
(*R*_a)-**99**

Enantioselectivity of **99** was measured with chiral HPLC analysis using a Daicel Corp. Chiralpak IC Column (4.6 mm ϕ \times 250 mL, Particle Size 5 μ M, Part No. 83325). *Method*: Hexanes:IPA (70:30), flow rate = 1.0 mL/min, *t*_R = 5.6 min (minor) and *t*_R = 6.7 min (major).

→ Determined, averaged of 3 trials: 25:75 e.r., 50 ee%

Sample Trace: 27:73 e.r., 46 ee%

Racemic Standard of **99**

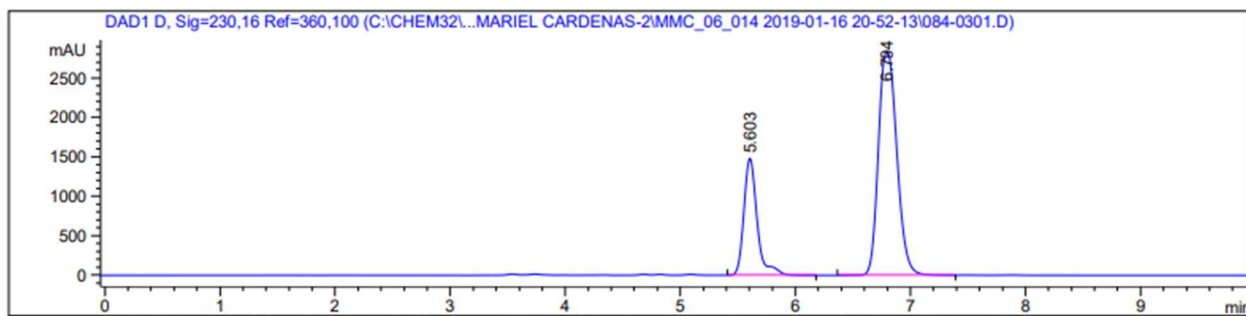


Signal 1: DAD1 A, Sig=254,4 Ref=360,100

Peak #	RetTime [min]	Type	Width [min]	Area [mAU*s]	Height [mAU]	Area %
1	5.589	VB	0.1182	1.69492e4	2241.87329	49.3357
2	6.774	VB	0.1586	1.74057e4	1711.80566	50.6643

Totals : 3.43549e4 3953.67896

Sample HPLC of **99**



Signal 4: DAD1 D, Sig=230,16 Ref=360,100

Peak #	RetTime [min]	Type	Width [min]	Area [mAU*s]	Height [mAU]	Area %
1	5.603	VB	0.1220	1.19545e4	1483.91077	27.4156
2	6.794	BB	0.1759	3.16502e4	2843.46167	72.5844

Totals : 4.36047e4 4327.37244

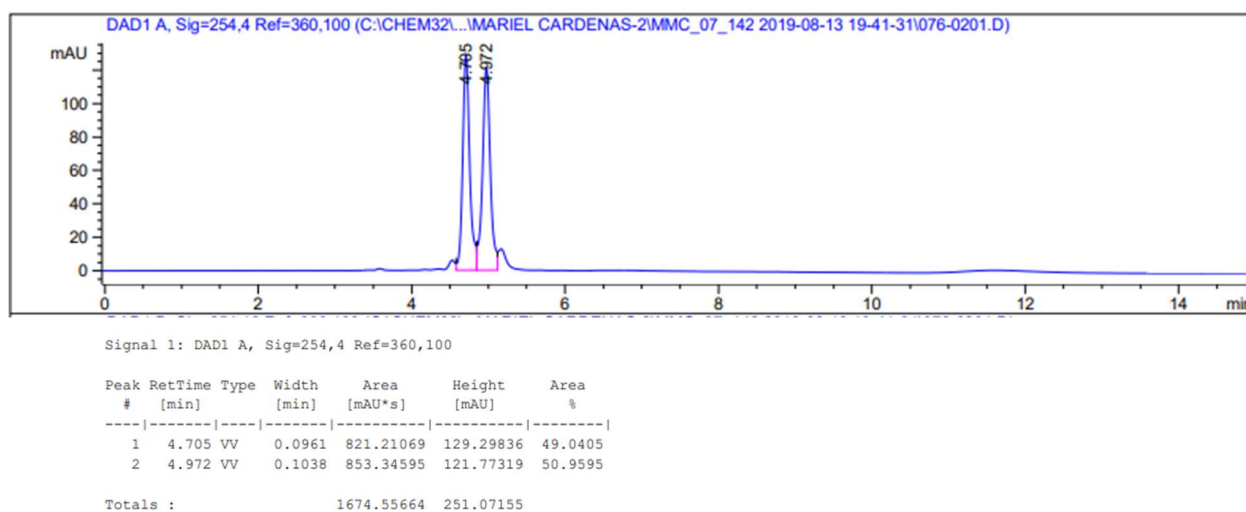
major enantiomer,
(*R*_a)-**102**

Enantioselectivity of **102** was measured with chiral HPLC analysis using a Daicel Corp. Chiralpak IA Column (4.6 mm ϕ \times 250 mL, Particle Size 5 μ M, Part No. 80325). *Method*: Hexanes:IPA (70:30), flow rate = 1.0 mL/min, *t*_R = 7.3 min (minor) and *t*_R = 7.6 min (major).

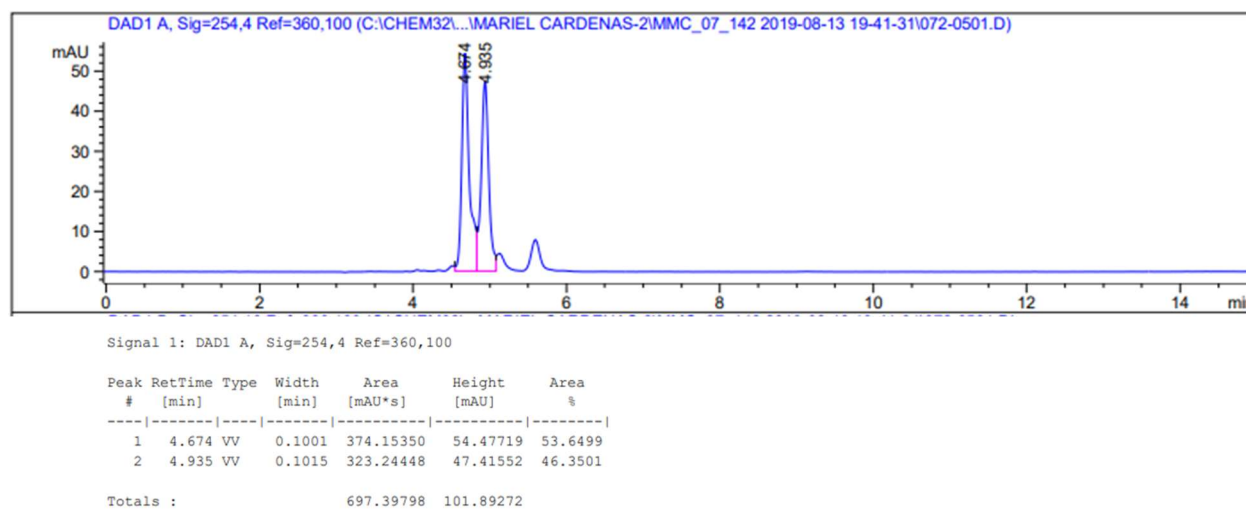
→ Determined, average of 3 trials: 54:46 e.r., 8 ee%

Sample Trace: 54:46 e.r., 8 ee%

Racemic Standard of **102**



Sample HPLC of **102**



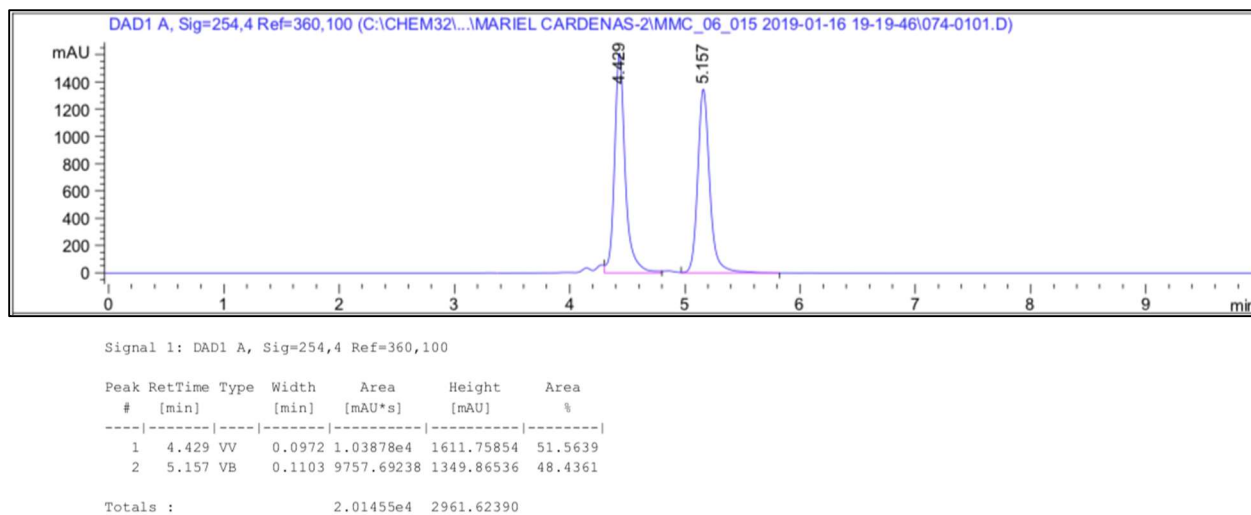
major enantiomer,
(*R*_a)-**101**

Enantioselectivity of **101** was measured with chiral HPLC analysis using a Daicel Corp. Chiralpak IA Column (4.6 mm ϕ \times 250 mL, Particle Size 5 μ M, Part No. 80325). *Method*: Hexanes:IPA (70:30), flow rate = 1.0 mL/min, *t*_R = 4.4 min (major) and *t*_R = 5.2 min (minor).

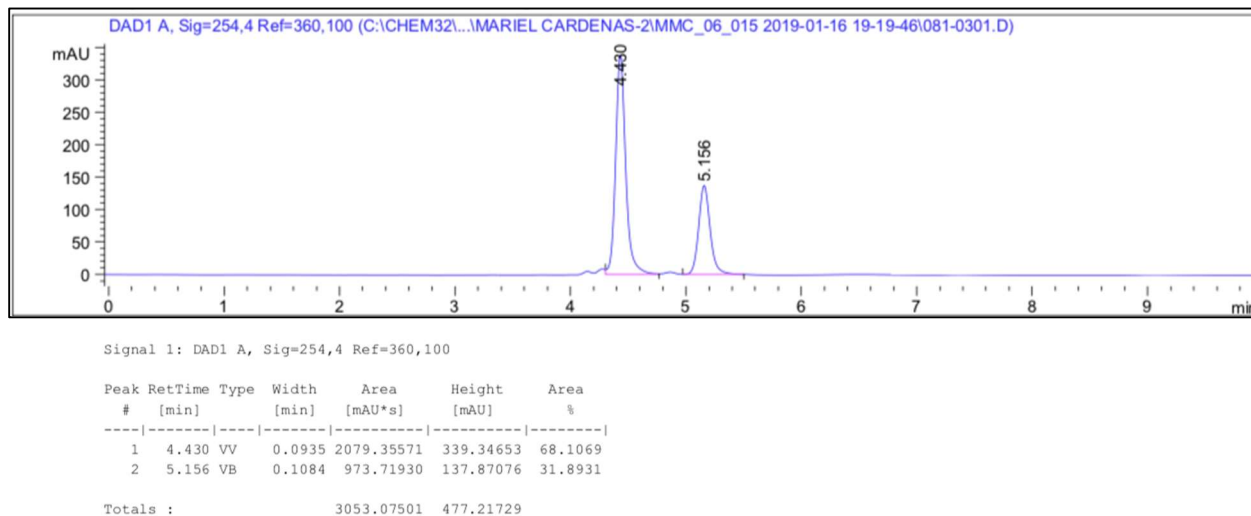
→ Determined, average of 6 trials: 68:32 e.r., 36 ee%

Sample Trace: 68:32 e.r., 36 ee%

Racemic Standard of **101**



Sample HPLC of **101**



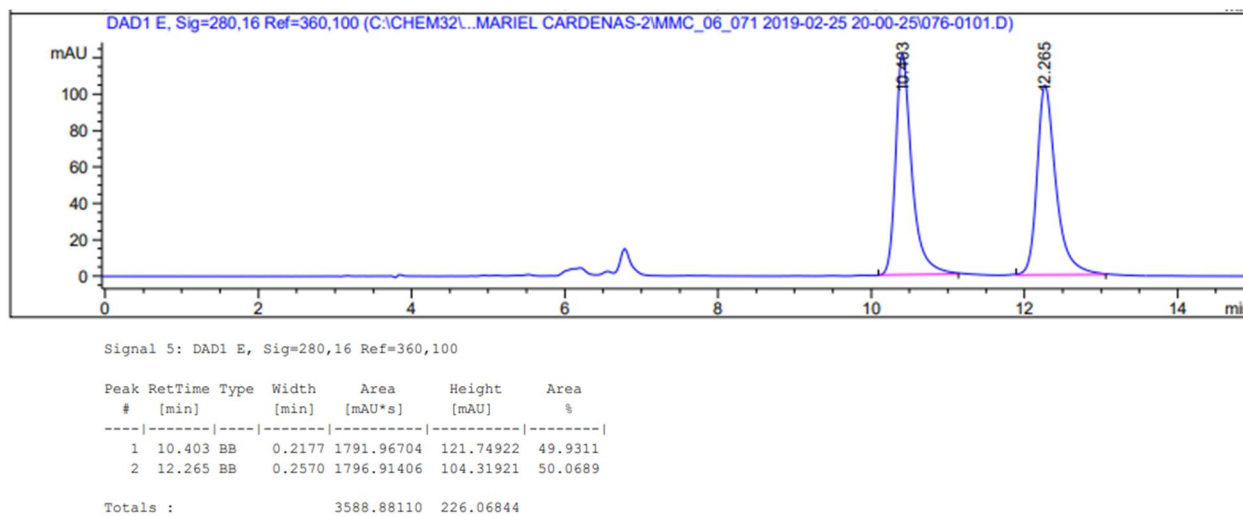
major enantiomer,
(S_a)-**104**

Enantioselectivity of **104** was measured with chiral HPLC analysis using a Daicel Corp. Chiralpak IA Column (4.6 mm ϕ \times 250 mL, Particle Size 5 μ M, Part No. 80325). *Method*: Hexanes:IPA (95:5), flow rate = 1.0 mL/min, *t*R = 10.4 (minor) and *t*R = 12.3 (major). Trace amounts of CH₂Cl₂ (to dissolve the sample) are present at 5.8 min.

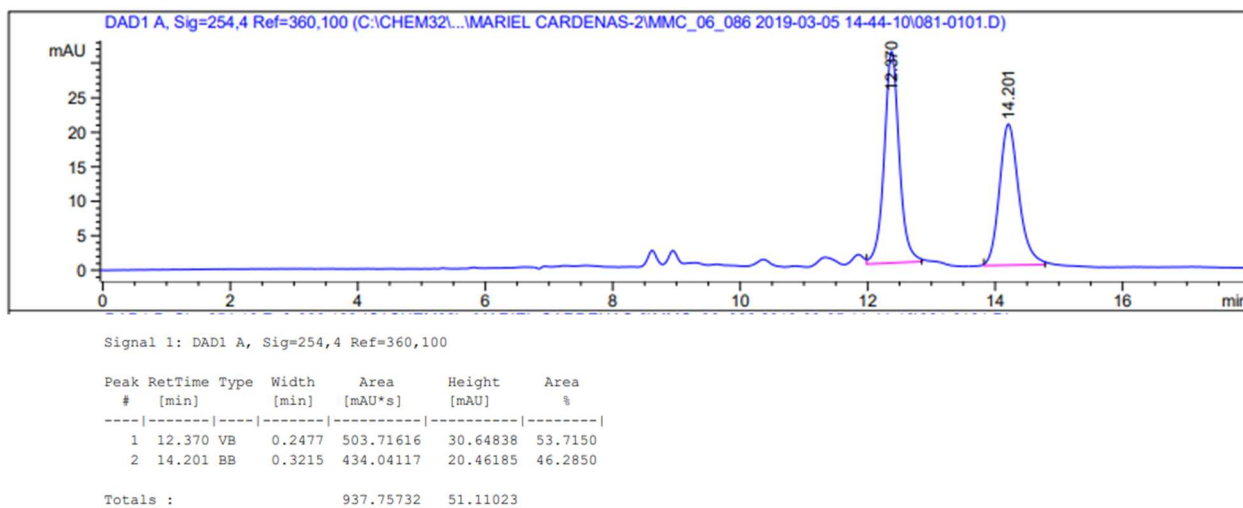
→ Determined, averaged of 5 trials: 63:37 e.r., 26 ee%

Sample Trace: 54:46 e.r., 8 ee%

Racemic Standard of **104**



Sample HPLC of **104**



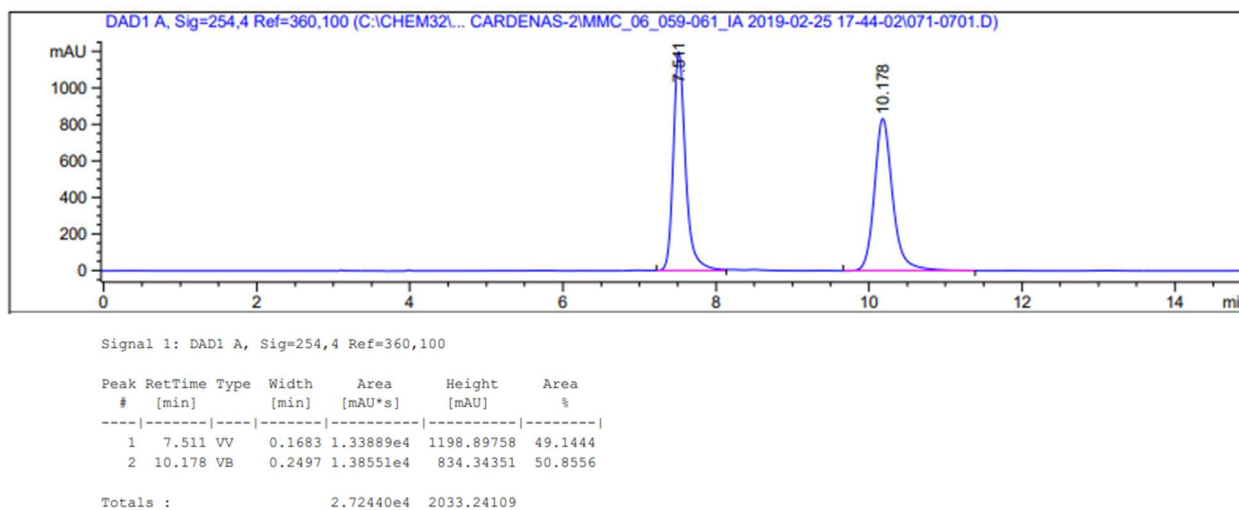
major enantiomer,
(*R*_a)-**103**

Enantioselectivity of **103** was measured with chiral HPLC analysis using a Daicel Corp. Chiralpak IA Column (4.6 mm ϕ \times 250 mL, Particle Size 5 μ M, Part No. 80325). *Method*: Hexanes:IPA (95:5), flow rate = 1.0 mL/min, *t*_R = 7.5 (minor) and *t*_R = 10.2 (major).

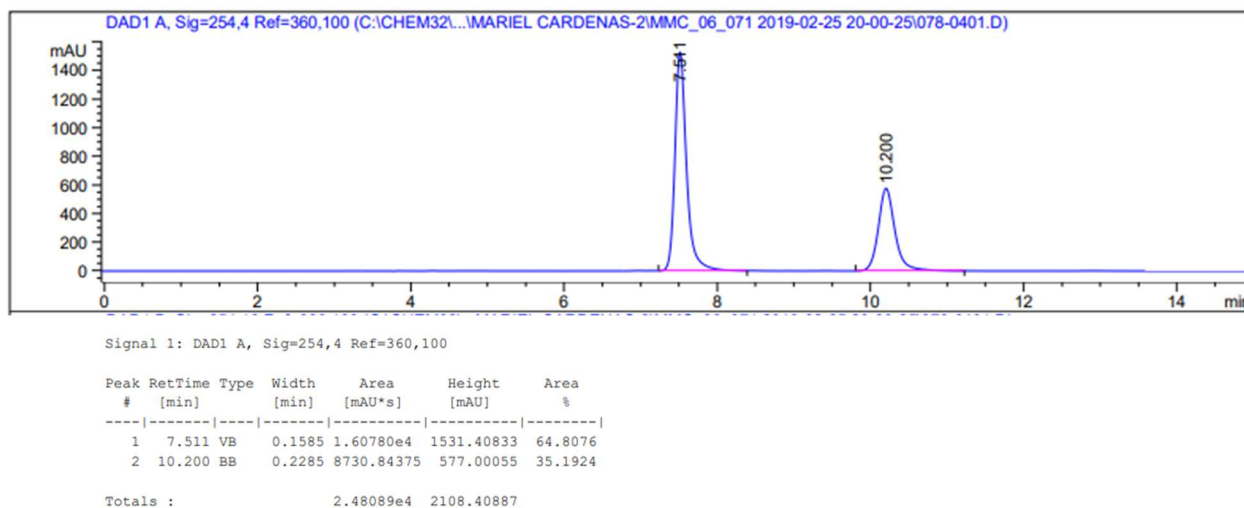
→ Determined, averaged of 3 trials: 74:26 e.r., 48 ee%

Sample Trace: 65:35 e.r., 30 ee%

Racemic Standard of **103**



Sample HPLC of **103**



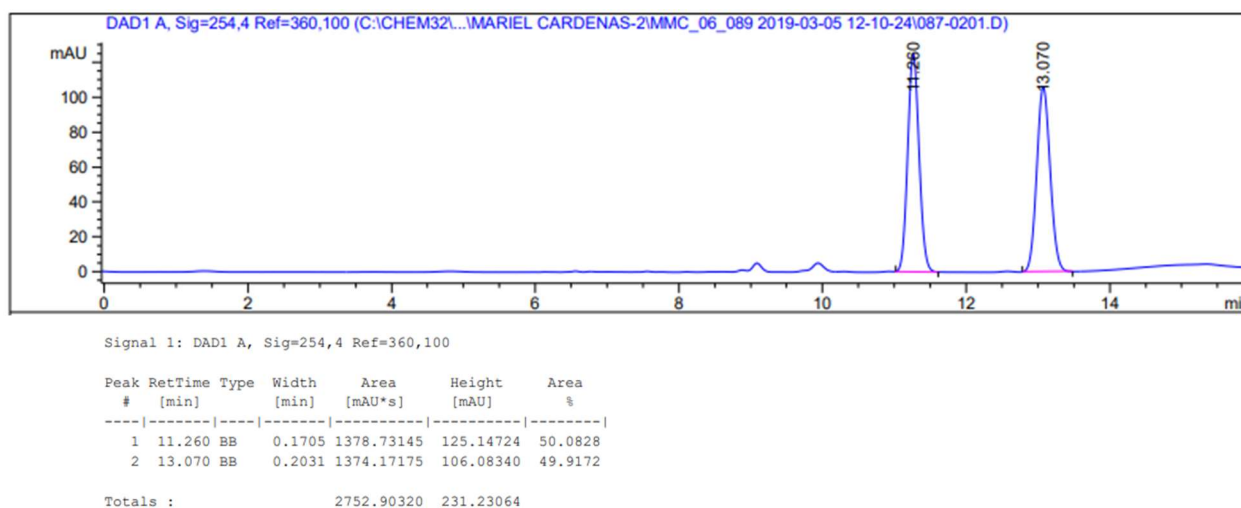
major enantiomer,
(*S*_a)-**106**

Enantioselectivity of **106** was measured with chiral HPLC analysis using a Daicel Corp. Chiralpak IC Column (4.6 mm ϕ \times 250 mL, Particle Size 5 μ M, Part No. 83325). *Method*: Hexanes:IPA (98:2), flow rate = 0.7 mL/min, *t*R = 16.4 min (major) and *t*R = 17.4 min (minor).

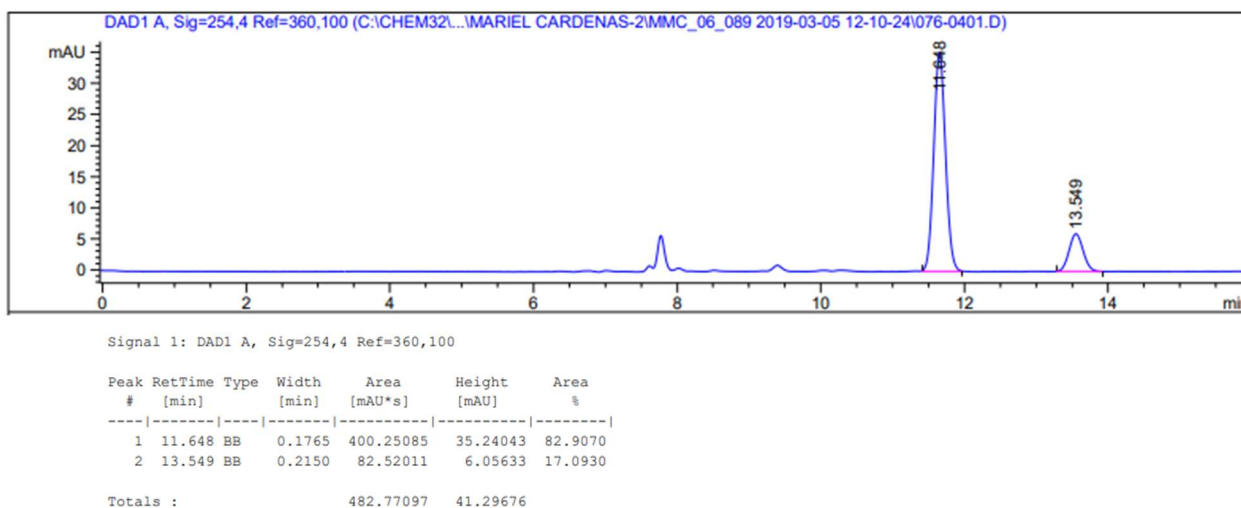
→ Determined, average of 3 trials: 83:17 e.r., 66 ee%

Sample Trace: 83:17 e.r., 66 ee%

Racemic Standard of **106**



Sample HPLC of **106**



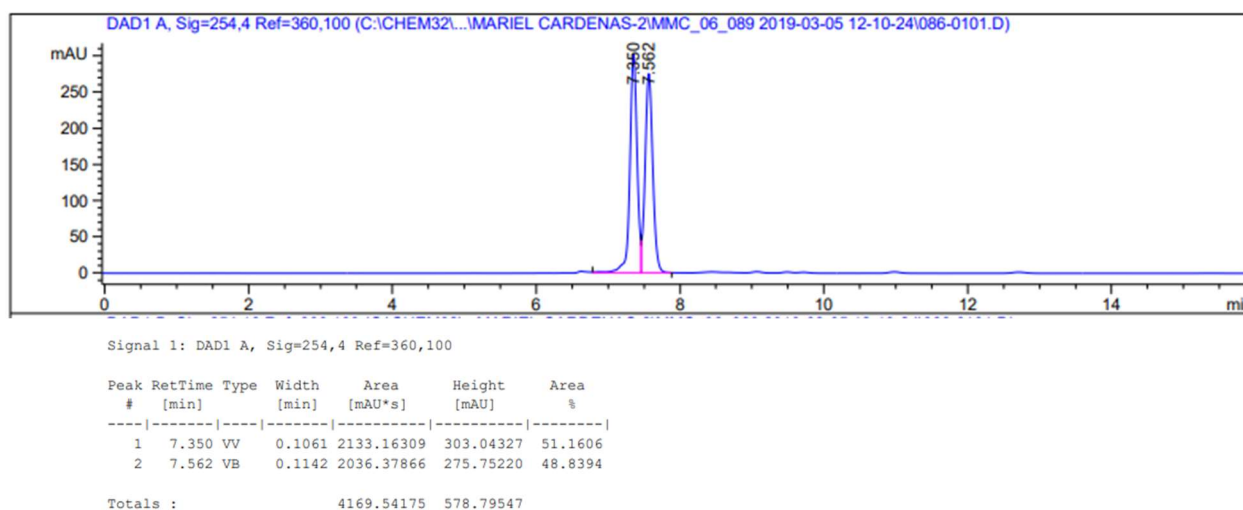
major enantiomer,
(*R*_a)-**105**

Enantioselectivity of **105** was measured with chiral HPLC analysis using a Daicel Corp. Chiralpak IC Column (4.6 mm ϕ \times 250 mL, Particle Size 5 μ M, Part No. 83325). *Method*: Hexanes:IPA (70:30), flow rate = 1.0 mL/min, *t*_R = 7.35 min (major) and *t*_R = 7.6 min (minor).

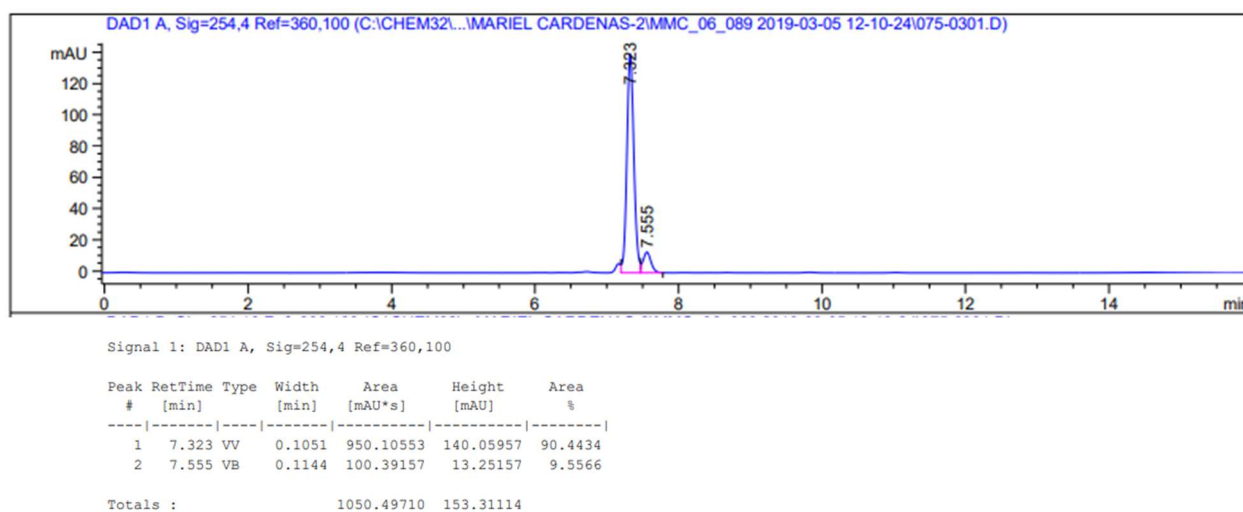
→ Determined, average of 3 trials: 9:91 e.r., 82 ee%

Sample Trace: 90:10 e.r., 80 ee%

Racemic Standard of **105**



Sample HPLC of **105**



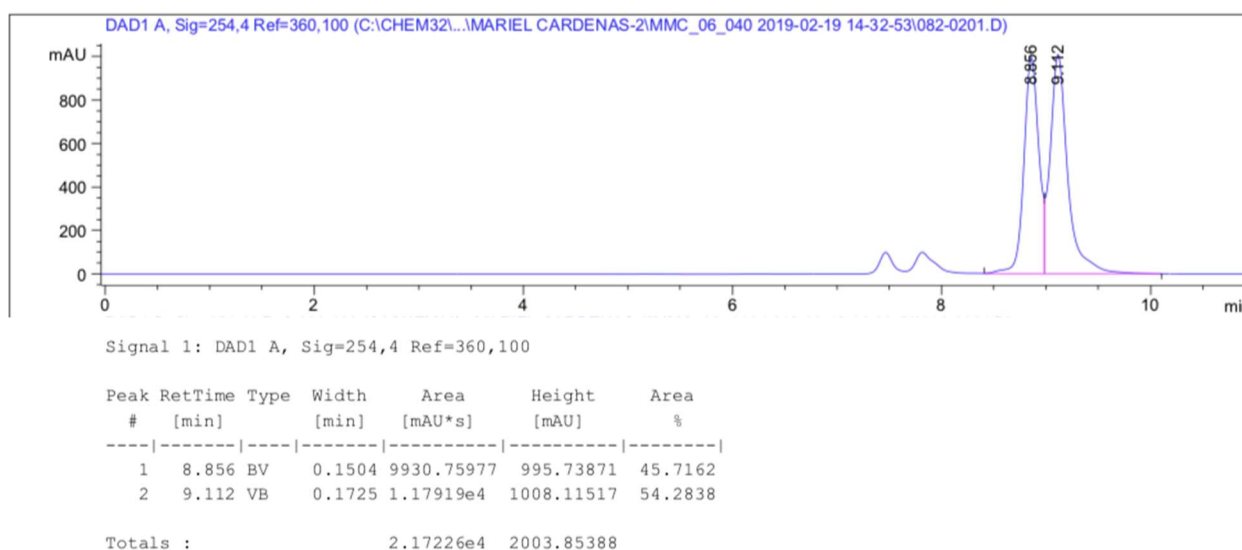
major enantiomer,
(S_a)-**108**

Enantioselectivity of **108** was measured with chiral HPLC analysis using a Daicel Corp. Chiralpak IA Column (4.6 mm ϕ \times 250 mL, Particle Size 5 μ M, Part No. 80325). *Method*: Hexanes:IPA (98:2), flow rate = 0.7 mL/min, *t*_R = 7.3 min (minor) and *t*_R = 7.6 min (major).

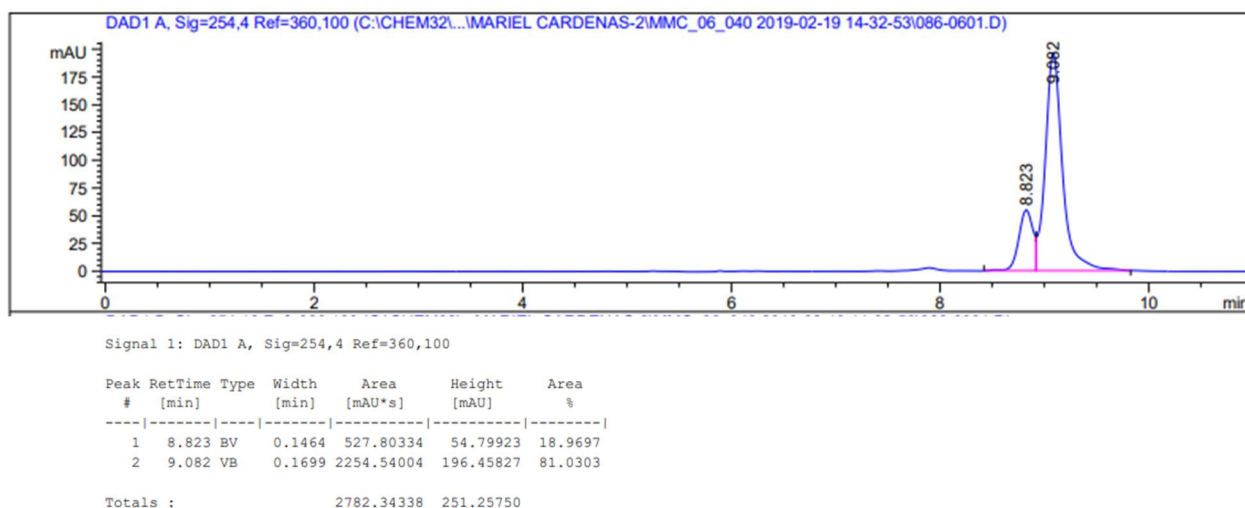
→ Determined, average of 3 trials: 82:18 e.r., 64 ee%

Sample Trace: 81:19 e.r., 62 ee%

Racemic Standard of **108**



Sample HPLC of **108**



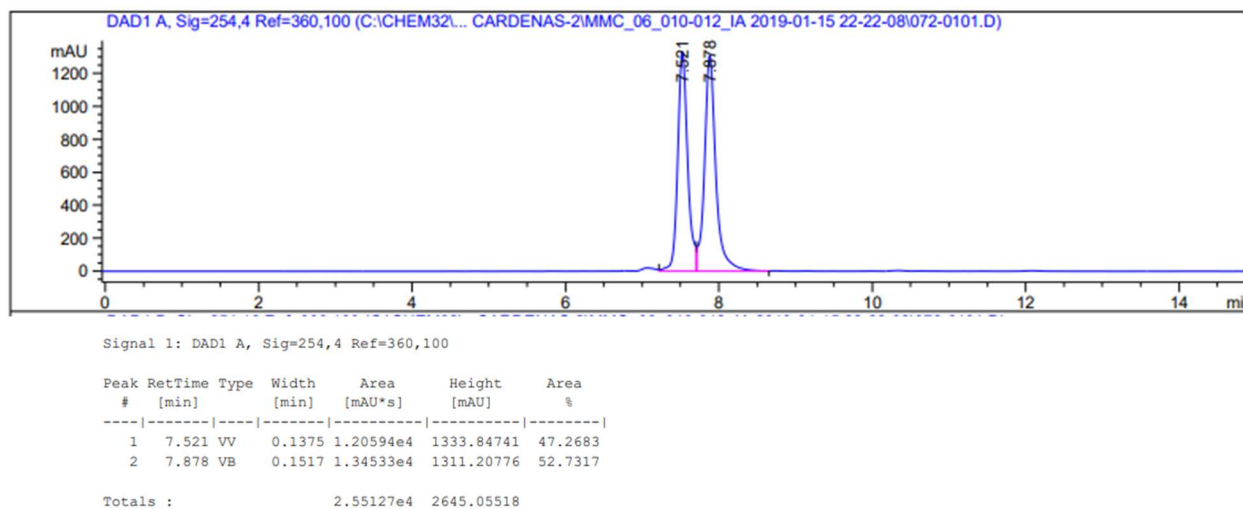
major enantiomer,
(*R*_a)-**107**

Enantioselectivity of **107** was measured with chiral HPLC analysis using a Daicel Corp. Chiralpak IA Column (4.6 mm ϕ \times 250 mL, Particle Size 5 μ M, Part No. 80325). *Method*: Hexanes:IPA (98:2), flow rate = 0.7 mL/min, *t*_R = 7.5 min (minor) and *t*_R = 7.9 min (major). Trace amounts of CH₂Cl₂ (to dissolve the sample) is present at 5.8 min.

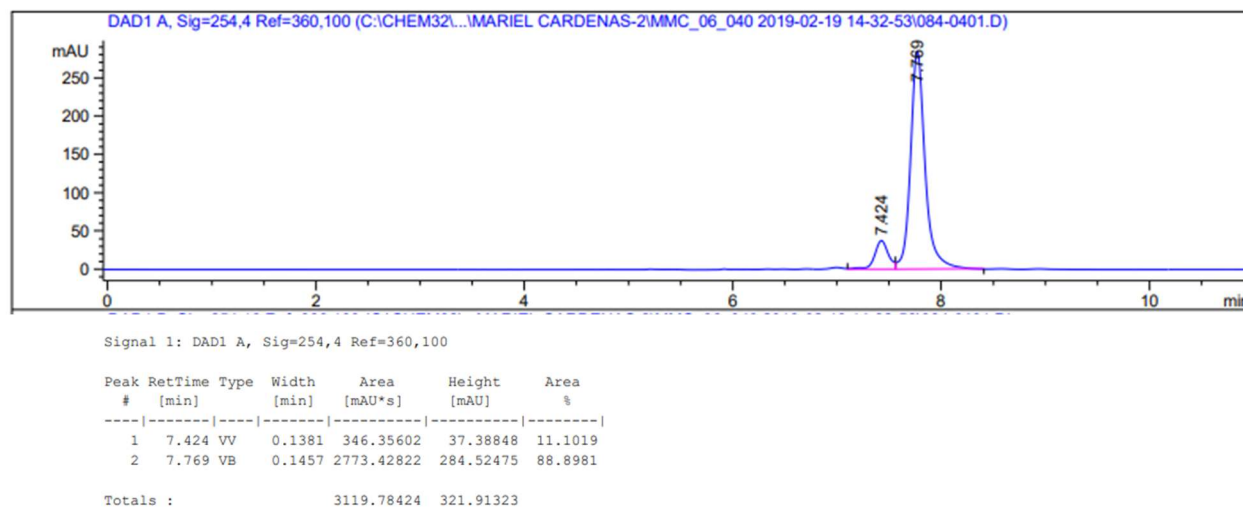
→ Determined, average of 3 trials: 11:89 e.r., 78 ee%

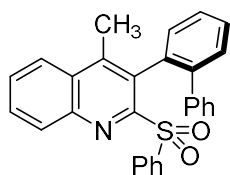
Sample Trace: 11:89 e.r., 78 ee%

Racemic Standard of **107**



Sample HPLC of **107**





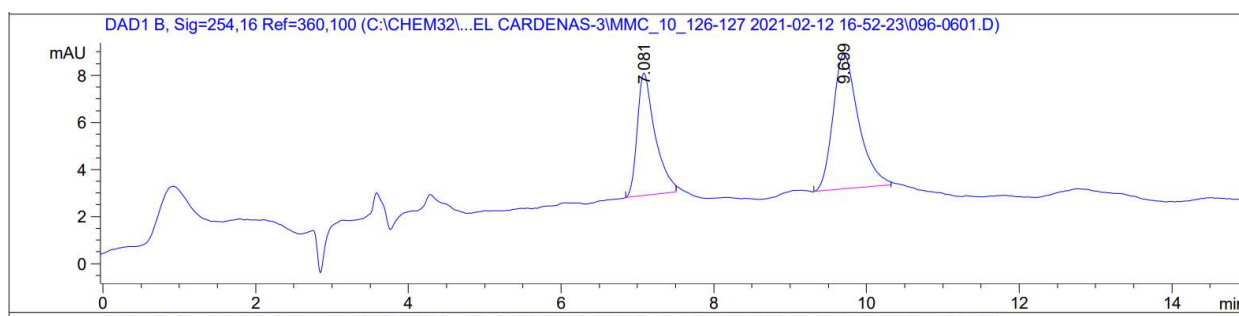
major enantiomer,
(*R_a*)-119

Enantioselectivity of **119** was measured with chiral HPLC analysis using a Daicel Corp. Chiralpak IA Column (4.6 mm ϕ \times 250 mL, Particle Size 5 μ M, Part No. 80325). *Method*: Hexanes:IPA (75:25), flow rate = 1.0 mL/min, *t_R* = 7.0 min (minor) and *t_R* = 9.7 min (major).

→ Determined, average of 3 trials: 15:85 e.r., 70 ee%

Sample Trace: 12:88 e.r., 76 ee%

Racemic Standard of 119

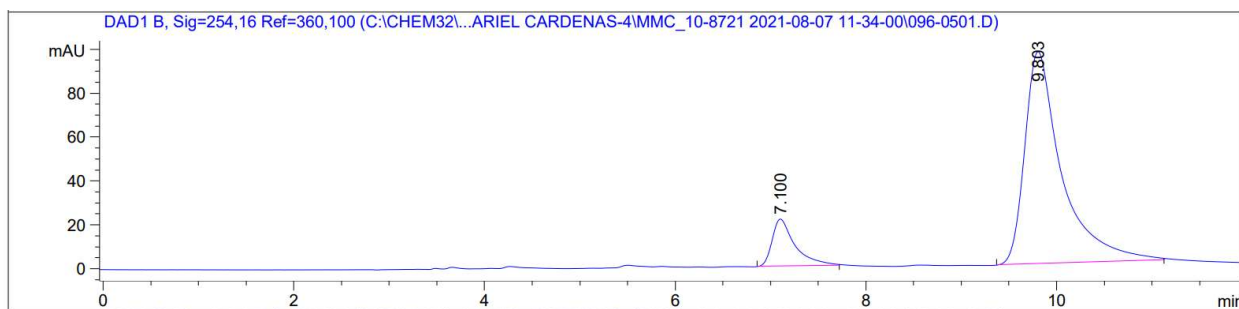


Signal 2: DAD1 B, Sig=254,16 Ref=360,100

Peak #	RetTime [min]	Type	Width [min]	Area [mAU*s]	Height [mAU]	Area %
1	7.081	BB	0.2357	84.86999	5.21904	38.8794
2	9.699	BB	0.3431	133.42049	5.74130	61.1206

Totals : 218.29047 10.96034

Sample HPLC of 119



Signal 2: DAD1 B, Sig=254,16 Ref=360,100

Peak #	RetTime [min]	Type	Width [min]	Area [mAU*s]	Height [mAU]	Area %
1	7.100	BB	0.2440	361.60696	21.51913	12.1576
2	9.803	BB	0.3913	2612.71729	96.66442	87.8424

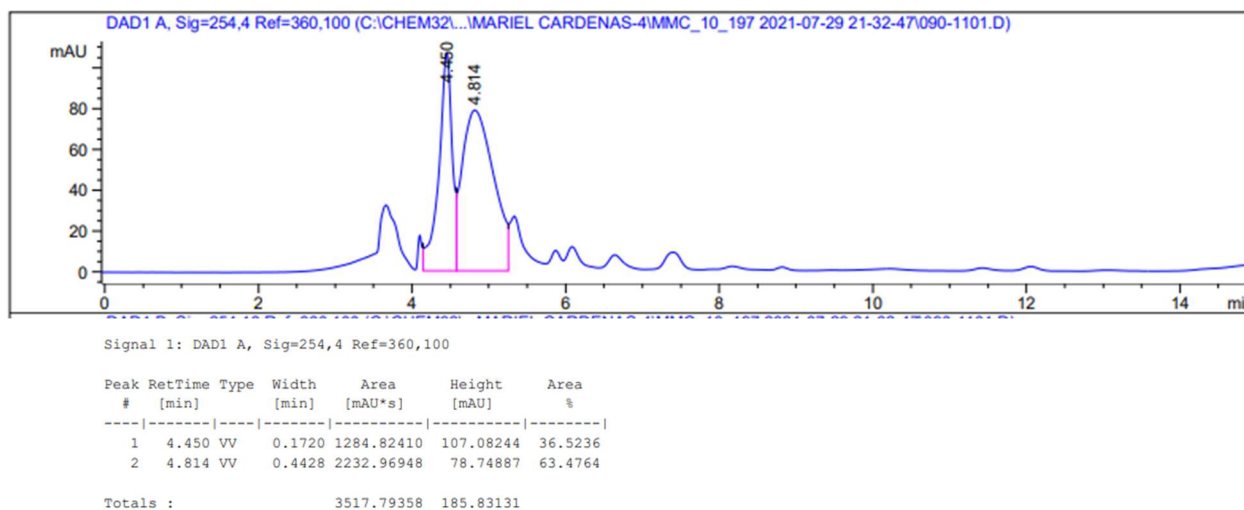
major enantiomer,
(*R*_a)-**120**

Enantioselectivity of **120** was measured with chiral HPLC analysis using a Daicel Corp. Chiralpak IA Column (4.6 mm ϕ \times 250 mL, Particle Size 5 μ M, Part No. 80325). *Method*: Hexanes:IPA (98:2), flow rate = 1.0 mL/min, *t*_R = 5.6 min (minor) and *t*_R = 6.7 min (major). This is an intermediate enroute to **121**. I was unable to achieve a resolved method. It is likely that the enantiopurity is in line with compound **121**. We included the traces to be thorough.

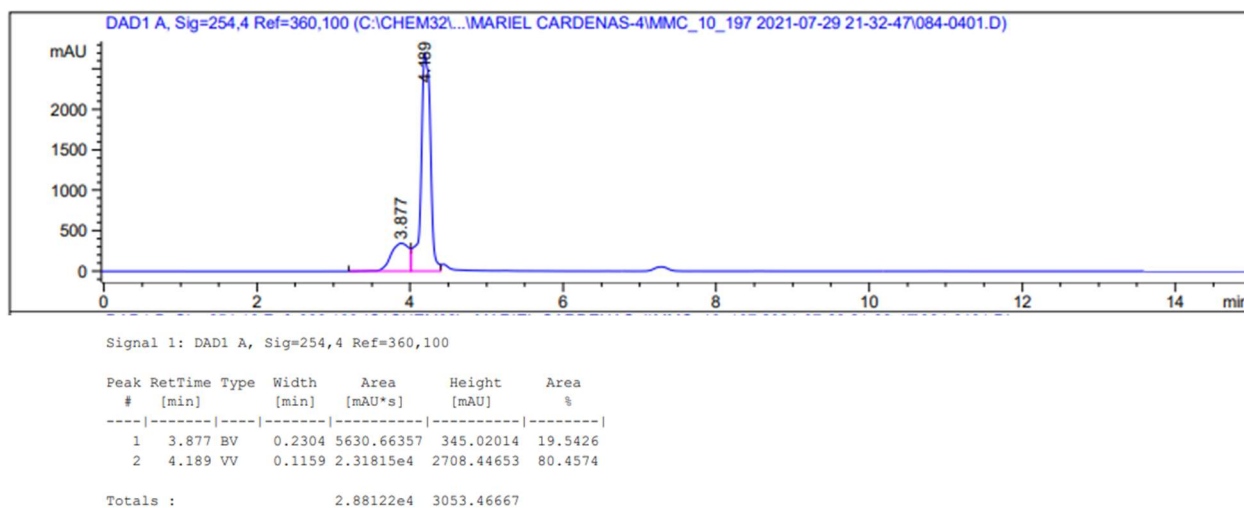
→ Determined, average of 3 trials: 16:84 e.r., 68 ee%

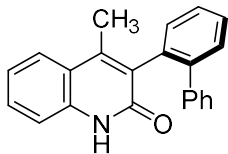
Sample Trace: 19.5:80.5 e.r., 61 ee%

Racemic Standard of **121**



Sample HPLC of **121**





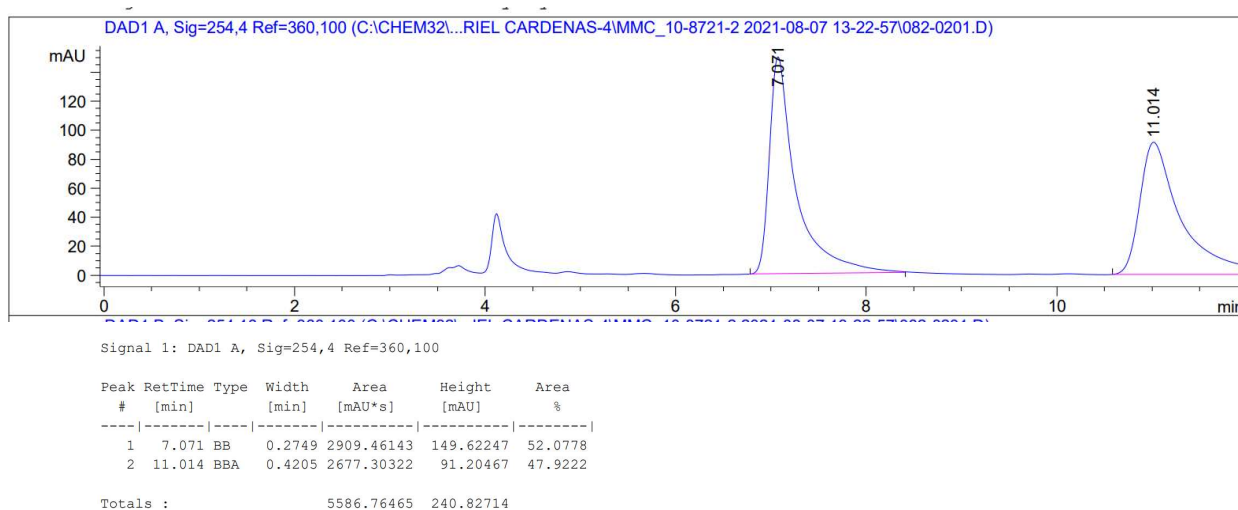
major enantiomer,
(*R*_a)-**121**

Enantioselectivity of **121** was measured with chiral HPLC analysis using a Daicel Corp. Chiralpak IA Column (4.6 mm ϕ \times 250 mL, Particle Size 5 μ M, Part No. 80325). *Method*: Hexanes:IPA (75:25), flow rate = 1.0 mL/min, *t*_R = 7.0 min (minor) and *t*_R = 11.0 min (major).

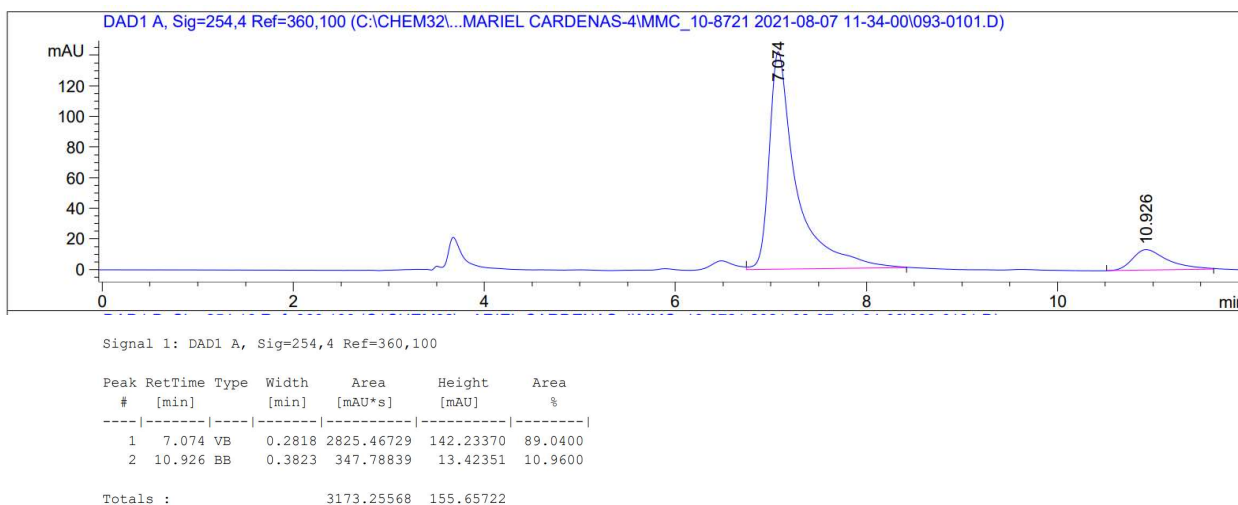
→ Determined, average of 3 trials: 16:84 e.r., 68 ee%

Sample Trace: 11:89 e.r., 78 ee%

HPLC Standard of **121** (racemized from a **121**; contains extra solvents)



Sample HPLC of **121**



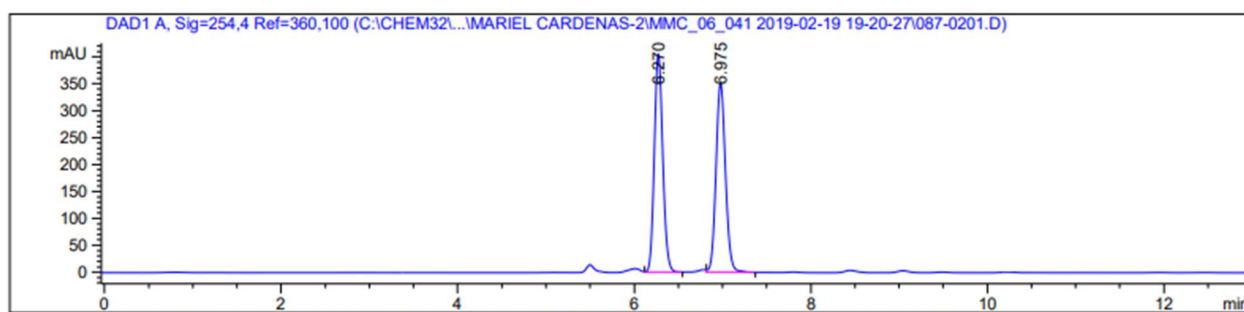
major enantiomer,
(*S*_a)-**110**

Enantioselectivity of **110** was measured with chiral HPLC analysis using a Daicel Corp. Chiralpak IA Column (4.6 mm ϕ \times 250 mL, Particle Size 5 μ M, Part No. 80325). *Method*: Hexanes:IPA (98:2), flow rate = 0.7 mL/min, *t*R = 12.0 min (major) and *t*R = 12.6 min (minor).

→ Determined, average of 2 trials: 83:17 e.r., 66 ee%

Sample Trace: 79:21 e.r., 58 ee%

Racemic Standard of **110**

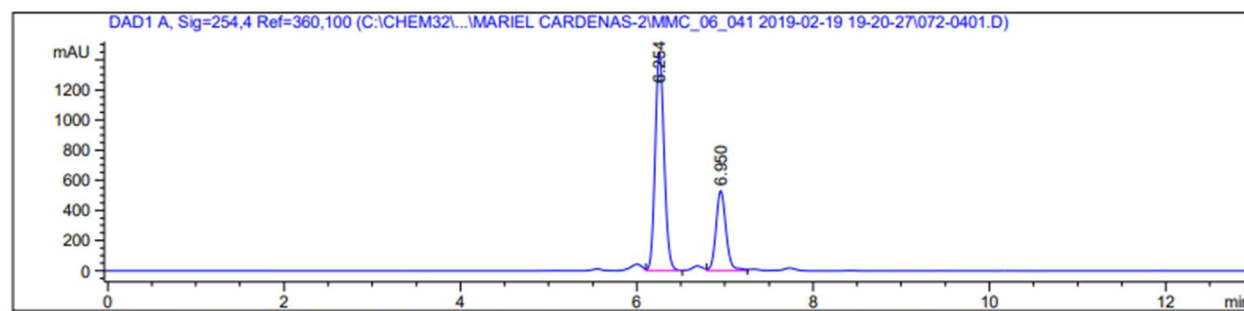


Signal 1: DAD1 A, Sig=254,4 Ref=360,100

Peak #	RetTime [min]	Type	Width [min]	Area [mAU*s]	Height [mAU]	Area %
1	6.270	VB	0.1036	2705.08984	406.76730	50.7156
2	6.975	VB	0.1171	2628.75391	352.06003	49.2844

Totals : 5333.84375 758.82733

Sample HPLC of **110**



Signal 1: DAD1 A, Sig=254,4 Ref=360,100

Peak #	RetTime [min]	Type	Width [min]	Area [mAU*s]	Height [mAU]	Area %
1	6.254	VV	0.1081	1.02222e4	1452.29602	70.6911
2	6.950	VV	0.1209	4238.16943	532.32648	29.3089

Totals : 1.44603e4 1984.62250

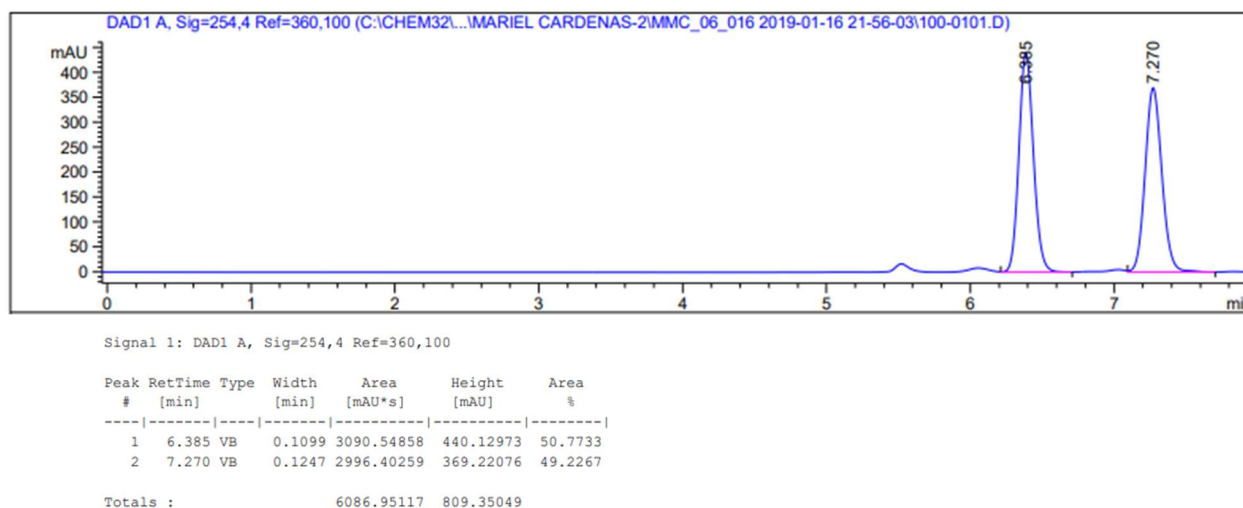
major enantiomer,
(*R*_a)-**109**

Enantioselectivity of **109** was measured with chiral HPLC analysis using a Daicel Corp. Chiralpak IA Column (4.6 mm ϕ \times 250 mL, Particle Size 5 μ M, Part No. 80325). *Method*: Hexanes:IPA (98:2), flow rate = 0.7 mL/min, *t*_R = 6.4 min (major) and *t*_R = 7.3 min (minor).

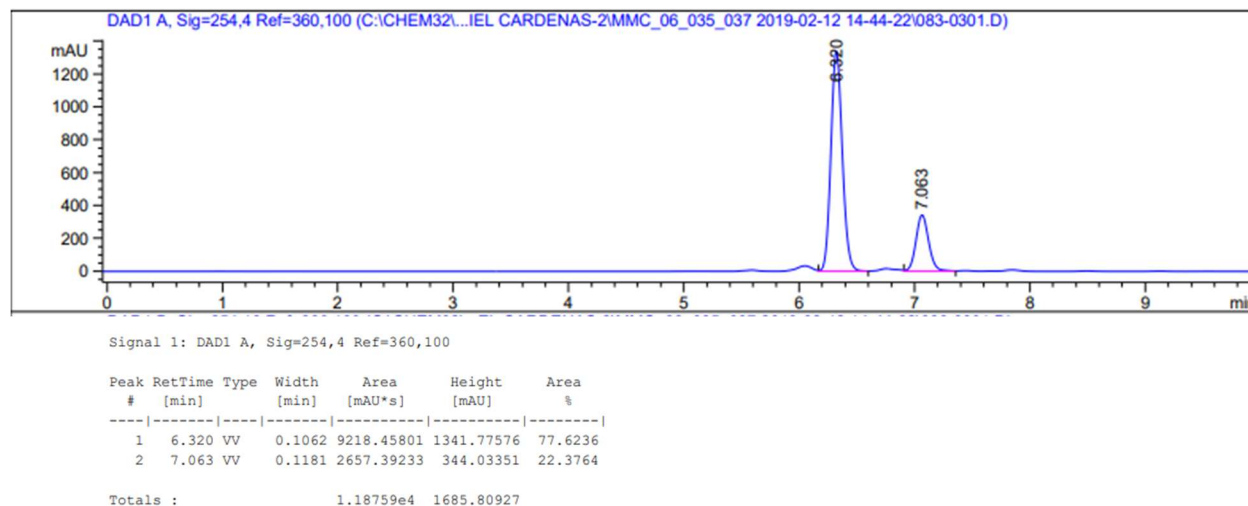
→ Determined, average of 2 trials: 23:77 e.r., 54 ee%

Sample Trace: 22:78 e.r., 56 ee%

Racemic Standard of **109**



Sample HPLC of **109**



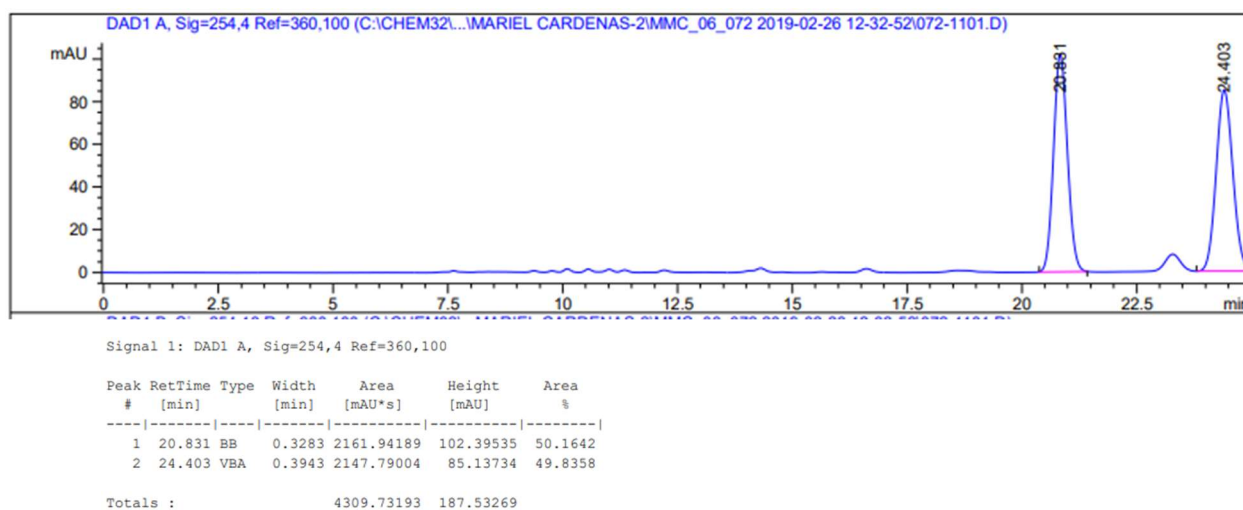
major enantiomer,
(*S_a*)-**112**

Enantioselectivity of **112** was measured with chiral HPLC analysis using a Daicel Corp. Chiralpak IC Column (4.6 mm ϕ \times 250 mL, Particle Size 5 μ M, Part No. 83325). *Method*: Hexanes:IPA (98:2), flow rate = 0.5 mL/min, *t*R = 20.8 min (major) and *t*R = 24.4 min (minor).

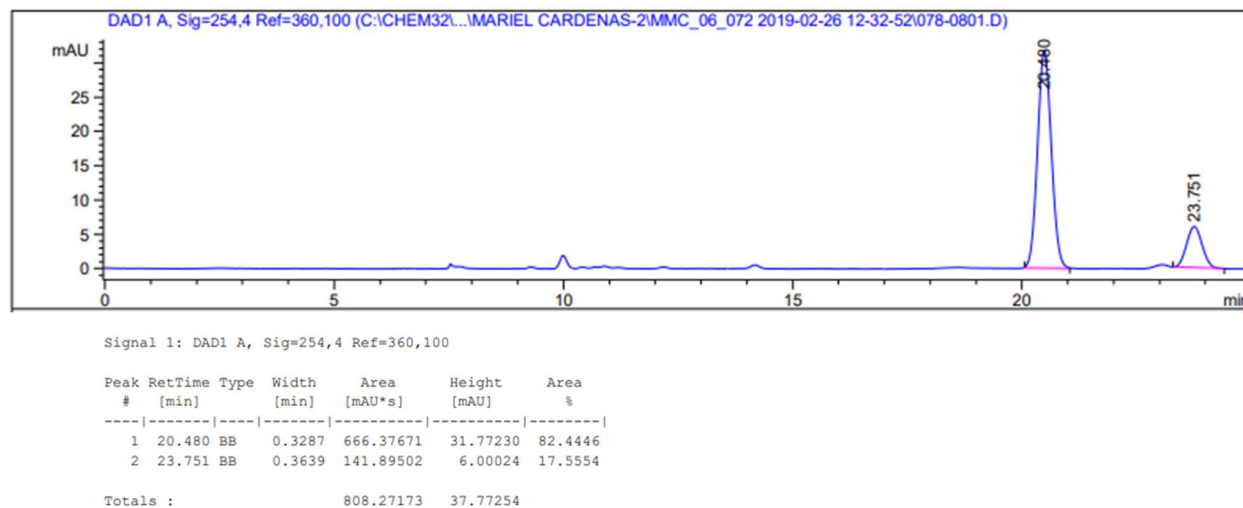
→ Determined, average of 2 trials: 82:18 e.r., 64 ee%

Sample Trace: 82:18 e.r., 64 ee%

Racemic Standard of **112**



Sample HPLC of **112**



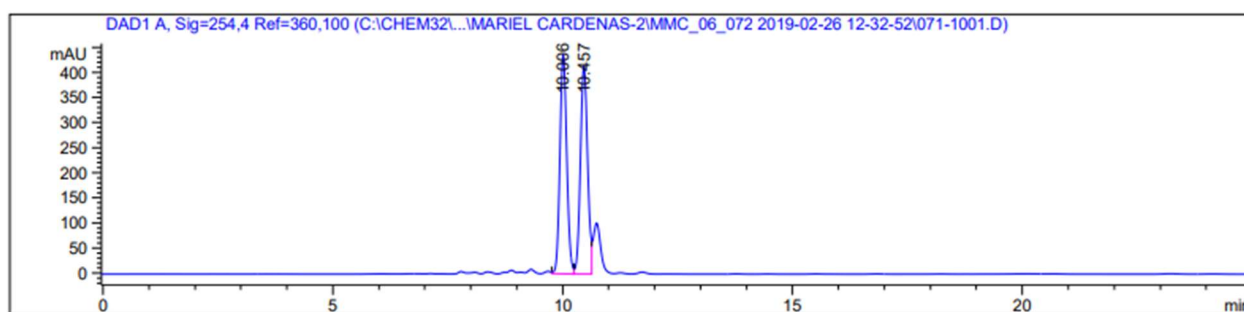
major enantiomer,
(*R*_a)-**111**

Enantioselectivity of **111** was measured with chiral HPLC analysis using a Daicel Corp. Chiralpak IC Column (4.6 mm ϕ \times 250 mL, Particle Size 5 μ M, Part No. 83325). *Method*: Hexanes:IPA (70:30), flow rate = 1.0 mL/min, *t*_R = 5.6 min (major) and *t*_R = 6.7 min (minor).

→ Determined, average of 2 trials: 13:87 e.r., 74 ee%

Sample Trace: 13:87 e.r., 74 ee%

Racemic Standard of **111**

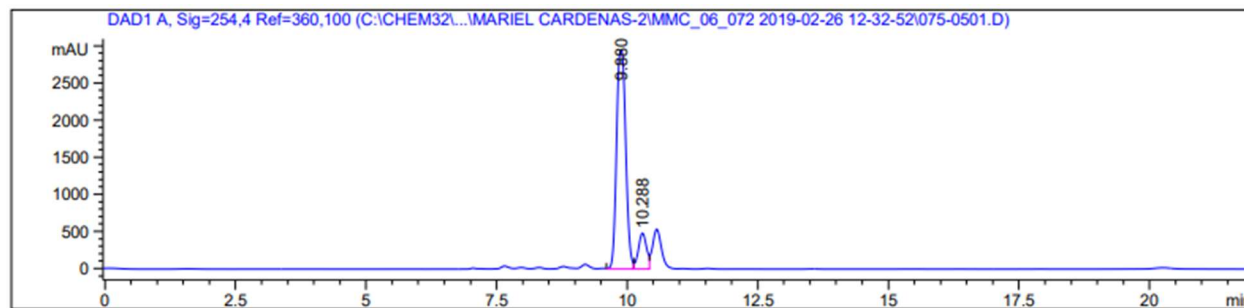


Signal 1: DAD1 A, Sig=254,4 Ref=360,100

Peak #	RetTime [min]	Type	Width [min]	Area [mAU*s]	Height [mAU]	Area %
1	10.006	VV	0.1605	4517.50293	437.53732	49.9859
2	10.457	VV	0.1692	4520.05322	414.70200	50.0141

Totals : 9037.55615 852.23932

Sample HPLC of **111**



Signal 1: DAD1 A, Sig=254,4 Ref=360,100

Peak #	RetTime [min]	Type	Width [min]	Area [mAU*s]	Height [mAU]	Area %
1	9.880	VV	0.1943	3.60445e4	2955.18799	87.2443
2	10.288	VV	0.1668	5269.92578	484.88898	12.7557

Totals : 4.13144e4 3440.07697

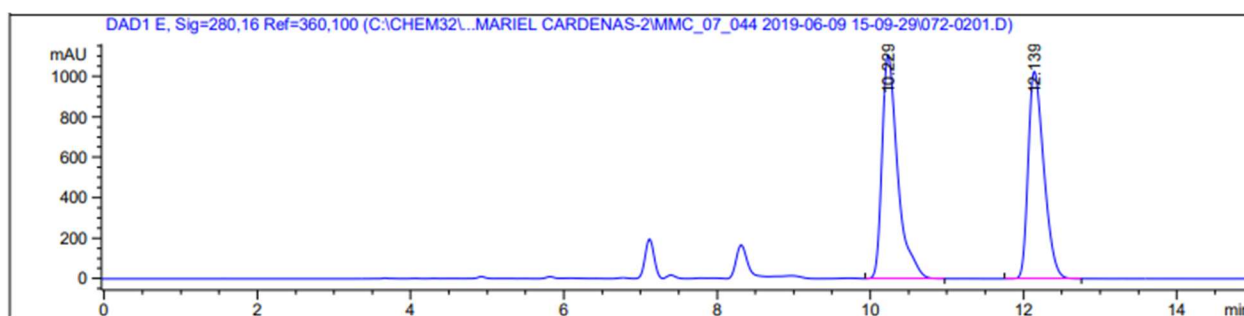
major enantiomer,
(*S*_a)-**114**

Enantioselectivity of **114** was measured with chiral HPLC analysis using a Daicel Corp. Chiralpak IC Column (4.6 mm ϕ \times 250 mL, Particle Size 5 μ M, Part No. 83325). *Method*: Hexanes:IPA (98:2), flow rate = 0.7 mL/min, *t*R = 10.2 min (major) and *t*R = 12.1 min (minor).

→ Determined, average of 2 trials: 81.5:18.5 e.r., 63 ee%

Sample Trace: 81.5:18.5 e.r., 63 ee%

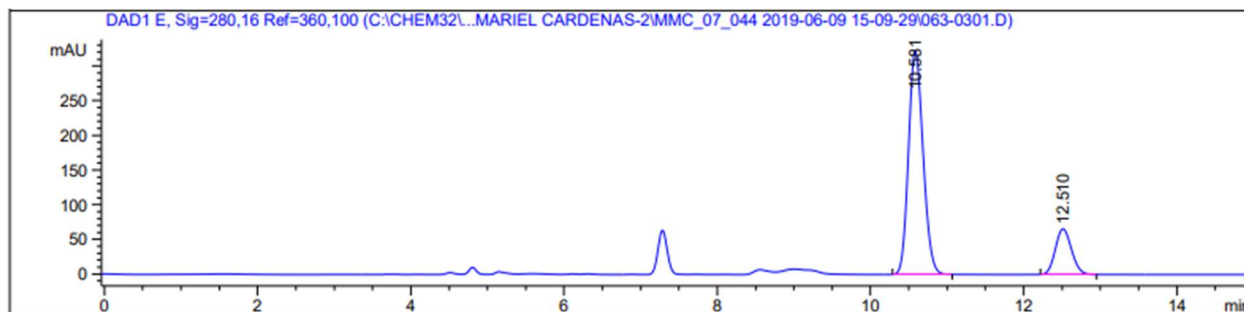
Racemic Standard of **114**



Signal 5: DAD1 E, Sig=280,16 Ref=360,100

Peak #	RetTime [min]	Type	Width [min]	Area [mAU*s]	Height [mAU]	Area %
1	10.229	VB	0.2164	1.57864e4	1106.62793	52.0617
2	12.139	BB	0.2174	1.45361e4	1025.34070	47.9383
Totals :				3.03226e4	2131.96863	

Sample HPLC of **114**



Signal 5: DAD1 E, Sig=280,16 Ref=360,100

Peak #	RetTime [min]	Type	Width [min]	Area [mAU*s]	Height [mAU]	Area %
1	10.581	BB	0.2060	4263.41211	322.99353	81.5102
2	12.510	BB	0.2293	967.11609	65.86954	18.4898
Totals :				5230.52820	388.86308	

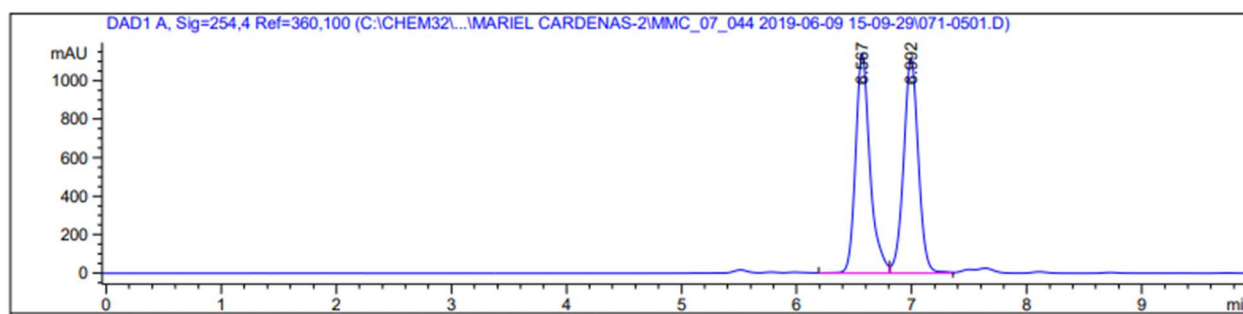
major enantiomer,
(*R*_a)-**113**

Enantioselectivity of **113** was measured with chiral HPLC analysis using a Daicel Corp. Chiralpak IC Column (4.6 mm ϕ \times 250 mL, Particle Size 5 μ M, Part No. 83325). *Method*: Hexanes:IPA (70:30), flow rate = 1.0 mL/min, *t*_R = 6.6 min (minor) and *t*_R = 7.0 min (major).

→ Determined, average of 2 trials: 19:81 e.r., 62 ee%

Sample Trace: 19:81 e.r., 62 ee%

Racemic Standard of **113**

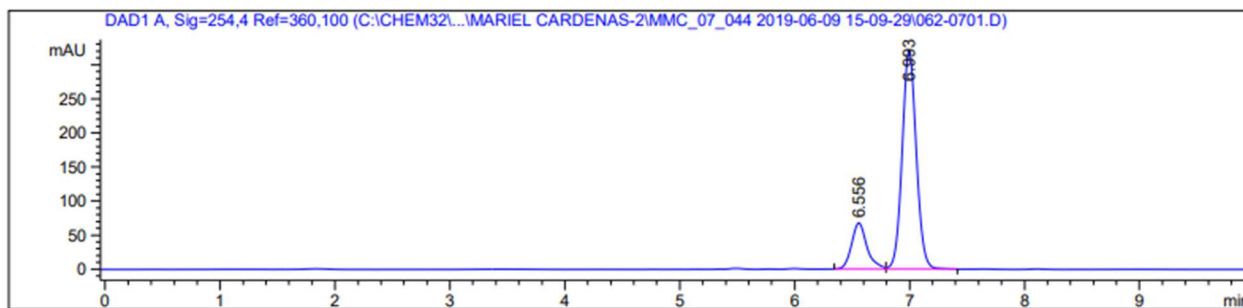


Signal 1: DAD1 A, Sig=254,4 Ref=360,100

Peak #	RetTime [min]	Type	Width [min]	Area [mAU*s]	Height [mAU]	Area %
1	6.567	VV	0.1297	9958.57129	1142.32532	50.0186
2	6.992	VV	0.1358	9951.17188	1118.47083	49.9814

Totals : 1.99097e4 2260.79614

Sample HPLC of **113**



Signal 1: DAD1 A, Sig=254,4 Ref=360,100

Peak #	RetTime [min]	Type	Width [min]	Area [mAU*s]	Height [mAU]	Area %
1	6.556	BV	0.1416	639.44904	68.06207	18.9030
2	6.993	VB	0.1315	2743.33667	321.54132	81.0970

Totals : 3382.78571 389.60339

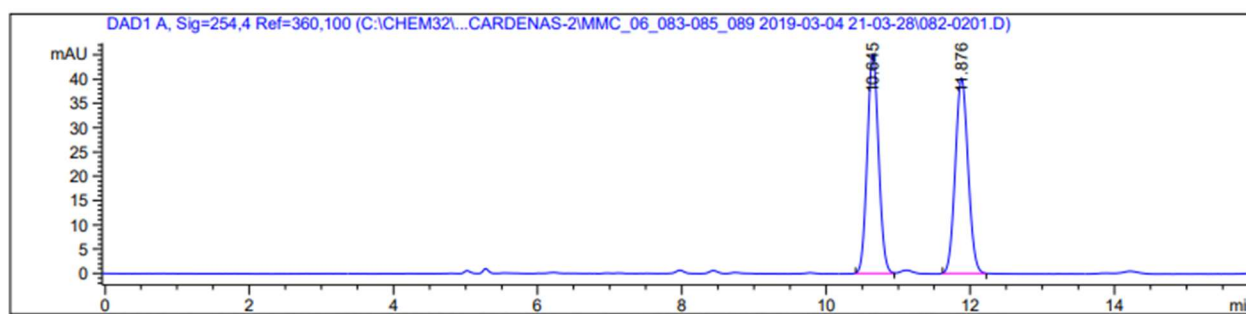
major enantiomer,
(*S*_a)-**115**

Enantioselectivity of **115** was measured with chiral HPLC analysis using a Daicel Corp. Chiralpak IC Column (4.6 mm ϕ \times 250 mL, Particle Size 5 μ M, Part No. 83325). *Method*: Hexanes:IPA (98:2), flow rate = 0.7 mL/min, *t*_R = 10.6 min (major) and *t*_R = 11.9 min (minor).

→ Determined, average of 2 trials: 69:31 e.r., 38 ee%

Sample Trace: 69:31 e.r., 38 ee%

Racemic Standard of **115**

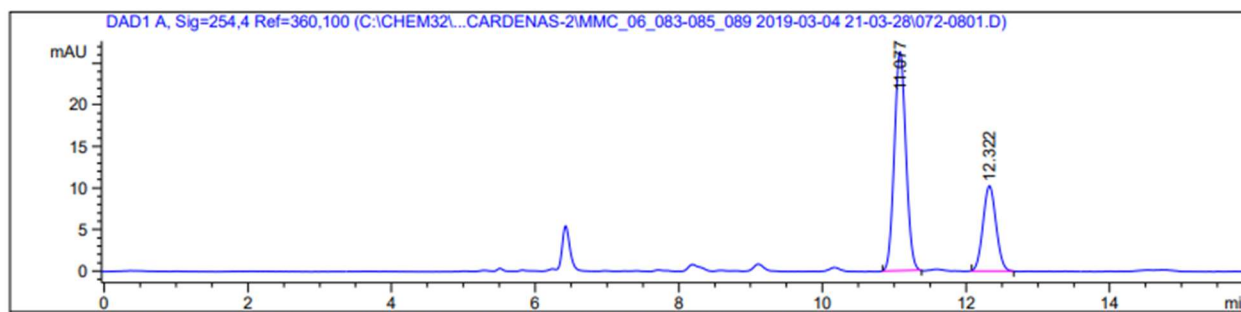


Signal 1: DAD1 A, Sig=254,4 Ref=360,100

Peak #	RetTime [min]	Type	Width [min]	Area [mAU*s]	Height [mAU]	Area %
1	10.645	BB	0.1700	497.05429	45.29067	49.9280
2	11.876	BB	0.1922	498.48715	40.32581	50.0720

Totals : 995.54144 85.61647

Sample HPLC of **115**



Signal 1: DAD1 A, Sig=254,4 Ref=360,100

Peak #	RetTime [min]	Type	Width [min]	Area [mAU*s]	Height [mAU]	Area %
1	11.077	BB	0.1749	295.82111	26.36147	69.4143
2	12.322	BB	0.1981	130.34605	10.26766	30.5857

Totals : 426.16716 36.62913

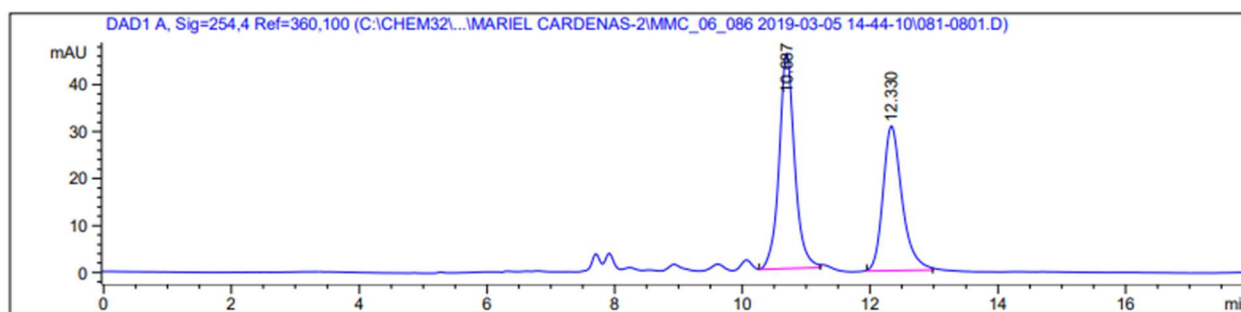
major enantiomer,
(*R*_a)-**73**

Enantioselectivity of **73** was measured with chiral HPLC analysis using a Daicel Corp. Chiralpak IC Column (4.6 mm ϕ \times 250 mL, Particle Size 5 μ M, Part No. 83325). *Method*: Hexanes:IPA (70:30), flow rate = 1.0 mL/min, *t*R = 10.7 min (minor) and *t*R = 12.3 min (major).

→ Determined, average of 2 trials: 5:95 e.r., 90 ee%

Sample Trace: 12:88 e.r., 76 ee%

Racemic Standard of **73**

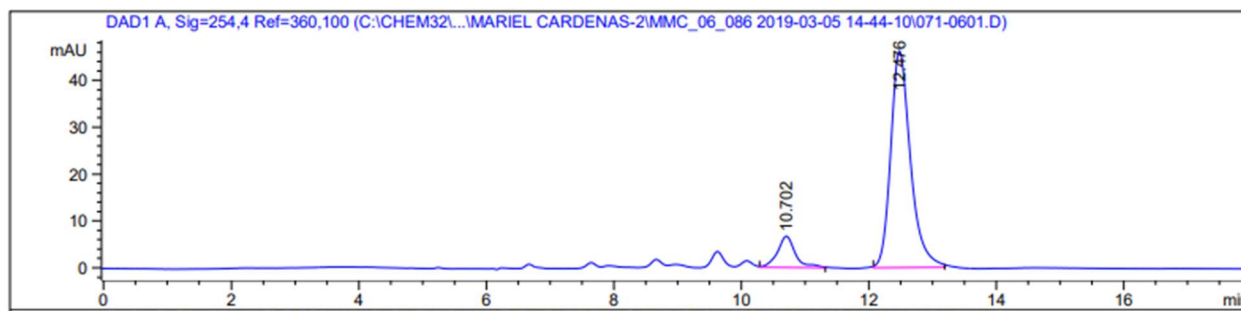


Signal 1: DAD1 A, Sig=254,4 Ref=360,100

Peak #	RetTime [min]	Type	Width [min]	Area [mAU*s]	Height [mAU]	Area %
1	10.687	VB	0.2519	777.85083	45.86111	54.7418
2	12.330	BB	0.3155	643.09375	30.81101	45.2582

Totals : 1420.94458 76.67212

Sample HPLC of **73**



Signal 1: DAD1 A, Sig=254,4 Ref=360,100

Peak #	RetTime [min]	Type	Width [min]	Area [mAU*s]	Height [mAU]	Area %
1	10.702	VB	0.2906	134.59886	6.74980	11.8804
2	12.476	BB	0.3259	998.35345	46.23511	88.1196

Totals : 1132.95232 52.98491

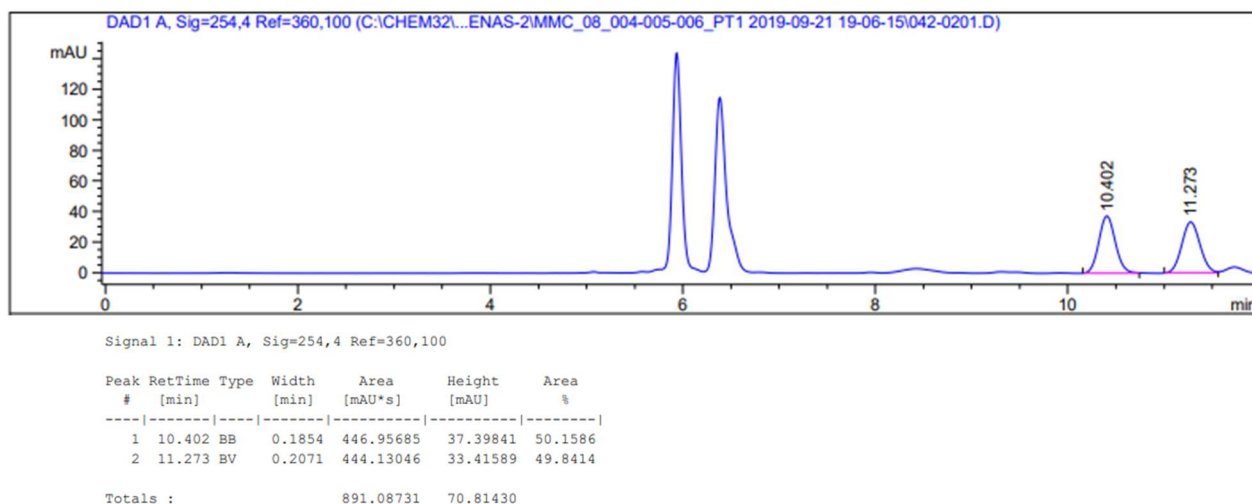
major enantiomer,
(S_a)-**108**

Enantioselectivity of **108** was measured with chiral HPLC analysis using a Daicel Corp. Chiralpak IA Column (4.6 mm ϕ \times 250 mL, Particle Size 5 μ M, Part No. 80325). Method: Hexanes:IPA (98:2), flow rate = 1.0 mL/min, *t*R = 16.4 min (major) and *t*R = 17.4 min (minor).

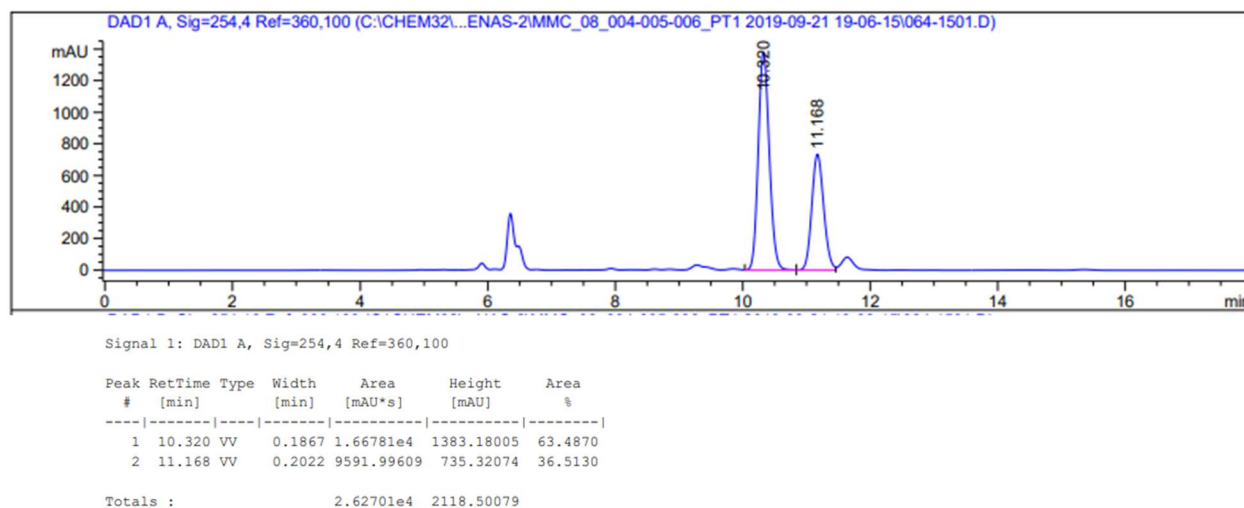
→ Determined, average of 2 trials: 64:36 e.r., 28 ee%

Sample Trace: 64:34 e.r., 28 ee%

Racemic Standard of **108**



Sample HPLC of **108**



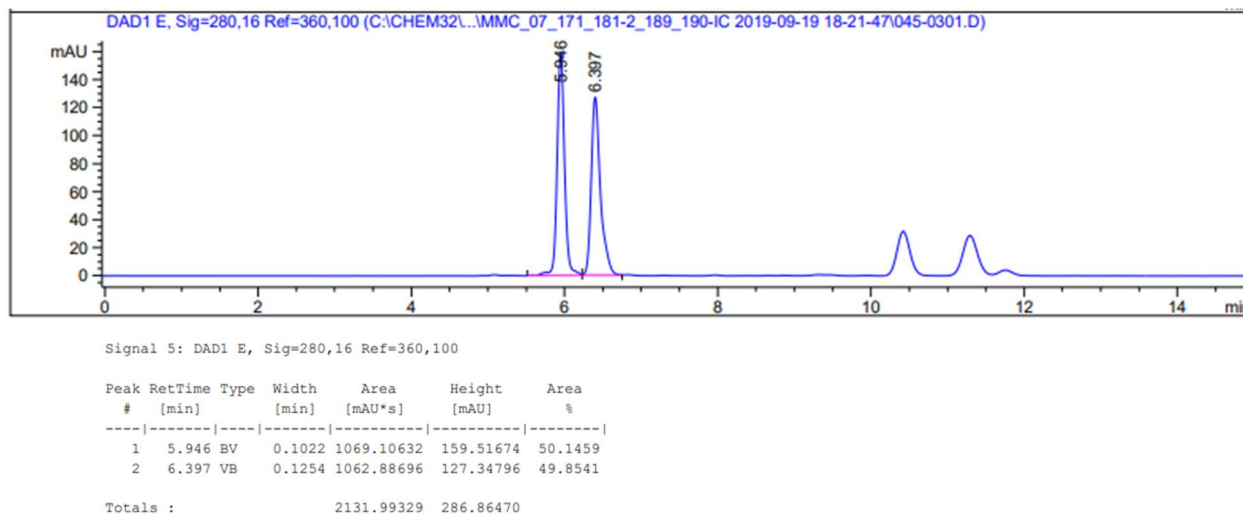
major enantiomer,
(*R*_a)-**107**

Enantioselectivity of **107** was measured with chiral HPLC analysis using a Daicel Corp. Chiralpak IA Column (4.6 mm ϕ \times 250 mL, Particle Size 5 μ M, Part No. 80325). *Method*: Hexanes:IPA (98:2), flow rate = 1.0 mL/min, *t*_R = 5.9 min (minor) and *t*_R = 6.4 min (major).

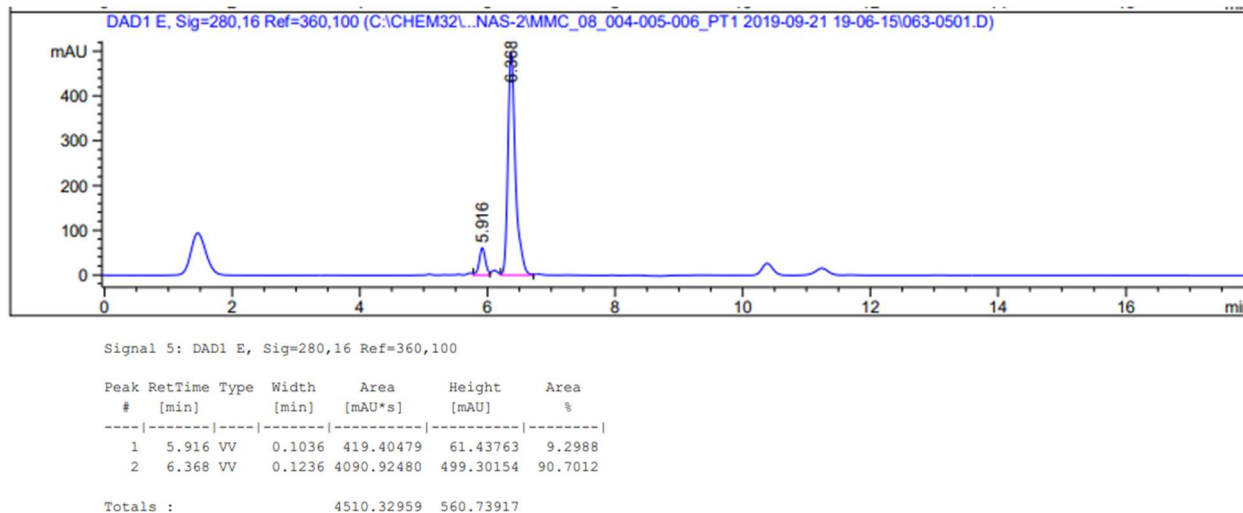
→ Determined, average of 4 trials: 9:91 e.r., 82 ee%

Sample Trace: 9:91 e.r., 82 ee%

Racemic Standard of **107**



Sample HPLC of **107**



2.2.20 X-ray Crystallography

Crystals of compounds **72**, **85**, **86**, and **107** were obtained by slow evaporation from deuterated chloroform, respectively. The crystals were mounted on a nylon loop in Paratone oil (Hampton Research). The diffraction data were collected on a Bruker APEX-II CCD area detector equipped with a graphite monochromator and MoK α radiation ($\lambda = 0.71073 \text{ \AA}$) at 100(2) K with 0.5 deg/frame scans. The data collection strategy was calculated on APEX3¹, the data integration was performed using SAINT program², the absorption correction based on multi-scan was obtained by SADABS³, and the space groups were assigned using XPREP⁴. The structures were solved by direct method with SHELXS⁵ and refined by full-matrix least-squares based on F^2 with SHELXL⁵ using Olex2 program⁶. Hydrogen atoms in **72**, **85**, **86**, and **107** were placed at idealized positions and were refined as riding atoms with uniform isotropic thermal parameters. The ORTEP models were drawn on Mercury⁷ in Cambridge Structural Database system software⁸. A summary of the crystallographic data is given in Table S.1 and S.2. The products, **107** and **86**, found from the asymmetric syntheses indicated Flack⁹/Hooft¹⁰ parameters with 0.05(7)/0.033(11) and -0.03(4)/-0.005(9), respectively. These crystal structures are shown in Figure S.1. The crystal structures of compounds **72** and **85** were found in the racemic crystals, shown in Figure S.2.

- (1) APEX3 (v2018.1-0), Bruker AXS Inc., Madison, Wisconsin, USA, 2018.
- (2) SAINT (V8.38A), Bruker AXS Inc., Madison, Wisconsin, USA, 2016.
- (3) SADABS (v2016/2), Bruker AXS Inc., Madison, Wisconsin, USA, 2016.
- (4) XPREP (v2014/2), Bruker AXS Inc., Madison, Wisconsin, USA, 2014.
- (5) G. M. Sheldrick, A short history of *SHELX*. *Acta Crystallogr., Sect. A: Found. Crystallogr.* **64**, 112–122 (2008).
- (6) O. V. Dolomanov, L. J. Bourhis, R. J. Gildea, J. A. K. Howard, H. Puschmann, *OLEX2*: a complete structure solution, refinement and analysis program. *J. Appl. Crystallogr.* **42**, 339–341 (2009).
- (7) C. F. Macrae, P. R. Edgington, P. McCabe, E. Pidcock, G. P. Shields, R. Taylor, M. Towler, J. van de Streek, *Mercury*: visualization and analysis of crystal structures. *J. Appl. Crystallogr.* **39**, 453–457 (2006).
- (8) F. H. Allen, The Cambridge Structural Database: a quarter of a million crystal structures and rising. *Acta Cryst Sect A Found Cryst.* **58**, 380–388 (2002).
- (9) H. D. Flack, G. Bernardinelli, The use of X-ray crystallography to determine absolute configuration. *Chirality*. **20**, 681–690 (2008).
- (10) R. W. W. Hooft, L. H. Straver, A. L. Spek, Determination of absolute structure using Bayesian statistics on Bijvoet differences. *J. Appl. Crystallogr.* **41**, 96–103 (2008).

Table 31. Crystallographic data of compounds **107** and **86**.

Compound	107	86
CCDC Number	1999111	1999112
Formula	C ₂₈ H ₂₁ NS	C ₂₃ H ₁₅ F ₄ NS
Formula weight, g/mol	403.52	413.42
<i>T</i> , K	100(2)	100(2)
Crystal system	Monoclinic	Orthorhombic
Space group	<i>P</i> 2 ₁	<i>P</i> 2 ₁ 2 ₁ 2 ₁
<i>a</i> , Å	10.0555(4)	9.8999(2)
<i>b</i> , Å	11.6803(5)	13.7881(3)
<i>c</i> , Å	18.1925(7)	27.3121(6)
α , °	90	90
β , °	100.9539(18)	90
γ , °	90	90
<i>V</i> , Å ³	2097.80(15)	3728.12(14)
<i>Z</i> , <i>Z'</i>	4, 2	8, 2
Radiation (λ , Å)	Mo <i>K</i> α , 0.71073	Mo <i>K</i> α , 0.71073
μ , mm ⁻¹	0.169	0.221
ρ_{calc} , g/cm ³	1.278	1.473
Color	Colorless	Colorless
2 θ range for data collection, °	2.28 to 54.20	5.88 to 54.20
Index ranges	-12 ≤ <i>h</i> ≤ 12 -14 ≤ <i>k</i> ≤ 14 -23 ≤ <i>l</i> ≤ 23	-12 ≤ <i>h</i> ≤ 12 -17 ≤ <i>k</i> ≤ 17 -35 ≤ <i>l</i> ≤ 35
Reflections collected	42835	86653
Independent reflections	9235 [<i>R</i> _{int} = 0.0217, <i>R</i> _{sigma} = 0.0201]	8217 [<i>R</i> _{int} = 0.0343, <i>R</i> _{sigma} = 0.0153]
Completeness to 2 θ = 50.48°, %	99.6	99.6
Goodness-of-fit on <i>F</i> ²	1.171	1.058
<i>R</i> ₁ / <i>wR</i> ₂ , % [<i>I</i> >= 2 σ (<i>I</i>)]	3.73/9.16	2.23/5.91
Largest diff. peak/hole, e Å ⁻³	0.360/-0.254	0.236/-0.197
Flack/Hooft parameters	0.05(7)/0.033(11)	-0.03(4)/-0.005(9)

Table 32. Crystallographic data of compounds **72** and **85**.

Compound	72	85
CCDC Number	1999113	1999114
Formula	C ₂₂ H ₁₆ FNS	C ₂₃ H ₁₈ FNS
Formula weight, g/mol	345.42	359.44
<i>T</i> , K	100(2)	100(2)
Crystal system	Monoclinic	Monoclinic
Space group	<i>P</i> 2 ₁ / <i>c</i>	<i>C</i> 2/ <i>c</i>
<i>a</i> , Å	9.8278(4)	35.7964(15)
<i>b</i> , Å	10.9691(5)	9.0412(4)
<i>c</i> , Å	32.1964(15)	11.4109(5)
α , °	90	90
β , °	91.4798(18)	98.271(2)
γ , °	90	90
<i>V</i> , Å ³	3469.7(3)	3654.6(3)
<i>Z</i> , <i>Z'</i>	8, 2	8, 1
Radiation (λ , Å)	Mo <i>K</i> α , 0.71073	Mo <i>K</i> α , 0.71073
μ , mm ⁻¹	0.200	0.192
ρ_{calc} , g/cm ³	1.322	1.307
Color	Colorless	Colorless
2 θ range for data collection, °	5.31 to 51.36	2.30 to 51.36
Index ranges	-11 ≤ <i>h</i> ≤ 11 -13 ≤ <i>k</i> ≤ 13 -39 ≤ <i>l</i> ≤ 39	-43 ≤ <i>h</i> ≤ 43 -11 ≤ <i>k</i> ≤ 11 -13 ≤ <i>l</i> ≤ 13
Reflections collected	81618	49364
Independent reflections	6576 [<i>R</i> _{int} = 0.0188, <i>R</i> _{sigma} = 0.0087]	3455 [<i>R</i> _{int} = 0.0575, <i>R</i> _{sigma} = 0.0170]
Completeness to 2 θ = 50.48°, %	99.9 99.9	
Goodness-of-fit on <i>F</i> ²	1.158	1.163
<i>R</i> ₁ / <i>wR</i> ₂ , % [<i>I</i> >= 2 σ (<i>I</i>)]	4.17/9.55	4.53/9.95
Largest diff. peak/hole, e Å ⁻³	0.313/-0.254	0.302/-0.319

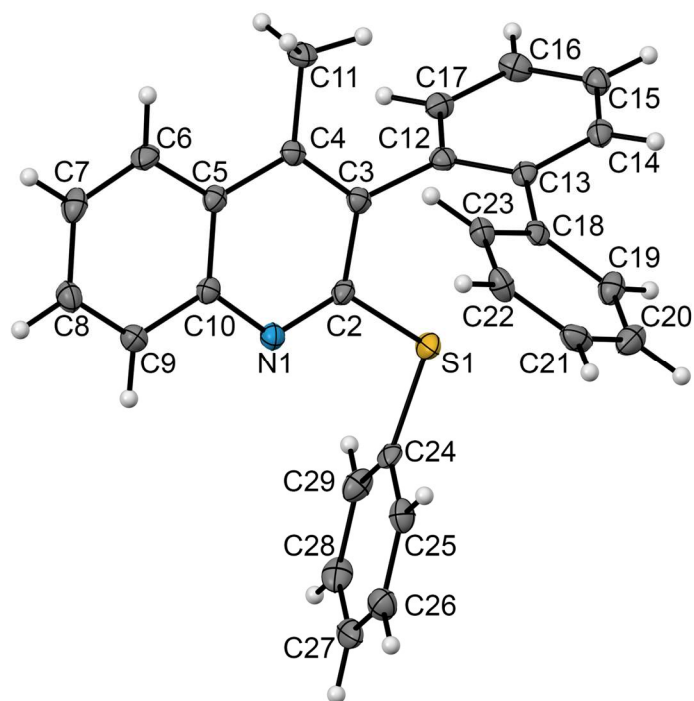


Figure 38. Crystal structures of compound **107** produced from the asymmetric syntheses. The thermal ellipsoids are drawn at the 50% probability level.

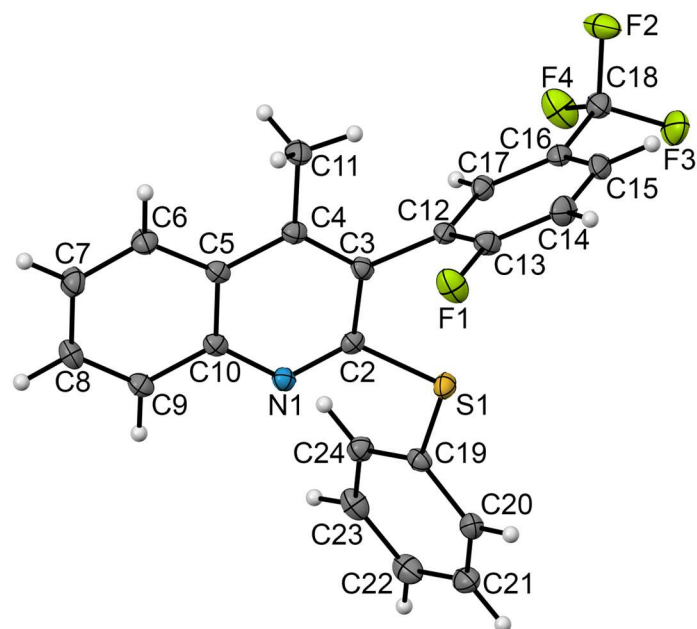


Figure 39. Crystal structures of compound **86** produced from the asymmetric syntheses. The thermal ellipsoids are drawn at the 50% probability level.

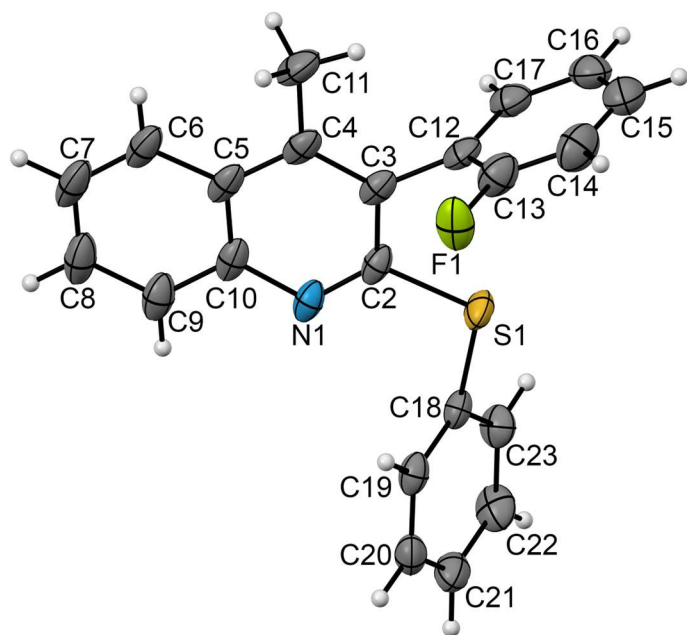


Figure 40. Crystal structures of compound **72** showing one of the enantiomers found in the racemic crystals. The thermal ellipsoids are drawn at the 50% probability level.

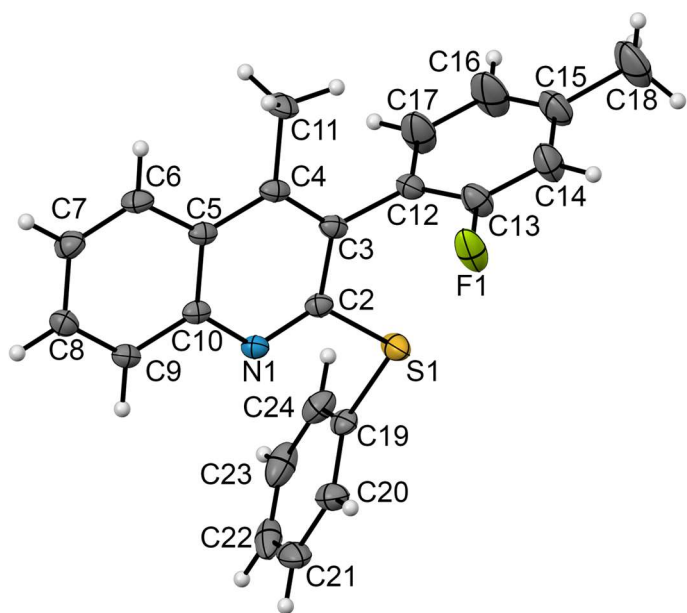
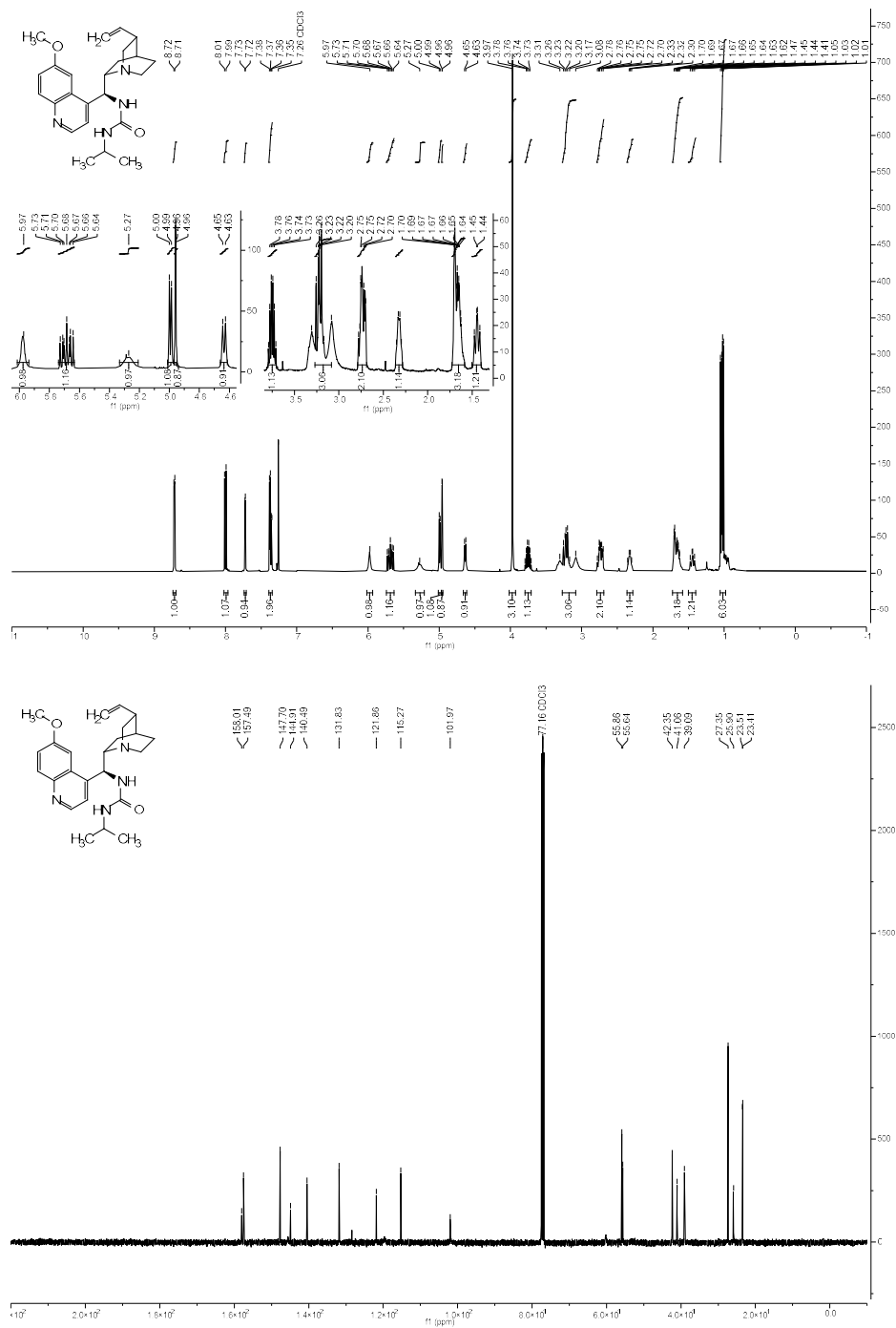


Figure 41. Crystal structures of compound **85** showing one of the enantiomers found in the racemic crystals. The thermal ellipsoids are drawn at the 50% probability level.

2.2.21. Spectral Data (NMR, HRMS-ESI MSpec)

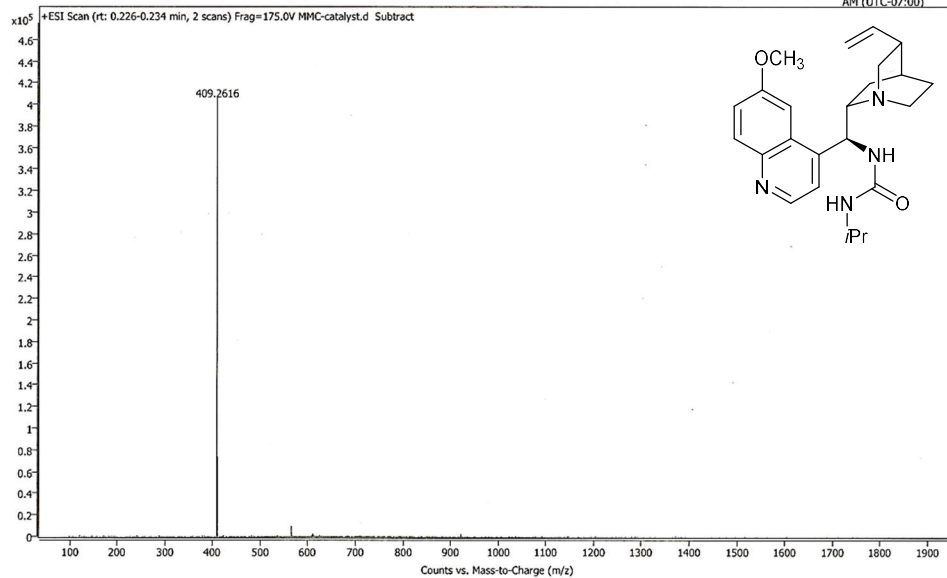
^1H and ^{13}C NMR and HRMS (ESI) Spectral Data of Catalyst 77



Spectrum Plot Report



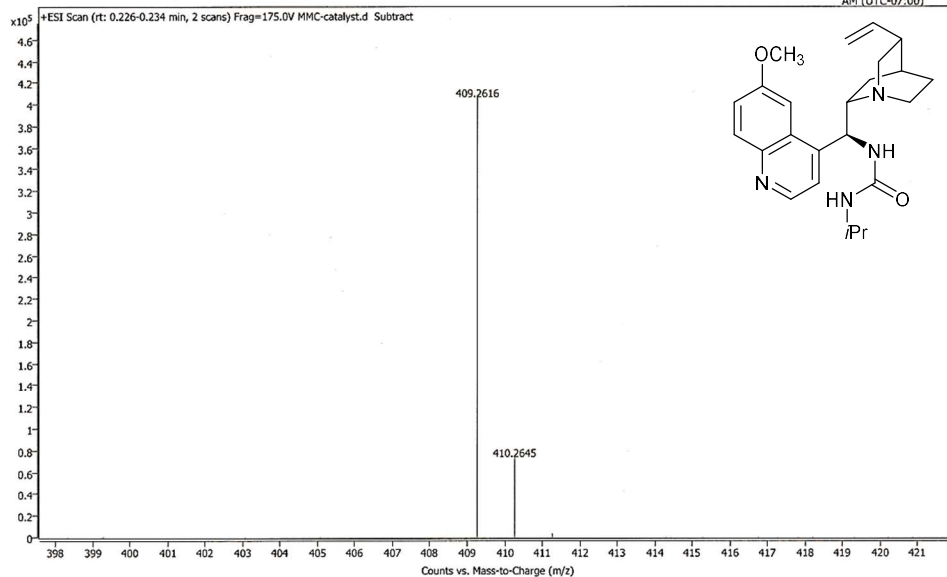
Name	MMC-catalyst	Rack Pos.	Instrument	Instrument 1	Operator
Inj. Vol. (ul)	2	Plate Pos.	IRM Status	Some ions missed	
Data File	MMC-catalyst.d	Method (Acq)	Column bypass.m	Comment	Acq. Time (Local)
					3/23/2020 11:22:10 AM (UTC-07:00)



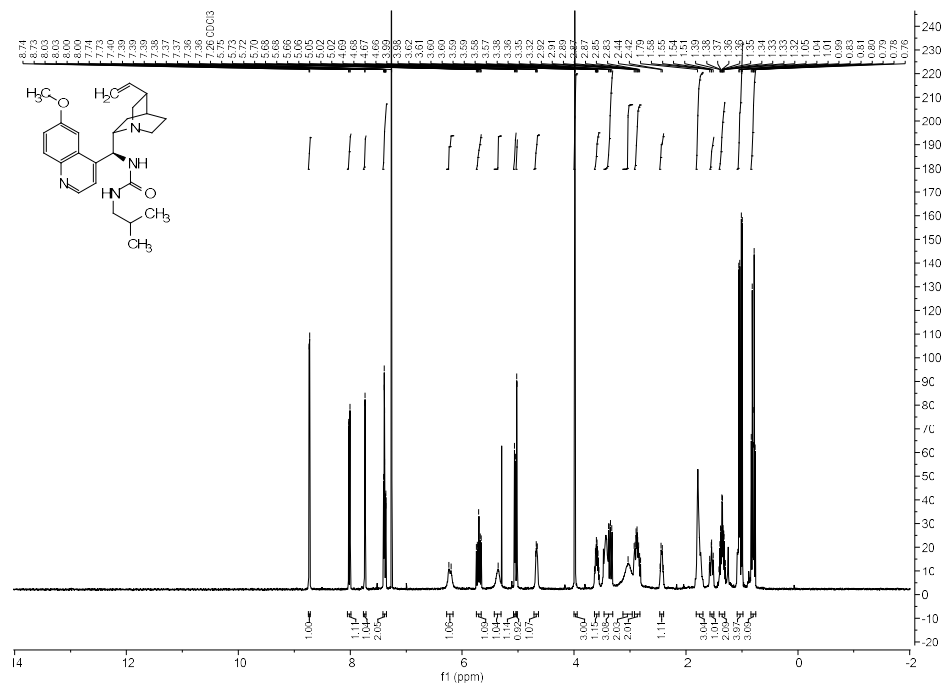
Spectrum Plot Report



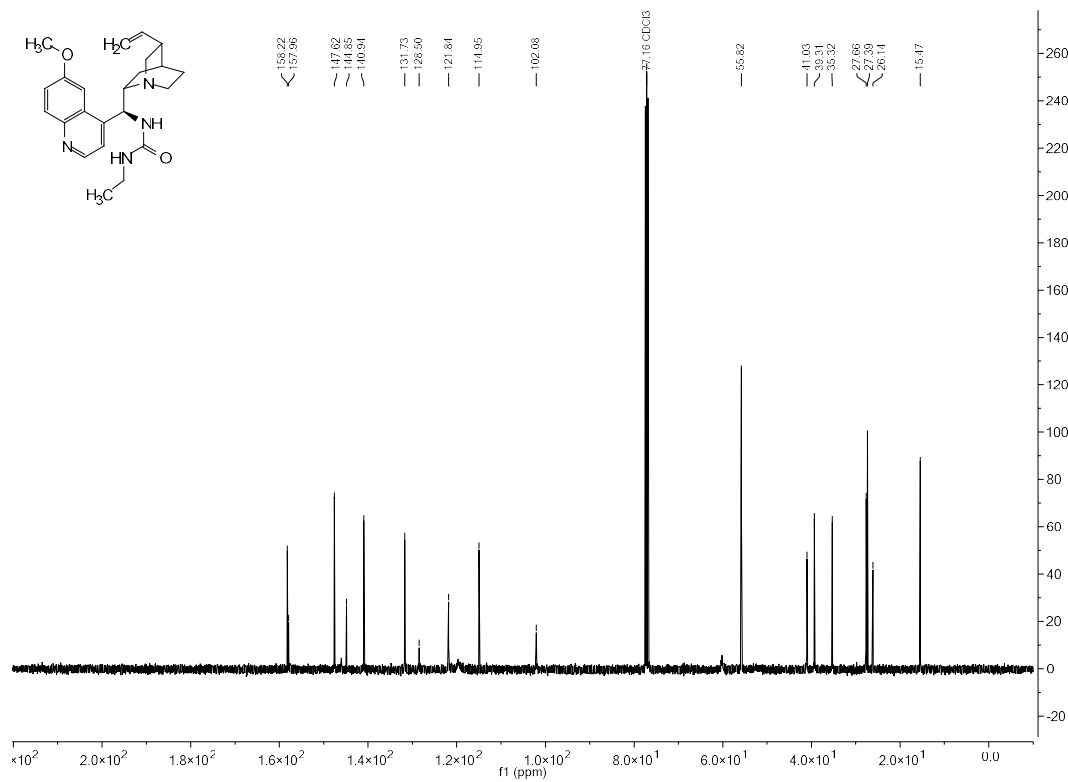
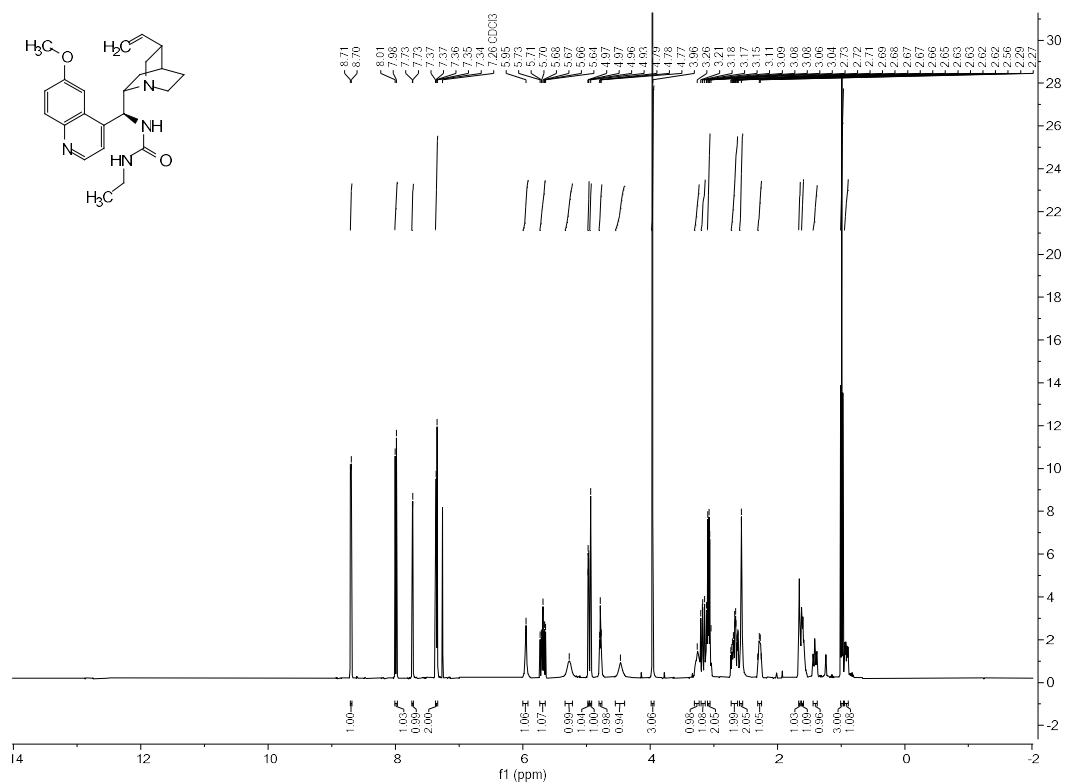
Name	MMC-catalyst	Rack Pos.	Instrument	Instrument 1	Operator
Inj. Vol. (ul)	2	Plate Pos.	IRM Status	Some ions missed	
Data File	MMC-catalyst.d	Method (Acq)	Column bypass.m	Comment	Acq. Time (Local)
					3/23/2020 11:22:10 AM (UTC-07:00)



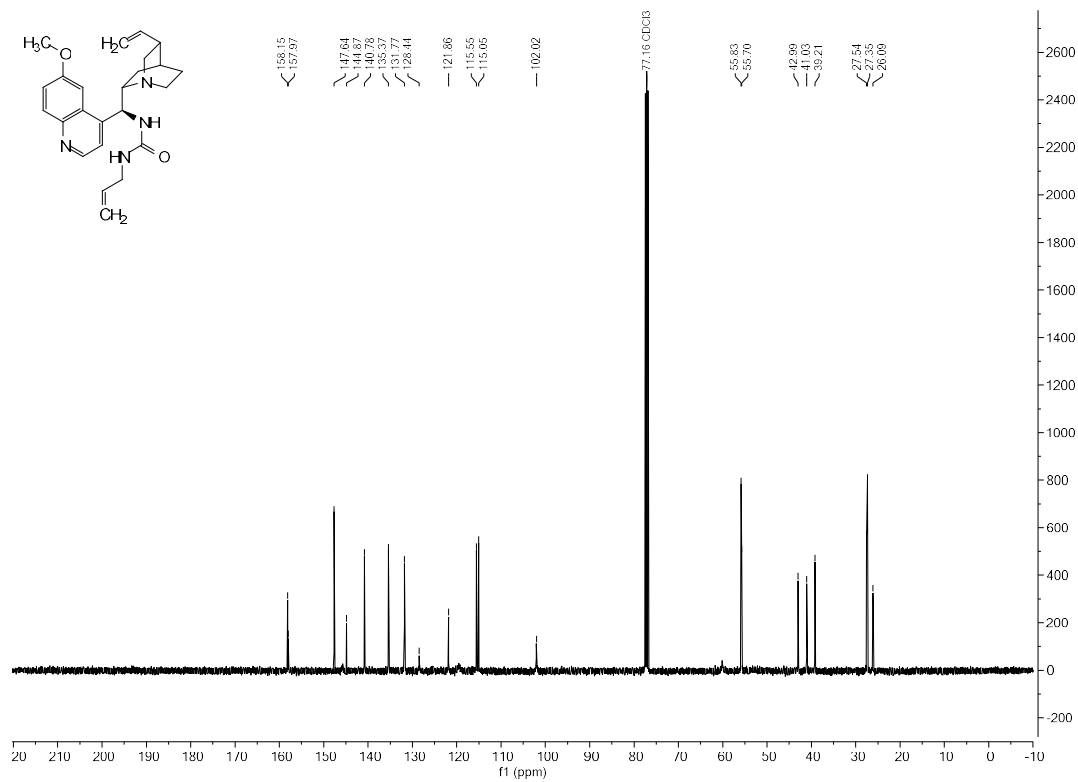
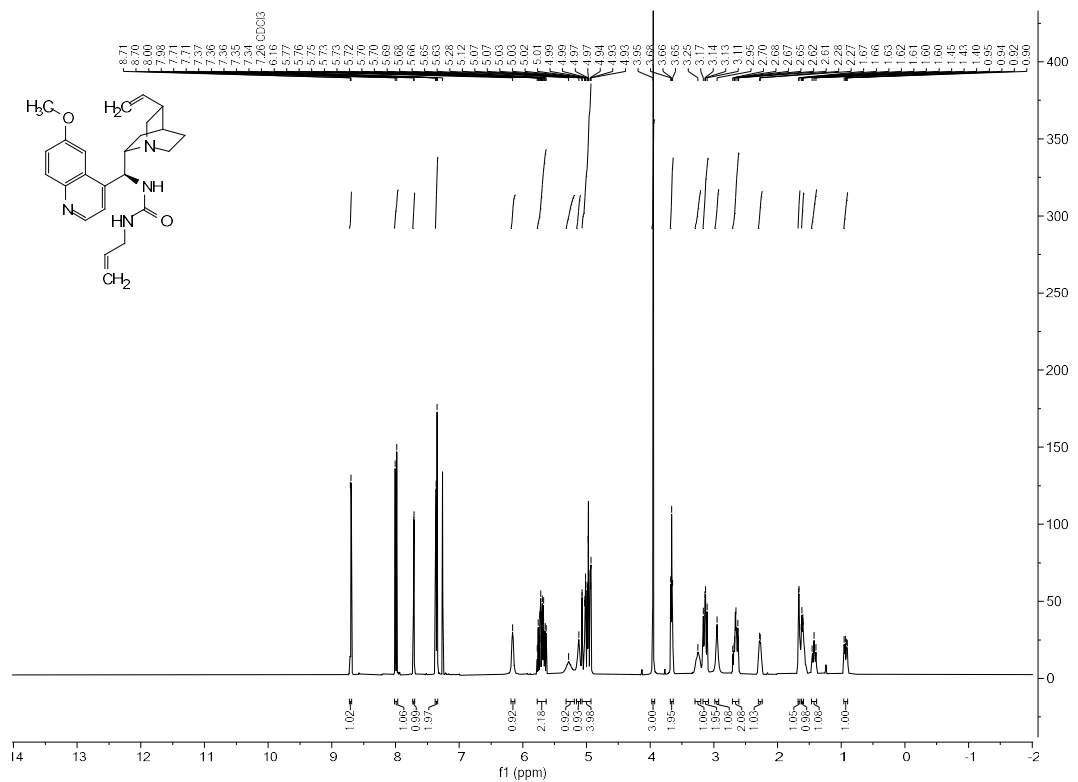
¹H Spectral Data of Catalyst CA10



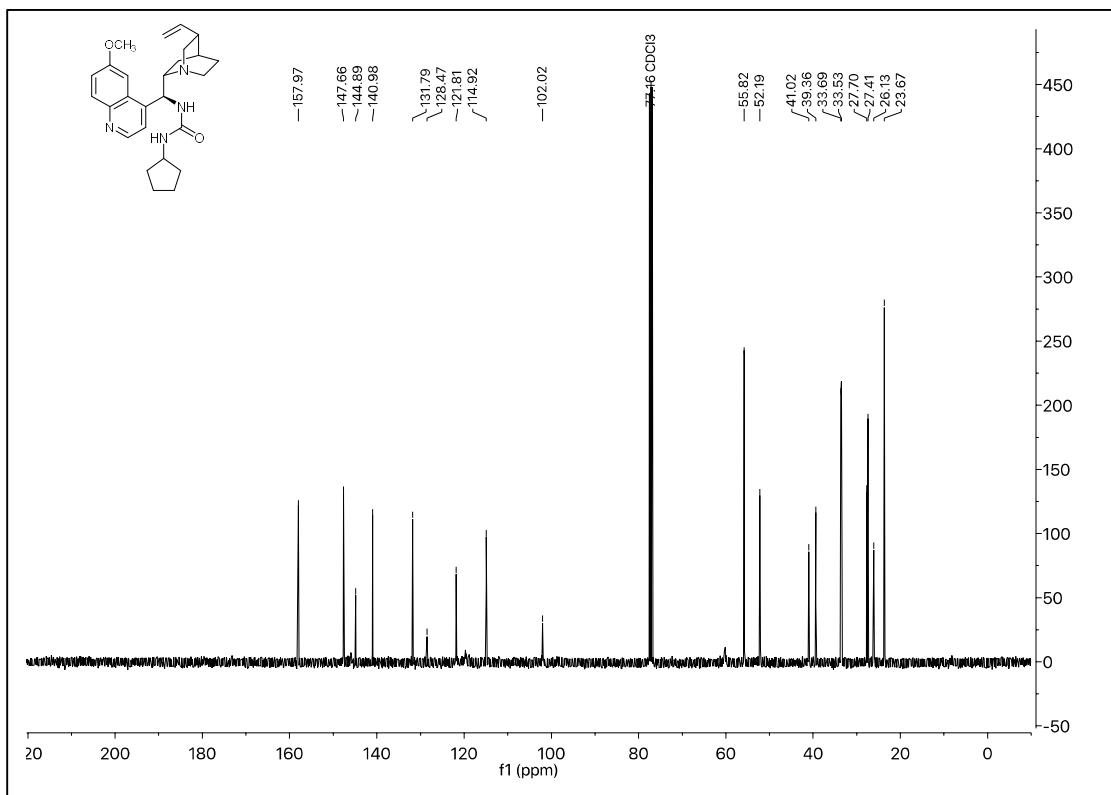
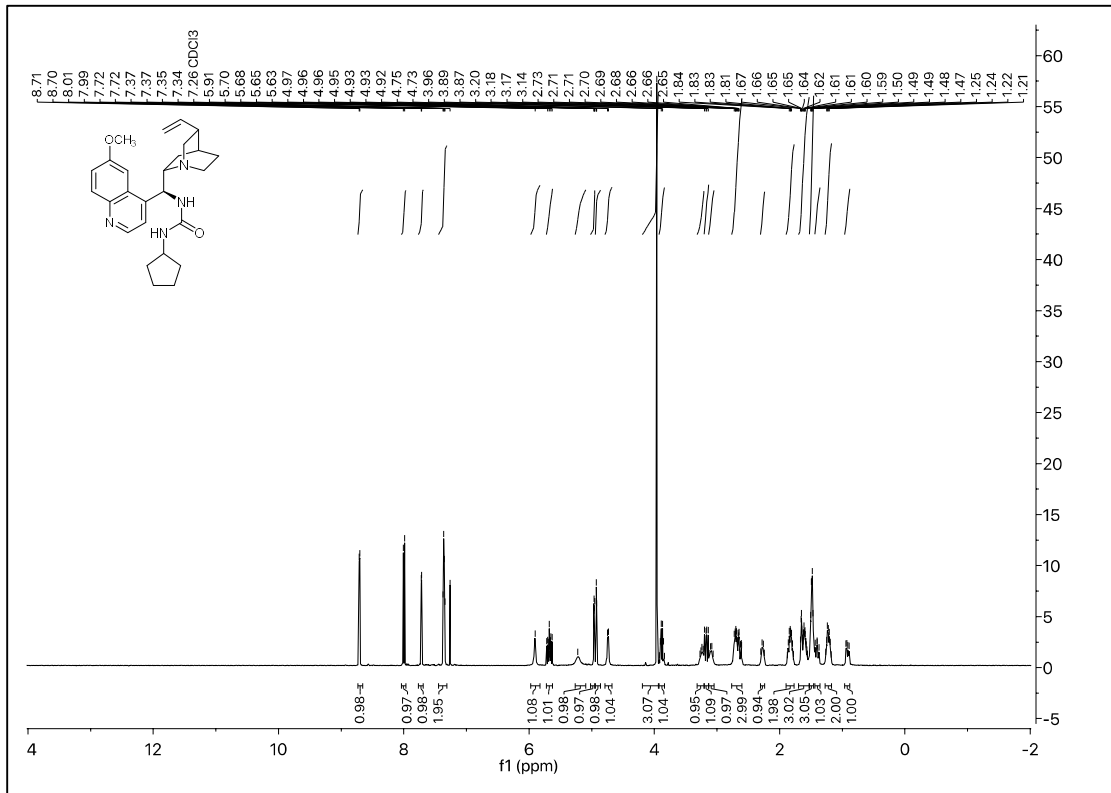
^1H and ^{13}C Spectral Data of Catalyst CA16



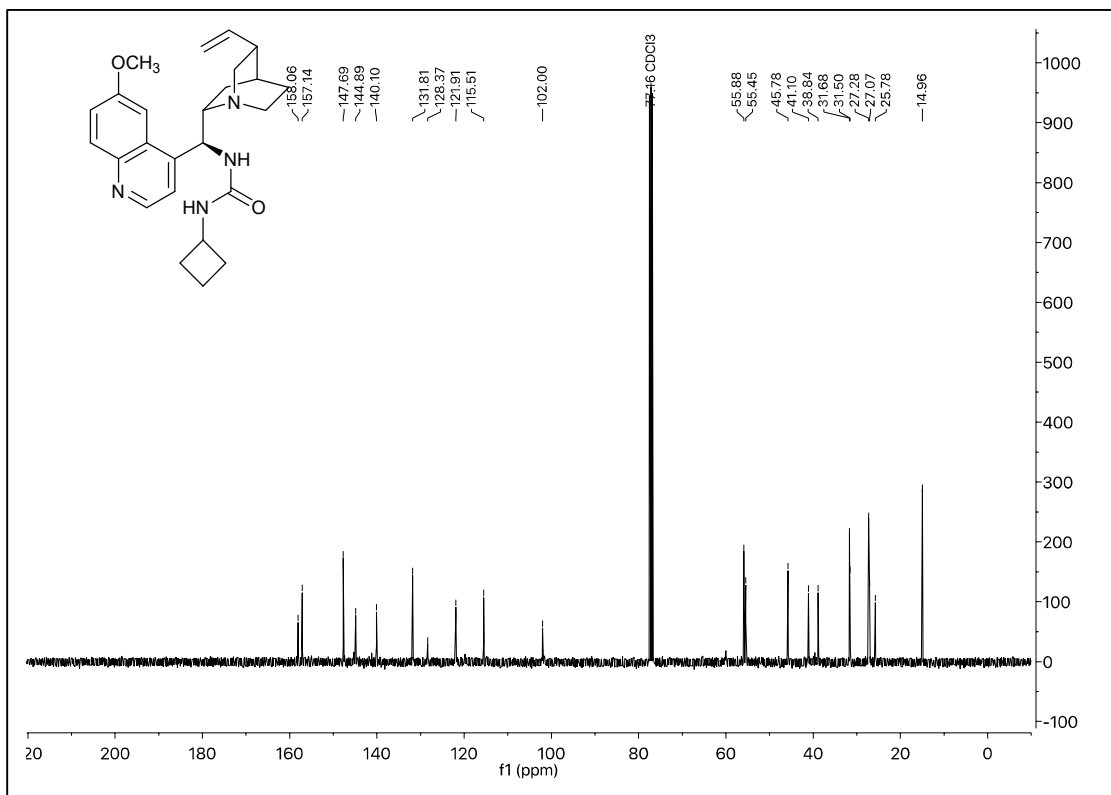
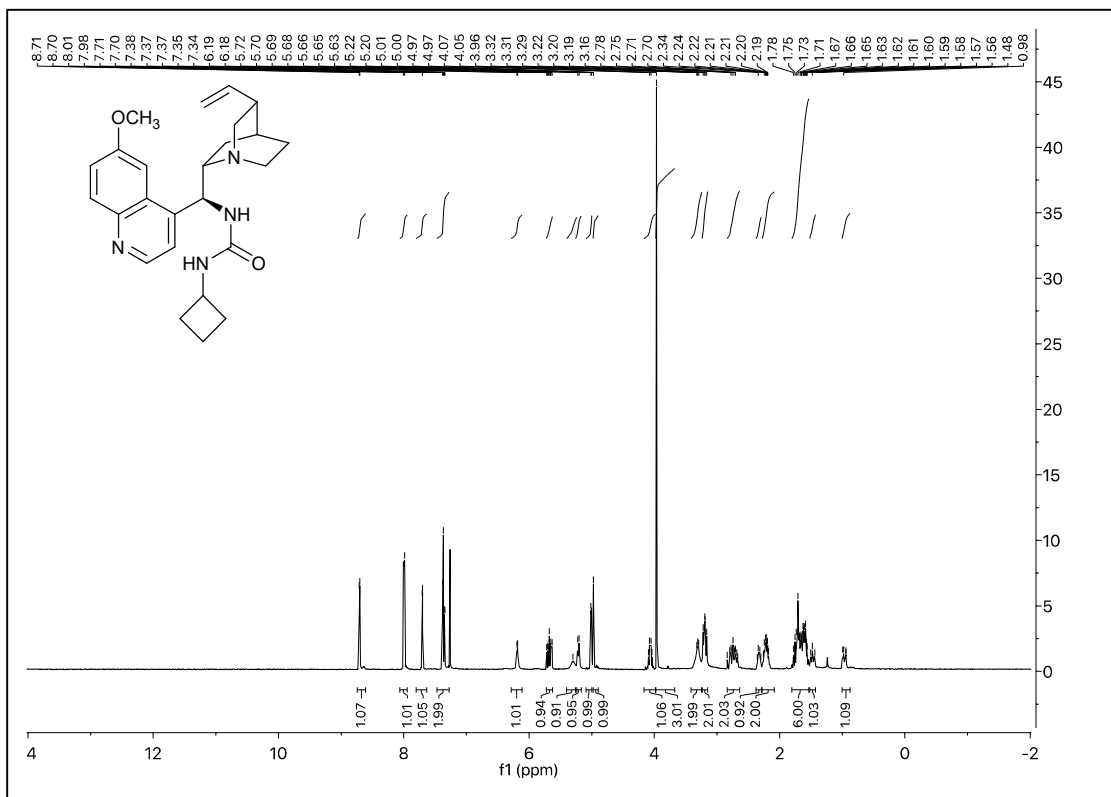
^1H and ^{13}C Spectral Data of Catalyst CA18



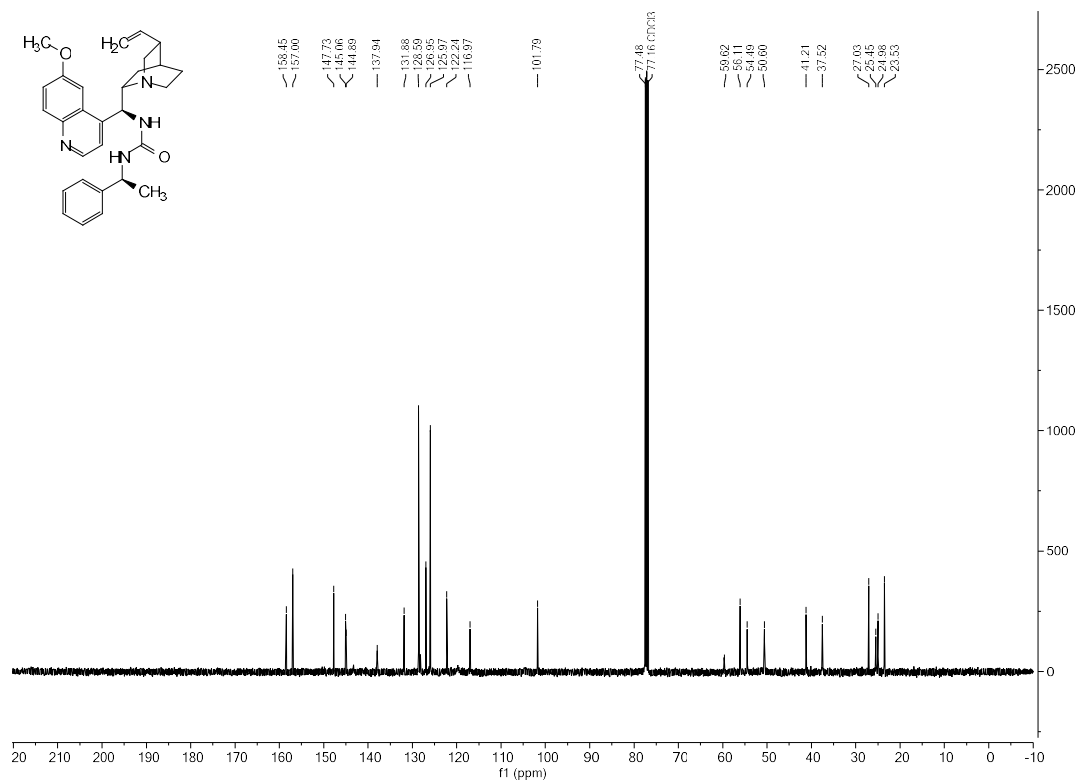
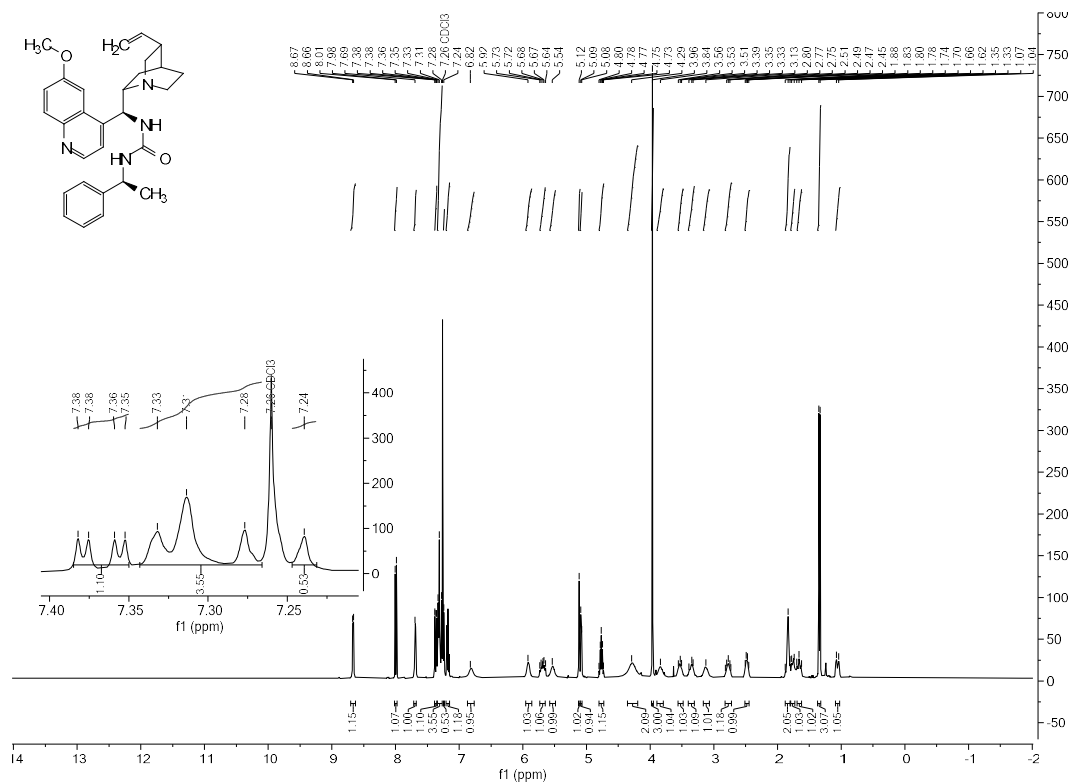
^1H and ^{13}C Spectral Data of Catalyst 79



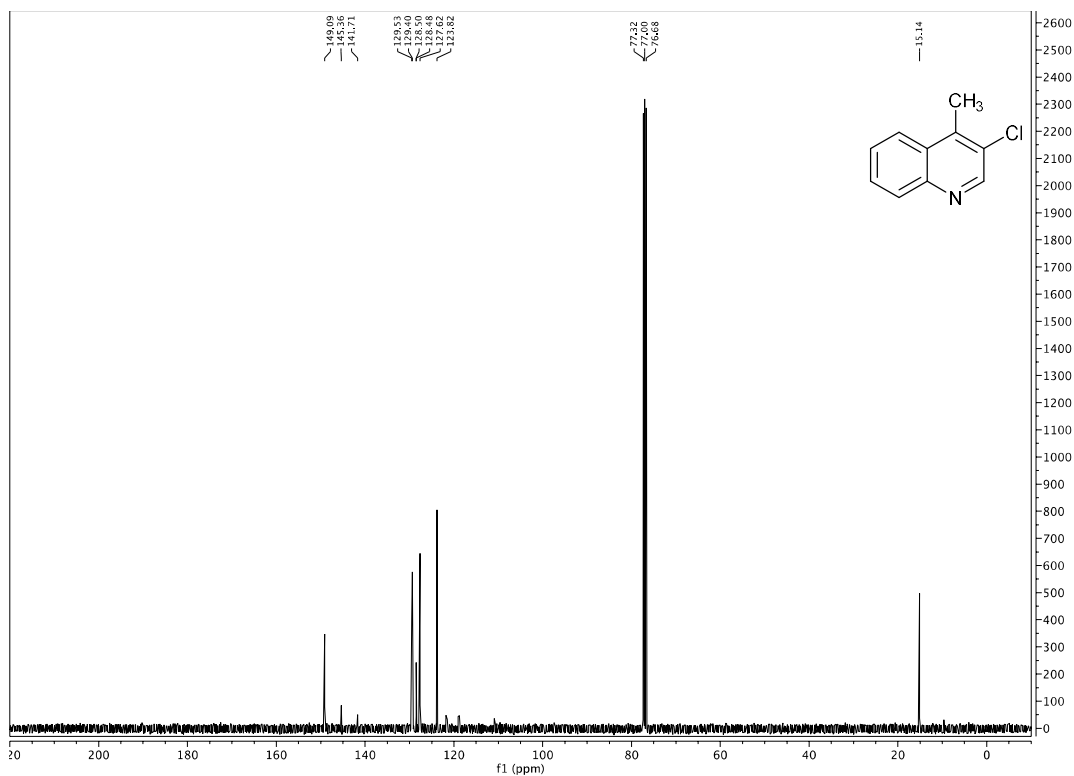
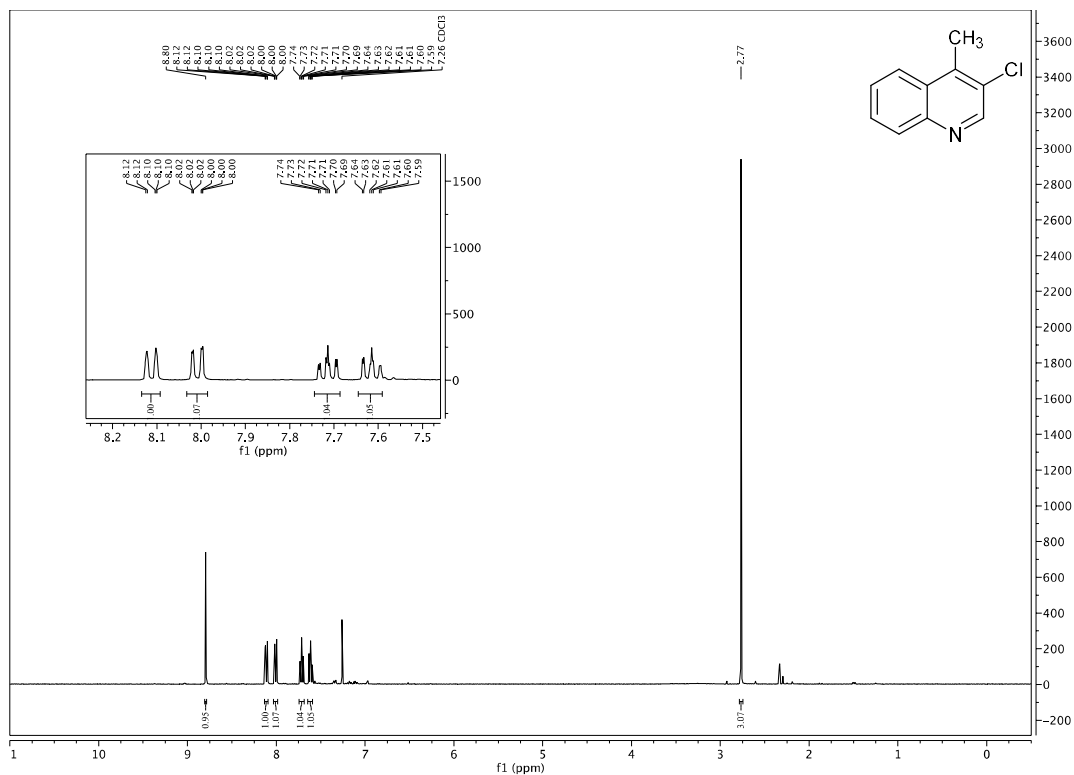
^1H and ^{13}C Spectral Data of Catalyst CA21



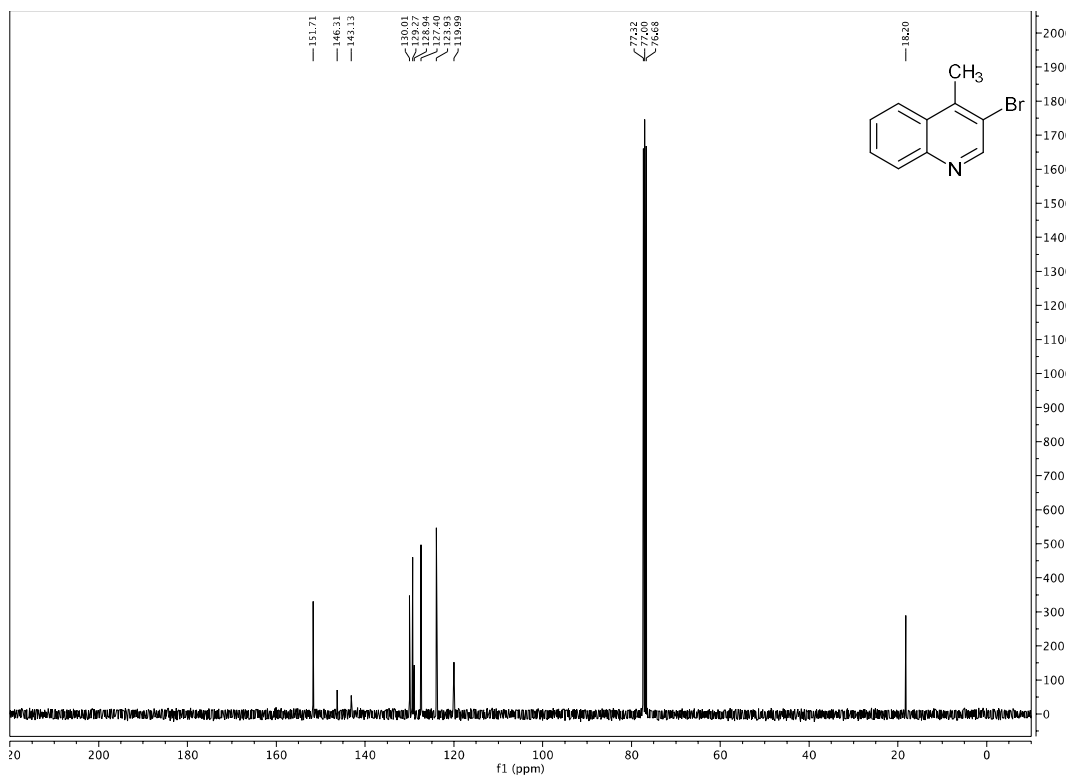
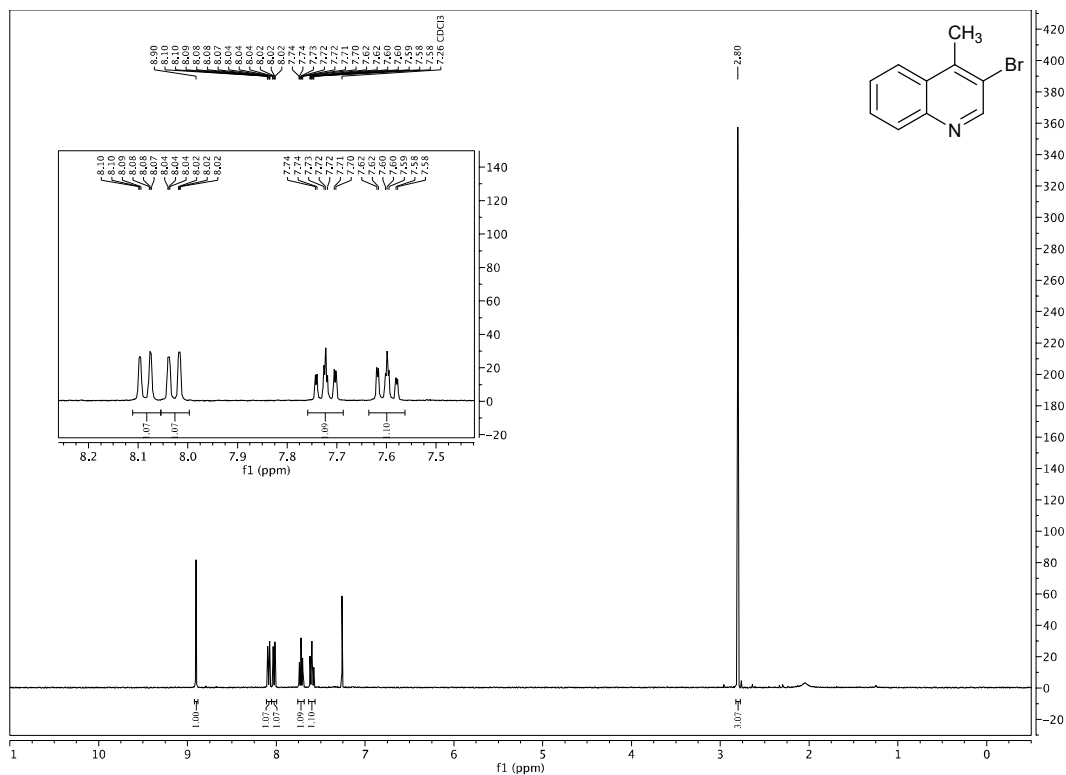
^1H and ^{13}C Spectral Data of Catalyst CA24



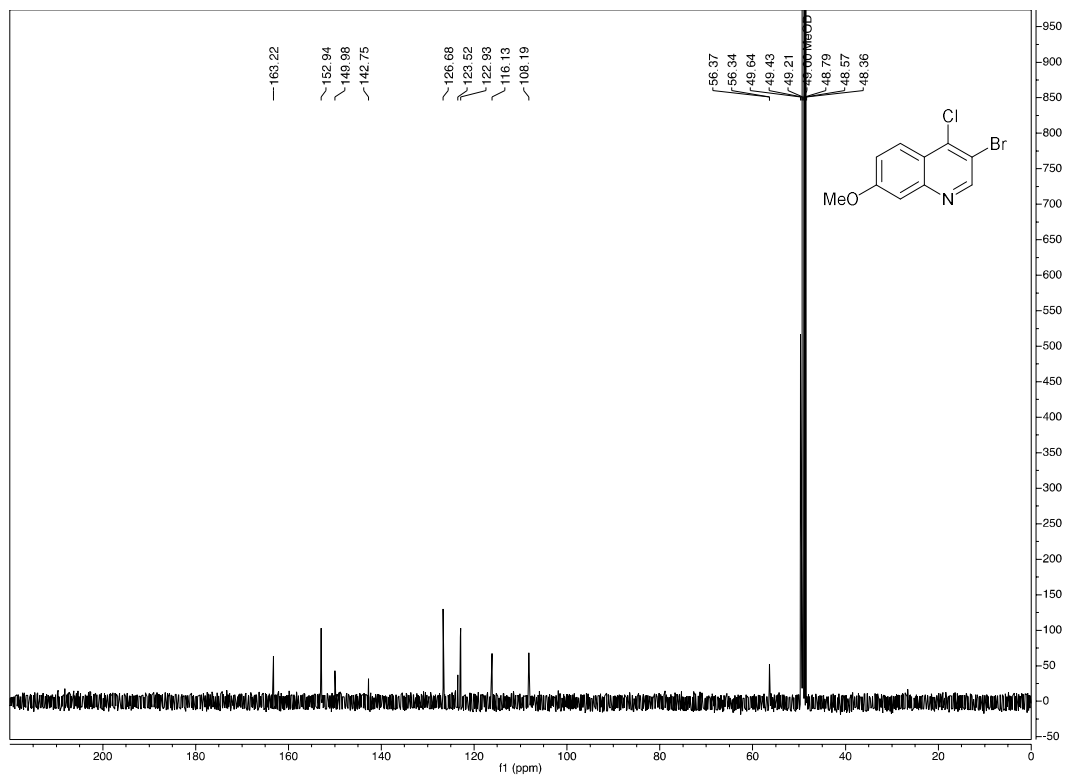
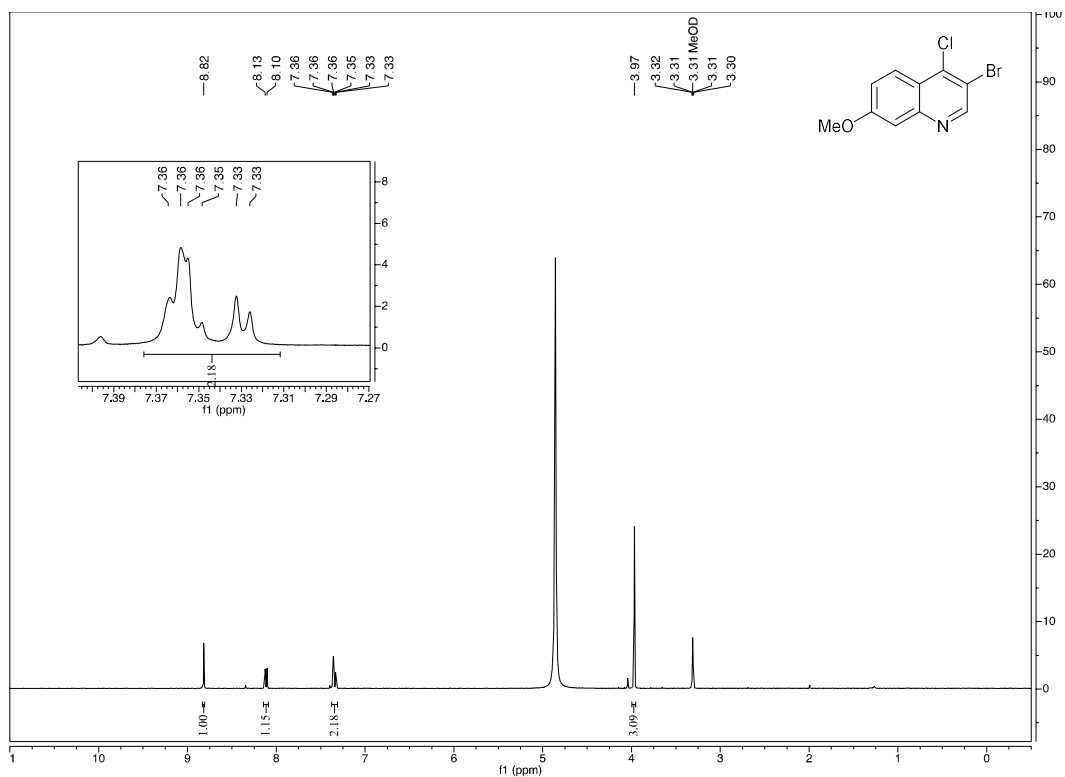
^1H and ^{13}C NMR Spectral Data of 3-chloro-4-methylquinoline



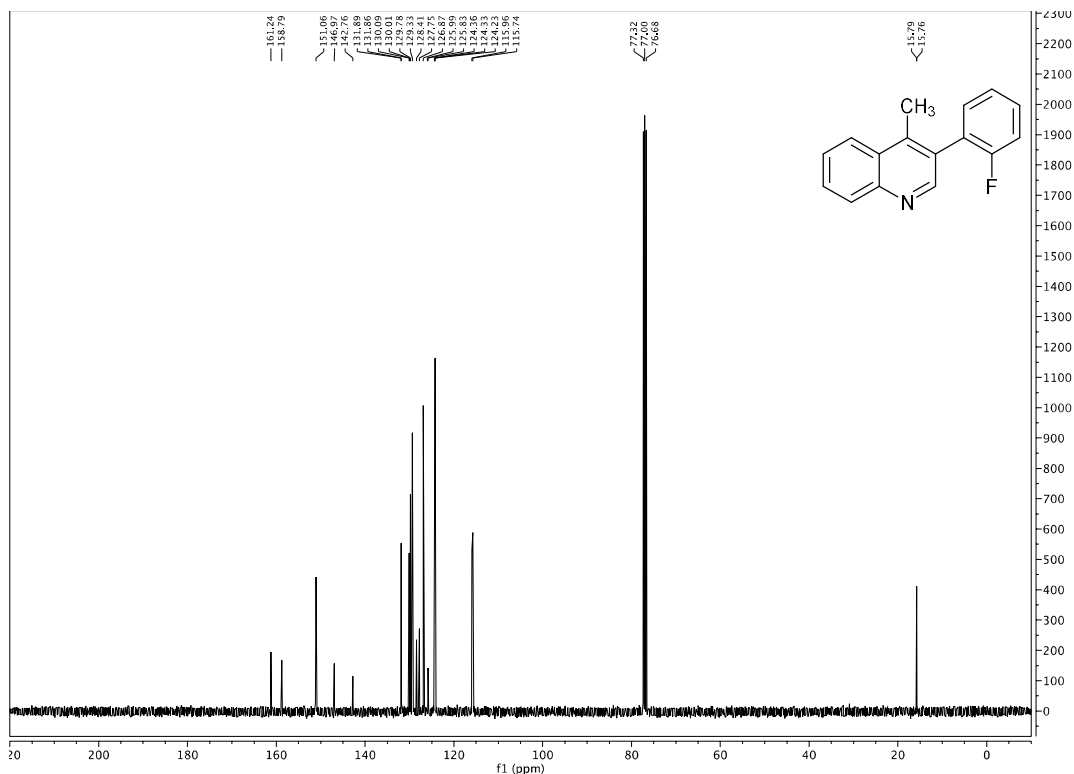
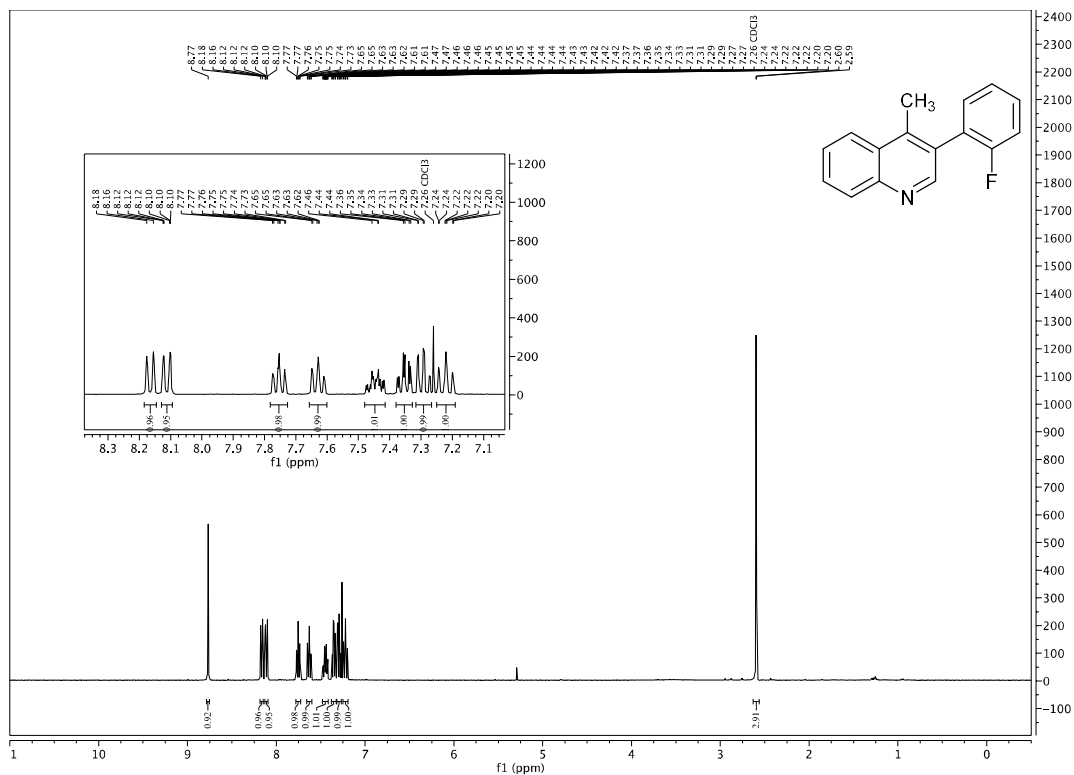
¹H and ¹³C NMR Spectral Data of 3-bromo-4-methylquinoline

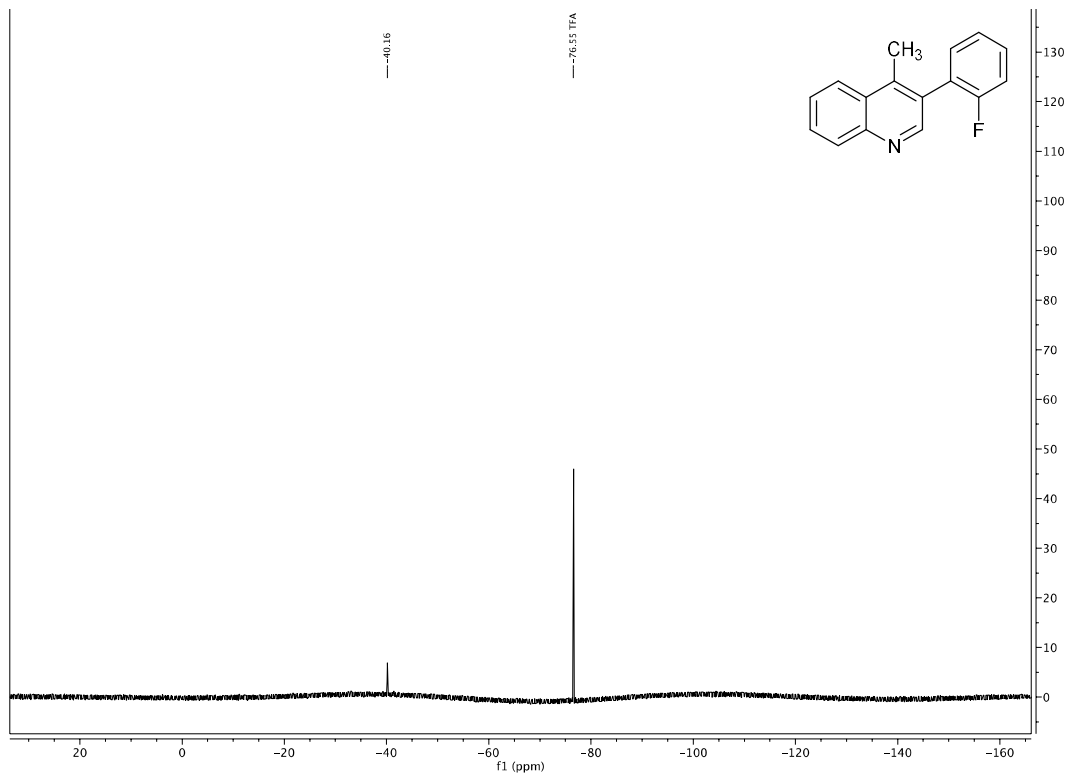


^1H and ^{13}C NMR Spectral Data of 3-bromo-4-chloro-7-methoxyquinoline

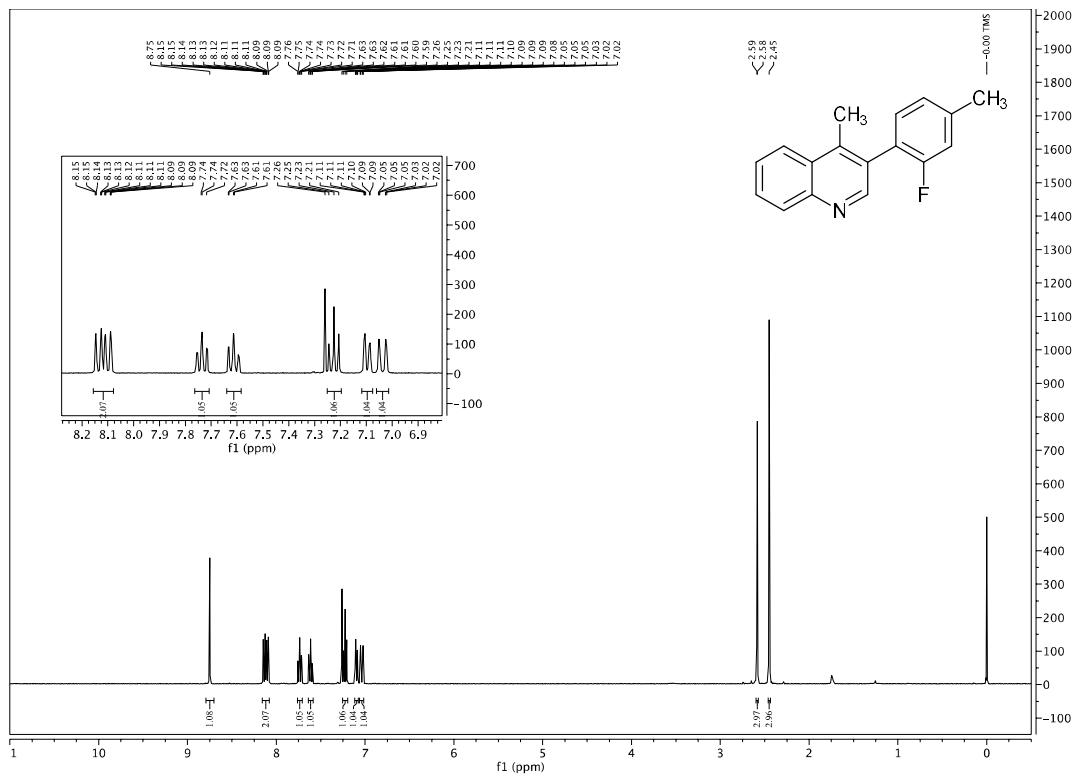


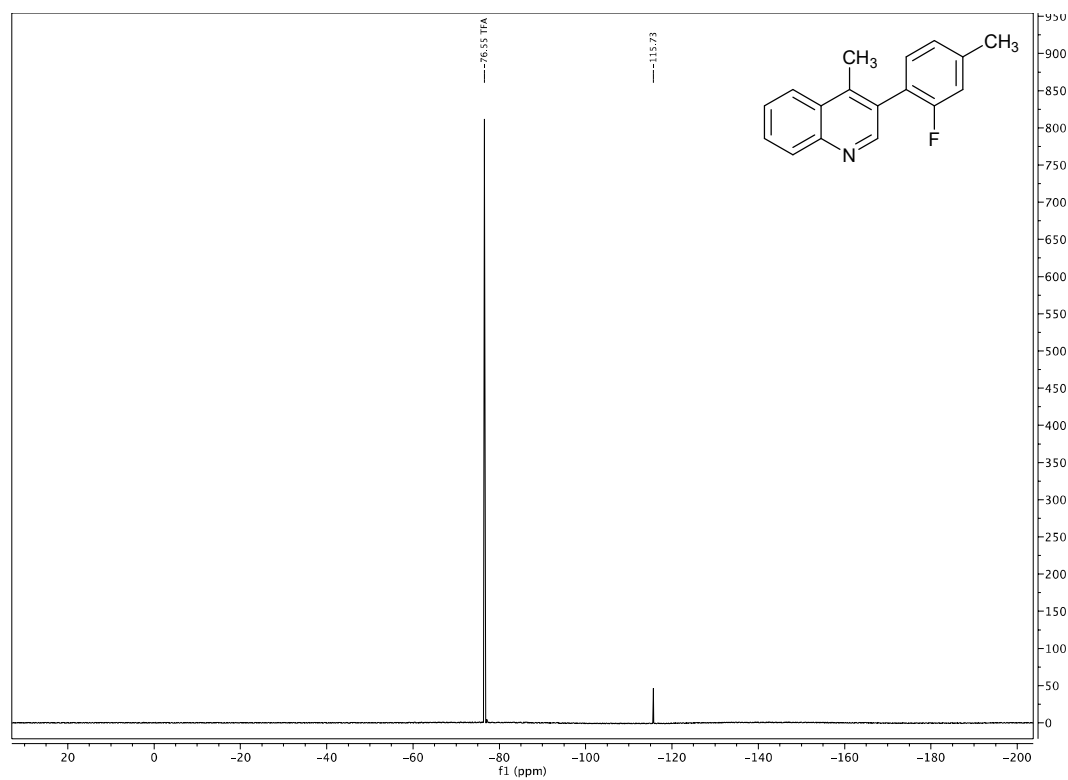
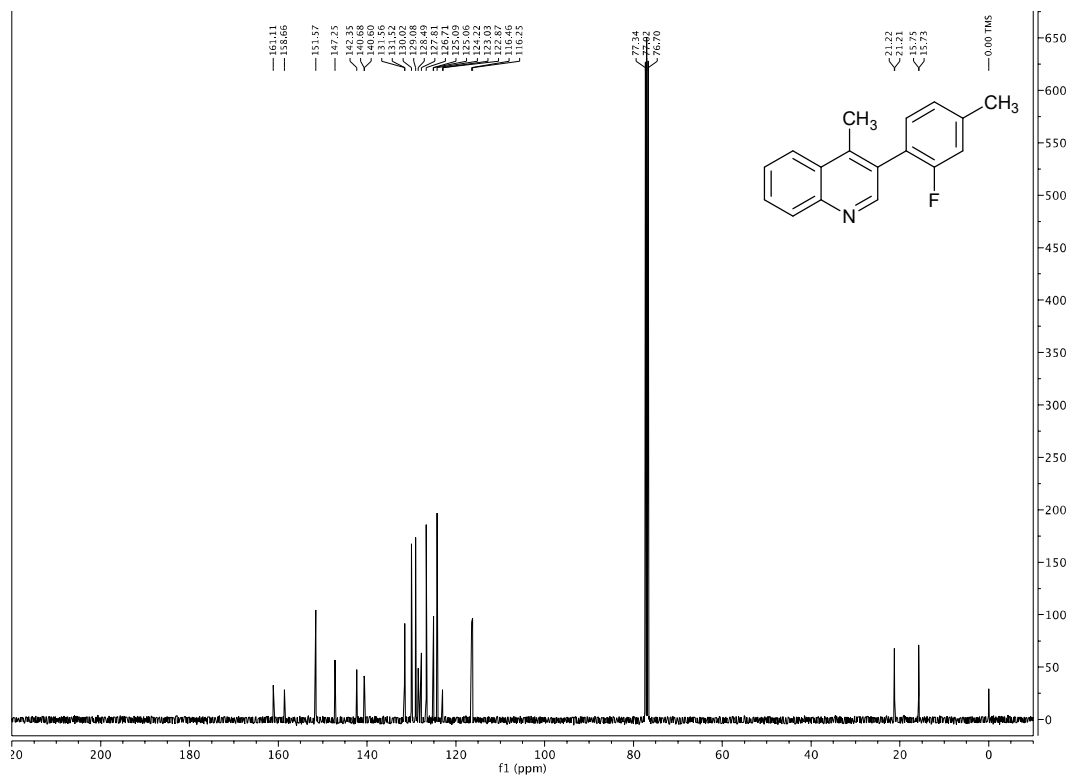
¹H, ¹³C, and ¹⁹F NMR Spectral Data of 3-(2-fluorophenyl)-4-methylquinoline



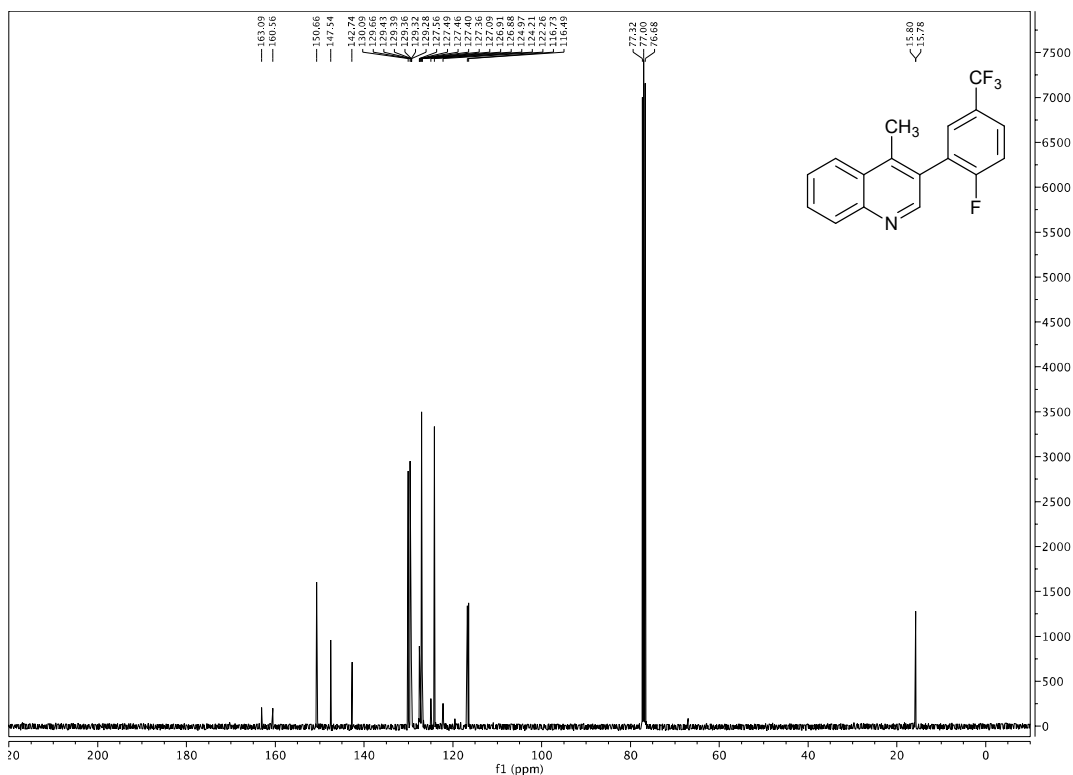
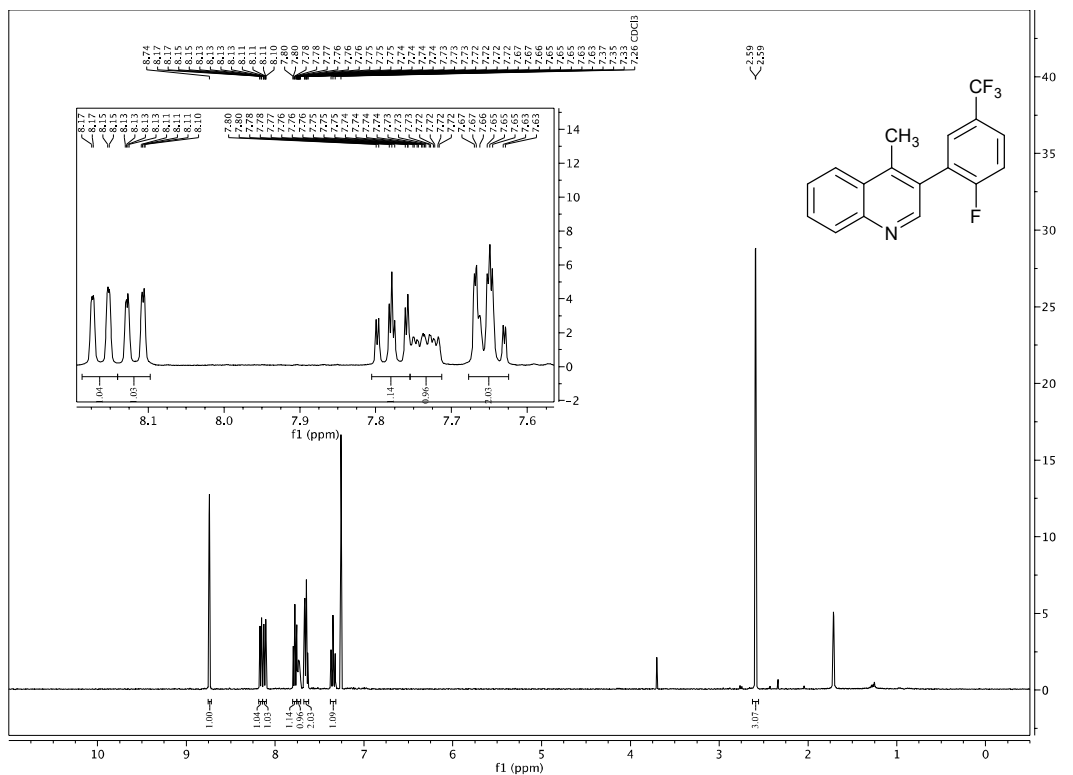


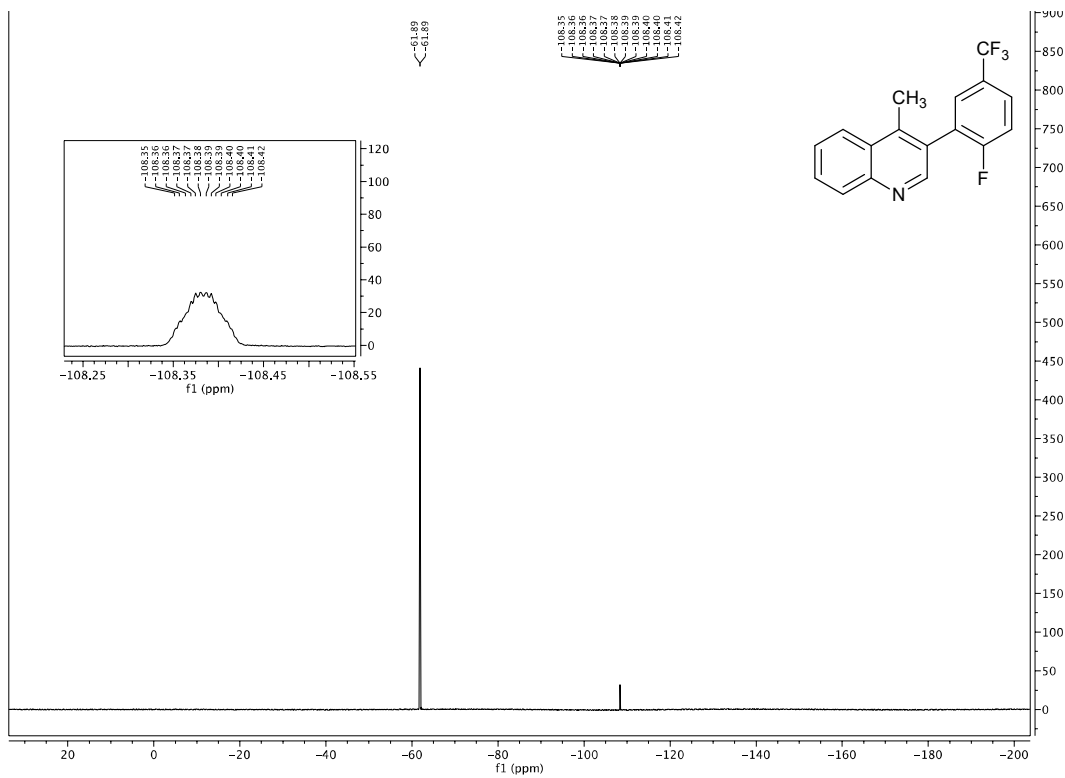
¹H, ¹³C, and ¹⁹F NMR Spectral Data of 3-(2-fluoro-4-methylphenyl)-4-methylquinoline



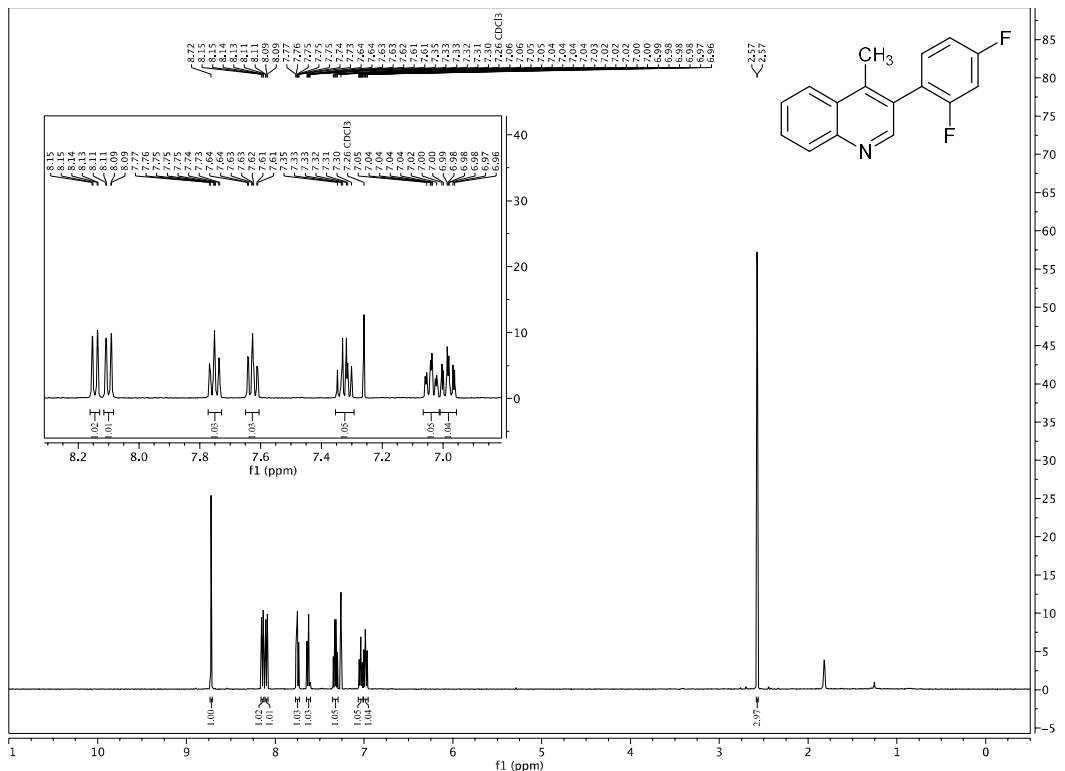


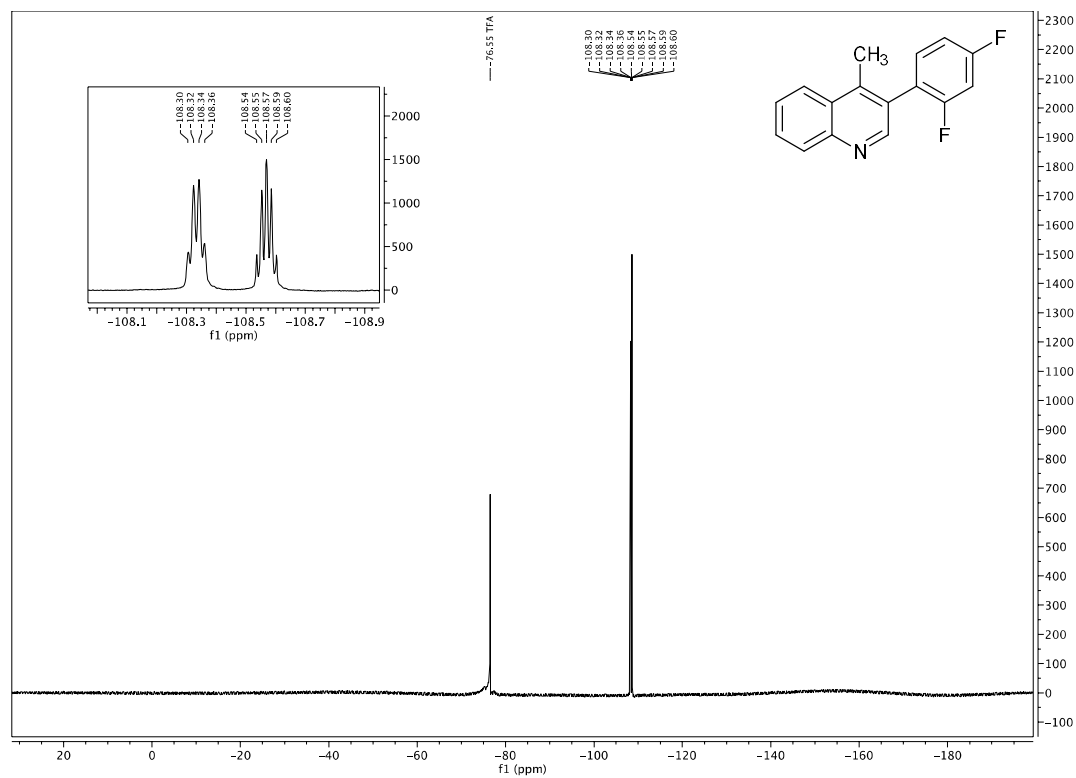
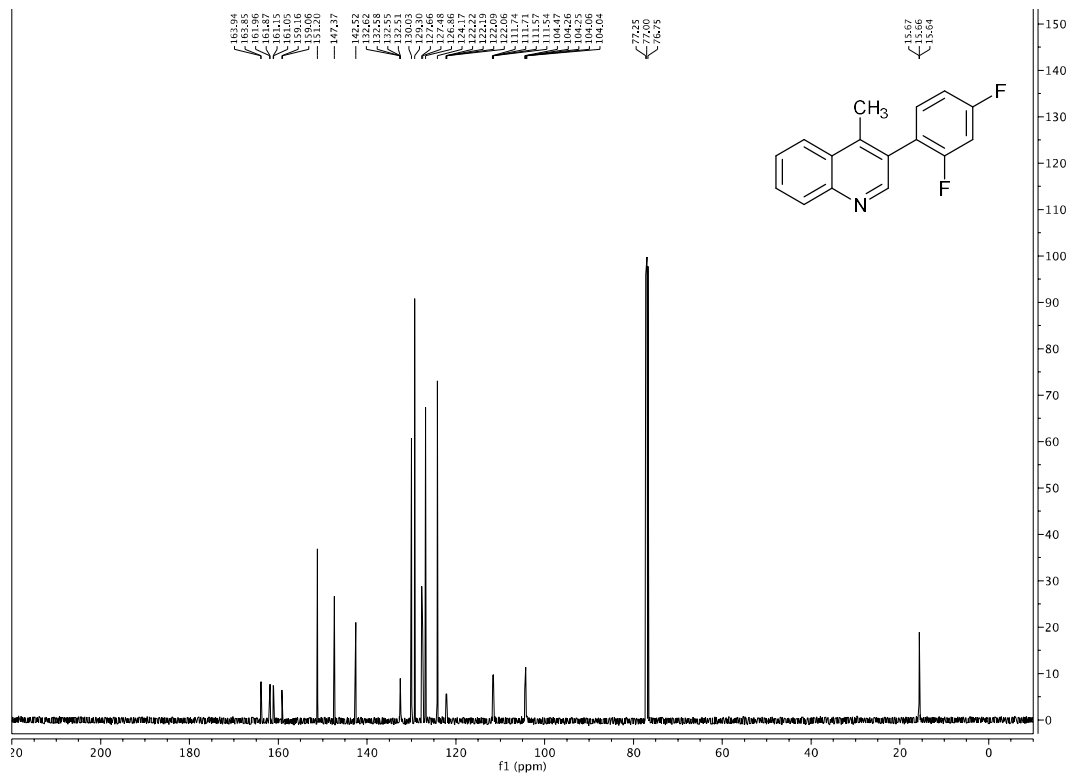
^1H , ^{13}C , and ^{19}F NMR Spectral Data of 3-(2-fluoro-5-(trifluoromethyl)phenyl)-4-methylquinoline



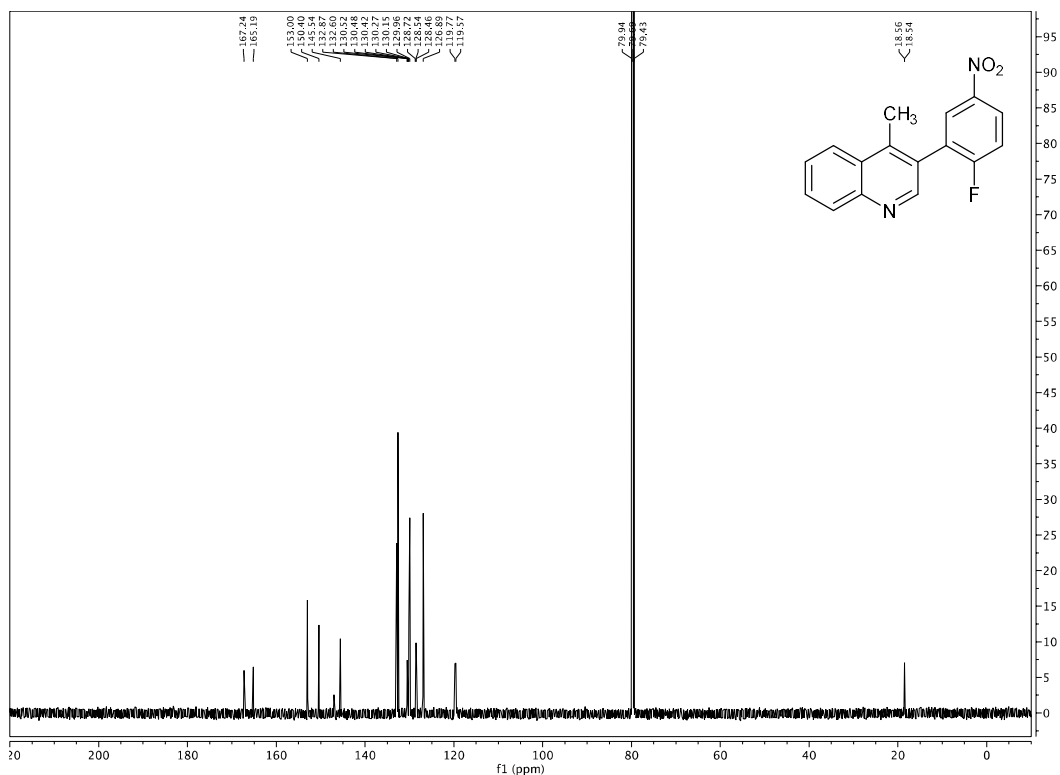
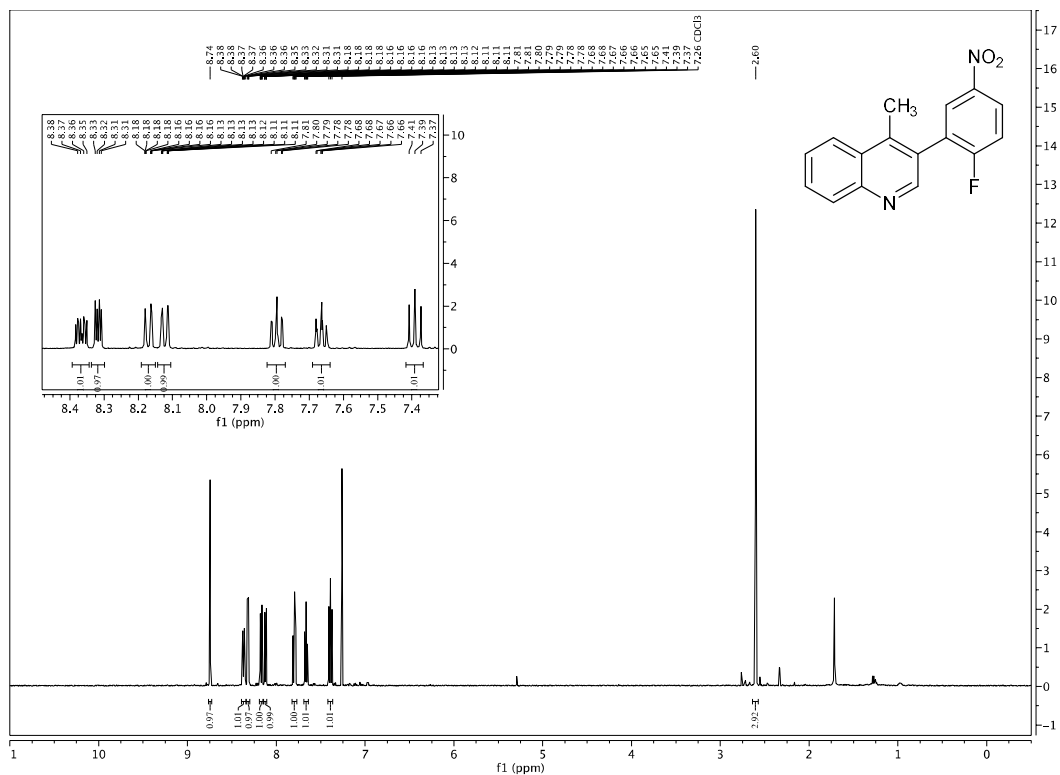


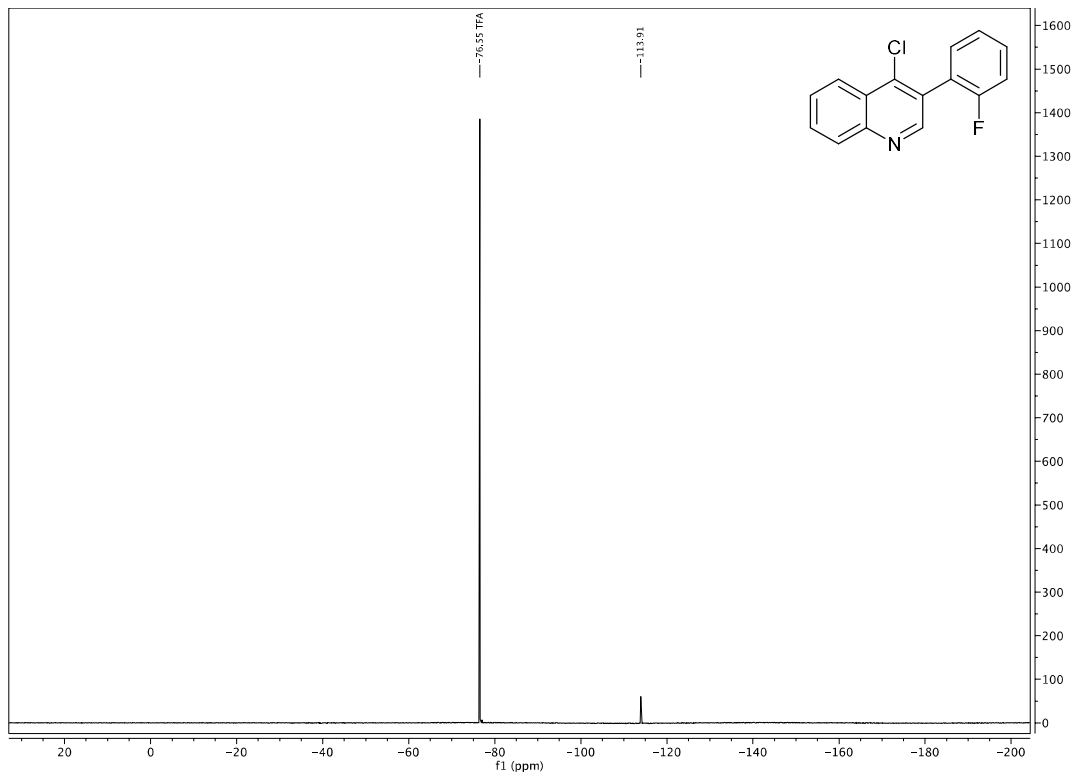
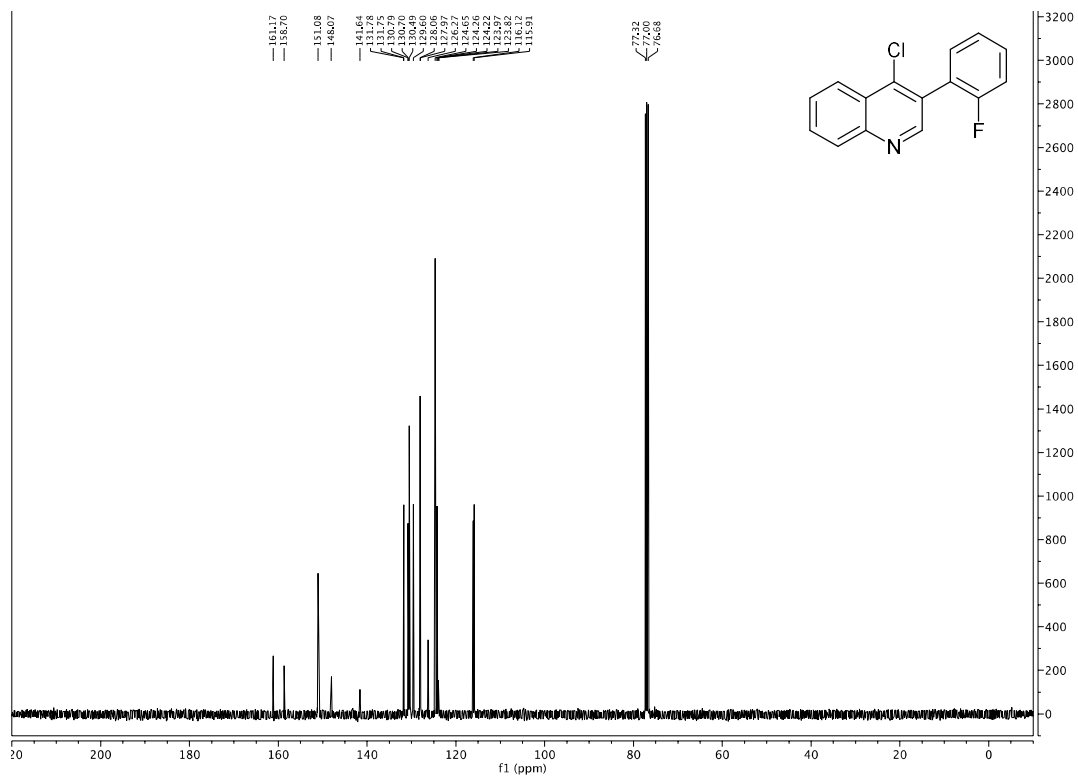
^1H , ^{13}C , and ^{19}F NMR Spectral Data of 3-(2,4-difluorophenyl)-4-methylquinoline



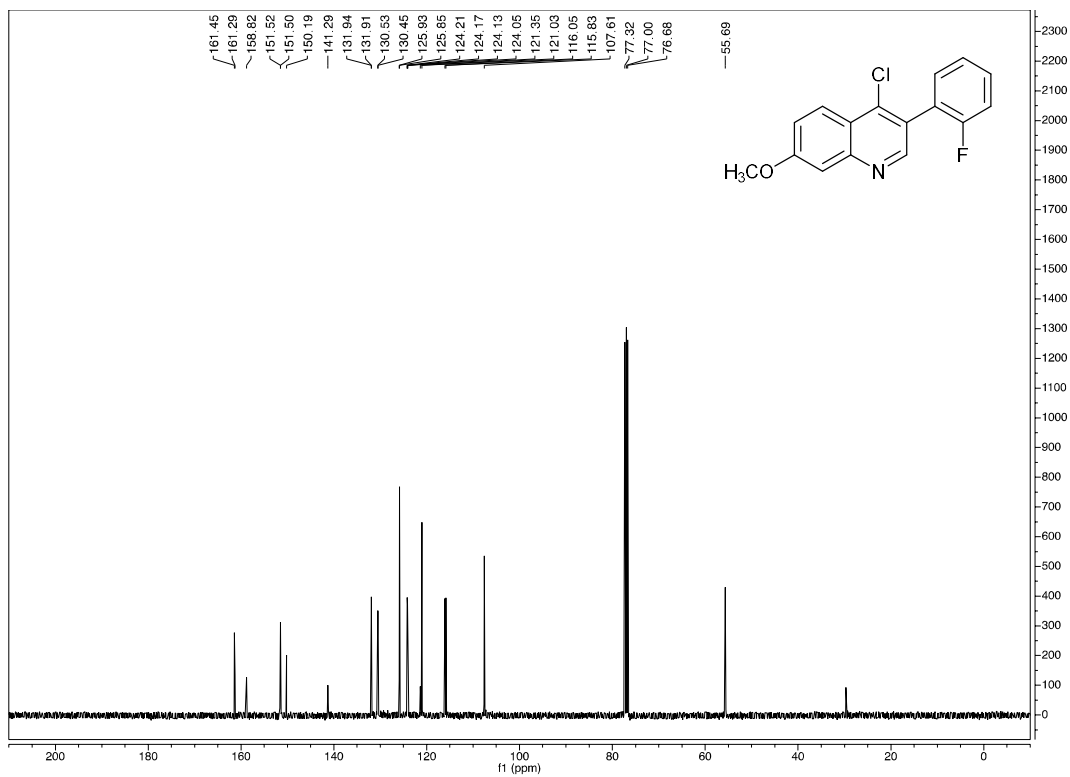
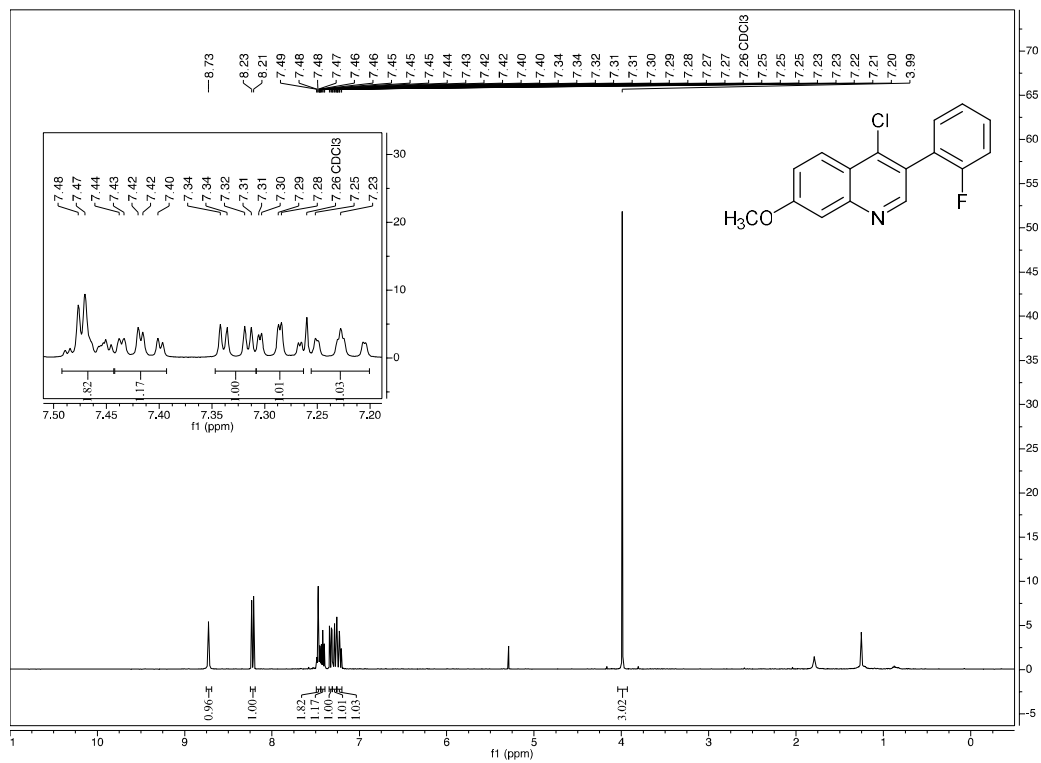


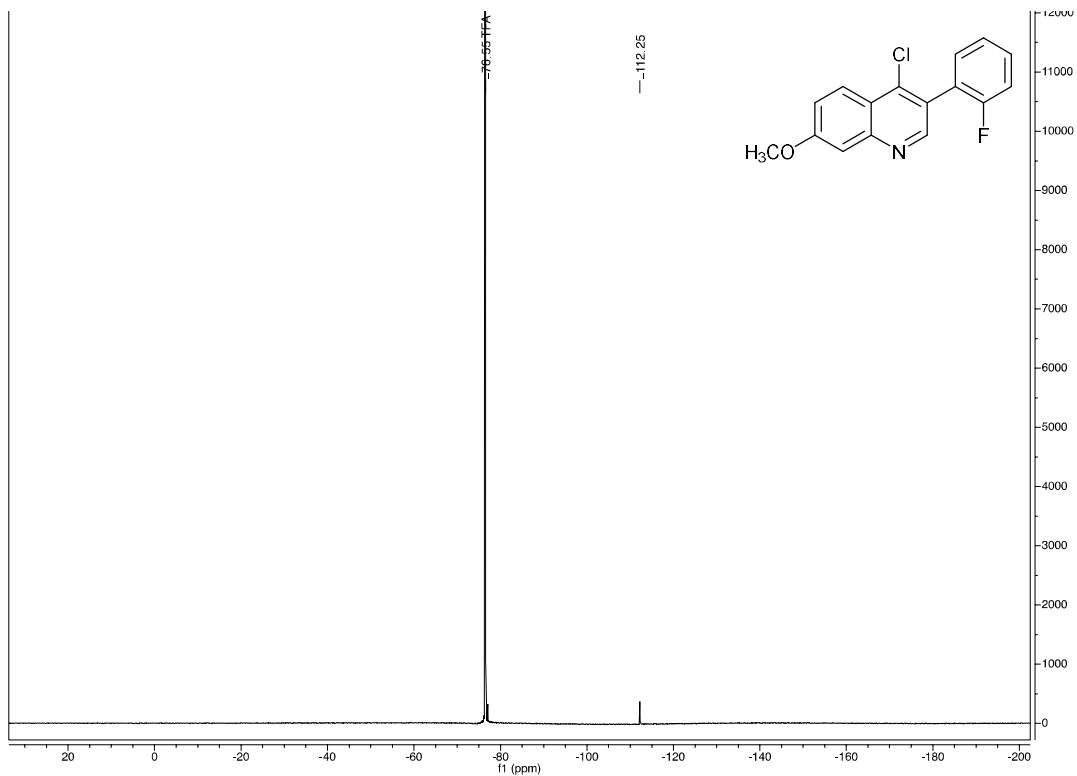
^1H , ^{13}C , and ^{19}F NMR Spectral Data of 3-(2-fluoro-5-nitrophenyl)-4-methylquinoline



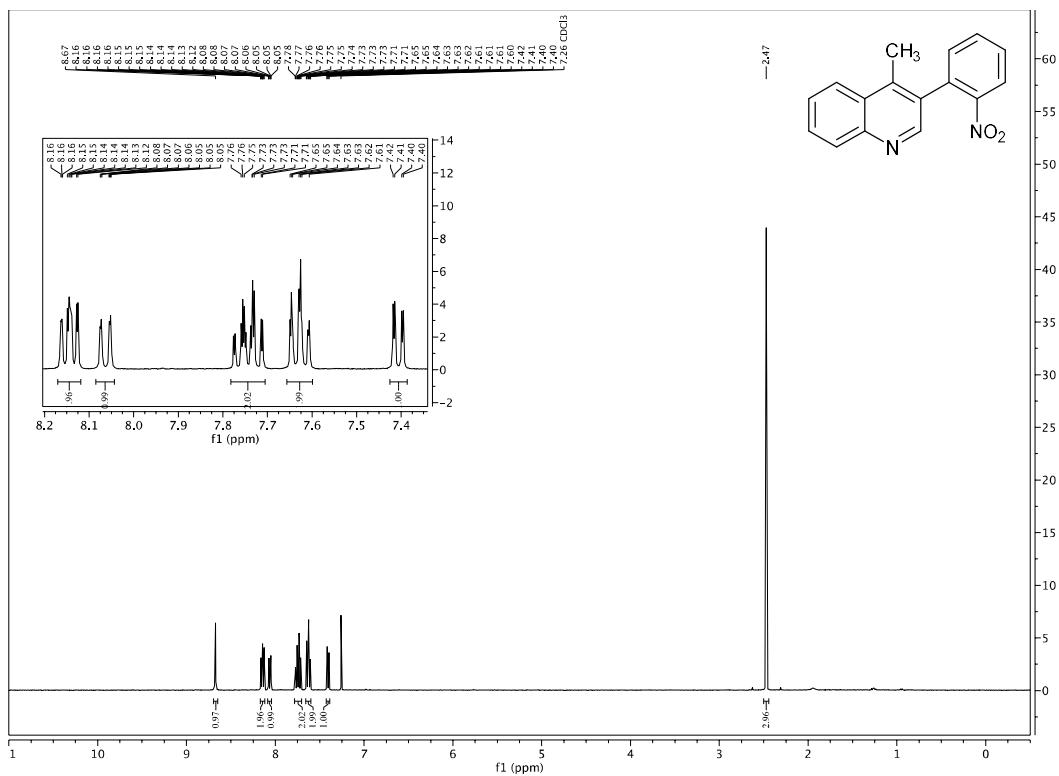


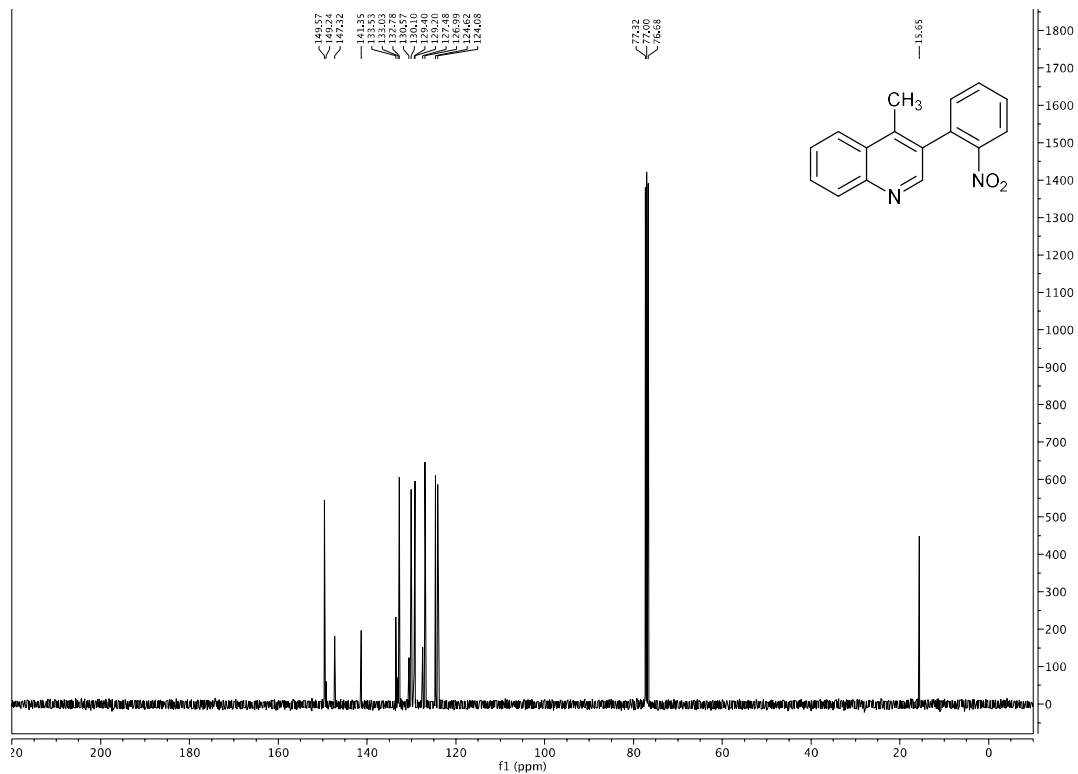
^1H , ^{13}C , and ^{19}F NMR Spectral Data of 4-chloro-3-(2-fluorophenyl)quinoline



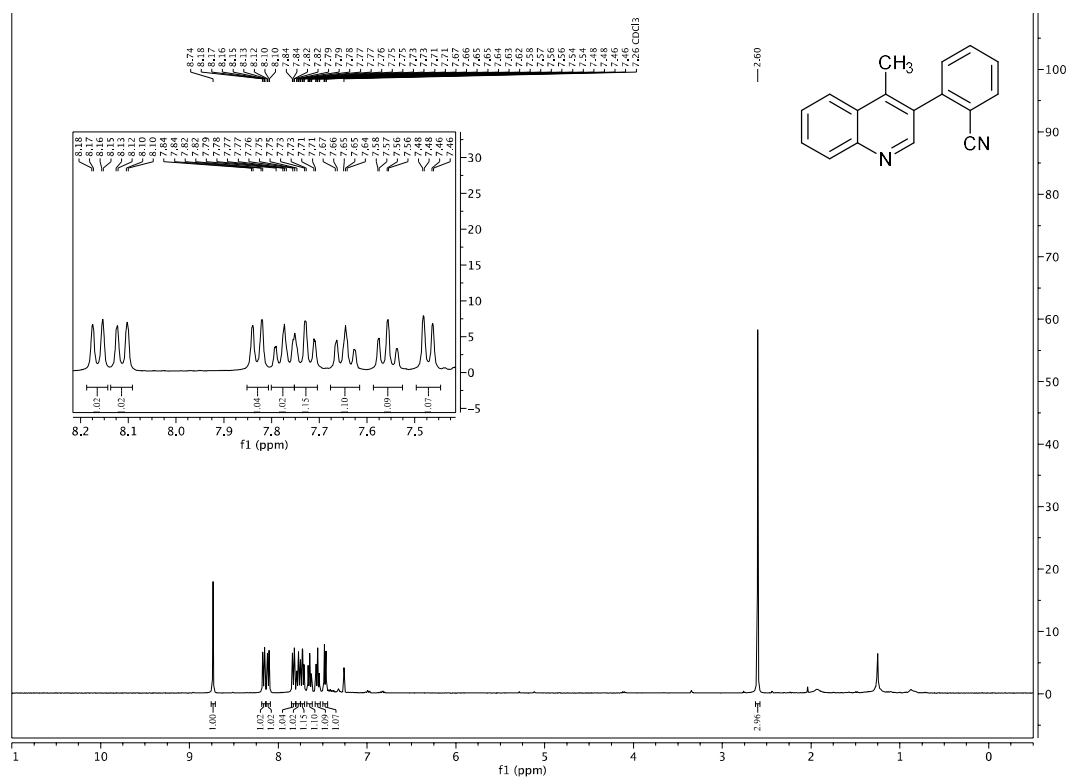


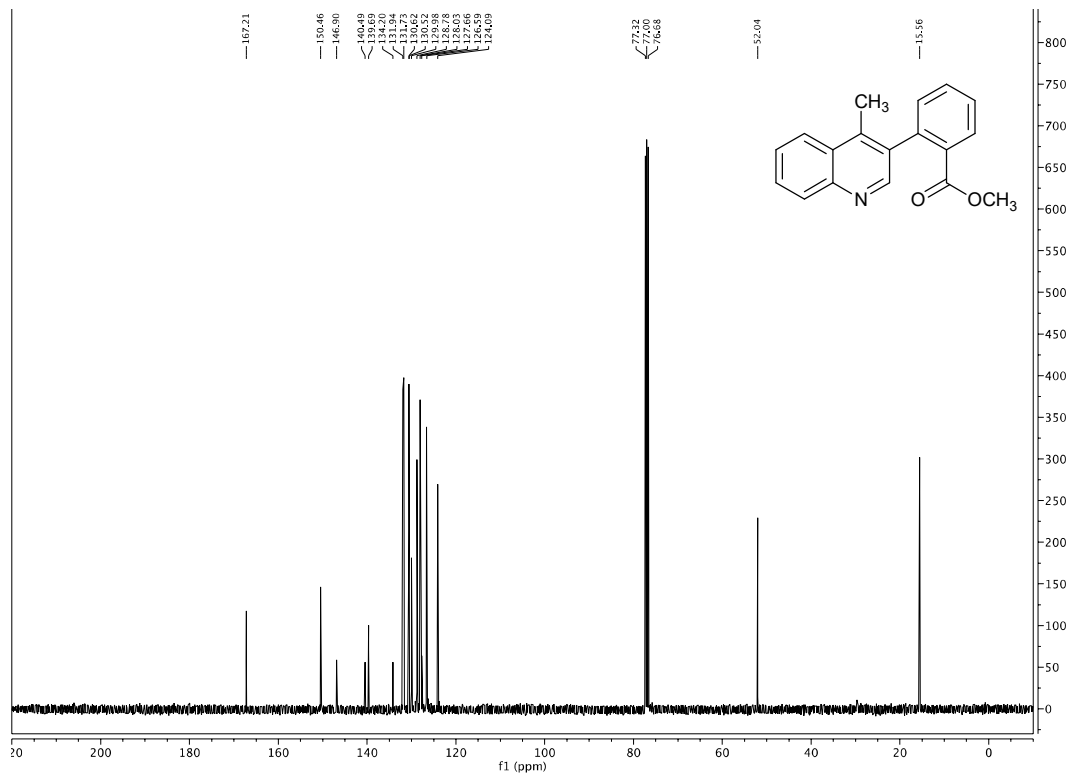
¹H and ¹³C NMR Spectral Data of 4-methyl-3-(2-nitrophenyl)quinoline



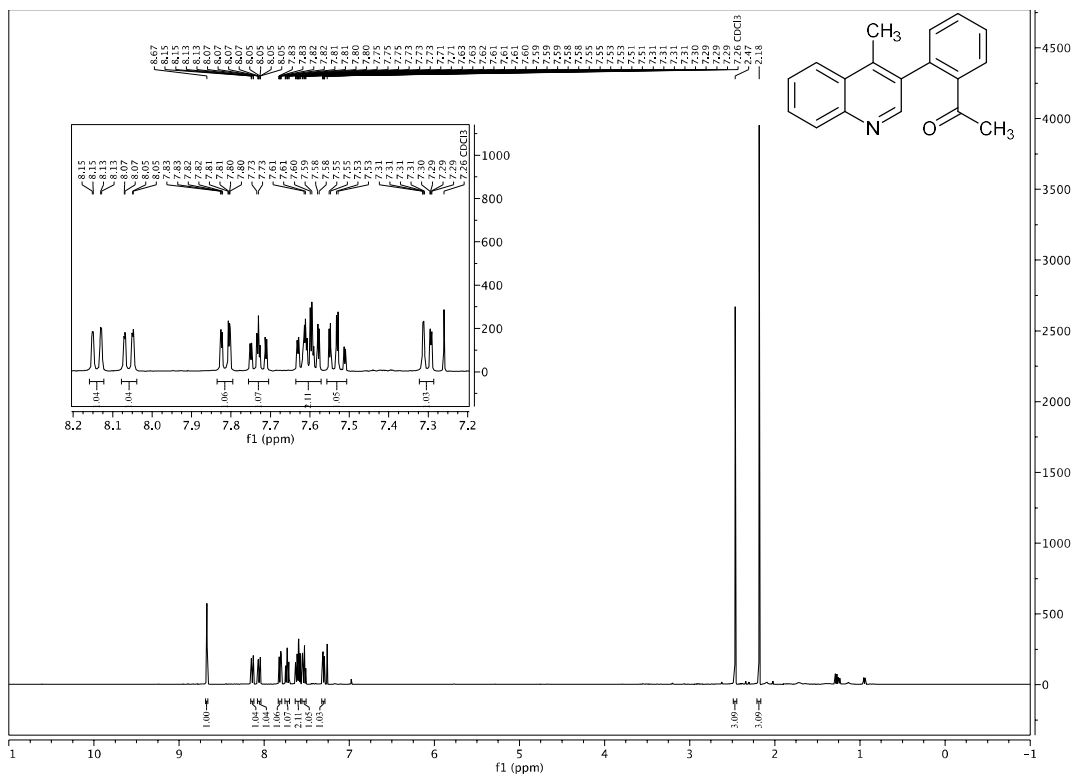


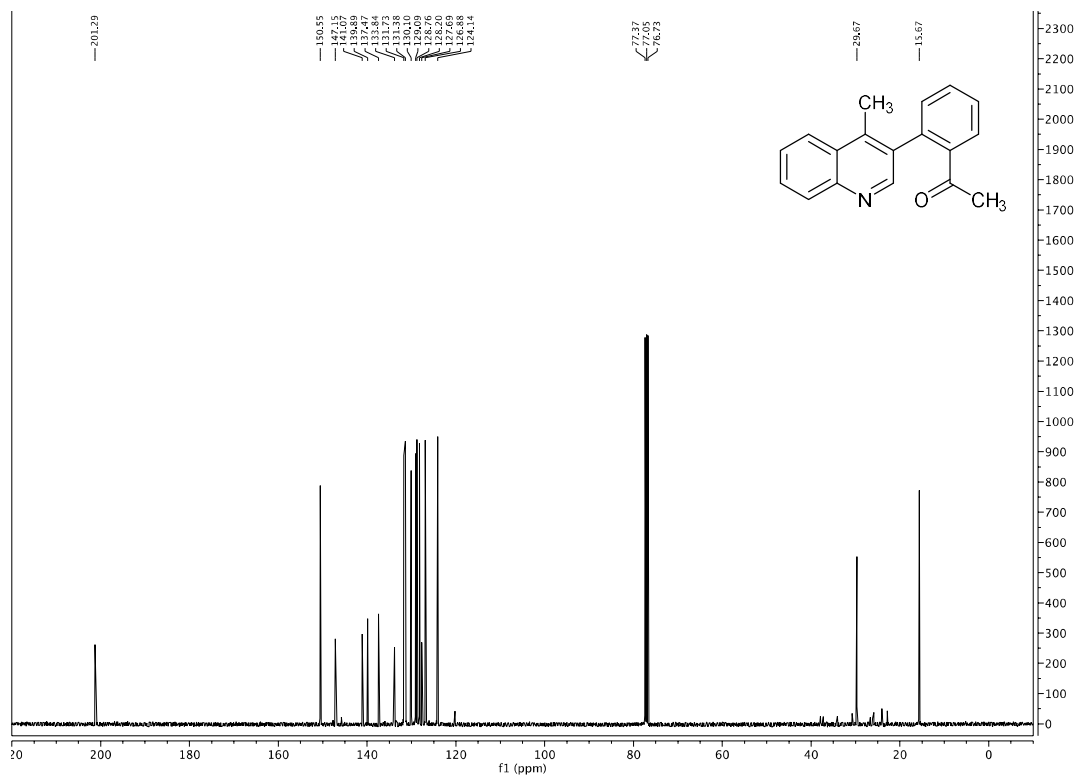
¹H and ¹³C NMR Spectral Data of 2-(4-methylquinolin-3-yl)benzonitrile



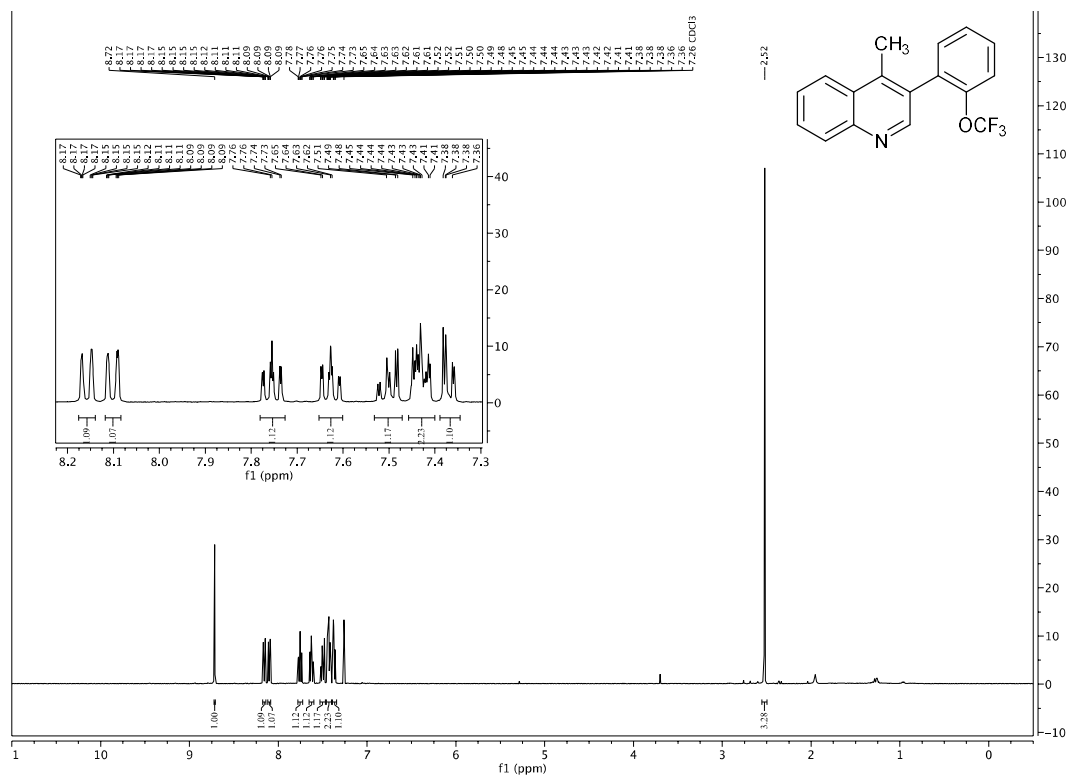


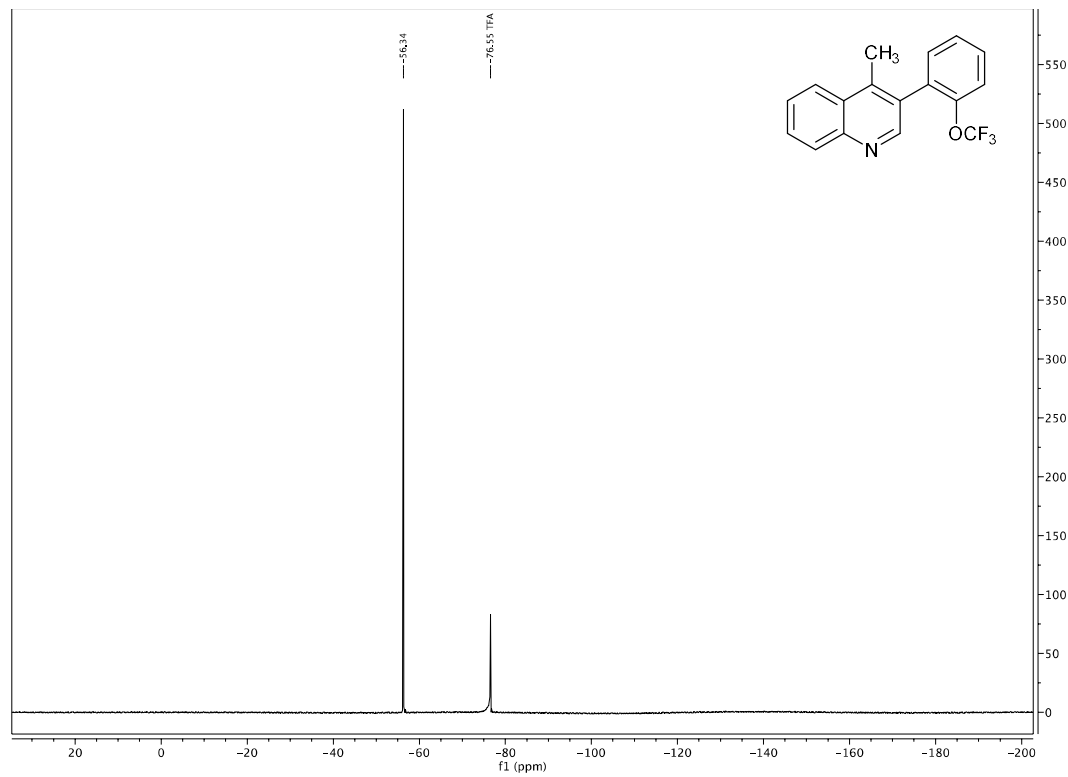
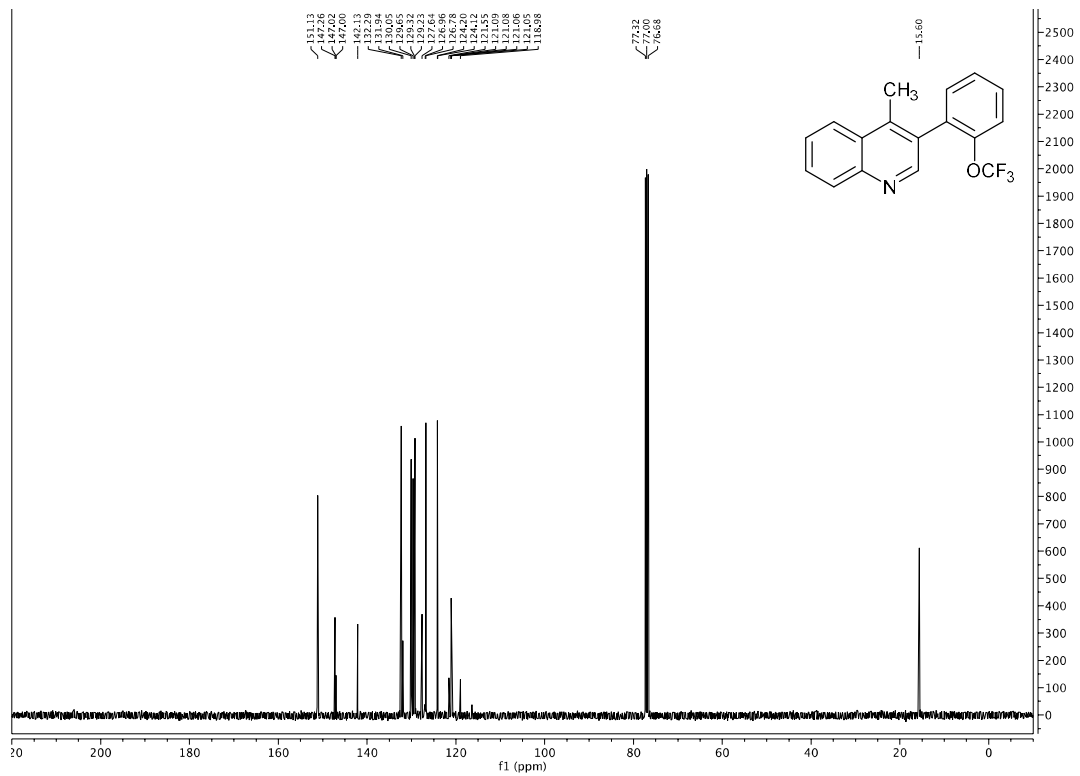
¹H and ¹³C NMR Spectral Data of 1-(2-(4-methylquinolin-3-yl)phenyl)ethanone



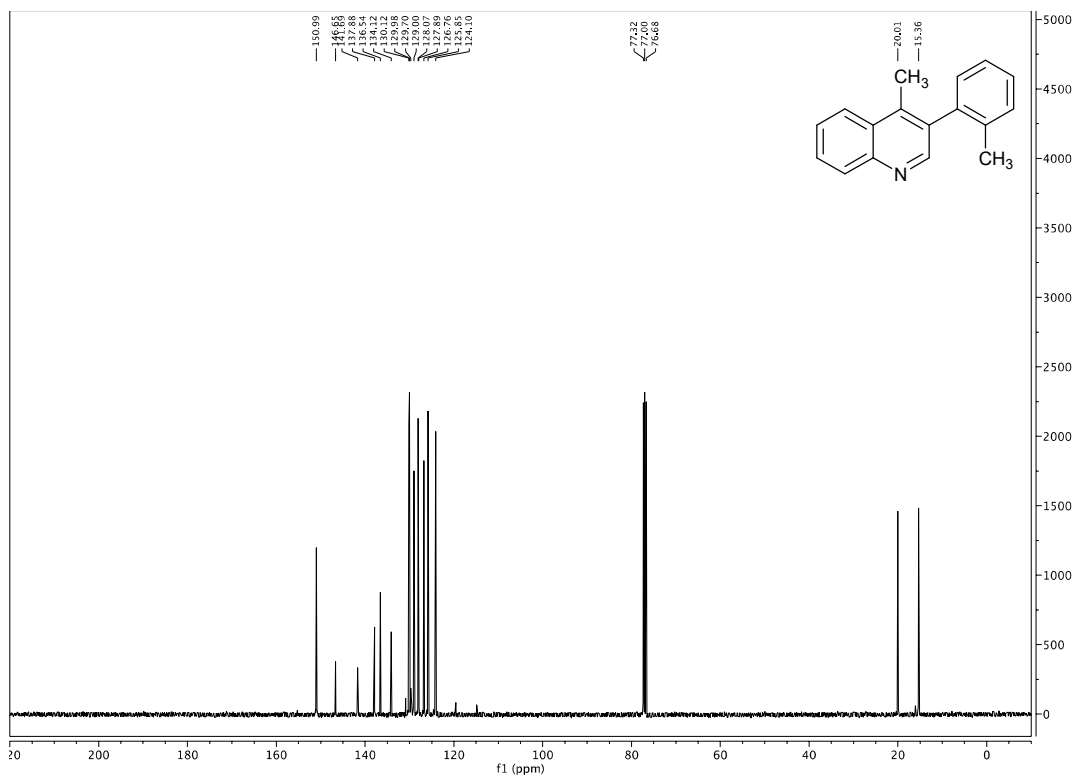
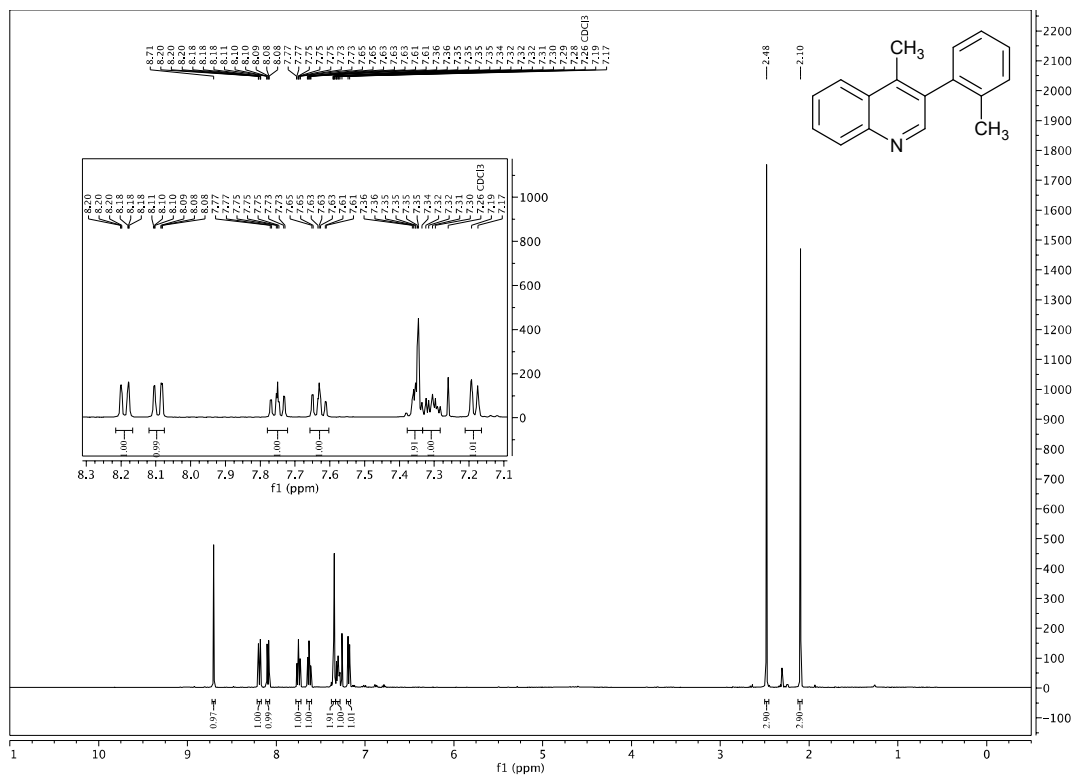


¹H and ¹³C NMR Spectral Data of 4-methyl-3-(2-(trifluoromethoxy)phenyl)quinoline

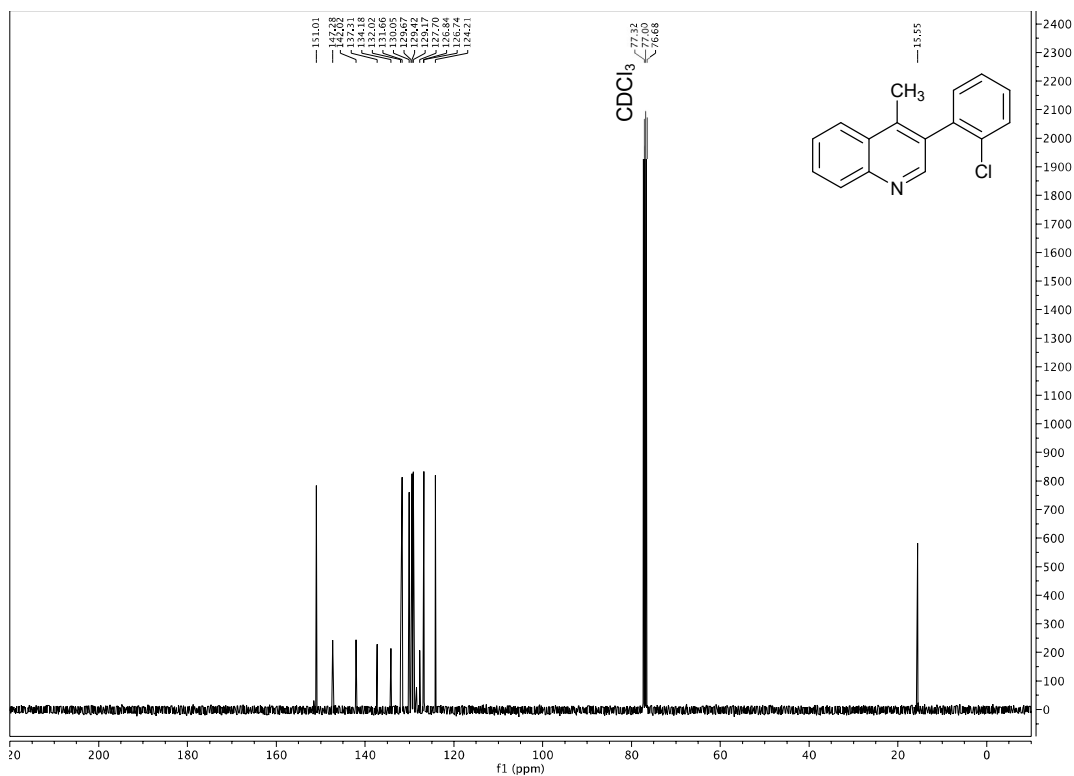
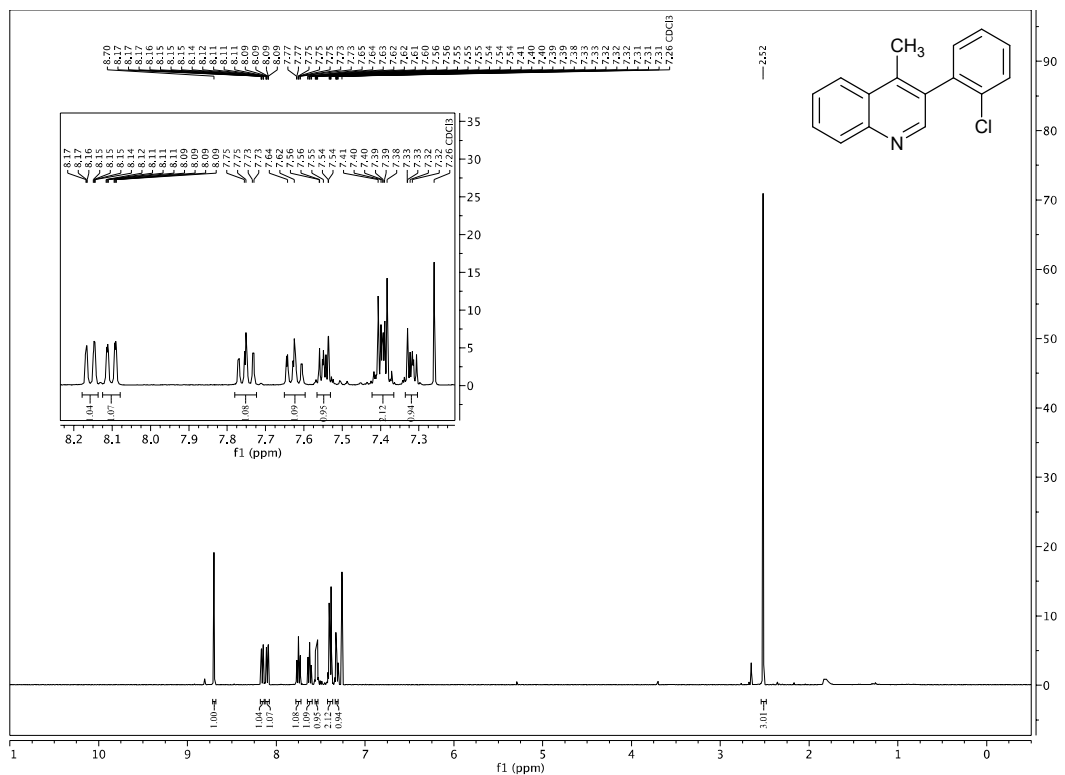




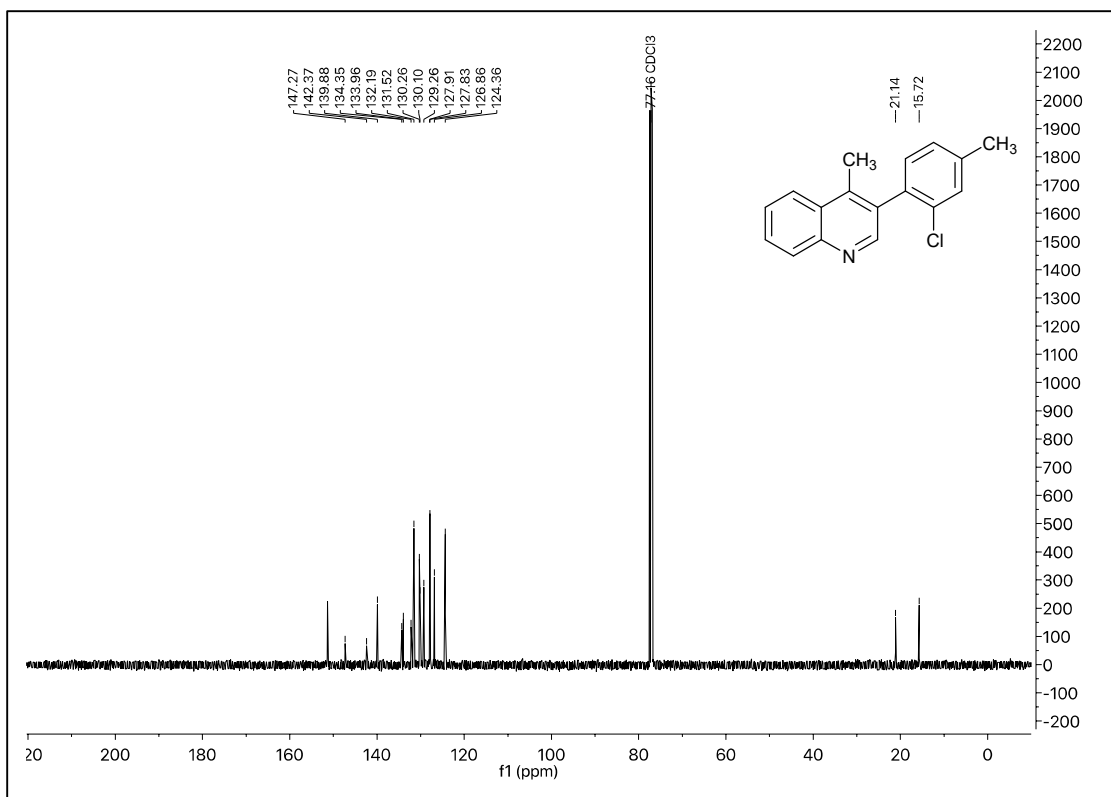
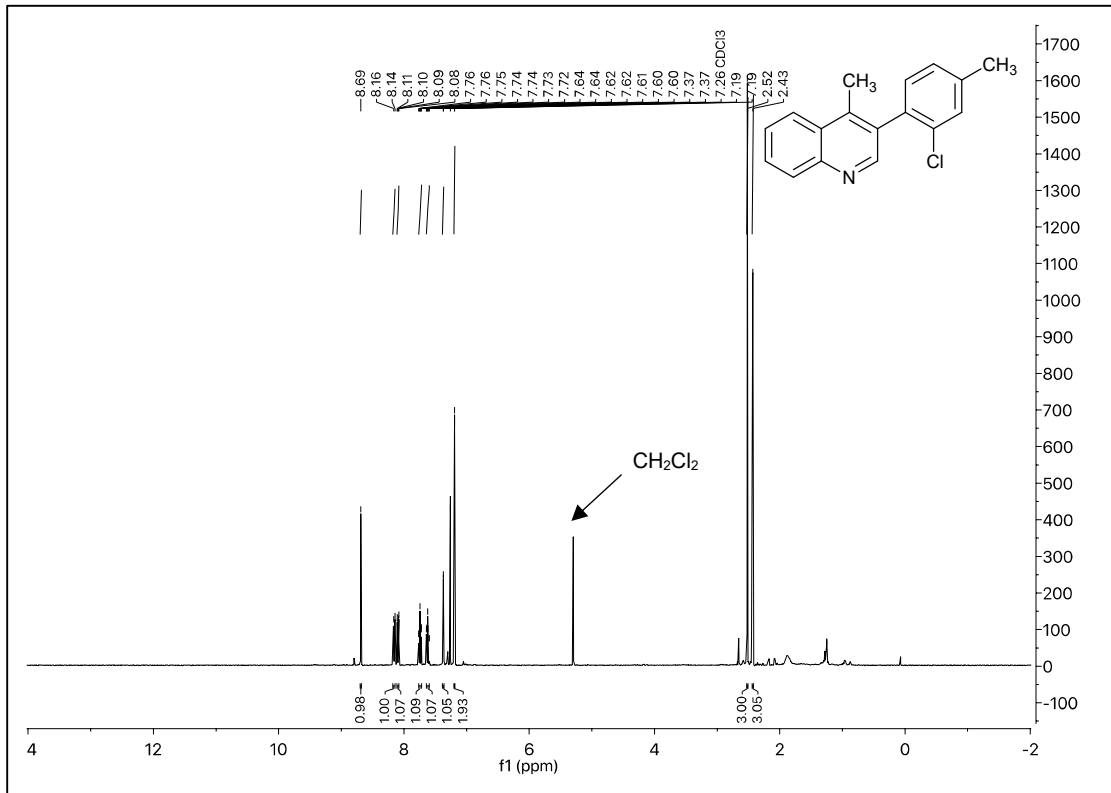
¹H and ¹³C NMR Spectral Data of 4-methyl-3-(o-tolyl)quinoline



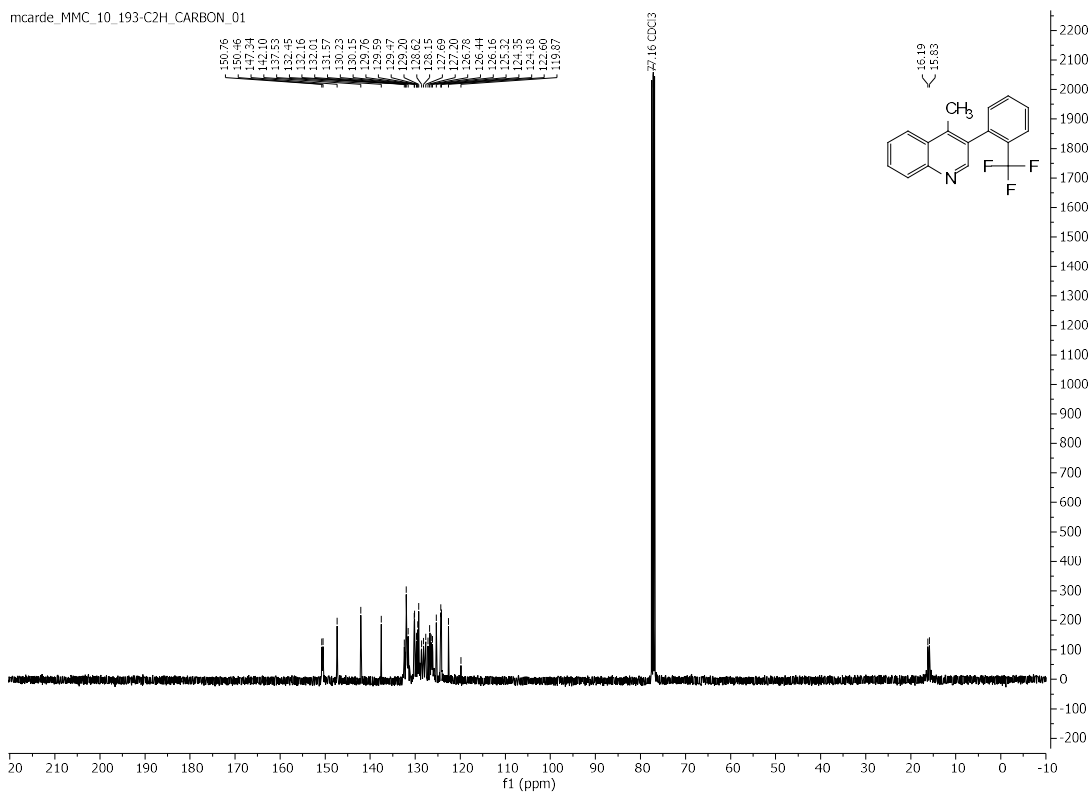
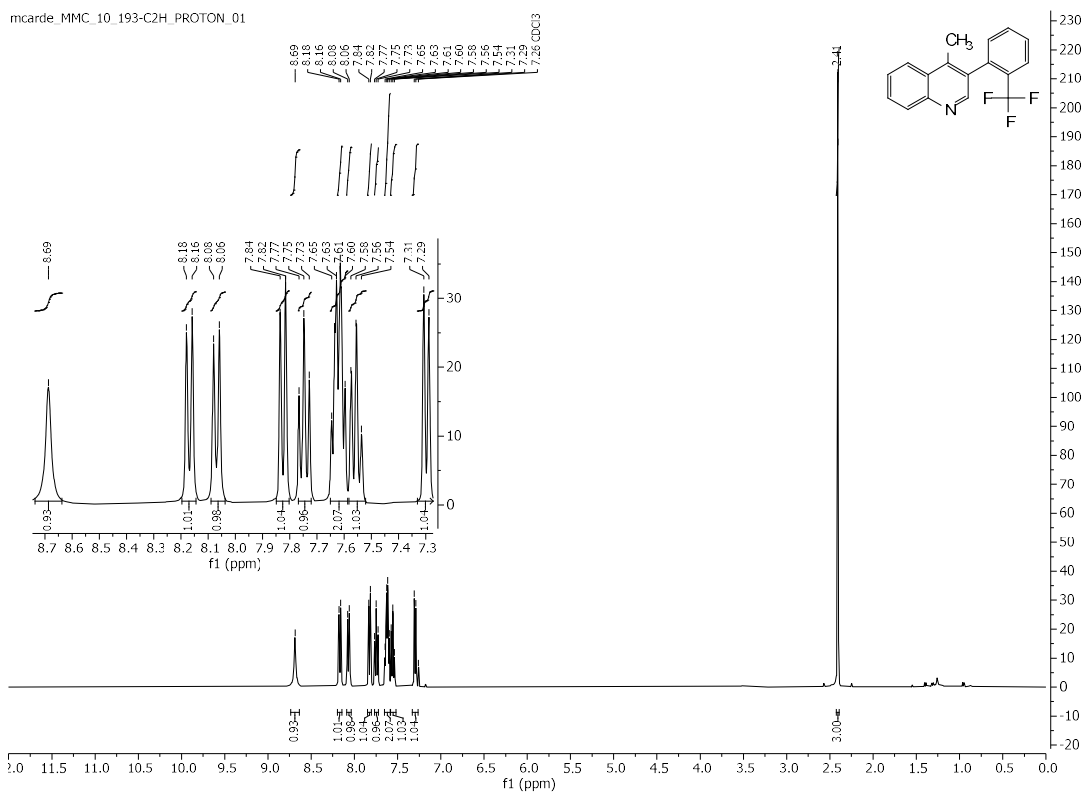
¹H and ¹³C NMR Spectral Data of 3-(2-chlorophenyl)-4-methylquinoline



^1H (trace CH_2Cl_2) and ^{13}C NMR Spectral Data of 3-(2-chloro-4-methylphenyl)-4-methylquinoline

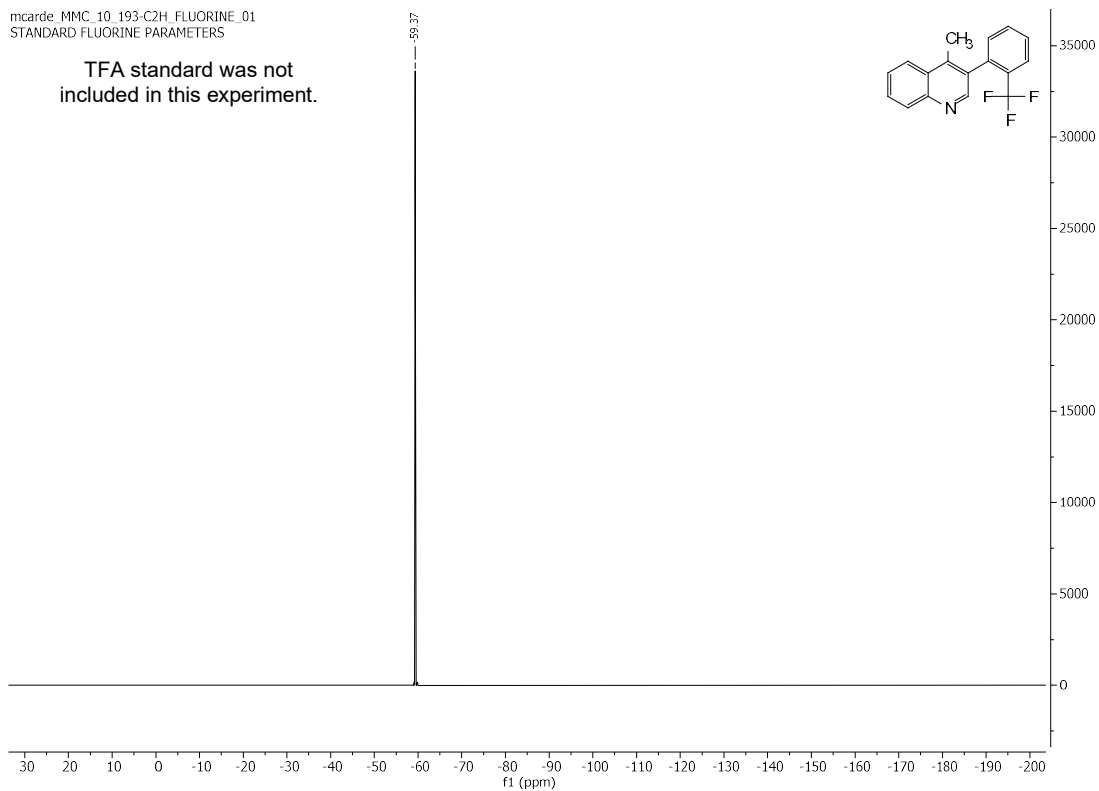


¹H and ¹³C NMR Spectral Data of 4-methyl-3-(2-(trifluoromethyl)phenyl)quinoline

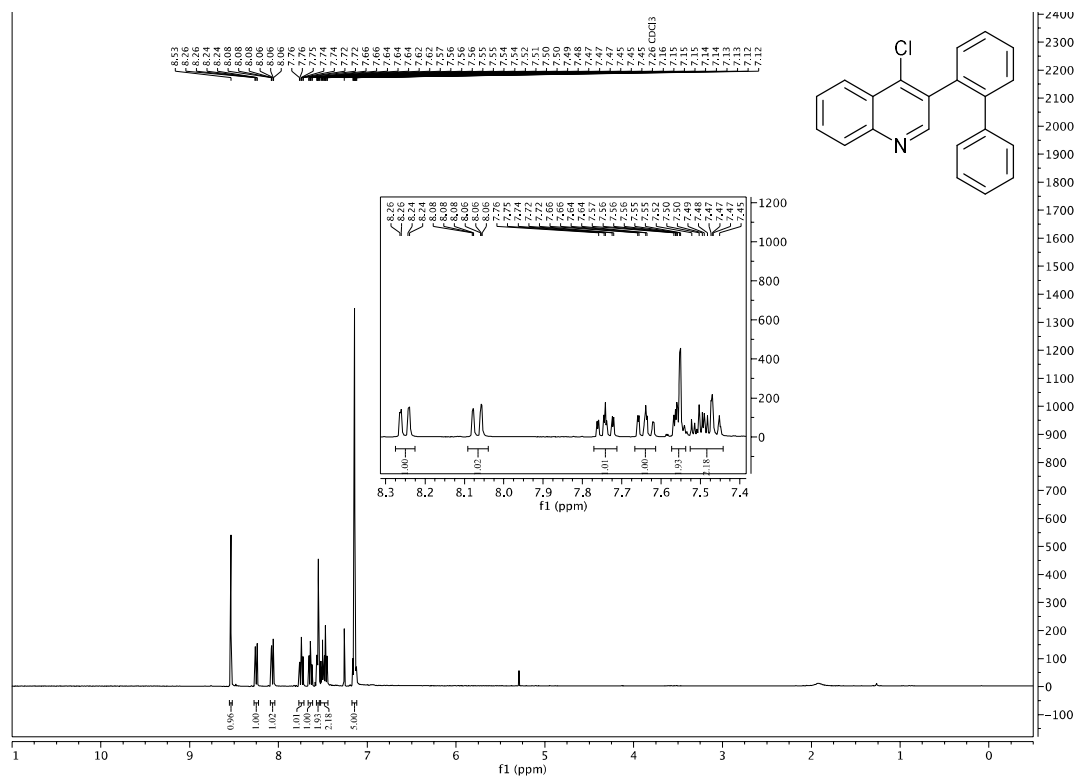


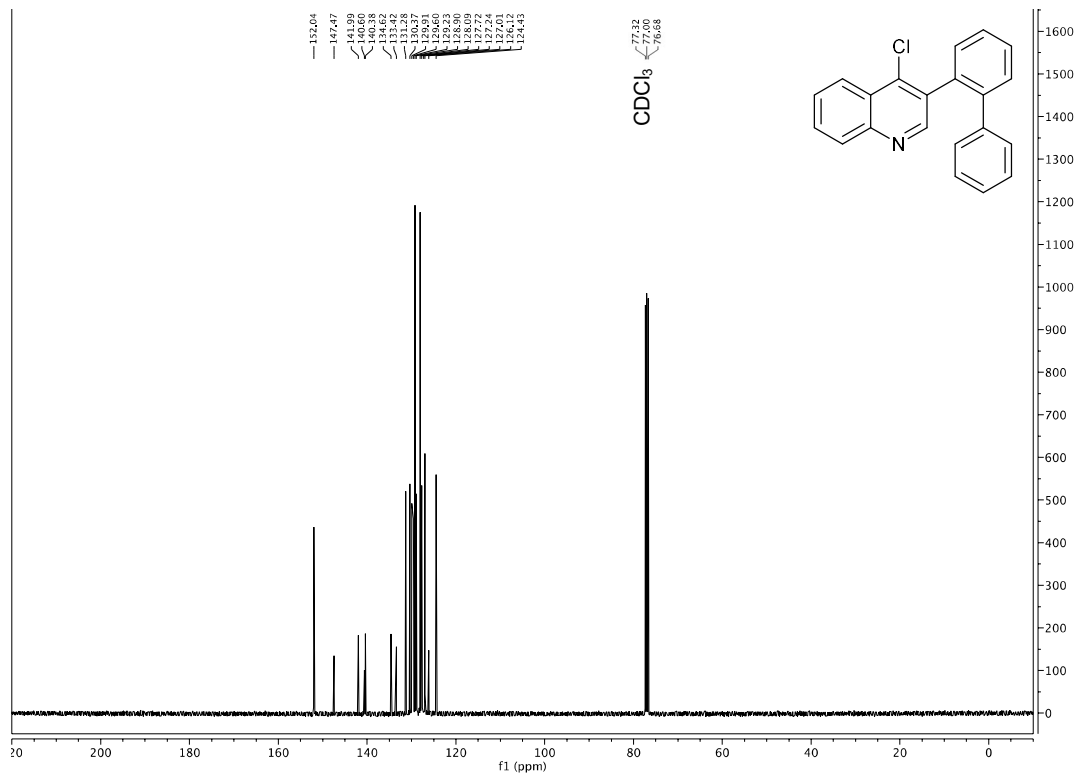
mcardr MMC_10_193-C2H_FLUORINE_01
STANDARD FLUORINE PARAMETERS

TFA standard was not
included in this experiment.

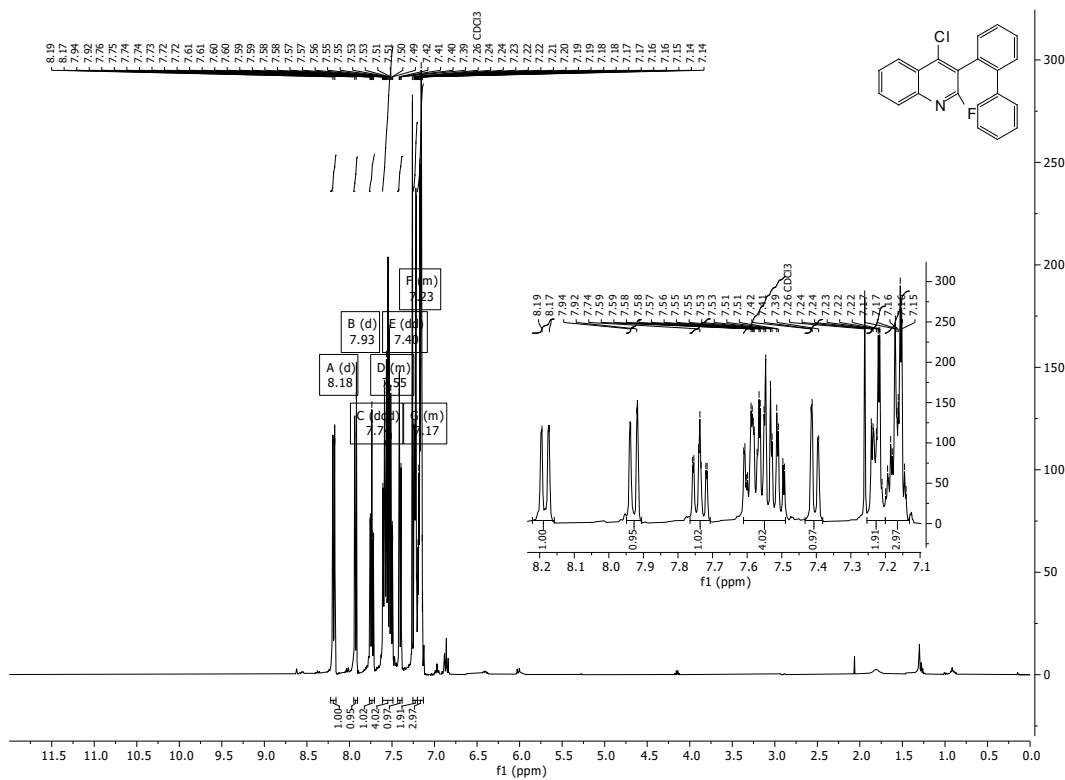


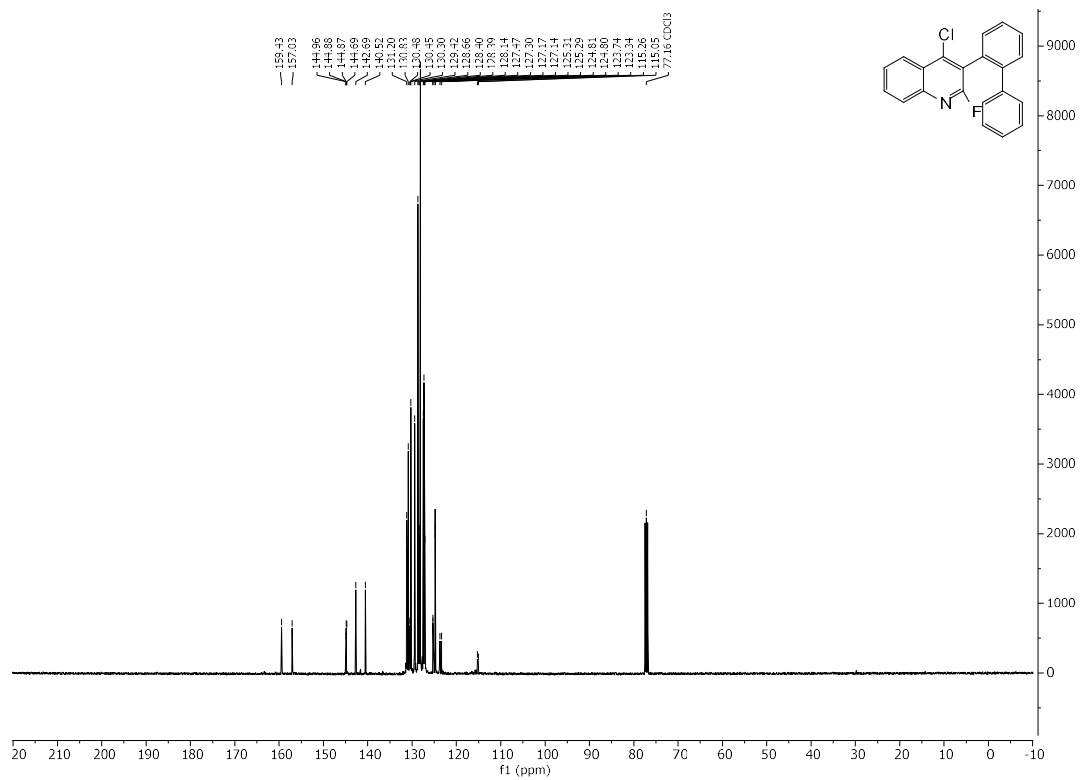
¹H and ¹³C NMR Spectral Data of 3-([1,1'-biphenyl]-2-yl)-4-chloroquinoline



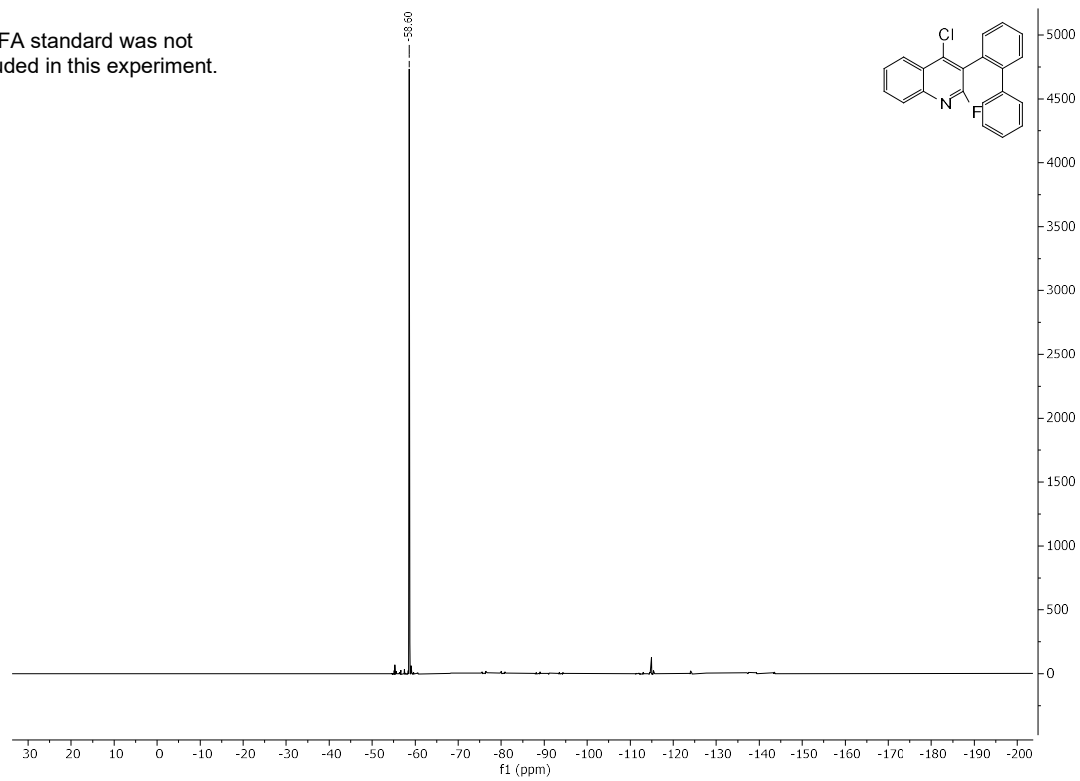


¹H, ¹³C, and ¹⁹F NMR Spectral Data of 3-([1,1'-biphenyl]-2-yl)-4-chloro-2-fluoroquinoline

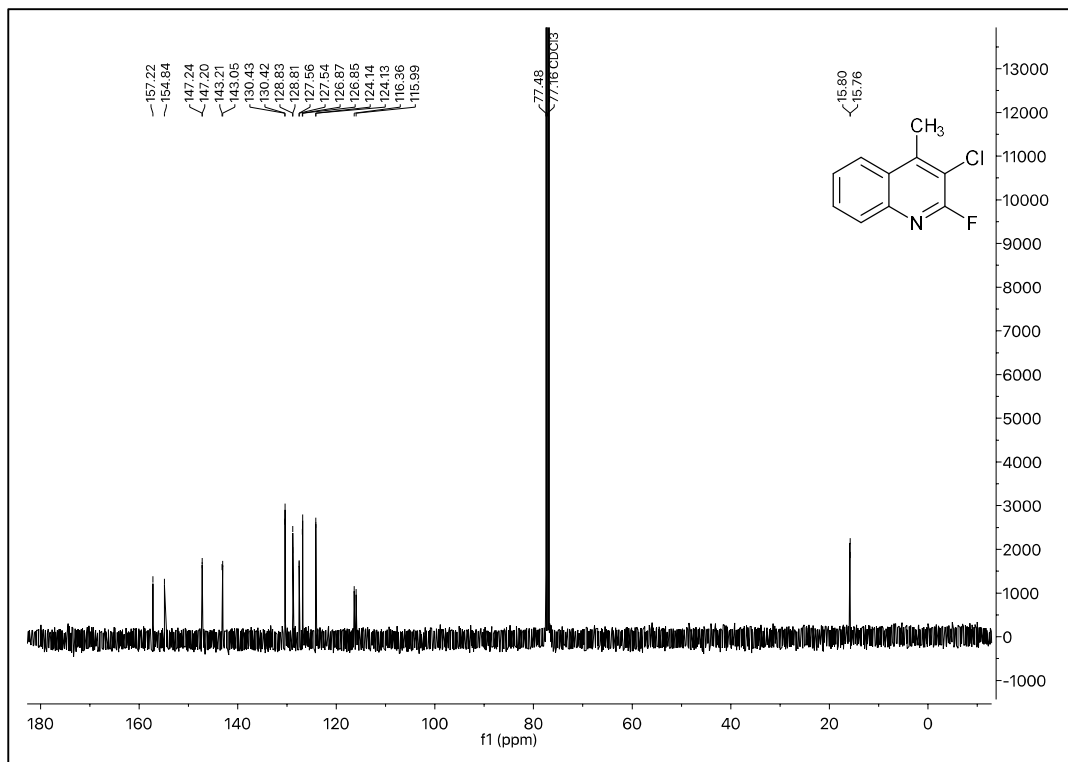
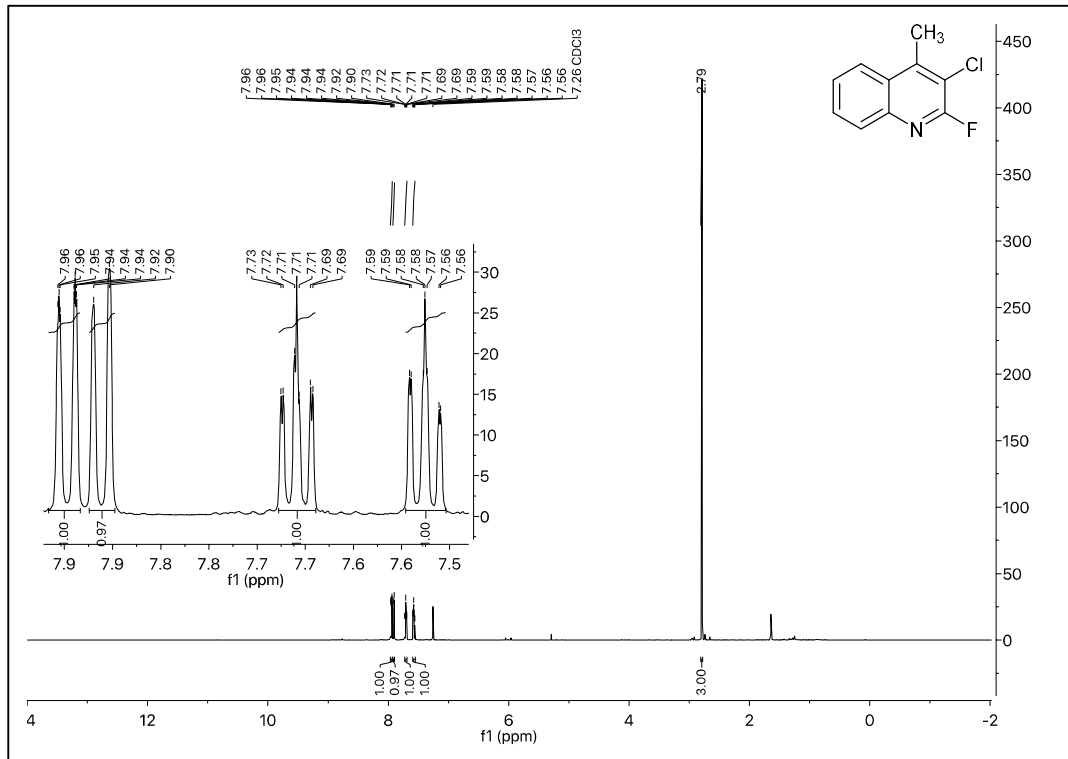


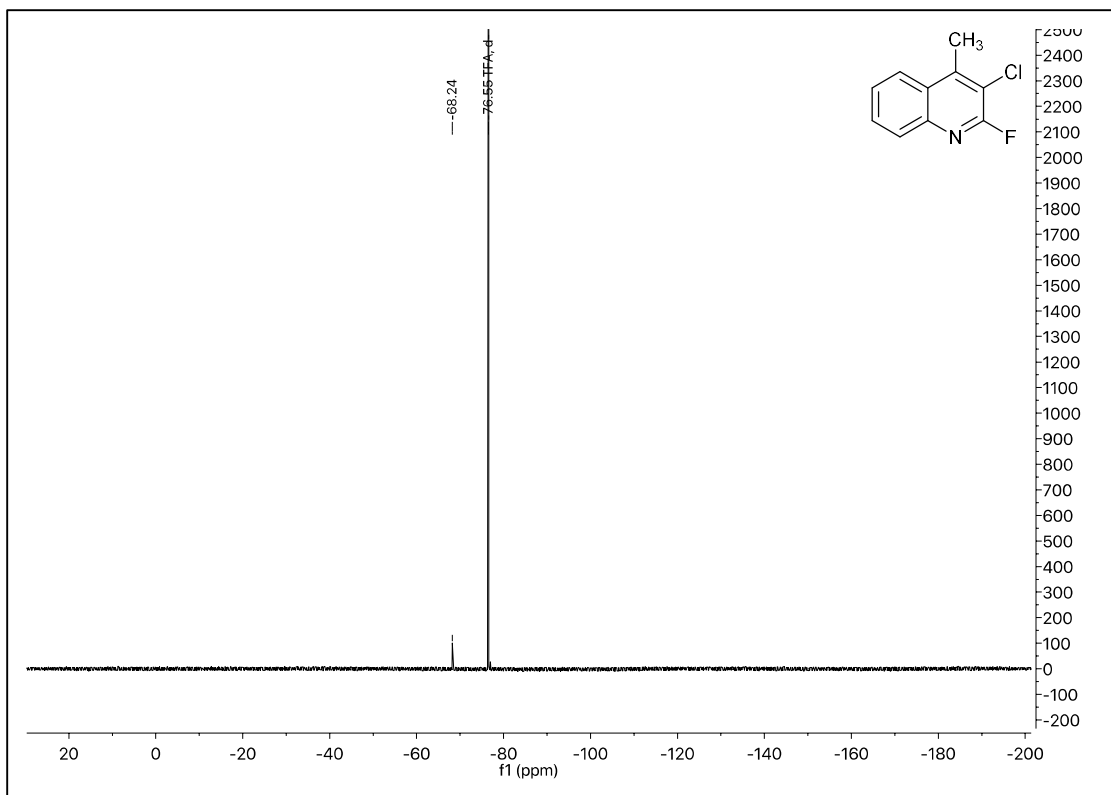


TFA standard was not included in this experiment.

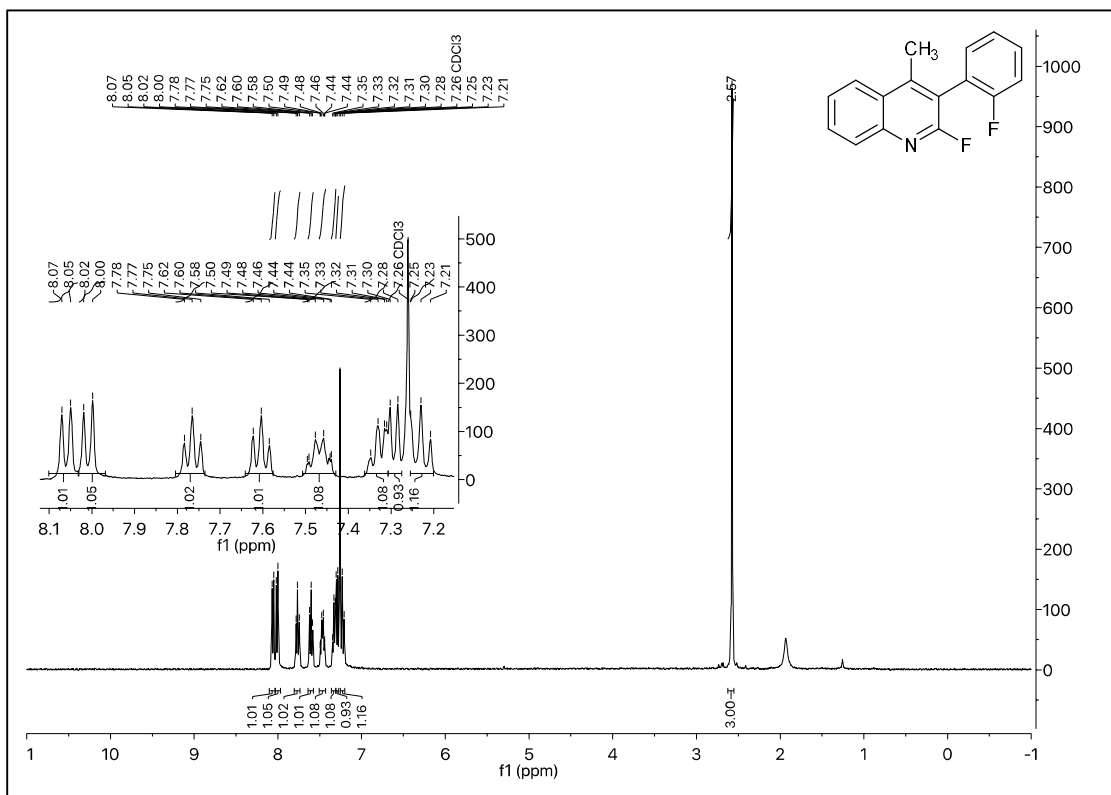


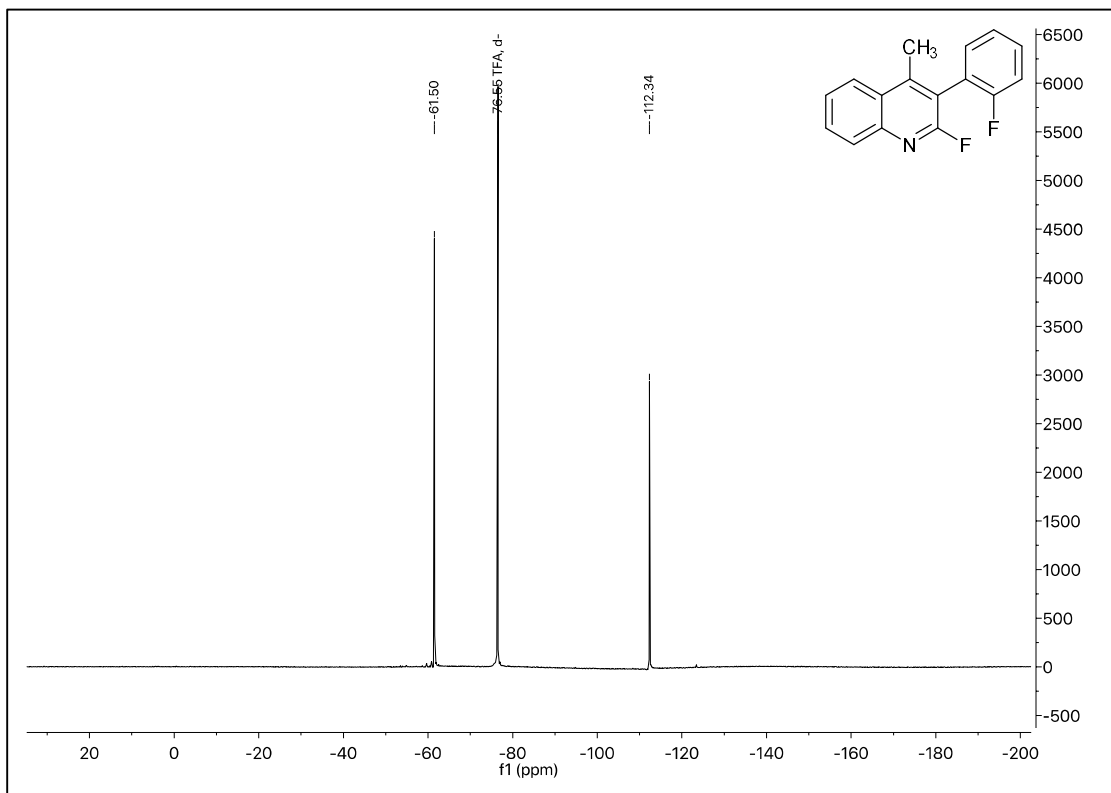
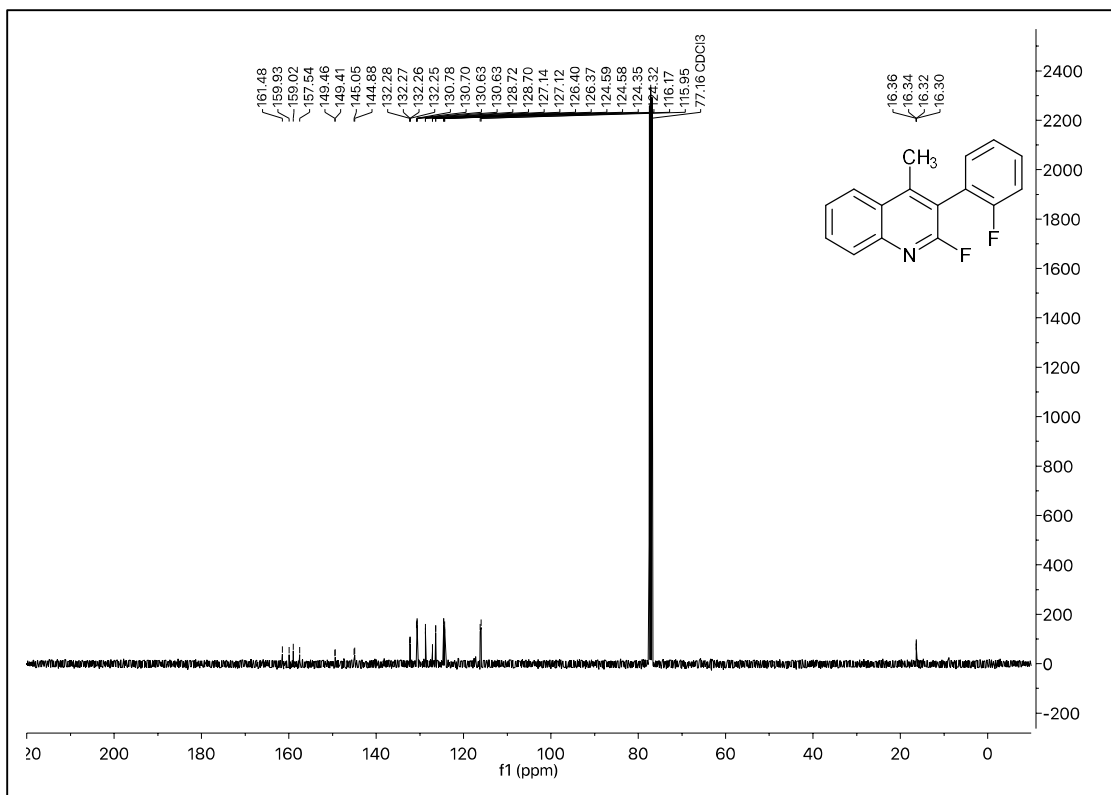
^1H , ^{13}C , and ^{19}F NMR Spectral Data of 3-chloro-2-fluoro-4-methylquinoline



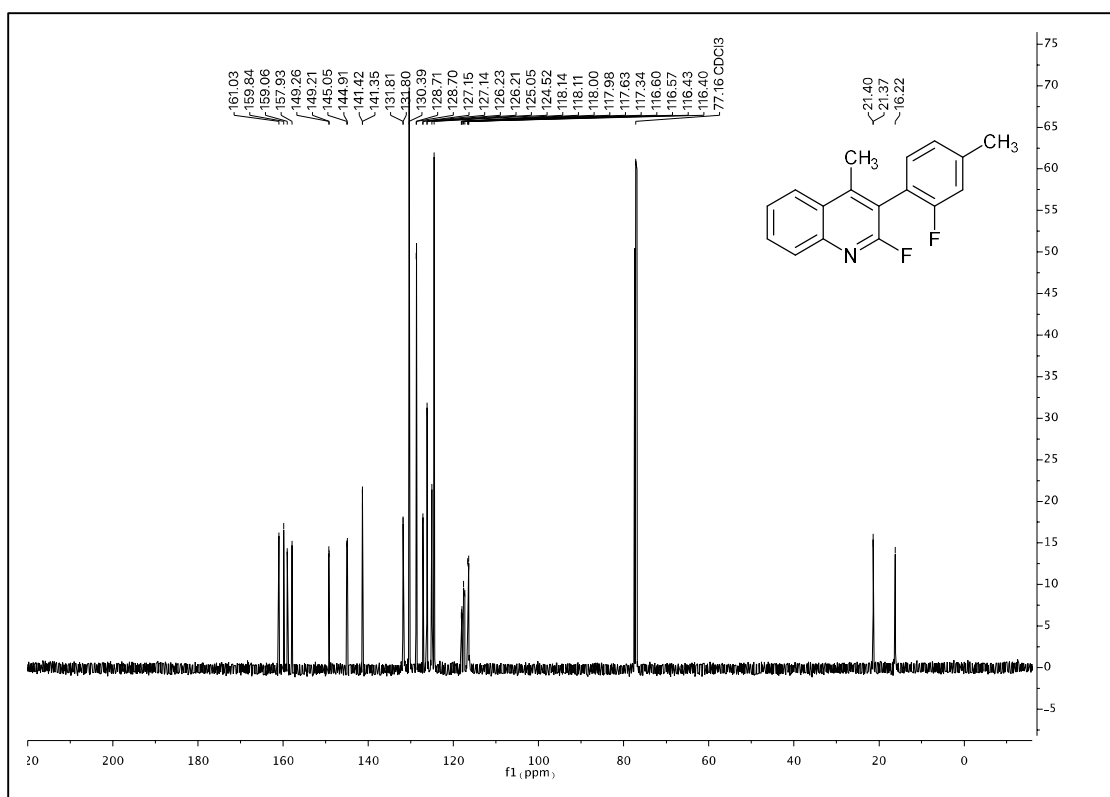
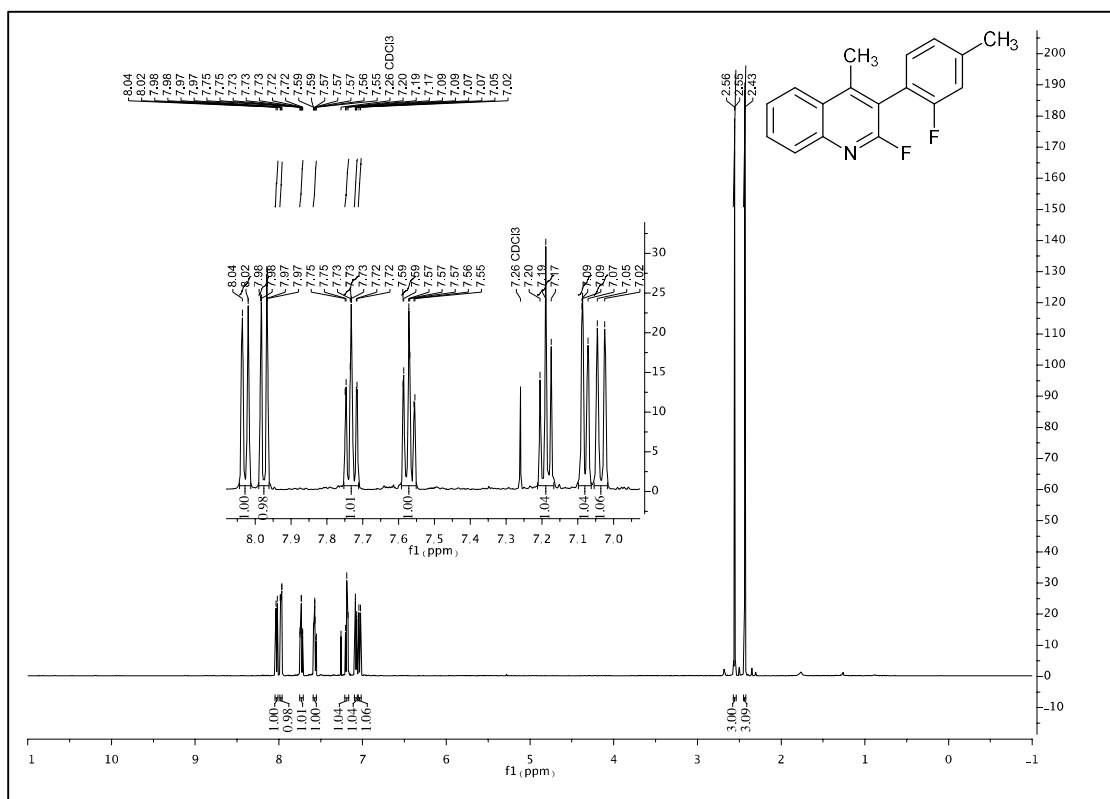


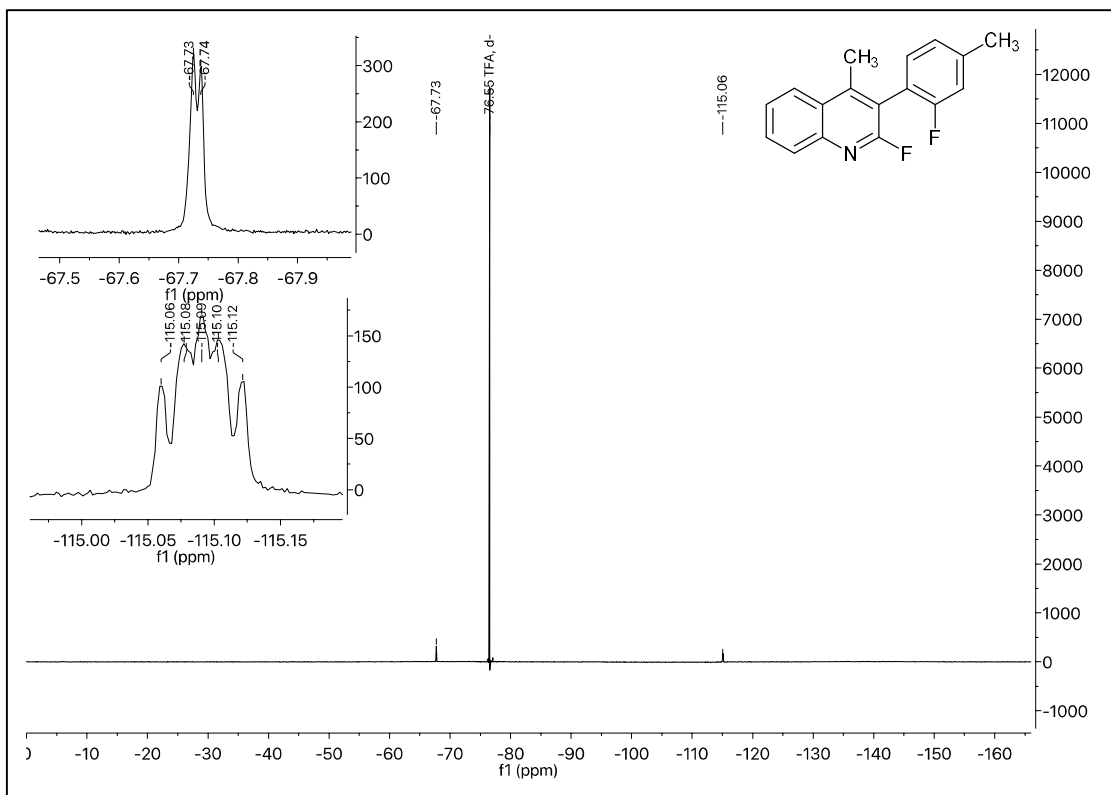
¹H, ¹³C, and ¹⁹F NMR Spectral Data of 2-fluoro-3-(2-fluorophenyl)-4-methylquinoline



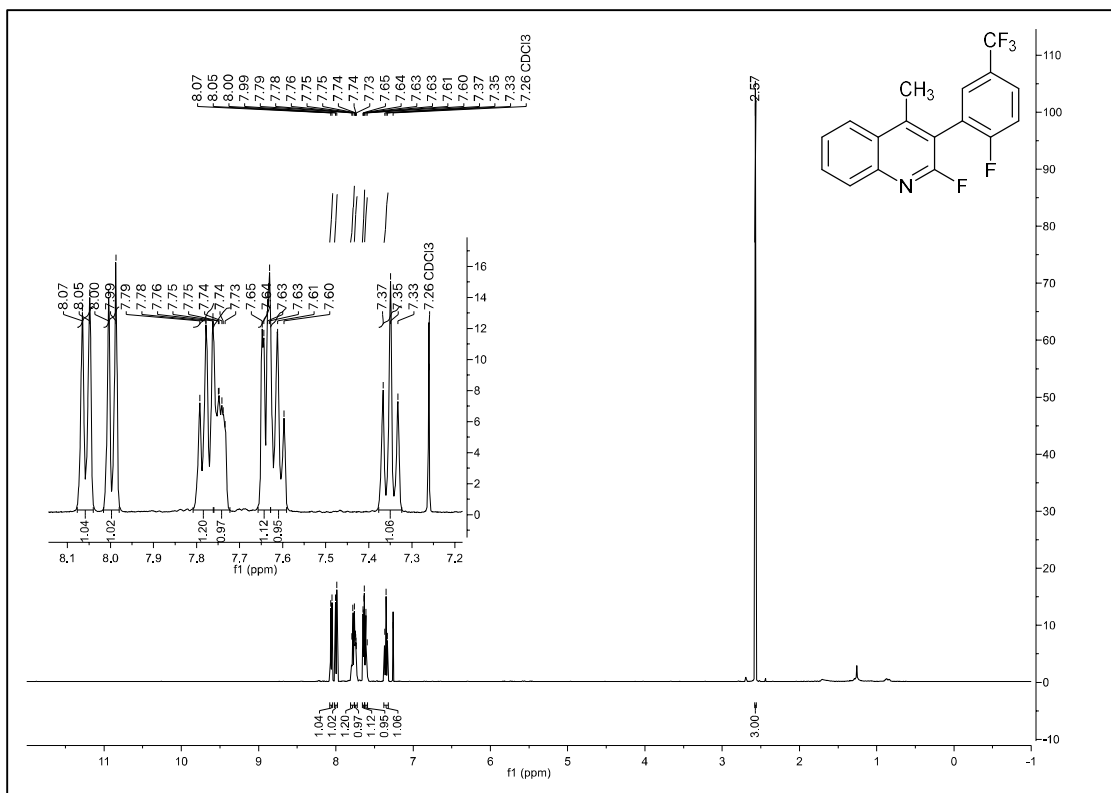


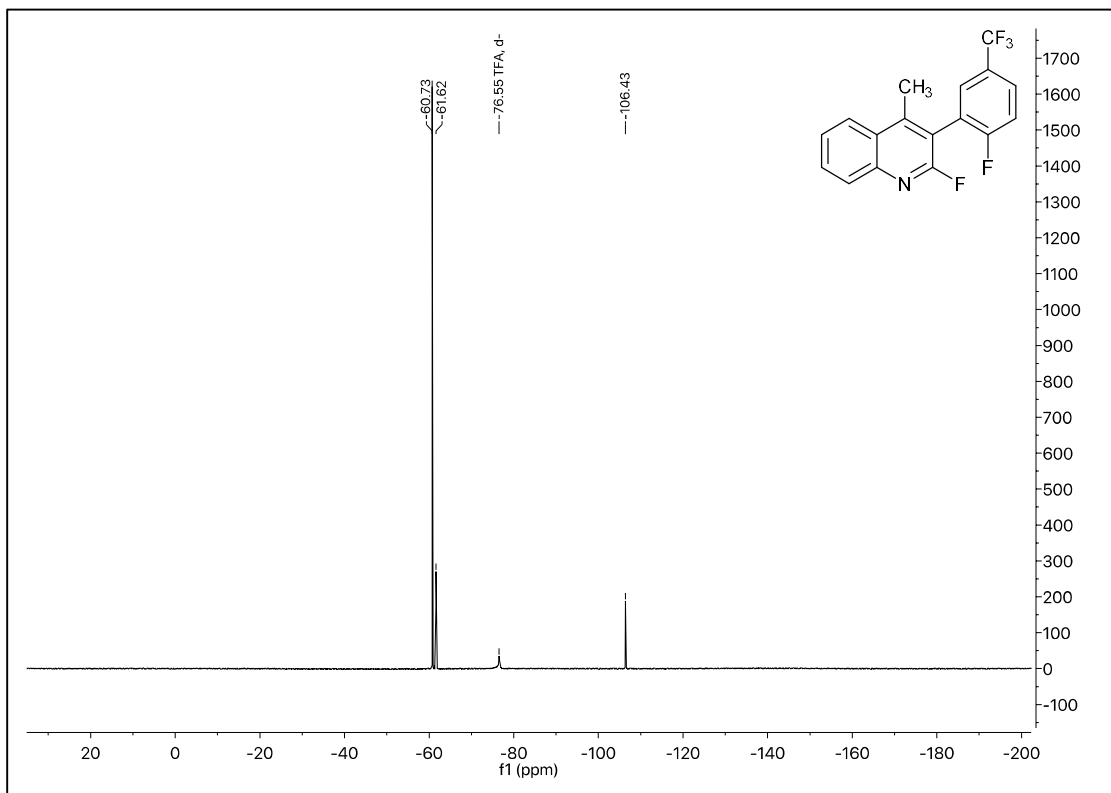
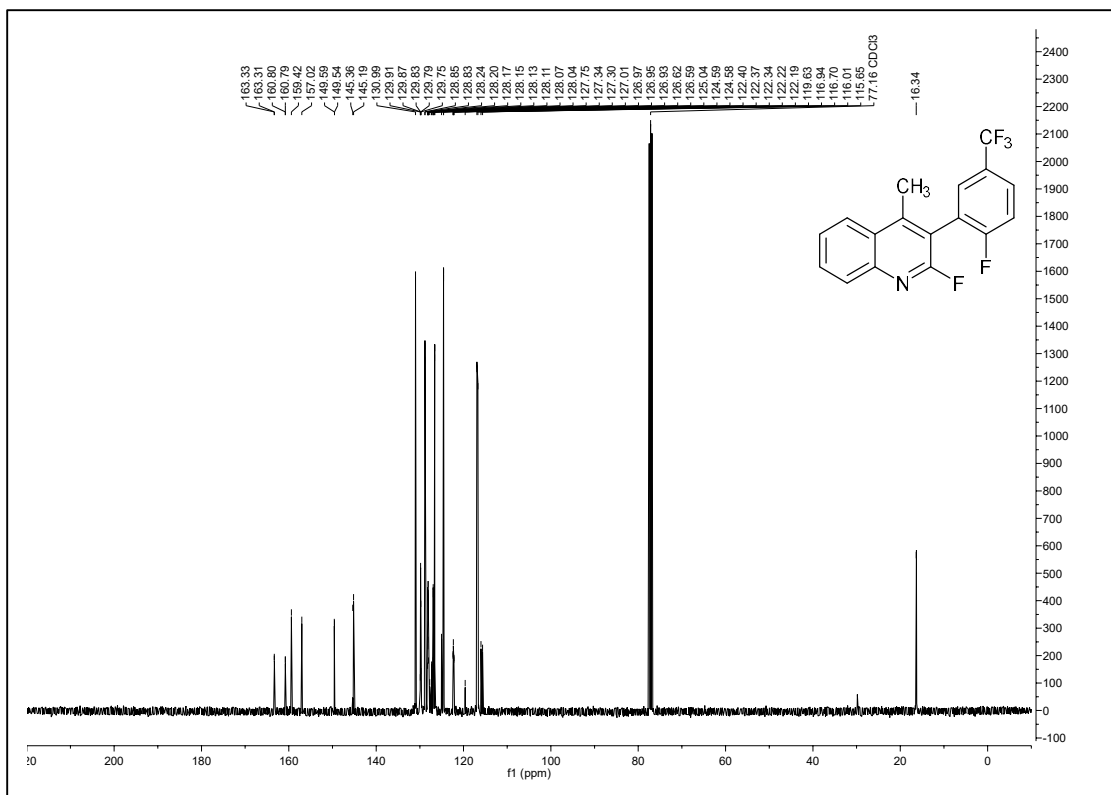
^1H , ^{13}C , and ^{19}F NMR Spectral Data of 2-fluoro-3-(2-fluoro-4-methylphenyl)-4-methylquinoline



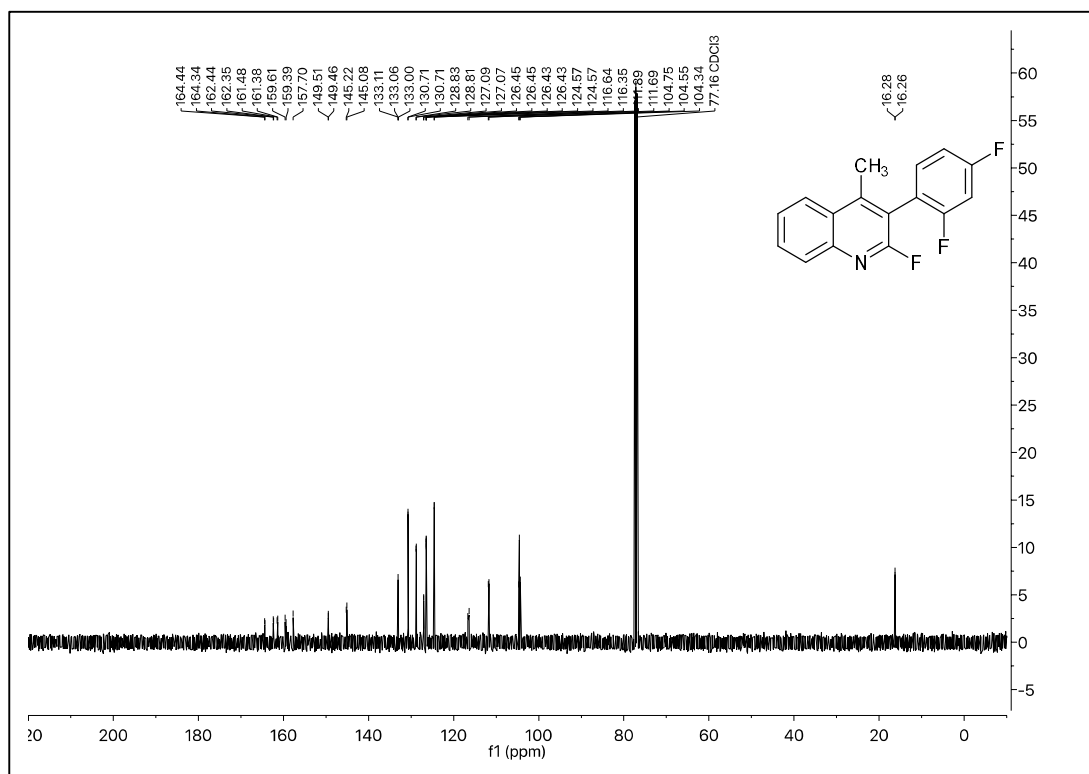
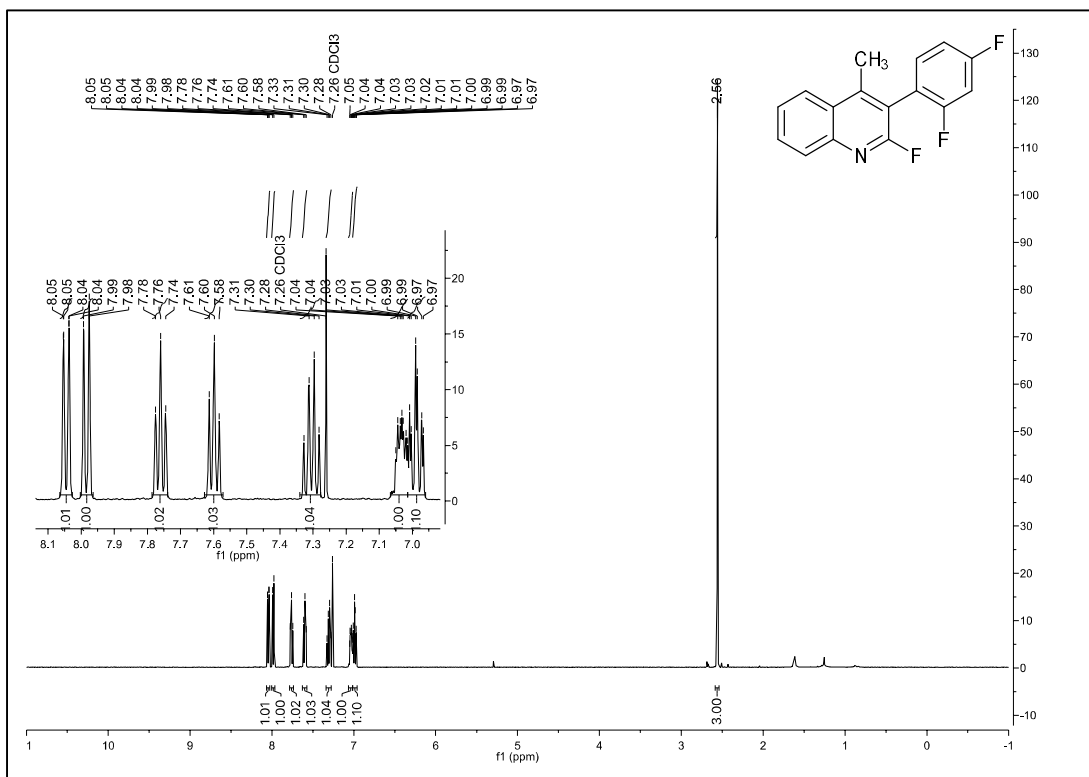


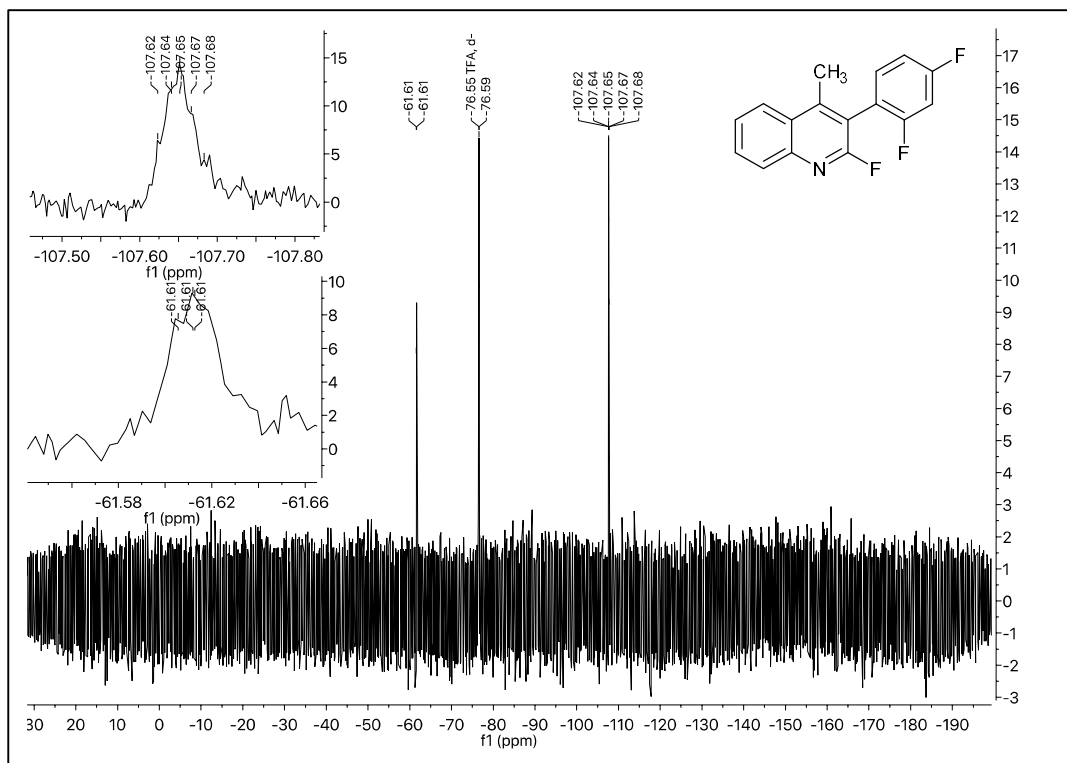
¹H, ¹³C, and ¹⁹F NMR Spectral Data of 2-fluoro-3-(2-fluoro-5-(trifluoromethyl)phenyl)-4-methylquinoline



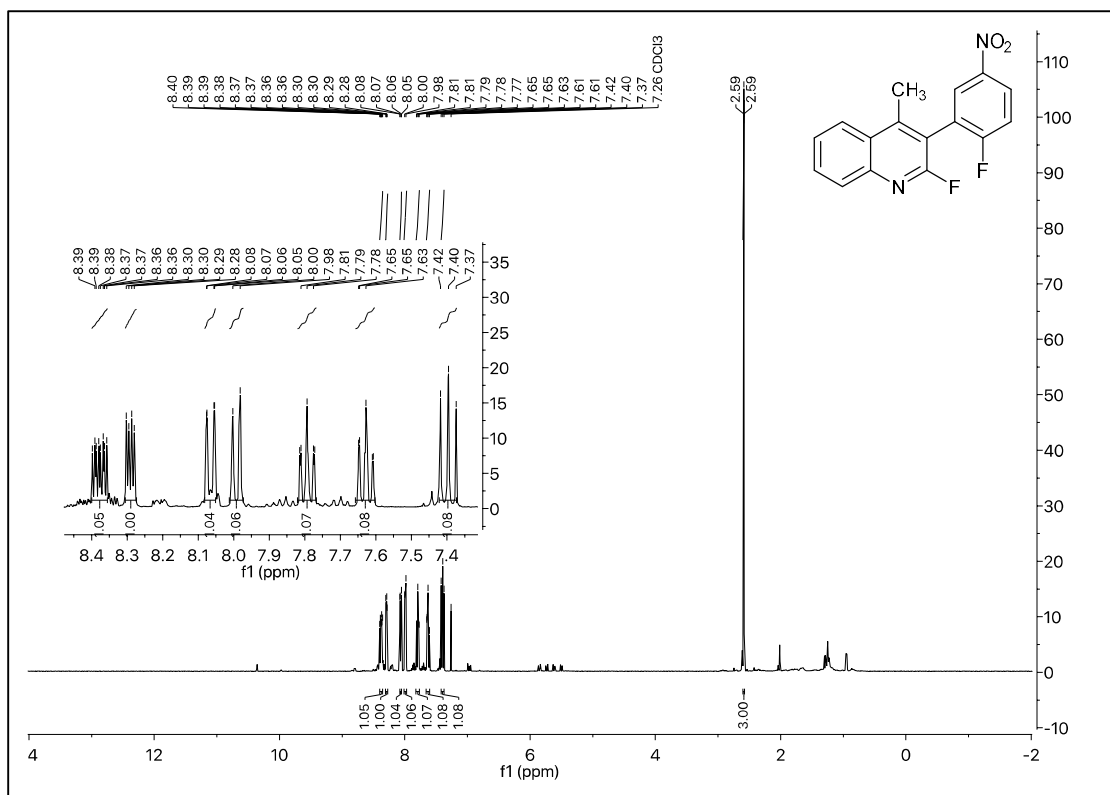


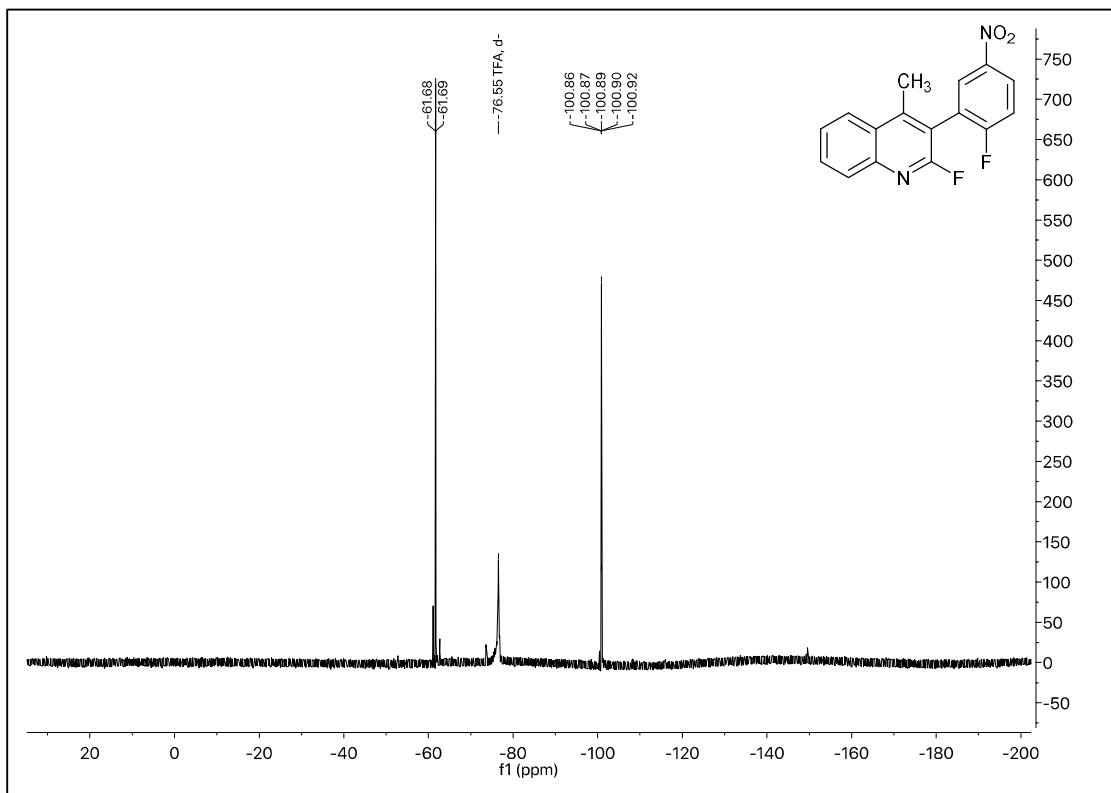
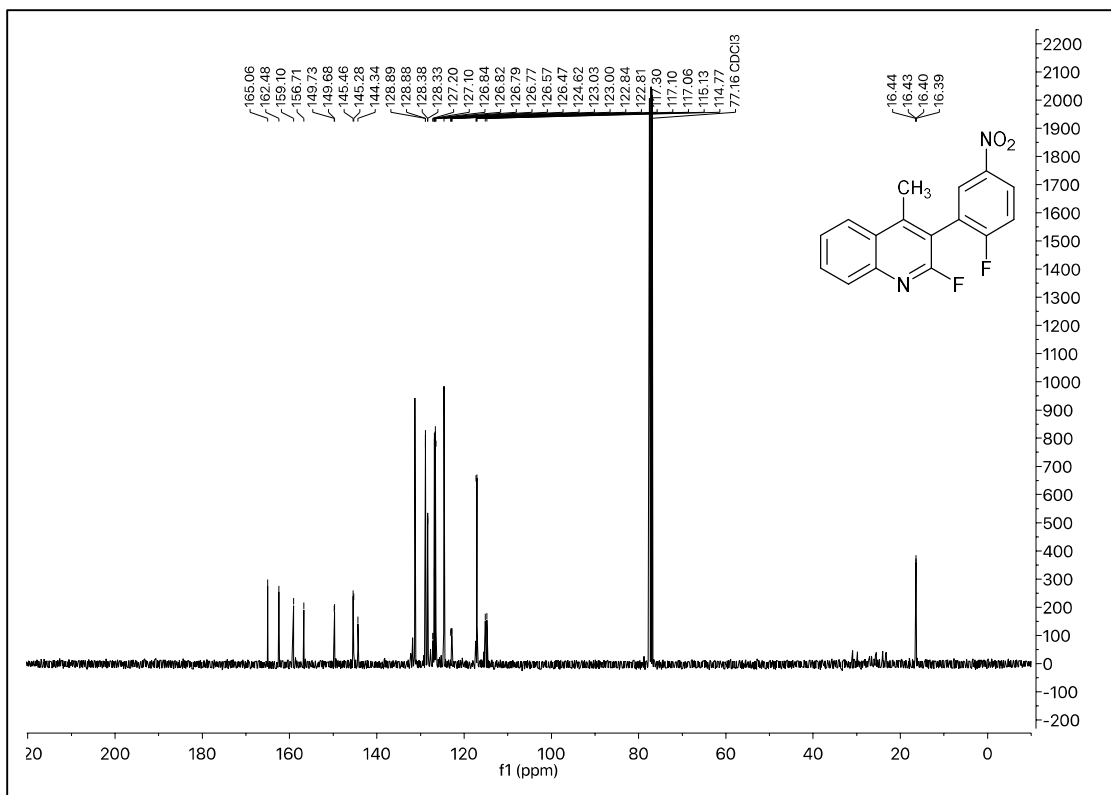
^1H , ^{13}C , and ^{19}F NMR Spectral Data of 2-fluoro-3-(2-fluoro-5-(trifluoromethyl)phenyl)-4-methylquinoline

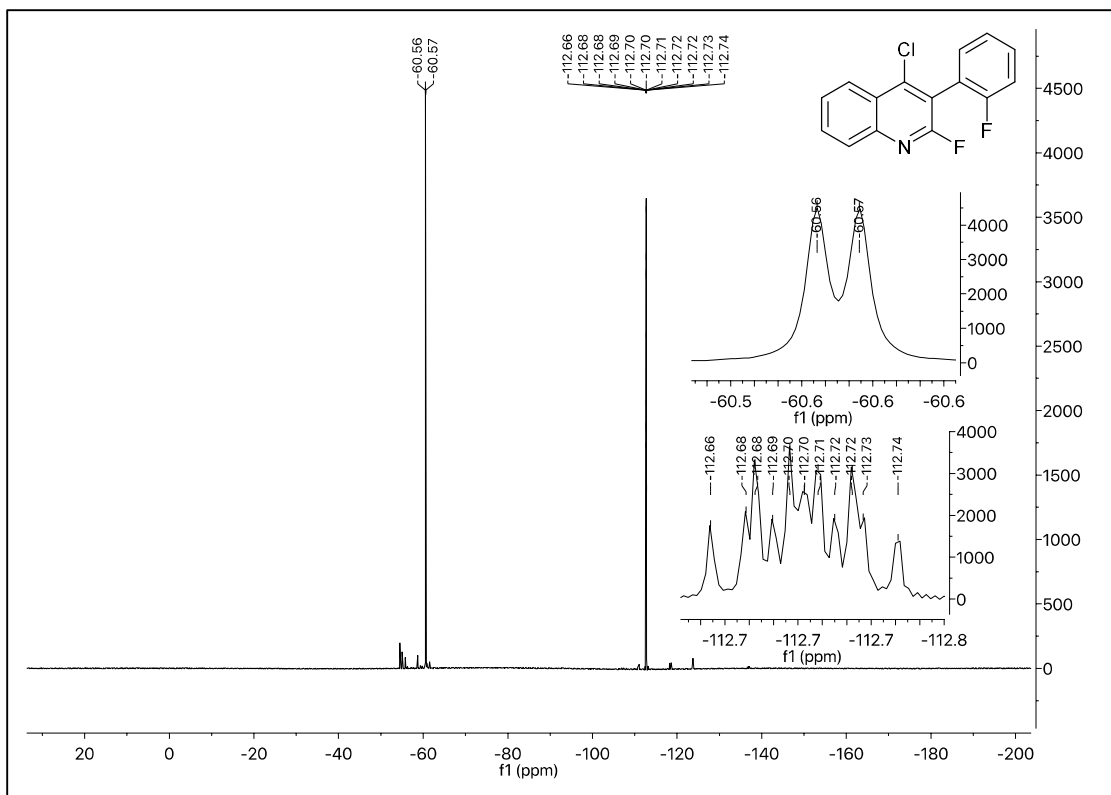




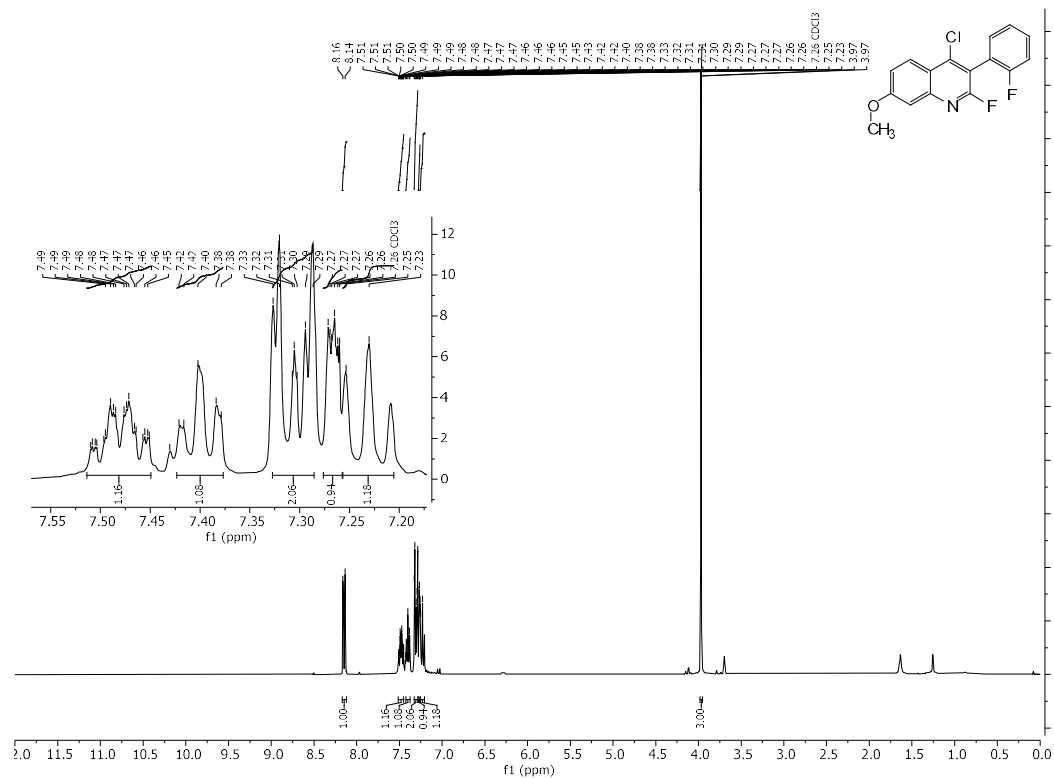
¹H, ¹³C, and ¹⁹F NMR Spectral Data of 2-fluoro-3-(2-fluoro-5-nitrophenyl)-4-methylquinoline

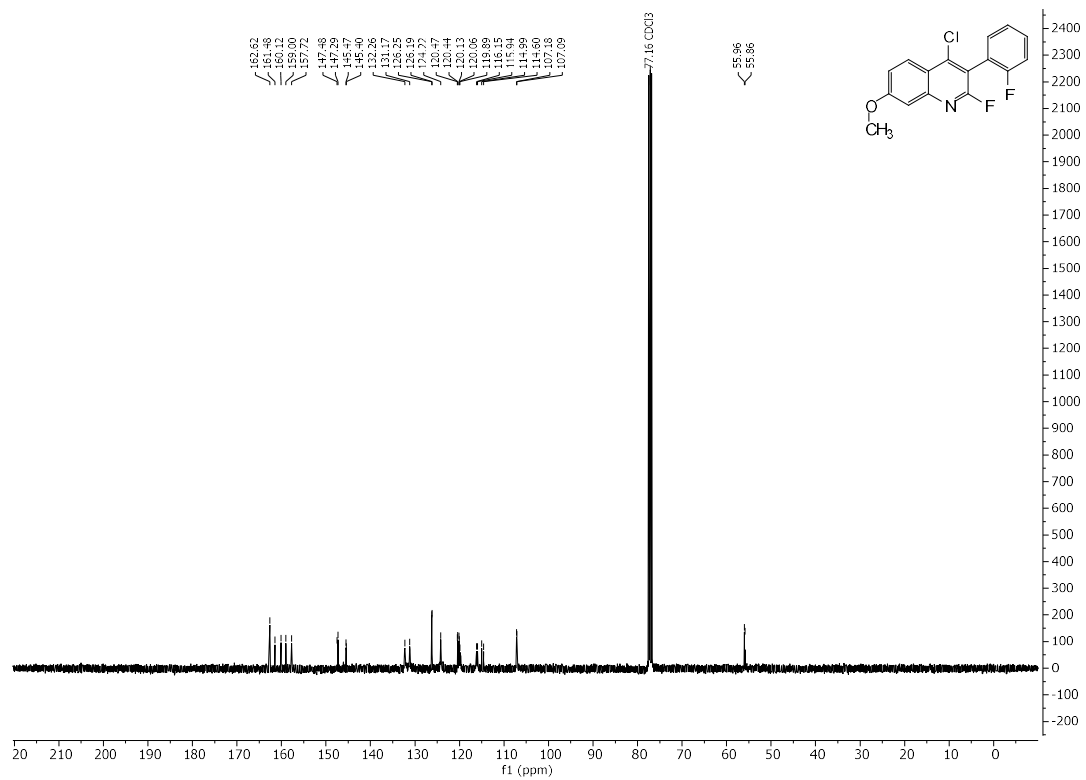




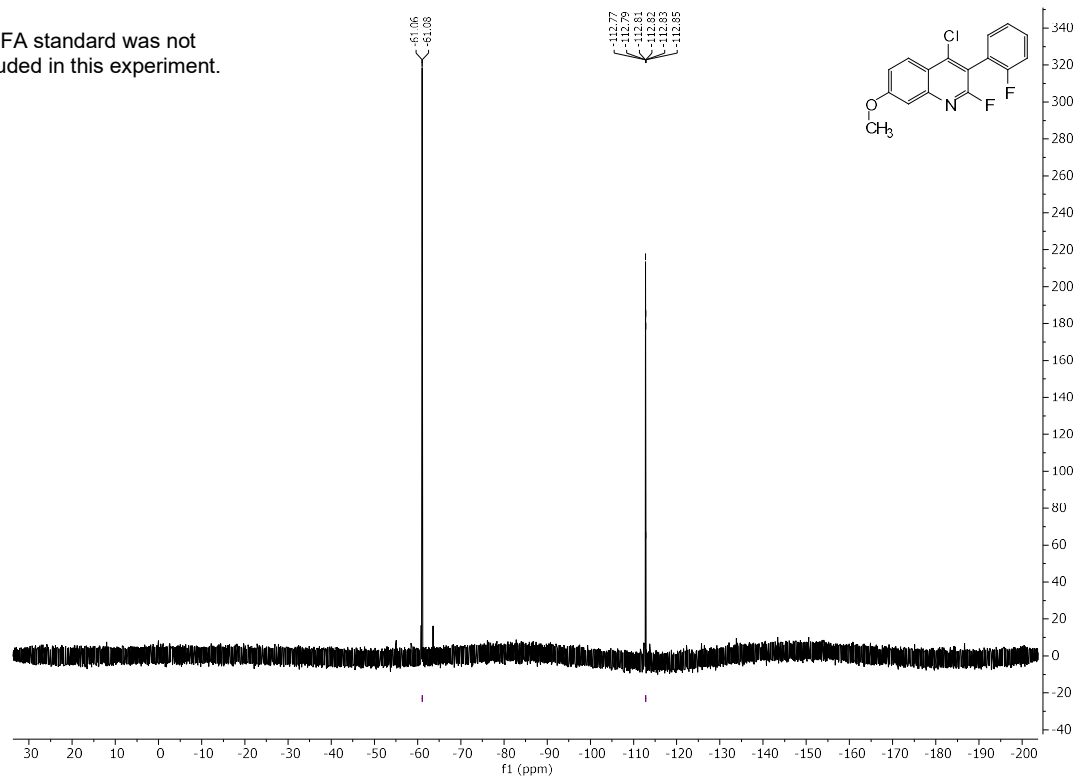


¹H, ¹³C, and ¹⁹F NMR Spectral Data of **1i**

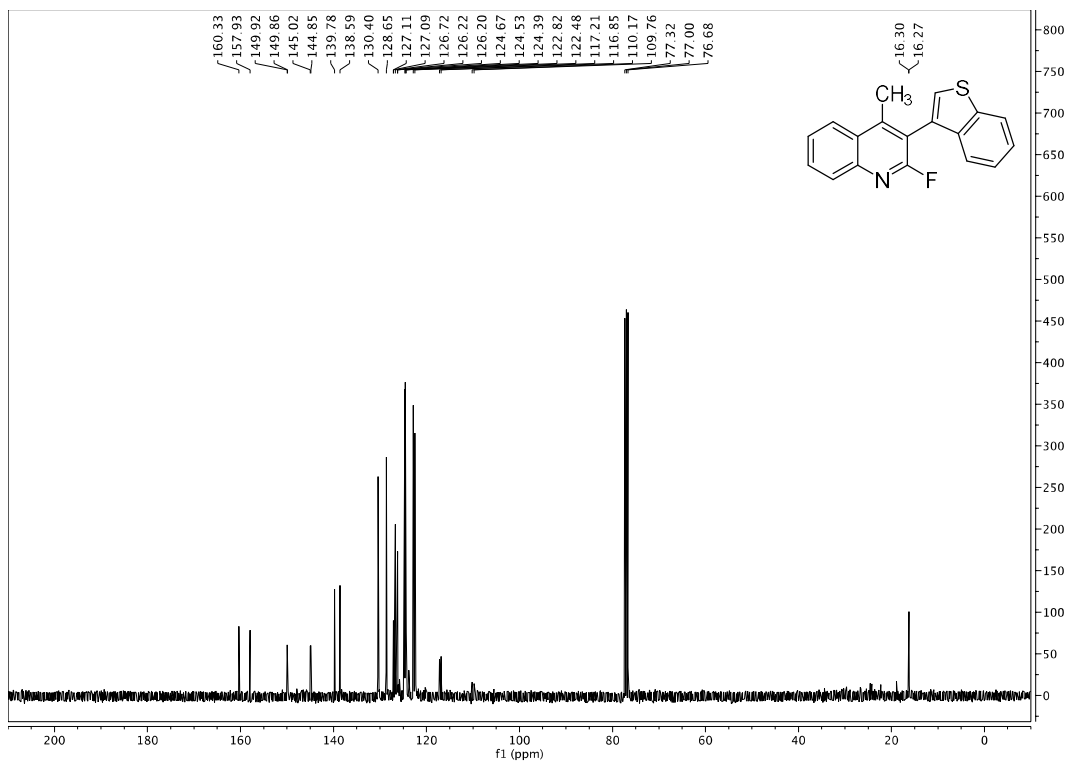
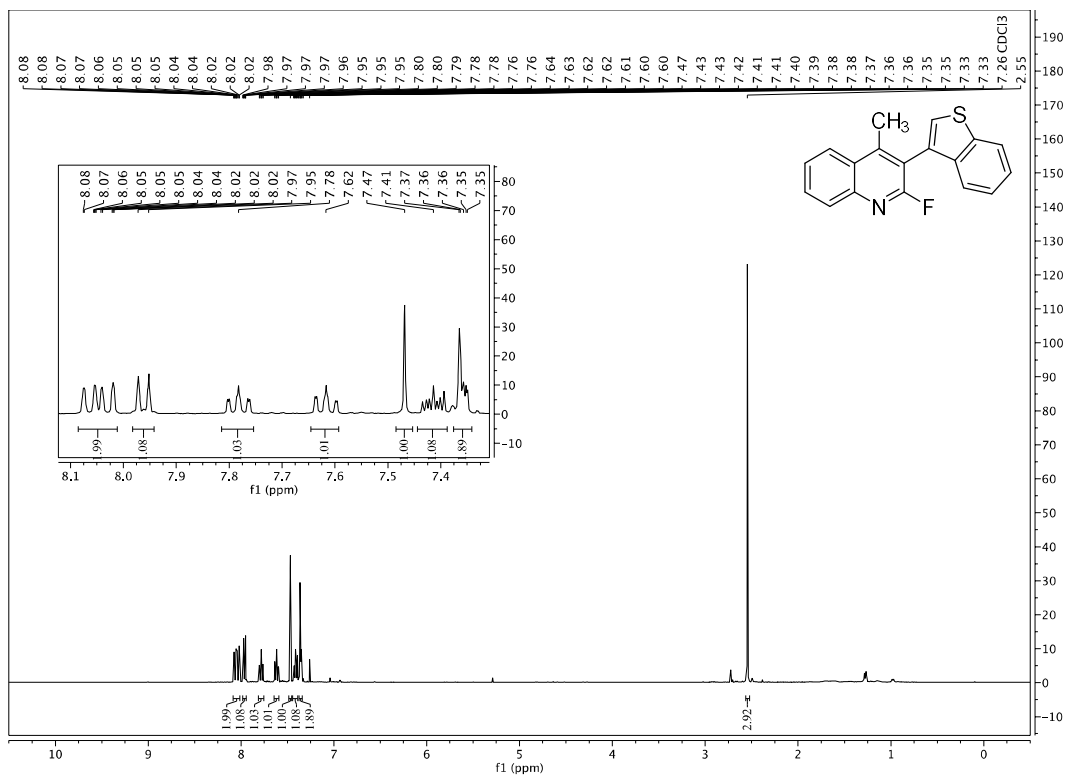


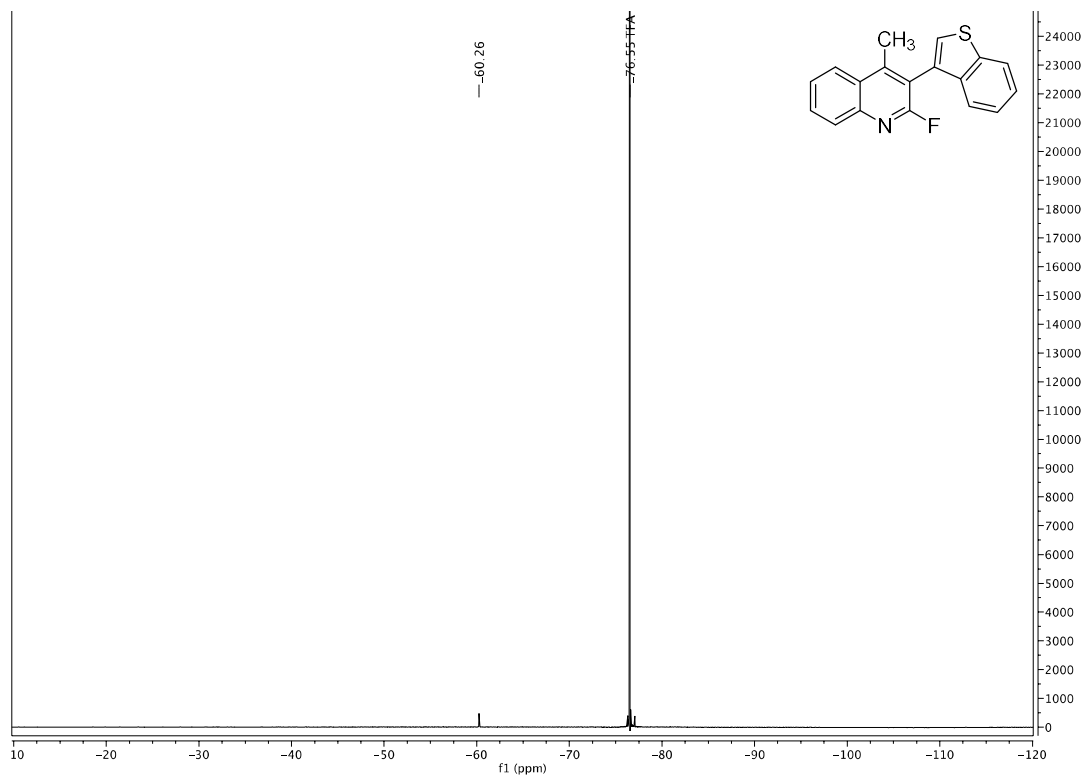


TFA standard was not included in this experiment.

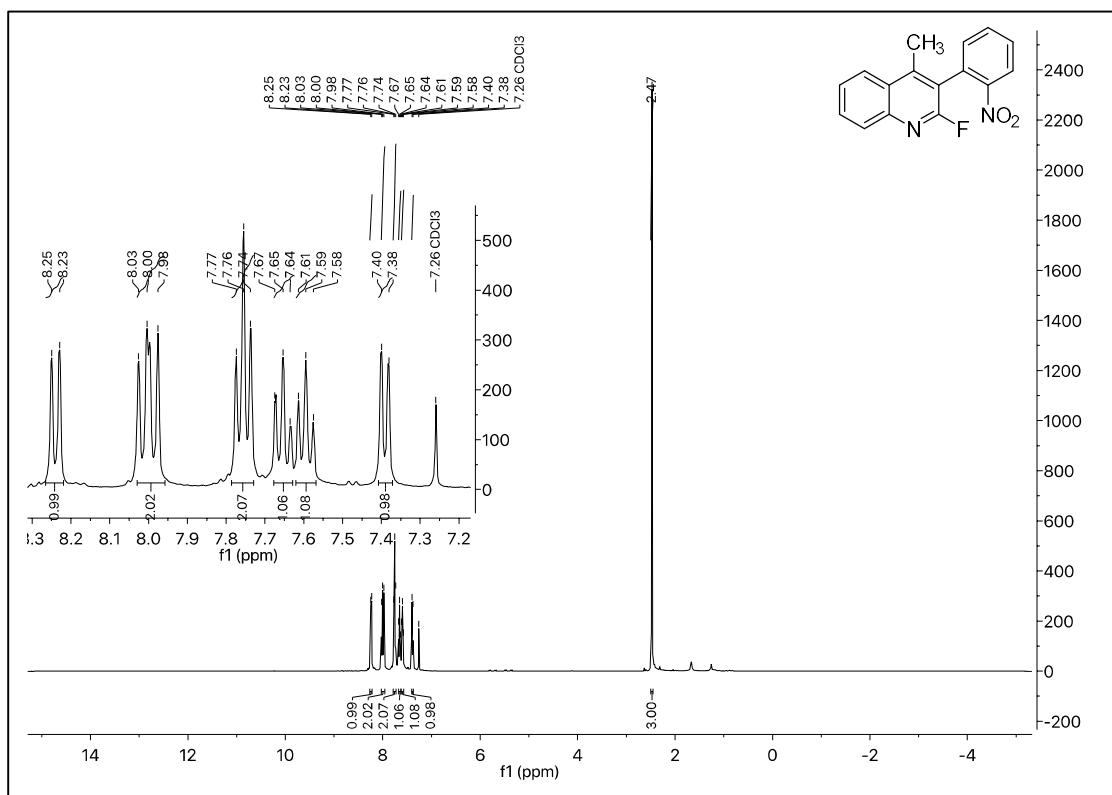


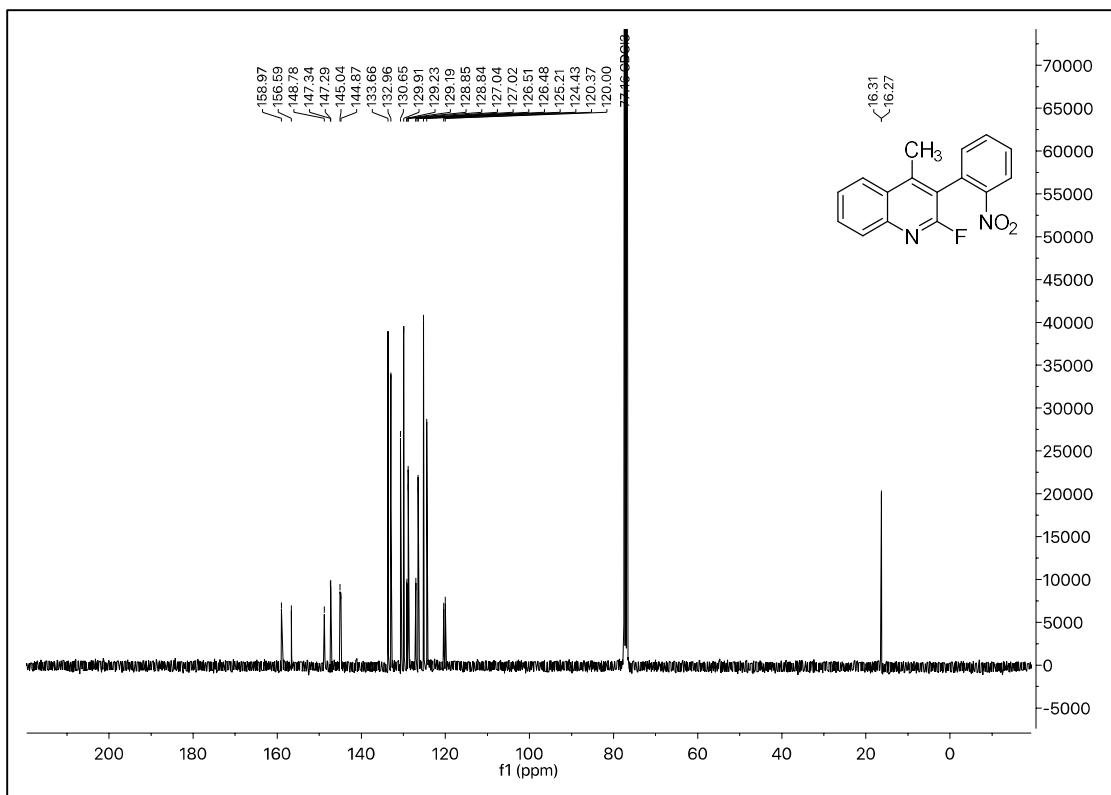
^1H , ^{13}C , and ^{19}F NMR Spectral Data of **1k**



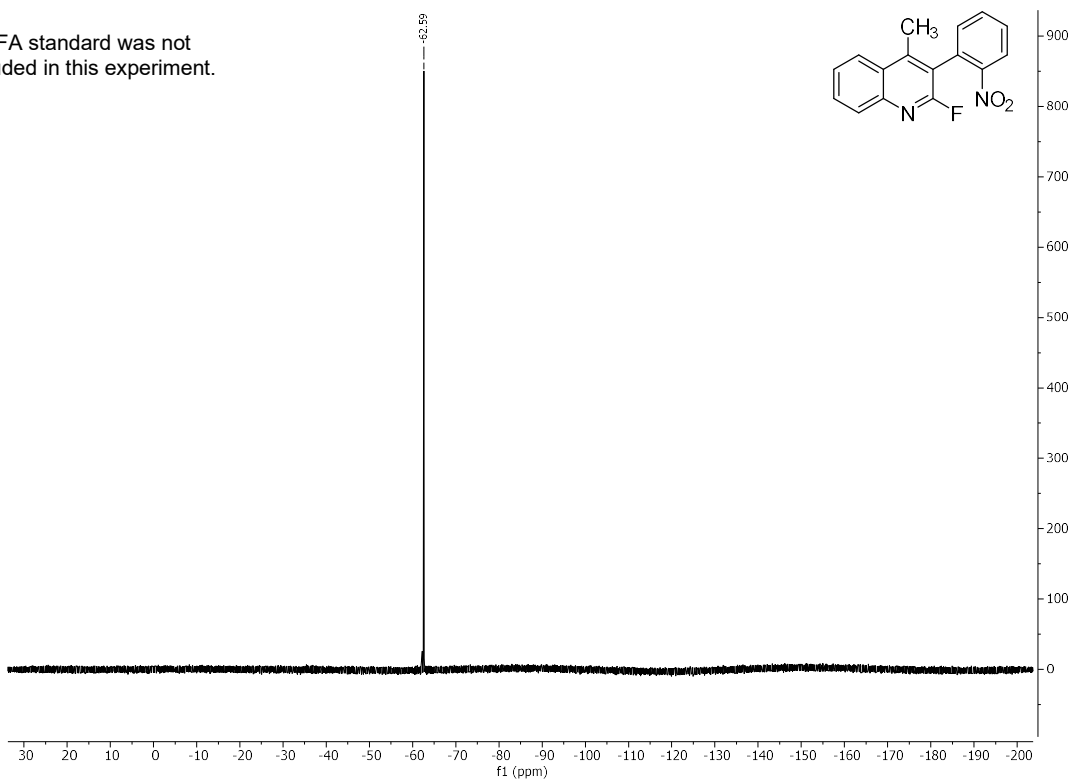


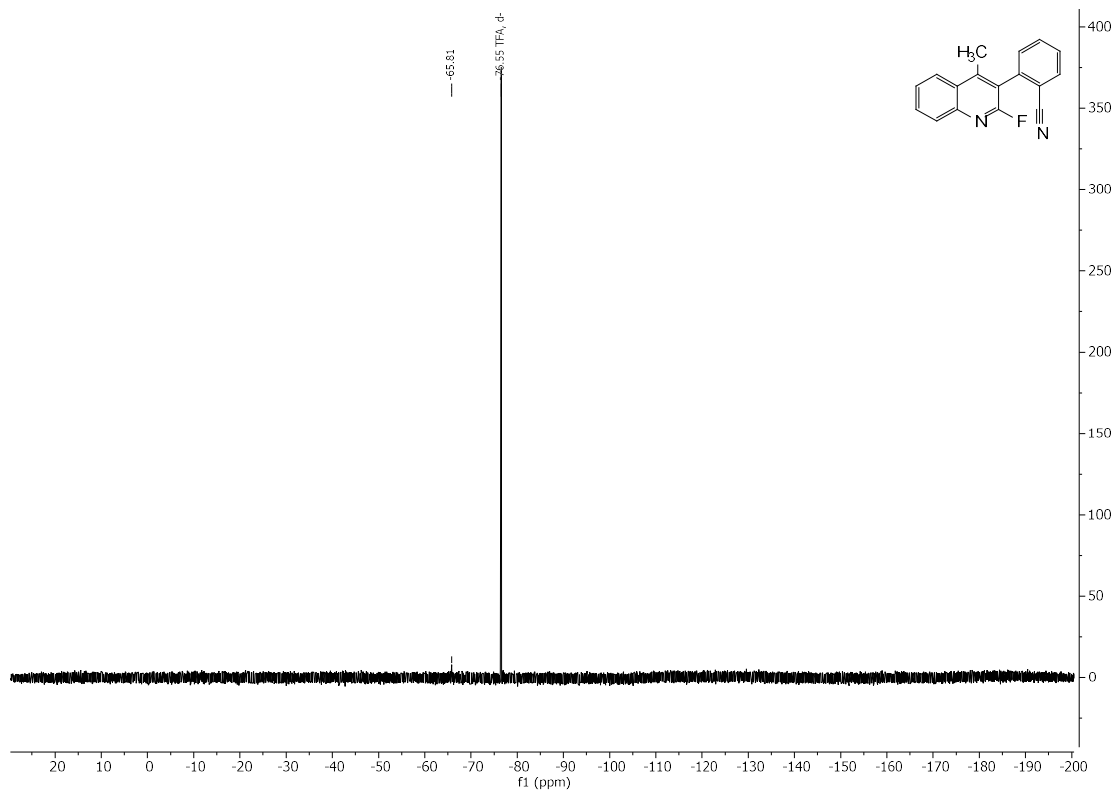
^1H , ^{13}C , and ^{19}F NMR Spectral Data of **98**



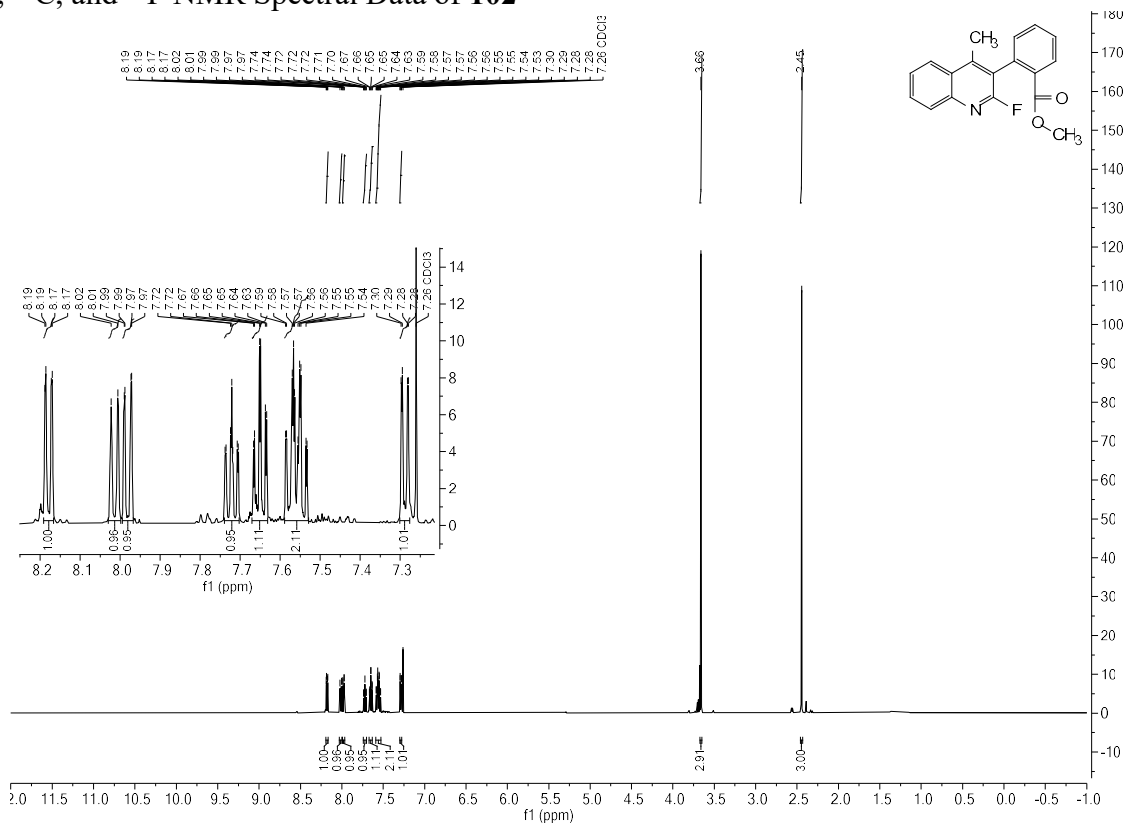


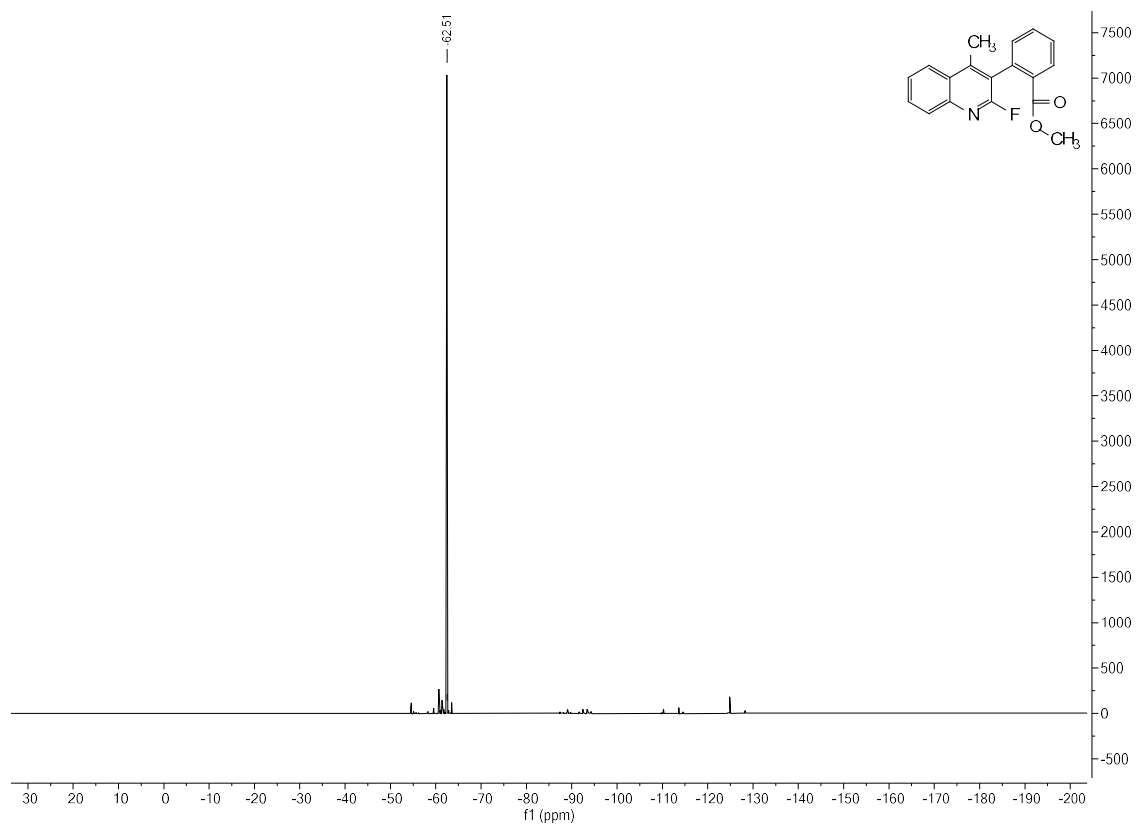
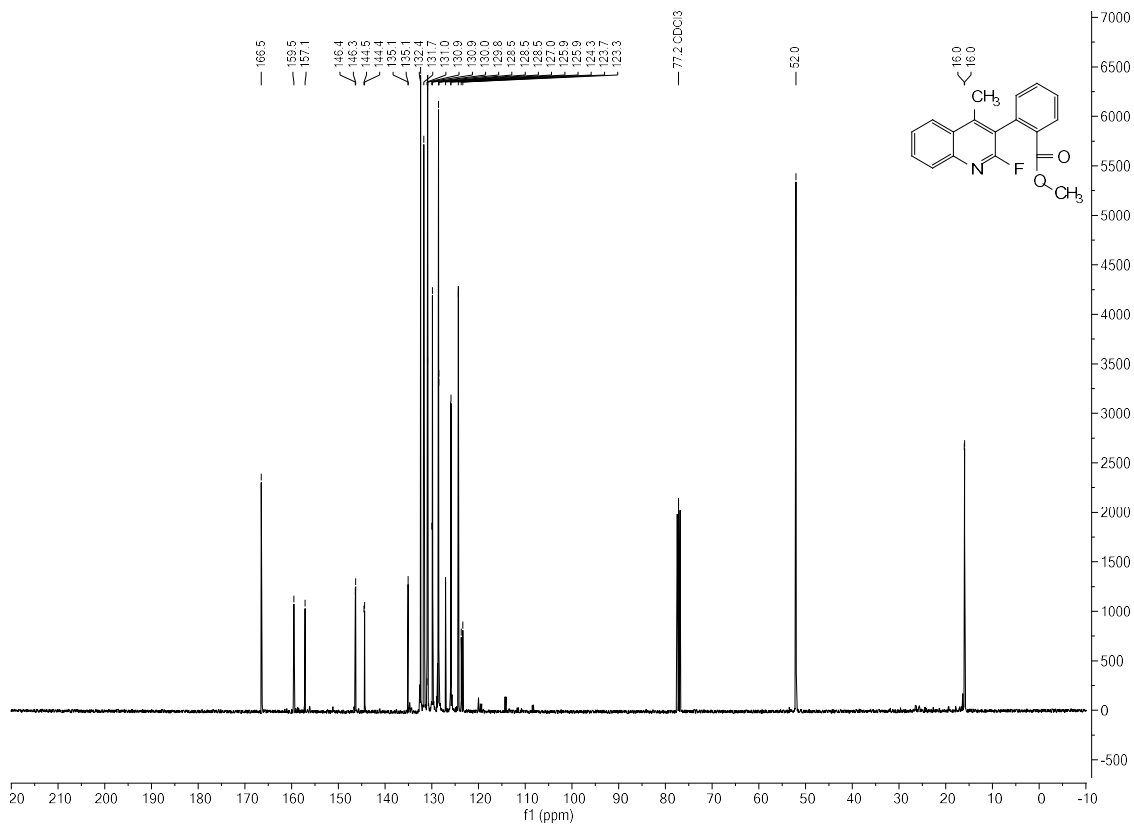
TFA standard was not included in this experiment.



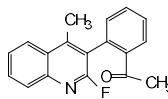
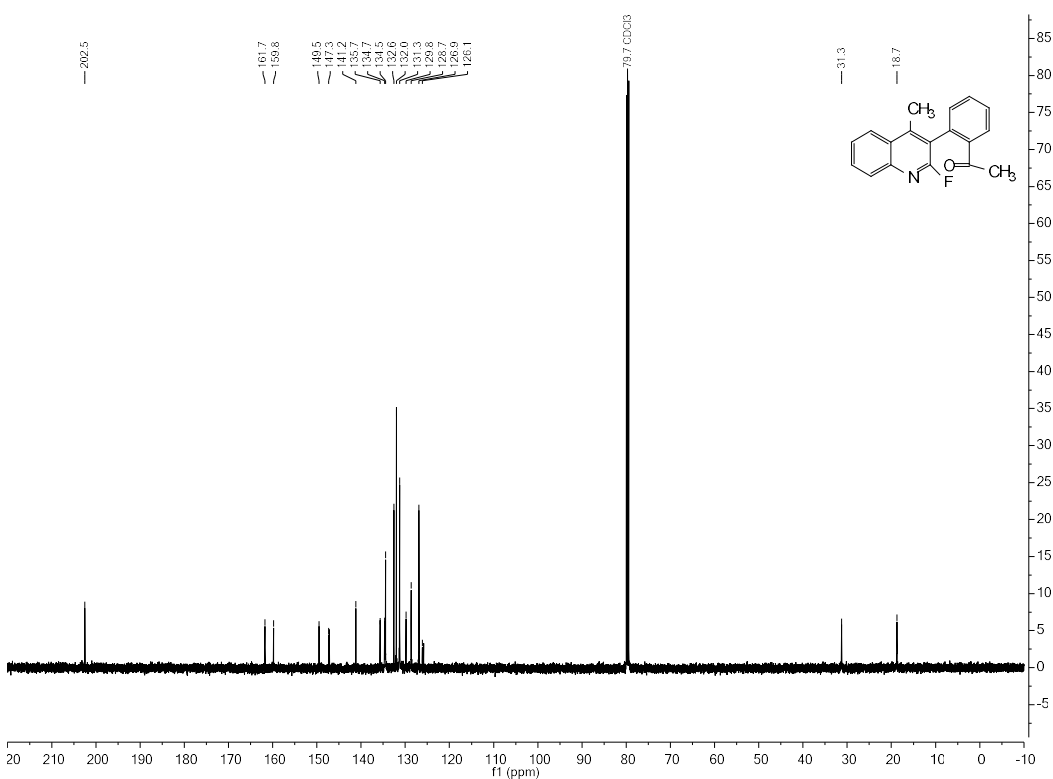
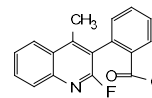
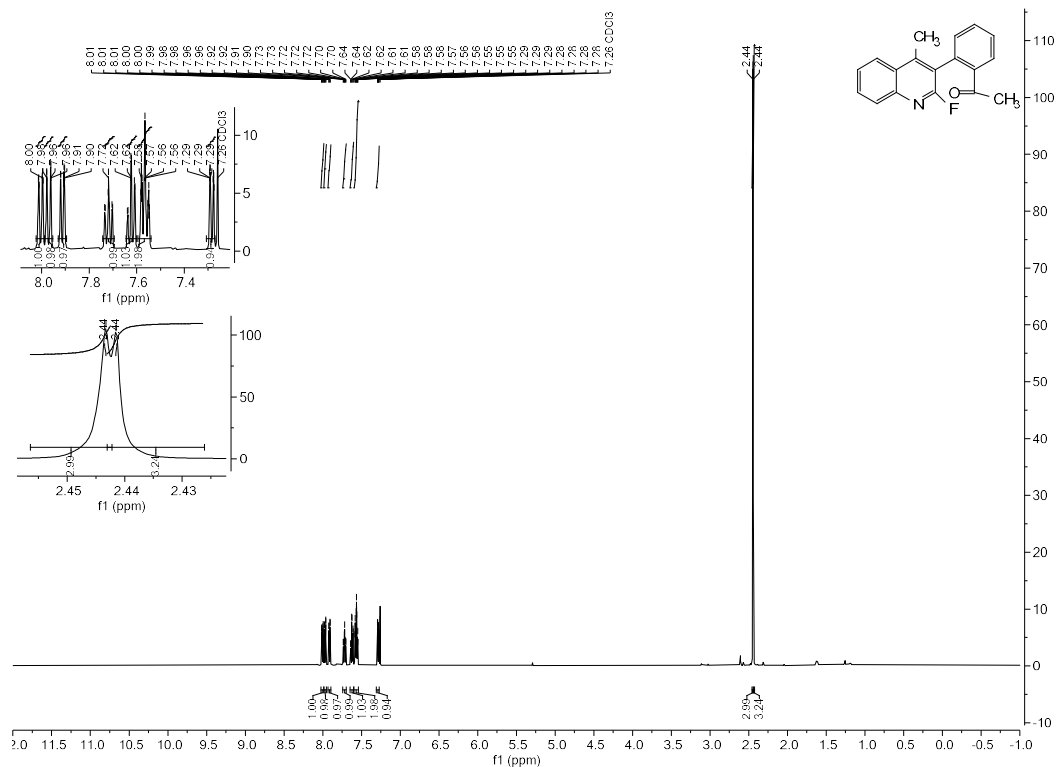


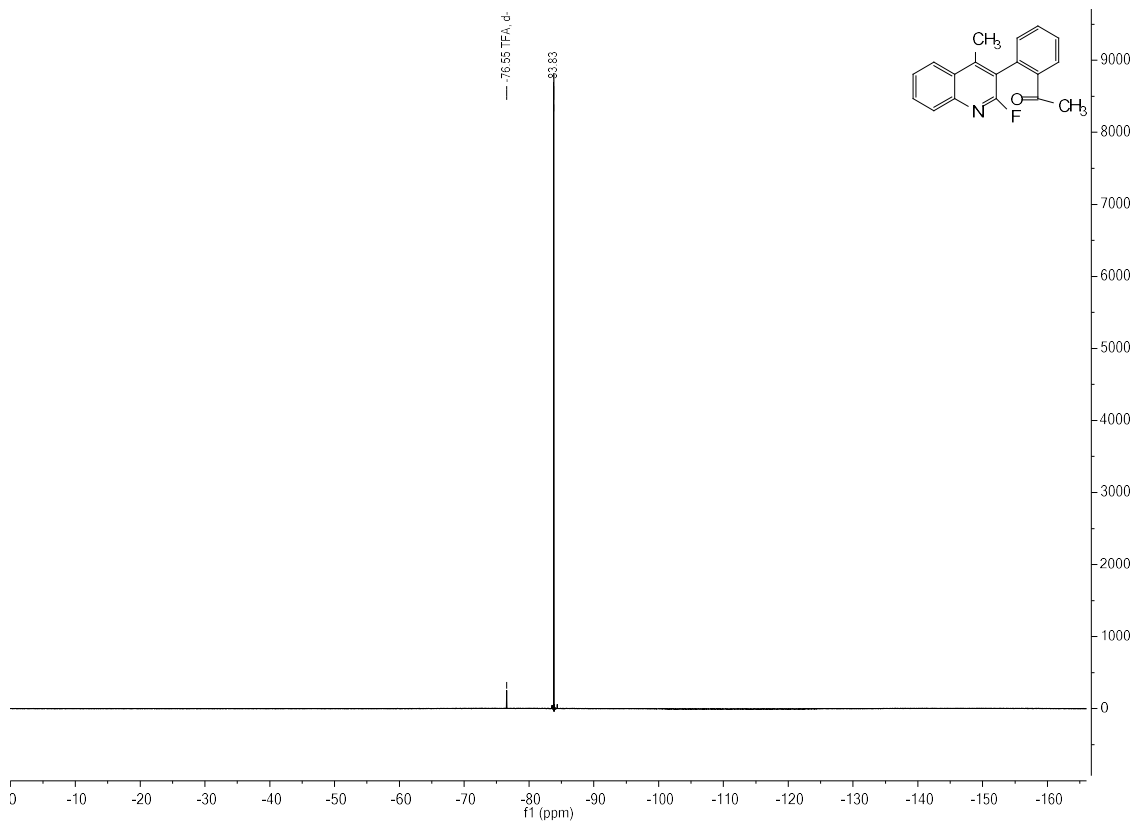
^1H , ^{13}C , and ^{19}F NMR Spectral Data of 102



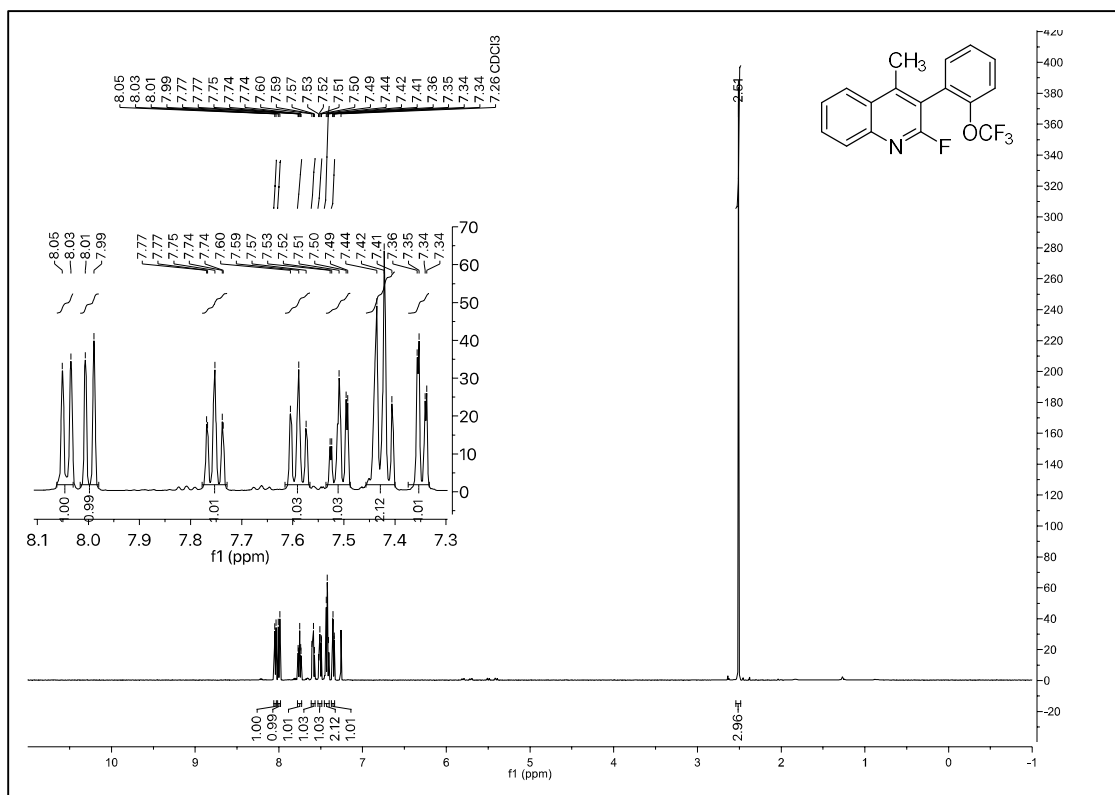


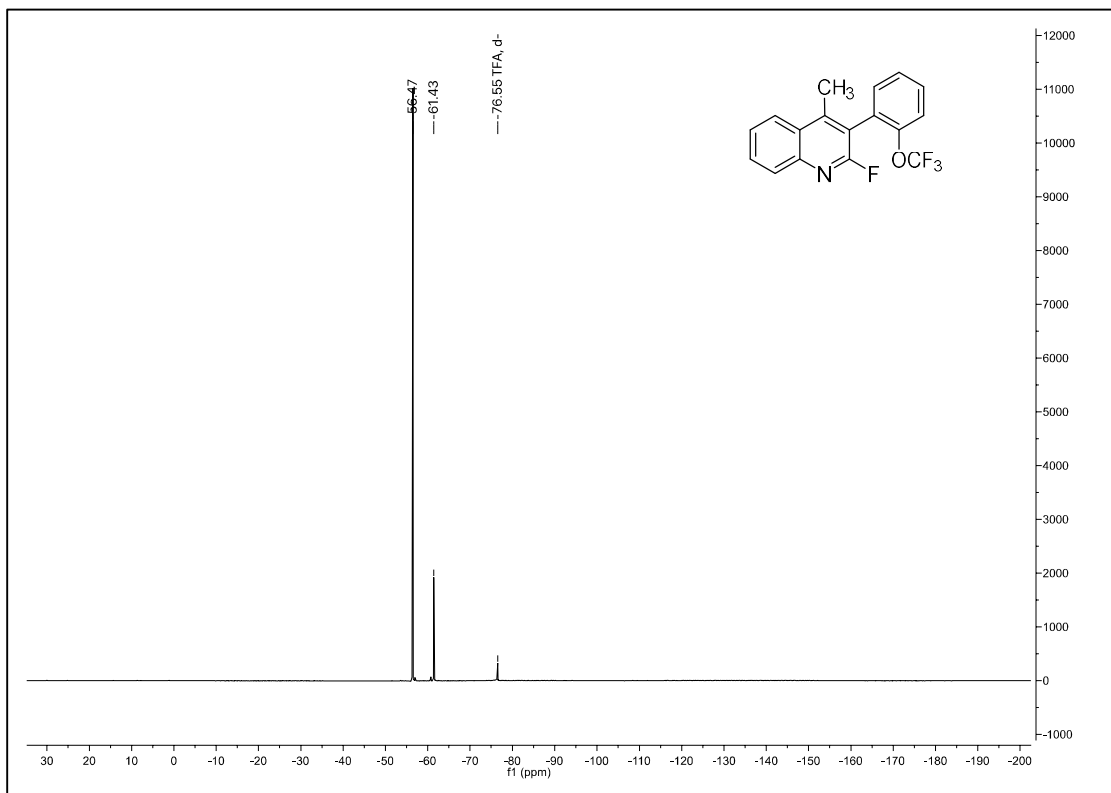
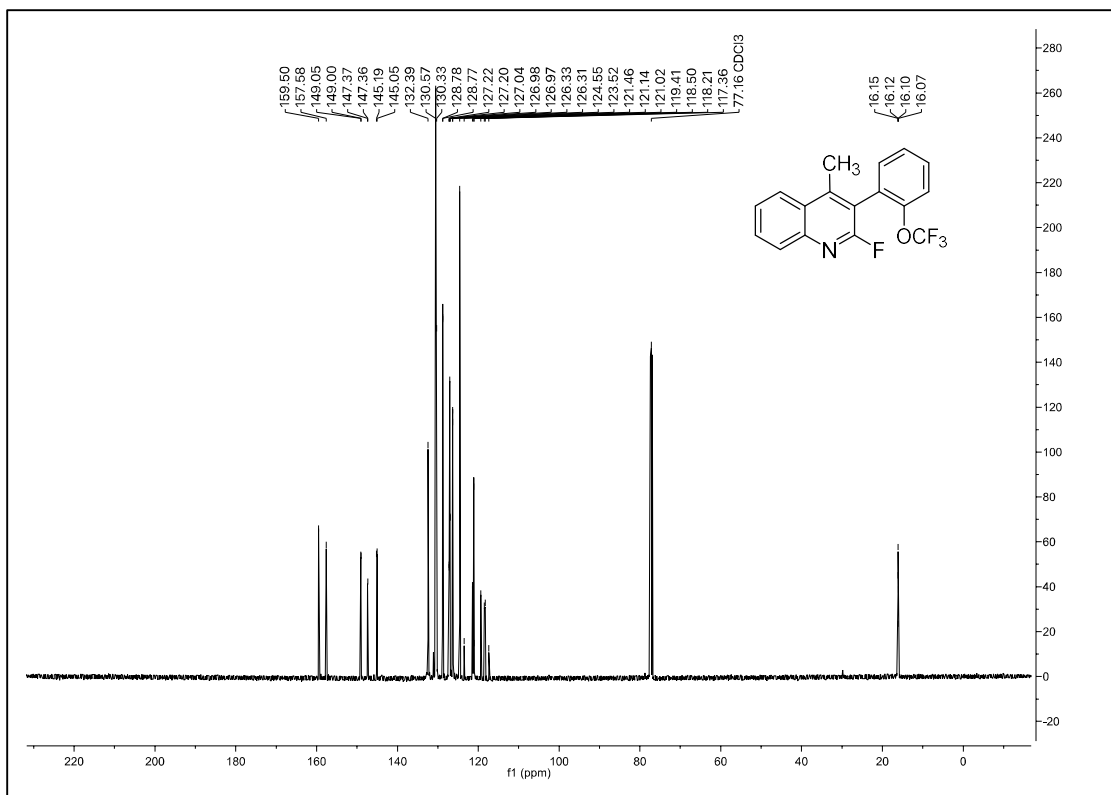
^1H , ^{13}C , and ^{19}F NMR Spectral Data of **104**



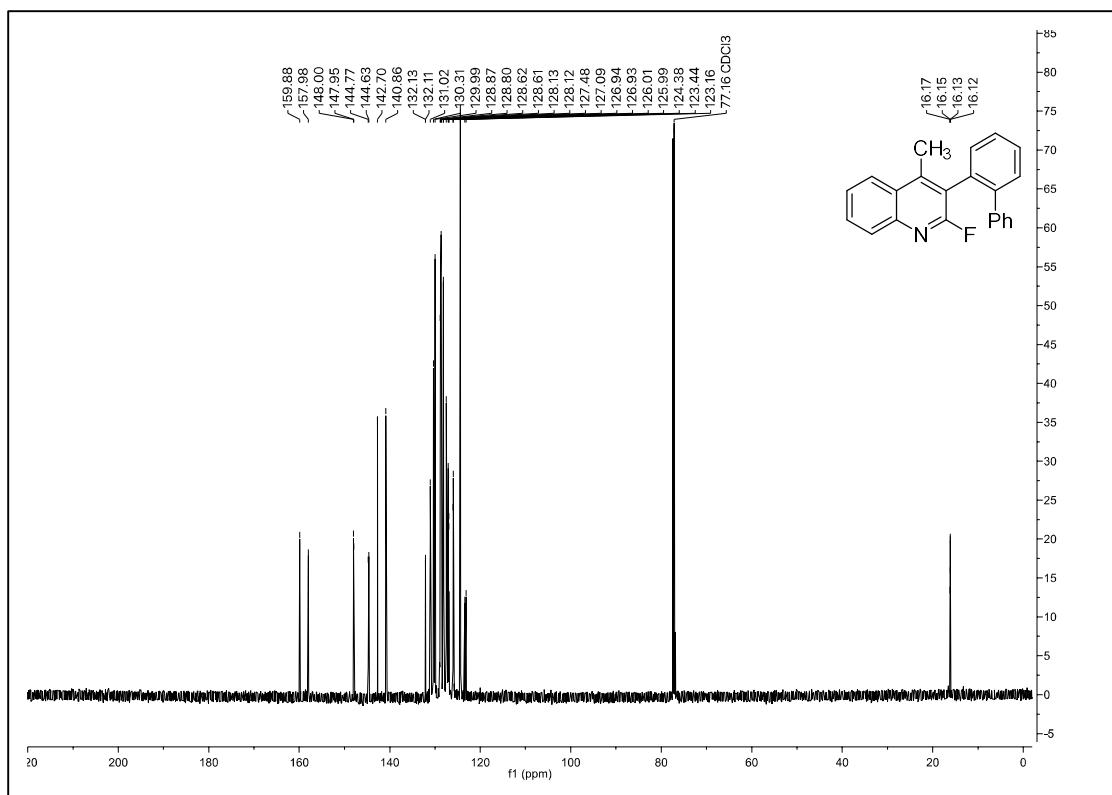
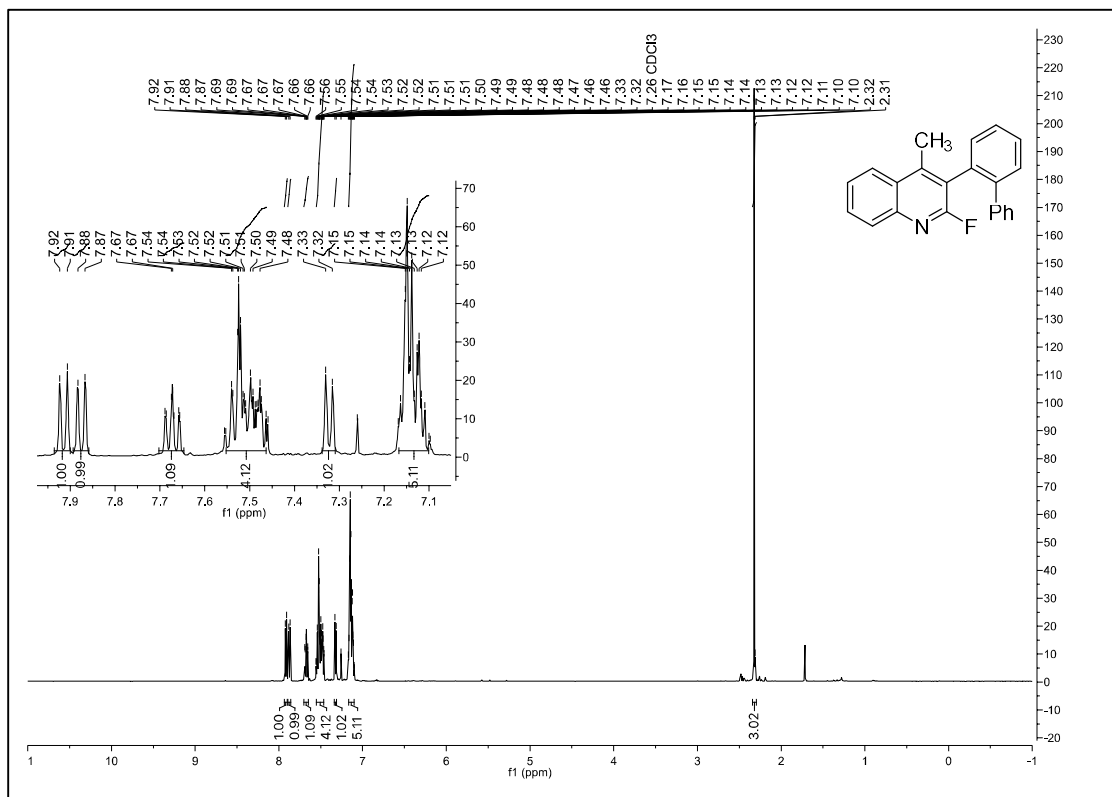


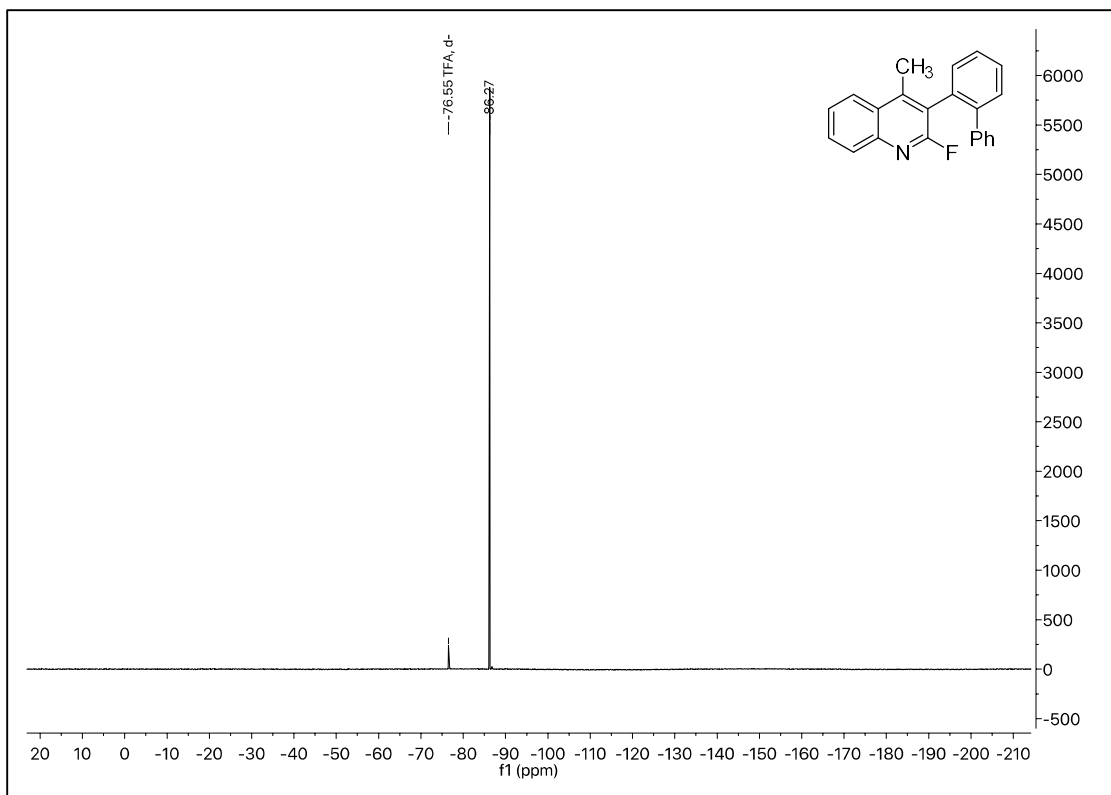
¹H, ¹³C, and ¹⁹F NMR Spectral Data of 106



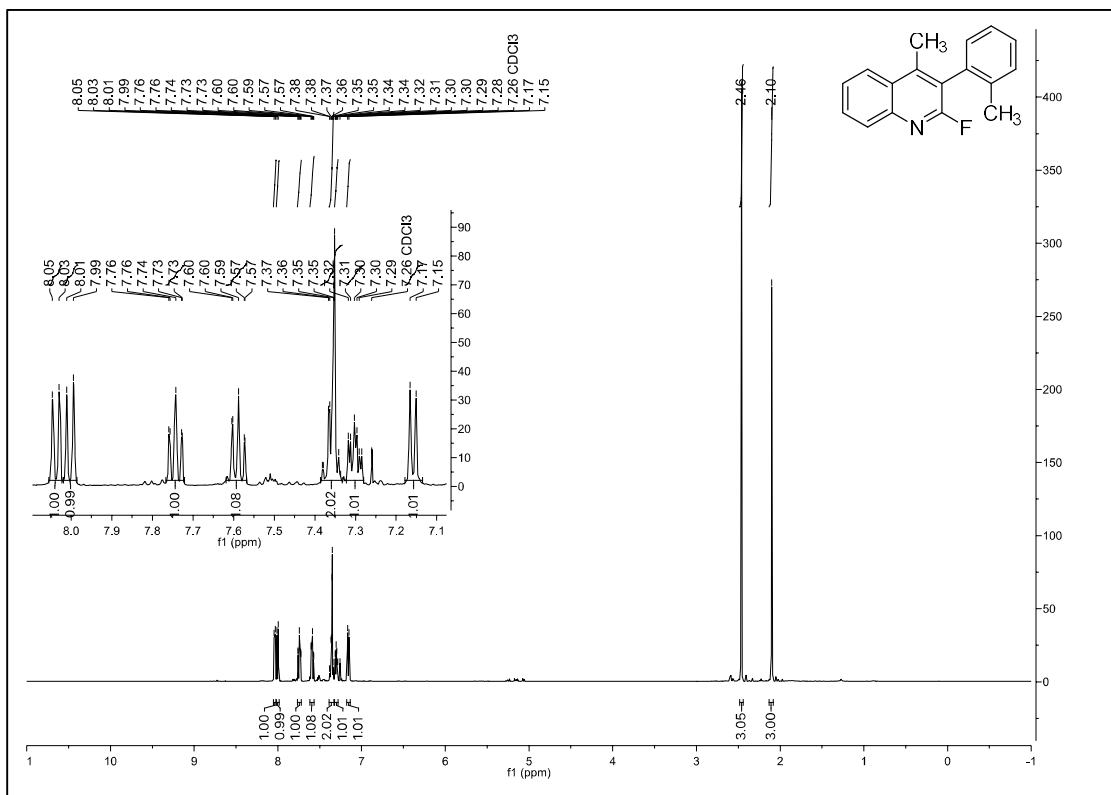


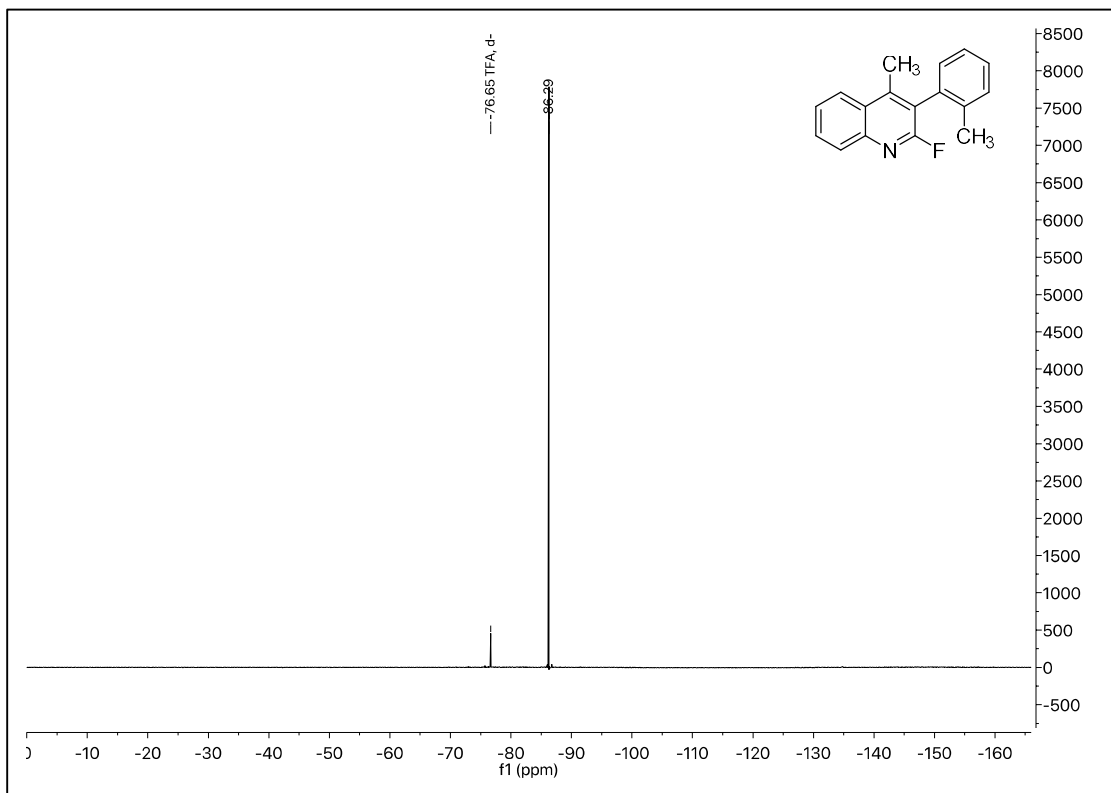
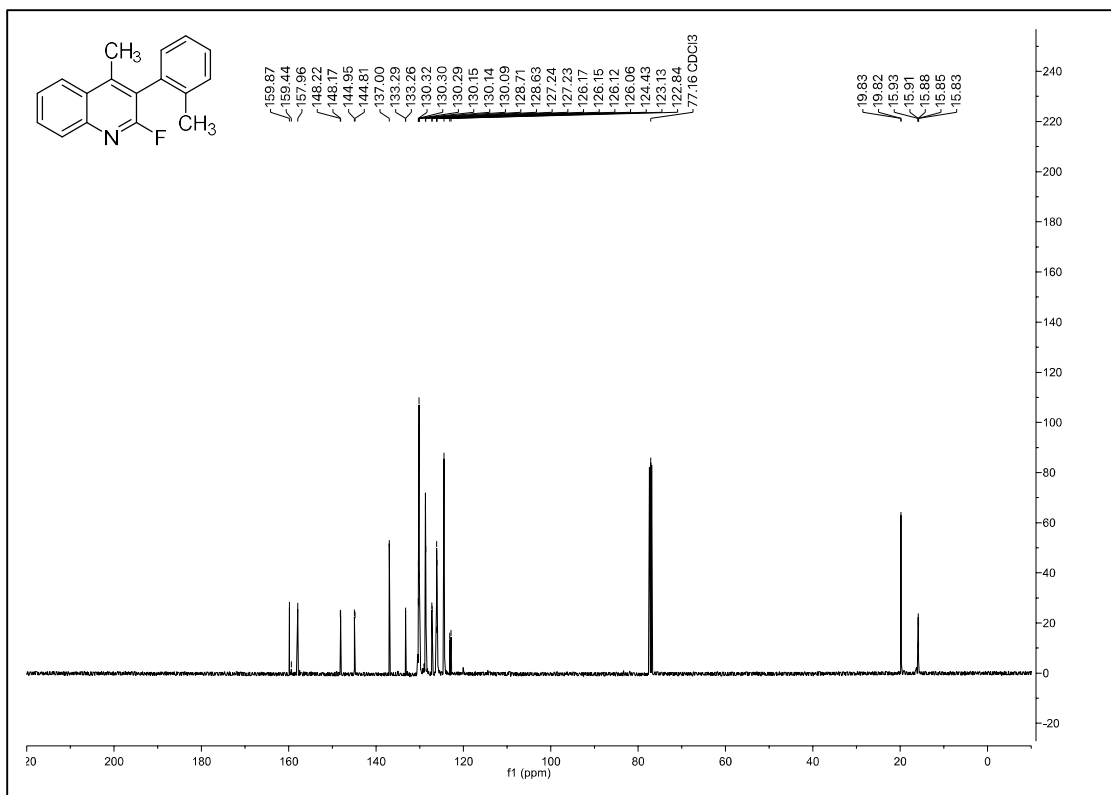
^1H , ^{13}C , and ^{19}F NMR Spectral Data of **108**



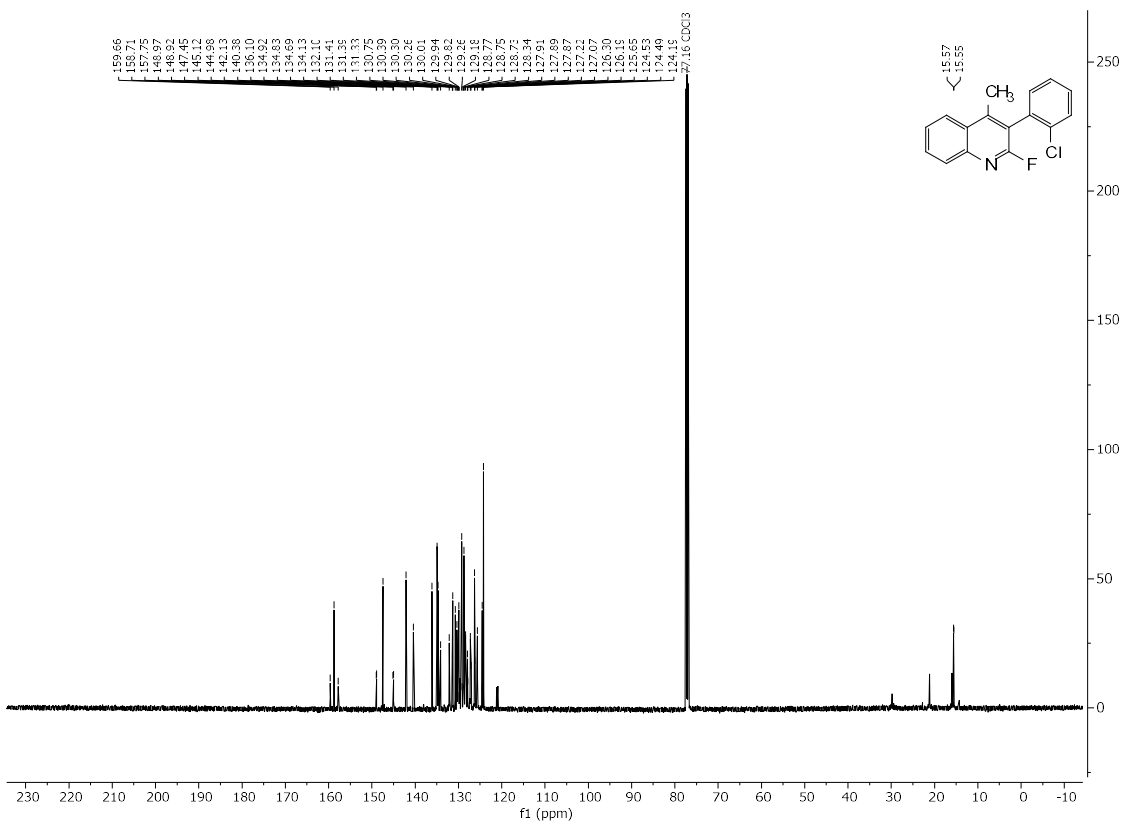
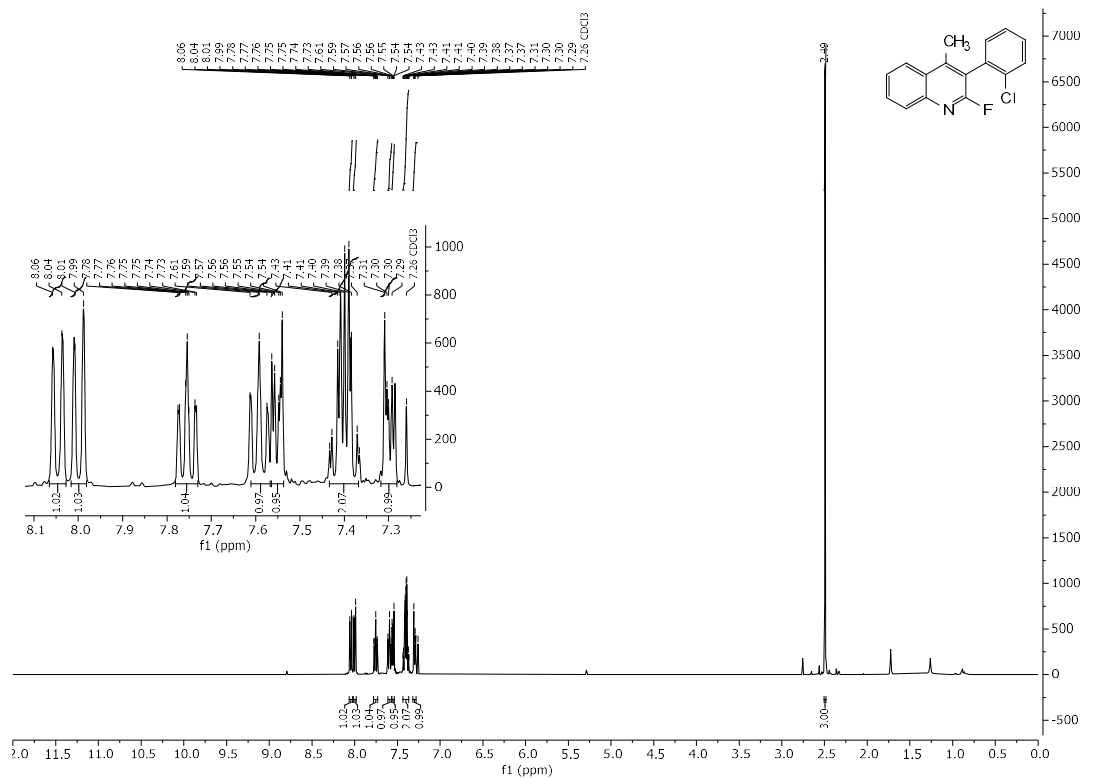


^1H , ^{13}C , and ^{19}F NMR Spectral Data of **110**

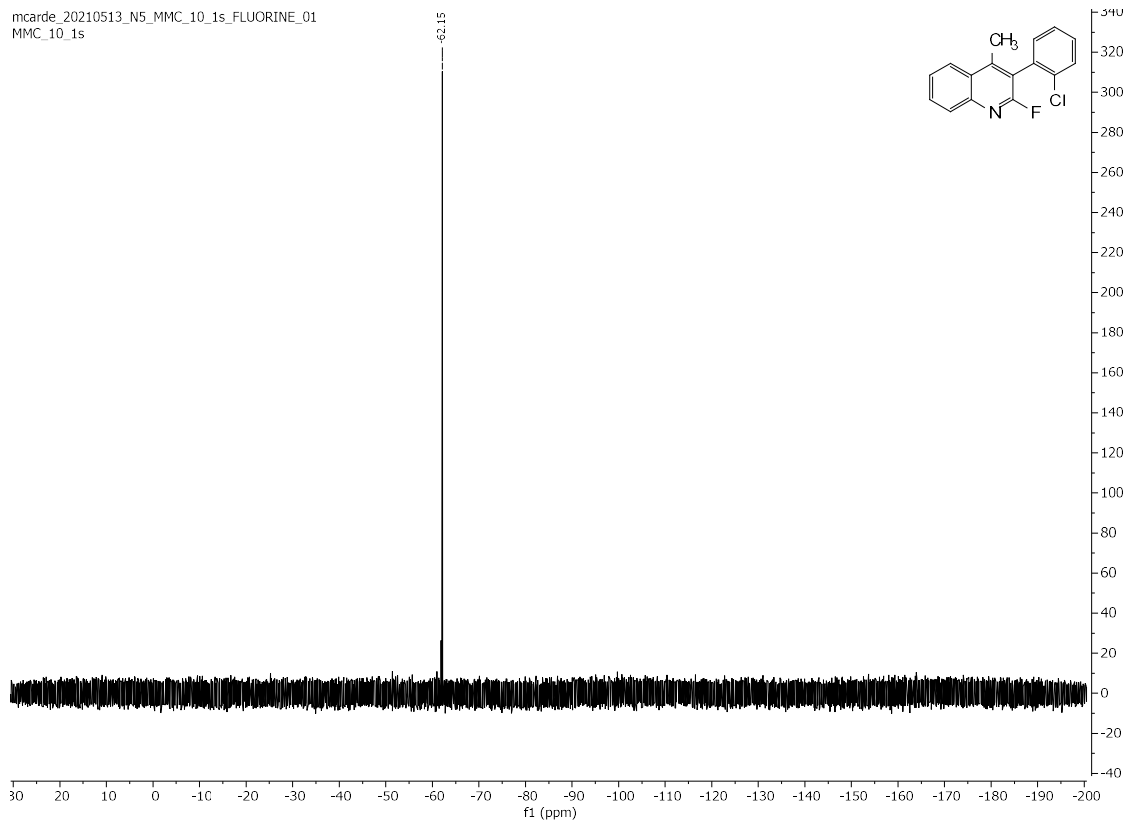




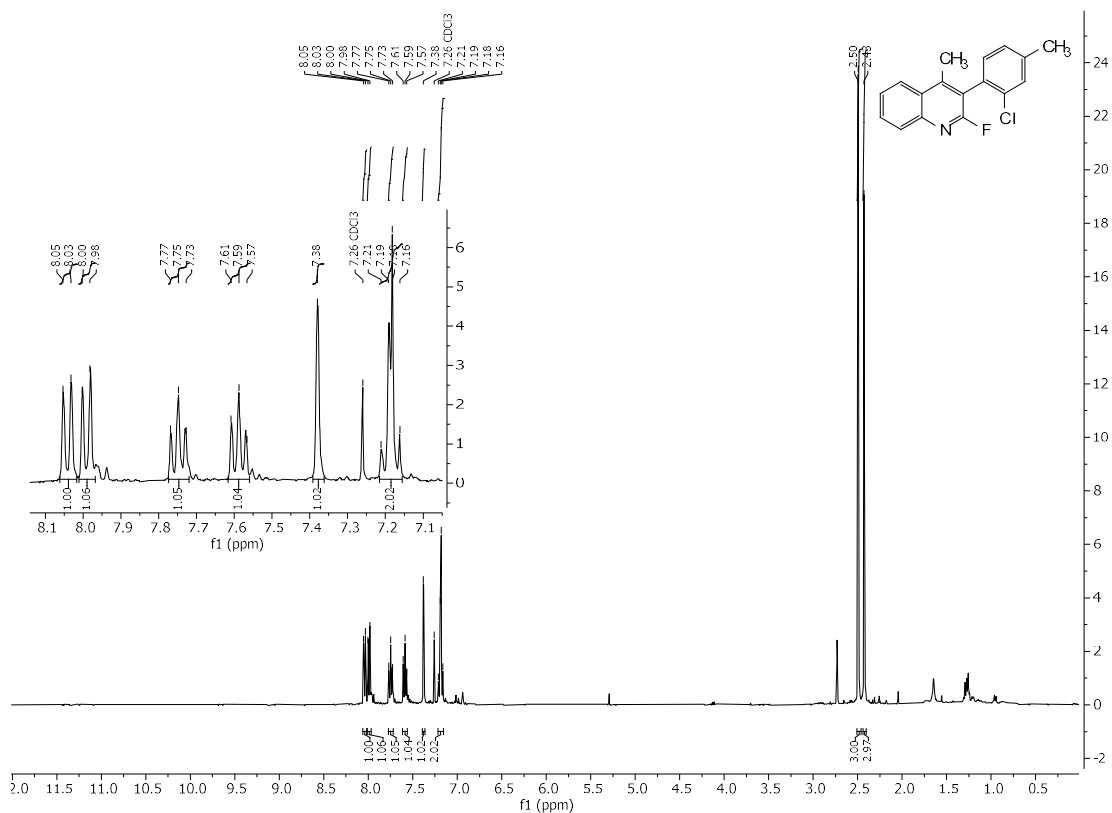
^1H , ^{13}C , and ^{19}F NMR Spectral Data of **112**

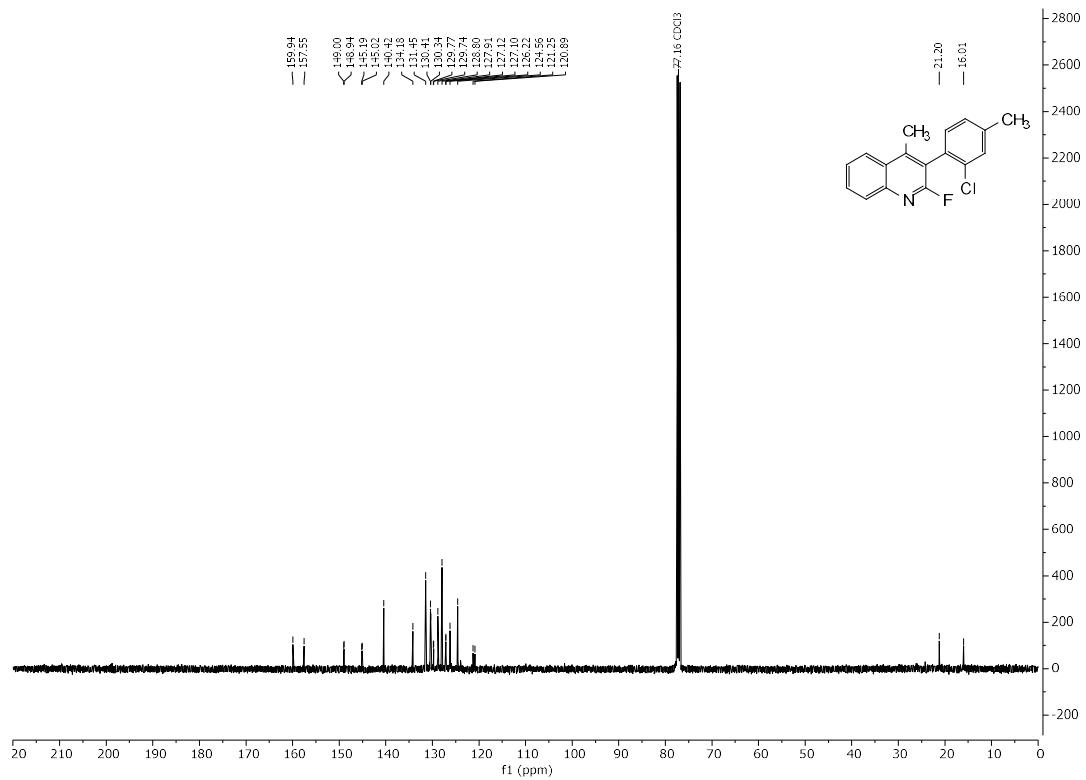


mcarde_20210513_N5_MMC_10_1s_FLUORINE_01
MMC_10_1s

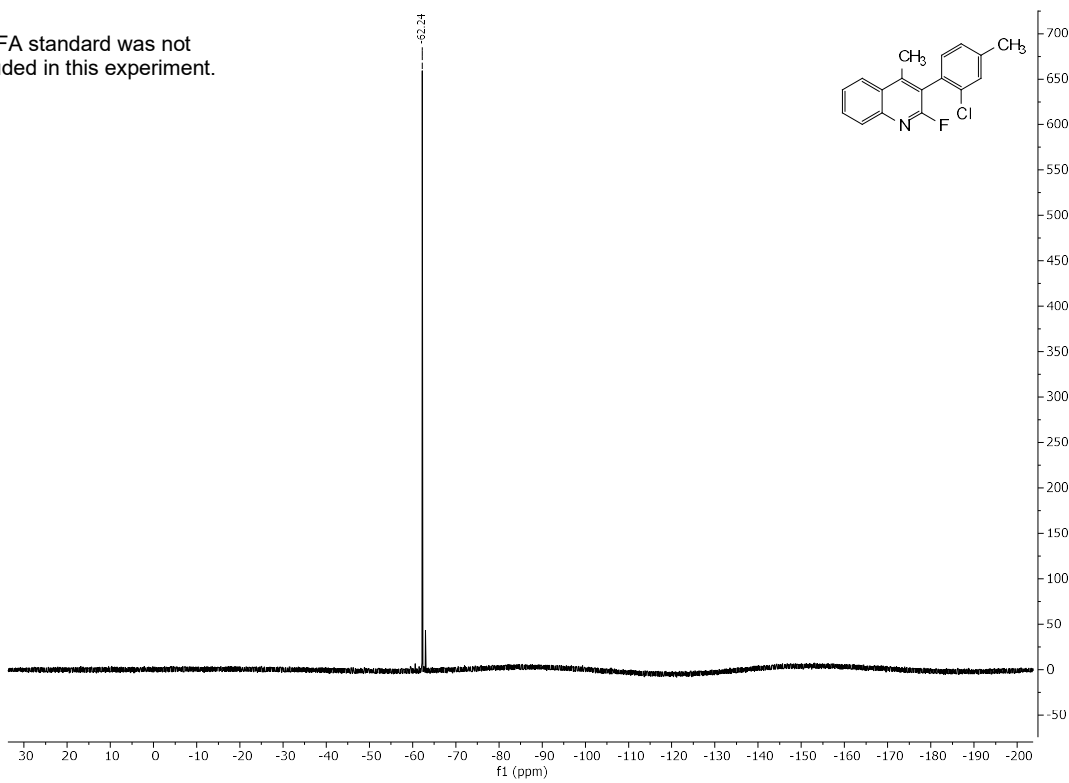


^1H , ^{13}C , and ^{19}F NMR Spectral Data of 114

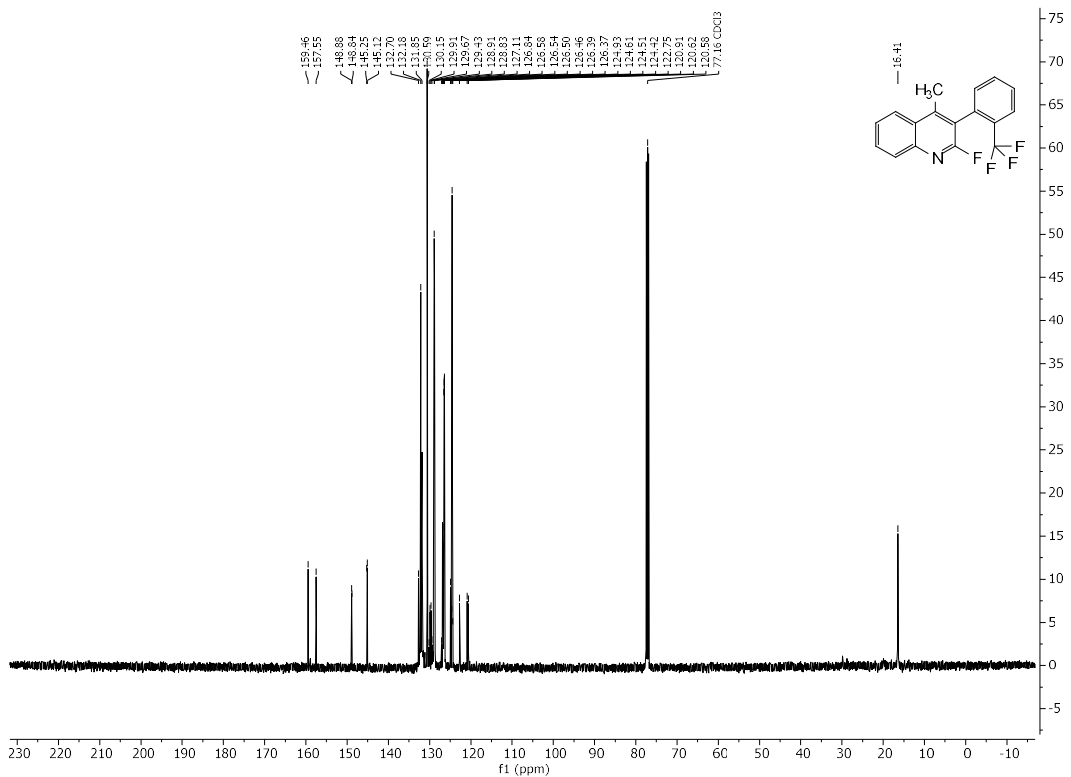
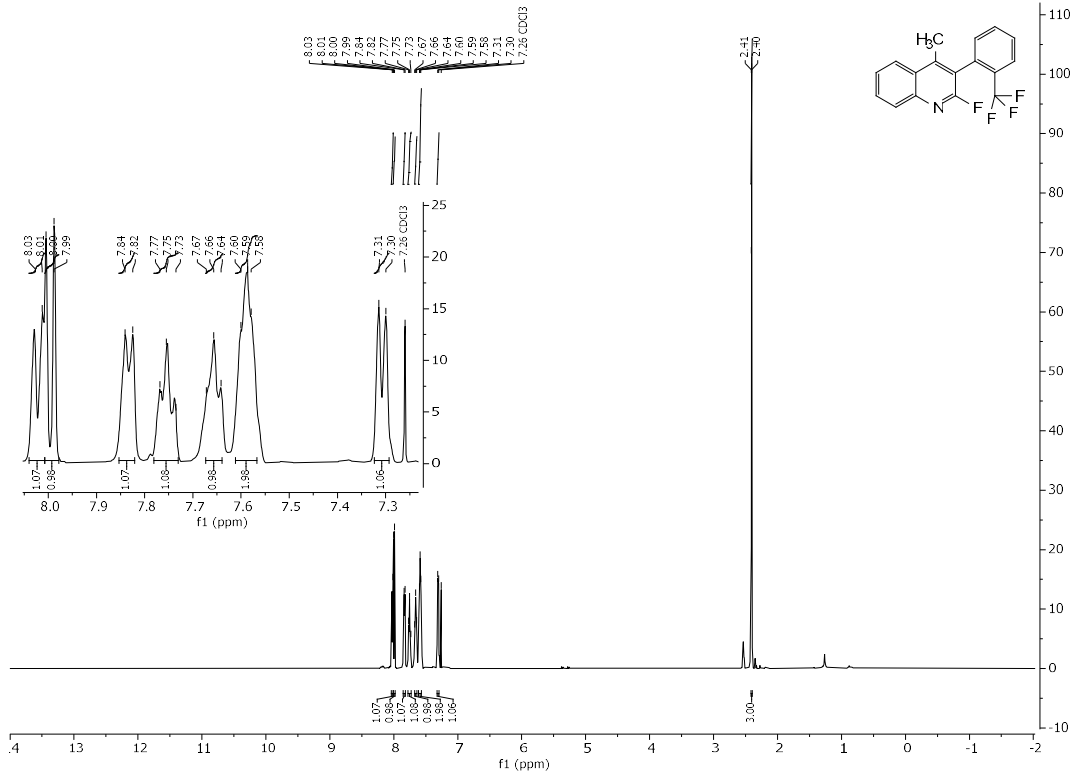




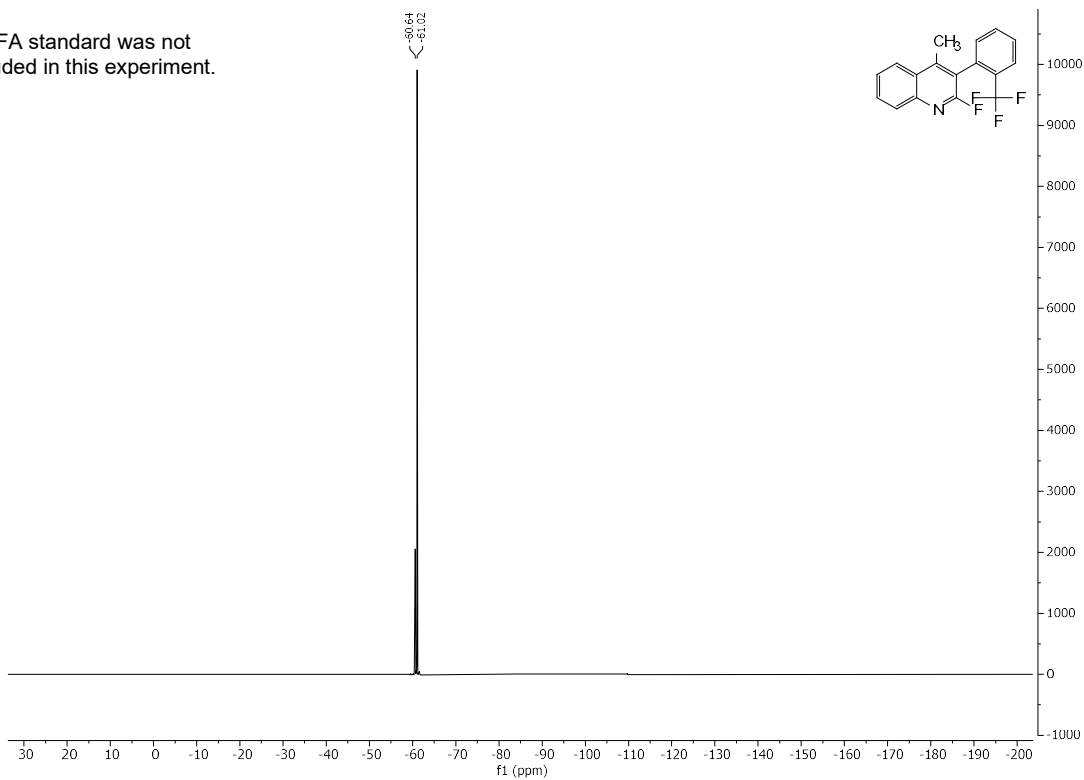
TFA standard was not included in this experiment.



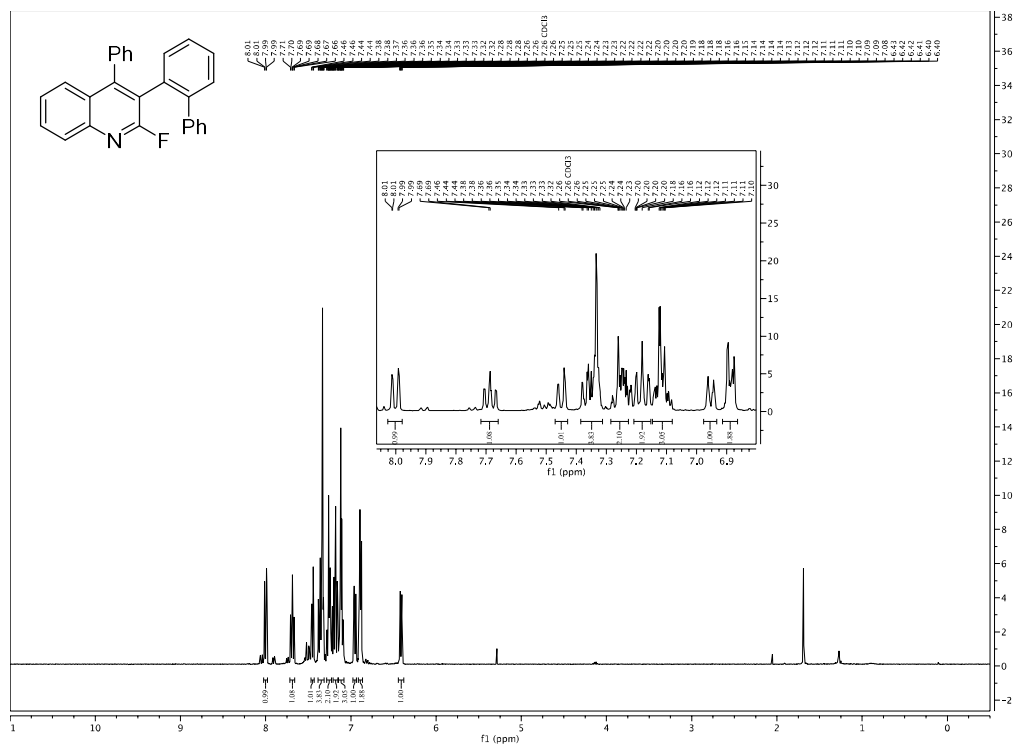
^1H , ^{13}C , and ^{19}F NMR Spectral Data of **115**

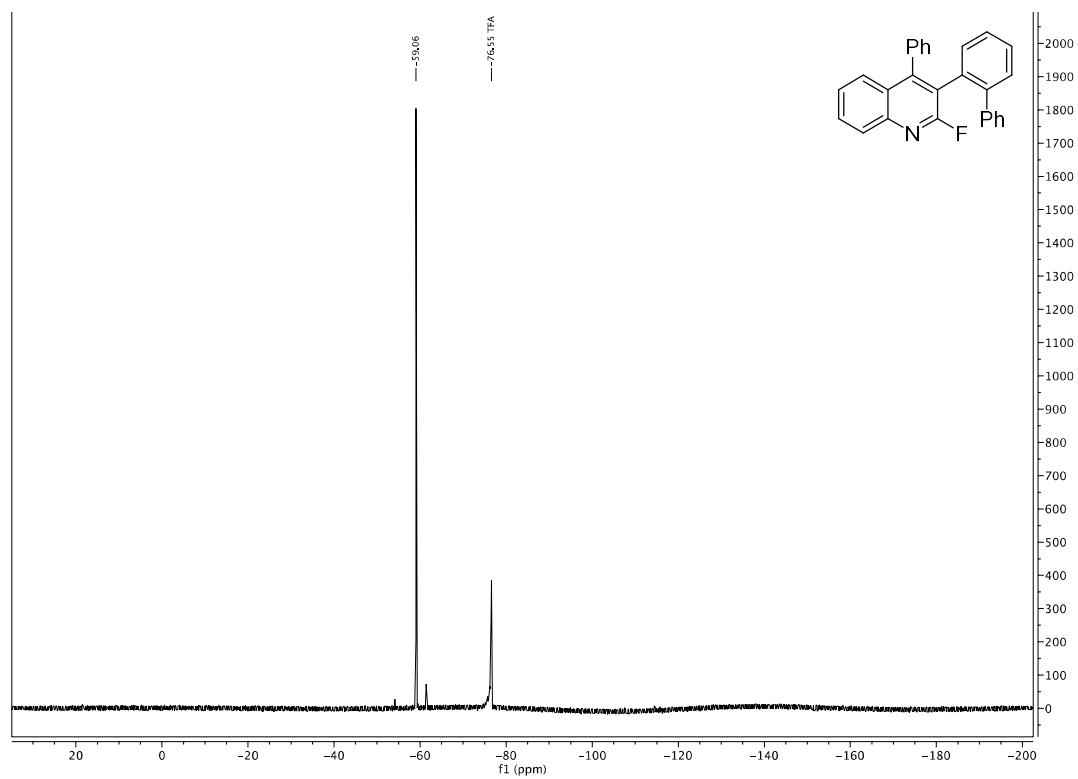
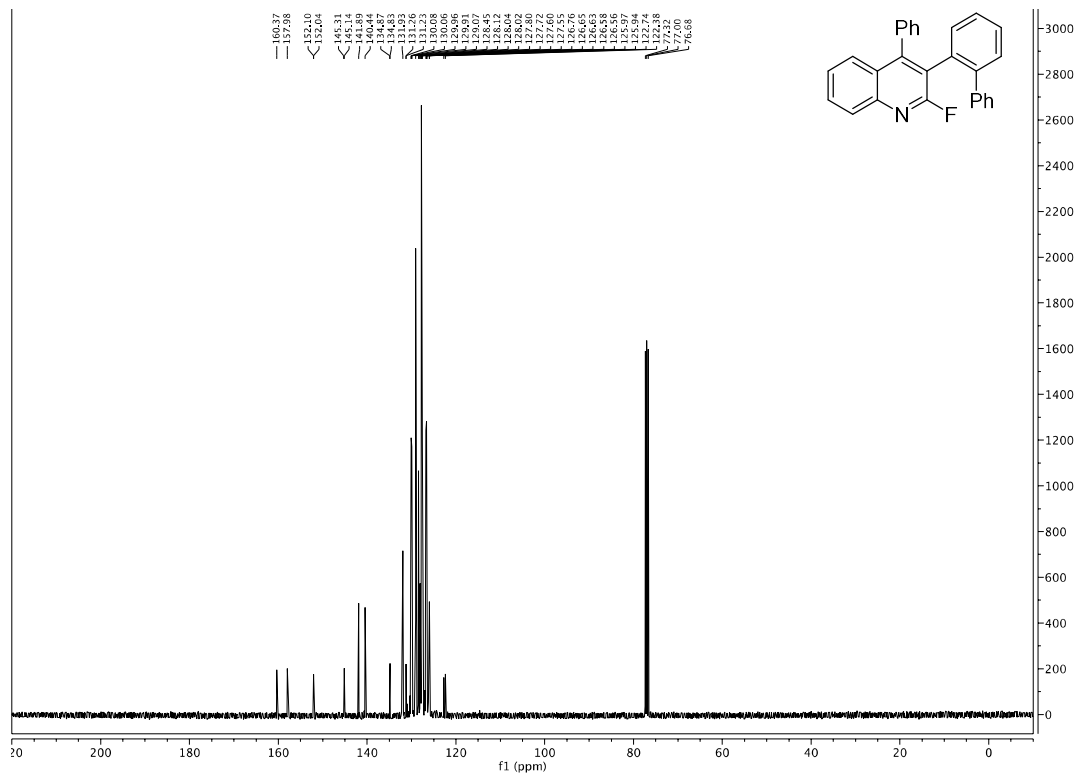


TFA standard was not included in this experiment.

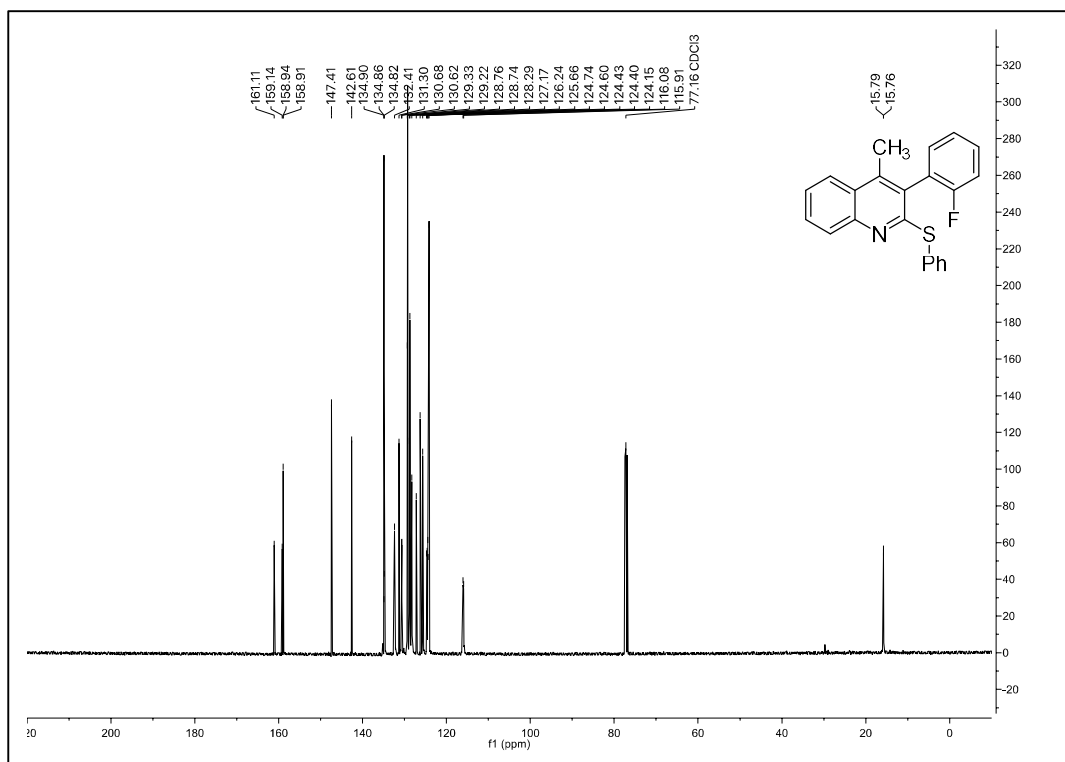
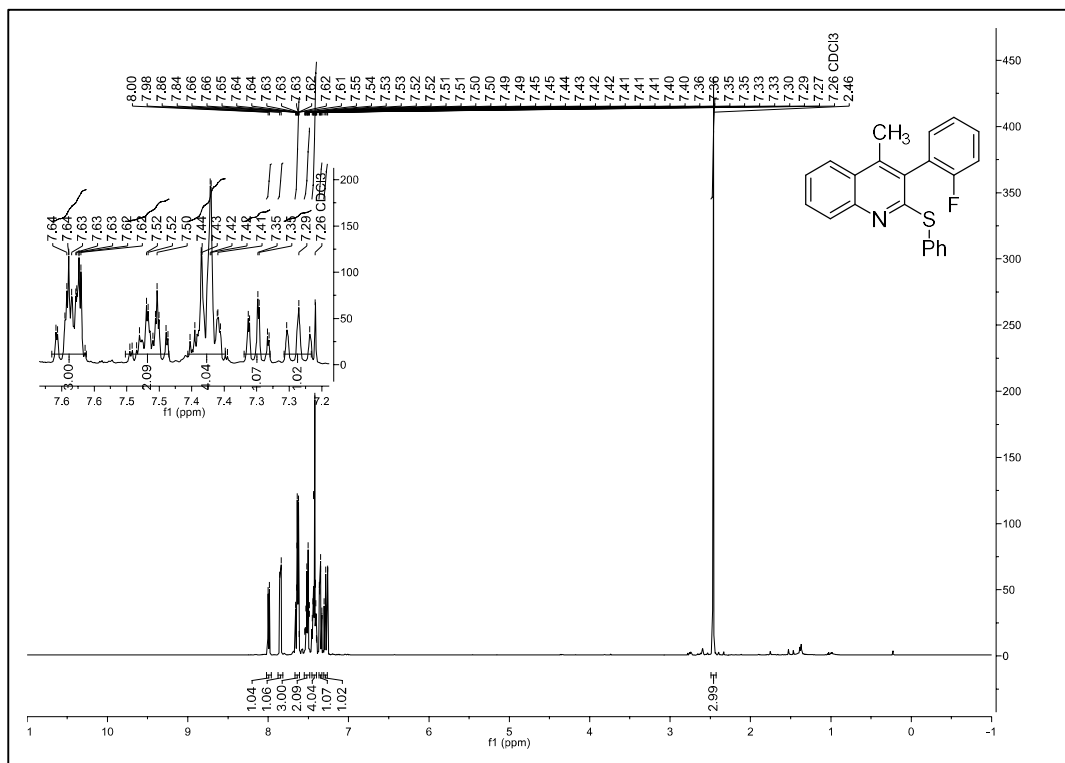


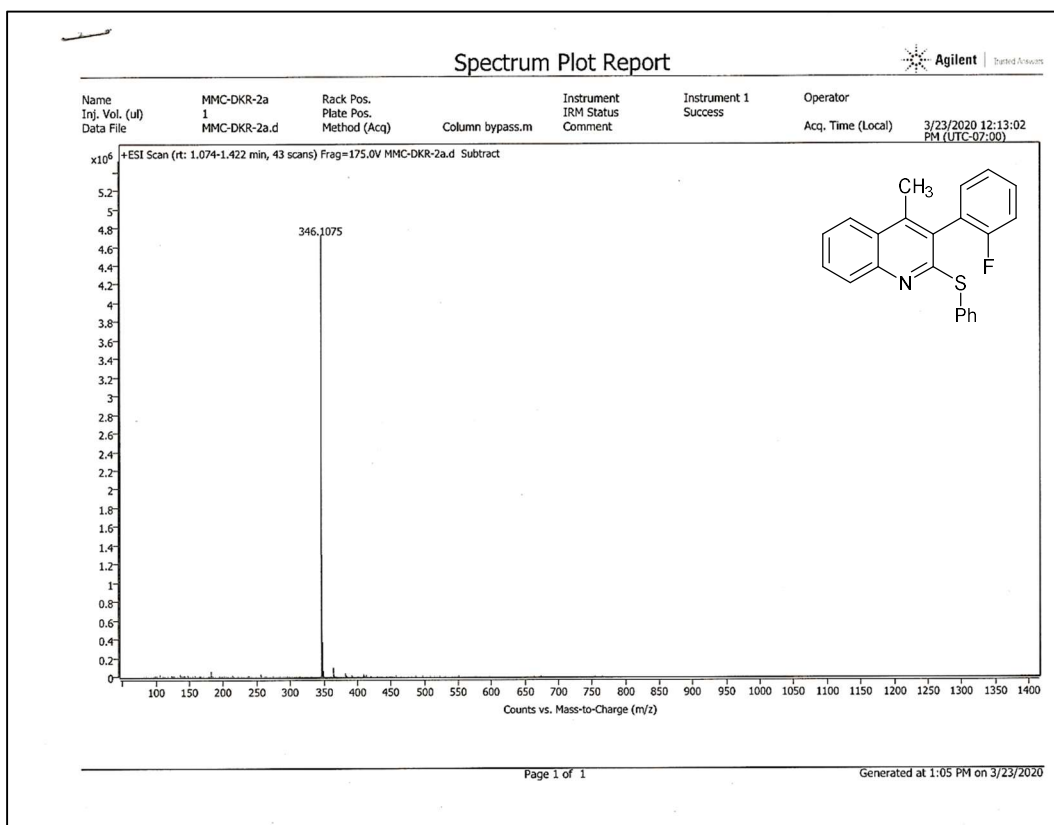
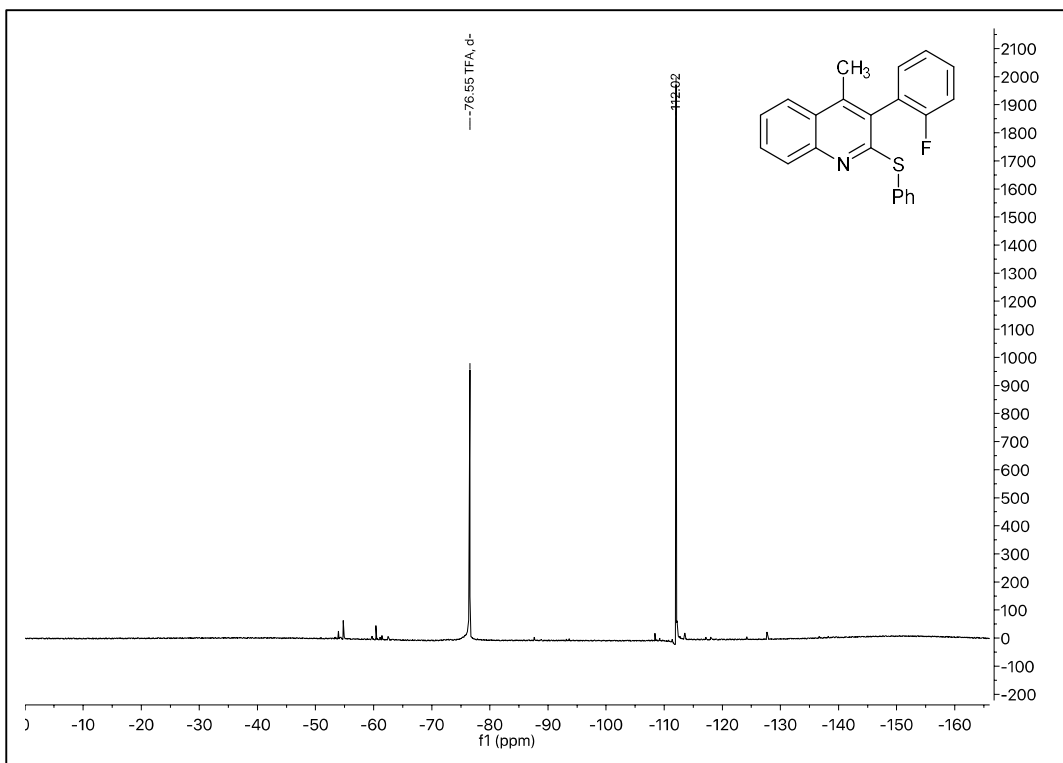
¹H, ¹³C, and ¹⁹F NMR Spectral Data of 1v



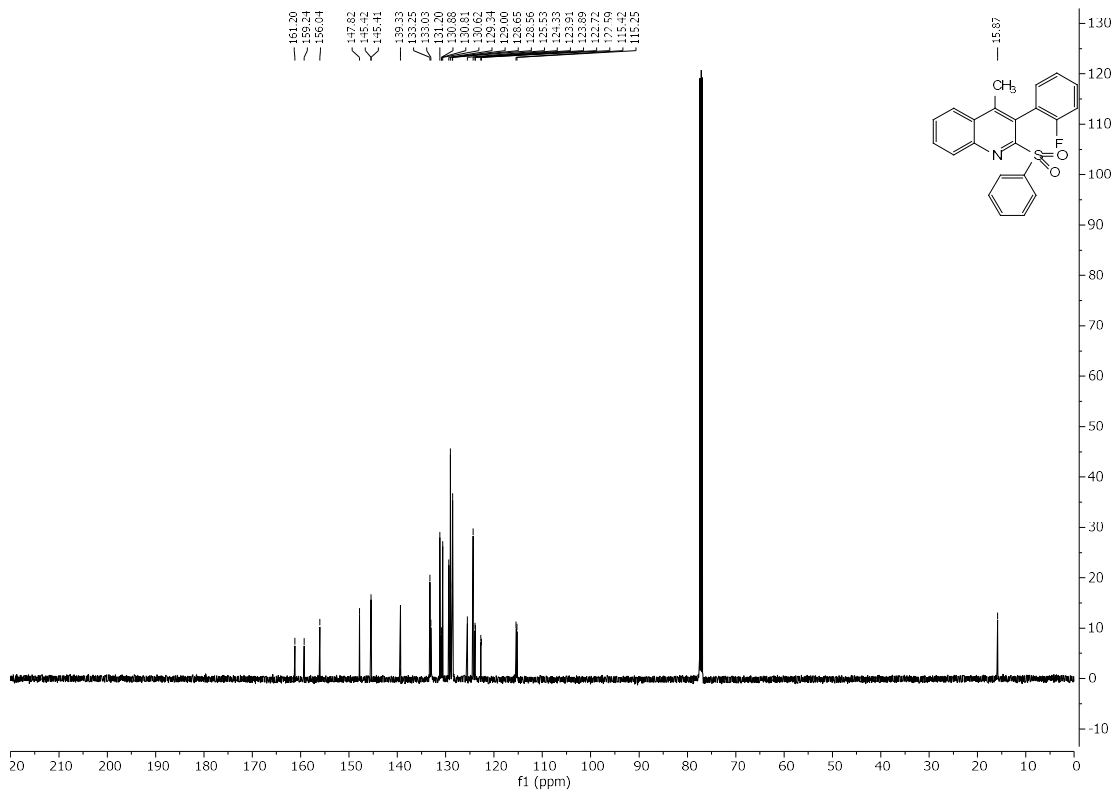
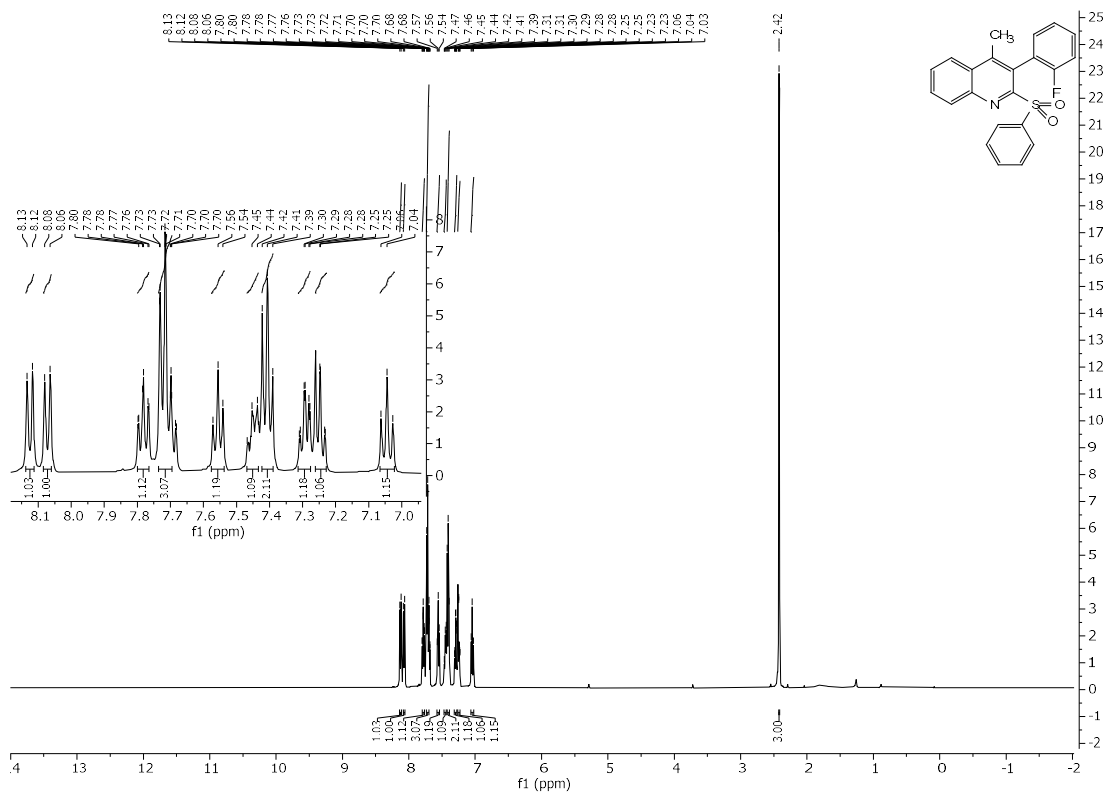


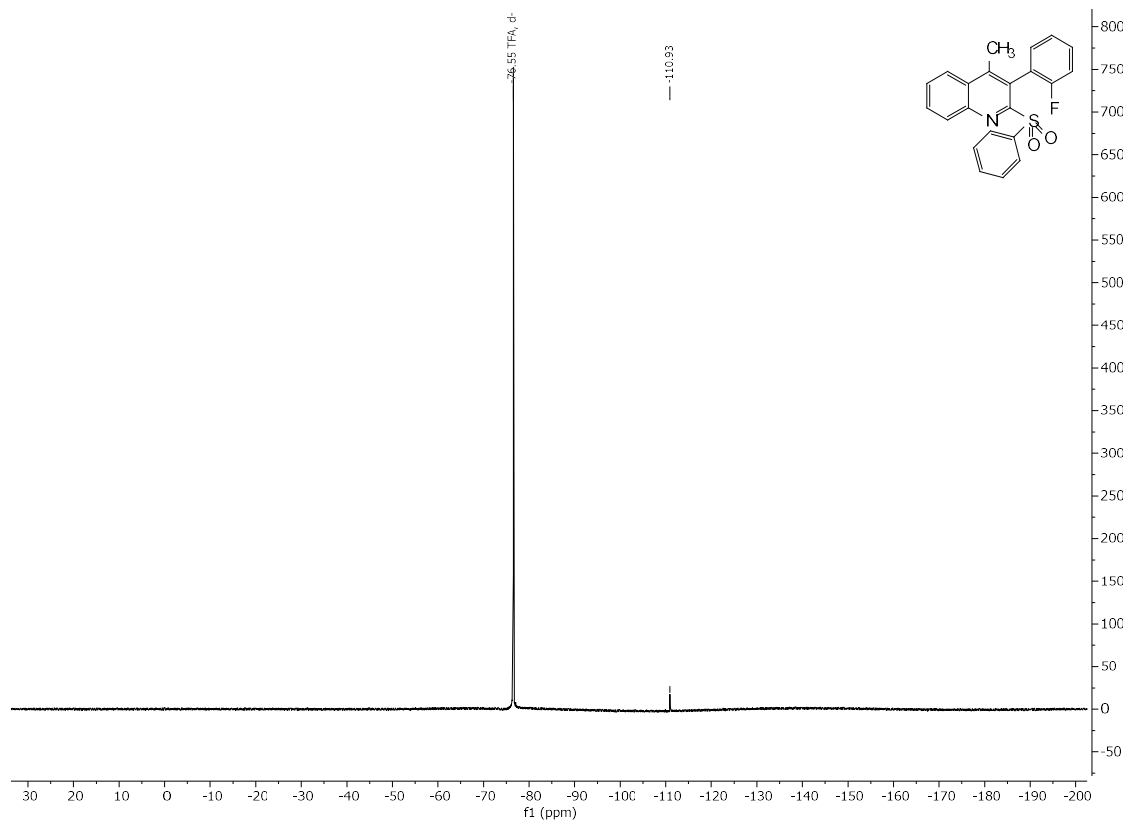
H, ¹³C, and ¹⁹F NMR and HRMS (ESI) Spectral Data of **72**



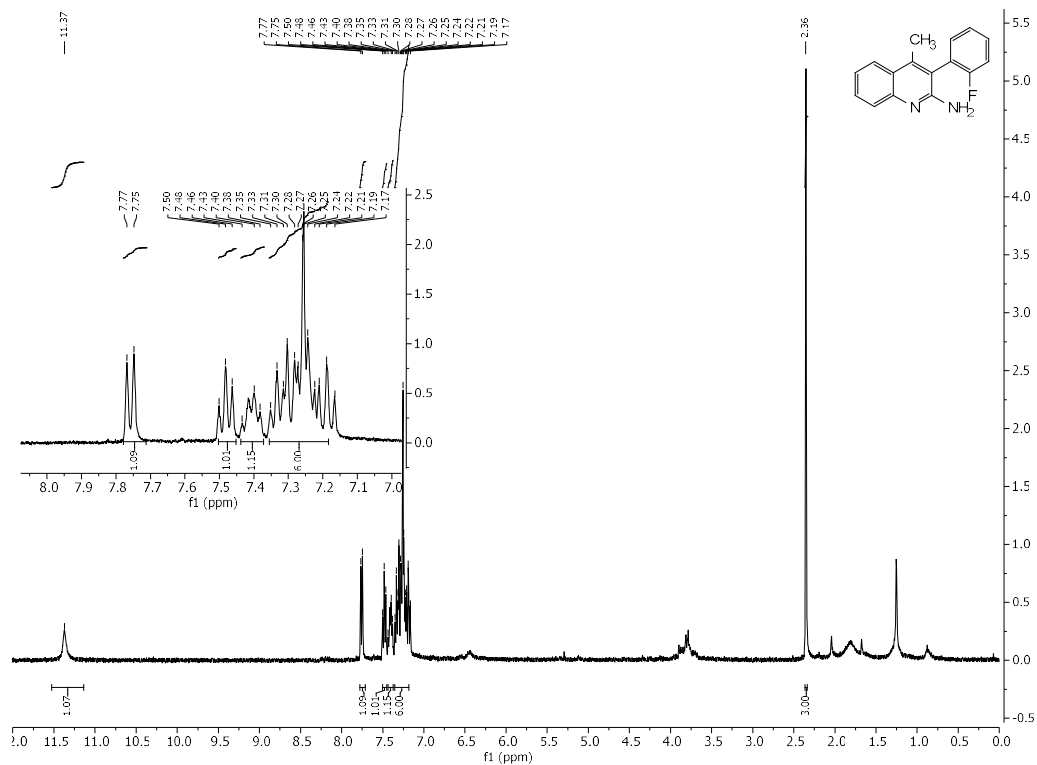


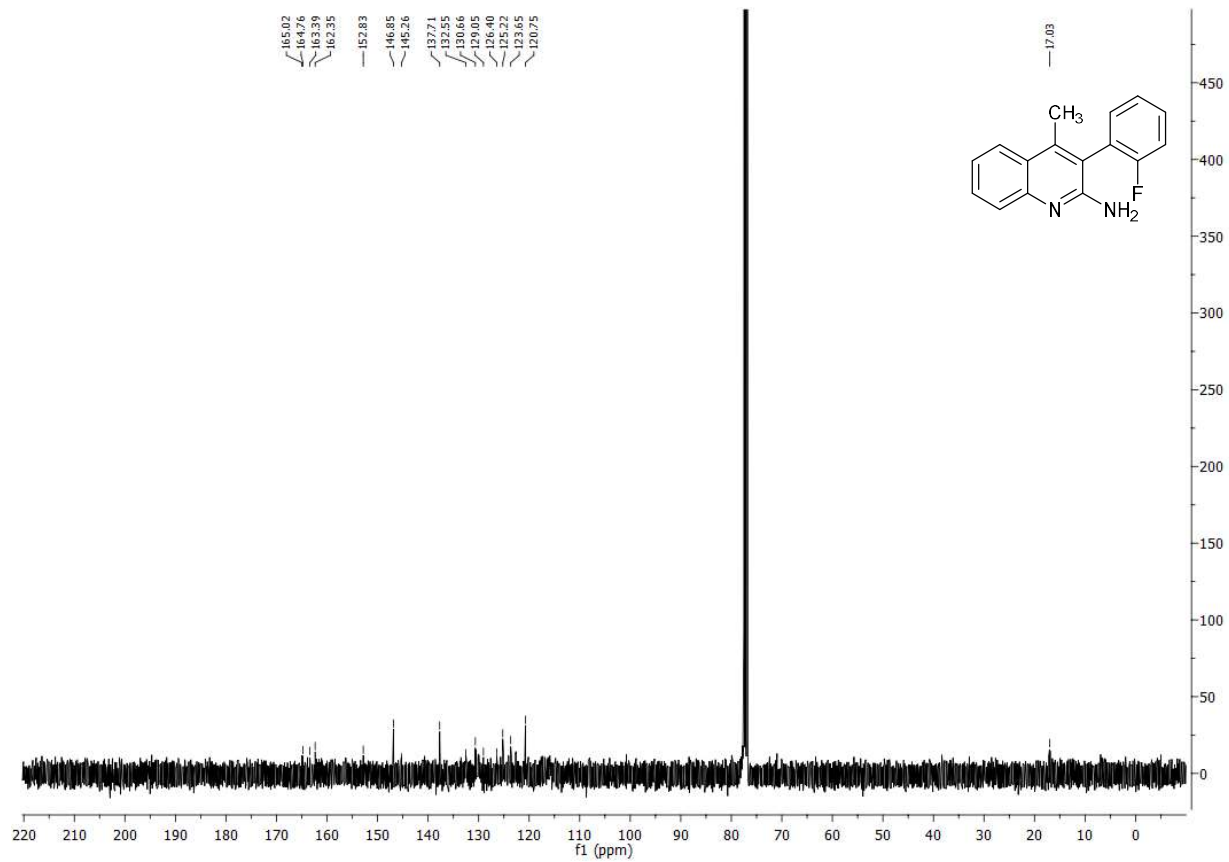
^1H , ^{13}C , and ^{19}F NMR and HRMS (ESI) Spectral Data of **80**



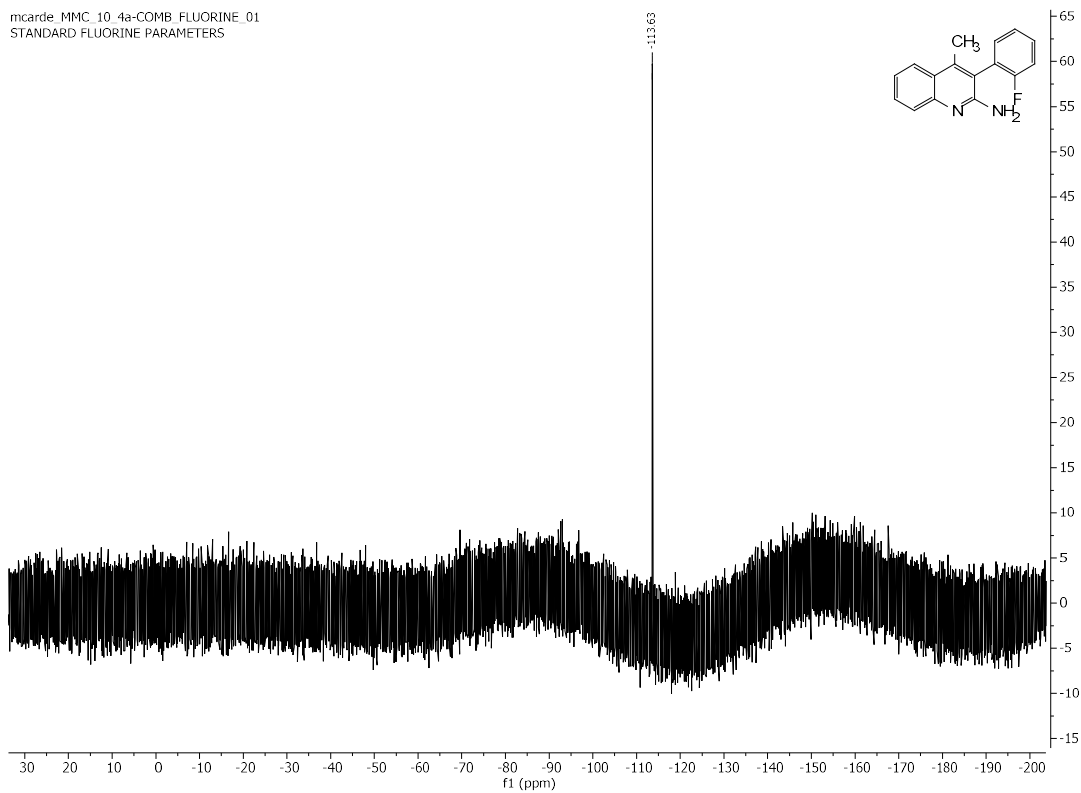


¹H (trace CDCl₃ grease), ¹³C, and ¹⁹F NMR and HRMS (ESI) Spectral Data of **118**



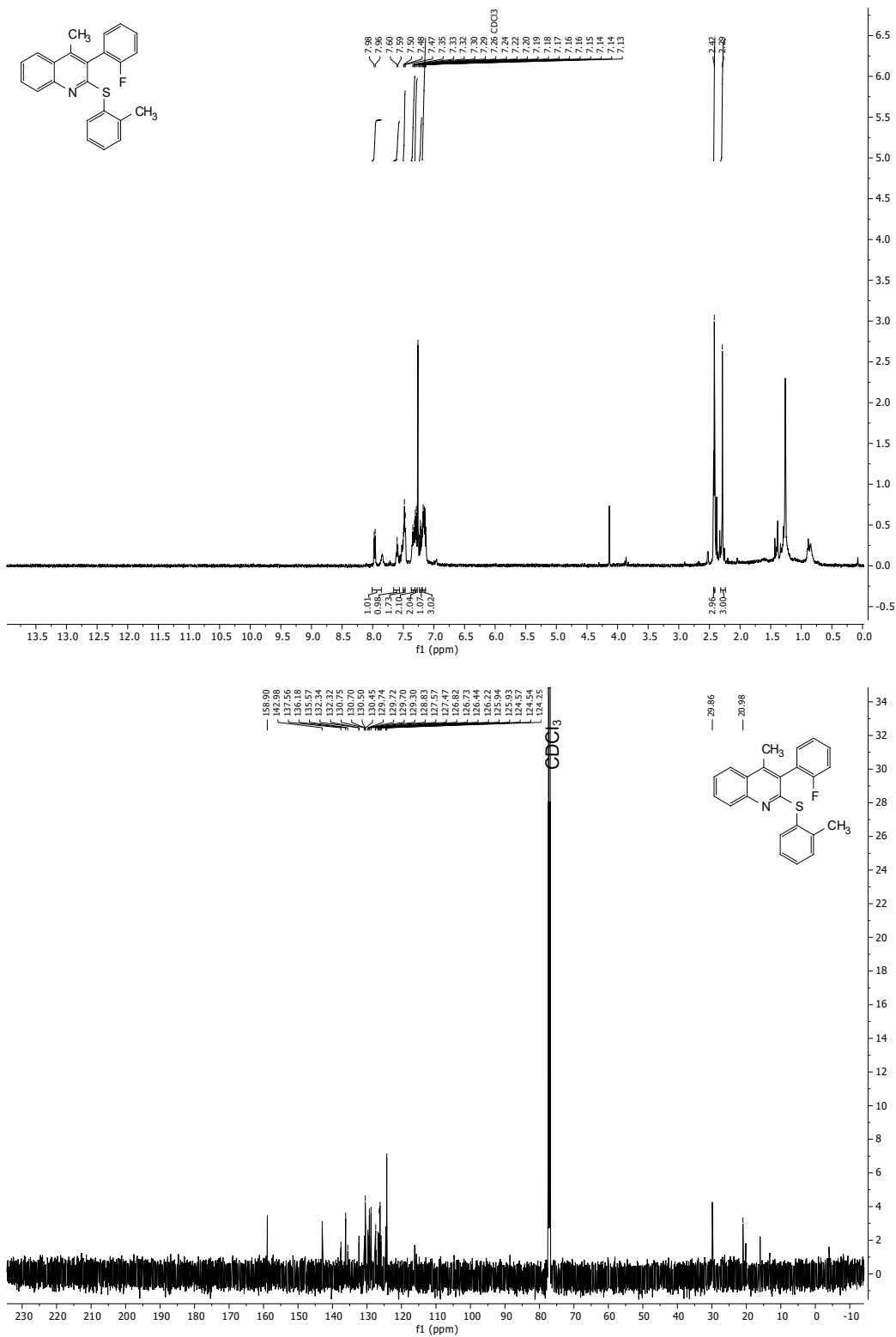


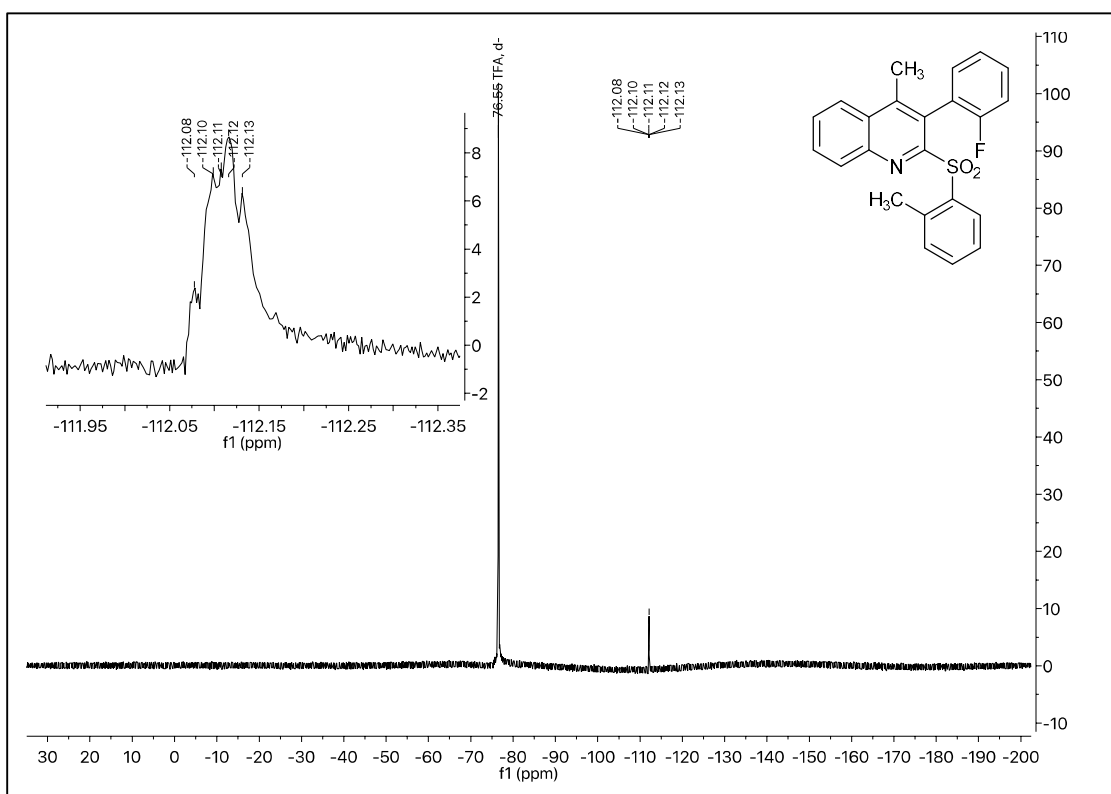
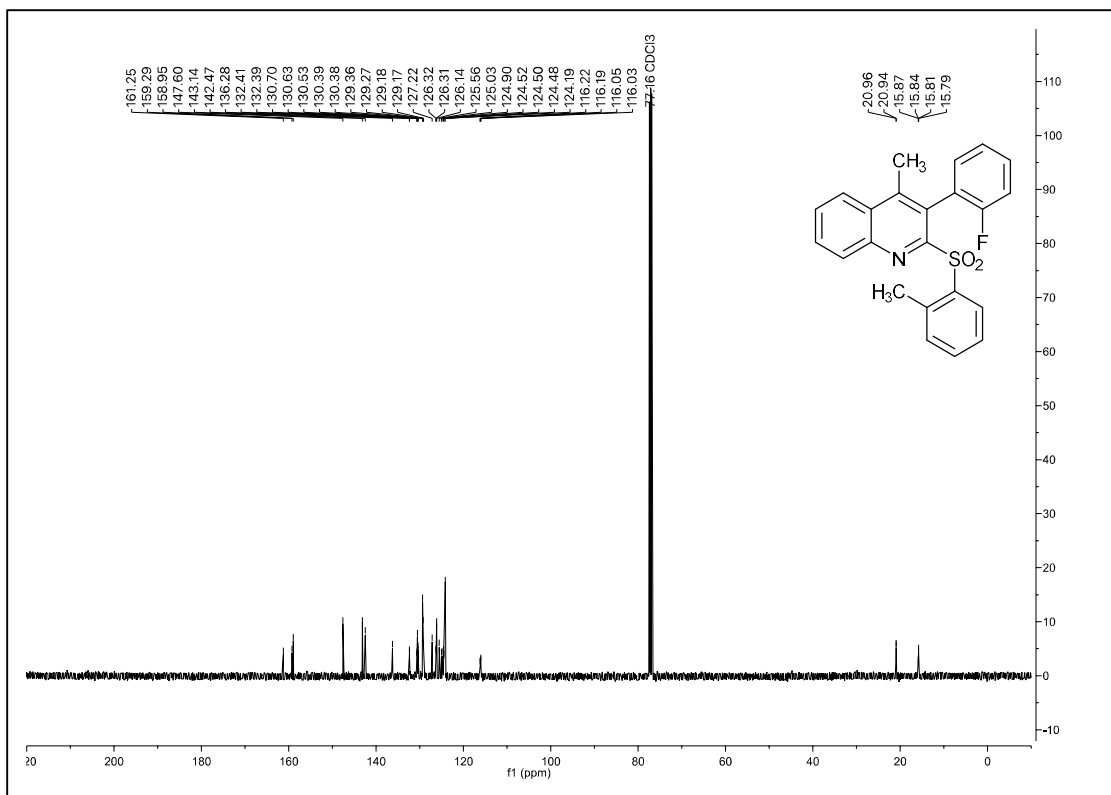
mcardc MMC_10 4a-COMB_FLUORINE_01
STANDARD FLUORINE PARAMETERS



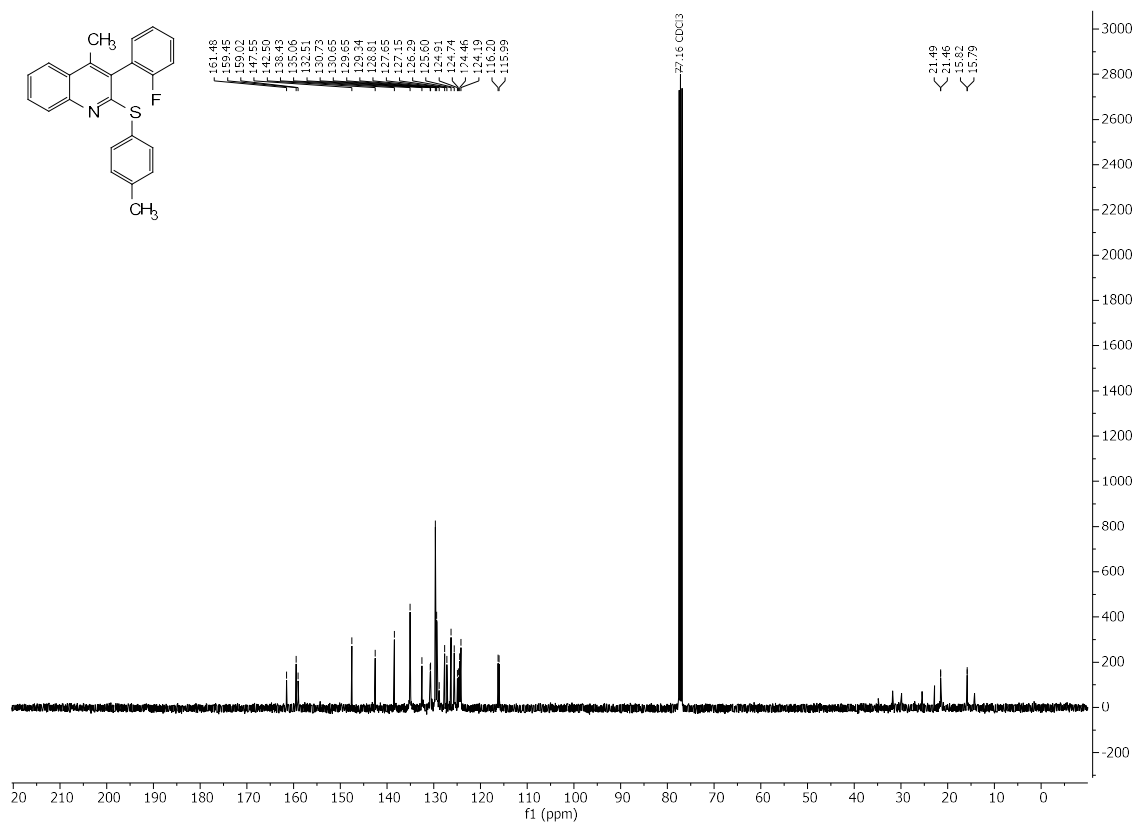
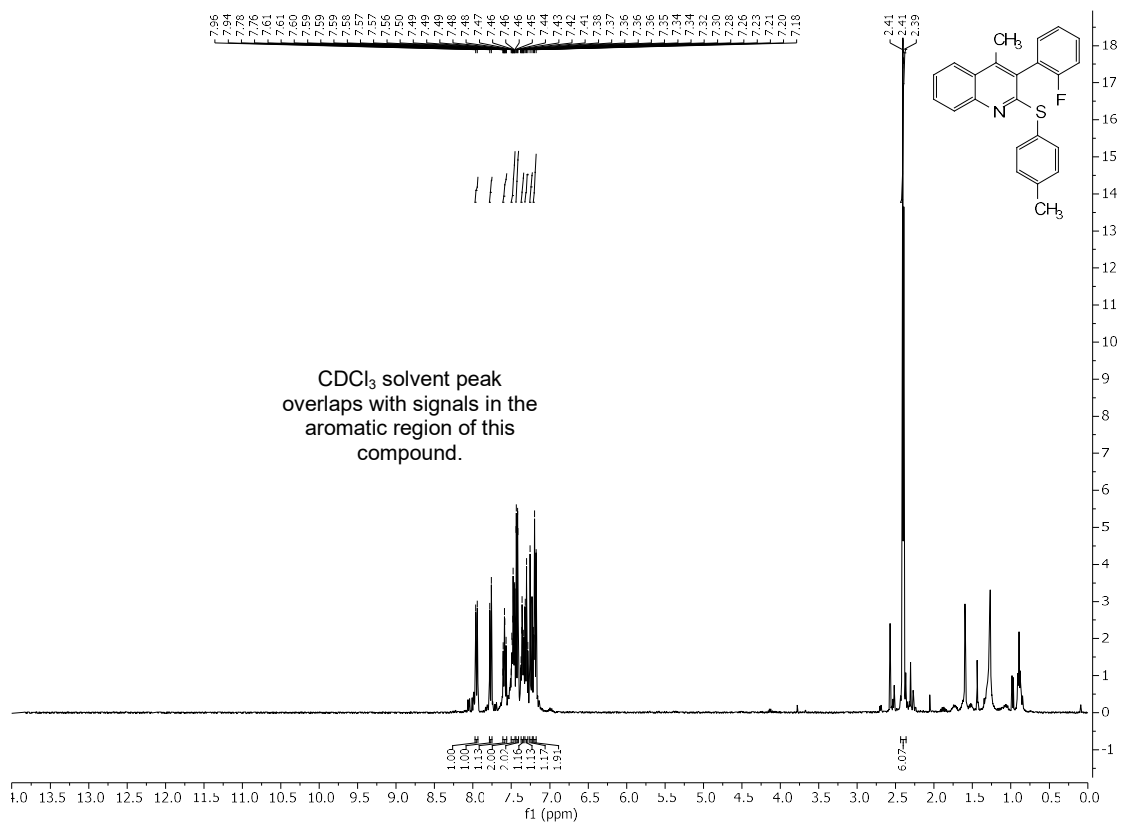
^1H (trace CDCl_3 grease, EtOAc and *n*-Hexane) ^{13}C , and ^{19}F NMR and HRMS (ESI) Spectral Data

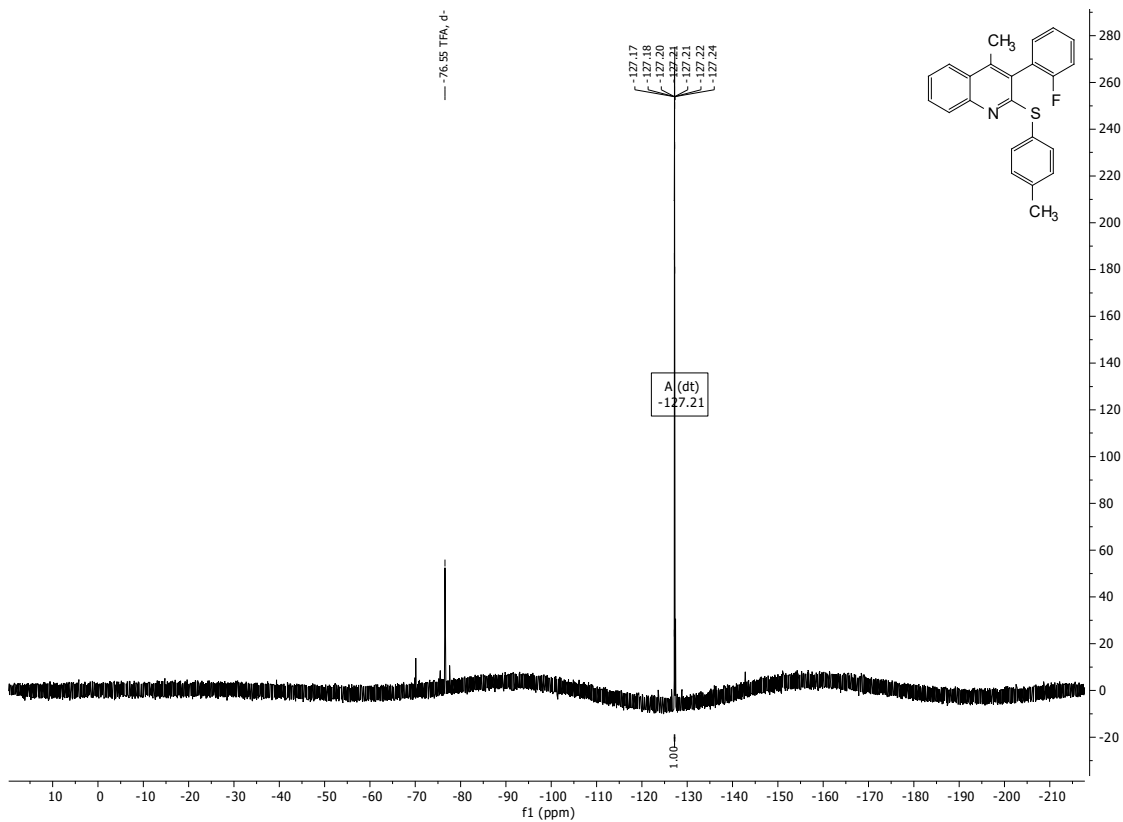
of **81**





^1H , ^{13}C , and ^{19}F NMR and HRMS (ESI) Spectral Data of **84**

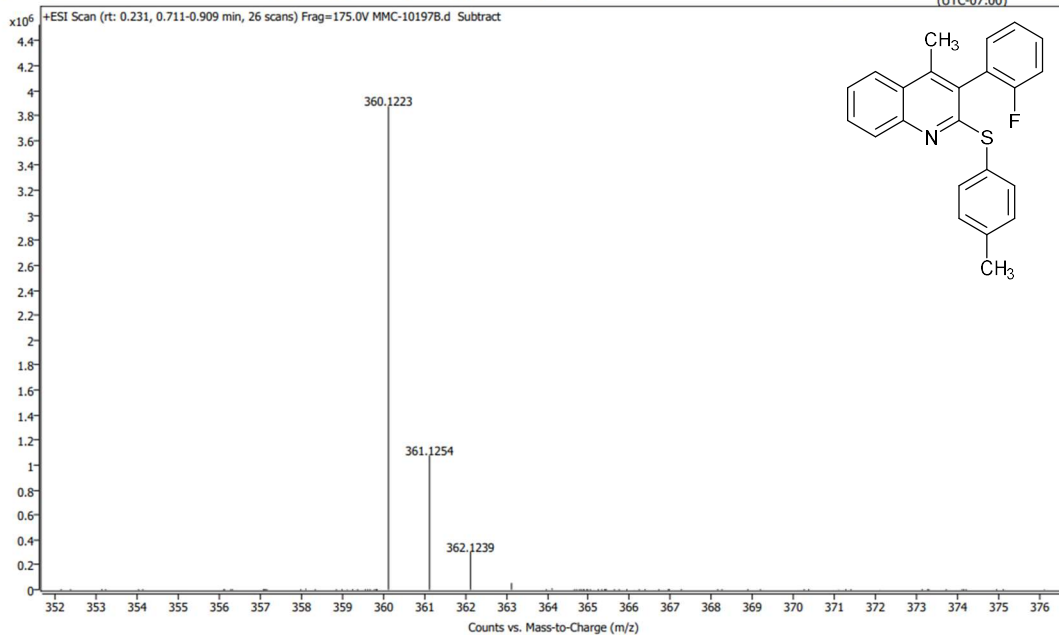




Spectrum Plot Report

Agilent | Trusted Answers

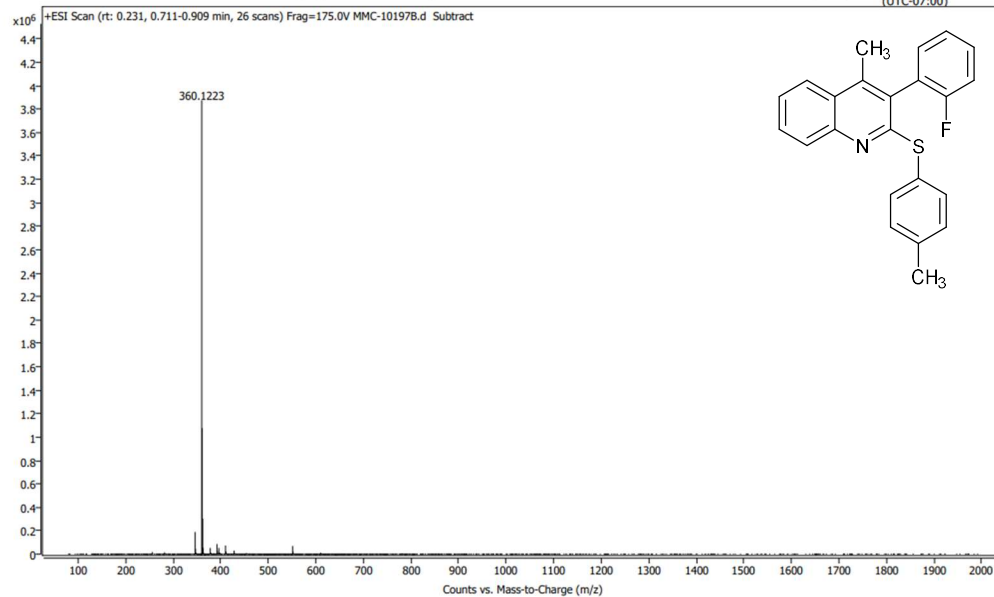
Name	Rack Pos.	Instrument	Instrument 1	Operator
Inj. Vol. (ul) 1	Plate Pos.	IRM Status	Success	
Data File	Method (Acq)	Column bypass.m		Acq. Time (Local) 8/6/2021 4:03:35 PM (UTC-07:00)



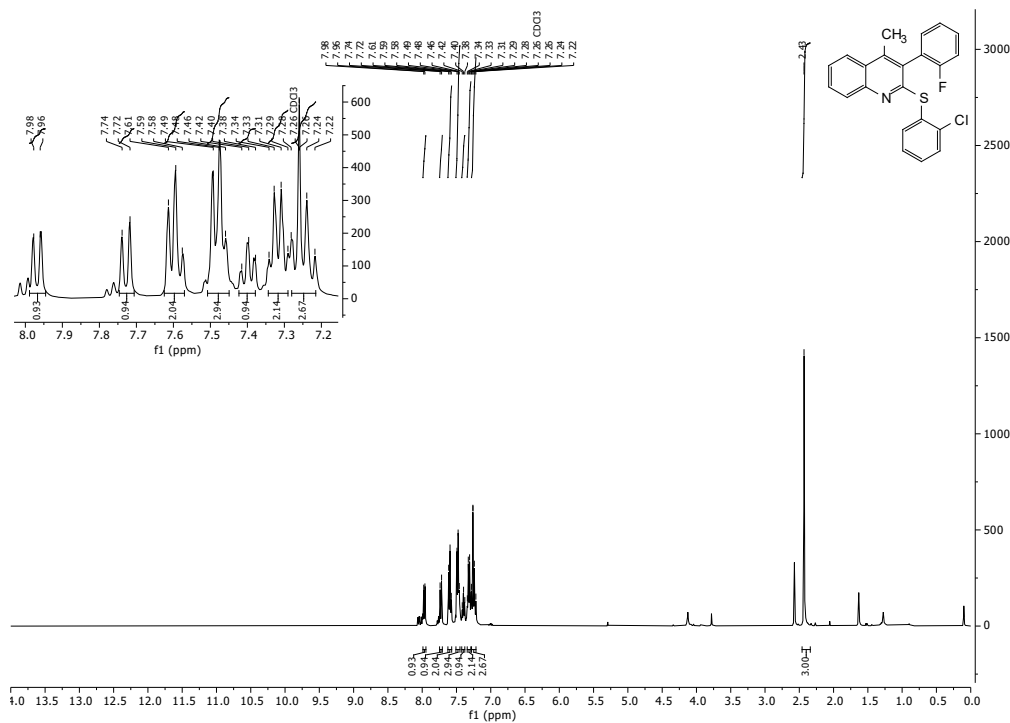
Spectrum Plot Report

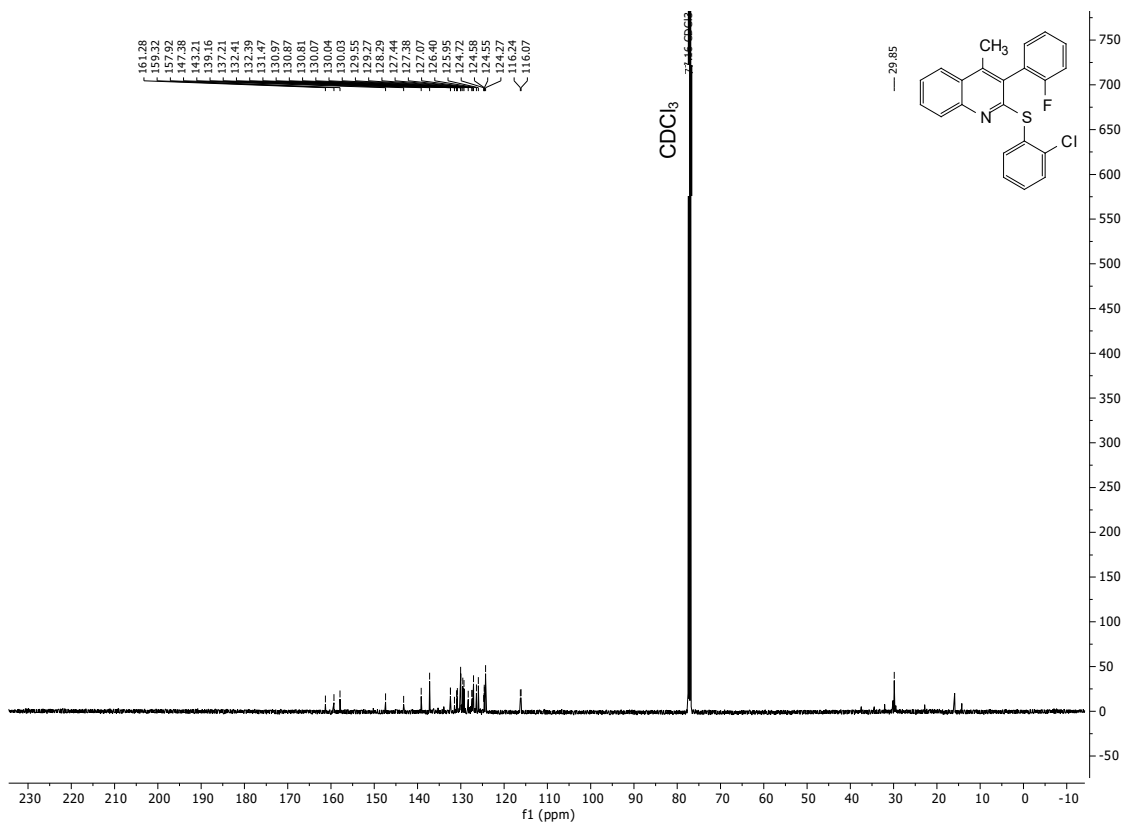


Name	1	Rack Pos.	Instrument	Instrument 1	Operator
Inj. Vol. (ul)		Plate Pos.	IRM Status	Success	
Data File		Method (Acq)	Column bypass.m	Comment	Acq. Time (Local) 8/6/2021 4:03:35 PM (UTC-07:00)

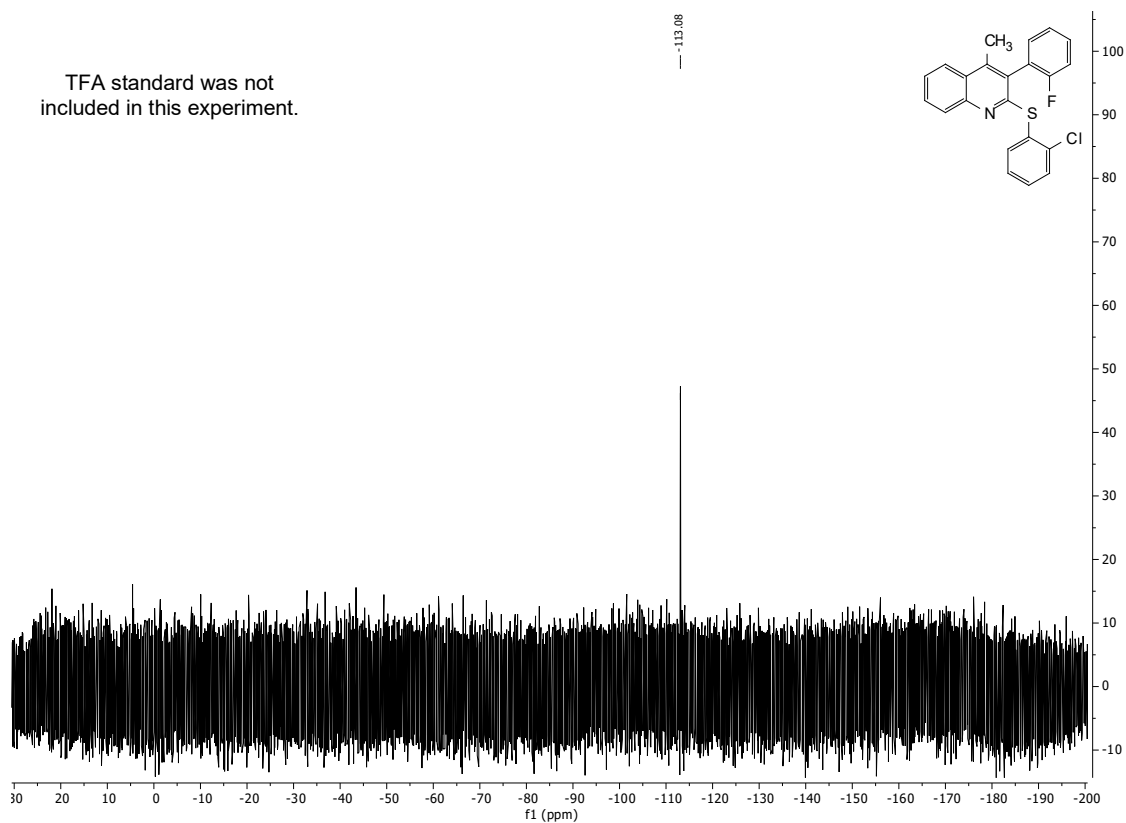


¹H, ¹³C (X-C coupling, X = F, Cl), and ¹⁹F NMR and HRMS (ESI) Spectral Data of **84**





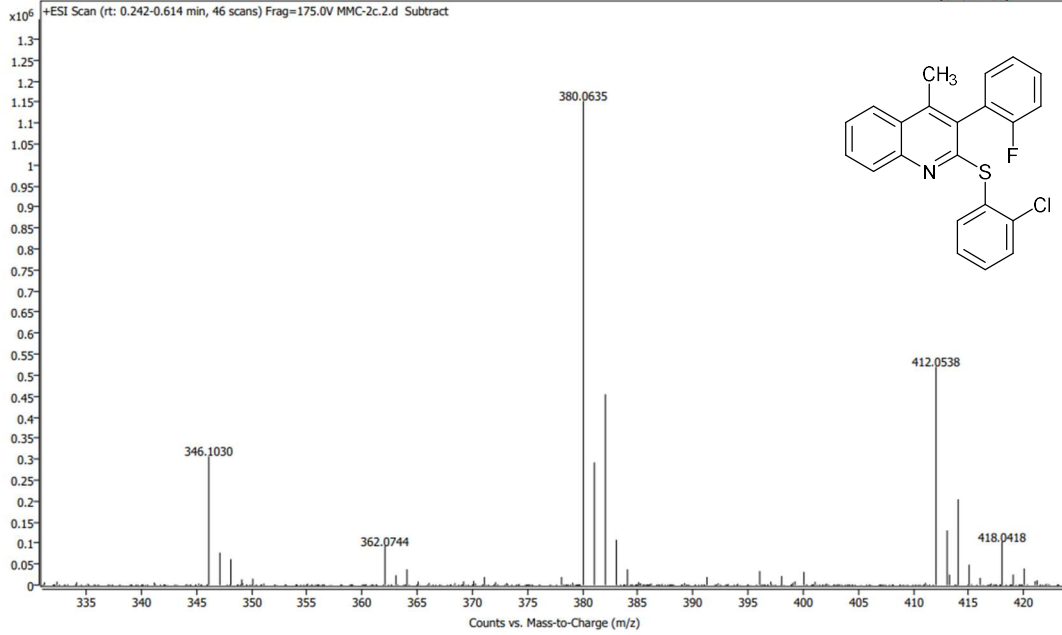
TFA standard was not included in this experiment.



Spectrum Plot Report

Agilent | Trusted Answers

Name	1	Rack Pos.	Instrument	Instrument 1	Operator
Inj. Vol. (ul)	1	Plate Pos.	IRM Status	Success	
Data File		Method (Acq)	Column bypass.m	Comment	Acq. Time (Local) 8/6/2021 2:31:37 PM (UTC-07:00)



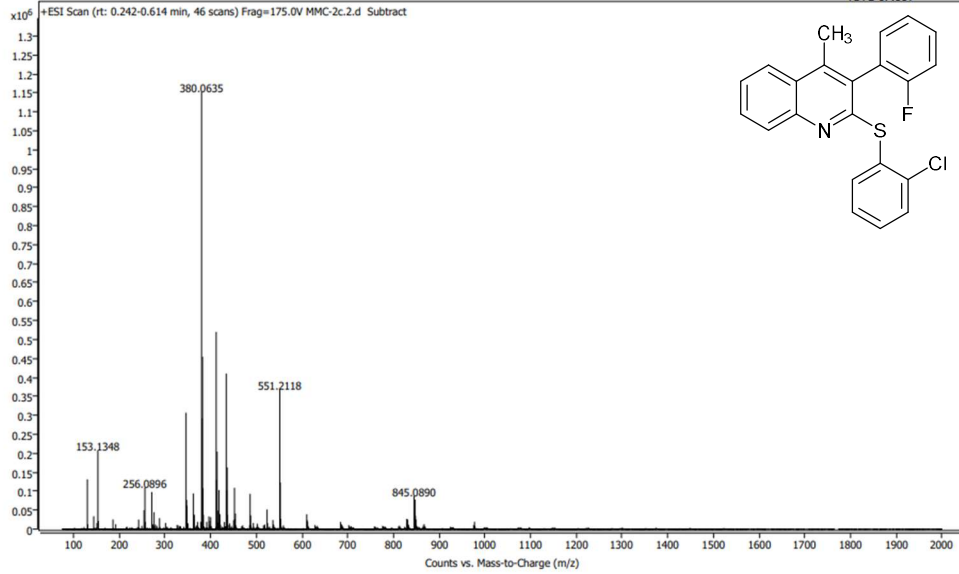
Page 1 of 1

Generated at 3:33 PM on 8/6/2021

Spectrum Plot Report

Agilent | Trusted Answers

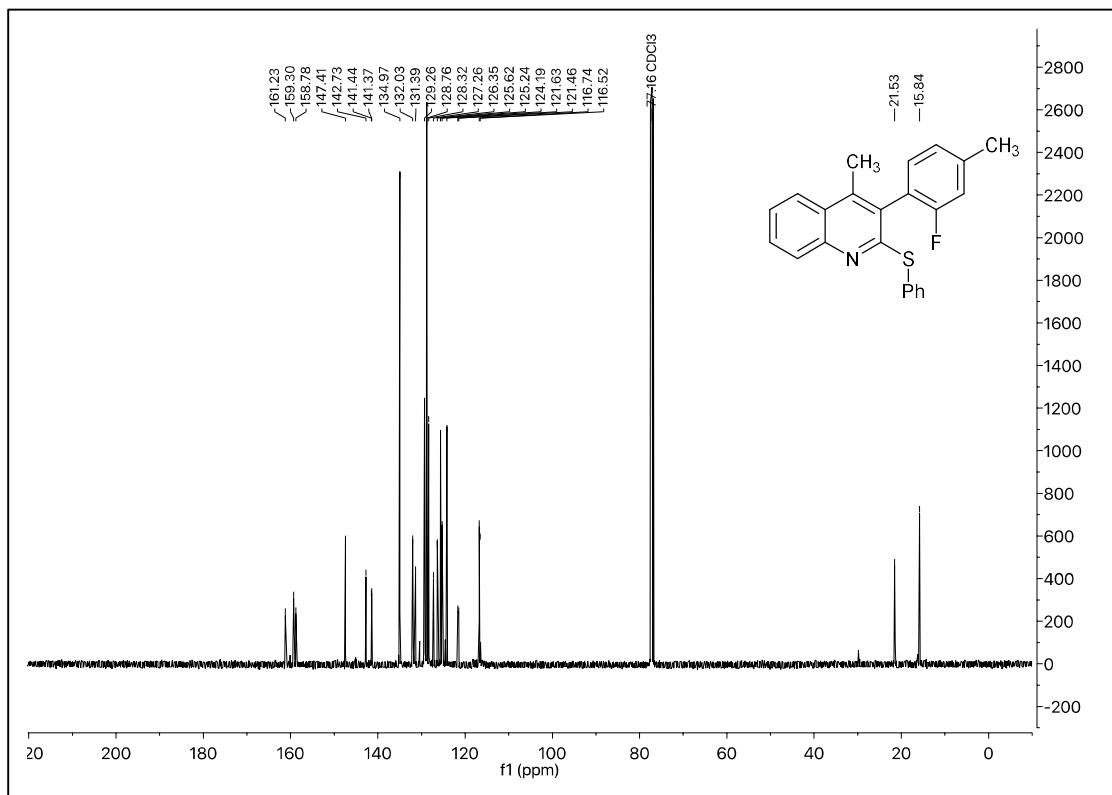
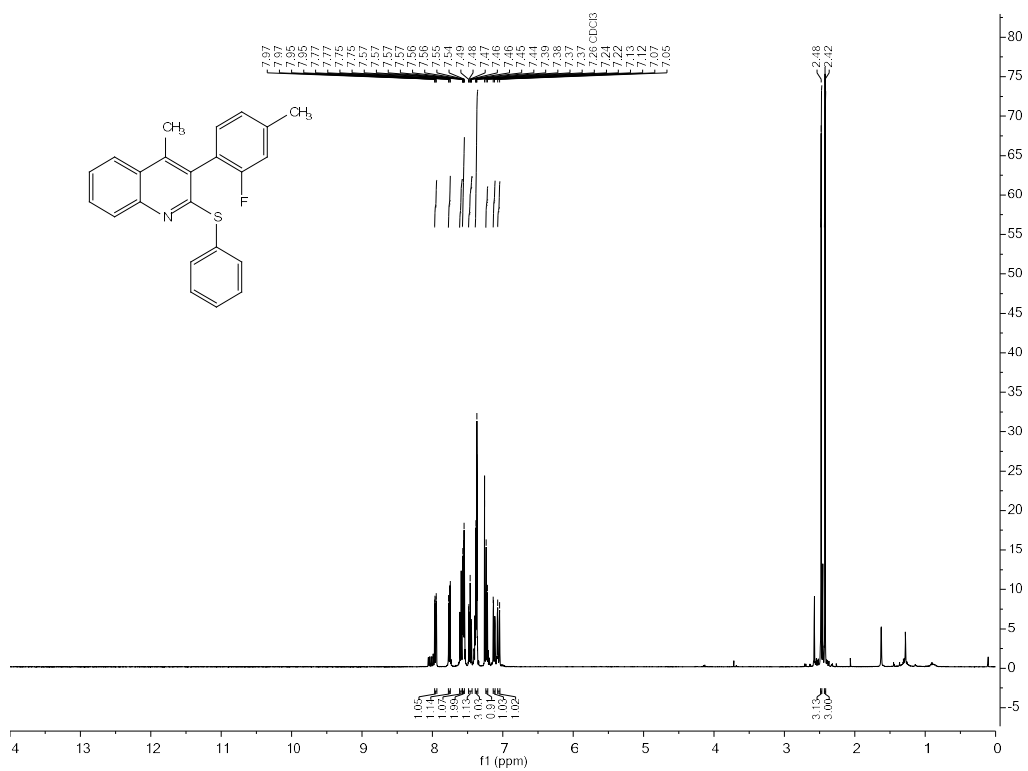
Name	1	Rack Pos.	Instrument	Instrument 1	Operator
Inj. Vol. (ul)	1	Plate Pos.	IRM Status	Success	
Data File		Method (Acq)	Column bypass.m	Comment	Acq. Time (Local) 8/6/2021 2:31:37 PM (UTC-07:00)



Page 1 of 1

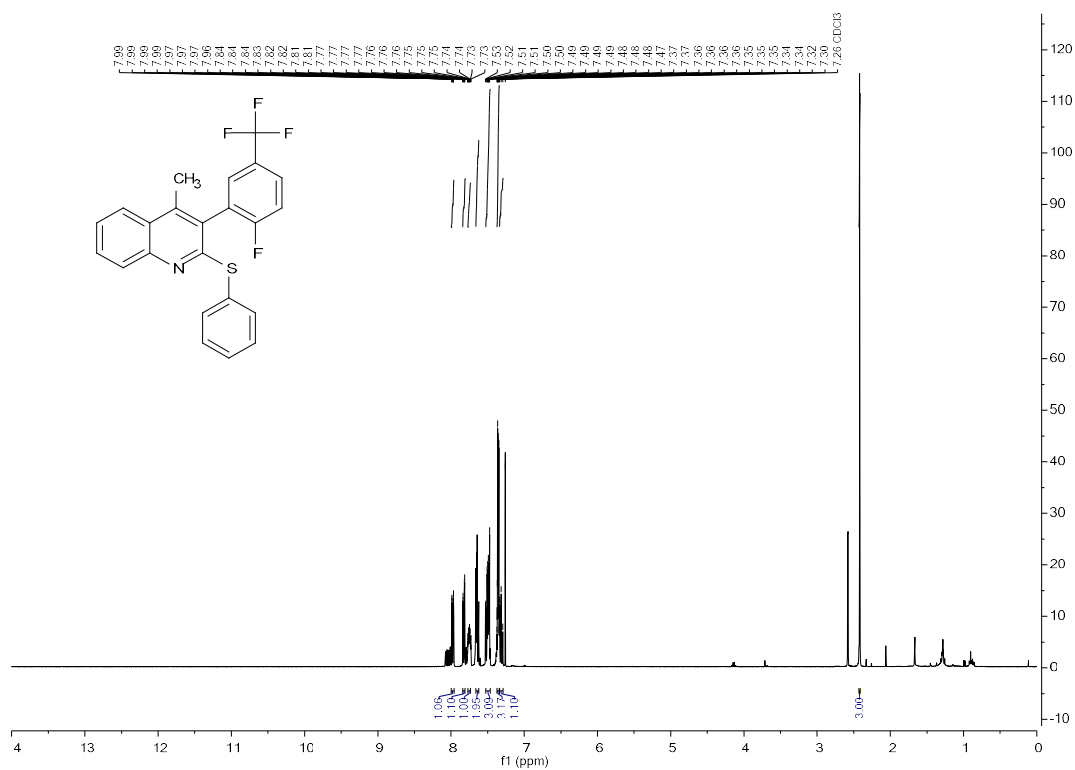
Generated at 3:34 PM on 8/6/2021

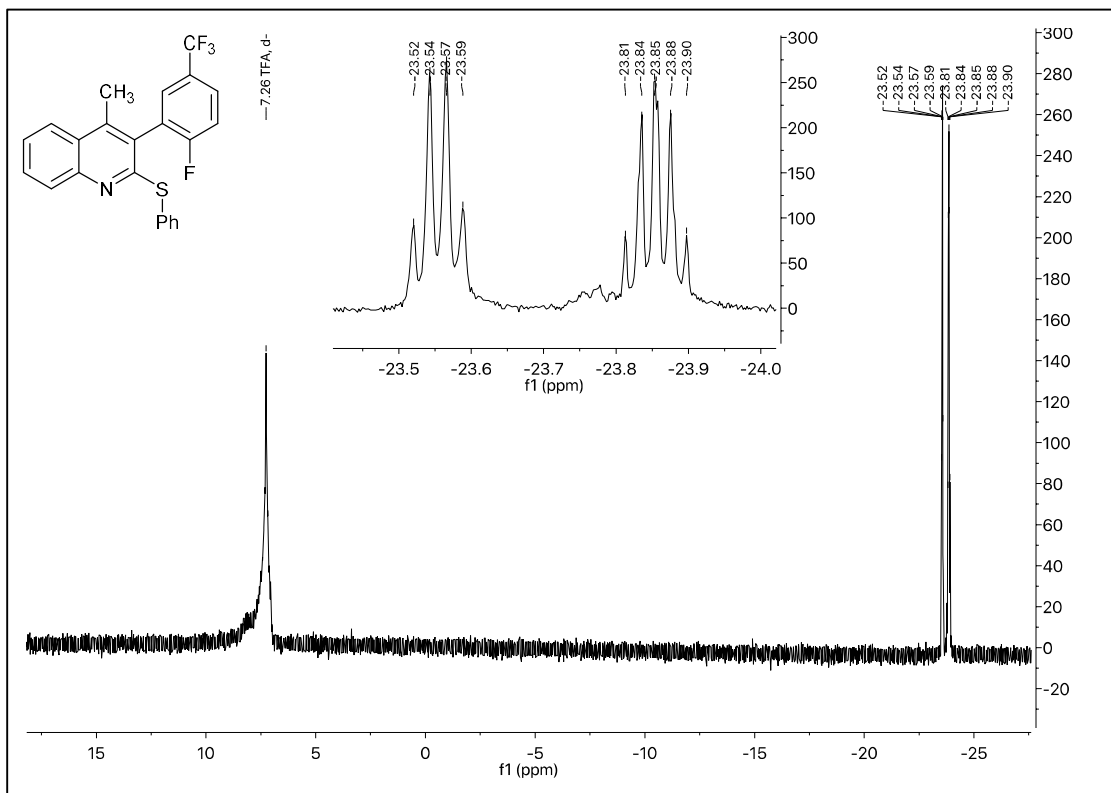
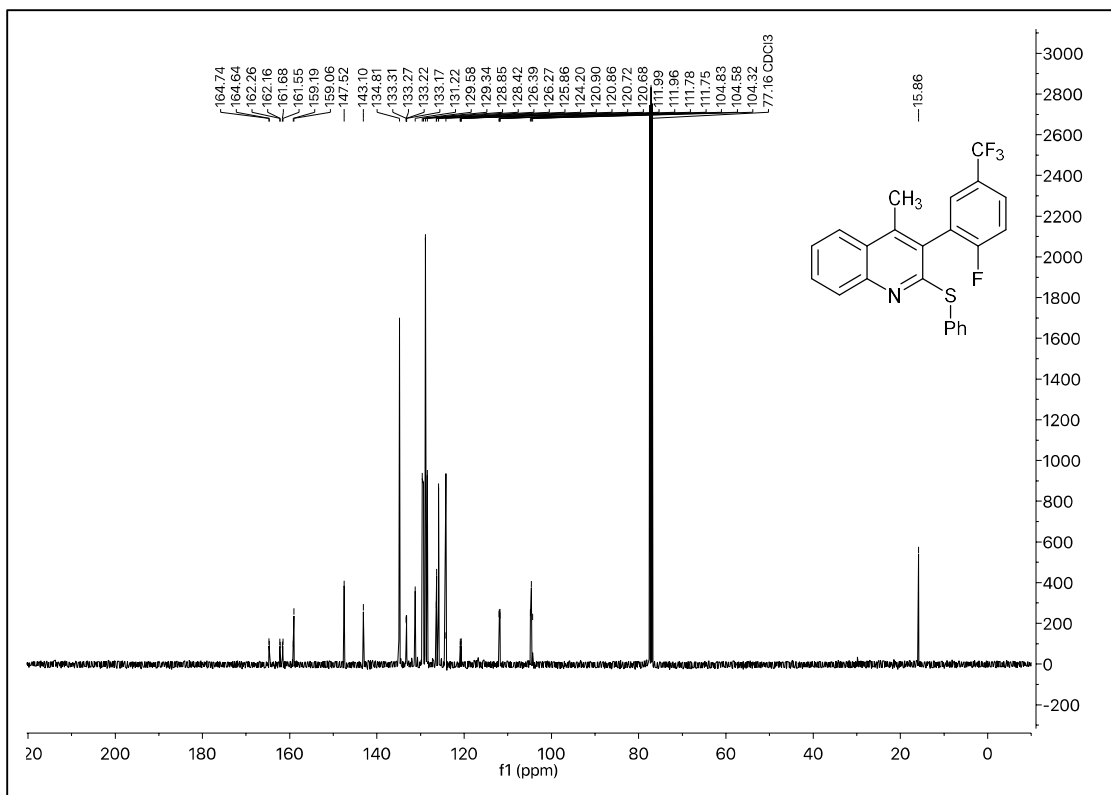
^1H , ^{13}C , and ^{19}F NMR of **85**

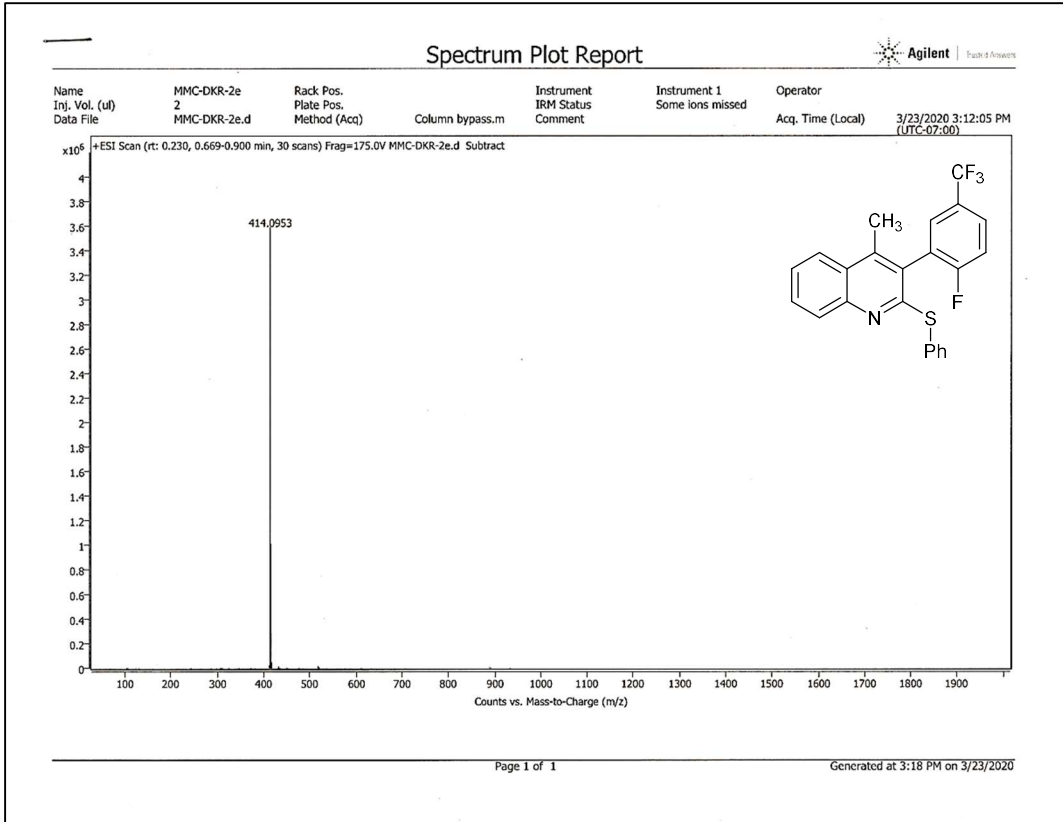




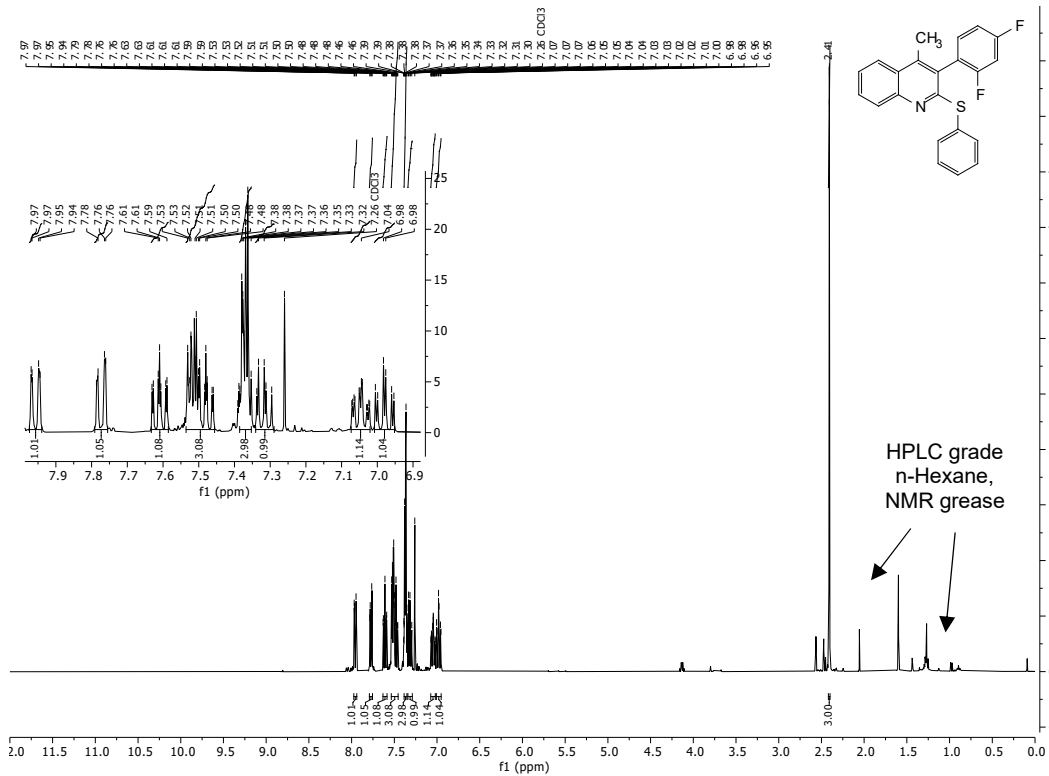
¹H, ¹³C, and ¹⁹F NMR and HRMS (ESI) Spectral Data of **86**

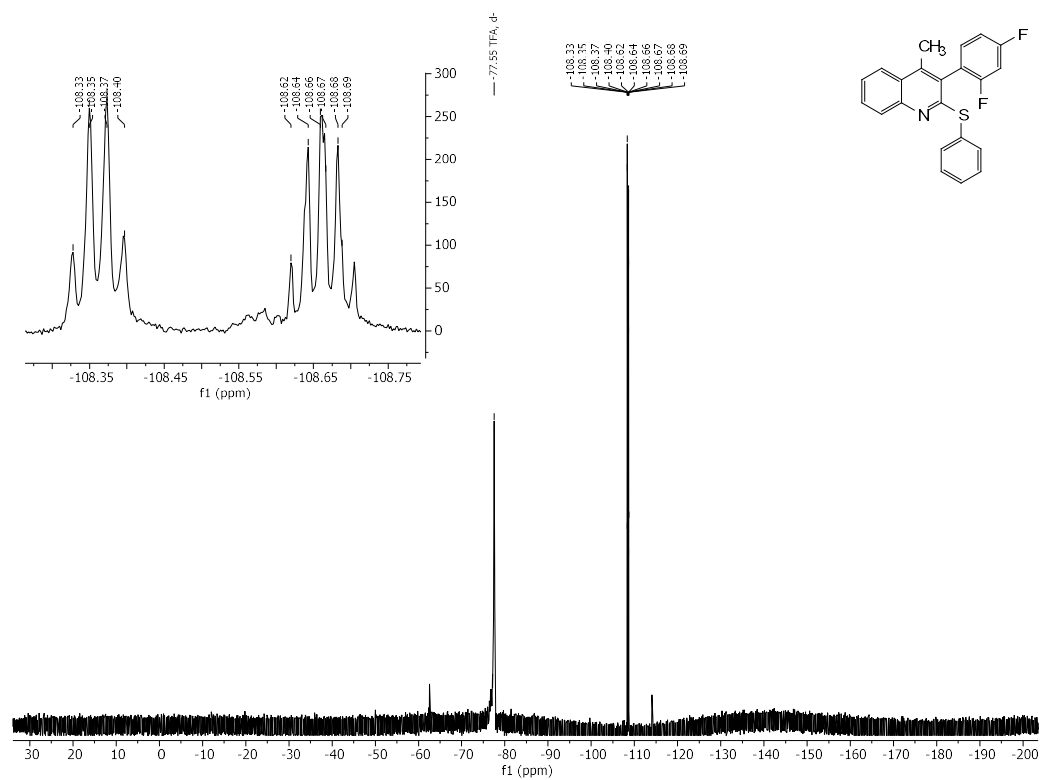
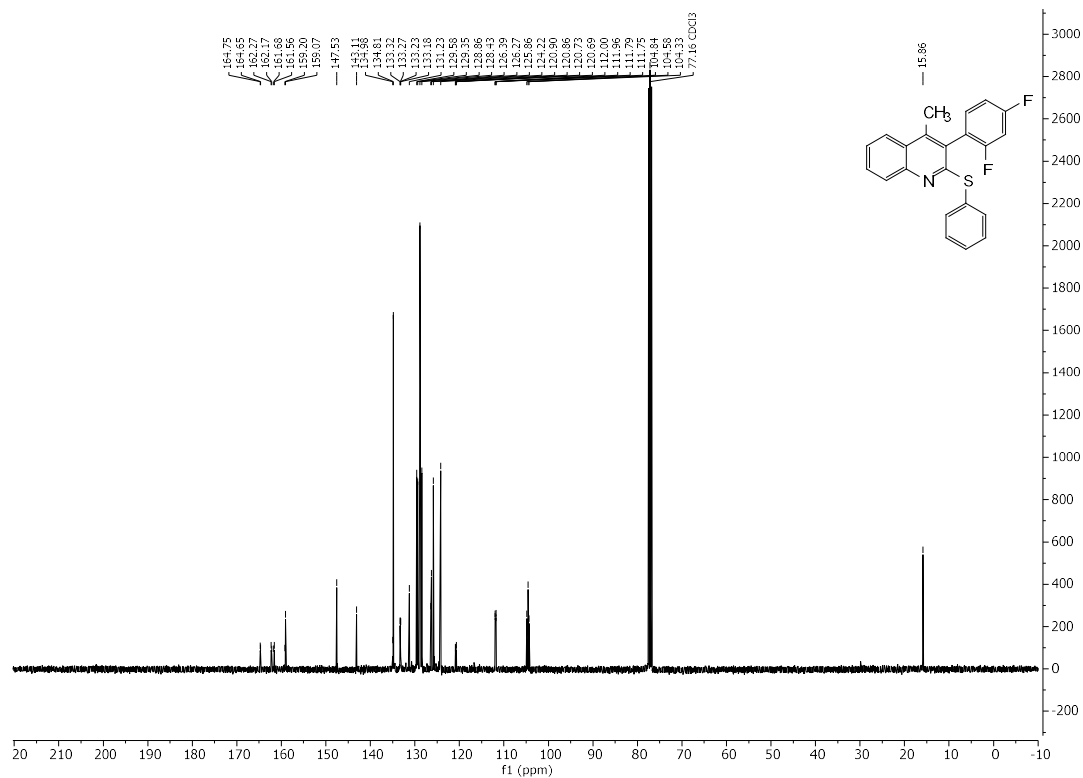


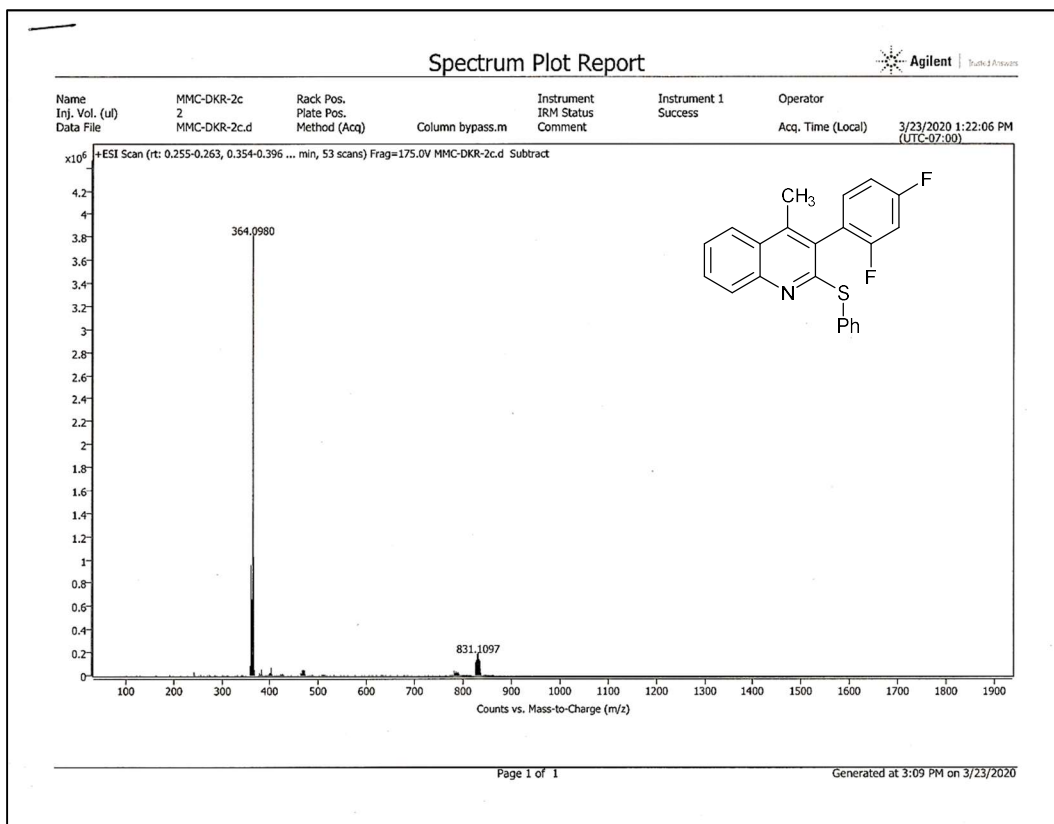




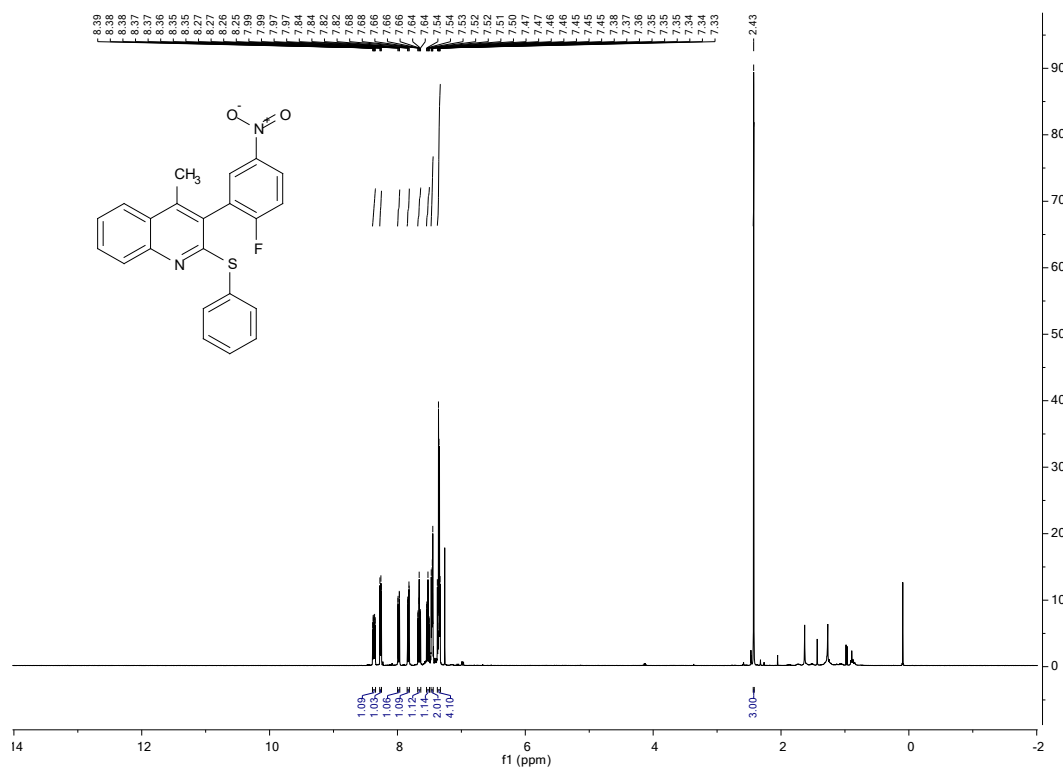
¹H (trace HPLC grade *n*-Hexane), ¹³C, and ¹⁹F NMR and HRMS (ESI) Spectral Data of **87**

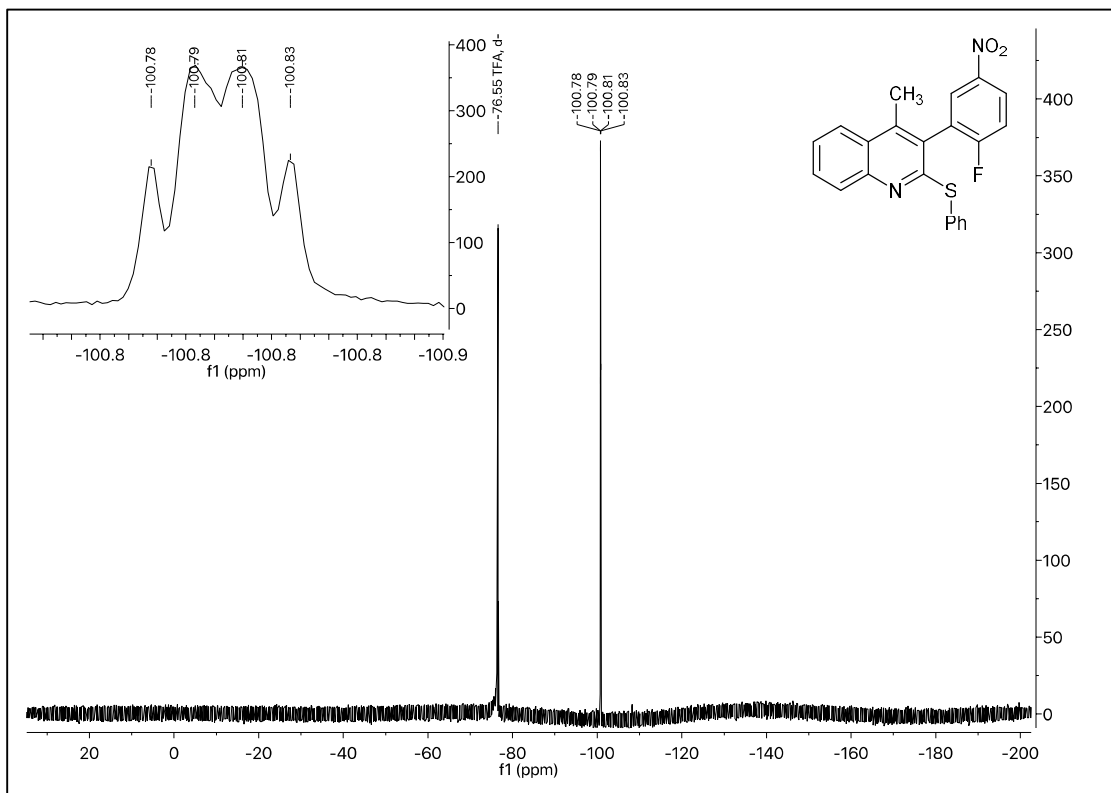
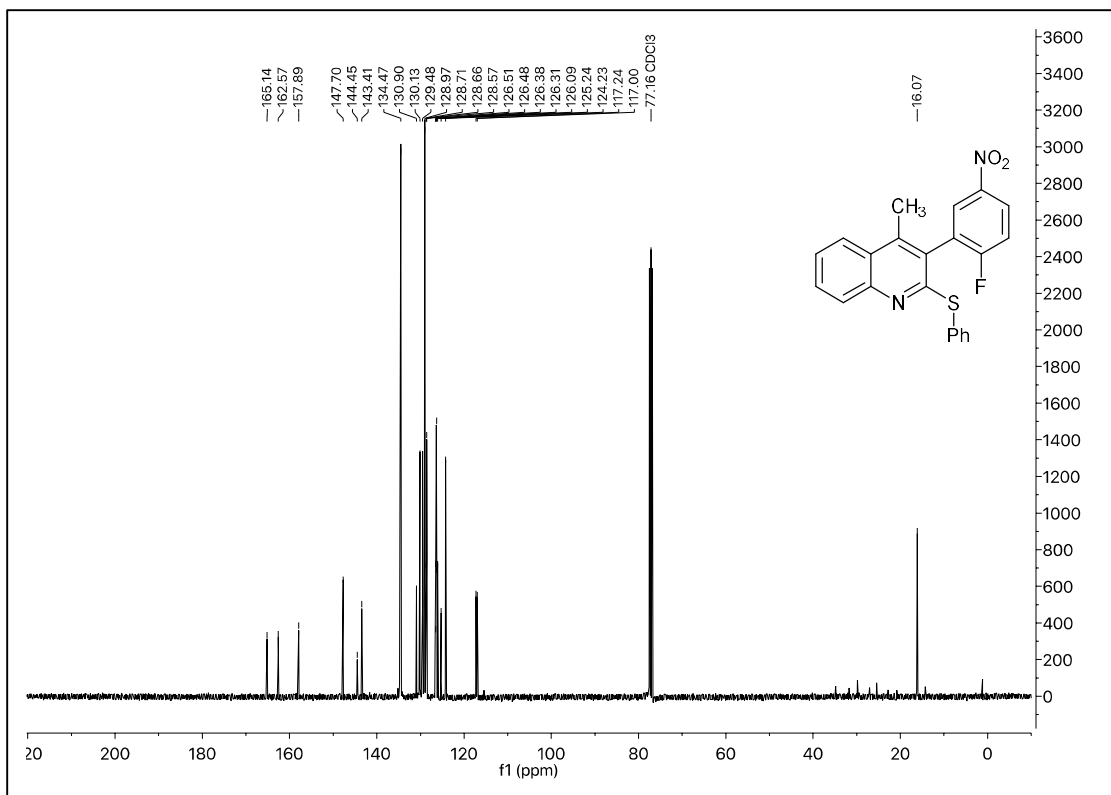


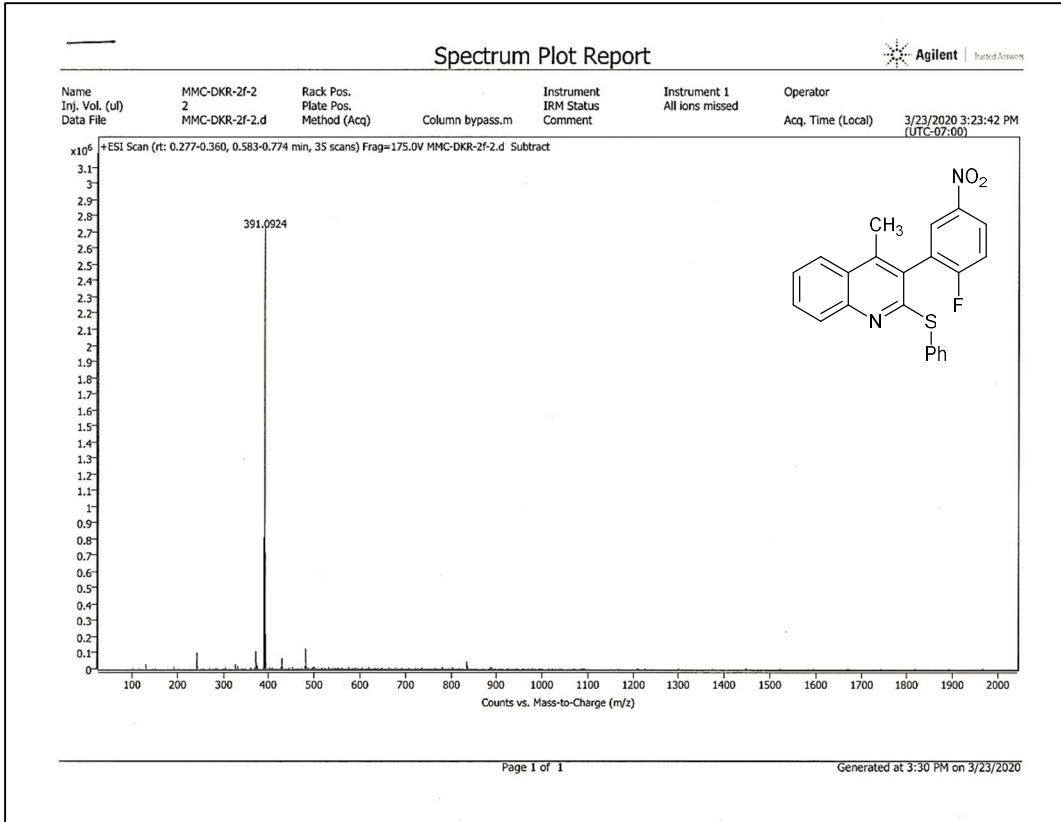




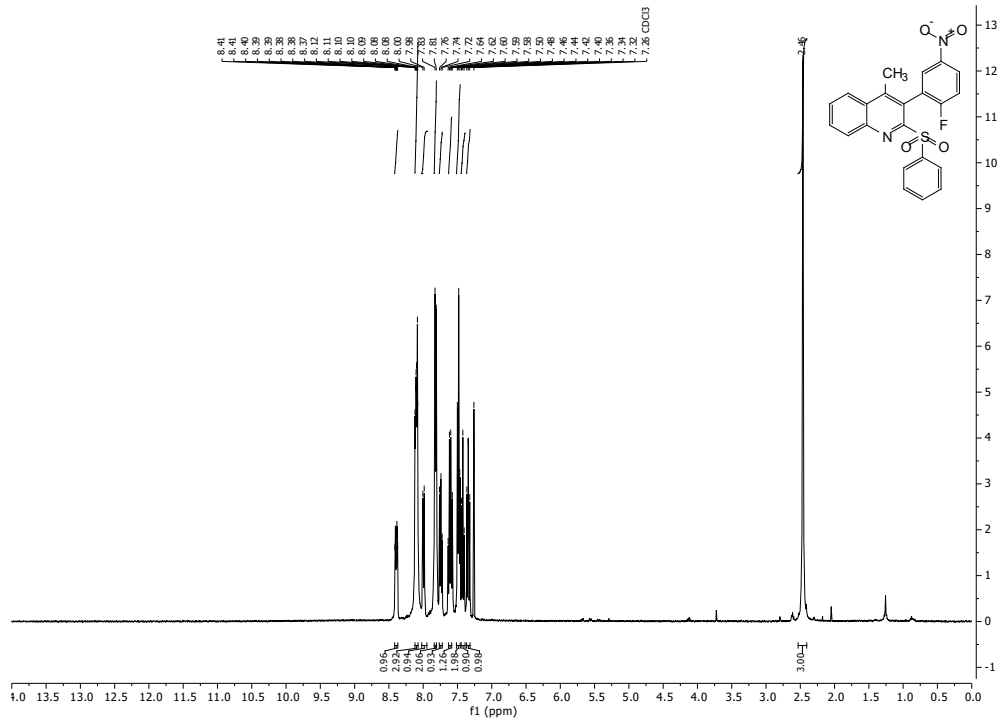
¹H, ¹³C, and ¹⁹F NMR and HRMS (ESI) Spectral Data of **2g**



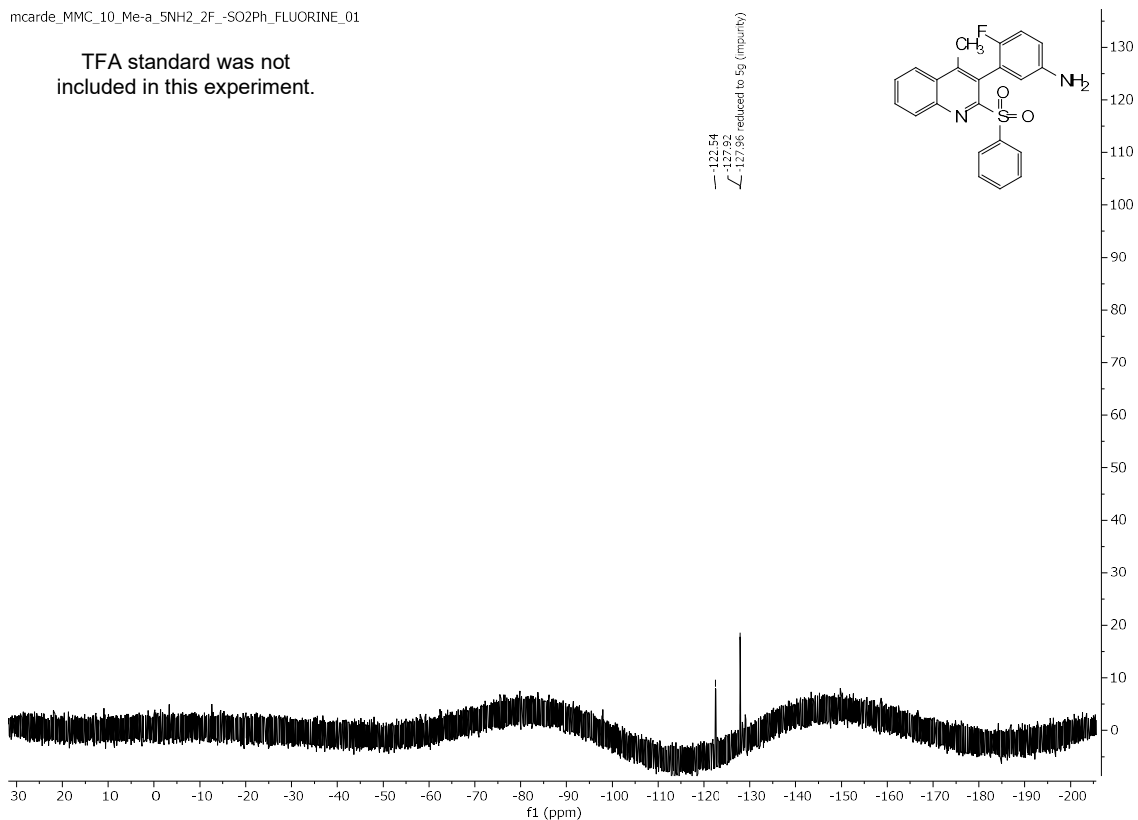




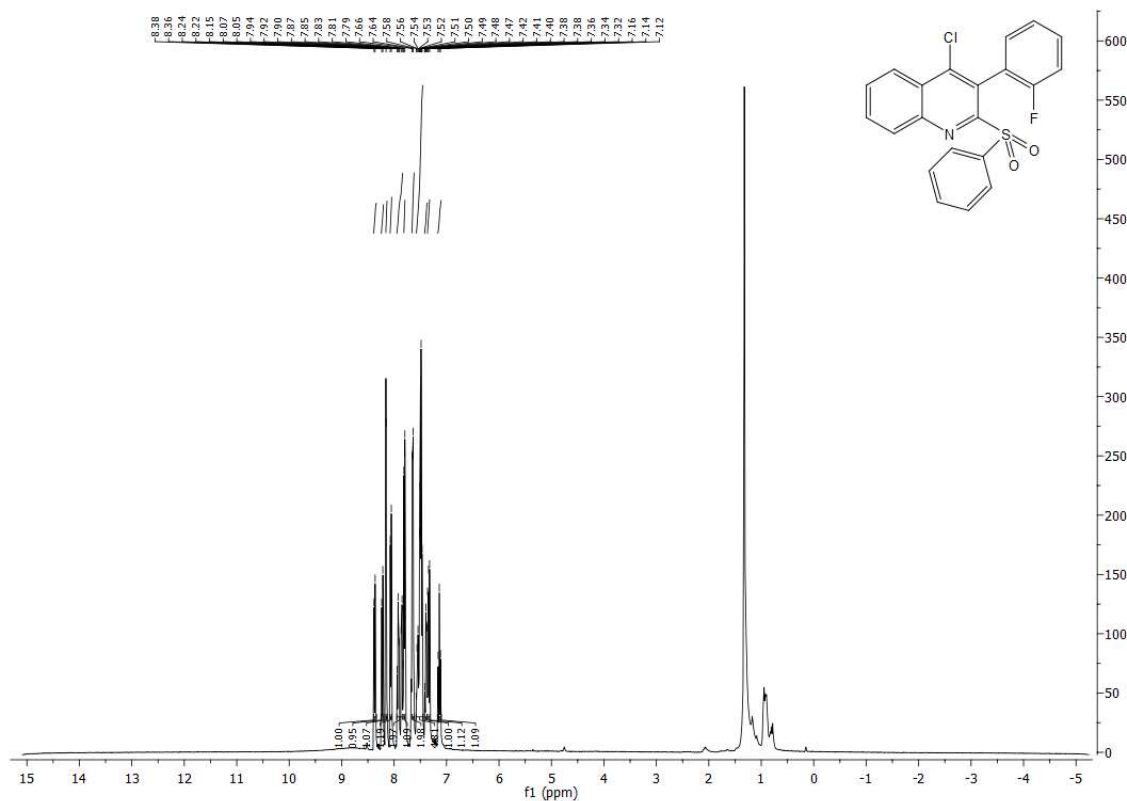
¹H, ¹³C, and ¹⁹F NMR Spectral Data of **122**

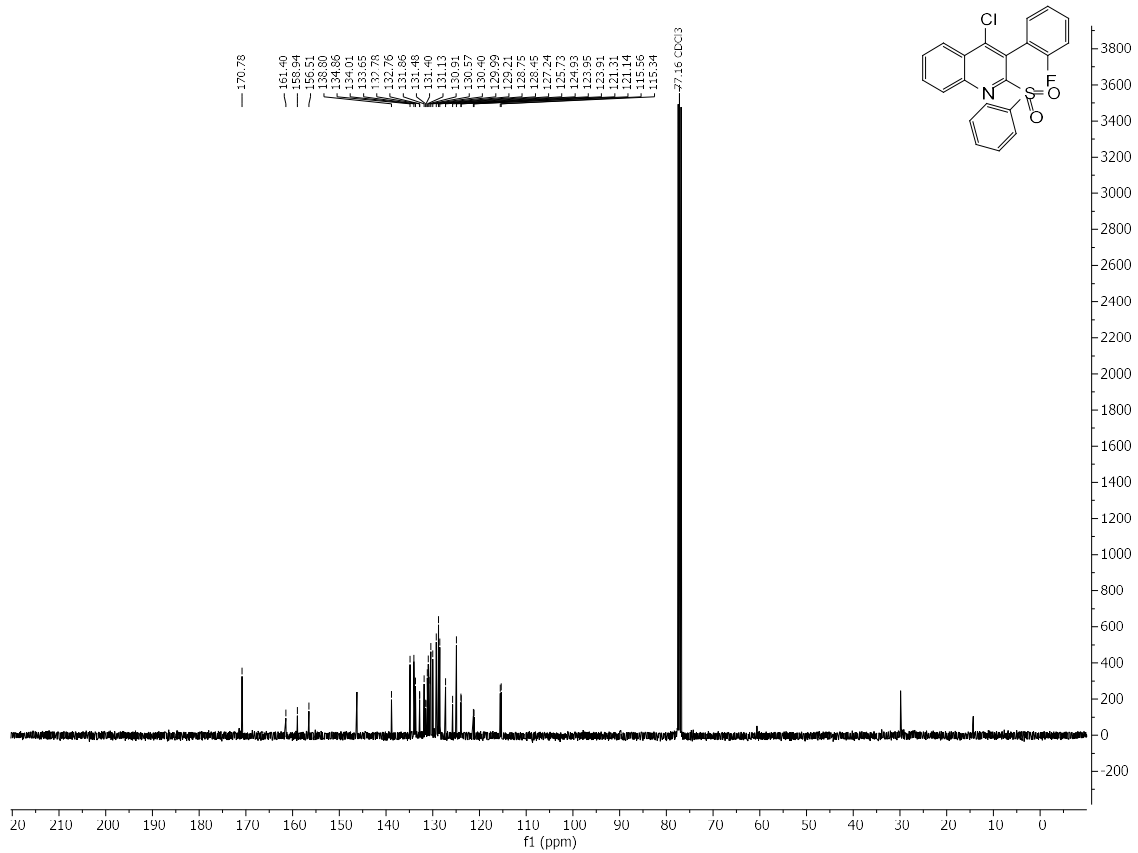


TFA standard was not included in this experiment.

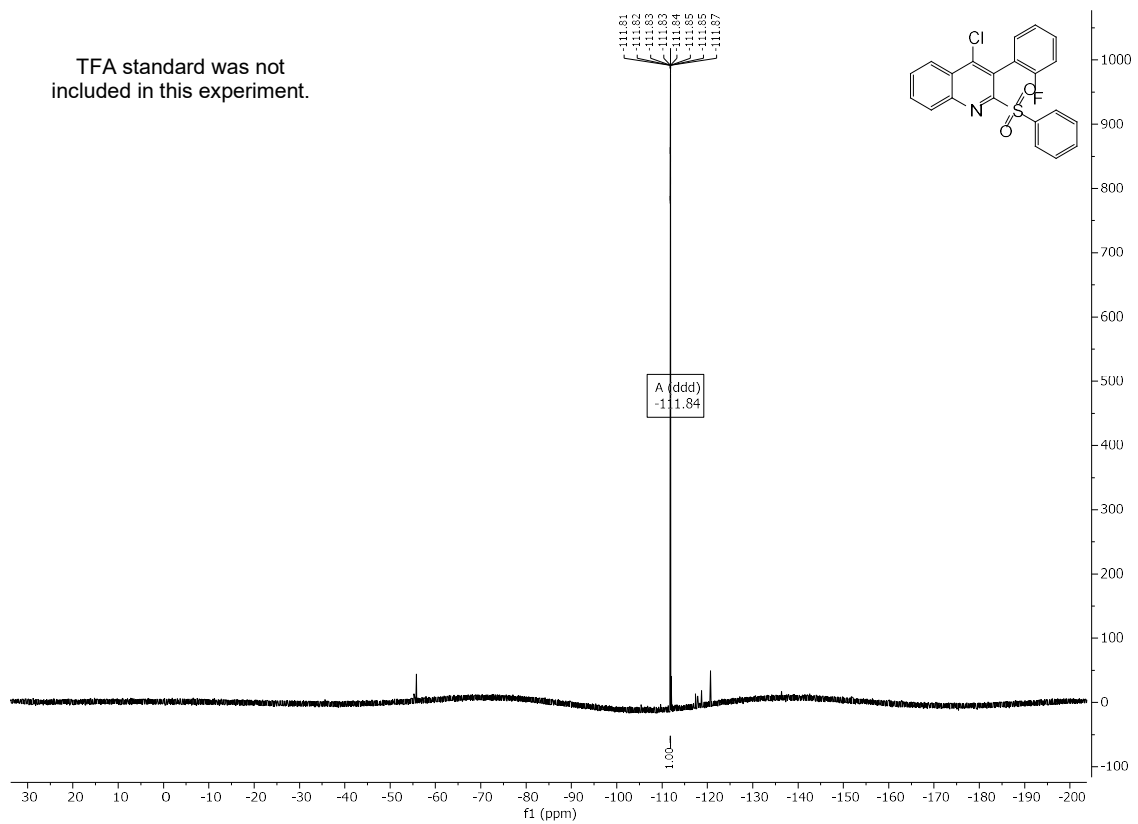


¹H (grease impurity), ¹³C, and ¹⁹F NMR and HRMS (ESI) Spectral Data of **91**





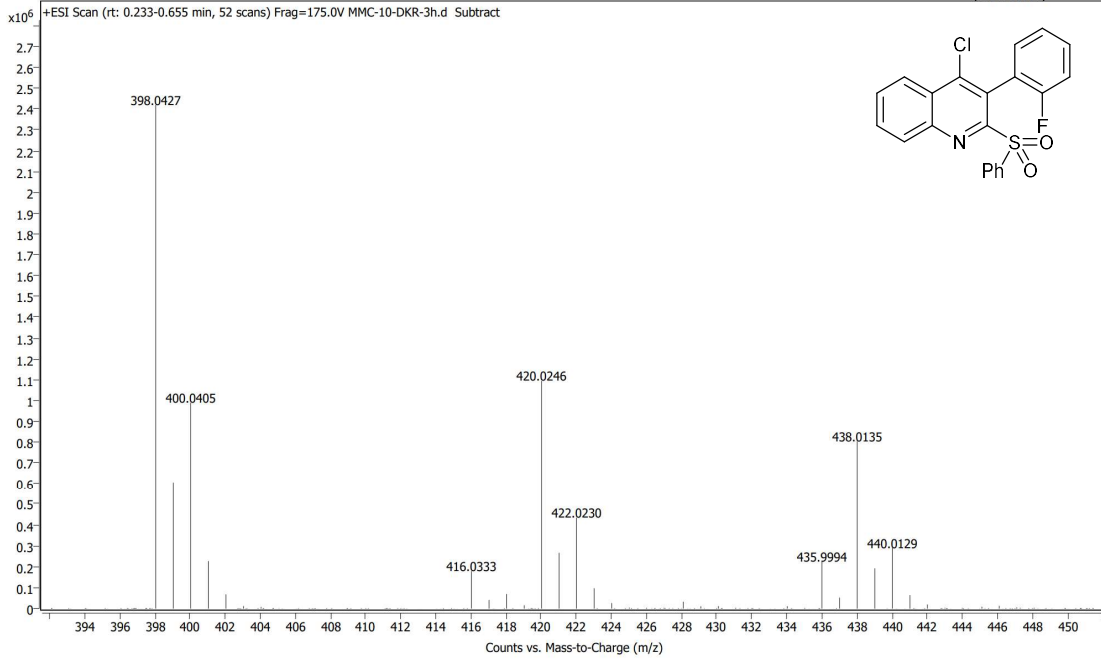
TFA standard was not included in this experiment.



Spectrum Plot Report



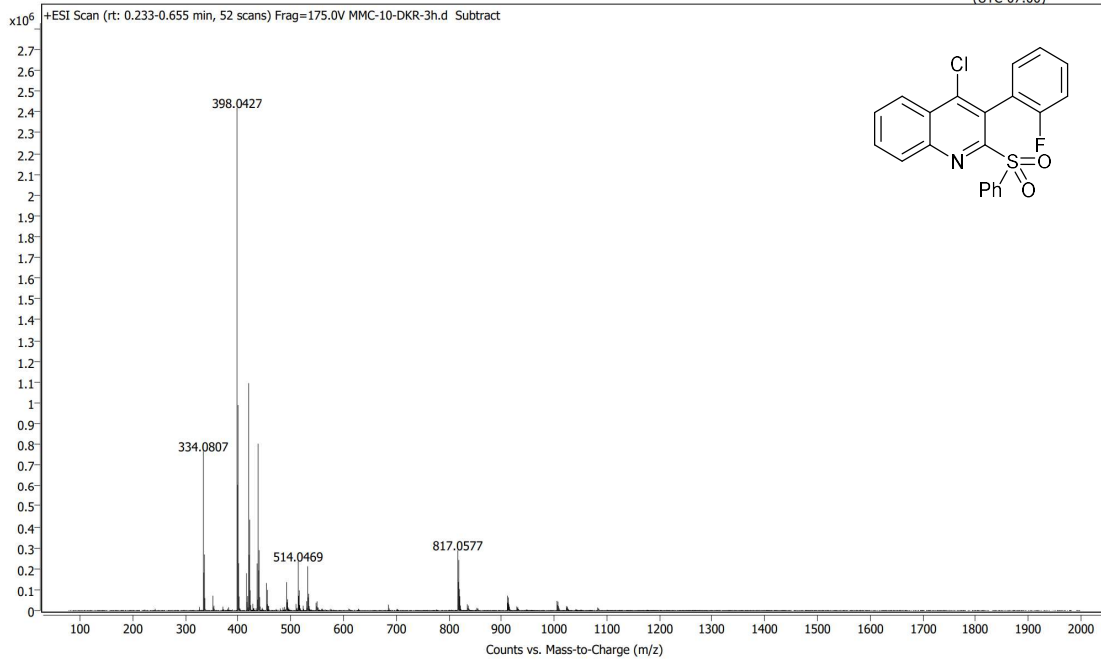
Name	MMC-10-DKR-3h	Rack Pos.	Instrument	Instrument 1	Operator
Inj. Vol. (ul)	1	Plate Pos.	IRM Status	Some ions missed	
Data File	MMC-10-DKR-3h.d	Method (Acq)	Column bypass.m		Acq. Time (Local) 5/13/2021 4:05:01 PM (UTC-07:00)



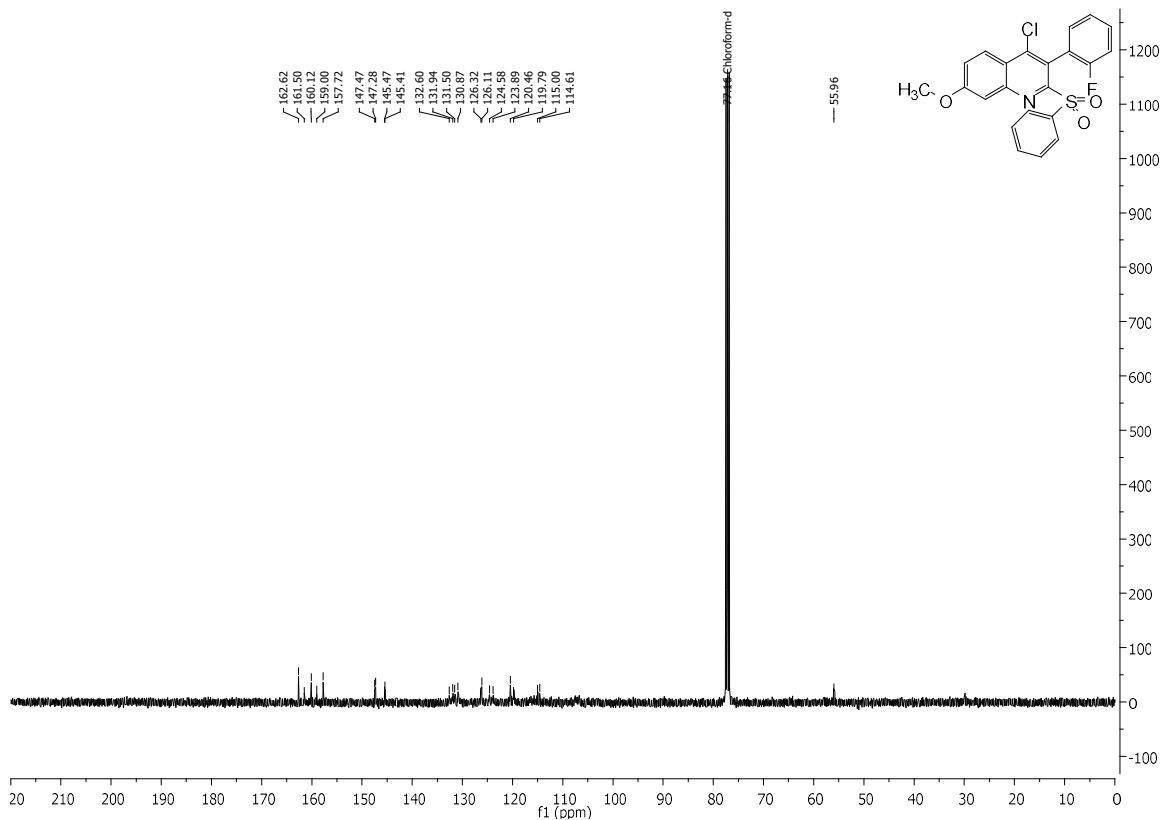
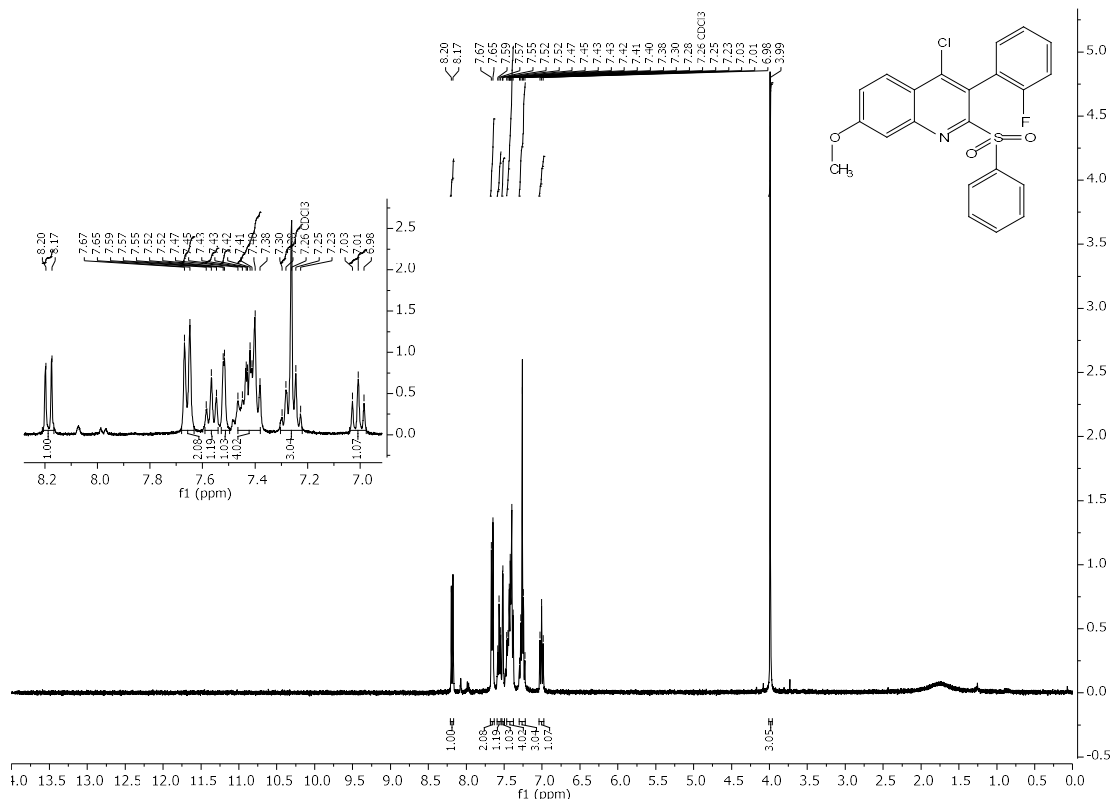
Spectrum Plot Report



Name	MMC-10-DKR-3h	Rack Pos.	Instrument	Instrument 1	Operator
Inj. Vol. (ul)	1	Plate Pos.	IRM Status	Some ions missed	
Data File	MMC-10-DKR-3h.d	Method (Acq)	Column bypass.m		Acq. Time (Local) 5/13/2021 4:05:01 PM (UTC-07:00)

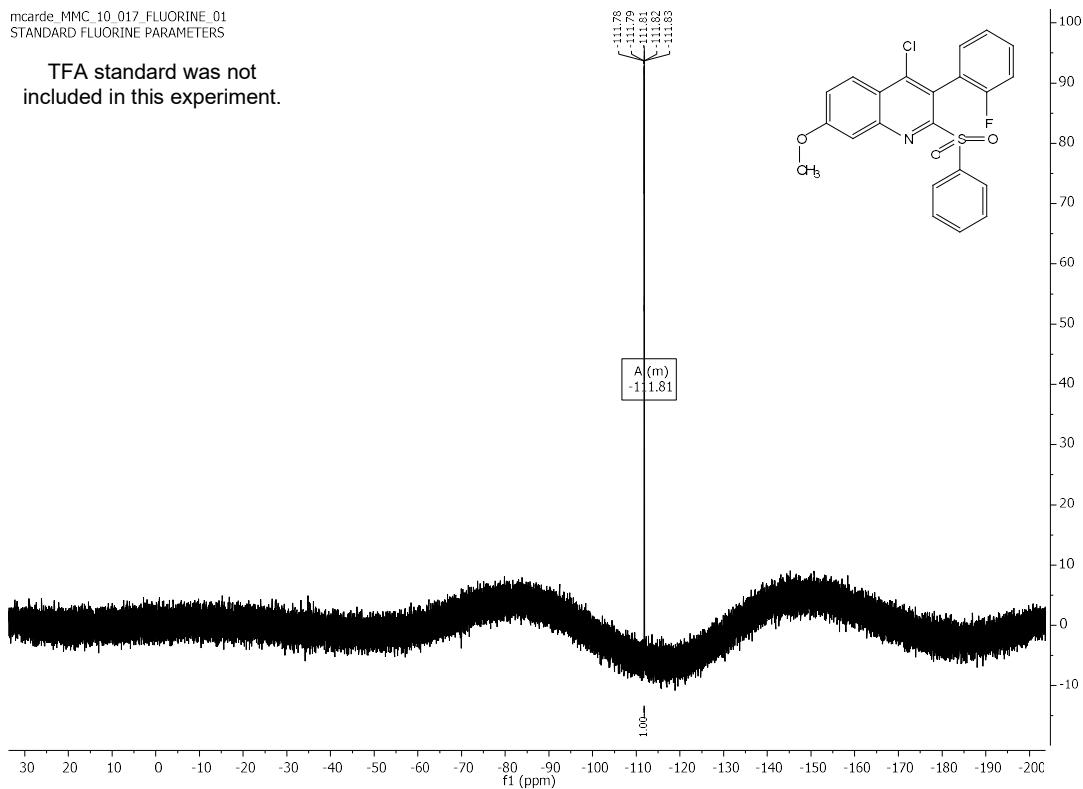


^1H , ^{13}C , and ^{19}F NMR and HRMS (ESI) Spectral Data of **93**



mcarde_MMC_10_017_FLUORINE_01
STANDARD FLUORINE PARAMETERS

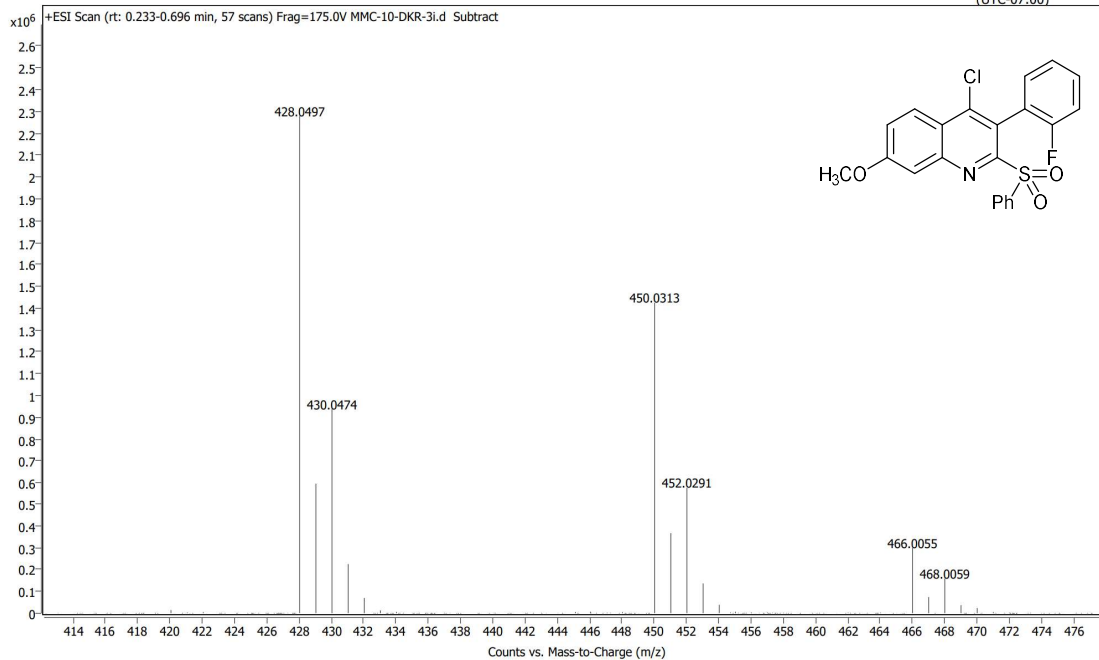
TFA standard was not included in this experiment.



Spectrum Plot Report



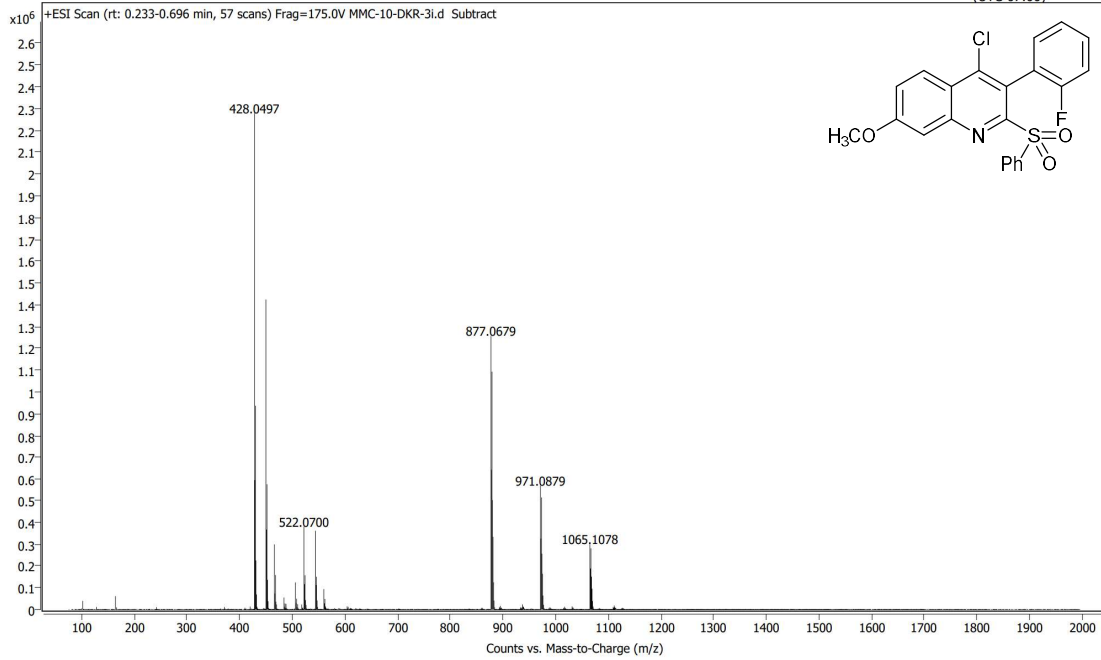
Name	MMC-10-DKR-3i	Rack Pos.		Instrument	Instrument 1	Operator
Inj. Vol. (ul)	1	Plate Pos.		IRM Status	Success	
Data File	MMC-10-DKR-3i.d	Method (Acq)	Column bypass.m	Comment		Acq. Time (Local) 5/13/2021 4:10:16 PM (UTC-07:00)



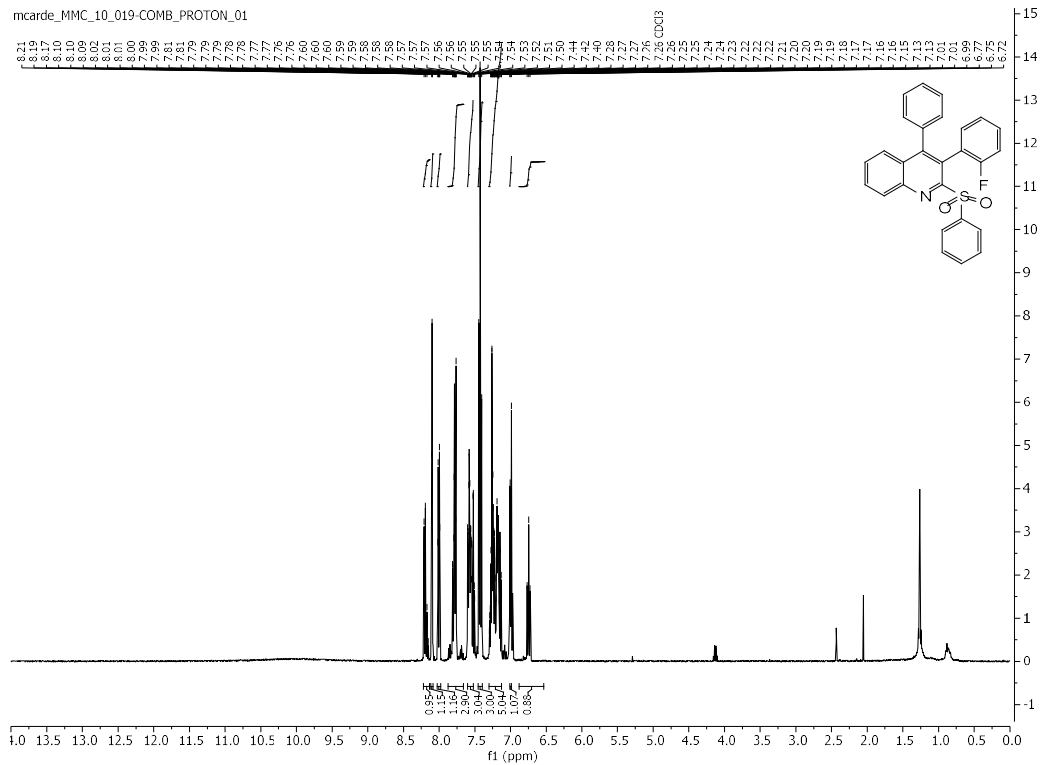
Spectrum Plot Report

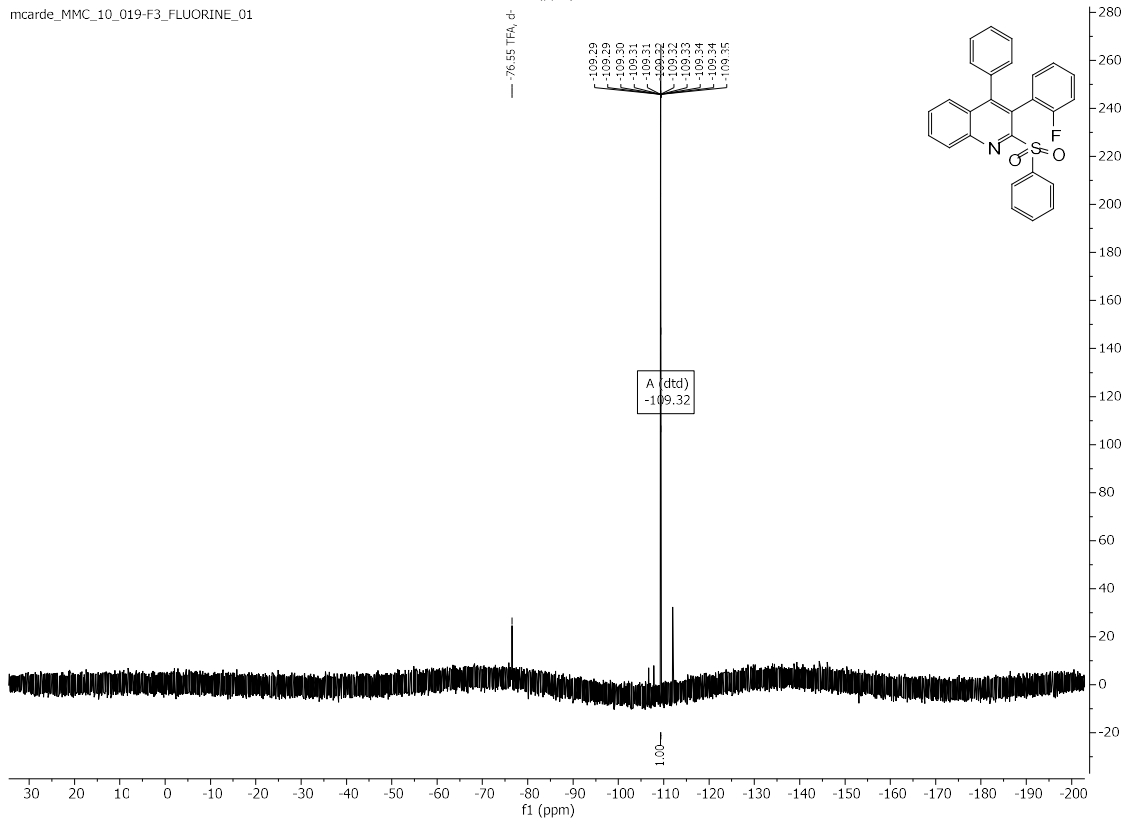
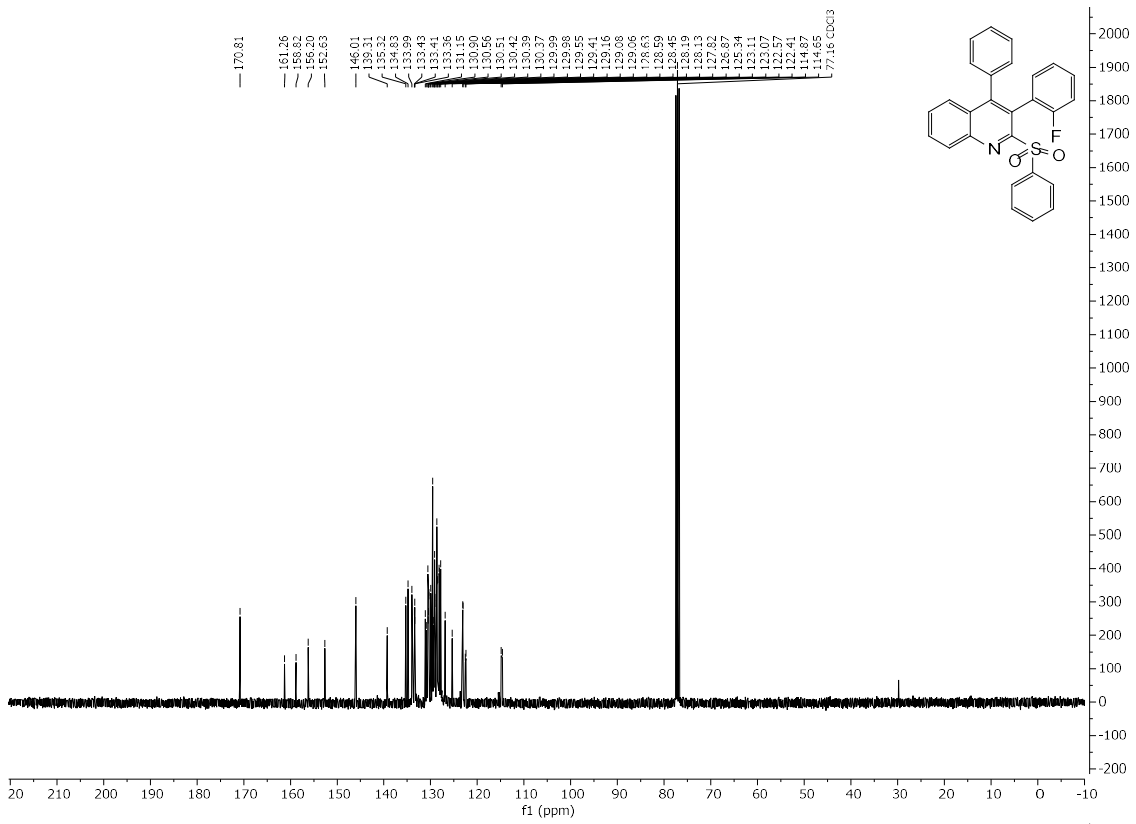


Name: MMC-10-DKR-3i Rack Pos.: Instrument: Instrument 1 Operator: Acq. Time (Local): 5/13/2021 4:10:16 PM
 Inj. Vol. (ul): 1 Plate Pos.: IRM Status: Success
 Data File: MMC-10-DKR-3i.d Method (Acq): Column bypass.m Comment: (UTC-07:00)



¹H, ¹³C, and ¹⁹F NMR and HRMS (ESI) Spectral Data of **95**

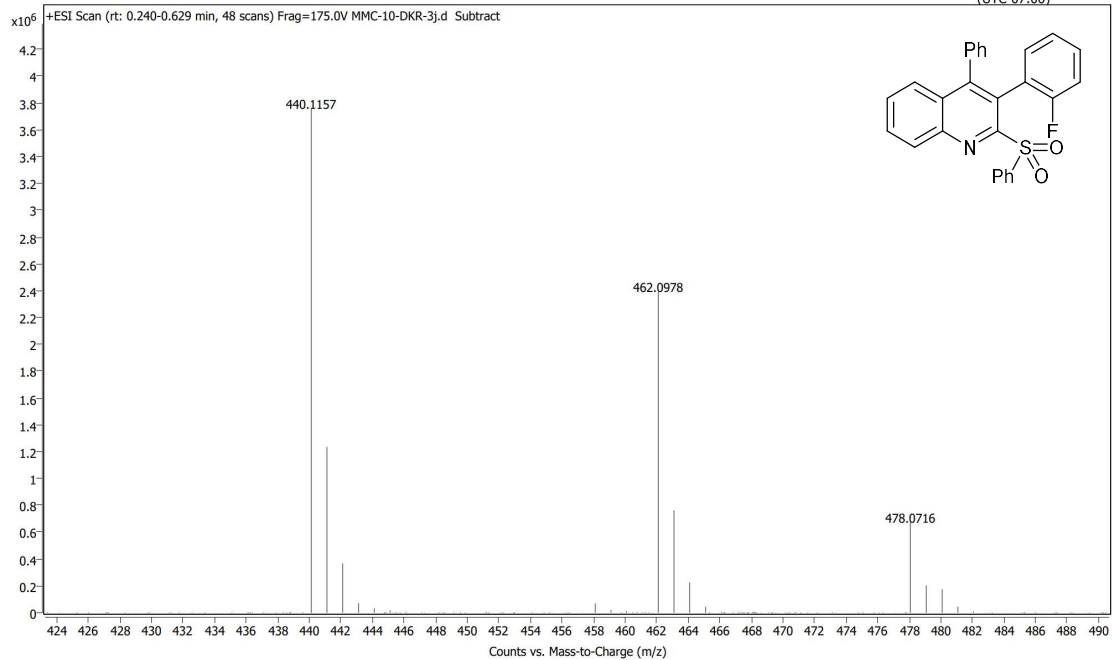




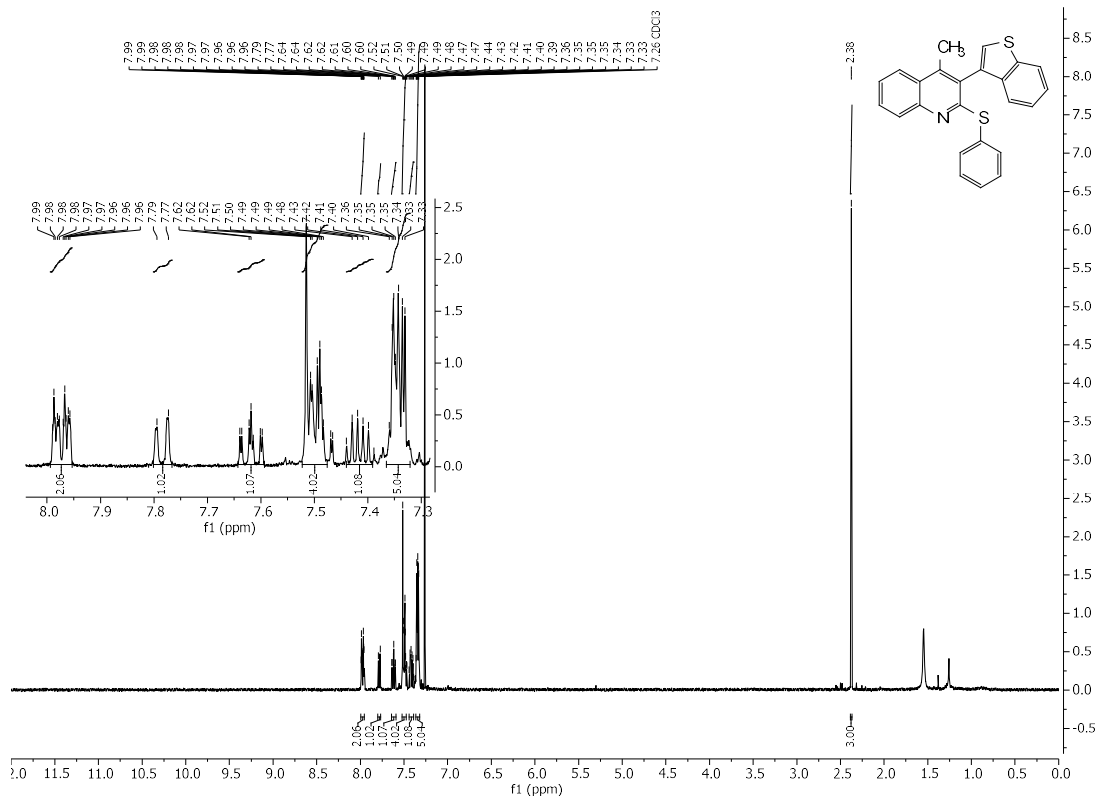
Spectrum Plot Report

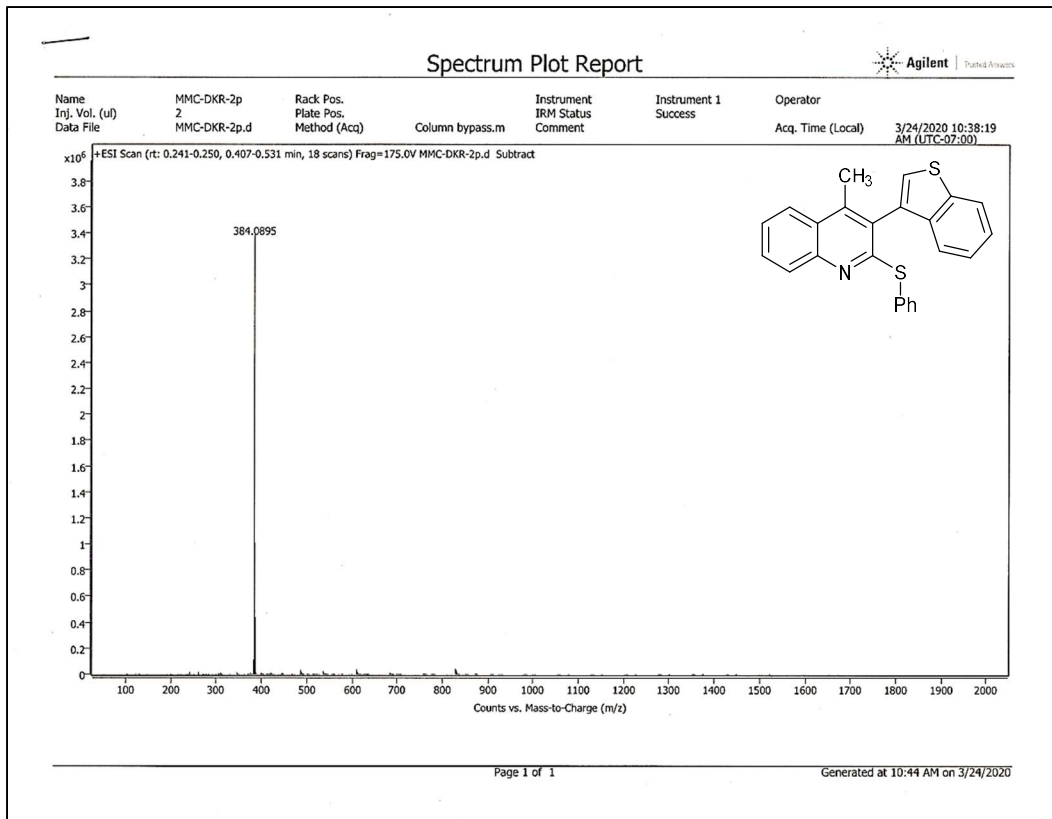
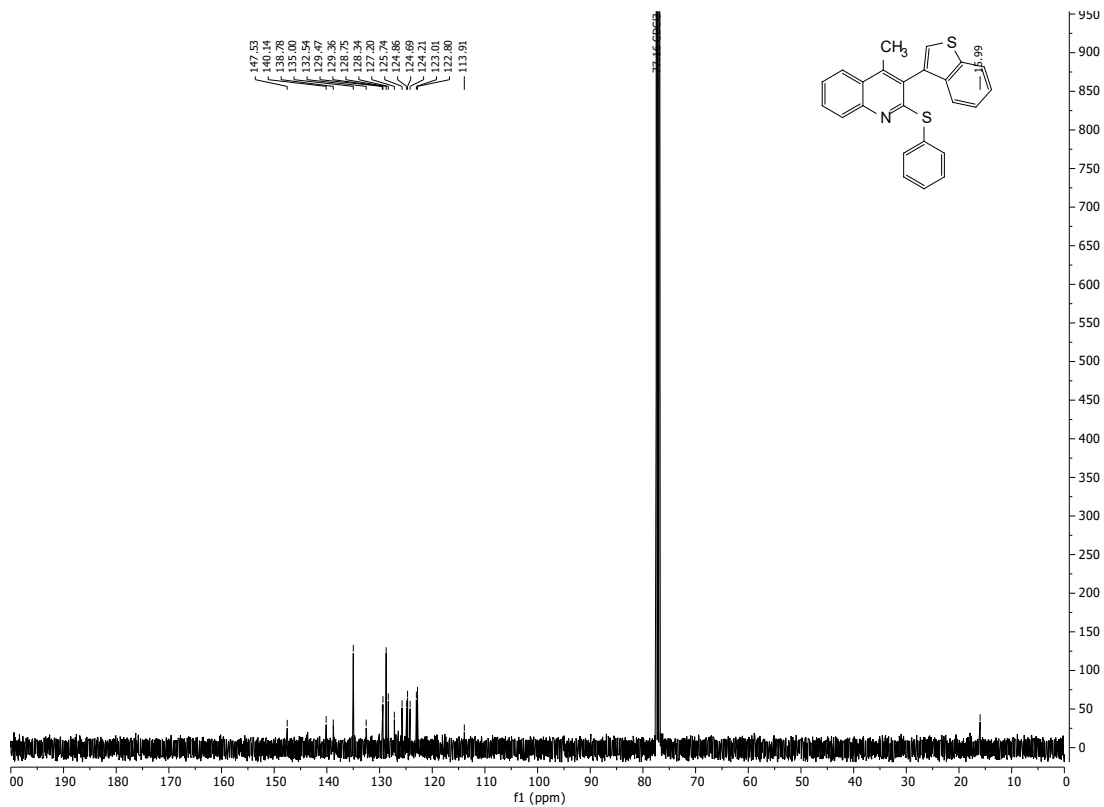


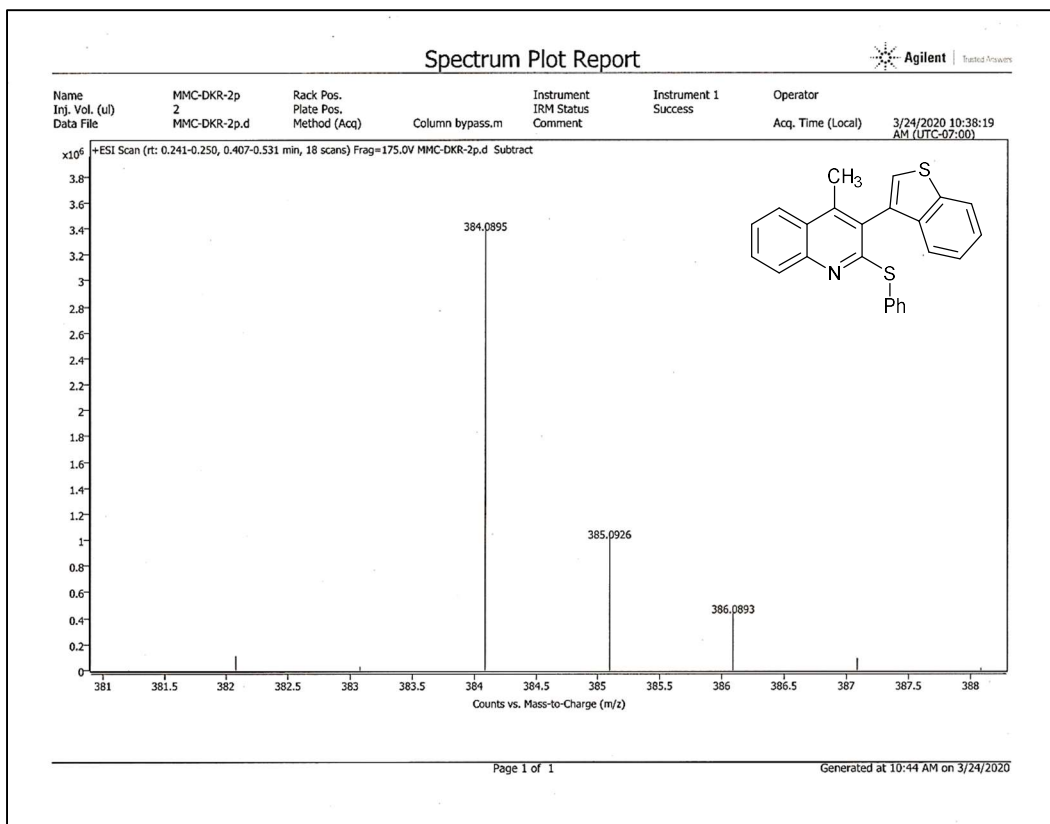
Name	MMC-10-DKR-3j	Rack Pos.		Instrument	Instrument 1	Operator
Inj. Vol. (ul)	1	Plate Pos.		IRM Status	Some ions missed	
Data File	MMC-10-DKR-3j.d	Method (Acq)	Column bypass.m	Comment		Acq. Time (Local) 5/13/2021 4:15:55 PM (UTC-07:00)



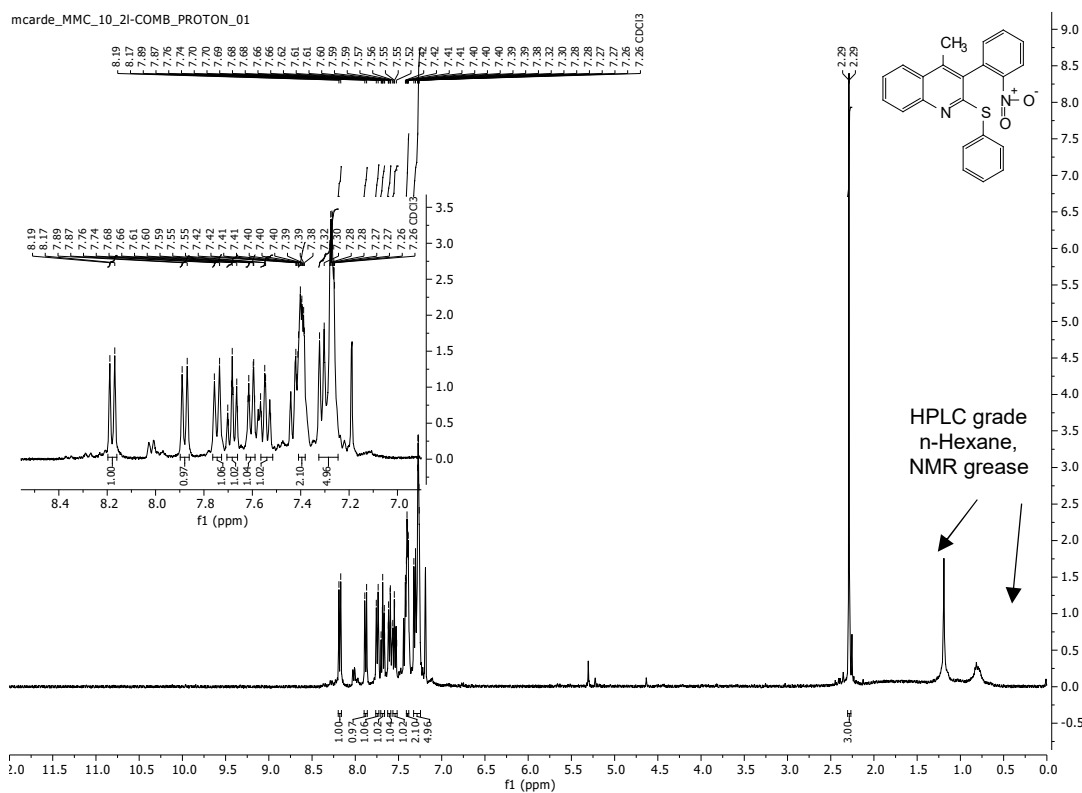
¹H, ¹³C, and ¹⁹F NMR and HRMS (ESI) Spectral Data of **96**



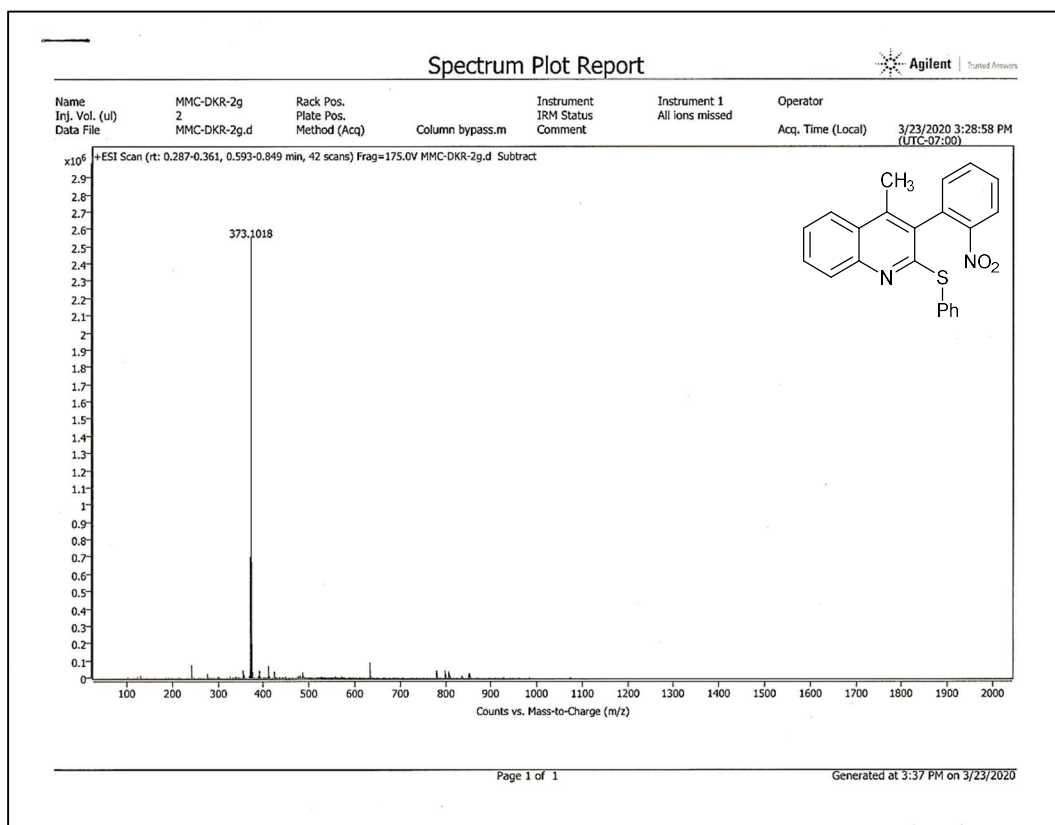
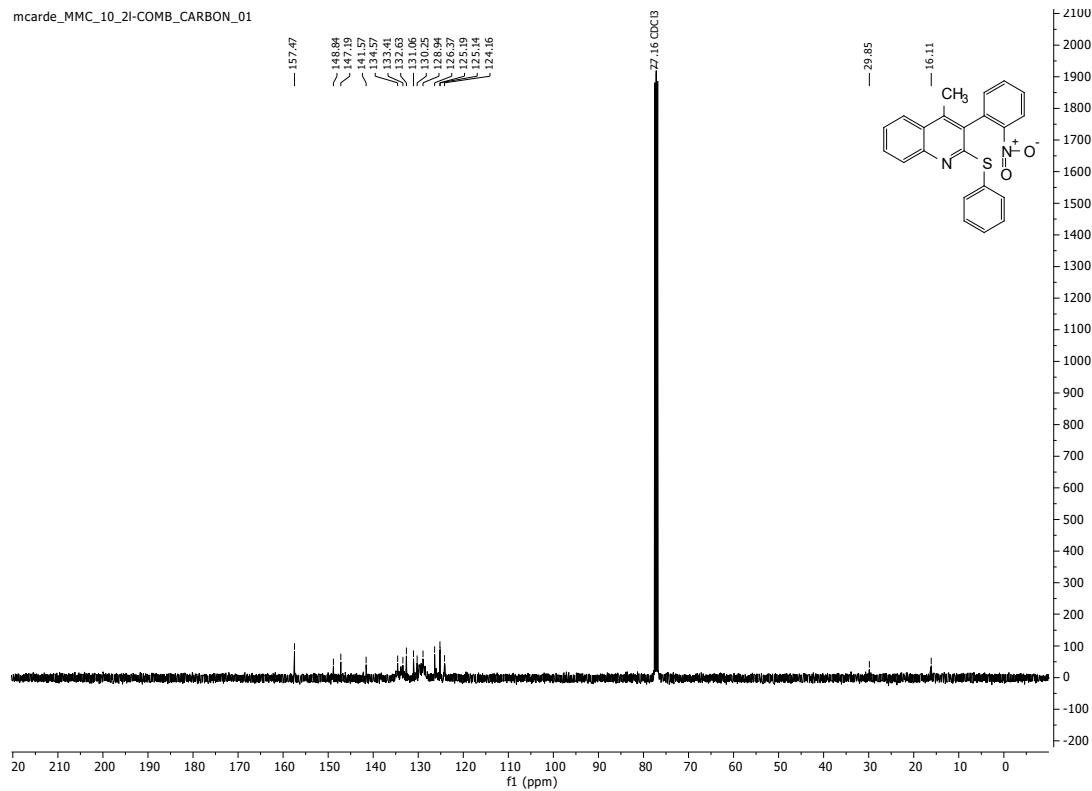




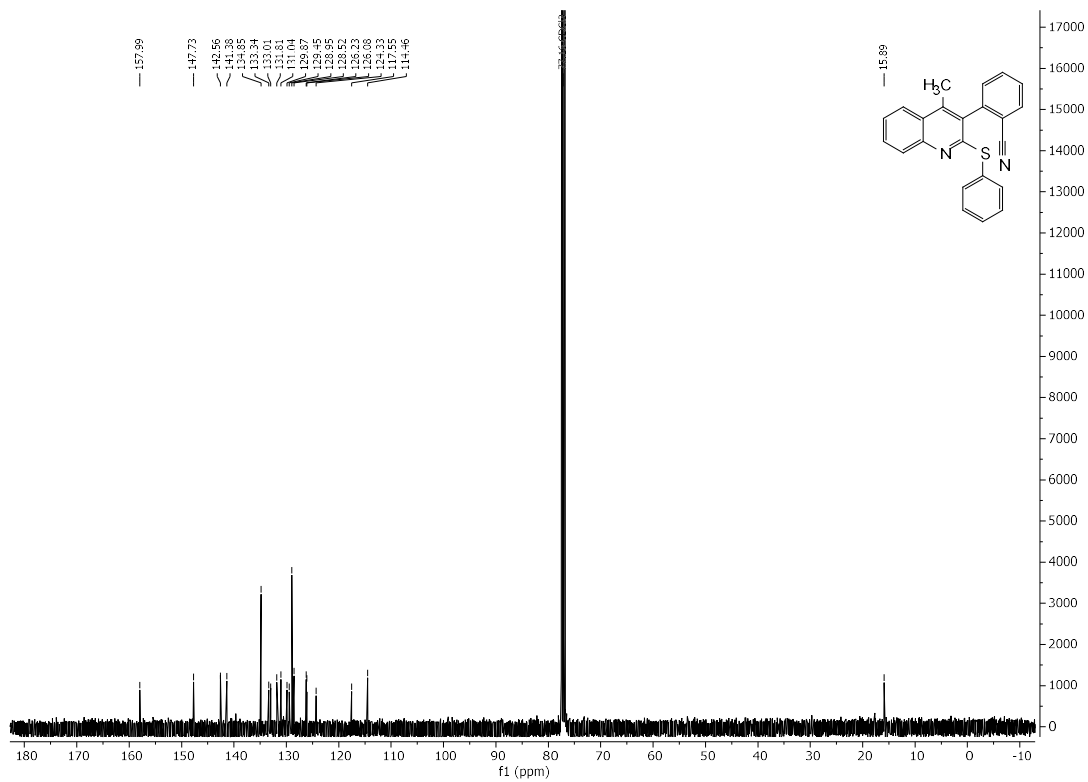
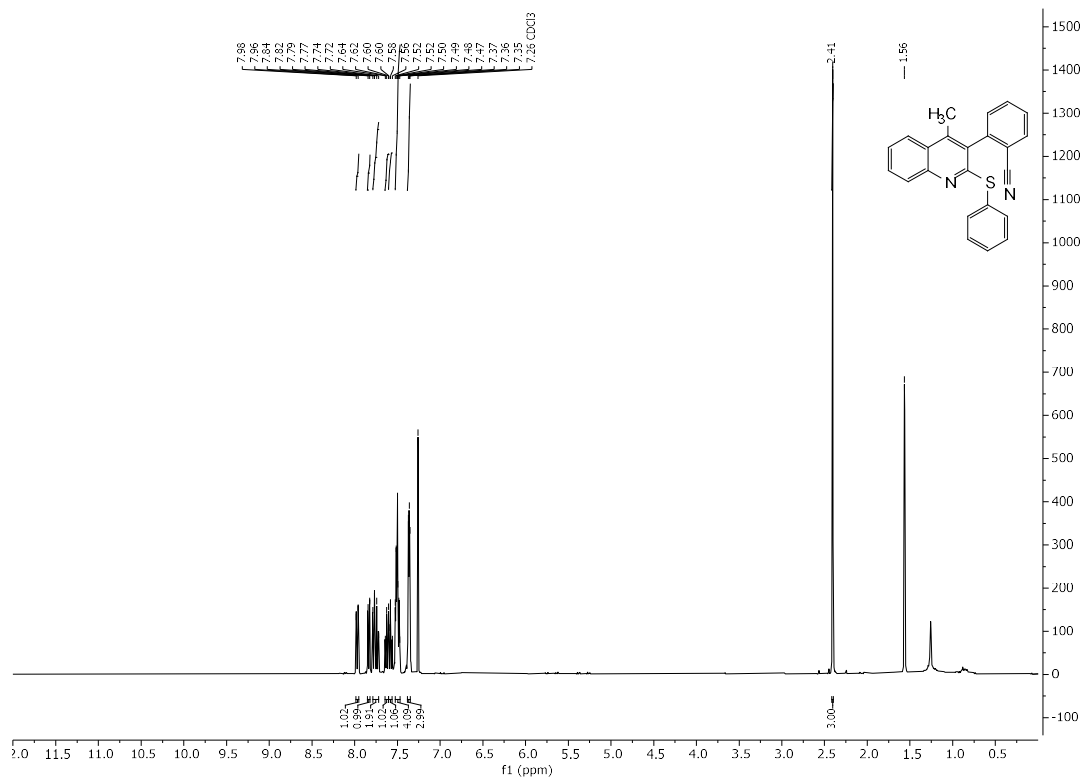
¹H (trace CDCl₃ grease), ¹³C and HRMS (ESI) Spectral Data of 97



mcardc MMC_10_2I-COMB CARBON_01

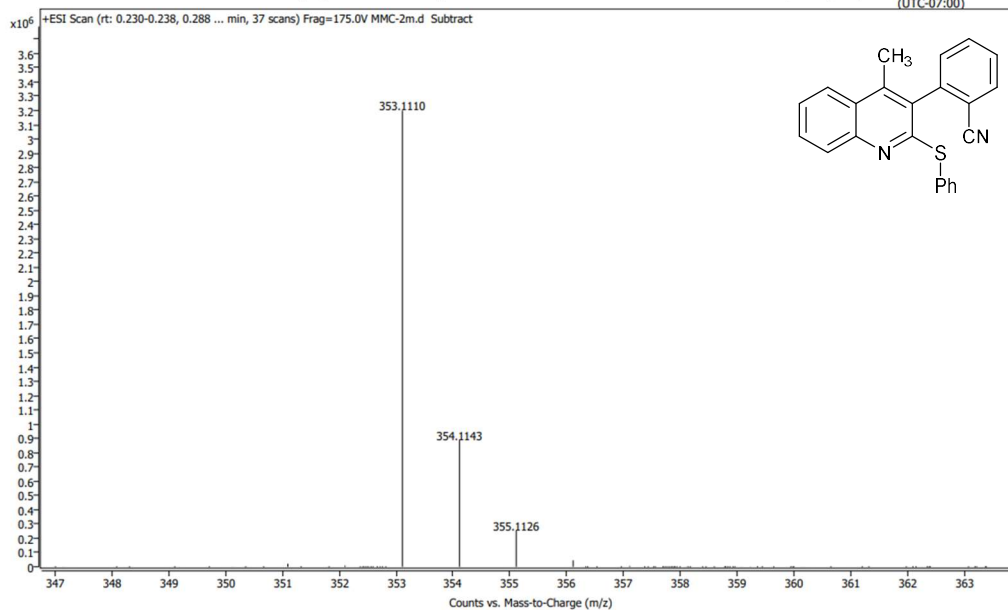


^1H , ^{13}C , and HRMS (ESI) Spectral Data of **99**

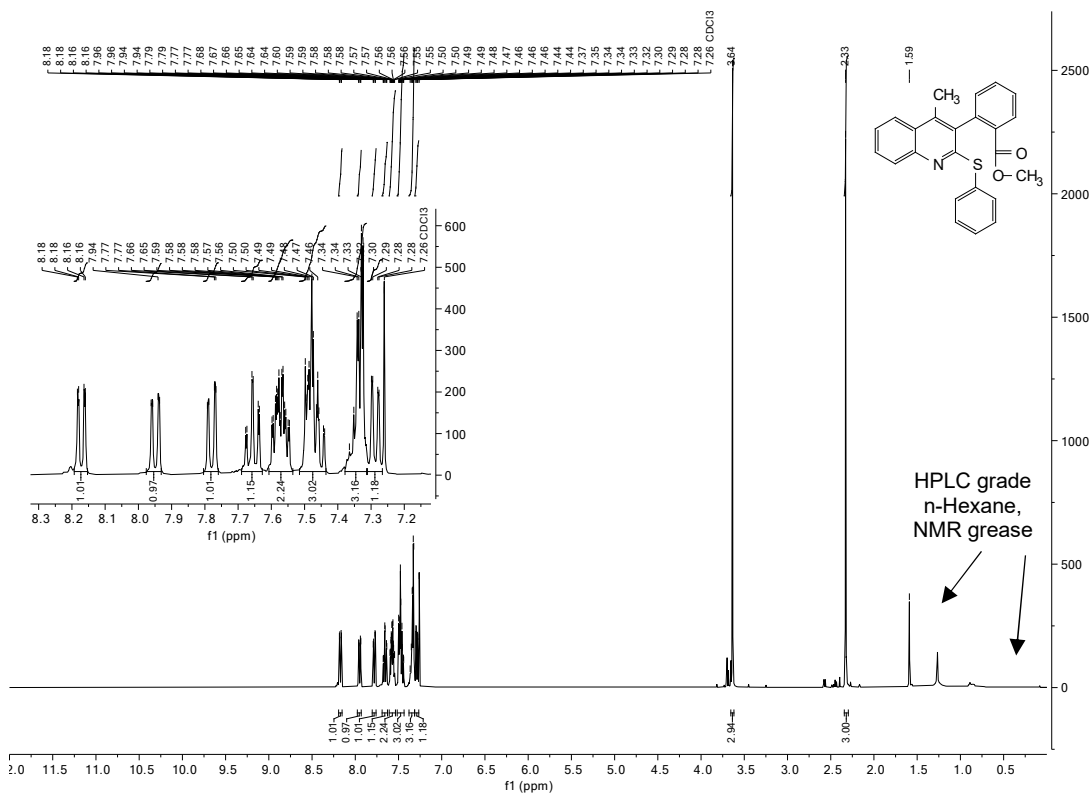


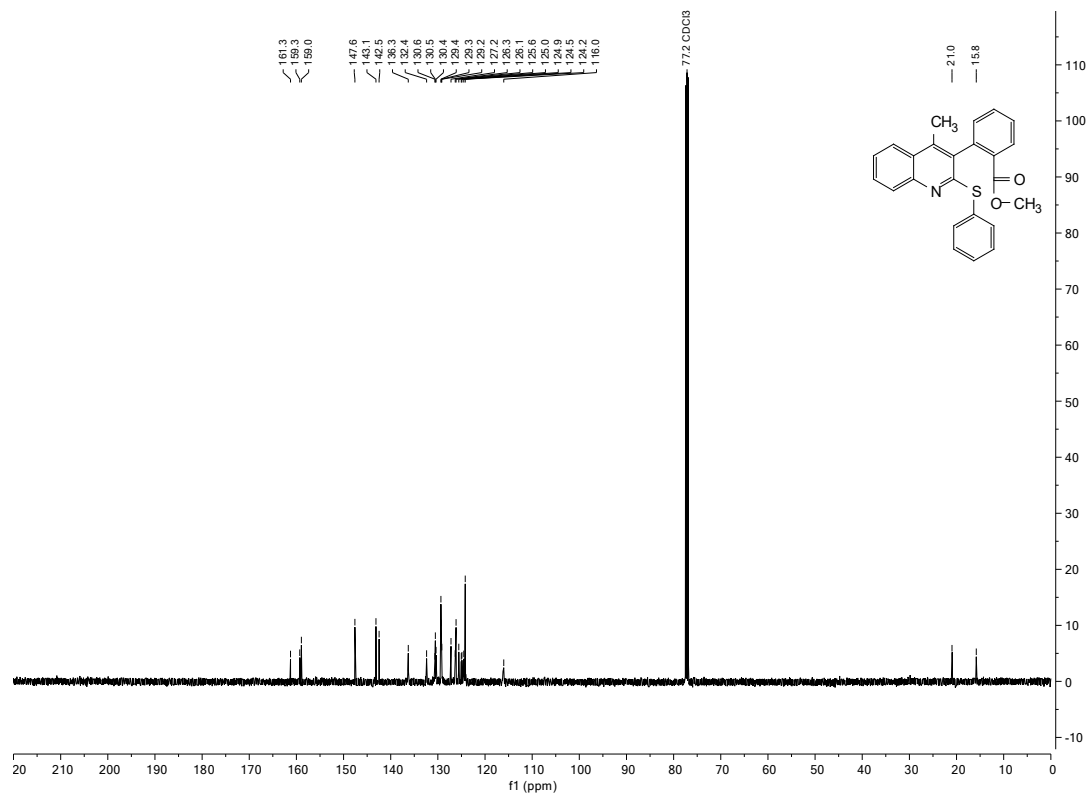
Spectrum Plot Report

Name	Inj. Vol. (ul)	Rack Pos.	Plate Pos.	Instrument	IRM Status	Instrument 1	Operator
Data File	1	Method (Acq)	Column bypass.m	Comment	Success	Acq. Time (Local)	8/6/2021 3:38:40 PM (UTC-07:00)

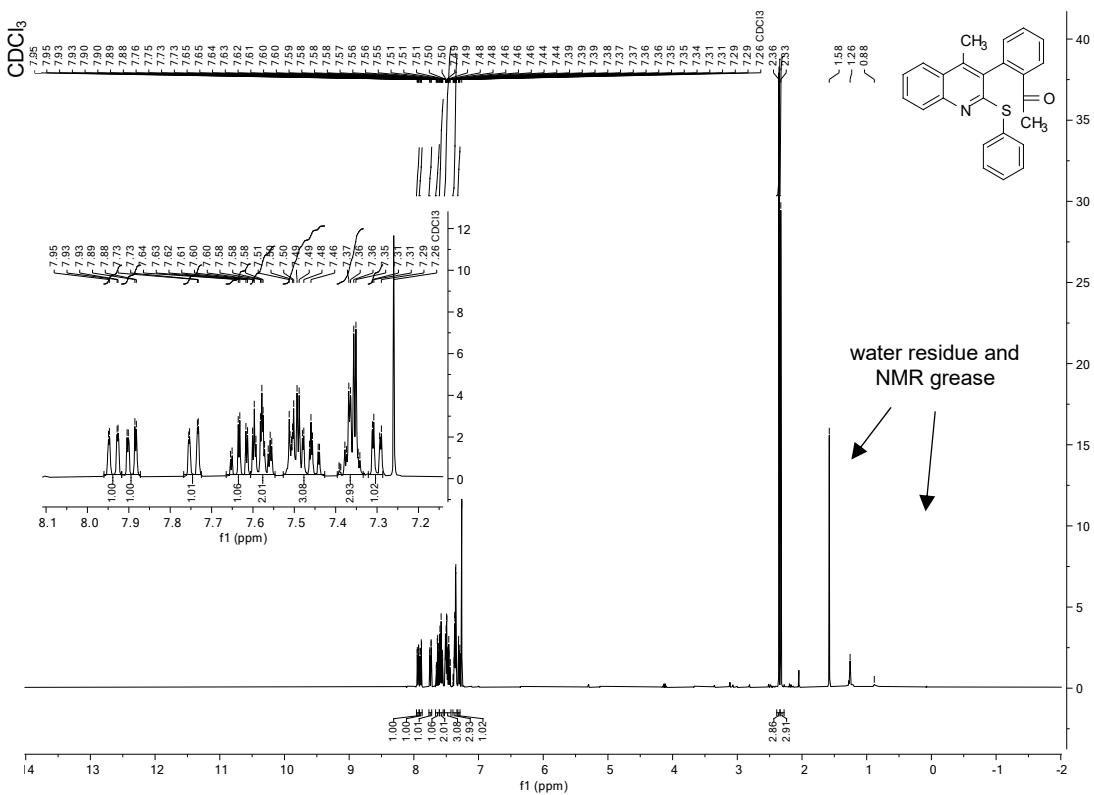


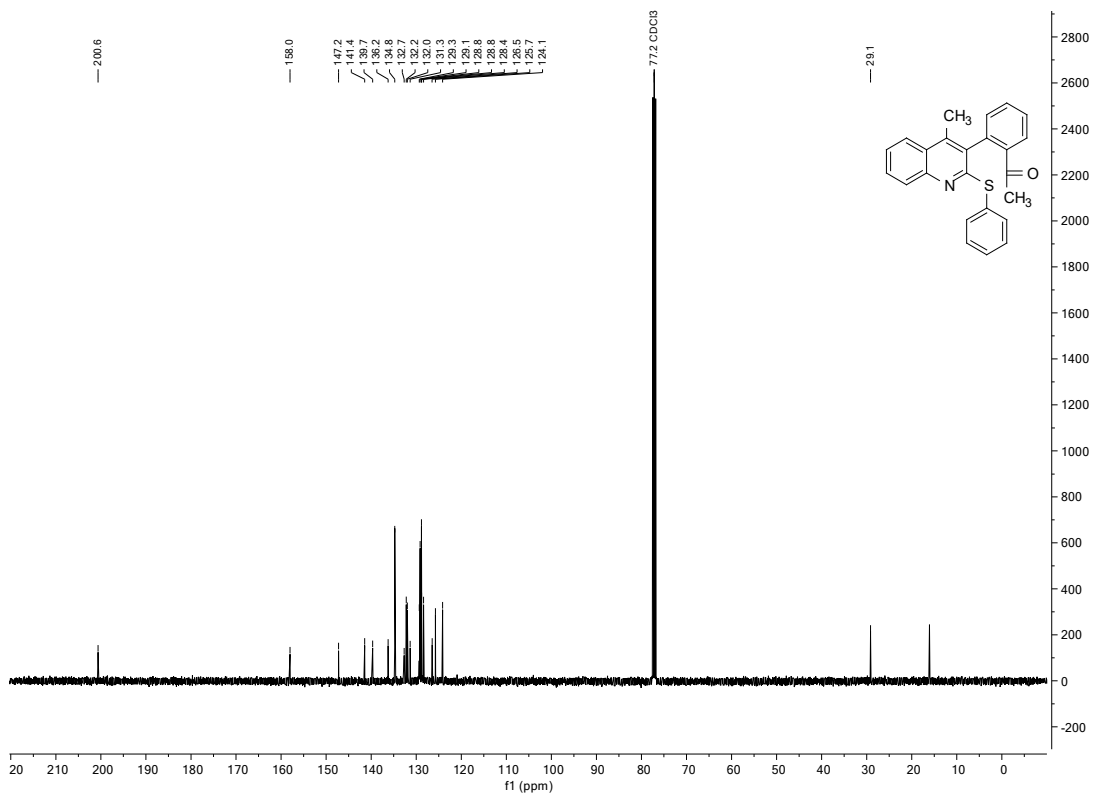
^1H (trace CDCl_3 grease) and ^{13}C NMR Spectral Data of **101**





^1H (trace CDCl₃ water and grease), ^{13}C , and HRMS (ESI) Spectral Data of **103**

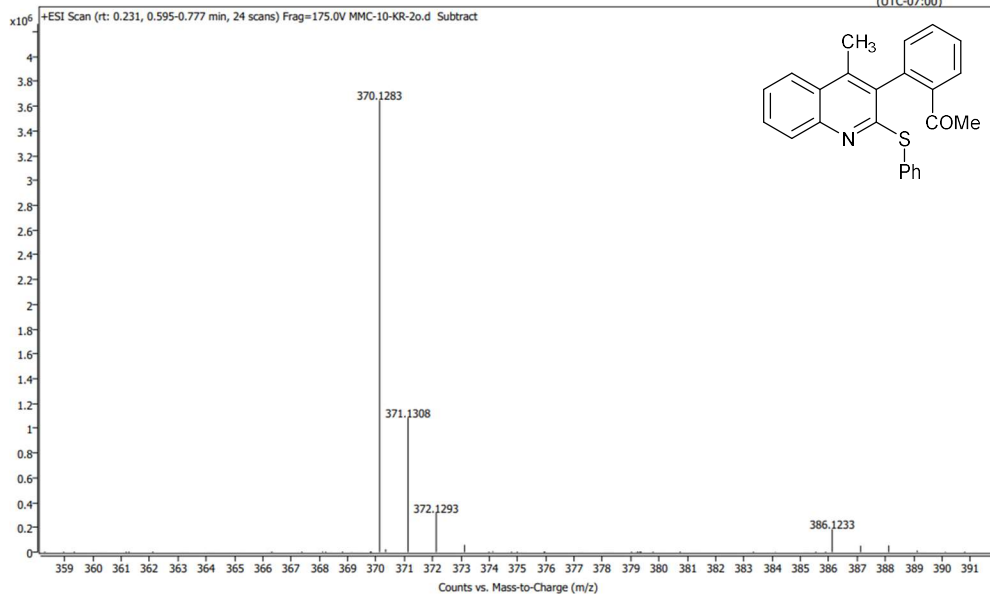




Spectrum Plot Report

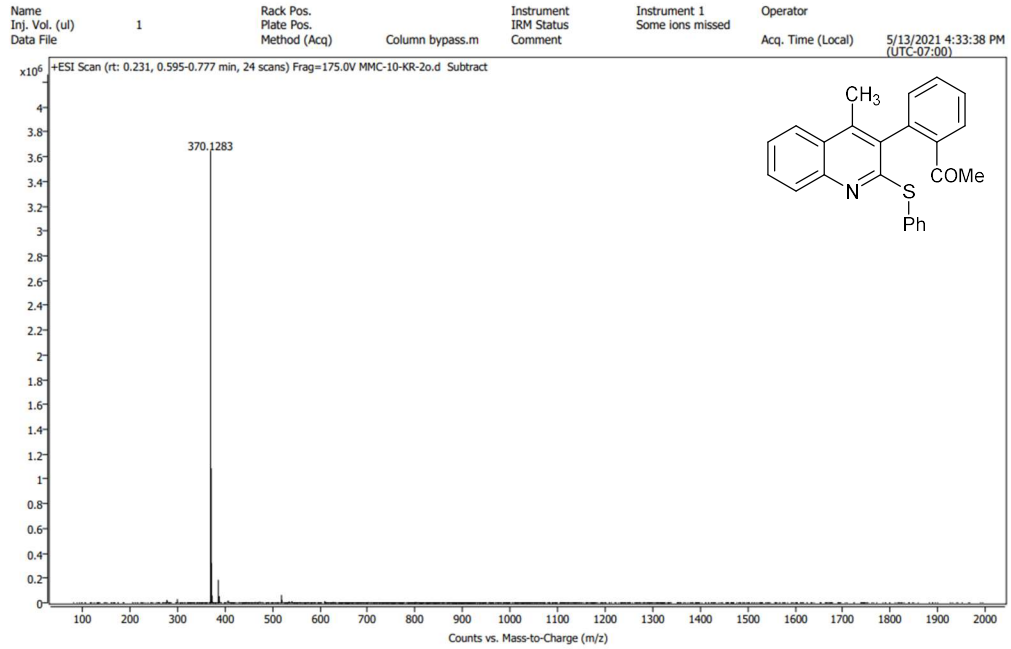
Agilent | Rapid Answer

Name	Inj. Vol. (ul)	1	Rack Pos.	Plate Pos.	Method (Acq)	Column bypass.m	Instrument	IRM Status	Instrument 1	Operator	Acq. Time (Local)
Data File							Comment	Some ions missed			5/13/2021 4:33:38 PM (UTC-07:00)



Spectrum Plot Report

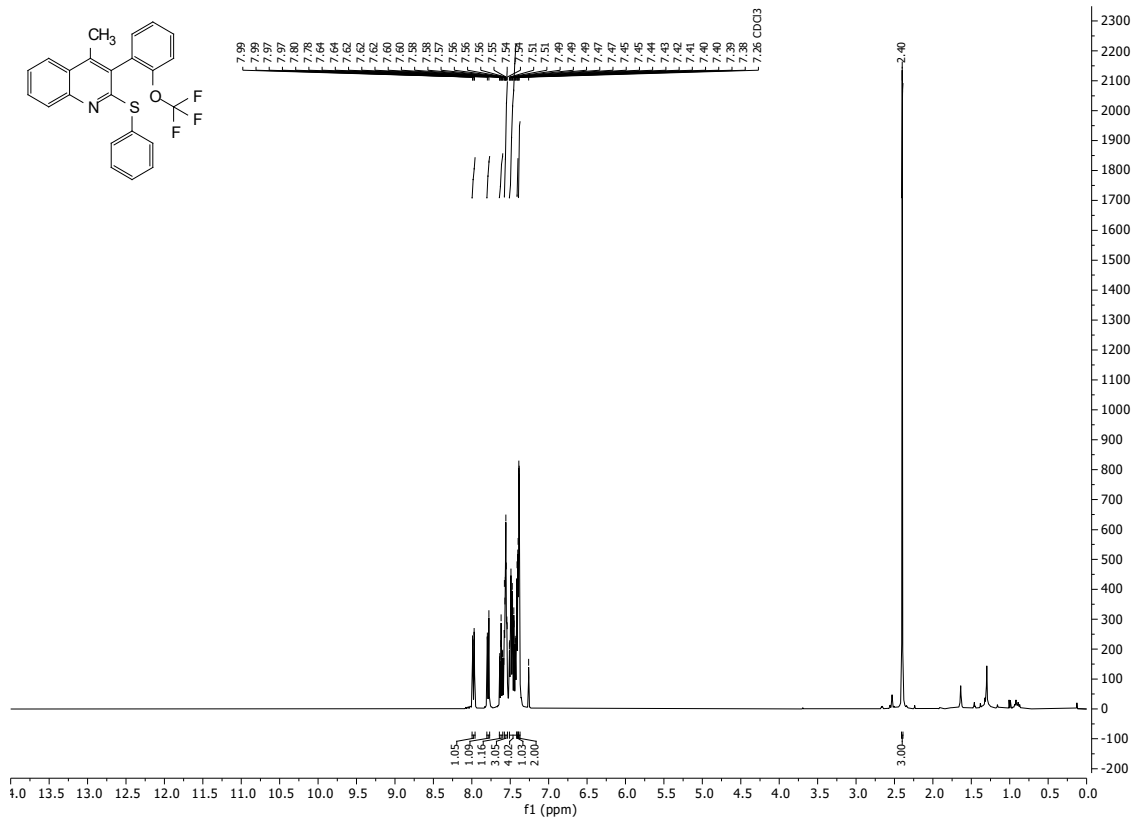
Agilent | Exact Analysis

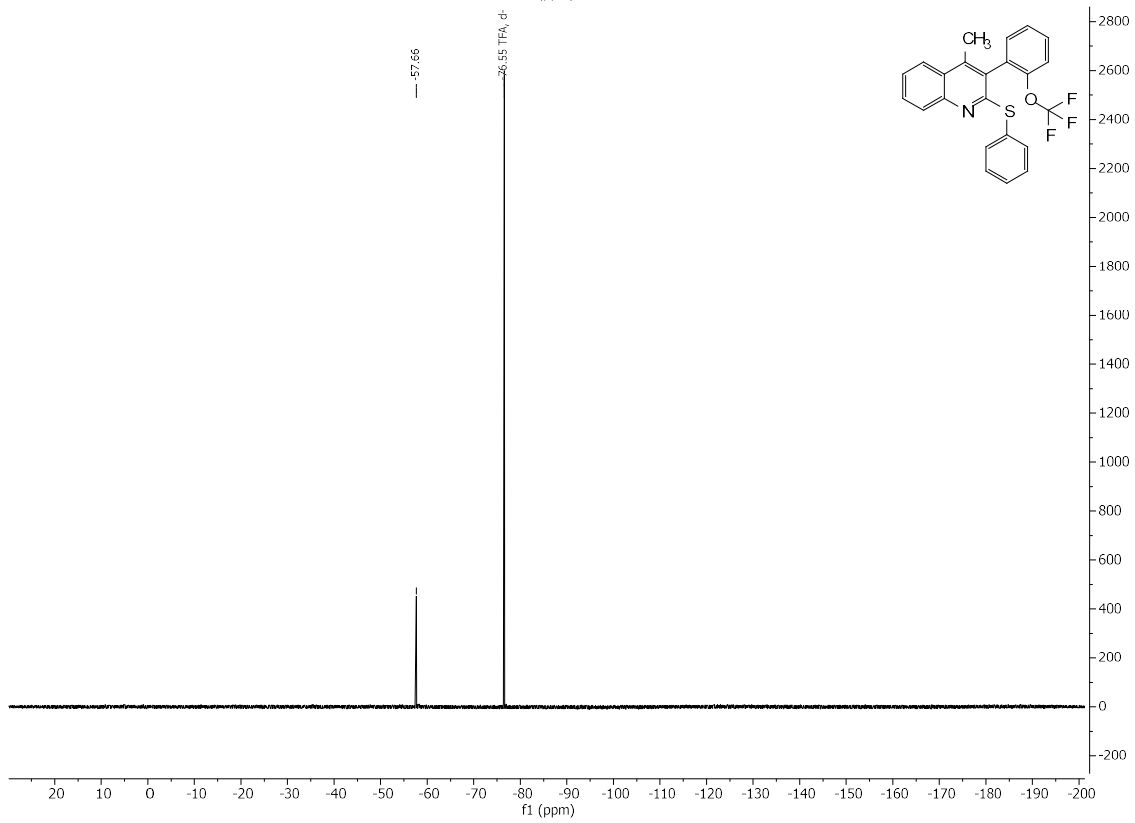
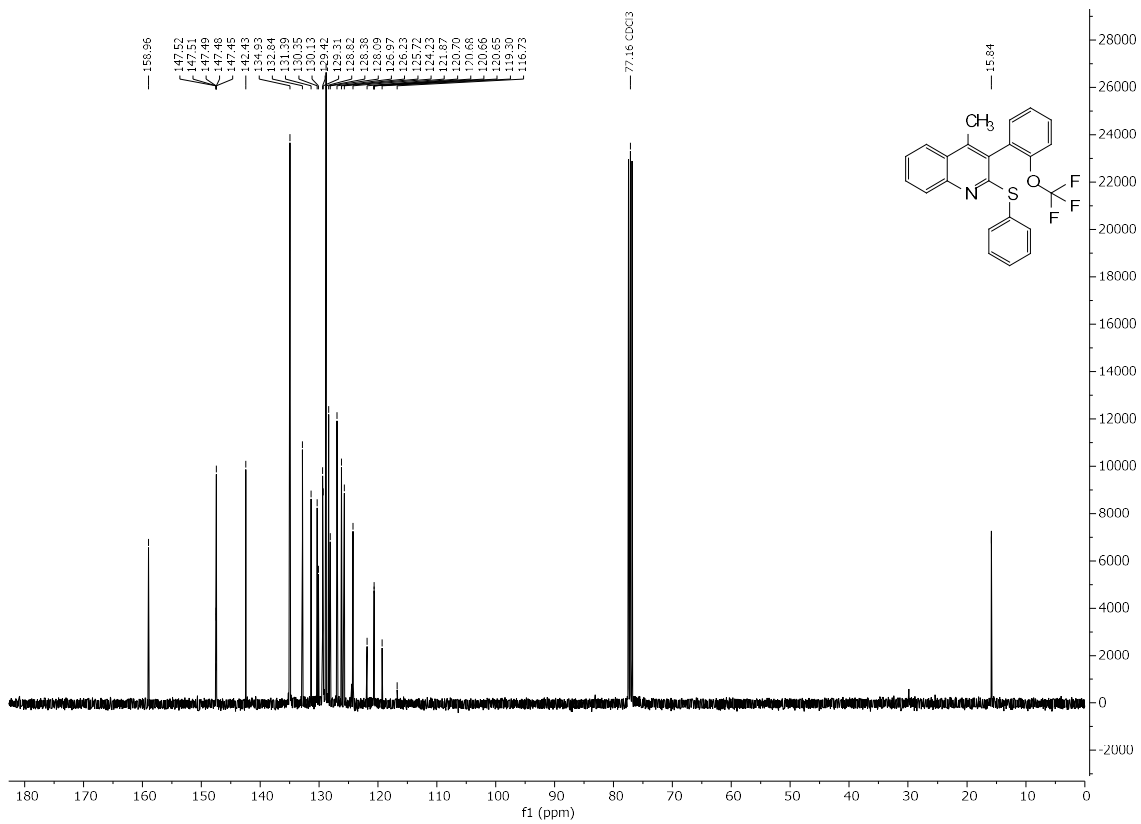


Page 1 of 1

Generated at 4:40 PM on 5/13/2021

¹H, ¹³C, and ¹⁹F NMR and HRMS (ESI) Spectral Data of 105

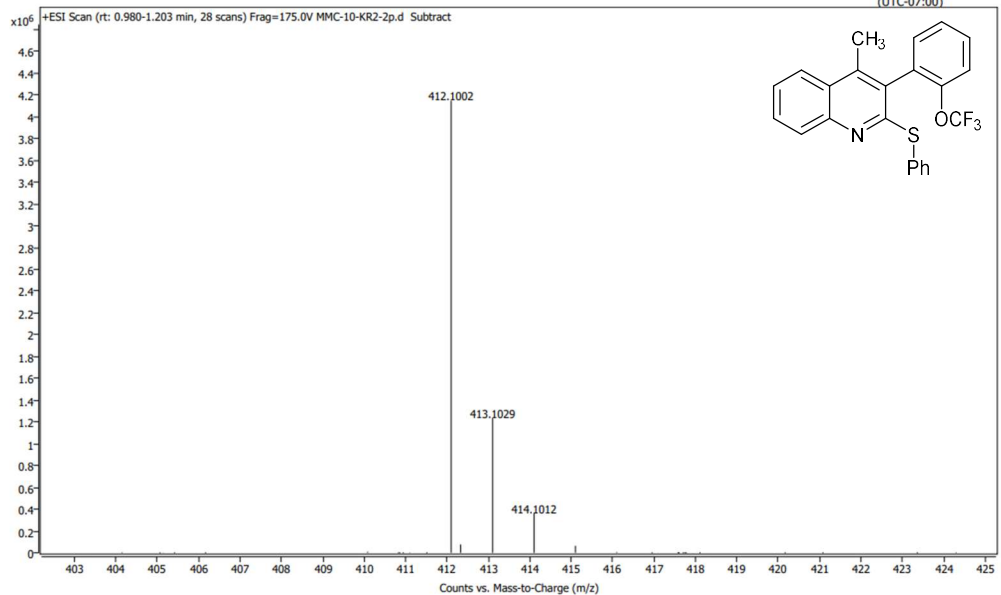




Spectrum Plot Report



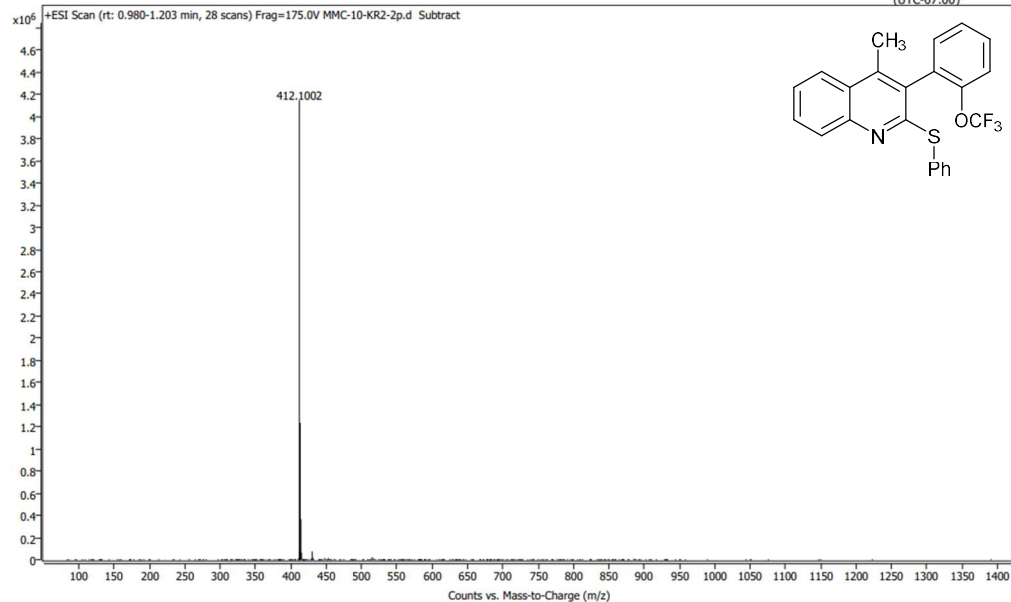
Name	MMC-10-KR2-2p	Rack Pos.	Instrument	Instrument 1	Operator
Inj. Vol. (ul)	1	Plate Pos.	IRM Status	Success	
Data File	MMC-10-KR2-2p.d	Method (Acq)	Column bypass.m	Comment	Acq. Time (Local) 5/13/2021 4:44:28 PM (UTC-07:00)



Spectrum Plot Report



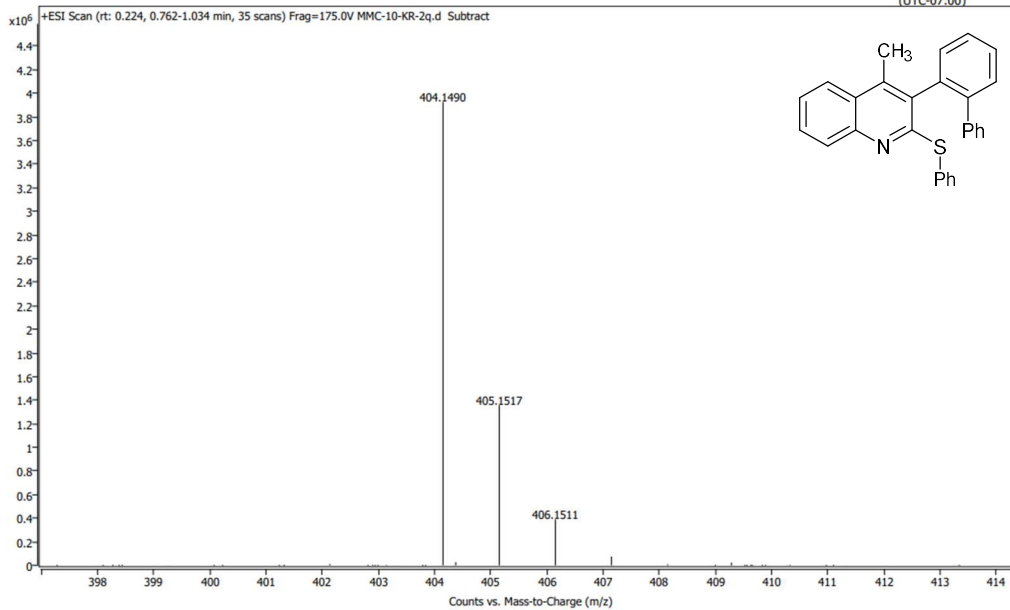
Name	MMC-10-KR2-2p	Rack Pos.	Instrument	Instrument 1	Operator
Inj. Vol. (ul)	1	Plate Pos.	IRM Status	Success	
Data File	MMC-10-KR2-2p.d	Method (Acq)	Column bypass.m	Comment	Acq. Time (Local) 5/13/2021 4:44:28 PM (UTC-07:00)



Spectrum Plot Report

Agilent | Trusted Answers

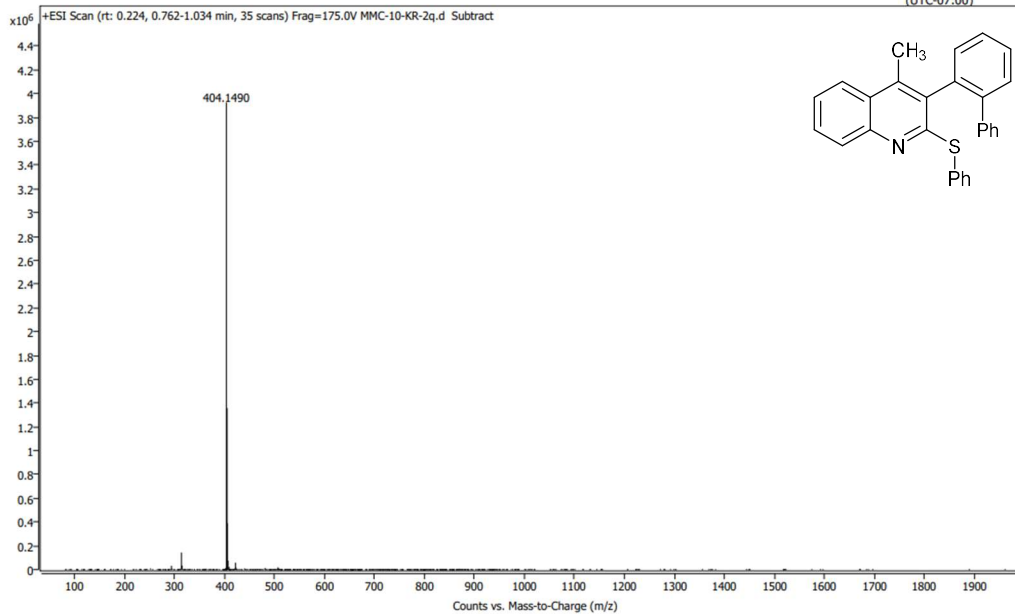
Name	MMC-10-KR-2q	Rack Pos.	Instrument	Instrument 1	Operator
Inj. Vol. (ul)	1	Plate Pos.	IRM Status	Some ions missed	
Data File	MMC-10-KR-2q.d	Method (Acq)	Column bypass.m	Comment	Acq. Time (Local) 5/13/2021 4:52:13 PM (UTC-07:00)



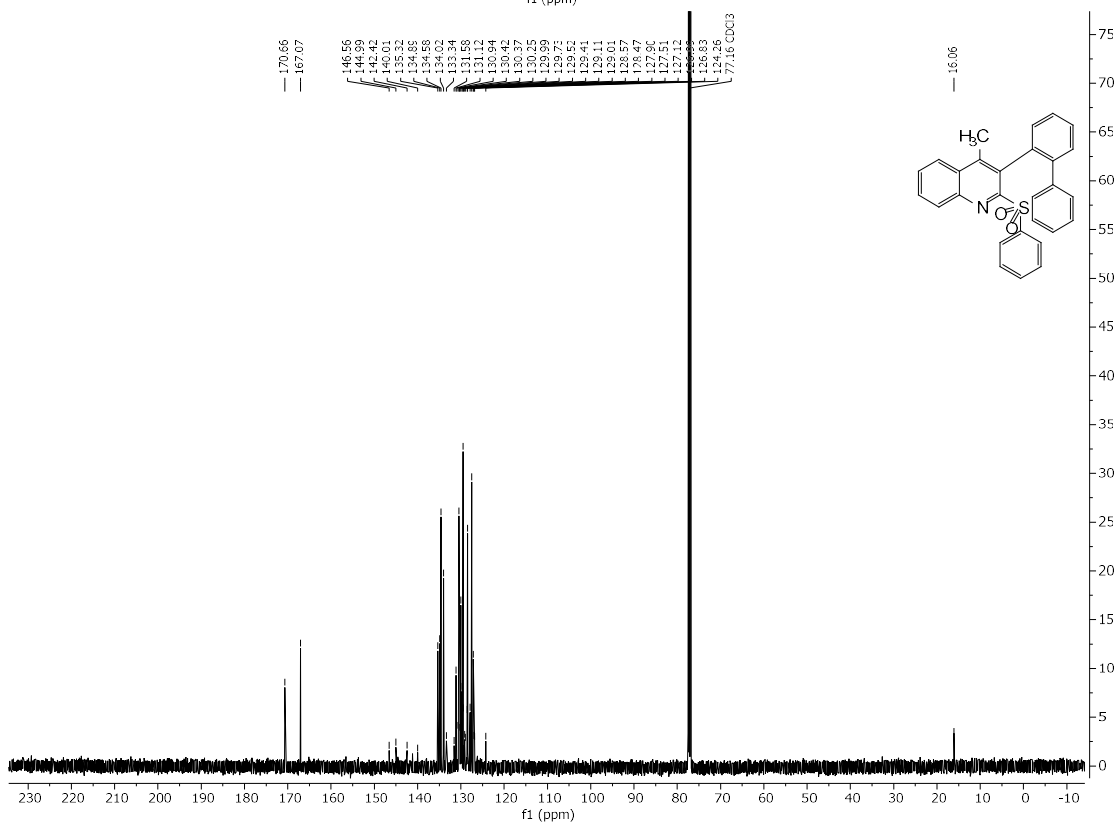
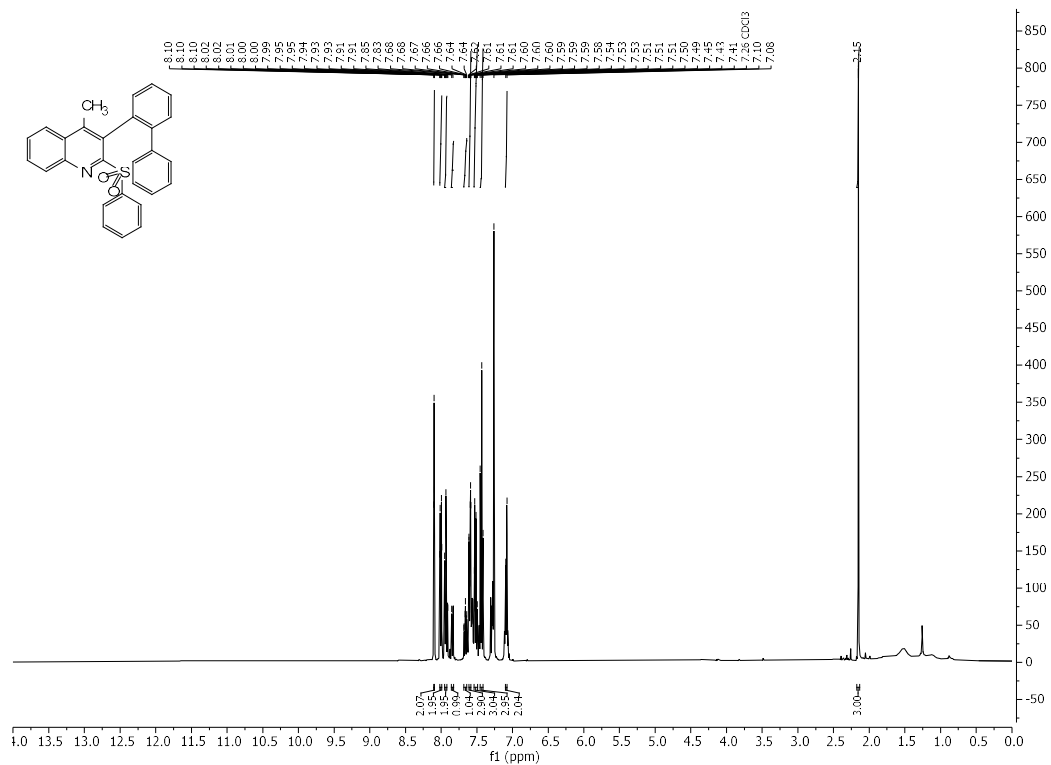
Spectrum Plot Report

Agilent | Trusted Answers

Name	MMC-10-KR-2q	Rack Pos.	Instrument	Instrument 1	Operator
Inj. Vol. (ul)	1	Plate Pos.	IRM Status	Some ions missed	
Data File	MMC-10-KR-2q.d	Method (Acq)	Column bypass.m	Comment	Acq. Time (Local) 5/13/2021 4:52:13 PM (UTC-07:00)



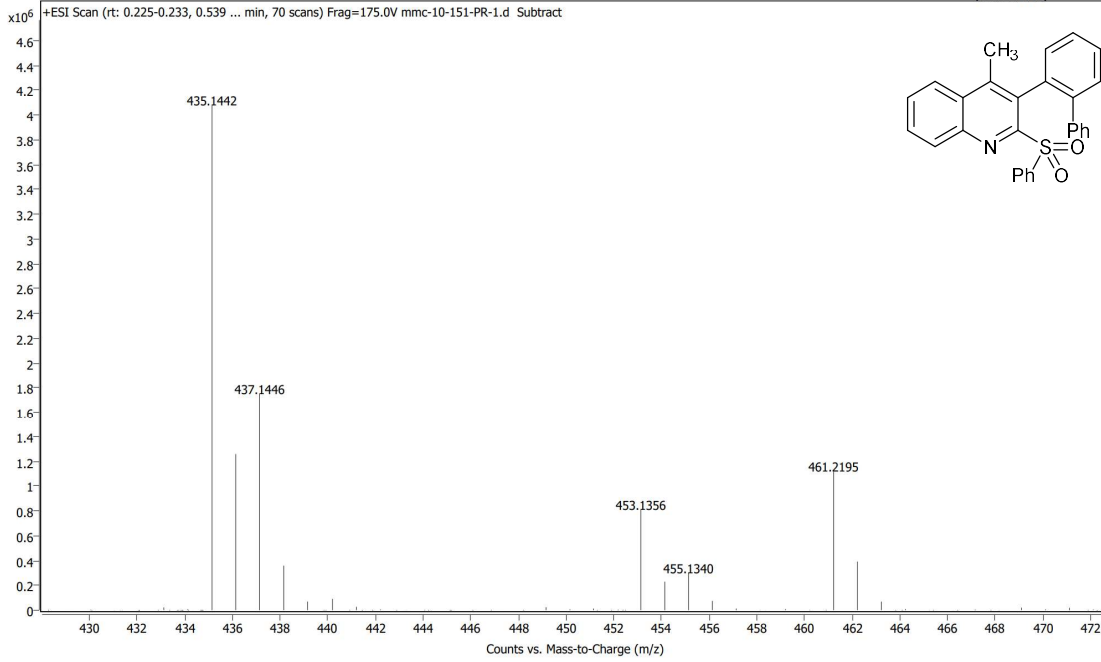
^1H , ^{13}C and HRMS (ESI) Spectral Data of **119**



Spectrum Plot Report



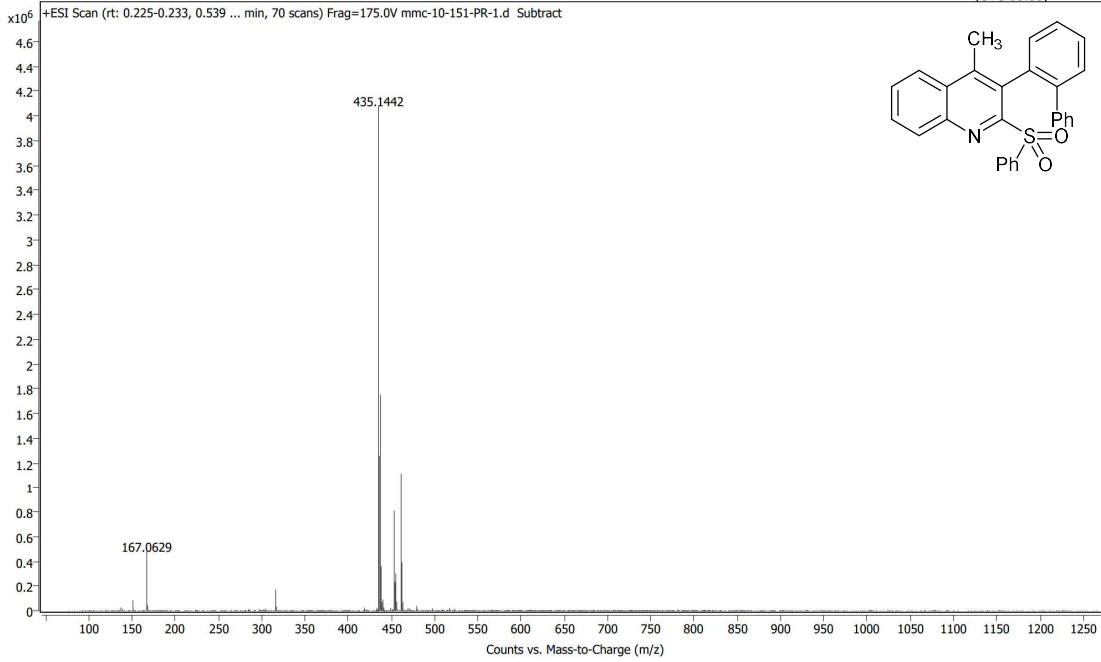
Name: mmc-10-151-PR Rack Pos.: Instrument: Instrument 1 Operator:
Inj. Vol. (ul): 1 Plate Pos.: IRM Status: All ions missed
Data File: mmc-10-151-PR-1.d Method (Acq): Column bypass.m Comment: Acq. Time (Local): 3/10/2021 9:25:04 AM (UTC-08:00)



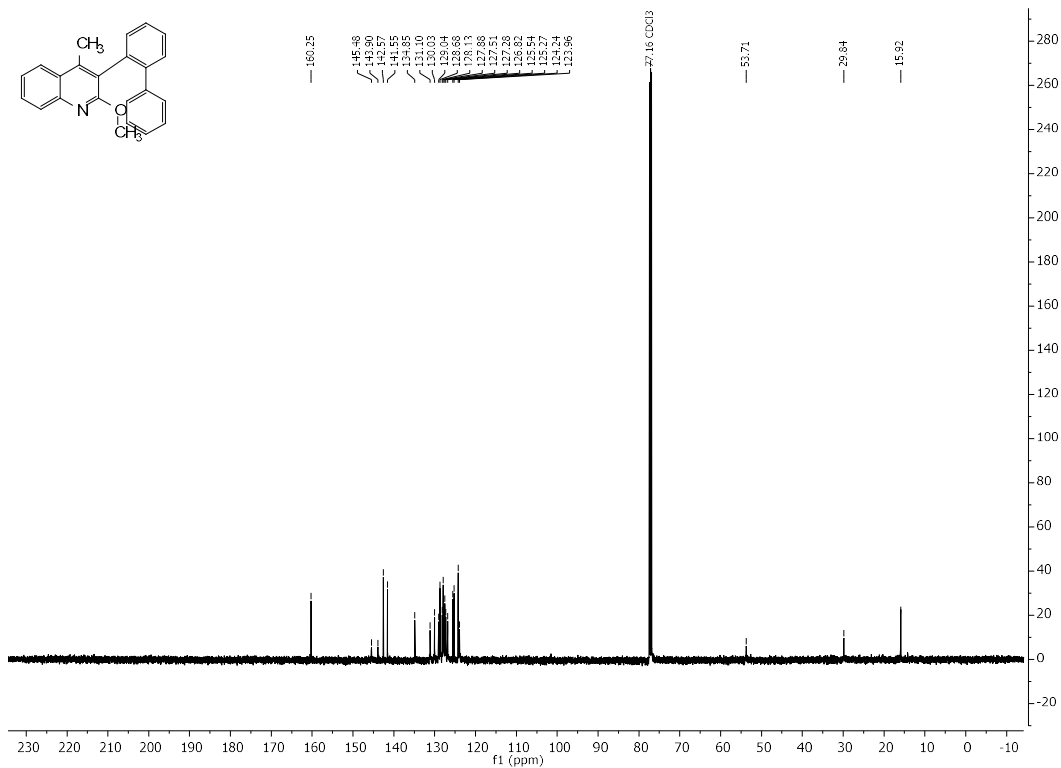
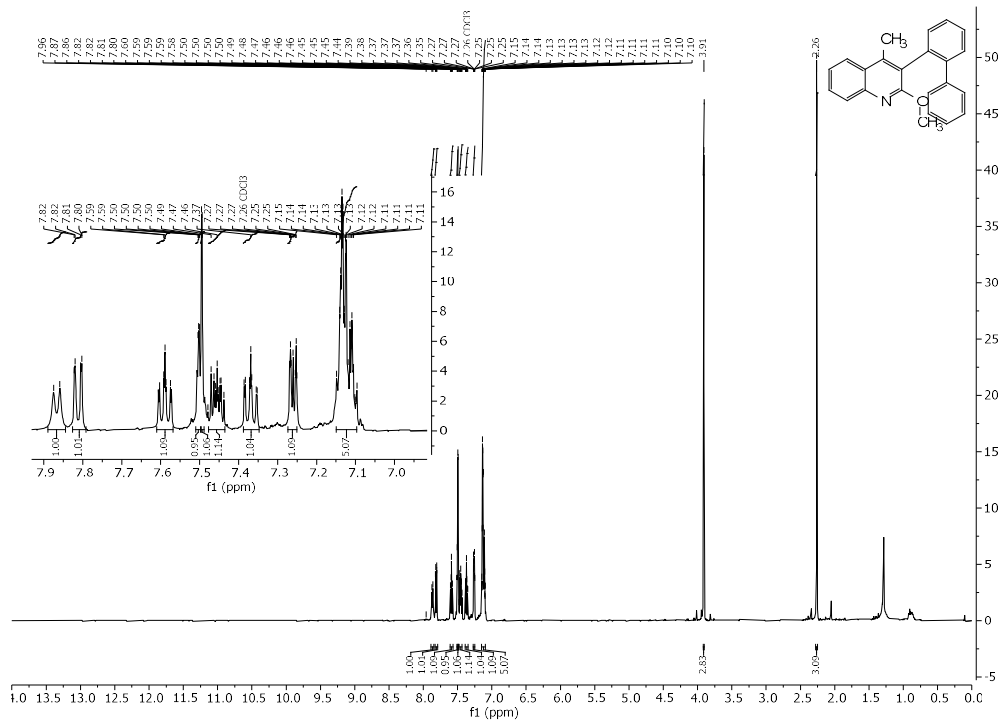
Spectrum Plot Report



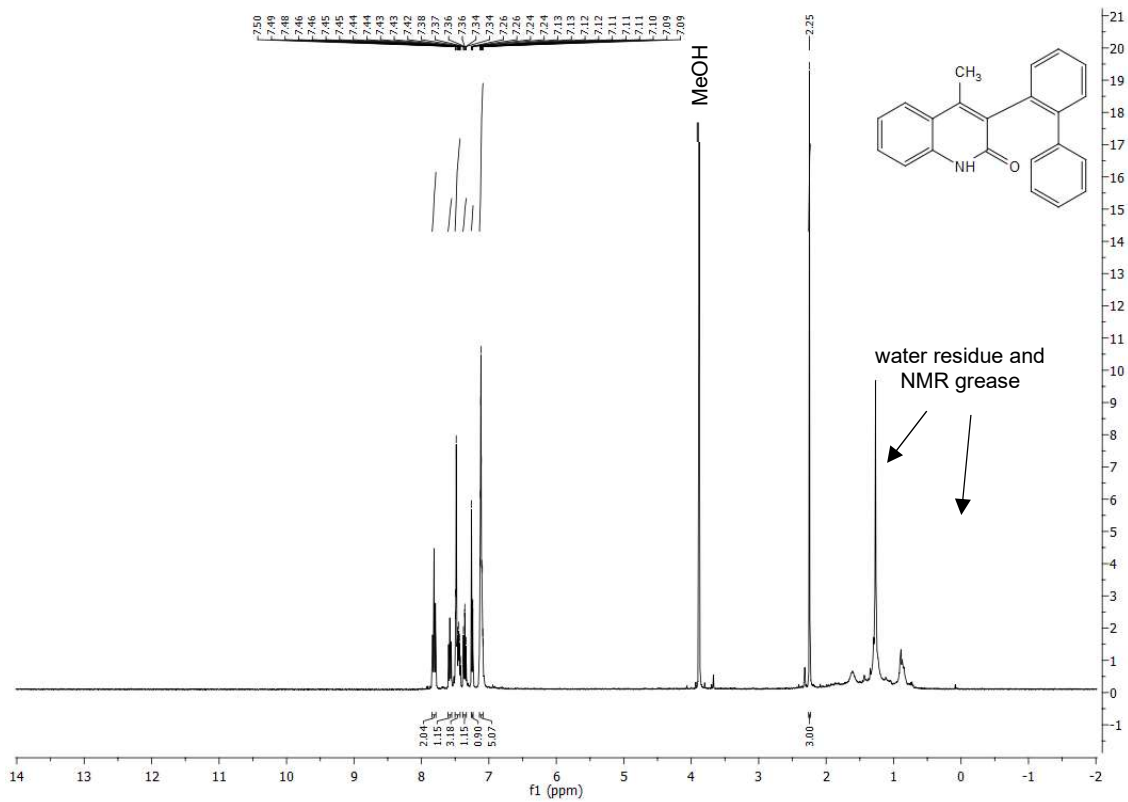
Name: mmc-10-151-PR Rack Pos.: Instrument: Instrument 1 Operator:
Inj. Vol. (ul): 1 Plate Pos.: IRM Status: All ions missed
Data File: mmc-10-151-PR-1.d Method (Acq): Column bypass.m Comment: Acq. Time (Local): 3/10/2021 9:25:04 AM (UTC-08:00)

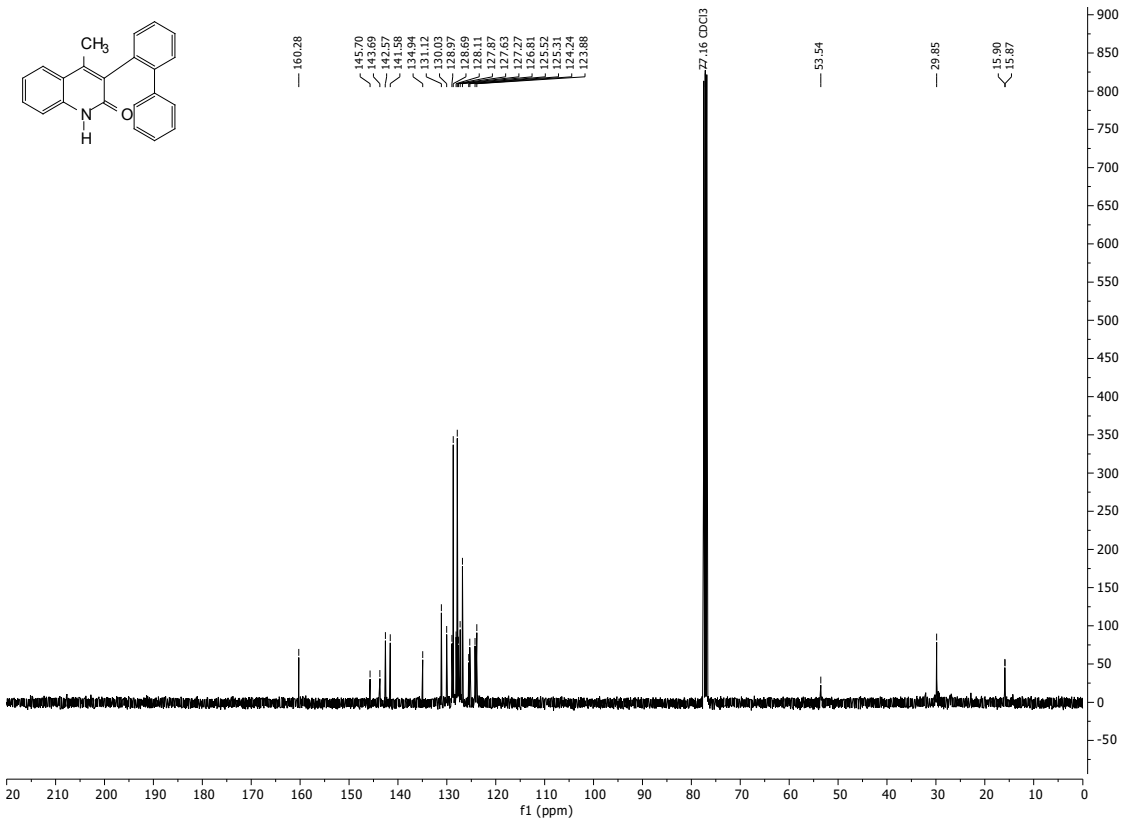


¹H and ¹³C Spectral Data of 120



^1H (residual CH_3OH , grease impurity), ^{13}C and HRMS (ESI) Spectral Data of **121**

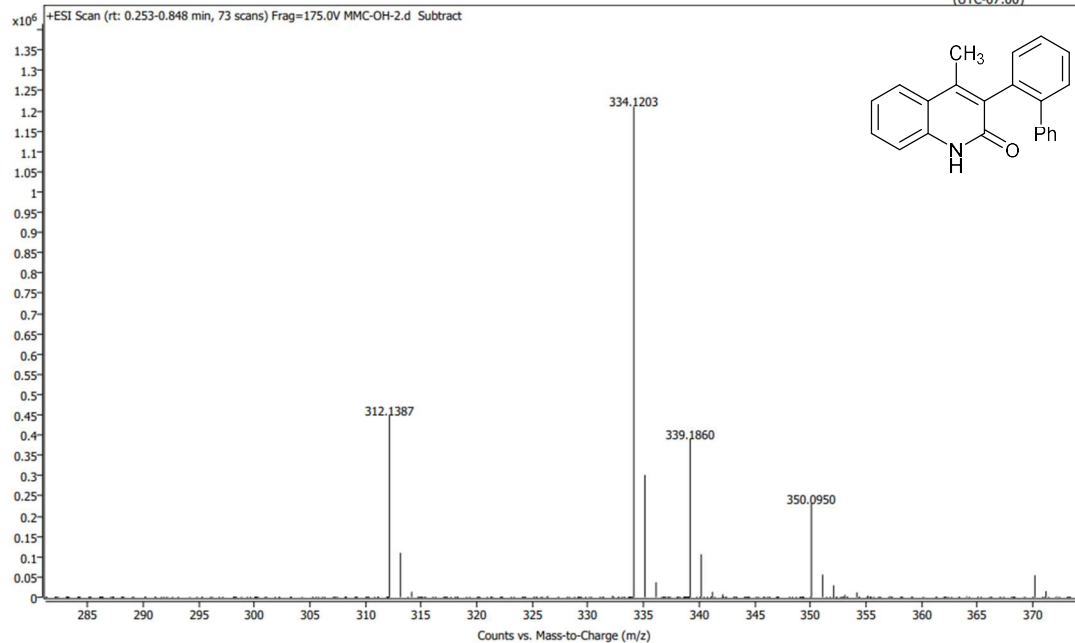




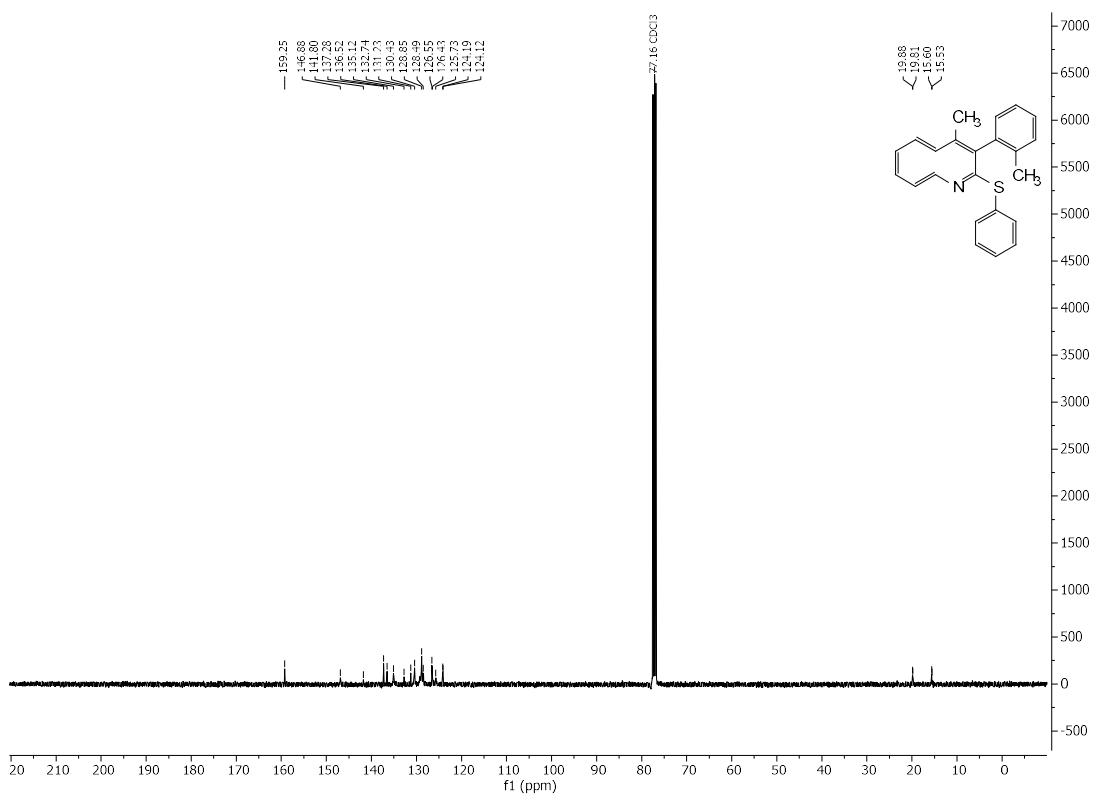
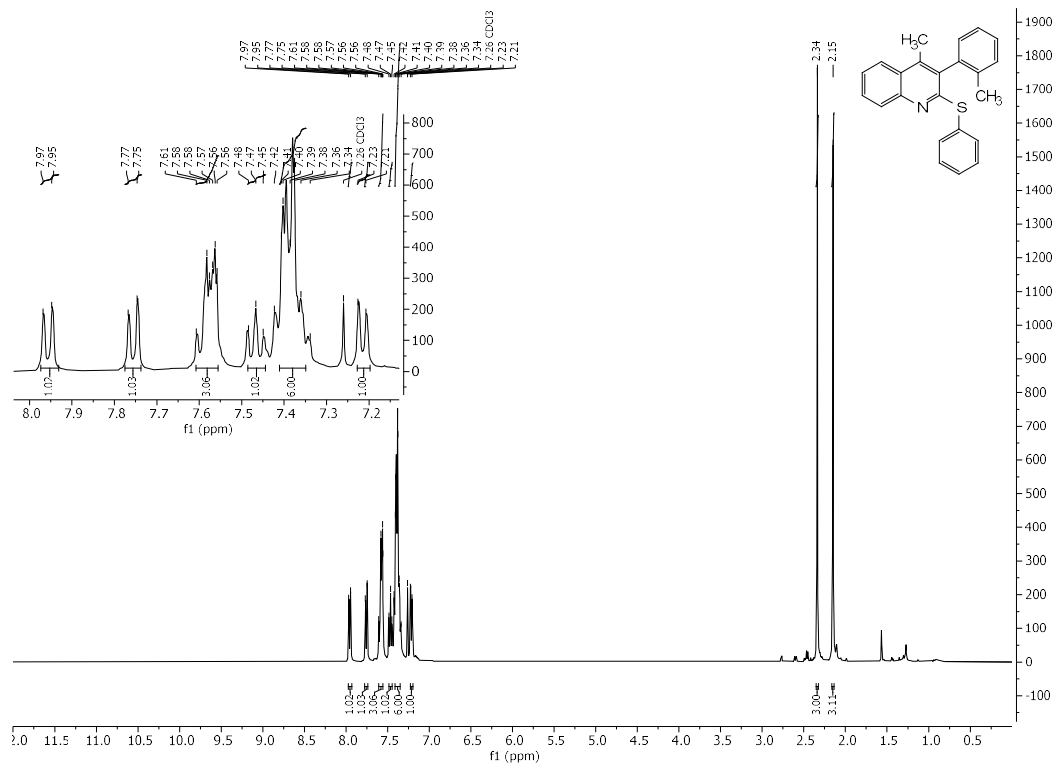
Spectrum Plot Report

Agilent | Rapid Answer

Name	1	Rack Pos.		Instrument	Instrument 1	Operator	
Inj. Vol. (ul)	1	Plate Pos.		IRM Status	All ions missed		
Data File		Method (Acq)	Column bypass.m	Comment		Acq. Time (Local)	8/6/2021 10:09:34 AM (UTC-07:00)



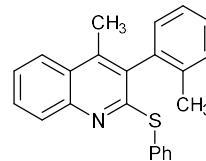
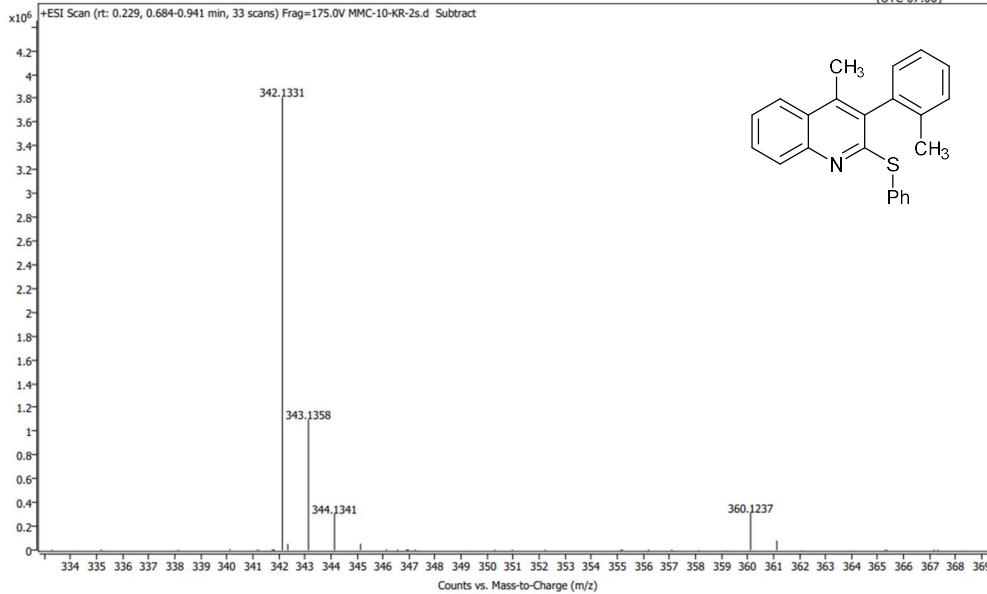
^1H , ^{13}C and HRMS (ESI) Spectral Data of **109**



Spectrum Plot Report



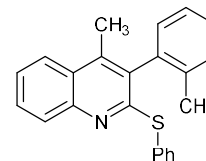
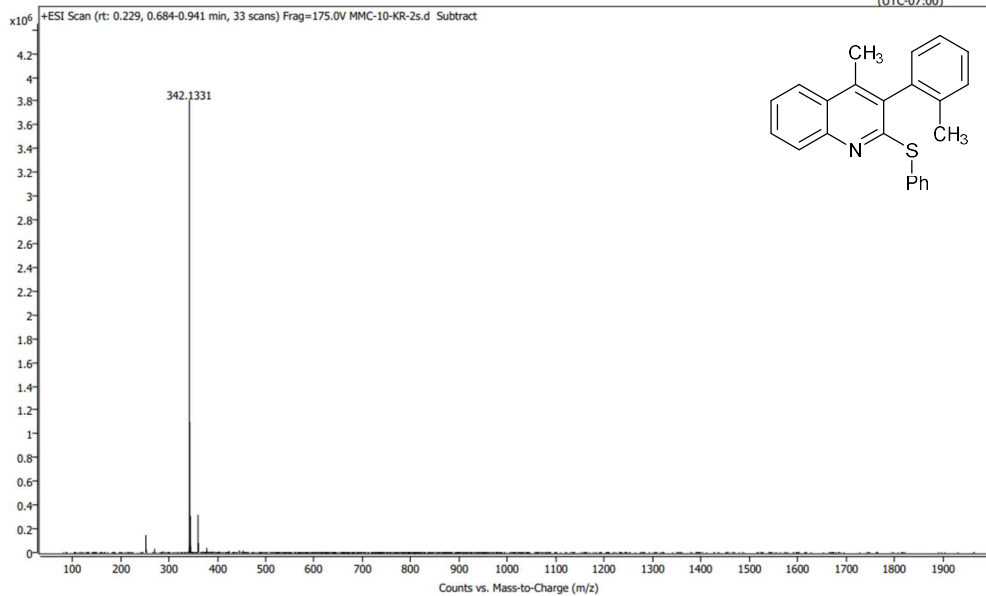
Name		Rack Pos.		Instrument	Instrument 1	Operator
Inj. Vol. (ul)	1	Plate Pos.		IRM Status	Some ions missed	
Data File		Method (Acq)	Column bypass.m	Comment		Acq. Time (Local) 5/13/2021 5:03:24 PM (UTC-07:00)



Spectrum Plot Report



Name	MMC-10-KR-2s	Rack Pos.		Instrument	Instrument 1	Operator
Inj. Vol. (ul)	1	Plate Pos.		IRM Status	Some ions missed	
Data File	MMC-10-KR-2s.d	Method (Acq)	Column bypass.m	Comment		Acq. Time (Local) 5/13/2021 5:03:24 PM (UTC-07:00)

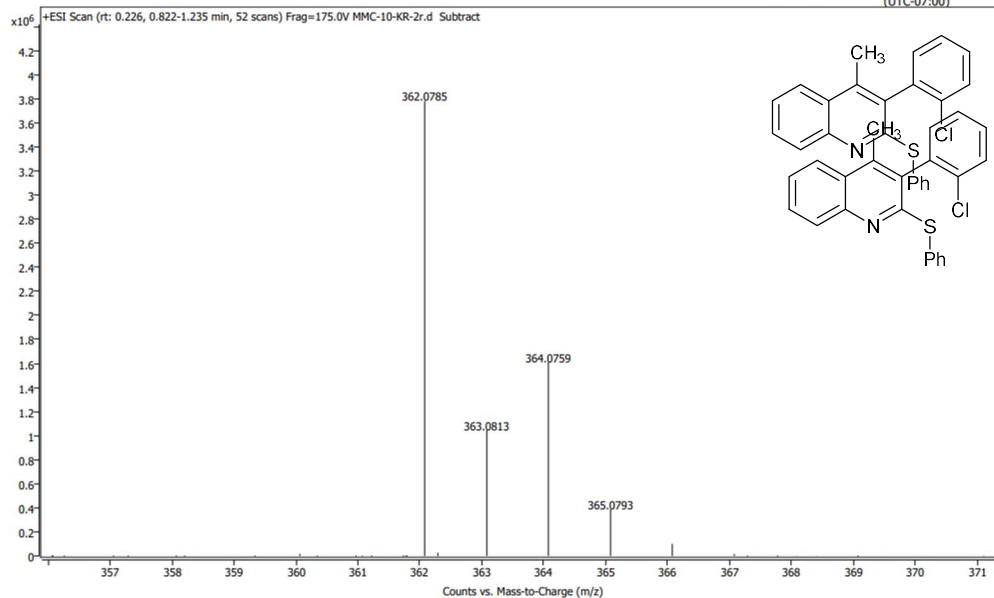


¹H, ¹³C and HRMS (ESI) Spectral Data of **111**

Spectrum Plot Report

Agilent | Trusted Analysis

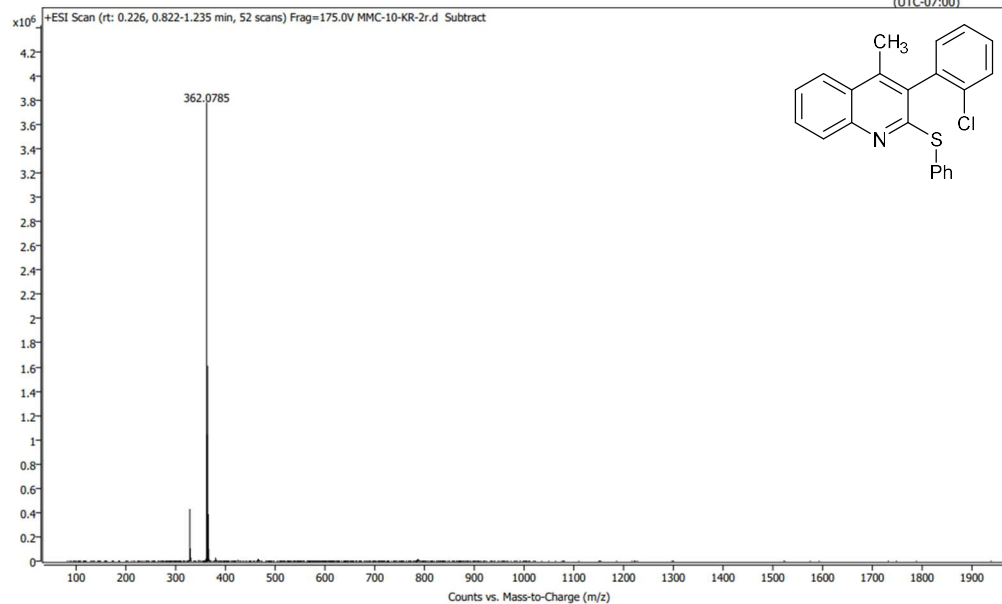
Name	Inj. Vol. (ul)	1	Rack Pos.	Plate Pos.	Method (Acq)	Column bypass.m	Instrument	IRM Status	Comment	Instrument 1	Some ions missed	Operator	Acq. Time (Local)	5/13/2021 4:57:28 PM (UTC-07:00)
------	----------------	---	-----------	------------	--------------	-----------------	------------	------------	---------	--------------	------------------	----------	-------------------	----------------------------------



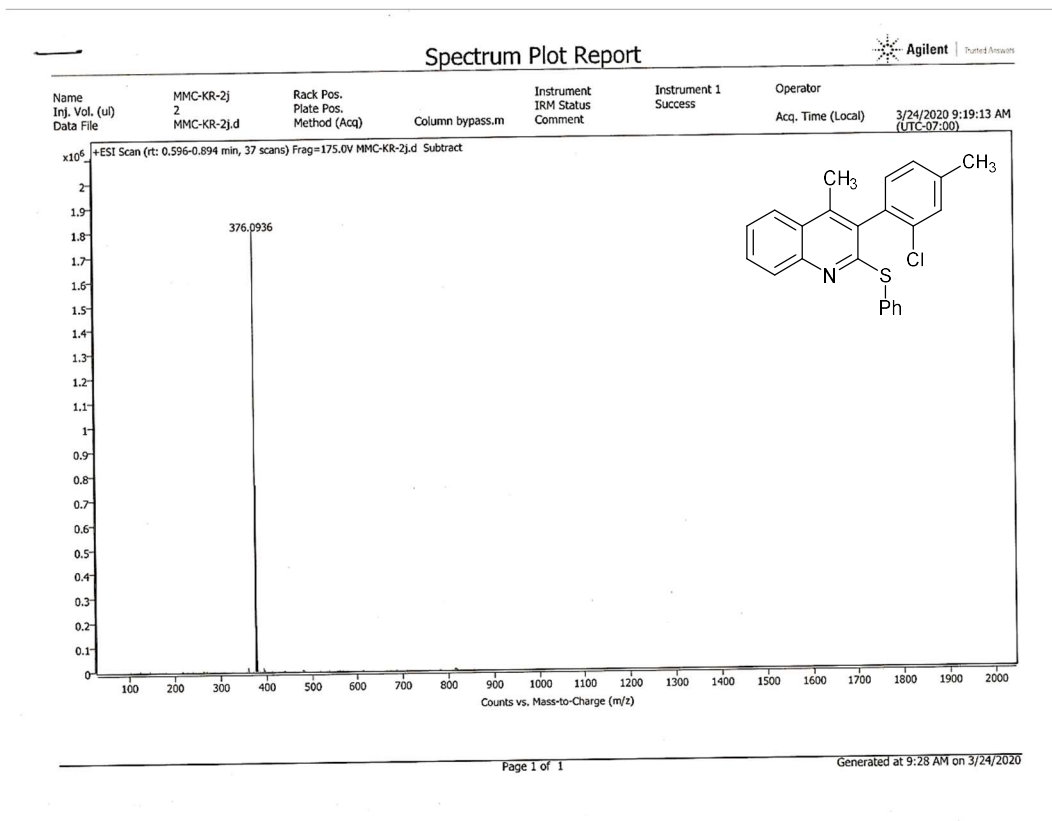
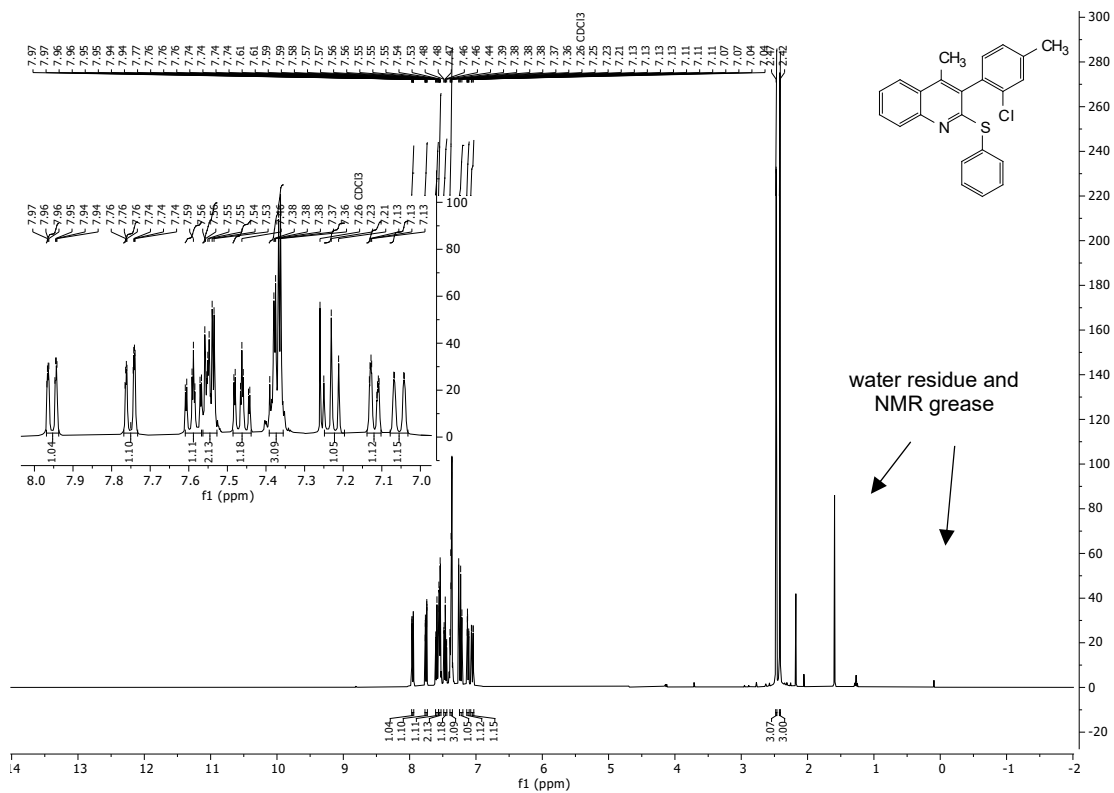
Spectrum Plot Report

Agilent | Trusted Analysis

Name	MMC-10-KR-2r	Rack Pos.	Plate Pos.	Method (Acq)	Column bypass.m	Instrument	IRM Status	Comment	Instrument 1	Some ions missed	Operator	Acq. Time (Local)	5/13/2021 4:57:28 PM (UTC-07:00)
------	--------------	-----------	------------	--------------	-----------------	------------	------------	---------	--------------	------------------	----------	-------------------	----------------------------------



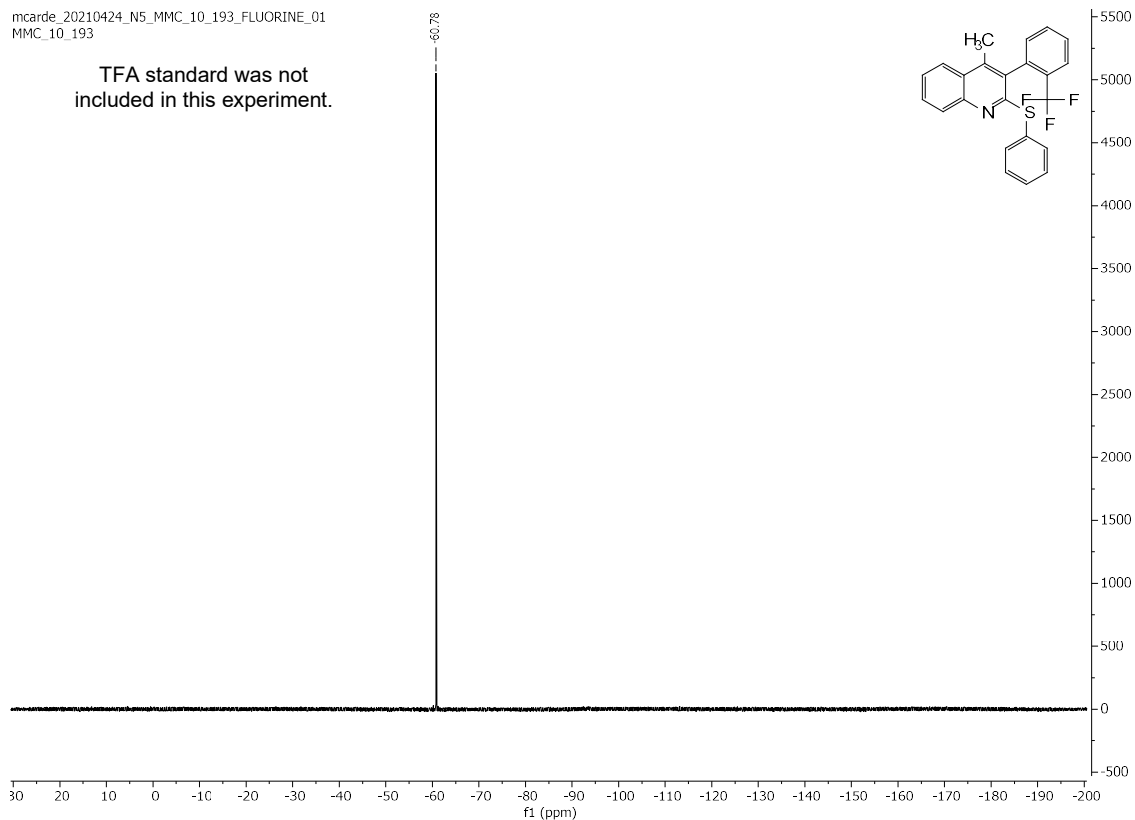
¹H and HRMS (ESI) Spectral Data of **113**



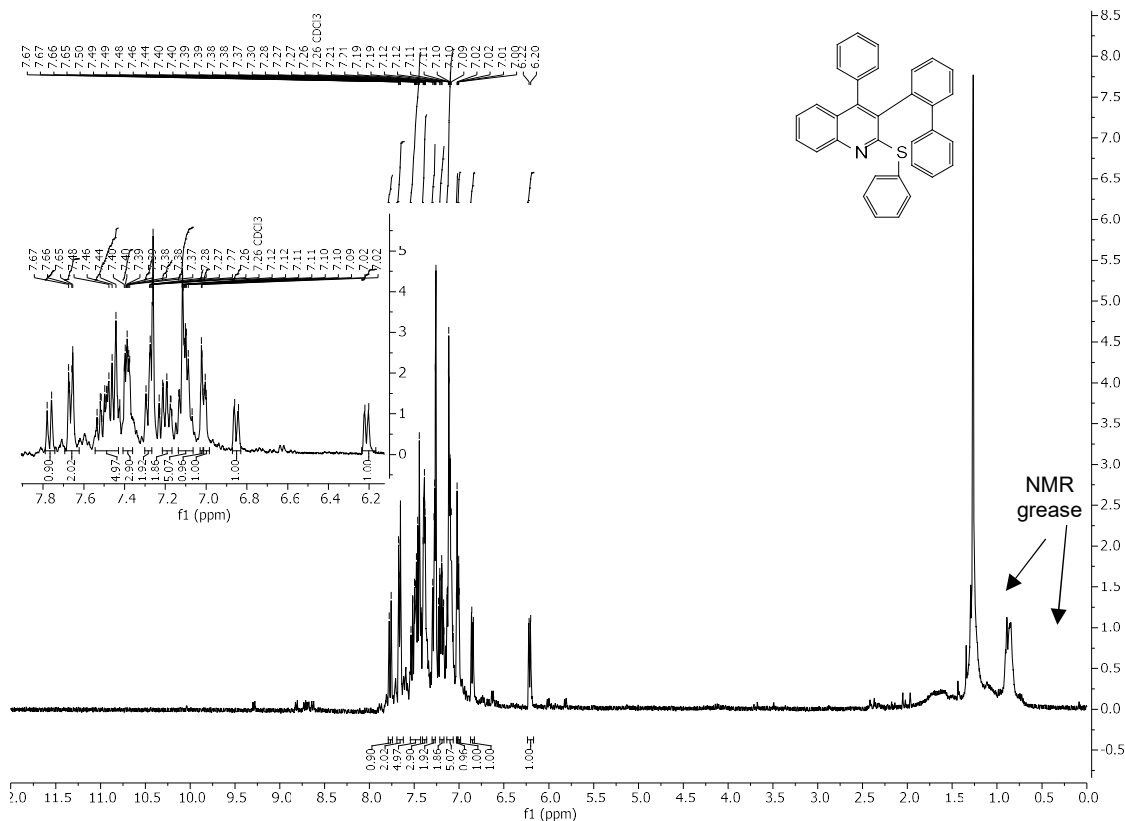
^1H , ^{13}C , and ^{19}F NMR and HRMS (ESI) Spectral Data of 72

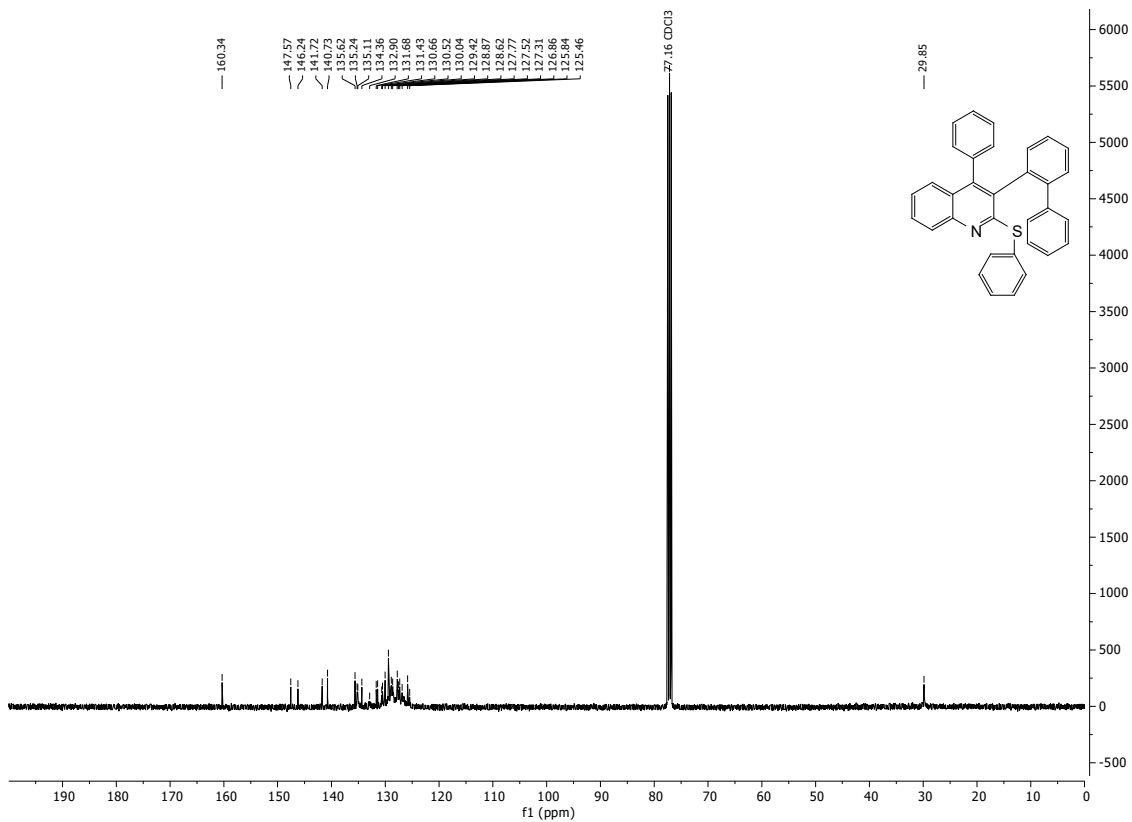
mcarde_20210424_N5_MMC_10_193_FLUORINE_01
MMC_10_193

TFA standard was not
included in this experiment.



¹H (trace CDCl₃ grease) and ¹³C and HRMS (ESI) Spectral Data of 116

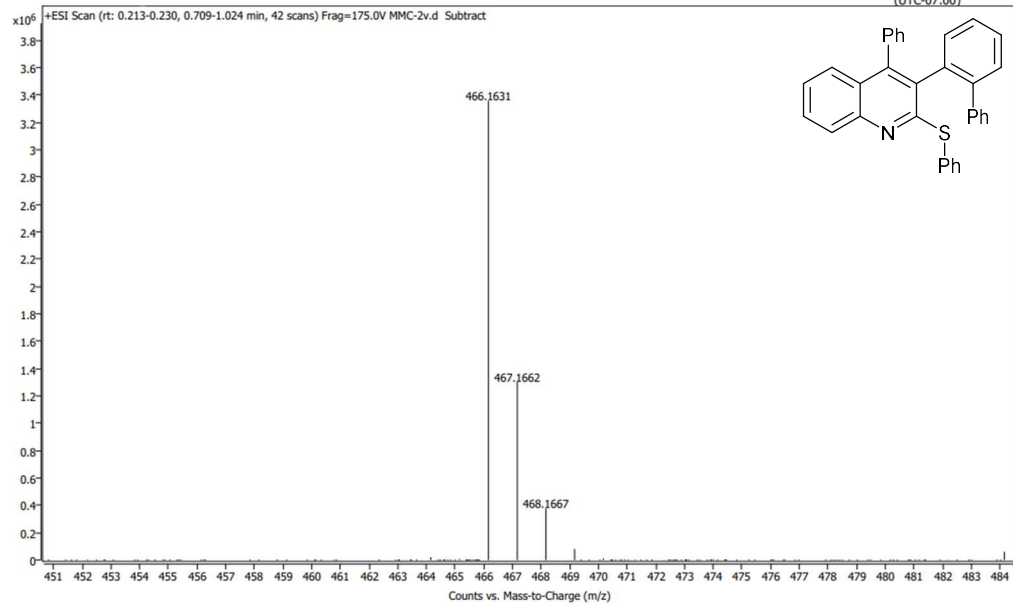




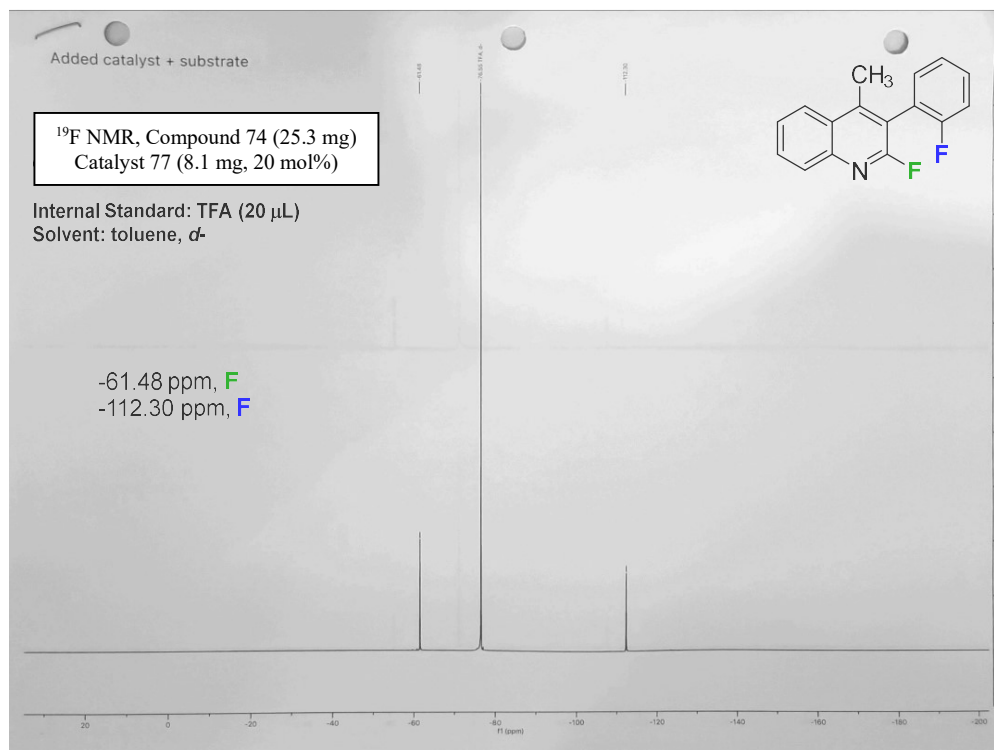
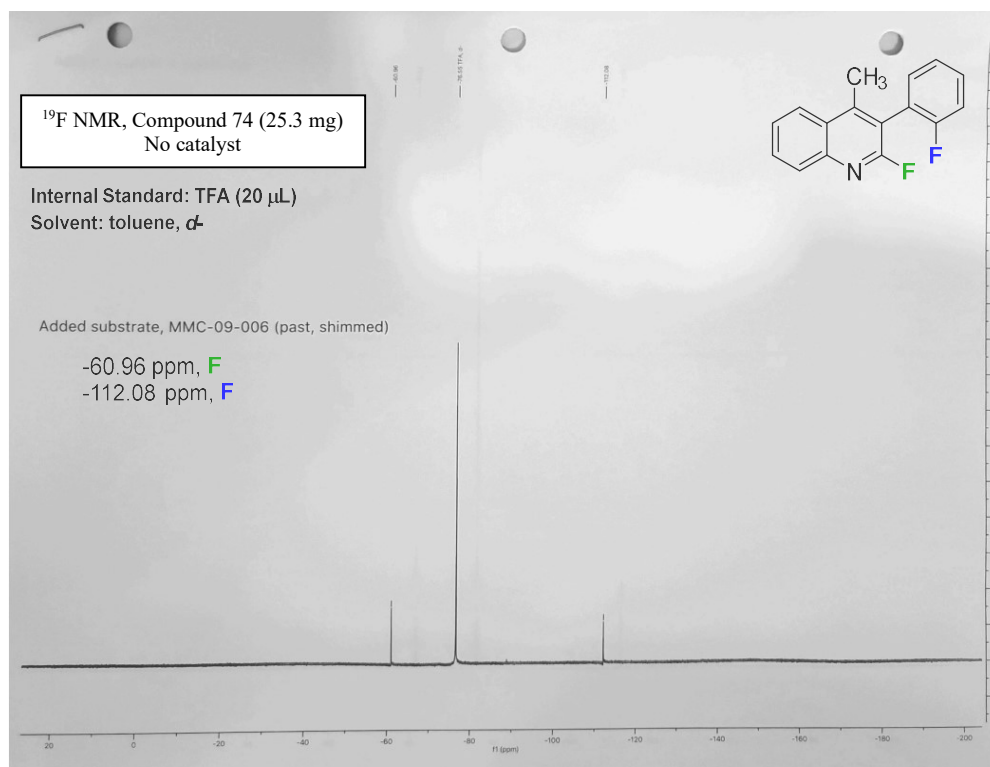
Spectrum Plot Report

Agilent Trusted Analysis

Name	1	Rack Pos.		Instrument	Instrument 1	Operator
Inj. Vol. (ul)		Plate Pos.		IRM Status	Success	
Data File		Method (Acq)	Column bypass.m	Comment		Acq. Time (Local)
						8/6/2021 2:06:29 PM (UTC-07:00)



Preliminary Studies, ^{19}F NMR Experiments of Substrate 74-Catalyst 77



Chapter 3 ACCESSING ATROPISOMERIC CHEMICAL PROBES FOR NEW DISEASE TARGETS

Copyright

Chapter 3 contains material that will be utilized in a future publication. The dissertation author was a supplemental researcher and coauthor for each of these manuscripts. Support of this work by the National Institute of General Medical Science (R35GM124637) is acknowledged. Work shared in this chapter is ongoing, and likely will be pursued in a pivotal direction by other members in the Gustafson group.

3.1 Background – Chemical Probes Role in Medicinal Chemistry

We ventured into exploring other types of promiscuous scaffolds to which conformational control of the atropisomeric axes would lead to selectivity for new and unique targets. All efforts would lead us to new types of compounds which might exhibit desirable potency and selectivity if we could leverage stable Class-3 atropisomerism to tune the dihedral angle. At the time of these ongoing projects, we became more focused on developing the SAR for many of these compounds. In many cases, we were enabled to study and then improve our analogues' biological profiles through iterative structural-based design (SBDD), where we were able to curate what specific functional groups to be the key pharmacophore for each scaffold. Our group had proof-of-concept supported by the success of the Class-3 atropisomeric PPY-based RET kinase inhibitor project.³⁷ In addition, we addressed many synthetic challenges and limitations to the scalability and diverse 'late-stage' functionalization for these types of pharmaceutically relevant compounds without observable racemization. In the next phases of the projects, our team began new opportunities to

improve target selectivity and potency for other types of pharmaceutically relevant scaffolds (most of which are *N*-heterocycles).

One important highlight of our previous approach was heavy reliance on the available crystallographic data. For our new projects, this reliance of SBDD can pose a limitation to examining only well-studied target classes and atropisomeric scaffolds. A cursory search of public domains (e.g., the RCSB Protein Data Bank, i.e., PDB) finds at least 1600 unique Class-1 atropisomeric small molecule and protein co-crystal structures. Previous ‘SBDD-driven medicinal chemistry’ campaigns towards PP/PPY-based kinase inhibitors were quite straightforward since RET (and other kinases) are extremely well-studied and as such there were plethora of models available from the PDB for the team to access. However for new disease areas in which the field is still quite young, access to helpful crystallographic and Cryo-EM models can be quite scarce or privatized for patent reasons. In certain industries these types of limitations might not present as challenges, as many companies are able to funnel finances and springboard a lot of effort to obtain this information for their disease target. However, at an academic institution, this bottleneck might require extra investments that many research groups likely would not be able to spare. Also, these efforts typically require a lot of compounds to be made, of which potency and selectivity is often elusive.

Today there are new technologies that continue to be developed for implications in the modern age of drug discovery. One method to circumvent SBDD is to improve drug properties and use activity as the focus in medicinal chemistry exploration. If biological assays are developed and align with the adverse event that the disease outcome represents, then measure of potency or selectivity would be used as the key driver for furthering new designs irrespective of available structures. However, this itself is also challenging since curation of the biological assay is

paramount and critical. Ideally, the assays our group would like to use must replicate the pharmacology of the disease and show clearly that there is a change in activity when a small molecule is introduced. This is difficult to probe if there are off-targeted activities or chances of false positives. Another issue looms if the compound is not able to have ideal properties to engage with the target, and in industry is referred to as the “Rule of 5” or “Beyond Rule of Five.”^{113,114}

In these sensitive *in vivo* assays, if the compounds are not permeable it makes it challenging to build further SAR and design new small molecules. Within this last decade, development of new types of ‘drugging systems’ like PROTACs,¹¹⁵ RIPTACs,¹¹⁶ and ADCs¹¹⁷ are reshaping the way that small-molecule drug discovery is performed. Before the end of these early studies, some of my colleagues were dedicated to using this approach to improve the properties of the PPY-kinase inhibitor specifically as a ‘proof-of-concept’ as well as acquire ‘drug-like’ properties. I am very excited to see if they have made progress moving forward. Another method is emerging to advance current computational programming, where AI-assisted machine-learning¹¹⁸ can take all existing structures to perform SBDD via averaging datasets. This said, many of these technologies are far from perfected and often require new input data from crystallizing target structures with new scaffolds possessing even better potency and selectivity.

3.2 Diazirine Atropoproboscopes – Activated by UV Light

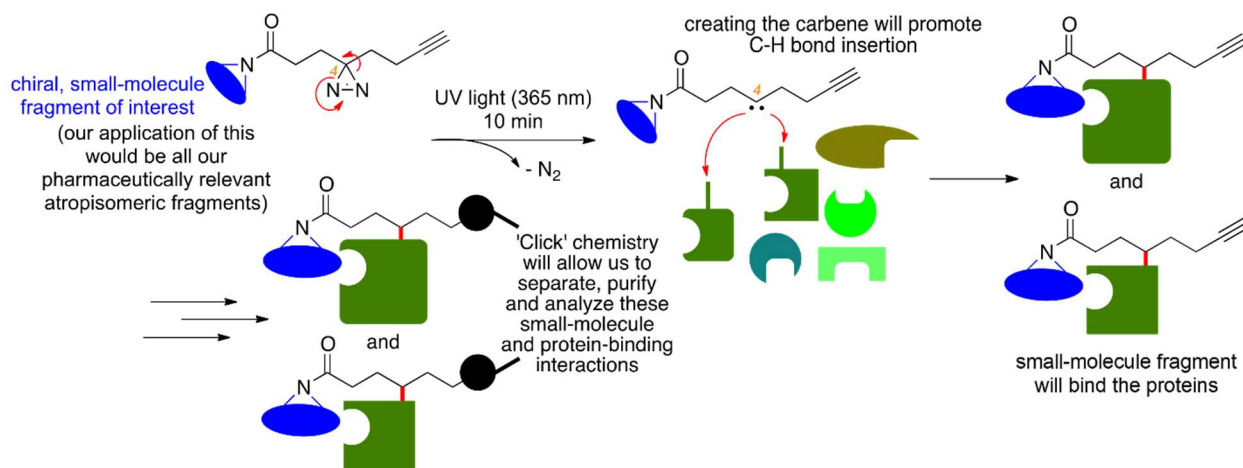


Figure 42. Chemical Probes via Fragment-Based Ligand and Targeted Discovery^{108,119}

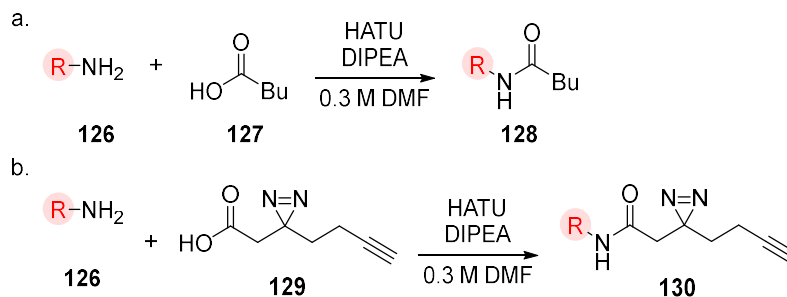
One common practice within drug discovery (if crystallographic or Cryo-EM information cannot be an option) is to apply a chemoproteomics approach to find targets to which a compound can engage with. Through use of a chemical probe, biological targets can be studied through various assays and technologies which have been developed in the last two decades. Ideally if a compound (as an inhibitor) is potent and selective, then it becomes a proxy starting point; a “molecular scalpel” which can then drive further development towards an even more efficient compound. However, in many cases chemical probes analogous to “molecular Swiss Army blades” which often can engage with multiple targets resulting in polypharmacology. In many ways, the chemoproteomics’ methods are quite like fragment-based drug discovery and exploration.^{108,119,120} Chemoproteomics was a very feasible approach to study new disease areas and possibly cover diverse pharmacological space.^{108,119} In addition to this, we were able to find other applications for our Class-3 atropisomeric scaffolds especially important for non-inhibitor type small-molecules or allosteric binders. While wrapping up the efforts made to the 3-aryl quinoline S_NAr project, the Gustafson group took a few Class 1-4 atropisomeric PPYs and quinolines and prepared a few

chemical probes to leverage this recent approach. Equation 42 shows the general method of how these chemical probes function, based on Parker and coworkers' previous work.

Parker and coworkers previously pioneered a new method of fragment-based discovery, where compounds synthesized with a 'diazirene/alkyne' handle were easily obtained through amide formation – the most widely used reaction of all medicinal chemistry. Under UV irradiation, the diazirene would break and release N₂ and leave a stable, yet reactive carbene which can perform C-H insertion to covalently link to many unique targets. Selectivity is driven through the fragments that are attached to this chemical probe, since the small-molecule protein-binding interactions will facilitate these C-H insertions to occur more prevalently. The terminal alkyne is used in purification of the protein samples via mass-exchange chromatography, since biotinylated tags can be attached at this terminus using Click chemistry.¹²¹ These tags can then be removed allowing us to uncover what proteins are associated through readout masses.

In our collaboration, I and the team synthesized a few of these atropisomerically stable and unstable 3-aryl quinolines, PPYs, *N*-aryl pyridones, and *N*-arylquinoids that possess a diazirene photoreactive group containing a clickable alkyne handle⁵⁴ to look at the effects of atropisomer conformation on selectivity across the entire proteome. We hypothesize that synthesizing these chemical probes (i.e., referred to these compounds as 'atropoprobes') approach will uncover new targets that prefer specific atropisomers of a given scaffold, independent of available structural data. From this work, we envisioned that these Class-3 atropisomeric 'fragments' would be much more selective as analogues to known kinase inhibiting scaffolds. This was confirmed in my colleagues' efforts in the RET kinase inhibitor program (i.e., atropisomeric PPY) through examining *in vitro* potency and selectivity data.

3.3 Current Results and Future Directions



Equation 48. General Syntheses for Atropoprobes. a. Synthesis of the control chemical probes. b. Synthesis of chemical probes.

Our atropoprobes were synthesized by following prep associated with Dr. Parker's chemistry. Using either EDC-HOBt or HATU-mediated conditions, these diazirene-containing 'clickable' linkers were attached to our atropisomeric fragments using amide bond formation. While each atropisomer of stereochemically stable compounds can be obtained through HPLC chiral separation, atroposelective S_NAr can be particularly useful to access larger amounts of enantioenriched sulfide precursors, wherein synthesizing the final chemical probe will not lead to observable racemization. I was co-leading the development of this project, and synthesized many compounds described above that were inspired from previous compounds I synthesized. More details of the syntheses and summaries of characterization results are all found in Section 3.3, "Experiment Section" of this thesis. Please also refer to "Section 2.2.6 Post-functionalization of Atropisomeric 3-arylquinolines" to see how these apply in these cases. Notably, there is not much data summarized from this reporting, however several examples of the profiles for these compounds are featured in this thesis.

Table 33. 3-aryl Pyrrolopyrimidine-based diazirines

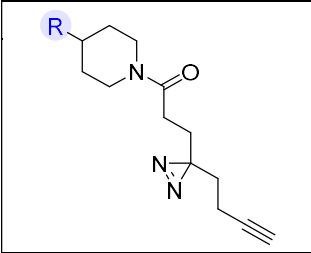
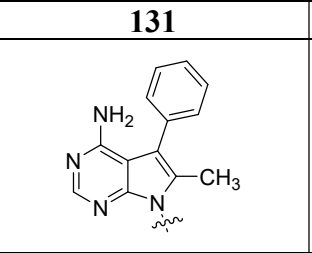
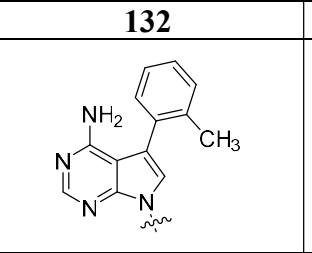
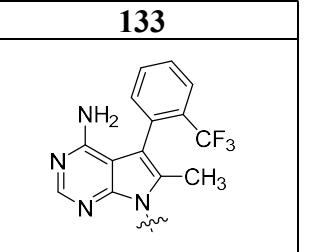
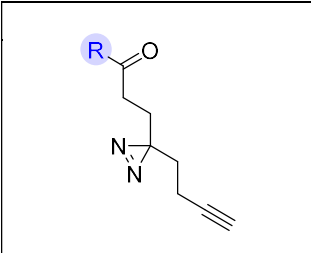
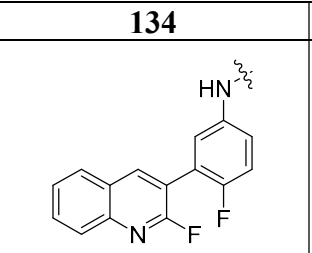
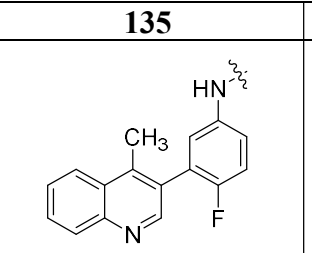
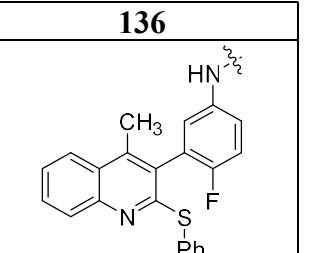
	131	132	133
			
Purity	>98% purity	>98% purity	E1 ^[a] : <100% purity E2: >98% purity
HPLC Method	50:50 Hex/EtOH (IA)	20:80 Hex/EtOH (IA)	50:50 Hex/EtOH (IA)
Unstable or Stable Atropisomerism	unstable	unstable	stable

Table 34. 3-aryl Quinoline-based diazirines

	134	135	136
			
Purity	>98% purity	>98% purity	E1 ^[a] : <100% purity E2: <100% purity
HPLC Method	70:30 Hex/IPA (IA)	20:80 Hex/IPA (IA)	70:30 Hex/EtOH (IC)
Unstable or Stable Atropisomerism	unstable	unstable	stable

^[a]E1 = enantiomer 1, E2 = enantiomer 2 (stereochemistry was not elucidated)

Our collaborators in the Parker group profiled our atropoprobes across the proteome to identify new atroposelective protein-small molecule interactions. Our focus for this set was on the PPY-based and 3-aryl quinolines, which were first profiled in K562 cells (i.e., common transfected cell-lines for modeling human leukemia, https://www.cellosaurus.org/CVCL_0004). Early results from these studies were quite successful, and identified two atropoprobes which were able find targets that possess high degrees of atropisomeric preferences for these types of compounds. While

these were still early results, this inspired confidence served as a great foundation for this emerging project. Results from this set are a great marker for a ‘proof-of-concept’ that we can use chemoproteomics to discover new targets when reliance of SBDD is quite challenging.

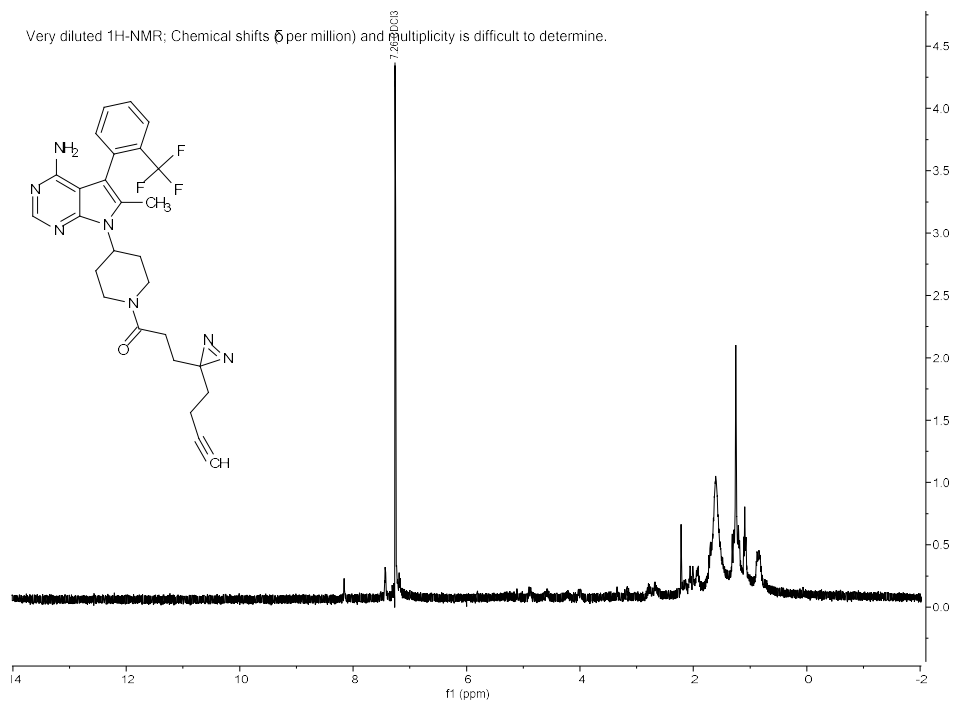
There are still important additions that would refine this project that the continuing team is considering. Firstly, this assay was selected for discovering several targets that display large atropisomer preferences (Figure 8). Moving forward, the Gustafson group will synthesize new atropoprobates based on *N*-aryl quinoids and quinazolines. In addition, it is important to profile across multiple cell lines to both validate and strengthen this preliminary data. Lastly, using *in vitro* and *in vivo* assays will also confirm the binding data we obtained. This work is significant as it provides a discovery platform that allows for the assessment of novel drug-like atropisomeric chemical space across the proteome. In future works, I encourage my colleagues to investigate any respective small-molecule interactions we observed from our atropisomeric probes from secondary assay validated targets.

This method will represent exploration of new atropisomeric scaffolds since future structure optimization studies for potentially understudied targets can be performed when visualization is not available.

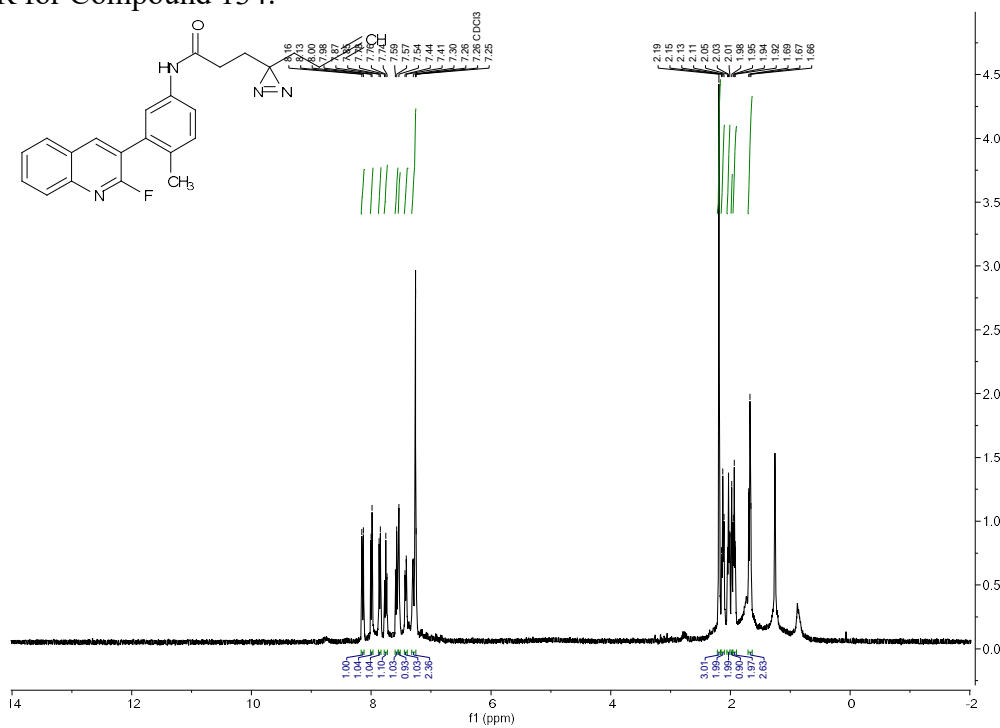
3.3 Experimental Section

3.1.1 Example NMR Spectra for Atropoprobates

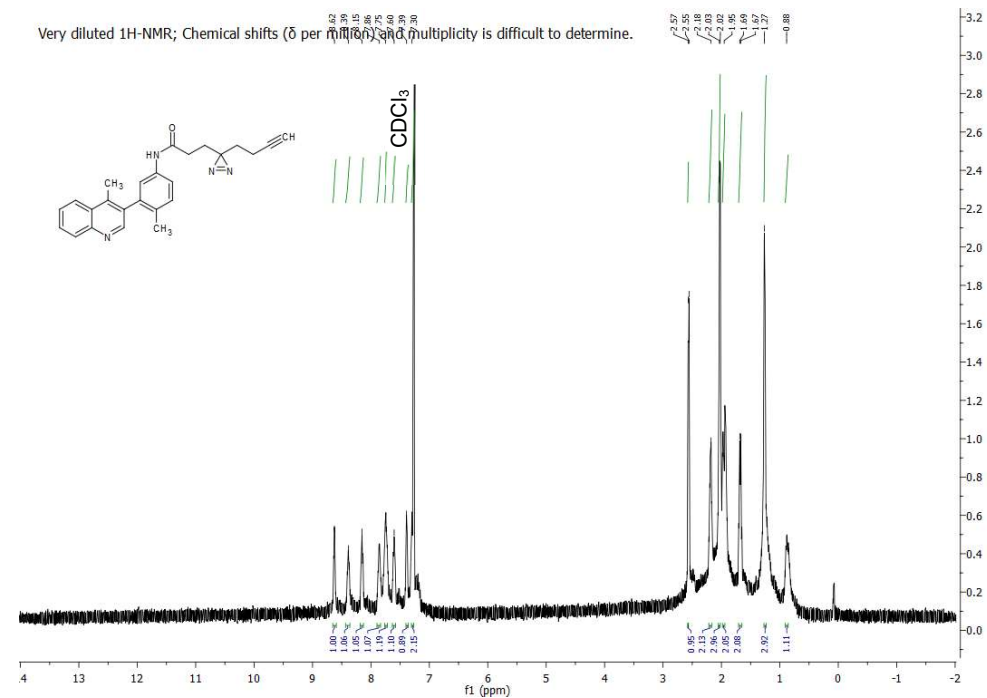
¹H NMR for Compound 133 (sample is too dilute to analyze outside of generalities)



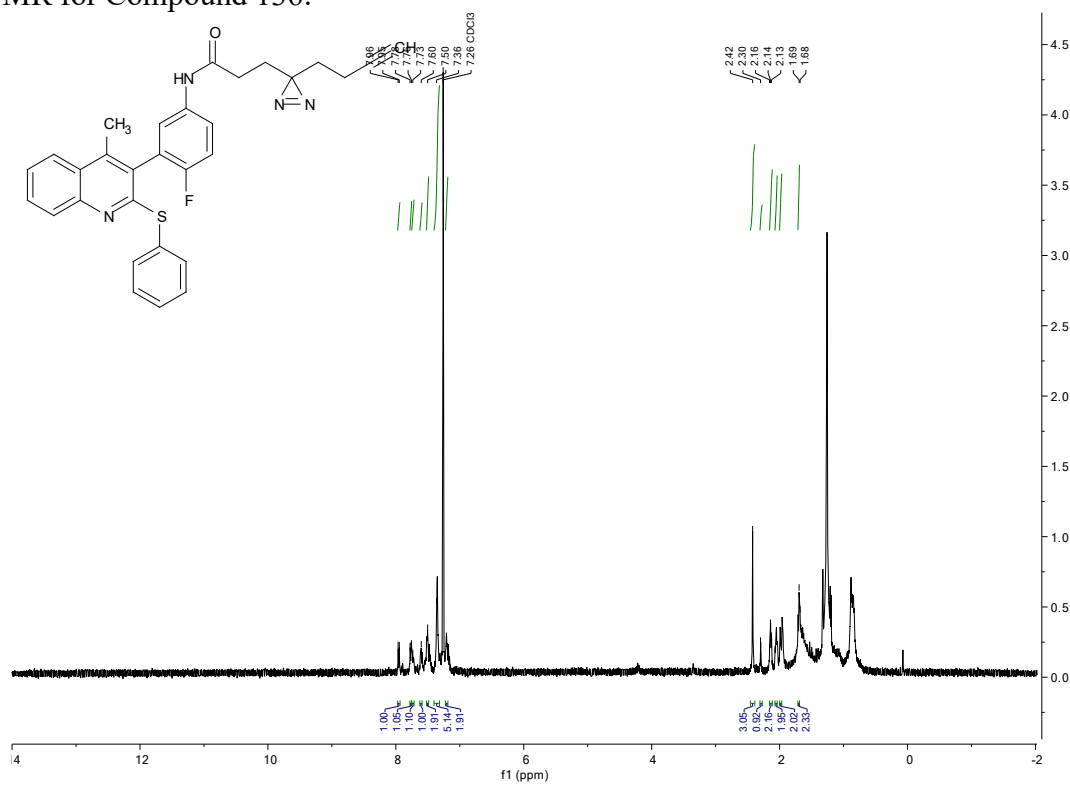
$^1\text{H NMR}$ for Compound 134:



$^1\text{H NMR}$ for Compound 135:



^1H NMR for Compound 136:



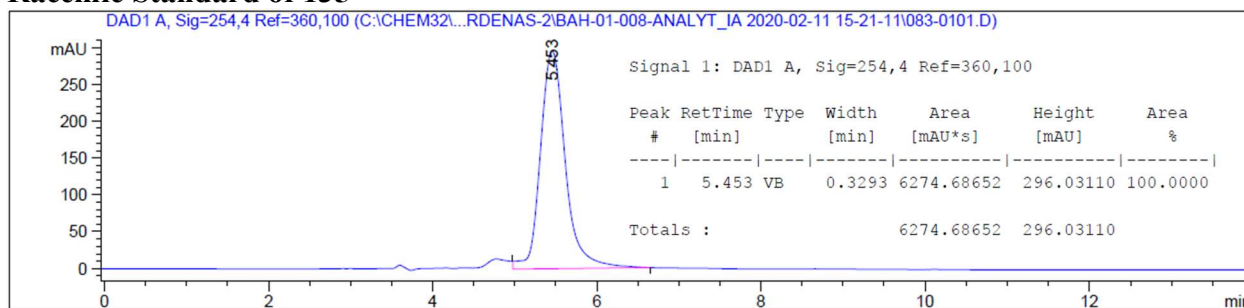
3.3.2 Chiral HPLC Traces

135

135 was measured with HPLC analysis using Chiralpak IA Hexanes/IPA (70:30), flow rate = 1.0 mL/min, t_R = 5.4 min.

→ Determined 100 ee%

Racemic Standard of 135

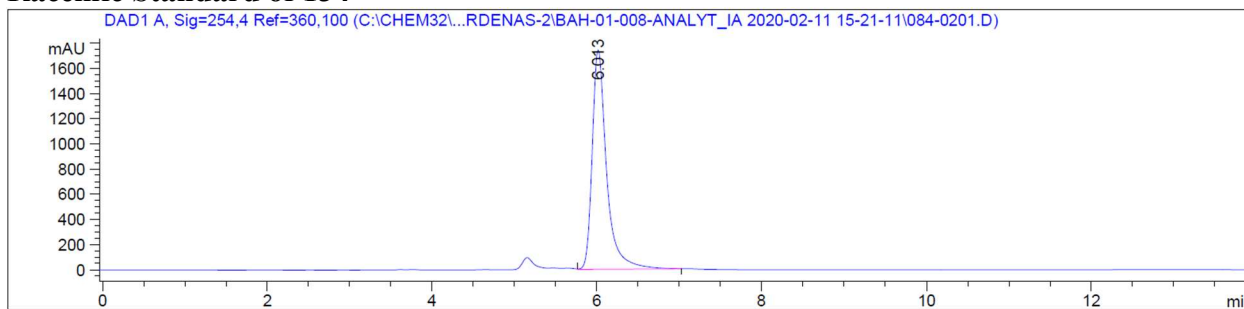


134

134 was measured with HPLC analysis using Chiralpak IA Hexanes/IPA (70:30), flow rate = 1.0 mL/min, t_R = 5.4 min.

→ Determined 100 ee%

Racemic Standard of 134



Signal 1: DAD1 A, Sig=254,4 Ref=360,100

Peak #	RetTime [min]	Type	Width [min]	Area [mAU*s]	Height [mAU]	Area %
1	6.013	VB	0.1825	2.12804e4	1742.24573	100.0000

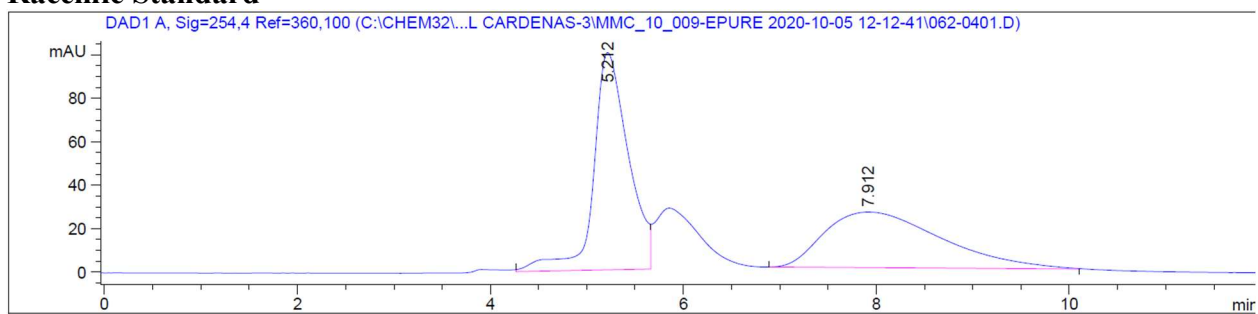
Totals : 2.12804e4 1742.24573

E1 of 136 was measured with HPLC analysis using Chiralpak IA Hexanes/EtOH (70:30), flow rate = 1.0 mL/min, tR = 5.4 min.

→ Determined 100 ee%

[enantiopure]
Enantiomer 1

Racemic Standard

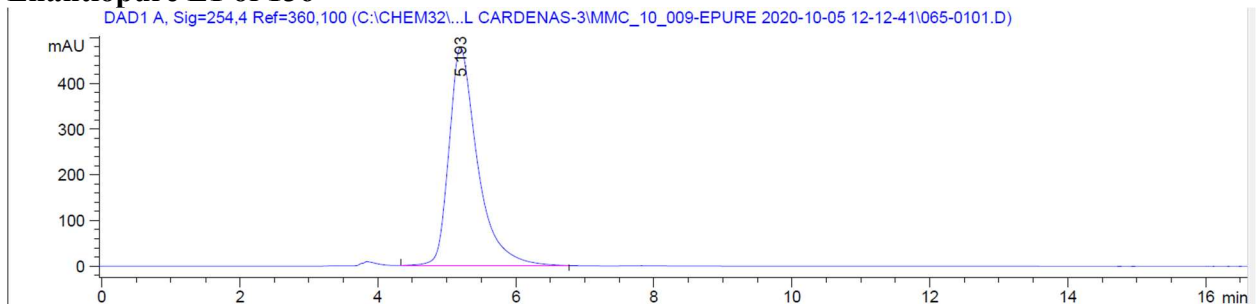


Signal 1: DAD1 A, Sig=254,4 Ref=360,100

Peak #	RetTime [min]	Type	Width [min]	Area [mAU*s]	Height [mAU]	Area %
1	5.212	BV	0.3777	2536.72046	100.06839	53.9040
2	7.912	BB	1.0430	2169.27808	25.59001	46.0960

Totals : 4705.99854 125.65840

Enantiopure E1 of 136



Signal 1: DAD1 A, Sig=254,4 Ref=360,100

Peak #	RetTime [min]	Type	Width [min]	Area [mAU*s]	Height [mAU]	Area %
1	5.193	BB	0.4221	1.38042e4	479.12216	100.0000

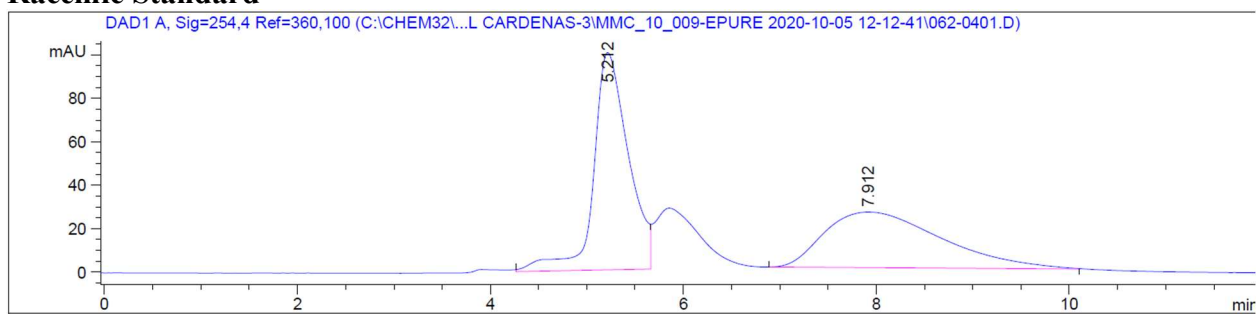
Totals : 1.38042e4 479.12216

E2 of 136 was measured with HPLC analysis using Chiralpak IA Hexanes/EtOH (70:30), flow rate = 1.0 mL/min, tR = 5.4 min.

→ Determined 100 ee%

[enantiopure]
Enantiomer 2

Racemic Standard

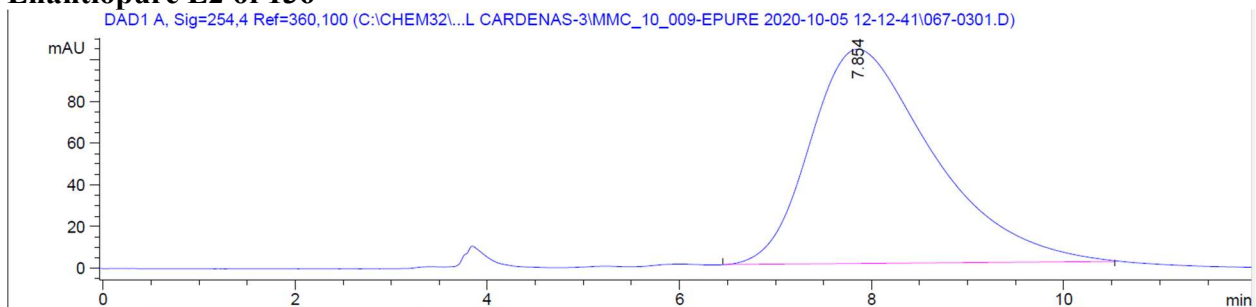


Signal 1: DAD1 A, Sig=254,4 Ref=360,100

Peak #	RetTime [min]	Type	Width [min]	Area [mAU*s]	Height [mAU]	Area %
1	5.212	BV	0.3777	2536.72046	100.06839	53.9040
2	7.912	BB	1.0430	2169.27808	25.59001	46.0960

Totals : 4705.99854 125.65840

Enantiopure E2 of 136



Signal 1: DAD1 A, Sig=254,4 Ref=360,100

Peak #	RetTime [min]	Type	Width [min]	Area [mAU*s]	Height [mAU]	Area %
1	7.854	BB	1.3020	9173.08398	102.90110	100.0000

Totals : 9173.08398 102.90110

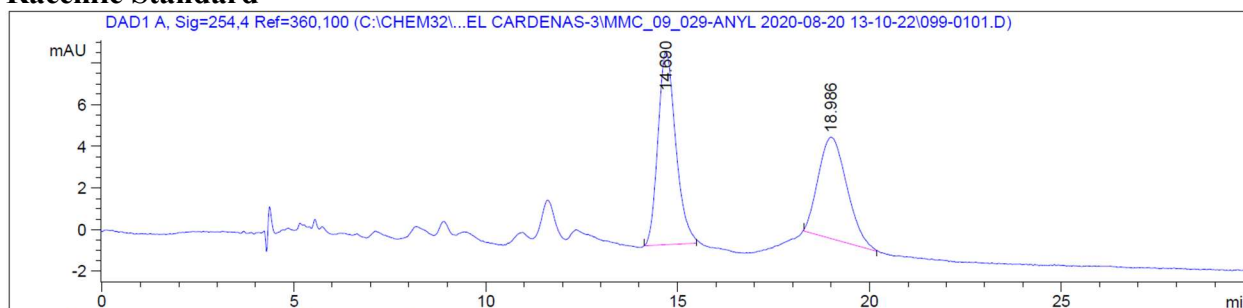
E1 of 133 was measured with HPLC analysis using Chiralpak IA Hexanes/EtOH (50:50), flow rate = 1.0 mL/min, tR = 5.4 min.

→ Determined 100 ee%

[enantiopure]

Enantiomer 1

Racemic Standard

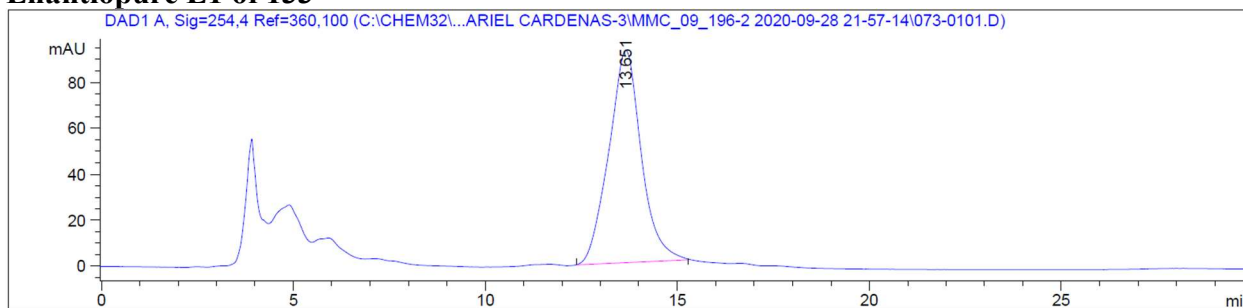


Signal 1: DAD1 A, Sig=254,4 Ref=360,100

Peak #	RetTime [min]	Type	Width [min]	Area [mAU*s]	Height [mAU]	Area %
1	14.690	BB	0.4959	300.59988	9.28051	54.3436
2	18.986	BB	0.6232	252.54704	4.86813	45.6564

Totals : 553.14693 14.14864

Enantiopure E1 of 133



Signal 1: DAD1 A, Sig=254,4 Ref=360,100

Peak #	RetTime [min]	Type	Width [min]	Area [mAU*s]	Height [mAU]	Area %
1	13.651	BB	0.8558	5459.10547	92.59670	100.0000

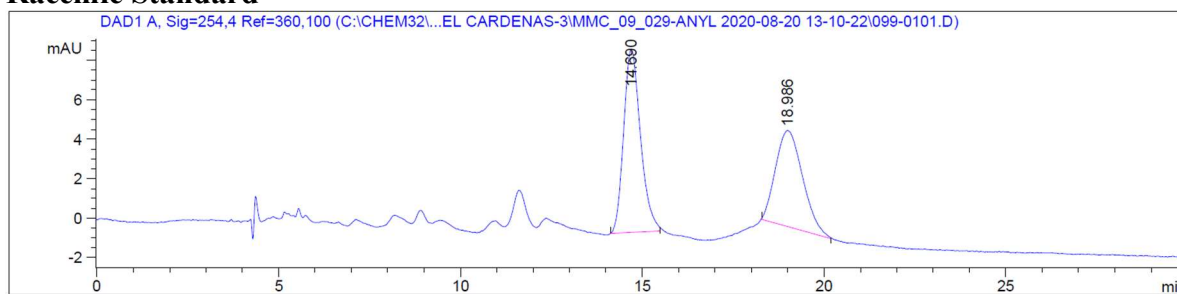
Totals : 5459.10547 92.59670

E2 of 133 was measured with HPLC analysis using Chiralpak IA Hexanes/EtOH (50:50), flow rate = 1.0 mL/min, tR = 5.4 min.

→ Determined 1.9:98.1 e.r., 96.2 ee%

[enantiopure]
Enantiomer 2

Racemic Standard

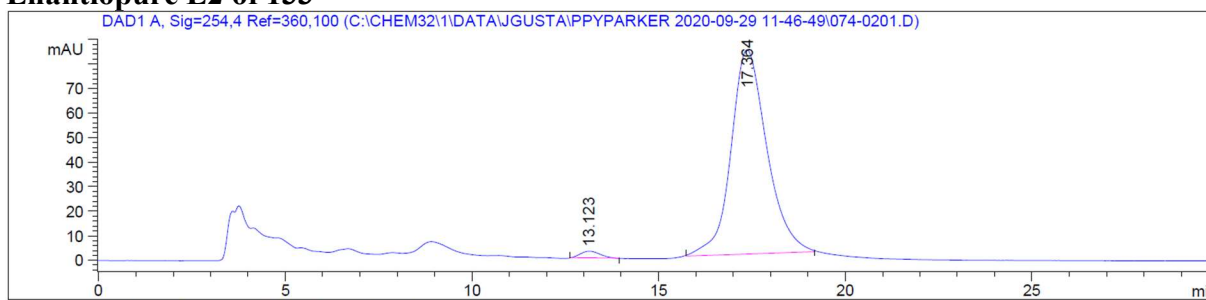


Signal 1: DAD1 A, Sig=254,4 Ref=360,100

Peak #	RetTime [min]	Type	Width [min]	Area [mAU*s]	Height [mAU]	Area %
1	14.690	BB	0.4959	300.59988	9.28051	54.3436
2	18.986	BB	0.6232	252.54704	4.86813	45.6564

Totals : 553.14693 14.14864

Enantiopure E2 of 133

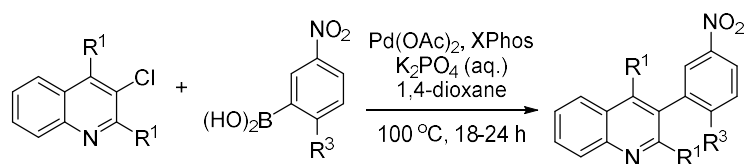


Signal 1: DAD1 A, Sig=254,4 Ref=360,100

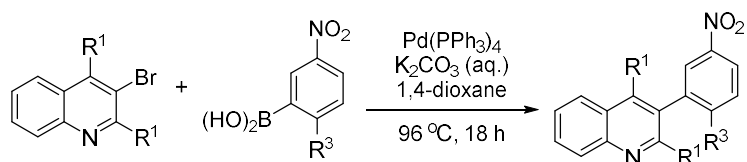
Peak #	RetTime [min]	Type	Width [min]	Area [mAU*s]	Height [mAU]	Area %
1	13.123	BB	0.4685	107.86214	2.86951	1.8953
2	17.364	BB	0.9900	5583.11572	83.29853	98.1047

Totals : 5690.97787 86.16804

3.3.3. Cross-coupling Procedure for Synthesis of Intermediates

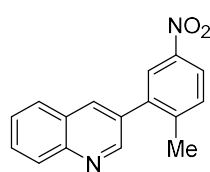


Equation 49. **Method A. Buchwald-Hartwig Cross-Coupling**



Equation 50. **Method B. Suzuki-Miyaura Cross-Coupling**

3-(2-methyl-5-nitrophenyl)quinoline

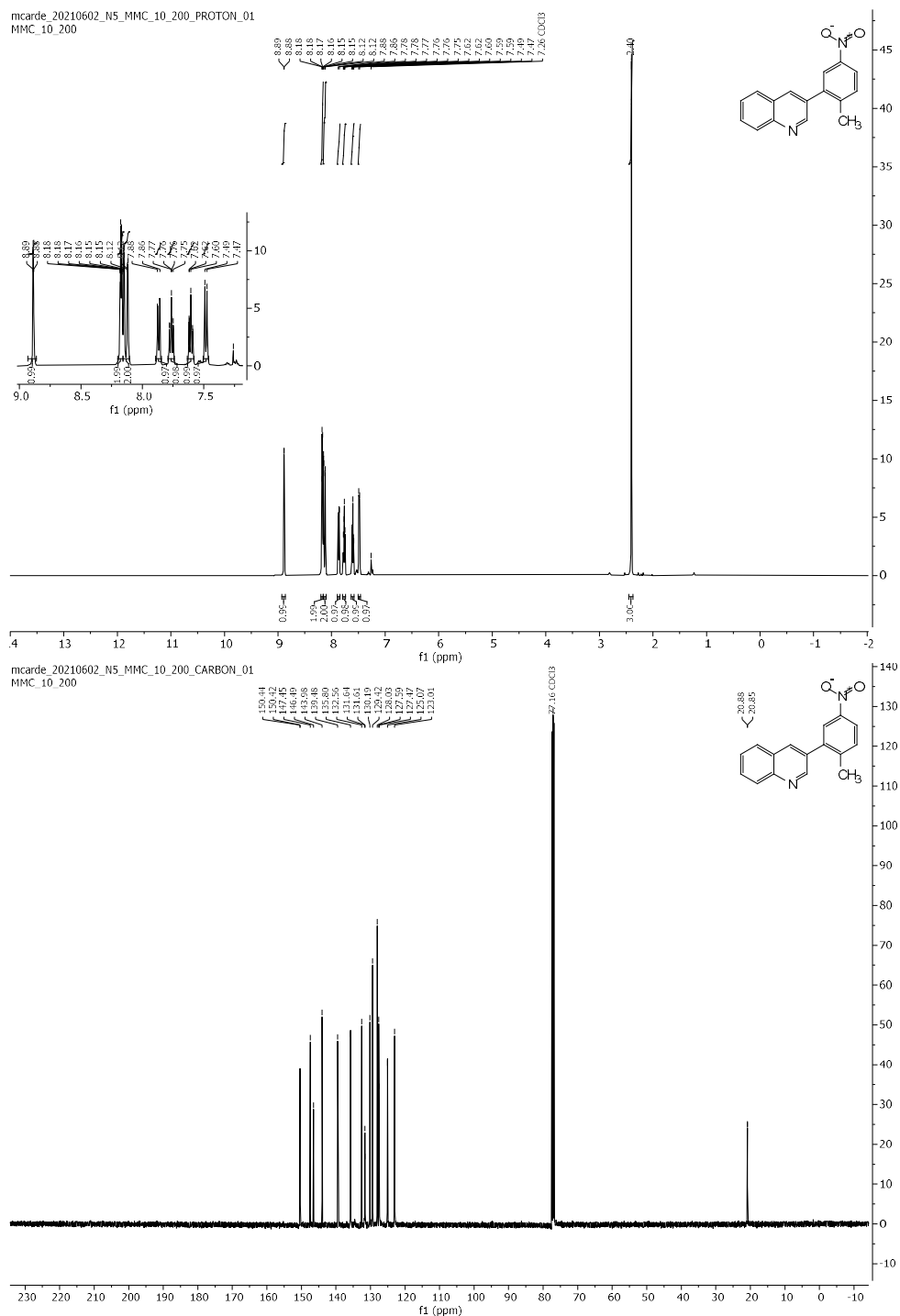


To 3-bromoquinoline (600 mg, 2.884 mmol, 1.0 equiv) was added (2-methyl-5-nitrophenyl)boronic acid (677 mg, 3.742 mmol, 1.3 equiv), potassium carbonate (916.7 mg, 6.6332 mmol, 2.3 equiv), Pd(PPh₃)₄ (166 mg, 0.1442 mmol, 0.05 equiv), 3.8 mL degassed, deionized H₂O and 11.5 mL 1,4-dioxane. The reaction conditions and workup procedure were followed according to the procedure outlined in Section “2.2.6.9 Synthesis of 3-aryl quinoline intermediates.” Purification was carried out via FCC 0% → 60% EtOAc in n-hexane to afford product as a brown solid (559.3 mg, 72%).

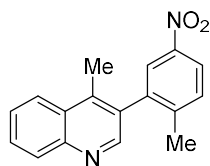
¹H NMR (500 MHz, CDCl₃) δ (ppm) = 8.89 (d, J = 2.3 Hz, 1H), 8.20 – 8.16 (m, 2H), 8.13 (dd, J = 15.1, 2.3 Hz, 2H), 7.87 (d, J = 9.9 Hz, 1H), 7.79 – 7.74 (m, 1H), 7.63 – 7.58 (m, 1H), 7.48 (d, J = 8.3 Hz, 1H), 2.40 (s, 3H).

^{13}C NMR (126 MHz, CDCl_3) δ (ppm) = 150.43 (d, $J = 2.4$ Hz), 147.45, 146.49, 143.98, 139.48, 135.80, 132.56, 131.62 (d, $J = 4.3$ Hz), 130.19, 129.42, 128.03, 127.59, 127.47, 125.07, 123.01, 20.86 (d, $J = 3.3$ Hz).

MS (APCI) = 264.3 m/z calculated for $\text{C}_{16}\text{H}_{12}\text{N}_2\text{O}_2$; experimental 264.1.



4-methyl-3-(2-methyl-5-nitrophenyl)quinoline



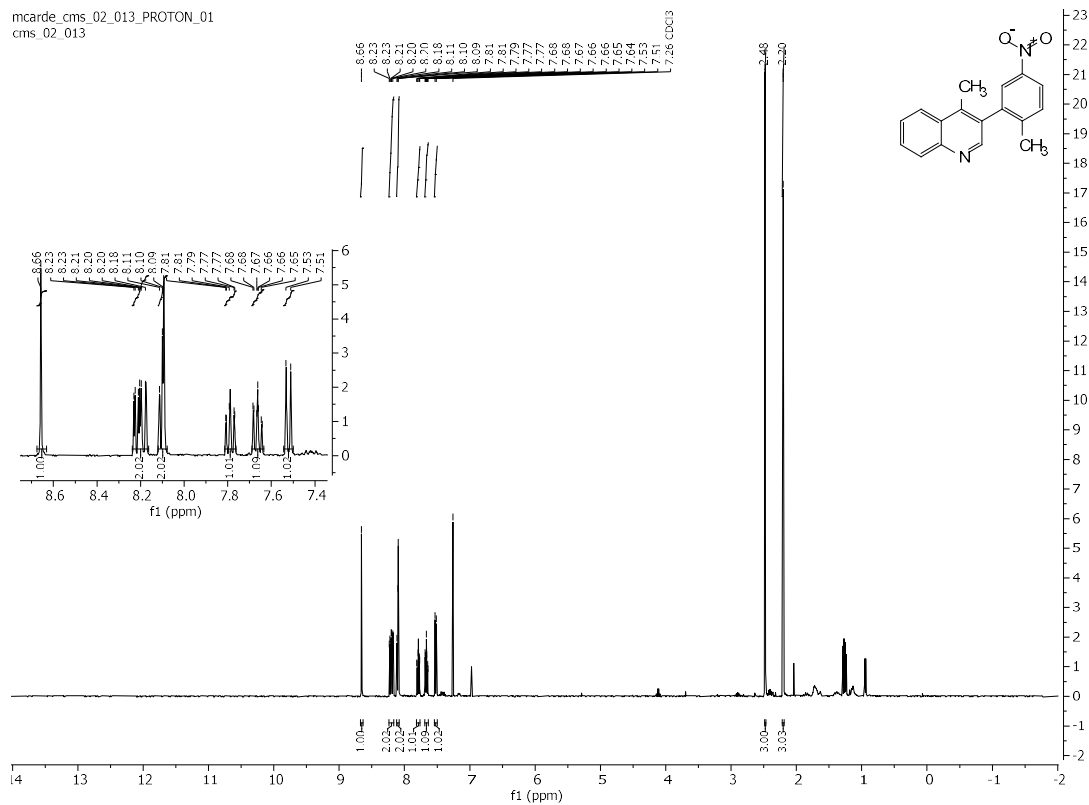
To 3-chloro-4-methylquinoline (650 mg, 3.779 mmol, 1.0 equiv) was added (2-methyl-5-nitrophenyl)boronic acid (889 mg, 4.913 mmol, 1.3 equiv), potassium phosphate tribasic (1.844 g, 8.692 mmol, 2.3 equiv), Pd(OAc)₂ (84.6 mg, 0.3779 mmol, 0.1 equiv), XPhos (360 mg, 0.7558 mmol, 0.2 equiv), 5.03 mL degassed, deionized H₂O and 15.1 mL 1,4-dioxane. The reaction conditions and workup procedure were followed according to the procedure outlined in Section “2.2.6.9 Synthesis of 3-aryl quinoline intermediates.” Purification was carried out via FCC 0% → 60% EtOAc in *n*-hexane to afford product as a brown solid (704 mg, 67%).

¹H NMR (400 MHz, CDCl₃) δ (ppm) = 8.66 (s, 1H), 8.24 – 8.16 (m, 2H), 8.12 – 8.08 (m, 2H), 7.81 – 7.76 (m, 1H), 7.66 (ddd, J = 8.5, 7.0, 1.5 Hz, 1H), 7.52 (d, J = 8.5 Hz, 1H), 2.48 (s, 3H), 2.20 (s, 3H).

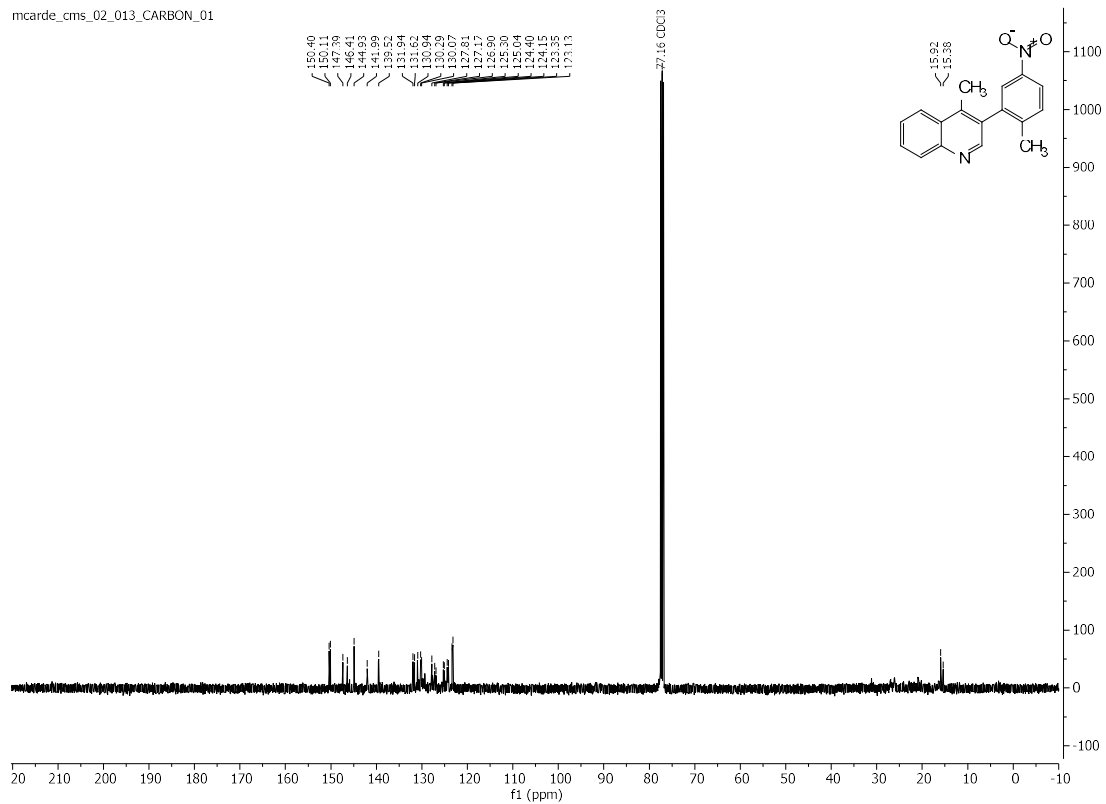
¹³C NMR (101 MHz, CDCl₃) δ (ppm) = 150.26 (d, J = 29.0 Hz), 147.39, 146.41, 144.93, 141.99, 139.52, 131.94, 131.62, 130.94, 130.18 (d, J = 22.3 Hz), 127.81, 127.04 (d, J = 27.2 Hz), 125.17 (d, J = 26.1 Hz), 124.27 (d, J = 25.1 Hz), 123.24 (d, J = 21.9 Hz), 15.92, 15.38.

MS (APCI) = 278.3 m/z calculated for C₁₇H₁₄N₂O₂; experimental 278.1.

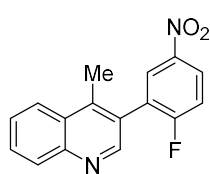
mcarde_cms_02_013_PROTON_01
cms_02_013



mcarde_cms_02_013_CARBON_01



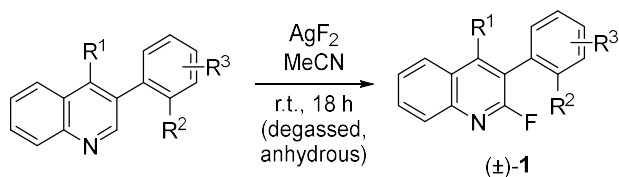
3-(2-fluoro-5-nitrophenyl)-4-methylquinoline



To 3-chloro-4-methylquinoline (2.615 g, 15.2 mmol, 1.0 equiv) was added (2-fluoro-5-nitrophenyl)boronic acid (3.65 g, 19.76 mmol, 1.3 equiv), potassium phosphate tribasic (7.42 g, 34.96 mmol, 2.3 equiv), Pd(OAc)₂ (340 mg, 1.52 mmol, 0.1 equiv), XPhos (1.45 g, 8.04 mmol, 0.2 equiv), 20 mL degassed, deionized H₂O and 60.8 mL 1,4-dioxane. The reaction conditions, workup, and purification procedure were followed according to the general procedure and characterization of this compound is in accordance with the report in Section “2.2.6.9 Synthesis of 3-aryl quinoline intermediates.” A yellowish orange amorphous solid, (4.1 g, 96%).

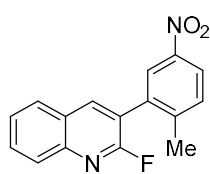
MS (APCI) = 282.3 m/z calculated for C₁₆H₁₁FN₂O₂; experimental 282.1.

3.3.4 Hartwig Fluorination Towards 3-aryl-2-fluoroquinolines



Equation 51. The modified Hartwig fluorination procedure is followed in accordance conditions reported in **Cardenas, M. M.**; Saputra, M. A.; Gordon, D. A.; Sanchez, A. N.; Yamamoto, N.; Gustafson, J. L. *Chem. Commun.*, **2021**, 57, 10087–10090.

2-fluoro-3-(2-methyl-5-nitrophenyl)quinoline



To 3-(2-methyl-5-nitrophenyl)quinoline (559.3 mg, 2.085 mmol) was added silver (II) fluoride (1.06 g, 7.298 mmol) and 4.2 mL degassed MeCN. The reaction conditions and workup procedure were followed according to the procedure outlined in **Cardenas, M. M.**; Saputra, M. A.; Gordon, D. A.; Sanchez, A. N.;

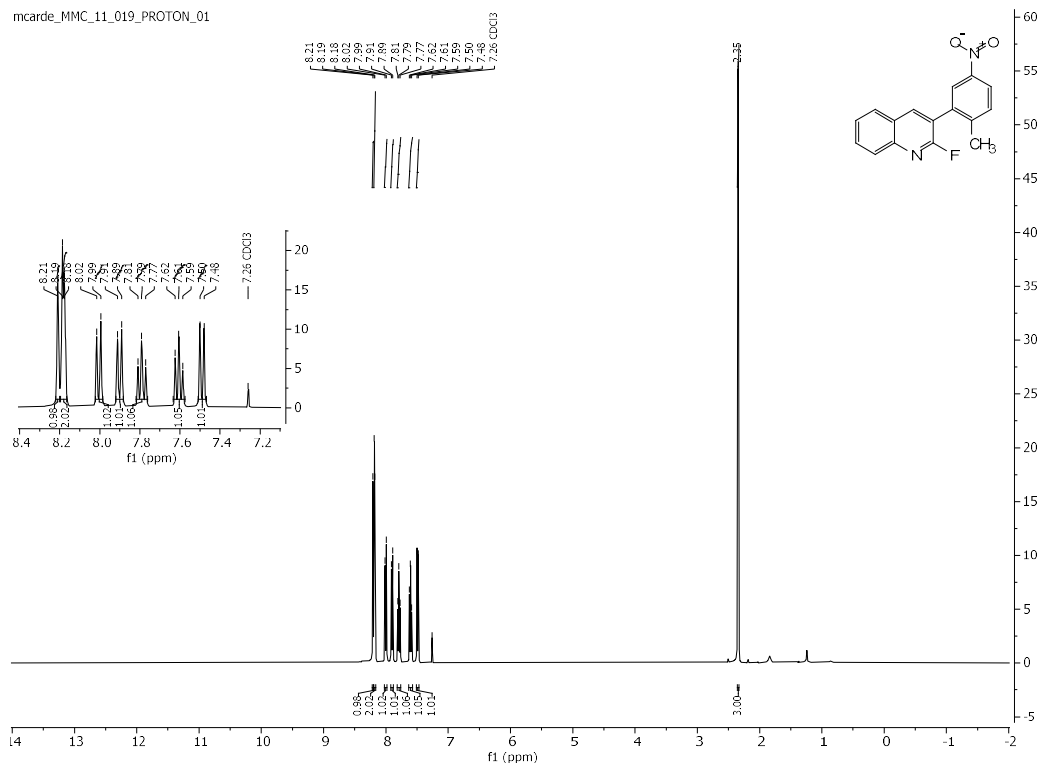
Yamamoto, N.; Gustafson, J. L. *Chem. Commun.*, **2021**, 57, 10087–10090. Purification was carried out via FCC 0% → 45% EtOAc in n-hexane to afford the product as a beige solid (380 mg, 64%).

¹H NMR (400 MHz, CDCl₃) δ (ppm) = 8.21 (s, 1H), 8.18 (d, J = 3.7 Hz, 2H), 8.01 (d, J = 8.5 Hz, 1H), 7.90 (d, J = 8.2 Hz, 1H), 7.82 – 7.76 (m, 1H), 7.63 – 7.57 (m, 1H), 7.49 (d, J = 8.1 Hz, 1H), 2.35 (s, 3H).

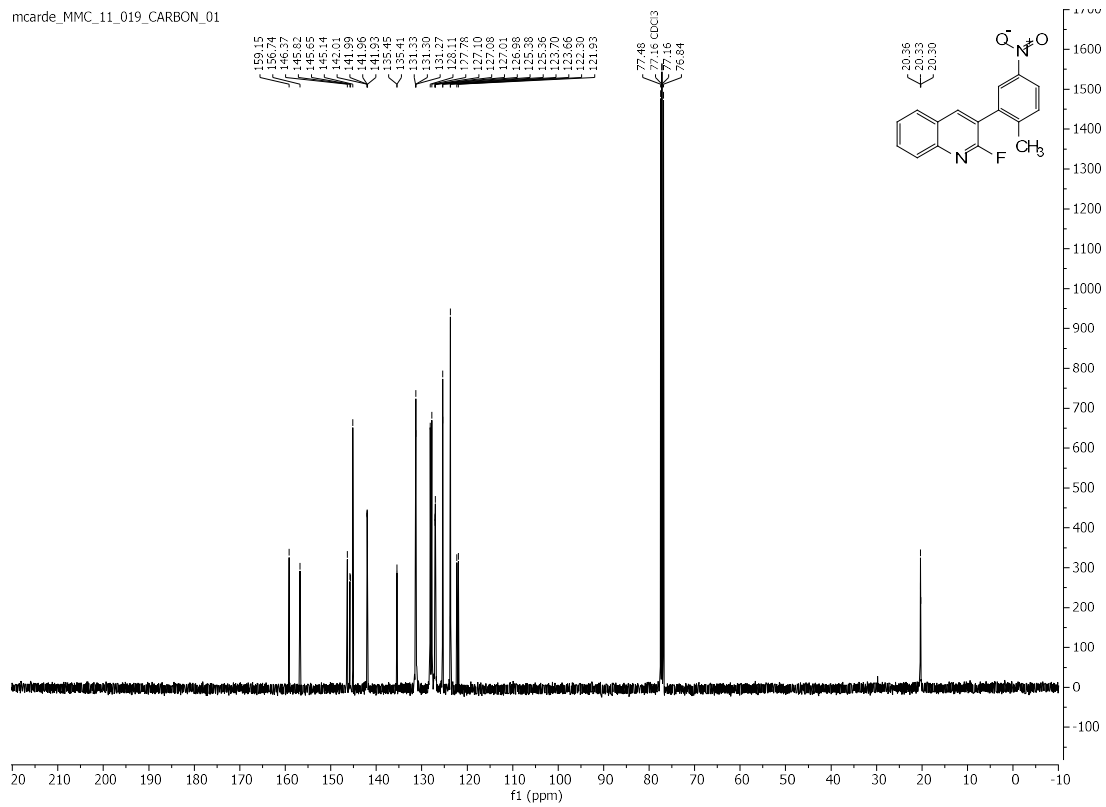
¹³C NMR (101 MHz, CDCl₃) δ (ppm) = 159.15, 156.74, 146.37, 145.73 (d, J = 16.6 Hz), 145.14, 142.00 (d, J = 2.1 Hz), 141.94 (d, J = 2.1 Hz), 135.43 (d, J = 3.9 Hz), 131.38 – 131.22 (m), 127.94 (d, J = 33.2 Hz), 127.09 (d, J = 2.1 Hz), 126.99 (d, J = 2.5 Hz), 125.37 (d, J = 1.8 Hz), 123.66, 122.11 (d, J = 37.4 Hz), 20.33 (t, J = 3.2 Hz).

¹⁹F NMR (376 MHz, CDCl₃) δ (ppm) = -63.47 (d, J = 9.5 Hz).

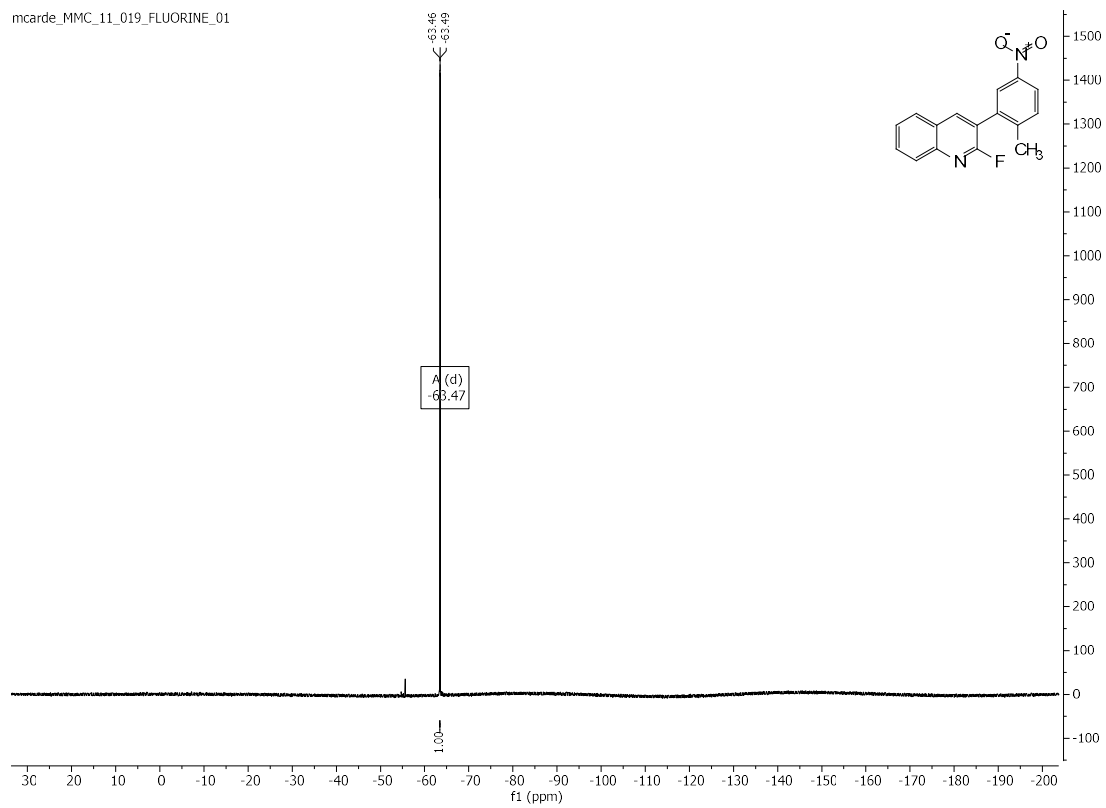
MS (APCI) = 282.3 m/z calculated for C₁₆H₁₁FN₂O₂; experimental 282.1.



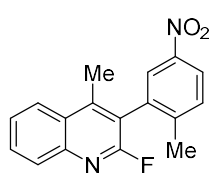
mcarde MMC_11_019 CARBON_01



mcarde MMC_11_019 FLUORINE_01



2-fluoro-4-methyl-3-(2-methyl-5-nitrophenyl)quinoline



To 4-methyl-3-(2-methyl-5-nitrophenyl)quinoline (800 mg, 2.836 mmol, 1.0 equiv) was added silver (II) fluoride (1.5 g, 10.072 mmol, 3.5 equiv) and 5.1 mL degassed MeCN. The reaction conditions and workup procedure were followed according to the procedure outlined in **Cardenas, M. M.**; Saputra, M. A.; Gordon, D. A.; Sanchez, A. N.; Yamamoto, N.; Gustafson, J. L. *Chem. Commun.*, **2021**, 57, 10087–10090. Purification was carried out via FCC 0% → 45% EtOAc in n-hexane to afford **[insert #]** as a beige solid (345 mg, 41%).

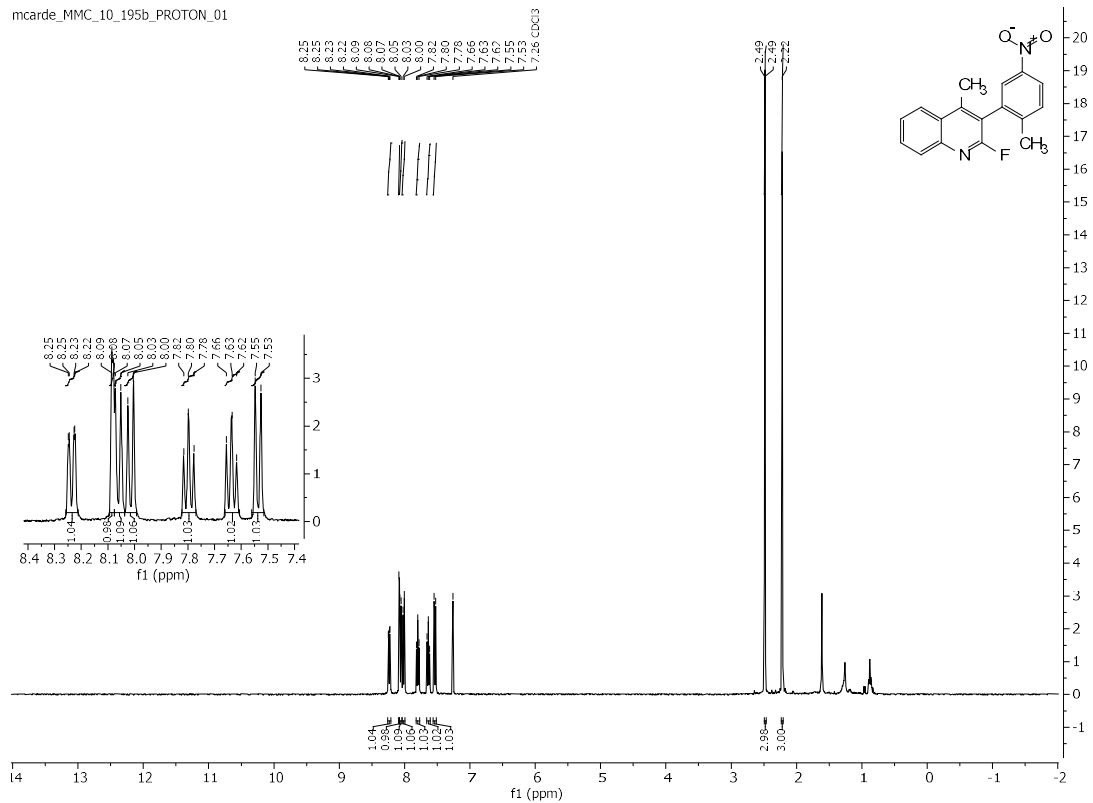
¹H NMR (400 MHz, CDCl₃) δ (ppm) = 8.24 (dd, J = 8.5, 1.2 Hz, 1H), 8.08 (d, J = 2.4 Hz, 1H), 8.06 (d, J = 8.4 Hz, 1H), 8.02 (d, J = 8.3 Hz, 1H), 7.82 – 7.77 (m, 1H), 7.66 – 7.61 (m, 1H), 7.54 (d, J = 8.4 Hz, 1H), 2.49 (d, J = 1.4 Hz, 3H), 2.22 (s, 3H).

¹³C NMR (101 MHz, CDCl₃) δ (ppm) = 158.16 (d, J = 239.8 Hz), 148.57 (d, J = 6.0 Hz), 146.56, 145.38, 145.20, 134.87 (d, J = 2.8 Hz), 131.37, 130.92, 128.94 (d, J = 1.8 Hz), 127.05 (d, J = 2.1 Hz), 126.70 (d, J = 2.5 Hz), 125.44, 124.53, 123.70, 120.66 (d, J = 37.1 Hz), 20.21, 16.08.

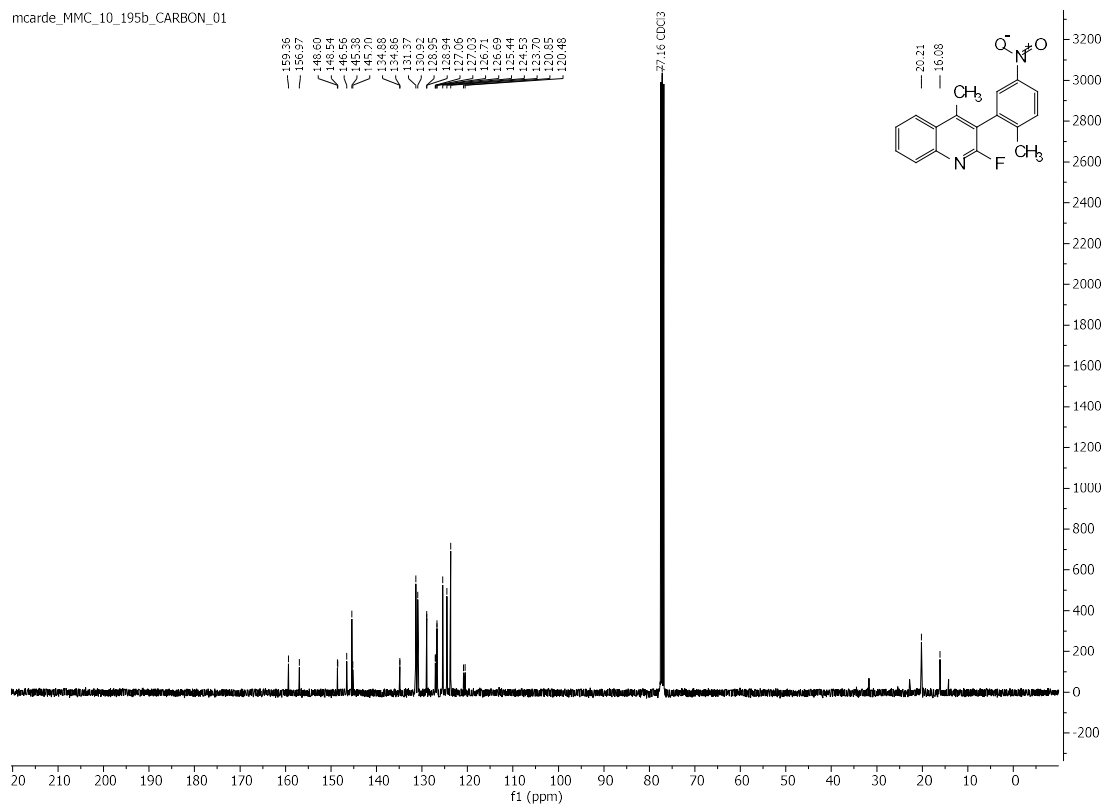
¹⁹F NMR (376 MHz, CDCl₃) δ (ppm) = -62.38.

MS (APCI) = 296.3 m/z calculated for C₁₇H₁₃FN₂O₂; experimental 296.1.

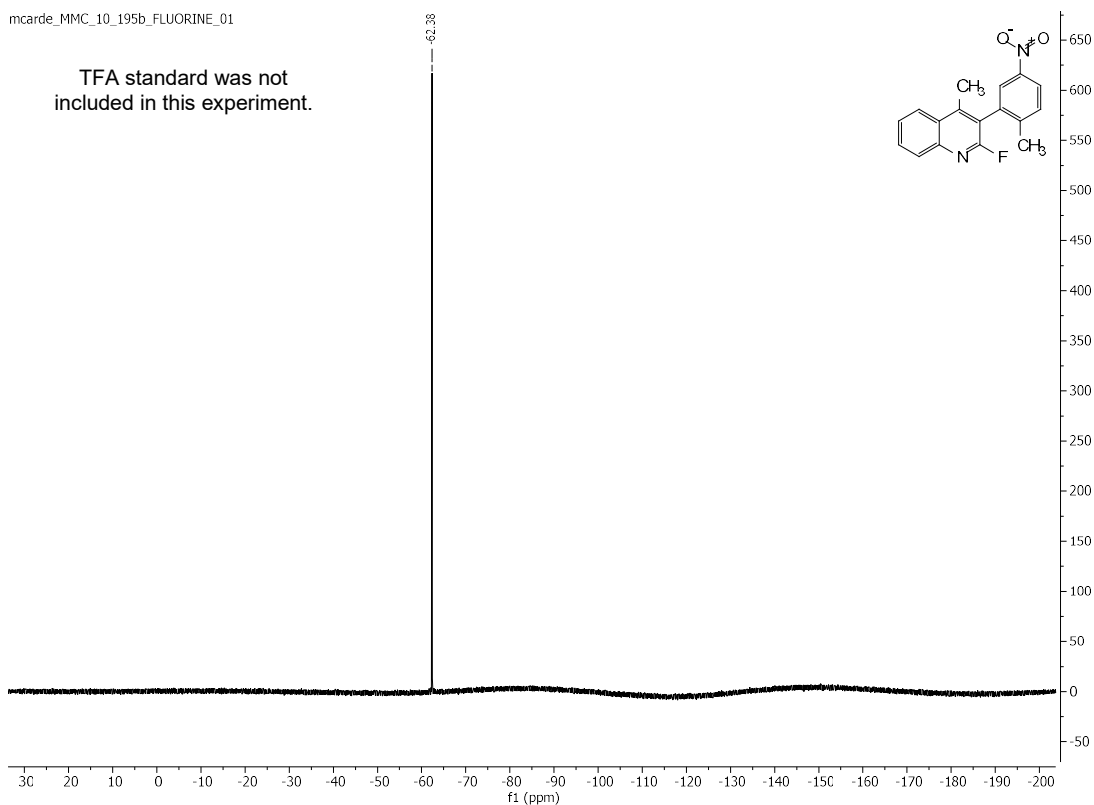
mcarde MMC_10_195b_PROTON_01



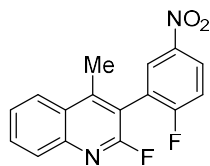
mcarde MMC_10_195b_CARBON_01



mcarde_MMC_10_195b_FLUORINE_01



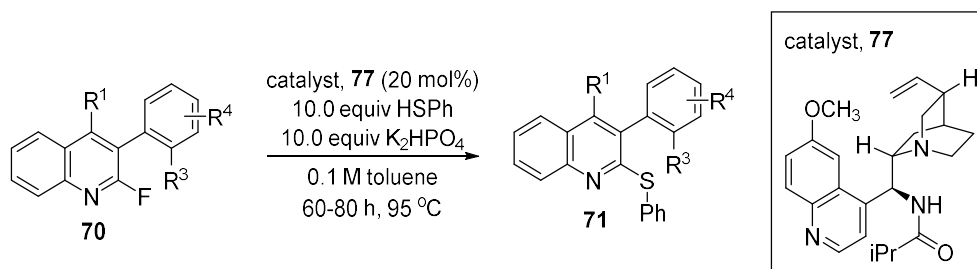
2-fluoro-3-(2-fluoro-5-nitrophenyl)-4-methylquinoline



To 3-(2-fluoro-5-nitrophenyl)-4-methylquinoline (800 mg, 2.836 mmol) was added silver (II) fluoride (1.5 g, 10.072 mmol) and 5.1 mL degassed MeCN. The reaction conditions, workup, and purification procedure were followed according to the general procedure and characterization of this compound is in accordance with the report in **Cardenas, M. M.**; Saputra, M. A.; Gordon, D. A.; Sanchez, A. N.; Yamamoto, N.; Gustafson, J. L. *Chem. Commun.*, **2021**, 57, 10087–10090. A yellowish orange amorphous solid, (4.1 g, 96%). Refer to Section 2.2.12 for the synthesis of this compound.

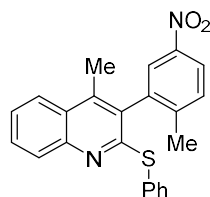
MS (APCI) = 300.3 m/z calculated for C₁₆H₁₀F₂N₂O₂; experimental 300.6.

3.3.5 General Thiolation Towards 3-aryl-2-(phenylthio)quinolines



Equation 52. The nucleophilic aromatic substitution of thiophenol into a 3-aryl-2-fluoroquinoline was reported by Section “2.2.6.11 General S_NAr Strategy to yield enantioenriched 3-aryl-2-(phenylthio)quinolines (2).” A modification was used where 10.0 equiv of potassium phosphate is used and the reaction is heated at 95 °C.

4-methyl-3-(2-methyl-5-nitrophenyl)-2-(phenylthio)quinoline



To 2-fluoro-4-methyl-3-(2-methyl-5-nitrophenyl)quinoline (187 mg, 0.6311 mmol, 1.0 equiv) was added thiophenol (643.8 mL, 6.311 mmol, 10.0 equiv), potassium phosphate dibasic (1.098 g, 6.311 mmol, 10 equiv), catalyst **77** and

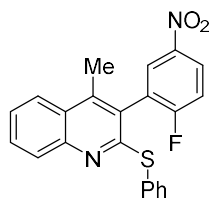
6.3 mL toluene. The resulting reaction was heated at 95 °C for 30 h. The workup procedure and purification were followed according to the procedure outlined in **Cardenas, M. M.**; Saputra, M. A.; Gordon, D. A.; Sanchez, A. N.; Yamamoto, N.; Gustafson, J. L. *Chem. Commun.*, **2021**, 57, 10087–10090. Product is a white solid (156 mg, 46%). Refer to Section 2.2.13 for more details.

¹H NMR (500 MHz, CDCl₃) δ (ppm) = 8.25 (dd, J = 8.4, 2.4 Hz, 1H), 8.07 (d, J = 2.4 Hz, 1H), 7.97 (dd, J = 8.3, 1.7 Hz, 1H), 7.80 (d, J = 7.0 Hz, 1H), 7.64 (ddd, J = 8.3, 6.9, 1.4 Hz, 1H), 7.54 (s, 1H), 7.51 (ddt, J = 5.5, 3.8, 2.1 Hz, 3H), 7.38 (dd, J = 4.5, 2.3 Hz, 3H), 2.34 (s, 3H), 2.25 (s, 3H).

¹³C NMR (126 MHz, CDCl₃) δ (ppm) = 158.13, 147.53, 146.76, 145.69, 141.81, 138.14, 134.86, 131.40, 130.71, 130.41, 129.70, 129.39, 128.93, 128.66, 126.24, 126.03, 125.82, 124.15, 123.65, 20.16, 15.67.

MS (APCI) = 386.1 m/z calculated for C₂₃H₁₈N₂O₂S; experimental 386.4.

3-(2-fluoro-5-nitrophenyl)-4-methyl-2-(phenylthio)quinoline, 89

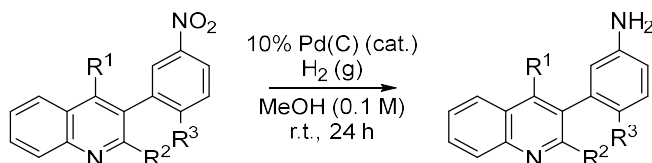


This substrate was previously synthesized and obtained in **Cardenas, M. M.**; Saputra, M. A.; Gordon, D. A.; Sanchez, A. N.; Yamamoto, N.; Gustafson, J. L. *Chem. Commun.*, **2021**, 57, 10087–10090. Please refer to Section 2.2.13 for

more details on the synthesis and the characterization of this compound.

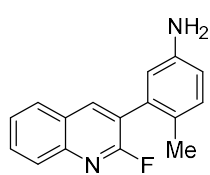
MS (APCI) Calculated: 391.1 m/z calculated for C₂₂H₁₅FN₂O₂S; experimental 389.9, 391.6.

3.3.6 Synthesizing Intermediates: General Amination Towards 3-aryl-2-(phenylthio)quinolines



Equation 53. The nucleophilic aromatic substitution of thiophenol into a 3-aryl-2-fluoroquinoline was reported by **Cardenas, M. M.**; Saputra, M. A.; Gordon, D. A.; Sanchez, A. N.; Yamamoto, N.; Gustafson, J. L. *Chem. Commun.*, **2021**, 57, 10087–10090. A modification was used where 10.0 equiv of potassium phosphate is used and the reaction is heated at 95 °C.

3-(2-fluoroquinolin-3-yl)-4-methylaniline



Following the general procedure: to 2-fluoro-3-(2-methyl-5-nitrophenyl)quinoline (380 mg, 1.328 mmol, 1.0 equiv) was added Pd(C) (141 mg, 1.328 mmol, 1.0 equiv) and 5.0 mL degassed MeOH. The reaction

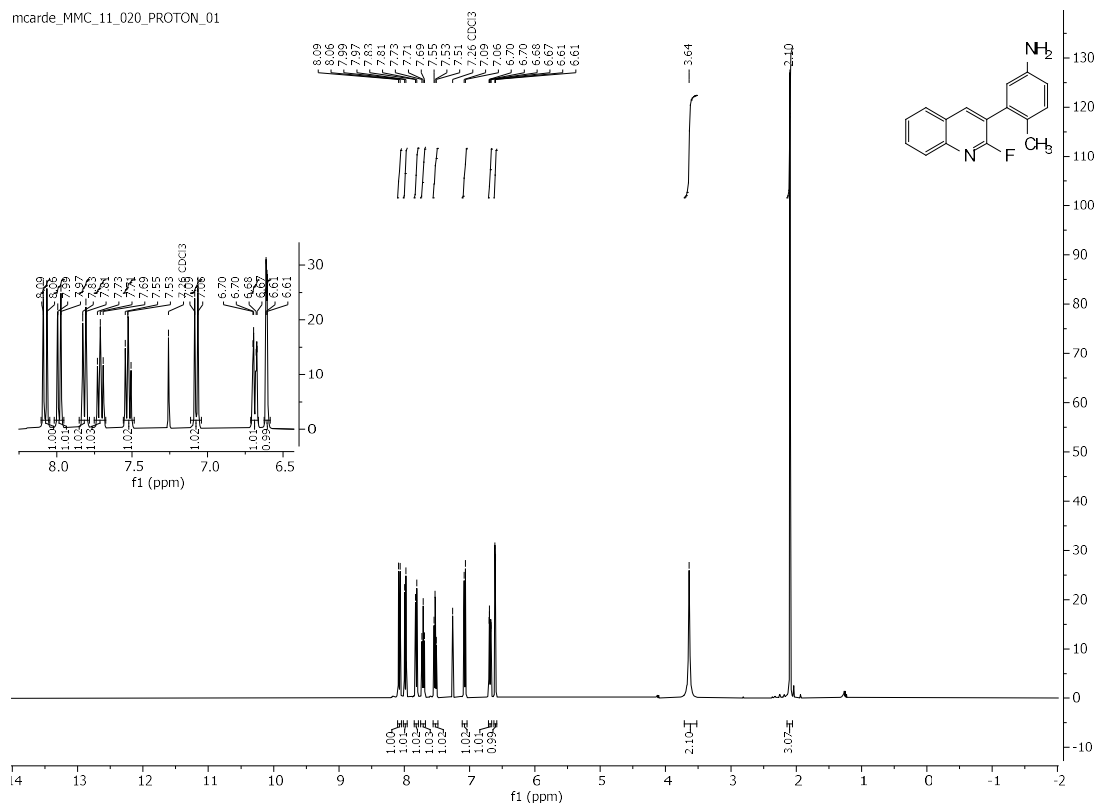
conditions and workup procedure were followed according to the procedure outlined in Section “2.2.6.12 Post Functionalization of Enantioenriched PR (2) and SM (1).” Purification was carried out via FCC 0% → 75% EtOAc in *n*-hexane to afford product as a white solid (156 mg, 46%).

¹H NMR (400 MHz, CDCl₃) δ (ppm) = 8.08 (d, J = 9.6 Hz, 1H), 7.98 (d, J = 8.4 Hz, 1H), 7.82 (d, J = 8.2 Hz, 1H), 7.75 – 7.67 (m, 1H), 7.56 – 7.49 (m, 1H), 7.08 (d, J = 8.1 Hz, 1H), 6.69 (dd, J = 8.6, 2.2 Hz, 1H), 6.61 (d, J = 2.9 Hz, 1H), 3.64 (s, 2H), 2.10 (s, 3H).

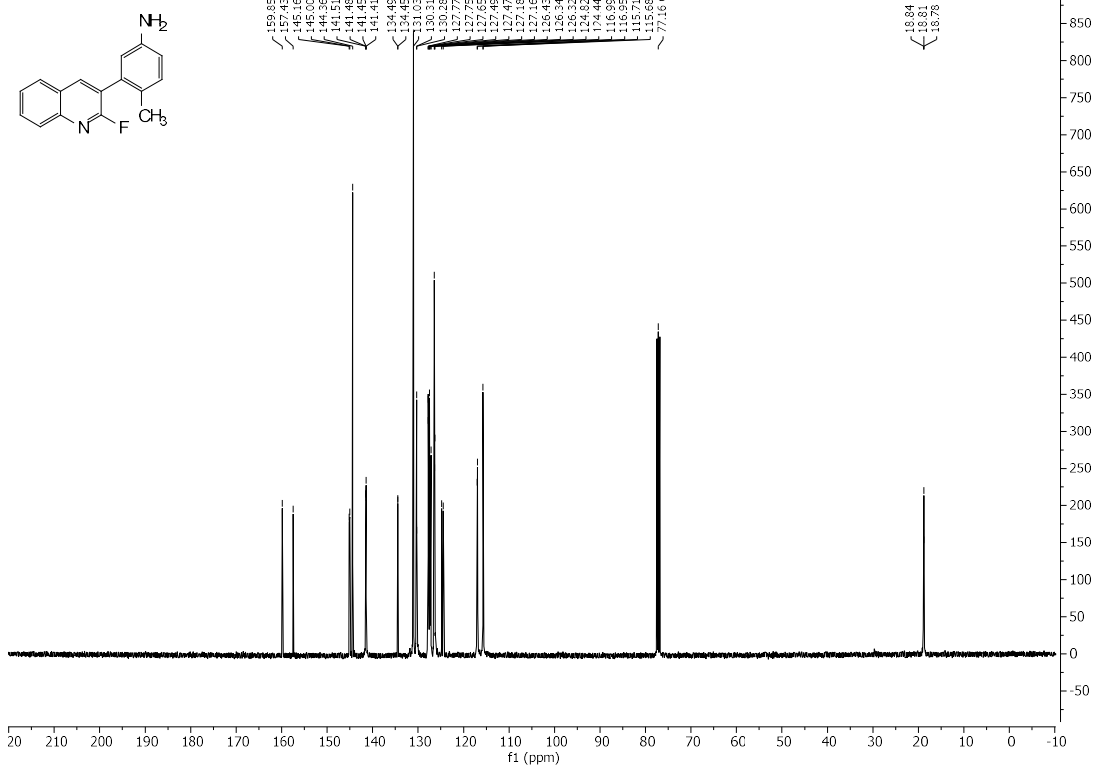
¹³C NMR (101 MHz, CDCl₃) δ (ppm) = 158.64 (d, J = 242.7 Hz), 145.08 (d, J = 16.6 Hz), 144.36, 141.46 (dd, J = 6.5, 3.0 Hz), 134.47 (d, J = 3.5 Hz), 131.03, 130.29 (d, J = 2.8 Hz), 127.62 (dd, J = 28.3, 1.8 Hz), 127.17 (d, J = 1.8 Hz), 126.43, 126.33 (d, J = 2.5 Hz), 124.63 (d, J = 37.4 Hz), 116.97 (d, J = 4.6 Hz), 115.70 (d, J = 2.8 Hz), 18.93 – 18.69 (m).

¹⁹F NMR (376 MHz, CDCl₃) δ (ppm) = -63.18 (d, J = 9.5 Hz).

MS (APCI) = 252.3 m/z calculated for C₁₆H₁₃FN₂; experimental 253.6, 252.9.

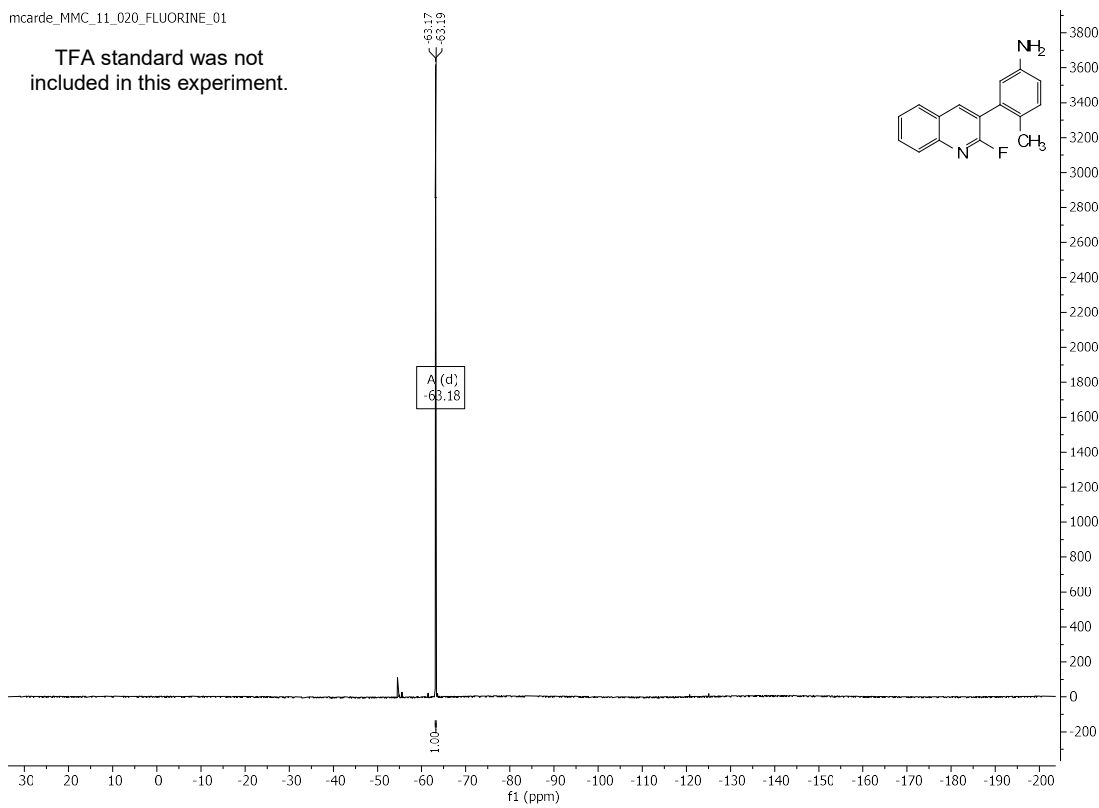


mcardc MMC_11_020 CARBON_01

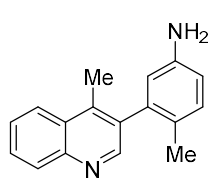


mcardc MMC_11_020 FLUORINE_01

TFA standard was not included in this experiment.



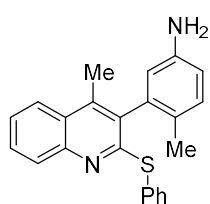
4-methyl-3-(4-methylquinolin-3-yl)aniline



Following the general procedure: to 4-methyl-3-(2-methyl-5-nitrophenyl)quinoline (155 mg, 0.557 mmol, 1.0 equiv) was added Pd(C) (40 mg, 0.375 mmol, 0.70 equiv) and 5.0 mL degassed MeOH. The reaction conditions and workup procedure were followed according to the procedure outlined in **Cardenas, M. M.**; Saputra, M. A.; Gordon, D. A.; Sanchez, A. N.; Yamamoto, N.; Gustafson, J. L. *Chem. Commun.*, **2021**, 57, 10087–10090. Purification was carried out via FCC 0% → 75% EtOAc in *n*-hexane to afford product as a white solid (72 mg, 52%).

MS (APCI) = 248.1 m/z calculated for C₁₇H₁₆N₂; experimental 249.6.

4-methyl-3-(4-methyl-2-(phenylthio)quinolin-3-yl)aniline, 123



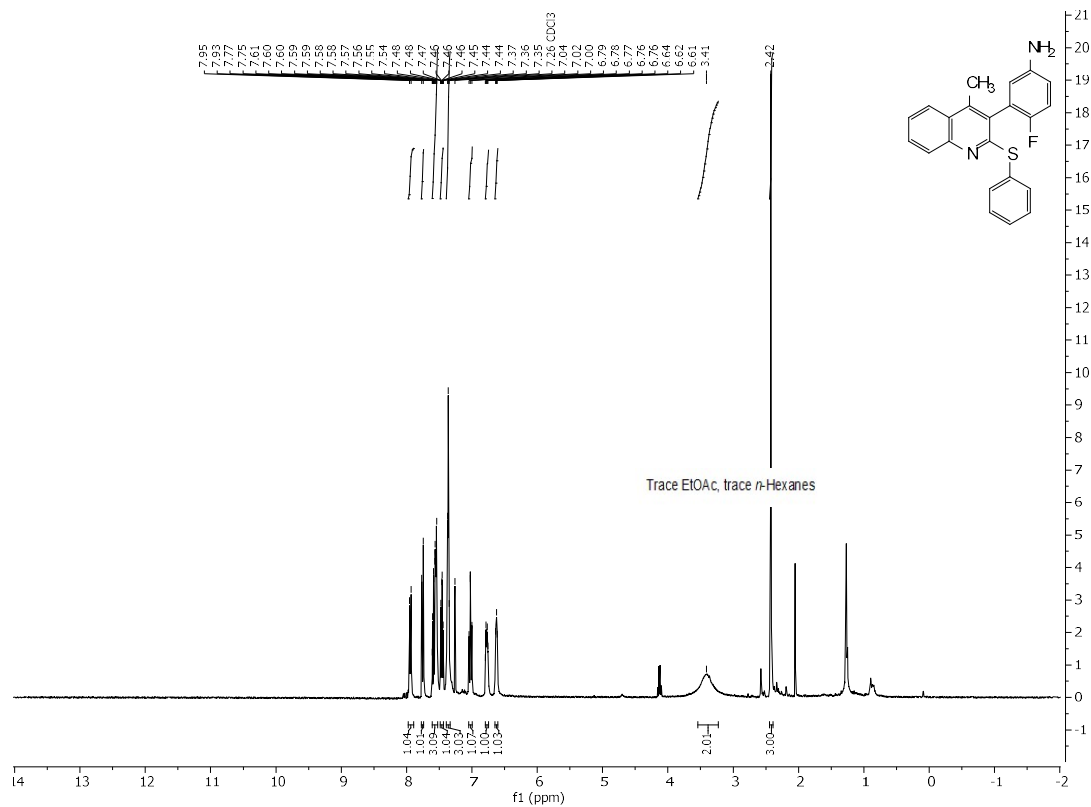
Following the general procedure: to 4-methyl-3-(2-methyl-5-nitrophenyl)quinoline (50 mg, 0.129 mmol, 1.0 equiv) was added Pd(C) (15 mg, 0.129 mmol, 1.0 equiv) and 2.0 mL degassed MeOH. The reaction conditions and workup procedure were followed according to the procedure outlined in **Cardenas, M. M.**; Saputra, M. A.; Gordon, D. A.; Sanchez, A. N.; Yamamoto, N.; Gustafson, J. L. *Chem. Commun.*, **2021**, 57, 10087–10090. Purification was carried out via FCC 0% → 75% EtOAc in *n*-hexane to afford **123** as a white solid (72 mg, 52%). Please refer to Section 2.2.15 for more details regarding the preparation of these compounds.

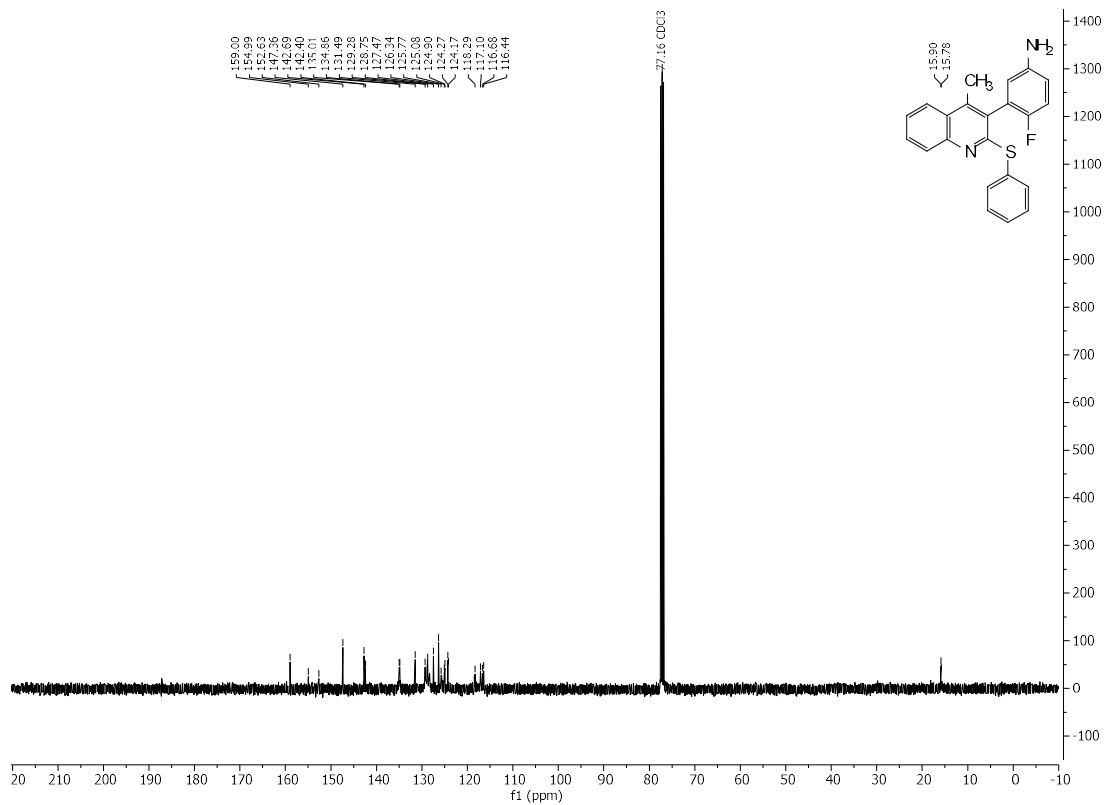
¹H NMR (400 MHz, CDCl₃) δ (ppm) = 7.94 (d, J = 8.4 Hz, 1H), 7.76 (d, J = 8.4 Hz, 1H), 7.61 – 7.52 (m, 3H), 7.49 – 7.44 (m, 1H), 7.36 (t, J = 5.2 Hz, 3H), 7.05 – 6.99 (m, 1H), 6.79 – 6.75 (m, 1H), 6.65 – 6.60 (m, 1H), 3.41 (s, 2H), 2.42 (s, 3H).

^{13}C NMR (101 MHz, CDCl_3) δ (ppm) = 159.00, 154.99, 152.63, 147.36, 142.69, 142.40, 135.01, 134.86, 131.49, 129.28, 128.75, 127.47, 126.34, 125.77, 125.08, 124.90, 124.27, 124.17, 118.29, 117.10, 116.68, 116.44, 15.90, 15.78.

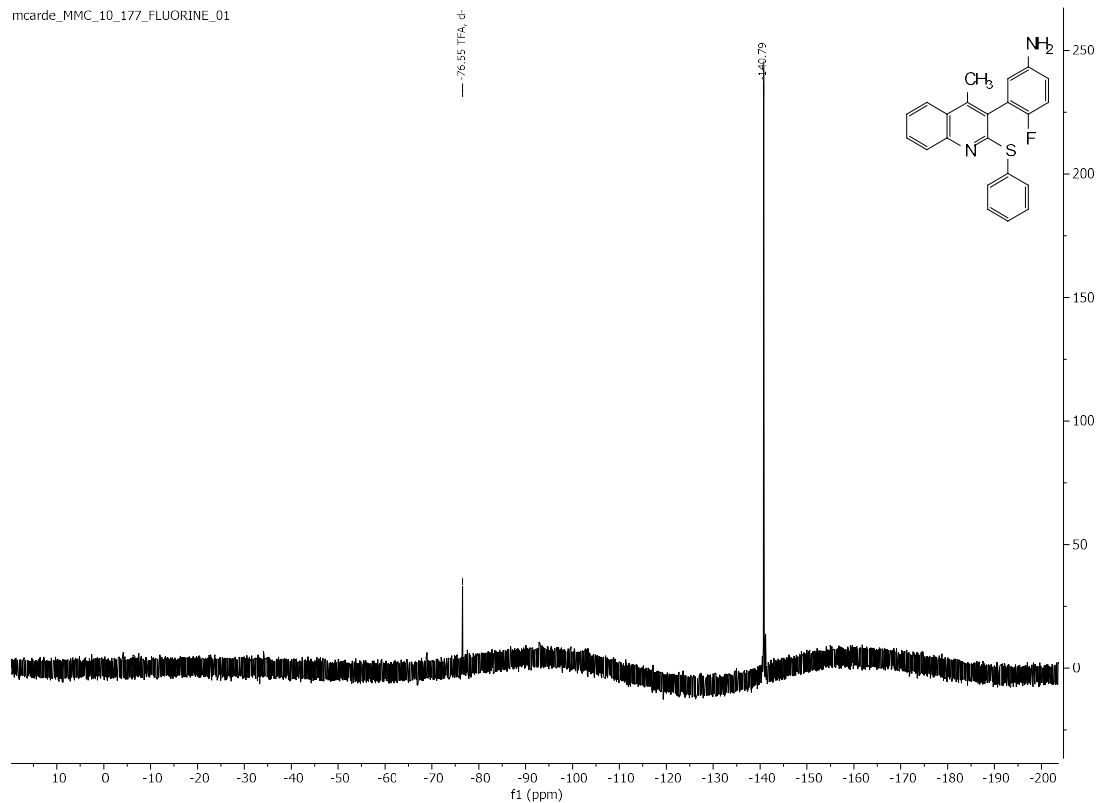
^{19}F NMR (376 MHz, CDCl_3) δ (ppm) = -140.79.

MS (APCI) = 356.5 m/z calculated for $\text{C}_{23}\text{H}_{20}\text{N}_2\text{S}$; experimental 356.3.

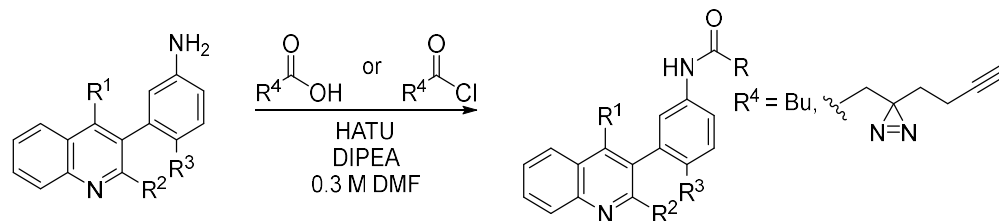




mcarde MMC_10_177_FLUORINE_01



3.3.7 General Procedure: HATU Amide Coupling Towards Atropisomeric Quinoline Scaffolds



Equation 54. Amide coupling was conducted in accordance with the report from Conway, L. P.; Jadhav, A.M.; Homan, R. A.; Li, W.; Rubiano, J.S.; Hawkins, R.; Lawrence, R.M.; Parker, C.G. *Chem. Sci.*, 2021, 12, 7839–7847 (*i.e.*, General Procedure 2 of ‘Synthesis of Diazirine Containing Tags’).

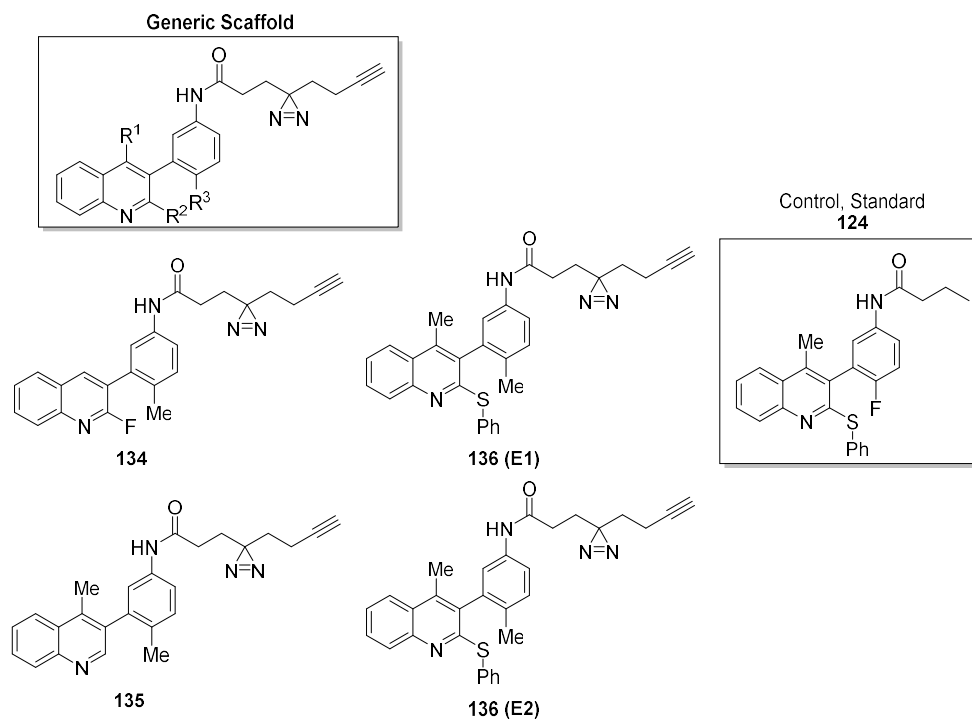
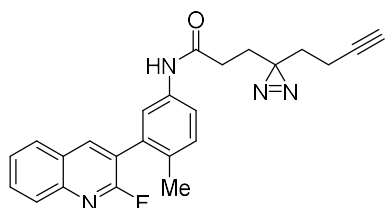


Figure 43. Scope of Chemical Probes

General Amide Coupling Synthesis: A 4.0 mL dram scintillation vial equipped with a stir bar was charged with 0.3 – 0.5 M DMF. The resulting vial was charged with variable substituted 3-arylquinoline (1.0 equiv), HATU (1.25 equiv), and DIPEA (4.0 equiv). The resulting reaction

solution was stirred at room temperature for 15 minutes. Respective acid chloride or carboxylic acid (1.15 equiv) was added to the reaction slowly. The reaction was left to stir at this temperature for up to 20 h. The resulting reaction was diluted with EtOAc or DCM (~0.2 V) and washed with brine (~0.2 V). Organic layer was separated and dried over Na₂SO₄. The crude product was isolated after concentration *in vacuo*. Purification of the crude product was performed in FCC 0% → 80% EtOAc in n-hexane to afford the quinoline-based chemical probe in ~80% yields.

3-(3-(but-3-yn-1-yl)-3H-diazirin-3-yl)-N-(3-(2-fluoroquinolin-3-yl)-4-methylphenyl)propanamide, 134



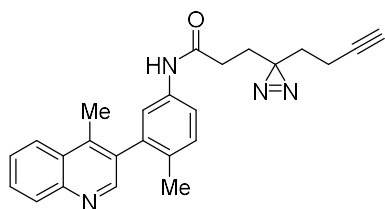
Following the general procedure: 3-(2-fluoroquinolin-3-yl)-4-methylaniline (156 mg, 0.164 mmol, 1.0 equiv), 3-(3-(but-3-yn-1-yl)-3H-diazirin-3-yl)propanoic acid (118 mg, 0.7061 mmol, 1.15 equiv), HATU (291.65 mg, 0.7675 mmol, 1.25 equiv), DIPEA (430 μ L, 2.45 mmol, 4.0 equiv), and 2.0 mL DMF were added to a 2 dram vial equipped with a stir bar. The reaction conditions, workup procedure, and purification were conducted according to the general procedure to afford **134** as a beige solid (45 mg, 69%).

¹H NMR (400 MHz, CDCl₃) δ (ppm) = 8.14 (t, J = 6.6 Hz, 1H), 7.99 (t, J = 6.0 Hz, 1H), 7.85 (t, J = 6.1 Hz, 1H), 7.78 – 7.73 (m, 1H), 7.60 – 7.55 (m, 1H), 7.54 (d, J = 5.4 Hz, 1H), 7.42 (t, J = 6.8 Hz, 1H), 7.32 – 7.26 (m, 1H), 2.19 (d, J = 4.2 Hz, 1H), 2.15 – 2.10 (m, 1H), 2.03 (dd, J = 10.1, 4.9 Hz, 1H), 1.98 (d, J = 7.0 Hz, 1H), 1.92 (s, 40H), 1.66 (s, 1H).

MS (APCI) = 400.5 m/z calculated for C₂₄H₂₁FN₄O; experimental 401.0.

HRMS (ESI) = 400.4574 calculated; found 401.1777

3-(3-(but-3-yn-1-yl)-3H-diazirin-3-yl)-N-(4-methyl-3-(4-methylquinolin-3-yl)phenyl)propanamide, 135



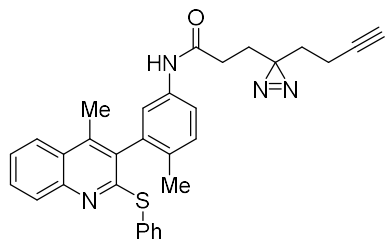
Following the general procedure: 4-methyl-3-(4-methylquinolin-3-yl)aniline (72 mg, 0.29 mmol, 1.0 equiv), 3-(3-(but-3-yn-1-yl)-3H-diazirin-3-yl)propanoic acid (54.8 mg, 0.33 mmol, 1.15 equiv), HATU (137.6 mg, 0.3623 mmol, 1.25 equiv), DIPEA (278 μ L, 1.16 mmol, 4.0 equiv), and 966 μ L DMF were added to a 2 dram vial equipped with a stir bar. The reaction conditions, workup procedure, and purification were conducted according to the general procedure to afford **135** as a beige solid (86.3 mg, 75%).

$^1\text{H NMR}$ (400 MHz, CDCl_3) δ (ppm) = 8.63 (s, 1H), 8.39 (s, 1H), 8.15 (s, 1H), 7.87 (s, 1H), 7.76 – 7.72 (m, 1H), 7.60 (s, 1H), 7.39 (s, 1H), 7.27 (d, $J = 1.7$ Hz, 1H), 2.57 (s, 1H), 2.19 (s, 1H), 2.03 (s, 1H), 1.94 (s, 1H), 1.68 (d, $J = 7.2$ Hz, 1H), 1.27 (s, 1H), 0.89 (s, 1H).

$\text{MS (APCI)} = 396.2$ m/z calculated for $\text{C}_{25}\text{H}_{24}\text{N}_4\text{O}$; experimental 397.0.

$\text{HRMS (ESI)} = 396.4940$ calculated; found 397.2025

3-(3-(but-3-yn-1-yl)-3H-diazirin-3-yl)-N-(4-methyl-3-(4-methyl-2-(phenylthio)quinolin-3-yl)phenyl)propanamide, 136



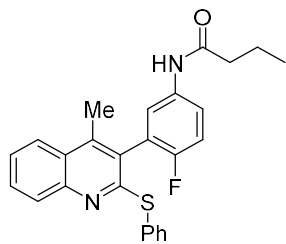
Following the general procedure: 4-methyl-3-(4-methyl-2-(phenylthio)quinolin-3-yl)aniline (38 mg, 0.106 mmol, 1.0 equiv), 3-(3-(but-3-yn-1-yl)-3H-diazirin-3-yl)propanoic acid (20.4 mg, 0.1228 mmol, 1.15 equiv), HATU (50.4 mg, 0.1325 mmol, 1.25 equiv), DIPEA (74 μ L, 0.424 mmol, 4.0 equiv), and 353 μ L DMF were added to a 2 dram vial

equipped with a stir bar. The reaction conditions, workup procedure, and purification were conducted according to the general procedure to afford **136** as a white solid (43.4 mg, 81%).

MS (APCI) = 504.7 m/z calculated for C₃₁H₂₈N₄OS; experimental 397.0.

HRMS (ESI) = 504.6520 calculated; found 505.2062

***N*-(4-fluoro-3-(4-methyl-2-(phenylthio)quinolin-3-yl)phenyl)butyramide**



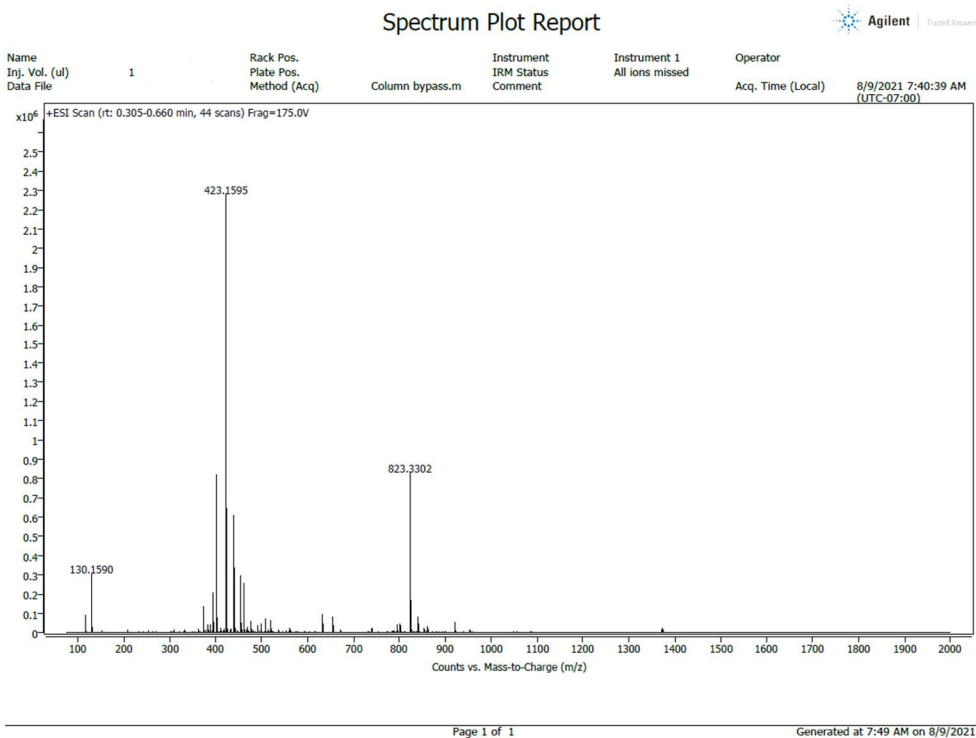
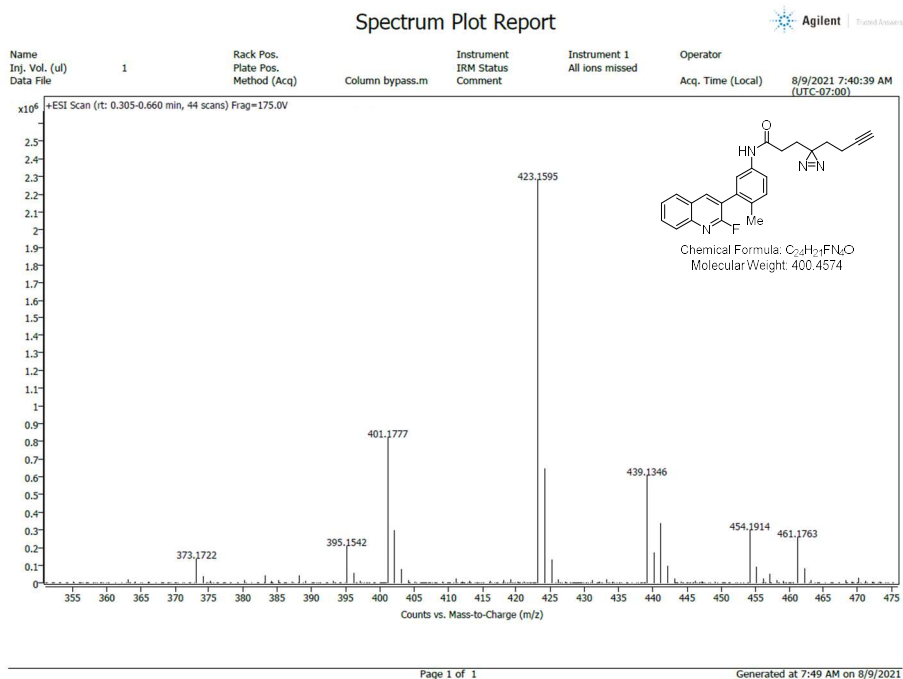
Following the general procedure: 4-fluoro-3-(4-methyl-2-(phenylthio)quinolin-3-yl)aniline (16.4 mg, 0.0457 mmol, 1.0 equiv), butyryl chloride (5.57 μ L, 0.0526 mmol, 1.15 equiv), HATU (21.7 mg, 0.0572 mmol, 1.25 equiv), DIPEA (32 μ L, 0.1828 mmol, 4.0 equiv), and

152 μ L DMF were added to a 2 dram vial equipped with a stir bar. The reaction conditions, workup procedure, and purification were conducted according to the general procedure to afford product as a white solid (15 mg, 84%).

MS (APCI) = 430.5 m/z calculated for C₂₆H₂₃FN₂OS; experimental 430.1.

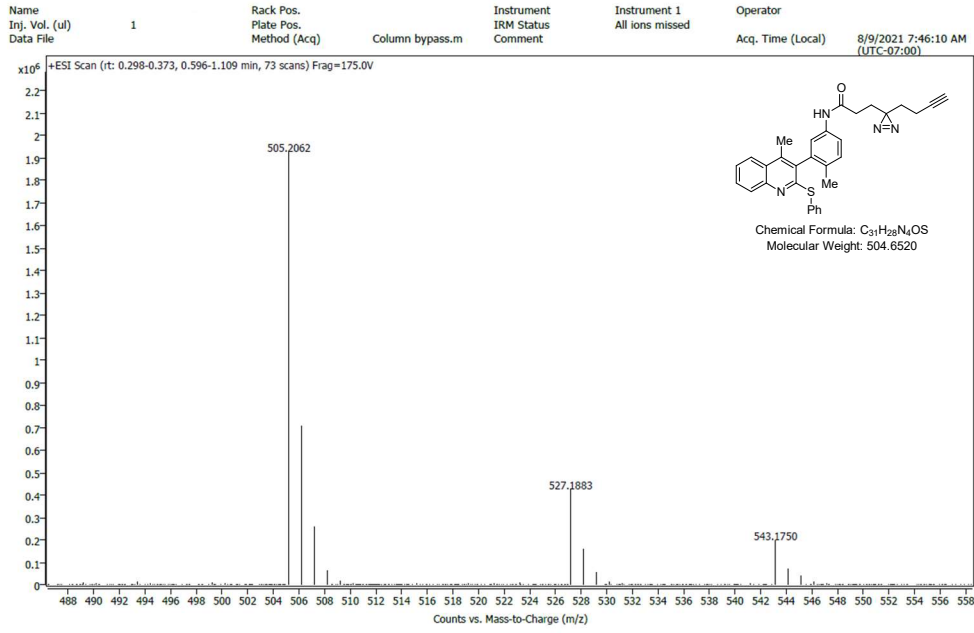
3.3.8 Sample Mass Spectrometry of Atropoprobes

HRMS of Compound 134 (major ion is [M+Na])

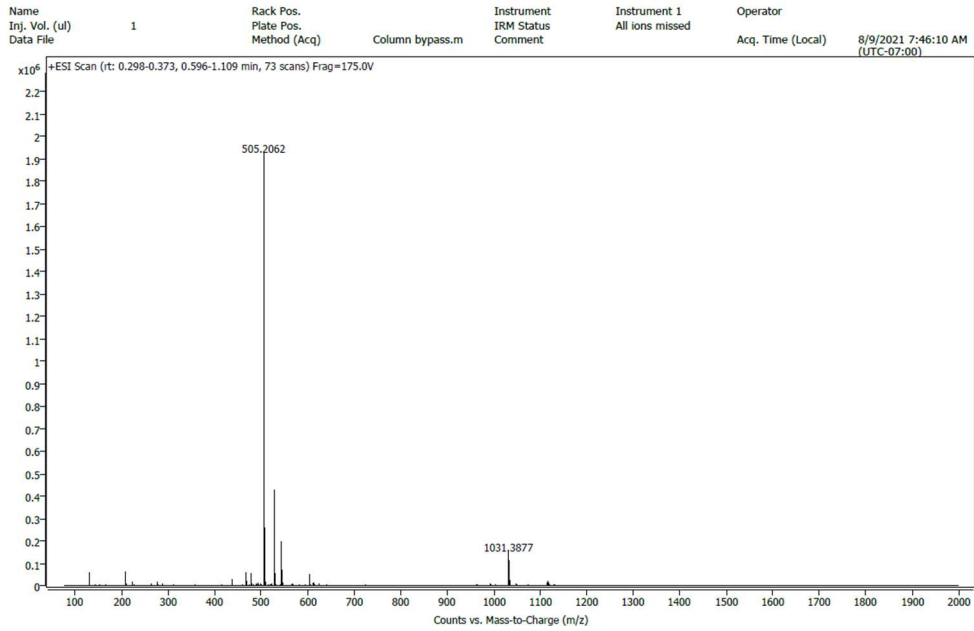


HRMS of Compound 136

Spectrum Plot Report



Spectrum Plot Report



Acknowledgements

Chapter 3 in full is an ongoing project and the manuscript is still in progress. The work that appears in this thesis dissertation was completed before June 2021. The dissertation author is one of the primary investigators, and this work will likely be pivoted in another direction. The dissertation author was the primary researcher responsible for this early work.

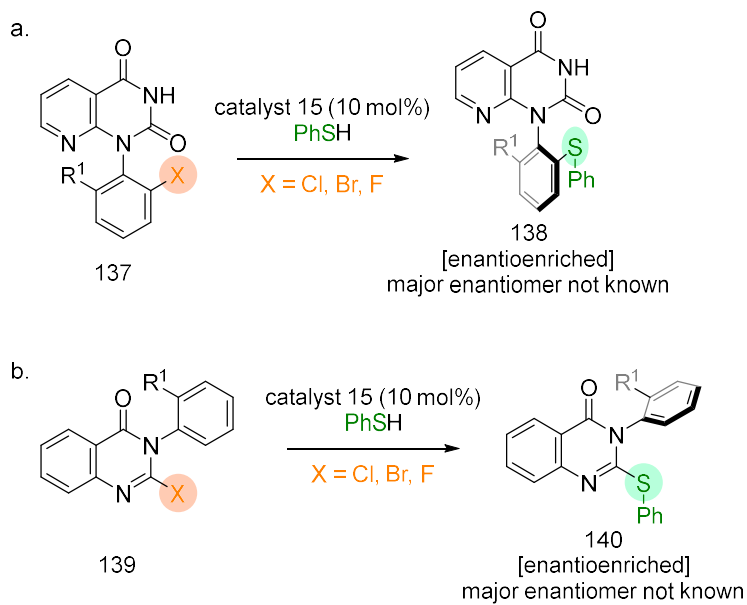
Chapter 4 FUTURE DIRECTIONS FOR NEW ATROPOSELECTIVE NUCLEOPHILIC SUBSTITUTIONS

Copyright

Chapter 4 is a compilation of material that may be utilized in future publications. The following are co-authors for these projects: Cardenas, M. M.; Gustafson, J. L. The dissertation author was a supplemental researcher and coauthor for the data presented for future manuscripts. Support of this work by the National Science Foundation (CHE-1664565) and the National Institute of General Medical Science (R35GM124637) are acknowledged.

4.1 Background Information

We have shown that atroposelective S_NAr is a suitable synthetic method to obtain pharmaceutically relevant pyrrolopyrimidines and quinolines. I am excited to see the implications of this S_NAr approach in the Gustafson group, and hope that it will springboard its applications towards other classes of heteroarene pharmaceuticals. Early results are finding that atroposelective S_NAr of thiophenol to synthesize pharmaceutically relevant scaffolds as the quinoxalines and quinoxalinones (inspired from the KRAS inhibitors of Amgen's Sotorasib²³ and Mirati Therapeutics' MRTX1719)²² are possible. Preliminary results using the optimized chiral catalyst 15 from the PPY work leads to respective enantioselectivity of *s*-factor at 6.

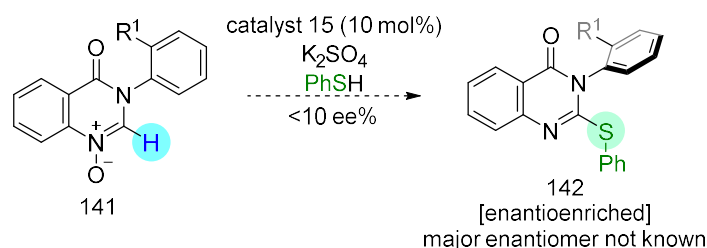


Equation 55. S_NAr of atroposelective pharmaceutically relevant scaffolds. a. Synthesis of Enantioenriched Scaffold derived from Sotorasib. b. Synthesis of scaffold derived from MRTX1719.

S_NAr is extremely useful as late-stage functionalization of medicinally relevant sulfides, methoxy- or hydroxy-groups and most importantly amines. However, we have found specific alkyl-groups can impart drastically increased potency (Figure 8, the C-2 methylated position led to an extremely potent inhibitor of BRK). In these instances, S_NAr has not been an amenable strategy to access alkylated, (e.g., methyl-groups, etc.) bioactive heterocycles. It was challenging to retain enantioselectivity whilst reducing the size of the smallest possible leaving group for atroposelective S_NAr to still proceed through some degree of dynamic kinetic resolution. As a result the conversion limitation of a classical kinetic resolution persists across these projects. Particularly, we have seen from atroposelective S_NAr towards 3-arylquinolines where the background kinetic resolution can noticeably affect enantioselectivity at the 50% conversion limit.

4.1 Preliminary Results: Vicarious Nucleophilic Substitution

While there are not many leaving groups that are smaller than fluorine, there are specific nucleophilic reactions to pursue a mechanism where a reactive, aromatic “proton” is replaced. If we presumed that a majority of S_NAr effort would lead to KR, perhaps reactions such as atroposelective Vicarious Nucleophilic Substitutions (VNS) on these scaffolds would be facilitated through only DKR. In VNS, a hydrogen atom is replaced by the nucleophile. My colleagues in my tenure have previously developed successful atroposelective VNS via the addition of thiophenols or nitroalkanes into naphthoquinones.

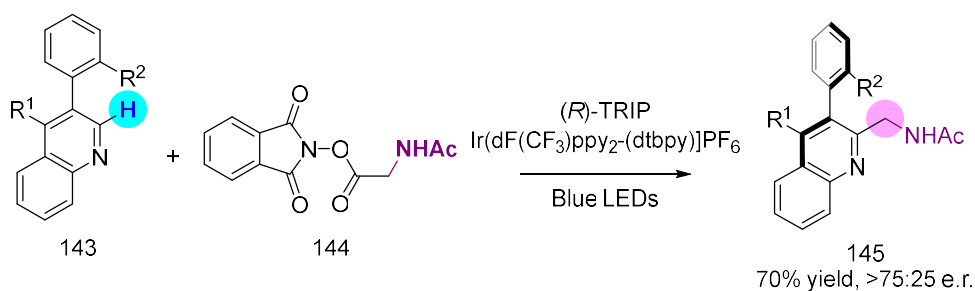


Equation 56. General synthetic scheme of atroposelective S_NAr of Quinazolinones

To address this, we attempted an atroposelective VNS of thiophenols into heterocyclic *N*-oxides of 3-arylquinolines (Equation 56). Unfortunately, a lot of this effort overlapped with the S_NAr projects and were unable to be completed. In addition, chiral catalyst-controlled VNS is very challenging, since the starting materials are much more activated and the quinoline is more reactive. As a result, early optimization has exclusively led to reactions where products are less than 10 ee%. Most of this ongoing effort will take place in future works from the Gustafson group. However, these preliminary results demonstrate that the S_NAr and VNS projects will be significant as they will allow for facile and flexible access to privileged atropisomeric scaffolds with the potential to expedite medicinal chemistry efforts.

4.2 Preliminary Results: Minisci Chemistry

Within this last decade, the ‘state of the art’ C-H functionalization¹²² of pharmaceutically relevant heteroarenes used widely in industry involves ‘nucleophilic’ radicals, in what is typically referred as Minisci chemistry.¹²³ Seminal work from Baran,^{124,125} Molander,¹²⁶ DiRocco,¹²⁷ and MacMillan¹²⁸ have all employed variants of Minisci chemistry on medically relevant heteroarenes. However, regiochemistry is still largely an unsolved problem, more specifically with pyridines and quinolines that have multiple reactive sites. Depending on the reaction conditions, the regioisomeric mixtures can become extremely varied. In acidic conditions, the regiochemistry can be controlled for the C-2 position of pyridines and quinolines. However, there is currently no precedence to obtain selectivity for the C-3 or C-4 positions. Furthermore, many pharmaceutically relevant scaffolds can have multiple heteroarenes that are reactive towards Minisci chemistry, which can lead to more regio- and chemoselectivity issues. Though these are concerning issues, the vast undertaking of diverse functionalization is extremely valuable since a larger ‘chemical space’ can be investigated in the iterative SAR and ADMET cycles during the preliminary stages of drug discovery.



Equation 57. General synthetic scheme of atroposelective Minisci on 3-arylquinolines

We are very interested in tackling the problem of regioselectivity, however are more agnostic with respect to the mode of catalysis needed to accomplish this. Phipps and coworkers¹²⁹

have recently shown that enantioselective Minisci reactions can be achieved using chiral phosphoric acids assuming that the radical possesses a N-H bonding handle. Jiang and coworkers¹³⁰ also showed they could perform similar enantioselective photoredox-catalyzed Minisci chemistry to obtain isoquinolines. Inspired by these studies, we hypothesized that H-bonding of chiral Brønsted-acid catalysts^{101,131–133} (e.g. phosphoric acids, etc.) can influence the regioselectivity and atroposelectivity of Minisci chemistry in biarylated pyridine and quinolines (Equation 57). While I will not be able to pursue this project also, I was delighted to find preliminary results that demonstrated that this was indeed possible. I am excited and hope these results inspire others in the group to pursue a catalyst-controlled regioselective Minisci chemistry for alkylation in other pharmaceutically relevant heteroarenes.

Acknowledgements

Chapter 4 in full, is an ongoing project and the manuscript is still in progress. The work that appears in this thesis dissertation was completed before June 2021. Authors on this project were set to be Zanolini, Ryan; Basilaia, Mariam; Cardenas, Mariel M.; Gustafson, Jeffrey L. The dissertation author was one of the primary investigators for the manuscript in progress.

REFERENCES

- (1) Clayden, J.; Moran, W. J.; Edwards, P. J.; LaPlante, S. R. The Challenge of Atropisomerism in Drug Discovery. *Angew. Chem. Int. Ed.* **2009**, *48* (35), 6398–6401.
- (2) Toenjes, S. T.; Gustafson, J. L. Atropisomerism in Medicinal Chemistry: Challenges and Opportunities. *Future Med. Chem.* **2018**, *10* (4), 409–422.
- (3) Dinh, A.; Gustafson, J. L. A Catalytic Cycle of Discovery: Asymmetric Catalysis Gives Rise to New Chiral Catalyst Scaffolds. *Chem. Elsevier Inc.* **2020**, 810–812.
- (4) Toenjes, S. T.; Basilaia, M.; Gustafson, J. L. Leveraging Conformational Control about a Potential Atropisomeric Axis as a Strategy in Medical Chemistry. *Future Med. Chem.* **2021**, 443–446.
- (5) Leroux, F. Atropisomerism, Biphenyls, and Fluorine: A Comparison of Rotational Barriers and Twist Angles. *ChemBioChem* **2004**, *5* (5), 644–649.
- (6) Alkorta, I.; Elguero, J.; Roussel, C.; Vanthuyne, N.; Piras, P. Atropisomerism and Axial Chirality in Heteroaromatic Compounds. *Ad. Het. Chem.* **2012**, *105*, 309-351.
- (7) Cardenas, M. M.; Nguyen, A. D.; Brown, Z. E.; Heydari, B. S.; Heydari, B. S.; Vaidya, S. D.; Gustafson, J. L. Atropisomerism as Inspiration for New Chemistry. *Arkivoc* **2021**, *2021*, 20–47.
- (8) Cardenas, M. M.; Saputra, M. A.; Sanchez, A. N.; Valle, E.; Robinson, C. J.; Gustafson, J. L. *Developing Atroposelective Syntheses to Access Pharmaceutically Relevant Compounds*. Poster Presentations.
- (9) Cardenas, M. M.; Toenjes, S. T.; Nalbandian, C. J.; Gustafson, J. L. Enantioselective Synthesis of Pyrrolopyrimidine Scaffolds through Cation-Directed Nucleophilic Aromatic Substitution. *Org. Lett.* **2018**, *20* (7), 2037–2041.
- (10) Cardenas, M. M.; Saputra, M. A.; Gordon, D. A.; Sanchez, A. N.; Yamamoto, N.; Gustafson, J. L. Catalytic Atroposelective Dynamic Kinetic Resolutions and Kinetic Resolutions towards 3-Arylquinolines via S_NAr. *Chem. Comm.* **2021**, *57* (78), 10087–10090.
- (11) Donovan, K. A.; An, J.; Nowak, R. P.; Yuan, J. C.; Fink, E. C.; Berry, B. C.; Ebert, B. L.; Fischer, E. S. Thalidomide Promotes Degradation of SALL4, a Transcription Factor Implicated in Duane Radial Ray Syndrome. *eLife Digest*.
- (12) Lenza, W.; Pfeiffer, R. A.; Kosenow, W.; Hayman, D. J. THALIDOMIDE AND CONGENITAL ABNORMALITIES. *The Lancet* **1962**, *269* (7219), 45–46.

- (13) Hirsch, D. R.; Metrano, A. J.; Stone, E. A.; Storch, G.; Miller, S. J.; Murelli, R. P. Troponoid Atropisomerism: Studies on the Configurational Stability of Tropone-Amide Chiral Axes. *Org. Lett.* **2019**, *21* (7), 2412–2415.
- (14) Beutner, G.; Carrasquillo, R.; Geng, P.; Hsiao, Y.; Huang, E. C.; Janey, J.; Katipally, K.; Kolotuchin, S.; La Porte, T.; Lee, A.; Lobben, P.; Lora-Gonzalez, F.; Mack, B.; Mudryk, B.; Qiu, Y.; Qian, X.; Ramirez, A.; Razler, T. M.; Rosner, T.; Shi, Z.; Simmons, E.; Stevens, J.; Wang, J.; Wei, C.; Wisniewski, S. R.; Zhu, Y. Adventures in Atropisomerism: Total Synthesis of a Complex Active Pharmaceutical Ingredient with Two Chirality Axes. *Org. Lett.* **2018**, *20* (13), 3736–3740.
- (15) Takahashi, H.; Wakamatsu, S.; Tabata, H.; Oshitari, T.; Harada, A.; Inoue, K.; Natsugari, H. Atropisomerism Observed in Indometacin Derivatives. *Org. Lett.* **2011**, *13* (4), 760–763.
- (16) Brunel, J. M. BINOL: A Versatile Chiral Reagent. *Chem Rev* **2005**, *105* (3), 857–897.
- (17) Chen, Y.; Yekta, S.; Yudin, A. K. Modified BINOL Ligands in Asymmetric Catalysis. *Chem. Rev.* **2003**, *103* (8), 3155–3211.
- (18) Jones, B. A.; Balan, T.; Jolliffe, J. D.; Campbell, C. D.; Smith, M. D. Practical and Scalable Kinetic Resolution of BINOLs Mediated by a Chiral Counterion. *Angew. Chem. Int. Ed.* **2019**, *131* (14), 4644–4648.
- (19) Jones, B. A.; Balan, T.; Jolliffe, J. D.; Campbell, C. D.; Smith, M. D. Practical and Scalable Kinetic Resolution of BINOLs Mediated by a Chiral Counterion. *Angew. Chem. Int. Ed.* **2019**, *58* (14), 4596–4600.
- (20) LaPlante, S. R.; Edwards, P. J.; Fader, L. D.; Jakalian, A.; Hucke, O. Revealing Atropisomer Axial Chirality in Drug Discovery. *ChemMedChem* **2011**, *6* (3), 505–513.
- (21) Wang, J.; Zeng, W.; Li, S.; Shen, L.; Gu, Z.; Zhang, Y.; Li, J.; Chen, S.; Jia, X. Discovery and Assessment of Atropisomers of (±)-Lesinurad. *ACS Med. Chem. Lett.* **2017**, *8* (3), 299–303.
- (22) Smith, C. R.; Aranda, R.; Bobinski, T. P.; Briere, D. M.; Burns, A. C.; Christensen, J. G.; Clarine, J.; Engstrom, L. D.; Gunn, R. J.; Ivetac, A.; Jean-Baptiste, R.; Ketcham, J. M.; Kobayashi, M.; Kuehler, J.; Kulyk, S.; Lawson, J. D.; Moya, K.; Olson, P.; Rahbaek, L.; Thomas, N. C.; Wang, X.; Waters, L. M.; Marx, M. A. Fragment-Based Discovery of MRTX1719, a Synthetic Lethal Inhibitor of the PRMT5•MTA Complex for the Treatment of MTAP-Deleted Cancers. *J. Med. Chem.* **2022**, *65* (3), 1749–1766.
- (23) Halford, B. Amgen Unveils Its KRas Inhibitor in Human Clinical Trials. *Drug Discovery* **2019**, 12–14.
- (24) Fleeman, N.; Houten, R.; Chaplin, M.; Beale, S.; Boland, A.; Dundar, Y.; Greenhalgh, J.; Duarte, R.; Shenoy, A. A Systematic Review of Lenvatinib and Sorafenib for Treating

- Progressive, Locally Advanced or Metastatic, Differentiated Thyroid Cancer after Treatment with Radioactive Iodine. *BMC Cancer* **2019**, *19* (1209), 1-16.
- (25) Das, P.; Delost, M. D.; Qureshi, M. H.; Smith, D. T.; Njardarson, J. T. A Survey of the Structures of US FDA Approved Combination Drugs. *J. Med. Chem.* **2019**, 4265–4311.
- (26) Lopez, M. S.; Choy, J. W.; Peters, U.; Sos, M. L.; Morgan, D. O.; Shokat, K. M. Staurosporine-Derived Inhibitors Broaden the Scope of Analog-Sensitive Kinase Technology. *J. Am. Chem. Soc.* **2013**, *135* (48), 18153–18159.
- (27) Vallee, F., Dupuy, A. RCSB PDB - 5LQ9 CRYSTAL STRUCTURE OF HSP90 IN COMPLEX WITH SAR200323. **2017**.
- (28) Biswal, B. K.; Morisseau, C.; Garen, G.; Cherney, M. M.; Garen, C.; Niu, C.; Hammock, B. D.; James, M. N. G. The Molecular Structure of Epoxide Hydrolase B from Mycobacterium Tuberculosis and Its Complex with a Urea-Based Inhibitor. *J. Mol. Biol.* **2008**, *381*, 897–912.
- (29) Vitaku, E.; Smith, D. T.; Njardarson, J. T. Analysis of the Structural Diversity, Substitution Patterns, and Frequency of Nitrogen Heterocycles among U.S. FDA Approved Pharmaceuticals. *J. Med. Chem.* **2014**, *57* (24), 10257–10274.
- (30) Wu, P.; Nielsen, T. E.; Clausen, M. H. FDA-Approved Small-Molecule Kinase Inhibitors. *Trends in Pharmacological Sciences.* **2015**, 422–439.
- (31) Toenjes, S. T.; Basilaia, M.; Gustafson, J. L. Leveraging Conformational Control about a Potential Atropisomeric Axis as a Strategy in Medical Chemistry. *Future Med. Chem.* **2021**, *13* (5), 443–446.
- (32) Bott, G.; Field, L. D.; Sternhell, S. Steric Effects. A Study of a Rationally Designed System. *J. Am. Chem. Soc.* **1980**, *102* (17), 5618–5626.
- (33) Smith, D. E.; Marquez, I.; Lokensgard, M. E.; Rheingold, A. L.; Hecht, D. A.; Gustafson, J. L. Exploiting Atropisomerism to Increase the Target Selectivity of Kinase Inhibitors. *Angew. Chem. Int. Ed.* **2015**, *127* (40), 11920–11925.
- (34) Carlomagno, F.; Vitagliano, D.; Guida, T.; Napolitano, M.; Vecchio, G.; Fusco, A.; Gazit, A.; Levitzki, A.; Santoro, M. The Kinase Inhibitor PP1 Blocks Tumorigenesis Induced by RET Oncogenes. *Cancer Res* **2002**.
- (35) Piotrowska, Z.; Isozaki, H.; Lennerz, J. K.; Gainor, J. F.; Lennes, I. T.; Zhu, V. W.; Marcoux, N.; Banwait, M. K.; Digumarthy, S. R.; Su, W.; Yoda, S.; Riley, A. K.; Nangia, V.; Lin, J. J.; Nagy, R. J.; Lanman, R. B.; Dias-Santagata, D.; Mino-Kenudson, M.; Iafrate, A. J.; Heist, R. S.; Shaw, A. T.; Evans, E. K.; Clifford, C.; Ou, S. H. I.; Wolf, B.; Hata, A. N.; Sequist, L. V. Landscape of Acquired Resistance to Osimertinib in EGFR-Mutant

- NSCLC and Clinical Validation of Combined EGFR and RET Inhibition with Osimertinib and BLU-667 for Acquired RET Fusion. *Cancer Discov.* **2018**, *8* (12), 1529–1539.
- (36) Plaza-Menacho, I.; Barnouin, K.; Goodman, K.; Martínez-Torres, R. J.; Borg, A.; Murray-Rust, J.; Mouilleron, S.; Knowles, P.; McDonald, N. Q. Oncogenic RET Kinase Domain Mutations Perturb the Autophosphorylation Trajectory by Enhancing Substrate Presentation in Trans. *Mol. Cell* **2014**, *53*, 738–751.
- (37) Toenjes, S. T.; Garcia, V.; Maddox, S. M.; Dawson, G. A.; Ortiz, M. A.; Piedrafita, F. J.; Gustafson, J. L. Leveraging Atropisomerism to Obtain a Selective Inhibitor of RET Kinase with Secondary Activities toward EGFR Mutants. *ACS Chem. Biol.* **2019**, *14* (9), 1930–1939.
- (38) Espinosa, A. V.; Gilbert, J.; Fagin, J. RET M918T Mutations in Thyroid Cancer. *My Cancer Genome* **2017**, 1–2.
- (39) Jhiang, S. M. The RET Proto-Oncogene in Human Cancers. *Oncogene* **2000**, 5590–5597.
- (40) Plaza-Menacho, I.; Mologni, L.; Sala, E.; Gambacorti-Passerini, C.; Magee, A. I.; Links, T. P.; Hofstra, R. M. W.; Barford, D.; Isacke, C. M. Sorafenib Functions to Potently Suppress RET Tyrosine Kinase Activity by Direct Enzymatic Inhibition and Promoting RET Lysosomal Degradation Independent of Proteasomal Targeting. *J. Biol. Chem.* **2007**, *282*(40), 29230–29240.
- (41) Eng, C.; Clayton, D.; Schuffenecker, I.; Lenoir, G.; Cote, G.; Gagel, R. F.; Ploos Van Amstel, H. K.; Lips, C. J. M.; Nishisho, I.; Takai, S. I.; Marsh, D. J.; Robinson, B. G.; Frank-Raue, K.; Raue, F.; Xue, F.; Noll, W. W.; Romei, C.; Pacini, F.; Fink, M.; Niederle, B.; Zedenius, J.; Nordenskjöld, M.; Komminoth, P.; Hendy, G. N.; Gharib, H.; Thibodeau, S. N.; Lacroix, A.; Frilling, A.; Ponder, B. A. J.; Mulligan, L. M. The Relationship between Specific Ret Proto-Oncogene Mutations and Disease Phenotype in Multiple Endocrine Neoplasia Type 2: International RET Mutation Consortium Analysis. *J. Am. Med. Assoc.* **1996**, *276* (19), 1575–1579.
- (42) Knowles, P. P.; Murray-Rust, J.; Kjær, S.; Scott, R. P.; Hanrahan, S.; Santoro, M.; Ibáñez, C. F.; McDonald, N. Q. Structure and Chemical Inhibition of the RET Tyrosine Kinase Domain. *J. Biol. Chem.* **2006**, *281* (44), 33577–33587.
- (43) Chen, H.; Ma, J.; Li, W.; Eliseenkova, A. V.; Xu, C.; Neubert, T. A.; Miller, W. T.; Mohammadi, M. A Molecular Brake in the Kinase Hinge Region Regulates the Activity of Receptor Tyrosine Kinases. *Mol. Cell* **2007**, *27*, 717–730.
- (44) Schindler, T.; Bornmann, W.; Pellicena, P.; Miller, W. T.; Clarkson, B.; Kuriyan, J. Structural Mechanism for STI-571 Inhibition of Abelson Tyrosine Kinase. *Science* **2000**, *289* (5486), 1938–1942.

- (45) Hsu, K.-C.; Sung, T.-Y.; Lin, C.-T.; Chiu, Y.-Y.; Hsu, J. T.-A.; Hung, H.-C.; Sun, C.-M.; Barve, I.; Chen, W.-L.; Huang, W.-C.; Huang, C.-T.; Chen, C.-H.; Yang, J.-M. Anchor-Based Classification and Type-C Inhibitors for Tyrosine Kinases. *Scientific Reports* **2015**, *5* (10938), 1-14.
- (46) Manley, P. W.; Drueckes, P.; Fendrich, G.; Furet, P.; Liebetanz, J.; Martiny-Baron, G.; Mestan, J.; Trappe, J.; Wartmann, M.; Fabbro, D. Extended Kinase Profile and Properties of the Protein Kinase Inhibitor Nilotinib. *Biochim. Biophys. Acta. Proteins Proteom.* **2010**, *1804* (3), 445–453.
- (47) Palmieri, L.; Rastelli, G. Alpha-C Helix Displacement As a General Approach for Allosteric Modulation of Protein Kinases. *Drug Discov. Today* **2013**, *18* (7–8), 407–414.
- (48) Opencourseware, M.I.T. Kinase Domains: Structure and Inhibition. **2009**.
- (49) Kalaivani, R.; Srinivasan, N. A Gaussian Network Model Study Suggests That Structural Fluctuations Are Higher for Inactive States than Active States of Protein Kinases. *Mol. BioSyst.* **2015**, *11* (11), 1079–1095.
- (50) Manoharan, G. B.; Enkvist, E.; Kasari, M.; Viht, K.; Zenn, M.; Prinz, A.; Filhol, O.; Herberg, F. W.; Uri, A. FRET-Based Screening Assay Using Small-Molecule Photoluminescent Probes in Lysate of Cells Overexpressing RFP-Fused Protein Kinases. *Anal. Biochem.* **2015**, *481*, 10–17.
- (51) Levinson, N. M.; Boxer, S. G. Structural and Spectroscopic Analysis of the Kinase Inhibitor Bosutinib and an Isomer of Bosutinib Binding to the Abl Tyrosine Kinase Domain. *PLoS One* **2012**, *7* (4). e29828–e29828.
- (52) Lovering, F.; McDonald, J.; Whitlock, G. A.; Glossop, P. A.; Phillips, C.; Bent, A.; Sabnis, Y.; Ryan, M.; Fitz, L.; Lee, J.; Chang, J. S.; Han, S.; Kurumbail, R.; Thorarensen, A. Identification of Type-II Inhibitors Using Kinase Structures. *Chem. Biol. Drug. Des.* **2012**, 1–8.
- (53) Müller, S.; Chaikuad, A.; Gray, N. S.; Knapp, S. The Ins and Outs of Selective Kinase Inhibitor Development. *Nat. Chem. Biol.* **2015**, *11*, 818–821.
- (54) Nagar, B.; Hantschel, O.; Young, M. A.; Scheffzek, K.; Veach, D.; Bornmann, W.; Clarkson, B.; Superti-Furga, G.; Kuriyan, J. Structural Basis for the Autoinhibition of C-Abl Tyrosine Kinase. *Cell* **2003**, *112* (6), 859–871.
- (55) Johnson, T. K.; Soellner, M. B. Bivalent Inhibitors of C-Src Tyrosine Kinase That Bind a Regulatory Domain. *Bioconjug. Chem.* **2016**, *27* (7), 1745–1749.
- (56) Jiang, J.; Gui, F.; He, Z.; Li, L.; Li, Y.; Li, S.; Wu, X.; Deng, Z.; Sun, X.; Huang, X.; Huang, W.; Han, S.; Zhang, T.; Wang, Z.; Jiao, B.; Song, S.; Wang, H.; Chen, L.; Zhou, D.; Liu, Q.; Ren, R.; Zhang, J.; Deng, X. Targeting BRK-Positive Breast Cancers with Small-Molecule Kinase Inhibitors. *Cancer Res.* **2017**, *77* (1), 175–186.

- (57) Patel, L.; Chandrasekhar, J.; Evarts, J.; Forseth, K.; Haran, A. C.; Ip, C.; Kashishian, A.; Kim, M.; Koditek, D.; Koppenol, S.; Lad, L.; Lepist, E. I.; McGrath, M. E.; Perreault, S.; Puri, K. D.; Villaseñor, A. G.; Somoza, J. R.; Steiner, B. H.; Therrien, J.; Treiberg, J.; Phillips, G. Discovery of Orally Efficacious Phosphoinositide 3-Kinase δ Inhibitors with Improved Metabolic Stability. *J. Med. Chem.* **2016**, *59* (19), 9228–9242.
- (58) Steen, E.; Basilaia, M.; Kim, W.; Getz, T.; Gustafson, J. L.; Zage, P. E. Targeting the RET Tyrosine Kinase in Neuroblastoma: A Review and Application of a Novel Selective Drug Design Strategy. *Biochemical Pharmacology. Elsevier Inc.* **2023**, *216* (115751), 1–17.
- (59) Saputra, M. A.; Cardenas, M. M.; Gustafson, J. L. Asymmetric Synthesis of Nonbiaryl Atropisomers. *Wiley-VCH GmbH*, **2021**, 109-140.
- (60) Jolliffe, J. D.; Armstrong, R. J.; Smith, M. D. Catalytic Enantioselective Synthesis of Atropisomeric Biaryls by a Cation-Directed O-Alkylation. *Nat. Chem.* **2017**, *9*, 558.
- (61) Armstrong, R. J.; Smith, M. D. Catalytic Enantioselective Synthesis of Atropisomeric Biaryls: A Cation-Directed Nucleophilic Aromatic Substitution Reaction. *Angew. Chem. Int. Ed.* **2014**, *53*, 12822–12826.
- (62) Blackmond, D. G. Kinetic Resolution Using Enantioimpure Catalysts: Mechanistic Considerations of Complex Rate Laws. *J. Am. Chem. Soc.* **2001**, *123* (4), 545–553.
- (63) Johnson, D. W.; Singleton, D. A. Nonlinear Effects in Kinetic Resolutions. *J. Am. Chem. Soc.* **1999**, *121* (40), 9307–9312.
- (64) Goodman, J. M.; Köhler, A. K.; Alderton, S. C. M. Interactive Analysis of Selectivity in Kinetic Resolutions. *Tetrahedron Lett.* **1999**, *40* (49), 8715–8718.
- (65) Kagan, H. B.; Fiaud, J. C. Kinetic Resolution. In *Topics in Stereochemistry*; New York: John Wiley and Sons, Inc. **1988**, *18*, 249–340.
- (66) Rios, R.; Jimeno, C.; Carroll, P. J.; Walsh, P. J. Kinetic Resolution of Atropisomeric Amides. *J. Am. Chem. Soc.* **2002**, *124* (35), 10272–10273.
- (67) Keith, J. M.; Larrow, J. F.; Jacobsen, E. N. Practical Considerations in Kinetic Resolution Reactions. *Adv. Synth. Catal.* **2001**, *343*, 5–26.
- (68) Blackmond, D. G. Kinetic Resolution Using Enantioimpure Catalysts: Mechanistic Considerations of Complex Rate Laws. *J. Am. Chem. Soc.* **2001**, *123* (4), 545–553.
- (69) Abula, A.; Xu, Z.; Zhu, Z.; Peng, C.; Chen, Z.; Zhu, W.; Aisa, H. A. Substitution Effect of the Trifluoromethyl Group on the Bioactivity in Medicinal Chemistry: Statistical Analysis and Energy Calculations. *J. Chem. Inf. Model* **2020**, *60* (12), 6242–6250.

- (70) Yale, H. L. The Trifluoromethyl Group in Medicinal Chemistry. *J. Med. Pharma. Chem.* **1959**, *1* (2), 121–133.
- (71) Yoon, T. P.; Jacobsen, E. N. Privileged Chiral Catalysts. *Science (1979)* **2003**, *299* (5613), 1691–1693.
- (72) Kagan, H. B.; Fiaud, J. C. “Kinetic Resolution” in Topics in Stereochemistry. *Wiley-VCH*, **2007**, *18*, 249–330.
- (73) Maddox, S. M.; Nalbandian, C. J.; Smith, D. E.; Gustafson, J. L. A Practical Lewis Base Catalyzed Electrophilic Chlorination of Arenes and Heterocycles. *Org. Lett.* **2015**, *17* (4), 1042–1045.
- (74) Kalvet, I.; Magnin, G.; Schoenebeck, F. Rapid Room-Temperature, Chemoselective Csp²–Csp² Coupling of Poly(Pseudo)Halogenated Arenes Enabled by Palladium (I) Catalysis in Air. *Angew. Chem. Int. Ed.* **2017**, *56* (6), 1581–1585.
- (75) Bruno, N. C.; Tudge, M. T.; Buchwald, S. L. Design and Preparation of New Palladium Precatalysts for C–C and C–N Cross-Coupling Reactions. *Chem. Sci.* **2013**, *4* (3), 916–920.
- (76) Organ, M. G.; Abdel-Hadi, M.; Avola, S.; Dubovyk, I.; Hadei, N.; Kantchev, E. A. B.; O’Brien, C. J.; Sayah, M.; Valente, C. Pd-Catalyzed Aryl Amination Mediated by Well Defined, N-Heterocyclic Carbene (NHC)-Pd Precatalysts, PEPPSI. *Chem. Eur. J.* **2008**, *14* (8), 2443–2452.
- (77) Zeng, H.; Belanger, D. B.; Curran, P. J.; Shipps, G. W.; Miao, H.; Bracken, J. B.; Arshad Siddiqui, M.; Malkowski, M.; Wang, Y. Discovery of Novel Imidazo[1,2-a]Pyrazin-8-Amines as Brk/PTK6 Inhibitors. *Bioorg. Med. Chem. Lett.* **2011**, *21* (19), 5870–5875.
- (78) Nakano, K.; Kitamura, M. Dynamic Kinetic Resolution (DKR) from Separation of Enantiomers: Synthetic Methods. *Wiley-VCH*, **2014**, 161–216.
- (79) Chan, V.; Kim, J. G.; Jimeno, C.; Carroll, P. J.; Walsh, P. J. Dynamic Kinetic Resolution of Atropisomeric Amides. *Org. Lett.* **2004**, *6* (12), 2051–2053.
- (80) Gustafson, J. L.; Lim, D.; Miller, S. J. Dynamic Kinetic Resolution of Biaryl Asymmetric Bromination. *Science* **2010**, *328* (4), 1251–1255.
- (81) Bhat, V.; Wang, S.; Stoltz, B. M.; Virgil, S. C. Asymmetric Synthesis of QUINAP via Dynamic Kinetic Resolution. *J. Am. Chem. Soc.* **2013**, *135* (45), 16829–16832.
- (82) Gustafson, J. L.; Lim, D.; Miller, S. J. Dynamic Kinetic Resolution of Biaryl Atropisomers via Peptide- Catalyzed Asymmetric Bromination. *Science* **2010**, *328* (5983), 1251–1255.

- (83) Fugard, A. J.; Lahdenperä, A. S. K.; Tan, J. S. J.; Mekareeya, A.; Paton, R. S.; Smith, M. D. Hydrogen-Bond-Enabled Dynamic Kinetic Resolution of Axially Chiral Amides Mediated by a Chiral Counterion. *Angew. Chem. Int. Ed.* **2019**, *131* (9), 2821–2824.
- (84) Staniland, S.; Adams, R. W.; McDouall, J. J. W.; Maffucci, I.; Contini, A.; Grainger, D. M.; Turner, N. J.; Clayden, J. Biocatalytic Dynamic Kinetic Resolution for the Synthesis of Atropisomeric Biaryl N-Oxide Lewis Base Catalysts. *Angew. Chem. Int. Ed.* **2016**, *128* (36), 10913–10917.
- (85) Dinh, A. N.; Noorbehesht, R. R.; Toenjes, S. T.; Jackson, A. C.; Saputra, M. A.; Maddox, S. M.; Gustafson, J. L. Catalytic Atroposelective Synthesis of Diaryl Ethers via C(Sp²)-H Alkylative Dynamic Kinetic Resolution. *Synlett* **2018**, *29* (16), 2155–2160.
- (86) Fugard, A. J.; Lahdenperä, A. S. K.; Tan, J. S. J.; Mekareeya, A.; Paton, R. S.; Smith, M. D. Hydrogen-Bond-Enabled Dynamic Kinetic Resolution of Axially Chiral Amides Mediated by a Chiral Counterion. *Angew. Chem. Int. Ed.* **2019**, *58* (9), 2795–2798.
- (87) Aly, R. M.; El-Motwally, A. M.; Al-Ansary, G. H. Quinoline-Based Small Molecules as Effective Protein Kinases Inhibitors. *J. Am. Sc.* **2016**, *12* (5), 10–32.
- (88) Cumming, J. N.; Smith, E. M.; Wang, L.; Misiaszek, J.; Durkin, J.; Pan, J.; Iserloh, U.; Wu, Y.; Zhu, Z.; Strickland, C.; Voigt, J.; Chen, X.; Kennedy, M. E.; Kuvelkar, R.; Hyde, L. A.; Cox, K.; Favreau, L.; Czarniecki, M. F.; Greenlee, W. J.; McKittrick, B. A.; Parker, E. M.; Stamford, A. W. Structure Based Design of Iminohydantoin BACE1 Inhibitors: Identification of an Orally Available, Centrally Active BACE1 Inhibitor. *Bioorg Med Chem Lett* **2012**, *22* (7), 2444–2449.
- (89) Brik, A.; Wong, C. HIV-1 Protease : Mechanism and Drug Discovery. *Org. Biomol. Chem.* **2003**, *3*, 5–14.
- (90) Ray, A. S.; Schinazi, R. F.; Murakami, E.; Basavapathruni, A.; Shi, J.; Zorca, S. M.; Chu, C. K.; Anderson, K. S. Probing the Mechanistic Consequences of 5-Fluorine Substitution on Cytidine Nucleotide Analogue Incorporation by HIV-1 Reverse Transcriptase. *Antivir. Chem Chemother.* **2003**, *14* (3), 115–125.
- (91) Zhang, H.; Hou, G.; Lu, M.; Ahn, J.; Byeon, I. J. L.; Langmead, C. J.; Perilla, J. R.; Hung, I.; Gor'Kov, P. L.; Gan, Z.; Brey, W. W.; Case, D. A.; Schulten, K.; Gronenborn, A. M.; Polenova, T. HIV-1 Capsid Function Is Regulated by Dynamics: Quantitative Atomic-Resolution Insights by Integrating Magic-Angle-Spinning NMR, QM/MM, and MD. *J. Am. Chem. Soc.* **2016**, *138* (42), 14066–14075.
- (92) Lemke, C. T.; Titolo, S.; von Schwedler, U.; Goudreau, N.; Mercier, J.-F.; Wardrop, E.; Faucher, A.-M.; Coulombe, R.; Banik, S. S. R.; Fader, L.; Gagnon, A.; Kawai, S. H.; Rancourt, J.; Tremblay, M.; Yoakim, C.; Simoneau, B.; Archambault, J.; Sundquist, W. I.; Mason, S. W. Distinct Effects of Two HIV-1 Capsid Assembly Inhibitor Families That Bind

- the Same Site within the N-Terminal Domain of the Viral CA Protein. *J. Virol.* **2012**, *86* (12), 6643–6655.
- (93) Lostes-Bardaji, M. J.; García-Illescas, D.; Valverde, C.; Serrano, C. Ripretinib in Gastrointestinal Stromal Tumor: The Long-Awaited Step Forward. *Ther. Adv. Med. Oncol.* **2021**, *13*, 1–12.
- (94) Hu, Y. L.; Wang, Z.; Yang, H.; Chen, J.; Wu, Z. B.; Lei, Y.; Zhou, L. Conversion of Two Stereocenters to One or Two Chiral Axes: Atroposelective Synthesis of 2,3-Diarylbenzoindoles. *Chem. Sci.* **2019**, *10* (28), 6777–6784.
- (95) Shao, Y. D.; Dong, M. M.; Wang, Y. A.; Cheng, P. M.; Wang, T.; Cheng, D. J. Organocatalytic Atroposelective Friedländer Quinoline Heteroannulation. *Org. Lett.* **2019**, *21* (12), 4831–4836.
- (96) Shah, P.; Westwell, A. D. The Role of Fluorine in Medicinal Chemistry. *J. Enzyme Inhib. Med. Chem.* **2007**, *22* (5), 527–540.
- (97) Hagmann, W. K. The Many Roles for Fluorine in Medicinal Chemistry. *J. Med. Chem.* **2008**, *51* (15), 4359–4369.
- (98) Connon, S. J. Asymmetric Catalysis with Bifunctional Cinchona Alkaloid-Based Urea and Thiourea Organocatalysts. *Chem. Comm.* **2008**, No. 22, 2499–2510.
- (99) Grayson, M. N.; Houk, K. N. Cinchona Urea-Catalyzed Asymmetric Sulfa-Michael Reactions: The Brønsted Acid-Hydrogen Bonding Model. *J. Am. Chem. Soc.* **2016**, *138* (29), 9041–9044.
- (100) Çelebi-Ölçüm, N.; Aviyente, V.; Houk, K. N. Mechanism and Selectivity of Cinchona Alkaloid Catalyzed [1,3]-Shifts of Allylic Trichloroacetimidates. *J. Org. Chem.* **2009**, *74* (18), 6944–6952.
- (101) Grayson, M. N.; Houk, K. N. Cinchona Urea-Catalyzed Asymmetric Sulfa-Michael Reactions: The Brønsted Acid-Hydrogen Bonding Model. *J. Am. Chem. Soc.* **2016**, *138* (29), 9041–9044.
- (102) Shirakawa, S.; Yamamoto, K.; Maruoka, K. Phase-Transfer-Catalyzed Asymmetric SNAr Reaction of α -Amino Acid Derivatives with Arene Chromium Complexes. *Angew. Chem. Int. Ed.* **2015**, *54* (3), 838–840.
- (103) Purser, S.; Moore, P. R.; Swallow, S.; Gouverneur, V. Fluorine in Medicinal Chemistry. *Chem. Soc. Rev.* **2008**, *37* (2), 320–330.
- (104) Pupo, G.; Vicini, A. C.; Ascough, D. M. H.; Ibba, F.; Christensen, K. E.; Thompson, A. L.; Brown, J. M.; Paton, R. S.; Gouverneur, V. Hydrogen Bonding Phase-Transfer Catalysis with Potassium Fluoride: Enantioselective Synthesis of β -Fluoroamines. *J. Am. Chem. Soc.* **2019**, *141* (7), 2878–2883.

- (105) Pupo, G.; Ibba, F.; Ascough, D. M. H.; Vicini, A. C.; Ricci, P.; Christensen, K. E.; Pfeifer, L.; Morphy, J. R.; Brown, J. M.; Paton, R. S.; Gouverneur, V. Asymmetric Nucleophilic Fluorination under Hydrogen Bonding Phase-Transfer Catalysis. *Science* **2018**, *360* (6389), 638–642.
- (106) Liu, J. Y.; Yang, X. C.; Liu, Z.; Luo, Y. C.; Lu, H.; Gu, Y. C.; Fang, R.; Xu, P. F. An Atropo-Enantioselective Synthesis of Benzo-Linked Axially Chiral Indoles via Hydrogen-Bond Catalysis. *Org. Lett.* **2019**, *21* (13), 5219–5224.
- (107) Patel, N. D.; Wei, X.; Byrne, D.; Narayanan, B. A.; Pennino, S.; Sarvestani, M.; Saha, A.; Haddad, N.; Kapadia, S.; Lorenz, J. C.; Decroos, P.; Ye, A.; Lee, H.; Grinberg, N.; Hossain, A.; Busacca, C. A.; Yee, N. K.; Senanayake, C. H. Sulfone-Mediated S_NAr Reaction as a Powerful Tool for the Synthesis of 4-Quinolinylnyl Ethers and More-Application to the Synthesis of HCV NS3/4a Protease Inhibitor BI 201420. *J. Org. Chem.* **2020**, *85* (13), 8339–8351.
- (108) Parker, C. G.; Galmozzi, A.; Wang, Y.; Correia, B. E.; Sasaki, K.; Joslyn, C. M.; Kim, A. S.; Cavallaro, C. L.; Lawrence, R. M.; Johnson, S. R.; Narvaiza, I.; Saez, E.; Cravatt, B. F. Ligand and Target Discovery by Fragment-Based Screening in Human Cells. *Cell* **2017**, *168* (3), 527–541.
- (109) Saunders, C.; Khaled, M. B.; Weaver, J. D.; Tantillo, D. J. Prediction of ¹⁹F NMR Chemical Shifts for Fluorinated Aromatic Compounds. *J. Org. Chem.* **2018**, *83* (6), 3220–3225.
- (110) Shcherbakov, A. A.; Roos, M.; Kwon, B.; Hong, M. Two-Dimensional ¹⁹F–¹³C Correlation NMR for ¹⁹F Resonance Assignment of Fluorinated Proteins. *J. Biomol. NMR* **2020**, *74* (2–3), 193–204.
- (111) Mishra, S. K.; Suryaprakash, N. Intramolecular Hydrogen Bonding Involving Organic Fluorine: NMR Investigations Corroborated by DFT-Based Theoretical Calculations. *Molecules* **2017**, *22* (3), 423–467.
- (112) Persson, J.; Matsson, O. Use of Fluorine Kinetic Isotope Effects in the Study of Steric Effects in Nucleophilic Aromatic Substitution Reactions. *J. Org. Chem.* **1998**, *63* (25), 9348–9350.
- (113) Benet, L. Z.; Hosey, C. M.; Ursu, O.; Oprea, T. I. BDDCS, the Rule of 5 and Drugability. *Advanced Drug Delivery Reviews*. **2016**, 89–98.
- (114) DeGoey, D. A.; Chen, H. J.; Cox, P. B.; Wendt, M. D. Beyond the Rule of 5: Lessons Learned from AbbVie’s Drugs and Compound Collection. *J. Med. Chem.* **2018**, 2636–2651.
- (115) Liu, Z.; Hu, M.; Yang, Y.; Du, C.; Zhou, H.; Liu, C.; Chen, Y.; Fan, L.; Ma, H.; Gong, Y.; Xie, Y. An Overview of PROTACs: A Promising Drug Discovery Paradigm. *Mol. Biomed.* **2022**, *3* (46), 1–26.

- (116) Raina, K.; Forbes, C. D.; Stronk, R.; Rappi, J. P.; Eastman, K. J.; Gerritz, S. W.; Yu, X.; Li, H.; Bhardwaj, A.; Forgione, M.; Hundt, A.; King, M. P.; Posner, Z. M.; Denny, A.; McGovern, A.; Puleo, D. E.; Garvin, E.; Chenard, R.; Zaware, N.; Mousseau, J. J.; Macaluso, J.; Martin, M.; Bassoli, K.; Jones, K.; Garcia, M.; Howard, K.; Smith, L. M.; Chen, J. M.; De Leon, C. A.; Hines, J.; Kayser-Bricker, K. J.; Crews, C. M. Regulated Induced Proximity Targeting Chimeras (RIPTACs): A Novel Heterobifunctional Small Molecule Therapeutic Strategy for Killing Cancer Cells Selectively. *bioRxiv* **2023**, 1–26.
- (117) Pettinato, M. C. Introduction to Antibody-Drug Conjugates. *Antibodies* **2021**, *10* (42) 1–11.
- (118) Qureshi, R.; Irfan, M.; Gondal, T. M.; Khan, S.; Wu, J.; Hadi, M. U.; Heymach, J.; Le, X.; Yan, H.; Alam, T. AI in Drug Discovery and Its Clinical Relevance. *Heliyon* **2023**, *9* (e17575), 1–23.
- (119) Forrest, I.; Parker, C. G. Proteome-Wide Fragment-Based Ligand and Target Discovery. *Isr. J. Chem.* **2023**, *63* (e202200098), 1–13.
- (120) Kirsch, P.; Hartman, A. M.; Hirsch, A. K. H.; Empting, M. Concepts and Core Principles of Fragment-Based Drug Design. *Molecules* **2019**, *24*, 1–22.
- (121) Baskin, J. M.; Prescher, J. A.; Laughlin, S. T.; Agard, N. J.; Chang, P. V.; Miller, I. A.; Lo, A.; Codelli, J. A.; Bertozzi, C. R. Copper-Free Click Chemistry for Dynamic in Vivo Imaging. *Proceedings of the National Academy of Sciences* **2007**, *104* (43), 16793–16797.
- (122) Bissonnette, N. B.; Boyd, M. J.; May, G. D.; Giroux, S.; Nuhant, P. C-H Functionalization of Heteroarenes Using Unactivated Alkyl Halides through Visible-Light Photoredox Catalysis under Basic Conditions. *J. Org. Chem.* **2018**, *83* (18), 10933–10940.
- (123) Duncton, M. A. J. Minisci Reactions: Versatile CH-Functionalizations for Medicinal Chemists. *MedChemComm* **2011**, *2* (12), 1135–1161.
- (124) O'Hara, F.; Blackmond, D. G.; Baran, P. S. Radical-Based Regioselective C-H Functionalization of Electron-Deficient Heteroarenes: Scope, Tunability, and Predictability. *J. Am. Chem. Soc.* **2013**, *135* (32), 12122–12134.
- (125) Smith, J. M.; Dixon, J. A.; Degruyter, J. N.; Baran, P. S. Alkyl Sulfinates: Radical Precursors Enabling Drug Discovery. *J. Med. Chem.* **2019**, *62* (5), 2256–2264.
- (126) Molander, G. A.; Colombel, V.; Braz, V. A. Direct Alkylation of Heteroaryls Using Potassium Alkyl- and Alkoxyethyltrifluoroborates. *Org. Lett.* **2011**, *13* (7), 1852–1855.
- (127) DiRocco, D. A.; Dykstra, K.; Krska, S.; Vachal, P.; Conway, D. V.; Tudge, M. Late-Stage Functionalization of Biologically Active Heterocycles through Photoredox Catalysis. *Angew. Chem. Int. Ed.* **2014**, *53* (19), 4802–4806.

- (128) Wang, J.; Li, G. X.; He, G.; Chen, G. Photoredox-Mediated Minisci Alkylation of N-Heteroarenes Using Carboxylic Acids and Hypervalent Iodine. *Chem. Sci.* **2016**, *7* (7), 6407–6412.
- (129) Proctor, R. S. J.; Davis, H. J.; Phipps, R. J. Catalytic Enantioselective Minisci-Type Addition to Heteroarenes. *Science* **2018**, *360* (6387), 419–422.
- (130) Liu, X.; Liu, Y.; Chai, G.; Qiao, B.; Zhao, X.; Jiang, Z. Organocatalytic Enantioselective Addition of α -Aminoalkyl Radicals to Isoquinolines. *Org. Lett.* **2018**, *20* (19), 6298–6301.
- (131) Genov, G. R.; Douthwaite, J. L.; Lahdenperä, A. S. K.; Gibson, D. C.; Phipps, R. J. Enantioselective Remote C-H Activation Directed by a Chiral Cation. *Science* **2020**, *367*, 1246–1251.
- (132) Čorić, I.; List, B. Asymmetric Spiroacetalization Catalysed by Confined Brønsted Acids. *Nature* **2012**, *483* (7389), 315–319.
- (133) Tsuji, N.; Kennemur, J. L.; Buyck, T.; Lee, S.; Prévost, S.; Kaib, P. S. J.; Bykov, D.; Farès, C.; List, B. Activation of Olefins via Asymmetric Brønsted Acid Catalysis. *Science* **2018**, *359* (6383), 1501–1505.